



كلية العلوم والهندسة
College of Science & Engineering

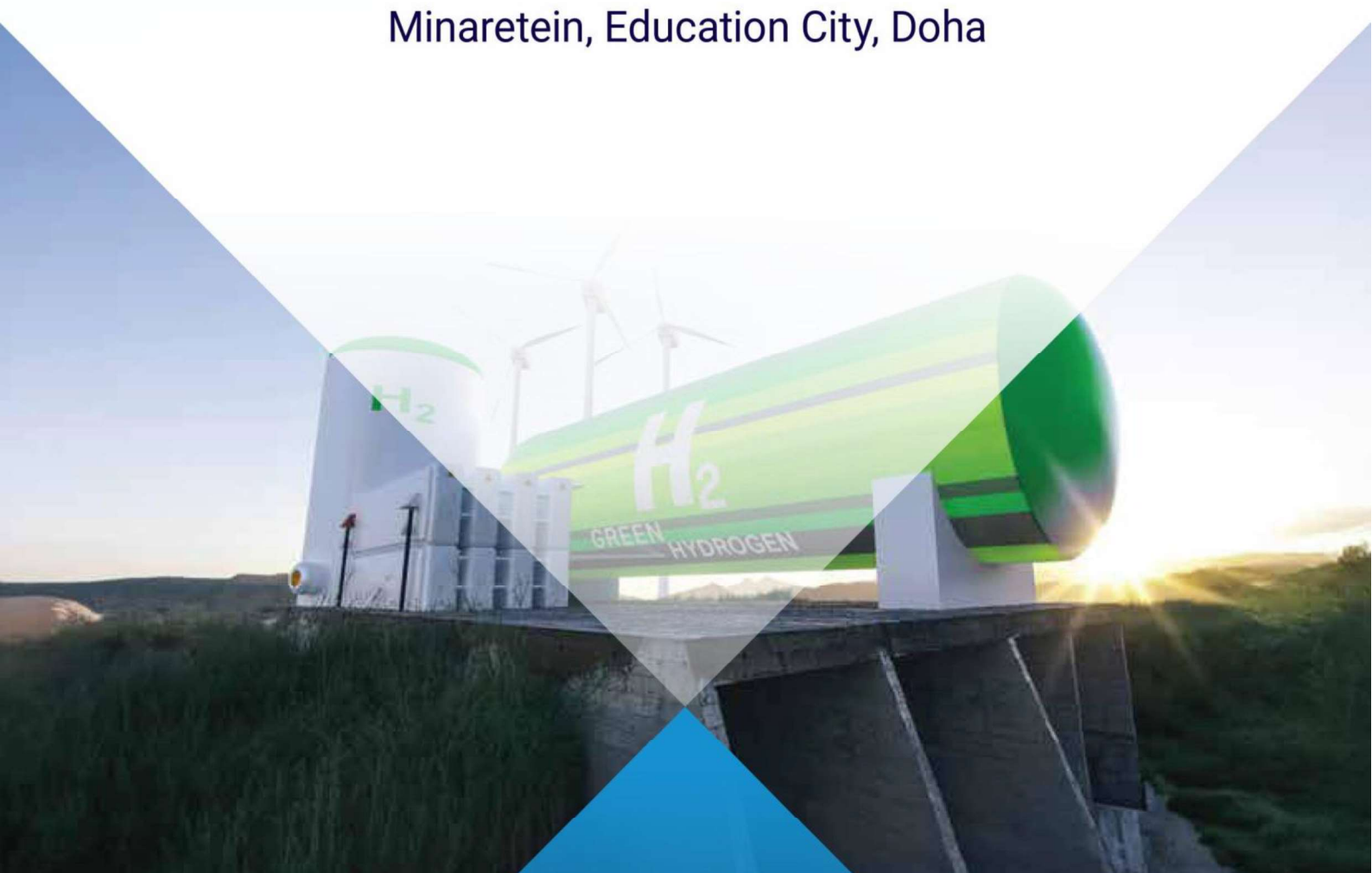
جامعة حمد بن خليفة
HAMAD BIN KHALIFA UNIVERSITY



14TH INTERNATIONAL CONFERENCE ON HYDROGEN PRODUCTION (ICH2P-2023)

DECEMBER 19 - 21, 2023

Minaretein, Education City, Doha



Program Layout

Day 1 | Tuesday, December 19, 2023

08:00 am-9:00 am	Conference Registration	Exhibition Hall
09:00 am-10:00 am	Opening Ceremony (Welcoming Talks)	Auditorium
10:00 am-10:45 am	Keynote Talks	Auditorium
10:45 am-11:15 am	Coffee Break	Exhibition Hall
11:15 am-12:45 pm	Keynote Talks	Auditorium
12:45 pm-02:00 pm	Lunch	Exhibition Hall
02:00 pm-03:30 pm	Industry Panel Session	Auditorium
03:30 pm-04:00 pm	Coffee Break (with Poster Presentations)	Exhibition Hall
04:00 pm-05:30 pm	Parallel Scientific Sessions	Conference Rooms

Day 2 | Wednesday, December 20, 2023

09:00 am-10:30 am	Plenary Sessions	Auditorium
10:30 am-10:45 am	Coffee Break (with Poster Presentations)	Exhibition Hall
10:45 am-12:30 pm	Parallel Scientific Sessions	Conference Rooms
12:30 pm-02:00 pm	Lunch	Exhibition Hall
02:00 pm-03:30 pm	Parallel Scientific Sessions	Conference Rooms
03:30 pm-04:00 pm	Coffee Break (with Poster Presentations)	Exhibition Hall
04:00 pm-05:30 pm	Parallel Scientific Sessions	Conference Rooms
06:30 pm-08:30 pm	Gala Dinner and Awards Ceremony	

Day 3 | Thursday, December 21, 2023

09:00 am-06:15 pm	Hydrogen Energy Course	Auditorium
09:00 am-10:30 am	Parallel Scientific Sessions	Conference Rooms
10:30 am-11:00 am	Coffee Break (with Poster Presentations)	Exhibition Hall
11:00 am-12:30 pm	Parallel Scientific Sessions	Conference Rooms
12:30 pm-02:00 pm	Lunch	Exhibition Hall
02:00 pm-03:30 pm	Parallel Scientific Sessions	Conference Rooms
03:30 pm-04:00 pm	Coffee Break (with Poster Presentations)	Exhibition Hall
04:00 pm-05:30 pm	Parallel Scientific Sessions	Conference Rooms
06:15 pm-06:30 pm	Closing Ceremony	Auditorium
06:30 pm-09:30 pm	Optional Social Tour	

Day 1 | Tuesday, December 19, 2023

Time	Program	Location
08:00 am-09:00 am	Conference Registration	Exhibition Hall
09:00 am-10:00 am	<p style="text-align: center;">OPENING CEREMONY</p> <p style="text-align: center;">Dr. Ala Al-Fuqaha Associate Provost Hamad Bin Khalifa University</p> <p style="text-align: center;">Dr. Yusuf Bicer Co-Chair of the Conference Hamad Bin Khalifa University</p> <p style="text-align: center;">Dr. Tareq Al-Ansari Co-Chair of the Conference Hamad Bin Khalifa University</p> <p style="text-align: center;">Dr. Mounir Hamdi Dean, College of Science and Engineering Hamad Bin Khalifa University</p> <p style="text-align: center;">H.E. Dr. Mohammed Bin Saleh Al-Sada Former Minister of Energy and Industry in Qatar Chairman of the Joint Advisory Board of Texas A&M University at Qatar Chairman of the Board of Trustees of the Doha University of Science and Technology</p>	Auditorium
Keynote Talks		
10:00 am-10:45 am	<p style="text-align: center;">ICH2P14-KN1</p> <p style="text-align: center;">New Horizons in Hydrogen Production Technologies</p> <p style="text-align: center;">Keynote Speaker - Dr. Ibrahim Dincer</p> <p style="text-align: center;">Professor, Ontario Tech University, Canada</p>	Auditorium
10:45 am-11:15 am	Coffee Break	Exhibition Hall

Day 1 | Tuesday, December 19, 2023

11:15 am-12:00 pm	<p style="text-align: center;">ICH2P14-KN2</p> <p style="text-align: center;">Development of Manufacturing Techniques for Highly Performing Polymer Electrolyte Membrane Fuel Cells</p> <p style="text-align: center;">Keynote Speaker – Dr. Xianguo Li</p> <p style="text-align: center;">Professor, University of Waterloo, Canada</p>	Auditorium
12:00 pm-12:45 pm	<p style="text-align: center;">ICH2P14-KN3</p> <p style="text-align: center;">Hydrogen and Fuel Cell Development and the Benefit of Digital Twin and Artificial Intelligence in this field</p> <p style="text-align: center;">Keynote Speaker - Dr. Abdul Ghani Olabi</p> <p style="text-align: center;">Professor, University of Sharjah, UAE</p>	Auditorium
12:45 pm-02:00 pm	Lunch	Exhibition Hall
02:00 pm-03:30 pm	<p style="text-align: center;">Industry Panel Session</p> <p style="text-align: center;"><u>Moderator:</u> Sean van der Post Global Offshore Business Director, Lloyd's Register</p>	Auditorium

Day 1 | Tuesday, December 19, 2023

Poster Number	Poster Presentations 3:30 PM - 4:00 PM Chair: Dr. Burak Yuzer	Exhibition Hall
ICH2P14 – PP175	Turquoise Hydrogen Production: Carbon Management and Conversion to Sustainable Energy Carriers <u>Aliya Banu, Yusuf Bicer</u>	
ICH2P14 – PP166	Evaluation of Hydrogen Production from Ammonia Reforming on Ni/ZnO Nanowire Catalysts <u>Hiroya Tamai, Hironori Nakajima</u>	
ICH2P14 – PP114	Photocatalytic Hydrogen Generation from Seawater Using High Performance Polymeric Materials <u>Noora Al-Subaiej, Ghalya Abdulla, Mohammed Al-Hashimi, Konstantinos E Kakosimos</u>	
ICH2P14 – PP008	Long-Term Assessment of Hydrogen Technology Deployment for Large Scale Decarbonisation of Power Production <u>Kamran Khammadoy, Damian Flynn, Eoin Syron</u>	
ICH2P14 – PP 013	Use of Refinery Off Gas (ROG) as CO ₂ Emission Reduction and Natural Gas (Ng) Savings in Hydrogen (H ₂) Production <u>Marcelo Tagliabue</u>	
ICH2P14 – PP139	Performances of Commercial Zeolites with Different Acidities for Catalytic CO ₂ Hydrogenation to Dimethyl Ether Using Copper/Zinc/Alumina Catalyst <u>Abdelbaki Benamor, Assem Mohamed, Abdul Hakeem Anwer, Siham AlQaradawi, Mohammed Saad</u>	
ICH2P14 – PP075	Modeling of Hydrogen Liquifaction Process Parameters Using Advanced Artificial Intelligence Technique <u>A. Abdallah El Hadj, Ait yahia, Hamza. K, M. Laidi, S. Hanini</u>	
ICH2P14 – PP066	Hydrogen Protection of the Mechanical Properties and Electrochemical Effects by Bio-Corrosion Inhibitors on Carbon Steel in the Presence of Aggressive Media <u>Mouna Amara, Azedine Belalia, Mohammed HadjMeliani, Hadjer Didouh, Rami K.Suleiman, Guy Pluvinage</u>	
ICH2P14 - PP192	Hydrogen from Catalytic Steam Reforming of Biomass <u>Sergio Rapaqñà, Alessandro Antonio Papa, Andrea Di Carlo</u>	
ICH2P14 - PP161	Textile Wastewater Treatment and Hydrogen Generation with Ion-Exchange Resins on Solar-Assisted Bipolar Membrane Electrolysis Process <u>Burak Yuzer, Ragad F. Alshebli, Nadira Salsabila, Yusuf Bicer</u>	
ICH2P14 - PP170	In-Situ Current Distribution Measurements of a Planar Solid Oxide Fuel Cell for a Three-Dimensional Finite Element Model Train a Machine-Learning Surrogate Model <u>Yutaro Ito, Yingtian Chi, Hironori Nakajima</u>	

Day 1 | Tuesday, December 19, 2023

Parallel Sessions 1

Time	Auditorium	Conference Room – A048	Conference Room – A046
04:00 pm-05:30 pm	<p>Session 1A: Clean Hydrogen Production Chair: Dr. Fadwa ElJack Co-Chair: Dr. Fares A. Almomani</p>	<p>Session 1B: Waste to Hydrogen Energy Chair: Dr. Tareq Al-Ansari Co-Chair: Dr. Mohammad Alherbawi</p>	<p>Session 1C: Hydrogen Production Catalysts Chair: Dr. Abdulkarem Amhamed Co-Chair: Dr. Ahmed Abdala</p>
04:00 pm-04:15 pm	<p>Invited Talk</p> <p>ICH2P14-IT1</p> <p>Green Hydrogen Production: Solar Chimney Power Plant Integrated with Water Desalination Plant</p> <p>Dr. Fares A. Almomani</p> <p>Department of Chemical Engineering, Qatar University</p>	<p>ICH2P14 - OP010</p> <p>A Novel Cost-Effective Approach for Production of Hydrogenase Enzymes and Molecular Hydrogen from Whey-Based By-Products</p> <p><i>Anna Poladyan, Meri Iskandaryan, Ofelya Karapetyan, Ela Minasyan, Anait Vassilian, Karen Trchounian, Garabed Anatronikian</i></p>	<p>ICH2P14 - OP037</p> <p>Synergizing Hydrogen and Chlorine Gas Production for Enhanced Resource Utilization Using Earth-Abundant Electrocatalysts</p> <p><i>Ahmed Badreldin, Ahmed Abdel-Wahab</i></p>
04:15 pm-04:30 pm		<p>ICH2P14 - OP044</p> <p>Biotechnological Potential of Spent Coffee Grounds for Large-Scale Hydrogen Production</p> <p><i>Liana Vanyan, Anait Vassilian, Anna Poladyan, Karen Trchounian</i></p>	<p>ICH2P14 - OP171</p> <p>Ni-Cu Bimetallic Catalysts for Effective Syngas Production via Low-Temperature Methane Steam Reforming</p> <p><i>Martin Khzouz, Babak Fakhim, Saleh Babaa, Mohammad Ghaleeh, Faraooq Sher, Evangelos I. Gkanas</i></p>
04:30 pm-04:45 pm	<p>ICH2P14 – OP095</p> <p>A Solar Pond Integrated with Bifacial Solar Panels for Power and Hydrogen Generation</p> <p><i>Dogan Erdemir, Ibrahim Dincer</i></p>	<p>ICH2P14 – OP069</p> <p>Biohydrogen Production from Various Industrial Wastewater of Chalawa, Kano, Nigeria</p> <p><i>Garba Uba, Abdulhadi Yakub, Salisu Ahmed, Ibrahim Abdulganiyyu</i></p>	<p>ICH2P14 - OP017</p> <p>Kinetic Modelling and Process Optimization for Blue Hydrogen Production Via Ammonia Cracking</p> <p><i>Raqad Aldilajjan, Sai Katikaneni, Osamah Siddiqui, Mohammad Rakib, Bandar Solami</i></p>
04:45 pm-05:00 pm	<p>ICH2P14 – OP205</p> <p>PV-AWG-H₂: A Potential Method for Sustainable Hydrogen Production in Qatar</p> <p><i>Aiyad Gannan, Nagi Abdussamie</i></p>	<p>ICH2P14 – OP102</p> <p>Syngas Production Using Catalyst Based on Local Minerals Extruded as Honeycomb Monolith</p> <p><i>Tarik Chafik</i></p>	<p>ICH2P14 – OP122</p> <p>Synthesis, Characterization, and Application of Bio-Templated Ni-Ce/Al₂O₃ Catalyst for Clean H₂ Production in the Steam Reforming of Methane Process</p> <p><i>Mohammad Reza Rahimpour, Maryam Koohi-Saadi</i></p>
05:00 pm-05:15 pm	<p>ICH2P14 - OP083</p> <p>Design and Performance Analysis of Green Hydrogen Production from Hybrid Solar PV/Wind Turbine Energy System</p> <p><i>Chaouki Ghenai</i></p>	<p>ICH2P14 – OP125</p> <p>Green Energy from Waste: A Systems Engineering Approach to Bio-Hydrogen Production</p> <p><i>Salman Raza Naqvi, Bilal Kazmi, Syed Ali Ammar Taqvi, Imtiaz Ali, Muhammad Shahbaz</i></p>	<p>ICH2P14 – OP211</p> <p>Integrated SMR System for Efficient Hydrogen and Power Production</p> <p><i>Abdullah A. AlZahrani, Mansur Aliyu</i></p>
05:15 pm-05:30 pm	<p>ICH2P14 – OP123</p> <p>Green Hydrogen Based Ammonia Production Process: Insight into Energy and CO₂ Emissions Minimization</p> <p><i>Swaprabha P. Patel, Ashish M. Gujarathi, Piyush Vanzara</i></p>	<p>ICH2P14 – OP113</p> <p>Development of a Hydrogen Production Model for The Gasification of Municipal Solid Waste and Its Constituents Using Aspen Plus Using Cao for CO₂ Capture</p> <p><i>Muhammad Shahbaz, Prakash Parthasarathy, Mohammad Alherbawi, Gordon McKay, Tareq Al-Ansari</i></p>	<p>ICH2P14 - OP144</p> <p>Hydrogen Production Via Steam Reforming of Methanol (SRM) Using Cu/ZnO/Al₂O₃ Catalyst</p> <p><i>Masresha Adasho Achomo, P. Muthukumar, Nageswara Rao Peela</i></p>

End of the Day

Day 2 | Wednesday, December 20, 2023




Time	Plenary Session	Location
09:00 am - 09:45 am	<p style="text-align: center;">ICH2P14-KN4</p> <p style="text-align: center;">Sustainable Feedstocks and Integrated Bioprocess for Biohydrogen Production in Arid and Desert Regions</p> <p style="text-align: center;">Keynote Speaker - Dr. Moktar Hamdi</p> <p style="text-align: center;">Professor, National Institute of Applied Sciences and Technology, University Carthage, Tunisia</p>	Auditorium
09:45 am - 10:30 am	<p style="text-align: center;">ICH2P14-KN5</p> <p style="text-align: center;">A Framework to Evaluate Economics and CO2 Fixation potential of New Carbon Capture and Utilization (CCU) Reaction Pathways – Towards Golden Hydrogen Production</p> <p style="text-align: center;">Keynote Speaker - Dr. Nimir Elbashir</p> <p style="text-align: center;">Professor, Chemical Engineering, Director TEES Gas and Fuels Research Center, Texas A&M University at Qatar</p>	Auditorium
10:30 am - 10:45 am	Coffee Break with Poster Presentations	Exhibition Hall

Poster Number	Poster Presentations 10:30 am-10:45 am Chair: Dr. Burak Yuzer	Exhibition Hall
ICH2P14 – PP117	Redox Regulation of Hydrogen Production in Escherichia Coli During Growth on Byproducts of the Wine Industry <i>Lusine Baghdasaryan, Ofelya Karapetyan, Karen Trchounian, Garabed Antranikian, Anna Poladyan</i>	
ICH2P14 – PP118	Comparative Economic Analysis of Small Modular Reactor Hydrogen Cogeneration and Conventional Gas-Fired Plant for Load Following: A Case Study <i>Derrick Whelan, Lixuan Lu</i>	
ICH2P14 – PP124	Ship Design Adaptations for LNG Propulsion, Carbon Capture Utilization, and Hybrid Technologies <i>Aisha Al-Asmakh, Yusuf Bicer, Tareq Alansari</i>	
ICH2P14 – PP128	Green Hydrogen Production: A Cost Comparison of Different Electrolysis Technologies <i>Hafiz Muhammad Uzair Ayub, Sabla Y. Alnouri</i>	
ICH2P14 – PP012	Comparative Study Between GBO and BES Optimization Algorithms for Optimal PEMFC Parameters Identification <i>Ahmed Zouhir Kouache, Ahmed Djafour, Khaled Mohammed Said Benzaoui, Souheil Touili</i>	📶
ICH2P14 – PP172	Integrated Hydrogen Production and Purple Phototrophic Bacteria Biomass Recovery via Electrocoagulation <i>Ojima Wada, Burak Yuzer, Yusuf Bicer, Gordon McKay, Hamish Mackey</i>	
ICH2P14 – PP188	Hydrogen Naval Propulsion: Problems and Solutions <i>Remili Sadia, Mohamed Chaimaa</i>	
ICH2P14 - PP186	Study of the Energy and Financial Performance of Hydrogen Production with Solar Energy and Photoelectrolyzer/PEM in the Algerian Desert Region (OUARGLA) <i>Madjeda Ramdani, Ahmed Djafour, El Mouatez Billah Messini, Ahmed Zouhir Kouache, Zineb Bensaci</i>	📶
ICH2P14 – PP014	Investigating the Effect of Using Hydrogen as a Fuel on Performances of Gas Turbine Operating at Lean Condition in Site of Hassi R'MEL <i>Fethia AMROUCHE, Bouziane Mahmah, Lidya Boudjema, Oum Keltoum Bari</i>	

Day 2 | Wednesday, December 20, 2023

Parallel Sessions 2			
Time	Auditorium	Conference Room – A048	Conference Room – A046
10:45 am-12:30 pm	Session 2A: Hydrogen Storage Chair: Dr. Fadwa El Mellouhi Co-Chair: Dr. Dhabia M. Al-Mohannadi	Session 2B: Bio-Hydrogen Chair: Dr. Ibrahim M. Abu-Reesh Co-Chair: Dr. Burak Yuzer	Session 2C: Low-Carbon Hydrogen with Reforming Chair: Dr. Anand Kumar Co-Chair: Dr. Mohammad Alherbawi
10:45 am-11:00 am	Invited Talk ICH2P14-IT2 Iron Based Hydrogen Storage and Transport	ICH2P14 – OP024 Biogas Dry Reforming to Syngas Using Catalyst Based on Local Minerals Extruded as Honeycomb Monolith <u>Tarik Chafik</u>	Invited Talk ICH2P14-IT3 Analyzing Grey and Blue Hydrogen Production Costs in Steam-Methane, Auto-Thermal, and Non-Catalytic Partial Oxidation Reforming Plants
11:00 am-11:15 am	Dr. Viktor Hacker Professor, Graz University of Technology, Institute of Chemical Engineering and Environmental Technology, Austria	ICH2P14 – OP197 A Net-Zero Emission System with Biogas-Fed Solid Oxide Fuel Cell for Hydrogen Production to Advance Sustainability in the Textile Industry <u>Baraka Abbas, Hooreen Ansari, Kabsha Zain, Wasifa Umer, Abeeha Fatima, Khurram Kamal, Tahir A.H. Ratlamwala</u>	Mary Katebah, Ma'moun Al-Rawashdeh, Patrick Linke Texas A&M University at Qatar
11:15 am-11:30 am	ICH2P14 – OP133 Graded Gyroid-Enhanced Metal Hydride Container for Efficient Hydrogen Storage Application <u>Luthfan Adhy Lesmana, Muhammad Aziz</u>	ICH2P14 - OP048 Biogas Production from Date Palm Fruit Waste in Jigawa State Nigeria <u>Abdulhadi Yakubu, Garba Uba, Zainab Abbas Abdulhadi, Ahmed Muhammad Gumel</u>	ICH2P14 - OP091 Piston Reactor Capabilities to Make Hydrogen from Methane Via Steam and Autothermal Reforming – Modeling Study <u>Aya Abousrafa, Patrick Linke, Ma'moun Al-Rawashdeh</u>
11:30 am-11:45 am	ICH2P14 - OP027 Transportation and Storage of Hydrogen by LOHC: Design and Simulation of the Dehydrogenation Reactor <u>Pietro Delogu, Elena Barbera, Andrea Mio, Alberto Bertucco, Maurizio Fermeqlia</u>	ICH2P14 – OP049 Production of Bioethanol from Groundnut Shell as a Substrate <u>Abdulhadi Yakubu, Garba Uba, Zainab Abbas Abdulhadi</u>	ICH2P14 – OP023 Membrane Reformer Technology for Sustainable Hydrogen Production from Hydrocarbon Feedstocks <u>Alaa Albasry, Ahmed Naimi, Abdulbari Alqarni, Minseok Bae, Bandar Solami, Stephen Paglieri, Aadesh Harale</u>
11:45 am-12:00 pm	ICH2P14 – OP126 Methods of Hydrogen Production, Storage and Transportation <u>Sayel M. Fayyad, A.m. Maqableh</u>	ICH2P14 - OP165 Hydrogen Gas and Biochar Production from Kitchen Waste Via Dark Fermentation <u>Sniqdhendubala Pradhan, Burak Yuzer, Yusuf Bicer, Gordon Mckay</u>	ICH2P14 – OP057 Catalytic Conversion of CO ₂ to CO Via Methane Dry Reforming and Reverse Water Gas Shift Reaction <u>Parisa Ebrahimi, Mohammed Al-Marri, Majeda Khraisheh, Anand Kumar</u>
12:00 pm-12:15 pm	ICH2P14 – OP109 Multi-Response Optimization of Absorption and Desorption Parameters in a Metal Hydride Based Hydrogen Storage System <u>Alok Kumar, Purushothaman Nandagopalan, P. Muthukumar, Ranjith Thangavel</u>	ICH2P14 – OP067 An Optimum Approach for Biohydrogen Production Using Poplar <u>A. Yaqmur Goren, Muratcan Kenez, Ibrahim Dincer, Ali Khalvati</u>	ICH2P14 - OP155 Enhancing Ni-Supported Catalysts for Efficient Dry Reforming of Methane: Effects of Halloysite Nanotubular Clay Surface Activation <u>Ahmed Abotaleb, Dema Al-Masri, Alaa Alkhateb, Kamal Mroue, Atef Zekri, Yasmin Mashhour, Alessandro Sinopoli</u>
12:15 pm-12:30 pm	ICH2P14 - OP031 Experimental Investigation on Novel Multi-Tube Metal Hydride Reactor for Large Capacity Hydrogen Storage Applications <u>Shubham Parashar, P. Muthukumar, Atul Kumar Soti</u>	ICH2P14 – OP087 Biomethanol and Hydrogen Production from Pinecone Biomass Using Steam Gasification <u>Hilal Sayhan Akci Turqut, Ibrahim Dincer</u>	ICH2P14 - OP047 The Hydrogen Production Using Steam Methane Reforming Based on Central Receiver <u>Ali Alaidaros, Abdullah A. AlZahrani</u>
12:30 pm-02:00 pm Lunch Exhibition Hall			





Day 2 | Wednesday, December 20, 2023

Parallel Sessions 3			
Time	Conference Room – A047	Auditorium	Conference Room – A046
02:00 pm-03:30 pm	Session 3A: Electrochemical Hydrogen Chair: Dr. Ahmed Abdala Co-Chair: Dr. Dogan Erdemir	Session 3B: Decarbonization through Hydrogen Chair: Dr. Marcello Contestabile Co-Chair: Dr. Luluwah Al-Fagih	Session 3C: Hydrogen in Transportation Applications Chair: Dr. Sertac Bayhan Co-Chair: Dr. Abdulla Al Wahedi
02:00 pm-02:15 pm	ICH2P14 - OP064 Effect of Volume Concentration and Sonication Time on the Performance of Hybrid Solar Collector Based Hydrogen Production System with Hybrid Nanofluid: An Experimental Investigation M.Baskaran, S.Senthilraja R. Gangadevi, Mohamed M. Awad	Invited Talk ICH2P14-IT4 In the Green Zone: Navigating Carbon Management in the Hydrogen Shift Dr. Muftah El-Naas	ICH2P14 - OP007 Carbon Emission Reductions in the University of Sao Paulo's Transportation Sector Using Hydrogen-Powered Vehicles Beethoven Narváez-Romo, Danilo Perecin, Thiago Lopes, Daniel Lopes, Karen Mascarenhas, Suani Coelho, Julio R. Meneghini
02:15 pm-02:30 pm	ICH2P14 - OP073 Solar Energy Driven Silicon Photovoltaic Monolithic Electrochemical Cells for Efficient Hydrogen Production from Water Mourad Frites, Shahed Khan	Professor, Chemical Engineering, Qatar University	ICH2P14 – OP020 Experimental Investigation of Diesel Engine in Dual Fuel Mode by Using Hydrogen and Low Carbon Ether Blended Diesel Vasanthakumar Ravisankar, Loganathan Marimuthu, Vikneswaran Malaiperumal
02:30 pm-02:45 pm	ICH2P14 - OP163 Seawater Desalination and Hydrogen Production Using Monovalent Selective Membranes Assisted with Ion-Exchange Resins for Hydroponic Solution Production Ragad F. Alshebli, Nadira Salsabila, Burak Yuzer, Yusuf Bicer	ICH2P14 - OP159 Developing A Sustainable Production Framework for Green Hydrogen to Decarbonize Existing Industrial Clusters Afreenuzzaman Badruzzaman, Fadwa Eljack, Seckin Karagoz	ICH2P14 - OP150 Driving Toward Hydrogen Mobility: A Life Cycle Cost Analysis of Traditional, Electric, And Hydrogen Fuel Cell Vehicles in Qatar Carlos Méndez, Marcello Contestabile, Yusuf Biçer
02:45 pm-03:00 pm	ICH2P14 - OP085 Design Considerations of Artificial UV Light-Driven Photocatalytic Water Splitting for Production of Hydrogen in a Combined Solar/Artificial Light Reactor Ahmed Abbas, Shohda Makki, Konstantinos E. Kakosimos	ICH2P14 - OP164 Decarbonizing ASEAN By 2050: From the Lens of a Hydrogen Economy Archana Kumaraswamy, Sushant S Garud, Iftekhar A Karimi, Shamsuzzaman Farooq	ICH2P14 – OP099 An Adaptation of The Conventional LNG Floating Storage and Regasification Unit to Hydrogen and Ammonia Dindha Andriani, Muhammad Usman Sajid, Yusuf Bicer
03:00 pm-03:15 pm	ICH2P14 - OP174 Electrochemical Conversion of Carbon Dioxide into Formic Acid as Hydrogen Carrier: Role of Anolyte Muhammad Arsalan, Muftah H. El-Naas	ICH2P14 - OP177 Shades Of Sustainability: An In-Depth Analysis of The Direct and Indirect Carbon Footprint in Blue Ammonia Manufacturing Hussein Al-Yafei, Ahmed AlNouss, Saleh Aseel	ICH2P14 – OP130 Exergetic Analysis of the Process for Hydrogen Rich Syngas Production Through Biomass Gasification and Its Onsite Use in HCCI Engine for Land Transportation Tawfiq Al-Mughanam, Abdul Khaliq
03:15 pm-03:30 pm	ICH2P14 - OP074  Evaluation of a Novel Hybrid Photoelectrochemical-Conventional Hydrogen Generator Mehmet Gursoy, Ibrahim Dincer	ICH2P14 – OP190  Feasibility Study of Backing Up Energy Supply For Electric Charging Stations With Hydrogen Integration Huseyin Biyikci, Yusuf Bicer	ICH2P14 – OP110  Development of a Hybrid Powering System with Ammonia Fuel Cells and Internal Combustion Engine for Submarines Ibrahim Akgun, Ibrahim Dincer
Coffee Break with Poster Presentations Exhibition Hall			

Day 2 | Wednesday, December 20, 2023

Poster Number	Poster Presentations 03:30 pm-04:00 pm Chair: Dr. Burak Yuzer	Exhibition Hall
ICH2P14 – PP041	Fast Modeling Method of Gas Diffusion Layers of Polymer Electrolyte Membrane Fuel Cells <i>Hamid Reza Taheri, <u>Mohsen Shakeri</u></i>	
ICH2P14 – PP101	$La_{0.6}Sr_{0.4}Co_{0.2}Fe_{0.8}O_{3-\delta}$ (LSCF) Cathode Supported on Gadolinium-Doped Ceria Electrolyte Prepared by Screen-Printing Method and Performances Evaluation as Solid Oxide Fuel Cell at Intermediate Temperature <i>Oumaima Ettalibi, Hicham Ben Brahim Sbitri, Abdessamad Samid, Ouafae Achak, Raphael Ihringer, <u>Tarik Chafik</u></i>	
ICH2P14 – PP015	Sorption Properties of Ball-Milled Porous Silicon for Hydrogen Storage Up to 80 Bar <i>Rama Chandra Mudulij, Paresh Kale</i>	
ICH2P14 – PP016	Evaluation of Synergistic Integration of Nickel, Porous Silicon, and Thermally Reduced Graphene Oxide for Hydrogen Storage <i>Rama Chandra Mudulij, Neeraj Kumar Nishad, Paresh Kale</i>	
ICH2P14 – PP108	Hydrogen Adsorption Characteristics of Activated Carbon Derived from Prickly Pear Seed Cake <i>Rimene Dhahri, Imen Tlili</i>	
ICH2P14 – PP154	Facilitating Production of Acetate and Hydrogen Through Enhanced Electron Transfer and Substrate Mass Transfer Using a Multifunctional Photocathode with NiO/G-C ₃ N ₄ /Polythiophene <i>Abdul Hakeem Anwer, Assem Mohamed, Nafees Ahmed, Abdelbaki Benamor</i>	
ICH2P14 – PP167	Recovery Of Spent Acidic and Alkaline Liquors Generated in Metal Industry and Hydrogen Production by An Integrated System <i>Huseyin Selcuk, Yusuf Gunes, Ayse Elif Ates, Burak Yuzer, Yusuf Bicer</i>	
ICH2P14 – PP105	Neural network for the prediction of Biohydrogen Production during Dark Waste Organic Biomass Fermentation <i>Fares Almomani</i>	
ICH2P14 – PP201	Recent Technological Development and Advancements in Hydrogen Storage Technologies <i>Abhishek Sharma, Mohit Nayal, Siddharth Jain, Varun Pratap Singh</i>	

Day 2 | Wednesday, December 20, 2023

Parallel Sessions 4			
Time	Conference Room – A047	Auditorium	Conference Room – A046
04:00 pm-05:30 pm	Session 4A: Green Hydrogen Production Chair: Dr. Hicham Hamoudi Co-Chair: Dr. Ahmed AlNouss	Session 4B: Hydrogen Techno-Economics Chair: Dr. Ahmed Khalifa Co-Chair: Dr. Ikhlas Ghiat	Session 4C: Integrated Hydrogen Production Systems Chair: Dr. Ahmad K. Sleiti Co-Chair: Dr. Abdullah A. AlZahrani
04:00 pm-04:15 pm	ICH2P14 – OP082 Green Hydrogen Production and Solar to Hydrogen Ratio Using Bifacial Solar Photovoltaics and High Roof Surface Albedo Fahad Ahmad Faraz, Oussama Rejeb, Chaouki Ghenai	Invited Talk ICH2P14-IT5 Future and Potential of Hydrogen for Qatar Under Its Energy and Economic Transformation Quest	ICH2P14 - OP094 Innovative Integrated Multigeneration System for Sustainable Power, Hydrogen, and Ammonia Production Ahmad K. Sleiti, Wahib A. Al-Ammari, Mohammad Azizur Rahman
04:15 pm-04:30 pm	ICH2P14 – OP029 Green Hydrogen Production by Hydrolysis of Aluminum and Waste Recycling Pedro Ayala, Edgar Borja, P.J. Sebastian	Dr. Muammer Koc Professor, Division of Sustainable Development, College of Science and Engineering, Hamad Bin Khalifa University	ICH2P14 - OP009  Transient Simulation and Comparative Assessment of Two Concentrated-Solar Based Hydrogen Production Systems Integrated with Vanadium-Chlorine Thermochemical Cycle Erfan Zand, Mohammadreza Khosravi, Pouria Ahmadi, Mehdi Ashjaee
04:30 pm-04:45 pm	ICH2P14 – OP018 Solar Hydrogen Production with Direct and Indirect Design System Ilyès Nouicer, Sabah Menia, Fares Meziane, Nourine Kabouche, Chaouki Ghenai	ICH2P14 - OP036 A Techno-Economic Evaluation of the Integration of Direct Air Capture with Hydrogen and Solar Fuel Production Enric Prats-Salvado, Nathalie Monnerie, Christian Sattler	ICH2P14 – OP104 Green Hydrogen Production via Integrated Triple Technologies: Downdraft Tower, Photovoltaic and Electrolysis Emad Abdelsalam, Fares Almomani
04:45 pm-05:00 pm	ICH2P14 - OP025 Thermoelectric Condensation of Ambient Humidified Air for Green Hydrogen Production Hilal Ahmad, Taqi Ahmad Cheema, Hadeed Ahmed Sher	ICH2P14 - OP176 Flowsheet Safety and Techno-Economic Analysis of Optimum Ammonia and Urea Production Route Amzan Alsabri, Ahmed AlNouss, Fadwa ElJack	ICH2P14 – OP089 Electricity Hydrogen and Heat (EHH) Production in Stand-Alone Renewable Energy System El Manaa Barhoumi, Ikram Ben Belgacem, Manaf Zghaibeh, Mohamed Ouda
05:00 pm-05:15 pm	ICH2P14 – OP187 Optimum Green Hydrogen Production Through Biomass Feedstock Blending Ahmed AlNouss, Gordon Mckay, Tareq Al-Ansari	ICH2P14 - OP096 Techno-Economic Evaluation of Various Hydrogen Carriers Ahmad K. Sleiti, Laveet Kumar, Wahib A. Al-Ammari	ICH2P14 – OP080  A Clean Option for Potential Hydrogen Production Via Nuclear in Canada Gorkem Kubilay Karayel, Ibrahim Dincer
05:15 pm-05:30 pm	ICH2P14 – OP111  An Integrated Solar-Driven Chlor-Alkali System for Hydrogen and Chlorine Production Sümeyya Ayça, Ibrahim Dincer	ICH2P14 – OP193 Strategy Of Turkiye on Hydrogen Energy Serpil Edeballi, Mustafa Ersoz	ICH2P14 – OP088  A Study on Nuclear-Based Hydrogen Production System Via Three- and Four-Step Magnesium Chlorine Cycles Sulenur Asa, Adem Acir, Ibrahim Dincer
06:30 pm-08:30 pm Gala Dinner and Awards Ceremony Hotel			





Day 3 | Thursday, December 21, 2023

Parallel Sessions 5			
Time	Conference Room – A047	Conference Room – A048	Conference Room – A046
09:00 am-10:30 am	<p style="text-align: center;">Session 5A: Life Cycle Assessment of Hydrogen Chair: Dr. Mohamed Haouari Co-Chair: Dr. Tareq A. Al-Ansari</p>	<p style="text-align: center;">Session 5B: Hydrogen in Grids and Communities Chair: Dr. Patrick Linke Co-Chair: Dr. Veronica Bermudez</p>	<p style="text-align: center;">Session 5C: Hydrogen Effects on Materials Chair: Dr. Ibrahim Galal Hassan Co-Chair: Dr. Afrooz Barnoush</p>
09:00 am-09:15 am	<p style="text-align: center;">ICH2P14 – OP084 Life Cycle Assessment of Green Hydrogen Supply Network <u>Dana Alghool</u>, <u>Mohamed Haouari</u>, <u>Paolo Trucco</u></p>	<p style="text-align: center;">ICH2P14 - OP056 Multi-Scenario Analysis of Levelized Cost of Hydrogen for Water Electrolysis-Photovoltaic Energy Technology in the Near Future (2025–2050) of Algeria <u>Hammou Tebibel</u>, <u>Abdelhamid M'raou</u></p>	<p style="text-align: center;">ICH2P14 – OP134 The Correlation of Porous Material's Properties Between Particle Geometry for Hydrogen Fuel And Electrolysis Cells <u>Jaeyeon Kim</u>, <u>Luthfan Adhy Lesmana</u>, <u>Muhammad Aziz</u></p>
09:15 am-09:30 am	<p style="text-align: center;">ICH2P14 – OP180 Life Cycle Assessment of a Direct Air Capture and CO₂ Utilization System <u>Aliya Banu</u>, <u>Namra Mir</u>, <u>Muftah H. El-Naas</u>, <u>Ahmed Ali Khalifa</u>, <u>Abdulkarem I. Amhamed</u>, <u>Yusuf Bicer</u></p>	<p style="text-align: center;">ICH2P14 - OP142 Optimizing Green Hydrogen and Power Generation from Urban Sewage Sludge in the Steel Industry: A Kerman Case Study <u>Saeed Edalati</u>, <u>Mohammadreza Khosravirad</u></p>	<p style="text-align: center;">ICH2P14 – OP112 Influence Of Hydrogen Uptake on Additively Manufactured and Conventional Austenitic Stainless Steels 316L <u>Qingyang Liu</u>, <u>Sumia Manzoor</u>, <u>Mohammad Tariq</u>, <u>Hanan Farhat</u>, <u>Afrooz Barnoush</u></p>
09:30 am-09:45 am	<p style="text-align: center;">ICH2P14 - OP178 Tank To Tank Life Cycle Assessment of Greenhouse Gas Emission from Methanol Plant <u>Hussein Al-Yafei</u>, <u>Ahmed AlNouss</u>, <u>Saleh Aseel</u>, <u>Mohannad AlJarrah</u>, <u>Tareq Al-Ansari</u></p>	<p style="text-align: center;">ICH2P14 - OP097 Maximizing Power Grid Resilience: Rolling Horizon Control for Output Power Smoothing in Islanded Wind-Solar Microgrids with Multiple Hydrogen Storage Tanks <u>Muhammad Bakr Abdelqahany</u>, <u>Ahmed Al-Durra</u></p>	<p style="text-align: center;">ICH2P14 – OP046 In-House Green Anti-Corrosion Inhibitor to Protect from Hydrogen Embrittlement Effect on the Structural Integrity of Api 5l Steel Pipeline <u>Mohammed HadjMeliani</u>, <u>Hadjer Didouh</u>, <u>Mouna Amara</u>, <u>Azedine Belalia</u>, <u>Rami K.Suleiman</u>, <u>Guy Pluvinage</u></p>
09:45 am-10:00 am	<p style="text-align: center;">ICH2P14 – OP106 An Integrated Life Cycle Assessment and Supply Chain Analysis of a Multi-Generation System for Renewable Clean Power and Green Hydrogen Production <u>Tahir Abdul Hussain Ratlamwala</u>, <u>Sheikh Muhammad Ali Haider</u>, <u>Khurram Kamal</u></p>	<p style="text-align: center;">ICH2P14 - OP173 Circular Economy of integrating Green Hydrogen Production within an Eco-Industry Park <u>Hajer Mkacher</u>, <u>Fadwa ElJack</u></p>	<p style="text-align: center;">ICH2P14 - OP072 Protection From Hydrogen Embrittlement Using Green Inhibitor on the Welding Joint of Api X65 Pipeline Steel in Dynamic Loading <u>Azedine Belalia</u>, <u>Mohammed Hadj Meliani</u>, <u>Hadjer Didouh</u>, <u>Mouna Amara</u>, <u>Rami K.Suleiman</u>, <u>Guy Pluvinage</u></p>
10:00 am-10:15 am	<p style="text-align: center;">ICH2P14 - OP151 Regeneration Energy Optimisation of Post-Combustion CO₂ Capture (PCC) Process Based on Amine Composition Using Artificial Neural Network (ANN) <u>Najamus Sahar Riyaz</u>, <u>Nancy Khalaf AbuZaid</u>, <u>AlAnkaa Al-Harbi</u>, <u>Abdelbaki Benamor</u></p>	<p style="text-align: center;">ICH2P14 - OP004 Monte Carlo Simulation Applications for Stakeholder Management on Hydrogen Production Projects: Toward Sustainable Development <u>Ayman Mashali</u></p>	<p style="text-align: center;">ICH2P14 - OP043 Advancing Hydrogen Production: High-Resolution Kinetic Analysis of Photocatalytic Water Splitting Using Covalent Organic Framework Catalyst and Ascorbic Acid <u>Suhde Makkj</u>, <u>Konstantinos E. Kakosimos</u></p>
10:15 am-10:30 am	<p style="text-align: center;">ICH2P14 – OP120 A Life Cycle Assessment of Hydrogen Production with Catalyst <u>Assem Abdurakhmanova</u>, <u>Ibrahim Dincer</u></p>	<p style="text-align: center;">ICH2P14 - OP052 Assessment of Hydrogen Trading Within Blockchain and Artificial Intelligence: A Review <u>Sofya Morozova</u>, <u>Arif Karabuga</u>, <u>Zafer Utlu</u></p>	<p style="text-align: center;">ICH2P14 – OP140 A Critical Review of Hydrogen (H₂) Flow Assurance in the Presence of Impurities <u>Mohammad Azizur Rahman</u>, <u>Ibrahim Hassan</u>, <u>Rashid Hasan</u>, <u>Faisal Khan</u>, <u>Eduardo Gildin</u>, <u>Ahmad Sleiti</u></p>

Day 3 | Thursday, December 21, 2023

Poster Number	Poster Presentations 10:30 am-11:00 am Session Chair: Dr. Burak Yuzer	Exhibition Hall
ICH2P14 – PP005	Efficiency Hydrogen Production Via Water Photoreduction Over Fenps Elaborated Via Green Way <i>Meriem Guouasmi, <u>Amel Boudjema</u>, Chahrazed Benhamidech, Khaldoun Bachari</i>	
ICH2P14 – PP011	Field Investigation of Green Hydrogen Production Through the Pem Electrolyzer in Ouargla City <i>Ahmed Zouhir Kouache, Ahmed Djafour, Khaled Mohammed Said Benzaoui, Madjida Ramdani</i>	
ICH2P14 – PP028	Recent advances in Green Synthesis of Cu ₂ O as a Photocatalyst for Conversion of Solar Energy into H ₂ <i>S. Torres-Arellano, <u>P.J. Sebastian</u></i>	
ICH2P14 – PP030	Effect of Scale-Up in Membraneless Microbial Electrolysis Cells on Hydrogen Production <i>M. Mejía-López, O. Lastres, J.L. Alemán-Ramirez, L. Vereá, <u>P.J. Sebastian</u></i>	
ICH2P14 – PP153	Synthesis and Evaluation of Cu-Based Catalytic Materials for CO ₂ Hydrogenation to Value-Added Products <i>Rim Ismail, Assem Mohamed, Mohamed Ali H. Saad, Abdelbaki Benamor</i>	
ICH2P14 – PP168	Current and Temperature Distributions in a Planar Solid Oxide Electrolysis Cell In-situ Assessed with Segmented Electrodes <i>Kentaro Yokoo, Hironori Nakajima, Kohei Ito</i>	
ICH2P14 – PP181	Underground Gas Storage Systems: Natural Gas, Hydrogen, And Carbon Sequestration <i>Manal Al-Shafi, Yusuf Bicer, Ahmad Abushaikha</i>	
ICH2P14 – PP055	Forced Convection in Porous Medium Using Triply Periodical Minimum Surfaces: Experimental and Numerical Approach <i>M. Ziad Saghir</i>	

Day 3 | Thursday, December 21, 2023





Parallel Sessions 6			
Time	Conference Room – A047	Conference Room – A048	Conference Room – A046
11:00 am-12:30 pm	Session 6A: Bio-Hydrogen-2 Chair: Dr. Mohammad Alherbawi Co-Chair: Dr. Farhat Mahmood	Session 6B: Hydrogen Storage and Carriers Chair: Dr. Majeda Khraisheh Co-Chair: Dr. Alessandro Sinopoli	Session 6C: Electrolyzers Chair: Dr. Muhammed Iberia Aydin Co-Chair: Dr. Nurettin Sezer
11:00 am-11:15 am	ICH2P14 - OP157 Potential Evaluation and Optimization of Exoelectrogenic Activity of Rhodobacter Capsulatus: A Sustainable Strategy for Bioelectricity Production <u>Saima Mirza, Junaid Mahmood, Arjumand Shah Bano, Mohammad Morowvat, Mudassar Ali, Obaid ur-Rehman</u>	 ICH2P14 - OP145 Heat Transfer Optimization of a Metal Hydride Tank Targeted to Improve Hydrogen Storage Performance <u>Nadhir Lebaal, Djafar Chabane, Alaeddine Zereg, Nouredine Fenineche</u>	ICH2P14 - OP156 An Electrolyser Design for Membraneless Electrolysis by Using 3D Printing <u>Muhammed Iberia Aydin, Ibrahim Dincer</u>
11:15 am-11:30 am	ICH2P14 – OP135 Predictive Modeling of Biogas and Methane Production from Cow and Chicken Manure Using a Modified Gompertz Model Optimized by Particle Swarm Optimization <u>Nadjiba Sophy, Nour Elislam Mougari, Nabil Himrane, Luis Le Moyne</u>	ICH2P14 – OP137 Sodium Bicarbonates Production Through Carbon Mineralization for Hydrogen Storage: A Techno-Economic Assessment <u>Dina Ewis, Zeyad Moustafa Ghazi, Sabla Y. Alnouri, Abdelbaki Benamor, Muftah H. El-Naas</u>	ICH2P14 – OP179 Modeling For Multi-Mechanisms Permeability of Hydrogen Using a Membrane Process <u>Hamid Zentou, Mahmoud M. Abdelnaby, Abdullah A. AlZahrani</u>
11:30 am-11:45 am	ICH2P14 - OP079 Optimizing Hydrogen Production and Anaerobic Biodegradability in Pharmaceutical Industry Wastewaters Through Photocatalytic Oxidation <u>Ayşe Elif Ateş, Burak Yüzer, Adem Yurtsever, Sinan Ates</u>	ICH2P14 - OP146 Assessing the Potential and Viability of Renewable Methane and Hydrogen as Sustainable Energy Carriers <u>Mohammed Al-Breiki, Yusuf Bicer</u>	ICH2P14 - OP033 Degradation Modelling of Water Electrolyzers Using Hidden State Estimation and Deep Learning <u>Frank Hilden, Pourya Azadi, Stéphane Haag, Giuseppe Cusati, Vanessa Gepert</u>
11:45 am-12:00 pm	ICH2P14 – OP189 Biocatalytic Conversion of Lignocellulosic Biomass into Biohydrogen Via Photofermentation Route <u>Saima Mirza, Javed Iqbal Qazi, Shulin Chen</u>	ICH2P14 – OP184 Flexible Natural Gas Allocation to Blue-Hydrogen Monetised Products: An Agent-Based Modelling Approach <u>Noor Yusuf, Ahmed AlNouss, Tareq Al-Ansari</u>	ICH2P14 - OP141 Experimental And Numerical Analyses of A Cathode-Supported Monolithic Solid Oxide Electrolysis Cell <u>Hironori Nakajima, Yoshihiro Iwanaga, Kohei Ito</u>
12:00 pm- 12:15 pm	ICH2P14 – OP196  Mathematical Modeling of A Sustainable Energy System For Restaurant Communities: Waste-To-H2 Conversion, CO2 Mitigation, Clean Fuel Production, And Power Generation <u>Syed Muhammad Aun Rizvi, Khurram Kamal, Tahir A.H. Ratlamwala</u>	ICH2P14 – OP035 Power-To-Gas Process in the Upgrading of The CO ₂ Extracted from the Unprocessed Algerian Natural Gas <u>Rafika Boudries, Nourine Kabouche, Rafik Medjebour, Brahim Laoun, A. Khellaf</u>	ICH2P14 – OP065 Solar Hydrogen and Methanol Production with CSP/PV Driven Electrolyser <u>Nathalie Monnerie, Andreas Rosenstiel, Christian Sattler</u>
12:15 pm-12:30 pm	ICH2P14 - OP092  An Approach in Treating Biomass and Plastic Waste for Production of Hydrogen and Ethanol <u>Muhammad Ishag, Ibrahim Dincer</u>	ICH2P14 – OP183 Comparative Thermodynamic Analysis of Two Green Fuel Production and Power Generation Pathways <u>Amira Chebbi, Yusuf Bicer</u>	ICH2P14 - OP090  An Investigation of Metal Coated 3D-Printed Electrodes for Hydrogen Production <u>Muarij Khalil, Ibrahim Dincer</u>
12:30 pm-02:00 pm Lunch Exhibition Hall			

Day 3 | Thursday, December 21, 2023

Parallel Sessions 7			
Time	Conference Room – A047	Conference Room – A048	Conference Room – A046
02:00 pm-03:30 pm	Session 7A: Thermodynamic Analysis of Hydrogen Systems Chair: Dr. Hadi Genceli Co-Chair: Dr. Shoukat Alim Khan	Session 7B: Fuel Cells and Combustion Chair: Dr. Mohd Zamri Che Wanik Co-Chair: Dr. Tahir A.H. Ratlamwala	Session 7C: Photo-Electro-Catalytic Hydrogen Production Chair: Dr. Rima Isaifan Co-Chair: Dr. Khaled Abedrabboh
02:00 pm-02:15 pm	ICH2P14 - OP152 Design, development and investigation of solar-integrated co-electrolysis for methanol production Muhammad Sajid Khan, Muhammad Abid, Chen Chen, Juliana Hj Zaini, Tahir Ratlamwala	ICH2P14 - OP042 Feasibility Study of a Molten Carbonate Fuel Cell as a CO ₂ Separator for Various Industrial Exhaust Emissions Arkadiusz Szczęśniak, Aliaksandr Martsinchyk, Olaf Dybinski, Katsiaryna Martsinchyk, Kamil Futyma, Łukasz Szablowski, Jarosław Milewski, Małgorzata Dembowska	ICH2P14 - OP034 Synthesis and Application of Pd/Sr-NPs@TiO ₂ for Photocatalytic H ₂ Generation from Water Splitting Reactions Ejaz Hussain, Khezina Rafiq
02:15 pm-02:30 pm	ICH2P14 – OP160 Energy And Exergy Analysis of A Four-Step Copper Chlorine Cycle For Enhanced Efficiency And Performance Satyasekhar Bhogilla, Aman Pandoh, Uday Raj Singh	ICH2P14 - OP149 Sustainable Proton-Exchange-Membrane Fuel Cell (PEMFC) System Exergoeconomic Analysis Rodrigo Raimundo, Carlos Matiolo, Rhayssa Ribas, Lauber Martins, André Mariano, Stephan Och, Vanessa Kava, José Vargas	ICH2P14 – OP127 Dye-Sensitized Photocatalytic Hydrogen Production by Sepiolite Clay Yigit Osman Akyildiz, Emre Aslan, Mahmut Kus, Imren Hatay Patir, Mustafa Ersoz
02:30 pm-02:45 pm	ICH2P14 – OP054 Performance Evaluation of Different Working Fluids In S-ORC Based Hydrogen Production System Arif Karabuga, Zafer Utlu, Melik Ziya Yakut	ICH2P14 – OP136 3e Analysis and Multi-Objective Optimization of Solar-Thermal-Assisted Energy System: Supercritical CO ₂ Brayton Cycle and Solid Oxide Electrolysis/Fuel Cells Zhicong Fang, Zhichao Liu, Shuhao Zhang, Zekun Yang	ICH2P14 - OP032 Synthesis of Au–BaO@TiO ₂ /Cds Catalysts: H ₂ Generation from Water Splitting Reactions Khezina Rafiq, Ejaz Hussain
02:45 pm-03:00 pm	ICH2P14 - OP162 Thermodynamic Evaluation of a Renewable Energy Storage Concept Incorporating a Solid Oxide Electrolyzer and Metal Hydride Compressor Uday Raj Singh, Satyasekhar Bhogilla	ICH2P14 – OP203 A Review of The Feasibility of Utilising Hydrogen as a Marine Fuel in Australia Hongjun Fan, Naqi Abdussamie, Andrew Harris, Peggy Shu-Ling Chen, Irene Penesis	ICH2P14 – OP115 Photocatalytic Hydrogen Generation from Seawater Using High-Performance Polymeric Materials Noora Al-Subaiei, Ghalya Abdulla, Mohammed Al-Hashimi, Konstantinos E Kakosimos
03:00 pm-03:15 pm	ICH2P14 - OP053 Thermodynamic Analysis of PTC-Based Hydrogen Production System Arif Karabuga, Zafer Utlu, Hasan Ayarturk	ICH2P14 - OP143 Study Of Laminar Burning Speed Correlation' For Ammonia-Hydrogen Fueled Mixture Anas Rao, Muhammad Ihsan Shahid, Muhammad Farhan, Yongzheng Liu, Fanhua Ma	ICH2P14 - OP021 Efficient and Stable Seawater Electrolysis Over a Binder-Free Nio-Nanosheet Array Bifunctional Catalyst Khadijeh Hemmati
03:15 pm-03:30 pm	ICH2P14 – OP093 A Unique System for Hydrogen, Methanol, Fresh Water and Electricity Production with Carbon Capturing and Storage Mitra Ghannadi, Ibrahim Dincer	ICH2P14 – OP194 Proton Exchange Membrane based Fuel Cell Generation System Modeling for Power System Studies Mohd Zamri, Che Wanik	ICH2P14 – OP121 Piezocatalytic Hydrogen Evolution Activity of Seleno-Chevreol Phases Talha Kuru, Emre Aslan, Faruk Ozel, Imren Hatay Patir, Mustafa Ersoz
03:30 pm-04:00 pm Coffee Break with Poster Presentations Exhibition Hall			

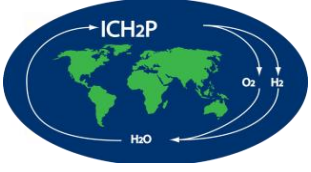
Day 3 | Thursday, December 21, 2023

Poster Number	Poster Presentations 03:30 pm-04:00 pm Chair: Dr. Burak Yuzer	Exhibition Hall
ICH2P14 – PP132	Modeling Of Supercritical Hydrogen Storage System Parameters Using Artificial Intelligence Technique <u>A. Abdallah El Hadj, Ait Yahia, Smain Sabour, Mohammed R Zahi, Maamar Laidi, S.Hanini</u>	
ICH2P14 – PP147	Photo-Electro-Electrolysis System Utilizing TiO ₂ -Coated Stainless Steel and FTO as Photoelectrodes for Enhanced Dye Removal in Wastewater and Hydrogen Production <u>Nadira Salsabila, Ragad F. Alshebli, Burak Yuzer, Yusuf Bicer</u>	
ICH2P14 – PP169	Dynamic Modelling Approach for Understanding the Influence of Carbon Policies on Electrofuels Utilisation Within the Aviation Sector <u>Ridab Khalifa, Yusuf Bicer, Tareq Al-Ansari</u>	
ICH2P14 – PP185	Multi-Purpose Charging Station for Electric and Hydrogen Vehicles Enabling Sustainable Transportation <u>Marawan Hussein, Sara Mohamed, Amira Chebbi, Luluwah Al-Fagih, Tareq Al-Ansari, Yusuf Bicer</u>	
ICH2P14 – PP068	Hydrogen Sulfide H ₂ S – for the Service of Humanity! <u>Anatolii Startsev</u>	

Time	Conference Room – A048	Conference Room – A046
04:00 pm-05:00 pm	Session 8A: Other Hydrogen Applications Chair: Dr. Dogan Erdemir Co-Chair: Dr. Hanadi G. Al-Thani	Session 8B: Hydrogen Utilization and Production Chair: Dr. Huseyin Selcuk Co-Chair: Dr. Muhammed Iberia Aydin
04:00 pm-04:15 pm	ICH2P14 - OP051 Enhancing Hydrogen Gas Production in Escherichia Coli Through a Crispr-Based Approach <u>Salisu Ahmed, Musa Abdullahi, Abubakar Ahmad</u>	ICH2P14 – OP182 A Techno-Economic Analysis of Hybrid Solar-Wind Energy Systems with Hydrogen Storage for Residential Communities <u>Sara Mohamed, Yusuf Bicer, Luluwah Al-Fagih</u>
04:15 pm-04:30 pm	ICH2P14 - OP148 State-Flow Based Energy Management System in Micro-Grid Including Fuel Cell <u>Hamid Bentarzi, Abderrahmane Ouadi, Abdelkader Zitouni, Abdelkader Abdelmoumene</u>	ICH2P14 – OP138 Design And Performance Analysis of Ammonia-Based Power Generation <u>Kazuki Ohira, Rahmat Waluyo, Muhammad Aziz</u>
04:30 pm-04:45 pm	ICH2P14 – OP191 Wind Power's Evolution: Unveiling Advances and Challenges in the Quest for Sustainable Energy <u>Abdelkader Abdelmoumene, Hamid Bentarzi</u>	ICH2P14 – OP071 Investigation of a New Energy System with Recycled Aluminum-Water Hydrogen Production <u>Andre Bolt, Ibrahim Dincer, Martin Agelin-Chaab</u>
04:45 pm-05:00 pm	ICH2P14 – OP213 An Investigation on the Magnetic Cooling Systems in Electric Vehicle <u>Nader Javani, Hadi Genceli</u>	ICH2P14 – OP195 Optimizing Green Hydrogen Production in the GCC: A Pilot Study of Capacity Factor Enhancement via Trans-Continental Energy Imports <u>Moiz Ali, Yusuf Bicer, Tareq Al-Ansari</u>
05:00 pm-05:15 pm	ICH2P14 – OP070  Bio-Inspired Optimization of Hydrogen Production Plants: Harnessing the Pollutants for Enhanced Efficiency of Fuel Cell <u>Khaled Abu Alfoul, Anaam Abu Foul</u>	ICH2P14 - OP098  Electro-Biomembrane Reactor for Concurrent Hydrogen Production and Desalination <u>Ahmet Faruk Kilicaslan, A. Yagmur Goren, Ibrahim Dincer, Ali Khalvati</u>
05:15 pm-05:30 pm	ICH2P14 – OP119  Low Price Photo and Thermal Production of Hydrogen Fuel from Hydrogen Sulfide Extracted from Petroleum Natural Gas <u>Salah Naman</u>	ICH2P14 - OP078  A Community Energy System Designed to Cover the Needs Including Hydrogen <u>Moslem Sharifishourabi, Ibrahim Dincer, Atef Mohany</u>
06:30 pm-09:30 pm Optional Social Tour		

Hydrogen Energy Course

Time	Hydrogen Energy Course (with registration)	Auditorium
09:00 am-09:15 am	Opening Talks	
09:15 am-11:15 am	Introduction to Hydrogen: H2-101 Professor Dr. Ibrahim Dincer, Ontario Tech University, Canada	
11:15 am-11:30 am	Break	
11:30 am-01:30 pm	Hydrogen Production: Electrolyzes, Methods and Processes Professor Dr. Fares Almomani, Qatar University, Qatar	
1:30 pm-02:00 pm	Lunch Break	
2:00 pm-04:00 pm	Hydrogen Storage and Transportation Dr. Yusuf Bicer, Hamad Bin Khalifa University, Qatar	
04:00 pm-04:15 pm	Break	
04:15 pm-06:15 pm	Hydrogen Utilization and Fuel Cells Professor Dr. Xianguo Li, University of Waterloo, Canada	
06:15 pm-06:30 pm	Certification Ceremony	



كلية العلوم والهندسة
College of Science & Engineering

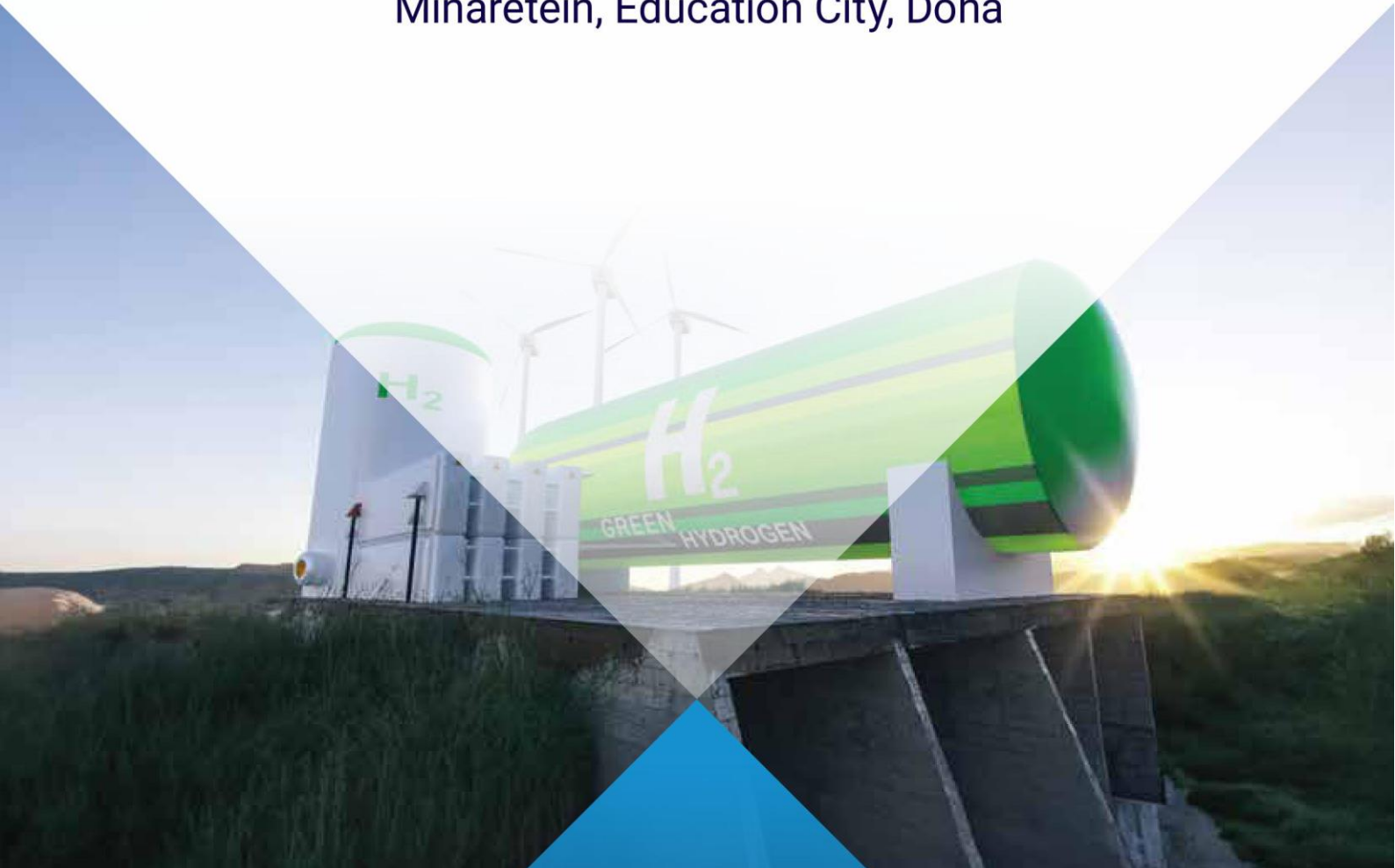
جامعة حمد بن خليفة
HAMAD BIN KHALIFA UNIVERSITY



14TH INTERNATIONAL CONFERENCE ON HYDROGEN PRODUCTION (ICH2P-2023)

DECEMBER 19 - 21, 2023

Minaretein, Education City, Doha



14th INTERNATIONAL CONFERENCE ON HYDROGEN PRODUCTION (ICH2P-2023)

December 19 – 21, 2023
Education City, Doha, Qatar

CONFERENCE PROCEEDINGS

EDITORS

Yusuf Bicer
Tareq Al-Ansari
Ibrahim Dincer
Omer Abedrabboh
Mohammad Alherbawi
Burak Yuzer

ISBN: 978-625-008-245-4

INDEX

About HBKU	X
Forewords	XI
Committees	XIV
Acknowledgement	XIX
Invited Speakers	1
IT#1. “Green Hydrogen Production: Solar Chimney Power Plant Integrated with Water Desalination Plant”, <i>Emad Abdelsalam, Fares Almomani</i>	2
IT#3. “Analyzing Grey and Blue Hydrogen Production Costs in Steam-Methane, Auto-Thermal, And Non-Catalytic Partial Oxidation Reforming Plants”, <i>Mary Katebah, Ma’moun Al-Rawashdeh, Patrick Linke</i>	17
Oral Presentations	21
OP#4. “Monte Carlo Simulation Applications for Stakeholder Management on Hydrogen Production Projects: Toward Sustainable Development”, <i>Ayman Mashali</i>	22
OP#7. “Carbon Emission Reductions in The University of Sao Paulo’s Transportation Sector Using Hydrogen-Powered Vehicles”, <i>Beethoven Narváez-Romo, Danilo Perecin, Thiago Lopes, Daniel Lopes, Karen Mascarenhas, Suani Coelho, Julio R. Meneghini</i>	29
OP#9. “Transient Simulation and Comparative Assessment of Two Concentrated-Solar Based Hydrogen Production Systems Integrated with Vanadium-Chlorine Thermochemical Cycle”, <i>Erfan Zand, Mohammadreza Khosravi, Pouria Ahmadi, Mehdi Ashjaee</i>	35
OP#10. “A Novel Cost-Effective Approach for Production of Hydrogenase Enzymes and Molecular Hydrogen from Whey-Based By-Products”, <i>Anna Poladyan, Meri Iskandaryan, Ofelya Karapetyan, Ela Minasyan, Anait Vassilian, Karen Trchounian, Garabed Anatronkian</i>	40
OP#17. “Kinetic Modelling and Process Optimization for Blue Hydrogen Production Via Ammonia Cracking”, <i>Ragad Aldilajjan, Sai Katikaneni, Osamah Siddiqui, Mohammad Rakib, Bandar Solami</i>	46
OP#23. “Membrane Reformer Technology for Sustainable Hydrogen Production from Hydrocarbon Feedstocks”, <i>Alaa Albasry, Ahmed Naimi, Abdulbari Alqarni, Minseok Bae, Bandar Solami, Stephen Paglieri, Aadesh Harale</i>	52
OP#25. “Thermoelectric Condensation of Ambient Humidified Air for Green Hydrogen Production”, <i>Hilal Ahmad, Taqi Ahmad Cheema, Hadeed Ahmed Sher</i>	58
OP#27. “Transportation and Storage of Hydrogen by LOHC: Design and Simulation of the Dehydrogenation Reactor”, <i>Pietro Delogu, Elena Barbera, Andrea Mio, Alberto Bertucco, Maurizio Fermeglia</i>	62

OP#33. “Degradation Modelling of Water Electrolysers Using Hidden State Estimation and Deep Learning”, <i>Frank Hilden, Pourya Azadi, Stéphane Haag, Giuseppe Cusati, Vanessa Gepert</i>	68
OP#36. “A Techno-Economic Evaluation of the Integration of Direct Air Capture with Hydrogen and Solar Fuel Production”, <i>Enric Prats-Salvado, Nathalie Monnerie, Christian Sattler</i>	74
OP#44. “Biotechnological Potential of Spent Coffee Grounds for Large-Scale Hydrogen Production”, <i>Liana Vanyan, Anait Vassilian, Anna Poladyan, Karen Trchounian</i>	79
OP#47. “The Hydrogen Production Using Steam Methane Reforming Based on Central Receiver”, <i>Ali Alaidaros, Abdullah A. AlZahrani</i>	85
OP#52. “Assessment of Hydrogen Trading Within Blockchain and Artificial Intelligence: A Review”, <i>Sofya Morozova, Arif Karabuga, Zafer Utlu</i>	92
OP#53. “Thermodynamic Analysis of PTC-Based Hydrogen Production System”, <i>Arif Karabuga, Zafer Utlu, Hasan Ayarturk</i>	96
OP#54. “Performance Evaluation of Different Working Fluids In S-ORC Based Hydrogen Production System”, <i>Arif Karabuga, Zafer Utlu, Melik Ziya Yakut</i>	100
OP#65. “Solar Hydrogen and Methanol Production with CSP/PV Driven Electrolyser”, <i>Nathalie Monnerie, Andreas Rosenstiel, Christian Sattler</i>	104
OP#67. “An Optimum Approach for Biohydrogen Production Using Poplar”, <i>A. Yagmur Goren, Muratcan Kenez, Ibrahim Dincer, Ali Khalvati</i>	107
OP#70. “Bio-Inspired Optimization of Hydrogen Production Plants: Harnessing the Pollutants for Enhanced Efficiency of Fuel Cell”, <i>Khaled Abu Alfoul, Anaam Abu Foul</i>	110
OP#71. “Investigation of a New Energy System with Recycled Aluminum-Water Hydrogen Production”, <i>Andre Bolt, Ibrahim Dincer, Martin Agelin-Chaab</i>	115
OP#73. “Solar Energy Driven Silicon Photovoltaic Monolithic Electrochemical Cells for Efficient Hydrogen Production from Water”, <i>Mourad Frites, Shahed Khan</i>	118
OP#74. “Evaluation of a Novel Hybrid Photoelectrochemical-Conventional Hydrogen Generator”, <i>Mehmet GURSOY, Ibrahim Dincer</i>	123
OP#78. “A Community Energy System Designed to Cover the Needs Including Hydrogen”, <i>Moslem Sharifishourabi, Ibrahim Dincer, Atef Mohany</i>	126
OP#80. “A Clean Option for Potential Hydrogen Production Via Nuclear in Canada”, <i>Gorkem Kubilay Karayel, Ibrahim Dincer</i>	129
OP#82. “Green Hydrogen Production and Solar to Hydrogen Ratio Using Bifacial Solar Photovoltaics and High Roof Surface Albedo”, <i>Fahad Ahmad Faraz, Oussama Rejeb, Chaouki Ghenai</i>	132
OP#83. “Design and Performance Analysis of Green Hydrogen Production from Hybrid Solar PV/Wind Turbine Energy System”, <i>Chaouki Ghenai</i>	139

OP#84. "Life Cycle Assessment of Green Hydrogen Supply Network", <i>Dana Alghool, Mohamed Haouari, Paolo Trucco</i>	146
OP#87. "Biomethanol and Hydrogen Production from Pinecone Biomass Using Steam Gasification", <i>Hilal Sayhan Akci Turgut, Ibrahim Dincer</i>	153
OP#88. "A Study on Nuclear-Based Hydrogen Production System Via Three- and Four-Step Magnesium Chlorine Cycles", <i>Şulenur Asal, Adem Acir, Ibrahim Dincer</i>	155
OP#90. "An Investigation of Metal Coated 3D-Printed Electrodes for Hydrogen Production", <i>Muarij Khalil, Ibrahim Dincer</i>	158
OP#91. "Piston Reactor Capabilities to Make Hydrogen from Methane Via Steam and Autothermal Reforming – Modeling Study", <i>Aya Abousrafa, Patrick Linke, Ma'moun Al-Rawashdeh</i>	161
OP#92. "An Approach in Treating Biomass and Plastic Waste for Production of Hydrogen and Ethanol", <i>Muhammad Ishaq, Ibrahim Dincer</i>	167
OP#93. "A Unique System for Hydrogen, Methanol, Fresh Water and Electricity Production with Carbon Capturing and Storage", <i>Mitra Ghannadi, Ibrahim Dincer</i>	170
OP#94. "Innovative Integrated Multigeneration System for Sustainable Power, Hydrogen, and Ammonia Production", <i>Ahmad K. Sleiti, Wahib A. Al-Ammari, Mohammad Azizur Rahman</i>	173
OP#95. "A Solar Pond Integrated with Bifacial Solar Panels for Power and Hydrogen Generation", <i>Dogan Erdemir, Ibrahim Dincer</i>	181
OP#96. "Techno-Economic Evaluation of Various Hydrogen Carriers", <i>Ahmad K. Sleiti, Laveet Kumar, Wahib A. Al-Ammari</i>	183
OP#97. "Maximizing Power Grid Resilience: Rolling Horizon Control for Output Power Smoothing in Islanded Wind-Solar Microgrids with Multiple Hydrogen Storage Tanks", <i>Muhammad Bakr Abdelghany, Ahmed Al-Durra</i>	191
OP#98. "Electro-Biomembrane Reactor for Concurrent Hydrogen Production and Desalination", <i>Ahmet Faruk Kilicaslan, A. Yagmur Goren, Ibrahim Dincer, Ali Khalvati</i>	194
OP#106. "An Integrated Life Cycle Assessment and Supply Chain Analysis of a Multi-Generation System for Renewable Clean Power and Green Hydrogen Production", <i>Tahir Abdul Hussain Ratlamwala, Sheikh Muhammad Ali Haider, Khurram Kamal</i>	197
OP#110. "Development of a Hybrid Powering System with Ammonia Fuel Cells and Internal Combustion Engine for Submarines", <i>Ibrahim Akgun, Ibrahim Dincer</i>	200
OP#111. "An Integrated Solar-Driven Chlor-Alkali System for Hydrogen and Chlorine Production", <i>Sümeyya Ayça, Ibrahim Dincer</i>	203
OP#112. "Influence Of Hydrogen Uptake on Additively Manufactured and Conventional Austenitic Stainless Steels 316L", <i>Qingyang Liu, Sumia Manzoor, Mohammad Tariq, Hanan Farhat, Afrooz Barnoush</i>	206

OP#119. “Low Price Photo and Thermal Production of Hydrogen Fuel from Hydrogen Sulfide Extracted from Petroleum Natural Gas”, <i>Salah Naman</i>	211
OP#120. “A Life Cycle Assessment of Hydrogen Production with Catalysts”, <i>Assem Abdurakhmanova, Ibrahim Dincer</i>	214
OP#122. “Synthesis, Characterization, and Application of Bio-Templated Ni-Ce/Al ₂ O ₃ Catalyst for Clean H ₂ Production in the Steam Reforming of Methane Process”, <i>Mohammad Reza Rahimpour, Maryam Koochi-Saadi</i>	216
OP#123. “Green Hydrogen Based Ammonia Production Process: Insight into Energy and CO ₂ Emissions Minimization”, <i>Swaprabha P. Patel, Ashish M. Gujarathi, Piyush Vanzara</i>	221
OP#130. “Exergetic Analysis of the Process for Hydrogen Rich Syngas Production Through Biomass Gasification and Its Onsite Use in HCCI Engine for Land Transportation”, <i>Tawfiq Al-Mughanam, Abdul Khaliq</i>	227
OP#133. “Graded Gyroid-Enhanced Metal Hydride Container for Efficient Hydrogen Storage Application”, <i>Luthfan Adhy Lesmana, Muhammad Aziz</i>	233
OP#134. “The Correlation of Porous Material’s Properties Between Particle Geometry for Hydrogen Fuel and Electrolysis Cells”, <i>Jaeyeon Kim, Luthfan Adhy Lesmana, Muhammad Aziz</i>	238
OP#135. “Predictive Modeling of Biogas and Methane Production from Cow and Chicken Manure Using a Modified Gompertz Model Optimized by Particle Swarm Optimization”, <i>Nadjiba Sophy, Nour Elislam Mougari, Nabil Himrane, Luis Le Moyne</i>	241
OP#137. “Sodium Bicarbonates Production Through Carbon Mineralization for Hydrogen Storage: A Techno-Economic Assessment”, <i>Dina Ewis, Zeyad Moustafa Ghazi, Sabla Y. Alhourri, Abdelbaki Benamor, Muftah H. El-Naas</i>	247
OP#138. “Design And Performance Analysis of Ammonia-Based Power Generation”, <i>Kazuki Ohira, Rahmat Waluyo, Muhammad Aziz</i>	252
OP#140. “A Critical Review of Hydrogen (H ₂) Flow Assurance in The Presence of Impurities”, <i>Mohammad Azizur Rahman, Ibrahim Hassan, Rashid Hasan, Faisal Khan, Eduardo Gildin, Ahmad Sleiti</i>	257
OP#141. “Experimental And Numerical Analyses of a Cathode-Supported Monolithic Solid Oxide Electrolysis Cell”, <i>Hironori Nakajima, Yoshihiro Iwanaga, Kohei Ito</i>	263
OP#142. “Optimizing Green Hydrogen and Power Generation from Urban Sewage Sludge in the Steel Industry: A Kerman Case Study”, <i>Saeed Edalati, Mohammadreza Khosravirad</i>	269
OP#145. “Heat Transfer Optimization of a Metal Hydride Tank Targeted to Improve Hydrogen Storage Performance”, <i>Nadhir Lebaal, Djafar Chabane, Alaeddine Zereg, Nouredine Fenineche</i>	279
OP#149. “Sustainable Proton-Exchange-Membrane Fuel Cell (PEMFC) System Exergoeconomic Analysis”, <i>Rodrigo Raimundo, Carlos Matiolo, Rhayssa Ribas, Lauber Martins, André Mariano, Stephan Och, Vanessa Kava, José Vargas</i>	285

OP#151. "Regeneration Energy Optimisation of Post-Combustion CO ₂ Capture (PCC) Process Based on Amine Composition Using Artificial Neural Network (ANN)", <i>Najamus Sahar Riyaz, Nancy Khalaf AbuZaid, AlAnkaa Al-Harbi, Abdelbaki Benamor</i>	291
OP#152. "Design, Development and Investigation of Solar-Integrated Co-Electrolysis for Methanol Production", <i>Muhammad Sajid Khan, Muhammad Abid, Chen Chen, Juliana Hj Zaini, Tahir Ratlamwala</i>	296
OP#156. "An Electrolyser Design for Membraneless Electrolysis by Using 3D Printing", <i>Muhammed Iberia Aydin, Ibrahim Dincer</i>	300
OP#162. "Thermodynamic Evaluation of a Renewable Energy Storage Concept Incorporating a Solid Oxide Electrolyzer and Metal Hydride Compressor", <i>Uday Raj Singh, Satyasekhar Bhogilla</i>	303
OP#163. "Seawater Desalination and Hydrogen Production Using Monovalent Selective Membranes Assisted with Ion-Exchange Resins for Hydroponic Solution Production", <i>Ragad F. Alshebli, Nadira Salsabila, Burak Yuzer, Yusuf Bicer</i>	306
OP#165. "Hydrogen Gas and Biochar Production from Kitchen Waste Via Dark Fermentation", <i>Snigdhendubala Pradhan, Burak Yuzer, Yusuf Bicer, Gordon Mckay</i>	311
OP#171. "Ni-Cu Bimetallic Catalysts for Effective Syngas Production via Low-Temperature Methane Steam Reforming", <i>Martin Khzouz, Babak Fakhim, Saleh Babaa, Mohammad Ghaleeh, Farooq Sher, Evangelos I. Gkanas</i>	318
OP#177. "Shades Of Sustainability: An In-Depth Analysis of The Direct and Indirect Carbon Footprint in Blue Ammonia Manufacturing", <i>Hussein Al-Yafei, Ahmed AlNouss, Saleh Aseel</i>	325
OP#178. "Tank To Tank Life Cycle Assessment of Greenhouse Gas Emission from Methanol Plant", <i>Hussein Al-Yafei, Ahmed AlNouss, Saleh Aseel, Mohannad AlJarrah, Tareq Al-Ansari</i>	332
OP#184. "Flexible Natural Gas Allocation to Blue-Hydrogen Monetised Products: An Agent-Based Modelling Approach", <i>Noor Yusuf, Ahmed AlNouss, Tareq Al-Ansari</i>	339
OP#196. "Mathematical Modeling of a Sustainable Energy System for Restaurant Communities: Waste-To-H ₂ Conversion, CO ₂ Mitigation, Clean Fuel Production, And Power Generation", <i>Syed Muhammad Aun Rizvi, Khurram Kamal, Tahir A.H. Ratlamwala, Muhammad Fahad Sheikh</i>	345
OP#197. "A Net-Zero Emission System with Biogas-Fed Solid Oxide Fuel Cell for Hydrogen Production to Advance Sustainability in The Textile Industry", <i>Baraka Abbas, Hooreen Ansari, Kabsha Zain, Wasifa Umer, Abeeha Fatima, Khurram Kamal, Tahir A.H. Ratlamwala</i>	348
Posters	352
PP#8. "Long-Term Assessment of Hydrogen Technology Deployment for Large Scale Decarbonisation of Power Production", <i>Kamran Khammadv, Damian Flynn, Eoin Syron</i>	353
PP#11. "Field Investigation of Green Hydrogen Production Through the Pem Electrolyzer in Ouargla City", <i>Ahmed Zouhir Kouache, Ahmed Djafour, Khaled Mohammed Said Benzaoui, Abdelmoumen Gougui</i>	359

PP#12. "Comparative Study Between GBO and BES Optimization Algorithms for Optimal PEMFC Parameters Identification", <i>Ahmed Zouhir Kouache, Ahmed Djafour, Khaled Mohammed Said Benzaoui, Mohammed Bilal Danoune</i>	365
PP#14. "Investigating the Effect of Using Hydrogen as a Fuel on Performances of Gas Turbine Operating at Lean Condition in Site of Hassi R'mel", <i>Fethia Amrouche, Bouziane Mahmah, Lidya Boudjemaa, Oum Keltoum Bari</i>	372
PP#15. "Sorption Properties of Ball-Milled Porous Silicon for Hydrogen Storage Up to 80 Bar", <i>Rama Chandra Muduli, Paresh Kale</i>	378
PP#16. "Evaluation of Synergistic Integration of Nickel, Porous Silicon, and Thermally Reduced Graphene Oxide for Hydrogen Storage", <i>Rama Chandra Muduli, Neeraj Kumar Nishad, Dinesh Dashbabu, E. Anil Kumar, Paresh Kale</i>	384
PP#41. "Fast Modeling Method of Gas Diffusion Layers of Polymer Electrolyte Membrane Fuel Cells", <i>Hamid Reza Taheri, Mohsen Shakeri</i>	390
PP#68. "Hydrogen Sulfide H ₂ S – for the Service of Humanity!", <i>Anatolii Startsev</i>	394
PP#75. "Modeling of Hydrogen Liquifaction Process Parameters Using Advanced Artificial Intelligence Technique", <i>A. Abdallah El Hadj, Ait Yahia, Hamza. K, M. Laidi, S. Hanini</i>	401
PP#117. "Redox Regulation of Hydrogen Production in Escherichia Coli During Growth on Byproducts of the Wine Industry", <i>Lusine Baghdasaryan, Ofelya Karapetyan, Karen Trchounian, Garabed Antranikian, Anna Poladyan</i>	405
PP#118. "Comparative Economic Analysis of Small Modular Reactor Hydrogen Cogeneration and Conventional Gas-Fired Plant for Load Following: A Case Study", <i>Derrick Whelan, Lixuan Lu</i>	411
PP#128. "Green Hydrogen Production: A Cost Comparison of Different Electrolysis Technologies", <i>Hafiz Muhammad Uzair Ayub, Sabla Y. Alnouri</i>	415
PP#139. "Performances of Commercial Zeolites with Different Acidities for Catalytic CO ₂ Hydrogenation to Dimethyl Ether Using Copper/Zinc/Alumina Catalyst", <i>Assem. T. Mohamed, Abdul Hakeem Anwer, Dina Ewis, Siham Y. Al-Qaradawi, Mohamed Ali H. Saad, Abdelbaki Benamor</i>	421
PP#154. "Facilitating Production of Acetate and Hydrogen Through Enhanced Electron Transfer and Substrate Mass Transfer Using a Multifunctional Photocathode with Nio/G-C ₃ N ₄ /Polythiophene", <i>Abdul Hakeem Anwer, Assem Mohamed, Nafees Ahmed, Abdelbaki Benamor</i>	427
PP#166. "Evaluation of Hydrogen Production from Ammonia Reforming on Ni/ZnO Nanowire Catalysts", <i>Hiroya Tamai, Hironori Nakajima</i>	434
PP#168. "Current and Temperature Distributions in a Planar Solid Oxide Electrolysis Cell In-Situ Assessed with Segmented Electrodes", <i>Kentaro Yokoo, Hironori Nakajima, Kohei Ito</i>	439

PP#170. "In-Situ Current Distribution Measurements of a Planar Solid Oxide Fuel Cell for a Three-Dimensional Finite Element Model to Train a Machine-Learning Surrogate Model", **443**
Yutaro Ito, Yingtian Chi, Hironori Nakajima

PP#188. "Hydrogen Naval Propulsion: Problems and Solutions", **447**
Remili Sadia, Mohamed Chaimaa



ABOUT HAMAD BIN KHALIFA UNIVERSITY

Hamad Bin Khalifa University (HBKU), a member of Qatar Foundation for Education, Science, and Community Development (QF), was founded in 2010 to continue fulfilling QF's vision of unlocking human potential.

HBKU is a homegrown research and graduate studies University that acts as a catalyst for positive transformation in Qatar and the region while having a global impact.

Located within Education City, HBKU seeks to provide unparalleled opportunities where inquiry and discovery are integral to teaching and learning at all levels utilizing a multidisciplinary approach across all focus areas.

HBKU is committed to actively contribute to achieving the Qatar National Vision 2030 by building and cultivating human capacity through an enriching academic experience and an innovative research ecosystem. Through applying creativity to knowledge, students will have the opportunity to discover innovative solutions that are locally relevant and have a global impact.

At Hamad Bin Khalifa University – our students, faculty, staff, partners, and leadership – all share a common belief in the power of higher education and research to make a positive impact in the development of nations.

FOREWORDS



Dean's Welcoming Message

On behalf of the College of Science and Engineering (CSE) at Hamad Bin Khalifa University, it is our honor to host and organize this prestigious international event, the 14th International Conference on Hydrogen Production (ICH2P-2023). I would like to extend my warmest greetings to all the attendees of this promising event.

The College of Science and Engineering aims to be a world-class multidisciplinary college with significant positive impact on the region and the world, in the fields of science, engineering, and technology. One of our key divisions is the Division of Sustainable Development with its mission of educating future leaders on Sustainable Energy and Sustainable Environment and all associated areas.

We look forward to contributing to the high-quality research results that will be presented during the symposium, which will help develop new policies and scientific progress towards achieving sustainable development, and be of great value to positioning our college in the midst of these extremely important fields of hydrogen research.

We look forward to welcoming you.

Dr. Mounir Hamdi

Dean of the College of Science and Engineering
Hamad Bin Khalifa University

FOREWORDS



Co-Chair's Welcoming Message

As Co-Chair of the Organizing Committee for the International Conference on Hydrogen Production (ICH2P-2023), I am honored to welcome you to this esteemed gathering held at Hamad Bin Khalifa University, Education City, in Qatar from December 19-21, 2023. Your presence here signifies a shared commitment to addressing the challenges of our time through innovative solutions in hydrogen production, storage, transportation, delivery, and utilization.

The scientific part of ICH2P-2023 will include talks by keynote speakers, invited speakers, and industry experts, as well as oral and poster presentations from academic participants. Conference proceedings will be published on the website after reviewing the submitted manuscripts. High-quality papers will be considered, in expanded form, for possible publication in specific reputable international journals mentioned on the conference website.

Throughout the conference days, we invite you to immerse yourself in the diverse discussions, presentations, and collaborative opportunities that this conference offers. The insights and knowledge shared here have the power to shape the future of sustainable energy.

We extend our deepest appreciation to the speakers, sponsors, and the dedicated organizing committee for their tireless efforts in making this event possible. Together, let us embark on a journey of discovery, collaboration, and progress towards a more sustainable and hydrogen-powered world.

Thank you for being part of this transformative experience.

Yusuf Bicer

Conference Co-Chair

Associate Professor, Division of Sustainable Development

College of Science and Engineering

Hamad Bin Khalifa University

FOREWORDS



Co-Chair's Welcoming Message

On behalf of the Division of Sustainable Development, it is my distinct pleasure to welcome you to the International Conference on Hydrogen Production (ICH2P-2023) at Hamad Bin Khalifa University. This gathering is a testament to our collective commitment to advancing sustainable solutions, and your presence amplifies the impact we can make together.

Hydrogen, as a clean and versatile energy source, is at the forefront of our shared vision for a more sustainable future. We encourage you to actively participate in the sessions, engage in discussions, and forge connections that transcend borders and disciplines. The interdisciplinary collaboration fostered during this conference has the potential to drive innovation and pave the way for a greener world.

We also plan to include a social program covering a welcome reception, lunches, coffee breaks, a gala dinner, and social tours in Doha. You will have the opportunity to experience and observe the distinctive Qatari culture, and the hospitality and beauty of Doha.

A heartfelt thank you to the organizers, speakers, and sponsors for their dedication to making this event a success. Together, let us explore the frontiers of hydrogen production and contribute to building a more sustainable and resilient world.

We endeavor to ensure that ICH2P-2023 will be a valuable, impactful, and enjoyable event.

Dr. Tareq Al-Ansari

Conference Co-Chair

Associate Professor, Head of the Division of Sustainable Development

College of Science and Engineering

Hamad Bin Khalifa University

ORGANIZING COMMITTEE

Honorary Chair

T. Nejat Veziroglu
USA

Founding Chair

Ibrahim Dincer
Ontario Tech University, Canada

Co-Chairs

Yusuf Bicer
Hamad Bin Khalifa University, Qatar

Tareq Al-Ansari
Hamad Bin Khalifa University, Qatar

Executive Committee

Abdulkarem Amhamed
Hamad Bin Khalifa University/QEERI, Qatar

Ahmad S. Abushaika
Hamad Bin Khalifa University, Qatar

Ahmed Khalifa
Qatar University, Qatar

Fares A. Almomani
Qatar University, Qatar

Gordon McKay
Hamad Bin Khalifa University, Qatar

H.E. Mohammed Bin Saleh Al-Sada
Texas A&M University at Qatar, Qatar

Executive Committee (Continues)

Luluwah Al-Fagih
Hamad Bin Khalifa University, Qatar

Marcello Contestabile
Hamad Bin Khalifa University/QEERI, Qatar

Mounir Hamdi
Hamad Bin Khalifa University, Qatar

Muammer Koc
Hamad Bin Khalifa University, Qatar

Muftah El-Naas
Qatar University, Qatar

Nimir Elbashir
Texas A&M University at Qatar, Qatar

Patrick Linke
Texas A&M University at Qatar, Qatar

Local and International Organizing Committee

Abdullah A. AlZahrani

Umm Al-Qura University, Saudi Arabia

Abdulla Al Wahedi

Qatar General Electricity and Water Corporation, Qatar

Burak Yuzer

Hamad Bin Khalifa University, Qatar

Farhat Mahmood

Hamad Bin Khalifa University, Qatar

Farrukh Khalid

Indian Institute of Technology, Guwahati, India

Fatih Sorgulu

Yildiz Technical University, Türkiye

Hanadi G. Al-Thani

Hamad Bin Khalifa University, Qatar

Ikhlas Ghiat

Hamad Bin Khalifa University, Qatar

Mehmet Akif Ezan

Dokuz Eylul University, Türkiye

Merve Ozturk

Yildiz Technical University, Türkiye

Mohammad Alherbawi

Hamad Bin Khalifa University, Qatar

Muhammad Luqman

King Fahd University of Petroleum and Minerals

Muhammad Usman Sajid

Hamad Bin Khalifa University, Qatar

Nader Javani

Yildiz Technical University, Türkiye

Nurettin Sezer

Hamad Bin Khalifa University/QEERI, Qatar

Shoukat Alim Khan

Texas A&M University at Qatar, Qatar

Tahir A.H. Ratlamwala

National University of Sciences and Technology, Pakistan

Local Scientific Committee

Abdulnasser Mabrouk

Hamad Bin Khalifa University/QEERI, Qatar

Ahmad Sleiti

Qatar University, Qatar

Ahmed Abdala

Texas A&M University at Qatar, Qatar

Ahmed Abdel-Wahab

Texas A&M University at Qatar, Qatar

Alessandro Sinopoli

Hamad Bin Khalifa University/QEERI, Qatar

Anand Kumar

Qatar University, Qatar

Awni Al-Otoom

The University of Doha for Science and
Technology, Qatar

Aziz Rahman

Texas A&M University at Qatar, Qatar

Brahim Aïssa

Hamad Bin Khalifa University/QEERI, Qatar

Dhabia M. Al-Mohannadi

Texas A&M University at Qatar, Qatar

Fadwa El Mellouhi

Hamad Bin Khalifa University/QEERI, Qatar

Fadwa ElJack

Qatar University, Qatar

Hamish Mackey

University of Canterbury, New Zealand / HBKU,
Qatar

Hicham Hamoudi

Hamad Bin Khalifa University/QEERI, Qatar

Ibrahim Galal Hassan

Texas A&M University at Qatar, Qatar

Ibrahim M. Abu-Reesh

Qatar University, Qatar

Ioannis Economou

Texas A&M University at Qatar, Qatar

Konstantinos Kakosimos

Texas A&M University at Qatar, Qatar

Majeda Khraisheh

Qatar University, Qatar

Mohamed Haouari

Qatar University, Qatar

Mohd Zamri Che Wanik

Hamad Bin Khalifa University/QEERI, Qatar

Ramazan Kahraman

Qatar University, Qatar

Rima Isaifan

Hamad Bin Khalifa University, Qatar

Sami G. Al-Ghamdi

KAUST, Saudi Arabia/HBKU, Qatar

Sertac Bayhan

Hamad Bin Khalifa University/
QEERI, Qatar

Shaheen Al-Muhtaseb

Qatar University, Qatar

Veronica Bermudez

Hamad Bin Khalifa University/
QEERI, Qatar

International Scientific Committee

Adnan Midilli

Yildiz Technical University, Türkiye

Aysel Kantürk Figen

Yildiz Technical University, Türkiye

Bestami Ozkaya

Yildiz Technical University, Türkiye

Bruce E Logan

Pennsylvania State University, USA

Can Ozgur Colpan

Dokuz Eylul University, Türkiye

Chao-Yang Wang

Pennsylvania State University, USA

Franco Barbir

University of Split, Croatia / USA

Giuseppe Spazzafumo

University of Cassino and Southern Lazio, Italy

Greg F. Naterer

Memorial University of Newfoundland, Canada

Hirohisa Uchida

Tokai University, Japan

Ilgi Karapinar

Dokuz Eylül University, Türkiye

Chao-Yang Wang

Pennsylvania State University, USA

İnci Eroglu

Middle East Technical University, Türkiye

Ioan Iordache

ICMET, Romania

John W. Sheffield

Purdue University, USA

Joris Proost

University catholique de Louvain, Belgium

Marc A. Rosen

Ontario Tech University, Canada

Matthew M. Mench

University of Tennessee, Knoxville, USA

Meng Ni

Hong Kong Polytechnic University, Hong Kong

Peter Strasser

Technische Universität Berlin, Germany

Ramazan Solmaz

Bingol University, Türkiye

Vasudevan Subramanian

CSIR, India

Vladimir Linkov

University of the Western Cape, South Africa

Wei-Hsin Chen

National Cheng Kung University, Taiwan

Xianguo Li

University of Waterloo, Canada

Yun Hang Hu

Michigan Technological University, USA

Ziad Saghir

Toronto Metropolitan University, Canada

Student Support Committee
(Hamad Bin Khalifa University, Qatar)

Aliya Banu

Amira Chebbi

Anas H. Karaki

Carlos Mendez

Dawood Hjeij

Dindha Andriani

Fabiha Sadaf Hussain

Fadi AlNoaimi

Haya Talib Hashim Shubbar

Manal AlShafi

Mohammed Al-Breiki

Moiz Maroof Ali

Nadira Salsabila

Namra Mir

Omer Abedrabboh

Ragad F. Alshebli

Razan Ezzeldin Hamza Sawaly

Ridab Awad Hamid Khalifa

Sami Sbahieh

Sara Adel Elsaïd Mohamed

Yasser M. Abdellatif

The ICH2P-2023 Organizing Committee expresses its sincere appreciation to the following organizations and sponsors.

Cooperating Institutions



Strategic Partner



Platinum Sponsor



Silver Sponsors



14th INTERNATIONAL CONFERENCE ON HYDROGEN PRODUCTION (ICH2P-2023)



December 19 – 21, 2023
Education City, Doha, Qatar

INVITED SPEAKERS



ICH2P14-IT1

GREEN HYDROGEN PRODUCTION: SOLAR CHIMNEY POWER PLANT INTEGRATED WITH WATER DESALINATION PLANT

¹Emad Abdelsalam, ²Fares Almomani

¹Electrical and Energy Engineering Department, Al Hussein Technical University, Amman 11831, Jordan

²Chemical Engineering Department, Qatar University, Qatar

*Corresponding author e-mail: Falmomani@qu.edu.qa

ABSTRACT

Modeling of a Solar Chimney Power Plant (SCPP) integrated with a water desalination power plant (WDPP) for synchronous electricity production, clean water, and hydrogen has been investigated for the Doha-Qatar climate. This study focuses on the performance of the SCPP when operating in standalone mode and when integrated with a WDPP. The SCPP produces electricity through a wind turbine, clean water through an evaporative process, and hydrogen using electrolysis. The excess heat from the WDPP boosts the temperature profile of the SCPP and results in continuous electrolysis to produce hydrogen. Results indicate that the combined SCPP and WDPP system enhanced the temperature and air velocity profiles, resulting in the maximum hydrogen production exceeding 39,018 kg annually compared to 13,351 kg for a standalone SCPP. Furthermore, electricity and clean water from the proposed system were 2.9 times and 1.6 times, respectively, greater than the standalone SCPP.

Keywords: Green Hydrogen, sustainability, solar energy, power plants

INTRODUCTION

Hybrid technologies, which integrate many energy technologies, indicate that the future energy sector will not rely solely on one energy source[1],[2]. Alongside the increasing energy demand, it is important to additionally take into account the diversity, efficacy, and sustainability of energy resources [3]-[5]. Increasing the utilization of additional renewable energy sources is vital for the purpose of achieving sustainability and enhancing energy efficiency. In recent years, there has been a growing trend towards adopting alternative energy sources that produce no carbon emissions. This shift is driven by the increasing disparity between energy supply and demand, as well as the detrimental environmental impact of fossil fuels [6],[7]. Fuel cells (FCs) are a prominent and promising power source alternative for the future. They are known for their reliability, silent operation, and high efficiency [8].

The projected hydrogen demand for 2020 is expected to reach 87 million metric tons (MT), and this figure is estimated to increase to 500-680 million MT by 2050. Between 2020 and 2021, the valuation of hydrogen production's share price was expected to be \$130 billion. It is projected to grow at an annual rate of 9.2% until 2030[8]-[11]. Currently, the production of "green" hydrogen is limited, resulting in fossil fuels being responsible for about 95% of total hydrogen generation. At present, hydrogen production relies on 2% of the world's coal and 6% of its natural gas[12][13]. Furthermore, the economic feasibility of producing green hydrogen has increased as a result of declining costs of clean energy, lower prices of electrolyzers, and improved efficiency resulting from advancements in technology. Bloomberg New Energy Finance predicts that by 2050, the cost of producing green hydrogen could range from \$0.70 to \$1.60 per kilogram in most parts of the world. This would make green hydrogen cost-competitive with natural gas, assuming that natural gas prices continue to decline. NEL, the leading global manufacturer of electrolyzers, asserts that the cost threshold for creating green hydrogen from fossil fuels could be achieved by 2025[14]. Research indicates that these advanced hydrogen generation systems have a distinct capacity to be powered by renewable energy sources such as hydro, geothermal, and solar. In 2017, hydrogen production systems that incorporate heat recovery (thermal) and photonic-based technologies outperformed other systems in terms of emissions, price, and efficiency [19]. Recent findings suggest that hydrogen might potentially become a financially feasible fuel option in the transportation sector, as long as it is exempt from carbon taxes, considering the existing expenses associated with alternative fuels [15], [16]. Various countries are developing national hydrogen roadmaps in reaction to the rapid progress of hydrogen technology and increasing energy needs. Hydrogen has the capacity to meet the increasing demands of social development across several energy sectors. Consequently, numerous countries have implemented measures to support the fuel cell industry and incorporate the hydrogen sector into their national objectives [17].

Japan's government has implemented a domestic policy to promote the production of hydrogen. This plan encompasses an advanced industrial system that is at the forefront of technology and commercialization. It has the capacity to manufacture over ten thousand Toyota Mirai vehicles[18]. Nevertheless, the progress in these technologies and significant improvements in the storage, transportation, and utilization of hydrogen fuel indicate a reduction in the country's reliance on imported fossil fuels. Consequently, green hydrogen will surpass traditional energy sources in importance[19]. The photonic alternatives obtain the highest average grade (7.60/10) for the hydrogen generating approach, followed by thermal choices (5/10) and bio options (4.80/10) [20].

Hydrogen production from the sun is often considered the optimal choice for sustainable energy, and solar energy has the capacity to be the most abundant and renewable energy source now accessible to mankind. The various methods for solar to hydrogen synthesis have been extensively studied, including the determination of exergy and the utilization of energy. Wang et al. [20] investigated the mechanisms of photochemical processes, which involve the utilization of photon-activated electrons from secondary components (sensitizer and catalyst) to activate and separate water. Additionally, they examined thermochemical cycles that employ heat energy to separate water molecules, electrolysis that utilizes electricity to break water molecules, and solar-to-hydrogen reactions.

The paper provides a comprehensive analysis of the theoretical aspects and current technological advancements in generating hydrogen from solar energy. It also explores the potential of a solar photovoltaic-based hydrogen system to operate for extended periods by improving energy efficiency and employing a continuity index[21]. Solar energy plays a vital role in the shift from carbon-based fuels to environmentally friendly energy sources. Solar energy has the potential to be a crucial and indispensable source for generating hydrogen, as it falls under the category of energy sources that can be used to produce hydrogen. There are three distinct categories of solar energy: photovoltaic, thermal, and photoelectrochemical [22]. Hydrogen can be produced by various methods, including solar thermolysis, mechanical-to-electrical energy conversion, solar thermochemical cycles, solar cracking, solar gasification, and electrolysis. Bio-photolysis and photoelectrolysis are the primary methods for directly producing hydrogen. The photovoltaic source is used to generate electricity, which is then employed in the process of electrolysis to produce hydrogen. The solar thermal energy source is utilized to generate hydrogen through sun gasification and solar ammonia reforming, hence extracting thermal energy. Conversely, the low productivity of solar-to-hydrogen systems and the exorbitant cost of photovoltaic cells are regarded as major impediments to the widespread economic advancement of solar-powered hydrogen production. Furthermore, the cost of generating green hydrogen from wind energy and solar sources should be at least four times cheaper than the price of retail power, as it has a significant impact on the final price of hydrogen [24]. Another major obstacle to improving overall hydrogen generation efficiency is the efficacy of solar energy conversion into electricity. On the other hand, solar electrolysis, photochemical technologies, and photoelectrochemicals offer greater convenience for hydrogen filling stations because they require fewer procedures and have the possibility to eliminate hydrogen distribution networks. Continued development of materials for high-temperature processes, with a specific emphasis on high-temperature membranes and heat exchangers for solar thermal processes, is crucial [25].

Jordan's limited natural resources have led to a reliance on imported fossil fuels, amounting to approximately 17% of GDP in 2017, equivalent to \$3.5 billion. This dependence has significant implications for the country's progress in modern society and its economy. Jordan achieved a remarkably effective energy transition by embracing renewable energy ahead of any other country in the MENA region. The authorities effectively decreased the expenses of the PV project, as evidenced by the pricing of renewable energy. The prices experienced a decline from 16.9 cents per kilowatt-hour (kWh) during a 200 MW bidding round in 2013 to a range of \$6-7 cents per kWh in 2015, and further dropped to approximately 2.5 cents per kWh in 2019. The findings suggesting the potential for green hydrogen production should be acknowledged as prompts, necessitating further research to verify the results of this study. An aspect of ambiguity in this analysis pertains to the future development of Qatar's hydrogen market; the demand for hydrogen is a critical apprehension. Nevertheless, there is an expectation that the demand for green hydrogen will experience a significant increase in the upcoming years. Qatar should actively monitor the trend towards hydrogen and, if possible, identify potential hydrogen consumers in Qatar and the neighboring nations. The findings indicated that solar-hydrogen fuel could serve as a viable substitute for Jordan [26]. A comparable investigation may be required for Qatar. By 2060, the manufacturing initiated in 2020 has the potential to meet a significant amount of the energy demand sector [27], [28]. In order to attract investments in the production of green hydrogen

and position Qatar as a hub for trading green hydrogen and its byproducts, such as green ammonia and green methanol, it may be necessary for Qatar to adopt a legislative and regulatory strategy plan similar to the one implemented in Jordan [29].

MATERIALS AND METHODS

System Description

The system depicted in Figure 1 works on the principle of natural convection. It consists of three main components: a solar collector, a chimney, and a water desalination and hydrogen production plant. The solar collector is a crucial component that absorbs solar radiation and converts it into heat. It is typically constructed using a dark material with high absorbance properties. When sunlight falls on the collector, the material absorbs a significant portion of the solar energy, which is then transformed into thermal energy.

The tall-vertical structure of the chimney causes an upward airflow due to the temperature difference between the hot air inside and the cooler air outside. The hydrogen production plant, located at the base of the chimney, uses solar heat and airflow to drive a series of processes that produce clean water and hydrogen fuel.

During the daytime, solar heat accumulates in the solar collector section; the inside air heats up, expands, and becomes less dense, causing it to rise and flow into the chimney. The solar heating creates a continuous airflow that drives a turbine connected to an electrical generator, producing electricity. As the excess heat from the solar desalination plant is channeled into the solar collector section, the temperature profile is further enhanced, resulting in more airflow velocity and boosting the power produced. Directing the excess heat also allows for uninterrupted electricity generation through nighttime as the desalination plant heat supply continues.

As the hot air rises, it also passes over a seawater pool, causing some water to evaporate and produce steam. The steam then condenses on a series of surfaces within the chimney, making clean water that can be collected through the gutters and distilled water pipes. This provides an additional water desalination system that aids the adjacent plant.

The remaining hot air then flows into the hydrogen production plant, which is used to split water molecules into hydrogen and oxygen through electrolysis. Hydrogen is collected and stored for use as a clean and renewable fuel source. Excess electricity from the turbine can be used to enhance the electrolysis process and produce hydrogen undisturbed. Overall, integrating the heat recovered from the water desalination plant would aid the SSCP in producing power, distilled water, and hydrogen fuel both in the daytime and nighttime.

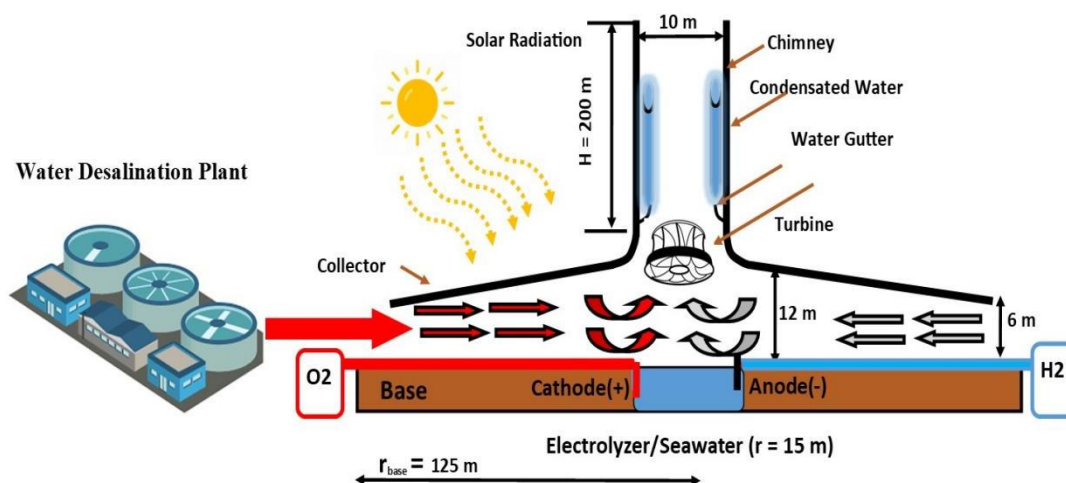


Figure 1. Illustration of the proposed SSCP system integrated with electrolysis station and water desalination power plant

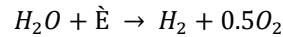
Properties	Value
Power	600-650MW
Flue gas mass flow rate	750-800 kg/s
Temp	150-200°C
Specific heat	1.131-1.134 kJ/kg K
Moisture Content	12-16%

Properties of the water desalination plant

Mathematical Model

Reaction (1) illustrates the complete Waterc reaction. Based on the energy requirements outlined in our earlier study (Almomani and Bohsale 2020), the energy necessary for producing PH₂ via the Waterc process has been calculated. Several authors extensively examined this system's energy and exergy analysis (Chase 1998) and (Ni et al. 2006).

In summary, equation (1) can be employed to calculate the energy (\dot{E} (K)) required for reaction (1) to convert water into oxygen and hydrogen gas. The Gibbs free energy (G) from equation (2) governs the decomposition of water, also known as Reaction (1).



$$\Delta G(T) = T \left(\frac{\Delta \dot{E}(T)}{T} - \Delta s(T) \right)$$

Where U stands for energy, G (K) for the change in Gibbs free energy, T for Kelvin temperature. When the pressure is constant, E, S, and G fluctuate as a function of temperature. The applied cell potential must be greater than the cell's reversible potential to electrolyzer water effectively. The applied cell potential should contain the additional possibility to account for irreversibilities produced within the cell, such as reactant/product transportation, charge transfer, and resistance of electrolytes and electrodes (P_{extra}). The potential for such would be removed by adding an internal impedance (Z_{in}) proportional to the anticipated P_{extra}. Equation (2) can calculate the rate at which heat (QH) developed owing to irreversibility.

The applied cell potential must exceed the cell's reversible potential to facilitate efficient water electrolysis. Additionally, the applied cell potential should incorporate the capacity to address the irreversibility arising within the cell, such as the transportation of reactants/products, charge transfer, and the resistance of electrolytes and electrodes (P_{extra}). This potential imbalance could be mitigated by introducing an internal impedance (Z_{in}) proportional to the anticipated P_{extra}. Equation (2) can be employed to compute the rate at which heat (QH) develops due to irreversibility.

$$P_{extra} = \frac{Q_H}{I}$$

Where:

$$P_{extra} = IZ_{in}$$

The energy required for water electrolysis can be provided by the generated (QH) inside the cell, which is why I, or the applied current (A), is used. If the cell's rate of QH is insufficient, additional external heat must be applied to maintain water electrolysis. The requisite values for water, oxygen, and hydrogen's E, Q, and G were all in the thermochemical tables (Chase 1998). The total energy needed to accomplish the electrolysis of water equals the theoretical energy demand plus any associated losses, as shown by equations 1 and 2. As a result, Equation (3) may be used to determine the efficiency of water electrolysis:

$$\eta_{En} = N_{H_2} \times LHV_{H_2} \times \sum \Delta H^{-1} \quad (3)$$

Where $LHV_{(H_2)}$ is the lower heating value of H_2 , $N (H_2, prod)$ is the flow rate of H_2 leaving the system, and H is the total of the system's electric energy input used to create oxygen, water, and hydrogen.

$$N_{H_2,prod} = N_{H_2O,reacted} = 0.5 \sqrt{(JF^{-1})^2}$$

$$N_{O_2,prod} = 0.25 \sqrt{(JF^{-1})^2}$$

The symbol J is the electrolysis cell's current density. Furthermore, F is the Faraday constant. Consequently, using equation (6) to determine the electrical energy involved in W_{atelc}

$$\sum \Delta H = J \sum (P_{irr} + P_{act,c} + P_{act,a} + P_{con,a} + P_{con,c} + P_{ohm}) \quad (6)$$

P_{irr} is the reversible potential calculated using the Nernst equation. The equations shown below were used to calculate these parameters $P_{(act,c)}$, $P_{(act,c)}$, $P_{(act,a)}$, $P_{(con,a)}$, $P_{(con,c)}$, and P_{ohm} .

The calculation of the aforementioned parameters is covered elsewhere (Todd and Young 2002; Hernández-Pacheco et al. 2004; Nam and Jeon 2006b; Ni et al. 2006; Ni et al. 2007). Equation 7 was then used to calculate the maximum amount of hydrogen (kg) that the SCPP system can produce.

$$P_{H_2} (kg) = \frac{E}{\Delta E(H_2)} \quad (7)$$

$$P_{ohm} = 2.99 \times 10^{-5} J L \exp(10300 T^{-1})$$

$$P_{act,i} = RTF^{-1} \sinh^{-1} \left(\frac{J}{2\gamma_i e^{\left(\frac{E_{act,i}}{RT}\right)}} \right)$$

$$P_{con,c} = \frac{RT}{2F} \ln \left(\sqrt{1 + \left(\frac{JRTd_c}{2fD_{H_2O}^{eff} P_{H_2O}^{In}} \right)} \times \sqrt{\left(1 - \left(\frac{JRTd_c}{2fD_{H_2O}^{eff} P_{H_2O}^{In}} \right) \right)^{-2}} \right)$$

$$P_{con,a} = 0.25 RTF^{-1} \ln \left(\sqrt{\left((P_{O_2}^{In})^2 + \frac{JRT\mu d_a}{2FBg} \right) \times (P_{O_2}^{In})^{-2}} \right)$$

SCPP Mathematical Model

In our previous articles (Abdelsalam et al. 2020; Abdelsalam et al. 2021a; Abdelsalam et al. 2021b; Alkasrawi et al. 2021), we extensively discussed the mathematical model and performance characteristics of the SCPP. However, the detailed model can be found in the supplemental material. The mathematical model was implemented using MATLAB programming. The application reads weather data from an input file containing hourly weather information for Doha, Qatar, spanning an entire year. This data includes relative humidity, wind speed, solar radiation, and outdoor temperature. All system parameters, including collector and absorber temperatures, as well as the temperature profile of the system's air, are computed by the software through a MATLAB genetic algorithm program. The software calculates the production of oxygen, hydrogen, and power hourly, along with quantifying the water desalination process.

RESULTS AND DISCUSSION

Figure 2 illustrates the weather information gathered in Doha, Qatar (at 25° 17' 9.9816" N and 51° 32' 5.3412" E). The two-dimensional plot displays annual radiation in watts per meter square as a function of time. The first axis is the vertical y-axis on the left-hand side of the plot and represents the 24-hour day, with time increasing from bottom to top. The second axis represents the 12 months of the year and is located on the horizontal x-axis, with January at the left and December at the right. The third axis is the vertical y-axis on the right-hand side of the plot and represents the intensity of the radiation, measured in watts per meter square, with values increasing from bottom to top. The plot shows that the highest radiation intensity occurs in July at noon, with values exceeding 650 W/m². Generally, radiation intensity is highest in the summer months and lowest in the winter months.

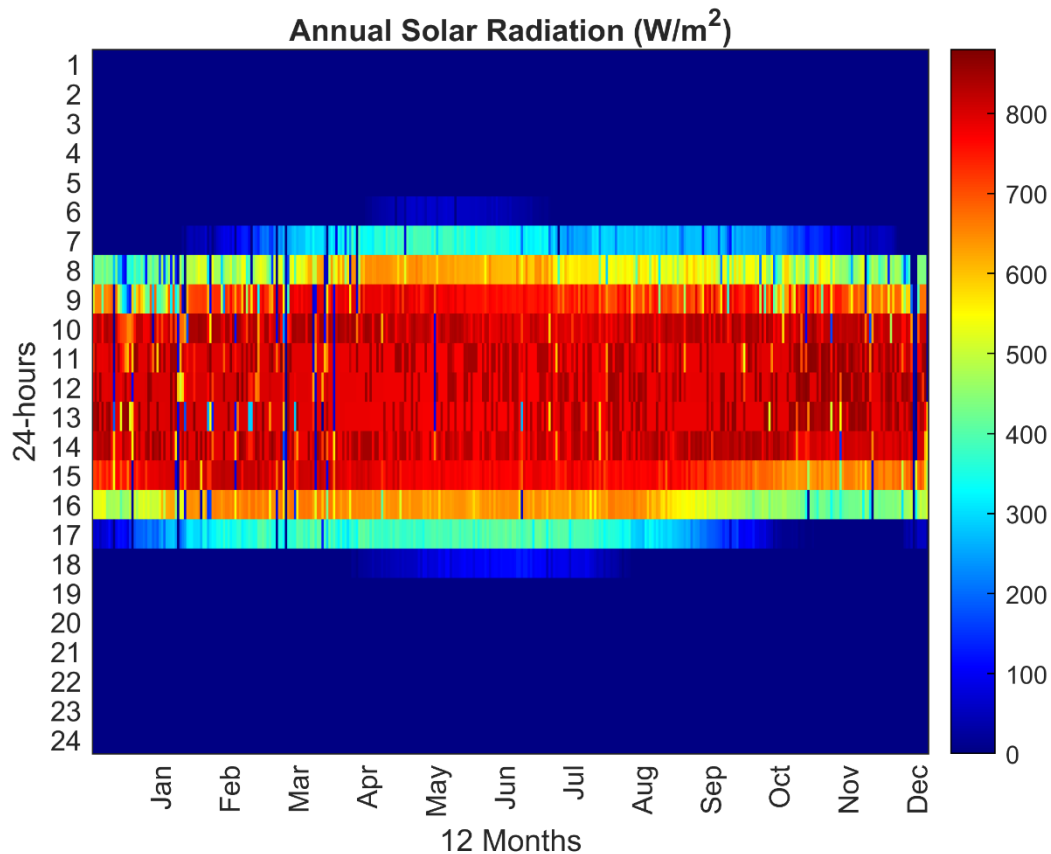


Figure 2. Display the yearly information on solar irradiance and measurements of solar irradiance for each hour.

Furthermore, the plot underscores the broader seasonal trends in radiation intensity. Summer months emerge as the leaders in solar energy, with their abundant sunlight resulting in heightened radiation levels. Conversely, the winter months witness a decline in radiation intensity due to reduced daylight hours and less direct sunlight. This insight into the annual radiation dynamics guides the optimization of hydrogen production strategies, promoting the utilization of solar-driven processes during peak radiation months to ensure maximum efficiency and output.

Figure 3 displays three variables: Ambient temperature, wind speed, and humidity, plotted over time. The x-axis represents time, with earlier times on the left and later times on the right. The y-axis on the left-hand side of the plot represents ambient temperature, while the y-axis on the right-hand side of the plot represents humidity and wind speed. The plot shows that humidity levels are highest at night, reaching a maximum of 85 °C. Wind speed fluctuates over time and does not show a clear pattern. Ambient temperature increases over the day, with maximum values occurring in the afternoon. Overall, the plot suggests that the weather conditions are cooler and more humid at night, with higher temperatures and lower humidity during the day.

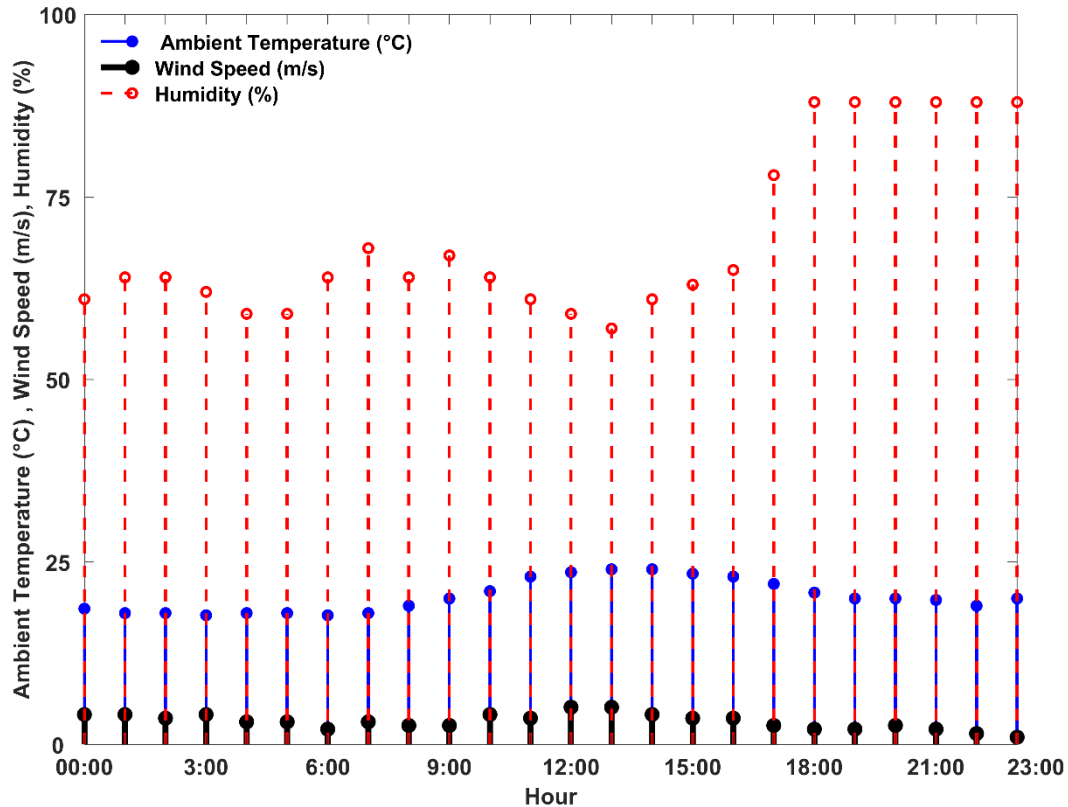


Figure 3. A 24-hour Weather Profile in Doha, Qatar

Each variable finds its representation on distinct y-axis strategically placed for clarity. The ambient temperature, a critical factor influencing energy processes, is elegantly positioned on the y-axis of the left-hand side. Simultaneously, the y-axis on the left-hand side accommodates humidity and wind speed, aligning with their respective values to avoid confusion.

The trajectory of ambient temperature charts a predictable course. As the sun ascends in the sky, temperatures steadily rise, culminating in their zenith during the afternoon hours. This trend aligns with the sun's intensity, illustrating the direct relationship between solar irradiance and temperature increase.

3.2 System Characteristics

Figure 4 displays the impact of exterior and interior temperatures on the performance of two systems, one with traditional SSCP and one with a SSCP+WDPP. The x-axis represents time in hours, with noon showing the maximum values. The y-axis represents air temperature. The plot shows that both systems are affected by changes in exterior and interior temperature. The performance of the traditional SSCP system SSCP decreases as external temperatures drop.

In contrast, the system's performance with a WDPP is less affected by changes in the external temperature. The interior temperature of both systems increases with time, with maximum values

occurring at 12 p.m. Overall, the plot suggests that the system with an SCPP performs better than the traditional system in maintaining interior temperatures in the face of changes in exterior temperature.

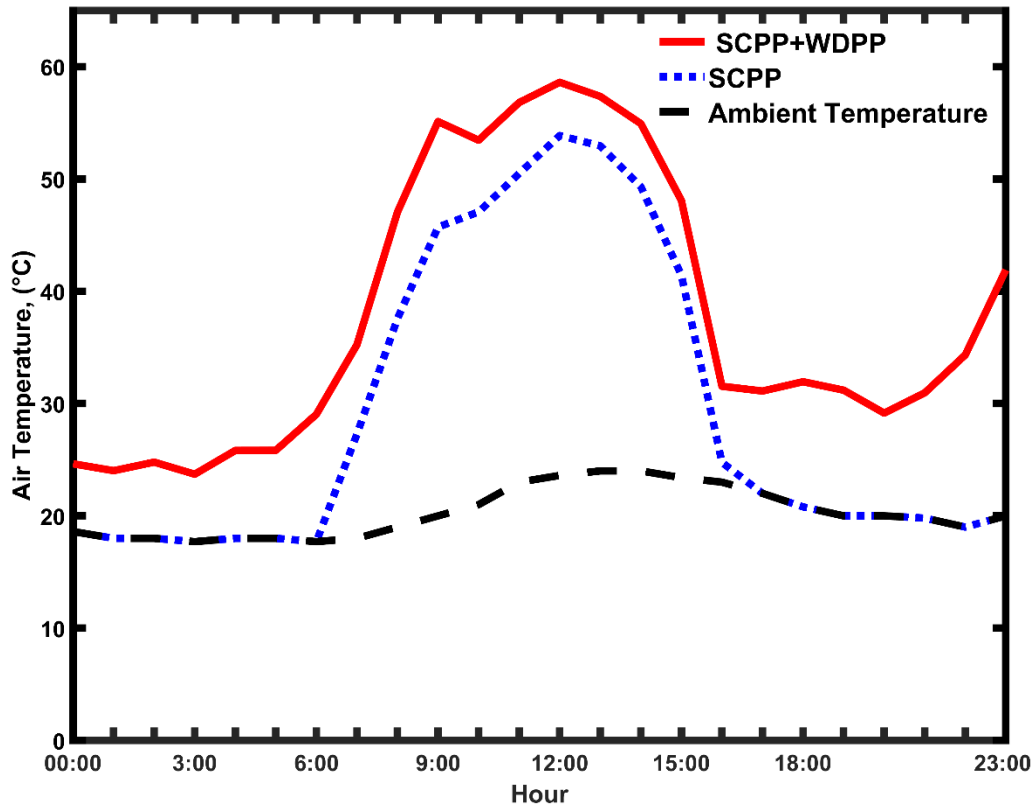


Figure 4. The variation of the temperature profile under the collector when the SCPP is in standalone mode and integrated with the WDPP.

Within this graphical narrative, both systems' performances are indicators of their response to external and internal temperature fluctuations. Notably, as the exterior temperature undergoes shifts, both the traditional SCPP and the SCPP+WDPP system display discernible alterations in performance. The traditional SCPP system is sensitive to diminishing exterior temperatures, reducing efficiency as the external environment cools. On the other hand, the system integrated with a WDPP demonstrates resilience against these external temperature changes, remaining relatively unfazed by such fluctuations. This divergence in behavior underscores the innovative potential of the WDPP system in maintaining consistent performance across varying external thermal conditions.

Figure 5 displays a 24-hour air velocity profile in the chimney in the case of the SCPP in a standalone mode and the SCPP+WDPP mode in Doha on January 1st. The x-axis represents time in hours, with earlier times on the left and later times on the right. The y-axis represents air velocity. The plot shows that both systems are affected by changes in external temperature, with air velocity decreasing as external temperature increases. The maximum air velocity occurs in the morning, although the exact time is not specified. Overall, the plot suggests that both systems experience a similar pattern of decreasing air velocity with increasing external temperature, although further details on the systems and their performance would be needed to make more specific conclusions.

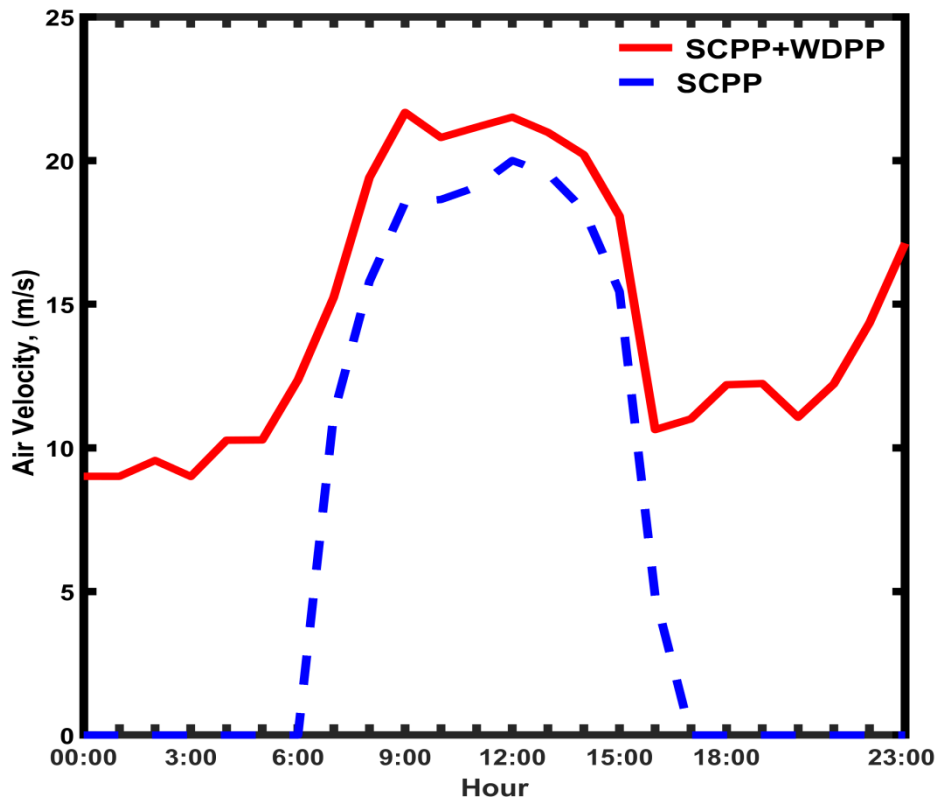


Figure 5. The air velocity profile changes within the chimney when the SCPP operates in standalone mode and when integrated with the WDPP.

Figure 5 paints a clear picture of the responsiveness of both systems to changes in external temperature. As the external temperature undergoes variations, both the SCPP Design and SCPP+WDPP systems display discernible fluctuations in air velocity. It becomes evident that air velocity experiences a decrease with the escalation of external temperature. This shared behavior underscores the sensitivity of both systems to thermal variations, mirroring the general trend of air velocity deceleration as temperatures rise.

The plot spotlights the morning hours as the period of peak air velocity, yet it refrains from specifying the precise time of this zenith. Despite this ambiguity, it is apparent that both systems converge in showcasing this peak in the early hours of the day. This shared temporal alignment further underscores the systems' parallel responses to the daily temperature cycle.

In summation, the plot hints at a common trend between the SCPP Design and SCPP+WDPP systems: a decrease in air velocity as external temperatures ascend. However, for a more in-depth understanding and to draw specific conclusions about the systems' performance nuances, additional details about the systems themselves, their underlying mechanics, and performance metrics would be required. The plot serves as an initial insight, underscoring the need for a deeper exploration into the systems' intricacies to substantiate any definitive observations or conclusions.

Figure 6 displays the annual electricity production in MWh for two systems, SCPP and SCPP+WDPP. The x-axis represents time in months, with January on the left and December on the right. The y-axis represents electricity production in MWh. The plot shows that both systems experience seasonal variations in electricity production. The maximum production for the SCPP system occurs in June, while the maximum production for the SCPP+WDPP system occurs in January and exceeds 100 MWh. Overall, the plot suggests that adding the WDPP system may improve electricity production during the winter months.

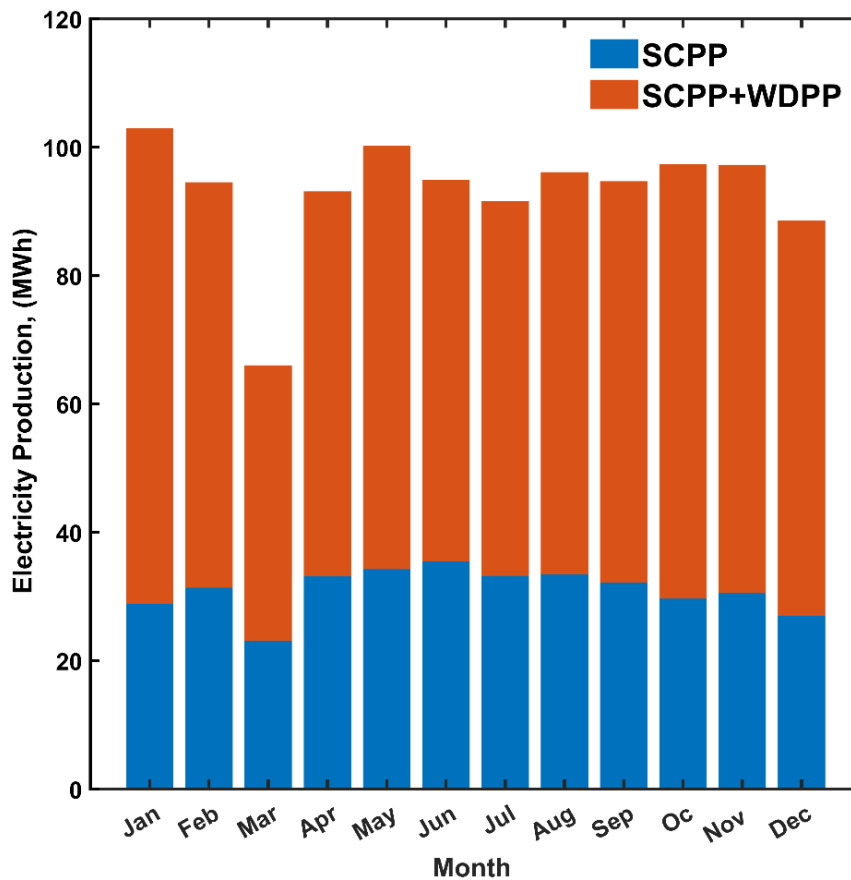


Figure 6. Monthly Profile of Electricity Production via the SCPP and SCPP+WDPP in Doha, Qatar.

In contrast, the SCPP+WDPP system carves a different path. Its zenith in electricity production arrives in January, characterized by lower temperatures and distinct energy consumption patterns. Remarkably, this peak transcends the 100 MWh mark, reflecting the impactful integration of the WDPP component. This enhancement underscores the potential of wind-driven energy to bolster electricity output during periods when conventional sources might face limitations.

Figure 7 displays the annual hydrogen production in kg for two systems, SCPP and SCPP+WDPP. The x-axis represents time in months, with January on the left and December on the right. The y-axis represents hydrogen production in kg. The plot shows that both systems experience seasonal variations in hydrogen production. The maximum production for the SCPP system occurs in May, while the maximum production for the SCPP+WDPP system occurs in December and exceeds 6500 kg. Overall, the plot suggests that adding the WDPP system may improve hydrogen production during the winter months, although further details on the systems and their performance would be needed to make more specific conclusions.

The SCPP+WDPP system charts a unique trajectory. Its pinnacle in hydrogen production emerges in December, a period defined by cooler temperatures and specific energy needs. Astonishingly, this crescendo surges beyond 6500 kg, a testament to the transformative effect of the integrated WDPP component. This achievement underscores the potency of harnessing wind energy to amplify hydrogen production, particularly when climatic conditions might otherwise pose challenges.

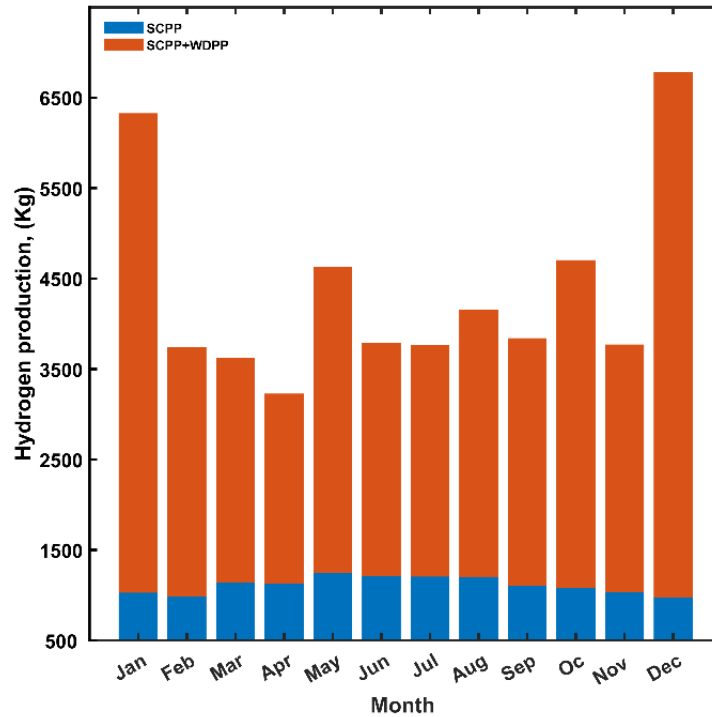


Figure 7. Monthly Profile of Hydrogen Production via the SCPP and SCPP+WDPP in Doha, Qatar.

Figure 8 displays the annual oxygen production in kg for two systems, SCPP and SCPP+WDPP. The x-axis represents time in months, with January on the left and December on the right. The y-axis represents oxygen production in kg. The plot shows that both systems experience seasonal variations in oxygen production. The maximum production for the SCPP system occurs in May, while the maximum production for the SCPP+WDPP system occurs in December and exceeds 50000 kg. Overall, the plot suggests that adding the WDPP system may improve oxygen production during the winter months.

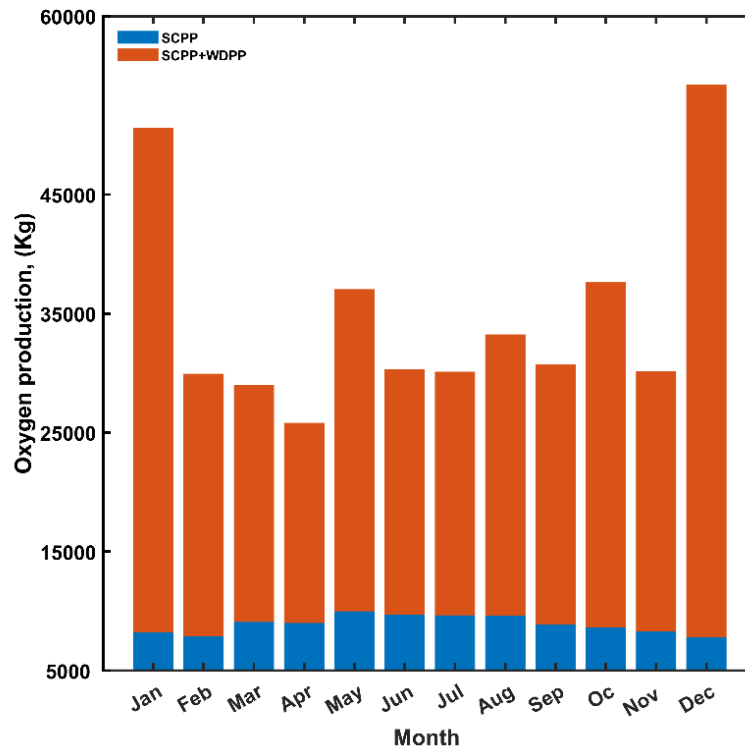


Figure 8. Monthly Profile of Oxygen Production via the SCPP and SCPP+WDPP in Doha, Qatar.

The SCPP+WDPP system charts its unique path. Its summit in oxygen production emerges firmly in December, a time characterized by cooler temperatures and distinct atmospheric conditions. Remarkably, this crescendo soars beyond 50000 kg, a testament to the transformative influence of the integrated WDPP component. This accomplishment underscores the synergistic power of harnessing wind energy to amplify oxygen production, especially when conventional conditions might not be conducive

CONCLUSIONS

This study has investigated the modeling of an SCPP integrated with a WDPP for the synchronous production of electricity, clean water, and hydrogen in the context of the Doha, Qatar climate. The analysis focused on comparing the performance of the SCPP when operating in a standalone mode and when integrated with the WDPP. This work provides insights into the system's performance, considering temperature, air velocity, and weather conditions. A key finding is that adding the WDPP component enhances the system's interior temperatures, especially during external temperature fluctuations. Electricity, Hydrogen, Oxygen, and water production show seasonal variations, with the SCPP+WDPP system outperforming the standalone SCPP during winter. The findings emphasize the importance of renewable energy sources, such as solar and wind, in meeting the growing demands for electricity, clean water, and hydrogen in a changing energy landscape. Further research and development are crucial to optimize and scale such integrated systems for practical applications to transition to a cleaner and more sustainable energy future.

REFERENCES

- [1] P. Das, B. K. Das, M. Rahman, and R. Hassan, "Evaluating the prospect of utilizing excess energy and creating employments from a hybrid energy system meeting electricity and freshwater demands using multi-objective evolutionary algorithms," in *Energy*, 2022. doi: 10.1016/j.energy.2021.121860.

- [2] N. S. Santarisi and S. S. Faouri, "Prediction of combined cycle power plant electrical output power using machine learning regression algorithms," *Eastern-European Journal of Enterprise Technologies*, vol. 6, no. 8, p. 114, 2021.
- [3] S. R. Paramati, U. Shahzad, and B. Doğan, "The role of environmental technology for energy demand and energy efficiency: Evidence from OECD countries," *Renewable and Sustainable Energy Reviews*, 2022, doi: 10.1016/j.rser.2021.111735.
- [4] A. Bani Yaseen, L. Al-Hyari, O. Almahmoud, and M. Hammad, "Performance of a new solar water heater design with natural circulation," *Energy Sources, Part A: Recovery, Utilization, and Environmental Effects*, pp. 1–16, 2020.
- [5] M. T. Nasir, D. Afaneh, and S. Abdallah, "Design Modifications for a Thermoelectric Distiller with Feedback Control," *Energies (Basel)*, vol. 15, no. 24, p. 9612, 2022.
- [6] A. Kalair, N. Abas, M. S. Saleem, A. R. Kalair, and N. Khan, "Role of energy storage systems in energy transition from fossil fuels to renewables," *Energy Storage*, 2021, doi: 10.1002/est2.135.
- [7] F. Dawood, M. Anda, and G. M. Shafiullah, "Hydrogen production for energy: An overview," *International Journal of Hydrogen Energy*, vol. 45, no. 7. Elsevier Ltd, pp. 3847–3869, Feb. 2020. doi: 10.1016/j.ijhydene.2019.12.059.
- [8] M. İnci and M. S. Aygen, "A modified energy management scheme to support phase balancing in grid interfaced photovoltaic/fuel cell system," *Ain Shams Engineering Journal*, 2021, doi: 10.1016/j.asej.2020.12.018.
- [9] S. G. Nnabuife, J. Ugbeh-Johnson, N. E. Okeke, and C. Ogonnaya, "Present and projected developments in hydrogen production: a technological review," *Carbon Capture Science & Technology*, p. 100042, 2022.
- [10] J. H. Nam and D. H. Jeon, "A comprehensive micro-scale model for transport and reaction in intermediate temperature solid oxide fuel cells," *Electrochim Acta*, vol. 51, no. 17, pp. 3446–3460, 2006, doi: <https://doi.org/10.1016/j.electacta.2005.09.041>.
- [11] A. Ebrahimi, G. D. Najafpour, and D. Y. Kebria, "Effect of batch vs. continuous mode of operation on microbial desalination cell performance treating municipal wastewater," *Iranian Journal of Hydrogen & Fuel Cell*, vol. 4, no. January, pp. 281–290, 2017, doi: 10.22104/IJHFC.2016.473.
- [12] S. Sevda, H. Yuan, Z. He, and I. M. Abu-Reesh, "Microbial desalination cells as a versatile technology: Functions, optimization and prospective," *Desalination*, vol. 371, pp. 9–17, 2015, doi: 10.1016/j.desal.2015.05.021.
- [13] P. Esmaili, I. Dincer, and G. F. Naterer, "Energy and exergy analyses of electrolytic hydrogen production with molybdenum-oxo catalysts," *Int J Hydrogen Energy*, vol. 37, no. 9, pp. 7365–7372, 2012, doi: <https://doi.org/10.1016/j.ijhydene.2012.01.076>.
- [14] L. Van Cappellen, H. Croezen, and F. Rooijers, "Feasibility study into blue hydrogen," Jul. 2018.
- [15] D. J. Jovan and G. Dolanc, "Can green hydrogen production be economically viable under current market conditions," *Energies (Basel)*, 2020, doi: 10.3390/en13246599.
- [16] Y. Khawaja, I. Qiqieh, J. Alzubi, O. Alzubi, A. Allahham, and D. Giaouris, "Design of cost-based sizing and energy management framework for standalone microgrid using reinforcement learning," *Solar Energy*, vol. 251, pp. 249–260, 2023.
- [17] L. F. Al-Hyari and M. Kassai, "Energetic investigation of energy recovery technologies in air handling units," *International Review of Applied Sciences and Engineering*, vol. 9, no. 1, pp. 49–57, 2018.
- [18] L. Fan, Z. Tu, and S. H. Chan, "Recent development of hydrogen and fuel cell technologies: A review," *Energy Reports*, vol. 7, pp. 8421–8446, 2021.

- [19] P. Nikolaidis and A. Poullikkas, "A comparative overview of hydrogen production processes," *Renewable and Sustainable Energy Reviews*. 2017. doi: 10.1016/j.rser.2016.09.044.
- [20] C. Acar and I. Dincer, "Review and evaluation of hydrogen production options for better environment," *J Clean Prod*, 2019, doi: 10.1016/j.jclepro.2019.02.046.
- [21] Z. Wang, R. R. Roberts, G. F. Naterer, and K. S. Gabriel, "Comparison of thermochemical, electrolytic, photoelectrolytic and photochemical solar-to-hydrogen production technologies," in *International Journal of Hydrogen Energy*, 2012. doi: 10.1016/j.ijhydene.2012.03.057.
- [22] M. Younas, S. Shafique, A. Hafeez, F. Javed, and F. Rehman, "An Overview of Hydrogen Production: Current Status, Potential, and Challenges," *Fuel*, vol. 316. Elsevier Ltd, May 2022. doi: 10.1016/j.fuel.2022.123317.
- [23] F. Calise, M. D. D'Accadia, M. Santarelli, A. Lanzini, and D. Ferrero, *Solar Hydrogen Production: Processes, Systems and Technologies*. 2019. doi: 10.1016/C2017-0-02289-9.
- [24] H. Ishaq, I. Dincer, and C. Crawford, "A review on hydrogen production and utilization: Challenges and opportunities," *Int J Hydrogen Energy*, vol. 47, no. 62, pp. 26238–26264, Jul. 2022, doi: 10.1016/j.ijhydene.2021.11.149.
- [25] S. E. Hosseini and M. A. Wahid, "Hydrogen production from renewable and sustainable energy resources: Promising green energy carrier for clean development," *Renewable and Sustainable Energy Reviews*. 2016. doi: 10.1016/j.rser.2015.12.112.
- [26] S. Koumi Ngoh and D. Njomo, "An overview of hydrogen gas production from solar energy," *Renewable and Sustainable Energy Reviews*, vol. 16, no. 9. pp. 6782–6792, Dec. 2012. doi: 10.1016/j.rser.2012.07.027.
- [27] M. Jaradat, O. Alsotary, A. Juaidi, A. Albatayneh, A. Alzoubi, and S. Gorjian, "Potential of Producing Green Hydrogen in Jordan," *Energies (Basel)*, vol. 15, no. 23, Dec. 2022, doi: 10.3390/en15239039.
- [28] K. Alrabie and M. N. Saidan, "A preliminary solar-hydrogen system for Jordan: Impacts assessment and scenarios analysis," *Int J Hydrogen Energy*, 2018, doi: 10.1016/j.ijhydene.2018.03.218.
- [29] M. Hammad, M. S. Y. Ebaid, and L. Al-Hyari, "Green building design solution for a kindergarten in Amman," *Energy Build*, vol. 76, pp. 524–537, 2014.
- [30] F. Almomani and R. R. Bohsale, "Nickel/Cobalt nanoparticles for electrochemical production of hydrogen," *Int J Hydrogen Energy*, 2020.
- [31] M. Chase, *NIST-JANAF Thermochemical Tables, 4th Edition*. American Institute of Physics, - 1, 1998.
- [32] M. Ni, M. K. H. Leung, and D. Y. C. Leung, "An electrochemical model of a solid oxide steam electrolyzer for hydrogen production," *Chem Eng Technol*, vol. 29, no. 5, pp. 636–642, May 2006, doi: 10.1002/ceat.200500378.
- [33] E. Hernández-Pacheco, D. Singh, P. N. Hutton, N. Patel, and M. D. Mann, "A macro-level model for determining the performance characteristics of solid oxide fuel cells," *J Power Sources*, vol. 138, no. 1, pp. 174–186, 2004, doi: <https://doi.org/10.1016/j.jpowsour.2004.06.051>.
- [34] B. Todd and J. B. Young, "Thermodynamic and transport properties of gases for use in solid oxide fuel cell modelling," *J Power Sources*, vol. 110, no. 1, pp. 186–200, 2002, doi: [https://doi.org/10.1016/S0378-7753\(02\)00277-X](https://doi.org/10.1016/S0378-7753(02)00277-X).
- [35] J. H. Nam and D. H. Jeon, "A comprehensive micro-scale model for transport and reaction in intermediate temperature solid oxide fuel cells," *Electrochim Acta*, vol. 51, no. 17, pp. 3446–3460, 2006, doi: <https://doi.org/10.1016/j.electacta.2005.09.041>.



- [36] M. Ni, M. K. H. Leung, and D. Y. C. Leung, "Energy and exergy analysis of hydrogen production by solid oxide steam electrolyzer plant," *Int J Hydrogen Energy*, vol. 32, no. 18, pp. 4648–4660, 2007, doi: <https://doi.org/10.1016/j.ijhydene.2007.08.005>.
- [37] M. Alkasrawi, E. Abdelsalam, H. Alnawafah, F. Almomani, M. Tawalbeh, and A. Mousa, "Integration of Solar Chimney Power Plant with Photovoltaic for Co-Cooling, Power Production, and Water Desalination," *Processes*, vol. 9, no. 12, p. 2155, 2021, doi: 10.3390/pr9122155.
- [38] E. Abdelsalam *et al.*, "An innovative design of a solar double-chimney power plant for electricity generation," *Energies (Basel)*, vol. 14, no. 19, 2021, doi: 10.3390/en14196235.
- [39] E. Abdelsalam *et al.*, "Performance analysis of hybrid solar chimney–power plant for power production and seawater desalination: A sustainable approach," *Int J Energy Res*, vol. 45, no. 12, pp. 17327–17341, Oct. 2021, doi: 10.1002/ER.6004.
- [40] E. Abdelsalam, F. Kafiah, M. Alkasrawi, I. Al-Hinti, and A. Azzam, "Economic Study of Solar Chimney Power-Water Distillation Plant (SCPWDP)," *Energies (Basel)*, vol. 13, no. 11, p. 2789, 2020.

ICH2P14-IT3

ANALYZING GREY AND BLUE HYDROGEN PRODUCTION COSTS IN STEAM-METHANE, AUTO-THERMAL, AND NON-CATALYTIC PARTIAL OXIDATION REFORMING PLANTS

Mary Katebah, Ma'moun Al-Rawashdeh, Patrick Linke

Department of Chemical Engineering, Texas A&M University at Qatar, Education City, Doha, Qatar

*Corresponding author e-mail: Patrick.linke@qatar.tamu.edu

ABSTRACT

Global hydrogen demand is seeing significant growth. Most of the hydrogen production is by natural gas (NG) reforming. The main production routes are steam-methane reforming (SMR), auto-thermal reforming (ATR), and partial oxidation (POX). Hydrogen plants are associated with substantial amounts of emissions, and reducing their carbon intensity is essential in the clean energy transition. Blue hydrogen production, where CO₂ emissions are captured and stored (CCS), is currently the most promising solution for carbon reduction. While the SMR route is widely studied, limited techno-economic analyses exist for ATR and POX. This study presents a comparative assessment on the three main routes. Given the substantial amount of excess heat, emissions reduction is investigated by two pathways: i) integration with an electrolyzer to produce more H₂, and ii) coupling with CCS where energy systems are designed to integrate heat and power across the hydrogen/CCS plants. Results show that integration with CCS is more economically and environmentally advantageous. SMR outperformed ATR and POX for both grey and blue hydrogen production. Outside the boundaries of the plants, life-cycle emissions are quantified and compared with electrolysis. Emissions from blue hydrogen production can compete with electrolysis for current electricity mixes, with green hydrogen costs being around 4-6 times higher than blue hydrogen.

Keywords: Hydrogen, Techno-economic analysis, CCS, heat integration.

INTRODUCTION

Global hydrogen demand has grown more than three-fold in the past five decades [1], and its consumption is projected to increase over six-fold by 2050 [2]. There are three main hydrogen production pathways: grey/black hydrogen generated from fossil fuels, where the CO₂ associated with the process is released to the atmosphere, blue hydrogen also from fossil fuels, but the produced CO₂ is stored/ utilized, and green hydrogen from renewable sources by electrolysis [3]. Almost 96% of the current hydrogen production is source from fossil fuels [4], with natural gas (NG) reforming being the primary source of hydrogen production [1]. Although hydrogen is a clean energy carrier, hydrogen production releases substantial amounts of CO₂ emissions. Producing low carbon hydrogen is key to sustainable future energy systems. Methods that are currently being explored for low-carbon hydrogen production are green and blue hydrogen. However, as long as fossil fuels dominate the global economy, the most promising short-term solution for CO₂ mitigation is blue hydrogen production from fossil fuels with CCUS [5]. There are three main NG reforming routes for hydrogen production: steam-methane reforming (SMR), auto-thermal reforming (ATR), and partial oxidation (POX) [5]. Although SMR is widely studied in the literature, there are little studies on ATR and POX. Moreover, there are no detailed analysis on heat and power integration of hydrogen plants with CCS. This study aims to address these gaps by conducting a comparative techno-economic assessment of hydrogen production by the three prominent routes. Given the large amounts of excess heat in the processes, two pathways are considered to reduce emissions. In the first pathway, additional hydrogen is produced using excess heat to enhance hydrogen production in an electrolyzer, whereas, in the second pathway, the excess heat is used to drive the CO₂ capture and compression processes. To obtain a comprehensive comparison, cost and emissions are compared with electrolysis technology based on a life-cycle assessment.

HYDROGEN PRODUCTION

Figure 1 illustrates the hydrogen production routes by NG reforming. In SMR, steam reacts with NG by an endothermic reaction to produce syngas at a H₂:CO ratio of 3:1. POX, on the other hand, is an exothermic reaction where NG reacts with oxygen producing syngas at a H₂:CO ratio of 2:1. ATR is essentially a combination of the two, where the exothermic POX generates the heat required in the endothermic SMR reaction.

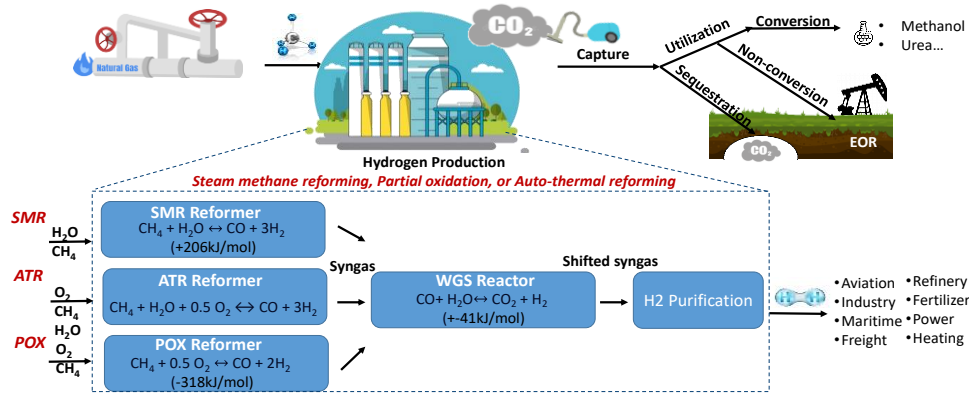


Figure 1: hydrogen production routes by NG reforming

Grey Hydrogen Production

For a proper comparison, the processes for the three main routes are designed to be standalone large-scale hydrogen plants with a 500 TPD production capacity. Optimum operating conditions presented in the literature are considered for the units, and a summary of the assumptions used in this analysis are listed in Table 1.

Table 1: Main design assumptions

	SMR	ATR	POX
NG Feed	50 bar, 50°C, 85% C1, 7% C2, 3% C3, 2% CO ₂ , 3% C4+		
Pre-reformer	500C, 25 bar, S/C: 2.7	500C, 25 bar, S/C:0.3	No pre-reformer
Reformer	700C, 24 bar, S/C: 3	700C, 24 bar, O/C: 0.5, S/C: 1.5	1,187C, 24 bar, O/C: 0.7
HT WGS	320°C, 6 bar		
LT WGS	190°C, 5.5 bar		
H ₂ Purification (PSA)	Pressure swing adsorption: 22 bar, 90% recovery, 99.99% H ₂ Purity		
Air separation Unit	No ASU	Power demand: 0.35 kWh/Nm ³ O ₂	
Hydrogen Product	500 TPD, 25°C, 20 bar (99.9% purity)		

All three processes are simulated in Aspen Plus to obtain the main results summarized in Table 2. Heat integration Pinch Analysis is performed to maximize heat recovery within the system, and a heat exchanger network is developed for all the processes. Excess heat is used to generate high-pressure steam at 90 bar for maximizing power generation in condensing turbines. For all three plants, the total process power demand was met using the power generated from the respective process, resulting in self-sufficient processes in terms of heating and power requirements. A techno-economic analysis is conducted following the approach presented in Katebah et al. [5] to obtain hydrogen prices of \$0.96, \$1.17, and \$1.19/kg H₂ for SMR, ATR, and POX, respectively, at a NG price of \$3.7/GJ.

Table 2: Main results for grey hydrogen production by SMR, ATR and POX

		SMR	ATR	POX
H ₂ Produced	Kg H ₂ /hr (TPD)	20,830 (500 TPD)		
NG Consumption	kg CH ₄ / kg H ₂	3.16	3.21	3.34
Excess heat after HI	kWh/ kg H ₂	2.9	1.3	1.7
Oxygen demand	kg O ₂ / kg H ₂	-	3.2	3.4
Specific CO ₂ Emissions	kg CO ₂ / kg H ₂	8.4	8.7	9
CAPEX	\$/ kg H ₂	0.15	0.34	0.33
OPEX	\$/ kg H ₂	0.81	0.83	0.86
Hydrogen Production Cost	\$/ kg H ₂	0.96	1.17	1.19

Results show that for a fixed production capacity, SMR has lowest emissions and cost due to the lower fuel demands and CAPEX as it has no air separation unit and less compression demands. It is also noteworthy to indicate that despite SMR being an endothermic reaction, it is associated with the largest amounts of excess heat, also as a result of the lower power requirements.

Blue Hydrogen Production

In the first pathway, the hydrogen plants are integrated with an electrolyzer as a means of reducing specific CO₂ emissions by producing additional hydrogen. A hydrogen production price of \$0.99/kg H₂ is calculated based on the study by Katebah et al. [5], thereby reducing the emissions from 8.4 to 8.3 kg CO₂/kg H₂. The limited hydrogen production and specific emissions are due to high electricity demands in the electrolyzer [5]. Since SMR is associated with the highest amounts of excess heat, emissions reduction in ATR and POX will be even lower. Therefore, this pathway will not be considered for subsequent analysis.

In the second pathway, the plants are integrated with CCS units. CCS is a highly energy-intensive process entailing several units: CO₂ capture and separation, followed by CO₂ compression and subsequent transportation and injection, or utilization. In all three cases, the plants are integrated with two carbon capture units: a pre-combustion unit before the PSA, and post-combustion units to maximize CO₂ removal. The capture plants are assumed to be amine-based (MDEA-Pz), with energy demands of 550 and 1,080 kWh/ tonne CO₂, respectively [5]. The pre-combustion unit is integrated before the PSA since its feed is associated with a higher CO₂ partial pressure, and upstream removal reduces the PSA capacity, which translates into a lower CAPEX. Energy systems are designed to meet the power and heat demands for the three processes such that excess heat utilization is maximized in the CCS, after which supplementary NG is employed for maximum CO₂ capture. Excess heat utilization can reduce the emissions by 40%, 20%, and 45%, in the SMR, ATR, and POX plants, respectively. Including the additional CAPEX requirements by the CCS, and supplementary fuel demands, hydrogen price increased to \$1.31, 1.52, and 1.5/kg H₂ respectively, for the SMR, ATR and POX processes. These results show that SMR outperforms ATR and POX for blue H₂ production.

To obtain a more holistic comparison, life-cycle emissions are included to those produced within the boundary of the plant based on the global warming potential (GWP). Emissions considered include upstream emissions, transportation, plant commissioning/decommissioning, and operation. Based on the assumptions presented in Katebah et al. [5], total emissions range from 2 to 7.6 kg CO_{2e}/kg H₂, 1.6-7.1 kg CO_{2e}/kg H₂, and 1.4-7 kg CO_{2e}/kg H₂ for SMR, ATR, and POX, respectively. Upstream emissions have the largest contribution to the overall emissions, dominated by the methane leak rate, which could be alleviated by proper control.

When compared to the state-of-the-art electrolysis, and assuming an alkaline electrolyzer with an electricity requirement of 50 kWh/kg H₂, electrolysis life-cycle emissions range from 8.5 to 41.1 kg CO_{2e}/kg H₂ for current electricity mixes [5]. The results are substantially higher than those associated with blue H₂ production by all three routes. Assuming an electricity price ranging from \$0.08-0.14/kWh, H₂ production costs by electrolysis range from around \$4-8/kg H₂, resulting in prices that are around 4-6 times higher than blue hydrogen production.

CONCLUSIONS

In this study, a comparative techno-economic assessment is conducted on the three production routes for grey and blue hydrogen. Two pathways are investigated for reducing the CO₂ emissions from hydrogen plants. The first pathway considers integrating the plants with an electrolyzer to reduce the specific emissions. In the second pathway, hydrogen plants are integrated with carbon capture and compression units. Results show that integration with CCS is more economically and environmentally advantageous. For both grey and blue hydrogen production, the analysis showed that SMR outperformed ATR and POX. Extending the analysis to include life-cycle emissions showed that methane leakage is the largest contributor to the overall emissions, necessitating further research to properly quantify upstream emissions. Compared to electrolysis, emissions for blue hydrogen for all the routes are lower as a result of current electricity mixes, and are achievable at significantly lower costs.

ACKNOWLEDGMENTS

This work was made possible by funding from the Qatar National Research Fund (QNRF) project number NPRP12S-0304-190222 and co-funding support from Shell Global Solutions International B.V. and Qatar Shell Research and Technology Center. The statements made herein are solely the responsibility of the author(s).

REFERENCES

1. IEA. 2019. The Future of Hydrogen.
2. Hydrogen Council. 2017. Hydrogen scaling up: A sustainable pathway for the global energy transition.
3. Y. Khojasteh Salkuyeh, B. A. Saville, and H. L. MacLean. 2017. Techno-economic analysis and life cycle assessment of hydrogen production from natural gas using current and emerging technologies. *International Journal of Hydrogen Energy*. 42: 18894–18909.
4. A. Al-Qahtani, B. Parkinson, K. Hellgardt, N. Shah, and G. Guillen-Gosalbez, 2021. Uncovering the true cost of hydrogen production routes using life cycle monetisation. *Applied Energy*. 281: 115958.
5. M. Katebah, M. Al-Rawashdeh, and P. Linke. 2022. Analysis of hydrogen production costs in Steam-Methane Reforming considering integration with electrolysis and CO₂ capture. *Cleaner Engineering Technology*. 10: 100552.

14th INTERNATIONAL CONFERENCE ON HYDROGEN PRODUCTION (ICH2P-2023)



December 19 – 21, 2023
Education City, Doha, Qatar

ORAL PRESENTATIONS



ICH2P14-OP004

MONTE CARLO SIMULATION APPLICATIONS FOR STAKEHOLDER MANAGEMENT ON HYDROGEN PRODUCTION PROJECTS: TOWARD SUSTAINABLE DEVELOPMENT

**Ayman Mashali*

**(Qatar General Electricity & Water Corporation “KAHRAMAA”), Zone 61, ST 875, Building 35, Doha, Qatar
Corresponding author e-mail: ayman.mashali@yahoo.com

ABSTRACT

This paper seeks to explore, investigate, and assess an innovative approach by implementing Monte Carlo Simulation applications for stakeholder management practices (MC-SMP) in Hydrogen Production projects (H2PPs) toward achieving sustainable development. The methodology/approach included a literature review, Stakeholder identification, Identification of stakeholder attributes and their importance level, and Validation and verification based on Monte-Carlo simulation analysis, “1000 iterations were run” to provide reliable results with affordable computational cost, and A 90% confidence interval was defined. The findings showed that the (MC-SMP) allowed the determination of the degree of uncertainty in achieving the stakeholder performance indicators. The developed approach is more appropriate for dealing with Stakeholder Management in (H2PP), giving the project manager a clear vision and a statistical indicator and predictor of stakeholder performance. The Practical implications lie in that it is the first research to study the synergy of “Monte Carlo simulation application and stakeholder management practice” (MC-SMP) that supports a theory with real-world data. It makes this research a starting point for other researchers. The Originality and value of this study lie in that it has produced valuable insights into a novel approach to synergy between (MC-SMP) that can reinforce SM practices in (H2PPs).

Keywords: Monte Carlo, stakeholder, management, hydrogen.

1. Introduction

The constant increase in global energy demand has led to an intensification of fossil fuel utilization that, today, still accounts for more than 80% of the overall primary energy consumption worldwide [1]. Such impediments necessitate a global shift from traditional energy sources to renewables. The global transition from traditional to renewable energy resources is a requirement for the global transition from fossil fuels to renewable energy resources [2]. In recent years, (H2PPs) and scale have shown a gradual upward trend, Where interest in hydrogen technologies to provide clean energy for the future has steadily grown. Besides, Hydrogen is experiencing unprecedented global hype. Moreover, Hydrogen can replace fossil fuels in the long term. Furthermore, Hydrogen production from renewable energies is a key part of the transition to realize a sustainable energy economy for developed and developing nations [3]. In this context, this study proposes an innovation that integrates (MC-SM) to address SM problems with substantial stability and reliability. Thus, employing an appropriate method to achieve reliable SM is challenging for decision-makers in the (H2PPs) process owing to its inherent complexity, sensitivity, and uncertainty. The use of (MC-SM) in (H2PPs) is a novel technique that can enhance the feasibility of projects. Project success hinges on how well the link between the project and its stakeholder environment is managed. Additionally, understanding how stakeholders affect a project helps managers modify and customize their SM techniques to fit various project scenarios. Furthermore, comprehending the various effects of stakeholders is crucial for managers as it aids in risk assessments and reaction planning [4].

2. Literature review

A significant portion of this rising energy demand is accounted for using fossil fuels, which also pose challenges due to the depletion of resources and growth in greenhouse gas emissions [5]. These factors contribute to rising energy demand from significant population growth and economic development. Within CO₂ emissions reduction, substituting fossil fuels with sustainably produced bioenergy can play an important role [6]. Several options for anthropogenic CO₂ emissions reduction are being investigated, and hydrogen can replace fossil fuels in the long term [7]. Hydrogen is experiencing unprecedented global hype and is regarded as the urgently needed building block for the much-needed carbon-neutral energy transition to mitigate the effects of global warming [8], Where Global Hydrogen Production to over 85 million tons [9]. Moreover, hydrogen reinforces the contribution

of renewables towards mitigating climate change. [10]. Effective SM has been deemed necessary for the successful execution of (H2PPs).

The term “stakeholder” was originally defined as: “Those groups without whose support the organization would cease to exist.”. Stakeholder theory was developed primarily to help managers understand their stakeholders and strategically manage them [11]. Previous research on stakeholders has offered a range of stakeholder definitions and conceptualizations, from expansive to restrictive perspectives[12]. The definition of a stakeholder offered by [11] is the most widely accepted and comprehensive. “Any group or individual who can affect or be affected by the achievement of the organization’s objectives” is considered a stakeholder.

Stakeholder management SM is thus understood as an essential tool, decision-making support of the management team making attainable the project objectives. Poor SM may lead to negative effects with significant impact, some even irretrievable, and disruption to project delivery [13,14]. A fresh approach incorporating a global long-term perspective based on the latest trends will be necessary to enable a more efficacious project management of stakeholder interactions [15]. The Monte Carlo approach is a multi-iterative statistical technique [16]. The invention of this method has been credited to Stanislaw Ulam, a mathematician working on the US’ Manhattan Project during World War II [17].

Although Monte Carlo simulation is documented as a valuable method for project management applications, it has not been mainly utilized by project managers in real-world concerns unless the organization’s project management processes need it, such as in cost and time management [18]. Application of Monte Carlo Simulation in SM problems is planned to serve as a decision support tool to assess project accomplishment.

Using (MC-SM) for (H2PPs) is a novel approach that can improve the feasibility of projects. Even though the Monte Carlo method is widely applicable, a guide is still needed to facilitate the straightforward incorporation of this method into SM procedures in businesses [19]. Using the Monte Carlo method through the software environment allows companies to implement simulations that Businesses will gain a realistic understanding of how their project and investments will develop. As far as the researcher knows, studies have yet to examine the implementation of the Monte Carlo Simulation in SM practices as undertaken in this study.

Gap in the Body of Knowledge

It is noteworthy that despite the increasing benefits and utility of Monte Carlo simulation in terms of schedule and cost, no current information is available about its application to stakeholder management. Literature in the publication, however, clarifies that there is still a knowledge gap between applying Monte Carlo simulation as a valuable tool for stakeholder management and the principal driver of project management, which is stakeholder management. This emphasizes the necessity of finding a practical solution once more.

3. Research methodology/approach

This study uses the Monte Carlo method to adopt a novel SM approach in (H2PPs). This consideration is depended on @RISK software has been used to carry out the simulation. The approach included: a) literature review; b) Stakeholder identification; c- Stakeholder register preparation within Primavera risk analysis software; d) Identification of stakeholder attributes and their importance level; e- Build the stakeholder impacts plan; f) Define the simulation model; g) Running primavera risk analysis; h) Simulate multiple iterations, “1000 iterations were run” to provide reliable results with affordable computational cost, and A 90% confidence interval was defined [20] (Sensitivity Analysis, and Modeling & Simulation).

4. Discussion

The challenges in (H2PPs) are not just technical but also possibly in managing varying stakeholders. The large number of stakeholders in the life cycle of (H2PPs) makes SM control difficult. Our target is how the quantitative stakeholder engagement assessment process is performing and what are the benefits of applying this process for the project’s success, where quantitative stakeholder engagement assessment is a numerical way to demonstrate the impact of stakeholder engagement on the project objectives and how these calculations provide a clear photo of the project stakeholder status. It also guides the project team to know where they have to focus on.

The author quoted and adapted the standard risk matrix and applied it to stakeholders. Five zones are present in the Probability Impact Matrix: Red (dark), Red (light), Yellow, Green (dark) and Green (light).

The matrix is 5 x 5 with the impact ranging from very low to very high on the horizontal axis and probability (with the same range) on the vertical axis. Figures 1&2 shows the standard stakeholder matrix, which is used to determine the stakeholder zone for each identified stakeholder.

Probability and Impact Stakeholder Matrix

- To assign a combined probability-impact rating to each stakeholder identified for a project.
- stakeholders are prioritized according to how they affect a project's objectives.
- created during the Plan Risk Management process.
- A probability and impact matrix that uses an **ordinal** scale identifies stakeholder priority based on **descriptions** of combined impact and probability, such as medium/low or high/medium.
- A **cardinal** probability and impact matrix identifies stakeholder priority based on a **numeric** score.

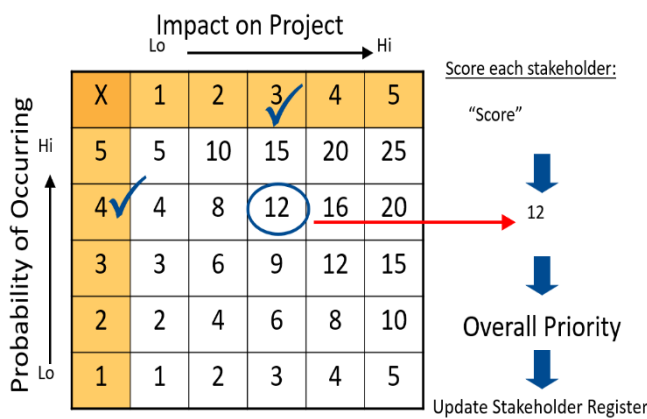


Figure 1: Probability Impact Matrix

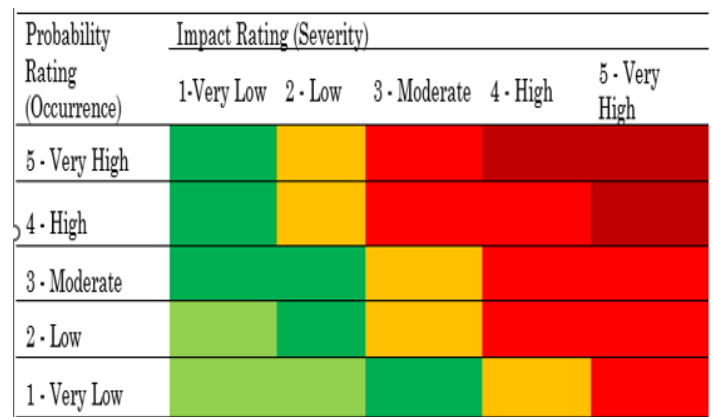


Figure 2: Level of Risk based on Probability Impact Matrix

Figure 3 illustrates the project stakeholder matrix; it provides a simple way to show stakeholder importance as follows:

- Four stakeholders (Kahramaa, Ashghal, Ministry of Interior, and Doha Port) were in the dark red zone because of their high critical impact, which is a top priority, and close attention should be paid to them. Therefore, the project management team must focus on and develop strategies to avoid the risks of this group.
- Three stakeholders (MMUP, Ministry of Transport and Communication, and neighbouring residents) were in the yellow zone because of their moderate importance and impact, which must be controlled.
- Two stakeholders (Mowasalat and Qatar Rail) were in the green zone because of their low impact, which can be monitored, controlled, or ignored.

Consequently, Risk management should thoroughly examine every facet of project management to provide an action plan or a stakeholder's risk mitigation plan for every controllable stakeholder event. Accordingly, best practices, organizational expertise, industry benchmarks, lessons gained, and experience are used to construct stakeholder risk mitigation plans. The stakeholder engagement scoring preparation process within Primavera risk analysis software illustrated in Figure 4.

Stakeholder's Sensitivity Analysis

The Monte Carlo simulation technique was selected for sensitivity analysis and simulations. Tornado diagrams can convey their results to decision-makers succinctly and clearly, which is the fundamental pillar for effective SM decisions with the project's goal. This diagram consists of several horizontal bars. (variation amplitude). Thus, the stakeholder bar with the most significant project impact will be the largest one. Fig. 5 presents the Monte Carlo simulation results in terms of a normal distribution. The maximum stakeholder sensitivity analysis results show that the most effective stakeholders (Kahramaa, Ashghal, Ministry of Interior and Doha Port) significantly affect the project. The analysis results identify the high stakeholders influence assumptions and provide a variation reference for the decision-makers

to define contingency allowance in the projects. So, Sensitivity analysis is essential to bridge the gap between decision-makers (who often do not directly work or develop the model) and analysts (who work directly on the model). The Tornado diagram show the prioritization of the project stakeholder risks before the mitigation actions applied as illustrated in Figure 5.

Risk			Pre-Mitigation (Data Date = 10/12/2022)					Post-mitigation					
ID	T/O	Title	Probability	Schedule	Cost	Performance	Score	Response	Probability	Schedule	Cost	Performance	Score
R01	T	KAHRAMAA	VH	VH	VH	VH	25	Reduce	M	M	M	M	9
R02	T	Ashghal	H	H	H	VH	20	Reduce	H	L	L	L	8
R03	T	MMUP	M	M	M	M	9	Reduce	L	L	L	L	4
R04	T	Ministry of Interior	VH	VH	VH	VH	25	Reduce	M	M	M	M	9
R05	T	Doha Port	VH	VH	VH	VH	25	Reduce	M	M	M	M	9
R06	T	Ministry of Transport and Communications	M	M	M	M	9	Reduce	L	L	L	L	4
R07	T	Mowasalat	VL	VL	VL	VL	1	Reduce	N	N	N	N	0
R08	T	Qatar Rail	L	L	L	L	4	Reduce	VL	VL	VL	VL	1
R09	T	Local Residents	M	L	L	L	6	Reduce	L	VL	VL	VL	2

Figure 3: Stakeholder Engagement Register preparation process within Primavera risk analysis software.

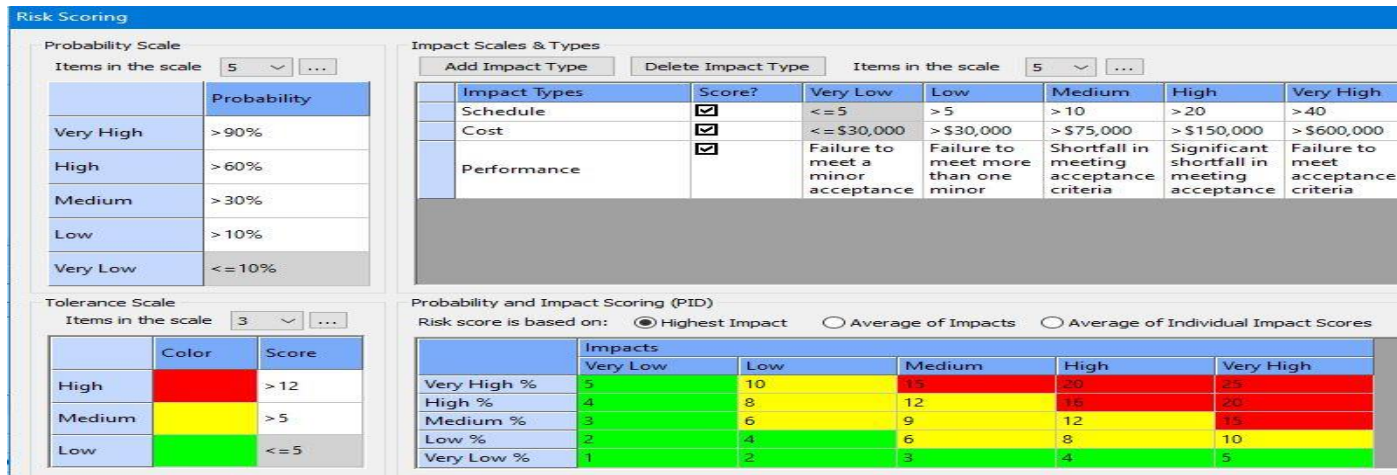


Figure 4: Stakeholder Engagement Scoring

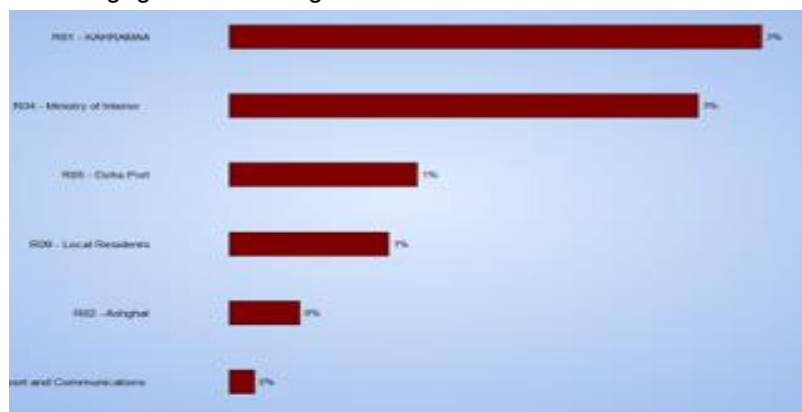


Figure 5: Tornado diagram (Pre-Mitigation)

The study's conclusions highlight how this study supports and guides managers in managing their interactions with stakeholders by offering new, insights into the project stakeholders and managerial responses to these effects. Besides, it is imperative that managers continually assess and manage stakeholders throughout a project because, depending on shifts in authority, urgency, and power, or because new stakeholder clusters may emerge, stakeholders' potential to influence the project may

alter. Additionally, managers need to be prepared to strike a balance between foreseeing stakeholder risks and building the ability to handle emergent and unanticipated stakeholder-related events in relation to novel SM techniques. However, to effectively use the different stakeholder analysis techniques, project managers need more hands-on training.

5. Innovation, Value, and Contribution to Knowledge and Practice

Practical implications – This is the first research to study the synergy of "Monte Carlo simulation application and SM practice" (MC-SM) that supports a theory with real-world data. It makes this research a starting point for other researchers and will provide profound contributions to theory and research besides industry practice.

Contributions to research on stakeholder

The study of the expected character of project stakeholders' effective engagement is a field of stakeholder research's shortcomings. Besides, the classification and characterization of various stakeholder influences quantitatively have yet to be previously presented in stakeholder research by implementing Monte Carlo Simulation applications, and it is, therefore, one of the contributions of this study. This paper provides a unique idea and a productive foundation for more reflections about (MC-SM) synergy. This subject has yet to get significant academic attention. Which further advances the field of stakeholder research. Additionally, In terms of research on (H2PPs), this study offers insightful information about a preliminary understanding of the nature of the Monte Carlo simulation-based stakeholder effects in the project. Moreover, it can be declared that the author has provided a new formulation of the definition of stakeholder engagement that reads as follows: Stakeholder engagement is a specific event that can have a positive or negative impact on a project.

6. Limitations of the research

The limitations related to this research are briefly outlined: The research was carried out in the State of Qatar in a specific cultural context. Due to the dynamic nature of stakeholder management, the identified list of top significant stakeholders and their attributes may vary with changes in the country or project-specific conditions thus should be subject to continuous updates. However, the study is still reasonable and, fortunately, suitable to evaluate SM in H2PPs.

7. Conclusion

This paper has reported on applying the Monte Carlo simulation method to study the SM practice within the (H2PPs). Using (MC-SM) for (H2PPs) is a novel approach that can improve the feasibility of projects. Monte Carlo Simulation is a numerical way to demonstrate the impact of the project stakeholders on the project objectives and how these calculations provide a clear photo of the project status and also guide the project team to know where they have to focus. However, Like other tools, simulations need to be used with care since the simulation's validity depends on the data's reliability, the variables' appropriateness, and applicability. The outcomes of this research are meaningful and expected to help government departments and other stakeholders involved in (H2PPs) decision-making and direct other research endeavours in that field. Moreover, it enables practitioners to identify critical stakeholders and the attributes affecting their criticality, thus facilitating effective response planning and control. Thus, this improves the decision-making process's stability, reliability, and applicability and enriches the existing system. Utilizing a tornado diagram, the sensitivity analysis produced the following:

- The most influential stakeholders are (Kahramaa, Ashghal, Qatar Rail, MOI, and Local Resident), in the dark red zone. They represent the top factors, which gives exceptional importance to the stakeholder that belong to these categories and requires attention and concentration of management on them significantly and try to avoid or transfer as well as share with other stakeholders or reduce the impact as much as possible. that can be controlled and reduced by improving the skills of the construction project team.
- The moderate influential stakeholders are (MMUP, Ministry of Transport and Communication, and neighbouring residents) located in the yellow zone.
- The low significant stakeholders are (Mowasalat and Qatar Rail) in the green zone.

It is noteworthy that the Benefits of Monte Carlo Simulation applications for SM on (H2PPs) include: a) Proactive approach; b) More and better information about stakeholders is available during planning and decision-making and its impact on the project objectives; c) Give a clear vision about the most critical stakeholder in the project with 80% confidence; d) Minimize the effects of adverse stakeholders (Risks);

e) Maximize the effect of positive stakeholders (opportunity); and f) Mitigate the project delay and cost overrun. The verbiage added by this paper indicates that further efforts are required to understand what end-users require while disseminating the message of the value of Monte Carlo Simulation applications for SM on (H2PPs) that may become in high demand in current and future times. This paper's conclusions can generate an innovative impetus to achieve (MC-SM) synergy on (H2PPs) to achieve holistic sustainability. Besides, the results show that (MC-SM) is an enabling applicable mechanism for SM in (H2PPs).

In addition to what was mentioned, The necessity for stakeholders' sensitive project managers as opposed to those who concentrate on technical matters and the significance of understanding the role of stakeholders in the project. Often, there is no formal mechanism for managing stakeholders; instead, the project risk analysis process includes a cursory examination of stakeholders. Project managers should get ongoing training and education regarding managing stakeholder influences from the project's environment and internal and technical project issues.

8. Recommendations

The following recommendations are described:

- Further studies should be investigated based on case studies in different countries for reinforcing the adoption and application of Monte Carlo simulation and SM practices in H2PPs to validate and further improve this developed approach.
- Therefore, this research recommends that construction key stakeholders adopt dynamic and positive attitudes to (MC-SM). Moreover, they are advised to adopt efficient proactive (MC-SM) approaches in their projects to ensure project success.
- Raise awareness among key stakeholders in the H2P industry around the advantages of (MC-SM) synergy to minimize the industry's opposition and resistance to change.

REFERENCES

- [1] International Energy Agency, 2015.
- [2] Ishaq, H., Dincer, I., & Crawford, C. (2022). A review on hydrogen production and utilization: Challenges and opportunities. *International Journal of Hydrogen Energy*, 47(62), 26238-26264.
- [3] Rahmouni, S., Negrou, B., Settou, N., Dominguez, J., & Gouareh, A. (2017). Prospects of hydrogen production potential from renewable resources in Algeria. *International Journal of Hydrogen Energy*, 42(2), 1383-1395.
- [4] Mashali A., Elbeltagi E., Motawa I., Elshikh M. Stakeholder Management: An Insightful Overview of Issues, 2020b. International Conference on Civil Infrastructure and Construction (CIC 2020), Doha, Qatar, 2-5 February 2020.
- [5] IEA, International Energy Agency. (2019). The future of hydrogen: seizing today's opportunities. <https://iea.blob.core.windows.net/assets/9e3a3493-b9a6-4b7d-b499-7ca48e357561/>
- [6] Carlsen, L., & Bruggemann, R. (2022). The 17 United Nations' sustainable development goals: A status by 2020. *International Journal of Sustainable Development & World Ecology*, 29(3), 219-229.
- [7] Nnabuife, S. G., Ugbeh-Johnson, J., Okeke, N. E., & Ogbonnaya, C. (2022). Present and projected developments in hydrogen production: A technological review*. *Carbon Capture Science & Technology*, 3, 100042.
- [8] Kopteva, A.; Kalimullin, L.; Tcvetkov, P.; Soares, A. Prospects and Obstacles for Green Hydrogen Production in Russia. *Energies* 2021, 14, 718. <https://doi.org/10.3390/en14030718>
- [9] Dawood F., Anda M., Shafiullah G.M. Hydrogen production for energy: An overview. *International Journal of Hydrogen Energy*. 2020. Vol. 45. N 7, p. 3847-3869. DOI: 10.1016/j.ijhydene.2019.12.059
- [10] V.M. Maestre, A. Ortiz, I. Orti, Challenges and prospects of renewable hydrogen-based strategies for full decarbonization of stationary power applications, *Renew. Sustain. Energy Rev.* 152 (2021), 111628, <https://doi.org/10.1016/j.rser.2021.111628> z.
- [11] Freeman, R.E., 1984. *Strategic Management: A Stakeholder Approach*, (Cambridge University Press: Cambridge, UK.).
- [12] PMI, 2017. A guide to the project management body of knowledge (PMBOK® guide), Sixth Edition, PMBOK® Guide, Project Management Institute, Newtown Square, Pennsylvania.

- [13] Mashali, A., Elbeltagi, E., Motawa, I., & Elshikh, M. (2023). Stakeholder management challenges in mega construction projects: critical success factors. *Journal of Engineering, Design and Technology*, 21(2), 358-375.
- [14] Mok, K. Y., Shen, G. Q., Yang, R. J., Li, C. Z. (2017). "Investigating key challenges in major public engineering projects by a network-theory based analysis of stakeholder concerns: A case study." *International Journal of Project Management*, 35(1), 78-94, <https://doi.org/10.1016/j.ijproman.2016.10.017>.
- [15] Edelenbos J. Managing stakeholder involvement in decision making: a comparative analysis of six interactive processes in the Netherlands. *J Public Adm Res Theory* 2005; 16:417–46.
- [16] Kwak, Y. H., & Ingall, L. (2007). Exploring Monte Carlo simulation applications for project management. *Risk management*, 9, 44-57.
- [17] Eckhardt, R. (1987). Stan Ulam, John von Neumann, and the Monte Carlo Method. *Los Alamos Science. Special Issue (15)*, pp. 131–137.
- [18] Qazi, A., & Simsekler, M. C. E. (2021). Risk assessment of construction projects using Monte Carlo simulation. *International journal of managing projects in business*, 14(5), 1202-1218
- [19] Binder, K. (2005). Monte-Carlo methods. *Mathematical tools for physicists*, 249-280.
- [20] Diaz, C. F., & Hadipriono, F. C. (1993). Nondeterministic networking methods. *Journal of construction engineering and management*, 119(1), 40-57.

ICH2P14-OP007

CARBON EMISSION REDUCTIONS IN THE UNIVERSITY OF SAO PAULO'S TRANSPORTATION SECTOR USING HYDROGEN-POWERED VEHICLES

^{1,2*}Beethoven Narváez-Romo, ²Danilo Perecin, ¹Thiago Lopes, ³Daniel Lopes, ¹Karen Mascarenhas, ^{1,2}Suani Coelho, ¹Julio R. Meneghini

¹University of Sao Paulo, Research Centre for Greenhouse Gas Innovation – RCGI, Av. Professor Mello Moraes, 2231, Sao Paulo-SP, Brazil

²University of Sao Paulo, Bioenergy Research Group – GBio, Av. Professor Luciano Gualberto, 1289, Sao Paulo-SP, Brazil

³Hytron - Energia e Gases | NEA GROUP Company, Rua Eritrina, 181 Condomínio Industrial Veccon Zeta - Jardim Dulce, Sumaré-SP, Brazil

*Corresponding author e-mail: betonarmo@usp.br

ABSTRACT

The energy-intensive transportation sector faces significant challenges in achieving decarbonization goals. According to the System Gas Emissions Estimation platform, the subset of this sector, specifically buses powered by internal combustion engines utilizing diesel fuel in Brazil, accounted for emissions equivalent to 19.76 million tonnes CO_{2-eq}. These are significant emissions for the country, considering that light vehicles are mostly powered by ethanol and ethanol gasoline blend. Therefore, this study aims to estimate and compare achievable emission reductions by implementing renewable hydrogen vehicles in the transport sector at the University of São Paulo. The methodological approach considers low-carbon hydrogen production using the ethanol steam reforming route, wherein energy and mass balances are carried out throughout the hydrogen chain. A baseline scenario for 2023 CO_{2-eq} emissions considers transportation specifics; frequencies, distances, routines, and embedded technologies with their consumption coefficients. A comparative assessment between renewable hydrogen technologies and the established baseline scenario is performed. Results displayed that replacing the current fleet of conventional internal combustion engine buses with hydrogen-based options leads to a significant annual reduction of 2658 tonnes CO_{2-eq}, approximately an 83% reduction as compared to the internal combustion-based operation. Furthermore, the total energy conversion efficiency, Well-to-Wheel, achieved 26.9 % and 11.8% for hydrogen and conventional vehicles, respectively, without air-conditioning system. Notably, CO_{2-eq} emissions surged by at least 16% due to the presence of air-conditioning system for conventional vehicles. This can be a significant contribution to reducing the country's GHG emissions and to achieve its NDC.

Keywords: Low-Carbon Hydrogen, Ethanol Steam Reforming, Fuel Cell, Transport, Well-to-Wheel.

INTRODUCTION

Nowadays, low-carbon intensity solutions for energy transition in the transportation sector worldwide are in progress to alleviate the growing energy crisis, such as battery electric vehicles (BEVs) and hydrogen-based (H₂) technologies, just to mention a few. The solution involving BEVs, besides necessitating a renewable electricity source, might require complex energy planning to mitigate direct impacts on the power grid [1,2,3,4] and sustainable actions for battery disposal and mining. For instance, there are temporal mismatches between renewable energy generation and electrical consumption [5]. On the other hand, the H₂ route also presents challenges, such as sourcing renewable energy for its production [6,7], for instance, the demand for electric power in the water electrolysis process [8,9].

Therefore, this study aims to estimate and compare achievable emission reductions by implementing renewable hydrogen vehicles in the urban transport sector at the University of São Paulo (USP), which involves producing H₂ via ethanol steam reforming (ESR). The pilot plant analyzed here will be the world's first ethanol-to-hydrogen energy conversion plant. The undergoing project is developed by the Research Centre for Greenhouse Gas Innovation (RCGI/USP), in partnership with Hytron, Shell Brasil, Raízen, Company of Urban Transportation of São Paulo (EMTU), and the National Service of Industrial Learning (SENAI). As part of this project, a pilot hydrogen refuelling station is under construction and will be launched by 2024.

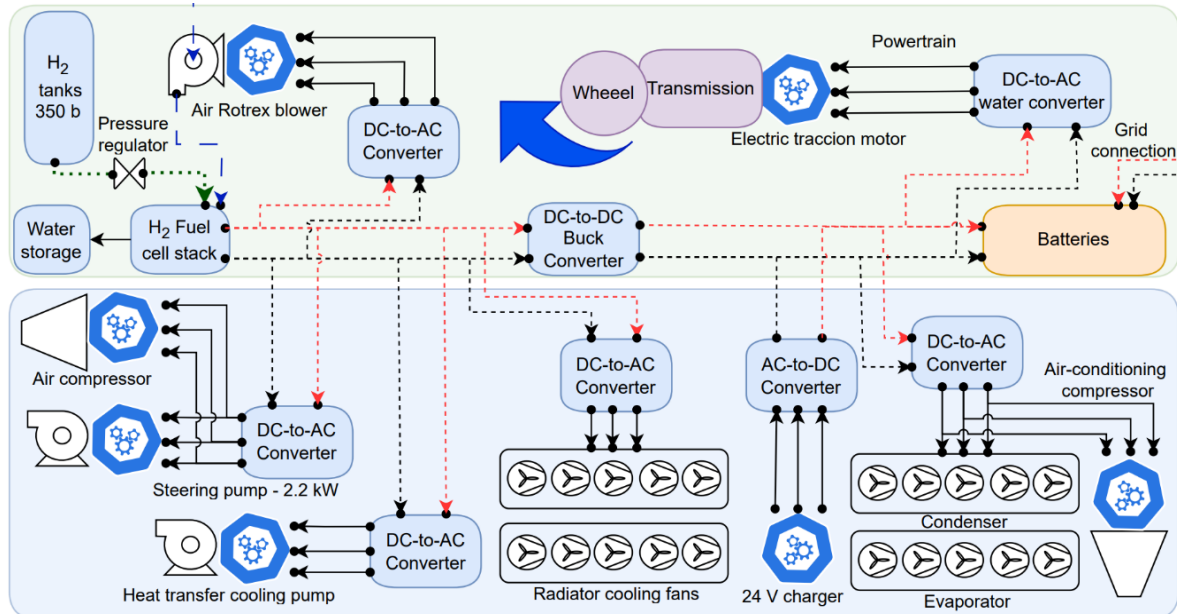


Fig. 1. Schematic representation of the hydrogen-based vehicle. The blue rectangle comprises the vehicle's auxiliary systems, including the air compressor, steering pump, heat transfer cooling pump, radiator cooling fans, and air conditioning system. The green rectangle shows the powertrain of the hydrogen-powered vehicle, involving H₂ storage tanks, a fuel cell stack, an electric converter, and batteries.

MATERIAL AND METHODS

Hydrogen-powered vehicles

Conventional internal combustion engine (ICE) buses share similarities with hydrogen-powered vehicles, as depicted in Fig. 1. These heavy vehicles for passenger transport primarily consist of two subsystems: the powertrain and auxiliary systems. It is worthwhile mentioning that while various components, such as the steering pump, require energy from embedded technology, particular focus was given to analyzing the influence of the air-conditioning system along with the powertrain type. To effectively compare both technologies, CO_{2-eq} greenhouse gas emissions (GHG) consider transportation specifics: frequencies, distances, routines, and embedded technologies with their consumption coefficients. Table 1 summarizes the technical specifications of both technologies.

Table 1. Summary of the technical specifications for ICE and Hydrogen-powered vehicles

Component:	Quant.	Weight, kg	Total weight, kg
Total weight of hydrogen-powered vehicle	1	14000	14000 ^a
HYDROGEN-POWERED VEHICLE			
Fuel cell model HD6Velocity 130 kW	1	450	450 ^a
Lithium batteries model UEV-18XP – 60 kWh	46	15	685 ^b
AC 165 kW Electric traction motor	1	500	500 ^c
CFW11 T Traction frequency inverter	1	75	75 ^c
Hydrogen storage tanks	4	175	700 ^a
Hydrogen weight	1	30	30 ^a
		Total, kg	2440
INTERNAL COMBUSTION ENGINE (ICE)			
4-stroke ICE model OM906-LA 188 kW (wet) 188 kW at 2200 rpm, 6 in-line cylinders with 7.2 l displacement, comp. ratio of 17.3:1 ^d	1	613	613 ^e
Diesel oil storage tank with 300 l of fuel	1	281	281
Transmission model ZF-EcoLife-6AP-1000B-(wet) Gear ratio: 1 st →3.36 (7.79 with torque converter); 2 nd →1.91; 3 rd →1.42; 4 th →1.0; 5 th →0.72; 6 th →0.62 ^d	1	421	421 ^f
		Total, kg	281
Total weight of diesel vehicle			1315
		Difference, kg	8.0%

^a Supplied by EMTU; ^b Technical data sheet of Lithium Battery [10]; ^c Technical data sheet of WEG [11]; ^d Technical data sheet of Mercedes-Benz, BO9916728 [12]; ^e Technical data sheet of Mercedes-Benz, 1044-004 [13]; ^f Frota and Cia Guide [14];

Methodological approach

The methodological approach considers low-carbon hydrogen production using the ethanol steam-reforming route, wherein energy and mass balances are carried out throughout the hydrogen chain. Two models were carried out to compute the CO_{2-eq} greenhouse gas emissions. The first one, a trivial model, only considers an average fuel consumption value along with the carbon intensity of each fuel type. The second one, a complex model, develops a detailed account based on a bus longitudinal dynamic model.

In the bus longitudinal dynamic model, from the perspective of a mass-point vehicle, the tractive force (F_{trac}) can be defined as a function of the set of forces (F) as given in Eq. (1). It is evident that bus acceleration (dV_{bus}/dt) is contingent upon both conservative and dissipative forces. Non-conservative forces, such as rolling resistance (F_{roll}) and aerodynamic resistance (F_{aero}), invariably act in opposition to the bus's direction of motion. Conversely, the road grade force (F_{grade}) can fluctuate depending on the incline of the road, thereby influencing the power requirements of the vehicle's powertrain, and this force is commonly referred to as the tractive or traction force (F_{trac}).

$$M_{bus} \frac{dV_{bus}}{dt} = F_{inertia} = F_{trac} - F_{roll} - F_{aero} - F_{grade} \quad (1)$$

The aerodynamic force, also known as drag force, acting over the frontal area (A_f) of a vehicle on motion, is determined by a function involving the square of the bus's velocity (V_{bus}), the air density (ρ_{air}), and the aerodynamic drag coefficient (C_d), Eq. (2). At 25°C and atmospheric pressure ($P=94.0$ kPa) in São Paulo, the air density is calculated as $\rho_{air} = 1.098$ kg/m³. A specific drag coefficient of $C_d = 0.79$ has been defined for the bus [17]. It is noteworthy that the maximum permissible velocity for the bus within the campus is restricted to 50.0 km/h (13.88 m/s).

$$F_{aero} = \frac{1}{2} \rho_{air} A_f C_d V_{bus}^2 \quad (2)$$

The rolling resistance force is expressed by Eq. (3). The coefficient of rolling resistance (c_{roll}) is influenced by several parameters, including vehicle speed, tire pressure, and road surface conditions, as noted by [18]. In this equation, g represents the acceleration due to gravity, and the $\text{Cos}(\alpha)$ function accounts the non-horizontal road effects. Serrao [19] suggest that c_{roll} can be treated as a constant value, typically falling within the range of 0.01 to 0.02, which might correspond to approximately 1% to 2% of the vehicle's weight.

$$F_{roll} = c_{roll} M_{bus} g \text{Cos}(\alpha) \quad (3)$$

The road grade force is linked to the component of weight in the longitudinal direction and given by Eq. (4). This value is positive when the inclined plane refers to an uphill direction. Consequently, steeper inclines demand greater traction power, with the maximum value occurring when the angle reaches unit, i.e., $\alpha = 90^\circ$. However, it's important to note that such a steep angle is not practically achievable. Conversely, on a horizontal plate, the grade force is null because the force acts orthogonal to the plane. Therefore, the tractive force can be defined by Eq (5).

$$F_{grade} = M_{bus} g \text{Sin}(\alpha) \quad (4)$$

$$F_{trac} = M_{bus} a_{bus} + c_{roll} M_{bus} g \text{Cos}(\alpha) + \frac{1}{2} \rho_{air} A_f C_d V_{bus}^2 + M_{bus} g \text{Sin}(\alpha) \quad (5)$$

As depicted in Fig. (2), carbon emission intensity was analyzed not only concerning the vehicle driving cycle on a specific route, but also encompassing the entire energy conversion process of each embedded vehicle. For ICEVs, energy from fossil fuel is supplied to the engine until it reaches the wheels. Similarly, the electric vehicle powertrain is powered by using ethanol-derived hydrogen fuel cells. A robust thermodynamic model was defined to calculate the mechanical energy required to manage the thermal load of a standard bus under operating conditions in São Paulo, Brazil.

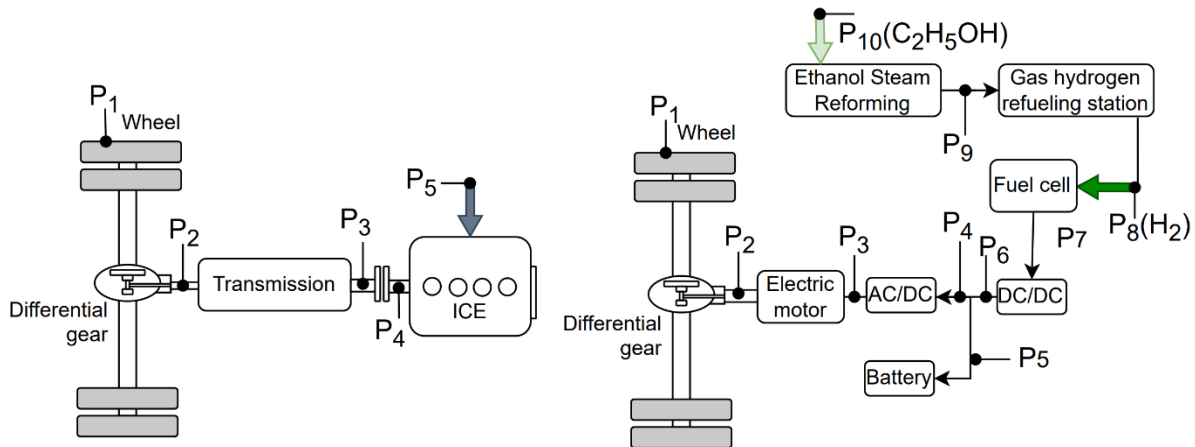


Fig. 2. Schematic representation of the powertrain for both embedded technologies: conventional internal combustion engines versus hydrogen-based vehicles. P_1 and P_2 stand for the mechanical power demanded by the wheel and the differential gear mechanism, respectively, to overcome the tractive force. This value was estimated by using the bus longitudinal model. ICEVs equipped with automatic transmission have a torque converter (P_3 to P_4), known for being highly inefficient at low-speed ratios.

RESULTS AND DISCUSSION

Despite ethanol is widely used in the light-duty transportation sector, its application for heavy-duty transportation sector will be made possible by ethanol steam reforming, presenting itself as a low-carbon alternative to diesel oil. Fossil fuels naturally exhibit a higher carbon intensity compared to biofuels. According to RenovaCalc^{RM} [15], while diesel oil has an average carbon intensity of 86.5 gCO_{2-eq}/MJ, ethanol stands at 25 gCO_{2-eq}/MJ [16], even though some biorefineries have a better sustainable performance with 15 gCO_{2-eq}/MJ. This metric involves the entire life-cycle assessment; production, distribution, and the combustion process within the respective engines, Well-to-Wheel (WtW). Consequently, the low-carbon hydrogen derived from ethanol route offers advantages as compared with conventional fossil routes. It means that the H₂ reaches a carbon intensity of approximately 30 gCO_{2-eq}/MJ when the thermal efficiency of the ethanol steam reforming is equivalent to 70%.

Technologically, it is well known that the efficiency of fuel cells is higher than that of ICEs, and industrial prototypes have demonstrated fuel cell efficiencies equivalent to 60%. Thus, hydrogen-powered vehicles benefit not only from higher thermal efficiency, but also from the energy management provided by electric motors; for instance, energy consumption can be reduced to zero during stops, when the air-conditioning is inactive, or when the vehicle is descending a hill. In addition, electric motors efficiently deliver the necessary mechanical power to the wheel, and power peaks can be handled by using the energy stored in the batteries (60 kWh). Furthermore, ICEs are coupled with inefficient components in transient driving cycles, such as the torque converter and transmission system. In addition, ICEs are projected to provide the maximum instantaneous power demand for a given route, leading to engine oversizing, i.e., while the hydrogen-powered bus was installed with a 130 kW fuel cell stack, the ICE bus was coupled with a 188 kW.

All previous comments are reflected in Fig. (3). The total energy conversion efficiency, WtW, for hydrogen and conventional vehicles was 26.9% and 11.8%, respectively, without air-conditioning system. Results showed that replacing the current fleet of conventional internal combustion engine buses with hydrogen-based options leads to a significant annual reduction of 2658 tonnes CO_{2-eq}, approximately an 83% reduction as compared to the internal combustion-based operation. Notably, CO_{2-eq} emissions increased by at least 16% due to the presence of air-conditioning systems.

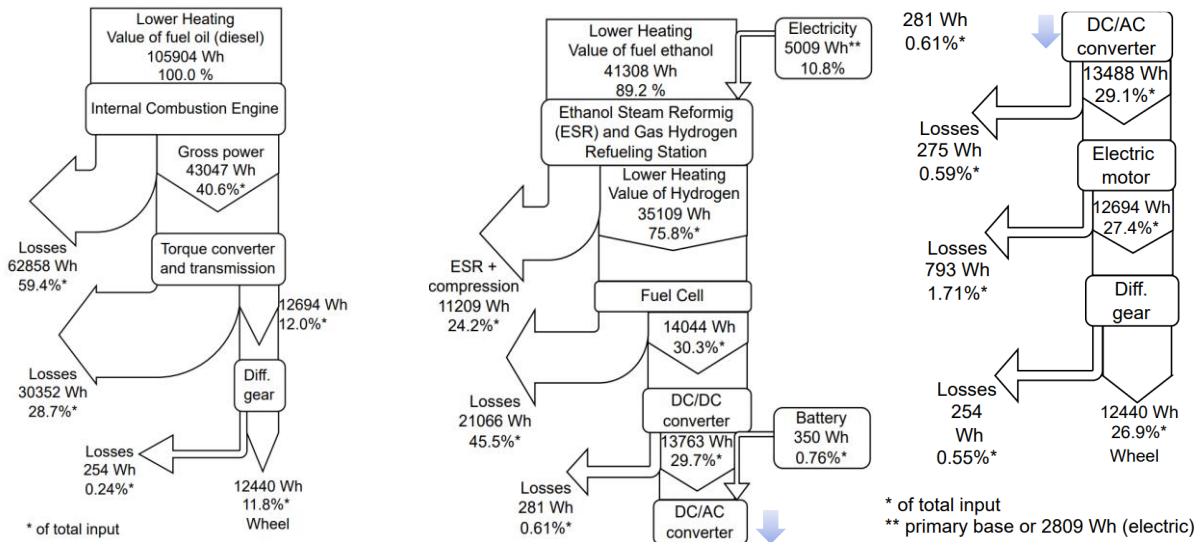


Fig. 3. Sankey diagrams illustrating energy flows for fossil fuel and hydrogen-powered vehicles. Percentages are based on the lower heating value of each fuel. The results pertain to a specific route at the University of São Paulo, considering 33 stop points with a 30-second stop cycle. Note that although batteries might be recharged using a regenerative braking system, this contribution has not been considered here.

CONCLUSIONS

Results displayed that replacing the current fleet of conventional internal combustion engine buses with hydrogen-based options leads to a significant annual reduction of 2658 tonnes CO_{2-eq}, approximately an 83% reduction as compared to the internal combustion-based operation. Furthermore, the total energy conversion efficiency, WtW, achieved 26.9% and 11.7% for hydrogen and conventional vehicles, respectively, without air-conditioning system. Notably, CO_{2-eq} greenhouse gas emissions surged by at least 16% due to the presence of air-conditioning systems for conventional vehicles.

ACKNOWLEDGEMENT

We gratefully acknowledge support of the RCGI – Research Centre for Greenhouse Gas Innovation, hosted by the University of São Paulo (USP) and sponsored by FAPESP – São Paulo Research Foundation (2020/15230-5; 2014/50279-4 and 2020/01177-5) and Shell Brasil, and the strategic importance of the support given by ANP (Brazil’s National Oil, Natural Gas and Biofuels Agency) through the R&DI levy regulation. Also, the first author thanks SGA-USPSustent Program for the personal financial support.

NOMENCLATURE

A	Area, m ²
a	Acceleration, m/s ²
c	Mass, kg
C_d	Aerodynamic drag coefficient, -
C_{roll}	Rolling resistance coefficient, -
F	Force, N
g	Acceleration of gravity, m/s ²
M	Mass, kg
M	Mass, kg
P	Pressure, kPa
P	Power, kW
t	Time, s
V	Velocity, m/s

Greek Letters

α	Plane tilt angle, °
ρ	Density, kg/m ³

Subscripts

a	Air
aero	Aerodynamic
bus	Bus/Vehicle
f	Frontal
grade	Grade
inertia	Inertial
roll	Rolling
trac	Tractive

REFERENCES

1. Hadley SW. and Tsvetkova AA. 2009. Potential impacts of plug-in hybrid electric vehicles on regional power generation. *The Electricity Journal*, 22(10):56-68.
2. Morrissey P. Weldon P. and O'Mahony M. 2016. Future standard and fast charging infrastructure planning: An analysis of electric vehicle charging behaviour. *Energy Policy*, 89:257-270.
3. Markel T. Meintz A. Hardy K. Chen B. Bohn T. Smart J. and Pratt R. 2015. Multi-lab EV smart grid integration requirements study. providing guidance on technology development and demonstration (No. NREL/TP-5400-63963). National Renewable Energy Lab.(NREL), Golden, CO (United States).
4. Muratori M. 2018. Impact of uncoordinated plug-in electric vehicle charging on residential power demand. *Nature Energy*, 3(3):193-201.
5. Needell Z, Wei W, and Trancik JE. 2023. Strategies for beneficial electric vehicle charging to reduce peak electricity demand and store solar energy. *Cell Reports Physical Science*, 4(3):101287.
6. Dincer I. 2012. Green methods for hydrogen production. *International Journal of Hydrogen Energy*, 37(2): 1954-1971.
7. Turner J. Sverdrup G. Mann MK. Maness PC. Kroposki B. Ghirardi M. and Blake D. 2008. Renewable hydrogen production. *International Journal Of Energy Research*, 32(5):379-407.
8. Ursua A. Gandia LM. and Sanchis P. 2011. Hydrogen production from water electrolysis: current status and future trends. *Proceedings of the IEEE*, 100(2):410-426.
9. Hassan N. S. Jalil, AA. Rajendran S. Khusnun NF. Bahari MB. Johari A. and Ismail M. 2023. Recent review and evaluation of green hydrogen production via water electrolysis for a sustainable and clean energy society. *International Journal of Hydrogen Energy (In Press)*.
10. Lithium Battery. Technical data sheet U-Charge XP Series, Lithium-Ion Battery Modules, Aug./2021. Accessed in Oct./2023. Available at: <https://www.lithionbattery.com/>.
11. WEG. Technical data sheet, Motor 165 kW, Aug./2021. Accessed in Oct./2023. Available at: <https://www.weg.net/institutional/BR/en/>.
12. Mercedes-Benz. Technical data sheet MB OM926 LA (Proconve), BO9916728, Oct./2016.
13. Mercedes-Benz, "RHB Dieselmotor OM906/926LA - Repair Manual, Service and Parts," 1044-004, Oct./2014.
14. Frota and Cia Guide - Internal Combustion Engines, Transmissions, and Lubricants (In Portuguese), pg. 31, 2012. Accessed in Oct./2023. Available at: <https://frotacia.com.br/>.
15. Matsuura MISF. et al. 2018. Método e Ferramenta para a Contabilidade da Intensidade de Carbono de Biocombustíveis no Programa Renovabio Método e Ferramenta para a Contabilidade da Intensidade de Carbono de Biocombustíveis no Programa Renovabio.
16. UNICA, 2023. Uniao da Industria de Cana-de-açúcar. Accessed in Oct./2023. Available at: www.unica.com.br.
17. Stanislovaitis C. 2014. Power Management for an Electrified Bus (Doctoral dissertation, The Ohio State University).
18. Guzzella L. Sciarretta A. 2007. *Vehicle propulsion systems* (Vol. 1). Springer-Verlag Berlin Heidelberg.
19. Serrao L. 2009. *A comparative analysis of energy management strategies for hybrid electric vehicles* [Doctoral dissertation, Ohio State University]. OhioLINK Electronic Theses and Dissertations Center. http://rave.ohiolink.edu/etdc/view?acc_num=osu1243934217

TRANSIENT SIMULATION AND COMPARATIVE ASSESSMENT OF TWO CONCENTRATED-SOLAR BASED HYDROGEN PRODUCTION SYSTEMS INTEGRATED WITH VANADIUM-CHLORINE THERMOCHEMICAL CYCLE

Erfan Zand, Mohammadreza Khosravi, Pouria Ahmadi, Mehdi Ashjaee

School of Mechanical Engineering, College of Engineering, University of Tehran, P.O. Box 11155-4563, Tehran, Iran

*Corresponding author e-mail: pouryaahmadi81@gmail.com

ABSTRACT

This research investigates the transient performance of two concentrated solar-based systems, namely E-1 and E-2, under various Middle Eastern climate conditions, both systems are capable of simultaneous production of Hydrogen and power along with other useful services such as fresh water, heating, and cooling. E-1 utilizes a solar power tower configuration with Thermal Energy Storage (TES) to provide heat to a Brayton power cycle. The exhaust gases of the turbine act as the heat source for a three-step V-Cl thermochemical cycle and a Rankine cycle which in turn powers a water production unit. Additionally, a portion of the generated power is allocated to an Alkaline electrolyzer unit for additional Hydrogen production. The generated Hydrogen is compressed to 700 bar in a 3-step Hydrogen compression process, facilitating storage and transportation. E-2 configuration combines Parabolic Trough Collector (PTC) with TES to supply heat to a Rankine and a V-Cl thermochemical cycle, while the other components remain similar to E-1. These setups showcase multigeneration adaptability with different solar concentrating technologies. The main objective of this study is to introduce and compare the performance of the two CSP-based systems, providing insights to help establish and enhance Hydrogen production and integration into the emerging Middle Eastern Hydrogen economy. Transient simulation and modeling are conducted using a coupling of TRNSYS and EES software. Key parameters affecting the system's performance such as solar irradiation and plant area, are identified and investigated. The results demonstrate that Hydrogen production is significantly influenced by seasonal climate changes furthermore, the study presents the produced Hydrogen and power for different cities, highlighting the superior CSP system for each city considering the available area.

Keywords: Hydrogen production, concentrated solar energy, thermochemical water splitting cycle, transient simulation.

INTRODUCTION

There has been a surge in global energy demand with the growth in population, improvements in living standards and industrialization of human society. Currently, fossil fuels partake 80% of primary global energy supply which translates to catastrophic environmental problems such as greenhouse gas emissions and air pollution. To prevent these unsavoury consequences international arrangements have been made to vigorously increase the share of renewable energies in the primary energy supply and it is estimated that this share will reach to 63% by 2050 [1]–[3]. Hydrogen is seen as the ideal alternative energy carrier of the future from the perspective of many researchers due to having numerous desirable properties such as higher energy density, environmental factors, and its ability of efficient conversion to electricity and vice versa. Among various forms of renewable energies, Concentrated Solar energy possesses a unique place, because it Provides high-quality thermal energy. This energy can directly be used in processes like steam methane reforming (SMR) and thermochemical water splitting cycles (TWSCs) to produce hydrogen and other valuable chemicals. Alternatively, it can be used to generate clean electricity which can later power electrolysis-based technologies for clean hydrogen production. Due to these favorable qualities, the global installed capacity of concentrated solar power (CSP) technology has increased dramatically and approached 7 GW by the end of 2020, a fivefold increase since 2010 [4]–[6]. Many Middle Eastern countries such as Qatar, Iran, Turkey, and Pakistan are blessed with locations with mostly sunny days and direct normal irradiance (DNI) ranging between 1900-2400 kWh/m². These resources makes them Ideal candidates for CSP based technologies for clean generation of Power and hydrogen. Many studies have highlighted the potential of Middle Eastern countries for utilizing CSP technologies. Sadeghi et al. [7] proposed a stand-alone solar power tower (SPT) system for a city in Iran (Isfahan), capable of producing 1530 kg/h of hydrogen, while Burulday et al. [8] designed a hybrid solar and biomass power plant for

Turkey (Manisa) which produces 7912.5 ton/year of hydrogen and 39.89 MW electricity. Most of the research available in literature either conducts a steady-state analysis or considers a single type of CSP technology or a single location. However, this study presents a comparative assessment of two CSP-based systems, E-1 and E-2, for five different cities in the Middle East using transient simulations. Both systems are capable of simultaneous production of hydrogen and power and are integrated with Vanadium-Chlorine (V-Cl) TWSC.

SYSTEM DESCRIPTION AND MODELING

The two CSP-based systems are schematized in Fig. 1. Fig. 1(a) displays the E-2 energy system, which consists of three subsystems: the solar subsystem, the power block, and the hydrogen block. The solar subsystem includes the parabolic trough collectors (PTC) with Concrete thermal storage acting as thermal energy storage (TES) and a heat transfer fluid (HTF) pump to circulate the HTF. Therminol VP-1 is selected as the HTF for this configuration. The HTF enters the PTC with a temperature of 297 °C and is heated to 390 °C. The power block considered for this system is a steam Rankine cycle with reheat similar to Solar Electric Generating Station VI [9]. After absorbing heat from TES at state 6, a portion of HTF enters the auxiliary heater to both satisfy the necessary temperature of 525 °C required to run a V-Cl cycle and provide enough heat for the power block on the days that the solar field can not produce enough heat. After leaving the auxiliary heater, HTF splits into two streams; stream 11 goes to the V-Cl unit for Hydrogen production, while stream 9 merges with stream 10 to provide the Rankine cycle heat. 20% of the HTF at state 12 is sent to the reheater (state 17), while the rest is utilized in the superheater, steam generator, and preheater of the Rankine cycle. The pump takes in saturated water leaving the condenser at state 29 and increases its pressure to 100 bar; water then is heated to approximately 370 °C before entering the high-pressure turbine at state 24; after passing through the turbine water is then reheated in the reheater, to 370 °C and enters the low-pressure turbine at state 27, water then enters the condenser at state 28 completing the cycle. The Hydrogen block consists of a three-step V-Cl cycle, an alkaline electrolyzer unit that, utilizes a portion of generated electricity to produce Hydrogen, and a 3-step compression unit (not displayed in the figure). Fig. 1(b) displays the E-1 energy system, which consists of three similar subsystems: solar, power, and hydrogen. The solar subsystem utilizes a heliostat field with an air receiver solar tower, rock bed thermal storage, and an air compressor. The power block is a Brayton cycle with a bottoming Rankine cycle; after leaving the TES at state 4, air enters a combustion chamber to provide the temperature required for the turbine. Exhaust gases at state 6 act as the heat source for the V-Cl cycle and a Rankine cycle identical to the one described for the E-2 system. The Hydrogen block is the same as the E-2 system. 5 cities (Doha, Shiraz, Zahedan, Nawabshah, Quetta) in the Middle East are chosen for this assessment based on factors such as DNI, land slope, and wind speed. The best fit for each city is highlighted, considering the total aperture area of 50,000 m² to 150,000 m². Solar thermal electric components (STEC) library [10] in TRNSYS software has been used for the modeling of solar and power subsystems, while the three-step V-Cl cycle proposed by Amendola [11] has been coded in EES and linked to TRNSYS to conduct the Transient simulation and analysis.

RESULT AND DISCUSSION

Figure 2 demonstrates the annual result of the TRNSYS simulation for the E-2 system for Shiraz for a total PTC aperture area of 200,000 m². It is evident from the figure that the performance of the solar field and, henceforth, the whole system is significantly influenced by seasonal changes. In the seasons with lower DNI, the system can not satisfy the designed HTF flow rate of 400 kg/s, so the power block is forced to operate under off-design conditions; this indicates the need for an auxiliary heating system in the colder season, while in the seasons with sufficient DNI the system can operate with no need of back up heaters. This trend is seen for both E-1 and E-2 systems in all locations investigated; locations with higher DNI require less powerful backup heating systems. Table 1 presents the annual power production of the E-1 system while only producing power. To ensure the smooth function of the system, additional heat is added to the system via a combustion chamber (values mentioned in Table 1 in parentheses). With the increase of aperture area, annual power production increases while the amount of additional heat decreases for all cities; also, cities with higher DNI, such as Shiraz and Quetta, require less additional heat and produce more power with the same amount of aperture area.

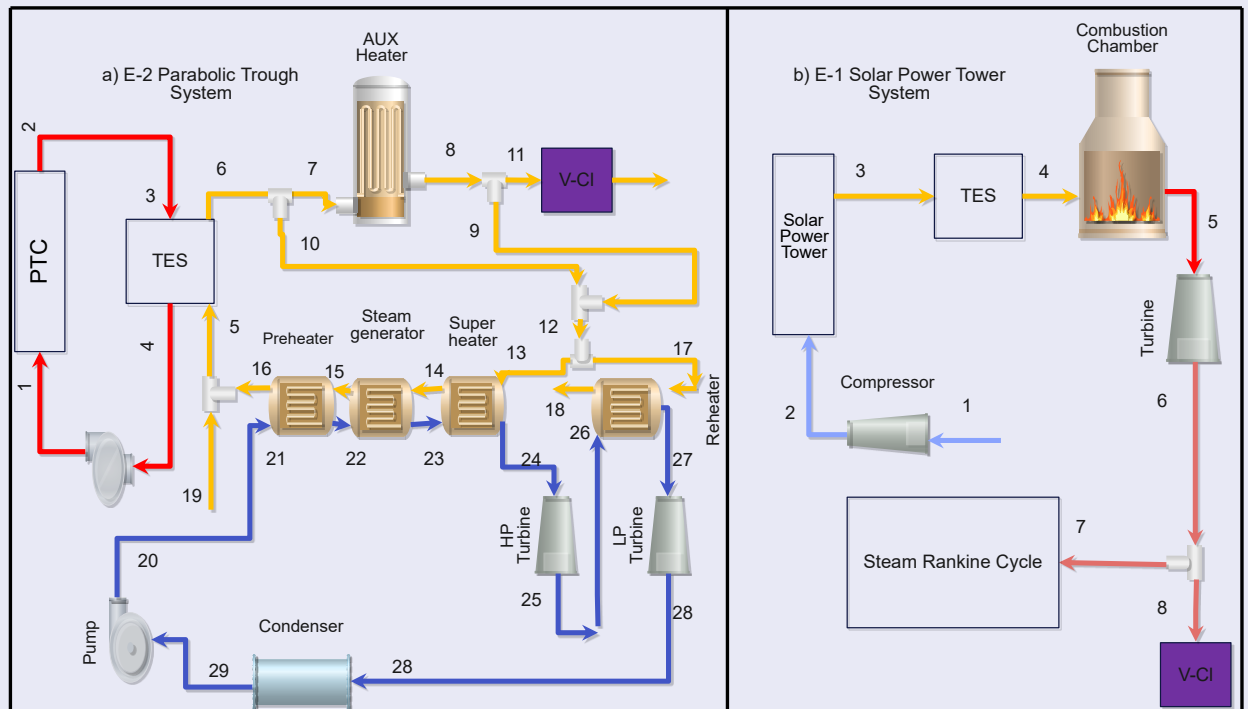


Figure 1. Schematic diagram of the two integrated systems

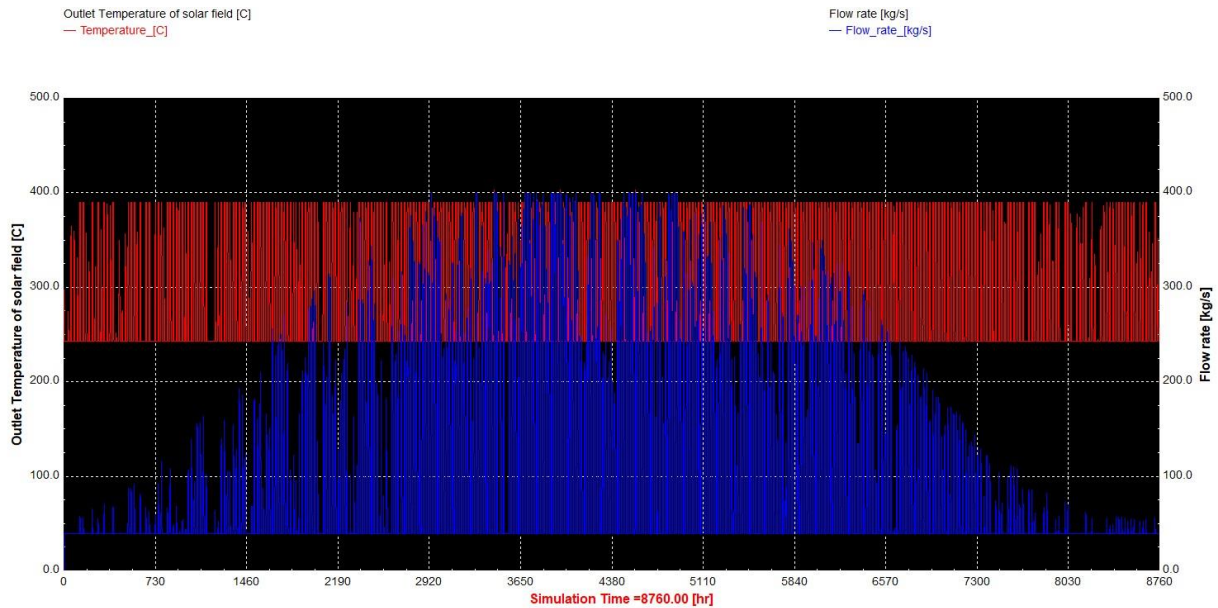


Figure 2 Outlet Temperature and the HTF flow rate of the PTC field for Shiraz during a year

Table 1 Annual Power production of E-1 system

City	Shiraz	Zahedan	Doha	Quetta	Nawabshah
Aperture area m ²	Annual Power Production (Additional Heat) GWh				
50000	73.26 (105)	72.39(116.48)	72.22(127.317)	72.91(116.23)	71.83(119.84)
100000	92.12(94.4)	83.55(103.6)	76.687(114.2)	85.20 (104)	78.196(103)
150000	112.9(90.58)	98.164(98.86)	85(108.3)	99.9 (99.38)	90.4(97.02)

Table 2 Annual Power production of E-2 system with no additional heat

City	Shiraz	Zahedan	Doha	Quetta	Nawabshah
Aperture area m ²	Annual Power Production GWh				
50000	3.94	2.26	0.46	2.64	0.38
100000	21.22	12.53	4.36	13.3	4.83
150000	40.2	24.47	10.42	25.51	12.61

The simulation results of the E-2 system for five different cities have been displayed in Table 2. These results are based on the annual power production of the cities while producing power only, and with no additional heat. It is observed that the annual power production of the cities increases by 10-33 times when the aperture area is increased from 50,000 m² to 150,000 m². Cities with lower DNI such as Doha and Nawabshah, benefit the most from the increase in aperture area. However, cities with higher DNI like Shiraz, Zahedan, and Quetta do not experience as much growth in power production, but they still produce the most power. The hydrogen subsystem consists of the V-CI cycle, and the electrolyzer unit is capable of producing hydrogen. 20% of the exhaust gases of the E-1 system (state 8, figure 1. b) goes into the V-CI cycle, while 10% of the electricity produced is allocated to the electrolyzer unit. E-2 system follows a similar procedure. E-1 system is capable of producing 100 – 186 tons of hydrogen per year, with Shiraz having the highest production among the five cities. E-2 system is capable of producing 14 – 38 tons of hydrogen per year, with Shiraz being the highest. The E-1 system can produce more hydrogen than the E-2 system since it utilizes a much higher auxiliary heat. To choose the best system for each city, two main factors should be considered: the amount of additional heat and total aperture area. The E-1 system is better suited for cities with lower DNI such as Nawabshah and Doha when the aperture area is lower than 100,00 m². This is because the PTC-based system cannot produce enough power and needs much additional heat. On the other hand, the E-2 system is better suited for cities with higher DNI such as Shiraz, Zahedan, and Quetta. These cities can produce enough power to be feasible with no additional heat for most of the year, which leads to lower environmental pollution.

Conclusion

In this study, the transient performance of two CSP-based systems integrated with a V-CI cycle was investigated for five Middle Eastern cities. The best fit for each city was determined based on factors such as aperture area and additional heat requirement. Shiraz was found to be the best city for both systems due to its superior DNI.

References

- [1] I. Dincer and C. Acar, "Potential Energy Solutions for Better Sustainability," *Exergetic, Energetic and Environmental Dimensions*, pp. 3–37, Jan. 2018, doi: 10.1016/B978-0-12-813734-5.00001-9.
- [2] "Key World Energy Statistics 2021 – Analysis - IEA." Accessed: Nov. 28, 2023. [Online]. Available: <https://www.iea.org/reports/key-world-energy-statistics-2021>
- [3] D. Gielen, F. Boshell, D. Saygin, M. D. Bazilian, N. Wagner, and R. Gorini, "The role of renewable energy in the global energy transformation," *Energy Strategy Reviews*, vol. 24, pp. 38–50, Apr. 2019, doi: 10.1016/J.ESR.2019.01.006.
- [4] S. Zhang, K. Li, P. Zhu, M. Dai, and G. Liu, "An efficient hydrogen production process using solar thermo-electrochemical water-splitting cycle and its techno-economic analyses and multi-objective optimization," *Energy Convers Manag*, vol. 266, p. 115859, Aug. 2022, doi: 10.1016/J.ENCONMAN.2022.115859.
- [5] "Solar energy." Accessed: Nov. 29, 2023. [Online]. Available: <https://www.irena.org/Energy-Transition/Technology/Solar-energy>
- [6] F. Safari and I. Dincer, "A review and comparative evaluation of thermochemical water splitting cycles for hydrogen production," *Energy Convers Manag*, vol. 205, p. 112182, Feb. 2020, doi: 10.1016/J.ENCONMAN.2019.112182.



- [7] S. Sadeghi and S. Ghandehariun, "A standalone solar thermochemical water splitting hydrogen plant with high-temperature molten salt: Thermodynamic and economic analyses and multi-objective optimization," *Energy*, vol. 240, p. 122723, Feb. 2022, doi: 10.1016/J.ENERGY.2021.122723.
- [8] M. E. Burulday, M. S. Mert, and N. Javani, "Thermodynamic analysis of a parabolic trough solar power plant integrated with a biomass-based hydrogen production system," *Int J Hydrogen Energy*, vol. 47, no. 45, pp. 19481–19501, May 2022, doi: 10.1016/J.IJHYDENE.2022.02.163.

ICH2P14-OP010

A NOVEL COST-EFFECTIVE APPROACH FOR PRODUCTION OF HYDROGENASE ENZYMES AND MOLECULAR HYDROGEN FROM WHEY-BASED BY-PRODUCTS

^{1,2*}Anna Poladyan, ^{1,2}Meri Iskandaryan, ^{1,2}Ofelya Karapetyan, ³Ela Minasyan, ²Anait Vassilian, ^{1,2}Karen Trchounian, ⁴Garabed Anatronikian

¹Department of Biochemistry, Microbiology and Biotechnology, Faculty of Biology, Yerevan State University, 1 A. Manoogian str., 0025 Yerevan, Armenia

²Scientific-Research Institute of Biology, Yerevan State University, 1 A. Manoogian str., 0025 Yerevan, Armenia

³Institute of Pharmacy, Yerevan State University, 1 A. Manoogian str., 0025, Yerevan, Armenia

⁴Hamburg University of Technology, Institute of Technical Biocatalysis, CBBS, Schwarzenberg-Campus 4, 21073 Hamburg, Germany

*Corresponding author e-mail: apoladyan@ysu.am

ABSTRACT

Heterotrophic *Escherichia coli* and chemolithoautotroph *Ralstonia eutropha* have significant implications in biotechnology. *R. eutropha* H16 is a pivotal model organism in the generation of O₂-tolerant [NiFe]-hydrogenases (Hyds), crucial biocatalyst for biological fuel cells (BFCs). *E. coli* is known for its ability to produce molecular hydrogen (H₂) through sugars and glycerol mixed acid fermentation. In this study, side streams from the dairy industry, a mixture of curd and cheese whey (CW), were explored for the two-phase growth of *R. eutropha* H16 and *E. coli* BW25113. Diverse parameters, including cell mass (OD), pH, oxidation-reduction potential (ORP) kinetics, H₂ production, and H₂-oxidizing Hyd activity, were examined. For *R. eutropha* H16, growth was observed in 4-fold diluted whey (15 g/L) under microaerophilic conditions over 7 days, both with and without glycerol supplementation. The maximum growth was achieved within 5 days across all samples. Notably, the most remarkable growth and Hyd activity enhancement were observed in the whey mixture supplemented with glycerol. The maximal H₂-oxidizing Hyd activity was measured on the 2nd day of *R. eutropha* H16 cultivation, reaching its maximum (~0.433 ± 0.05 U/min/mg CDW) in glycerol-added CW. The increase in Hyd activity correlated with a decline in pH and ORP. Interestingly, *R. eutropha* H16 could not utilize lactose, which is abundant in whey. High-performance liquid chromatography (HPLC) confirmed lactose presence in CW post *R. eutropha* growth. Consequently, wild-type *E. coli* BW25113 was introduced following *R. eutropha* cell removal. *E. coli* reached maximum growth after 72 hours, with the highest H₂ yields (~5.2 mmol/L/g dry whey) attained within 48 hours across all samples. This study's outcomes offer insights into the economically viable production of bacterial biomass, H₂, and Hyd enzymes using dairy industry by-products, opening new avenues for biotechnological advancement.

Keywords: Biohydrogen, hydrogenases, dairy industry side-streams.

INTRODUCTION

Approximately 70% of whole milk undergoes processing to create various dairy products, with the primary by-product of this process being liquid whey. The main part of whey is obtained from the production of cheese, and the rest from the production of casein. Dairy whey is divided into two main categories: sweet whey (SW) and acid whey (AW). Sweet whey is produced during the production of rennet-type cheeses, while acid whey is a by-product of the production of some acidic dairy products such as curd [1].

Dairy wastewater is distinguished by its substantial organic content, typically exhibiting elevated levels of chemical oxygen demand (COD) and biological oxygen demand (BOD), ranging from 1 to 10 g/L and 0.3 to 5.9 g/L, respectively [2]. Whey is a mixture of globular proteins and casein, so it has excellent nutritional properties. Casein is a phosphoprotein and may be used as a source of carbohydrates, amino acids, calcium and phosphorous [1]. Due to the composition dairy whey represents as a rich nutrient medium for different bacteria growth and cultivation, despite of this dairy whey is currently being discharged directly into aqueous systems, causing inadvertent harm to aquatic life forms and, consequently, negatively impacting the overall environment [3]. Handling this solid waste residue is a huge challenge and can cost up to 60% of total treatment cost in the processing unit [3, 4].

Our prior research has concentrated on identifying the optimal growth conditions for *Ralstonia eutropha* and *Escherichia coli* using two distinct dilutions of dairy waste, as described in Poladyan et al. (2023) [5]. However, the primary objective of our study is to develop and optimize a strategy for the

scalability, feasibility, and economic viability of the utilization of dairy wastes to obtain bacterial biomass with catalytically active enzymes for oxidation and reduction of H₂. The best candidate enzymes for hydrogen metabolism are hydrogenases (Hyds) presented in bacteria such as *R. eutropha* and *E. coli*. *R. eutropha* and *E. coli* are bacteria possessing significant biotechnological potential due to their O₂-tolerant Hyds. They hold promise for advancing future H₂-based biotechnology, facilitating the production of a wide range of commercially, environmentally, and medically valuable compounds.

R. eutropha is a chemolithoautotrophic β -proteobacterium with the remarkable capability to express four different O₂-tolerant [NiFe] Hyds: a membrane-bound Hyd (MBH), cytoplasmic soluble Hyd (SH), a regulatory Hyd (RH) and an actinobacterial type Hyd (AH) [6, 7]. The MBH plays a key role in H₂ uptake-driven respiration using O₂ as the terminal electron acceptor. In contrast, the SH is a bidirectional Hyd that directly reduces NAD⁺ to NADH using H₂, thus generates reducing equivalents. RH controls Hyd gene transcription according to the availability of H₂. AH it falls into the category of high affinity Hyds and displays notable tolerance to O₂ [6]. These Hyds can be presented as promising candidates as anodic biocatalysts in Enzymatic biofuel cells (EFC) or microbial fuel cells (MFC) and may lead to efficient electricity production. Additionally, biologically derived H₂ is an attractive source of electrons for electricity generation in EFCs.

Hydrogen is the most prevalent element in the universe, yet it doesn't naturally occur in a pure form on our planet. Abundant, cost-effective, and environmentally friendly, hydrogen has long been hailed as the fuel of tomorrow. However, in recent times, the emergence of 'green hydrogen': hydrogen produced without relying on fossil fuels, has emerged as a promising clean energy source, capable of propelling us toward a net-zero emissions future.

Molecular hydrogen (H₂) can be produced via Hyds during mixed-acid fermentation by *E. coli*. Among H₂-producing bacteria, *E. coli* is the best-characterized bacterium, having established metabolic pathways and, importantly, there are many strains to manipulate genetically [8]. The *E. coli* also has four different Hyds, but only two of them are an O₂-tolerant: Hyd1 and Hyd3. The Hyds of *E. coli* are performed not only H₂ formation, but also H₂ oxidation depend of experimental conditions [8].

In this context, it was important to find the optimal conditions when using dairy waste materials will be possible to obtain biomass with active Hyds as a H₂ synthesizing agents in case of *E. coli* and biocatalysts in case of *R. eutropha*. New approach is implemented in the current study: *R. eutropha* H16 could not utilize lactose, which is abundant in whey, consequently, *E. coli* BW25113 was introduced following *R. eutropha* cell removal and H₂ production was examined.

MATERIALS AND METHODS

Growth media and cultivation conditions of bacteria

R. eutropha H16 is pre-cultivated heterotrophically in Fructose-Nitrogen (FN) minimal mineral medium. The basic FN medium comprised 100 ml of 10 x H16 buffer, 850 ml of water, and the sterilized solutions listed below: 10 mL NH₄Cl (20 % w/v), 1 mL MgSO₄ x 7H₂O (20% w/v), 1 mL CaCl₂ x 2H₂O (1% w/v), 1 mL FeCl₃ x 6H₂O (0.5% w/v), and 10 mL fructose (40% w/v). The 10 x H16 buffer contained 90 g Na₂HPO₄ x 12 H₂O and 15 g KH₂PO₄ ad 1000 ml H₂O (final pH of 7.0). The bacteria were aerobically pre-cultivated on a shaker at 130 rpm and 30 °C [9].

E. coli BW25113 inocula were cultivated under fermentative conditions at pH 7.5 and 37°C in a peptone medium, which consisted of 20 g/L peptone, 2 g/L K₂HPO₄, and 5 g/L NaCl [8].

We conducted a study on bacterial growth parameters using different combinations of dairy waste materials, specifically cheese (SW) and curd whey (AW), in combination with 0.4% glycerol. The dairy waste materials had undergone hydrolysis, filtration, dilution fourfold with distilled water and sterilization. pH adjustment was achieved using a concentrated solution of sodium bicarbonate [5].

The bacterial cultivation process was carried out in two phases. In the first phase, 3% of *R. eutropha* pre-culture was inoculated into a dairy waste medium under microaerophilic conditions (conditions in 1000 mL baffled flasks containing 800 mL of solutions) for a period of 7 days. In the second phase, after the isolation of *R. eutropha* from the medium, it was co-inoculated with a wild-type and recombinant mutant strain of *E. coli* for duration of 5 days. This approach was chosen as *R. eutropha* does not utilize several carbon sources, such as sugars, present in both AW and SW.

Determination of bacterial growth characteristics

Bacterial growth was assessed by measuring the optical density (OD) at 600nm using a spectrophotometer (Spectro UV-VIS Auto, LaboMed, Los Angeles, CA, USA).

The pH of the medium was determined with a pH electrode on an HJ1131B pH meter (Hanna Instruments, Portugal). Adjustments to the medium's pH were made by adding 0.1 M NaOH or 0.1 N HCl solutions, depending on the initial pH of the medium. Bacterial culture medium oxidation reduction potential (ORP) and H₂ production of bacterial culture cells was determined by using a couple of glass oxidation-reduction platinum (Pt) (EPB-1, Measuring Instruments Enterprise, Gomel, Belarus, or PT42BNC, Hanna Instruments, Portugal) and titanium-silicate (Ti-Si) (EO-02, Measuring Instruments Enterprise, Gomel, Belarus) electrodes. The Pt electrode is sensitive to O₂ and H₂ levels in the medium, whereas the Ti-Si electrode remains unaffected by the presence of O₂ or H₂ and provides an overall ORP measurement.

This property allows H₂ detection in the growth medium, particularly under anaerobic conditions [10]. Before conducting the analysis, both electrode readings were calibrated using a control solution, consisting of a combination of 0.049 M potassium ferricyanide (K₃[Fe(CN)₆]) and 0.05 M potassium ferrocyanide (K₄[Fe(CN)₆]*3H₂O) at a pH 6.86. The readings of both electrodes in the solution at 25°C were found to be +245±10 mV.

The H₂-oxidizing activity of Hyds will be quantified in anaerobic cuvettes by monitoring H₂-dependent methylene blue reduction at 570 nm and 30 °C with a Cary 50 UV-vis spectrophotometer [11]. Pre-purified waste and end products of metabolism were analyzed on an Agilent 1260 Bio-inst HPLC equipped with columns for the determination of organic acids and sugars (Germany).

Data processing was carried out using the determination of Student's reliability criteria using Microsoft Excel 2016. The difference was valid when P<0.05. Various analytical grade reagents produced by Carl Roth GmbH (Germany), Sigma Aldrich (USA) were used.

RESULTS AND DISCUSSION

R. eutropha H16 was cultured using sweet whey (SW, 15 g/L) and acid whey (AW, 12.5 g/L) with or without glycerol supplementation (0.4%). Additionally, a combination of 7.5 g/L SW and 6.5 g/L AW was used with and without glycerol. Bacterial growth parameters and H₂-oxidizing Hyd activity were investigated under micro-aerobic conditions over a 7-day period. The obtained results were compared to a glucose-fructose-nitrogen (GFN) medium, identified as the optimal condition among all studied heterotrophic conditions for maximal Hyds production [9].

Unlike the GFN medium, the logarithmic growth phase of *R. eutropha* resulted in an observed increase in pH from 7.0 to 7.2-8.0. The maximum growth of *R. eutropha* was observed after the 5th day when utilizing a mixture of SW and AW, reaching an OD₆₀₀ of approximately 3.8 ± 0.02. Notably, there was no significant difference recorded between the SW and AW mixture and the mixture containing glycerol. In contrast to the gradual growth of bacteria in a GFN medium, a steady increase in growth was detected, with the maximal OD₆₀₀ recorded on the 7th day (approximately 3.9 ± 0.02) (Fig. 1).

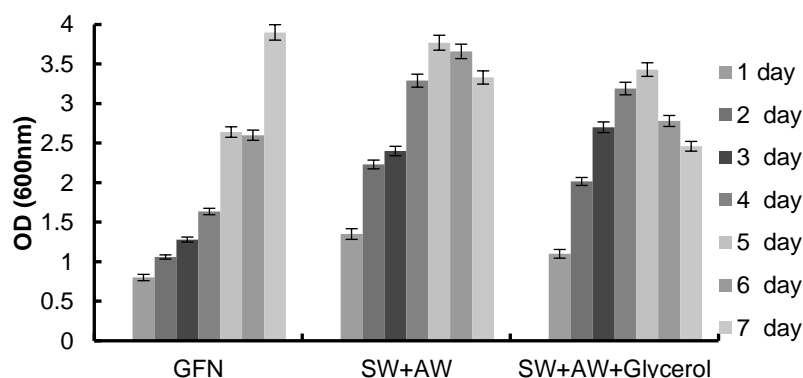


Fig.1. Biomass formation (OD₆₀₀) of *R. eutropha* on the mixture of 7.5 g/L SW and 6.5 g/L AW with and without glycerol and GFN. Bacteria were grown micro-anaerobically, at 30°C, 7 days (n=5, p<0.05).

The decrease in pH was correlated with a reduction in ORP, with the most significant change recorded on the 2nd day of bacterial growth, dropping from $+330 \pm 10$ mV to 79 ± 10 mV. This decline in ORP is also linked to Hyd activity. Higher H₂-oxidizing Hyd activity was observed from the 2nd day of *R. eutropha* cultivation in both the mixture with or without glycerol, in comparison to the GFN medium where Hyd activity started on the 1st day (24 hours). The maximum Hyd activity, approximately 0.433 ± 0.05 U/min/mg CDW, was detected in the CW and glycerol-containing sample on the 2nd day (48 hours). Moreover, the glycerol-containing sample exhibited twice the activity compared to the glycerol-free mixture. This heightened activity persisted until the 6th day of bacterial growth, and this phenomenon is attributed to the presence of glycerol, which facilitates the expression of the Hyds genes and sustains the notably slow growth of *R. eutropha* H16 [11]. Nevertheless, the impact of glycerol was more pronounced in the GFN medium, where the hydrogen-oxidizing activity of Hyds was consistently observed throughout the 7 days of the experiment with minor variations (Fig. 2).

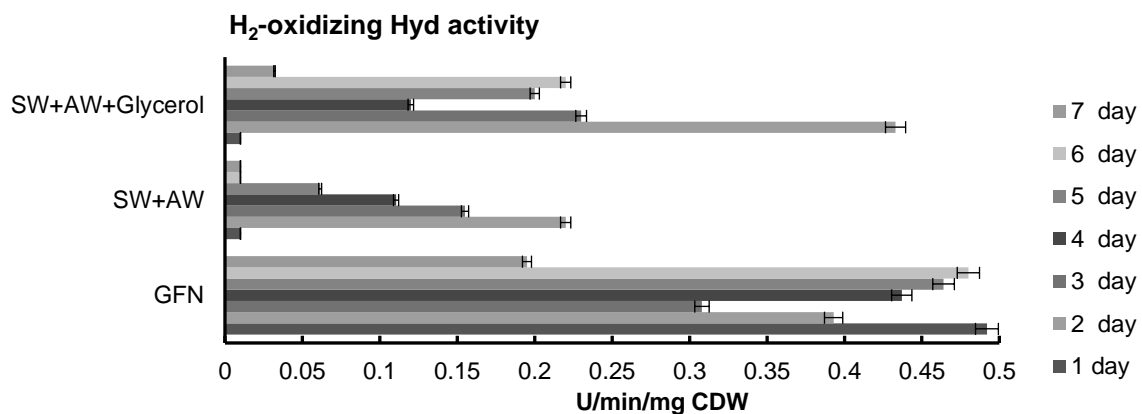


Fig.2. Hydrogen-oxidizing Hyd activity of *R. eutropha* on the mixture of 7.5 g/L SW and 6.5 g/L AW with and without glycerol and GFN. Activity was expressed in U/min/mg (7 days, n=5, p<0.05).

After culturing *R. eutropha* H16 for 72 hours and 120 hours, the cells were harvested, and the supernatant was reused for the cultivation of *E. coli* cells. The collected whey was subjected to HPLC analysis to determine its sugar composition both before and after microbial cultivation. Relying on the data concerning Hyd enzyme's involvement in H₂ production and aiming to direct the metabolism of *E. coli* towards H₂ production upon whey utilization, the next step of our experiments was to investigate the growth and H₂ production *E. coli* BW25113 and mutant (*hyaB hybC hycAfdG ldhA frdC aceE*). The bacteria were cultured overnight in a peptone medium with glucose, after which 3% of the bacterial pre-cultures were inoculated into growth media initially containing whey mixture of 7.5 g/L SW and 6.5 g/L AW with and without glycerol at a pH of 7.5. *E. coli* wild-type parental strain (PS) and mutant strain growth, ORP and pH kinetics, and H₂ production was investigated during 144 h on AW and SW alone and mixed with glycerol.

With the biomass formation pH and ORP (readings of Pt electrode) decline was shown (Figs. 3, 4). After growth more acidic pH was stated in the samples without glycerol supplementation. The results align with literature data, indicating that less acid is produced during the fermentation of glycerol (citation).

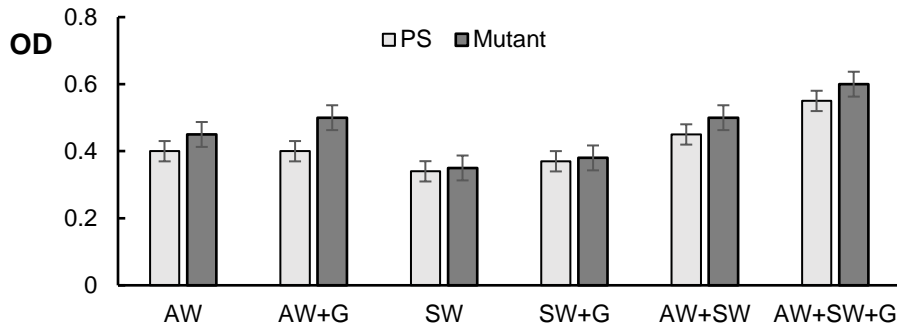


Fig.3. Growth of *E. coli* BW25113 (PS) and mutant strain (M) on sweet whey (SW, 15 g/L) and acid whey (AW, 12.5 g/L) with and without glycerol (G) supplementations or mixture of 7.5 g/L SW and 6.5 g/L AW with and without Glycerol. Bacteria were grown anaerobically, 37°C, (n=5, p<0.05).

Maximal (OD₆₀₀ 0.6) growth was achieved at 72 h of growth upon AW and SW mixture with glycerol supplementation. Maximal H₂ production was stated in all samples reaching up to the highest H₂ yields (~5.2 mmol/L/g dry whey) attained within 48 hours across all samples.

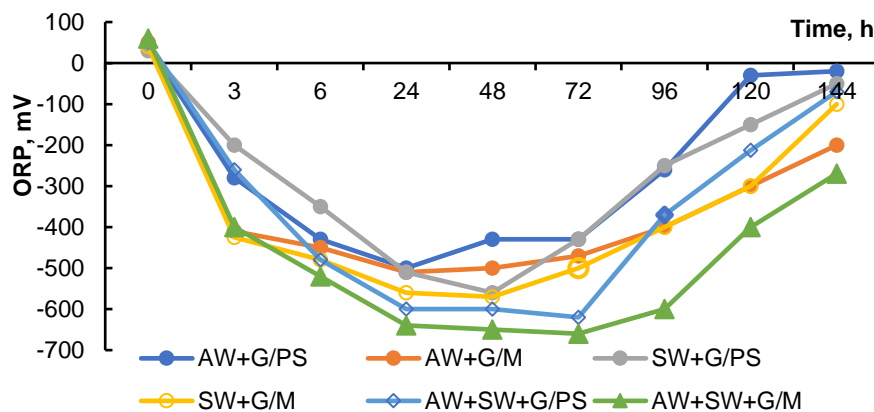


Fig.4. ORP kinetics (Pt electrode) of *E. coli* BW25113 (PS) and mutant strain (M) on sweet whey (SW, 15 g/L) and acid whey (AW, 12.5 g/L) with and without glycerol (G) supplementations.

However, H₂ production and biomass formation was stimulated in mutant strain: reading of Pt electrode reached up to -660 ± 10 mV (~6 mmol/L/g dry whey). The H₂ stimulation might be because of redirecting glucose metabolism to formate via deleting different genes (*hyaB* the large subunit of Hyd-1 and *hybC* the large subunit of Hyd-2) responsible for H₂ uptake or oxidation, formate transport, inactivating lactate, and acetate synthesis, etc. (Maeda et al., 2007; Bekbayev et al., 2022). The responsible Hyd enzymes for H₂ production during utilization of whey were revealed in *E. coli*, consequently, the application of genetic modification tools enhanced H₂ production.

CONCLUSIONS

The results have the potential for further application and scaling up of H₂ and Hyd enzyme production technology. They present a new opportunity for utilizing cost-effective industrial by-products in microbial cultivation, offering not only affordable energy generation but also a solution to the ecological challenge of waste disposal.

ACKNOWLEDGEMENT

This work was supported by the Foundation of Armenian Science and Technology (FAST) ADVANCE program to AP, KT, EM, and GA and the grant [21AG-1F043] from the State Committee of Science, Ministry of Education, Science, Culture and Sport of Armenia to AP.

REFERENCES

1. Ganju S and Gogate PR. 2017. A review on approaches for efficient recovery of whey proteins from dairy industry effluents. *Journal of Food Engineering* 215:84-96. <https://doi.org/10.1016/j.jfoodeng.2017.07.021>.
2. Kothari R, Kumar V, Pathak VV and Tyagi VV. 2017. Sequential hydrogen and methane production with simultaneous treatment of dairy industry wastewater: Bioenergy profit approach. *International Journal of Hydrogen Energy* 42:4870-4879.
3. Usmani Z, Sharma M, Gaffey J, Sharma M, Dewhurst RJ, Moreau B, Newbold J, Clark W, Thakur VK and Gupta VK. 2022. Valorization of dairy waste and by-products through microbial bioprocesses. *Bioresource Technology* 346.
4. Kwapinska M, Horvat A, Liu Y et al. 2020. Pilot Scale Pyrolysis of Activated Sludge Waste from Milk Processing Factory. *Waste Biomass Valor* 11:2887–2903. <https://doi.org/10.1007/s12649-019-00596-y>
5. Poladyan A, Trchounian K, Paloyan A, Minassyan E, Aghekyan H, Iskandaryan M, Khoyetsyan L, Aghayan S, Tsaturyan A and Antranikian G. 2023. Valorization of whey-based side streams for microbial biomass, molecular hydrogen, and hydrogenase production. *Appl Microbiol Biotechnol*. <https://doi.org/10.1007/s00253-023-12609-x>
6. Lenz O, Lauterbach L, Frielingsdorf S and Friedrich B. 2015. Oxygen-tolerant hydrogenases and their biotechnological potential. *Biohydrogen*, Chapter: 4, Edited by Matthias Rögner
7. Schäfer C, Friedrich B and Lenz O. 2013. Novel, Oxygen-Insensitive Group 5 [NiFe]-Hydrogenase in *R. eutropha*. *Applied and Env. Microb.* 79(17):5137-5145.
8. Trchounian K, Poladyan A, Vassilian A and Trchounian A. 2012. Multiple and reversible hydrogenases for hydrogen production by *Escherichia coli*: dependence on fermentation substrate, pH and the F₀F₁-ATPase, *Critical Reviews in Biochemistry and Molecular Biology* 47(3): 236–249.
9. Poladyan A, Blbulyan S, Sahakyan M, Lenz O and Trchounian A. 2019. Growth of the facultative chemolithoautotroph *Ralstonia eutropha* on organic waste materials: growth characteristics, redox regulation and hydrogenase activity. *Microb Cell Fact.* 18:201. doi.org/10.1186/s12934-019-1251-5
10. Vassilian A and Trchounian A. 2009. Environment oxidation-reduction potential and redox sensing by bacteria. *Bacterial membranes. Res. Signpost: Kerala, India*
11. Poladyan A, Blbulyan S, et al. 2019. Growth of the Facultative Chemolithoautotroph *Ralstonia eutropha* on Organic Waste Materials: Growth Characteristics, Redox Regulation and Hydrogenase Activity. *Microb. Cell Fact.* 18:201. <https://doi.org/10.1186/s12934-019-1251-5>
12. Wood TK, Maeda T, Sanchez-Torres V (2007) Enhanced hydrogen production from glucose by metabolically engineered *Escherichia coli*. *Appl. Microbiol. Biotechnol.* 77(4): 879–90.
13. Bekbayev K, Mirzoyan S, Toleugazykyzy A, Tlevlessova D, Vassilian A, Poladyan A, Trchounian K (2022) Growth and hydrogen production by *Escherichia coli* during utilization of sole and mixture of sugar beet, alcohol, and beer production waste. *Biomass Convers. Biorefinery*. DOI:10.1007/s13399-022-02692-x

ICH2P14-OP017

KINETIC MODELLING AND PROCESS OPTIMIZATION FOR BLUE HYDROGEN PRODUCTION VIA AMMONIA CRACKING

¹Ragad Aldilajjan, ¹Sai Katikaneni, ¹Osamah Siddiqui, ²Mohammad Rakib, ¹Bandar Solami

¹R&DC Saudi Aramco, Dhahran, Saudi Arabia

²RASD Saudi Aramco, Dhahran, Saudi Arabia

*Corresponding author e-mail: osamah.siddiqui@aramco.com

ABSTRACT

Ammonia is considered to be a promising hydrogen carrier as it comprises of 17.8 wt% of hydrogen and enables its transfer over long distances at lower costs. In efforts of optimizing the process of back-cracking ammonia to hydrogen, this study focuses on reactor optimization and analysis of energy sources required for blue ammonia cracking plants.

Aspen Plus was used to simulate an industrial scale ammonia cracking plant, consisting of a multi-tubular packed bed reactor loaded with a Co-Ba/CeO₂ catalyst to crack the ammonia to hydrogen and nitrogen using in-house developed kinetics. A sensitivity analysis was conducted to investigate the effects of changing reactor temperatures, reactor dimensions and number of tubes on the conversion of ammonia to aid in the optimization of the reactor dimensions and operating conditions. For example, with 30 tubes, a 72% decrease in the reactor length was observed as the temperature increased from 550 °C to 600 °C at 30 bars.

An overall plant energy efficiency of 76% had been estimated. In efforts of further optimizing the overall process, different case studies were investigated for providing the required energy for ammonia cracking which is an endothermic reaction. For scenarios providing the heat requirement using ammonia, hydrogen, or a mixture of hydrogen and ammonia (40 %mol H₂ and 60 %mol NH₃) as the fuel, efficiencies of 63%, 58% and 59% respectively were estimated. An in-depth analysis has also been conducted to include the NO_x emissions for each case.

Keywords: Ammonia cracking, Blue Hydrogen, Kinetic modelling, Process optimization

INTRODUCTION

In efforts of shifting towards more sustainable and environmentally friendly sources of energy, the world is racing towards developing hydrogen production technologies that would be economically and environmentally friendly. Nevertheless, long-distance transportation of hydrogen remains a challenge [1]. In parallel, efforts are being devoted into optimizing and upscaling the process of ammonia decomposition to hydrogen, as it is one of the most promising hydrogen carriers, given ammonia's high hydrogen and zero-carbon content, which presents it as a viable solution for the transportation of hydrogen to remote locations [2]. Yet, the combustion of fossil fuels to facilitate the ammonia decomposition using an industrial-fired furnace emits greenhouse gases [3]. In a previous work done by Morlanes et al., [4] experimental and process simulation results proved that a CoCe catalyst (80/20) promoted with 0.5% Barium deemed to have a performance only 11% lower than that of a 3%Ru10%K catalyst on CaO, but is a much cheaper alternative. Lezcano et al. [5] utilized a microkinetic approach to further elucidate the role of the Barium promoter in a CoCe catalysts. As of now, only a few studies have been published in regards to optimizing a commercial scale ammonia cracking process. Chen et al. [6] conducted an optimization study for conversion of ammonia decomposition in a membrane reactor by varying the operating conditions [6]. In a previous study by Devkota et al. [7], the reactor optimization for such a process has been looked into with an objective of increasing the process efficiency and lowering the greenhouse gas emissions. They proposed that dividing a single catalytic bed into multi-bed with intermediate heating using 9% of the ammonia feed and the unreacted ammonia and waste hydrogen yields an optimal case scenario. The current study focuses on optimizing the reactor configuration and dimensions to reach the optimal conversion, and into increasing the efficiency and decreasing the environmental impact using a part of the ammonia feed and the produced hydrogen for firing in the burners.

MODEL DESCRIPTION

Aspen Plus V.12 has been used to develop a process model for cracking fresh ammonia feed. A stream of ammonia with 0.5 wt% of moisture is first dried, heated up to the feed temperature and cracked to hydrogen, using a catalytic reactor. Water wash is used to separate the residual ammonia and the

hydrogen is purified from impurities using a PSA, producing hydrogen of a purity up to 99.99%. Fig. 1 shows a simplified schematic of the overall process model.

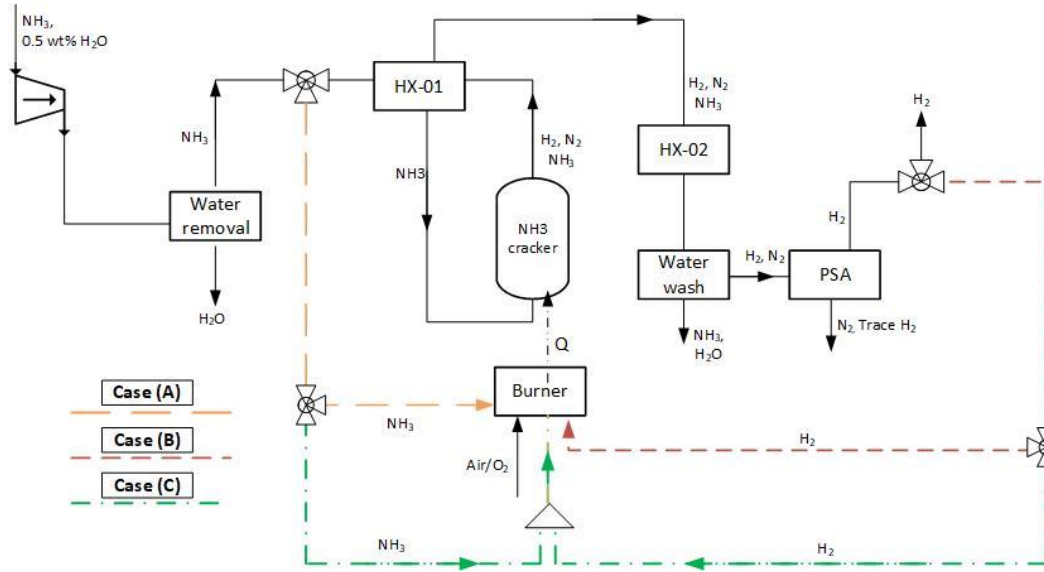


Figure 1. Schematic of the ammonia cracking process

A Temkin-Pyzhev type of kinetic rate expression described in Realpe et al. [8] based on a cobalt based catalyst, has been utilized, as presented in the following equations:

$$\Delta G_{rxn}^{\circ} = 95517 - 193.67T - 0.035293T^2 + (9.22 \times 10^{-6}T^3) \quad (1)$$

$$(-r_{NH_3}) = k_0 p_{NH_3}^a p_{H_2}^b \times \left(1 - \frac{1}{K_{eq}} \times \frac{p_{H_2}^3 p_{N_2}}{p_{NH_3}^2} \right) \quad (2)$$

A standard multi-tubular reactor averages between 20 to 400 tubes, with a length between 6 to 12 meters [9]. In this work, the effect of temperature on the conversion profile along the reactor was studied, with temperatures ranging from 500 – 600 °C. Moreover, the effect of number of tubes within the reactor at each temperature on the conversion of ammonia was also studied with an objective to minimize the number and length of required tubes for a targeted conversion of ammonia. For all cases studied, a reactor tube diameter of 101.6 mm was considered. Furthermore, given that the ammonia cracking reaction is significantly endothermic, efforts were devoted to process optimization to maximize the energy efficiency and minimize NO_x emissions. For this, three main cases were looked into:

- Case (a): burning a fraction of ammonia from the inlet stream.
- Case (b): burning a fraction of the produced hydrogen
- Case (c): utilizing a mixture of the fed ammonia and the produced hydrogen

The scenarios studied in this paper are summarized in table 1. Energy efficiency for the process was estimated using the process efficiency equation, as shown in Eqn. (3).

$$Energy\ Efficiency = \frac{\dot{m}_{H_2,product} * LHV}{(\dot{m}_{NH_3,input} * LHV) + P_{in}} \quad (3)$$

The efficiency calculation considers all equipment in the described process. For scenario (c), a sensitivity study was conducted for various compositions of hydrogen and ammonia in the fuel mixture to the furnace for the efficiencies and NO_x emissions. In the furnace combustion reactions, the default option of having either NO or NO₂ only and not both simultaneously as a side product, had been considered. For the combustion process, a case with air was compared against burning with pure oxygen. In the efficiency calculations, the energy requirement for generating the pure oxygen from air using a PSA was considered, with an energy requirement of 51.3 kWh per ton of pure oxygen produced [10]. The term P_{in} includes the energy required for the compressors, separators, columns and PSA to separate hydrogen from impurities.

Table 1. Summary of the case scenarios studied in this paper.

Reactor Optimization				
Scenario	Case	Varied variables	Fixed variables	Objective functions
Reactor Optimization	Optimizing the number of tubes of the reactor required	- Number of tubes: 30 – 100 tubes - Temperature: 500 – 600 °C	- Pressure: 30 bars - Feed flowrate of ammonia	Maximizing ammonia conversion and minimizing number and length of tubes required.
	Optimizing the length of the tubes required	- Length of tubes: 0.1 – 11 meters - Temperature: 500 – 600 °C		
Process Optimization				
Case	Sub-case	Burner feed	Dependent variables	
A	A.1	- NH ₃ from inlet feed - Air	Maximizing process efficiency and minimizing NOx emitted/H ₂ produced (gNOx/gH ₂)	
	A.2	- NH ₃ from inlet feed - Oxygen		
B	B.1	- Produced H ₂ - Air		
	B.2	- Produced H ₂ - Oxygen		
C	C.1	- NH ₃ + H ₂ - Air		
	C.2	- NH ₃ + H ₂ - Oxygen		

RESULTS AND DISCUSSION

Reactor optimization:

For this study, the reactor length was varied from 3 to 11 meters, and operating at 3 temperatures of 500, 550 and 600 °C. As shown in Fig. 2, at 550 °C, a higher number of tubes results to a higher conversion at the initial lengths of the reactor itself, leading to a shorter length of the reactor. As an example, with 50 reactor tubes, about 95.7% ammonia conversion is obtained with 5.3 meters of the reactor length. With 30 tubes, the same conversion requires 7.6 meters of reactor tube length.

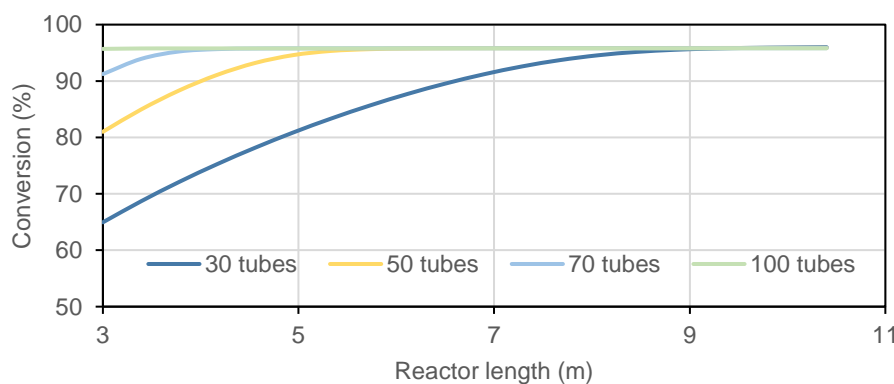


Figure 2. Conversion of ammonia at different lengths of the reactor for varying number of tubes at 550 °C and 30 bars.

Given the endothermic nature of the reaction, the reaction conversion is enhanced at higher temperatures. Another analysis was conducted with only 30 tubes of the reactor, at a constant temperature of 600 °C. As shown in Fig. 3, within only 3 meters of the reactor, 97.3% of ammonia is converted into hydrogen. This showcases the ability to optimize the overall process of ammonia cracking by mainly optimizing the reactor itself into what would be sufficient to obtain the targeted conversion.

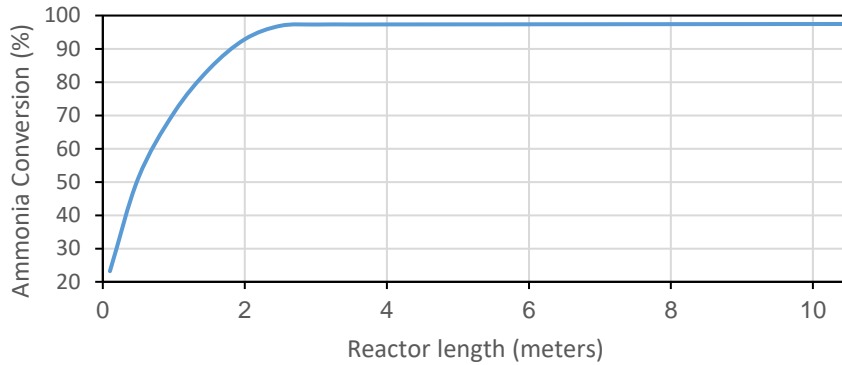


Figure 3. Ammonia conversion profile at 600 °C and 30 bars with 30 tubes of the reactor.

Process optimization:

As described earlier, three cases are considered for process optimization that include utilizing the ammonia from the feed in the burner, hydrogen from the produced outlet, and a mixture of both to produce the energy required for the ammonia cracking process. For all cases, the efficiency, NO_x emissions, and quantity of hydrogen produced were analysed. The process was maintained at 600 °C and 30 bars, for all the studied scenarios. For the case of using a part of pure ammonia from the inlet feed as the combustion fuel, an efficiency of 63% was achieved. For a case of using pure hydrogen from the product stream as fuel, an efficiency of 58% was achieved. Lastly, while using a mixed stream of various proportions of ammonia and hydrogen as combustion fuel, efficiencies up to 71% were obtained.

A parametric study was done for various combinations of combustion fuel as defined by case (c). Scenarios were also included for burning this fuel mixture with air or pure oxygen. As shown in Fig. 4, the efficiency is higher when pure oxygen is used as a feed compared to the cases of using air, which can be attributed to the energy utilized to heat up the inert nitrogen present in the air. The plot in Fig. 4 demonstrates the efficiency with varied amounts of hydrogen in the fuel mix to the burner. For all different compositions of the fuel mixture, increasing hydrogen fraction in fuel mixture increases the efficiency of the overall process.

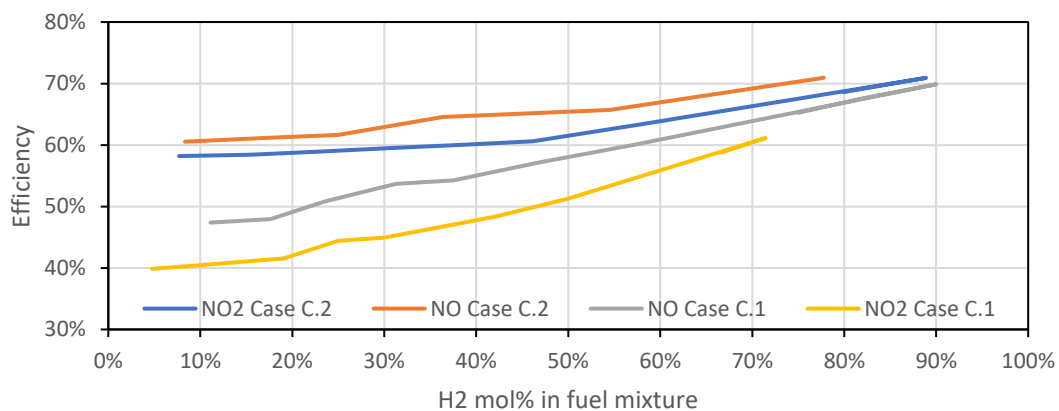


Figure 4. Overall process efficiency for different compositions of hydrogen and ammonia in fuel at 600 °C and 30 bars.

An analysis was conducted for the overall yield of hydrogen based on the total ammonia fed to the process, which also includes the ammonia used for combustion fuel. As shown in Fig. 5, overall hydrogen yield increases for pure oxygen versus air for the fuel combustion. This yield also increases with increase in the fraction of hydrogen in the fuel mixture.

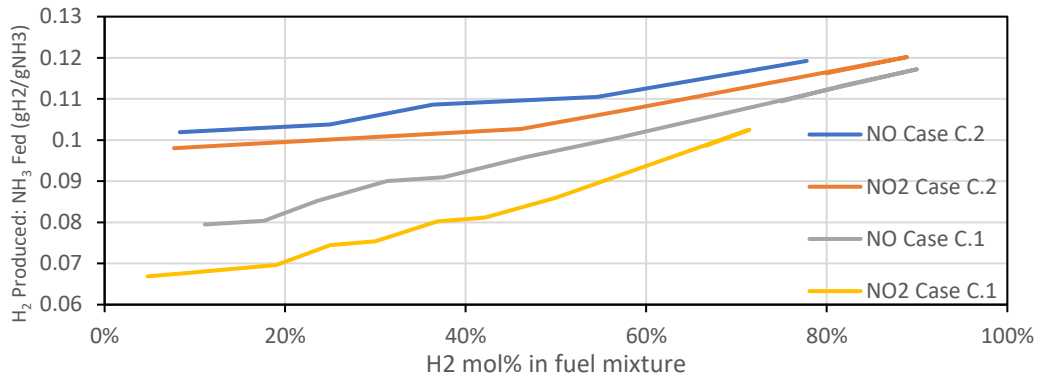


Figure 5. Effect of H₂ mol% on the ratio of hydrogen produced to ammonia fed at 600 °C and 30 bars.

An analysis of the amount of NO_x emissions in the flue gas per amount of hydrogen produced from the process is depicted in Fig. 6. Lower NO_x emissions were observed while using pure oxygen in the burners, compared to cases using air for fuel combustion. For instance, for the case of pure oxygen at 8 mol% of Hydrogen and balance ammonia, the ratio of NO₂:H₂ is 0.16 gNO_x/gH₂. However, with air, and 10 mol% of hydrogen, this ratio increases to 0.37 gNO_x/gH₂, which corresponds to more than a 100% increase.

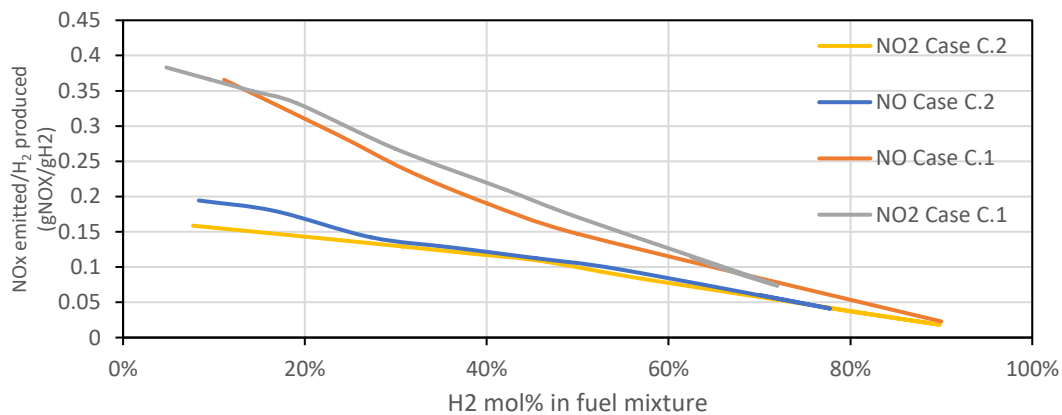


Figure 6. Ratio of NO_x emitted to H₂ produced at varying compositions of H₂ mol% at 600 °C and 30 bars.

CONCLUSIONS

This paper focused on the reactor optimization and process optimization of the ammonia cracking process to hydrogen. Reactor optimization deals with sensitivity studies with the number and length of tubes of the reactor to achieve a targeted conversion of ammonia. As an example, at 600°C, 30 tubes of 4-meter length yielded a 97.3% conversion of ammonia. This configuration was fixed for the overall process optimization. For the process optimization using this optimized reactor configuration, three main cases were studied, using pure ammonia or pure hydrogen, or a mixture in various proportions of ammonia and hydrogen. Among the scenarios studied, a fuel mixture comprising 90 mol% H₂ and 10 mol% NH₃ with pure oxygen demonstrated a comparatively high efficiency of 70%, a higher overall hydrogen yield and a lower NO_x emission per unit mass of hydrogen produced.

NOMENCLATURE

ΔG_{rxn}°	Gibbs free energy, kJ/mol
T	Temperature, K
k_0	Pre-exponential factor, mol/g.s.bar
p_i	Partial pressure of component i , bar
K_{eq}	Equilibrium constant
\dot{m}_i	mass flowrate of component i , kg/sec
LHV_i	Lower heating value of component i , MJ/kg
P_{in}	Total power requirement, MJ/sec

REFERENCES

1. Camel Makhloufi, Nouaamane Kezibri, Large-scale decomposition of green ammonia for pure hydrogen production, International Journal of Hydrogen Energy, Volume 46, Issue 70, 2021, Pages 34777-34787, ISSN 0360-3199, <https://doi.org/10.1016/j.ijhydene.2021.07.188>.
2. Zhijian Wan, Youkun Tao, Jing Shao, Yinghui Zhang, Hengzhi You, Ammonia as an effective hydrogen carrier and a clean fuel for solid oxide fuel cells, Energy Conversion and Management, Volume 228, 2021, 113729, ISSN 0196-8904, <https://doi.org/10.1016/j.enconman.2020.113729>.
3. Masato Tamura, Takahiro Gotou, Hiroki Ishii, Dirk Riechelmann, Experimental investigation of ammonia combustion in a bench scale 1.2 MW-thermal pulverised coal firing furnace, Applied Energy, Volume 277, 2020, 115580, ISSN 0306-2619, <https://doi.org/10.1016/j.apenergy.2020.115580>.
4. N. Morlanés , S. Sayas , G. Shterk , S. P. Katikaneni , A. Harale , B. Solami and J. Gascon , *Catal. Sci. Technol.*, 2021, **11** , 3014 —3024
5. Gontzal Lezcano, Natalia Realpe, Shekhar R. Kulkarni, Salvador Sayas, Jose Cerrillo, Natalia Morlanes, Hend O. Mohamed, Vijay K. Velisoju, Ragad F. Aldilajan, Sai P. Katikaneni, Mohammad Rakib, Bandar Solami, Jorge Gascon, Pedro Castaño. Unraveling the promoter role of Ba in Co–Ce catalysts for ammonia decomposition using microkinetic modeling, Chemical Engineering Journal, Volume 471, 2023, 144623, ISSN 1385-8947, <https://doi.org/10.1016/j.cej.2023.144623>.
6. Wei-Hsin Chen, Wei-Shan Chou, Rei-Yu Chein, Anh Tuan Hoang, Joon Ching Juan, Multiple-objective optimization on ammonia decomposition using membrane reactor, International Journal of Hydrogen Energy, 2023, ISSN 0360-3199, <https://doi.org/10.1016/j.ijhydene.2023.05.081>.
7. Sijan Devkota, Beom-Ju Shin, Ji-Hun Mun, Tae-Ha Kang, Hyung Chul Yoon, Shaukat Ali Mazari, Jong-Ho Moon, Process design and optimization of onsite hydrogen production from ammonia: Reactor design, energy saving and NOX control, Fuel, Volume 342, 2023, 127879, ISSN 0016-2361, <https://doi.org/10.1016/j.fuel.2023.127879>.
8. N. Realpe, S.R. Kulkarni, J.L. Cerrillo, N. Morlanés, G. Lezcano, S.P. Katikaneni, S. N. Paglieri, M. Rakib, B. Solami, J. Gascon, P. Castaño, Modeling-aided coupling of catalysts, conditions, membranes, and reactors for efficient hydrogen production from ammonia, React. Chem. Eng. 8 (2023) 989–1004, <https://doi.org/10.1039/D2RE00408A>.
9. Rostrup-Nielsen, J. R. Catalytic Steam Reforming. In Catalysis; Springer, 1984; pp 1–117.
10. Banaszkiwicz T, Chorowski M. Energy Consumption of Air-Separation Adsorption Methods. Entropy (Basel). 2018 Mar 28;20(4):232. doi: 10.3390/e20040232. PMID: 33265323; PMCID: PMC7512746.

ICH2P14-OP023

MEMBRANE REFORMER TECHNOLOGY FOR SUSTAINABLE HYDROGEN PRODUCTION FROM HYDROCARBON FEEDSTOCKS

*Alaa Albasry, Ahmed Naimi, Abdulbari Alqarni, Minseok Bae, Bandar Solami, *Stephen Paglieri, Aadesh Harale*

Carbon Management Division, R&D Center, Saudi Arabian Oil Company, Dhahran 31311, Saudi Arabia

*Corresponding author e-mail: stephen.paglieri@aramco.com

ABSTRACT

Hydrogen (H₂) is receiving growing interest as a clean energy carrier as the world's energy system transitions towards net zero. The International Energy Agency estimates that current global H₂ consumption will increase by > 200% to reach over 200 MMt annually by 2030. This increase will be accompanied by a significant rise in the demand for low-carbon H₂ from 10% in 2020 to 70% by 2030, and around half of this low-carbon H₂ will be derived from fossil fuels [1].

Today, H₂ is primarily produced from hydrocarbons using the steam methane reforming (SMR) process. This well-established method converts methane-rich gas into syngas, which is further treated with steam to increase H₂ yield via the water-gas-shift (WGS) process. However, this conventional route results in high carbon intensity of 10 tons CO₂ / ton of H₂. Therefore, there is a growing need for sustainable H₂ production technologies that utilize existing fossil energy sources and infrastructure while minimizing carbon emissions and costs.

This paper gives an overview of the work conducted by Saudi Aramco's Research and Development Center to develop membrane reactor (MR) technology as a promising method for sustainable H₂ production from hydrocarbons. A H₂-selective palladium-alloy (Pd-Au) membrane is integrated within the catalyst bed, creating a system where H₂ production and separation occur simultaneously in a single unit. This integration offers several advantages over the conventional system. Process intensification allows overcoming thermodynamic equilibrium conversion limitations while producing high purity (>99%) H₂ at milder operating temperatures of ~ 550 °C compared to 850 °C in conventional packed bed reactors. Downstream processes such as WGS reactors and pressure swing adsorption are eliminated, resulting in reduced capital and operating costs. Moreover, the by-product stream is pressurized at 25-40 bar and contains CO₂ at concentrations above 60%, enabling CO₂ capture at reduced costs by as much as \$15 per ton.

Keywords: Hydrogen production, steam methane reforming, palladium alloy membrane, membrane reactor.

INTRODUCTION

The world faces the challenge of finding sustainable and affordable energy sources to meet the ever-growing energy demand while achieving net zero goals. Hydrogen (H₂) is one of the potential solutions to this challenge and is envisioned to play an essential role in the future's energy mix. H₂ can be derived from various renewable and non-renewable sources such as water and fossil fuels, respectively, through different processes. However, due to its commercial maturity and higher efficiency, steam methane reforming (SMR) is recognized as the predominant industrial process for H₂ production [2]. In the SMR process, methane (CH₄) and steam are reacted under harsh conditions (800-1000 °C and 14-20 bar) in packed bed catalytic reactors to produce H₂ and CO as shown in Eq. 1:



This is followed by two stages of water-gas shift (WGS) processes to enhance H₂ yield by converting CO to CO₂ as per the following reaction:



Typically, processes such as pressure swing adsorption (PSA) and methanation are used downstream of the WGS reactors to separate and purify H₂ from carbon oxides [3].

Although this route is industrially mature, research is still ongoing in various aspects of the process to minimize the CO₂ emissions associated with H₂ production (10 tons of CO₂ per ton of H₂), to truly harness the potential benefits of H₂ as a sustainable energy carrier.

The reforming reactor configuration is one of the research areas where many efforts have been realized to achieve more sustainable production alternatives. In particular, the development of palladium (Pd)-based membrane reactors (MR) has gained significant attention in recent years. The MR consists of a fixed-bed catalytic reactor housing an integrated Pd perm-selective membrane to facilitate H₂ separation as it is being produced. In such reactors, the three main steps of the conventional SMR process, namely reforming, WGS, and H₂ separation are performed in a single unit. This results in process optimization in terms of the amount and size of equipment needed and associated capital expenditure. By removing H₂ in-situ, greater CH₄ conversions beyond the thermodynamic equilibrium can be achieved at milder conditions such as lower temperatures and less steam content [4, 5, 6]. Moreover, because the separation is driven by pressure, the CO₂ stream produced by the reactor is concentrated and at high pressure, allowing for carbon capture at reduced costs given that several stages of CO₂ purification and compression would be avoided [7, 5].

Several studies demonstrated both experimentally and numerically the achievable benefits from using MRs over conventional reactors (CR). Lin et al. [8] demonstrated the equilibrium shift in CH₄ conversions when integrating a 20 μm thick supported Pd membrane in the reactor. They showed that CH₄ conversions above 80% were realizable at 500°C and 9 bar in the Pd-based MR, whereas a temperature of 850°C was needed to achieve the same conversion levels in a CR. Sheu et al. [3] conducted a numerical evaluation of the performance of a Pd-Ru MR for SMR in terms of CH₄ conversion and H₂ recovery at different operating parameters; 96.5% conversion and near complete H₂ recovery was obtained at 550°C and 3.5 bar. Castro-Dominguez et al [9] evaluated the performance of a Pd-Au MR packed with two layers of SMR and WGS catalysts in series. They demonstrated that the dual catalyst MR configuration achieved 43% CH₄ conversions at 475°C and 5 bar while maintaining reduced CO content in the retentate as a result of the WGS catalyst addition. Barbieri et al. [10] presented a comprehensive analysis of a Pd-based MR used for SMR and discussed how the use of a MR improved the overall process performance. Moreover, Sweeney et al. [11] performed an economic analysis of an industrial scale SMR process with a Pd-based MR, and their results showed that using an optimized MR process offered reductions in natural gas consumption and overall annual costs even with the high capital costs usually associated with Pd membranes. In this work, the focus is placed on demonstrating the MR technology using different hydrocarbon feedstocks, namely CH₄ and synthetic pre-reformed naphtha (PRN), and assessing the performance of a Pd based MR at industrially relevant operating conditions to further understand its behaviour and the realizable advantages.

EXPERIMENTAL

A composite Pd-Au membrane supported on a symmetric porous alumina ceramic tube (CoorsTek) was obtained from TNO for the experimental tests, as shown in Figure 1. The membrane specifications reported by the manufacturer are summarized in Table 1.



Figure 1. Pd-Au membrane (before testing).

Table 1. Membrane specifications.

Parameter	Value
Effective length	15.1 cm
Outer diameter	1.4 cm
Thickness	5.67 μm (4.92 Pd μm + 0.75 μm Au)
Composition	19.7 wt.% Au
Active surface area	66.4 cm ²

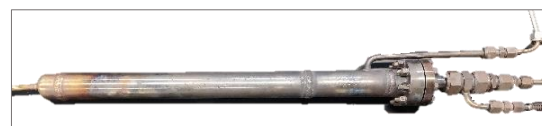


Figure 2. Membrane reactor module.

The Pd-Au membrane was placed in a tubular stainless-steel module (2.4 cm internal diameter), as shown in Figure 2. The annular space was packed with 64 cm³ (75.11 g) of a mixture of commercial catalysts (-12+20 mesh size); low-temperature SMR catalyst (R-88(R)-HEAT-X™) and high-temperature WGS catalyst (SK-501 Flex™) at a ratio of 3:1 by volume. Both catalysts were supplied by Topsøe.

The module was installed inside a vertical split four-zone electric furnace of a testing unit (AP Miniplant). A multipoint thermocouple was positioned inside the membrane near its centreline and kept at the testing temperature by regulating the furnace parameters. The gases used to make the simulated feed mixtures were CO, H₂, CH₄, CO₂, while N₂ was used as a trace gas for the gas chromatography (GC) analysis. The gas flowrates were controlled via mass flow controllers. Water was vaporized into steam in an evaporator unit before it was mixed with the other gases, and the flowrate of water was controlled by means of a high-pressure pump. The mixed stream was then heated to the set temperature in a pre-heater before it was fed to the catalyst bed of the MR. The permeate and retentate streams out of the reactor were passed through condensers to condense unreacted steam and remove any moisture. After that, with the aid of a backpressure regulator, a slip stream of the dry retentate or permeate was directed to an online GC (Agilent 7890A) for composition analysis, and GC readings were registered regularly every 15-20 minutes until reaching steady state. A sweep gas was not utilized in these tests. Alongside SMR testing, pure H₂ permeation tests were conducted periodically to monitor the performance and stability of the membrane. The permeation tests were conducted using 2500-3000 cm³ min⁻¹ (STP) pure H₂ feed at 550°C and 3 bar, while keeping the permeate side of the membrane at atmospheric pressure. The feed compositions and test conditions are shown in Table 2.

Table 2. SMR testing conditions for the membrane reactor.

Test	Feed	Steam to carbon ratio	Temperature (°C)	Pressure (bar)	GHSV (h ⁻¹)	Feed Composition (mol%)					
						CH ₄	H ₂ O	CO ₂	CO	H ₂	N ₂
Reforming	Methane (MN)	4	550	15 to 30 in 5 bar increments	976	18.4	73.4	-	-	5.8*	2.4
	Pre-reformed naphtha (PRN)**	2.6			1600	13.5	60.5	9.0	0.7	14.9	1.5
Permeation	H ₂	NA			3	NA	0	0	0	0	100

*A small amount of H₂ was fed to prevent oxidation of the catalyst.

** The synthetic PRN is based on the outlet composition of a pre-reformer reactor operated at 580°C and 15 bar.

RESULTS AND DISCUSSION

Methane Conversion

The performance of the Pd-Au MR for SMR was evaluated under the above conditions by analysing the CH₄ conversion, H₂ purity and flux, and CO₂ concentration in the retentate. CH₄ conversion, X_{CH_4} , was calculated as:

$$X_{CH_4} = \frac{F_{CH_4 in} - F_{CH_4 out}}{F_{CH_4 in}} \quad Eq. 3$$

Where $F_{CH_4 in}$ and $F_{CH_4 out}$ are the molar flowrates of CH₄ in the feed and retentate, respectively. Figure 3 shows the effect of the membrane on CH₄ conversions for both types of feed compositions tested at 550°C as a function of pressure, as well as the associated equilibrium conversions achievable in a CR calculated based on a simulation using AspenPlus.

The conversion enhancement is clearly seen in Figure 3. The conversions obtained in the MR exceeded the maximum conversions that can be attained in a CR at the same operating conditions, i.e. equilibrium conversions, for both feed types due to the continuous removal of H₂ through the membrane, which shifts the reforming reaction towards more products as per Le Chatelier's principle. In the case of MN feed, conversions as high as 91% were obtained at 30 bar, more than 5 times the equilibrium conversion in a CR at the same pressure (15.7%). With PRN feed however, the conversions achieved are lower than those with MN feed, as the maximum conversion achieved was approximately 65%. This is expected given that PRN feed contains more H₂ to begin with and the tests were run at a higher GHSV. Nonetheless, the enhancement in conversion is more prominent in the PRN case. For instance, at 15 bar, the conversion with the MN feed was 3.5x higher than the respective equilibrium conversion, while it was 25-fold greater for the PRN feed. Moreover, relatively high conversions were maintained between 52%-65% in the PRN case, whereas methanation of the synthetic PRN feed was expected to occur in a CR at pressures above 15 bar (indicated by the sub-zero conversions) as per the thermodynamic equilibrium calculations shown in Figure 3.

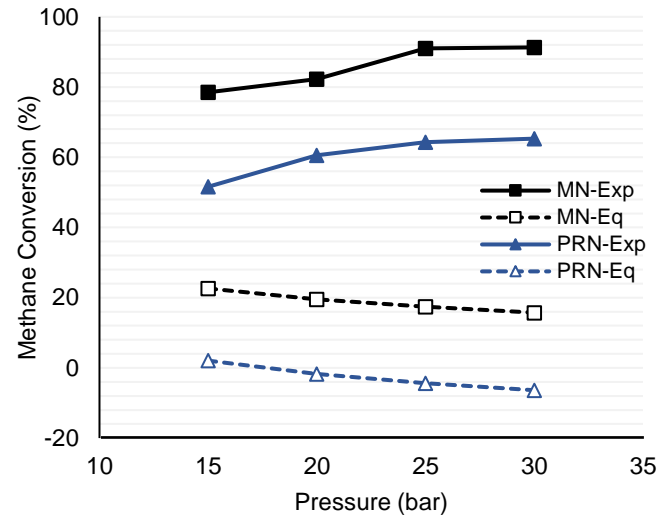


Figure 3. CH₄ conversion at 550°C as a function of feed pressure.

Furthermore, in contrast with the thermodynamic equilibrium trend, the conversion in the MR increased with increasing the pressure. This was due to the fact that H₂ permeation through the membrane is pressure-driven, hence resulting in greater H₂ recoveries that further shift the reaction towards more CH₄ conversion, which more than compensates for the decrease in conversion at higher pressures due to thermodynamics.

Hydrogen Purity

Figure 4 shows the H₂ purity achieved based on the molar composition of the permeate stream for each feed case at different pressures. The H₂ purity remained at high levels throughout in both cases with purities as high as 99.2% achieved at 15 bar. However, purity levels fell to ~98.7% as pressure increased to 30 bar. This slight reduction is attributed to the pressure-promoted permeation of non-selective species, such as CO₂ and CH₄ through small defects in the membrane layer [12]. So even though higher pressures are desirable for achieving greater H₂ recoveries and CH₄ conversions, the pressure needs to be optimized to ensure that the H₂ purity is not compromised too much.

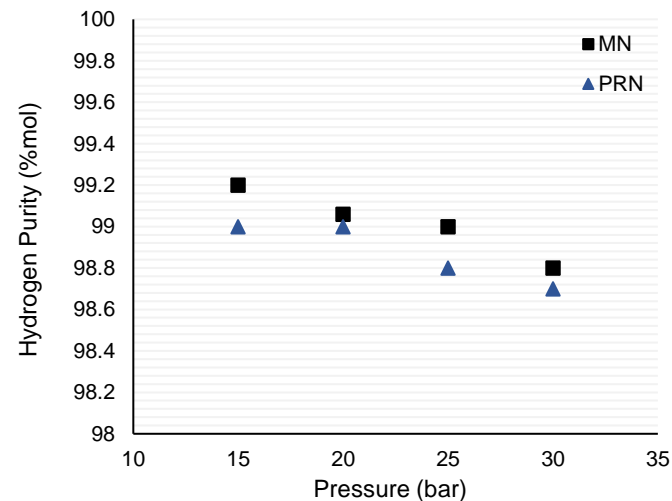


Figure 4. Purity of hydrogen produced in the MR at 550°C as a function of reaction pressure.

Hydrogen Flux

The H₂ flux was measured periodically at 500-550°C and 3 bar in between the reforming runs using pure H₂ feed. The flux remained relatively stable between 0.15 and 0.165 mol m⁻² s⁻¹ over the course of daily MR tests for more than 400 hours on stream with no measurable loss of permeation as shown in Figure 5, indicating the high stability of the membrane under the conditions tested.

CO₂ concentration

The concentrations of CO₂ in the retentate stream as well as the equilibrium concentrations at the same operating conditions are depicted in Figure 6. It can be clearly seen that with MR technology, the by-product stream contains higher concentrations of CO₂ than what would be achievable in a CR, as per the equilibrium calculations. The CO₂ concentration increased with pressure in the MR, which is in alignment with the same trend followed by the CH₄ conversion in the MR (Figure 3), as expected. The highest concentrations of nearly 76% and 60% CO₂ were reached at 30 bar for MN and PRN feeds, respectively, whereas only 8% and 24% CO₂ would be achieved in the CR at equilibrium. This would enable integration of carbon capture at lower associated cost and energy penalty as discussed previously.

CONCLUSIONS

The results of lab-scale testing of MR technology for SMR were presented and discussed. The tests were carried out using a Pd-Au composite membrane and a 3:1 mixture of SMR and WGS commercial catalysts in the MR. MN and PRN feeds were reformed at 550°C and pressures ranging from 10 to 30 bar. The results showed that the MR exhibited excellent performance in terms of CH₄ conversion and H₂ production and purity. Relatively high CH₄ conversions of 91% and 65% were achieved at 30 bars with MN and PRN feeds, respectively, with H₂ purity exceeding 98.5% over the course of testing. Therefore, this showcases both the potential and flexibility of MR technology for sustainable H₂ production from different hydrocarbon feedstocks in comparison to the thermodynamically-limited conventional packed-bed catalytic reactor process setup. This lab-scale demonstration constitutes a part of the efforts carried out in Saudi Aramco's Research and Development Center with the aim to ultimately deploy this technology at an industrial scale.

ACKNOWLEDGEMENT

The financial support of Saudi Aramco for this project is gratefully acknowledged. The authors would also like to thank TNO for providing the membrane and Topsøe for providing the SMR and WGS catalysts.

REFERENCES

- [1] IEA, "Net Zero by 2050," IEA, Paris, 2021, <https://www.iea.org/reports/net-zero-by-2050>, License: CC BY 4.0.
- [2] M. Abdollahi, J. Yu, P. K. Liu, R. Ciora, M. Sahimi and T. T. Tsotsis, "Ultra-pure hydrogen production from reformat mixtures using a palladium membrane reactor system," J of Membr Sci, vol. 390, pp. 32-42, 2012.

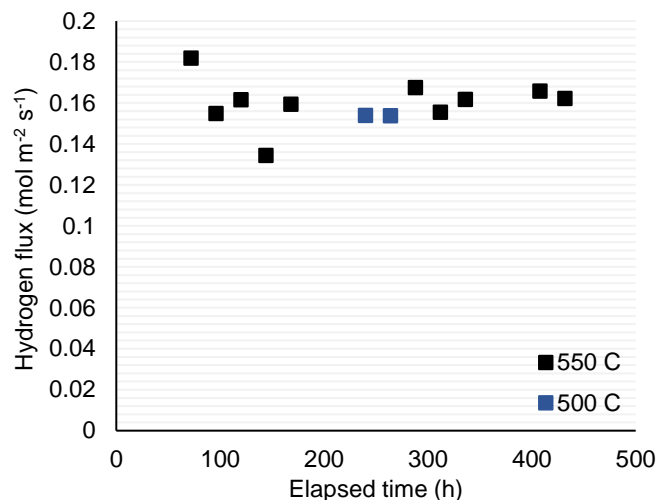


Figure 5. Hydrogen flux at 550°C and 3 bar over time.

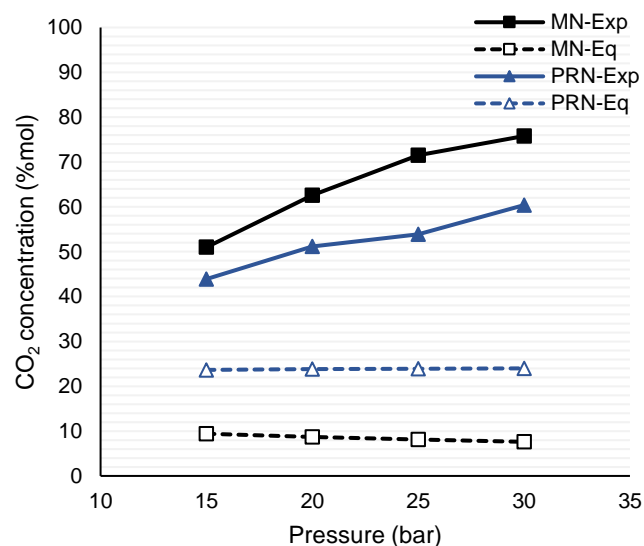


Figure 6. Concentration of CO₂ produced at 550°C in the retentate stream of a MR as a function of pressure.

- [3] W.-J. Sheu, Z.-W. Hsu, W.-H. Chen and Y.-C. Chen, "Investigation of steam methane reforming in a PdRu membrane reactor with a counter-current configuration," *Int J of Hydrogen Energy*, 2023.
- [4] M. A. Habib, A. Harale, S. Paglieri, F. S. Alrashed, A. Al-Sayoud, M. V. Rao, M. A. Nemitallah, S. Hossain, M. Hussien, A. Ali, M. A. Haque, A. Abuelyamen, M. R. Shakeel, E. M. A. Mokheimer, and R. Ben-Mansour "Palladium-Alloy Membrane Reactors for Fuel Reforming and Hydrogen Production: A Review," *Energy Fuels*, vol. 35, pp. 5558-5593, 2021.
- [5] T. Y. Amiri , K. Ghasemzageh and A. Iulianelli, "Membrane reactors for sustainable hydrogen production through steam reforming of hydrocarbons: A review," *Chemical Engineering and Processing - Process Intensification* , vol. 157, pp. 108148, 2020.
- [6] S. Tosti, "Overview of Pd-based membranes for producing pure hydrogen and state of art at ENEA laboratories," *International Journal of Hydrogen Energy*, vol. 35, no. 22, pp. 12650-12659, 2010.
- [7] E. Palo, A. Salladini, B. Morico, V. Palma, A. Ricca and G. Iaquaniello, "Application of Pd-Based Membrane Reactors: An Industrial Perspective," *Membranes*, vol. 8, no. 4, pp. 101, 2018.
- [8] Y.-M. Lin, S.-L. Liu , C.-H. Chuang and Y.-T. Chu, "Effect of incipient removal of hydrogen through palladium membrane on the conversion of methane steam reforming Experimental and modeling," *Catalysis Today*, vol. 82, pp. 127–139, 2003.
- [9] B. Castro-Dominguez, I. P. Mardilovich, L.-C. Ma, R. Ma, A. G. Dixon, N. K. Kazantzis and Y. H. Ma, "Integration of Methane Steam Reforming and Water," *Membranes* , vol. 6, no. 44, pp. 1-18, 2016.
- [10] G. Barbieri, G. Marigliano, G. Perri and E. Drioli, "Conversion-Temperature Diagram for a Palladium Membrane Reactor. Analysis of an Endothermic Reaction: Methane Steam Reforming," *Ind. Eng. Chem. Res.*, vol. 40, pp. 2017-2026, 2001.
- [11] D. M. Sweeney, V. Alves, S. Sakhai, S. Dinh and F. V. Lima, "Techno-economic Analysis and Optimization of Intensified, Large-Scale Hydrogen Production with Membrane Reactors," *Ind & Eng Chem Res*, vol. 62, no. 46, pp. 19740-19751, 2023.
- [12] P. Pinacci, M. Broglia, C. Valli, G. Capannelli and A. Comite , "Evaluation of the water gas shift reaction in a palladium membrane reactor," *Catalysis Today*, vol. 156, no. 3, pp. 165-172, 2010.

ICH2P14-OP25

THERMOELECTRIC CONDENSATION OF AMBIENT HUMIDIFIED AIR FOR GREEN HYDROGEN PRODUCTION

¹Hilal Ahmad, ²Taqi Ahmad Cheema, ³Hadeed Ahmed Sher

^{1,2}Faculty of Mechanical Engineering, Ghulam Ishaq Khan Institute of Engineering Sciences and Technology, Topi 23640, Pakistan

³Faculty of Electrical Engineering, Ghulam Ishaq Khan Institute of Engineering Sciences and Technology, Topi 23640, Pakistan

*Corresponding author e-mail: tacheema@giki.edu.pk

ABSTRACT

As the world moves towards decarbonization, green hydrogen produced using solar energy for alkaline electrolysis offers immense potential as a clean and green fuel. An innovative approach for green hydrogen production is condensing water vapor from moist air using thermoelectric coolers (TECs). The present study presents numerical modelling of a novel TEC-based condensation system, designed specifically for water production in remote locations with limited water resources. The system could facilitate solar-powered water generation for subsequent alkaline electrolysis to produce hydrogen under challenging environmental conditions, such as deserts, remote and arid regions, or hot and humid environments. Computational modelling reveals that parameter like air humidity, temperature difference, and flow rate impact important outcomes such as water condensation rate, efficiency, and energy needs. Moreover, the study explores the right balance between efficiently condensing a large volume of vapors using solar-powered TECs and minimizing electricity consumption to yield an optimal quantity of hydrogen through alkaline electrolysis. By optimizing carefully, the thermoelectric condensers seem to be a feasible alternative to move closer to cleaner fuel through a unique solar-powered process that turns humid air into hydrogen through efficient alkaline electrolysis, which is in line with global efforts to make the world more sustainable. The detailed and thoughtful modelling approach sets the groundwork for evaluating this new practical system designed for solar-powered water and hydrogen production using alkaline electrolysis in water-scarce regions.

Keywords: Green Hydrogen, Alkaline Electrolysis, Thermoelectric Cooler, Numerical Modelling, Ambient Humidified Air.

INTRODUCTION

Producing potable water for green hydrogen production in arid environments with scarce water resources poses a significant challenge and requires innovative solutions. Moist air condensation using solar powered Peltier modules presents a sustainable and cost-effective water resource for an alkaline electrolyzer. Researchers have explored various techniques for generating potable water, with atmospheric water generation emerging as a promising approach. Esfe et al. [1] numerically evaluated the effect of temperature reduction of TEC cold surface on the water production rate. And stated that condensation rate is directly related to cold surface temperature reduction. Alenezi et al. [2] numerically and experimentally investigated the impact of relative humidity on water generation using TEC. And observed that significant rise in water production was observed with increasing relative humidity. Eslami et al. [3] investigated the performance and optimization of TEC water production by finding optimum number of TEC and channel length at different temperature. Based on this study 26 ml/h of water extracted from air with minimal 20W electrical power at specific conditions. Jang et al. [4] studied the effect of temperature on stack efficiency and find out that minimizing temperature gradients across the stack substantially improves overall cell performance against constant current density and flowrate. Jesús Rodríguez and Ernesto Amores [5] investigated optimizing electrolyzer parameters and validated that high temperature, small electrode spacing, and concentrated electrolytes improved the overall performance aligning with experimental trends.

In the present study, a simulation-based study is carried out to numerically investigate a TEC moist air condensation optimization with electric current, air velocity, and humidity and alkaline electrolyzer to achieve the optimal quantity of water for green hydrogen production by minimizing electricity consumption in deserted, remote, and arid regions.

METHODOLOGY

The analysis of the TEC vapor condenser involved a commercial software to perform numerical analysis. The computational model has three domains, the Moist air domain, TEC domain and Alkaline electrolyzer domain as shown in Fig.1, which have an interface. The moist air domain consists of a 3D CAD model as shown on the right side of Fig.1 with dimensions of 4cm x 4cm x 4cm. while the TEC domain consists of TEC1-12706 with default dimensions. The electrolyzer cell consist of 2D model with dimensions of 0.8cm x 8.5cm with separator width (0.1cm). The TEC cold plate was coupled to a moist air domain to directly correlate applied current and condensation rate,

just like the real system. The bottom surface was the condenser and top were considered adiabatic. Ambient moist air entered at 308K and 80% RH. A saturated 100% RH was assumed on the cold surface for full moisture condensation. The moist air physics combined laminar flow, heat, and mass transport in a stationary study. A 2D (CFD) model of an alkaline electrolyzer cell includes the coupled physics of laminar flow, mass transport, and electrochemical reactions. The separator exchange OH⁻ ions. Butler-Volmer kinetics were implemented to relate overpotential to reaction rates for the hydrogen evolution and oxygen evolution half-cell reactions. Temperature-dependent physical properties were specified for the 8560mol/m³ KOH electrolyte along with binary diffusion coefficients. The mesh was refined near electrodes and membrane to ensure accuracy of gradients. Time dependent solutions were obtained for the electrolyte potential, polarization curve and concentration of continuous and dispersed phases.

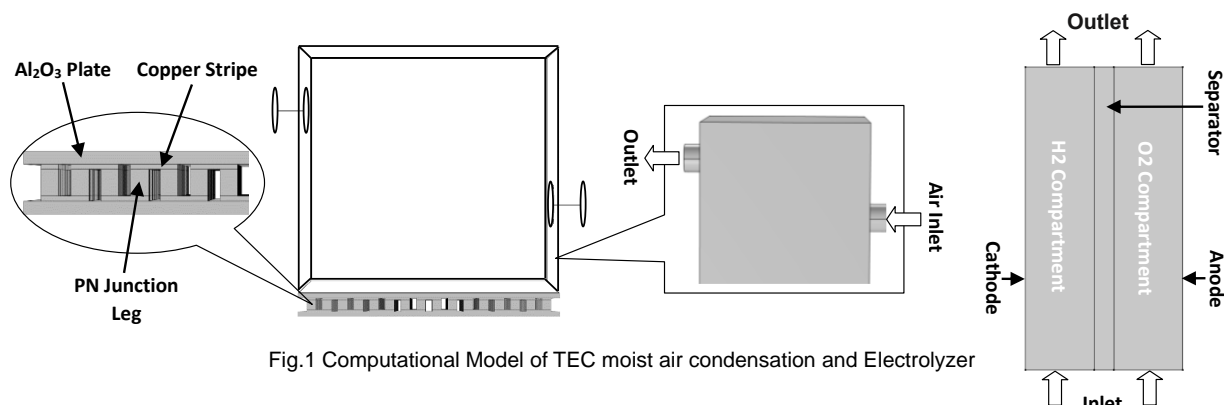


Fig.1 Computational Model of TEC moist air condensation and Electrolyzer

RESULT AND DISCUSSION

Fig. 6 shows that TEC cold face temperature approached 271.67K indicating effective Peltier cooling at 3.0A. Inlet air velocity distribution as shown in Fig. 2 demonstrate a uniform flow over the cold surface helping in longer contact of air with cold surface. Fig. 3 shows the temperature gradient in the moist air domain declining towards the cold plate. The relative humidity distribution exhibits a gradient increasing towards the cold plate, reaching a saturated value of 1.0 where air condenses vapor upon contact with the cold surface as shown in Fig. 4. Similarly increasing air velocities increases condensation, while excessive velocity reverses it. Also increasing absolute humidity from 70% to 85% directly related to condensation rates by increasing the moisture content in the inlet air as shown in Fig. 7. The normalized condensation rate showed a peak of 0.478 kg/m².h by reducing cold side temperature from 300K to 271.6K at constant humidity as shown in Fig. 7. The volume fraction gradient shows that gases produced near the electrode form a curtain type profile increasing the vertical volume fraction due to gases accumulation as shown in Fig. 5. Finally, Fig 8. shows the H₂ evolution rate at cathode with 0.133 kg/m².h H₂. Overall, this model provided the coupled heat and mass transport physics governing the condensation as well as electrolysis process.

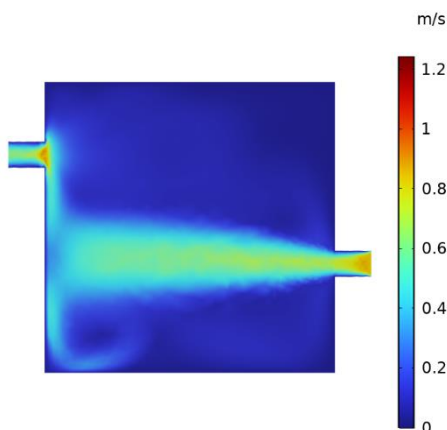


Fig 2. Velocity gradient of moist air domain at mid plane

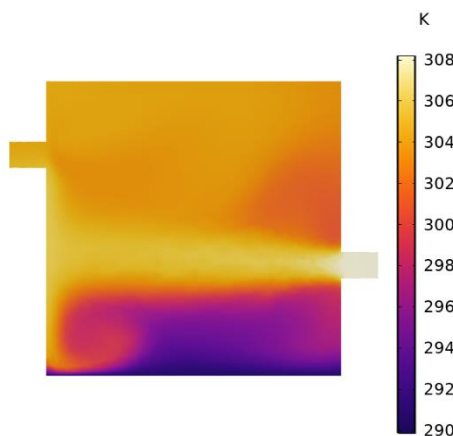


Fig 3. Temperature gradient of moist air domain at mid plane

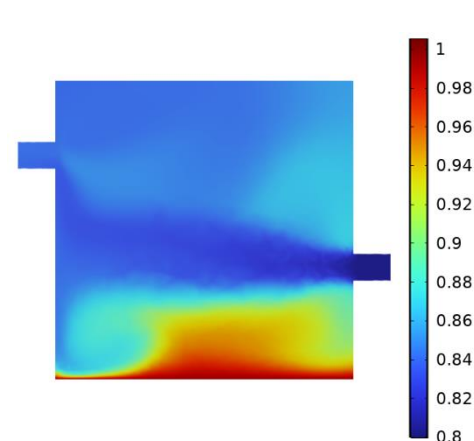


Fig 4. Relative Humidity gradient of moist air domain at mid plane

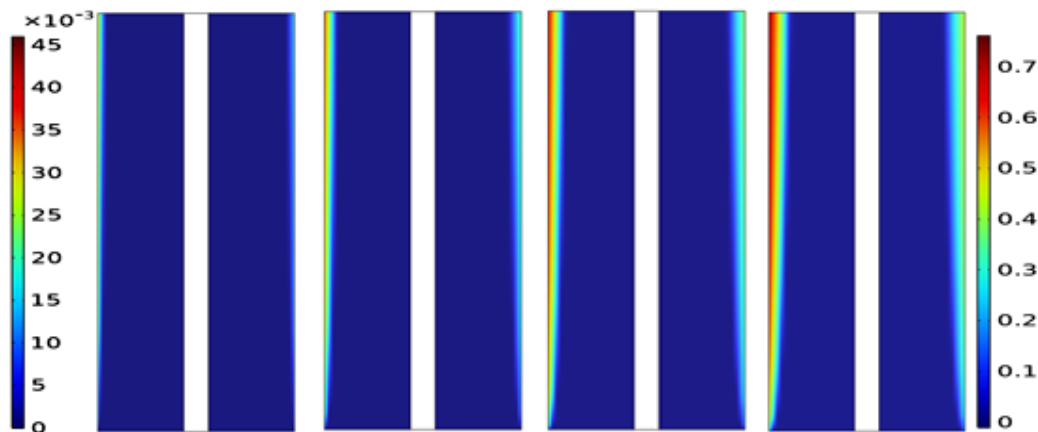


Fig 5. Volume Fraction gradient in H₂ and O₂ compartments at different current density values (model conditions: 70 deg C, 33 wt% KOH, and 0.1 m/s)

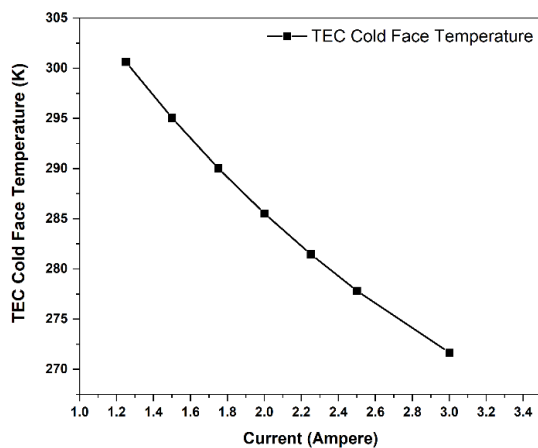


Fig 6. TEC cold face Temperature at different current input

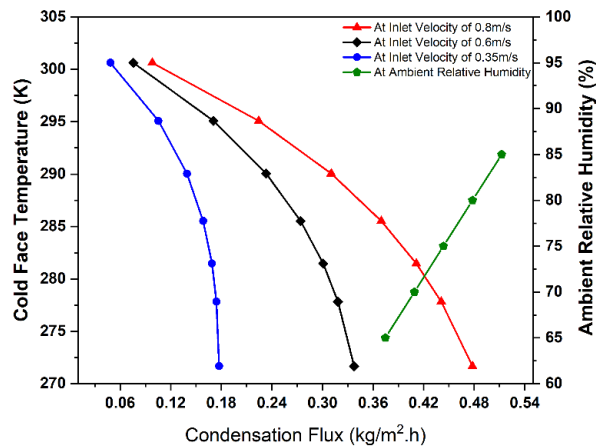


Fig 7. Amount of water vapor condensation with varying TEC cold plate temperature

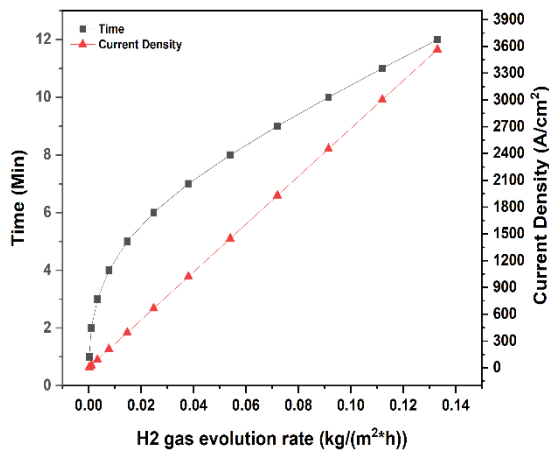


Fig 8. Hydrogen Evolution flux at different time and current density values

CONCLUSION

In this study a 3D numerical model of TEC moist air condensation and 2D model of alkaline electrolyzer cell were simulated. The model incorporated heat and mass transport, air flow dynamics, linearly coupled with thermoelectric effects, and electrochemical reactions. Systematic parametric simulations were conducted to study the impacts of electric current, air velocity, and relative humidity on the water condensation rate. It is concluded that:



- Increasing current enhances cooling by reaching 271.67K at 3A. Similarly increasing air velocities increases condensation, while excessive velocity reverses it. Increased humidity at 308K amplified condensate flux to 0.512kg/m².h at 85% humidity.
- It is observed that the hydrogen evolution rate at the cathode reached a maximum of 0.133 kg/m².h during electrolysis process.

REFERENCES

1. Hemmat Esfe, Mohammad, Saeed Esfandeh, and Davood Toghraie. 2021. "Numerical Simulation of Water Production from Humid Air for Khuzestan Province: Investigation of the Peltier Effect (Thermoelectric Cooling System) on Water Production Rate." *Case Studies in Thermal Engineering* 28: 101473.
2. Anwur Alenezi, Hyung-ho Jung, and Yousef Alabaiadly. 2023. "Experimental and Numerical Analysis of an Atmospheric Water Harvester Using a Thermoelectric Cooler." *Atmosphere* 2023, 14(2), 276.
3. M. Eslami, M. Eslami, Eslami, M.R, Tajeddini, F, Etaati, N, 2018. "Thermal Analysis and Optimization of a System for Water Harvesting from Humid Air Using Thermoelectric Coolers." *Energy Conversion and Management* 174: 417–29.
4. Rodríguez, Jesús, and Ernesto Amores. 2020. "CFD Modeling and Experimental Validation of an Alkaline Water Electrolysis Cell for Hydrogen Production." *Processes* 8(12): 1634.
5. Jang, Dohyung et al. 2021. "Numerical Modeling and Analysis of the Temperature Effect on the Performance of an Alkaline Water Electrolysis System." *Journal of Power Sources* 506: 230106.

ICH2P14-OP027

TRANSPORTATION AND STORAGE OF HYDROGEN BY LOHC: DESIGN AND SIMULATION OF THE DEHYDROGENATION REACTOR

¹Pietro Delogu, ²Elena Barbera, ^{3,5}Andrea Mio, ^{2,4}Alberto Bertuccio, ^{3,5*}Maurizio Fermeglia

¹SERICHEM, Italy

²Department of Industrial Engineering (DII), University of Padova, Italy

³Department of Engineering and Architecture (DIA), University of Trieste, Italy

⁴Centro Studi "Levi Cases" for Energy Economics and Technology, University of Padova, Italy

⁵Center for Energy, Environment and Transport Giacomo Ciamician, University of Trieste, Italy

*Corresponding author e-mail: maurizio.fermeglia@units.it

ABSTRACT

Long-distance transport and long-term storage of hydrogen can be realized with Liquid Organic Hydrogen Carriers (LOHC) based on a two-step cycle: (1) hydrogenation of the LOHC molecule (i.e., hydrogen is covalently bound to the LOHC) and (2) dehydrogenation after transport and/or storage. Since the (optimal) LOHC is liquid at ambient conditions and shows similar properties to crude oil-based liquids (e.g. diesel and gasoline), its handling and storage is realized by well-known processes; thus, a stepwise adaptation of the existing crude oil-based infrastructure is technically possible. LOHC show economic advantages compared to compressed hydrogen and liquid hydrogen for long-term storage/long distance transport applications. The energetic efficiency of the systems depends on the dehydrogenation step. In this paper we will consider the details of thermodynamic and kinetic fundamentals of hydrogenation and dehydrogenation of a typical LOHC, namely Perhydro-Dibenzyl-Toluene. The fundamental chemical equilibrium expressions as a function of temperature and the catalytic kinetic expression for the reaction rate at different conditions are evaluated for the design of a dehydrogenation Continuous Stirred Tank Reactor. A process simulator (Aspen Plus v.14.1™) is used to simulate the reactor at different operating conditions, focusing on the dynamic response of the reactor to any change in temperature, pressure, and inlet flow rate. The results obtained from the steady state simulation show a good agreement with experimental literature data. The results from dynamic simulation show that the time response of the reactor is compatible with the hydrogen production variations needed by fuel cells used for transportation.

Keywords: LOHC, dehydrogenation, CSTR, dynamics.

INTRODUCTION

Liquid organic hydrogen carriers (LOHCs) have gathered a lot of attention in recent years as a promising solution for the efficient, economical, and safe storage and transport of hydrogen. In LOHC systems, catalytic hydrogenation bonds hydrogen to an organic carrier molecule to create a hydrogen-rich storage liquid that resembles a fuel. The latter may be handled and transported using the petroleum infrastructure now in place at room conditions. A catalytic dehydrogenation process is then used for on-demand hydrogen release at the time and place of energy or hydrogen request.

Among the possible LOHC molecules, the dibenzyl toluene (H0-DBT) and the perhydro-dibenzyl toluene (H18-DBT) have drawn a lot of attention. DBT is made up of many isomers in both its hydrogen-rich (HX-DBT) and hydrogen-lean (H0-DBT) forms. DBT has been used extensively as a heat transfer fluid since the 1960s [1-5]. A hydrogen capacity of up to 6.2 weight percent, or a volumetric hydrogen content of 56 gH₂/L, is provided by the LOHC system H0-DBT/H18-DBT [6]. LOHC, and particularly DBT, show economic advantages compared to compressed hydrogen (GH₂) and liquid hydrogen (LH) for long-term storage/long distance transport applications [4]. Hurskainen et al. [7] showed the advantages of using LOHC in terms of CAPEX and net H₂ payload with respect to GH₂ trailers and in terms of lifetime with respect to trucks (table 1).

An example of the possibility of LOHC-based hydrogen transport for future international commerce of chemically bonded hydrogen is a tanker ship of the Suezmax class that is loaded with H18-DBT. Based on the Lower Heating Value (LHV) of the chemically bonded hydrogen, its 150,000 metric tons of liquid load would thus contain 9,300 metric tons of hydrogen, or 309.9 GWh of energy [6,8]. This indicates that a feasible alternative for the future is LOHC-based transcontinental hydrogen trade from wind- or sun-rich regions to industrialized nations that today import a large amount of energy.

Table 1: Comparison of different H₂ carriers [7]: LOHC tanker trailer is 36000 l; GH₂ trailer is 2 x 200 bar steel bottle ISO20 containers; Advanced GH₂ trailer is ISO40 HC 350 bar composite.

	Truck	LOHC tanker trailer	GH ₂ trailer	Advanced GH ₂ trailer
Investment cost	180 k€	140 k€	530 k€	420 k€
Lifetime	1.5 million km or 8 years	15 years	15 years	15 years
Fixed O&M		4% of CAPEX	2% of CAPEX	2% of CAPEX
Net H₂ payload		2000 kg (1400 kg useable)	400 kg	900 kg
Unloading & loading time (LOHC)		1 h + 1 h		
Drop-off & pick-up time (GH₂)			1 h + 1 h	1h + 1 h

The introduction of global emission pricing [9] and growing electricity costs as well as an increase in the demand for electricity (for example, battery vehicle mobility) will make the import of LOHC-bound hydrogen appealing already in the short to medium term [4, 10, 11].

The development of the hydrogenation/dehydrogenation equilibrium and kinetic models of the H0-DBT/H18-DBT system is the focus of the current investigation. Understanding equilibrium and kinetic data is essential for sizing of the reversible hydrogenation/dehydrogenation processes. The energetic efficiency of the systems depends on the dehydrogenation step. [12]. With the obtained models, the simulation of a Continuous Stirred Tank Reactor (CSTR) for the dehydrogenation process is performed and finally some preliminary results for the dynamic behaviour of the CSTR are shown.

THE REACTION SCHEME

H0-DBT is hydrogenated via a sequential, step-by-step process [13]. One outer benzyl ring is hydrogenated to create H6-DBT in the first stage, and the second outer benzyl ring is hydrogenated to form H12-DBT in the second step. The middle ring is hydrogenated to generate H18-DBT in the last and rate-limiting hydrogenation step. The equivalent H6-DBT, H12-DBT, and H18-DBT fractions are made up of the appropriate isomers since H0-DBT is a combination of many of them. The reactions that take place in a catalytic hydrogenation/dehydrogenation reactor of perhydro dibenzyl toluene can be summarized, both from a kinetic and thermodynamic point of view, in three fundamental steps (Figure 1) [10].

Experimental determination of the hydrogenation/dehydrogenation equilibrium of the LOHC system H0/H18 dibenzyl toluene have been recently reported using innovative methods based on ¹³C-NMR and GC-FID. [14] There are three phases in the system: (1) catalytic solid adsorbing reagents and products.; (2) liquid phase consisting mainly of tricyclic compounds and solubilized hydrogen and (3) gaseous phase containing essentially hydrogen and tricyclic compounds as a function of their vapour pressure in relation to the composition of the liquid phase and temperature.

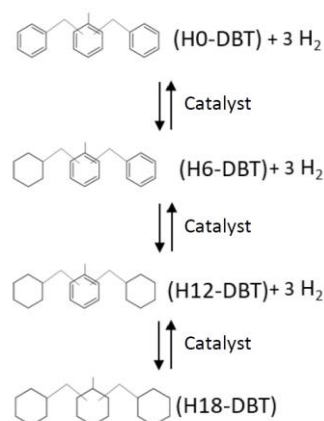


Figure 1: Proposed reaction scheme for hydrogenation of H0-DBT, and dehydrogenation of H18-DBT [10].

It can be assumed, as a first approximation, that phase and adsorption equilibria can be ideal. As a result, chemical equilibrium relationships for steps 1-3 can be represented by the following expressions:

$$K_3 = \frac{c_{L2}^e p_{H_2}^3}{c_{L3}^e}; K_2 = \frac{c_{L1}^e p_{H_2}^3}{c_{L2}^e}; K_1 = \frac{c_{L0}^e p_{H_2}^3}{c_{L1}^e} \quad \text{where } c_{Li}^e = \frac{n_{Li}^e}{V_{liq}} \text{ is the equilibrium liquid-phase molar concentrations of tricyclic compounds.}$$

The pressure of H₂ is given by the difference between the total pressure and the sum of the partial pressures of the tricyclics:

$$p_{H_2} = P_{tot} - \sum_i P_i^0(T) \frac{n_{Li}^e}{\sum_k n_{Lk}^e} \quad (1)$$

but for sake of simplicity, given the low vapour pressure of these components (about 0.1 bar at a temperature of 290 °C), in the following reference is made only to the hydrogen pressure.

The kinetics of each of the reactions taking place in the solid phase between the species adsorbed on the catalyst can be described by the following general equation, taking reaction 3 as an example:

$$r_3 \left[\frac{mol}{g_{cat}h} \right] = k_3 c_{cat} c_{L3} - k_{-3} c_{cat} c_{L2} p_{H_2}^q \quad (2)$$

and similar for reactions 1 and 2. The exponent q is the reaction order for hydrogen. Since the concentration of the catalyst appears in all equations with the same exponent, these can be simplified into the form:

$$r_3 \left[\frac{mol}{g_{cat}h} \right] = c_{cat} (k_3 c_{L3} - k_{-3} c_{L2} p_{H_2}^q) = \frac{m_{cat}}{V_{liq}} (k_3 c_{L3} - k_{-3} c_{L2} p_{H_2}^q) \quad (3)$$

The material balance of a CSTR reactor is then given by:

$$\frac{dn}{dt} = \underline{f} - \underline{u} + V_{liq} \underline{v}^T \underline{r} = \underline{0} \quad (4)$$

\underline{f} is the flow in and \underline{u} is the flow out of the CSTR. All variables are vectors. This form can be employed to all the specific reactions. As far as hydrogen is concerned, the overall equation is:

$$\frac{dn_{H_2}}{dt} = f_{H_2} - u_{H_2} + 3m_{cat} [(k_3 c_{L3} - k_{-3} c_{L2} p_{H_2}^q) + (k_2 c_{L2} - k_{-2} c_{L1} p_{H_2}^q) + (k_1 c_{L1} - k_{-1} c_{L0} p_{H_2}^q)] = 0 \quad (5)$$

Hydrogen pressure and hold-up are related to each other according to the volumes of the phases present in the reactor:

$$n_{H_2} = \frac{p_{H_2} V_{gas}}{RT} \quad (6)$$

Given the similarity of the liquid compounds present in the reactor, they can be assigned a density and an average molecular weight that are the same for all, so that it can be calculated from the volume of liquid N_{tot} , according to:

$$N_{tot} = \frac{V_{liq} \bar{p}}{PM} \quad (7)$$

while the total molar output flow rate must be equal to the sum of the feed flow rates:

$$U = \sum f_i \quad (8)$$

The closure constraint at 1 of the summation of molar fractions present in the liquid phase also applies.

Considering now the degree of freedom analysis, there are a total of 19 variables and 9 equations, so the system has 10 degrees of freedom. These can be saturated in various ways, but essentially the variables that could be fixed are: feed rates (5), the volumes of the 3 phases (3), H₂ pressure (1), and temperature (1), for a total of 10 variables. The parameters of the model consist of the 3 rate constants of the direct reactions, the 3 equilibrium constants for the inverse-reactions, and the hydrogen pressure exponent q . The estimation has been done starting from the experimental data of Dürr et al [14].

The temperature dependence of the equilibrium constants of the three reactions has been approximated by the equations:

$$K_i = \exp\left(-\frac{\Delta G_r(T)}{RT}\right) \quad (9)$$

$$\Delta G_r(T) = \frac{T}{T^0} \Delta G_r(T^0) + \Delta H_r(T^0) \left(1 - \frac{T}{T^0}\right) + \Delta C_p (T - T^0) - T \Delta C_p \ln \frac{T}{T^0} \quad (10)$$

whose adaptive parameters are $\Delta G_r(T^0)$, $\Delta H_r(T^0)$ and ΔC_p . Given the substantial identity of the 3 reactions involved in the model, a single value was used for $\Delta H_r(T^0)$ and ΔC_p , while a specific value of $\Delta G_{ri}(T^0)$ has been identified for each reaction. The reference temperature was 493 K. Figure 2 shows the comparison between experimental [14] and calculated degree of hydrogenation (DoH) data. It can be seen how the model developed is able to reproduce the available experimental trends and can therefore be used to describe the thermodynamics in the kinetic model of the reaction, thus minimizing the parameters to be optimized. The best estimation of the parameters of a kinetic model requires the availability of the evolution of the composition of the reactant system under conditions of constant temperature. Jorschick et al. [15] measured experimental data using a Pt on alumina catalyst (0.3% by weight) at a

single concentration of 3 g/100 g, at 30 bar absolute hydrogen pressure and temperatures between 201 and 311 °C. They measured the flow of hydrogen needed to maintain the pressure constant and calculated the degree of hydrogenation. Using the data of [14] combined with those of [15], we estimated the values of k_i and q .

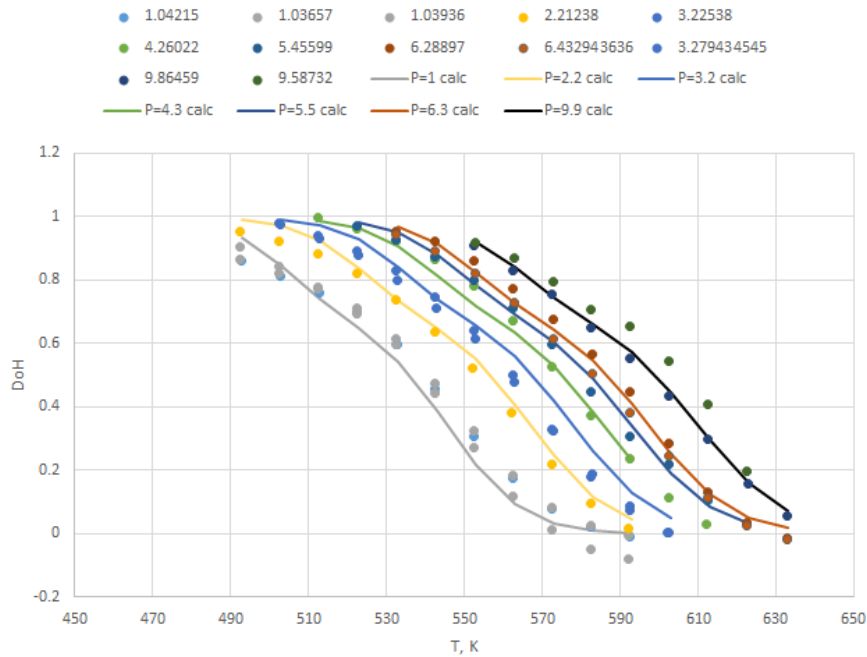


Figure 1: Comparison of experimental and calculated data for the degree of hydrogenation of DBT.

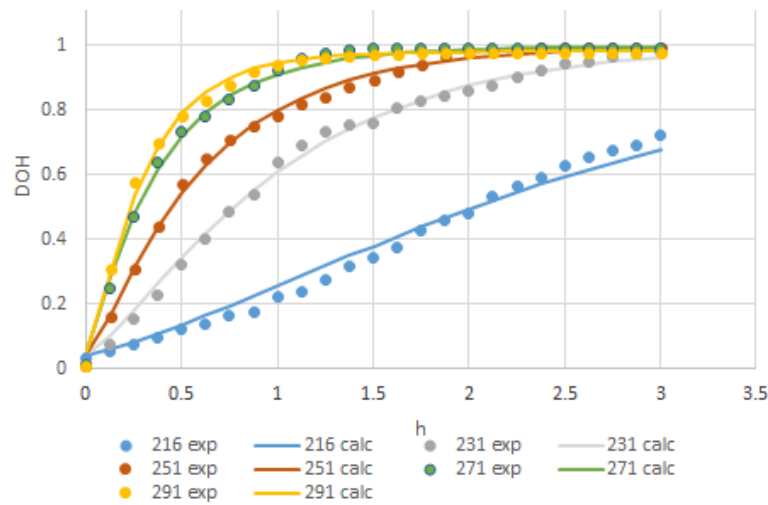


Figure 2: Comparison of experimental and calculated DoH data.

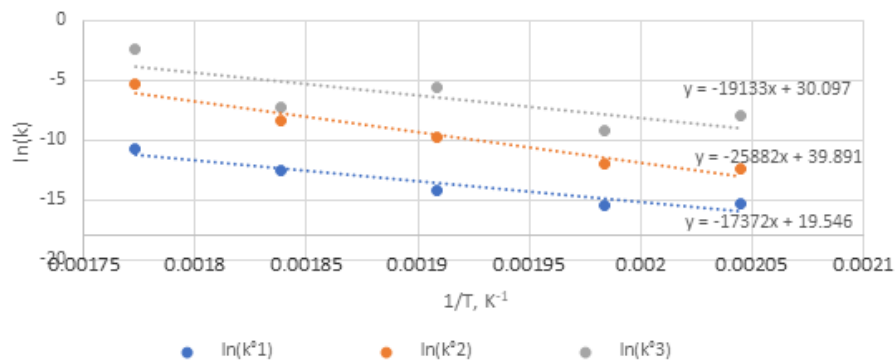


Figure 3: equilibrium constants ($\ln K$) versus $1/T$: comparison of calculated and experimental data.

Figure 3 shows the comparison between experimental values and calculated DoH curves obtained with the equilibrium and kinetic constant derived as reported above and implemented in a batch reactor of Aspen Plus v. 14.1™ process simulator..

The results obtained from the simulation show a good agreement with experimental literature data [14,15], thus allowing to state that the reactions implemented in Aspen Plus v. 14.1™ reliably describe the process of interest. The temperature dependence of the equilibrium constants for the 3 reactions is reported in figure 4, where the calculated values are compared with the experimental ones.

THE CSTR REACTOR PROCESS SIMULATION

The block flow diagram of the dehydrogenation process is shown in Figure 4.

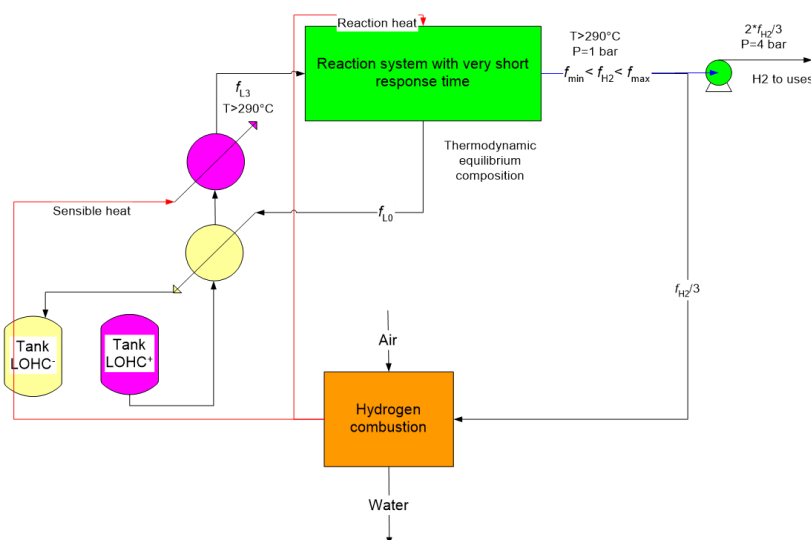


Figure 4: Diagram of operation of a hydrogen generator from LOHC

The output hydrogen pressure must be such that it can be fed to a fuel cell (around 4 atm). To obtain a high conversion at this pressure, it is necessary to operate at elevated temperatures, but not to exceed 300 °C, a temperature at which the decomposition reactions of dibenzyl toluene to volatile compounds become important. A temperature of 291 °C was used in the analysis. Consequently, it is necessary to supply the system with a quantity of heat equal to the sum of the sensible heat necessary to bring the temperature of the incoming flow up to 291 °C (minus the recovered heat) and the reaction heat. If the system is autonomous, this heat is generated by burning a portion of the hydrogen produced. From the data reported above, it is easy to calculate the heat needed to bring the temperature of one mole of LOHC from 25 to 291 °C, which is about 38 kcal. The CSTR model available in Aspen Plus v. 14.1™ was used to simulate the dehydrogenation reactions using the equilibrium and kinetic equations developed above.

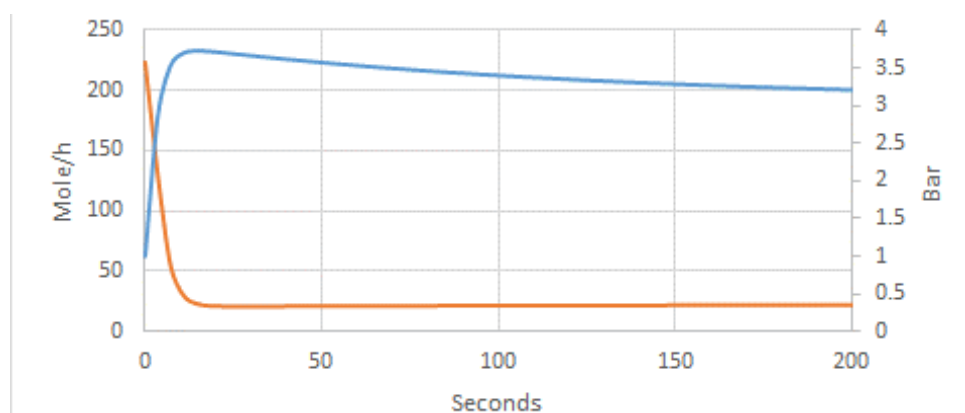


Figure 5: H2 flow rate (blue) and pressure initial changes (orange) as a function of time (s)

In addition, the transition dynamics between two different power demands of the CSTR reactor have been evaluated using differential equations. [16] The model calculates the time needed to reach the new steady state conditions starting from a reference steady state and the change in the composition of the liquid effluent, taken at the same total molar flow rate as the feed. The time to reach steady state is about 5 seconds. However, this only affects the internal conditions of the reactor, as both the LOHC supply and the hydrogen withdrawal are constant from the beginning of the variation.

In a first phase, the system produces more of the hydrogen withdrawn, and this leads to an increase in pressure; this is then compensated until the steady state is reached. As an example, figure 5 shows the hydrogen flow rate and pressure profiles as a function of time for a change in the hydrogen request from 10 kW to 100 kW.

CONCLUSIONS

The main result of this paper is the development of equilibrium and kinetic expressions and parameters from literature experimental data for describing hydrogenation and dehydrogenation of DBT LOHC. All chemical reactions occurring in the processes have been taken into account, including direct and reverse reactions. The expressions for the reactions' rate developed compare well with the experimental data of DoH. The reactions' rate expression have been used in the simulation of a steady state CSTR and for the dynamic simulation of a transient for the same CSTR.

REFERENCES

1. P. Preuster, C. Papp, P. Wasserscheid, *Liquid Organic Hydrogen Carriers (LOHCs): Toward a Hydrogen-free Hydrogen Economy*. Accounts of Chemical Research, 2017. **50**(1): p. 74-85.
2. K. Müller, Technologien zur Speicherung von Wasserstoff. Teil 1: Wasserstoffspeicherung im engeren Sinn. Chemie Ingenieur Technik, 2019.
3. P.M. Modisha, C.N.M. Ouma, R. Garidzirai, P. Wasserscheid, D. Bessarabov, The Prospect of Hydrogen Storage Using Liquid Organic Hydrogen Carriers. Energy & Fuels, 2019.
4. M. Niermann, S. Drünert, M. Kaltschmitt, K. Bonhoff, Liquid Organic Hydrogen Carrier (LOHC) – Techno-economic analysis of LOHCs in a defined process chain. Energy & Environmental Science, 2019.
5. P.T. Aakko-Saksa, C. Cook, J. Kiviaho, T. Repo, Liquid organic hydrogen carriers for transportation and storing of renewable energy—Review and discussion. Journal of Power Sources, 2018. **396**: p. 803-823.
6. N. Brückner, K. Obesser, A. Bösmann, D. Teichmann, W. Arlt, J. Dungs, P. Wasserscheid, Evaluation of Industrially Applied Heat-Transfer Fluids as Liquid Organic Hydrogen Carrier Systems. ChemSusChem, 2014. **7**(1): p. 229-235.
7. M. Hurskainen, J. Ihonen, "Techno-economic feasibility of road transport of hydrogen using liquid organic hydrogen carriers", International Journal of hydrogen energy, Vol. 45 (56), 2020, pagg. 32098-32112
8. Energie in Zahlen - Arbeit und Leistungen der AG Energiebilanzen, U.M. Hans-Joachim Ziesing, Michael Nickel et al., Editor. 2019, Arbeitsgemeinschaft Energiebilanzen e.V.: Berlin.
9. State and Trends of Carbon Pricing 2023, in © World Bank. <https://openknowledge.worldbank.org/items/58f2a409-9bb7-4ee6-899d-be47835c838f>
10. P. Runge, C. Sölch, J. Albert, P. Wasserscheid, G. Zöttl, V. Grimm, Economic comparison of different electric fuels for energy scenarios in 2035. Applied Energy, 2019. 233: p. 1078-1093.
11. D. Teichmann, W. Arlt, P. Wasserscheid, Liquid Organic Hydrogen Carriers as an efficient vector for the transport and storage of renewable energy. International Journal of Hydrogen Energy, 2012. **37**(23): p. 18118-18132.
12. Asif F., Hamayun M.H., Hussain M., Hussain A., M. Maafa I.M., Park Y-K., Performance Analysis of the Perhydro-Dibenzyl-Toluene Dehydrogenation System—A Simulation Study, Sustainability 2021, **13**, 6490.
13. G. Do, P. Preuster, R. Aslam, A. Bösmann, K. Müller, W. Arlt, P. Wasserscheid, Hydrogenation of the liquid organic hydrogen carrier compound dibenzyltoluene – reaction pathway determination by ¹H NMR spectroscopy. React. Chem. Eng., 2016. **1**(3): p. 313-320.
14. S. Dürr, S. Zilm, M. Geißelbrecht, Karsten Müller, P. Preuster, A. Bösmann, P. Wasserscheid, Experimental determination of the hydrogenation/dehydrogenation - Equilibrium of the LOHC system H₀/H₁₈-dibenzyltoluene, International Journal of Hydrogen Energy, Volume 46, Issue 64, 2021, Pages 32583-32594, ISSN 0360-3199, <https://doi.org/10.1016/j.ijhydene.2021.07.119>.
15. H. Jorschick, P. Preuster, S. Dürr, A. Seidel, K. Müller, A. Bosmann, P. Wasserscheid, Hydrogen Storage Using a Hot Pressure Swing Reactor. Energy & Environmental Science, 2017.
16. Delogu, P. personal communication 2023.

ICH2P14-OP033

DEGRADATION MODELLING OF WATER ELECTROLYSERS USING HIDDEN STATE ESTIMATION AND DEEP LEARNING

**Frank Hilden, Pourya Azadi, Stéphane Haag, Giuseppe Cusati, Vanessa Gepert*

Air Liquide Forschung und Entwicklung GmbH - Innovation Campus Frankfurt, Gwinnerstraße 27-33, 60388 Frankfurt, Germany

*Corresponding author e-mail: frank.hilden@airliquide.com

ABSTRACT

In the paradigm of energy transition, water electrolysis (WE) is a predominant route for the production of green hydrogen. Due to large capital costs, lifetime management is critical during operation. The main degradation phenomena in WE are related to the catalyst and the membrane. In large-scale electrolyzers, monitoring degradation is challenging due to a lack of suitable measurement techniques. This paper proposes an approach for the estimation of non-measurable degradation parameters in WE using a particle filter for a nonlinear state-space system. The WE is conceptualised as a Hidden Markov model with the degradation parameters as stochastic variables that are unobservable. The static equations of the degradation parameters are transformed into state transition equations. Using observable measurements, the likelihood for each particle is determined. A neural network is trained based on the hidden state estimations to handle measurement uncertainties and to forecast the rate of degradation parameters, using process inputs. This approach is validated by generated data.

Keywords: Water electrolysis, Degradation modelling, Machine learning, Neural networks, Sequential Monte Carlo method

INTRODUCTION

Green hydrogen (GH₂), produced from water and renewable energy sources, ensures zero greenhouse gas emissions and is widely viewed as a promising solution in regard to the energy transition. The efficacy and affordability of GH₂ as a widespread energy source depend on the efficiency and durability of WE. While technological advances have led to significant improvements, the longevity of these systems remains an area of concern [1]. Renewable energy sources exhibit a highly dynamic and volatile power profile. The operation of a WE in such energy systems is subject to frequent load changes and even periods with no available green electricity. This necessitates an enhanced flexibility and dynamism of the operation of WEs. However, it has been described in the literature that dynamic and intermittent operation can shorten the lifetime of an WE [1].

Comprehensive assessment regarding the durability and degradation mechanisms of WE and their respective components are available in the literature. Lopez et al. [1] delineated a thorough overview of the ageing mechanisms in WE, particularly concerning renewable energy sources. Feng et al. [2] provided an in-depth examination of degradation mechanisms inherent to essential components and outlined strategies for mitigation. Kuhnert et al. [3] recently published a review on accelerated stress tests of key degradation components in context with their individual accelerating conditions.

Whilst the observations concerning the main degradation phenomena are commonly consistent, there are divergences when it comes to quantifying the effects on cell performance. Possible reasons are related to different cell components, equipment and operating conditions [4]. Bender et al. [5] reported that cross-lab cell hardware tests varied up to three times more than single-lab tests, owing to non-standardized conditioning. These factors, coupled with the unsolved challenge of transferring and up-scaling from laboratory to large-scale stacks make lifetime prediction of WEs a remaining substantial challenge within the industry [3]. A common degradation indicator for large-scale WEs is upon today the gradual increase in cell voltage [4, 6, 7]. However, in the last few years, it has become evident that an increasing cell voltage as a single degradation indicator has several limitations for a reliable lifetime prediction as it solely reflects the loss of efficiency over time without revealing the underlying cause [4, 8]. In the long-term operation of a WE, several other failures such as pinhole formation and membrane thinning can occur and affect the lifetime and operation of a WE [4, 8]. In particular, safety issues are related to membrane thinning which over time becomes increasingly challenging to manage. During the GH₂ production, the renewable energy sources can decrease to an extent that hydrogen production may even lag behind by a rate at which hydrogen diffuses through the membrane. In these circumstances, there is an increased risk of gas crossover, forming a potentially volatile H₂/O₂ mixture in the oxygen-evolving site [1].

Despite extensive reports on predominant degradation mechanisms, models that adequately describe ageing under dynamic operating conditions of WEs do not exist. Bahr et al. [9] used a feed-forward artificial neural network to predict the increasing cell voltage. Papakonstantinou et al. [6] provided an empirical equation to forecast the cell voltage increase based on time and measured high frequency resistance. Chandesris et al. [10] related the fluoride release rate to membrane thinning for a limited number of data at different operating conditions. This paper proposes a novel approach for modelling degradation in water electrolyzers. In this approach, the WE is described by a Hidden Markov model (HMM) with the key degradation parameters as hidden states that are estimated using a particle filter. The added value of this approach compared to previous studies is the representation of degradation phenomena beyond only the increase in cell voltage. Incorporation of the current efficiency as an additional observation and degradation indicator into the modelling framework enhances the precision of the hidden state estimation and leads to a more comprehensive representation of degradation phenomena compared to previously reported works.

WATER ELECTROLYSIS PHYSICS-BASED MODEL

For the optimal operation of a WE, the overall efficiency ε has to be considered. The overall efficiency measures the total effectiveness of a WE in converting electrical energy into hydrogen and can be described as the product of voltage efficiency ε_V and current efficiency ε_I [11].

$$\varepsilon = \varepsilon_V \cdot \varepsilon_I \quad (1)$$

The current efficiency describes how effectively the electrical current is used in the water splitting reaction. In case it's sufficient to relate it only to hydrogen, it can be calculated as follows [11]:

$$\varepsilon_I = 1 - \frac{2F}{i} \cdot \dot{N}_{H_2}^{cross} \quad (2)$$

where i is the current density and F is the Faraday constant. $\dot{N}_{H_2}^{cross}$ denotes the mass transport related to the crossover of hydrogen into the oxygen evolving site due to convection and diffusion and can be calculated as follows [12]:

$$\dot{N}_{H_2}^{cross} = \dot{N}_{H_2}^{conv} + \dot{N}_{H_2}^{diff} = \frac{K_{mem}}{\eta_{H_2O}} \Delta p + \frac{D_{H_2}^{eff}}{d_{mem}^{wet}} \Delta c_{H_2} \quad (3)$$

where $D_{H_2}^{eff}$ is the effective diffusion coefficient, d_{mem}^{wet} the wet membrane thickness, η_{H_2O} the water viscosity, K_{mem} the membrane permeability, and Δp and Δc_{H_2} the pressure and H_2 concentration difference between cathode and anode.

The voltage efficiency describes how close the cell operates to its theoretical energy input. It depends on the thermoneutral, reversible, and cell voltages and can be calculated as follows [11]:

$$\varepsilon_V = \frac{U_{tn}}{U_{tn} + U_{cell} - U_{rev}} \quad (4)$$

The cell voltage as a function of process input variables, i.e. current I temperature T and pressure p is a superposition of different overpotentials [13]:

$$U_{cell} = U_{rev} + \eta_{act,el} + \eta_{ohm} \quad (5)$$

The voltage when the cell is operating at reversible conditions U_{rev} can be expressed as [13]:

$$U_{rev}(T, p) = -\frac{\Delta G(T, p)}{nF} \quad (6)$$

The total energy requisite to trigger the electrochemical reactions at the electrodes, the so-called activation overvoltage $\eta_{act,el} = \eta_{act,an} + \eta_{act,ca}$ can be expressed as [13]:

$$\eta_{act,el}(i, T, p) = \frac{RT}{2F\alpha_{an}} \sinh^{-1} \left(\frac{i}{2i_{0,an}(T, p)} \right) + \frac{RT}{2F\alpha_{ca}} \sinh^{-1} \left(\frac{i}{2i_{0,ca}(T, p)} \right) \quad (7)$$

where α is the charge transfer coefficient, $i_{0,el}$ the exchange current density at anode and cathode side, p operating pressure and T operating temperature of the electrolyser. For given operating conditions and a known electrochemical specific surface area A_c as a function of catalyst particle loading and active catalyst area, the exchange current density can be calculated as follows [14, 15]:

$$i_{0,el}(p, T) = i_{0,ref,el} A_c \left(\frac{p}{p_{ref}} \right)^Y \exp \left(\frac{\Delta G}{RT} \left(1 - \frac{T}{T_{ref}} \right) \right) \quad (8)$$

The ohmic overvoltage η_{ohm} reflects the overvoltage caused by the resistance of the electrolyser's components to the movement of electrons and protons. By distinguishing between membrane and electrical resistances, the ohmic overvoltage can be expressed as [13]:

$$\eta_{ohm}(i, T) = \eta_{mem}(i, T) + \eta_{elect}(i, T) \quad (9)$$

The resistance of the membrane overvoltage $\eta_{mem}(T)$ depends on the wet membrane thickness d_{mem}^{wet} and the membrane conductivity σ_{mem} [13].

$$\eta_{mem}(i, T) = \frac{d_{mem}^{wet}(T)}{\sigma_{mem}(T)} \cdot i \cdot A_{mem} \quad (10)$$

The wet membrane thickness is a function of the dry membrane thickness, the water content λ and the swelling factor r_{sf} [16]:

$$d_{mem}^{wet}(T) = d_{mem}^{dry} \cdot (1 + r_{sf}(T) \cdot \lambda(T)) \quad (11)$$

As previously elaborated, the increasing cell voltage over time is mainly due to a loss of catalyst activity caused by a decrease of the electrochemical specific surface area, which leads to decrease in exchange current density. In case one electrode has a much smaller overpotential than the other, it can be sufficient to only consider exchange current density i_0 of the electrode with the higher overpotential [12]. Membrane thinning leads to a decrease in cell voltage and can cause cell failures and safety issues. The membrane thickness is the sole parameter that influences both current and voltage efficiency. Thus, when modelling degradation, it is imperative to consider at least these two parameters.

STATE SPACE MODEL AND STOCHASTIC FILTERING

The two key degradation parameter $x = (i_0, d_{mem}^{wet})$ are in general unobservable (hidden) states during operation. In this section, a particle filter algorithm will be presented which enables monitoring these parameters at any time step k by approximating the posterior probability distribution using recursive state estimation. For the application of a particle filter, two sources of information are required. First, a state transition function f , which describes how the state x is expected to evolve over time based on a prior knowledge, the process input u , and the process model noise v [17].

$$x_{k+1} = f(x_k, u_k, v_k) \quad (12)$$

The second required information is the measurement function g which relates the observable measurement $y = (U_{cell}, \epsilon_I)$ to the internal states x , process inputs and measurement noise w [17].

$$y_k = g(x_k, u_k, w_k) \quad (13)$$

Within the realm of stochastic state estimation, Eqs. (12) and (13) are defining an input-output HMM, which is derived from Eqs. (2) and (5). The corresponding hidden states, defined by Eqs. (8) and (11), must be converted into a time discrete state transition function to be functional for the following stochastic state estimation [14].

$$i_{0,k+1} = i_{0,k} + \Delta i_0(T, p) \quad (14)$$

$$d_{mem,k+1}^{wet} = d_{mem,k}^{wet} + \Delta d_{mem}^{wet}(T) \quad (15)$$

The state transition equation can be obtained by discretizing the time derivatives in Eqs. (8) and (11) through the backward difference approximation $\left(\frac{dx}{dt} = \frac{x_t - x_{t-1}}{\Delta t}\right)$ [14].

The proposed algorithm for estimating the hidden states is shown in Alg. 1. The particles are initially derived from a prior distribution with equivalent weights. During each time iteration, these particles transition to predicted states, with their associated weights calculated and updated through the observation likelihood, followed by a normalisation process. Subsequently, a resampling procedure is conducted where particles with greater weights exhibit a higher propensity for replication. At the end of each time step k , the hidden states $x = (i_0, d_{mem}^{wet})$ are estimated. Based on this estimation, the loss of the electrochemical specific surface area A_c and the thickness (loss) of the dry membrane d_{mem}^{dry} can be calculated. These two parameters can be seen as an adaptation of the key degradation parameters to the process conditions at time step k [14]. Furthermore, this adaptation also reduces the feature dimensionality. Based on the obtained time series for these adjusted degradation parameters, a NARX Neural Network (NARX-NN) is trained, to predict the future evolution of these two parameters. Since its performance heavily relies on the quality of the estimated hidden states, the forward filtering approach is extended with a backward smoothing approach (Alg. 1). Backward smoothing in particle filters refines

Algorithm 1 Forward-Filter Backward-Smoothing (FFBS) Particle Filter for Estimation of i_0 and d_{mem}^{dret}

▷ **Forward Pass Filter**

For $k = 0$ **to** K **do**
If $k = 0$: // Initialization
 $\mathbf{x}_0^{(j)} \sim p(\mathbf{x}_0 | \mathcal{N}(T, \sigma_T), \mathcal{N}(p, \sigma_p))$ for $j = 1 \dots N$ // Sample from prior distribution
 $\omega_0^{(j)} = 1 / N$ $j = 1 \dots N$ // Set weights

Else: // Hidden State estimation loop
// Prediction
 $\mathbf{x}_k^{(j)} = f(\mathbf{x}_{k-1}, \mathbf{u}_k, \mathbf{v}_k)$, for $j = 1 \dots N$ // Predict states - Eq. (14) & (15)

// Update
 $\omega_k^{(j)} \propto \omega_{k-1}^{(j)} L(y_k | g(\mathbf{x}_k^{(j)}, \mathbf{u}_k, \mathbf{w}_k))$ for $j = 1 \dots N$ // Update weights for pred. observation - Eq. (2) & (5)

// Resampling
 $\mathbf{x}_k^{(j)} \sim \mathbf{x}_k^{(j)}, \omega_k^{(j)}$ for $j = 1 \dots N$ // Resample based on weights to get a new set of particles
 $\omega_k^{(j)} = \omega_k^{(j)} / \sum \omega_k^{(j)}$ $j = 1 \dots N$ // Normalise weights
 $\hat{\mathbf{x}}_k = \sum \omega_k^{(j)} \mathbf{x}_k^{(j)}$ // Estimate Hidden State at time step k

▷ **Backward Pass Smoother**

 $\mathbf{x}_{K|K}^{(j)} = \mathbf{x}_K^{(j)}$ // Initialisation - Set smoothed particles of last time step K equal to the filtered particles
For $k = K - 1$ **to** 0 **do**
 $\alpha_k^{(j)} \propto \omega_k^{(j)} p(\mathbf{x}_{k+1|k}^{(j)} | \mathbf{x}_{k|k}^{(j)})$ for $j = 1 \dots N$ // Transition density from k to $k+1$ given observation up to K
 $\alpha_k^{(j)} = \alpha_k^{(j)} / \sum \alpha_k^{(j)}$ $j = 1 \dots N$ // Normalise modified weights
 $\mathbf{x}_{k|k}^{(j)} \sim \mathbf{x}_{k+1|k}^{(j)}, \alpha_k^{(j)}$ for $j = 1 \dots N$ // Resample $\mathbf{x}_{k|k}^{(j)}$ based on $\alpha_k^{(j)}$
 $\hat{\mathbf{x}}_{k|k} = \sum \alpha_k^{(j)} \mathbf{x}_{k|k}^{(j)}$ // Estimate smoothed Hidden State at time step k

state estimates $\mathbf{x}_{k|k}$ by leveraging both past observations $y_{1:k}$ and future observations $y_{k+1:K}$. In contrast, forward-filtering determines states $\mathbf{x}_{k|k}$ solely based on observations up to time k ($y_{1:k}$). By integrating the future data, backward smoothing enhances the posterior distribution $p(\mathbf{x}_k | y_{1:K})$, yielding a more robust and accurate state representation [17]. This elevates the quality of the data used in the training phase of the data driven model, leading to a model with enhanced predictive capabilities.

DATA DRIVEN MODELLING

The Nonlinear Auto Regressive with eXogenous inputs (NARX) neural network is a variant of recurrent neural networks (RNNs). The architecture can be envisioned as a feed-forward neural network with feedback loops corresponding to past values. This design makes NARX networks suitable for modelling complex nonlinear time series data and capable of handling the supposed cumulative impact of operational stressors on degradation. Once trained, the model can predict future outputs based on both historical output and exogenous input values. The NARX model is defined by [18]:

$$\mathbf{z}(k) = \Gamma(\mathbf{z}(k-1), \dots, \mathbf{z}(k-r), \mathbf{u}(k-1), \dots, \mathbf{u}(k-s)) \quad (16)$$

where k represents the current time step, r and s are the auto-regressive and exogenous input lags, determining the depth of the time series history that the model considers, and Γ denotes the nonlinear function approximated by the neural network. The vector $\mathbf{z}(k) = [A_c(k), d_{mem}^{dry}(k)]^T$ represents the degradation parameters as outputs, calculated through Alg. 1 and Eqs. (8) and (11). The vector $\mathbf{u}(k) = [i(k), T(k)]^T$ corresponds to the process inputs which have an impact on degradation during Time on Stream (ToS). Here, the NARX-NN comprises four layers: an input layer, two hidden layers with ten neurons, and an output layer. The choice of ten neurons in the hidden layer was based on the Akaike Information Criterion (AIC), which was used to prevent overfitting and strike a balance between model complexity and performance. Given the varied scales and units of the variables, a min-max normalisation was performed to bring all data within the range $[0, 1]$, ensuring uniformity and aiding model convergence. A subset of 2800 hours was used to optimise the hyper parameters of the model. Afterwards, the NARX-NN was used to forecast the evolution of $\mathbf{z}(k)$. The result can be seen in Fig. 1, where the grey region indicates the training period.

RESULTS AND DISCUSSION

The process data of a WE was generated for 6000 hours of operation. To emulate a real-world power profile from renewable energy sources, a random walk was employed to simulate randomness for current and temperature, incorporating a minimum duration constraint before subsequent fluctuations to analyse the effects of varying operating conditions. Initial data inspection revealed periodic missing entries, which were estimated using cubic spline interpolation. Analysis of the scatter plot presented in Fig. 1 demonstrates that operating conditions strongly influence degradation. During Time on Stream, the operating conditions increasingly influence the degradation of a WE. This phenomenon is supposed to occur due to cumulative impact of operational stressors on the materials and on components of the WE over time. Notably, elevated temperatures and increased current densities are associated with a loss of catalytic activity. Additionally, high temperatures are observed to induce membrane thinning, whereas the impact of current density on membrane integrity appears to be comparatively minor. Fig. 2 shows the validation results of the developed NARX-NN for the cell voltage and current efficiency. The particle filter demonstrates proficiency in monitoring the measured cell voltage and current efficiency, while effectively mitigating the noise present in the measurements and input variables.

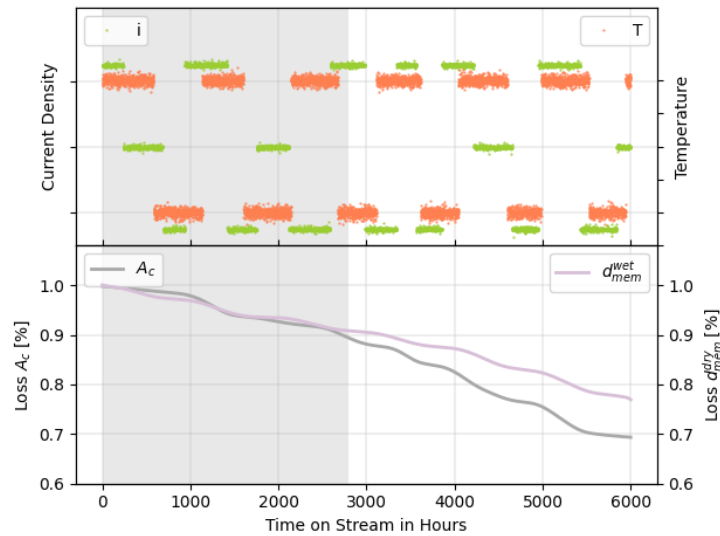


Fig. 1. Estimation of the loss of the electrochemical specific surface area and the dry membrane thickness based on process input variables (i : current density, T : stack temperature); grey region: training period.

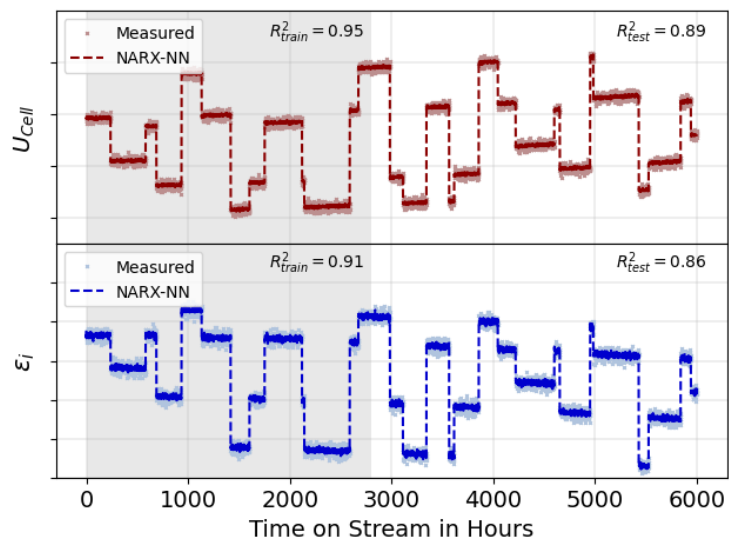


Fig. 2. Comparison between measured values and calculated values of cell voltage and current efficiency; grey region: training period.

CONCLUSIONS AND OUTLOOK

In conclusion, employing a particle filter as a stochastic filtering method facilitates the estimation of primary degradation parameters in WE, effectively overcoming challenges associated with up-scaling from laboratory to industrial scale. Incorporating current efficiency allows for a comprehensive model of the loss of the electrochemical specific surface area and the thinning of the membrane. However, to enhance the robustness of the model, additional operational key performance indicators, such as hydrogen crossover oxygen-evolving site (HTO), should be considered as well and might further improve the hidden state estimation. Moreover, it is worth mentioning that improper design and suboptimal operating conditions can precipitate the accumulation and release of gas bubbles, which in turn may cause fluctuations in voltage that complicates modelling and hidden state estimation. Furthermore, the implications of more frequent load variations and the ramping strategy have not been in the scope of this study and require further investigation to understand their full impact on system

performance and durability. The major next step is to complement the degradation modelling framework by the inclusion of other degradation origins such as foreign ion contamination and specific membrane failures.

REFERENCES

1. Lopez, V. M., Ziar, H., Haverkort, J. W., Zeman, M., & Isabella, O. (2023). Dynamic operation of water electrolyzers: A review for applications in photovoltaic systems integration. *Renewable and Sustainable Energy Reviews*, 182, 113407.
2. Feng, Q., Liu, G., Wei, B., Zhang, Z., Li, H., & Wang, H. (2017). A review of proton exchange membrane water electrolysis on degradation mechanisms and mitigation strategies. *Journal of Power Sources*, 366, 33-55.
3. Kuhnert, E., Hacker, V., & Bodner, M. (2023). A Review of Accelerated Stress Tests for Enhancing MEA Durability in PEM Water Electrolysis Cells. *International journal of energy research*.
4. Tomić, A. Z., Pivac, I., & Barbir, F. (2023). A review of testing procedures for proton exchange membrane electrolyzer degradation. *Journal of Power Sources*, 557, 232569.
5. Bender, G., Carmo, M., Smolinka, T., Gago, A., Danilovic, N., Mueller, M. (2019). Initial approaches in benchmarking and round robin testing for proton exchange membrane water electrolyzers. *International journal of hydrogen energy*, 44(18), 9174-9187.
6. Guilbert, D., & Papakonstantinou, G. (2022). Modeling, Degradation Study, Failures Diagnosis and Faulty Operating Management of Electrolyzers. *Membranes*, 12(12), 1195.
7. Lee, H., Gu, J., Lee, B., Cho, H. S., & Lim, H. (2023). Prognostics and health management of alkaline water electrolyzer: Techno-economic analysis considering replacement moment. *Energy and AI*, 13, 100251.
8. Suermann, M., Bensmann, B., & Hanke-Rauschenbach, R. (2019). Degradation of proton exchange membrane (PEM) water electrolysis cells: looking beyond the cell voltage increase. *Journal of The Electrochemical Society*, 166(10), F645.
9. Bahr, M., Gusak, A., Stypka, S., & Oberschachtsiek, B. (2020). Artificial neural networks for aging simulation of electrolysis stacks. *Chemie Ingenieur Technik*, 92(10), 1610-1617
10. Chandresis, M., Médeau, V., Guillet, N., Chelghoum, S., Thoby, D., & Fouda-Onana, F. (2015). Membrane degradation in PEM water electrolyzer: Numerical modeling and experimental evidence of the influence of temperature and current density. *International Journal of Hydrogen Energy*, 40(3), 1353-1366.
11. Lamy, C., & Millet, P. (2020). A critical review on the definitions used to calculate the energy efficiency coefficients of water electrolysis cells working under near ambient temperature conditions. *Journal of power sources*, 447, 227350.
12. Bernt, M., Schröter, J., Möckl, M., & Gasteiger, H. A. (2020). Analysis of gas permeation phenomena in a PEM water electrolyzer operated at high pressure and high current density. *Journal of The Electrochemical Society*, 167(12), 124502.
13. Ma, Z., Witteman, L., Wrubel, J. A., & Bender, G. (2021). A comprehensive modeling method for proton exchange membrane electrolyzer development. *International Journal of Hydrogen Energy*, 46(34), 17627-17643.
14. Aguilar, J. A., Andrade-Cetto, J., & Husar, A. (2022). Control-oriented estimation of the exchange current density in PEM fuel cells via stochastic filtering. *International Journal of Energy Research*, 46(15), 22516-22529.
15. Ojong, E. T., Kwan, J. T. H., Nouri-Khorasani, A., Bonakdarpour, A., Wilkinson, D. P., & Smolinka, T. (2017). Development of an experimentally validated semi-empirical fully-coupled performance model of a PEM electrolysis cell with a 3-D structured porous transport layer. *International journal of hydrogen energy*, 42(41), 25831-25847.
16. Ito, H., Maeda, T., Nakano, A., & Takenaka, H. (2011). Properties of Nafion membranes under PEM water electrolysis conditions. *International journal of hydrogen energy*, 36(17), 10527-10540.
17. Cappé, O., Godsill, S. J., & Moulines, E. (2007). An overview of existing methods and recent advances in sequential Monte Carlo. *Proceedings of the IEEE*, 95(5), 899-924.
18. Boussaada, Z., Curea, O., Remaci, A., Camblong, H., & Mrabet Bellaaj, N. (2018). A nonlinear autoregressive exogenous (NARX) neural network model for the prediction of the daily direct solar radiation. *Energies*, 11(3), 620.

ICH2P14-OP036

A TECHNO-ECONOMIC EVALUATION OF THE INTEGRATION OF DIRECT AIR CAPTURE WITH HYDROGEN AND SOLAR FUEL PRODUCTION

^{1,2*}Enric Prats-Salvado, ¹Nathalie Monnerie, ^{1,2}Christian Sattler

¹German Aerospace Center (DLR), Institute of Future Fuels, Linder Höhe, Cologne, Germany

²RWTH Aachen University, Chair for Solar Fuel Production, Templergraben 55, Aachen, Germany

*Corresponding author e-mail: enric.pratsalvado@dlr.de

ABSTRACT

Producing fuels such as hydrogen and its derivatives with a neutral carbon footprint is a critical step toward decarbonization. One promising approach is thermochemical cycles, in which water and CO₂ are split with heat to produce hydrogen and carbon monoxide. These can then be processed into liquid fuels such as methanol. The CO₂ used as a feedstock can be captured from the atmosphere to close the carbon cycle with direct air capture (DAC). In this study, we identify and quantify the benefits of several synergies between two DAC technologies and a solar redox thermochemical cycle. To this end, we build a comprehensive model in Aspen Plus® and HFLCAL, estimate the capital and operational expenses and calculate the levelized cost of fuel (LCOF) for a plant producing 9934 tons of methanol per year in Riyadh, Saudi Arabia. The results show that all configurations achieve a lower LCOF compared to a baseline without any integration, thus confirming the synergies between the technologies. Among the configurations studied, the most cost-effective one integrates a solid DAC system, which has the lowest capital investment and allows for waste heat utilization. We also conclude that the LCOF is mainly driven by the plant's capital investment.

Keywords: Thermochemical Cycle, Direct Air Capture, Solar Fuels, Methanol, Techno-economic Assessment.

INTRODUCTION

Without action, global temperatures could rise by 2.7°C by 2100, disrupting nearly every ecosystem in the world [1,2]. Tackling climate change will involve transitioning away from fossil fuels, which in turn calls for a major technological breakthrough [3,4]. Here, we explore two important technologies that can foster the energy transition: direct air capture of CO₂ and solar thermochemical cycles.

Direct air capture of CO₂ (DAC) has attracted considerable attention in recent years due to its ability to remove and concentrate very dilute carbon dioxide from the atmosphere. The removed CO₂ can either be sequestered or used as a feedstock for the carbon capture and utilization industry (CCU) [5]. While relatively expensive compared to other carbon dioxide sources, DAC differs from other alternatives in that it does not have obvious biophysical limitations (as biogenic sources do) and can produce truly carbon-neutral CO₂ when powered by renewable energy (as opposed to point-source carbon capture) [6–8].

Solar thermochemical cycles, unlike the currently most mature processes that rely on electricity, can produce hydrogen directly from heat. This avoids the energy losses involved in power generation and greatly increases the potential efficiency of the technology [9,10]. Another advantage of solar thermochemical cycles is the possibility of simultaneous production of hydrogen and carbon monoxide when water and carbon dioxide are fed [11,12]. The mixture of hydrogen and carbon monoxide can be used as synthesis gas for the production of liquid fuels such as kerosene, which is critical for the decarbonization of sectors like aviation [13,14].

For hydrogen-derived liquid fuels to be carbon-neutral, it is essential that the CO₂ is not of fossil origin. Therefore, it seems logical to integrate a DAC unit into a solar thermochemical fuel plant. However, most research to date has focused on improving DAC independently of CCU. By focusing on the synergies between DAC and solar thermochemical cycles, we intend to fill this knowledge gap.

At the present time, there is a broad portfolio of DAC technologies. Two of these are considered in this study on the basis of their superior readiness, namely solid sorbent and liquid solvent direct air capture, frequently referred to simply as S-DAC and L-DAC respectively. While S-DAC employs a solid sorbent that chemically combines with carbon dioxide, the L-DAC process relies on a liquid solvent that reacts

with CO₂ in the air. Notably, the former can release the capture carbon dioxide by applying heat at low temperatures (i.e., 100 °C), while the latter requires elevated temperatures for regeneration (as high as 900 °C) [5,15,16].

Similarly, there are several types of solar thermochemical cycles. Here, we focus on a technology called redox cycles, where a metal oxide (e.g., cerium dioxide) is reduced at elevated temperatures and low oxygen partial pressures to form oxygen vacancies in the metal oxide structure. The material is then oxidized again in the presence of steam at slightly lower temperatures to produce hydrogen. This process can also occur in the presence of CO₂, resulting in the formation of carbon monoxide. The reactions do not consume any metal oxide and the cycle can start again with the reduction step [17,18].

MODELLING

We have defined 4 scenarios, each with a different configuration of the DAC with the solar thermochemical cycle [19,20]. Scenarios A and B are based on L-DAC, with Scenario A including a new concept of L-DAC powered entirely by solar energy. Scenario B, on the other hand, is based on the commercial L-DAC concept of oxyfuel natural gas combustion (allowing in-situ use of the oxygen produced by the thermochemical cycle). Scenario C employs an S-DAC system installed in the solar fuel plant and capable of utilizing low-quality waste heat from the thermochemical cycle. S-DAC is also used in Scenario D, but in a decentralized manner by capturing the heating, ventilation, and air conditioning (HVAC) systems of buildings in urban areas near the plant and compensates their additional energy needs by providing the excess electricity generated for free [21]. An overview of the different scenarios is shown in Fig. 1.

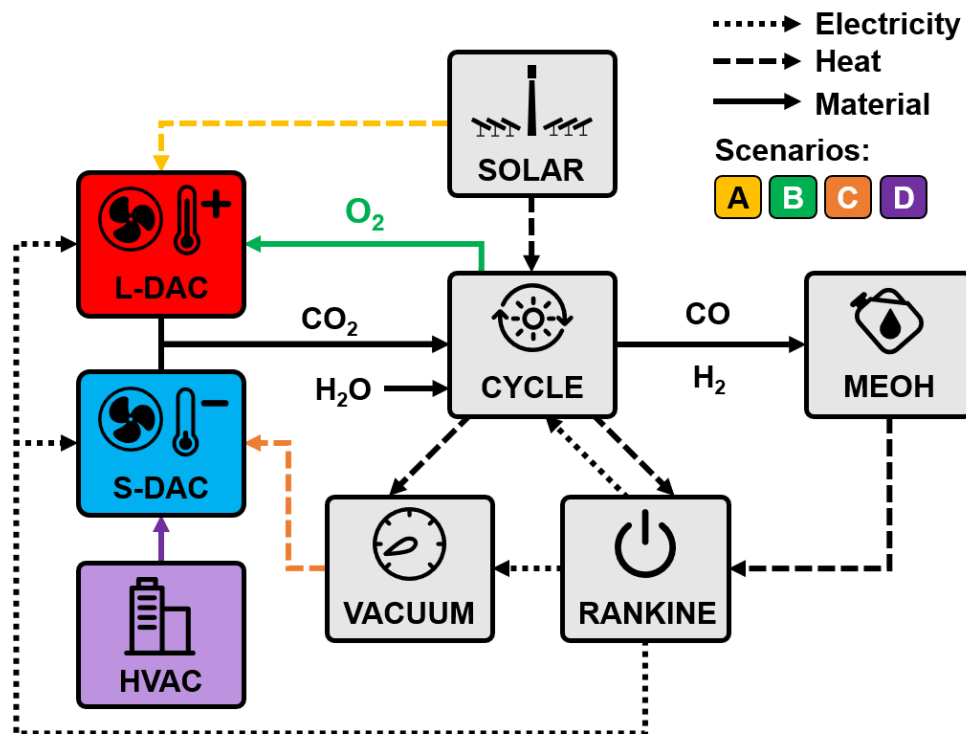


Fig. 1. Schematic overview of the different scenarios. The abbreviations in the figure stand for: "L-DAC" = liquid direct air capture; "S-DAC" = solid direct air capture; "HVAC" = heating, ventilation, and air conditioning; "SOLAR" = concentrated solar power; "CYCLE" = thermochemical cycle; "MEOH" = methanol synthesis; "VACUUM" = vacuum system; and "RANKINE" = Rankine cycle. Adapted from [20].

Simulations were then built for each part of the process. The thermochemical cycle, the methanol synthesis and the auxiliary systems (i.e., the vacuum system and the Rankine cycle) were simulated in Aspen Plus[®], while the heliostat field and solar tower were modelled with the DLR software HFLCAL [22]. The DAC data were extracted from the relevant literature, except for Scenario A, which used an innovative solar L-DAC approach that had to be modelled in Aspen Plus[®]. The location selected for the study was Riyadh, Saudi Arabia, and the model considered the locally available solar irradiance

(provided with hourly resolution by Meteonorm[®] software) and the regional weighted average cost of capital (WACC) of 6.8% [23].

The solar field was designed to provide 280 MW of thermal power under design conditions, which is consistent with the capacity of existing large power towers according to available databases [24]. The next step was to screen a range of sizes of the solar thermochemical cycle and find the design capacity that would lead to the minimum levelized cost of fuel (LCOF) for the produced methanol. According to our calculations, this design capacity should be 202 MW of thermal power fed into the solar reactor. Taking into account the local solar resources and a capacity utilization of 90%, this corresponds to an annual methanol production of 9934 metric tons. The remaining units (namely the DAC system, the methanol plant, and auxiliary equipment) were sized to match the above capacity.

Capital expenditure (CAPEX) was calculated using the results of the simulations and a combination of available correlations for mature process equipment [25] and cost estimation techniques from existing studies for non-standard units [26]. In addition, the operational expenditure (OPEX) was determined by considering fixed (i.e., maintenance) and variable costs (i.e., raw materials, utilities and labour).

The LCOF was calculated from the annualized CAPEX, assuming local WACC and a 25-year operating life, the OPEX, and by-product revenues. To determine the uncertainty of the results, the standard deviation of the final CAPEX was extracted from a 1000-sample Monte Carlo simulation by assigning a confidence interval of 30 and 50% to the costs of high- and low-maturity units, respectively. Complementing this study, a sensitivity analysis was conducted to determine the variables that dominate the LCOF.

RESULTS AND DISCUSSION

The results of the scenarios described were compared to a baseline consisting of an L-DAC unit and a solar thermochemical cycle without any integration between them (i.e., as two stand-alone units). The main results of the techno-economic assessment are shown in Fig. 2. All scenarios with integrations between DAC and solar fuels production show a cost reduction compared to the baseline LCOF. Scenario C stands out as the most cost-effective configuration because it has the lowest CAPEX (due to the most inexpensive DAC unit) without sacrificing variable OPEX or by-product revenues. From the LCOF breakdown, we can see that the largest contributors to the final cost are the fixed OPEX (basically maintenance) and the CAPEX for the Rankine cycle and solar equipment.

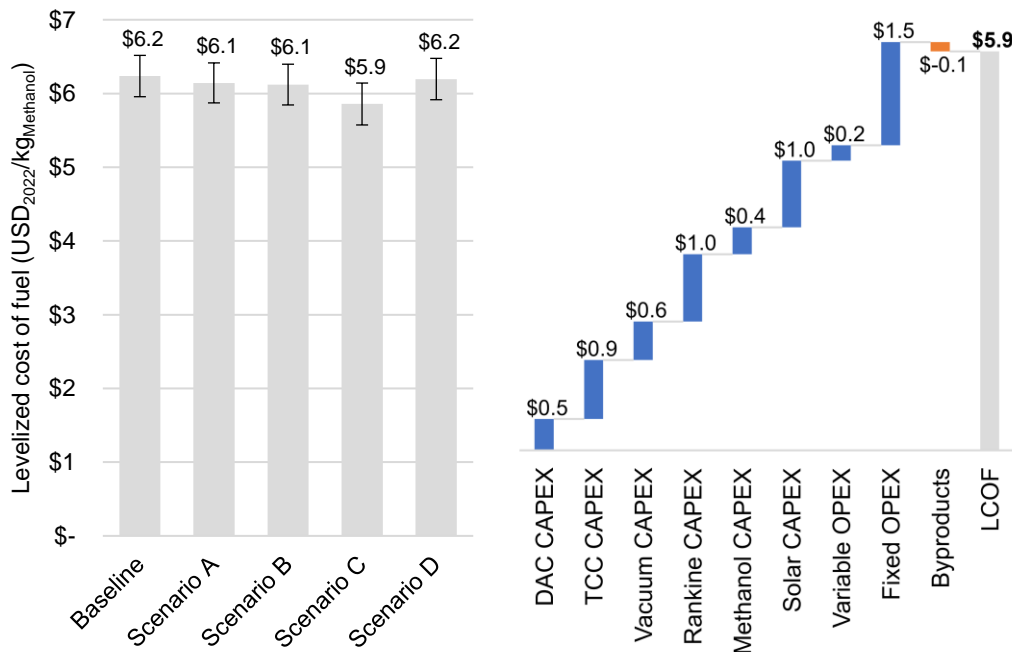


Fig. 2. Levelized cost of fuel (LCOF) for the methanol produced in each scenario and the baseline (left) and breakdown in individual contributions to the LCOF for the scenario C (right).

The sensitivity analysis in Fig. 3 shows that increasing the overall system efficiency and reducing the Lang factor and capital cost are the main drivers for improving the cost of methanol in Scenario C. Interestingly, the cost of water or the revenue from low pressure steam (LPS) have almost negligible impact.

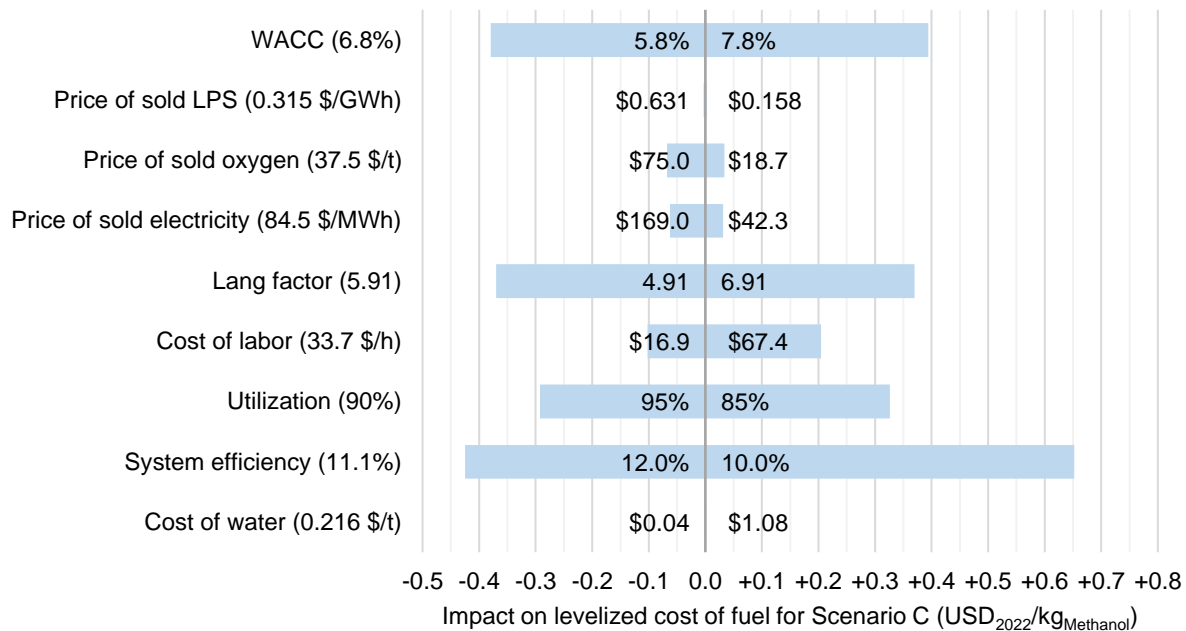


Fig. 3. Impact on the levelized cost of fuel (LCOF) for the methanol produced in Scenario C (LCOF = 5.9 USD₂₀₂₂/kg_{Methanol} under reference conditions). The value of each parameter under reference conditions is shown in parentheses. The abbreviations “WACC” and “LPS” stand for weighted average cost of capital and low-pressure steam, respectively.

CONCLUSIONS

This work explores the potential integration of DAC and methanol production via a solar thermochemical cycle and shows that there are significant synergies that lead to lower fuel production costs. Based on the results, S-DAC system integration is recommended over L-DAC due to the possibility of waste heat utilization from the solar thermochemical cycle and lower DAC CAPEX.

The breakdown of the methanol price shows that more than three-quarters of the cost is attributable to the capital investment required for the construction of the infrastructure. This phenomenon is also underlined by the sensitivity analysis, where parameters with a significant impact on CAPEX, such as the Lang factor or the WACC, are among the top three most influential variables. It is noteworthy that the cost of water, assumed to be obtained from desalination, has an almost negligible impact, which opens the door to the operation of solar fuel plants in regions with water shortages but abundant solar resources.

In summary, DAC-integrated solar thermochemical cycles may be a promising future pathway due to their synergies and potential high efficiencies. However, the technology needs to be further developed to reduce capital investment and increase system efficiency in order to be competitive with fossil and synthetic fuels produced by other routes.

REFERENCES

1. United Nations Environment Programme. Emissions Gap Report 2021: The Heat Is On - A World of Climate Promises Not Yet Delivered. Nairobi, Kenya.
2. Blunden J and Arndt DS. 2020. State of the Climate in 2019. Bulletin of the American Meteorological Society 101: S1-S429.
3. Lüthi D, Le Floch M, Bereiter B, Blunier T, Barnola J-M, Siegenthaler U, Raynaud D, Jouzel J, Fischer H, Kawamura K and Stocker TF. 2008. High-resolution carbon dioxide concentration record 650,000-800,000 years before present. Nature 453: 379-82.

4. PLASS GN. 1956. The Carbon Dioxide Theory of Climatic Change. *Tellus* 8: 140-54.
5. International Energy Agency. 2022. Direct Air Capture: A key technology for net zero. France.
6. Hanna R, Abdulla A, Xu Y and Victor DG. 2021. Emergency deployment of direct air capture as a response to the climate crisis. *Nature Communications* 12.
7. Madhu K, Pauliuk S, Dhathri S and Creutzig F. 2021. Understanding environmental trade-offs and resource demand of direct air capture technologies through comparative life-cycle assessment. *Nature Energy* 6: 1035-44.
8. Deutz S and Bardow A. 2021. Life-cycle assessment of an industrial direct air capture process based on temperature–vacuum swing adsorption. *Nature Energy* 6: 203-13.
9. Lua Y, Zhua L, Agrafiotis C, Vieten J, Roeb M and Sattler C. 2019. Solar fuels production: Two-step thermochemical cycles with cerium-based oxides. *Progress in Energy and Combustion Science* 75.
10. Agrafiotis C, Roeb M and Sattler C. 4.18 Solar Fuels. In: Dincer I, editor. *Comprehensive energy systems*. Amsterdam, Netherlands: Elsevier. 2018.
11. Marxer D, Furler P, Takacs M and Steinfeld A. 2017. Solar thermochemical splitting of CO₂ into separate streams of CO and O₂ with high selectivity, stability, conversion, and efficiency. *Energy Environ. Sci.* 10: 1142-9.
12. Rytter E, Souskova K, Lundgren MK, Ge W, Nannestad AD, Venvik HJ and Hillestad M. 2016. Process concepts to produce syngas for Fischer–Tropsch fuels by solar thermochemical splitting of water and/or CO₂. *Fuel Processing Technology* 145: 1-8.
13. Koepf E, Zoller S, Luque S, Thelen M, Brendelberger S, González-Aguilar J, Romero M and Steinfeld A. 2019. Liquid fuels from concentrated sunlight: An overview on development and integration of a 50 kW solar thermochemical reactor and high concentration solar field for the SUN-toLIQUID project 2126.
14. Romero M, González-Aguilar J, Sizmann A, Batteiger V, Falter C, Steinfeld A, Zoller S, Brendelberger S and Liefertink D. 2019. Solar-Driven Thermochemical Production of Sustainable Liquid Fuels from H₂O and CO₂ in a Heliostat Field.
15. Fasihi M, Efimova O and Breyer C. 2019. Techno-economic assessment of CO₂ direct air capture plants. *Journal of Cleaner Production* 224: 957-80.
16. National Academies of Sciences, Engineering, and Medicine. 2019. *Negative Emissions Technologies and Reliable Sequestration: A Research Agenda*.
17. Bulfin B, Vieten J, Agrafiotis C, Roeb M and Sattler C. Applications and Limitations of Two Step Metal Oxide Thermochemical Redox Cycles; A Review. *Journal of Materials Chemistry*.
18. Pein M, Agrafiotis C, Vieten J, Giasafaki D, Brendelberger S, Roeb M and Sattler C. 2020. Redox thermochemistry of Ca-Mn-based perovskites for oxygen atmosphere control in solar-thermochemical processes. *Solar Energy* 198: 612-22.
19. Prats-Salvado E, Monnerie N and Sattler C. 2021. Synergies between Direct Air Capture Technologies and Solar Thermochemical Cycles in the Production of Methanol. *Energies* 14: 4818.
20. Prats-Salvado E, Monnerie N and Sattler C. 2022. Techno-Economic Assessment of the Integration of Direct Air Capture and the Production of Solar Fuels. *Energies* 15: 5017.
21. Dittmeyer R, Klumpp M, Kant P and Ozin G. 2019. Crowd oil not crude oil. *Nature Communications* 10.
22. Schwarzbözl P, Pitz-Paal R, Schmitz M. 2009. Visual HFLCAL - A Software Tool for Layout and Optimisation of Heliostat Fields. 15th International SolarPACES Symposium.
23. Ameli N, Dessens O, Winning M, Cronin J, Chenet H, Drummond P, Calzadilla A, Anandarajah G and Grubb M. 2021. Higher cost of finance exacerbates a climate investment trap in developing economies. *Nature Communications* 12: 4046.
24. <https://solarpaces.nrel.gov/>. Accessed on June, 2022.
25. Peters MS, Timmerhaus KD and West RE. 2003. *Plant design and economics for chemical engineers*. Boston, London, McGraw-Hill.
26. Remer DS and Chai LH. 1993. *Process Equipment, Cost Scale-up*. New York, Marcel Dekker, Inc.

ICH2P14-OP044

BIOTECHNOLOGICAL POTENTIAL OF SPENT COFFEE GROUNDS FOR LARGE-SCALE HYDROGEN PRODUCTION

^{1,2,3}Liana Vanyan, ²Anait Vassilian, ^{1,2}Anna Poladyan, ^{1,2,3*}Karen Trchounian

¹Department of Biochemistry, Microbiology and Biotechnology, Faculty of Biology, Yerevan State University, 1 A. Manoogian str., 0025 Yerevan, Armenia

²Scientific-Research Institute of Biology, Yerevan State University, 1 A. Manoogian str., 0025 Yerevan, Armenia

³Microbial Biotechnologies and Biofuel Innovation Center, Yerevan State University, 1 A. Manoogian str., 0025 Yerevan, Armenia

*Corresponding author e-mail: k.trchounian@ysu.am

ABSTRACT

Currently hydrogen (H₂) has emphasized as a clean and versatile solution for sustainable development. This study aims to investigate the large-scale production of hydrogen to assess the biotechnological potential of coffee waste utilization. *Escherichia coli* wild-type and septuple mutant ($\DeltahyaB \DeltahybC \DeltahycA \DeltafdoG \DeltaldhA \DeltafrdC \DeltaaceE$) were used. Bacteria were grown in coffee waste processing solution (65 g L⁻¹ SCG hydrolyzed with diluted sulphuric acid) [1] at pH 7 in 5 L reactor, additional glycerol at a concentration of 10 mL L⁻¹, was added.

In wild type without the presence of glycerol, the cumulative hydrogen yield was ~4 L (0.13 L Day⁻¹), and in the mutant, the production of ~5.3 L lasted for a month, accumulating ~0.4 L of hydrogen per day. During glycerol co-fermentation, the cumulative amount of hydrogen in the wild type was ~5.2 L, accumulating 0.2 L of hydrogen per day, while the septuple mutant produced 15 L of hydrogen, accumulating 0.5 L of hydrogen per day, and the maximum hydrogen was produced in the 24th hour.

It has been shown that hydrogen equal to 33 kWh of energy was possible to produce during batch culturing of 200 g SCG and glycerol, which can be used in large semi-technological productions.

Keywords: Renewable energy, Spent Coffee Grounds (SCG), *E. coli*.

INTRODUCTION

The investigation and development of ways to obtain alternative and renewable energy sources is a priority area of modern research, given the irreversible decline in fossil fuel reserves. The hydrogen energy industry, positioned as a frontrunner in the quest for carbon-free and environmentally friendly energy carriers, plays a pivotal role in the global transition towards sustainable energy solutions. With its combustion energy released five times higher than the calorific value of certain carbon fuels, hydrogen not only promises superior energy yield but also significantly reduces greenhouse gas emissions into the atmosphere [1,2]. Furthermore, its versatile applications in the production of ammonium, methanol, and various industries, including oil and gas and chlor-alkali, underscore its strategic importance in the broader context of industrial processes[2,3].

To achieve substantial hydrogen production, employing fermenting bacteria is recommended and efficient. These bacteria exhibit rapid growth and demonstrate high hydrogen production rates. Notably, their independence from light allows them to decompose organic matter irrespective of light presence. Extensive research has revealed that bacteria can generate hydrogen from agricultural and organic waste, with fermentative production proving to be the most effective method [4]. In the wake of increasing global energy demand and the imperative to transition towards sustainable and renewable energy sources, the exploration of unconventional yet abundant biomass for biohydrogen production has gained significant attention. Among the diverse array of biomass resources, spent coffee grounds emerge as a promising candidate for large-scale hydrogen production, standing at the intersection of waste management and bioenergy innovation.

Coffee, one of the world's most consumed beverages, generates vast quantities of spent coffee grounds as a byproduct of the brewing process [5,6]. Traditionally viewed as waste, these grounds possess latent biotechnological potential that extends far beyond their initial role in caffeine infusion. Recent advancements in bioengineering and bioprocessing techniques have unveiled the possibility of harnessing the intrinsic content of spent coffee grounds to produce hydrogen, biofuels and other value-added products, with minimal environmental impact[6–9].

This study aims to investigate the biotechnological landscape of employing *Escherichia coli* (*E. coli*) for the utilization of spent coffee grounds (SCG) as a carbon source. In tandem, glycerol, a byproduct from biodiesel production [10], will be incorporated into the study to enhance the H₂ production yield. This dual-source approach aims to maximize the potential for sustainable bioenergy production, presenting a novel paradigm at the confluence of waste management and bioenergy innovation.

The overarching goal is to investigate the pH effect on hydrogen production in the hydrolyzate of SCG using *E. coli* wild type and septuple mutant. As well as to investigate the large-scale production of hydrogen to evaluate the biotechnological potential of using waste.

In essence, our study unfolds in two key stages: the identification of optimal pH conditions and the subsequent investigation of large-scale hydrogen production under a singular, selected pH setting. Through this dual approach, we aim to offer a comprehensive understanding of both the nuanced factors influencing hydrogen production and the scalability potential of the biotechnological processes explored.

EXPERIMENTAL PROCEDURES

Spent Coffee Grounds (SCGs) generated from coffee preparation containing mixture of Robusta and Arabica were exposed to pretreatment with acidic hydrolysis in an autoclave (WiseClave WACS1100, Daihan Scientific, South Korea) at 121°C for 45 min as described before. Optimally 40 g L⁻¹ SCG with 0.4 % diluted H₂SO₄ were used as described before [7,11]. The pH of the SCG hydrolysate was separately adjusted to pH 6.0; pH 7.0; pH 8.0 by addition of K₂HPO₄. 13.6 g L⁻¹ glycerol was added as a substrate in the SCG medium when indicated [11].

Escherichia coli wild-type (wt) BW25113 and septuple mutant were used (Table 1). 3% (v/v) inoculum grown overnight in peptone medium (peptone 20 g L⁻¹, KH₂PO₄ 2g L⁻¹, NaCl 5 g L⁻¹) were suspended into SCG hydrolyzate. During batch culturing redox potential (ORP in mV) was determined by ORP electrode Pt BNC (HI3131, HANNA Instruments, Portugal), medium pH was determined by pH meter (HI1131, HANNA Instruments, Portugal) [12–14]. H₂ yield expressed in mmol L⁻¹ was calculated as described by Piskarev et al[15].

Cumulative H₂ production was determined separately in 5000 mL (large-scale) glass vessels under permanently stirring conditions; the gases (H₂ and CO₂) bubbled were treated by 1 M NaOH solution (to eliminate CO₂ from gas mixture); and further sole H₂ gas was collected and estimated by the water displacement volume as described before[13,14,16] and expressed as [ml H₂ (g SCG)⁻¹] or [ml H₂ (g SCG)⁻¹ 0.3 g (glyc)⁻¹]:

Table 1. Characteristics of *E. coli* strains used

Strains	Genotype	Subunits lacking	Reference
BW25113	<i>rrBA lacZ4787 HsdR514Δ(araBAD)567Δ(rhaBAD)568 rph-1</i>	Wild type	[17]
BW25113hyaB hybC hycA fdoG ldhA frdC aceE	BW25113 <i>ΔhyaB ΔhybC ΔhycA ΔfdoG ΔldhA ΔfrdC ΔaceE</i>	Large subunit of Hyd-1 and 2, repressor of FHL, α-subunit of formate dehydrogenase-N, lactate dehydrogenase	[18]

RESULTS AND DISCUSSION

ORP changes were assessed in both wild-type and seven-gene disruption mutant strains under varying pH conditions. In both pH 6 and pH 7 medium, ORP drop ≥ -400 mV [15] commenced at 3rd hour of growth, whereas the mutant strain exhibited a delayed onset at the 6th hour (Fig. 1 AB). At pH 6 without glycerol, the wild type showed the highest hydrogen yield at 24 hours (3.60 mmol L⁻¹), which increased to 5.07 mmol L⁻¹ at 72 hours with glycerol. In the pH 6 without addition of glycerol, hydrogen production was observed until the 120th hour of growth with an output of 0.73 mmol L⁻¹, and in the glycerol-containing medium with an output of 0.78 mmol L⁻¹ until the 144th hour. In case of pH 7 condition, the maximum hydrogen yield was observed in the 48th hour of growth in both glycerol-containing and non-glycerol samples, amounting to 5.2 mmol L⁻¹, but in the glycerol-free sample, hydrogen production lasted until the 120th hour of growth, and in the glycerol-containing sample, 192th hour. This data corresponds to the results obtained in previous studies that glycerol is assimilated in a longer period of time or hydrogen production is prolonged with the presence of glycerol, which is more beneficial in productions [19].

In both pH 8 conditions, hydrogen production was observed at the 24th hour of growth, and in contrast to pH 6 and pH 7, here the hydrogen production time was significantly reduced, with growth up to 72th hour, and in the sample containing glycerol - the 120th hour [Fig.1C]. In the septuple mutant, a drop in ORP value to -400 mV in samples with and without glycerol at pH 6 and pH 7 was observed at 6 h of growth, identical to the wild type.

In the septuple mutant, the maximum yield of H₂ in the sample without glycerol was observed at the 48th hour of growth: 5.07 mmol L⁻¹, which is 1.4 times more than in the wild type under the same condition. And in the sample containing glycerol, the maximum yield was 3.55 mmol L⁻¹ in the 24th hour, which is less than the wild type under the same condition. The duration of hydrogen production in both cases was not significantly different compared to the wild type. Data suggest that the results obtained using the mutant at pH 6 and pH 7 are partially reproducible

compared to the use of pure culture of the mutant [18], but is still effective using for wastes rich in carbohydrates, it is advisable to use a seven-gene mutant because it shows a higher yield than the wild type.

In the septuple mutant at pH 8, H₂ production began at the 6th hour under glycerol-containing conditions. Without glycerol, production and output lasted until the 24th hour, yielding 2.24 mmol L⁻¹, whereas the glycerol-containing sample endured until the 72 hour, reaching a maximum output of 5.24 mmol L⁻¹ at the 48th hour.

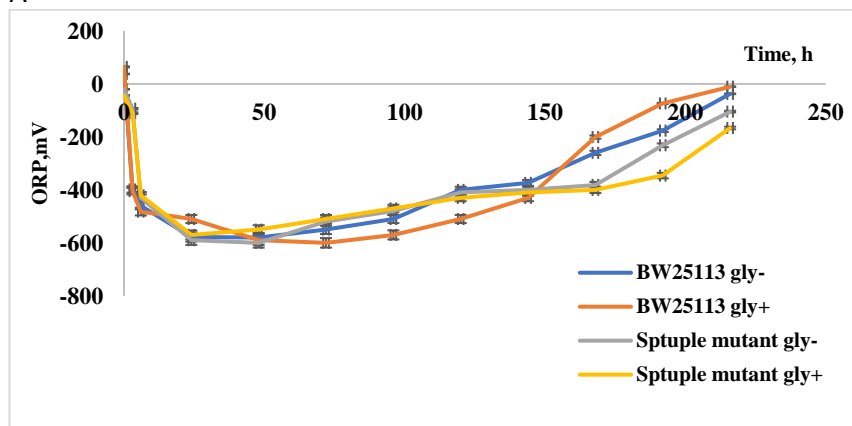
Further 5 L reactor was used for volumetric H₂ production measurements during batch culturing. It is worth to mention that against data obtained during growth in volumetric measurements in pH 6 H₂ production was significantly lower compared to wild type (data not shown), thus further researches were done only in pH 7.

In the wild type without the presence of glycerol, the cumulative yield of hydrogen was 3.9 L, accumulating 0.13 L per day, and in the seven-gene mutant, the production of 5.3 L lasted for a month, accumulating 0.17 L of hydrogen per day (Fig. 2). During added glycerol fermentation, the wild type accumulated 0.17 L of hydrogen daily, while the mutant produced 15 L in the same conditions, accumulating 0.5 L of hydrogen daily, with the maximum hydrogen produced in the 24th hour.

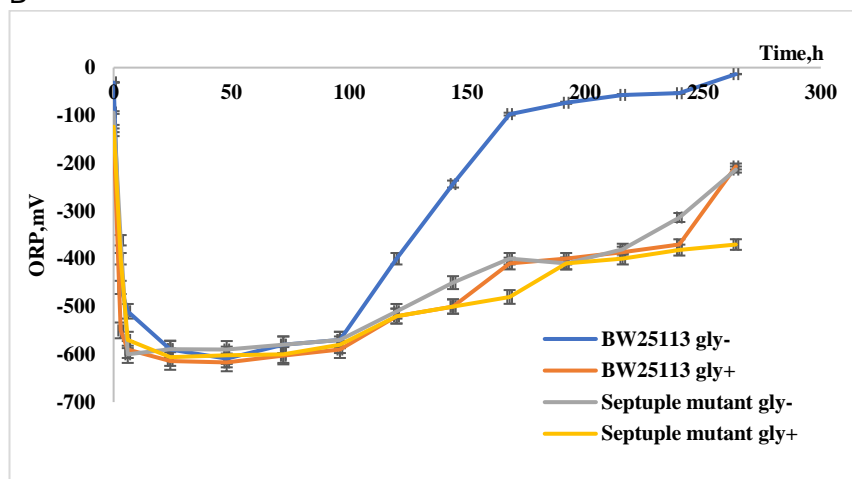
It turns out, that in mutant during co-utilization of glycerol H₂ yield was 56.5±1,7 ml H₂ (g SCG)-1 0.3 g(glyc)-1, which is twice higher compared to wild type of the same condition, meanwhile in experiments without glycerol it was 1.4, which means the the usage of the mutant is more effective whlie using mixtures of carbon sources.

This extensive analysis suggests that utilizing the seven-gene mutant with glycerol allows the potential production of approximately 1 kg of hydrogen, equivalent to 33 kWh of energy, presenting promising prospects for hydrogen generation from waste in the context of a circular economy [16].

A



B



C

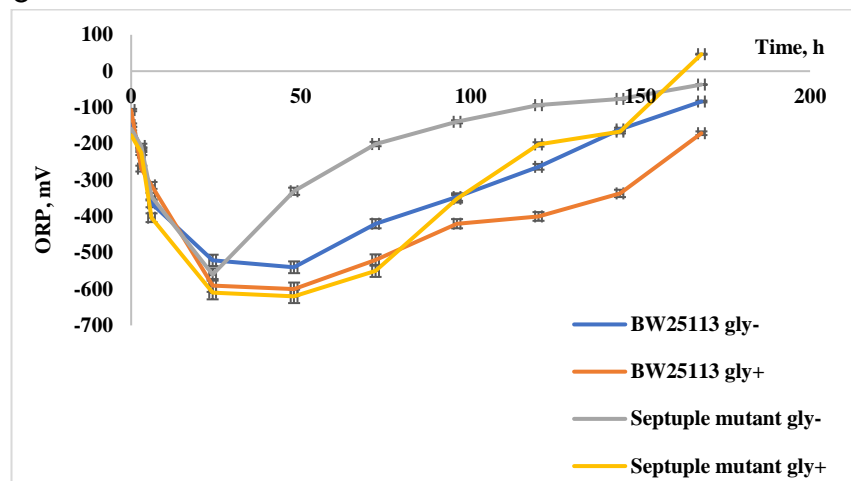


Figure 1 ORP and H₂ production during growth of *E. coli* wild type and septuple mutant at pH 6 (A), pH 7 (B), pH 8 (C). Bacteria were grown upon utilization of 45 min hydrolyzed SCG for 260 h at 37°C.

Table 2. Cumulative hydrogen production yield in *E. coli* wild type and septuple mutant. Bacteria were grown for 45 min in hydrolyzed and twice diluted SCG medium at 37 °C at pH 7.

day	SCG		SCG+glycerol	
	Wild type	Mutant	Wild type	Mutant
1	1740±50	958±29	1960±59	1160±35
2	1090±33	2610±78	880±27	4490±135
3	630±19	710±21	640±19.2	3030±100
5	200±6	1135±34	580±17.4	2620±79
7	220±7	325±9.8	230±7	915±28
14	-	872±26.16	580±17	2165±65
30	-	530±16	360±11	480±15
Total (ml)	3880±117	7465±224	5230±157	14860±445
Yield ml day ⁻¹	130±4	248±7,44	174±5,2	500±15
Yield [ml H ₂ (g SCG) ⁻¹] or [ml H ₂ (g SCG) ⁻¹ 0.3 g(glyc) ⁻¹]:	19.4±0,59	28±0,84	26±0,78	56.5±1,7

CONCLUSION

In conclusion, our study underscores the substantial promise of the SCG by using septuple mutant for large-scale hydrogen production, particularly in the presence of glycerol. This emphasizes its pivotal role in advancing sustainable practices within the circular economy, offering significant potential for efficient and scalable hydrogen generation from waste resources.

ACKNOWLEDGEMENT

This work was supported by a research grant from the Science Committee of the Ministry of Education, Science, Culture and Sports of Armenia to AP (21AG-1F043).

REFERENCES

- [1] Mazloomi K, Gomes C 2012 Hydrogen as an energy carrier: Prospects and challenges. *Renewable and Sustainable Energy Reviews* 16:3024–33.
- [2] Ivanenko AA, Laikova AA, Zhuravleva EA, Shekhurdina SV, Vishnyakova AV, Kovalev AA, et al. 2023 Biological production of hydrogen: From basic principles to the latest advances in process improvement. *International Journal of Hydrogen Energy*, in press.
- [3] Nazir H, Muthuswamy N, Louis C, Jose S, Prakash J, Buan MEM, et al. 2020. Is the H₂ economy realizable in the foreseeable future? Part III: H₂ usage technologies, applications, and challenges and opportunities. *Int J Hydrogen Energy* 45:28217–39.
- [4] Trchounian K, Poladyan A, Vassilian A, Trchounian A. 2012. Multiple and reversible hydrogenases for hydrogen production by *Escherichia coli*: dependence on fermentation substrate, pH and the F₀ F₁ - ATPase. *Crit Rev Biochem Mol Biol* 47:236–49.
- [5] Mussatto SI, Carneiro LM, Silva JPA, Roberto IC, Teixeira JA 2011. A study on chemical constituents and sugars extraction from spent coffee grounds. *Carbohydr Polym* 83:368–74.
- [6] Kovalcik A, Obruca S, Marova I. Valorization of spent coffee grounds: A review 2018. *Food and Bioproducts Processing* 110:104–19.
- [7] Vanyan L, Cenian A, Trchounian K. 2022. Biogas and Biohydrogen Production Using Spent Coffee Grounds and Alcohol Production Waste. *Energies (Basel)* 5935.
- [8] Kang B-J, Jeon J-M, Bhatia SK, Kim D-H, Yang Y-H, Jung S, et al. 2023 Two-Stage Bio-Hydrogen and Polyhydroxyalkanoate Production: Upcycling of Spent Coffee Grounds. *Polymers (Basel)* 15:681.
- [9] Andrade C, Perestrelo R, Câmara JS 2022. Bioactive Compounds and Antioxidant Activity from Spent Coffee Grounds as a Powerful Approach for Its Valorization. *Molecules* 27:7504.
- [10] Clomburg JM, Gonzalez R. 2013. Anaerobic fermentation of glycerol: a platform for renewable fuels and chemicals. *Trends Biotechnol* 31:20–8.
- [11] Petrosyan H, Vanyan L, Mirzoyan S, Trchounian A, Trchounian K. 2020. Roasted coffee wastes as a substrate for *Escherichia coli* to grow and produce hydrogen. *FEMS Microbiol Lett* 367.
- [12] Mirzoyan S, Trchounian A, Trchounian K. 2019. Hydrogen production by *Escherichia coli* during anaerobic utilization of mixture of lactose and glycerol: Enhanced rate and yield, prolonged production. *Int J Hydrogen Energy* 44:9272–81.
- [13] Poladyan A, Trchounian K, Vassilian A, Trchounian A. 2018. Hydrogen production by *Escherichia coli* using brewery waste: Optimal pretreatment of waste and role of different hydrogenases. *Renew Energy* 115:931–6.
- [14] Bekbayev K, Mirzoyan S, Toleugazykyz A, Tlevlessova D, Vassilian A, Poladyan A, et al. 2022 Growth and hydrogen production by *Escherichia coli* during utilization of sole and mixture of sugar beet, alcohol, and beer production waste. *Biomass Conversion and Biorefinery*
- [15] Piskarev IM, Ushkanov VA, Aristova NA, Likhachev PP, Myslivets TS 2010. Establishment of the redox potential of water saturated with hydrogen. *Biophysics (Oxf)* 55:13–7.
- [16] Mirzoyan S, Aghekyan H, Vanyan L, Vassilian A, Trchounian K. 2022 Coffee silverskin as a substrate for biobased production of biomass and hydrogen by *Escherichia coli*. *International Journal of Energy Resource* 46:23110–21.
- [17] Baba T, Ara T, Hasegawa M, Takai Y, Okumura Y, Baba M, et al. 2006. Construction of *Escherichia coli* K-12 in-frame, single-gene knockout mutants: the Keio collection. *Mol Syst Biol* 2.
- [18] Maeda T, Sanchez-Torres V, Wood TK 2007. Enhanced hydrogen production from glucose by metabolically engineered *Escherichia coli*. *Appl Microbiol Biotechnol* 77:879–90.



- [19] Trchounian K, Trchounian A. 2015. Hydrogen production from glycerol by Escherichia coli and other bacteria: An overview and perspectives. Applied Energy 156:174–84.

ICH2P14-OP047

THE HYDROGEN PRODUCTION USING STEAM METHANE REFORMING BASED ON CENTRAL RECEIVER

**Ali Alaidaros, Abdullah A. AlZahrani,*Department of Mechanical Engineering, Umm Al-Qura University, PO Box 715, Makkah, 21955, Saudi Arabia
*Corresponding author e-mail: s44280568@st.uqu.edu.sa

ABSTRACT

In pursuing sustainable and efficient energy solutions, integrating renewable technologies has emerged as a promising option. The primary source of industrial hydrogen is steam methane reforming (SMR); however, this process is based on fossil fuels with massive carbon byproduct emissions. The solar thermal tower appears to be a suitable renewable source for powering SMR by providing heat at a high temperature to drive the process reactions. This approach aims to harness the abundance of solar energy while simultaneously utilizing natural gas as a feedstock for hydrogen production with minimum environmental impact. This research establishes the viability of combining external central receiver concentrated solar power with SMR, revealing general insights into the system's energy and exergy performance. The analysis of the current system is performed using the thermodynamic, and thermochemical approaches to conduct a parametric study. A 220 MW central receiver is first modeled with a high-temperature molten salt as a working fluid. The SMR process model is then developed, considering both reforming and shift reactions, and solved using Engineering Equation Solver (EES). The subsystem models are validated before being integrated into the overall system model. The performance of the SMR reactor is found to considerably affect the overall system performance. The results also show that when increasing the temperature above 750°C, no remarkable improvement in the reforming process is observed. In contrast, the higher the temperature in the water gas shift reactor, the lower the performance that the system achieved. Moreover, due to the large central receiver surface area, the impact of wind velocity on the overall system is considered. At low velocities, the effect is limited up to 5 m/s, but at higher velocities, the efficiency declines by less than 1%. The system's overall performance in terms of energy and exergy efficiencies are 68% and 67%, respectively, additionally, the amount of hydrogen produced at a central receiver of 220 MWth capacity, is about 7.3 kg/s at a 2.1 steam-to-carbon ratio. This integration mitigates a minimum of 12 kg/s of CO₂ emissions that would be generated due to methane combustion.

Keywords: Steam methane reforming, Central receiver, energy and exergy analysis, hydrogen production.

INTRODUCTION

The escalating global energy demand and urgent need to curb greenhouse emissions drive the research for sustainable and efficient energy technologies. Hydrogen as a versatile and clean energy carrier, holds an immense potential to revolutionize various sectors including transportation, industrial, and power generation [1]. Most of the current hydrogen is produced using the conventional steam methane reforming (SMR) process by injecting the methane as a feedstock to produce hydrogen and carbon emissions. This SMR process is dominating the hydrogen production technologies for various applications due to the reduced cost, about \$1.25 per kg for natural gas cost at \$3 per thousand cubic feet [2]. The SMR is a well-established process, in general, it occurs by reacting the methane (CH₄) with steam (H₂O) at high temperatures in the range of (700°C to 1000°C) [3] to produce hydrogen and carbon monoxide (CO). Subsequently, the water gas shift (WGS) reaction is utilized to produce additional hydrogen by consuming carbon monoxide and steam. Thus, the final products of both reactions are hydrogen and carbon dioxide (CO₂). The performance of the SMR process is evaluated using thermodynamics at equilibrium to estimate the hydrogen production rate. An SMR system was presented by Simpson et al. [4]. They presented a thermodynamic analysis of the SMR process showing that for one mol of CH₄ 2.25 mol of hydrogen was produced with energy and exergy efficiencies of about 66.65% and 62.69 % respectively. Soria et al. [5] investigated adding steam to the methane on the reforming activity and products in an attempt to combine SMR and dry methane reforming (DMR). They found that co-feeding of steam increases methane conversion rate hydrogen yield, but decreases carbon dioxide conversion and carbon monoxide yield. Furthermore, they confirmed that their

thermodynamic analysis results were in acceptable agreement with experimental data. Several other studies focused on catalysts development further information can be found in the recent review article [6].

The use of solar energy to power SMR can reduce CO₂ emissions by up to 35-40% compared to the conventional SMR process that relies on fossil fuel combustion [7]. Various solar energy technologies can be utilized to drive SMR processes such as the volumetric reformer and tubular reformer receiver [8]. A designed configuration of volumetric receiver on a parabolic dish on a commercial scale was demonstrated in the Enhanced Solar Absorption Receiver (CAWSAR) [9]. The system was operated during either steady-state or solar fluctuation conditions, this system was reported to achieve a 70% methane conversion factor and the thermal efficiency reached up to 85%. Utilizing a decoupled fluid to transfer the solar energy concept was established by a Spanish-German project [10], the hot air was generated in the solar tower at 1000°C to reform the methane inside a tubular receiver, the final methane conversion was reported between 68% and 93% depending on reformer's operating temperature that ranged from 702 °C and 803 °C.

The central receiver (CR) appears to be a suitable alternative source to maintain the SMR operating conditions based on solar renewable sources. The CR purpose is to collect the solar irradiance using mirrors, installed either around or north -for northern hemisphere- the CR tower, and reflect it to the CR tubes to heat the working fluid. Compared to other solar technologies, CRs can provide a higher temperature up to 1000°C [11]. The performance of the solar tower is affected by energy losses from the receiver and the field. These losses, mainly heat, are radiation and convection losses in addition to reflected losses. On the other hand, field loss occurs due to various imperfections such as cosine loss, reflectivity, shading, and blocking. More details on CR design and performance can be found in the literature [12]. One of the earliest CR pilot projects is the 10 MWe Solar One project located in Barstow, California. In this project, the CR working fluid was water which passes through the cylindrical receiver's tubes to generate steam that can be used in the power cycle to generate electric power [13]. The performance measurements of the Solar One project revealed a CR conversion efficiency of 77%, and it was increased to 82% after the repainting of the receiver surface [12]. The molten salt was a promising working fluid; therefore, the Solar Two project was developed to utilize the molten salt in the CR integrated with thermal energy storage to serve as a heat transfer fluid and a storage medium. Compared with Solar One, Solar Two CR achieved a higher efficiency of about 88% [14]. The current paper proposes using molten salt in the CR not only as a heat transfer fluid but also as a storage medium, enabling a continuous energy supply for SMR. In contrast to previous studies, the current work considered large-scale hydrogen production using SMR powered by a fully dedicated solar thermal system with storage to enable continuous hydrogen production. The proposed integrated system is modeled and the model is validated. Furthermore, a parametric analysis is conducted considering various operating conditions to determine the optimum system performance using energy and exergy approaches.

SYSTEM DESCRIPTION

The system developed for this study consists of a central receiver (CR), thermal energy storage (TES), and steam methane reforming (SMR). The system's purpose is to produce hydrogen in steady-state conditions utilizing solar energy as a renewable source. The hydrogen production starts by feeding the SMR system with methane and steam as shown in Figure 1. The feeding fluid passes through three heating processes and heat recoveries to reach the SMR operating temperature. At 12 and 13 state points, the inlet fluids react inside the SMR reactor, the SMR reaction is an endothermic process, thus, additional energy is required to complete the reaction. Due to the high operating temperature of the SMR system about 720°C as listed in Table 1, the CR technology is suggested to maintain the SMR temperature. The cylindrical central receiver type is used with heliostats to reflect the sun wave to the receiver's tubes. The working fluid in the CR is molten salt with (46.5%LiF_11.5%NaF_42%KF) composition in weight percentage (wt%) [15], the molten salt enters the CR tubes in two paths to be circulated within the CR panels and eventually exits at a higher temperature carrying energy to the SMR reactor. In addition, the solar issues for instance: fluctuation, clouds, and night operating are considered by integrating thermal energy storage to stabilize the system's energy source. The next process in hydrogen production is the water gas shift (WGS) process, in this process, more hydrogen is generated by consuming the carbon monoxide with the rest of the water. In WGS exothermic reaction the expelled

heat is recovered to increase the feeding fluids temperature. In general, the hydrogen mostly is generated in the SMR reactor, and the rest is produced in WGS. The last process is to separate the hydrogen from the carbon dioxide, which occurs in the separator.

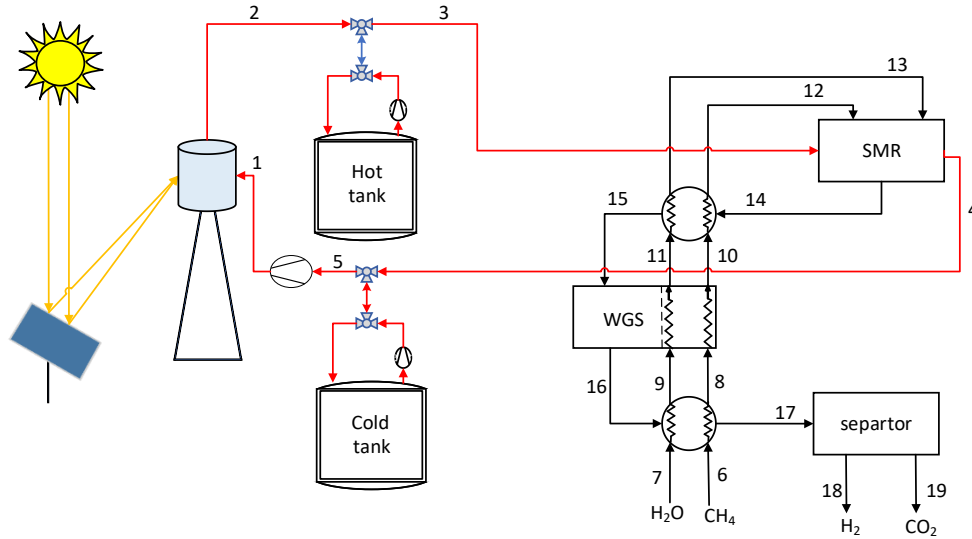


Figure 1 schematic diagram of the hydrogen production system

Table 1. Operating conditions

Parameter	Value/type
Reformer temperature	720 [°C]
Reformer pressure	1 [bar]
Water gas shift reactor temperature	300 [°C]
Water gas shift reactor pressure	1 [bar]
S:C ratio	2.1
Beam radiation	874 [W/m ²]
Working fluid	Salt(46.5%LiF_11.5%NaF_42%KF) [15]
Central receiver diameter	11.8 [m]
Tube diameter	0.029 [m]
Central receiver outlet temperature	850 [°C]
Central receiver inlet temperature	700 [°C]

ANALYSIS

In this section, the mathematical models of the physical subsystems are presented based on the thermodynamics laws and the assumptions considered. First, the analysis of the solar tower is presented followed by SMR. Last, the performance of the overall integrated system is analyzed.

Solar tower

The energy balance of the solar tower is presented as follows:

$$\dot{Q}_s = \dot{Q}_{abs} + \dot{Q}_{cv,loss} + \dot{Q}_{rad} + \dot{Q}_{ref,loss} + \dot{Q}_{opt,loss} \quad (1)$$

Where (\dot{Q}_s) is the solar radiation, (\dot{Q}_{abs}) is the absorbed power in CR, ($\dot{Q}_{cv,loss}$) is the convection loss from CR to the ambient, (\dot{Q}_{rad}) is the radiation loss of CR to ambient, ($\dot{Q}_{ref,loss}$) is the reflected loss due to tube material emissivity, and ($\dot{Q}_{opt,loss}$) is the optical loss. Each term in the balance equation is defined as per the following equations.

$$\dot{Q}_s = A_{hel} I_b \quad (2)$$

$$\dot{Q}_{abs} = \dot{m}_{MS}(h_2 - h_1) \quad (3)$$

$$Q_{cv,loss} = h_{mix} A_{rec}(T_{rec} - T_a) \quad (4)$$

$$\dot{Q}_{rad,loss} = \sigma \varepsilon A_{rec} \left[0.5(T_{rec} - T_{sky})^4 + 0.5(T_{rec} - T_a)^4 \right] \quad (5)$$

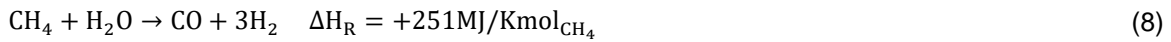
$$\dot{Q}_{ref,loss} = (\dot{Q}_s - \dot{Q}_{opt,loss})(1 - \alpha_{paint}) \quad (6)$$

$$\dot{Q}_{opt,loss} = (1 - \eta_{opt})\dot{Q}_s \quad (7)$$

Were (A_{hel}) is the heliostats area, (I_b) is the beam radiation, (\dot{m}_{MS}) is molten salt mass flow rate, (h_2), (h_1) are the enthalpies of exit and inlet states, (h_{mix}) is the convection heat transfer coefficient, (A_{rec}) is the CR surface area, (T_a) is the ambient temperature, (T_{rec}) is the surface temperature of the CR, (σ) is the Steven Boltzmann constant, (ε) is the emissivity of CR material, (T_{sky}) is the sky temperature, (α_{paint}) is the absorptivity of the CR surface layer, and (η_{opt}) is the optical efficiency of the solar heliostate field.

SMR

To analyze the thermodynamic equilibrium of the SMR and WGS, the overall reactions can be written as the following:



For both reactions, the mole fraction for each element can be found by solving the equilibrium and molar balance equations.

$$\dot{N}_{in,i} = \dot{N}_{out,i} + \dot{N}_{gen,i} \quad (10)$$

$$K_{SMR} = \frac{\left(\frac{y_{CO}P_{SMR}}{P_o}\right) \left(\frac{y_{H_2}P_{SMR}}{P_o}\right)^3}{\left(\frac{y_{CH_4}P_{SMR}}{P_o}\right) \left(\frac{y_{H_2O}P_{SMR}}{P_o}\right)} \quad (11)$$

$$K_{WGS} = \frac{\left(\frac{y_{CO_2}P_{WGS}}{P_o}\right) \left(\frac{y_{H_2}P_{WGS}}{P_o}\right)}{\left(\frac{y_{CO}P_{WGS}}{P_o}\right) \left(\frac{y_{H_2O}P_{WGS}}{P_o}\right)} \quad (12)$$

Where (\dot{N}) is the molar rate of any (i) substance, (P_{SMR}), (P_{WGS}), are the pressure of reforming and shift reactions, (P_o) is the reference pressure, (y) is the molar fraction for (i) substance.

Overall

The overall analysis is defined as shown:

$$\eta_{en,OV} = \frac{\dot{m}_{H_2} \cdot LHV_{H_2}}{\dot{Q}_s + \dot{m}_{CH_4} \cdot LHV_{CH_4}} \quad (13)$$

$$\eta_{ex,OV} = \frac{\dot{m}_H \cdot ex_H}{\dot{E}x_s + \dot{m}_{CH_4} \cdot ex_{CH_4}} \quad (14)$$

Where (\dot{m}_{H_2}) is the hydrogen mass flow rate, (LHV_{H_2}) is the lower heating value of hydrogen, (\dot{m}_{CH_4}) is the methane mass flow rate, (LHV_{CH_4}) is the lower heating value of methane, (ex_H) is the chemical exergy of hydrogen, (ex_{CH_4}) is the chemical exergy of methane, and ($\dot{E}x_s$) the solar exergy.

RESULT

In this section, the solutions obtained are based on the mathematical models that are solved simultaneously using Engineering Equation Solver (EES) software. The chemical equations are considered at equilibrium assuming that reactions occur instantaneously. These models are first validated by comparing the results with those of experimental data then the analyses are conducted as presented in the following

Validation

The verification of the system is conducted by comparing individual subsystem results with established literature findings. Validation of the central receiver model involves comparing it with the Solar One central receiver [12], which has a capacity of 34 MW_{th}, as depicted in Figure 2. This process includes an analysis of the energy efficiency of the receiver in our model, contrasted against the efficiency of Solar One under varying levels of energy absorption in the central receiver. Furthermore, the validation of the steam methane reforming (SMR) system, which operates at a pressure of 1 bar and a steam-to-carbon ratio of 2:1, is shown in Figure 3. This illustration shows how the methane conversion factor and the hydrogen molar fraction change with increasing temperature, comparing these variations to those documented in the prior paper [16].

The comparative validations shown in both Figure 2 and Figure 3 for the receiver and the SMR agree well with the published work and confirm that the model results are acceptable.

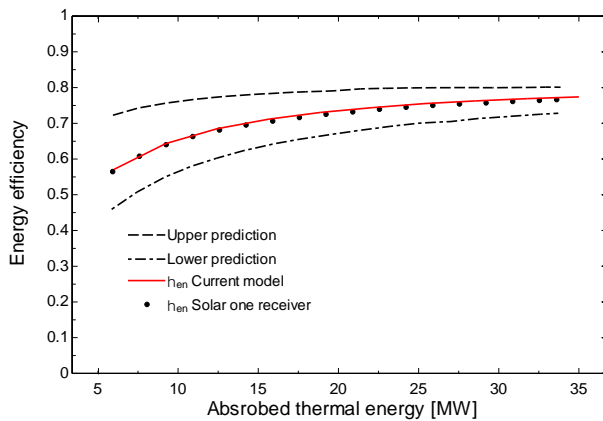


Figure 2. Validation of current central receiver model efficiency with solar one project [12].

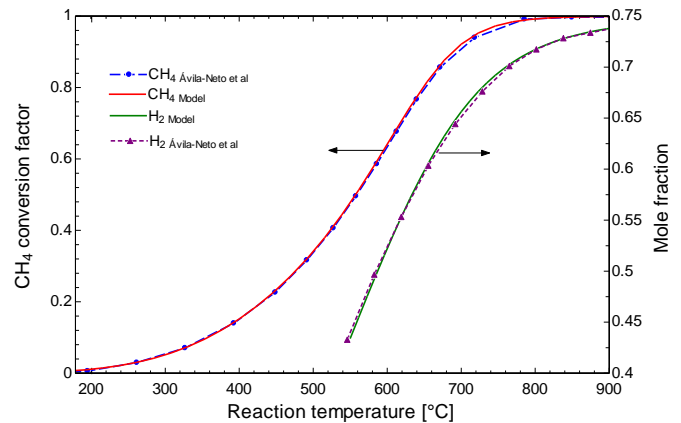


Figure 3. Comparison of hydrogen mole fraction at 1 bar, S:C of 1, and methane conversion at 1 bar, S:C of 2 with literature [16]

Parametric analysis Results

A parametric analysis is conducted to assess the system's performance in producing hydrogen using the energy and exergy approaches as defined in the analysis section. Most hydrogen is generated during the reforming process as clarified in the reaction equation (8). Thus, Figure 4 presents the effect of reforming temperature on the overall efficiencies including energy and exergy efficiencies and the amount of hydrogen within the reforming reaction.

It is noticed that the efficiencies increase from 500°C, however, above 750°C the efficiencies curves leveled and there is no improvement in the performance. Similarly, the mass flow rate rises to 750°C, and no more mass is generated at higher temperatures. The rest amount of the hydrogen is generated in the WGS reaction by consuming the carbon monoxide with steam and the final products are hydrogen

and carbon dioxide. In contrast to the reformer, the higher the temperature in the shift reaction, the less hydrogen can be produced, thus, the system efficiencies decrease marginally with high temperature. Nonetheless, the reaction normally occurs at high temperatures, e.g. at 300°C, this limitation is regraded to the reaction rate, which at low temperatures it's not sufficient to operate due to the long-time of the reaction. Figure 5 illustrates the effect of shift reaction on the system efficiencies and the total mass flow rate of the hydrogen at different operating temperatures. While the shift reaction affects the overall system performance, it's not as significant as the reforming process.

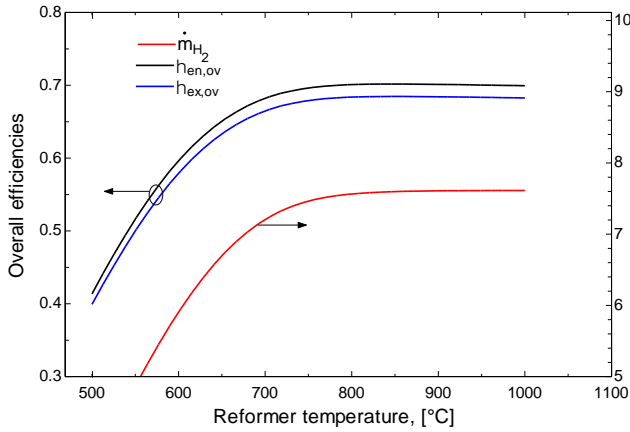


Figure 4. The effect of reformer temperature on overall energy and exergy efficiencies and the hydrogen mass flow rate

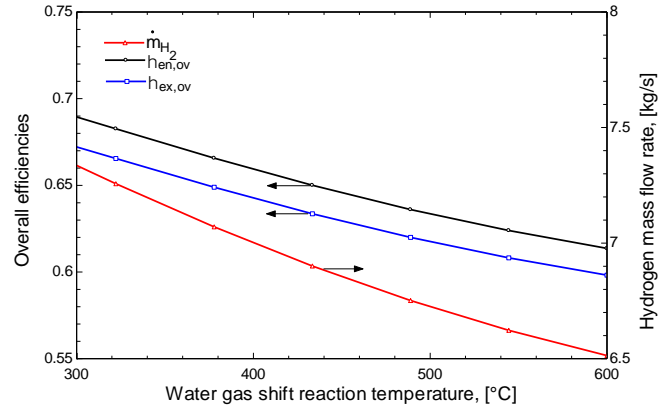


Figure 5. The effect of shift reaction temperature on the overall system's energy and exergy efficiencies and hydrogen mass flow rate

One of the major factors in steam reforming is the amount of added steam represented in the steam-to-carbon ratio (S:C). Usually, the added steam is favorable to increase the hydrogen molecules; however, not all hydrogen can be extracted from steam. Figure 6, shows that the performance and the hydrogen mass flow rate of the overall system accelerate up to 4 ratio and then no more improvement is progressed. Figure 7 is associated with central receiver performance and due to the large surface area of the receiver tubes and the height of the tower, the wind velocity has a noticeable effect on the overall performance. As shown in Figure 7 up to 5 m/s wind speed the change is slightly sighted while above it, the decline is increased along with wind velocity. Even, the amount of the decline is still less than 1% for both energy and exergy efficiencies.

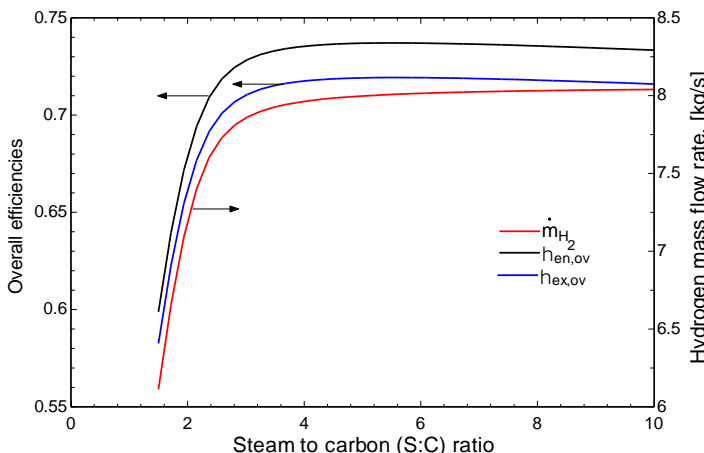


Figure 6 the effect of steam to carbon ratio on the overall system's energy and exergy efficiencies and hydrogen mass flow rate.

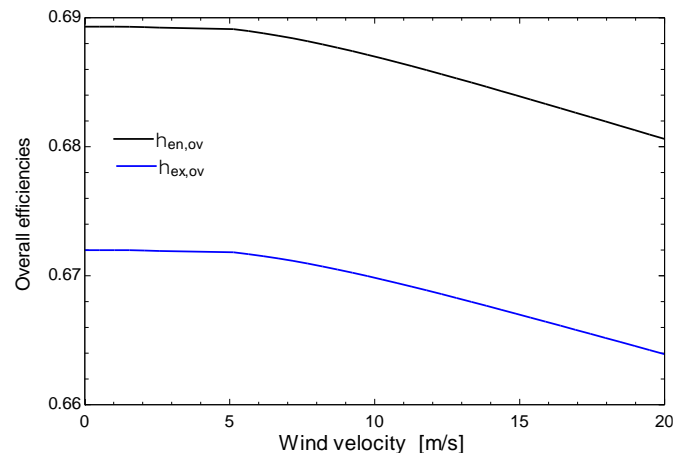


Figure 7 the effect of wind velocity on the overall system's energy and exergy efficiencies and hydrogen mass flow rate

Conclusion

This research demonstrates the potential of combining concentrated solar power with SMR for sustainable hydrogen production. By utilizing the abundant solar energy, methane feedstock can be converted to hydrogen with a minimum amount of carbon emissions. The current paper addresses the overall performance of the solar tower-based SMR system to reveal the system's preferable conditions. The reformer temperature appears to be the main factor that affects the overall performance and

hydrogen production. The results show that 750°C is the optimal operating temperature, and 7.3 kg/s of hydrogen is generated at a solar tower scale of 220 MWth at the operating conditions of Almadina city as provided in the system description. Moreover, the wind velocity has a slight effect on the overall performance ultimately less than 1%. It should be emphasized that the proposed integration of the solar tower with SMR mitigates a minimum of 12 kg/s of CO₂ emissions that would be generated due to methane combustion.

Reference

- [1] I. Dincer, "Green methods for hydrogen production," *Int. J. Hydrog. Energy*, vol. 37, no. 2, pp. 1954–1971, Jan. 2012, doi: 10.1016/j.ijhydene.2011.03.173.
- [2] A. Boretti and B. K. Banik, "Advances in Hydrogen Production from Natural Gas Reforming," *Adv. Energy Sustain. Res.*, vol. 2, no. 11, p. 2100097, 2021, doi: 10.1002/aesr.202100097.
- [3] "Hydrogen Production: Natural Gas Reforming," Energy.gov. Accessed: Oct. 09, 2023. [Online]. Available: <https://www.energy.gov/eere/fuelcells/hydrogen-production-natural-gas-reforming>
- [4] A. P. Simpson and A. E. Lutz, "Exergy analysis of hydrogen production via steam methane reforming," *Int. J. Hydrog. Energy*, vol. 32, no. 18, pp. 4811–4820, Dec. 2007, doi: 10.1016/j.ijhydene.2007.08.025.
- [5] M. A. Soria, C. Mateos-Pedrero, A. Guerrero-Ruiz, and I. Rodríguez-Ramos, "Thermodynamic and experimental study of combined dry and steam reforming of methane on Ru/ ZrO₂-La₂O₃ catalyst at low temperature," *Int. J. Hydrog. Energy*, vol. 36, no. 23, pp. 15212–15220, Nov. 2011, doi: 10.1016/j.ijhydene.2011.08.117.
- [6] S. Wang, S. A. Nabavi, and P. T. Clough, "A review on bi/polymetallic catalysts for steam methane reforming," *Int. J. Hydrog. Energy*, vol. 48, no. 42, pp. 15879–15893, May 2023, doi: 10.1016/j.ijhydene.2023.01.034.
- [7] E. Shagdar, B. Guene Lougou, Y. Shuai, E. Ganbold, O. Paul Chinonso, and H. Tan, "Process analysis of solar steam reforming of methane for producing low-carbon hydrogen," *RSC Adv.*, vol. 10, no. 21, pp. 12582–12597, 2020, doi: 10.1039/C9RA09835F.
- [8] I. Spiewak, C. E. Tyner, and U. Langnickel, "Applications of solar reforming technology," Sandia National Lab. (SNL-NM), Albuquerque, NM (United States), SAND-93-1959, Nov. 1993. doi: 10.2172/10131314.
- [9] J. F. Muir, R. E. Hogan, R. D. Skocypec, and R. Buck, "Solar reforming of methane in a direct absorption catalytic reactor on a parabolic dish: I—Test and analysis," *Sol. Energy*, vol. 52, no. 6, pp. 467–477, Jun. 1994, doi: 10.1016/0038-092X(94)90654-8.
- [10] M. Böhmer, U. Langnickel, and M. Sanchez, "Solar steam reforming of methane," *Sol. Energy Mater.*, vol. 24, no. 1, pp. 441–448, Dec. 1991, doi: 10.1016/0165-1633(91)90081-U.
- [11] L. L. Vant-Hull, "Chapter 8 - Central tower concentrating solar power systems," in *Concentrating Solar Power Technology (Second Edition)*, K. Lovegrove and W. Stein, Eds., in Woodhead Publishing Series in Energy. , Woodhead Publishing, 2021, pp. 267–310. doi: 10.1016/B978-0-12-819970-1.00019-0.
- [12] A. F. Baker, "10 MWe Solar Thermal Central Receiver Pilot Plant Receiver Performance Final Report".
- [13] A. F. Baker *et al.*, "US-Spain evaluation of the Solar One and CESA-I receiver and storage systems," Sandia National Lab. (SNL-CA), Livermore, CA (United States), SAND88-8262, Feb. 1989. doi: 10.2172/6425928.
- [14] R. Bradshaw *et al.*, "Final Test and Evaluation Results from the Solar Two Project," SAND2002-0120, 793226, Jan. 2002. doi: 10.2172/793226.
- [15] M. S. Sohal, M. A. Ebner, P. Sabharwall, and P. Sharpe, "Engineering Database of Liquid Salt Thermophysical and Thermochemical Properties," Idaho National Lab. (INL), Idaho Falls, ID (United States), INL/EXT-10-18297, Mar. 2010. doi: 10.2172/980801.
- [16] C. N. Ávila-Neto *et al.*, "Hydrogen production from methane reforming: Thermodynamic assessment and autothermal reactor design," *J. Nat. Gas Sci. Eng.*, vol. 1, no. 6, pp. 205–215, Dec. 2009, doi: 10.1016/j.jngse.2009.12.003.

ICH2P14-OP052

ASSESSMENT OF HYDROGEN TRADING WITHIN BLOCKCHAIN AND ARTIFICIAL INTELLIGENCE: A REVIEW

¹*Sofya Morozova*, ²*Arif Karabuga*, ³*Zafer Utlu*

¹Haliç University, Department of International Trade and Business, Istanbul, Turkey

²Haliç University, Sustainable Energy Systems Application and Research, Istanbul, Turkey

³Haliç University, Department of Mechanical Engineering, Istanbul, Turkey

*Corresponding author Email: 22051060279@ogr.halic.edu.tr; sofyatoo1@gmail.com

ABSTRACT

This paper showcases the idea of using blockchain technology and subfields of Artificial Intelligence (AI) to establish an efficient hydrogen trading mechanism. A review literature study was conducted in order to understand the abilities of the blockchain to run hydrogen trading contracts. Furthermore, to establish and characterize an example of a smart contract that would cover needed aspects of the hydrogen trading mechanism. As a key outcome, blockchain technology with AI-based predictions can organize the hydrogen trading market under one decentralized network, where all traders are connected and transaction costs and risks associated with intermediaries are decreased. Subfields of AI are able to provide accurate and efficient hydrogen predictions by using train models that collect historical and real-time data. Results given by AI algorithms should help participants to determine future demand for hydrogen credits, leading to more accurate pricing and distribution on the market. Also it was found that for the implementation of prediction model to the blockchain a special structure like oracle, service that enables predicted data to flow from the off-chain environment to on-chain, needs to be used. As a result, hybrid smart contract structure with AI-based predictions suitable for hydrogen trading were described.

Keywords: hydrogen trading, blockchain, artificial intelligence.

INTRODUCTION

The impact of climate change and environmental degradation becomes more obvious, so concern over clear ways of energy production has rapidly increased. New sources for energy production were taken under account and usage worldwide, crucially in countries where elaboration of the natural gas is difficult. Renewable energy such as wind, solar and hydrogen are examples of a global approach to reduce pollution. However, achieving reliable management of an energy market and economic assets requires better and more efficient organization. Hydrogen market is a new mechanism compared to other energy facilities. Green hydrogen (H₂) is a clean energy source that is produced by splitting water into hydrogen and oxygen using electricity from renewable sources. It does not rely on fossil fuels and can replace them in various applications. In order to spread domestically and globally with a larger number of participants hydrogen needs an optimized market. The development of the hydrogen market in the European Union is guided by the strategic goals of prioritizing safety, affordability and autonomy [1]. Countries in Europe have all the power to become a leader in their region and continue influence abroad [2]. Nevertheless, market systems have their limitations. As an example from another field - carbon emissions trading mechanism that already has several running systems. The application of blockchain technology for multi-tier supply chain and carbon trading was tested [3]. One of the biggest challenges facing carbon trading is the establishment of a decentralized system for companies, where in registries the data and transactions will be stored and monitored [4]. In the case of hydrogen, a hydrogen credits framework referenced to carbon credits was established, with the needed policies for the international market [5]. That allows us to suggest the implementation of blockchain infrastructure to create a hydrogen market with decentralized secure connection between parties.

BLOCKCHAIN

Blockchain is a distributed ledger system, the core technology of cryptocurrencies, NFTs, and smart contracts, that was founded by Satoshi Nakamoto in 2008. Technology itself presents “blocks” inside the “chain” where all the data is connected with a previous and the next one. Blockchain begins with a genesis block that does not have previous hash, all next blocks on the chain have hashes with a unique

cryptographic information about previous and the next hash, all these hashes are linked and correlated. This supposes that any change inside the one block will affect the whole system and gives an error as the result. Blockchain solves the double spending problem - duplication of digital content, and creates an immutable record. On account of this, the transaction process is recorded in the entire decentralized ledger network with the same code at the same time without financial intermediaries [6]. Inside the system, no organization can manipulate or compromise the data, to change one block or data the whole chain needs to be re-mined. Thus blockchain provides security, transparency, and permanence, as an example Bitcoin has never been hacked. Blockchain-based Ethereum allows hosting of smart contracts, script software imitation of a traditional contract that runs if agreed conditions have been met. To achieve the agreement between nodes - and users and gain a new block, blockchain has consensus mechanisms such as Proof of Stake is a mechanism used by the new version of Ethereum. PoS requires validation of its tokens in order to become a participant in a consensus. From afar it works like a lottery where you need to buy your invitation to create a new block.

Blockchain technology has the capability to increase the effectiveness of the hydrogen trading process. Blockchain can ensure that all information related is tamper-proof, secure, and decentralized. In addition, blockchain technology could enable the tracking of hydrogen units offset data such as renewable energy certificates, making the process more reliable and easier to verify [7]. The smart contracts of blockchain-enabled new hydrogen trading platforms can automate the process of rewarding companies for their clean energy efforts and encourage greater participation in renewable energy trading.

To enable blockchain system with artificial intelligence subfields as prediction models, information and data from outside the blockchain must be used. This can be achieved using oracles, by oracles resources from off the decentralized system could be taken inside the smart contract structure and some of the blind spots could be closed [8]. ML as a field of AI takes huge energy for data operation and prediction, thus it could be wasteful to build an ML-model directly into the blockchain. Ethereum for an off-chain environment suggests using oracles. It helps smart contracts access and use various ML models and algorithms that can enhance their capabilities and performance. Oracles use data such as market prices, and weather forecasts, as well as to interact with other systems, such as payment platforms, cloud services, and Internet of Things (IoT) devices.

ARTIFICIAL INTELLIGENCE

To start from afar, artificial intelligence (AI) is a software technology, a complicated operation of AI similar to the human brain, and provides the most suitable option from a variety of possible [9]. AI covers neural networks, deep learning (DL), machine learning (ML), forecasting, methods, data analysis, and problem-solving topics [10]. One of the suggestions is that we can use underlying techniques of AI to manage and enhance trading systems. As for the blockchain and smart contracts, machine learning models can provide more reliable data and predictions. Machine learning can predict production of hydrogen, allowing market participants to make more informed decisions. Predictive analytics can help companies and traders determine future demand for hydrogen units, leading to more accurate pricing in the market. On the one hand, AI-based systems can provide control and predict more accurate data. On the other hand, it can establish interactions inside the software system as between traders in further evaluation. By doing so, underlying AI algorithms can provide control and predict more accurate data for big data analytics, and establish interactions inside the software system as between traders in further evaluation for blockchain applications.

PROPOSED SYSTEM

One of the main objectives of this research is to try to establish and characterize a smart contract with an opportunity for prediction models implementation, that can create secure trading transactions on a blockchain platform in a case of hydrogen. In the process a Solidity and Remix - Ethereum IDE is being used to test and debug the smart contract [11]. For an implementation of the AI subfield to the smart contract. an oracle is needed to be used. For example, oracles enable smart contracts to use Google Cloud's BigQuery ML to train and deploy ML models using SQL, and then send the results back to the system.. Adding oracles also helps Veridium's smart contracts use IBM Watson's natural language processing to analyze news articles and social media posts about climate change and carbon policies. Another example is Google Cloud building hybrid blockchain in collaboration with Chainlink provides weather prediction for the services [12]. Out of existing systems, to provide input and output data from

the oracle, the Chainlink – decentralized oracle was taken under closer assessment. Chainlink uses a network of nodes that provide market data, weather data, automation, randomness and API, and information from off-chain sources to on-chain smart contracts from trusted sources via oracles. Thus, Chainlink can use Google Cloud's BigQuery ML to train and deploy machine learning models using SQL, and then send the results to smart contracts via oracles [12].

Writing a smart contract that uses Chainlink and Google Cloud ML contains several stages. First, a machine learning model needs to be created and deployed on Google Cloud ML that can make unit predictions based on some input data. Second, an oracle service needs to be chosen and integrated with the smart contract and the machine learning model. The oracle service can be either centralized or decentralized, depending on the security and reliability requirements. For example, Chainlink is a decentralized oracle service that can connect the smart contract to any external data source or system in a secure and transparent way. Third, the logic and parameters for input and output data from the oracle service need to be defined in the smart contract. The final result of running the code that depends on the data from the oracle service also needs to be specified in the smart contract. For example, a smart contract for hydrogen trading can request the prediction of produced units from the machine learning model using SQL queries, and use it to determine the cost. A smart contract for proposed hydrogen trading can use Chainlink and Google Cloud ML to request the prediction of hydrogen units from a Google Cloud ML model using SQL queries. Generally, and for APIs and for cloud platform function with proper request is built into the smart contract code.

The smart contract expects to include several components and functions that enable the following features:

Registration: The smart contract provides a mechanism for parties to join the blockchain network as either buyers or sellers of hydrogen units. Each party has a unique identifier and a balance of hydrogen units. The smart contract also maintains a list of registered participants and their roles on the network.

Trading: The smart contract facilitates the exchange of hydrogen units between buyers and sellers. The smart contract allows buyers and sellers to create, accept, or cancel offers for hydrogen. Each offer has a price, quantity, and expiration time that are specified by the offer creator. It also keeps track of the completed transactions on the blockchain ledger and updates the balances of the involved entities accordingly.

Prediction: The smart contract leverages machine learning models to forecast the future trends of hydrogen production and market prices. The smart contract uses historical and current data from the blockchain ledger and other sources as inputs for the models. The smart contract also refreshes the models periodically with new data to improve their accuracy and reliability.

Verification: The smart contract ensures the integrity and quality of the hydrogen data that are reported by the parties. The smart contract uses oracles to access external data sources that can verify and validate the data provided by the entities. Oracles are trusted third-party services that can communicate with the smart contract and feed it with external data like a bridge. The smart contract also rewards or penalizes the participants based on their actual hydrogen units compared to their allowances or credits.

RESULTS AND DISCUSSIONS

In this paper, the potential of blockchain technology and AI subfields to enable smart contracts for efficient hydrogen trading was explored. A literature review was conducted to understand how blockchain can run hydrogen trading contracts.

Main findings are:

Blockchain technology with AI-based predictions can create a decentralized hydrogen trading network, where all traders are connected and transaction costs and risks are reduced.

AI subfields can provide accurate and efficient hydrogen predictions by using trained models that collect historical and real-time data. These predictions can help traders to determine the future demand for hydrogen credits, leading to more optimal pricing and distribution in the market.

To implement prediction models on the blockchain, a special structure like an oracle is needed. An oracle is a service that allows predicted data to flow from the off-chain environment to the on-chain smart contract.

A description of a hybrid smart contract with ML-based predictions that is suitable for hydrogen trading was given.

CONCLUSIONS

In conclusion, both blockchain technology and artificial intelligence are popular and discussable topics nowadays, with high expectations for the future. We still need professionals who can continuously write such smart contracts. Hopefully, this idea will continue its development and bring us new models and achievements in the hydrogen trading system.

REFERENCES

1. Nuñez-Jimenez, A., & De Blasio, N. (2022). Competitive and secure renewable hydrogen markets: Three strategic scenarios for the European Union. *International Journal of Hydrogen Energy*, 47(84), 35553–35570. <https://doi.org/10.1016/j.ijhydene.2022.08.170>
2. Caglayan, D. G., Heinrichs, H., Robinius, M., & Stolten, D. (2021). Robust design of a future 100% renewable European energy supply system with hydrogen infrastructure. *International Journal of Hydrogen Energy*, 46(57), 29376–29390. <https://doi.org/10.1016/j.ijhydene.2020.12.197>
3. Lee, A. W. L., Toyoda, K., Yeow, I., Yeo, Z., Low, J. S. C., & Lu, W. F. (2023). Blockchain-enabled carbon emission management system in a multi-tier supply chain. *Procedia CIRP*, 116, 233–238. <https://doi.org/10.1016/j.procir.2023.02.040>
4. Hafner, M., Luciani, G. (2022). *The Palgrave Handbook of International Energy Economics*. In Springer eBooks. <https://doi.org/10.1007/978-3-030-86884-0>
5. Yang, J., Yu, L., Daiyan, R., & Amal, R. (2022b). A green hydrogen credit framework for international green hydrogen trading towards a carbon neutral future. *International Journal of Hydrogen Energy*, 47(2), 728–734. <https://doi.org/10.1016/j.ijhydene.2021.10.084>
6. Nakamoto S., Wright, C. S. (2008). Bitcoin: a Peer-to-Peer electronic cash system. *Social Science Research Network*. <https://doi.org/10.2139/ssrn.3440802>
7. OECD (2019), *The Policy Environment for Blockchain Innovation and Adoption: 2019 OECD Global*
8. Ethereum. (2023). Oracles | Ethereum.org. [ethereum.org. https://ethereum.org/en/developers/docs/oracles/](https://ethereum.org/en/developers/docs/oracles/)
9. Li, J., Herdem, M. S., Nathwani, J., & Wen, J. T. (2023). Methods and applications for Artificial Intelligence, Big Data, Internet of Things, and Blockchain in smart energy management. *Energy and AI*, 11, 100208. <https://doi.org/10.1016/j.egyai.2022.100208>
10. Loureiro, S., Guerreiro, J. F., & Tussyadiah, I. P. (2021). Artificial intelligence in business: State of the art and future research agenda. *Journal of Business Research*, 129, 911–926. <https://doi.org/10.1016/j.jbusres.2020.11.001>
11. Remix - Ethereum IDE. (2023). <https://remix.ethereum.org/>
12. Day, A. (2019, June 13). Building hybrid blockchain/cloud applications with Ethereum and Google Cloud. *Google Cloud Blog*. <https://cloud.google.com/blog/products/data-analytics/building-hybrid-blockchain-cloud-applications-with-ethereum-and-google-cloud>

ICH2P14-OP053

THERMODYNAMIC ANALYSIS OF PTC-BASED HYDROGEN PRODUCTION SYSTEM

¹Arif Karabuga, ²Zafer Utlu, ³Hasan Ayarturk

¹Haliç University, Sustainable Energy Systems Application and Research Center, Istanbul, Türkiye

²Haliç University, Faculty of Engineering, Mechanical Engineering, Istanbul, Türkiye

³RePG Energy Systems Inc., Bursa, Türkiye

*Corresponding author e-mail: arif.karabuga@gmail.com

ABSTRACT

In this study, hydrogen production at low temperatures is experimentally investigated. The presented study consists of three main stages. The first of these is thermal energy production, the second is electricity generation, and the third is hydrogen production. Parabolic trough collector (PTC) is used for thermal energy generation, organic Rankine cycle (ORC) is used for electricity generation, and proton exchange membrane (PEM) electrolyzer is used for hydrogen production. All of the electricity obtained from the ORC system, which has a unique design, is used for hydrogen production. In the presented study, the turbine output power is calculated as 1.956 kW and the net power of the ORC system is calculated as 1.381 kW.

Keywords: PTC, Hydrogen production, Green hydrogen, Thermodynamic analysis.

INTRODUCTION

The prominent option to cope with the global energy and climate crises is using alternative energy technologies. The most important alternative source to fossil fuels is renewable energy. Among the renewable energy sources, the most economical and applicable energy source is solar energy. There are two options to benefit from solar energy. These systems produce direct electricity (PV systems) and indirect electricity production (collector systems). In this study, the parabolic trough collector (PTC) system, which is a type of thermal collector system that produces indirect electricity, was examined experimentally. PTC systems are widely used in renewable energy power plants because they produce thermal energy at high temperatures [1]. PTC systems are used to produce steam energy for electricity generation, in addition to being used in heating processes, air conditioning and cooling applications [2]. There are various studies in the literature using PTC systems. Some of these are; Razmi et al. (2022) [3] presented the thermodynamic and economic analysis of the solar energy-assisted hydrogen production system in their study. As a result of the study, the exergy efficiency and cost of the presented system were found to be 17.6% and 592.4 \$/hour, respectively. Sathish et al (2023) [4] examined the thermodynamics and cost analysis of the PTC-assisted hydrogen production system. The highest amount of heat energy obtained in the PTC system was calculated as 25.489 MW and the thermal efficiency was 82%. In addition, the cost of daily hydrogen production was found to be 212.3 \$/kg.

In this study, the thermodynamic analysis of the PTC-assisted electricity and hydrogen production system is discussed experimentally. In the study, the amount of hydrogen to be obtained and the parameters affecting the energy efficiency of the system are evaluated holistically. In addition, it is aimed to determine ideal operating conditions to increase hydrogen production.

MATERIALS AND METHODS

In this section, the working principle of the experimental set and the formulas required for thermodynamic analysis are presented. The flow chart of the presented experimental set is presented in Figure 1. The collector has a mouth opening of 1.54 m². Figure 2 shows the PTC used in the study. Thermal energy coming out of the collector (point 2) is transferred to the ORC system through the heat exchanger. R1234yf fluid is used as the working fluid in the ORC system. The fluid temperature at the turbine inlet is approximately 122°C. Some of the energy produced by the turbine is spent in pumps. After subtracting the energy expenditures on the pumps, the net work obtained from the ORC system is found. All of the energy produced is transferred to the proton exchange membrane electrolyzer (PEMe) for hydrogen production. There are two basic requirements for the production of green

hydrogen, in other words, by the electrolysis of water using a renewable energy source. One of them is electricity and the other is water. The water used in PE must be ultrapure water. The main reason for this is that the membrane pores are not clogged.

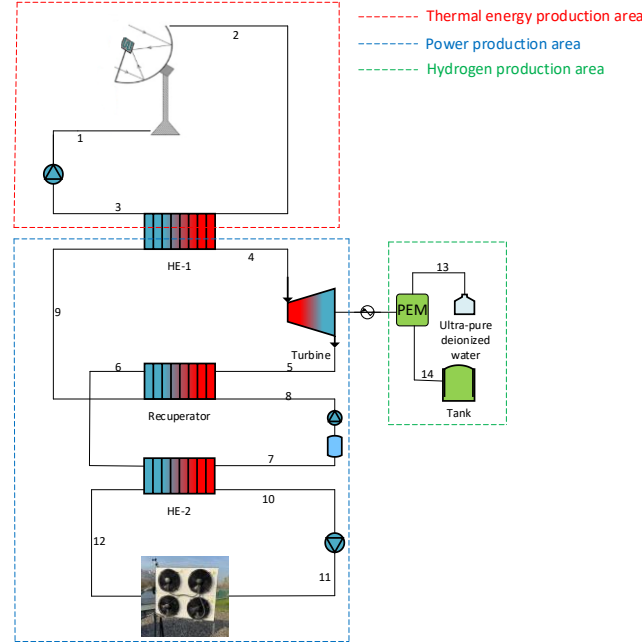


Fig. 1. Flow chart of PTC based hydrogen production system

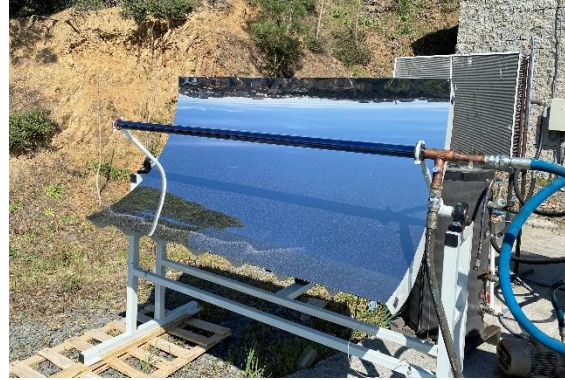


Fig. 2. PTC used in the experimental study

While performing thermodynamic performance analysis, energy analysis method was used for various parameters that ambient temperature, mass flow, and turbine inlet temperature, and a package program called Engineering Equation Solver (EES) was used. The energy equations applied to each component in the proposed system are given below [5];

$$\sum \dot{m}_{in} = \sum \dot{m}_{out} \quad (1)$$

$$\Delta E = \sum \dot{Q} - \sum \dot{W} + \sum \dot{m}_{in} h_{in} - \sum \dot{m}_{out} h_{out} \quad (2)$$

$$\dot{Q}_{solar} = IA\sigma\alpha \quad (3)$$

$$\eta = \frac{\dot{m}_{hydrogen} LHV}{\dot{Q}_{solar}} \quad (4)$$

RESULTS AND DISCUSSION

In this section, the graph obtained as a result of the thermodynamic analysis of the experimental study presented is shared. Figure 3 shows the change in the energy efficiency of the system and the amount of hydrogen production depending on the turbine inlet temperature. If the turbine inlet temperature increases from 100°C to 200°C, the energy efficiency of the entire system increases from 1.30% to 6.46%. Moreover, as another result of this increase in the turbine inlet temperature, the amount of hydrogen production increases from 0.000002211 kg/s to 0.00001045 kg/s. In the thermodynamic analysis of the system, the radiation intensity was measured as 550 W/m², the fluid flow rate in the ORC system was 0.04 kg/s and the collector outlet temperature was measured as 126°C. As a result of the study, turbine inlet temperature is an important parameter of system efficiency and hydrogen production amount.

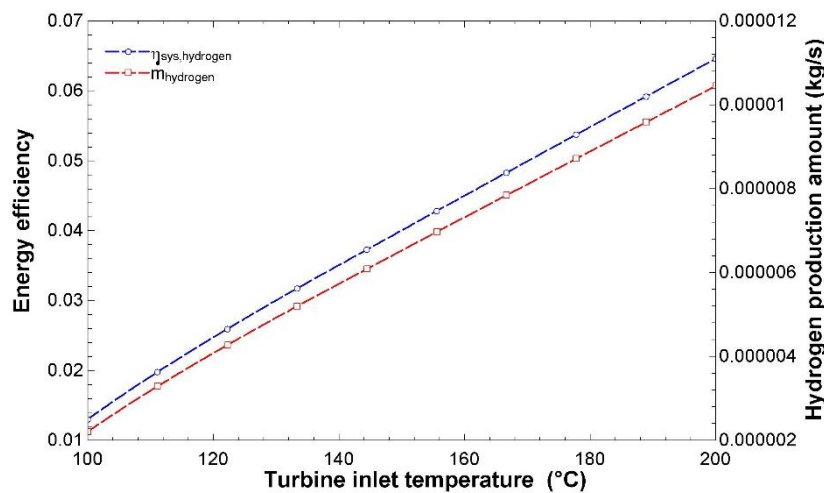


Fig. 3. Change in energy efficiency and hydrogen production amount of the presented system depending on turbine inlet temperature

CONCLUSIONS

In this study, PTC supported electricity and hydrogen production system used to benefit from solar energy is discussed. It has been observed that the turbine inlet temperature has a significant effect on the amount of electricity production, the energy efficiency of the system and the amount of hydrogen produced. The main results obtained as a result of the study are given below.

- The amount of energy produced from the turbine was measured as 1.9 kW.
- The energy efficiency of the system is calculated as 2.24%.
- The amount of hydrogen obtained from PEMe is 0.00000372 kg/s.

NOMENCLATURE

A	Area, m ²
\dot{E}	Energy rate, kW
h	Specific enthalpy, kJ/kg
\dot{m}	Mass flow rate, kg/s
\dot{Q}	Heat energy, kW
\dot{W}	Work, kW

Greek Letters

η	Energy efficiency
--------	-------------------

REFERENCES

1. Bedakhanian A, Maleki A, and Haghghat S. 2022. Utilizing the multi-objective particle swarm optimization for designing a renewable multiple energy system on the basis of the parabolic trough solar collector. *International Journal of Hydrogen Energy* 47(86): 36433-36447.
2. Damarseckin S, Atiz A and Karakilcik M. 2023. Solar pond integrated with parabolic trough solar collector for producing electricity and hydrogen. *International Journal of Hydrogen Energy* (In Press).
3. Razmi AR, Alirahmi SM, Nabat MH, Assareh E, and Shabakhti M. 2022. A green hydrogen energy storage concept based on parabolic trough collector and proton exchange membrane electrolyzer/fuel cell: Thermodynamic and exergoeconomic analyses with multi-objective optimization. *International Journal of Hydrogen Energy* 47(62): 26468-26489.
4. Sathish T, Sailaja C, Saravanan R, Suresh P, Anish M, Rajasimman M, Sambath U, Sabarirajan N, Muthukumar K, Joo SW, and Vasseghian Y. An absorber of parabolic trough collector for hydrogen production in a solid oxide fuel cell. *Fuel* 343:127982.
5. Karayel GK, and Dincer I. 2023. Green hydrogen production potential of Canada with solar energy. *Renewable Energy* (In Press)

ICH2P14-OP054

PERFORMANCE EVALUATION OF DIFFERENT WORKING FLUIDS IN S-ORC BASED HYDROGEN PRODUCTION SYSTEM

¹Arif Karabuga, ²Zafer Utlu, ³Melik Ziya Yakut

¹Haliç University, Sustainable Energy Systems Application and Research Center, Istanbul, Türkiye

²Haliç University, Faculty of Engineering, Mechanical Engineering, Istanbul, Türkiye

³Isparta University of Applied Sciences, Faculty of Technology, Mechatronics Engineering, Isparta, Türkiye

*Corresponding author e-mail: arif.karabuga@gmail.com

ABSTRACT

In this study, the hydrogen production system integrated into the solar-organic Rankine cycle (S-ORC) system is discussed. An evacuated tube solar collector (ETSC) is used to benefit from solar energy. The thermal energy obtained from the collector is produced in the integrated ORC system. Different fluids are examined comparatively in the S-ORC system. As a result of the study, the energy efficiency of the whole system for hydrogen production was calculated as 47.86%, 50.7%, 65.75% and 53.55% by using R134a, R1234yf, R410a and R32 fluids in the ORC system.

Keywords: Solar-ORC, Hydrogen production, Green hydrogen, Energy efficiency.

INTRODUCTION

The global climate crisis is a prevalent problem for all countries. For this reason, developed and developing countries base their energy policies on decarbonization. There are three main reasons for the global climate crisis. These; anthropological effects, volcanic activities and solar radiation. Among these three factors, the only parameters that can be avoided and that we can focus on in solving the climate crisis are anthropological factors [1]. Hydrogen energy is the prominent solution option among existing energy technologies to protect against the consequences of industrial activities with anthropological effects. In particular, hydrogen energy obtained from renewable energy sources by electrolysis of water, in other words, green hydrogen production, forms the basis of states' hydrogen policies. Solar, wind and geothermal energy are widely used in green hydrogen production [2, 3]. Roy and Samanta, (2024) [4] made a thermodynamic and economic analysis of solar energy-assisted hydrogen production. A parabolic trough solar collector and solid oxide electrolyzer were used in the presented study. The exergy efficiency of the entire presented system was calculated as 10.16% and its cost was 1.021 \$/kg. Karayel and Dincer, (2023) [5] examined solar energy-supported hydrogen production for different regions of Canada. Hydrogen was produced using alkaline, proton exchange membrane and anion exchange membrane electrolyzers. The highest hydrogen production was obtained in the anion exchange membrane with 211.17 Mt.

In this study, solar energy-assisted hydrogen production is discussed. The main purpose of this study is to examine energy changes depending on different working fluids in the ORC system used at low and medium temperature intensity.

MATERIALS AND METHODS

In this section, information about the experimental study will be given and details of the thermodynamic analysis of the experimental set will be shared. In the presented experimental study, an evacuated tube heat pipe solar collector (ETHPSC) with low and medium temperature density is used to benefit from solar energy, organic Rankine cycle (ORC) for electricity production and proton exchange membrane electrolyzer (PEMe) for hydrogen production. The flow chart of the presented study is shown in Figure 1. Terminal VP-1, a heat transfer oil, is used as the working fluid in ETHPSC. The heat transfer oil coming out of the collector is transferred to the ORC system through the heat exchanger. Four different working fluids are used respectively in the ORC system. The fluids used in the ORC system are R134a, R1234yf, R410a and R32. The net energy obtained from the ORC system is transferred to PE for hydrogen production. Ultrapure water is used to clean the PEMe membrane pores. The purity of the water used directly affects the usage time of the electrolyzer. Water in PEMe is approximately 0.045µS.

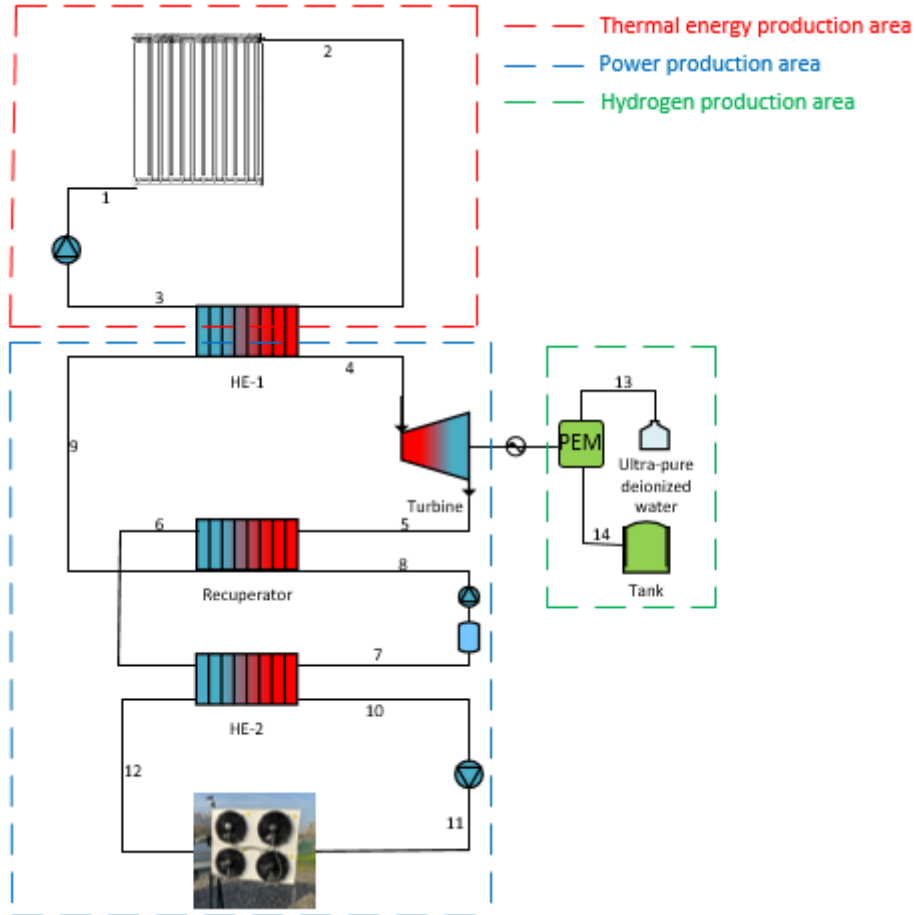


Fig. 1. ETHPSC based hydrogen production system [6]

While performing thermodynamic performance analysis, energy analysis method was used for various parameters that ambient temperature, mass flow, and turbine inlet temperature, and a package program called Engineering Equation Solver (EES) was used. The energy equations applied to each component in the proposed system are given below [7];

$$\sum \dot{m}_{in} = \sum \dot{m}_{out} \quad (1)$$

$$\Delta E = \sum \dot{Q} - \sum \dot{W} + \sum \dot{m}_{in} h_{in} - \sum \dot{m}_{out} h_{out} \quad (2)$$

$$\dot{Q}_{col} = I \rho_{ref} \rho_{rec} \varepsilon_{rec} A_n A_{rec} \quad (3)$$

$$\dot{Q}_{solar} = IA\sigma\alpha \quad (4)$$

$$\eta = \frac{\dot{Q}_{col}}{\dot{Q}_{solar}} \quad (5)$$

RESULTS AND DISCUSSION

In this section, the data obtained as a result of thermodynamic analysis are shared. Table 1 presents the energy efficiency and hydrogen production amount depending on four different fluids in the system operating at 95°C collector outlet temperature and 0.09 kg/s ORC working fluid flow rate. When the presented table is examined, the highest energy efficiency is obtained in R410a fluid with 65.75%. The lowest energy efficiency is achieved with R134a fluid. In addition, the highest annual hydrogen production is 131.3 kg/annual when R410a fluid is used. Figure 2 shows the change in energy efficiency of the entire system depending on the increase in turbine inlet temperature. All fluids show an increasing trend depending on the increase in turbine inlet temperature. Even though the highest energy efficiency is achieved in R410a fluid, the most notable change in inlet temperature occurs in R1234yf fluid. System efficiency increases from 15.47% to 78.91%.

Table 1. Obtained results from presented study

	R134a	R1234yf	R410a	R32
Energy efficiency (%)	47.86	50.7	65.75	53.55
Hydrogen production amount (kg/annual)	91.59	97.91	131.3	104.2

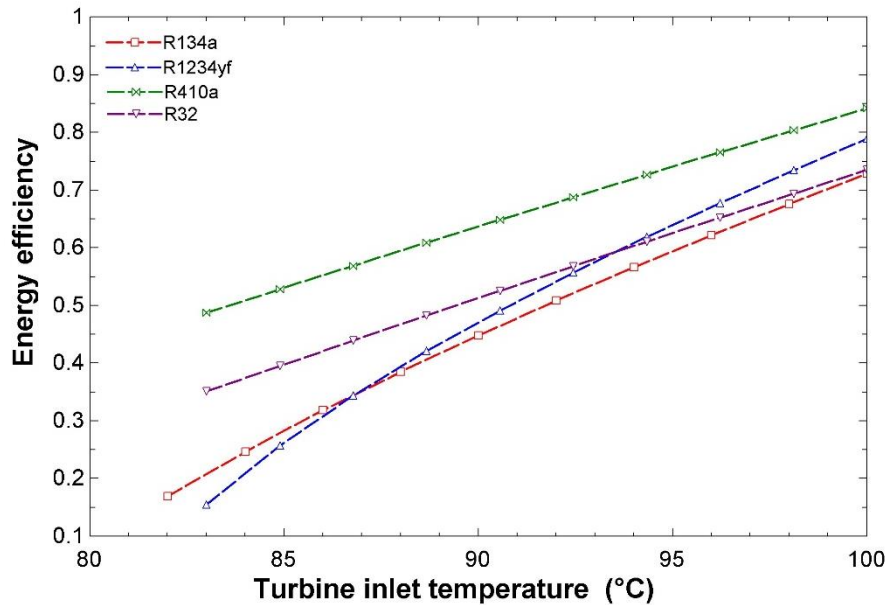


Fig.2. Change in energy efficiency of the presented system depending on turbine inlet temperature

CONCLUSIONS

In this study, thermodynamic analysis of an ETHPSC-based hydrogen production system to benefit from solar energy is presented. The results obtained from the analysis based on the turbine inlet temperature are as follows;

- The highest energy efficiency is when R410a fluid is used, with 65.75%.
- The highest hydrogen production amount was calculated as 131.3 kg/annual.
- Change in turbine inlet temperature is the basic parameter affecting system efficiency.

NOMENCLATURE

A	Area, m ²
\dot{E}	Energy rate, kW
h	Specific enthalpy, kJ/kg
\dot{m}	Mass flow rate, kg/s
\dot{Q}	Heat energy, kW
\dot{W}	Work, kW

Greek Letters

η	Energy efficiency
--------	-------------------

REFERENCES

1. Shakouri H. 2019. The share of cooling electricity in global warming: Estimation of the loop gain for the positive feedback. *Energy* 179:747-761.
2. Morrison A, Bhatelia T, Acquarola C, and Shah M. 2024. Low-carbon methanol production using solar thermal energy: A techno-economic assessment. *Green Technologies and Sustainability* 2(1):100059.
3. Shang R, Shi P, Yue Y, and Sardari F. 2023. Simulation and multi-aspect investigation of a geothermal-based power, hydrogen, oxygen, and fresh water production integrated into a flue gas-driven combined power plant. *Process Safety and Environmental Protection* 180: 648-668.
4. Roy D, and Samanta S. 2024. A solar-assisted power-to-hydrogen system based on proton-conducting solid oxide electrolyzer cells. *Renewable Energy* 220:119562.
5. Karayel GK, and Dincer I. 2023. Green hydrogen production potential of Canada with solar energy. *Renewable Energy* (In Press)
6. Karabuga A, Yakut MZ, and Utlü Z. 2023. Assessment of thermodynamic performance of a novelty solar-ORC configuration based hydrogen production: An experimental study. *International Journal of Hydrogen Energy* 48(99):39154-39168
7. Dincer I., Rosen M.A. (2020). *Exergy: Energy, Environment and Sustainable Development*, Third Edition.

ICH2P14-OP065

SOLAR HYDROGEN AND METHANOL PRODUCTION WITH CSP/PV DRIVEN ELECTROLYSER

¹*Nathalie Monnerie*, ¹*Andreas Rosenstiel*, ^{1,2}*Christian Sattler*

¹German Aerospace Center (DLR), Institute of Future Fuels, Linder Höhe, Cologne, Germany

²RWTH Aachen University, Chair for Solar Fuel Production, Templergraben 55, Aachen, Germany

*Corresponding author e-mail: nathalie.monnerie@dlr.de.

ABSTRACT

Hydrogen and its derivatives produced using renewable energy can have an important contribution to the energy transition and play a significant role in cutting greenhouse gas emissions. If produced with CO₂ from a sustainable source, synthetic fuels like e.g. methanol have the potential to replace some current fuels and to assist the chemical sector in moving away from fossil feedstocks. Amongst the renewable energies, solar energy has a huge potential, especially in the Earth's sunbelt which could become a large exporter of green hydrogen and methanol.

Nevertheless, the cost-efficiently production of hydrogen and methanol using solar energy is quite challenging. On one side, the use of photovoltaics (PV) can provide low levelized cost of electricity, but power availability is limited to daytime and can fluctuate depending on solar radiation. Using batteries for storage is possible but too expensive for storing large amounts of electricity. On the other side, the concentrated solar power (CSP) with thermal storage technology enables to store energy at lower costs and to generate electricity round-the-clock but the levelized costs of electricity are higher than those from PV.

Therefore, the combination of a concentrated solar power plant including a thermal molten salt storage with a photovoltaic power plant seems to be a good solution to ensure a relatively continuous power supply at low cost for the electrolysis and other process units. As these systems achieve more full-load times, they are expected to be more economical than systems without a storage option. This CSP/PV hybrid concept for hydrogen production can be e.g. coupled with a methanol production process. Models for both processes have been created and dynamic annual simulations were carried out. The full solar hydrogen and methanol production process chain has been evaluated and techno-economic analyses have been realized. In the case of solar hydrogen, production cost of 3.09 USD/kg has been calculated considering the anticipated cost reduction in the next years. In case of Methanol, a production cost of 726 €/t is expected, which demonstrate the attractive potential of this hybrid technology.

Keywords: Hydrogen, Methanol, Solar Fuels, Concentrated Solar Power, Techno-economic Assessment.

INTRODUCTION

In order to achieve climate neutrality and to facilitate the breakthrough of renewable energies across all industries, hydrogen technologies will be crucial [1,2]. Green hydrogen and its derivatives, which is generated by renewable energy sources and traded globally, is largely seen as a key component of a future hydrogen economy [3] and its production in the earth's sunbelt with the combination of available land and strong solar radiation is particularly promising. For this, alkaline electrolysis, which is a viable and well-established technique [4], can be used and be powered by solar energy, meaning photovoltaics (PV) and concentrated solar power (CSP). However, it is difficult to produce hydrogen and methanol using solar energy in a cost-effective manner. On the one hand, using photovoltaics (PV) can result in low levelized electricity costs; nevertheless, power availability is dependent on solar radiation and is only available during the day. It is possible to store electricity using batteries, but the cost is still prohibitive. Conversely, thermal storage technology combined with concentrated solar power (CSP) allows for more cost-effective energy storage and continuous electricity generation; however, the levelized costs of electricity are greater than those of photovoltaic (PV) systems.

Hence coupling photovoltaics with the concentrated solar power technology and thermal energy storage appears to be a good way to meet these requirements in locations with high solar irradiance. When solar radiation is not available, the stored heat can be used to generate electricity in the steam cycle or fed directly into the synthesis process. Thus, a concept based on the combination of these established

technologies and therefore suitable for short-term implementation for the solar production of hydrogen and methanol was developed and analysed in terms of economic viability.

MATERIALS AND METHODS

Alkaline electrolysis is combined with the provision of electricity from a CSP/PV hybrid power plant (See Figure 1). Models of the individual process components are created and annual yield calculations based on meteorological data carried out. A techno-economic assessment is carried out for three reference years (2020, 2030, 2045) considering possible decreasing costs for CSP and PV [5, 6] and for three locations to show the impact of various solar resources. An amortisation period of 20 years and an interest rate of 5% was assumed. Selling excess electricity and oxygen as a by-product is not considered. The models contain cost functions in order to optimise the capacity of the individual process components with regard to minimising the product costs. Based on this hydrogen and methanol production costs were determined. A sensitivity analysis shows how a variation in the cost assumptions effects the final results.

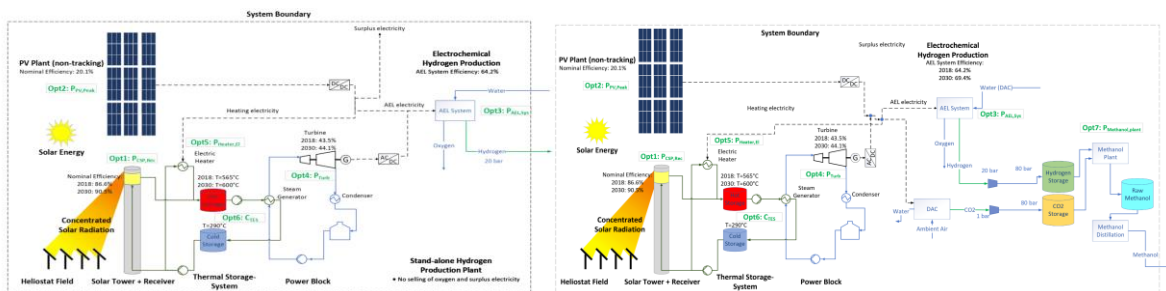


Fig. 1. CSP/PV hybrid electrolyser driven concept (for hydrogen and for methanol production)

RESULTS AND DISCUSSION

Production costs are heavily dependent on solar irradiation and lowest costs are therefore achieved for the location with the highest solar resource. For hydrogen, the lowest levelized cost of hydrogen LCOH are calculated to 4.04 USD/kg for the current PV and CSP investment costs and to 3.09 USD/kg for the future scenario (See Figure 2) For methanol, depending of the CO₂ source required for its production, production costs are in range of 726 to 974 €/t. In all cases, integrating concentrated solar power with photovoltaic technology is the most economically promising concept according to the assumptions made.

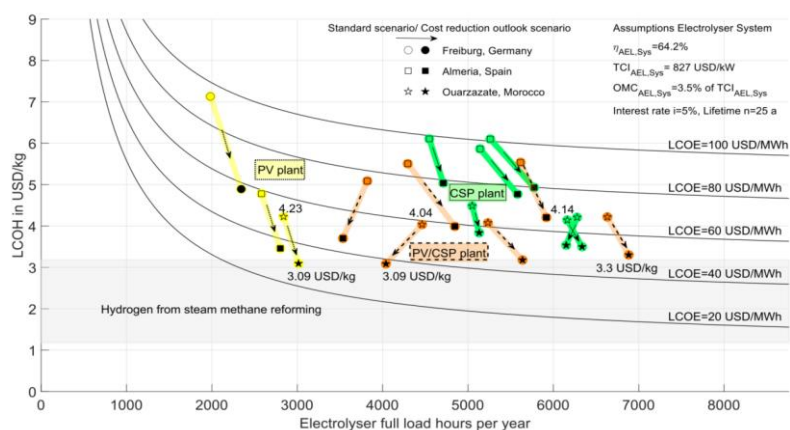


Fig. 2. Results of the hydrogen production costs [<https://www.mdpi.com/1996-1073/14/12/3437>]

CONCLUSIONS

In order to produce hydrogen and methanol cost-efficiently with renewable solar energy, an alkaline electrolyser system and a methanol production plant driven by a hybrid CSP/PV power plant has been modelled and optimized. Dynamic annual simulations were carried out for different locations. Techno-

economic assessments have been conducted and the entire solar hydrogen and methanol generation process chain assessed. In the case of solar hydrogen production, the estimated cost decrease of PV and CSP components in the upcoming years has led to a production cost of 3.09 USD/kg. A production cost of 726 €/t is anticipated for methanol, illustrating the hybrid technology's appealing potential.

ACKNOWLEDGEMENT

The authors of this paper gratefully acknowledge the funding of the project SolareKraftstoffe (Grant agreement Nr. 03EIV221), MENA-Fuels (Grant agreement Nr. 03EIV181A-C) and TUNol (Grant agreement Nr. 03EE5123E) by the Federal Ministry for Economic Affairs and Energy, on the basis of a decision by the German Bundestag as well as the financial support from DLR's basic funding for the project Neofuels.

REFERENCES

1. European Commission. The European Green Deal COM/2019/640 Final; European Commission: Brussels, Belgium, 2019.
2. FCH JU. Hydrogen Roadmap Europe. A Sustainable Pathway for the European Energy Transition, 1st ed.; FCH JU: Luxembourg, 2019.
3. The National Hydrogen Strategy; Federal Ministry for Economic Affairs and Energy, P.R. Division: Berlin, Germany, 2020
4. Buttler, A.; Spliethoff, H. Current status of water electrolysis for energy storage, grid balancing and sector coupling via power-to-gas and power-to-liquids: A review. *Renew. Sustain. Energy Rev.* 2018, 82, 2440–245
5. Dersch, J.; Dieckmann S.; Hennecke K.; Pitz-Paal R.; Taylor M.; Ralo P., LCOE reduction potential of parabolic trough and solar tower technology in G20 countries until 2030 , AIP Conference Proceedings, 2303, 1, 2020, <https://doi.org/10.1063/5.0028883>
6. IRENA. Future of Solar Photovoltaic: Deployment, Investment, Technology, Grid Integration and Socio-Economic Aspects (A Global Energy Transformation: Paper); International Renewable Energy Agency: Abu Dhabi, United Arab Emirates, 2019.

CH2P14-OP067

AN OPTIMUM APPROACH FOR BIOHYDROGEN PRODUCTION USING POPLAR

^{1,2*}A. Yagmur Goren, ¹Muratcan Kenez, ¹Ibrahim Dincer, ³Ali Khalvati

¹Ontario Tech University, Faculty of Engineering and Applied Science, 2000 Simcoe Street North, Oshawa, Ontario L1H 7K4, Canada

²Izmir Institute of Technology, Faculty of Engineering, Department of Environmental Engineering, Urla, Izmir, 35430, Türkiye

³Agro-Environmental Innovation and Technology, Research and Development Company, Thornhill, Ontario, L3T 0C6, Canada

*Corresponding author e-mail: Aysegul.Kara@ontariotechu.ca

ABSTRACT

Biohydrogen (Bio-H₂), a sustainable and environmentally friendly energy alternative, is critical in transitioning towards a more energy-efficient future. This research investigated the potential of utilizing poplar leaves as a substrate for bio-H₂ production with dark fermentation process, an underexplored area. Through a series of fifty-eight experimental runs according to the Box-Behnken Design (BBD), insightful findings were obtained about the bio-H₂ production process. The ideal maximum bio-H₂ production rate was estimated at approximately 0.2 mL/h, with an optimal time constant of about one hour. This study also identified optimal operational conditions for maximizing bio-H₂ production using Design-Expert statistical software with the BBD tool: an acid concentration of 10 %, a biomass quantity of 2.009 g, an initial pH of 7.65, a temperature of 39.9 °C, and a mixing ratio of 325.66 rpm. These conditions were projected to produce a maximum bio-H₂ production of 0.76 mL/g.

Keywords: Biohydrogen, Poplar leaves, Dark fermentation, Box-Behnken design, Optimization.

INTRODUCTION

At present, the conversion of natural gas and other fossil-based products, which is fairly cost-effective but has negative environmental effects, is the main source of H₂ generation on an industrial scale. Typical H₂ production technologies are not sustainable since they rely on supplies that are not renewable. On the other hand, the production of biohydrogen (bio-H₂) from algae, agricultural waste, and energy crops has been described as a source of green and sustainable energy [1]. To address the shortcomings of traditional or industrial-scale H₂ production procedures, biological approaches such as dark fermentation (DF), photofermentation (PF), and hybrid methods have attracted a significant amount of interest [2]. In more recent research, complex feedstock has gained significant attention, such as agricultural residues, industrial wastes, livestock waste, energy crops, and organic fractions of municipal waste [3]. Energy crops have been utilized to generate bio-H₂ more sustainably among these biomass resources. In general, lignocellulosic energy crops may produce more in less ideal conditions with low risk and need fewer fertilizer supplies.

So, one viable method for obtaining sustainable biomass is to grow lignocellulosic energy crops on degraded areas. It is vital to evaluate the biomass produced by energy crops on marginal or degraded lands to understand the potential of bioenergy systems. However, there is limited study on using energy crops for bio-H₂ production. Besides, to our best knowledge, the optimization studies with the Box-Behnken design (BBD) tool for bio-H₂ production using poplar leaves are insufficient and limited. Also, there is no study on bio-H₂ production using the DF process in the presence of a commercial microorganism source. Therefore, there is a crucial need for a comprehensive study on optimizing the DF process, which is performed using poplar leaves and commercially available microorganism sources.

Further to note that this is the amplest study on bio-H₂ production from poplar biomass with the help of commercial and cheap microorganism sources. The effects of operational factors such as acid concentration (AC), biomass concentration (BC), initial pH (pH_i), temperature (T), mixing ratio (MR), and microorganism concentration (MC) were studied to evaluate the optimum conditions. The BBD was carried out to evaluate the impact of the variables on the production of bio-H₂ and to optimize the process performance with the least amount of experiments. A mathematical model of BBD may also be used to forecast process results without the need for running tests, which suggests a good potential for use in pilot or real-scale applications.

MATERIALS AND METHODS

Bio-H₂ production using anaerobic DF was performed in 250 ml flasks with a volume of 100 mL on batch operating mode. The specified volume of acid-treated hydrolysate and inoculum (commercial microorganisms) was fed into the flasks and the pH was adjusted to the desired values. Each flask was covered using aluminium foil to prevent light intrusion into the reactor and the caps of the flasks were tightly closed with an airtight stopper, allowing the reactor to remain in oxygen-free conditions. Then, the bottles were placed on a heated magnetic stirrer, and anaerobic condition was guaranteed by purging the airtight flasks with pure N₂ gas. The operating time of fermentation experiments was 12 hours. The produced gas from the reactor was analyzed with an H₂ gas sensor.

The poplar leaves utilized in this study were harvested from the private garden in Thornhill, Canada. In the pre-treatment step, the specified amount of poplar leaves (2-10 g) was mixed at 150 rpm with various concentrations (1-6%, v/v) of 10 mL HCl acid solution in 25 mL flasks to obtain a slurry and pre-treatment experiments were conducted in an autoclave at 120 °C for 30 min. The response surface methodology (RSM) with the BBD tool was used for experimental design and optimization. The BBD consists of three basic steps: evaluating the model's suitability, predicting the response variables, and identifying the minimal number of carefully selected statistically constructed experimental runs. The BBD was performed to enhance bio-H₂ production and obtain maximum H₂ production rate, and consider the combined and individual impact of operational variables. Design Expert 13 was used for the statistical design and data analysis.

RESULTS AND DISCUSSION

The combined effects of several operational parameters on bio-H₂ production were investigated. Among all operational parameters, the acid concentration was found to be the most effective operational parameter on bio-H₂ production. Results revealed that the bio-H₂ production decreased with the increasing biomass amount at constant acid concentrations (Fig. 1a). For instance, the bio-H₂ production decreased from 0.4 to 0.2 mL/g with increasing biomass concentration from 2 to 10 g at the acid concentration of 10%. Similar results were observed for the other acid concentrations. The inadequacy of the fermentable sugars could explain the decrease in bio-H₂ production at high biomass amounts. Namely, the low bio-H₂ production obtained at high biomass concentrations shows that the acid utilized in the pre-treatment step cannot adequately decompose the biomass into valuable sugars. Therefore, increasing the biomass by keeping the acid concentration constant will not increase bio-H₂ production alone. On the contrary, as seen in the results, the remaining biomass without being degraded into sugars causes agglomeration in the environment, creating an unsuitable environment for microorganisms, and causing a decrease in hydrogen production. However, there was no significant change in bio-H₂ production considering the combined effect of microorganism amount and temperature (Fig. 1b).

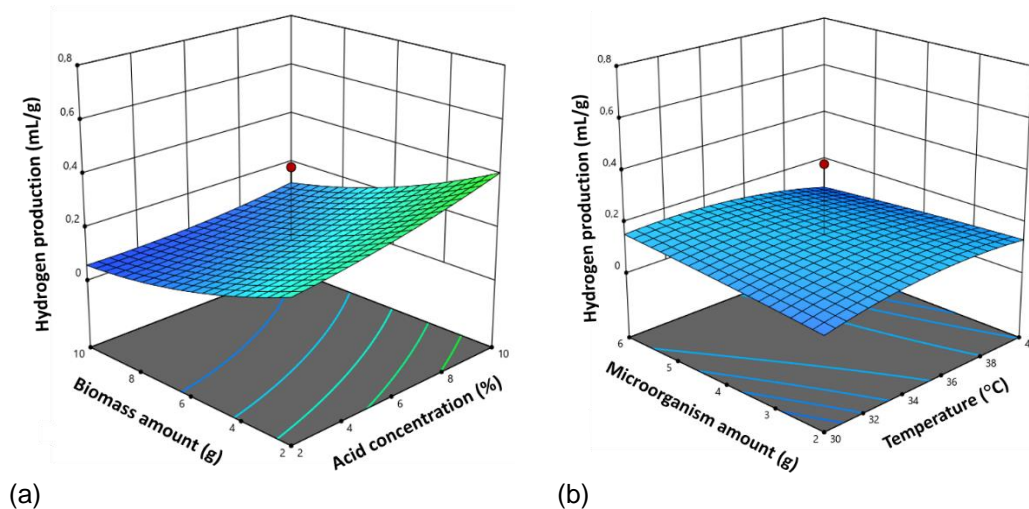


Fig. 1. Combined effects of parameters on production: (a) Biomass amount-acid concentration and (b) microorganism amount-temperature.

CONCLUSIONS

This study has presented a novel approach to generating renewable bio-H₂ using poplar leaves. Moreover, the BBD methodology was performed to optimize the efficiency of the DF for bio-H₂ production. In total, fifty-eight experimental runs were performed, and the combined effects of operational parameters were investigated. The optimum operational parameters predicted using BBD were an acid concentration of 10%, a biomass quantity of 2.009 grams, an initial pH of 7.65, a temperature of 39.9 °C, and a mixing ratio of 325.66 rpm considering the highest bio-H₂ production of 0.76 mL/g. In conclusion, this study offers significant benefits as one of the limited number of studies investigating the combined effect of operational parameters on bio-H₂ production using the DF process.

REFERENCES

1. Machineni L, Deepanraj B, Chew KW, Rao AG. 2023. Biohydrogen production from lignocellulosic feedstock: Abiotic and biotic methods. *Renewable and Sustainable Energy Reviews* 182:113344.
2. Anjum S, Aslam S, Hussain N, Bilal M, Boczka G, Smulek W, 2023. Bioreactors and biophoton-driven biohydrogen production strategies. *International Journal of Hydrogen Energy* 48:21176-21188.
3. Goren AY, Dincer I, Khalvati A. 2023. Comparative environmental sustainability assessment of biohydrogen production methods. *Science of the Total Environment* 166613.

ICH2P14-OP070

BIO-INSPIRED OPTIMIZATION OF HYDROGEN PRODUCTION PLANTS: HARNESSING THE POLLUTANTS FOR ENHANCED EFFICIENCY OF FUEL CELL

^{*1,2}*Khaled Abu Alfoul, ^{1,2}Anaam Abu Foul*

¹Albayt University, College of Engineering, Renewable and Sustainable Energy, Amman, Jordan

²Yarmouk university, Business, Business Administration, Amman, Jordan

*Corresponding author e-mail: kabwalfwl@gmail.com

ABSTRACT

This research explores the use of pollutants generated by hydrogen production plants to enhance efficiency while reducing environmental impact. The introduction traces the history of fuel cell development and highlights the environmental concerns associated with hydrogen production, focusing on the growing demand for this versatile energy carrier. To achieve the objectives of the study, computer experiments were used to simulate the chemical equations that occur inside luminous insects. The research hypothesis assumes a positive relationship between the use of emissions and reduced environmental impact, as well as increased fuel cell efficiency. In conclusion, this research seeks to address pressing environmental concerns related to hydrogen production. The study also aims to benefit from emissions resulting from hydrogen production, reduce environmental impact, increase the efficiency of fuel cells, and enhance global energy security. By reducing 60% of emissions, especially those associated with sulfur, nitrogen and carbon emissions, they will be used and exploited to generate a new type of energy.

Keywords: Hydrogen, Energy, Fuel cell, Pollution, Renewable.

INTRODUCTION

The summary of the introduction provided covers the history, current state, and potential future developments in the field of fuel cells and hydrogen energy.

Sir William Robert Grove developed the concept of fuel cells in 1838, pioneering the creation of a device that generates electricity by combining oxygen and hydrogen. Subsequent notable contributions were made by Friedrich Wilhelm Ostwald, who elucidated the relationship between various components of a fuel cell, and Francis Thomas Bacon, who developed a high-pressure nickel electrode fuel cell (Rayment and Sherwin, 2003). According to the 2022 International Energy Agency report, global hydrogen demand reached 94 million tons in 2021, mainly produced from natural gas, coal, and oil, with a small percentage from green hydrogen. Hydrogen production is associated with significant CO₂ emissions, with China being a major producer (Meng et al., 2021). The increase in hydrogen production, largely from fossil fuels, contributes to harmful emissions and global warming. Fuel cells offer a solution for remote areas lacking grid access. However, the production of hydrogen, especially gray and blue hydrogen, results in pollutants and toxic gases..(Niakolas et al., 2016).

The Russian-Ukrainian war led to a significant rise in natural gas prices, especially in the European Union countries, where the data of the International Energy Agency indicate that Russia represents the largest source of natural gas to the European continent by 45%(IEA, 2022), which made many countries to invest and move towards renewable energy and hydrogen energy, where hydrogen is considered It is one of the most abundant sources in the atmosphere, but it does not come in a natural or independent form, as some processes must be performed in order to extract it in its pure form, which results in many pollutants from these processes, and some of these gases are considered toxic, especially when manufacturing gray and blue hydrogen, which dominate the energy market Hydrogen, as they constitute more than 96% of the hydrogen currently generated around the world (Howarth and Jacobson, 2021) due to the low cost of these two types compared to green hydrogen.

The study aims to develop a technology to reduce emissions and economic costs associated with hydrogen energy production. It proposes using the Firefly technique, a form of bioluminescence involving luciferin, and oxygen, to improve fuel cell efficiency. This technique has applications in various fields including biotechnology, space study, medicine, and pest control. This summary encapsulates

the evolution of fuel cell technology, its current challenges in terms of environmental impact and economic feasibility, and the potential innovative solutions being researched to address these issues.

The summary highlights the challenges and opportunities in the context of global population growth, which has reached 8 billion, leading to increased energy demand. This demand surge has contributed to higher greenhouse gas emissions, with fossil fuels making up about 80% of the global energy mix. This scenario, outlined by the Environmental and Energy Studies Institute (EESI), underscores the need for solutions to reduce emissions, which are a major contributor to climate change and droughts worldwide. The study introduces the concept of the 'hydrogen contract', a response to the extensive development of hydrogen utilization technologies. Hydrogen is seen as a promising energy source due to its high energy density. The study aims to reduce and repurpose emissions from hydrogen production, converting them into a new form of energy, rather than releasing them into the atmosphere.

However, previous research has been inconclusive, particularly regarding the effective use of emissions from hydrogen production facilities. The study, therefore, sets out five main objectives: 1) Utilizing pollutants from hydrogen production as an energy source, inspired by the bioluminescence of fireflies; 2) Increasing the efficiency of fuel cells; 3) Reducing the environmental impact of hydrogen production facilities; 4) Enhancing energy supply through the successful development of this technology; and 5) Strengthening global energy security. These goals are crucial in addressing the increasing energy demands while mitigating environmental damage.

The study also points out a gap in existing research. To date, there appears to be no comprehensive study on the utilization of pollutants from gray and blue hydrogen production stations across the globe. While many studies have focused on reducing emissions from these stations, there is a noted lack of research on how to beneficially use the emissions they generate. This identifies a significant area for potential study and innovation in the field of energy production and environmental management.

LITREATURE REVIEW

The literature review in this study broadly examines the environmental, economic, and technological aspects of hydrogen production and the impact of various pollutants on fuel cell performance.

Impact of Pollutants on Fuel Cells:

(Cheng et al., 2007) his study discussed the impact of pollution on the fuel cell. Highlighted that even small amounts of pollutants like CO, CO₂, H₂S, and NH₃ significantly impair fuel cell performance, especially at low temperatures. According to (Krishnan et al., 2008) Focused on the adverse effects of pollutants in coal-derived gas on fuel cells, notably H₂S, AsH₃, PH₃, and CH₃Cl. They found that H₂S and AsH₃ particularly deteriorate cell performance.

Environmental and Economic Aspects of Hydrogen Production:

(Kothari et al., 2008) the aim of the study is to measure the effect of pollutants in coal-derived gas and their effect on the performance of the fuel cell. Emphasized the benefits of using renewable energy for hydrogen production to achieve zero emissions.

According to (Dufour et al., 2009) Investigated the steam reforming process, including thermal and catalytic decomposition of methane gas.

(Acar and Dincer, 2013) his study aimed to compare the methods of hydrogen production from renewable and non-renewable sources. Compared hydrogen production methods in Turkey, considering environmental impacts, production costs, and energy efficiency. The results of the study indicate that different regions and the availability of raw materials in these regions have different options for hydrogen production.

(Chai et al., 2021) Analyzed the pros and cons of different hydrogen production technologies, focusing on China's development in this area. The result of the study showed many disadvantages and

advantages of hydrogen production technology through electrolysis of water, which is characterized by being free of pollution, high purity of hydrogen, in addition to cleanliness. As for the disadvantages, they are the high-energy consumption, and the high hydrogen production cost. (Ullman and Kittner, 2022)The study concluded indicated that autocatalytic decomposition is one of the most environmentally friendly processes .Found autocatalytic decomposition to be environmentally friendly and noted a decrease in CO₂ emissions with steam reforming combined with CO₂ storage.

Specific Studies on Hydrogen Production Technologies:

(Suleman, 2014) his study has two aims. First, study the process of re-forming methane gas with steam derived from natural gas. How much has been the study of electrical hydrogen production with renewable energy. The results of the study indicated that hydrogen production by natural gas had the greatest impact on the environment in terms of pollutants

(Acar and Dincer, 2015) Examined the economic, environmental, and social effects of hydrogen production, contrasting fossil fuels and renewable energy sources. It found through the study that systems that depend on renewable energy sources to produce hydrogen achieved zero emissions harmful to the environment, but were less efficient and more expensive. While it showed that coal-based, methods gave higher efficiency and lower cost

(Nikolaidis and Poullikkas, 2017) Discussed the economic aspects of various hydrogen production methods, emphasizing the cost-effectiveness of the SMR process. the result of the study showed that the SMR process is one of the most cost-effective hydrogen production processes

(Golmakani et al., 2020) Aimed to demonstrate the efficacy of steam methane reforming technology for high purity hydrogen production, addressing the challenges of removing impurities like nitrogen gas. . It found through the study that the alternating current layer was capable of removing methane, carbon dioxide and carbon monoxide. It also found that the zeolite layer was insufficient to get rid of from nitrogen gas. The effect of N₂ impurity on PVSA performance further investigated by simulating two feeds with 3.1% and 1.1% N₂.

In summary, the literature review covers a range of studies that collectively analyze the impact of pollutants on fuel cells, the environmental and economic implications of hydrogen production technologies, and the potential of various methods to achieve efficient, clean, and cost-effective hydrogen production. Some previous studies examined the reduction of emissions from hydrogen production plants, and studies on the issue of exploiting these emissions and using them in energy production were not discussed.

RESEARCH METHODOLOGY

Computer models were used to predict the results of various experiments before they were actually conducted, where software was used MATLAB to provide a comprehensive understanding and optimization of the energy production process, identify influential variables such as temperature, pressure, and proportions of chemicals, and analyze their impact on energy production. The laboratory experiment was represented in computer models to achieve identical or close results to laboratory experiments due to the lack of laboratories in our country. Optimal codes were used to determine the best efficiency increase and cost reduction.

EQUATIONS

It is this reaction that takes place inside the luminous insects that triggers the process of bioluminescence: The lighting process inside the firefly takes place with a series of chemical equations, starting first with the process of combining luciferin with ATP to produce luciferyl adenylylate and ppi.

These are the equations that were used in computer modeling:



Luciferin=C₁₁H₈N₂O₃S₂

ATP –C₁₀H₁₆N₅O₁₃P₃ Energy in the body gotten through eating.(Lanza and Nair, 2009).

Luciferyl Adenylate: So large it is not given a chemical formula, breaks to from the light producing chemicals. ppi: inorganic pyrophosphate, a catalyst enzyme, not used later in the reaction, but used in other bodily functions (Lanza and Nair, 2009).

Then the process reaches the process of merging luciferyl adenylate with oxygen to produce oxyluciferin, which is the most important element in the process, as it is the element responsible for the lighting process.

These fireflies usually emit light in the yellow to green range, which means that the light range will be within 520-590 nm, which indicates that the light is within the visible light.

Luciferly Adenylate+O₂→Oxyluciferin+AMP+Light

Luciferly Adenylate: so large it is not given a chemical formula, breaks to from the light producing chemical. O₂: peroxide causes a redox a reaction. Oxyluciferin:C₁₀H₆N₂O₂S₂ ,The actual luminescent chemical; AMP: The switch, A increase its proportion is what causes the Oxyluciferin to begin to emit light; Light: photons emitted by the Oxyluciferin (Lanza and Nair, 2009).

RESULTS

The research conducted at the yielded significant findings in the field of hydrogen production optimization. The primary focus was on utilizing pollutants from hydrogen production plants to enhance the efficiency of fuel cells.

Pollutant Utilization Efficiency: The study successfully demonstrated that by harnessing pollutants such as sulfur, nitrogen, and carbon emissions, it is possible to reduce environmental impact significantly. Our results indicated a reduction of up to 60% in these emissions.

Enhanced Fuel Cell Performance: Incorporating bio-inspired techniques, notably mimicking the firefly bioluminescence process, showed a marked improvement in fuel cell efficiency. This novel approach led to a more effective conversion of chemical energy into electrical energy.

Economic and Environmental Benefits: The research underscored the potential economic benefits of this innovative approach. By reducing reliance on traditional energy sources and minimizing waste, the bio-inspired method presents a cost-effective solution. Environmentally, this approach contributes to reduced greenhouse gas emissions, aligning with global sustainability goals..

Challenges and Opportunities: The study also identified key challenges, including the need for advanced materials for efficient pollutant capture and the scalability of the bio-inspired process. However, the opportunity to revolutionize hydrogen production with a sustainable and efficient method was widely recognized.

Comparative Analysis: Compared to traditional methods of hydrogen production, this bio-inspired approach not only reduces emissions but also offers an innovative way to utilize waste by-products. This represents a significant shift from current practices, which predominantly focus on emission reduction alone.

CONCLUSION

The findings of this research carry profound implications for the future of hydrogen production. By demonstrating the feasibility of using pollutants to enhance fuel cell efficiency, the study paves the way for more sustainable and environmentally friendly hydrogen production methods. The successful application of bio-inspired techniques opens up new avenues for research and development in this field,

potentially leading to groundbreaking changes in energy production technologies. To the best of my knowledge, no research has been conducted on the utilization of pollutants from gray and blue hydrogen production stations across the world, as studies have focused on reducing these emissions where there is a lack of studies on benefiting from the emissions generated from these stations.

REFERENCES

- (IEA), I. E. A. 2022. How Europe can cut natural gas imports from Russia significantly within a year. *In: ENERGY*, R. (ed.).
- ACAR, C. & DINCER, I. 2013. Comparative environmental impact evaluation of hydrogen production methods from renewable and nonrenewable sources. *Causes, impacts and solutions to global warming*, 493-514.
- ACAR, C. & DINCER, I. 2015. Impact assessment and efficiency evaluation of hydrogen production methods. *International journal of energy research*, 39, 1757-1768.
- CHAI, S., ZHANG, G., LI, G. & ZHANG, Y. 2021. Industrial hydrogen production technology and development status in China: A review. *Clean Technologies and Environmental Policy*, 23, 1931-1946.
- CHENG, X., SHI, Z., GLASS, N., ZHANG, L., ZHANG, J., SONG, D., LIU, Z.-S., WANG, H. & SHEN, J. 2007. A review of PEM hydrogen fuel cell contamination: Impacts, mechanisms, and mitigation. *Journal of Power Sources*, 165, 739-756.
- DUFOUR, J., SERRANO, D., GÁLVEZ, J., MORENO, J. & GARCIA, C. 2009. Life cycle assessment of processes for hydrogen production. Environmental feasibility and reduction of greenhouse gases emissions. *International journal of hydrogen energy*, 34, 1370-1376.
- GOLMAKANI, A., NABAVI, S. A. & MANOVIĆ, V. 2020. Effect of impurities on ultra-pure hydrogen production by pressure vacuum swing adsorption. *Journal of Industrial and Engineering Chemistry*, 82, 278-289.
- HOWARTH, R. W. & JACOBSON, M. Z. 2021. How green is blue hydrogen? *Energy Science & Engineering*, 9, 1676-1687.
- KOTHARI, R., BUDDHI, D. & SAWHNEY, R. 2008. Comparison of environmental and economic aspects of various hydrogen production methods. *Renewable and Sustainable Energy Reviews*, 12, 553-563.
- KRISHNAN, G., JAYAWEERA, P., BAO, J., PEREZ, J., LAU, K., HORNBOSTEL, M., SANJURJO, A., ALBRITTON, J. & GUPTA, R. 2008. Effect of coal contaminants on solid oxide fuel system performance and service life. SRI International, Menlo Park, CA (United States).
- LANZA, I. R. & NAIR, K. S. 2009. Functional assessment of isolated mitochondria in vitro. *Methods in enzymology*, 457, 349-372.
- MENG, X., GU, A., WU, X., ZHOU, L., ZHOU, J., LIU, B. & MAO, Z. 2021. Status quo of China hydrogen strategy in the field of transportation and international comparisons. *International Journal of Hydrogen Energy*, 46, 28887-28899.
- NIAKOLAS, D. K., DALETOU, M., NEOPHYTIDES, S. G. & VAYENAS, C. G. 2016. Fuel cells are a commercially viable alternative for the production of "clean" energy. *Ambio*, 45, 32-37.
- NIKOLAIDIS, P. & POULLIKKAS, A. 2017. A comparative overview of hydrogen production processes. *Renewable and sustainable energy reviews*, 67, 597-611.
- RAYMENT, C. & SHERWIN, S. 2003. Introduction to fuel cell technology. *Department of Aerospace and Mechanical Engineering, University of Notre Dame, Notre Dame, IN*, 46556, 11-12.
- SULEMAN, F. 2014. *Comparative Study of Various Hydrogen Production Methods for Vehicles*, University of Ontario Institute of Technology (Canada).
- ULLMAN, A. N. & KITTNER, N. 2022. Environmental impacts associated with hydrogen production in La Guajira, Colombia. *Environmental Research Communications*, 4, 055003.

ICH2P14-OP071

INVESTIGATION OF A NEW ENERGY SYSTEM WITH RECYCLED ALUMINIUM-WATER HYDROGEN PRODUCTION

**Andre Bolt, Ibrahim Dincer, Martin Agelin-Chaab*

Clean Energy Research Laboratory (CERL), Faculty of Engineering and Applied Science, Ontario Tech. University, 2000 Simcoe Street North, Oshawa, Ontario L1H 7K4, Canada

*Corresponding author e-mail: Andre.Bolt@ontariotechu.ca

ABSTRACT

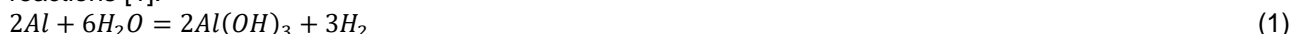
The presented study illustrates the design and investigation of a new renewable multigeneration system capable of hydrogen production through the aluminium water chemical reaction and electrolysis. The system can also produce other useful outputs such as electrical power, space heating and space cooling. The system achieved hydrogen production rates of 0.01277 kgs⁻¹ and 0.02299 kgs⁻¹, respectively, for the electrolysis system and from the aluminium-water reaction. Additionally, the system achieved an electrical energy output, heating load, and cooling load of 2571 kW, 2576 kW, and 344.7 kW, respectively.

Keywords: Hydrogen, Aluminium-Water, Electrolysis, Solar Power, Wind Power, Energy.

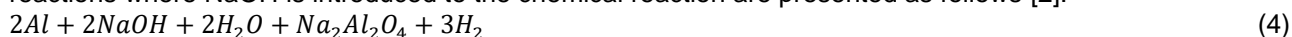
INTRODUCTION

As issues revolving around climate change and global warming become a growing concern, hydrogen as an energy carrier and fuel source is considered highly beneficial. This is attributed to the high energy density of hydrogen and the fact that it does not produce carbon dioxide during its combustion. In order to synthesize hydrogen sustainably, water-splitting techniques such as electrolysis have tremendous benefits, given that the earth's surface is primarily covered with water. However, hydrogen production through the Aluminium-Water Chemical Reaction is another water-splitting technique that has not been thoroughly investigated.

By reacting water and aluminium, hydrogen gas can be produced as depicted by the following chemical reactions [1]:



However, a protective oxide layer on the exterior surface of aluminium usually forms when it comes in contact with oxygen; this layer inhibits the reaction from continuously occurring. To mitigate the formation of the oxide layer, various techniques can be used, such as adding reaction promoters to the process. The net chemical reactions where NaOH is introduced to the chemical reaction are presented as follows [2]:

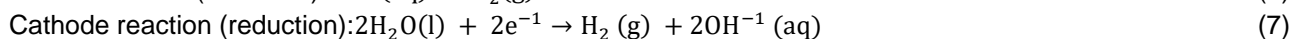


The NaOH used in the chemical reaction can be produced through many techniques, such as the Chlor-Alkali process. This process uses the membrane electrolysis of brine to produce Cl₂(g), H₂(g), and NaOH (aq) simultaneously. The Cl₂ and the H₂ can be stored for later use; however, the NaOH (aq) can potentially react directly with Al to produce additional H₂.

The proposed multigeneration system presents the design of a novel integrated system located within Calgary Alberta, which is capable of producing H₂, and several other additional useful outputs. The system will utilize wind turbines for its electrical energy input for the chlor-alkali process and to contribute toward the total amount of electrical power produced. Additionally, the system contains concentrating solar collectors to provide the necessary thermal energy input to operate the system. These other useful outputs of the system include electrical power, space heating, and space cooling. In the past, conventional multigeneration systems did not integrate aluminium-water hydrogen reactions as a proposed method to produce H₂. Furthermore, the system provides a viable approach to generate the NaOH consumed during the reaction while producing additional H₂ from electrolysis.

ANALYSIS

Fig. 1 illustrates the proposed multigeneration system capable of producing four useful outputs: hydrogen, electricity, space cooling, and space heating. In order to synthesize H₂ and NaOH simultaneously, the electrolysis of brine can be implemented. The chemical reaction at the anode, cathode, and the overall reaction can be presented as follows:



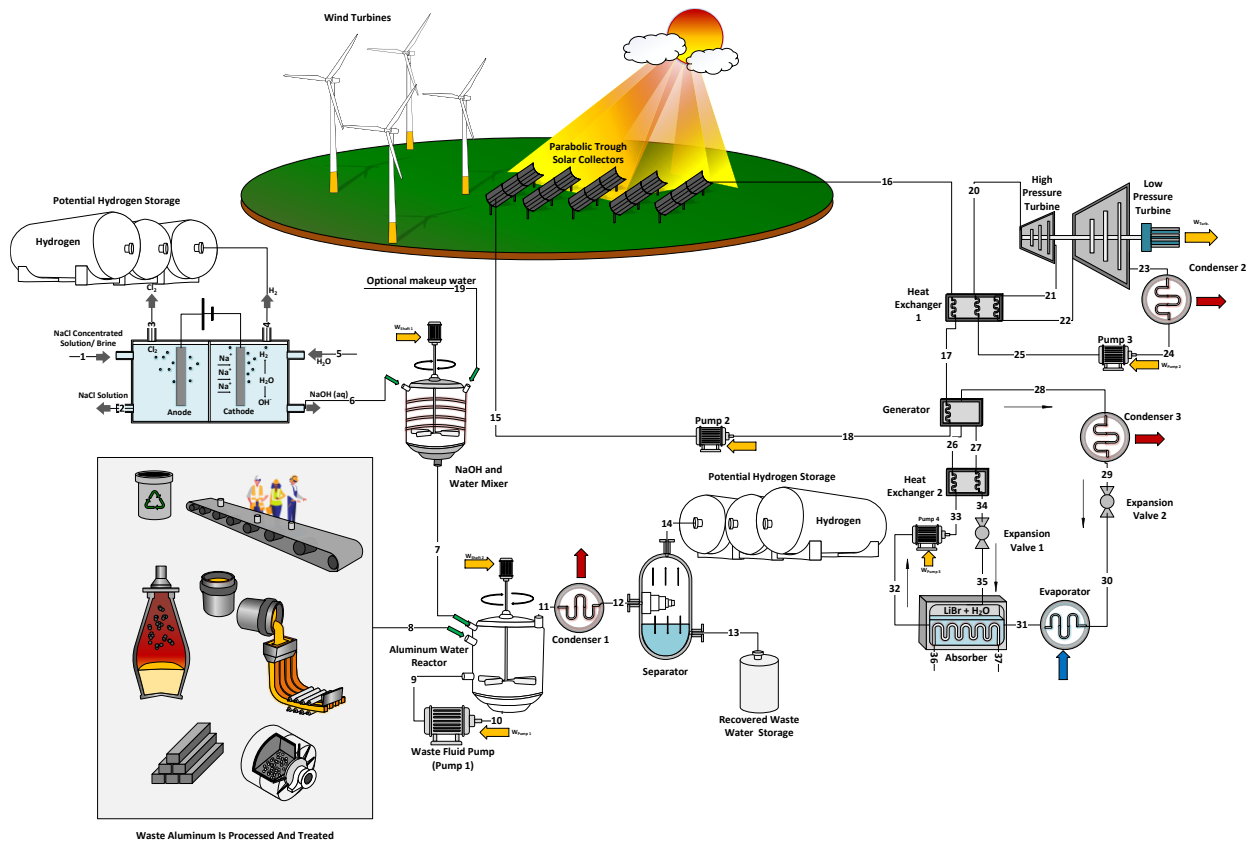
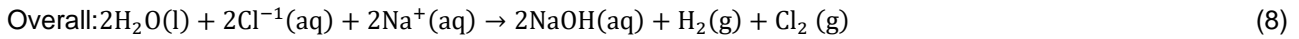


Fig. 1. A layout of the proposed multigeneration system.

RESULTS AND DISCUSSION

Given that the electrolyser system requires an electrical energy input to operate, the wind speed will significantly dictate the amount of NaOH and H₂ produced. Therefore, a parametric study was conducted, which varied the wind speed by the month, to observe the impact on the hydrogen production rate from electrolysis and the aluminium-water chemical reaction. The results of this parametric study are illustrated in Figure 2.

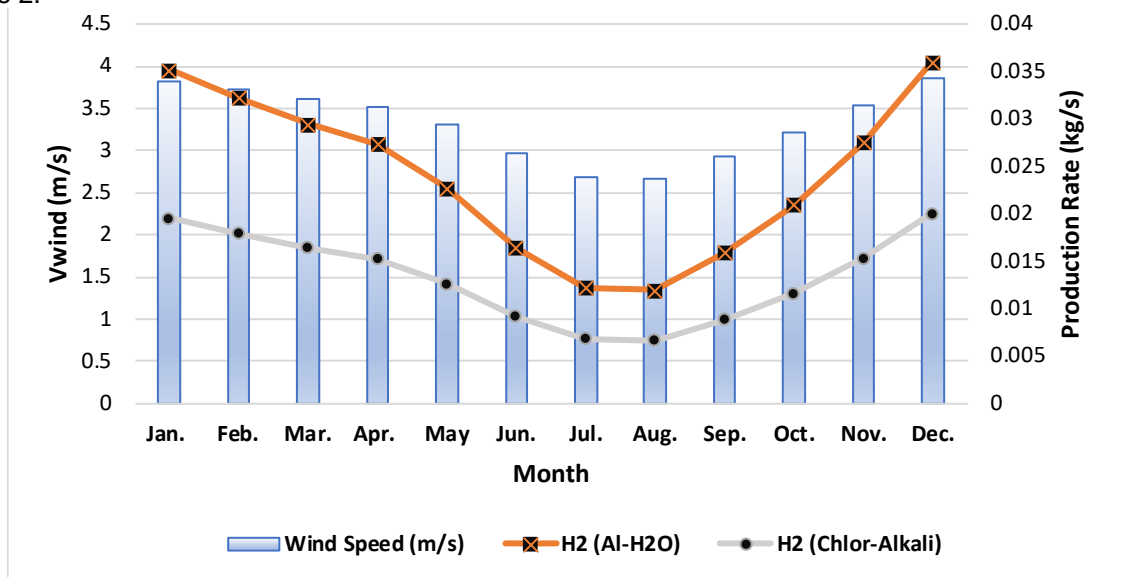


Fig. 2. Comparison between H₂ and CH₄ with varying volumetric flow rates

It was observed from the results presented that there is a strong correlation between the wind speed and the hydrogen produced from both sources. Based on the parametric study, it is expected that during December,



the highest average H₂ production rate of 0.02003 kgs⁻¹ and 0.03605 kgs⁻¹ will occur for the chlor-alkali process and the Al-H₂O reaction, respectively. However, during August, the hydrogen production rate decreased to 0.006778 kgs⁻¹ and 0.01193 kgs⁻¹ for the chlor-alkali process and the Al-H₂O reaction, respectively. The numerical value for all system's useful outputs during standard operating conditions have been summarized in Table 1.

Table 1. System Outputs During Standard Conditions

Useful Output	Value
H ₂ Production Rate (kgs ⁻¹)	0.03576
Net Power Output (kW)	2571
Heating Load (kW)	2576
Cooling load (kW)	344.7

CONCLUSIONS

The presented study illustrates the design of a new novel multigeneration system that is capable of producing four useful outputs, including hydrogen, electricity, space heating, and space cooling. In order to produce hydrogen, the system utilized a combination of electrolysis and the aluminium-water chemical reaction. The system achieved a total hydrogen production of 0.03576 kgs⁻¹, in which 64% of the hydrogen produced was attributed to the aluminium-water reaction. Furthermore, the system was believed to have the highest hydrogen production rate of 0.05608 kgs⁻¹ during December due to the wind speed of 3.86 ms⁻¹. The electrical power within the system was produced through the addition of a Rankine reheat cycle and the power allocated from the wind turbine. By considering the total power produced and power required to operate the system, the net power produced by the system was 2571 kW. The system also provided space heating by harnessing the waste heat generated from the condenser of the Rankine cycle. Whereas space cooling was achieved through the addition of a Li-Br absorption cooling sub-cycle. The space heating and cooling loads were calculated to be 2576 kW and 344.7 kW, respectively.

REFERENCES

- [1] US DOE, "Reaction of Aluminum with Water to Produce Hydrogen," *US DOE Rep.*, pp. 1–26, 2008, [Online]. Available: <http://scholar.google.com/scholar?hl=en&btnG=Search&q=intitle:Reaction+of+Aluminum+with+Water+to+Produce+Hydrogen#0>.
- [2] A. Bolt, I. Dincer, and M. Agelin-Chaab, "Experimental study of hydrogen production process with aluminum and water," *Int. J. Hydrogen Energy*, vol. 45, no. 28, pp. 14232–14244, 2020, doi: 10.1016/j.ijhydene.2020.03.160.

ICH2P14-OP073

SOLAR ENERGY DRIVEN SILICON PHOTOVOLTAIC MONOLITHIC ELECTROCHEMICAL CELLS FOR EFFICIENT HYDROGEN PRODUCTION FROM WATER

¹Mourad Frites, ^{2*}Shahed Khan

¹School of Natural, Health, Social and Behavioral Sciences, Centenary University, 400 Jefferson Street, Hackettstown, NJ 07840, USA

²Renewable Energy Technology, 4280 Breckenridge Court, Presto, PA 15142, USA

*Corresponding author e-mail: shahedumkhan@gmail.com

ABSTRACT

A novel bench-top solar energy driven silicon photovoltaic electrochemical cell (Si-PV-EC) has been meticulously designed for the purpose of generating hydrogen from water. The primary objectives of this project were to achieve high efficiency and long-term stability. The design incorporates a Si-PV cell sealed within an evacuated transparent glass capsule. The front and the back surface of the capsule was coated with spray pyrolytically deposited thin layer electrodes of earth abundant transition metal oxides. In the initial, Si-PV-EC-I, a thin layer semi-transparent Co-oxide anode was deposited on the front window of the glass capsule, which was pre-coated with conducting fluorine doped tin oxide (FTO). Under these conditions Si-PV-EC-I exhibited a percent solar to hydrogen efficiency (% STHE) of 5.42 %. In the second design, Si-PV-EC-II (A), the anode consisted of a thin layer of opaque mixed Co-Ni-oxide deposited onto the back window of the glass capsule, also precoated with conducting FTO. This configuration yielded a % solar to hydrogen efficiency of 8.67 %. In second design, Si-PV-EC II (B), the anode was similarly composed of an opaque layer of mixed Co-Ni-oxide, but it was deposited onto the back window formerly coated with a conducting graphite layer. In this case, the % STHE increased to 8.82 %. This enhanced efficiency was anticipated due to superior conductivity of the graphite layer compared to the FTO coating. All efficiencies were calculated using the volumes of actual hydrogen gas collected under the light illumination intensity of 0.1Watt cm⁻² (1 sun) from a solar simulator equipped with an AM 1.5 G filter. These high values of % STHEs were attributed to the photovoltage of 3.6 V generated by the Si-PV used and as well as to enhanced electrocatalytic activity of the transition metal Ni-Co mixed oxide anodes. No degradation of these Si-PV-ECs was observed even for continuous run during hydrogen gas collection.

Keywords: Photovoltaic, Hydrogen, Monolithic, Electrochemical, Cell.

INTRODUCTION

The Sun supplies to the Earth an astounding 1.2×10^5 trillion joules of energy in every second [1]. Hence, photoelectrochemical water splitting which converts solar energy to hydrogen fuel, offers an ultimate alternative energy solution which is clean and renewable [2-8]. Hence, the direct splitting of water to hydrogen and oxygen in solar energy driven monolithic silicon photovoltaic electrochemical cells (Si-PV-EC) is of paramount importance at present. This will also provide a useful method of storing solar energy in the form of clean hydrogen fuel.

At present the solar energy driven hydrogen production from water encounters important challenges such as, to maintain stable hydrogen evolution reaction (HER) rate, robustness, compactness and high percentage of solar to hydrogen efficiency (% STHE) of the Si-PV-EC. In this study, we address these challenges by reporting efficient splitting of water in a compact monolithic solar energy driven silicon photovoltaic-electrochemical cells (Si-PV-ECs) with the use of efficient Si-PV and the earth-abundant transition metal oxide anodes for oxygen evolution reaction (OER) and Pt or Ni metal cathodes for HER in Si-PV-ECs.

EXPERIMENTAL

For robustness, we encapsulated the Si-PV in an evacuated transparent glass enclosure to protect it from the corrosive electrolyte solution. For compactness the monolithic freestanding design was adopted as shown in Fig. 1. Such a freestanding monolithic Si-PV-EC system was fabricated by utilizing the presently available efficient Si-PV to drive the thermodynamically uphill water splitting reaction as well as overcoming the extra ohmic losses due to O₂ and H₂ gas evolution on the surfaces of anode and cathode respectively. To maintain constant HER rate, the Si-PV was chosen such that it supplies at least photovoltage of 3.6 V at its maximum power point. Such a photovoltage was found earlier [9]

to surmount the extra resistances or ohmic losses caused by H₂ and O₂ gas evolution on the surfaces of the electrodes and thus facilitated constant of rate of water splitting reaction overtime.

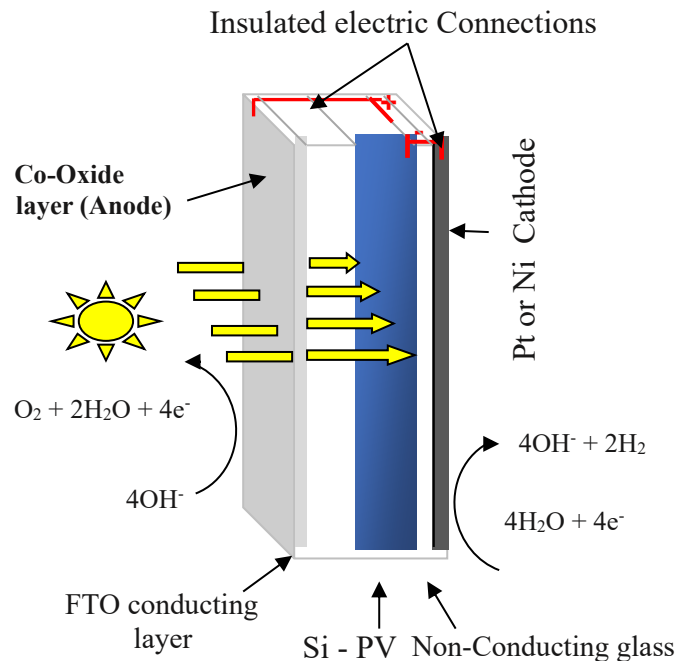


Figure 1: Freestanding monolithic self-driven water splitting Si-PV-EC- I

In the first design, Si-PV-EC-I, the anode, Co-oxide deposit (optically semi-transparent) on FTO coated conducting glass was used as the protective front window of the Si-PV sealed in an evacuated glass enclosure (Fig. 1). In the second design, Si-PV-EC-II (A), the anode consisted of a thin layer of opaque mixed Co-Ni-oxide deposited onto the back window of the glass capsule, also pre-coated with conducting FTO. In another such design, Si-PV-EC II (B), the anode was similarly composed of an opaque layer of mixed Co-Ni-oxide, but it was deposited on the back window pre-coated with a conducting *graphite layer*. Each anode was connected to positive pole of Si-PV. The photoactive surface area of each Si-PV was 12.21 cm². In all arrangements the negative pole Si-PV was connected to platinum or nickel metal sheet that acted as a cathode where hydrogen evolution reaction (HER) occurred when the Si-PV was exposed to solar simulated light of intensity 0.1 W cm⁻² (1 sun). Inverting an electrolyte filled graduated tube (not shown) on the top of Pt or Ni cathode as in Fig. 2, the hydrogen gas was collected by displacing the electrolyte solution of 2.5 M KOH in a single compartment.

The volumes of H₂ gas collected in Si-PV-EC-II (B) as a function of time of exposure to solar simulated light of 1 sun is given in Fig. 3 and those in Si-PV-EC-I and Si-PV-EC-II(A) are not shown. From the slopes of the fitted straight line of these plots the H₂ evolution rates were obtained. The steady state H₂ generation rate was found to be 0.423 mL min⁻¹ when Co-oxide on FTO coated glass as anode and Pt metal sheet as cathode were used in Si-PV-EC-I design. Importantly, enhanced H₂ generation rate of 0.6765 mL min⁻¹ was observed when mixed Ni-Co-oxide on FTO coated glass as anode and Pt metal sheet as cathode were used in the Si-PV-EC-II (A) configuration. Such a significant difference in the observed H₂ generation rate between these two Si-PV-ECs can be attributed to loss of light prior to reaching the Si-PV due to its absorption by the front semi-transparent Co-oxide layer in Si-PV-EC-I design (Fig. 1). However, in Si-PV-EC-II design as shown in Fig. 2, no such losses of light occurred since the opaque mixed Ni-Co-oxide was placed in the back of the sealed Si-PV in the evacuated transparent glass enclosure. Also, the mixed Ni-Co-oxide acted as a highly active anode for OER due to synergistic effect [10] compared to Co-oxide itself.

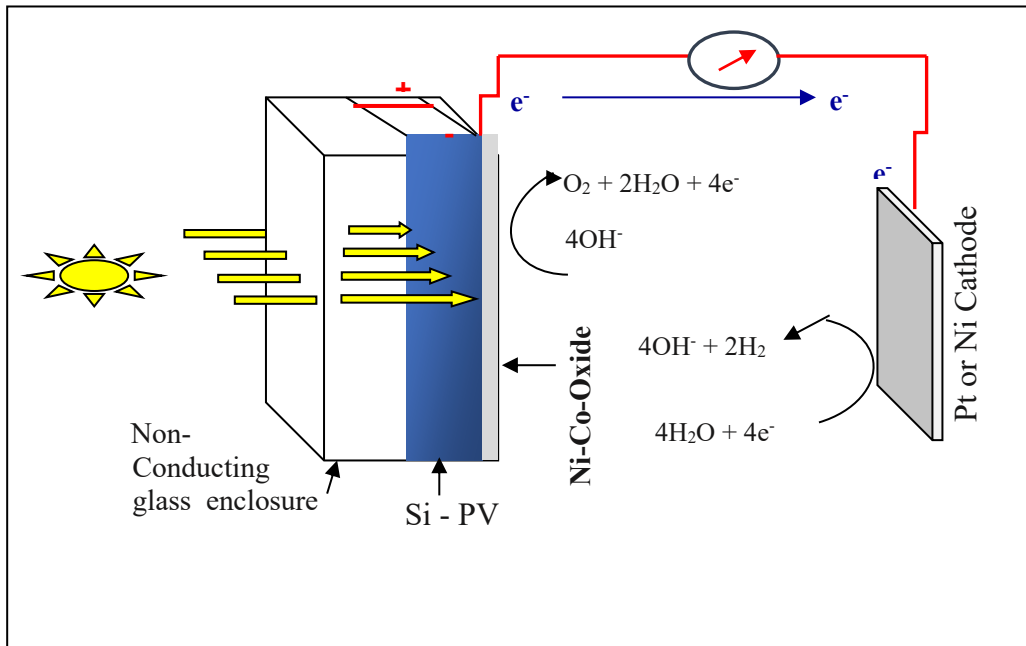


Figure 2: freestanding monolithic self-driven water splitting Si-PV-EC-II(A) and Si-PV-EC-II (B) designed to facilitate the collection of H₂ gas and determined the solar to H₂ production efficiency.

A further enhancement in H₂ generation rate of 0.6882 mL/min was observed in Fig. 3 when mixed Ni-Co oxide was deposited on graphite as anode and Ni metal sheet as cathode were used in the Si-PV-EC-II (B) configuration. This was due to enhanced conductivity of graphite compared to FTO coated glass in the Si-PV-PEC-II (A) (Fig. 2) configuration.

RESULTS AND DISCUSSION

From the volumes of hydrogen generated per second, V_{H₂}, the moles of H₂ gas produced per second, n_{H₂} was calculated using the ideal gas law, $n_{H_2} = (P_{atm} - P_{water\ vapor})V_{H_2}/RT$ by assuming hydrogen to behave as an ideal gas at atmospheric pressure, P_{atm} = 1.0 atm and considering the vapor pressure of water, P_{water vapor} = 0.031263 atm (= 23.76 mm Hg) in the electrolyte solution as equal to that of pure water at room temperature, T = 298.15 K and R = 0.0821 L atm K⁻¹ mol⁻¹. The moles H₂, n_{H₂} calculated from its collected volumes, V_{H₂} (= 0.6882 mL min⁻¹ = 1.147x10⁻⁵ L sec⁻¹) was found to be n_{H₂} = 4.54x10⁻⁷ moles sec⁻¹.

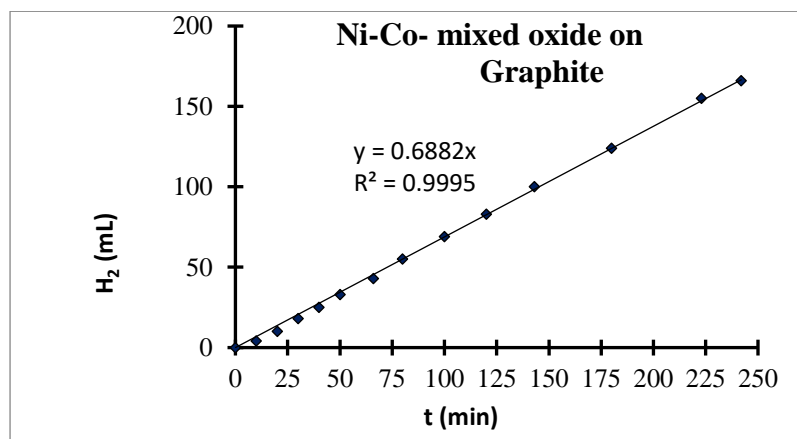


Figure 3: Volumes of H₂ collected versus time in Si-PV-EC-II (B) given in Fig. 2 exposed under solar simulated light illumination of 0.1W cm⁻² (1 sun) from a solar simulator with AM 1.5G filters using Ni - Co mixed oxide deposited on graphite sheet as an anode and Ni-metal sheet as a cathode.

The percentage of solar to hydrogen efficiency STHE (%) was calculated directly from the moles of H₂, n_{H2} collected in these Si-PV-PECs. The solar to hydrogen efficiencies, STHE (%) was calculated using Eq. (1) given in ref. [11] for Si-PV-EC-I and Si-PV-EC-II (A) and (B). The STHE (%) were found to be 5.42 % in Si-PV-EC-I and 8.67 % in Si-PV-EC-II (A). Noticeably, when mixed Ni-Co-oxide deposited on graphite sheet was used as anode and Ni sheet as a cathode in monolithic Si-PV-EC-II (B), the STHE (%) was found to 8.82 %. These results indicate the importance of potential electrocatalytic effect of earth abundant transition metal oxide and mixed metal oxide materials [12] used in the Si-PV-EC-I and Si-PV-EC-II for OER during water splitting. Also, due to synergistic effect the mixed transition metal oxides exhibited better electrocatalytic effect compared to single transition metal oxides.

CONCLUSION

In conclusion, it should be pointed out that the robust design of the monolithic water splitting Si-PV-EC-II(B), which generated the maximum solar to hydrogen efficiency of 8.82 % is exploitable by any other higher efficiency multi-junction tandem solar cells with needed stability for ≥ 10 years [7]. This is due to use of Si-PV in an evacuated glass enclosure sealed by glass itself. The practical efficiency of Si-PV-PEC-II for water splitting can be enhanced further to ≥ 10 % (US department of Energy's bench mark) using the smart electrocatalytic anodes like earth abundant mixed triple transition metal oxide as anodes and non-noble metal based CoNiFe-phosphide [13] and MoS₂ as cathodes [14]. The anodes and cathodes placed outside the evacuated glass enclosures will be easier to reactivate, improve or replace when needed. Thus, we provide in this report a solution of the intractable problem of having both highly efficient and as well as stable low-cost compact water splitting SI-PV-EC for the large-scale production of clean hydrogen fuel and oxygen in a self-driven monolithic manner. This work is consistent with the concept reported earlier [15] that at this time a balance is needed for an immediate solution for clean hydrogen production in large scale using existing technology and the continued fundamental research to provide better solutions in near future. Such systems of Si-PV-EC-II can be used also as a "floating water splitting photovoltaic- EC" for efficient green hydrogen generation for years to power the planet.

REFERENCES

1. Crabtree GW and Lewis NS. 2007. Solar energy conversion. *Physics Today*. 60 (3): 37-42.
2. Lewis NS and Nocera DG. 2006. Powering the planet: Chemical challenges in solar energy utilization. *Proceedings National Academy of Science*. U.S.A.,103:15729-15735.
3. Walter MG, Warren EL, McKone JR, Boettcher SW, Mi Q, Elizabeth A. Santori EA and Lewis NS. 2010. Solar Water Splitting Cells. *Chemical Review*. 110:6446-6473.
4. Osterlohand FE and Parkinson BA. 2011. Recent developments in solar water-splitting photocatalysis. *MRS Bulletin*, 36:17-22.
5. Khan SUM, Al-Shahry M, Ingler Jr. WB. 2002. Efficient Photochemical Water Splitting by a Chemically Modified n-TiO₂. *Science* 297:2243-2245.
6. Kanan KW and Nocera DG. 2008. In Situ Formation of an Oxygen-Evolving Catalyst in Neutral Water Containing Phosphate and Co²⁺. *Science* 321:1072-1075.
7. Park H. Vecitis CD. Choi W. Weres O. and Hoffmann R. 2008. Solar-Powered Production of Molecular Hydrogen from Water. *Journal of Physical Chemistry C* 112:885-889.
8. Shaban YA and Khan SUM. 2007. Surface Grooved Visible Light Active Carbon Modified (CM)-n-TiO₂ Thin Films for Efficient Photoelectrochemical Splitting of Water, *Chemical Physics*. 339:73-85.
9. Frites M and Khan SUM. 2013. Optimum Conditions for Efficient Hydrogen Generation by Water Electrolysis in an Electrochemical Cells Powered Either by Power Supply or Solar Cells, *Electrochemical Chemical Society Transactions* 50 (49):3-8.
10. Frites M. Ingler Jr. WB. and Khan SUM. 2011. Efficient Anode and Cathode Materials for Amorphous Silicon Solar Cell Driven all Solar Electrolysis of Water. *Green* 1: 97-103.
11. Solar to hydrogen efficiency can be expressed as [7, 10],

$$\text{STHE (\%)} = [(-\Delta G_{f, H_2O(l)}^\circ \times n_{H_2}) / (A_{Si-PV} \times P_{light})] \times 100 \quad (1)$$

where $\Delta G_{f, H_2O(l)}^\circ = -237.13 \text{ kJ mole}^{-1}$ is the free energy of formation of H₂O (l) from H₂(g) and O₂ (g) at the standard state, n_{H2} is the moles H₂ collected per second (moles sec⁻¹), A_{Si-PV} is the active surface area of Si-PV (which is 12.21 cm²) used in this study and P_{light} is the power density of solar simulated light of global AM 1.5 which is 0.1 watt cm⁻² for 1 sun. Note that 1 J sec⁻¹ = 1 watt.



12. Abid A, Dure N, Arif N, Ali H, Munawar I, Nora A, Abidal K and Azhar A. 2023. Fabrication of Efficient Electrocatalysts for Electrochemical Water Oxidation Using Bimetallic Oxides System. American Chemical Society Omega 8: 9539–9546.
13. Chen J. et al. 2022. Stoichiometry design in hierarchical CoNiFe phosphide for highly efficient water oxidation. Science China Material 65(10): 2685–2693.
14. Yan Yang et al. 2019, Hierarchical Nano-assembly of MoS₂/Co₉S₈/Ni₃S₂/Ni as a Highly Efficient Electrocatalyst for Overall Water Splitting in a Wide pH Range Journal of American Chemical Society 141: 10417-1043.
15. Whitesides GM. and Crabtree GW. 2007. Don't Forget Long-Term Fundamental Research in Energy. Science 315: 796-798.

ICH2P14-OP074

EVALUATION OF A NOVEL HYBRID PHOTOELECTROCHEMICAL-CONVENTIONAL HYDROGEN GENERATOR

**Mehmet Gursoy, Ibrahim Dincer*

Clean Energy Research Laboratory (CERL), FEAS, Ontario Tech University, Oshawa, Ontario, L1H 7K4, Canada
Corresponding author e-mail: mehmet.gursoy@ontariotechu.net

ABSTRACT

The main aim of this study is to investigate the integrated power process that utilizes solar power for various multigeneration applications, such as electricity generation, freshwater output, production of hydrogen, heating, and cooling. The research being suggested involves the integration of many components, including a solar power tower system, a combination Brayton-Rankine cycle, a multi-effect desalination (MED) unit, a unique hybrid electrolyzer system, an absorption cooling cycle, and a hydrogen storage and refuelling station. The power generated served a dual purpose, both as an input for hydrogen synthesis and as meeting the electrical needs of the local population. The thermodynamic assessment is used to assess the efficiency of the system being studied. The investigation focused on analysing the variation in hydrogen generation inside a combined photoelectrochemical (PEC) and conventional hybrid electrolyzer, with respect to solar irradiation levels, under ambient conditions. Based on the study conducted, it is seen that the hydrogen production rate is 1823.4 mL/h under conditions of no sun irradiation. However, this value increases to 1905.3 mL/h when subjected to a solar intensity of 1200 W/m².

Keywords: Solar energy, Hydrogen production, Hybrid water electrolysis.

INTRODUCTION

The use of water electrolysis for hydrogen production has significant potential as a viable pathway for the development of clean energy. Traditional electrolysis techniques have been widely accepted, but they often need a significant amount of energy. The process of photochemical-conventional hybrid electrolysis integrates the fundamental principles of solar technology with traditional electrolysis to improve the overall efficiency of hydrogen generation.

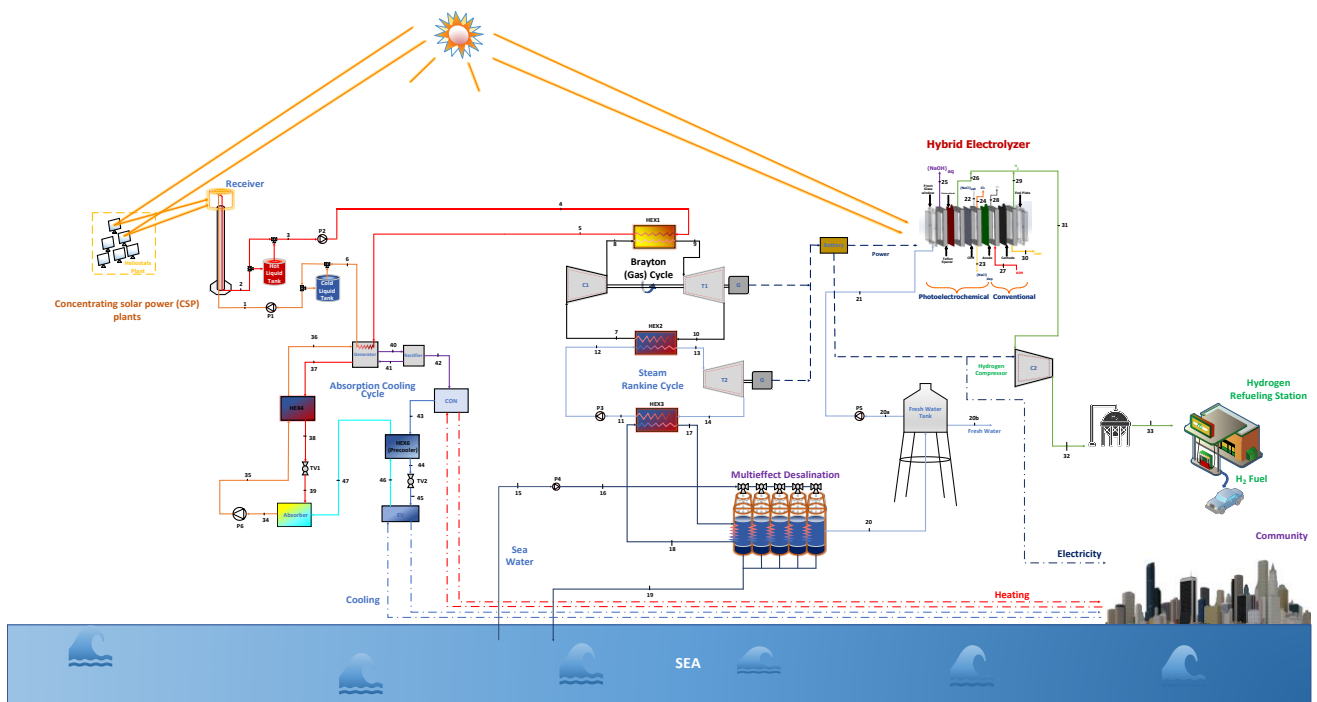


Fig. 1. An illustration of the proposed system's layout

Acar and Dincer [1] performed an experimental study to evaluate the thermodynamics of a novel hybrid chloralkali-photoelectrochemical system. This system was specifically developed to efficiently produce hydrogen

by splitting water. In another study conducted by Pinhassi et al. [2], the photocatalytic activity of thylakoid membranes and the overall water splitting in a bio-photo-electro-chemical (BPEC) cell were investigated by a simple process.

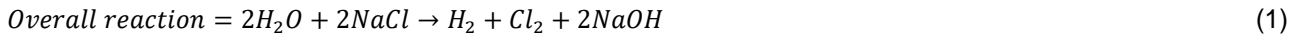
The fundamental concept behind photoelectrochemical-conventional hybrid electrolysis involves harnessing solar energy, particularly via the use of photovoltaic cells, to provide the necessary electrical energy for the process of water electrolysis. The field of photoelectrochemical hydrogen production presents a promising opportunity for the sustainable and environmentally friendly creation of hydrogen. Through continuous research and development endeavours, the field of PEC technology exhibits the potential to enable the transition towards a more environmentally friendly and sustainable energy infrastructure. This is achieved by solving various problems and enhancing the properties of materials used in the technology. The objective of this research is to enhance the efficiency of hydrogen generation via the development of a combined electrolyzer while considering certain criteria. Additionally, the aim is to ensure the continuous functioning of the system even in the absence of solar energy.

SYSTEM MODELING

Figure 1 illustrates the schematic layout of the proposed system. The energy and exergy assessments of the planned system were performed using the EES (Engineering Equation Solver) software tool. The research focuses on design from the perspective of hydrogen production at high efficiency and in a variety of situations. The employing of the photoelectrochemical-conventional hydrogen production system is a promising opportunity for the sustainable and environmentally friendly production of hydrogen. Additionally, it enables the generation of hydrogen from water by using power generated by the combined cycle. Subsequently, the generated hydrogen is sent to a storage tank, while the hydrogen refuelling station facilitates the provision of services to the community. The reactor has two distinct electrolysis cells, namely the photoelectrochemical cell and the conventional one. The PEC has an anode, a cation exchange membrane, and a photocathode. The critical point of the study is the common anode for both cells. 3 different electrolytes (NaCl_{sat} , fresh water from the MED unit, KOH) are used.

Furthermore, the membrane serves to counteract the presence of OH^- ions in the cathode compartment by the selective facilitation of Na^+ ion movement from the anode to the cathode partition. The reactor is equipped with optically transparent windows to facilitate the irradiation of the photocathode. The chemical process involving hydrogen synthesis in the hybrid electrolyzer may be represented by the following equation:

For the PEC cell:



For the conventional cell:



The equations given below are used to calculate the comprehensive energy and exergy efficiencies of the system respectively:

$$\eta_{\text{overall}} = \frac{\dot{m}_{20b}h_{20b} + \dot{Q}_{\text{cooling}} + \dot{Q}_{\text{heating}} + \dot{m}_{33}\text{LHV}_{\text{H}_2} + W_{\text{net}}}{\dot{Q}_{\text{in,SPT}}} \quad (7)$$

and

$$\psi_{\text{overall}} = \frac{\dot{m}_{20b}ex_{20b} + Ex^{\dot{Q}_{\text{cooling}}} + Ex^{\dot{Q}_{\text{heating}}} + \dot{m}_{33}(ex_{33} + ex_{\text{H}_2}^{\text{ch}}) + W_{\text{net}}}{Ex^{\dot{Q}_{\text{in,st}}}} \quad (8)$$

RESULTS AND DISCUSSION

The impact of solar irradiation, namely sunlight, on the rates of hydrogen generation in a PEC cell may be substantial. This is due to the fact that sunlight serves as the major energy source that propels the water-splitting process responsible for generating hydrogen. The hydrogen generation rate in the PEC cell has a direct proportionality to the intensity of sunshine. Elevated levels of light intensity provide accelerated formation of electron-hole pairs and heightened rates of hydrogen synthesis, whilst diminished light intensities correspond to decreased hydrogen production. In this regard, the effect of solar radiation on hydrogen production can be seen in Fig.2.

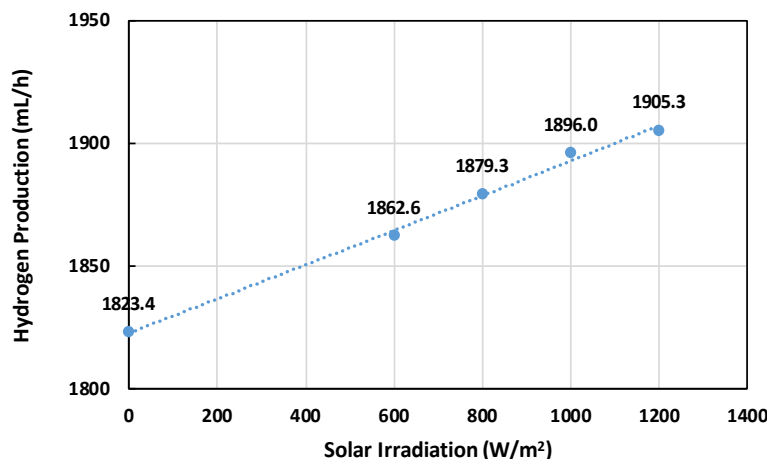


Fig. 2. The effect of solar radiation on hydrogen production

CONCLUSIONS

The present work has attempted to experimentally explore and thermodynamically assess a hybrid PEC-conventional system. The hybrid system being examined employs a water-splitting mechanism to produce hydrogen, while concurrently converting the resultant by-products into important industrial compounds such as chlorine (Cl₂) and sodium hydroxide (NaOH). Furthermore, the combination of the PEC and conventional electrolysis processes in this hybrid system significantly maximizes the use of the solar spectrum. At an ambient temperature, throughout a period of 1 hour, 1823 mL hydrogen gas was produced in the absence of light. There was an increase of 56 mL while an incident light intensity was 800 W/m². The light intensity was further augmented to 1200 W/m², and then 1905.3 mL hydrogen was obtained.

REFERENCES

1. C. Acar and I. Dincer, "Experimental investigation and analysis of a hybrid photoelectrochemical hydrogen production system," *Int. J. Hydrog. Energy*, vol. 42, no. 4, pp. 2504–2511, Jan. 2017, doi: 10.1016/j.ijhydene.2016.03.099.
2. R. I. Pinhassi *et al.*, "Hybrid bio-photo-electro-chemical cells for solar water splitting," *Nat. Commun.*, vol. 7, no. 1, p. 12552, Aug. 2016, doi: 10.1038/ncomms12552.

ICH2P14-OP078

A COMMUNITY ENERGY SYSTEM DESIGNED TO COVER THE NEEDS INCLUDING HYDROGEN

**Moslem Sharifishourabi, Ibrahim Dincer, Atef Mohany*

Clean Energy Research Laboratory, Faculty of Engineering and Applied Science, Ontario Tech. University, 2000 Simcoe Street North, Oshawa, Ontario, L1H 7K4, Canada

*Corresponding author e-mail: moslem.sharifishourabi@ontariotechu.ca

ABSTRACT

This article introduces a new multigeneration system designed to address the pressing demand of energy. Harnessing the power of solar and biomass energy sources, this system is designed to meet a diverse range of energy demands. Its capabilities extend beyond conventional systems, generating not only hydrogen but also providing hot water, heating, cooling, fresh water, and electricity. To comprehensively assess the system's performance and sustainability, this study conducts an analysis covering energy, exergy, and environmental impact assessments. By taking this holistic approach, valuable insights can be gained into the system's operation and its impact on the environment. The engineering equation solver is used for the analysis and the results of this investigation show that the overall energy and exergy efficiencies of the system are founded to be 55.46 % and 49.34 %, respectively. In addition, the energy and exergy coefficients of performance (COPs) of the absorption system are found to be 1.67 and 0.64, respectively. These findings signify the system's efficiency and potential to significantly contribute to a cleaner and more sustainable energy future.

Keywords: Biomass, Solar, Multigeneration, Water treatment, Hydrogen production.

INTRODUCTION

Energy serves as the backbone of economic growth and the sustenance of societies. It is crucial for human development and, by extension, the advancement of civilization. However, the generation and consumption of energy are also the leading causes of climate change. Principally, fossil fuels like coal, oil, and natural gas are employed to generate electricity, fuel vehicles, and heat buildings and industrial processes. These fossil fuels, when burned, not only fulfil our energy requirements but also exacerbate global warming by emitting substantial amounts of carbon dioxide. These emissions are a leading factor in trapping heat in the Earth's atmosphere, which contributes to climate change. Moreover, the localized pollution resulting from fossil fuel usage has detrimental effects on the environment. Consequently, there is a rising demand in the global energy sector to transition from fossil fuel-based systems to more sustainable alternatives like solar and biomass [1]. Despite these advantages, renewables currently make up a minor fraction of global energy consumption. However, this share is steadily rising, particularly in developed nations with supportive policies. To further improve efficiency and meet diverse energy needs, multigeneration systems have been developed. These systems integrate various cycles and technologies to produce multiple forms of useful energy.

In the context of this article, we introduce a novel multigeneration system that utilizes solar and biomass energy to meet various residential needs. Uniquely, this system incorporates ultrasound technology for water treatment and hydrogen production. Additionally, the heat from the chiller's absorber is repurposed to warm the sonohydrogen reactor. The primary goals of this article are to present this innovative multigeneration system, which integrates sonohydrogen production, and to explore the effects of various parameters on its performance. Rashwan et al. [2] have reviewed the fundamentals of sonohydrogen production, which focuses on the critical role of process parameters and operating conditions in sonic-hydrogen generation.

SYSTEM DESCRIPTION

The system design is displayed in Fig.1. It contains different sub-systems such as Solar and biomass system, steam Rankine cycle, Brayton cycle, organic Rankine cycle and chiller. In addition, the system includes the process of water treatment and hydrogen production using ultrasounds. In the system, there are some storages such as hot water and hydrogen storage.

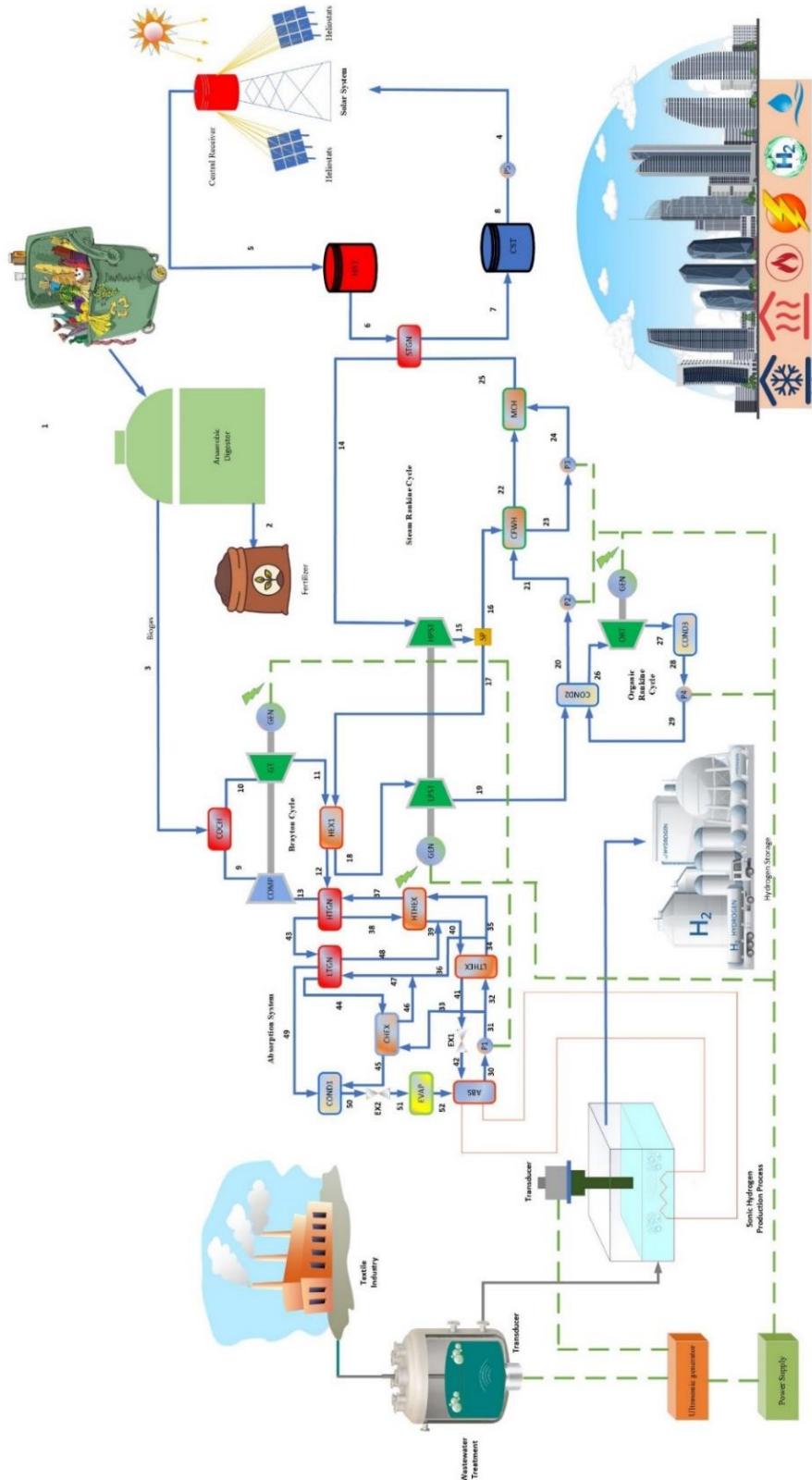


Fig. 1. The developed multigeneration system.

The working fluid in the solar system is molten salt which transfers the heat to the steam Rankine cycle via the steam generator. The steam Rankine cycle utilizes heat from the Brayton cycle to produce power and to operate the organic Rankine cycle. In the organic Rankine cycle, isobutane serves as the working fluid for power generation. Additionally, energy can be harvested from a biomass system using waste foods. This heat is then transfers into the Brayton cycle, which produces power and operates the

absorption system. The absorption system employs a mixture of ammonia and water to provide both heating and cooling for the community.

RESULTS AND DISCUSSION

Fig.2 illustrates the influence of changes in the reference temperature on both the exergetic COP (COP_{ex}) and energetic COP (COP_{en}) of the chiller. The graph highlights that as the reference temperature rises from 280 to 320 K, the COP_{ex} increases while the COP_{en} stays fixed. This phenomenon is due to the fact that a lower reference temperature results in a reduced driving force for heat transfer, resulting in a decrease of the COP_{ex} . Conversely, a higher ambient temperature enhances the driving force for heat transfer, thereby improving the COP_{ex} of the system.

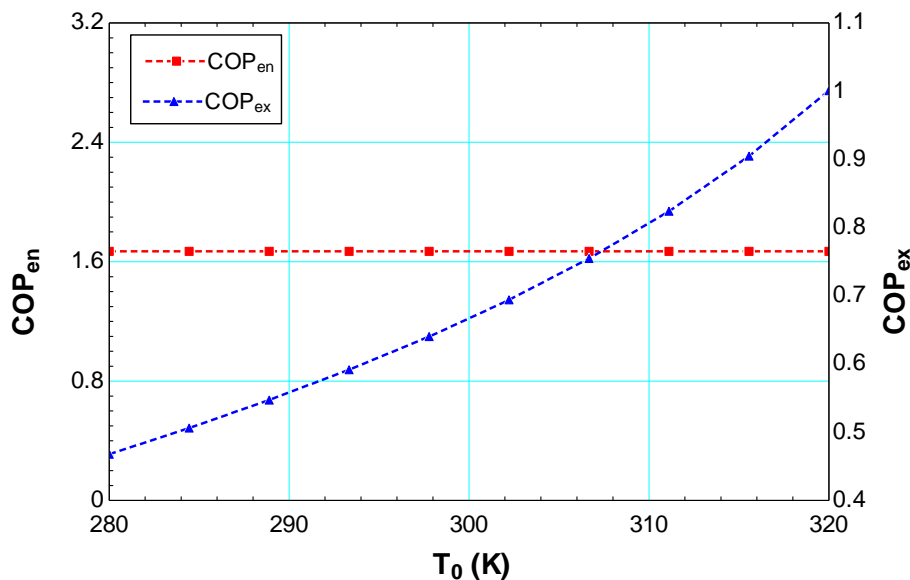


Fig. 2. The effect of reference temperature on the exergetic and energetic COPs

CONCLUSIONS

The primary focus of this paper has been the investigation of a recently developed multigeneration system. It benefits the potential utilization of solar and biomass energy to meet a diverse range of energy demands. This system is designed to generate multiple productions, including electricity, hot water, heating, cooling, fresh water, and hydrogen. Throughout this article, an evaluation encompassing energy, exergy, and environmental impact assessments are conducted to thoroughly assess the system's performance. This holistic examination has yielded valuable insights into the potential and sustainability of the proposed system. The findings reveal that the absorption system exhibits energy and exergy Coefficients of Performance (COPs) of 1.67 and 0.64, respectively. In addition, the overall energy and exergy efficiencies of the system are founded to be 55.46 % and 49.34 %, respectively. These metrics provide crucial benchmarks for evaluating the system's effectiveness and efficiency.

REFERENCES

- [1] I. Dincer and M. I. Aydin, "New paradigms in sustainable energy systems with hydrogen," *Energy Conversion and Management*, vol. 283, p. 116950, May 2023, doi: 10.1016/j.enconman.2023.116950.
- [2] S. S. Rashwan, I. Dincer, and A. Mohany, "A review on the importance of operating conditions and process parameters in sonic hydrogen production," *International Journal of Hydrogen Energy*, vol. 46, no. 56, pp. 28418–28434, Aug. 2021, doi: 10.1016/j.ijhydene.2021.06.086.

ICH2P14-OP080

A CLEAN OPTION FOR POTENTIAL HYDROGEN PRODUCTION VIA NUCLEAR IN CANADA

**Gorkem Kubilay Karayel, Ibrahim Dincer*

Clean Energy Research Laboratory, Faculty of Engineering and Applied Science, Ontario Tech University, Ontario, Canada

*Corresponding author e-mail: gkubilaykarayel@gmail.com

Abstract

The current study investigates clean hydrogen production using nuclear energy in various power plants located in Canada. Currently active Canadian Deuterium-Uranium (CANDU) reactors and small modular reactors considered in the calculations. The total clean hydrogen production is 2.014 Mt using electricity generated from nuclear energy. 1.84 Mt hydrogen can be produced using currently active nuclear power plants and 166.74 kt can be produced from small modular reactors. It shows promising potential for Canada to be on the list of hydrogen-producing countries.

Keywords: Clean hydrogen, electrolyser, nuclear energy, small modular reactor, Canada.

Introduction

In the foreseeable future, there is a possibility that nuclear energy will constitute a substantial portion of the global energy mix, thereby exerting a noteworthy influence. Renewable energy sources with low carbon emissions have the potential to serve as a sustainable electricity generation option, thereby aiding in the mitigation of greenhouse gas emissions. According to the World Nuclear Association (2023), the utilization of nuclear power has led to a noteworthy decrease in CO₂ emissions, amounting to more than 60 Gt during the span of the previous five decades. This reduction is about similar to the emissions produced by global energy-related activities over a period of nearly two years. Nevertheless, it is noteworthy that in affluent economies, the use of nuclear power has experienced a downward trend, characterized by the closure of existing facilities and a scarcity of fresh investments. This loss is occurring precisely during a period when there is a growing global demand for electricity sources that exhibit little carbon emissions. Conversely, it is noteworthy that the mean age of the nuclear infrastructure in developed nations stands at 35 years, with a number of reactors approaching their designated operational lifespan. In Canada, there are 19 nuclear reactors, with the exception of one, are all situated in Ontario, and in 2019, they were responsible for producing 61% of the province's total power (90,4 TWh) (IESO, 2023). The operational nuclear reactor in Canada at now is the Canada Deuterium Uranium (CANDU, 2023) using pressurized heavy-water reactor (PHWR), which stands as the sole type of its kind. In a previous study (Karaca et al., 2020), the abiotic depletion potential (ADP), acidification potential (AP), global warming potential (GWP), ozone depletion potential (ODP), and human toxicity potential (HTP) of a nuclear power plant investigated using a life cycle assessment (LCA) methodology. The GWPs (Global Warming Potentials) of various hydrogen production methods, including high temperature electrolysis (HTE), conventional electrolysis (CE), and 3-, 4-, and 5-step Cu-Cl cycles, were determined by experimental results and computations. The GWPs for these methods were found to be 0.4768, 0.7071, 1.320, 1.201, and 1.346 kg CO_{2eq} per kilogram of hydrogen, respectively. The primary objective of the present study is to assess the potential for hydrogen production in various parts of Canada using nuclear energy, employing a proton exchange membrane electrolyser (PEMEL). An analysis of each province reveals specific regions that exhibit higher prospects for hydrogen generation. Moreover, it is expected that the collected data would be utilized in the development of the country's energy infrastructure, including both domestic and global contexts, with a specific emphasis on hydrogen-based technology.

System Description and Analysis

Hydrogen production with nuclear energy can be achieved by employing many methods, namely radiolysis, electrolysis, high-temperature steam electrolysis, and hybrid thermochemical water splitting. These procedures include the decomposition of water to generate hydrogen. The initial approach, known as radiolysis, involves the utilization of nuclear radiation to induce the direct dissociation of the water molecule, resulting in the production of hydrogen and oxygen. The second technique, known as electrolysis, involves the utilization of electricity generated from nuclear energy sources to facilitate the process of electrolyzing water. Hybrid technologies, namely high-temperature steam electrolysis and hybrid thermochemical water splitting, are characterized by their utilization of both electrical energy and

high-temperature heat for the purpose of water splitting. The technical characteristics of the PEM electrolyser, used in the calculations for hydrogen generation, are presented in Table 1.

Table 1. Specification list for PEM electrolyser

Specification	PEM Electrolyser [22]
Model	Nell MC250 PEM Electrolyser (Nell Electrolyser)
Average Power Consumption at Stack (kWh/Nm ³)	4.5
Purity (with Optional High Purity Dryer) (%)	99.9995
Delivery Pressure (bar)	30
Net Production Rate (Nm ³ /h @ 0°C, 1 bar)	246
Net Production Rate (kg/24 h)	531

In the current system, currently active nuclear reactors located in Ontario, and New Brunswick and 11 small modular reactors (SMR) considered in the calculations. The CANDU reactors Bruce, Darlington, Pickering, and Point Lepreau and their electric capacities (MWe) considered. 100% of the generated electricity is used for clean hydrogen production. CANDU (Canadian Deuterium-Uranium) reactor is the only type of reactor used in nuclear power plants in Canada. This heavy water pressurized reactors use natural uranium as their fuel and heavy water as their coolant and moderator. However, small modular reactors use different systems rather than pressurized heavy water. The capacity and electricity generation values are taken directly from governmental and respective companies' sources.

Results and discussion

In this study, every active nuclear power plant and government supported small modular reactor initiatives considered in the calculations. Based on the generated electricity 100% of it used for producing clean hydrogen with PEM electrolyser. Table 2 shows each nuclear power plant and small modular reactors clean hydrogen production capacities.

Table 2. Clean hydrogen production in each nuclear reactor in Canada

Reactor	Type	Capacity (MWe)	Hydrogen production potential (kt)
Bruce	CANDU	6,225	852.88
Darlington	CANDU	3,524	482.82
Pickering	CANDU	3,080	421.99
Point Lepreau	CANDU	660	90.43
Terrestrial Energy	SMR	200	27.40
Ultra Safe Nuclear Corpo.	SMR	10	1.37
LeadCold Nuclear	SMR	3	0.41
ARC Nuclear Canada	SMR	100	13.70
Moltex Energy	SMR	300	41.10
SMR-160, LLC (Holtec)	SMR	160	21.92
NuScale Power	SMR	60	8.22
U-Battery Canada	SMR	4.00	0.55
GE Hitachi Nuclear Energy	SMR	300.00	41.10
X-energy	SMR	75.00	10.28
Westinghouse	SMR	5.00	0.69
Total		14,706	2,014.85

Conclusions

Data are taken from respective companies' and governmental sources. Using PEM electrolyzers, clean hydrogen production from nuclear energy in Canada is 2.014 Mt. Based on provinces, clean hydrogen can be produced from nuclear reactors in Ontario, and New Brunswick are 1.75 Mt, and 90.43 kt, respectively. Small modular reactors can be utilized in different locations and have capacity to produce 166.74 kt. Outcome of this study indicates that the potential for nuclear energy is promising substitute for producing hydrogen in various parts of Canada.

References

- CANDU, The Canada Deuterium Uranium Reactor, website, Accessed 09.27, 2023, from <https://canteach.candu.org/Info/Pages/CANDUReactors.aspx>
- IESO, The Independent Electricity System Operator, Supply Report, Accessed 09.27, 2023, from <https://www.ieso.ca/power-data/supply-overview/transmission-connected-generation>



- Karaca, A. E., Dincer, I., & Gu, J. (2020). Life cycle assessment study on nuclear based sustainable hydrogen production options. *International Journal of Hydrogen Energy*, 45(41), 22148-22159.
- Nell Hydrogen, Product Brochure, Accessed 09.27, 2023, from <https://nelhydrogen.com/product/m-series-containerized/>
- World Nuclear Association and IAEA Power Reactor Information Service (PRIS), website, Accessed 09.27, 2023, from <https://www.world-nuclear.org/getmedia/9dafaf70-20c2-4c3f-ab80-f5024883d9da/World-Nuclear-Performance-Report-2022.pdf.aspx>

ICH2P14-OP082

GREEN HYDROGEN PRODUCTION AND SOLAR TO HYDROGEN RATIO USING BIFACIAL SOLAR PHOTOVOLTAICS AND HIGH ROOF SURFACE ALBEDO

¹Fahad Ahmad Faraz, ¹Oussama Rejeb, ^{2*}Chaouki Ghenai

¹Renewable Energy and Energy Efficiency Research Group, Sustainable Energy and Power Systems Research Centre, Research Institute for Sciences and Engineering, University of Sharjah, Sharjah, UAE

²Sustainable and Renewable Energy Engineering Department, College of Engineering, University of Sharjah, Sharjah, UAE

*Corresponding author e-mail: cghenai@sharjah.ac.ae

ABSTRACT

Green hydrogen is a key factor for the decarbonization of the energy sector and to foster the clean energy transition but has the highest cost when compared to grey and blue hydrogen. This is due to the high cost of the generation of energy from renewable sources and the efficiency of the water electrolyzer. Future innovative energy technologies are needed to boost the power production from solar PV systems, reduce the cost of renewable electricity and enhance hydrogen production from electrolyzers. The main objective of this study is to investigate green hydrogen production enhancement using a bifacial solar PV system integrated with cool roof technology (high-albedo roof coatings). The best operating conditions of the bifacial solar PV (albedo, height from the ground, tilt angle, and distance between the solar panels) need to be determined to maximize the power output from the bifacial solar PV system and the green hydrogen production. The originality and novelty of this study lie in the fact that it integrates innovative technologies such as bifacial solar PV and building cool roofs to boost the power generation output and green hydrogen production. The experimental set-up is composed of bifacial solar PV, a building roof with high solar reflective material, microinverter, electrolyzer, metal hydride hydrogen tank, and an integrated data acquisition system. The results will show the daily performance of the bifacial solar PV and the green hydrogen production with different building roof coatings (green, grey, and white). The percentage changes in renewable energy production (kWh), green hydrogen production (L/hr), and solar-to-hydrogen conversion ratio using bifacial solar PV with cool roof technology compared to mono-facial solar PV system will be presented in this study.

Keywords: Green Hydrogen, Bifacial Solar PV, Cool Roof Technology, Albedo, Performance Analysis.

INTRODUCTION

Developing clean and sustainable energy systems and novel alternative fuels is vital to meet future energy needs in sectors including power production, residential and commercial buildings, transportation, and industrial usage[1]. A solar or wind energy unit, an electrolyser, a hydrogen storage tank, and a fuel cell are the four main parts of a renewable hydrogen system that generates clean hydrogen. The electrolyser produces hydrogen through water electrolysis using excess electricity from renewable sources[2–8]. Using solar photovoltaics (PV), electrolyser and a fuel cell, Ghenai et al.[1] propose an off-grid hybrid power system. This hybrid system was developed to meet the daily demand of 4,500 kWh for a residential community of 150 units. The distributed hybrid energy system generated 52% of its total electrical output from solar photovoltaic panels and 48% from a fuel cell. The most eco-friendly method to produce hydrogen (H₂) is through water electrolysis, which can be accomplished through several different technologies (including alkaline electrolysers, PEM electrolysers, AEM electrolysers, and solid oxide electrolysers). PEM electrolysers, in particular, are effective across a wide range of current densities[9], making them well-suited for integration with renewable energy sources. Compressed hydrogen gas can be held at low pressures and temperatures, liquid hydrogen at very low temperatures, or solid hydrogen stored in metal hydride tanks thanks to a chemical process.

Clean energy generation and hydrogen production both benefit from the use of bifacial solar panels and an electrolyser. To maximise their energy harvesting potential, bifacial solar panels are designed to receive light from both the front and back. The effect of albedo, tilt angle, and height above ground on the performance of a bi-facial solar PV system was investigated in a study by Ghenai et al[10]. The results showed that the maximum energy yield for mono PV (160.6 kWh/kWp) and bifacial PV (192.4 kWh/kWp) occurs in May under hot and humid conditions. In the same context, solar photovoltaic (PV) system performance on flat roof structures with surface albedo control has been proposed by Ghenai et al[11]. The innovative aspect of their research is the use of advanced bifacial solar PV and cool roof technologies to increase the power output of solar PV panels and proactively control electricity generation to balance supply and demand. According to their research, raising the

surface albedo from 0.2 to 0.5 can increase yearly bifacial solar PV power production by 7.75%, while increasing it from 0.2 to 0.8 can increase output by 14.96%.

Hydrogen is a clean and sustainable energy storage option or adaptable fuel that can be produced when extra electricity is used to electrolyse water in an electrolyser. Efforts to improve the effectiveness and reliability of renewable energy technology are ongoing, and this integrated system is a component of those efforts. No studies have examined how combining a bifacial solar PV system with cool roof technology, typified by high-albedo roof coatings, could improve green hydrogen production. This is the first investigation into this innovative idea, which involves producing hydrogen by electrolyser using a bifacial solar PV system and reflecting materials, including green cardboard, grey cardboard, white wallpaper, and cool roof paint. The research also compares the system's effectiveness at solar-to-hydrogen conversion (STH) using bifacial solar PV with cool roof technology compared to mono-facial solar PV system.

EXPERIMENTAL SETUP AND METHODOLOGY

A grid connected bifacial solar PV system is designed and studied to produce green hydrogen through an electrolyzer and stored in a metal hydride hydrogen storage tank. The system is mainly composed of two sub-systems, a solar PV system to meet the load demand and a hydrogen production and storage system as demonstrated in Fig. 1.

Bifacial Solar PV system

The solar PV system is further composed of bifacial solar PV panels (bPV), microinverters and data acquisition. Bifacial PV panels are characterized by dual active sides, front and rear. bPV panels produce electricity from direct solar radiation on the front side as conventional mono-facial PV panels. Besides, the active rear side enables bPV panels to also produce electricity from reflected irradiance (albedo) reaching to the rear side. It creates an opportunity to enhance the albedo as much as possible in order to increase the electricity generation by bPV panels. For this, various highly reflecting materials are studied to increase the albedo and hence the energy generation.

The bPV panel consists of 72 bPV cells with a rated power of 365W, an area of 1.96 m² and an efficiency of 18.6% from Jollywood. While reference mono-facial PV panel is 365W, an area of 1.94m² with an efficiency of 18.81% from Jinko Solar. Three bifacial and one mono-facial solar PV panels are installed at a fixed tilt angle of 25°, azimuth of 0° (south) and height of 0.76 m. Smart grid connected microinverters (HM-1500) are deployed to convert DC power from PV panels to AC power. The AC power is used to meet the load requirement of an electrolyzer (Hy-PEM-XP) from the H₂ planet. In grid connected configuration, the electrical grid is considered as an infinite storage of electricity. In the case of surplus PV energy, it is supplied to the grid, while in the case of insufficient PV power, the load demand is met with the grid power. The schematic of the experimental setup is demonstrated in Fig. 1.

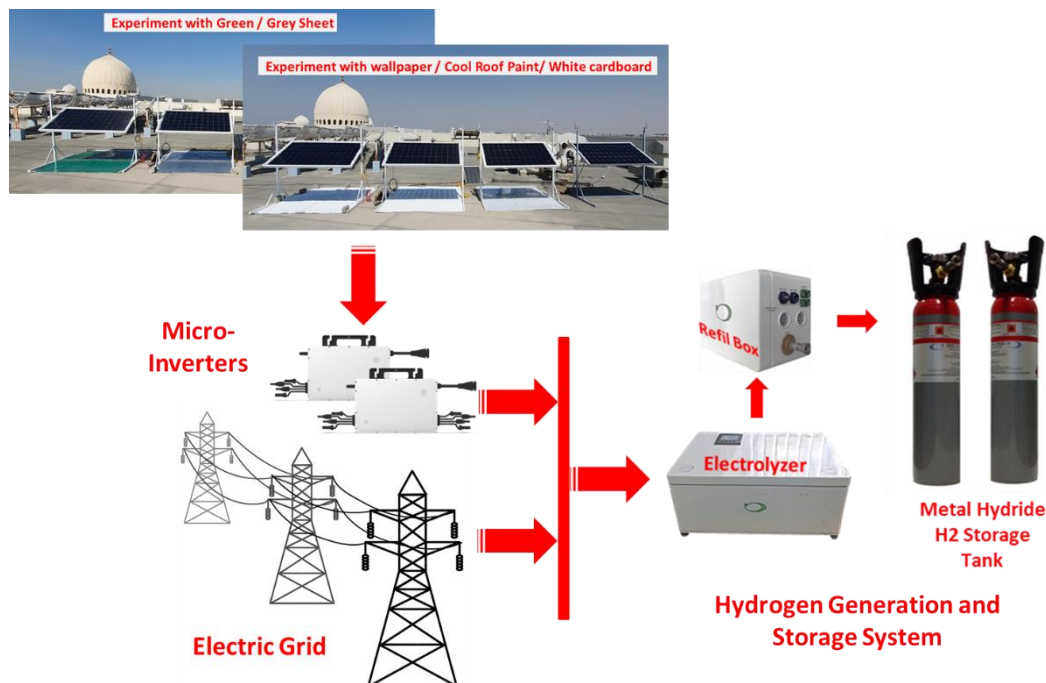


Fig. 1. Experimental Setup for Hydrogen Generation and Storage System

Reflection Surfaces & Spectral Analysis

Albedo is the part of solar radiation that is reflected from the surface. The rear surface of the bPV panel is exposed to the reflected radiations from the ground and produces extra energy as compared to conventional mono-facial PV. A sensitivity analysis study [10] of installation parameters concludes that the albedo is the most dominating factor impacting the output power of bPV panels among others such as tilt angle, and height from the ground level. It is significant to investigate the various materials and colours to understand the impact of albedo on bPV panels. The green and grey PVC sheets, white wallpaper, whiteboard, and highly reflecting cool roof paint are utilized as reflecting material to enhance the albedo.

A spectroradiometer SR-3500 from Spectral Evolution has been used to determine the spectrum of reflected light from the reflecting surfaces. The spectroradiometer analyses the spectrum of reflected light from 350 nm to 2500 nm. The figure demonstrates the full light spectrum of reflected light from different surfaces as compared to the calibrated reference surface. The spectrum is subdivided into ultraviolet, visible, and infrared regions. The spectrum analysis of reflected light from each surface is carried out as shown in Fig. 2.

Green surface: It reflects 2.65% in ultraviolet, 5.23% in visible and 29.43% in infrared region. The overall reflection is 25.54%. Grey Surface: It reflects 20% UV, 25.30% visible and 23.46% infrared radiation. The overall reflection is 23.79%. White cardboard: It reflects 12.40% UV, 63.64% visible, 35.87% infrared and 39.13% over the entire spectrum. White wallpaper: The whitewall paper has a certain pattern. It reflects 13.10% UV, 76.75% visible and 64.55% infrared light. The overall spectral reflection is 64.70%. Cool Roof Paint: It is a paint having a high reflecting index and is used on the rooftop of a building to reduce the heat transfer from the roof to the lower level by increasing the amount of reflected light. A coat of cool roof paint is applied. The spectral analysis shows that it reflects 15.90% UV, 79.90% visible and 87.48% infrared radiation. The overall reflection is 84.64% as given in Table 1.

The PV cells are made up of semiconductor material. The visible light is the most useful light region for electricity production [12]. More reflection in the visible region means more useful light for PV panels. Besides visible light, ultraviolet and infrared light also absorb the solar PV cell and cause a heating effect which negatively impacts the performance of the PV cell. Ideally, the reflecting surface of bPV should be highly reflected in the visible region and least reflective in the UV or IR regions. From the spectral analysis of the reflecting materials, it can be deduced that white colour is optimal for enhancing the albedo, especially cool roof paint that shows exceptionally high (79.90%) reflection in the visible region.

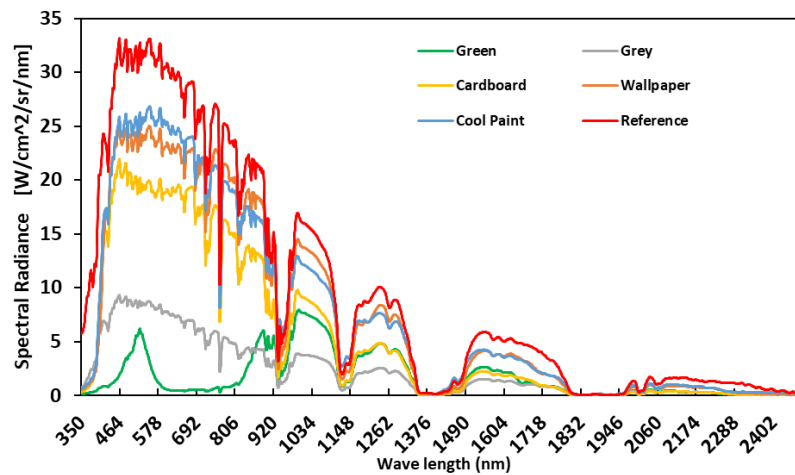


Fig. 2. Spectral Radiance of Reflecting material used for bPV.

Table 1. Percentage of Reflection of Light by the Reflecting Material used for bPV.

Description of Material	Ultraviolet	Visible	Infrared	Overall
	Avg. (350-400)	Avg. (401-800)	Avg.(801-2500)	Avg. (350-2500)
Green sheet	2.65	5.23	29.43	25.54
Grey Sheet	20.00	25.30	23.46	23.79
White cardboard	12.40	63.64	35.87	39.13
White Wallpaper	13.10	76.75	64.55	64.70
Cool Roof Paint	15.90	79.90	87.48	84.64

Performance of Solar PV panel: bPV vs mPV

To observe the impact of albedo enhancement on bPV panel energy production, bPV and ref mPV panels are installed under the same environmental conditions. The reflecting materials are placed under the bPV panels and power generation is recorded.

Albedo enhancement: Green & Grey vs mPV

Two bPV panels with green and grey reflecting material and reference mPV panels are installed. The experiment is carried out on a fairly sunny day. The front and rear irradiances and power output of PV panels are recorded accordingly from 9:15 am to 4:30 pm with a resolution of 15 minutes. The average front irradiance is 814.97 W/m², with rear side irradiances of 134.21 W/m² and 143.96 W/m² in the case of green and grey reflecting materials, respectively. The power produced by the mPV panel is observed at 230.91 W. The rear irradiance in addition to front irradiance improves the overall PV power production. The bPV-green has shown 17.33% more power generation as compared to mPV with avg. value of 270.93 W. While the bPV-grey has shown 19.70% more power production as compared to ref. mPV with avg. value of 276.41 W.

Table 2. Irradiance and power: bPV with green, grey and mPV

Description of Material	Irradiance		Power	Inc. in Power
	Front	Rear		
	W/m ²	W/m ²	W	%
m-Ref	-	-	230.91	-
bPV-Green	814.97	134.21	270.93	17.33
bPV-Grey	-	143.96	276.41	19.70

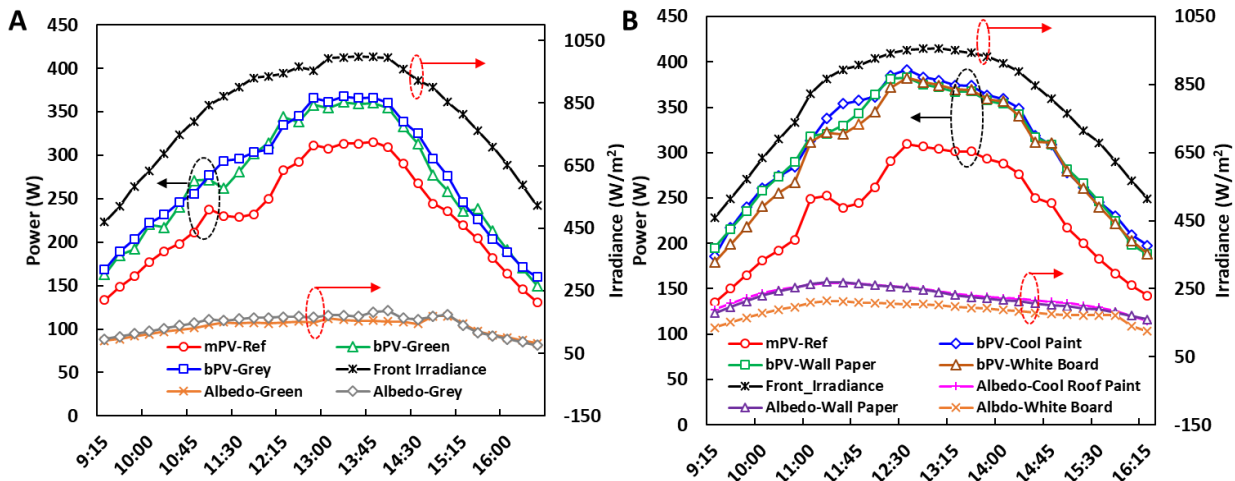


Fig. 3. (A) Green, Grey: Irradiance and Power by bPV and mPV, (B) White cardboard, wallpaper, cool roof paint: Irradiance and Power by bPV and mPV

Table 3. Irradiance and power: bPV with White cardboard, wallpaper, cool roof paint and mPV

Description of Material	Irradiance		Power	Inc. in Power
	Front	Rear		
	W/m ²	W/m ²	W	%
m-Ref	-	-	232.37	-
bPV-White cardboard	785.04	184.05	296.71	27.69
bPV-White Wallpaper	-	223.03	302.74	30.28
bPV-Cool Roof Paint	-	227.22	307.03	32.13

Albedo enhancement: White cardboard, wallpaper & cool roof paint

In this case, white cardboard, wallpaper and cool roof paint are used as reflecting material with bPV panels to increase the albedo. The front and rear irradiances and PV panel's power outputs are recorded from 9:15 am to 4:15 pm on the sunny day. Average front side irradiance is recorded as 785.04 W/m², while rear side irradiances are 184.05 W/m², 223.03 W/m² and 227.22 W/m² for cardboard, wallpaper and cool roof paint, respectively. The ref. mPV panel produces 232.37 W. The bPV-cardboard shows a 27.69% increment with a power generation of 296.71 W. The bPV wallpaper has shown 30.28% power enhancement with avg. value of 302.74 W while a 32.13% improvement in power generation (307.03W) is observed in the case of bPV with cool roof paint.

The generated power from bPV panels and mPV panels is sent to the microinverter which has a nominal MPPT efficiency of 99.8%. The microinverter is connected by an AC bus bar where the hydrogen generation and storage system are connected as load.

Hydrogen generation system

The hydrogen generation system consists of an electrolyzer, a control box and a storage tank. The electrolyzer is Hy-PEM-XP from H2 planet with a rated power consumption of 1300W with max. hydrogen generation capacity of 120 L/hr and pressure adjustment from 1-16 bar. The hydrogen from the electrolyzer is fed to the control box which is connected to the tank and supervises the hydrogen generation and storage. As long as the tank is filled, it sends a signal to the electrolyzer in order to reduce the production rate and go to standby mode. The storage tank is a metal hydride-based low-pressure storage tank. It can support a pressure of up to 30 bar. An energy meter is employed to record the power consumption by the electrolyzer, and the rate of hydrogen production is logged through the built-in sensor. A linear relationship is determined between power consumption and hydrogen production rate as follows:

$$H_2 \text{ (L/min)} = 2.3798 \times P(\text{kW}) + 0.0977 \quad (1)$$

Where P is the power consumption by the electrolyzer in kW. The hydrogen generation from the electrolyzer utilizing power produced from each solar PV panel is calculated through Eq. 1.

Table 4. Hydrogen Production Rate and STH: bPV with green, grey and mPV

Description of Material	Power W	Hydrogen Generation		STH %	Inc. in STH %
		Rate of H ₂ production L/hr	Increase %		
		m-Ref	230.91		
bPV-Green	270.93	44.55	14.71	9.00	13.74
bPV-Grey	276.41	45.33	16.73	9.16	15.77

Solar to hydrogen conversion efficiency (STH) is defined as the ratio of hydrogen power with the solar input power and can be determined by the following relationship as given in[13]:

$$STH (\%) = \frac{P_{H_2}}{P_{in}} = \frac{H_2 \text{ Production Rate} \times HHV_{H_2} \times \text{Density}_{H_2}}{\text{Area}_{PV} \times \text{Irradiance}} \times 100 \quad (2)$$

Where the production rate of H₂ is in L/hr, HHV is 39.39 kWh/kg, the density factor of H₂ is 0.002 kg/ 24.45 L, the area of PV in m² and the irradiance is in kW/m².

The Rate of H₂ production is 38.83 L/hr for the mPV reference panel. In the case of green reflecting material, a 44.55 L/hr hydrogen production rate is observed which is a 14.71% increase. In the case of grey, 16.73% enhancement is observed with an average production rate of 45.33 L/hr as given in Table 4. The Solar to Hydrogen conversion efficiency is 7.91%, 9.00% and 9.16% in the case of mPV, bPV with green and bPV with grey reflecting material respectively. An improvement of 13.74% and 15.77% has been observed in the case of green and grey reflecting material with bPV respectively. The hydrogen production rate and STH trends are illustrated in the Fig. 4 (A).

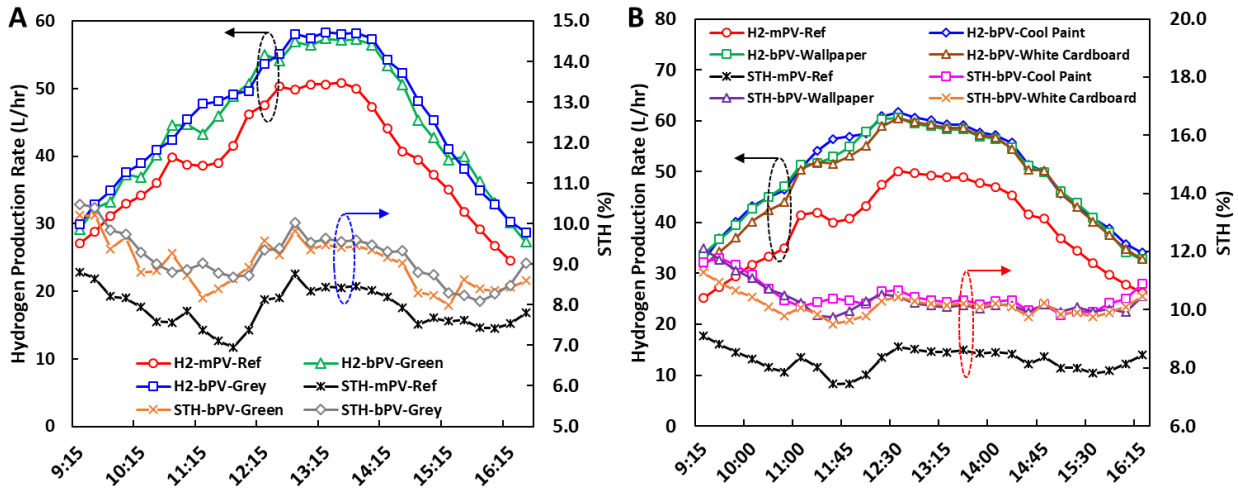


Fig. 4. (A) Green, Grey: Hydrogen Production and STH by bPV and mPV, (B) White cardboard, wallpaper, cool roof paint: Hydrogen Production and STH by bPV and mPV

The rate of H₂ production is 39.04 L/hr with 8.27% STH in the case of the mPV reference panel. An enhancement of 23.53% with 48.23 L/hr is observed in the case of bPV with white cardboard. The increment of 25.73% with a hydrogen production rate of 49.09 L/hr was observed from the electrolyzer in the case of bPV with white wallpaper. An enhancement of 27.31% was observed from the electrolyzer powered by bPV with cool roof paint as a reflecting material. In term of STH, 8.27% was achieved with mPV while 10.15%, 10.36% and 10.48% was achieved with bPV with cardboard, wallpaper, and cool roof paint, respectively. The improvements in STH are 22.70%, 25.26% and 26.69% for bPV with cardboard, wallpaper, and cool roof paint.

Table 5. Hydrogen Production Rate and STH: bPV with White cardboard, wallpaper, cool roof paint and mPV

Description of Material	Power W	Hydrogen Generation		STH %	Inc. in STH %
		Rate of H ₂ production L/hr	Increase %		
m-Ref	232.37	39.04		8.27	
bPV-White cardboard	296.71	48.23	23.53	10.15	22.70
bPV-White Wallpaper	302.74	49.09	25.73	10.36	25.26
bPV-Cool Roof Paint	307.03	49.70	27.31	10.48	26.69

CONCLUSIONS

A bifacial solar PV system with green, grey, white cardboard, white wallpaper and cool roof paint as reflecting material is investigated for hydrogen production through an electrolyzer. The performance of the system is evaluated in terms of power production through bPV panels vs mPV panel, hydrogen production rate (L/hr) and solar to hydrogen conversion efficiency (STH).

- The green colour sheet reflects 5.23% visible light, resulting in 134.21 W/m² irradiance on the rear side of the bPV panel and producing 17.33% more electrical power than the mPV panel.
- The grey sheet reflects 25.30% visible light, causing 143.96 W/m² irradiance reaching to the bPV panel on the rear surface and enhancing 19.70% electrical power production.
- The white cardboard is characterised by 64.63% visible light reflection, which improves the bPV panel power production by 27.69% as that of the mPV panel.
- The white wallpaper shows 76.75% reflection in the visible region which enhances the bPV panel production by 30.28%.
- The cool roof paint reflects the 79.90% visible light of the solar spectrum. The rear side irradiance of 227.22 W/m² was observed on the bPV panel, causing 32.13% more electrical energy production by the bPV panel.

- A 13.74% and 15.77% improvement in solar to hydrogen conversion efficiencies of the system is observed with green and grey reflecting material with bPV Panel.
- A 22.70%, 25.26% and 26.69% enhancement in STH efficiencies of the system are observed with white cardboard, white wallpaper, and cool roof paint as reflecting materials due to improvement in the albedo and power availability of the bPV panels.

REFERENCES

- [1] C. Ghenai, T. Salameh, A. Merabet, Technico-economic analysis of off grid solar PV/Fuel cell energy system for residential community in desert region, *Int. J. Hydrogen Energy*. 45 (2020) 11460–11470. <https://doi.org/https://doi.org/10.1016/j.ijhydene.2018.05.110>.
- [2] O. Rejeb, S.M. Alirahmi, E. Assareh, M. El Haj Assad, A. Jemni, M. Bettayeb, C. Ghenai, Innovative integrated solar powered polygeneration system for green Hydrogen, Oxygen, electricity and heat production, *Energy Convers. Manag.* 269 (2022) 116073. <https://doi.org/https://doi.org/10.1016/j.enconman.2022.116073>.
- [3] N. Khelfaoui, A. Djafour, C. Ghenai, I. Laib, M.B. Danoune, A. Gougui, Experimental investigation of solar hydrogen production PV/PEM electrolyser performance in the Algerian Sahara regions, *Int. J. Hydrogen Energy*. 46 (2021) 30524–30538. <https://doi.org/https://doi.org/10.1016/j.ijhydene.2020.11.193>.
- [4] G. Soy Turk, O. Kizilkan, M.A. Ezan, C.O. Colpan, Sizing of a solar and hydrogen-based integrated energy system of a stand-alone house in Izmir, *Int. J. Hydrogen Energy*. (2023). <https://doi.org/https://doi.org/10.1016/j.ijhydene.2023.05.159>.
- [5] A. Ibáñez-Rioja, L. Järvinen, P. Puranen, A. Kosonen, V. Ruuskanen, K. Hynynen, J. Ahola, P. Kauranen, Off-grid solar PV–wind power–battery–water electrolyzer plant: Simultaneous optimization of component capacities and system control, *Appl. Energy*. 345 (2023) 121277. <https://doi.org/https://doi.org/10.1016/j.apenergy.2023.121277>.
- [6] P. Pal, V. Mukherjee, Off-grid solar photovoltaic/hydrogen fuel cell system for renewable energy generation: An investigation based on techno-economic feasibility assessment for the application of end-user load demand in North-East India, *Renew. Sustain. Energy Rev.* 149 (2021) 111421. <https://doi.org/https://doi.org/10.1016/j.rser.2021.111421>.
- [7] M.S. Herdem, D. Mazzeo, N. Matera, C. Baglivo, N. Khan, Afnan, P.M. Congedo, M.G. De Giorgi, A brief overview of solar and wind-based green hydrogen production systems: Trends and standardization, *Int. J. Hydrogen Energy*. (2023). <https://doi.org/https://doi.org/10.1016/j.ijhydene.2023.05.172>.
- [8] Q. Hassan, Optimisation of solar-hydrogen power system for household applications, *Int. J. Hydrogen Energy*. 45 (2020) 33111–33127. <https://doi.org/https://doi.org/10.1016/j.ijhydene.2020.09.103>.
- [9] T. Oi, Y. Sakaki, Optimum hydrogen generation capacity and current density of the PEM-type water electrolyzer operated only during the off-peak period of electricity demand, *J. Power Sources*. 129 (2004) 229–237. <https://doi.org/https://doi.org/10.1016/j.jpowsour.2003.11.050>.
- [10] C. Ghenai, F.F. Ahmad, O. Rejeb, A.K. Hamid, Sensitivity analysis of design parameters and power gain correlations of bi-facial solar PV system using response surface methodology, *Sol. Energy*. 223 (2021) 44–53. <https://doi.org/https://doi.org/10.1016/j.solener.2021.05.024>.
- [11] C. Ghenai, F.F. Ahmad, O. Rejeb, M. Bettayeb, Artificial neural networks for power output forecasting from bifacial solar PV system with enhanced building roof surface Albedo, *J. Build. Eng.* 56 (2022) 104799. <https://doi.org/https://doi.org/10.1016/j.jobe.2022.104799>.
- [12] G. Huang, K. Wang, C.N. Markides, Efficiency limits of concentrating spectral-splitting hybrid photovoltaic-thermal (PV-T) solar collectors and systems, *Light Sci. Appl.* 10 (2021) 28. <https://doi.org/10.1038/s41377-021-00465-1>.
- [13] T.L. Gibson, N.A. Kelly, Optimization of solar powered hydrogen production using photovoltaic electrolysis devices, *Int. J. Hydrogen Energy*. 33 (2008) 5931–5940. <https://doi.org/https://doi.org/10.1016/j.ijhydene.2008.05.106>.

ICH2P14-OP083

DESIGN AND PERFORMANCE ANALYSIS OF GREEN HYDROGEN PRODUCTION FROM HYBRID SOLAR PV/WIND TURBINE ENERGY SYSTEM

^{1,2*} *Chaouki Ghenai*¹Sustainable and Renewable Energy Engineering Department, College of Engineering, University of Sharjah, Sharjah, UAE²Renewable Energy and Energy Efficiency Research Group, Sustainable Energy and Power Systems Research Centre, Research Institute for Sciences and Engineering, University of Sharjah, Sharjah, UAE

*Corresponding author e-mail: cghenai@sharjah.ac.ae

ABSTRACT

The primary objective of this techno-economic analysis is to look at the viability of producing environmentally friendly hydrogen from a water electrolyzer using a power system that combines solar photovoltaic cells and wind turbines. Modelling and simulation analysis was used in this study to test the performance of renewable power systems and green hydrogen production. To evaluate the efficiency and dependability of the proposed system, the city of Adrar, Algeria, which is located in the middle of the Sahara Desert, was chosen as the testing ground. Wind and solar resources are abundant in this oasis city. Solar photovoltaic, wind turbine, and PEM fuel cell systems are all capable of producing sufficient energy to meet the daily electrical loads of thousands of houses (15,000 kWh). Green hydrogen for PEM fuel cells and other hydrogen-based technologies (50 kg/day for industrial/transportation applications) was generated using surplus energy from renewable sources like solar panels and wind turbines. The results show the system's performance on a daily, monthly, and annual basis as well as the price of producing hydrogen and electricity. The potential and challenges for green hydrogen production and utilization in the Algerian desert for clean energy transition will be presented.

Keywords: Green Hydrogen, Solar PV, Wind Turbine, Desert Climate, Energy Transition.

INTRODUCTION

Hydrogen's potential as a clean and adaptable energy carrier is one of the main reasons for its rising profile in the energy mix. Hydrogen is so vital to the energy industry, the energy transition and net zero emissions by 2050. Hydrogen is very important for the clean energy and climate change mitigation strategies. It is considered a clean energy source because its combustion or fuel cell use results in just water. This makes it a potentially viable strategy for mitigating climate change by lowering GHG emissions. Energy storage and grid stability are two other crucial areas where hydrogen shines. Hydrogen has the potential to be a useful energy storage medium. Hydrogen produced via electrolysis from renewable energy sources such as wind and sun can be stored and used as a fuel or transformed back into electricity as needed. This facilitates grid stabilization and mitigates the intermittent nature of renewable energy. Hydrogen can be used as a replacement for fossil fuels in industries such as heavy manufacturing, aviation, and long-distance transportation, where direct electrification of processes is challenging, hence aiding in the decarbonization of these sectors. For the transportation sector, hydrogen fuel cells are being incorporated into a wide range of transportation options, from cars and trucks to buses. These fuel cells are preferable to electric batteries in some situations because of their greater range and faster refuelling times. For the manufacturing processes, hydrogen is used in chemical synthesis, refining, and metalworking. Many manufacturing processes can reduce their environmental effect by producing hydrogen from renewable resources. In the power sector, hydrogen can be utilized in gas turbines or blended with natural gas to reduce emissions during the power generation process. The power generation industry's carbon emissions may be lowered with the use of hydrogen. For residential and commercial buildings, hydrogen boilers and fuel cells can replace natural gas for space heating and water heating applications. New infrastructure building will also benefit from the expansion of hydrogen market. Investments in hydrogen production, storage, transportation, and distribution infrastructure are being made due to the rising popularity of hydrogen as an energy carrier. Building out this infrastructure is crucial for expanding the use of hydrogen-based power sources. Hydrogen is seen as a global solution for clean energy, and many countries are investing in research, development, and infrastructure to support the hydrogen economy. International collaboration on hydrogen production, transportation, and trade is increasing. The economy and job market will benefit from the development and expansion of the hydrogen market. The hydrogen sector has the potential to create new jobs in various industries, including research

and development, manufacturing, and maintenance of hydrogen-related technologies. However, it's important to note that the production of hydrogen, especially using current methods like steam methane reforming, can still involve emissions if not paired with carbon capture and storage. Additionally, hydrogen faces challenges related to cost, energy efficiency, and infrastructure development. Despite these challenges, hydrogen is considered a critical component of the transition to a more sustainable and low-carbon energy future.

Green hydrogen is produced by a renewable energy system such as a solar or wind energy unit, an electrolyser, a hydrogen storage tank. The electrolyser uses extra electricity from renewable sources to create hydrogen by electrolyzing water[1-8]. An off-grid hybrid power system based on solar photovoltaics (PV), an electrolyser, and a fuel cell was proposed by Ghenai et al.[1]. This hybrid setup was designed to supply the 4,500-kWh needed daily for a neighbourhood of 150 houses. Solar photovoltaic panels accounted for 52% of the distributed hybrid energy system's electrical output, while a fuel cell contributed the other 48%. Water electrolysis is the greenest way to make hydrogen, and it may be done in a variety of ways using technologies like alkaline electrolysers, PEM electrolysers, AEM electrolysers, and solid oxide electrolysers. Particularly well-suited for integration with renewable energy sources are PEM electrolysers, which are effective across a wide range of current densities[9]. Compressed hydrogen gas at low pressures and temperatures, liquid hydrogen at extremely low temperatures, and solid hydrogen held in metal hydride tanks are all chemically viable means of storing hydrogen. The usage of bifacial solar panels and an electrolyser is beneficial for both the creation of clean energy and the manufacture of hydrogen. Bifacial solar panels are double-sided, so they can absorb light from both sides and generate more electricity. In a study published in *Energy & Environmental Science*[10], Ghenai et al. looked at how albedo, tilt angle, and height above ground affected the efficiency of a bi-facial solar PV system. According to the findings, both mono PV (160.6 kWh/kWp) and bifacial PV (192.4 kWh/kWp) produce their highest energy yields in May, when temperatures are high, and humidity is high. Ghenai et al.[11] have made a similar suggestion for improving the efficiency of solar photovoltaic (PV) systems on flat roof structures by manipulating the roof's surface albedo. The novel component of their study is the incorporation of cutting-edge bifacial solar PV and cool roof technologies to boost solar panel efficiency and proactively regulate energy production to meet peak demand. According to their findings, annual bifacial solar PV power generation can be increased by 7.75% for an increase in surface albedo from 0.2 to 0.5, and by 14.96% for an increase in albedo from 0.2 to 0.8.

The main objective of this techno-economic study is to investigate the potential for creating green hydrogen from a water electrolyser with the help of a power system consisting of solar photovoltaic cells and wind turbines. The effectiveness of renewable power systems and green hydrogen production was evaluated in this study by modelling and simulation analysis. The city of Adrar, Algeria, situated in the heart of the Sahara Desert, was chosen as the testing site to assess the efficacy and dependability of the proposed system. There are many reasons why hybrid power systems are crucial for sustainable hydrogen generation. This guarantees that the hydrogen produced is completely carbon neutral, making for a more environmentally friendly energy process overall. Maintaining a steady and reliable electrical system is difficult when using renewable energy sources due to their intermittent nature. Combining renewable energy with other forms of generation, such as energy storage (hydrogen storage), creates a hybrid power system that can mitigate the intermittent nature of renewable energy. This allows for more reliable and productive hydrogen production. Hybrid systems can improve overall system efficiency by making the most of electricity from renewable sources and integrating it with existing generation methods. As a result, the production of hydrogen is more efficient, both monetarily and ecologically. The price at which green hydrogen can be produced is a major obstacle to its widespread use. By facilitating the use of low-cost renewable energy when available and the conversion to alternate energy sources when necessary, hybrid systems can aid in the reduction of these costs. Because of this versatility, green hydrogen may be able to compete with other energy carriers on price. Hybrid power systems are essential to the production of green hydrogen because they guarantee a steady and long-lasting source of clean energy for electrolysis. The challenges of renewable energy intermittency, grid stability, and cost-effectiveness are addressed by green hydrogen, which is both a viable and environmentally benign energy carrier for a variety of applications.

MODELING AND SIMULATION ANALYSIS

The hybrid solar PV/wind turbine/hydrogen fuel cell power system used in this study is shown in Figure 1. The effectiveness of renewable power systems and green hydrogen production was evaluated in this study by modelling and simulation analysis. The city of Adrar, Algeria, situated in the heart of the Sahara Desert, was chosen as the testing site to assess the efficacy and dependability of the proposed system. This oasis city has plentiful wind and solar resources (GHI annual average 5.68 kWh/m²/day and annual average speed of 5.86 m/s). The electrical loads needed for a thousand of homes can be met daily (15,000 kWh/day or 15 kWh/day per house) using solar photovoltaic, wind turbine, and PEM fuel cell systems. The extra power from solar panels and wind turbines were used to produce green hydrogen (50 kg/day for industrial/transportation applications – hydrogen load) for use in PEM fuel cells and other hydrogen-based technologies. Table 1 summarizes the characteristics of each part of the hybrid power system for hydrogen production. Ghenai et al. [1] provides more details on the solar PV, inverters, electrolyser, and fuel cell equations solved for the modelling and simulation analysis.

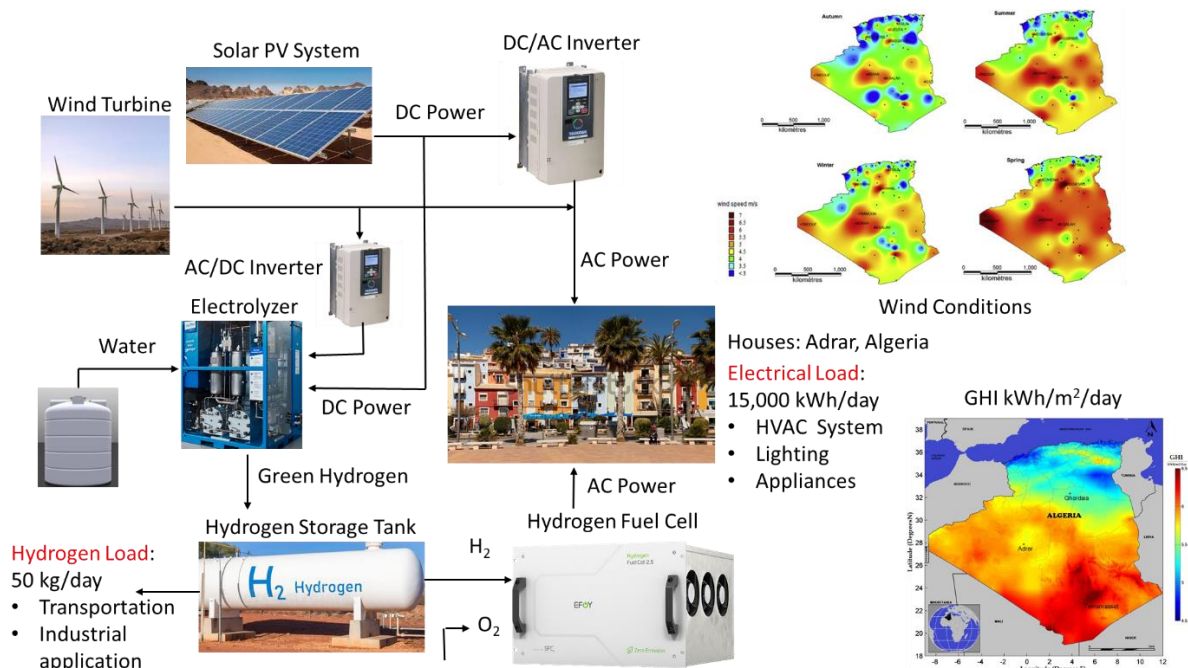


Fig. 1. Hybrid Solar PV/Wind Turbine/Hydrogen Fuel Cell Power System

Table 1. Characteristics of the Hybrid Solar PV/Wind Turbine/Hydrogen Fuel Cell Power System for Hydrogen production

	Capacity	Characteristics
Primary Loads	15,000 kWh/day	1000 houses, 15 kWh/day per house
Hydrogen Load	50 kg/day	Industrial/transportation applications
Solar PV	Rated Capacity: 972 kW	
Wind Turbine	Rated Capacity: 200 kW	
Electrolyser	500 kW	PEM electrolyser
Hydrogen Tank	5000 kg	Compressed hydrogen tank
Fuel Cell	Rated Capacity: 120 kW	Mean electrical efficiency of 60%

ARTIFICIAL NEURAL NETWORK (ANN) MODELS FOR RENEWABLE POWER OUTPUT AND HYDROGEN PRODUCTION

Figure 2 depicts the procedures required for the Artificial Neuro Networks (ANN) model to estimate the power output from solar PV and wind turbines and green hydrogen production. The Artificial Neural Network (ANN) can learn through the utilization of interconnected nodes, also known as neurons, as depicted in Figure 2. In this investigation, the Neural net time-series application was used to create, visualize, and train dynamic neural networks. The neural network program, which is illustrated in Figure 2, derives its projections of future values from the values that occurred in the previous iterations of one or more time series. The non-linear autoregressive with exogenous input (NARX) model was the one that we utilized, as shown in Figure 2. The neural net time-series program is created by following these steps in order: The input $x(t)$ and output $y(t)$ yearly simulation data from the modeling and simulation analysis is first imported; (2) the imported data is then divided into three sets: training, validation, and test; (3) a new neural network is created and trained; (4) a mean squared error and regression analysis are used to assess network performance; and (5) the prediction data is then analyzed using visualization charts such as validation performance, training state, and regression mode. It will eventually be feasible to feed the network the appropriate historical outputs as it gets educated to provide the appropriate present outputs. Levenberg-Marquardt optimization is utilized to effect changes to the weight and bias variables. To train the dataset, Levenberg-Marquardt was utilized. Even though it has a higher memory requirement, it is the most efficient approach for training. For the non-linear autoregressive with external input (NARX) network (t), you will need an input series $x(t)$ or predictors, as well as an output series $y(t)$. This neural network can predict the actual values of $y(t)$ based on the values of $x(t-1)$, $x(t-d)$, $y(t-1)$, and $y(t-d)$ that have been seen in the past, as depicted in Figure 2. The regression correlation R and the mean squared error, which are utilized in the process of performance analysis on the neural network.

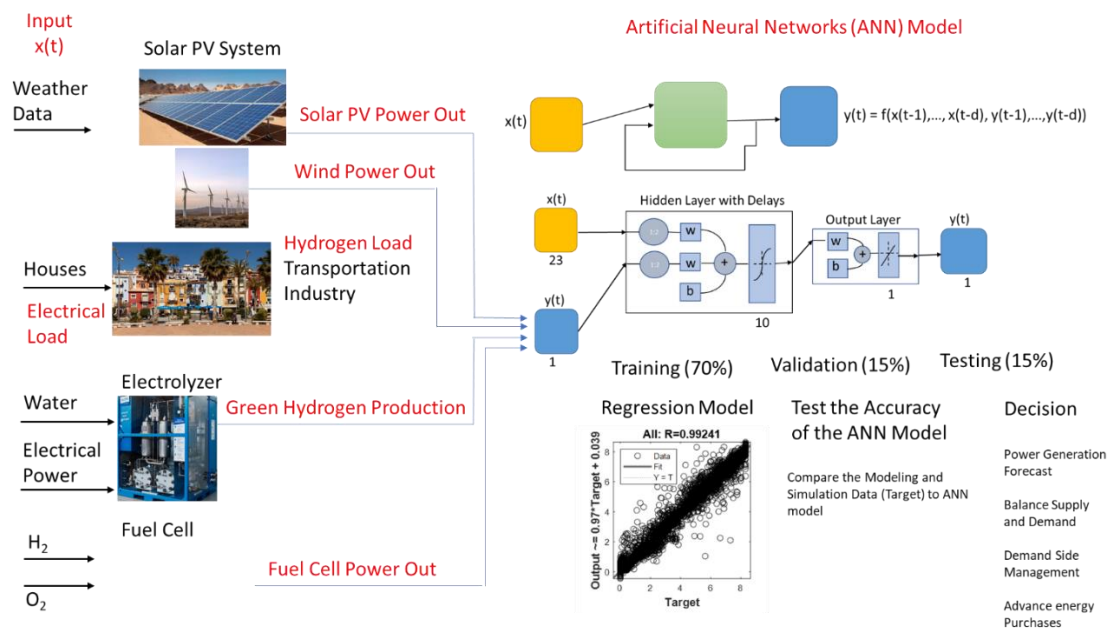


Fig. 2. Artificial Neural Network Models for Power Output and Green Hydrogen Production

RESULTS AND DISCUSSION

For the production (supply: 100% renewables), the total electrical energy production was 1,959,720 kWh/year with 69.5% of electrical power from solar PV (1,362.373 kWh/year), 8.68% from fuel cell (170,073 kWh/year) and 21.8% from wind turbines (427,274 kWh/year). Figure 3.a shows the monthly electric production from the solar PV, wind turbine and fuel cell. For the solar PV, the total rated capacity was 972 kW with a mean output of 3,733 kWh/day, 16% capacity factor and 4,248 hours of operation. The wind turbine has a total rated capacity of 200 kW with 24.4% capacity factor, and 6955 hours of operation. The fuel cell total electrical production was 170,073 kWh/year with maximum power output of 118 kW, and hydrogen consumption of 8,504 kg/year. The average fuel consumption per day and per

hour of the fuel cell were respectively 23.3 kg/day and 0.971 kg/hr. The electrolyser has a capacity of 500 kW with a total input energy of 1,245,611 kWh/year and a capacity factor of 28.4%. Figure 3.b shows the monthly electrolyser input power for hydrogen production. The mean output from the electrolyser was 3.06 kg/hr with a maximum output of 10.8 kg/hr. The total yearly hydrogen production from the electrolyser was 26,842 kg/year with a specific electrical consumption of 46.4 kWh per kg. The daily performance of the hybrid solar PV/Wind Turbine/Green Hydrogen fuel cell power system and hydrogen production in the electrolyser and consumption in the fuel cell and other hydrogen loads is shown in Fig.4. It is also noted that the storage tank has a maximum capacity of 5000 kg of hydrogen with energy storage capacity of 166,667 kWh and tank autonomy of 2,667 hours. The total electrical consumption was 1,792,944 kWh/year (91.5% of the total production) with 1,245,611 kWh/year (69.5%) for the electrolyser and 547,333 kWh/year (30.5%) for the primary electrical loads (houses). The excess electricity (dumped power) was 123,147 kWh (6.28%) and the rest (2.2%) are the losses in the inverters. The capacity shortage of the system was 538 kWh/year (0.0983%).

The ANN-based regression models that were developed for the hybrid solar PV/wind/hydrogen fuel cell power system to match the electrical and hydrogen loads are presented. Figure 5 provides illustrations of some examples of regression models for the solar PV power output and green hydrogen. The findings are presented, and they demonstrate the regression models that were used for training, validating, and testing. The values that were acquired from the ANN-based forecasting model are shown as output on the y axis, while the data that was received from the modelling and simulation study is shown as Target on the x axis. The findings also provide the equation that best describes the fit of the predictive data generated using the neural network, which is $Y = T$ (the perfect relation between predictive and target or predicted = target). The discrepancy between what is observed (the data from the simulation) and what is expected or predicted (the data from the ANN predictive model) is what is referred to as the ANN predictive model loss. In addition, the correlation coefficient (R) is presented in figure 5. The R^2 coefficient of determination is a measure that indicates how well the regression predictions (ANN model) line up with actual data (simulation or experimental data – target). Figure 5 shows that the R values for training, validation, and test conditions for solar PV power output and green hydrogen production are, respectively, 0.97566 – 0.98112 and 0.96621 – 0.97082. According to the values of R that are presented in Figure 5, the ANN models that were developed are quite accurate in their projections of the power output from the solar PV system and the production of green hydrogen from the electrolyser.

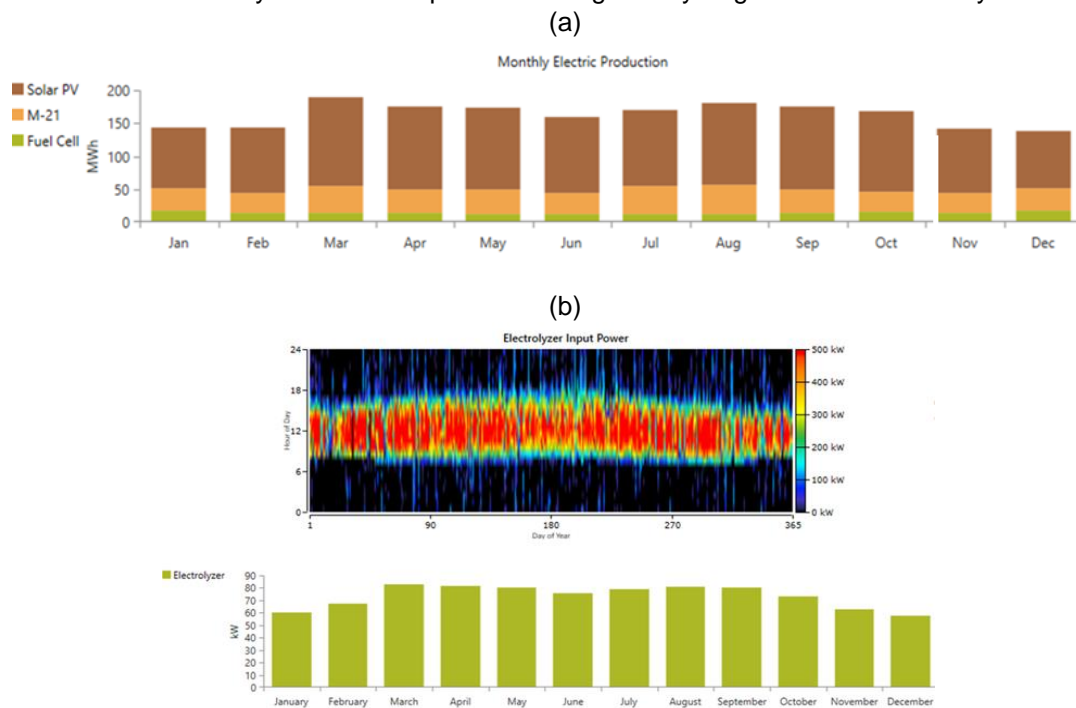


Fig. 3. Monthly Electrical Output and Input Powers: (a) Supply – Output Power: Solar PV, Wind Turbine and Fuel Cell, and (b) Demand - Electrolyser Input power

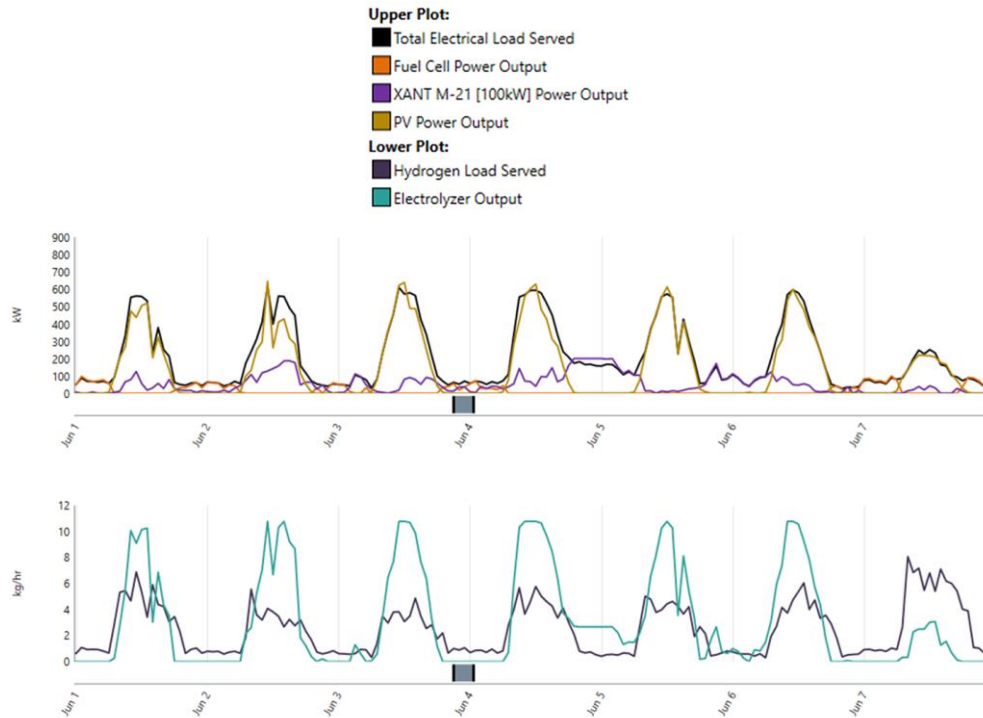


Fig. 4. Daily Performance of the Hybrid Solar PV/Wind Turbine/Green Hydrogen Fuel Cell Power System

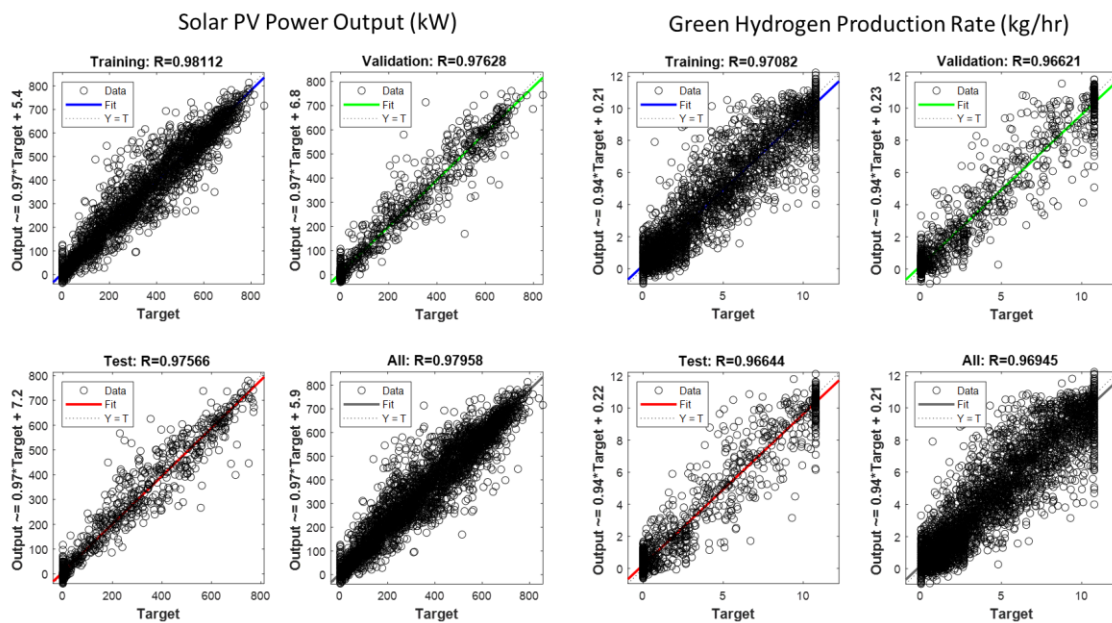


Fig. 5. Short-term Forecasting Models of Solar PV Power Output and Green Hydrogen Production

CONCLUSIONS

Modelling and simulation analysis of green hydrogen production in Adrar, Algeria (Algerian Desert) was performed in this study. Solar PV/Wind Turbine/ green hydrogen Fuel cell power system was used to meet electrical (15,000 kWh/day – 1000 houses) and Hydrogen (50 kg/day) Loads. The modelling and simulation analysis was used to test and assess the performance of renewable power systems and green hydrogen production. The results show:

- For the supply of renewable electricity for green hydrogen production and meet the electrical loads of the houses, the solar PV, wind turbine, and fuel cell were providing respectively 69.5%, 21.8% and 8.7% of the total production.

- For the demand or power consumption, 30.5% for electrical loads are used for the houses, and 63.5% for the green hydrogen production in the electrolyser.
- Daily performance of the off-grid power system shows a 100% Renewable energy system with zero carbon emissions and the electrical and hydrogen loads are met most of the time (no power shortage).
- The electrolyser's annual electricity input needs (1,245,611 kWh) are covered by the solar photovoltaic and wind turbine systems.
- The daily average and maximum green hydrogen production in the electrolyser are 3.06 and 10.8 kg/hr respectively with a specific energy consumption of 46.4 kWh/kg.
- For the fuel cell, the green hydrogen consumption was 8,604 kg/year, 23.3 kg/day and 0.917 kg/hr, with a specific fuel consumption of 0.05 kg of H₂/kWh.
- For the ANN-based forecasting models, the R values obtained for the training, validation, and test for the solar-driven green hydrogen production are 0.96621 – 0.98112. Accurate models for predicting 1 hour ahead the power output from solar PV system and green hydrogen production from the electrolyser were obtained in this study.
- The forecasting models will help resolve industry-related issues by forecasting power production to balance supply and demand, development of advanced power control systems, building operation and maintenance, demand-side management, and advance purchase of energy.

REFERENCES

1. C. Ghenai, T. Salameh, A. Merabet, Technico-economic analysis of off grid solar PV/Fuel cell energy system for residential community in desert region, *Int. J. Hydrogen Energy*. 45 (2020) 11460–11470. <https://doi.org/https://doi.org/10.1016/j.ijhydene.2018.05.110>.
2. O. Rejeb, S.M. Alirahmi, E. Assareh, M. El Haj Assad, A. Jemni, M. Bettayeb, C. Ghenai, Innovative integrated solar powered polygeneration system for green Hydrogen, Oxygen, electricity and heat production, *Energy Convers. Manag.* 269 (2022) 116073. <https://doi.org/https://doi.org/10.1016/j.enconman.2022.116073>.
3. N. Khelfaoui, A. Djafour, C. Ghenai, I. Laib, M.B. Danoune, A. Gougui, Experimental investigation of solar hydrogen production PV/PEM electrolyser performance in the Algerian Sahara regions, *Int. J. Hydrogen Energy*. 46 (2021) 30524–30538. <https://doi.org/https://doi.org/10.1016/j.ijhydene.2020.11.193>.
4. G. Soyuturk, O. Kizilkan, M.A. Ezan, C.O. Colpan, Sizing of a solar and hydrogen-based integrated energy system of a stand-alone house in Izmir, *Int. J. Hydrogen Energy*. (2023). <https://doi.org/https://doi.org/10.1016/j.ijhydene.2023.05.159>.
5. A. Ibáñez-Rioja, L. Järvinen, P. Puranen, A. Kosonen, V. Ruuskanen, K. Hynynen, J. Ahola, P. Kauranen, Off-grid solar PV–wind power–battery–water electrolyzer plant: Simultaneous optimization of component capacities and system control, *Appl. Energy*. 345 (2023) 121277. <https://doi.org/https://doi.org/10.1016/j.apenergy.2023.121277>.
6. P. Pal, V. Mukherjee, Off-grid solar photovoltaic/hydrogen fuel cell system for renewable energy generation: An investigation based on techno-economic feasibility assessment for the application of end-user load demand in North-East India, *Renew. Sustain. Energy Rev.* 149 (2021) 111421. <https://doi.org/https://doi.org/10.1016/j.rser.2021.111421>.
7. M.S. Herdem, D. Mazzeo, N. Matera, C. Baglivo, N. Khan, Afnan, P.M. Congedo, M.G. De Giorgi, A brief overview of solar and wind-based green hydrogen production systems: Trends and standardization, *Int. J. Hydrogen Energy*. (2023). <https://doi.org/https://doi.org/uoseresources.remotexs.xyz/10.1016/j.ijhydene.2023.05.172>.
8. Q. Hassan, Optimisation of solar-hydrogen power system for household applications, *Int. J. Hydrogen Energy*. 45 (2020) 33111–33127. <https://doi.org/https://doi.org/10.1016/j.ijhydene.2020.09.103>.
9. T. Oi, Y. Sakaki, Optimum hydrogen generation capacity and current density of the PEM-type water electrolyzer operated only during the off-peak period of electricity demand, *J. Power Sources*. 129 (2004) 229–237. <https://doi.org/https://doi.org/10.1016/j.jpowsour.2003.11.050>.
10. C. Ghenai, F.F. Ahmad, O. Rejeb, A.K. Hamid, Sensitivity analysis of design parameters and power gain correlations of bi-facial solar PV system using response surface methodology, *Sol. Energy*. 223 (2021) 44–53. <https://doi.org/https://doi.org/10.1016/j.solener.2021.05.024>.
11. C. Ghenai, F.F. Ahmad, O. Rejeb, M. Bettayeb, Artificial neural networks for power output forecasting from bifacial solar PV system with enhanced building roof surface Albedo, *J. Build. Eng.* 56 (2022) 104799. <https://doi.org/https://doi.org/10.1016/j.jobbe.2022.104799>.

ICH2P14-OP084

LIFE CYCLE ASSESSMENT OF GREEN HYDROGEN SUPPLY NETWORK

¹Dana Alghool, ²Mohamed Haouari, ¹Paolo Trucco

¹Politecnico Di Milano, Milan, Italy

²Qatar University, Doha, Qatar

*Corresponding author e-mail: dana.alghool@polimi.it

ABSTRACT

Green hydrogen has garnered significant attention from numerous countries as a promising energy source to replace traditional fossil fuels, dramatically reduce greenhouse gas emissions, and foster the transition toward net-zero energy systems. Green hydrogen can be produced in various ways (i.e., coupling standard PV panels, PV-T collectors, or CPV-T collectors with electrolyzer), conditioned to different states or carriers (i.e., liquefied hydrogen, compressed hydrogen, ammonia, and methanol), stored in various methods, transported by different means according to its state, and reconditioned to its original state at end-customers. In other words, hydrogen can go through various pathways (i.e., different processes and stages) in the hydrogen supply network (HSN), resulting in different greenhouse gas emission levels. This paper reports on a life cycle assessment (LCA) study of twelve different green hydrogen pathways for analyzing and comparing their emission profiles. The paper uses GaBi software for this purpose. The results indicate that the pathway with the lowest emissions, measuring just 2.67 kgCO₂eq/ kgH₂, involves coupling CPV-T collectors with an electrolyzer for hydrogen production. Hydrogen is subsequently compressed in a compression process, stored, transported in a compressed hydrogen container, and eventually delivered as compressed hydrogen to end-customers.

Keywords: Life Cycle Assessment, Green Hydrogen, Hydrogen Supply Network, CO₂ emissions.

INTRODUCTION

Hydrogen (H₂), the most abundant element in the universe, has garnered significant attention in recent years as a potential game-changer in the quest for sustainable energy solutions. Its importance lies in its role as a versatile energy carrier and its potential to revolutionize various sectors of the economy, from transportation to industry and even residential energy consumption. Nowadays, H₂ production is estimated at 70 million tons per annum (MTPA), mainly produced from natural gas and coal, resulting in high carbon dioxide (CO₂) emissions. According to the H₂ Council, H₂ is projected to contribute greatly to the transportation sector, industrial sector, and power generation by satisfying around 150, 110, and 140 MTPA, respectively [39]. Hence, large-scale production of green H₂ from cleaner sources is essential to meet the rising demand for H₂ in all sectors. However, realizing the full benefits of green hydrogen requires a thorough understanding of its life cycle, encompassing production, conditioning, transportation, storage, and reconditioning, which is where the concept of Life Cycle Assessment (LCA) comes into play.

LCA is a systematic approach that helps us quantify and evaluate the green hydrogen supply network (HSN) environmental aspects across its entire life cycle. By conducting LCAs, this paper can make informed decisions about green hydrogen technologies, identify areas for improvement, and develop strategies to minimize its environmental footprint while maximizing its efficiency and utility.

Looking at the extant literature on the topic, in [1], the authors conducted an LCA for green and grey Hydrogen supply chains (HSC) to investigate their environmental impact. The LCA of the green HSC considered hydrogen production (i.e., coupling electrolyzers with photovoltaic (PV) panels or wind turbines) and conditioning hydrogen into compressed hydrogen. They did not consider storage and distribution in the HSC. In [2], the authors conducted an LCA for blue and green HSC to investigate their environmental impact. The green hydrogen is produced by coupling wind turbines with electrolyzers and then could be conditioned to ammonia. In [3], the authors carried out an LCA for green HSC, where green hydrogen is produced by coupling wind turbines with electrolyzers. The HSC included production, conditioning, transportation, and post-processing to its original state. Hydrogen could be conditioned into compressed gaseous hydrogen, liquefied hydrogen, liquid organic hydrogen carrier (LOHC), or ammonia. The LCA results indicated that hydrogen transport using ammonia is the most attractive option. Additionally, in [4], the authors conducted an LCA for seven green HSC pathways: compressed hydrogen gas via pipeline, compressed hydrogen gas via tube trailer, liquid hydrogen, LOHC with natural gas as a heating source, liquid ammonia, liquid organic hydrogen carrier with hydrogen as a heating source, and the direct utilization of ammonia in direct ammonia fuel cell vehicle. The hydrogen is produced by coupling wind turbines with an electrolyzer. The LCA results showed

that compressed hydrogen gas via pipeline had the lowest global warming potential (GWP), while the liquid organic hydrogen carrier had the highest emissions. Similarly, in [5], the authors conducted an LCA for green hydrogen HSC here hydrogen is produced by coupling wind turbines with electrolyzers. However, they focused on investigating the environmental impact of different transport and distribution options, such as LOHC for transport and storage, compressed hydrogen storage in salt caverns with pipelines, and pressurized gas truck transport. The LCA results highlighted that the compressed hydrogen with pipelines has the least GWP. In [6], the authors coupled solar, wind, or hydropower with electrolyzers to produce green hydrogen. Additionally, the authors considered hydrogen transportation, delivery, storage, and refueling stations. The produced hydrogen could be transported and delivered in gaseous or liquid form.

Notably, none of the existing literature examines the environmental impacts of various HSN configurations and pathways, including different hydrogen production, conditioning, transportation, storage, and reconditioning technologies. This paper aims to make two main research contributions:

- Analyzing the environmental impacts of producing green hydrogen from coupling PV panels, photovoltaic thermal (PV-T) collectors, or concentrated photovoltaic thermal (CPV-T) collectors with electrolyzers. The existing literature only investigates the environmental impacts of coupling standard PV panels or mainly wind turbines with electrolyzers.
- Comparing the environmental impacts of twelve green hydrogen pathways to determine the one with the lowest GWP. The existing literature investigates common pathways such as compressed or liquified hydrogen. Nevertheless, this paper differs from [3] in that it considers in the LCA different types of PV panels for producing green hydrogen, the storage stage in the HSC, and different transportation means.

MATERIALS AND METHODS

This paper performs an LCA for different green HSN pathways. The LCA aims to assess the environmental impact of the different HSN pathways. The LCA consists of four phases: goal and scope definition, life cycle inventory (LCI), life cycle impact assessment (LCIA), and life cycle interpretation.

1. Goal and Scope Definition

The LCA aims to assess the environmental impacts associated with each possible pathway of the HSN over its life cycle. The LCA focuses only on the GWP impact on the environment, measured in CO₂ emissions. While the scope of the LCA covers the cradle to the grave of the HSN. In other words, the LCA considers the construction, production, operation and maintenance, and end-of-life stages of each component/ process in the HSN.

The considered HSN includes different hydrogen production methods, conditioning, transportation means, storage types, and reconditioning processes. Green hydrogen is produced from an electrolysis process that uses industrial-produced (IP) water or treated sewage effluent (TSE) water as a feedstock. Before that, the feedstock is deionized through a water-deionizing process. The electrolysis process is coupled with renewable energy in the form of PV panels for the energy source. This paper considers three types of PV panels: standard PV panels, PV-T collectors, and CPV-T collectors.

After green hydrogen is produced, it goes through four stages in the HSN: conditioning, storage, overseas transportation, and reconditioning stages. In each stage, the hydrogen can go through four possible pathways: CH₂, LH₂ – H₂, NH₃ – H₂, and CH₃OH – H₂. The CH₂ pathway includes compressing hydrogen via a compression process in the conditioning stage, storing it in a compressed hydrogen storage in the storage stage, and transporting it overseas to the consumer as compressed hydrogen in a compressed hydrogen container in the transportation stage. The LH₂ – H₂ pathway includes liquefying hydrogen via a liquefaction process in the conditioning stage, storing it in the liquid hydrogen storage in the storage stage, transporting it overseas to the consumer as liquified hydrogen in a liquid hydrogen tanker, and then regasifying it to hydrogen at the consumer side in a regasification process in the reconditioning stage. The NH₃ – H₂ pathway includes synthesizing hydrogen to ammonia via the Haber Bosch process in the conditioning stage, storing it in the ammonia storage in the storage stage, transporting it overseas to the consumer as ammonia in an ammonia tanker, and then cracking it to hydrogen at the consumer side in an ammonia cracking process in the reconditioning stage. The CH₃OH – H₂ pathway includes hydrogenating hydrogen to methanol via the CO₂ hydrogenation process in the conditioning stage, storing it in the methanol storage in the storage stage, transporting it overseas to the consumer as methanol in a methanol tanker, and then dehydrogenating it to hydrogen at the consumer side in a CO₂ dehydrogenation process in the reconditioning stage. It is noteworthy to mention that in the green HSN, the PV panels (i.e., standard PV panels, PV-T collectors, and CPV-T collectors) supply the required energy to all processes in the HSN, apart from the reconditioning process, since it is carried out at the consumer side.

This paper includes Fig. 1, highlighting the green HSN - CH₂ pathway as a sample. The other pathways differ in conditioning, storage, transportation, and reconditioning stages. To summarize, this paper investigates twelve possible pathways to determine the pathways with the highest and lowest CO₂ emissions. The functional unit of this LCA is the quantity of carbon dioxide emitted during the life cycle of the HSN. Hence, the functional unit is the quantity of CO₂ in kilogram emitted from the HSN when one kilogram of hydrogen is produced (i.e., kgCO₂/kgH₂).

2. Life Cycle Inventory

This paper determines the system inputs (i.e., feedstock and utility) and outputs (i.e., emissions) for each HSN process. It describes the LCI of each process below and collects the LCI from various sources such as literature, commercial websites, GaBi database, technical reports, etc. Here, this paper reports only the energy values required to produce, condition, or store depending on the stage. However, the full LCI can be viewed from the resources mentioned in Table 1, as it is not included here due to page limitations. This paper considers boil-off rates for conditioning, storage, transportation, and reconditioning stages.

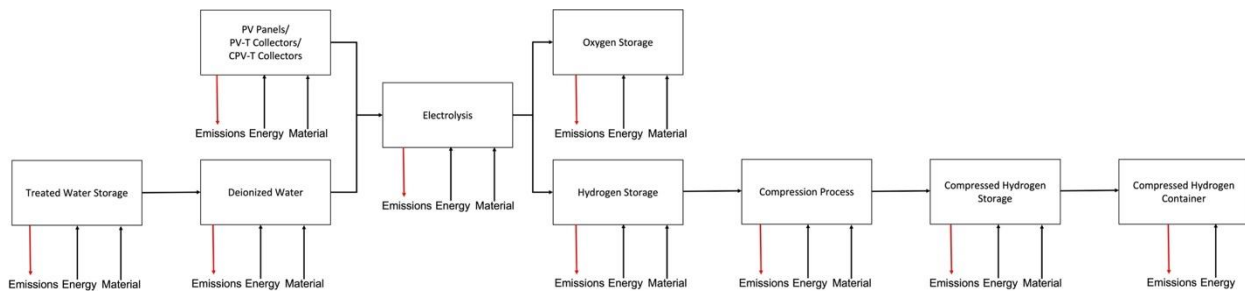


Fig. 1. The green HSN - CH₂ pathway

Table 1. LCI of the LCA processes

HSN Stage	Process		Energy Value	Unit	Resources
Production	Water Deionizing		1.1	kWh/ kgH ₂ O	GaBi database
	Renewable Energy	Standard PV Panels	-	-	GaBi database
		PV-T Collectors	-	-	Estimated & [7][8]
		CPV-T Collectors	-	-	Estimated & [9][10]
	Hydrogen Electrolysis		50	kWh/ kgH ₂	GaBi database
Conditioning	Hydrogen Compression		0.57	kWh/ kgH ₂	[22– 25][34]
	Hydrogen Liquefaction		10	kWh/ kgH ₂	[25 – 28][34]
	Ammonia Synthesis		11.2	kWh/ kgH ₂	GaBi database
	CO ₂ Hydrogenation		10.9	kWh/ kgH ₂	[29 – 35]
Storage	Compressed Hydrogen Storage		0.03	kWh/ kgH ₂	[25][34]
	Liquefied Hydrogen Storage		0.042	kWh/ kgH ₂	[34][24]
	Ammonia Storage		0.014	kWh/ kgH ₂	[34][23]
	Methanol Storage		0.012	kWh/ kgH ₂	[23][36]
Reconditioning	Hydrogen Regasification		2.53	kWh/ kgH ₂	[25][28][23][26]
	Ammonia Cracking		1.93	kWh/ kgH ₂	[28][23][37]
	CO ₂ Dehydrogenation		10.37	kWh/ kgH ₂	[34][36][38]

For the transportation stage, the LCI considers only the transportation and excludes vessel production, end-of-life treatment of the vessel, and the fuel supply chain. The compressed hydrogen is transported overseas via compressed hydrogen containers. The container uses heavy fuel oil as fuel for transportation. This paper uses the available LCI on GaBi software for containers, which is based on calculating the specific fuel consumption and its associated greenhouse gas (GHG) emissions. The equation is derived from [40].

The liquefied hydrogen, ammonia, and methanol are transported overseas via tankers. This paper uses the available LCI on GaBi software for liquefied natural gas tankers. However, this paper considers the density of the transported product in calculating the specific fuel consumption and its associated GHG emissions. In other words, the density ratio of liquefied natural gas to liquefied hydrogen, ammonia, and methanol is 0.167, 1.33, and

1.76, respectively. Additionally, this paper considers the losses that occur during the trip. The equations are derived from [40].

3. Life Cycle Impact Assessment

This paper quantifies the GHG in units of CO₂-equivalent based on the LCI flow results. It uses the CML 2001 – Jan 2016 method where GWP for a 100-year time horizon characterizes the GHG emissions values. It interprets the results in the next section.

RESULTS AND DISCUSSION

The LCA study's primary objective is to assess each pathway's environmental impact and determine which pathway has the lowest environmental impact. In this context, Fig. 2 compares the GWP of four pathways when different panels are employed. The LCA results highlight that the GWP decreases when CPV-T collectors are employed instead of standard PV panels, regardless of the pathway.

The GWP decreases by 26.4%, 22.2%, 18.2%, and 10.5% when CPV-T collectors are employed instead of standard PV panels for the CH₂, LH₂ – H₂, NH₃ – H₂, and CH₃OH – H₂ pathways, respectively. This decrease can be explained by the fact that the efficiency of CPV-T collectors is around 80%, while the efficiency of standard PV panels is about 18%. This high efficiency of the CPV-T collectors allows them to produce more hydrogen quantities than the standard PV panels for the same period. Thus, this reduces the GWP per one kg of hydrogen of CPV-T collectors compared to standard PV panels.

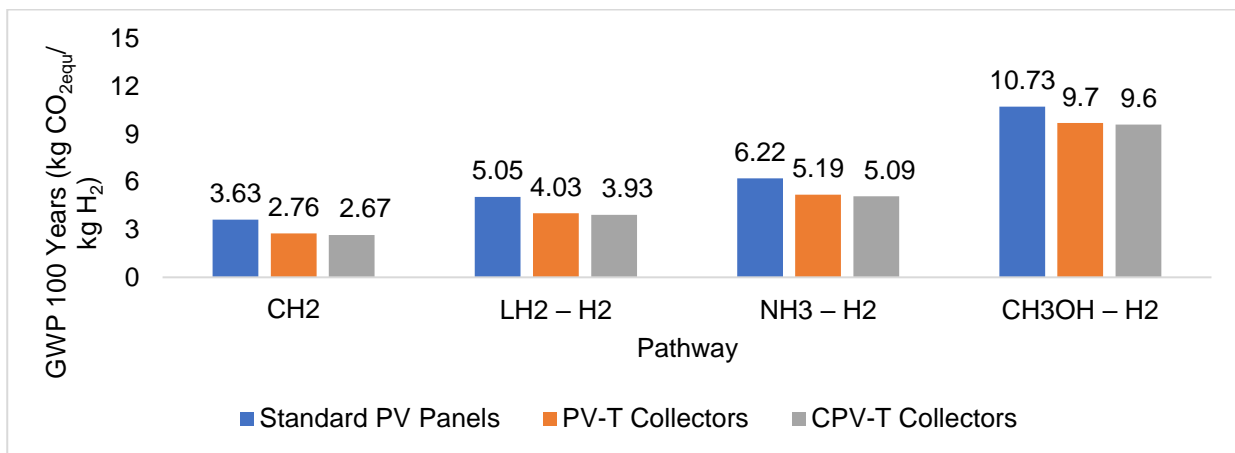


Fig. 2. The GWP of the green hydrogen pathways

Fig. 3 depicts the GWP of each stage in the HSN for each pathway when the CPV-T collectors are employed since they result in the lowest GWP compared to other collectors. Overall, this paper concludes that the CH₂ pathway has the lowest GWP, which is 2.67 kgCO_{2equ}/ kgH₂, compared to other pathways (i.e., lower by 47.2%, 90.6%, and 259.6% for LH₂ – H₂, NH₃ – H₂, and CH₃OH – H₂ pathways, respectively). The reason is that the compression process does not require much energy to compress hydrogen (i.e., 0.57 kWh/ kgCH₂), and no reconversion process occurs in this pathway compared to other pathways. The GWP of the compression process represents 5.4% of the total GWP (i.e., the GWP is 2.67 kgCO_{2equ}/ kgH₂). However, the CH₃OH – H₂ pathway has the highest GWP of 9.60 kgCO_{2equ}/ kgH₂ compared to other pathways, though it's less energy-intensive than the NH₃ – H₂ pathway. This can be explained by the fact that the CO₂ dehydrogenation process is an endothermic process that requires much heat to dehydrogenate methanol to hydrogen; hence, burning natural gas to supply the required heat emits CO₂. The CO₂ dehydrogenation process emits 5.43 kgCO_{2equ}/ kgH₂, while ammonia cracking process emits 1.12 kgCO_{2equ}/ kgH₂. In addition, the CO₂ hydrogenation process includes capturing CO₂ to be used as a feedstock in the hydrogenation process. Thus, the capturing process emits CO₂. Therefore, the CO₂ hydrogenation process emits 1.66 kgCO_{2equ}/ kgH₂, while the ammonia synthesis emits 1.46 kgCO_{2equ}/ kgH₂. The GWP of the CO₂ hydrogenation and dehydrogenation process represents 17.3% and 56.6% of the total GWP (i.e., the GWP is 9.60 kgCO_{2equ}/ kgH₂), respectively.

Looking at each stage independently, from the production stage, this paper highlights that all pathways emit the same amount of CO₂, which is 2.5 kg CO_{2equ}/ kgH₂, since one kg of hydrogen is produced from the electrolysis. However, the CO₂ emissions from this stage contribute differently where represents 93.6%, 63.7%, 49.1%, and 26.1% of the total GWP for the CH₂, LH₂ – H₂, NH₃ – H₂, and CH₃OH – H₂ pathways, respectively.

From the conditioning stage, this paper points out that the CH₂ pathway emits the least CO₂ (i.e., 0.14 kgCO₂_{2equ}/ kgH₂) since the compression process does not consume much energy (i.e., 0.57 kWh/ kg CH₂) compared to other conditioning processes in other pathways. Thus, the compression process represents only 5.4% of the total GWP. While the conditioning stage in the LH₂ – H₂ and NH₃ – H₂ pathways contribute to 29.6% (i.e., 1.17 kgCO₂_{2equ}/ kgH₂) and 28.6% (i.e., 1.46 kgCO₂_{2equ}/ kgH₂) of the total GWP, respectively. They have a higher GWP than the CH₂ pathway as the conditioning process in these pathways consumes more electricity than the compression process in the CH₂ pathway; hence, they have more emissions. While the CO₂ hydrogenation process in the CH₃OH – H₂ pathway emits the most CO₂ (i.e., 1.66 kgCO₂_{2equ}/ kgH₂) compared to other conditioning processes in other pathways as this process consumes 10.9 kWh/ kgH₂. In addition, it includes capturing CO₂ to use as a feedstock for the process. However, the GWP of this CO₂ hydrogenation process contributes only 17.3% of the total GWP in the CH₃OH – H₂ pathway, as the reconditioning stage of this pathway contributes the most to the total GWP.

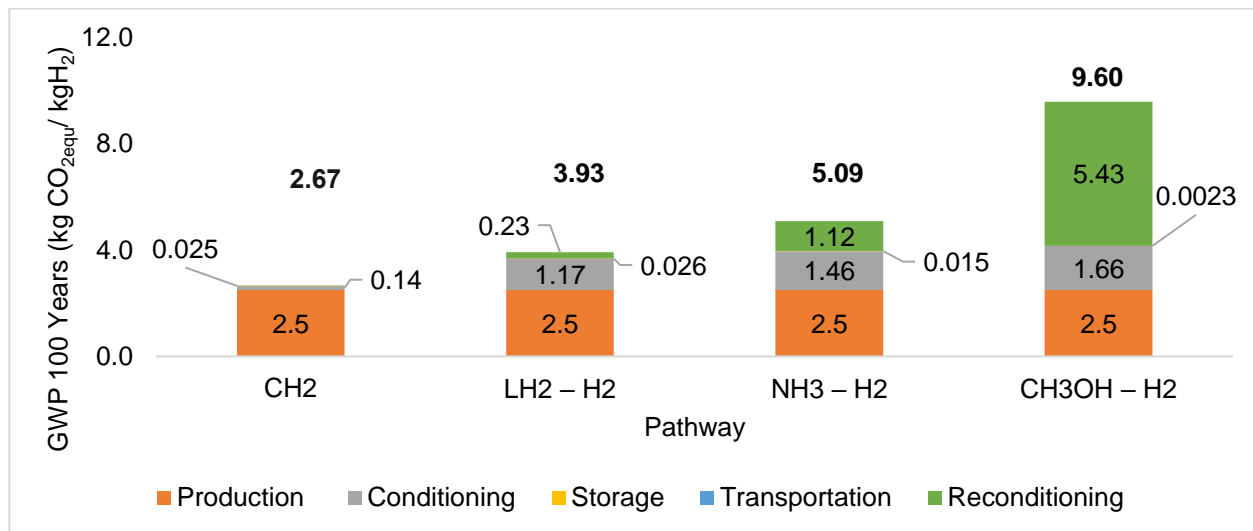


Fig. 3. The GWP of each stage in the HSN of each pathway when CPV-T collectors are employed

From the transportation stage, the emissions from each pathway are insignificant since this paper considers transporting one kg of hydrogen over 100 km. However, transporting compressed hydrogen in containers emits the lowest CO₂ (i.e., 0.00082 kgCO₂_{2equ}/ kgH₂) as it has the lowest density, 38 kg/ m³. While transporting methanol in tankers emits the highest CO₂ (i.e., 0.003 kgCO₂_{2equ}/ kgH₂) as it has the highest density, 792 kg/ m³. As the density of the product increases, more quantities can be transported overseas. Thus, more fuel is consumed during the voyage, which results in more emissions.

From the storage stage, storing methanol in the CH₃OH – H₂ pathway emits the least CO₂ emissions (i.e., 0.0023 kgCO₂_{2equ}/ kgH₂) as not much energy (i.e., 0.012 kWh/ kgCH₃OH) is required to store the methanol compared to other products. This is because methanol can be stored as a liquid at ambient temperature and pressure, typically not requiring refrigeration. In addition, methanol has the lowest boil-off (i.e., 0.005%) and low boiling points. The methanol storage contributes to 0.02% of the total GWP. While storing liquid hydrogen in the LH₂ – H₂ pathway emits the highest CO₂ emissions (i.e., 0.026 kgCO₂_{2equ}/ kgH₂) as a significant quantity of energy (i.e., 0.042 kWh/ kgLH₂) is needed to store the liquid hydrogen compared to other products. This is because liquid hydrogen must be cooled to a very low temperature (-253°C) to maintain its liquid state, which requires significant energy. In addition, liquid hydrogen has the highest boil-off (i.e., 0.18%). The liquid hydrogen storage contributes to 0.7% of the total GWP.

From the reconditioning stage, the CH₂ pathway does not include a reconditioning process, as compressed hydrogen is delivered to the end consumer. Therefore, the regasification process in the LH₂ – H₂ pathway emits the least CO₂ (i.e., 0.23 kgCO₂_{2equ}/ kgH₂) as it consumes 0.047 kWh/ kgH₂ compared to ammonia cracking (i.e., 1.93 kWh/ kgH₂) and CO₂ dehydrogenation (i.e., 0.37 kWh/ kgH₂ and 10 kWh/ kgH₂ of thermal energy). Thus, the regasification process contributes to 5.4% only of the total GWP. However, the CO₂ dehydrogenation process in the CH₃OH – H₂ pathway emits the most CO₂ (i.e., 5.43 kgCO₂_{2equ}/ kgH₂) compared to other reconditioning processes in other pathways, as it is an endothermic process that requires much heat and electricity to dehydrogenate methanol to hydrogen; hence burning natural gas emits CO₂. The CO₂ dehydrogenation process contributes to 56.6% of the total GWP as this process consumes the most electricity compared to other processes in other stages of this pathway. Hence, it produces the most emissions.

CONCLUSION

The environmental impact associated with different green hydrogen supply chains is a relevant factor in the energy transition toward Net Zero. So far, this issue received limited attention from scholars. The present paper conducted LCAs for twelve green hydrogen pathways to determine the one with the lowest GWP. The proposed HSC consisted of five stages: production, conditioning, storage, transportation, and reconditioning. Three different primary energy production are considered to be coupled with an electrolyzer, for hydrogen production: PV panels, PV-T collectors, and CPV-T collectors. The LCA results indicate that the HSN pathway with the lowest emissions, measuring just 2.67 kgCO_{2eq}/ kgH₂, involves coupling CPV-T collectors with an electrolyzer. In this pathway, the produced green hydrogen is subsequently compressed in a compression process, stored, transported in a compressed hydrogen container, and delivered as compressed hydrogen to end-customers. The LCA results coincide with findings from the literature where [4] and [5] reported that compressed hydrogen is the most environmentally friendly pathway when considering the same scope as them. For future work, this paper can extend the LCA by including other pathways, such as delivering ammonia or methanol as end products to customers instead of reconditioning them back to hydrogen. Afterward, it can compare all pathways to determine the one with the lowest GWP.

REFERENCES

- [1] Weidner, T., Tulus, V., & Guillén-Gosálbez, G. (2023). Environmental Sustainability Assessment of large-scale hydrogen production using prospective life cycle analysis. *International Journal of Hydrogen Energy*, 48(22), 8310–8327. <https://doi.org/10.1016/j.ijhydene.2022.11.044>
- [2] Park, C., Jeong, B., & Zhou, P. (2022). Lifecycle energy solution of the electric propulsion ship with live-life cycle assessment for Clean Maritime Economy. *Applied Energy*, 328, 120174. <https://doi.org/10.1016/j.apenergy.2022.120174>
- [3] Noh, H., Kang, K., & Seo, Y. (2023). Environmental and energy efficiency assessments of offshore hydrogen supply chains utilizing compressed gaseous hydrogen, liquefied hydrogen, liquid organic hydrogen carriers and ammonia. *International Journal of Hydrogen Energy*, 48(20), 7515–7532. <https://doi.org/10.1016/j.ijhydene.2022.11.085>
- [4] Akhtar, M. S., Dickson, R., & Liu, J. J. (2021). Life cycle assessment of inland green hydrogen supply chain networks with current challenges and future prospects. *ACS Sustainable Chemistry & Engineering*, 9(50), 17152–17163. <https://doi.org/10.1021/acssuschemeng.1c06769>
- [5] Wulf, C., Reuß, M., Grube, T., Zapp, P., Robinius, M., Hake, J.-F., & Stolten, D. (2018). Life cycle assessment of hydrogen transport and distribution options. *Journal of Cleaner Production*, 199, 431–443. <https://doi.org/10.1016/j.jclepro.2018.07.180>
- [6] Li, J., Zhu, X., Djilali, N., Yang, Y., Ye, D., Chen, R., & Liao, Q. (2022). Comparative well-to-pump assessment of fueling pathways for Zero-carbon transportation in China: Hydrogen economy or methanol economy? *Renewable and Sustainable Energy Reviews*, 169, 112935. <https://doi.org/10.1016/j.rser.2022.112935>
- [7] Life cycle greenhouse gas emissions from solar photovoltaics (fact sheet). (2012). <https://doi.org/10.2172/1056745>
- [8] Ardente, F., Beccali, G., Cellura, M., & Lo Brano, V. (2005). Life cycle assessment of a solar thermal collector. *Renewable Energy*, 30(7), 1031–1054. <https://doi.org/10.1016/j.renene.2004.09.009>
- [9] Cellura, M., Grippaldi, V., Lo Brano, V., Longo, S., & Mistretta, M. (2011). Conference: Life Cycle Management Conference LCM 2011. In Life cycle assessment of a solar PV/T concentrator system.
- [10] Payet, J., & Greffe, T. (2019). Life cycle assessment of new high concentration photovoltaic (HCPV) modules and multi-junction cells. *Energies*, 12(15), 2916. <https://doi.org/10.3390/en12152916>
- [22] Ghandehariun, S., & Kumar, A. (2016). Life cycle assessment of wind-based hydrogen production in Western Canada. *International Journal of Hydrogen Energy*, 41(22), 9696–9704. <https://doi.org/10.1016/j.ijhydene.2016.04.077>
- [23] Hong, X., Thaore, V. B., Karimi, I. A., Farooq, S., Wang, X., Usadi, A. K., Chapman, B. R., & Johnson, R. A. (2021). Techno-enviro-economic analyses of hydrogen supply chains with an ASEAN Case Study. *International Journal of Hydrogen Energy*, 46(65), 32914–32928. <https://doi.org/10.1016/j.ijhydene.2021.07.138>
- [24] Knop, V. (2022). A world of energy - hydrogen compression. A World Of Energy - Hydrogen Compression. Retrieved March 7, 2023, from <http://awoe.net/Hydrogen-Compression-LCA.html>
- [25] Weiszflog, E., & Abbas, M. (2022). (rep.). Life Cycle Assessment of Hydrogen Storage Systems for Trucks.
- [28] Stolzenburg, K., & Mubbala, R. (2013). (rep.). Integrated Design for Demonstration of Efficient Liquefaction of Hydrogen (IDEALHY).

- [29] Cordero-Lanzac, T., Ramirez, A., Navajas, A., Gevers, L., Brunialti, S., Gandía, L. M., Aguayo, A. T., Mani Sarathy, S., & Gascon, J. (2022). A techno-economic and life cycle assessment for the production of Green Methanol from CO₂: Catalyst and process bottlenecks. *Journal of Energy Chemistry*, 68, 255–266. <https://doi.org/10.1016/j.jechem.2021.09.045>
- [30] Rigamonti, L., & Brivio, E. (2022). Life cycle assessment of methanol production by a carbon capture and utilization technology applied to steel mill gases. *International Journal of Greenhouse Gas Control*, 115, 103616. <https://doi.org/10.1016/j.ijggc.2022.103616>
- [31] Soler, A., Gordillo, V., Lilley, W., Schmidt, P., Werner, W., Houghton, T., & Dell'Orco, S. (2022). (rep.). E-Fuels: A techno-economic assessment of European domestic production and imports towards 2050.
- [32] Demirel, Y. (2015). Technoeconomics and sustainability of renewable methanol and ammonia productions using wind power-based hydrogen. *Journal of Advanced Chemical Engineering*, 5(3). <https://doi.org/10.4172/2090-4568.1000128>
- [33] Lee, J.-S., Cherif, A., Lee, C.-J., Yoon, H.-J., Seo, S.-K., Bae, J.-E., Shin, H.-J., Lee, C., & Kwon, H. (2022). Large-scale overseas transportation of hydrogen: Comparative techno-economic and environmental investigation. *SSRN Electronic Journal*. <https://doi.org/10.2139/ssrn.4032602>
- [34] Kaiser, S., Siems, F., Mostert, C., & Bringezu, S. (2022). Environmental and economic performance of CO₂-based methanol production using long-distance transport for H₂ in combination with CO₂ Point Sources: A case study for Germany. *Energies*, 15(7), 2507. <https://doi.org/10.3390/en15072507>
- [35] Al-Breiki, M., & Bicer, Y. (2021). Comparative life cycle assessment of sustainable energy carriers including production, storage, Overseas Transport and Utilization. *Journal of Cleaner Production*, 279, 123481. <https://doi.org/10.1016/j.jclepro.2020.123481>
- [36] Patonia, A., & Poudineh, R. (2022). (rep.). Global trade of hydrogen: what is the best way to transfer hydrogen over long distances?
- [37] Dilshani, A., Wijayananda, A., & Rathnayake, M. (2022). Life cycle net energy and global warming impact assessment for hydrogen production via decomposition of ammonia recovered from source-separated human urine. *International Journal of Hydrogen Energy*, 47(57), 24093–24106. <https://doi.org/10.1016/j.ijhydene.2022.05.188>
- [38] Voelker, S., Deutz, S., Burre, J., Bongartz, D., Omari, A., Lehrheuer, B., Mitsos, A., Pischinger, S., Bardow, A., & von der Assen, N. (2022). Blend for all or pure for few? well-to-wheel life cycle assessment of blending electricity-based ome_{3–5} with fossil diesel. *Sustainable Energy & Fuels*, 6(8), 1959–1973. <https://doi.org/10.1039/d1se01758f>
- [39] IEA. (2019a). The Future of Hydrogen - Seizing today's opportunities. Technology report, <https://www.iea.org/reports/the-future-of-hydrogen>.
- [40] International Maritime Organization. (2015). (rep.). Third IMO GHG Study 2014 - Executive Summary and Final Report.

ICH2P14-OP087

BIOMETHANOL AND HYDROGEN PRODUCTION FROM PINECONE BIOMASS USING STEAM GASIFICATION

*Hilal Sayhan Akci Turgut, Ibrahim Dincer

Clean Energy Research Laboratory, FEAS, Ontario Tech University, Oshawa, Ontario, L1H 7K4, Canada

*Corresponding author e-mail: Hilal.Akci@ontariotechu.ca

ABSTRACT

The integrated system is designed to simulate the production of biomethanol and hydrogen, aiming to mitigate the pine beetle problem in British Columbia. The model incorporates robotic harvesting and steam gasification of woody bioresources derived from pinecones. Aspen Plus and MATLAB software are used to run the simulation. Gasification, syngas post-treatment, and methanol synthesis are the three primary stages of the procedure. The analysis of the system is conducted based on thermodynamic evaluations. The present system produces 0.17 kg/s of methanol and 0.025 kg/s of hydrogen, respectively.

Keywords: Methanol, Hydrogen, Biomass, Gasification.

INTRODUCTION

Global energy consumption has experienced a tremendous and alarming increase recently. Concerningly more greenhouse gas (GHG) emissions have been released as a result of this peak. The amount of CO₂ in the atmosphere is mostly influenced by emissions that result from the burning of fossil fuels. In British Columbia, the mountain pine beetle (MPB) has caused significant damage to trees. The health of the forestry sector and the viability of numerous communities in particular regions of the province are seriously threatened by this infestation. An environmentally beneficial and renewable option is bio-based energy. One of the most potential substitutes for traditional fuels among them is biofuels. Zhang et al. [1] suggested that the results of the economic evaluation point to the possibility for the manufacture of bio-methanol from charcoal to be a compelling and alluring option. Sattar et al. [2] determined that according to the results, increasing steam flow and temperature also results in a significant increase in dry gas yield and carbon conversion. While differences in particle size have little effect on the composition of the gaseous products, there is a drop in the volume percentage of hydrogen at high temperatures. Schweitzer et al. [3] proposed dual fluidized bed steam gasification process, product gas is produced that has a high calorific value. This technology has been successfully demonstrated at a small scale in research using clean biomass sources like wood pellets or wood chips, demonstrating its potential for practical applications. A new method is used for producing bio methanol and hydrogen by the steam gasification process of pinecone biomass, post-syngas treatment, and methanol synthesis. The objectives are solving the mountain pine beetle problem in BC with developing a new multigeneration system with clean energy sources, modelling and analysing the developed system thermodynamically, and evaluating the performance of the system.

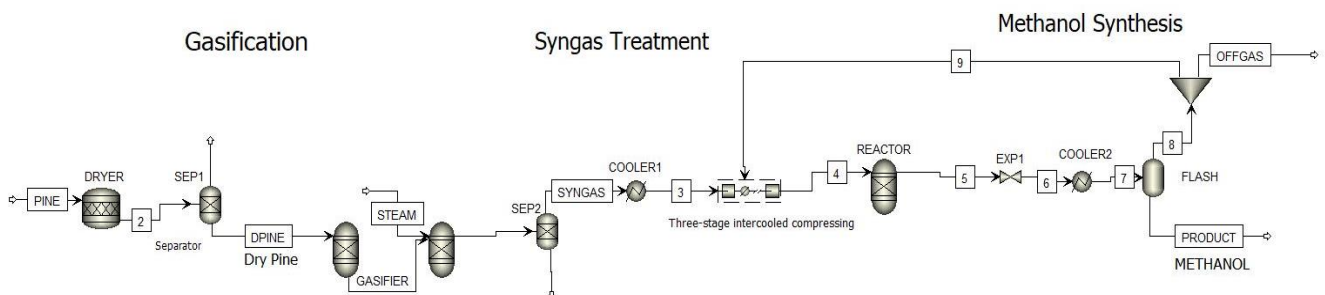


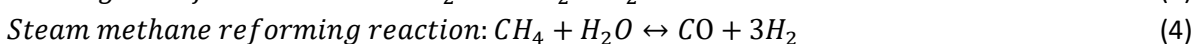
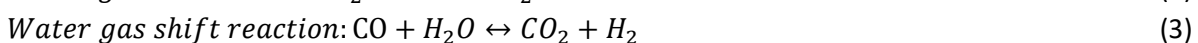
Fig. 1. The Aspen Plus simulation diagram of the designed system.

SYSTEM AND SIMULATION

Fig. 1 illustrates the Aspen Plus schematic diagram of the presently developed system which produces biomethanol from hydrogen. In order to synthesize methanol, the chemical reaction is given as follows:



The production of gases and steam in the process are presented as follows:



RESULTS AND DISCUSSION

The mass flow rates of every stream that exists in the process of the system are shown in Fig 2. In product, biomethanol production has the highest value of the stream which is 0.17 kg/s of methanol. In syngas, the hydrogen production value is estimated as 0.025kg/s of hydrogen. In both off-gas and syngas, CO₂ production is determined as 0.064kg/s.

It is estimated that 57.5% of pinecone biomass is successfully converted into bio-methanol. In comparison to the average range of 50–60% for such conversions, this result shows that a sizable amount of the energy content in the input biomass is efficiently transformed into bio-methanol. The intended system has been fully automated because of the robotic harvesting method's implementation, and it therefore has a radically entirely novel viewpoint.

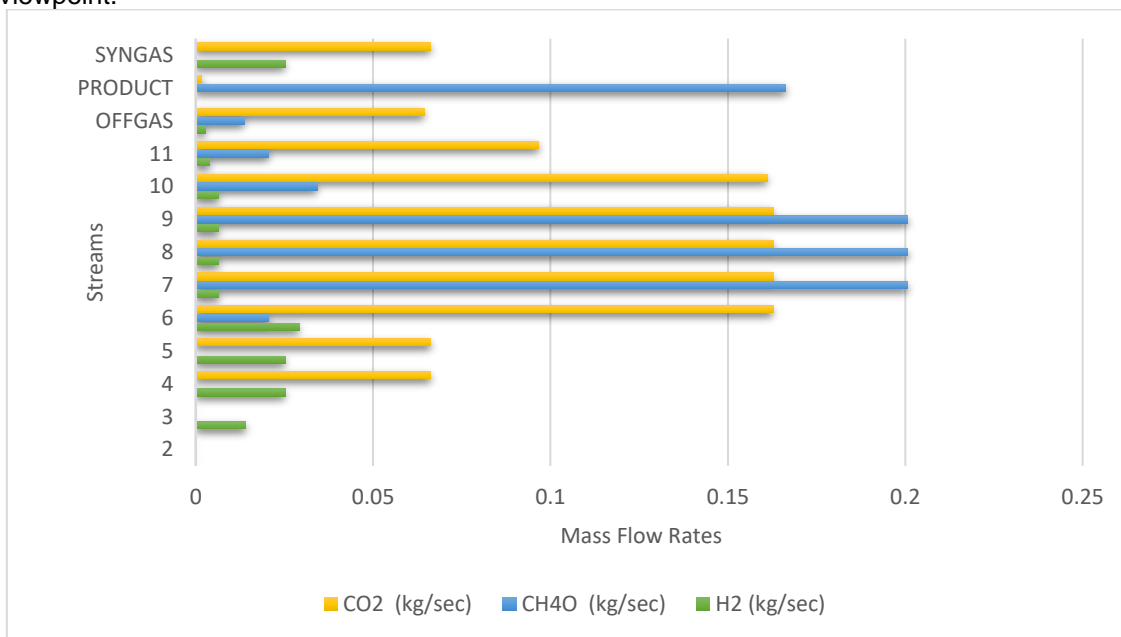


Fig. 2. The production flow rates of CO₂, CH₄O and H₂ gases of all streams

CONCLUSIONS

In this system, results show that the steam gasification, following syngas treatment and methanol synthesis processes successfully transforms a sizeable percentage of the energy present in the raw pinecone biomass into bio-methanol and hydrogen. The system has integrated the robotic harvesting approach to reach full automation, and this study shows that increasing level of efficiency have been attained.

REFERENCES

- 1) Zhang, Z., Delcroix, B., Rezazgui, O., & Mangin, P. (2021). Simulation and techno-economic assessment of bio-methanol production from pine biomass, biochar and pyrolysis oil. *Sustainable Energy Technologies and Assessments*, 44, 101002.
- 2) Sattar, A., Leeke, G. A., Hornung, A., & Wood, J. (2014). Steam gasification of rapeseed, wood, sewage sludge and miscanthus biochars for the production of a hydrogen-rich syngas. *biomass and bioenergy*, 69, 276-286.
- 3) Schweitzer, D., Gredinger, A., Schmid, M., Waizmann, G., Beirow, M., Spörl, R., & Scheffknecht, G. (2018). Steam gasification of wood pellets, sewage sludge and manure: Gasification performance and concentration of impurities. *Biomass and Bioenergy*, 111, 308-319.

ICH2P14-OP088

A STUDY ON NUCLEAR-BASED HYDROGEN PRODUCTION SYSTEM VIA THREE- AND FOUR-STEP MAGNESIUM CHLORINE CYCLES

^{1,2*}*Şulenur Asal, ¹Adem Acir, ²Ibrahim Dincer*

¹Gazi University, Faculty of Technology, Ankara, Türkiye

²Clean Energy Research Laboratory, Faculty of Engineering and Applied Science, Ontario Tech. University, Oshawa, ON, Canada

*Corresponding author e-mail: Sulenur.Asal@ontariotechu.ca

ABSTRACT

This study presents a nuclear-based hydrogen production system where a high-temperature gas-cooled reactor (pebble bed module) is used to meet the required energy demand of a hydrogen production facility. The 3-step and 4-step magnesium-chlorine (Mg-Cl) cycles are considered to examine hydrogen production capacities. The studies are carried out by comparing different reaction conversion ratios for both cycles. Also, the 3-step Mg-Cl cycle is found to be more efficient for hydrogen production compared to the 4-step Mg-Cl cycle. Moreover, the hydrogen production rate decreases as the conversion ratio decreases.

Keywords: Nuclear hydrogen production, HTR-PM, Magnesium-chlorine cycles.

INTRODUCTION

Hydrogen is clearly recognized as a sustainable solution for continually increasing energy demand. Hydrogen which is an energy carrier can be produced by using different methods including thermochemical cycles and electrolysis. The required high thermal energy can be met from renewable energy sources or nuclear reactors. Nuclear reactors can be a good option for high temperature requirements to produce hydrogen. In this context, there are lots of studies. Naterer et al. (2010) examined Canada's nuclear hydrogen production program by using the copper-chlorine (Cu-Cl) cycle. A cogeneration system which consists of high-temperature gas-cooled reactor (HTR-PM), sulfur-iodine (S-I) thermochemical cycle and seawater desalination facilities, was investigated elsewhere (Rodriguez et al. 2022). Temiz and Dincer (2021) designed and assessed a new hybrid system, which this system comprises a solar energy system, high-temperature nuclear reactor (HTR-10), fresh water and high temperature solid oxide electrolysis unit. Asal and Acir (2023) investigated hydrogen production potential of LIFE fusion reactor via various hydrogen production methods, cobalt-chlorine (Co-Cl), copper-chlorine (Cu-Cl) and sulfur-iodine (S-I) cycles. In this present study, high-temperature gas-cooled pebble bed module (HTR-PM) and 3-,4-step magnesium chlorine cycles were integrated and the hydrogen production amounts of both cycles were examined. While the calculations were made, different reaction conversion ratios (0.5, 0.6, 0.7, 0.8 and 0.9) were used for both 3-step and 4-step Mg-Cl cycles.

SYSTEM DESCRIPTION

The high-temperature gas-cooled reactor – pebble bed module (HTR-PM) was designed by the Tsinghua University of China (Hong et al. 2006). The thermal capacity of the reactor is 500.00 MW_{th} (2 units) and the coolant inlet and outlet temperatures are 250°C and 750°C, respectively (IAEA 2011). The required thermal to produce hydrogen power and electricity were met from the nuclear reactors. Figure 1 shows the system layout for present system by considering some earlier studies as a guiding sources (Ates and Ozcan 2022; IAEA 2011).

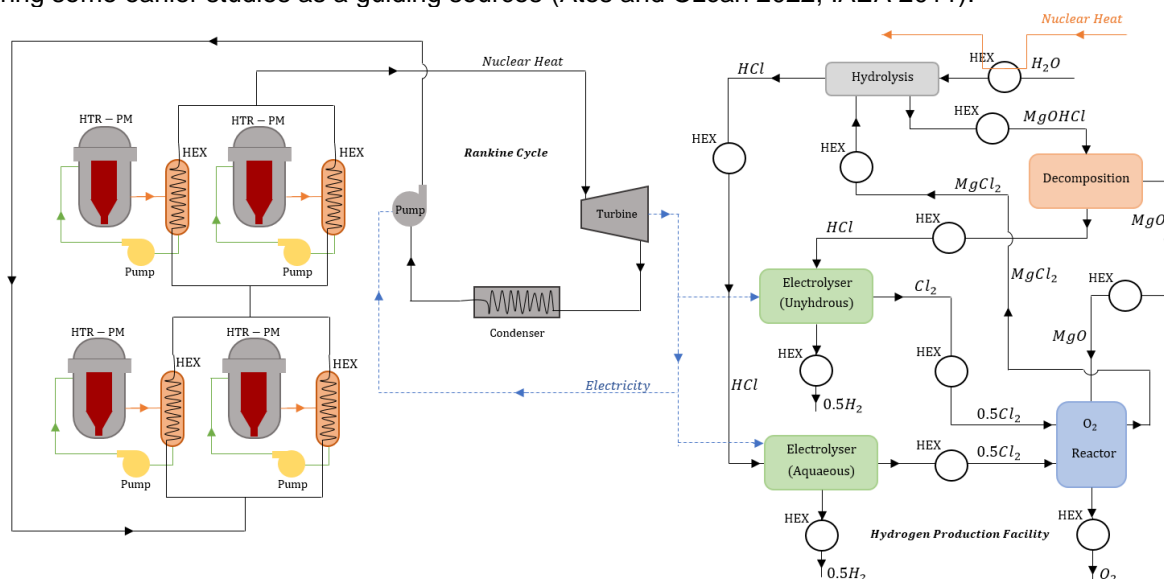


Fig. 1. A schematic diagram of the current nuclear-based hydrogen production system

The producing hydrogen amounts were calculated using flow mass ratio balance equations as follows:

$$\sum \dot{m}_{in} = \sum \dot{m}_{out} \quad (1)$$

$$\dot{m}_x = \frac{P_{hpf}}{q_{tot}} \quad (2)$$

$$\dot{m}_y = \dot{m}_x \cdot \frac{u_y}{u_x} \cdot \eta \quad (3)$$

where, \dot{m} is mass flow rate (kg/s), u is molar mass of compounds (g/mol), η is the efficiencies of reactions and q_{tot} is the total energy value (MJ/kg) which was assessed via the Energy Balance and Shomate Equations as

$$\dot{E}_{in} = \dot{E}_{out} \quad (4)$$

$$\dot{Q}_{in} + \dot{W}_{in} + \sum n_{in} H_{in} = \dot{Q}_{out} + \dot{W}_{out} + \sum n_{out} H_{out} \quad (5)$$

$$Q = \sum n_{out} (\bar{h}_f^o + \bar{h}(T) - \bar{h}_0)_{out} - \sum n_{in} (\bar{h}_f^o + \bar{h}(T) - \bar{h}_0)_{in} \quad (6)$$

$$\bar{h}(T) - \bar{h}_0 = AT + B \frac{T^2}{2} + C \frac{T^3}{3} + D \frac{T^4}{4} - \frac{E}{T} + F - H \quad (7)$$

where, \dot{E} shows total energy transfer (kW), \dot{Q} is the energy transfer by heat (kW), \dot{W} is the energy transfer by work (kW), \bar{h}_f^o is enthalpy of formation (kJ/mol), $\bar{h}(T)$ is sensible enthalpy of a given state (kJ/mol), \bar{h}_0 is standard sensible enthalpy at 25°C and 1 atm (kJ/mol), T is the specified temperature's 1/1000 in K. Also A, B, C, D, E, F and H are constants (NIST Chemistry WebBook) which are given in Table 1.

Table 1. The required parameters for Shomate equations (NIST Chemistry WebBook)

Compound	\bar{h}_f^o (kJ/mol)	A	B	C	D	E	F	G	H
MgCl ₂ (s)	-641.62	78.307330	2.435888	6.858873	-1.728967	-0.729911	-667.5823	179.2639	-641.6164
H ₂ O (g)	-241.83	30.092	6.832514	6.793435	-2.534480	0.082139	-250.8810	2233967	-241.8264
MgO (s)	-601.24	47.25995	5.68162	-0.872665	0.104300	-1.053955	-619.1316	764618	-601.2408
HCl (g)	-92.31	32.12392	-13.45805	19.86852	-6.853936	-0.049672	-101.6206	228.6866	-92.31201
Cl ₂ (g)	0	33.0506	12.2294	-12.0651	4.38533	-0.159494	-10.8348	259.029	0
O ₂ (g)	0	30.0235	8.772972	-3.988133	0.788313	-0.741599	-11.32468	236.16630	0
H ₂ (g)	0	33.066178	-11.363417	11.432816	-2.772874	-0.158558	-9.980797	172.707974	0

There are lots of studies about nuclear hydrogen production, which uses various hydrogen production methods including steam methane reforming (SMR), high temperature electrolysis (HTE), copper-chlorine (Cu-Cl), cobalt-chlorine (Co-Cl), sulphur-iodine (S-I) and magnesium-chlorine (Mg-Cl) cycles. Whilst the reactions are named as hydrolysis, chlorination, electrolysis and decomposition in the 4-step Mg-Cl cycle, the decomposition reaction is eliminated in 3-step Mg-Cl reaction. In Fig. 2, the schematic representations of cycles were illustrated. While the maximum temperature is 500°C for 3-step Mg-Cl cycle, this value is 475°C for 4-step cycle (Ozcan and Dincer 2016).

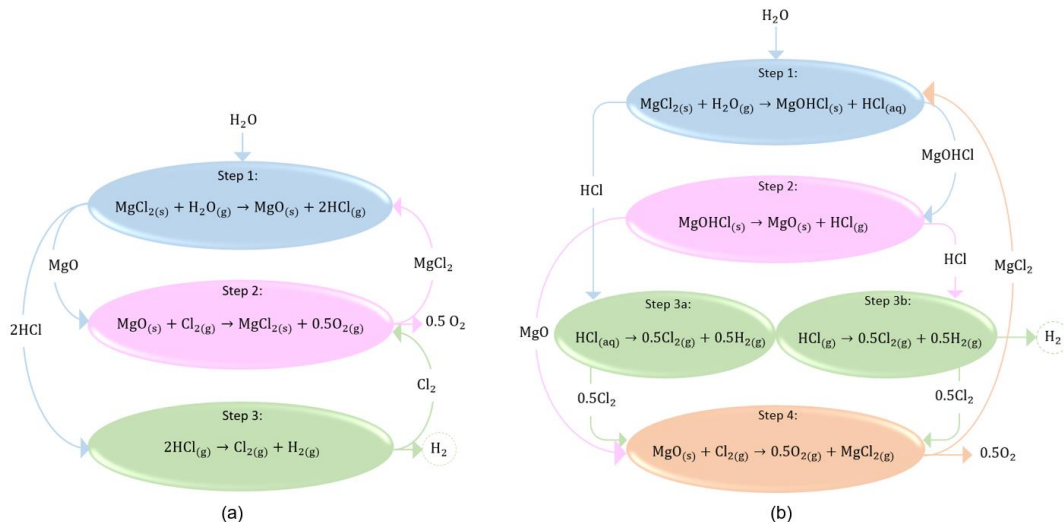


Fig. 2. The schematic representations of the cycles (a) 3-step Mg-Cl cycle; (b) 4-step Mg-Cl cycle.

RESULTS AND DISCUSSION

In this section, hydrogen production results were evaluated. In Fig.3 (a), the required H₂O mass flow rates and produced O₂ values are given. While the H₂O mass flow rates are constant for all conversion ratios, produced O₂ amounts go up with rising conversion ratios. The produced O₂ amount of 3-step Mg-Cl cycle is calculated as 53.2 kg/s for 0.9 conversion ratio. Moreover, this value is 13.7 kg/s for 4-step Mg-Cl cycle. Fig. 3 (b) illustrates produced hydrogen amounts via Mg-Cl cycles. More hydrogen is produced by using the 3-step Mg-Cl cycle than 4-step Mg-Cl cycle. The highest amount of produced hydrogen is obtained with 3-step Mg-Cl cycle and 0.9 conversion ratio.

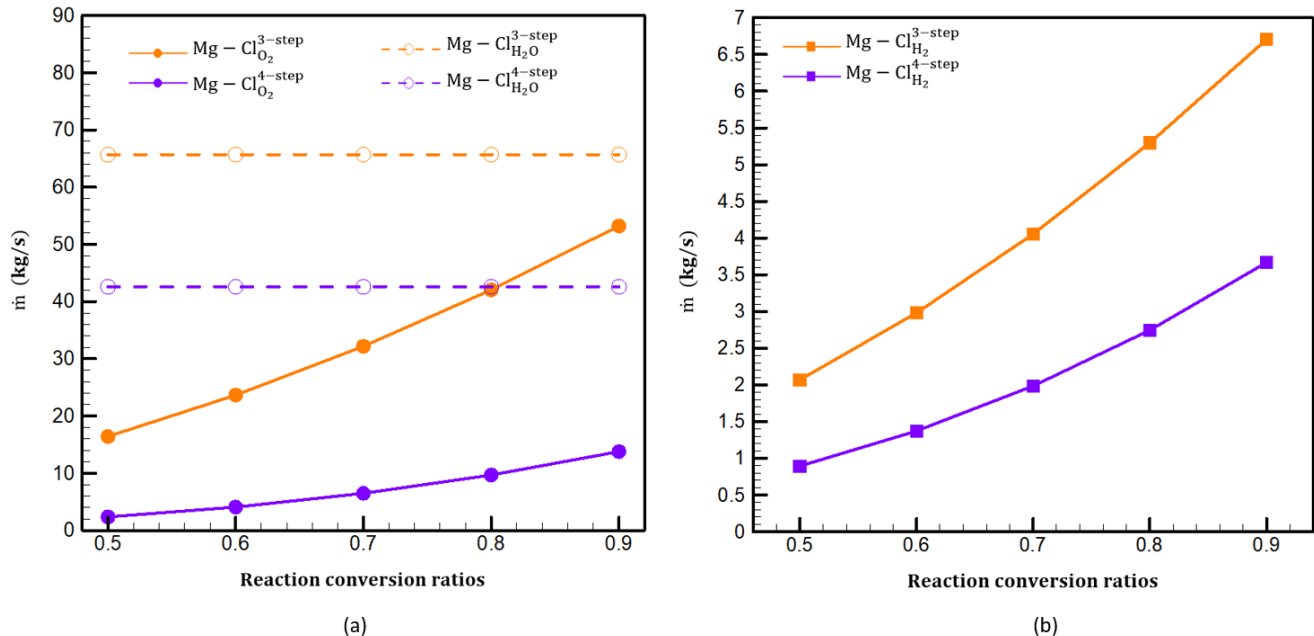


Fig. 3. Mass flow rates of H₂O and produced O₂; (b) Produced H₂ amounts according to conversion ratios.

CONCLUSIONS

The analysis carried out in this study obtains: (a) The HTR-PM integrated 3-step Mg-Cl system produced more hydrogen than the HTR-PM integrated 4-step Mg-Cl system for this presented system, (b) As the reaction conversion ratios increase, the producing hydrogen amounts rise steadily and (c) For the 0.9 conversion ratio, the 3-step and 4-step Mg-Cl cycles produce 6.7 kg/s and 3.7 kg/s H₂, respectively.

REFERENCES

- Asal, Şulenur, and Adem Acir. 2023. "Evaluation and Comparison of Hydrogen Production Potential of the LIFE Fusion Reactor by Using Copper-Chlorine (Cu-Cl), Cobalt-Chlorine (Co-Cl) and Sulfur-Iodine (S-I) Cycles." *International Journal of Hydrogen Energy* 48(60): 22791–805.
- Ates, Funda, and Hasan Ozcan. 2022. "Turkey's Industrial Waste Heat Recovery Potential with Power and Hydrogen Conversion Technologies: A Techno-Economic Analysis." *International Journal of Hydrogen Energy* 47(5): 3224–36.
- González Rodríguez, Daniel, Carlos Alberto Brayner de Oliveira Lira, Fernando Roberto de Andrade Lima, and Carlos García Hernández. 2022. "Exergy Study of Hydrogen Cogeneration and Seawater Desalination Coupled to the HTR-PM Nuclear Reactor." *International Journal of Hydrogen Energy* 48(7): 2483-2509.
- Hong, C. et al. 2006. "Thorium-Based Fuel Cycles in The Modular High Temperature Reactor." *Tsinghua Science and Technology* 11(6): 731-738.
- IAEA. 2011. "Status Report 96 - High Temperature Gas Cooled Reactor - Pebble-Bed Module." *IAEA Status Report for Advanced Nuclear Reactor Designs - Report 96*: 1–18.
- Naterer, G. F. et al. 2010. "Canada's Program on Nuclear Hydrogen Production and the Thermochemical Cu-Cl Cycle." *International Journal of Hydrogen Energy* 35(20): 10905–26.
- NIST Chemistry WebBook. <http://Webbook.Nist.Gov/Chemistry/>; 2018.
- Ozcan, Hasan, and Ibrahim Dincer. 2016. "Modeling of a New Four-Step Magnesium-Chlorine Cycle with Dry HCl Capture for More Efficient Hydrogen Production." *International Journal of Hydrogen Energy* 41(19): 7792–7801.
- Temiz, Mert, and Ibrahim Dincer. 2021. "Design and Analysis of a New Renewable-Nuclear Hybrid Energy System for Production of Hydrogen, Fresh Water and Power." *e-Prime - Advances in Electrical Engineering, Electronics and Energy* 1(July): 100021.

ICH2P14-OP090 AN INVESTIGATION OF METAL COATED 3D-PRINTED ELECTRODES FOR HYDROGEN PRODUCTION

*Muarij Khalil, Ibrahim Dincer

Ontario Tech University, Faculty of Engineering and Applied Science, Clean Energy Research Laboratory (CERL), 2000 Simcoe Street North, Oshawa, Ontario, L1H 7K4, Canada

*Corresponding author e-mail: Muarij.Khalil@ontariotechu.ca

ABSTRACT

In the presented paper, a new approach where the electrolysis cathodes are 3D-printed and coated for alkaline water electrolysis is investigated. Alloys including copper and iron are considered with nickel as coatings using electrodeposition. A new flow-through electrode design is compared with the traditionally designed electrodes. The flow-through electrodes were shown to have 70% higher efficiency than the coated 3D-printed electrode of the conventional design. 3D printing provides a safe design place for exploring unconventional electrode designs for improving electrolysis performance and efficiency.

Keywords: Hydrogen production, electrolysis, cathodes, energy, efficiency.

1. INTRODUCTION

Recently, hydrogen has been emerging as a popular clean fuel. Hydrogen can be produced from many sources and produces zero emissions when used as a fuel. Hydrogen is critical for tackling climate goals. It has many advantages, it has the potential to store, produce, and move energy [1]. 3D printing is an additive manufacturing technique that has become a popular approach in recent years for fabricating a variety of objects and geometries. Researchers have looked at various techniques for electroplating materials using electrodeposition. The general technique consists of a circuit using an anode, cathode, and electrolytic bath. For example, Huner et al. [2] conducted a study where they tested a nickel and platinum (Ni-Pt) coating on 3D-printed electrodes printed with graphene-based PLA. The 3D-printed and coated electrodes were investigated for hydrogen evolution reactions.

2. EXPERIMENTAL

A two-electrode electrodeposition system is implemented as the experimental setup to coat the electrodes. There are two main metal coatings that are investigated for electrodeposition on the 3D-printed electrodes, printed using conductive PLA and a 3D printer. Nickel and copper and nickel and iron are electroplated. The electroplating system consists of a platinum-coated titanium mesh electrode which is used as the counter electrode (anode). The part being coated (3D-printed electrode) is used as the cathode. Direct current is applied to the anode (+) and the cathode (-) which breaks down ions from the electrolyte bath and plates the part being coated (cathode). The composition of the electrolyte bath varied depending on the metal which was being coated. For hydrogen testing, a setup was implemented to test the electrodes using a cell to imitate the conditions of water electrolysis. Figure 1 shows the hydrogen testing apparatus used to test the prepared electrodes for the hydrogen evolution reaction. A 316 stainless steel electrode was used for the anode. The coated 3D-printed electrodes were used as the cathode. The produced hydrogen was collected and measured using the MQ-8 hydrogen gas sensor with Arduino.

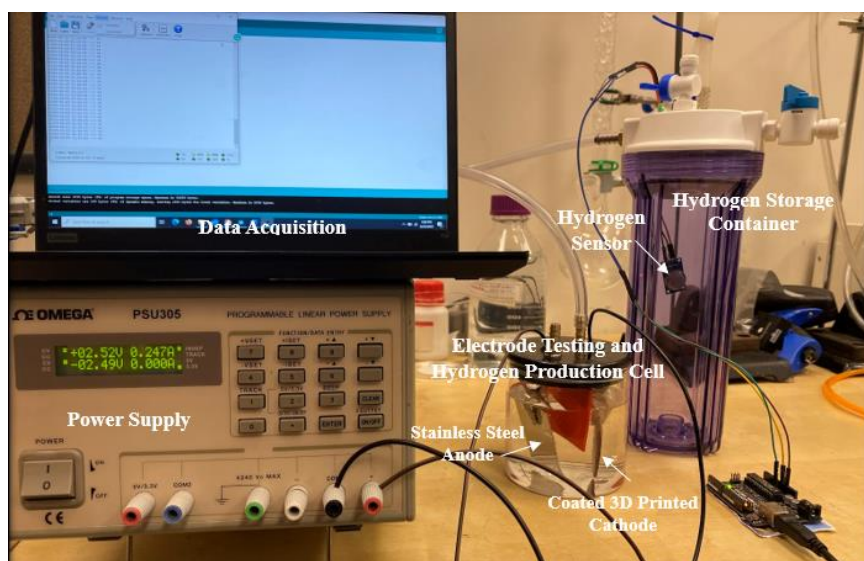


Fig. 1. Electrolysis cathodic testing and hydrogen measurement setup

Figure 2 shows the coated electrodes using electrodeposition of the two designs investigated for hydrogen production. The coated electrodes were then tested for hydrogen flow rate.

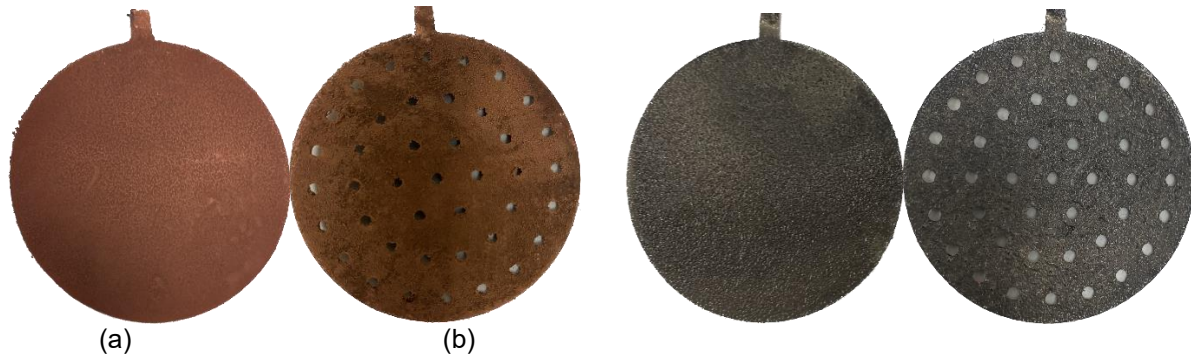


Fig. 2: (a) Nickel-copper coated electrodes (b) Nickel-iron coated electrodes

3. ANALYSIS

The amount of metal coating deposited during the electrodeposition is considered in this section. The metal deposited onto the electrode during electrodeposition can be calculated using Faraday's law as given as follows:

$$W = \frac{ItM}{nF} \quad (1)$$

where W is the amount of coating deposited on the electrode in grams (g), I is the current in amps (A), t is the deposition time in seconds (s), M is the molar mass of the metal plated (g/mol), n is the number of electrons involved and F is the Faraday's constant (96485 C/mol).

The energy and exergy efficiency of the electrode testing system is given as:

$$\eta_{en} = \frac{\dot{m}LHV}{\dot{E}_{in}} \quad (2)$$

$$\eta_{ex} = \frac{\dot{m}ex^{ch}}{\dot{E}_{in}} \quad (3)$$

where LHV is the low heating value of hydrogen (120 MJ/kg), \dot{m} is the mass flow rate of the hydrogen produced, and ex^{ch} (116.6 MJ/kg) is the chemical exergy.

For alkaline water electrolysis water is supplied with the addition of either potassium hydroxide or sodium hydroxide. Direct current is applied at the anode and cathode to split water. Oxygen and hydrogen are produced as the resulting gasses from the reaction. The reaction at the cathode is given by equation 4.



The composition of the electrolyte bath for copper coating consisted of 25 g copper sulfate with approximately 0.1 to 0.5 ml sulfuric acid with a pH of 2.5 to 3. An iron electrolyte bath with the composition of 33.3 g of iron sulfate, 8.4 g of iron chloride, and 2.67 g of ammonium chloride in 200 ml of distilled water was prepared for electrodeposition of iron Table 1 shows the parameters used to coat the 3D-printed electrodes along with the amount of coating of each metal coated.

Tab. 1: Electrodeposition parameters and metal coating amounts

Metal Coating	Nickel Coating			Alloy Metal Coating		
	Current (A)	Time (h)	Deposition (g)	Current (A)	Time (h)	Deposition (g)
Ni-Cu	0.8	2	1.75	0.7	2	1.66
Ni-Fe	0.8	4	3.5	0.8	2	1.67

4. RESULTS AND DISCUSSION

The energy efficiencies of the flow-through and conventional electrodes are directly compared. To evaluate the performance of the coated electrodes, the nickel-copper samples were tested for 1 hour three times to obtain average results. From the results of the experiments conducted three times (15 min, 30 min, and 1 h) a relation between the hydrogen mass flow rate and the operation time was developed. The tests were performed for the

nickel-copper coated flow-through, and the initial design coated CPLA 3D-printed electrodes.

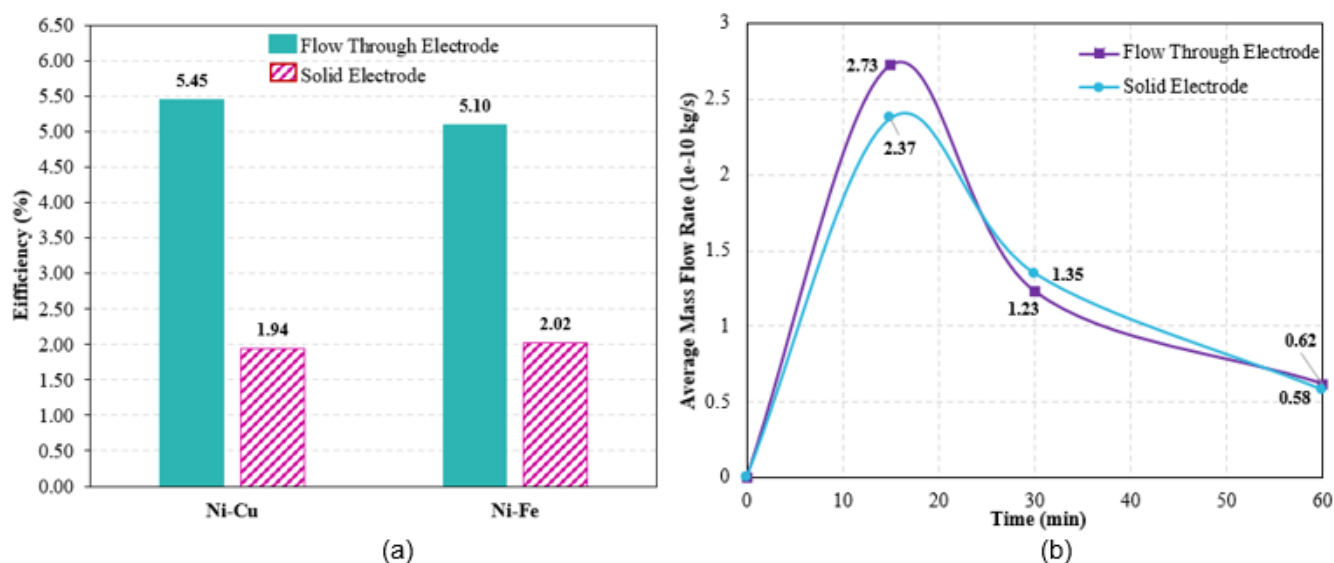


Fig. 3: (a) Efficiency (b) Average hydrogen mass flow rate for coated flow through and traditional electrodes

The mass flow rate is high in the first 15 minutes, when the flow rate decreases until it is stabilized. It can be observed that the flow-through electrode has a higher flow rate at the start compared to the initial design. With time the mass flow rate of the two electrodes is relatively similar. It can be seen that the efficiencies of the coated flow through electrodes are much higher than the initial design of coated 3D-printed electrodes. The efficiencies of the flow-through electrodes for the same coating metal is approximately 74% higher. The higher efficiency is directly a result of faster mass transport and higher hydrogen production rate for the flow-through design. In addition, the flow through electrodes requires less energy for the hydrogen produced compared to the initially designed electrodes. The increase in mass transport reduces the losses due to ohmic overpotential that occur between the electrolyte and the electrode. The presented study shows that the flow-through design has higher hydrogen production rates and much higher efficiencies compared to conventional electrode designs.

5. CONCLUSIONS

Hydrogen is an emerging clean fuel for the replacement of fossil fuels. No emissions are released when hydrogen is used as a fuel. Electrolysis is a common device used for hydrogen production, more commonly for green hydrogen production. Better solutions are needed to reduce hydrogen production costs, increase feasibility, and make hydrogen production more easily accessible. This paper presents a new approach for preparing the electrodes used in electrolysis for hydrogen production. A water-memberless alkaline electrolysis is considered, and the performance of the cathodes (coated 3D-printed electrodes) is evaluated in a 1M potassium hydroxide (KOH) added to the water supplied. The method considered for coating the 3D-printed electrodes using electrodeposition as the coating technique. Two electrode designs are investigated for hydrogen production, the conventional design and a flow-through electrode design. The flow-through electrode design was found to be the better design as the hydrogen production rate was increased. In addition, the energy efficiency of the flow-through electrode was ~70% higher compared to the traditional coated solid electrode design coated with the same metals. the efficiencies of the coated 3D-printed were low for commercial applications. However, this technology can be beneficial as a design space that can help improve the respective efficiencies and hence performance of conventional electrode designs.

REFERENCES

- [1] "The Future of Hydrogen – Analysis - IEA." <https://www.iea.org/reports/the-future-of-hydrogen> (accessed May 23, 2023).
- [2] B. Hüner, N. Demir, and M. F. Kaya, "Ni-Pt coating on graphene-based 3D printed electrodes for hydrogen evolution reactions in alkaline media," *Fuel*, vol. 331, p. 125971, Jan. 2023, doi: 10.1016/J.FUEL.2022.125971

ICH2P14-OP091

PISTON REACTOR CAPABILITIES TO MAKE HYDROGEN FROM METHANE VIA STEAM AND AUTOHERMAL REFORMING – MODELING STUDY

**Aya Abousrafa, Patrick Linke, Ma'moun Al-Rawashdeh*

Department of Chemical Engineering, Texas A&M University at Qatar, Education City, Doha, Qatar.

*Corresponding author e-mail: mamoun.al-rawashdeh@qatar.tamu.edu

ABSTRACT

The piston reactor is a novel chemical reactor concept with many unique offerings. It is a repurposed internal combustion engine but is now used as a chemical reactor to make valuable products in the exhaust while offering the possibility for integration with electricity via mechanical work. Low-carbon hydrogen is considered an important energy carrier for the future of energy transition. The implementation of electrified, downsized, and compact methane conversion has been identified as a promising direction to intensify hydrogen production and reduce carbon footprints. To date, the applications studied for the piston reactor have been limited to a few reaction routes with limited experimental work. All work on hydrogen production has been limited to partial oxidation till now. This study wants to assess the feasibility of steam methane reforming (SMR) and auto thermal refining (ATR) for hydrogen production in piston reactors under typical ICE engine conditions, targeting small-scale hydrogen plants at a scale of 25 TPD capacity. To enable an early-stage screening of the reaction before intensive experimental validation, a model-based approach is proposed based on coupling a zero-dimensional thermodynamic model with kinetics from the literature. It is used to explore the reactor operating conditions and generate full mass and energy balance. Process level considerations are accounted for right from the early stage of exploration. This approach narrows down the exploration space and provides informed decisions on the direction of the experimental work and process development. The SMR route revealed poor performance in the piston reactor while the ATR route showed superior performance (conversions > 90%). The ATR piston reactor process has a lower blue hydrogen production cost compared to that of the conventional process while keeping comparable CO₂ emissions. The availability of a power integration option with the heat generated provides a key advantage for the carbon capture and compression part. Overall, the used methodology proves valuable in assisting early-stage exploration. Also, the piston reactor shows some promise as a compact reactor suitable for small-scale hydrogen production facilities.

Keywords: Piston Reactor, Sustainability, Hydrogen, electrification.

INTRODUCTION

The piston-reactor is a novel concept that converts electrical energy into mechanical-work, and subsequently to chemical products [1,2]. It offers a simple and compact technology to carry out chemical reactions within a unique operating window at very high temperatures around 1500K, and pressures up to hundreds of bars within milliseconds. The rapid gas expansion leads to quenching of the reacting mixture which hinders secondary reactions of metastable species toward undesired by-products. The emerging piston reactor offers a unique, compact platform for chemical reactions, presenting opportunities for electrically driven operations distinct from conventional methods. To date, the applications studied for the piston reactor have been limited to a few reaction routes [3-5] with limited experimental work.

Hydrogen is considered an important energy carrier for low-carbon and net-zero economies [6]. Today, most hydrogen is produced from natural gas [7]. There are currently three commercial routes for hydrogen production from natural gas, namely partial oxidation of methane (POM), autothermal reforming (ATR), and steam reforming (SMR) [8, 9], with over 95% of global hydrogen being produced via SMR [8]. All three routes are commercially mature, but also associated with high CO₂ footprints [10]. The implementation of electrified and down-sized, compact reformers has been identified as a direction to intensify hydrogen production and reduce carbon footprints [11]. This could potentially enable hydrogen production facilities in regions with small gas reserves, biomethane produced from many

decentralized feedstock locations, and the utilization of stranded gas that would otherwise be flared [12, 13]. An example of such technology is an electrified reformer based on resistive heating supplied with renewable electricity to drive the catalytic SMR reactions to provide compact hydrogen production with reduced emissions compared to current reforming technologies [11].

The emerging piston reactor offers a unique, compact platform for chemical reactions, presenting opportunities for electrically driven operations distinct from conventional methods. This reactor is similar to the traditional internal combustion engine, compressing gas or liquid streams to generate high pressures and temperatures within milliseconds, fostering non-equilibrium states and inhibiting undesired reactions. While past studies on hydrogen production in piston reactors largely focused on POM, avenues exploring SMR and ATR remain underexplored due to their catalyst-dependent, endothermic nature. Existing attempts like the CHAMP-SORB membrane-based piston reactor or patented systems showed promise but lacked comprehensive data, hindering conclusive feasibility assessments. Despite the potential shown, commercializing piston reactors faces technical and interdisciplinary challenges, necessitating optimization for overall chemical production process design.

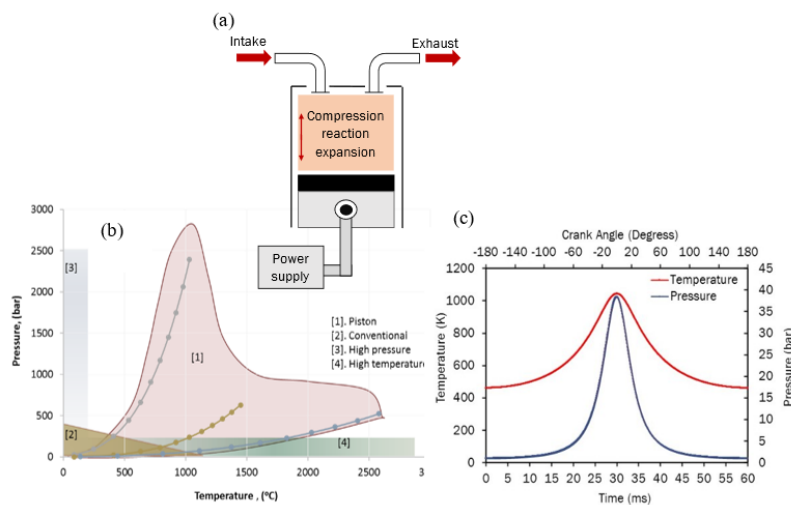


Figure 1. Schematic of a piston reactor (a), and operating temperature and pressure window compared to other reactors (b), in-cylinder pressure and temperature profiles (c).

This work aims to theoretically evaluate if steam methane reforming (SMR) and methane autothermal reforming (ATR) constitute promising routes for hydrogen production using piston reactor technology for typical parameters and conditions encountered in automotive internal combustion engines (ICE). Specifically, the aim is to use reactor modeling and consider process design aspects in the early stages of investigation to provide direction and justify the next research and development stages involving experimentation, while eliminating infeasible options from further expensive analysis. The piston reactor is first modeled using a zero-dimensional thermodynamic single-zone piston model coupled with available steady-state kinetic models for these routes. A model-based analysis is conducted to explore the operating window and limitations of SMR and ATR in the piston reactor. If the reaction underperforms under best-case conditions, then the reaction route is eliminated from further assessments and studies. For the promising route and conditions, process intensification potential is evaluated versus conventional reactor technology. Afterward, the implementation of the piston reactors into grey and blue hydrogen production process designs is explored to understand overall performance and economy of scale effects. This work wants to demonstrate and highlight the value of the implemented approach for quickly identifying promising directions for further detailed experimental and modeling studies during early-stage exploration.

MODEL DEVELOPMENT

A Zero-dimensional single-zone thermodynamic model is established for a four-stroke single-cylinder piston reactor. The model accounts for the temporal change of cylinder volume, pressure, temperature, and species concentrations. A homogeneous gas mixture is assumed for each state; thus, spatial variations inside the piston chamber are neglected. The simulated model starts with a prefilled cylinder that self-ignites due to compression without an external influence; consequently, no flame propagation or spark ignition is modeled in this work. The model handles only the closed part of the thermodynamics cycle, including compression, reaction, and expansion; without considering gas exchange processes. The simulation starts at the bottom dead center (BDC) and at inlet valve closing time (IVC). A full crankshaft rotation is then carried out until the exhaust valve opening time (EVO). Thermodynamic properties of the chemical species, including enthalpy and heat capacity, are represented by the seven-term NASA polynomials reported by Gordon and McBride [25, 26]. The closed cycle model was discretized into small crank angle/time steps. The source for the reaction rate is predicted using steady-state catalytic kinetic models available from the literature. The reactor model is pseudo-homogenous in which the catalyst amount is used to compute the rate of the reaction. The catalyst location is not relevant in this model but its total volume relative to the cylinder volume is accounted for to ensure a realistic value is being implemented. The amount of catalyst is treated as a theoretical model value. It is adjusted till a reasonable reaction rate is achieved which was 5 g in this work. The pseudo-homogenous assumption means there are no mass transfer limitations considered between the gas phase and the solid particles at this stage. Piston dimensions of 400 cc displacement volume, 16.5 compression ratio, and RPM of 3000 all similar to typical ICE engine specifications.

RESULTS AND DISCUSSION

STEAM REFORMING – BASE CASE IN PISTON REACTOR

A base case scenario for the piston reactor operating under steam reforming conditions is defined. The piston RPM, dimensions, and intake conditions were selected to be in a typical operating window range used in automotive engines. In this case scenario, the selected intake temperature and pressure were at 660K and 1 bar respectively [1]. An H₂O/CH₄ ratio of 3.56 and a speed of 3000 RPM were used with piston dimensions of 400 cc displacement volume and 16.5 compression ratio. Figure 2 displays the evolution of species mole fractions and temperature across the crank angle. Although the reaction was initiated, resulting in the production of synthesis gas and CO₂, methane conversion reaches only 13%, hindered by the insufficient in-cylinder temperatures of approximately 1011 K at maximum, unable to drive SMR reactions effectively. Compression-generated adiabatic heating is insufficient to drive the highly endothermic SMR reaction at adequate rates. Additionally, high in-cylinder pressure, caused by compression, promotes backward reactions, impacting methane consumption. The feed intake temperature is a key parameter to increase the SMR conversion. However, it has limitations on how much it can be increased and cannot increase the methane conversion to a level similar to those reached in industrial SMR reactors. Diluting the feed with argon is another method that can be used to decrease the heat capacity of the intake gas mixture and hence increase the temperature during the compression phase. However, this simultaneously reduces the absolute mole percentage of the produced species in the exhaust stream.

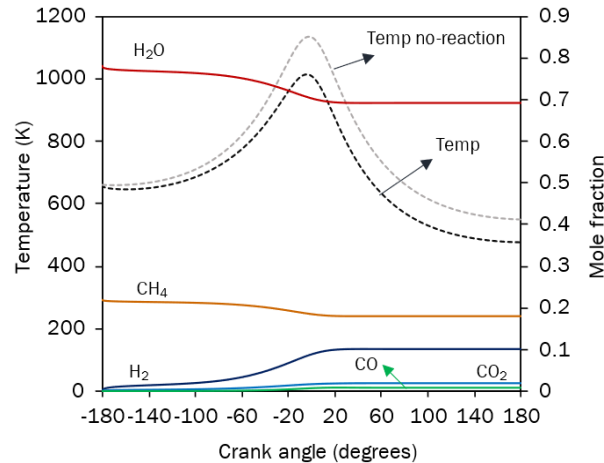


Figure 2: Evolution of species and in-cylinder temperature and temperature of the non-reacting mixture as a function of the crank angle at $N = 3000$ RPM, $T_{\text{intake}} = 660$ K, $P_{\text{intake}} = 1$ bar, $\text{H}_2\text{O}/\text{CH}_4 = 3.561$.

AUTOTHERMAL REFORMING – BASE CASE IN PISTON REACTOR

ATR combines the principles of SMR with methane combustion into one unit by adding some oxygen to the methane and steam feed mixture [14, 15]. The presence of oxygen triggers the exothermic oxidation reaction via auto-igniting methane, and the heat released during the reaction fulfills the energy demand of the endothermic SMR reactions. Thus, the main advantage of ATR is that the process is thermally neutral because the heat generated by the exothermic reaction sufficiently meets the energy requirement of SMR [16, 17]. A base case scenario for the piston reactor operating under ATR conditions is defined similarly to the discussed SMR base case. Figure 3 shows the species evolution and temperature changes throughout the crank angle. At the start of compression, reactant concentrations remain steady due to insufficient temperature. Approximately 18° before TDC, methane ignites at 1160 K, leading to a swift temperature surge from 1036 K to 2306 K. The reaction unfolds in two phases: first, oxygen consumption generates partial oxidation and full combustion products, peaking H_2O , and CO_2 . Second, the remaining CH_4 reacts with H_2O and some CO_2 , yielding synthesis gas with 89% methane conversion and 44 mol% hydrogen. An advantage of ATR in the piston reactor is the potential for work extraction from the exothermic reaction, surpassing heat used by endothermic reactions. Calculating the network per cycle, an estimate of 1.69 KW of co-generated work highlights the piston reactor's poly-generation potential under ATR conditions.

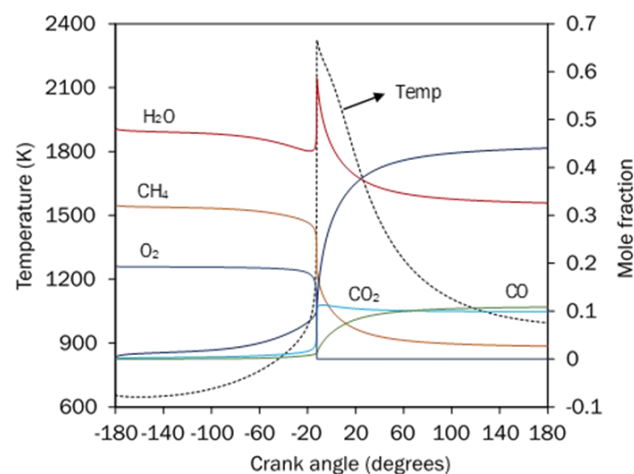


Figure 3: Evolution of species and in-cylinder temperature as a function of the crank angle at $N = 3000$ RPM, $T_{\text{intake}} = 660$ K, $P_{\text{intake}} = 1$ bar, $\text{H}_2\text{O}/\text{CH}_4 = 1.5$ and $\text{O}_2/\text{CH}_4 = 0.6$.

A parametric study was done to tune the performance of the piston reactor operating under ATR conditions including the rotational speed, intake temperature, and feed composition. Then a case study for ATR was selected and a process flowsheet was designed embedding the piston reactor for ATR to understand the economics and emissions associated with hydrogen production in a piston reactor as shown in Figure 3. The hydrogen plant, designed for a 25 TPD capacity, uses Aspen Plus software with HYSYS Peng-Robinson as the equation of state. It employs a piston reactor model, maximizing heat recovery and integrating excess heat for power generation. The process meets most power demands internally, with minimal external heating and cooling needs. A techno-economic study for 25 TPD production shows a CAPEX of \$80 million, resulting in an overall production cost of \$2/kg H₂. Scale analysis reveals a 70% cost reduction when scaling up to 300 TPD. Integration of excess heat reduces emissions and costs for low-CO₂ hydrogen. Comparisons with conventional methods indicate lower costs for the piston reactor ATR process, emphasizing the potential cost-effectiveness of reactor-based technology and the need for experimental validation.

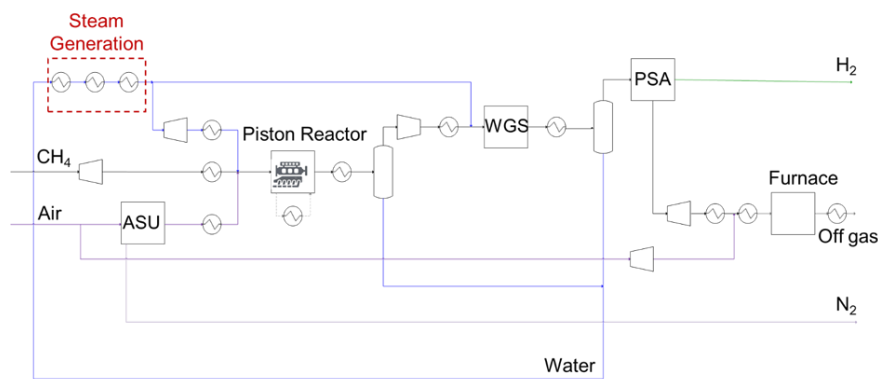


Figure 3: Process flow diagram of the ATR piston reactor process.

CONCLUSIONS

This study aimed to assess the feasibility of SMR and ATR for hydrogen production in piston reactors under typical ICE engine conditions. Key findings reveal:

- SMR proved unfeasible across wider conditions due to extreme temperature requirements (>1700 K) for reasonable conversion.
- ATR is an attractive route for hydrogen production in the piston reactor and is the choice to investigate in more detail in the future. Compared to industrial conventional ATR, the piston reactor reaches a similar methane conversion between 89% and 97% while operating at much lower pressures of 1 bar, and the intake feed temperature is lower by 283 K; it has much higher hydrogen production per catalyst at a 287-fold increase.
- Thermal coupling of endothermic and exothermic reactions in the piston reactor offers process intensification, enhancing catalyst efficiency and energy savings.
- The ATR piston reactor-based process has a lower blue hydrogen production cost compared to that of the conventional process while keeping comparable CO₂ emissions. This was enabled by the integration of power and heat generated from the piston reactor within an overall process and the integration of carbon capture and compression.

Overall, the piston reactor shows some promise as a compact reactor suitable for small-scale hydrogen production facilities. This conclusion was reached by following the modeling-based approach which incorporates the process level consideration right from the early stage of exploration. In the future, a detailed model accounting for catalysts and the experimental proof is the logical way forward to further evaluate and support the development end of the promising ATR route in the piston reactor for the production of blue hydrogen.

REFERENCES

1. Rudolph, C. and B. Atakan, *Investigation of natural gas/hydrogen mixtures for exergy storage in a piston engine*. Energy, 2021. **218**: p. 119375.
2. Ashok, A., et al., *Review of piston reactors for the production of chemicals*. Reviews in Chemical Engineering, 2021.
3. Gossler, H. and O. Deutschmann, *Numerical optimization and reaction flow analysis of syngas production via partial oxidation of natural gas in internal combustion engines*. International Journal of Hydrogen Energy, 2015. **40**(34): p. 11046-11058.
4. Karim, G.A. and I. Wierzba, *The production of hydrogen through the uncatalyzed partial oxidation of methane in an internal combustion engine*. International journal of hydrogen energy, 2008. **33**(8): p. 2105-2110.
5. Morsy, M.H., *Modeling study on the production of hydrogen/syngas via partial oxidation using a homogeneous charge compression ignition engine fueled with natural gas*. International journal of hydrogen energy, 2014. **39**(2): p. 1096-1104.
6. Oni, A., et al., *Comparative assessment of blue hydrogen from steam methane reforming, autothermal reforming, and natural gas decomposition technologies for natural gas-producing regions*. Energy Conversion and Management, 2022. **254**: p. 115245.
7. Yan, Y., et al., *Process simulations of blue hydrogen production by upgraded sorption enhanced steam methane reforming (SE-SMR) processes*. Energy Conversion and Management, 2020. **222**: p. 113144.
8. El-Emam, R.S. and H. Özcan, *Comprehensive review on the techno-economics of sustainable large-scale clean hydrogen production*. Journal of Cleaner Production, 2019. **220**: p. 593-609.
9. *H2A: Hydrogen Analysis Production Models*. Available from: <https://www.nrel.gov/hydrogen/h2a-production-models.html>.
10. Ferreira-Aparicio, P., M. Benito, and J. Sanz, *New trends in reforming technologies: from hydrogen industrial plants to multifuel microreformers*. Catalysis Reviews, 2005. **47**(4): p. 491-588.
11. Wismann, S.T., et al., *Electrified methane reforming: A compact approach to greener industrial hydrogen production*. Science, 2019. **364**(6442): p. 756-759.
12. Anderson, D.M., et al., *Sorption-Enhanced Variable-Volume Batch–Membrane Steam Methane Reforming at Low Temperature: Experimental Demonstration and Kinetic Modeling*. Industrial & Engineering Chemistry Research, 2015. **54**(34): p. 8422-8436.
13. Yelvington, P.E., et al., *On Piston Engines as Hydrocarbon Gas Reformers for Modular, Distributed Chemical Production*. Applications in Energy and Combustion Science, 2023: p. 100117.
14. Holladay, J.D., et al., *An overview of hydrogen production technologies*. Catalysis today, 2009. **139**(4): p. 244-260.
15. Lamb, J.J., et al., *Traditional routes for hydrogen production and carbon conversion, in Hydrogen, biomass and bioenergy*. 2020, Elsevier. p. 21-53.
16. Carapellucci, R. and L. Giordano, *Steam, dry and autothermal methane reforming for hydrogen production: A thermodynamic equilibrium analysis*. Journal of Power Sources, 2020. **469**: p. 228391.
17. Chaubey, R., et al., *A review on development of industrial processes and emerging techniques for production of hydrogen from renewable and sustainable sources*. Renewable and Sustainable Energy Reviews, 2013. **23**: p. 443-462.

ICH2P14-OP092

AN APPROACH IN TREATING BIOMASS AND PLASTIC WASTE FOR PRODUCTION OF HYDROGEN AND ETHANOL

**Muhammad Ishaq, Ibrahim Dincer*

Clean Energy Research Laboratory (CERL), Faculty of Engineering and Applied Science, Ontario Tech. University, 2000 Simcoe St, Oshawa, ON L1H 7K4, Canada

*Corresponding author e-mail: Muhammad.ishaq@ontariotechu.net

ABSTRACT

A novel configuration of using plastic waste and biomass-based energy to produce liquid fuel, hydrogen, thermal heat, and condensable gases is proposed in this study. The system aims to take advantage of key features of co-pyrolysis and gasification of plastic waste and biomass. The ASPEN plus V14.0 is employed to predict the efficiency of the process. The proposed waste processing energy system generates 658 kg/h of liquid fuel and 639 kg/h of hydrogen. The sensitivity analysis demonstrates that maximum hydrogen production mass flow rate is achieved at steam to carbon (S/C) ratio of 4.0 and gasification temperature of 700°C. A considerable trend in liquid fuel production rate is obtained at S/C of 0.4, 0.8, 1.2, and a temperature range of 200-800°C.

Keywords: Co-pyrolysis and gasification, Biomass and plastic waste, steam to carbon ratio.

INTRODUCTION

In the era of a circular economy, liquid fuels, for example, ethanol, and energy carriers, for example, hydrogen are the main priorities of researchers. Therefore, a new integrated approach for plastic waste and biomass-based energy systems is proposed and analyzed in this work. The objectives and scope of the present work are to develop a novel biomass-plastic waste-based energy system for the synthesis of hydrogen, biofuel, thermal heat, and non-condensable gases and hence to evaluate it thermodynamically by employing energy and exergy analysis. To conduct various sensitivity analyses so that potential operating variables can be identified.

STUDY AND ANALYSIS

Ontario contains 122 million tons of landfilling volume. In 2021, 240,945 tonnes of total municipal solid waste were generated in Oshawa. Among these, the share of leaf and yard waste is around 28,892 tonnes and the share of household plastic waste is around 41,886 tonnes which is 12% and 17.3% of the total MSW respectively. According to the report published by the Ministry of Government Conversation and Park, Oshawa is going to face waste problems. It stated that Ontario will utilize all its waste landfilling capacity by 2032 and dangerous pollutants (CO₂, CH₄) will be reverting to further landfilling [1]. Therefore, it is a high need to utilize this waste in an efficient way.

In the proposed configuration, biomass and plastic wastes from Oshawa city are considered major feedstock that undergoes drying, co-pyrolysis, and gasification to produce useful commodities of hydrogen and biofuel obtained in stream SP26 and SP31. The simulation of co-pyrolysis and gasification of both feedstocks is conducted in the ASPEN plus software V14.0 and its schematic is presented in Fig. 1. Redlich-Kwong-Soave cubic equation of state with Boston-Mathias alpha function (RKS-BM) was employed as base property method for all the thermodynamic properties [2]. The model has been developed by considering the following assumptions. (1). Steady-state operational conditions are respected in simulation. (2). Heat losses within the plant are ignored.

RESULTS AND DISCUSSION

Fig. 2 presents the influence of pyrolysis operating parameters such as temperature and steam-to-carbon ratio on the final flow rate of liquid fuel at output in stream SP31. The variation in pyrolysis temperature (T_{pyro}) is drawn on the x-axis while the variation in steam to carbon ratio (S/C) is shown in legends with different colored lines and the resulting production of liquid fuel (\dot{m}_{LF}) is plotted on the y-axis. The range of T_{pyro} is taken from 200 to 1200°C and steam to carbon molar flow ratio is considered from 0.4 to 4. The calculated sensitivity analysis depicts that pyrolysis temperature and steam-to-carbon ratios support the final liquid fuel production. It can be seen that the liquid fuel mass flow rate increases by around 52.8% and 43.6% as the temperature of the pyrolysis reactor is increased from 200 to 1200°C

at S/C molar flow ratio of 0.4 and 0.6 respectively. However, high values of S/C molar flow ratio ($S/C = 3.2$ and 3.6) result a lower production of liquid fuel by around 7.51 and 3.57% over the same variation of pyrolysis temperature. Even at ($S/C = 4.0$), the outlet fuel production increases by only 0.01% that demonstrates that higher values of steam to carbon ratio are not favorable for the fuel synthesis therefore, higher temperature from 1000-1200°C does not support the fuel synthesis at higher steam to carbon ratio. Hence, a gradual increase in the liquid fuel production mass flow rate is evident at lower values of T_{pyro} and S/C .

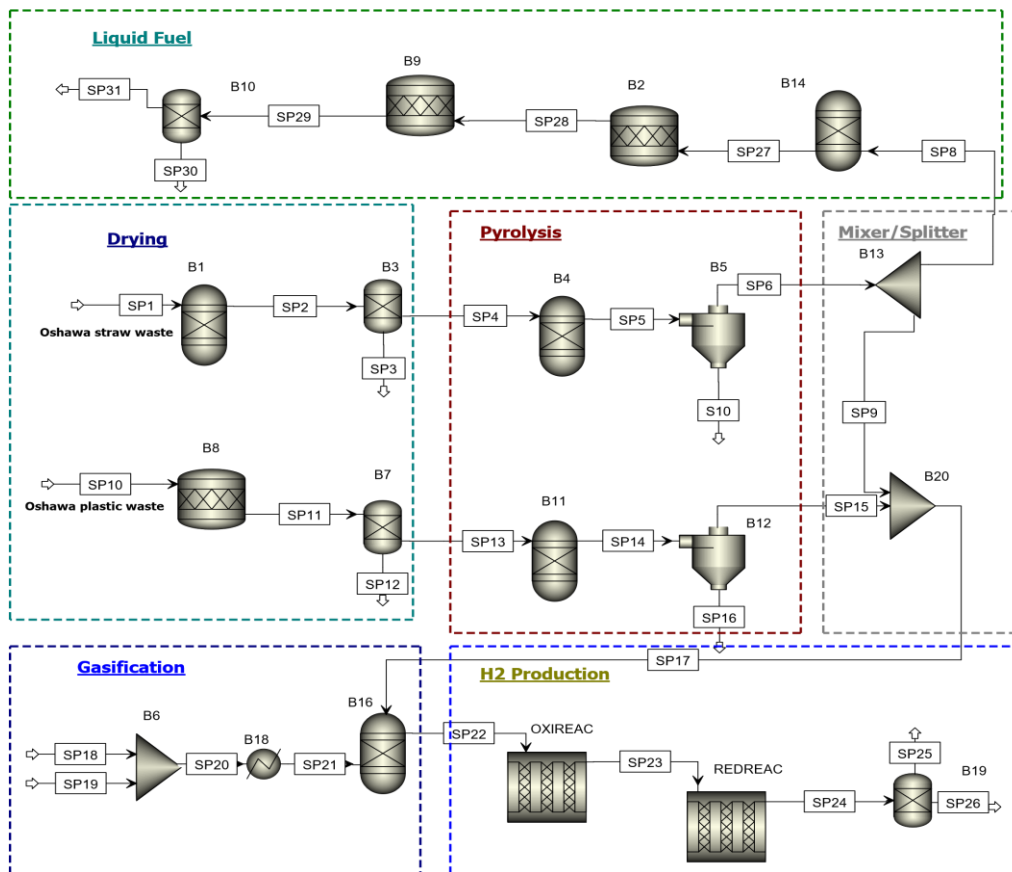


Fig. 1. The ASPEN plus schematic of the proposed conceptual design for the processing of biomass and plastic waste

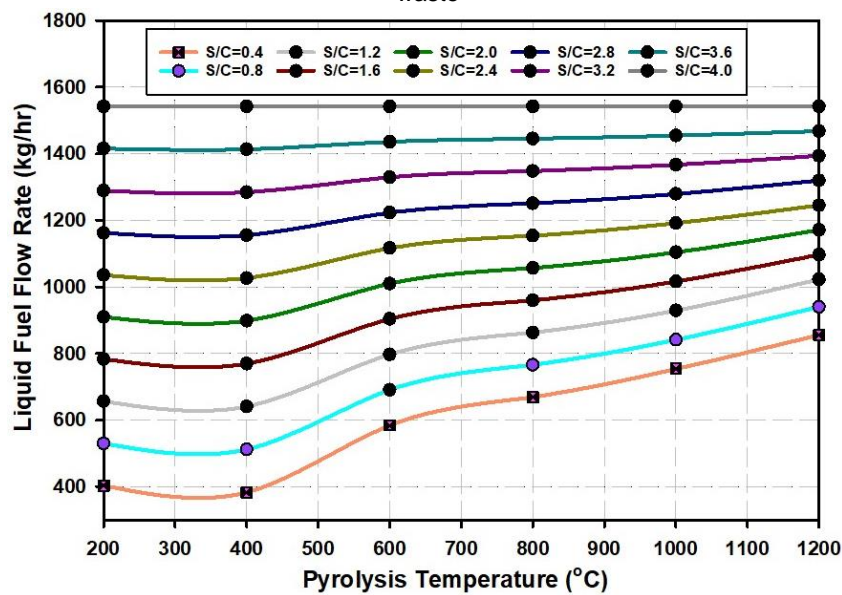


Fig. 2. The calculated sensitivity to variations in the pyrolysis T_{pyro} and S/C input to the PYRO REAC of the final liquid fuel mass flow rate produced at the output.

Fig. 3 represents the influence of gasification temperature and steam-to-carbon ratio on the hydrogen production at the output of the gasification reactor in stream SP22 while keeping the air mass flow rate constant. The range of T_{gasif} is considered from 200 to 1200°C and steam to carbon molar ratio is taken from 0.4 to 4.0 and the trend of hydrogen production is monitored. The calculated sensitivity analysis demonstrates that gasification temperature and steam-to-carbon ratio motivate the hydrogen production rate.

Overall, as the steam-to-carbon ratio improves, the hydrogen production flow rate peaks between 600 to 700°C temperature. At lower values of steam to carbon ratio ($\frac{S}{C} = 0.4$ and 0.8), the hydrogen synthesis rate grows by around 99.1% and 99.6% as the gasification reactor temperature range is varied from 200-700°C. One of the possible reasons is the activation of steam methane reforming and water gas shift reactions within the gasification reactor. At higher values of steam to carbon ratio ($\frac{S}{C} = 1.6$ and 2.0), the hydrogen production flow rate is maximum at around 700°C and after that, it decreases by around 14.7 and 16.5% respectively. It represents that high temperature does not drive the hydrogen synthesis flow rate. Furthermore, it can also be depicted those lower values of S/C and lower operating T_{gasif} suppress the H_2 production rate.

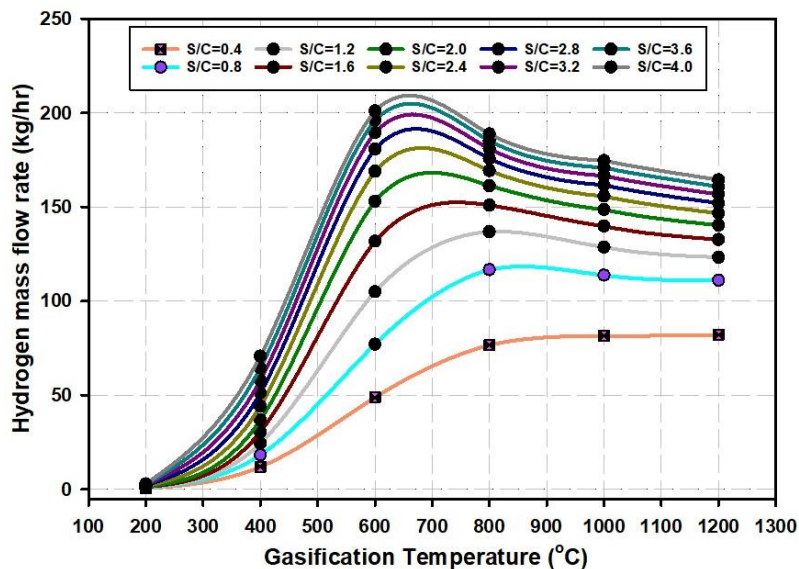


Fig. 3. The calculated sensitivity to variations in the gasification temperature and steam-to-carbon ratio input to the GASIF REAC of the hydrogen production mass flow rate produced at the output in stream SP22.

CONCLUSIONS

The present work has developed the ASPEN design of co-pyrolysis and gasification of biomass and plastic waste for liquid fuel and H_2 production. The influence of steam to carbon ratio and operating temperature on the final output commodities. The liquid fuel mass flow rate increases by 52.8% at S/C ratio of 0.4, while the hydrogen mass flow rate increases by 99.1% at the same value of the steam-to-carbon ratio.

Subscripts

pyro Pyrolysis
gasif Gasification

REFERENCES

- [1] Owma, "State of Waste in Ontario: Landfill Report, January 2021," 2021.
- [2] Y. Zhao *et al.*, "Energy, efficiency, and environmental analysis of hydrogen generation via plasma co-gasification of biomass and plastics based on parameter simulation using Aspen plus," *Energy Convers Manag*, vol. 295, p. 117623, Nov. 2023, doi: 10.1016/j.enconman.2023.117623.

ICH2P14-OP093

A UNIQUE SYSTEM FOR HYDROGEN, METHANOL, FRESH WATER AND ELECTRICITY PRODUCTION WITH CARBON CAPTURING AND STORAGE

**Mitra Ghannadi, Ibrahim Dincer*

Clean Energy Research Laboratory (CERL), Faculty of Engineering and Applied Science, Ontario Tech. University, Oshawa, Ontario, Canada

*Corresponding author e-mail: mitra.ghannadi@ontariotechu.net

Abstract

This study aims to investigate an innovative, multifunctional system designed to achieve dual hydrogen generation via Fe-based chemical looping and electrolysis. This system also encompasses capturing carbon dioxide emissions from a steel production facility and subsequent methanol production through the reaction of hydrogen and carbon dioxide. The system integrates three interconnected cycles, Brayton, Rankine, and Organic Rankine, to meet the electrical demands. Furthermore, the system features the production of an auxiliary resource in freshwater, obtained through seawater desalination and subsequently stored for future utilization. The findings reveal that when utilizing 1.5 kg/s of flue gas at a temperature of 1400°C, the system achieves a carbon dioxide capture efficiency of 92.5% using an amine-based solution, yielding a total of 0.0027 kg/s of hydrogen and 0.0042 kg/s of methanol with the overall energy and exergy efficiencies of 48.6% and 42.5%, respectively.

Keywords: Hydrogen, Methanol, Carbon Capturing.

1. Introduction

Using renewable energy sources is an attractive strategy for mitigating greenhouse gas emissions to avoid climate change. Consequently, a coordinated worldwide effort and investigation is underway to accelerate the adoption and integration of renewable energy technology. Two significant technologies that have been proven to cut GHG emissions significantly are carbon capture and storage (CCS) and hydrogen generation [1]. There is a recent trend to highlight the increasing viability of hydrogen generation as an environmentally friendly and adaptable energy source for addressing the decarbonization of energy systems and sustainability concerns. It has a variety of uses, including fuelling hydrogen fuel cell vehicles and functioning as an energy storage in many integrated renewable energy sectors. Hydrogen is now recognized as a key player as we have gone into hydrogen economy era. Hydrogen production is vital in moving toward a more sustainable and carbon-neutral energy environment due to its clean combustion and versatility as an industrial feedstock [2]. The prevalence of methanol production is increasing owing to its versatile nature and significance in the pursuit of sustainability objectives. The attractiveness of methanol stems from its potential as an environmentally friendly energy carrier, enabling the achievement of environmental objectives while using readily available resources since it uses the captured carbon dioxide and the produced hydrogen. Another sustainable mature technology involves desalinating sea and brackish water, which provides a substantial and reliable source of freshwater to address global water scarcity, enhances water supply resilience in arid regions and lowers the freshwater price in various regions.

A unique integrated system capable of producing and storing various energy sources, including hydrogen and methanol, is presented in this research. This system includes an amine-based carbon capturing subsystem, which is used for both storing and using carbon dioxide and heating other sectors. Moreover, the system has two different hydrogen production subsystems working separately to store and use hydrogen. The third subsystem is generating methanol from hydrogen and CO₂ and storing it. The electricity of this system is produced by coupling 3 different cycles, including Brayton, Rankine and Organic Rankine cycles. Furthermore, fresh water is also produced and stored in another subsystem from seawater by using multiple desalination processes. The system's uniqueness is derived from its singular design, notable results, and ability to effectively tackle the persistent issue of escalating global greenhouse gas emissions. Compared to other renewable energy systems, this paper generates a diverse array of useful products such as fresh water, electricity, and hydrogen, while mitigating carbon emissions and converting it into methanol to utilize it as a sustainable energy source.

2. System Description and Analysis

Figure 1 is an illustration of the desired multigenerational system. In this system, first, carbon dioxide is captured from a steel production facility by using monoethanolamine solution in a subsystem including absorber, stripper, heat exchanger₁, boiler and condenser. After capturing CO₂, it is cooled by passing through the condenser and then compressed and stored in a CO₂ storage tank for further use. In the

meantime, carbon monoxide is extracted from the treated gases after the absorber by using a membrane separator in order to be used for chemical looping hydrogen production.

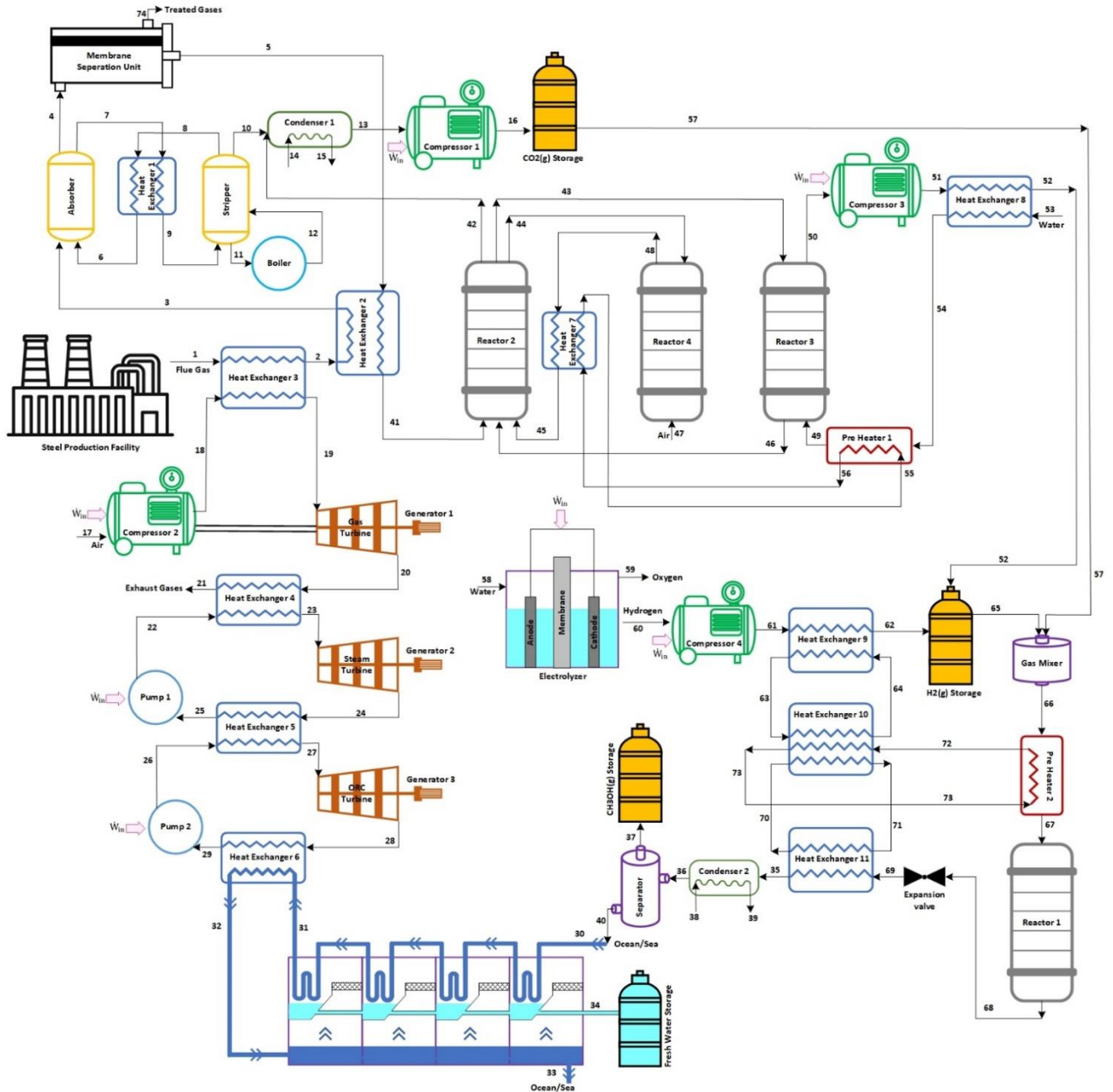
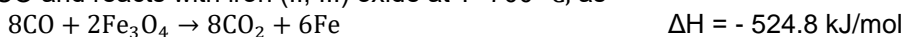


Fig. 1: Layout of the Proposed Multigeneration System

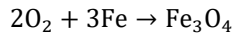
Before the carbon capturing process, the heat from the flue gas of the steel manufacturing processes is received by heat exchangers 2 and 3 and then heated the air for the combustion process in the Brayton cycle and carbon monoxide before going to reactor 2.

Hydrogen is the primary production of this system, which is generated using two different techniques: Fe-based chemical looping and electrolysis. In the first technique, reactor 2 uses the separated heated CO and reacts with iron (II, III) oxide at $T=700\text{ }^{\circ}\text{C}$, as



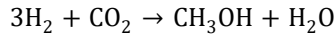
Then, as shown in reactions (2) and (3), in a cyclic manner, half of the iron produced in reactor 3 reacts with water vapor at a temperature of $700\text{ }^{\circ}\text{C}$ and produces hydrogen gas and iron (II, III) oxide. This produced hydrogen gas is then compressed and stored in the hydrogen tank. Also, the other half of the iron produced from reactor 2 goes to reactor 4, reacts with air oxygen at a temperature of $750\text{ }^{\circ}\text{C}$, and produces iron (II, III) oxide. Then iron (II, III) oxide from both reactors 3 and 4 return to reactor 2 and this cycle of hydrogen production is repeated in the same way.





$$\Delta H = - 1117.6 \text{ kJ/mol}$$

Hydrogen is also manufactured using a polymer electrolyte membrane (PEM) electrolyzer by consuming electricity. A compressor is used to compress the hydrogen that has been created, and it is then stored for later use. Afterwards, a specific amount of produced hydrogen and captured carbon dioxide, which have been stored in storage tanks, mixed, preheated, and then taken into reactor 1 at $T = 260 \text{ }^\circ\text{C}$ to produce methanol, as



$$\Delta H = - 49.3 \text{ kJ/mol}$$

The required electricity of this system is provided by combining 3 different cycles, which are the Brayton, Rankine and Organic Rankine cycles. The heat exchanger 6, used in the organic Rankine cycle, gives its heat to the seawater for desalination. Furthermore, fresh water will be produced by a multiple-stage thermal desalination process using ocean or sea water as an input.

3. Results and Discussion

As illustrated in Figure 2, elevating the flue gas mass flow rate within a steel production facility leads to a proportional increase in the generation of H_2 and CH_3OH . For instance, when a mere 0.1 kg/s of flue gas is introduced into the carbon capturing subsystem, it yields 0.0013 kg/s of hydrogen and 0.0015 kg/s of methanol. The comprehensive system has 48.6% and 42.5% of energy and exergy efficiencies, respectively.

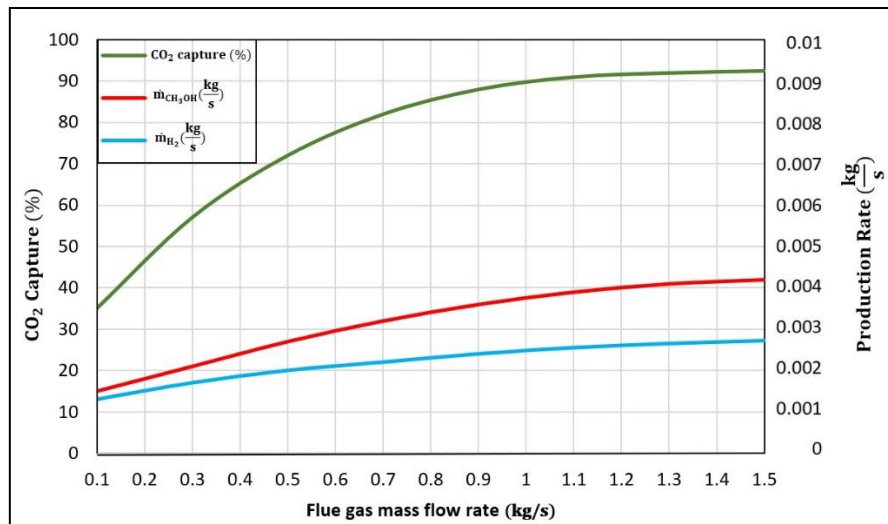


Fig. 2. Effect of flue gas mass flow rate on carbon capture percent and hydrogen and methanol production rate

4. Conclusions

The results show that by using 1.5 kg/s of flue gas at the temperature of $1400 \text{ }^\circ\text{C}$, it will capture 92.5% carbon dioxide by using an amine-based solution and will generate 0.0027 kg/s of H_2 in total and 0.0042 kg/s of CH_3OH . Moreover, it can be shown that the exergy destruction of all subsystems has a positive correlation with the ambient temperature, indicating that a rise in the ambient temperature leads to a corresponding increase in exergy destruction. The use of higher temperatures in the Organic Rankine heat exchanger will result in an increase in the rate of freshwater generation. The complete system exhibits total energy and exergy efficiencies of 48.6% and 42.5%, respectively.

References

1. Z. F. Toprak, N. Hamidi, Ş. Toprak, and Z. Şen, "Climatic identity assessment of the climate change," International Journal of Global Warming, vol. 5, no. 1, p. 30, 2013, doi: 10.1504/IJGW.2013.051480.
2. C. Acar and I. Dincer, "The potential role of hydrogen as a sustainable transportation fuel to combat global warming," Int J Hydrogen Energy, vol. 45, no. 5, pp. 3396–3406, Jan. 2020, doi: 10.1016/j.ijhydene.2018.10.149.

ICH2P14-OP094

INNOVATIVE INTEGRATED MULTIGENERATION SYSTEM FOR SUSTAINABLE POWER, HYDROGEN, AND AMMONIA PRODUCTION

¹Ahmad K. Sleiti, ¹Wahib A. Al-Ammari, ²Mohammad Azizur Rahman

¹Department of Mechanical & Industrial Engineering, College of Engineering, Qatar University, Doha, Qatar

²Petroleum Engineering Department, Texas A&M University at Qatar, Doha, Qatar

*Corresponding author e-mail: asleiti@qu.edu.qa

ABSTRACT

This study proposes an advanced sustainable multigeneration system for power, hydrogen (H₂), and ammonia (NH₃) production with a breakthrough liquid hydrogen (LH₂) production process using a dual mixed refrigerant (DMR) cryogenic technology. The proposed system integrates a direct oxy-combustion supercritical carbon dioxide (DOC-sCO₂) power plant with water electrolysis (WE) and the Haber-Bosch process for power, H₂, and NH₃ co-generation. To optimize the efficiency, the oxygen produced by the WE system is strategically used to significantly reduce the power consumption of the air separation unit (ASU), while the ASU's nitrogen gas is used for ammonia production, which results in minimizing the costs. Moreover, the WE system's feedwater is internally sourced from the DOC-sCO₂ power block, and the CO₂ is effectively captured, achieving near-zero emissions. In the liquefaction process, our proposed DMR-LH₂ process exhibits superior energy efficiency and flexibility compared to existing methods with energy consumption of 3.74 kWh/kg_{LH₂}. Thermo-economic analyses are performed for the integrated system. These analyses demonstrate impressive results: a levelized cost of electricity of 3.01¢/kWh, a levelized cost of LH₂ of 1.59 \$/kg_{LH₂}, and NH₃ levelized production cost of 0.24\$/kg_{NH₃}, all with energy efficiencies of 47.08% (DOC-sCO₂), 70.21% (WE), and 62.32% (NH₃), respectively. Moreover, the production costs of both H₂ and NH₃ are reduced by an average of 55% (compared to renewable-based systems).

Keywords: Hydrogen and ammonia production, Water electrolyzer, Liquid hydrogen, Dual mixed refrigerants, near-zero CO₂ emissions.

INTRODUCTION

The direct oxy-combustion (DOC) technology associated with the supercritical carbon dioxide (sCO₂) power cycle has gained much attention as one of the future power conversion breakthroughs [1]. This is due to that the DOC-based sCO₂ power system has several advantages over other conventional gas/steam power plants including (1) high energy efficiency (reaches 58% [2]) due to the burning of the fuel in the presence of pure oxygen (direct oxy-combustion), (2) compactness of the components due to the dense behavior of the CO₂ at supercritical conditions[3], and (3) the ability of DOC-sCO₂ cycle to automatically capture the produced CO₂ [4]. However, the requirement for pure oxygen for the combustion process increases the capital and operational costs of the plant as an energy-intensive air separation unit (ASU) is needed (20% of the net output power of the cycle [5]). On the other hand, hydrogen (H₂) and ammonia (NH₃) are considered promising free-carbon energy carriers[6] and are expected to play a crucial role in the global energy mix by 2050[7]. They can be produced from renewable[8], non-renewable (based on oxide fuel cell [9], and gas turbine [10] systems), or hybrid solar-based [11], [12] or biomass-based [13] low-carbon sources and transported for commercial applications in the energy import countries such as Japan, China, and Europe[14]. However, their relatively high production costs are one of the major barriers to their commercial applications. To minimize their costs, several multigeneration system for power, H₂, and NH₃ are proposed as discussed in the comparison section of this study.

Most of the available multigeneration systems use a renewable energy source to power the system, which introduces the challenge of intermittency. Other systems that use natural gas to drive the system utilize the steam-methane reformer to generate H₂ which yields the highest CO₂ emissions among the other H₂ production technologies. In addition, all of these systems have no internal use for the produced oxygen and required an external source of water for the H₂ production process, which minimizes the benefits of the system and increases its operating expenditures. Furthermore, most of these systems utilize Rankine or organic Rankine cycles to generate electricity. These Rankine cycles have much lower energy efficiencies (20-42%) than the DOC-sCO₂ power cycle (45-58%). Thus, this study

presents an innovative solution for the main issues of these systems by combining the DOC-sCO₂, WE, HBP, and H₂ liquefaction systems in an interactive structure as shown in Fig. 1. In this way, (i) the power consumption of the ASU is reduced by the partial O₂ production from the WE system, (ii) the feedwater of the WE is internally supplied from the DOC-sCO₂ system, (iii) the N₂ used for NH₃ production is provided by the same ASU of the DOC-sCO₂ system, which eliminates the need for extra ASU, (iv) part of the produced H₂ can be liquefied in the H₂ liquefaction system to transport LH₂ without suitable recovery for the flared H₂ gas, and (iv) the H₂ and NH₃ production is flexible to meet the technical requirements for both local and global energy markets.

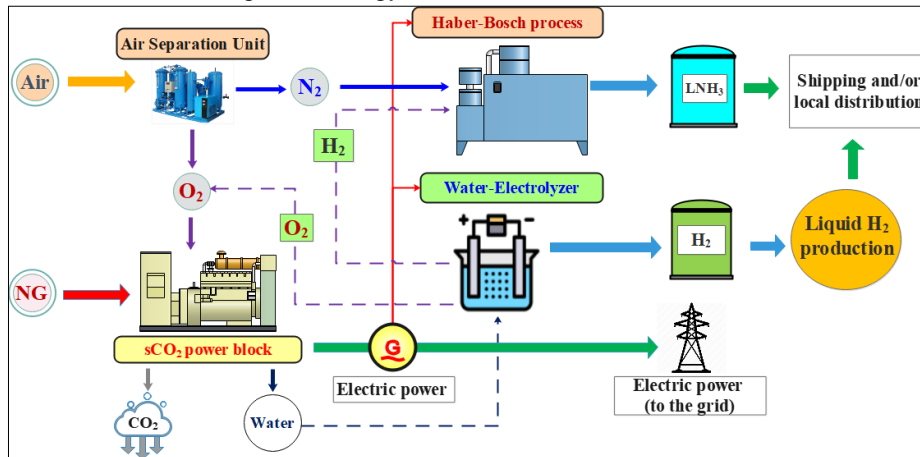


Fig. 1. Novelty aspects of the proposed system for hydrogen, ammonia, and power generation.

SYSTEM DESCRIPTION

The layout of the proposed system is presented in Fig. 2.

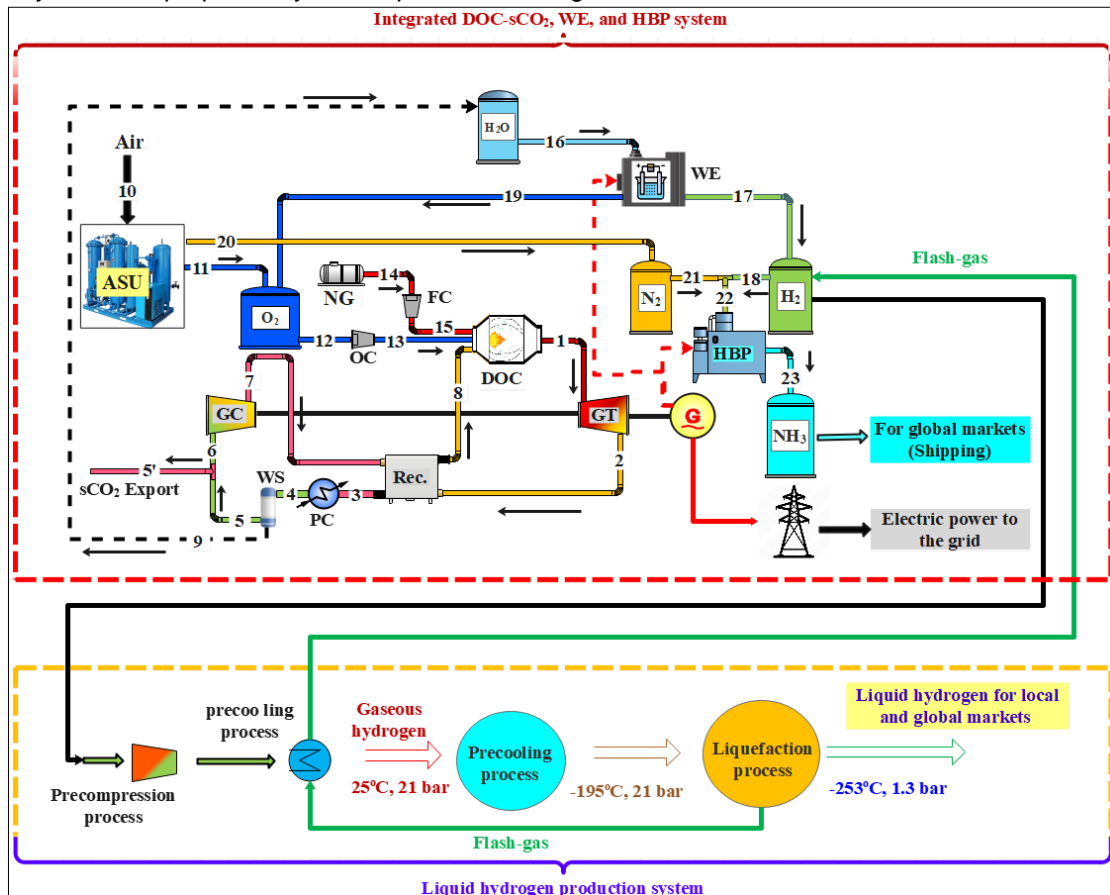


Fig. 2. The layout of the novel integration between the DOC-sCO₂ power cycle, water electrolyzer, and Haber-Bosch process systems.

On the high-pressure side, the combustion products (CO₂ and water vapor) enter the gas turbine (GT) at a maximum temperature (state 1) and expand to the low-pressure side to generate power. The outlet flow from the GT is passed through the recuperator (2-3) to preheat the recycled sCO₂ flow (7-8) and cooled in the precooler (PC,3-4). Then, the water vapor in the flow is separated in the water separator (WS, 4-5) and the produced water is stored in a storage tank to be used in H₂ generation. After that, the excess CO₂ produced through the combustion process is captured and transported for sequestration or commercial applications (5'). The other part is compressed to the maximum cycle pressure (state 7) and recycled to the DOC (8) after being preheated in the recuperator (7-8). The natural gas and O₂ are compressed to the operating pressure of the DOC using a fuel compressor (FC, 15) and O₂ compressor (OC, 13), respectively. The required O₂ is mainly provided by the ASU which draws ambient air (10) and splits it into N₂ (20) and O₂ (11). For H₂ production, the feedwater is fed to the WE system (state 16) that splits water into H₂(17) and O₂ (19). Part of the N₂ produced by the ASU is fed to the HBP to generate NH₃. The other is stored and distributed for commercial applications. The HBP is used to produce NH₃ from N₂ (21) and H₂ (18) gases following the explained mechanism in [15]. The produced NH₃ is liquefied by compressing it to high pressure (18 bar) and stored as a liquid at ambient temperature (25°C) with a purity of 99.95%[16]. Part of the produced H₂ will be liquefied in an efficient dual-mixed refrigerant (DMR) liquefaction process (shown in Fig. 3) to distribute H₂ in compact size with high energy density for local and/or global market. The flash H₂ gas produced at the final stage of the liquefaction process or storage system has a cryogenic temperature of -253°C, thus it is used to precool the H₂ gas that is fed to the liquefaction system and then directed to the H₂ storage tank of the integrated system. This will allow higher generation rate of ammonia.

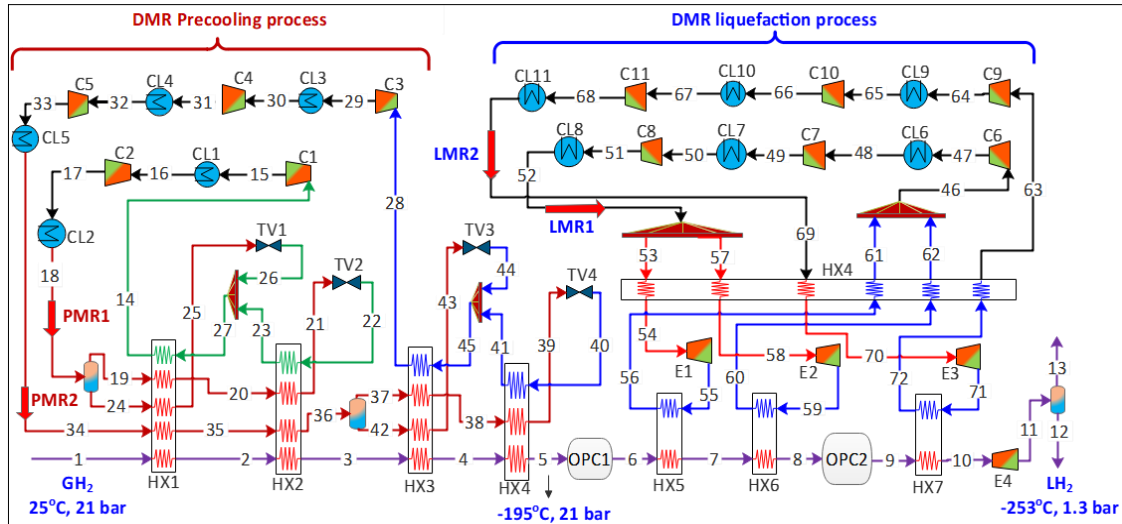


Fig. 3. Flowsheet of the new dual mixed refrigerant-based liquid hydrogen production system.

THERMO-ECONOMIC MODEL

The energy analysis of the proposed system is performed using Aspen HYSYS and Aspen Plus simulation platforms at steady-state conditions. The energy analysis in these platforms are established by implementing the mass, and energy balance principles on each component [17]:

$$\sum \dot{m}_i = \sum \dot{m}_o \quad (1)$$

$$\sum Q + \sum \dot{m}_i h_i = \sum \dot{W} + \sum \dot{m}_o h_o \quad (2)$$

Details models of the sCO₂-DOC components are available in [18]. For the sCO₂ power and HBP systems, Peng-Robinson equation of state is used to get the thermodynamic properties of the flow stream. For the WE system, it is simulated and validated in Aspen Plus according to the study provided by Sanchez et al. [19]. The specific energy consumption of the ASU, WE, HBP, and DMR H₂ liquefaction subsystems are determined by validated simulations and used as inputs in the simulation of the sCO₂-DOC system as presented in Table 1. Also, this table presents the main input parameters and assumptions that are made in the simulation process.

Table 1. Design values and ranges of the input parameters for the proposed system.

Parameter	Design value (Range)
Generation rate of NH ₃ , [TPD]	50
Generation rate of H ₂ , [TPD]	5
Power to the grid (P_{Grid}), [MW]	5
Percent of pressure drop, [%]	3% for DOC [20], 1% for Rec. (high pressure side) [20], 3% for Rec. (low pressure side) [20], 2% for PC [20].
Isentropic efficiency of gas turbine, [%]	93 [18]
Isentropic efficiency of compressors, [%]	90 [18]
Lifetime of the plant, [years]	20 [18]
Interest rate, [%]	10 [18]
Power utilization factor, [%]	85 [18]
Fuel cost, [\$/kWh _e]	0.07 [20]
Operating and maintenance cost, [\$/kWh _e]	0.008 [20]

To evaluate the energy performance indicators, the net output power of the sCO₂ power is defined as:

$$P_{net} = \eta_g (\dot{W}_{GT} - \dot{W}_{GC} - \dot{W}_{OC} - \dot{W}_{FC} - \dot{W}_{ASU}) \quad (3)$$

Where η_g , \dot{W}_{GT} , \dot{W}_{GC} , and \dot{W}_{ASU} are the generator efficiency, work rate of the gas turbine, gas compressor, and ASU, respectively. As part of the net output power of the sCO₂ power block is directed to the grid (P_{Grid}) and the other parts are consumed by the WE (\dot{W}_{WE}) and HBP (\dot{W}_{HBP}) process, then the net output power can also be expressed as $P_{net} = P_{Grid} + \dot{W}_{WE} + \dot{W}_{HBP} + \dot{W}_{DMR-LH2}$. The energy efficiency of the sCO₂ power cycle is defined as[20]:

$$\eta_{sCO_2} = P_{net} / Q_{DOC} \quad (4)$$

The energy efficiency of the WE system and the HBP system are defined in Eqs. 5, and 6, [21]:

$$\eta_{WE} = (\dot{m}_{17}h_{17} + \dot{m}_{19}h_{19}) / (\dot{W}_{WE} + \dot{m}_{16}h_{16}) \quad (5)$$

$$\eta_{HBP} = (\dot{m}_{23}h_{23}) / (\dot{W}_{HBP} + \dot{m}_{18}h_{18} + \dot{m}_{21}h_{21}) \quad (6)$$

where Q_{DOC} , \dot{W}_{WE} , and \dot{W}_{HBP} are the heat rate provided by the DOC, the work rate of the WE, and the work rate of the HBP, respectively. h_{17} , h_{16} , h_{23} , h_{18} , and h_{21} are specific enthalpies of the fluid at the state points shown in Fig. 2 and calculated at typical conditions of (1 bar, 35oC). The overall energy efficiency of the proposed integrated system is defined similarly to the integrated system in[21]:

$$\eta_{overall} = (P_{Grid} + (\dot{m}_{17} - \dot{m}_{18})LHV_{H_2} + \dot{m}_{23}LHV_{NH_3}) / Q_{DOC} \quad (7)$$

where P_{Grid} is the electric power supplied to the electric grid, LHV_{H_2} is the lower heating value of hydrogen (120MJ/kg) and LHV_{NH_3} is the lower heating value of ammonia (18.8MJ/kg).

The economic evaluation of the proposed system is carried out in terms of the levelized cost of electricity (LCOE) of the sCO₂ cycle, levelized cost of hydrogen (LCOH), and levelized cost of ammonia (LCOA). The LCOE is accounting for the subsystems that generate the electric power of the overall system which are: the sCO₂ power block, ASU, FC, and OC. The costs of the WE and HBP systems are not included in the LCOE but are accounted for in the LCOH and LCOA, respectively. The LCOE is defined as[22]:

$$LCOE = (CRF \times Z_{tot,sCO_2} + Z_{om,sCO_2}) / (P_{net} \times N) \quad (8)$$

where Z_{tot} is the total capital cost of the sCO₂ components, which were calculated based on the correlations given in [20], [22], [23]. Indirect costs for the equipment installation, labor, and other expenses are added as a percentage of the direct cost of each component as 2% of the total capital cost. Z_{om} is the annual operating and maintenance cost was set as 0.008\$/kWh_e and a fuel cost of 0.07\$/kWh_e [20]. N is the annual number of operation hours of the plant (7446 hrs. with a power utilization factor of 85%) [20]. CRF is the capital recovery factor, which is defined to annualize the capital cost and depends on the interest rate (i , 10%), and the plant lifetime (20 years), and given as[22]:

$$CRF = i \times (1 + i)^n / ((1 + i)^n - 1) \quad (9)$$

The equipment cost is updated from the reference year to the target year (2023) using the chemical engineering plant cost index (CEPCI) as [24]:

$$Z_{k,2023} = Z_{ref} \times \frac{CEPCI_{2023}}{CEPCI_{ref}} \quad (10)$$

The LCOH (including liquefaction cost) is defined as [25]:

$$LCOH = (CRF \times (Z_{tot,WE} + Z_{tot,DMR}) + Z_{om,WE} + Z_{om,DMR}) / (\dot{m}_{H_2} \times N) \quad (11)$$

where $Z_{tot,WE}$ is the capital cost of the electrolyzer system including the water and hydrogen storage tanks (see Table 2). $Z_{om,WE}$ is the operating and maintenance cost of the WE system, and \dot{m}_{H_2} is the hourly production rate of H₂ (kg/h). Similarly, the LCOA is defined as:

$$LCOA = (CRF \times Z_{tot,HBP} + Z_{om,HBP}) / (\dot{m}_{NH_3} \times N) \quad (12)$$

where $Z_{tot,HBP}$ is the capital cost of the HBP system including N₂ and NH₃ storage tanks (see [20], [22], [23]). $Z_{om,HBP}$ is the operating and maintenance cost of the HBP system, and \dot{m}_{NH_3} is the hourly production rate of NH₃ (kg/h).

RESULTS AND DISCUSSION

In this section, the performance of the proposed system is analyzed in terms of the overall energy efficiency, LCOE, LCOH, and LCOA.

Energy performance results

Table 2 shows the characteristics of the proposed system at the design conditions presented in Table 1. It is found that the total generated power by the GT must be 68.43 MW, where 3% is consumed for fuel compression, 5.2% for O₂ compression, 15% for sCO₂ recycled flow compression, and 5.1% for the ASU. The remaining part of the GT power is used to drive the WE and HBP subsystems with 5 MW is directed to the electricity grid. To generate 5 TPD as pure H₂ and 50 TPD as NH₃. Then the WE must produce H₂ at rate of 0.142 kg/s (12.27 TPD) and water supply of 1.03 kg/s must be secured. This amount of water is easily provided by the sCO₂ power block as it produces water at flow rate higher than needed by the WE (2.61 kg/s). In addition, the generated O₂ by the WE (0.888 kg/s) forms about 16% of the total O₂ that is needed by the sCO₂ power block. Furthermore, the amount of the produced N₂ from the ASU (13.95 kg/s) is much higher than needed by the HBP (0.40 kg/s). This implies that excess N₂ and water can be stored and exported for local market or local consumption. Economically, the integration of the DOC-sCO₂ power cycle with the WE and HBP subsystems reduces the levelized cost of the system outputs (electricity, H₂, and NH₃). In particular, the LCOE is 3.1 ¢/kWh, which is 50% lower than in conventional standalone DOC-sCO₂ power systems (6.35 ¢/kWh) [17]. Furthermore, the use of single ASU for both DOC and HBP reduces the cost of NH₃ synthesis to 0.24 \$/kg_{NH3} (without H₂ cost) or (1.34 with H₂ cost). As the H₂ cost is accounted within the levelized cost of H₂ production, it can be stated that the ammonia synthesis cost is reduced by 70% compared to typical NH₃ production systems [26]. Finally, with the use of DMR hydrogen liquefaction system, the proposed system produce liquid hydrogen at levelized cost of 1.59 \$/kg_{LH2}, which is 33% [27] lower than in single mixed refrigerant processes and 74% [28] lower than H₂ cost in standalone WE small-scale systems .

Table 2. Output of the proposed system at the design point conditions [17].

Characteristics of sCO ₂ power cycle	
Net output power, [MW]	26.89
Turbine inlet temperature, [°C]	764.3
Minimum cooling temperature, [°C]	34.0
Maximum cycle pressure, [bar]	245.0
Minimum cycle pressure, [bar]	74.0
Fuel flow rate, [kg/s]	1.36
O ₂ flow rate, [kg/s]	5.44
Recycled sCO ₂ flow rate, [kg/s]	234.0
Exported sCO ₂ flow rate, [kg/s]	5.24
Produced water flow rate, [kg/s]	2.61
Total cycle flow rate, [kg/s]	240.80
Fuel compression power, [MW]	2.08
O ₂ compression power, [MW]	3.59
sCO ₂ compression power, [MW]	10.35
sCO ₂ cycle efficiency, [%]	47.08
LCOE, [¢/kWh]	3.09

Characteristics of air separation unit	
Mass flow of air, [kg/s]	18.32
Mass flow of N ₂ , [kg/s]	13.95
Mass flow of O ₂ , [kg/s]	4.21
Consumed power, [MW]	3.47
Characteristics of Water electrolyzer system	
Mass flow of water, [kg/s]	1.028
Mass flow of H ₂ , [kg/s]	0.142
Mass flow of O ₂ , [kg/s]	0.888
Consumed power (including pumping and fan power), [MW]	20.52
WE energy efficiency, [%]	70.21
LCOH (without liquefaction cost), [\$/kg _{LH2}]	1.13
Characteristics of ammonia production system	
Mass flow of N ₂ , [kg/s]	0.400
Mass flow of H ₂ , [kg/s]	0.084
Mass flow of NH ₃ , [kg/s]	0.580
Consumed power	1.53
LCOA (liquid, without including H ₂ cost), [\$/kg _{NH3}]	0.24
LCOA (including H ₂ production cost), [\$/kg _{NH3}]	1.34
NH ₃ energy efficiency, [%]	66.58
Characteristics of DMR H2 liquefaction process	
H ₂ feed flow, [kg/s]	0.058
Total liquefaction power, [MW]	0.800
Cost of H ₂ liquefaction, [\$/kg _{LH2}]	0.46
LCOH (including liquefaction), [\$/kg _{LH2}]	1.59
Overall energy efficiency, [%]	43.2

Economic model

There are a few systems in the literature that were proposed for the cogeneration of power, H₂, and NH₃. The configurations and overall energy efficiencies of these systems are summarized in Table 3 alongside that for the present system. Although renewable-based systems have high energy efficiency (up to 75%), they are suffering from the intermittency issue or the high capital cost if thermal energy storage is used. Economically, the study presented by Yuksel et al.[22] reported the LCOH with an average of 2.55\$/kg_{H2} over the variation range of the solar radiation intensity from 400-1000W/m². However, the present proposed system achieves LCOH of 1.59\$/kg_{LH2} (38 lower than in [22] including the liquefaction cost) [29]. Moreover, an average ammonia production cost of 0.87 \$/kg_{NH3} (based on solar and wind energy sources) is reported by Campion et al. in [26]. This cost is three times higher than the cost of ammonia in the proposed system of this study (0.24 \$/kg_{NH3}). Thus, it can be stated that the proposed system in this study reduces the H₂ and NH₃ production costs by about 72% compared to the renewable energy-based multigeneration systems. Thus, an average of 55% reduction is achieved in the H₂ and NH₃ costs compared to renewable systems.

Table 3. Comparison between the present and other proposed multigeneration system in literature.

Ref.	Energy source	Integrated systems	Energy eff., (%)	Exergy eff., (%)	LH ₂ cost, (\$/kg _{H2})	NH ₃ cost, (\$/kg _{NH3})
[30]	Wind/CSP	SRC+PSA+PEM+ASR+FC	63	56	-	-
[22]	CSP	SRC+ORC+PEM+ASR+USU+AC	66	62	2.55	-
[21]	GTP	KPC+PEM+ASR	75	72	-	-
[31]	CSP	ORC+SMR+ASU+HPB+LNG-RU	47	57	-	-
[26]	PV/Wind	WE + HBP	-	-	-	0.87
This study	NG	DOC-sCO ₂ +ASU+WE+HBP+DMR	44	65	1.49	0.28

* CSP = concentrated solar power, SRC = steam Rankine cycle, PSA = pressure swing adsorption, PEM = proton exchange membrane, ASR = ammonia synthesis reactor, FC = fuel cell, ORC = organic Rankine cycle, MU = methanation unit, USU = urea synthesis unit, AC = absorption cooling, GTP = geothermal power, KPC = Kalina power cycle, SDC = solar dish collector, SMR = steam methane reformer, ASU = air separation unit, HBP = Haber-Bosch process, LNG-RU = liquefied gas regasification unit, CRS = cascade refrigeration system.

CONCLUSIONS

In this study, a novel integrated system for power, hydrogen, and ammonia generation is introduced using a direct oxy-combustion supercritical carbon dioxide (DOC-sCO₂) power cycle, water electrolyzer (WE), and Haber-Bosch process (HBP) subsystems. In addition, a novel dual-mixed cryogenic liquefaction process is combined with the proposed multigeneration system to produce liquid hydrogen (LH₂). The main conclusions of this study are summarized as follows:

- In comparison to renewable-based multigeneration systems, the proposed DOC-sCO₂/WE/HBP system in this study reduces the production costs of both hydrogen and ammonia by approximately 55%.
- The proposed integrated system has an overall energy efficiency of 43.20%, LCOE of 3.09 ¢/kWh, LCOH of 1.59\$/kg_{H₂}, and LCOA of 0.24\$/kg_{NH₃}.
- The integration of the WE with the DOC-sCO₂ system reduces the load of the ASU by 16% without additional cost for the consumed water and nitrogen in the H₂ and ammonia production.
- Due to the utilization of DOC technology, there are no NO_x emissions, and the low-carbon emissions of the power block are captured to realize near-zero emissions to the ambient air.

In closing, the proposed system introduces a feasible economic solution for clean energy production and free-carbon energy transmission into local and global energy markets.

ACKNOWLEDGEMENT

The work presented in this publication was made possible by NPRP-S grant # [NPRP14S-0321-210080] from the Qatar National Research Fund (a member of Qatar Foundation). The findings herein reflect the work, and are solely the responsibility, of the authors.

REFERENCES

- [1] S. Alharbi, M. L. Elsayed, and L. C. Chow, "Exergoeconomic analysis and optimization of an integrated system of supercritical CO₂ Brayton cycle and multi-effect desalination," *Energy*, vol. 197, p. 117225, 2020, doi: 10.1016/j.energy.2020.117225.
- [2] R. Scaccabarozzi, M. Gatti, and E. Martelli, "Thermodynamic analysis and numerical optimization of the NET Power oxy-combustion cycle," *Appl. Energy*, vol. 178, pp. 505–526, 2016, doi: 10.1016/j.apenergy.2016.06.060.
- [3] A. Rogalev, E. Grigoriev, V. Kindra, and N. Rogalev, "Thermodynamic optimization and equipment development for a high efficient fossil fuel power plant with zero emissions," *J. Clean. Prod.*, vol. 236, p. 117592, 2019, doi: 10.1016/j.jclepro.2019.07.067.
- [4] A. K. Sleiti and W. A. Al-Ammari, "Energy and exergy analyses of novel supercritical CO₂ Brayton cycles driven by direct oxy-fuel combustor," *Fuel*, vol. 294, no. February, p. 120557, 2021, doi: 10.1016/j.fuel.2021.120557.
- [5] W. Chan, X. Lei, F. Chang, and H. Li, "Thermodynamic analysis and optimization of Allam cycle with a reheating configuration," *Energy Convers. Manag.*, vol. 224, no. August, p. 113382, 2020, doi: 10.1016/j.enconman.2020.113382.
- [6] A. Odenweller, F. Ueckerdt, G. F. Nemet, M. Jensterle, and G. Luderer, "Probabilistic feasibility space of scaling up green hydrogen supply," *Nat. Energy*, vol. 7, no. 9, pp. 854–865, 2022, doi: 10.1038/s41560-022-01097-4.
- [7] F. Eljack and M.-K. Kazi, "Prospects and Challenges of Green Hydrogen Economy via Multi-Sector Global Symbiosis in Qatar," *Front. Sustain.*, vol. 1, pp. 1–15, 2021, doi: 10.3389/frsus.2020.612762.
- [8] A. Hasan and I. Dincer, "Development of an integrated wind and PV system for ammonia and power production for a sustainable community," *J. Clean. Prod.*, vol. 231, pp. 1515–1525, 2019, doi: 10.1016/j.jclepro.2019.05.110.
- [9] A. Perna, M. Minutillo, E. Jannelli, V. Cigolotti, S. W. Nam, and J. Han, "Design and performance assessment of a combined heat, hydrogen and power (CHHP) system based on ammonia-fueled SOFC," *Appl. Energy*, vol. 231, no. August, pp. 1216–1229, 2018, doi: 10.1016/j.apenergy.2018.09.138.
- [10] M. F. Ezzat and I. Dincer, "Energy and exergy analyses of a novel ammonia combined power plant operating with gas turbine and solid oxide fuel cell systems," *Energy*, vol. 194, p. 116750, 2020, doi: 10.1016/j.energy.2019.116750.
- [11] W. Wang, Y. Ma, A. Maroufmashat, N. Zhang, J. Li, and X. Xiao, "Optimal design of large-scale solar-aided hydrogen production process via machine learning based optimisation framework," *Appl. Energy*, vol. 305, no. May 2021, p. 117751, 2022, doi: 10.1016/j.apenergy.2021.117751.
- [12] H. Ishaq and I. Dincer, "Analysis and optimization for energy, cost and carbon emission of a solar driven steam-autothermal hybrid methane reforming for hydrogen, ammonia and power production," *J. Clean. Prod.*, vol. 234, pp. 242–257, 2019, doi: 10.1016/j.jclepro.2019.06.027.
- [13] K. Miyahira and M. Aziz, "Hydrogen and ammonia production from low-grade agricultural waste adopting chemical looping process," *J. Clean. Prod.*, vol. 372, no. August, p. 133827, 2022, doi: 10.1016/j.jclepro.2022.133827.
- [14] B. A. Franco, P. Baptista, R. C. Neto, and S. Ganiha, "Assessment of offloading pathways for wind-powered offshore hydrogen production: Energy and economic analysis," *Appl. Energy*, vol. 286, no. January, 2021, doi: 10.1016/j.apenergy.2021.116553.
- [15] J. Allen, S. Panquet, and A. Bastiani, "Electrochemical Ammonia: Power to Ammonia Ratio and Balance of Plant Requirements for Two Different Electrolysis Approaches," *Front. Chem. Eng.*, vol. 3, no. November, pp. 1–16, 2021, doi: 10.3389/fceng.2021.765457.

- [16] C. Fúnez Guerra, L. Reyes-Bozo, E. Vyhmeister, M. Jaén Caparrós, J. L. Salazar, and C. Clemente-Jul, "Technical-economic analysis for a green ammonia production plant in Chile and its subsequent transport to Japan," *Renew. Energy*, vol. 157, pp. 404–414, 2020, doi: 10.1016/j.renene.2020.05.041.
- [17] A. K. Sleiti, W. Al-Ammari, S. Ahmed, and J. Kapat, "Direct-fired oxy-combustion supercritical-CO₂ power cycle with novel preheating configurations -thermodynamic and exergoeconomic analyses," *Energy*, vol. 226, no. July, p. 120441, 2021, doi: 10.1016/j.energy.2021.120441.
- [18] W. A. Al-Ammari and A. K. Sleiti, "Comprehensive thermoeconomic, exergoeconomic, and optimization analyses of direct oxy-combustion supercritical CO₂ intercooled and reheated cycles under design and off-design conditions," *Energy Sci. & Eng.*, vol. 10, no. 4, pp. 1272–1295, 2022, doi: 10.1002/ese3.1101.
- [19] M. Sánchez, E. Amores, D. Abad, L. Rodríguez, and C. Clemente-Jul, "Aspen Plus model of an alkaline electrolysis system for hydrogen production," *Int. J. Hydrogen Energy*, vol. 45, no. 7, pp. 3916–3929, 2020, doi: 10.1016/j.ijhydene.2019.12.027.
- [20] A. K. Sleiti, W. A. Al-Ammari, L. Vesely, and J. S. Kapat, "Thermoeconomic and optimization analyses of direct oxy-combustion supercritical carbon dioxide power cycles with dry and wet cooling," *Energy Convers. Manag.*, vol. 245, no. 1 October 2021, p. 114607, 2021, doi: 10.1016/j.enconman.2021.114607.
- [21] Y. E. Yuksel, M. Ozturk, and I. Dincer, "Development and assessment of a novel geothermal power-based multigenerational system with hydrogen and ammonia production options," *Energy Convers. Manag.*, vol. 243, p. 114365, 2021, doi: 10.1016/j.enconman.2021.114365.
- [22] Y. E. Yuksel, M. Ozturk, and I. Dincer, "Design and analysis of a new solar hydrogen plant for power, methane, ammonia and urea generation," *Int. J. Hydrogen Energy*, vol. 47, no. 45, pp. 19422–19445, 2022, doi: 10.1016/j.ijhydene.2021.12.162.
- [23] N. T. Weiland, B. W. Lance, and S. R. Pidaparti, "SCO₂ power cycle component cost correlations from DOE data spanning multiple scales and applications," in *Proceedings of the ASME Turbo Expo*, 2019, vol. 9, no. June 2019, pp. 1–17. doi: 10.1115/GT2019-90493.
- [24] G. Rodríguez Hervás and F. Petrakopoulou, "Exergoeconomic Analysis of the Allam Cycle," *Energy and Fuels*, vol. 33, no. 8, pp. 7561–7568, 2019, doi: 10.1021/acs.energyfuels.9b01348.
- [25] S. K. Seo, D. Y. Yun, and C. J. Lee, "Design and optimization of a hydrogen supply chain using a centralized storage model," *Appl. Energy*, vol. 262, no. December 2019, p. 114452, 2020, doi: 10.1016/j.apenergy.2019.114452.
- [26] N. Champion, H. Nami, P. R. Swisher, P. Vang Hendriksen, and M. Münster, "Techno-economic assessment of green ammonia production with different wind and solar potentials," *Renew. Sustain. Energy Rev.*, vol. 173, no. November 2022, p. 113057, 2023, doi: 10.1016/j.rser.2022.113057.
- [27] M. S. Sadaghiani and M. Mehrpooya, "Introducing and energy analysis of a novel cryogenic hydrogen liquefaction process configuration," *Int. J. Hydrogen Energy*, vol. 42, no. 9, pp. 6033–6050, 2017, doi: 10.1016/j.ijhydene.2017.01.136.
- [28] A. Naquash *et al.*, "Hydrofluoroolefin-based mixed refrigerant for enhanced performance of hydrogen liquefaction process," *Int. J. Hydrogen Energy*, no. xxxx, pp. 1–15, 2022, doi: 10.1016/j.ijhydene.2022.02.010.
- [29] D. Hjeij, Y. Biçer, and M. Koç, "Hydrogen strategy as an energy transition and economic transformation avenue for natural gas exporting countries: Qatar as a case study," *Int. J. Hydrogen Energy*, vol. 47, no. 8, pp. 4977–5009, 2022, doi: 10.1016/j.ijhydene.2021.11.151.
- [30] O. Siddiqui and I. Dincer, "Design and transient analyses of a new renewable energy system for multigeneration of power, heat, hydrogen and ammonia," *J. Clean. Prod.*, vol. 270, p. 122502, 2020, doi: 10.1016/j.jclepro.2020.122502.
- [31] M. Moradi, B. Ghorbani, A. Ebrahimi, and M. Ziabasharhagh, "Process integration, energy and exergy analyses of a novel integrated system for cogeneration of liquid ammonia and power using liquefied natural gas regasification, CO₂ capture unit and solar dish collectors," *J. Environ. Chem. Eng.*, vol. 9, no. 6, p. 106374, 2021, doi: 10.1016/j.jece.2021.106374.

ICH2P14-OP095

A SOLAR POND INTEGRATED WITH BIFACIAL SOLAR PANELS FOR POWER AND HYDROGEN GENERATION

^{1,2*}*Dogan Erdemir*, ^{1,2}*Ibrahim Dincer*

¹Ontario Tech University, Clean Energy Research Laboratory, Oshawa, Ontario, Canada

²Yildiz Technical University, Department of Mechanical Engineering, Istanbul, Turkey

*Corresponding author e-mail: dogan.erdemir@ontariotechu.ca

ABSTRACT

This study develops a unique integrated system which combines the bifacial solar panels and solar pond. These technologies are integrated to create a synergistic system capable of supplying electricity, hydrogen, and heating for community use. The performance of the system is rigorously evaluated using thermodynamic assessments based on energy and exergy efficiencies. Hourly solar data for Antalya, Turkey, sourced from the Photovoltaic Geographical Information System (PVGIS), is utilized for calculations. The results demonstrate the potential to produce electricity, hydrogen, and recover heat energy efficiently, showcasing the viability of integrating bifacial solar panels with solar ponds. The overall energy and exergy efficiencies are calculated as 28.33% and 23.67%, respectively. This integrated approach presents a promising solution for meeting the multifaceted energy demands of a community while utilizing solar energy effectively.

Keywords: Solar energy, solar pond, Bifacial solar panel, hydrogen, energy storage.

INTRODUCTION

Solar energy is one of the most abundant and clean sources of renewable energy on Earth. However, harnessing solar energy efficiently and cost-effectively remains a challenge for many applications. A solar pond is a large body of water that can store solar energy in the form of heat at the bottom layer, while the upper layer acts as an insulator. The bottom layer is saturated with salt or brine, which prevents heat from rising to the surface and allows temperatures to reach up to near boiling. A solar pond can act as a year-round energy storage system that can be used for various purposes, such as industrial heating, desalination, chemical production, and electricity generation. After the energy crisis in 1979, renewable energy sources, especially solar thermal applications, including solar ponds, became a major attraction. After the 1990s, interest in solar energy largely shifted to PV applications. Photovoltaic modules that are bifacial can absorb light from both sides. In contrast to conventional solar panels, which capture light only from the front, bifacial solar panels can also receive reflected light from the surface beneath the panel. The transparency of bifacial solar PV panels refers to the ability of the panels to allow light to pass through them from both sides. The transparency of bifacial solar PV panels is achieved by using transparent glass or back sheets as the encapsulation materials, and by minimizing the use of metal frames or grid lines that could block the light. It can vary depending on the design and configuration of the panels, such as the thickness and type of glass, the number and size of busbars, and the spacing and arrangement of solar cells.

This work explores the integration of two innovative solar technologies: solar ponds and bifacial solar panels to meet the various demands of a community. Thus, the proposed integrated system meets the electricity, hydrogen and heating demands of the community. Thermodynamic assessment tools based on the first and second laws of thermodynamics are used for evaluating the system performance. For this purpose, the energy and exergy efficiencies of the system are defined.

SYSTEM AND ASSESSMENT

Figure 1 demonstrates the schematic representation of the proposed system. As seen from Figure 1, bifacial solar panels are used for generating electricity. While bifacial solar panels allow to generate electricity both side of the panels, it also allows to transmit solar lights through them, which provides the energy input for the solar pond. Back-face of the solar panels collects the solar energy reflected from the surface of the solar pond. Thus, this integrated creates an effective synergy for advance use of the salinity gradient solar pond. The size of the solar pond is 50 m x 50 m. Its depth is 5 m. The thickness of the heat storage zone of the solar pond is 3 m. A tube bank placed inside the solar pond is used for heat extraction from the pond, which is connected to a heat exchanger to deliver the extracted heat to the useful purposes. The PEM electrolyser is included into the system to produce hydrogen. In order to assess the system performance, a complete thermodynamic analysis based on energy and exergy efficiencies have been applied to the system. For this purpose, first, the mass, energy, entropy and exergy balance equations are written for each component of the system. Then, energy and exergy efficiencies are defined to calculate the system performance. Finally, parametric studies have been performed based on the key drivers in the system performance.

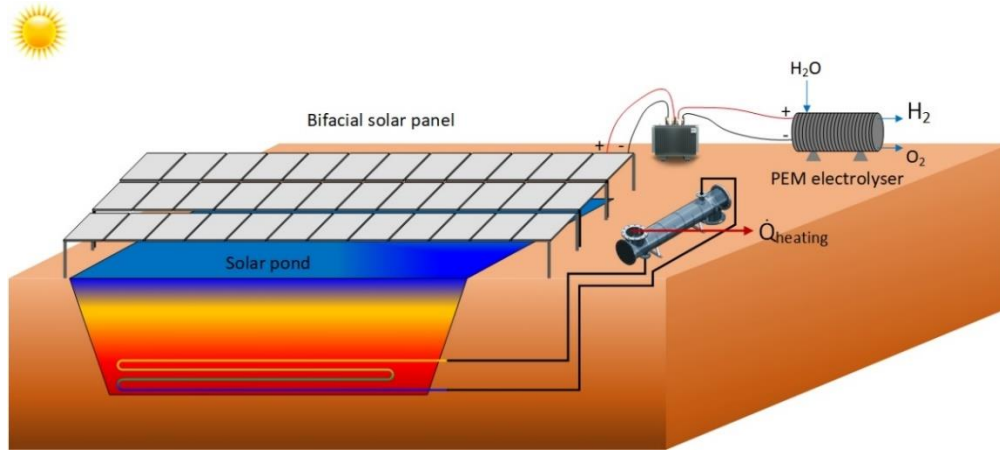


Figure 1. The schematic illustration of the solar pond covered with bifacial solar panels.

RESULTS AND DISCUSSION

The yearly dynamic solar data for Antalya, Turkey are used in this work. The data is retrieved from Photovoltaic Geographical Information System (PVGIS) [1]. The energy inputs and outputs are calculated based on yearly annual data for 2020 on hourly basis. For hydrogen production, it is assumed that 50 kWh of energy is required for 1 kg of hydrogen. Heat loss from the solar pond is assumed negligible. While the heat is charged from the beginning of the May to end of the October, it is discharged on January, February, March, April, November, and December. The half of the electricity produced in the bifacial solar panels is used for hydrogen generation. Figure 2 shows both the energy and exergy flows in the system. As seen from Figure 2, the yearly total solar energy and exergy inputs are 5281 and 5008 MWh, respectively. Annual electricity generation via bifacial solar panels are found to be 631.5 kWh. It is possible to produce 12,632 kg of hydrogen with 50% of the generated electricity. Under Antalya, Turkey conditions, the temperature of the brine in solar pond may reach up to 53 °C. Thus, it is possible to recover a 282 MWh of heat via solar pond, which corresponds 24 MWh of exergetic content.

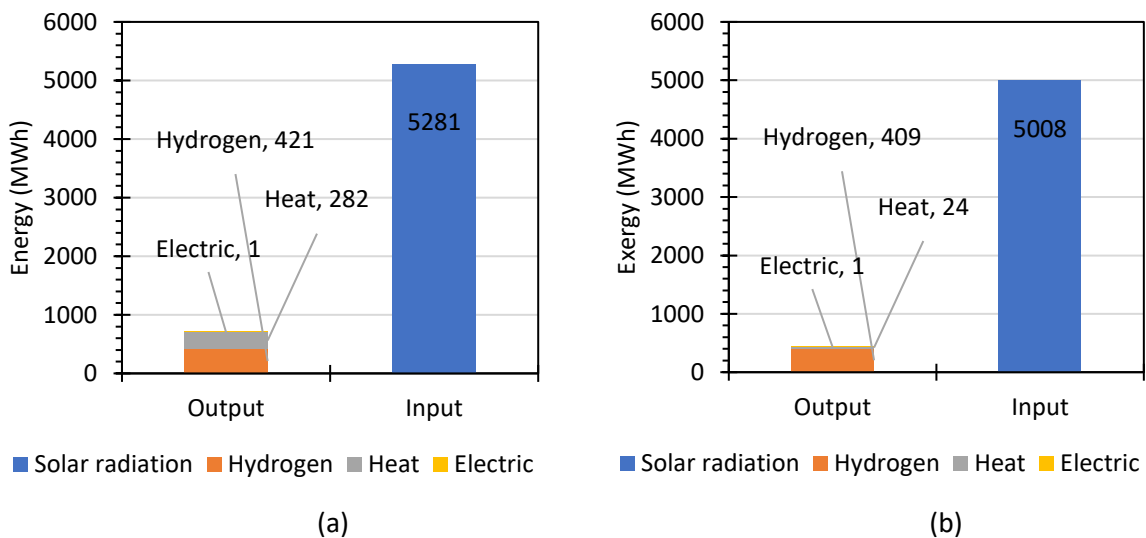


Figure 2. (a) Energy and (b) exergy flows in the system.

CONCLUSIONS

This study deals with the integration of solar pond and bifacial solar panel to meet the multiple demand of a community. Antalya, Turkey has been selected as the location. Hourly basis yearly solar data is used for calculation the inputs and outputs of the system. The overall energy and exergy efficiencies are calculated as 28.33% and 23.67%, respectively. Consequently, it has been reached that bifacial solar panels and solar ponds have a good synergy in meeting the electricity and heating demands. While bifacial solar panels delivering electricity for meeting demands and hydrogen production, the solar pond can store heat for later use.

REFERENCES

1. Photovoltaic Geographical Information System (PVGIS), EU Science Hub, 2023. Data accessed on 2023-10-01: https://re.jrc.ec.europa.eu/pvg_tools/en/

ICH2P14-OP096

TECHNO-ECONOMIC EVALUATION OF VARIOUS HYDROGEN CARRIERS**Ahmad K. Sleiti, Laveet Kumar, Wahib A. Al-Ammari*Department of Mechanical & Industrial Engineering, College of Engineering, Qatar University, Doha, Qatar
*Corresponding author's email: asleiti@qu.edu.qa**ABSTRACT**

The shift from a fossil fuel-based economy to one focused on low-carbon pathways is fundamentally dependent on the mode of energy transportation. Hydrogen can play a pivotal role in the future global energy landscape, facilitating the achievement of carbon-neutral goals by 2050. Nevertheless, the large-scale transportation of hydrogen presents technological and economic challenges that need to be addressed within existing energy infrastructures. Also, research examining the economic viability of exporting hydrogen from nations that primarily export natural gas is very limited. Therefore, a comprehensive study on the techno-economic evaluation (TEE) of these hydrogen transportation pathways is analytically investigated to promote economical and large-scale hydrogen energy carrier development. This paper investigates and compares four different modes of hydrogen energy carrier including liquid hydrogen (LH₂), Ammonia (NH₃), Methanol (MeOH), and Dimethyl ether (DME) transportation. This study concluded that NH₃ followed by LH₂ are the most cost-effective options to transport hydrogen. The total SEC of NH₃ is 7.67 kWh/kg-H₂ which is 51% lower than LH₂ pathway at 600 tons/day capacity. Therefore, the overall operational expenditure (OPEX) of NH₃ will be much lower than that of the LH₂ and other pathways. This results in the lowest levelized cost of hydrogen (LCOH) of the NH₃ pathway which is 4.76 \$/kg-H₂ because the main cost for conditioning and reconditioning is higher for MeOH and DME. It is recommended to consider NH₃ pathway as a promising alternative for efficient and sustainable energy transportation, thereby contributing to the establishment of an environmentally friendly hydrogen economy. However, it is crucial to emphasize that substantial research efforts are required to make this approach both technologically and economically viable.

Keywords: Hydrogen transportation, Techno-Economic, Liquid Hydrogen (LH₂), Ammonia (NH₃), Methanol (MeOH), Dimethyl ether (DME).

INTRODUCTION

Large-scale hydrogen production facilities, which are centralized and utilize diverse energy sources, are currently in operation. However, the transportation of hydrogen from these production sites to distribution points poses a challenge, especially when the energy source is situated in a distant location [1]. Hydrogen in its various forms, whether it is in liquid, gas, or metal hydride form, can be transported via road, pipeline, or ocean. For short distances and smaller quantities, especially when dealing with CGH₂, road transport is feasible. However, for transporting substantial amounts of hydrogen over extensive distances, pipelines prove to be a more effective choice. Liquid hydrogen, in particular, can be efficiently transported over long distances through road or sea routes. On the other hand, the transport of low-pressure hydrogen stored in metal hydrides is constrained to smaller quantities and shorter distances [2][3].

Fig. 1. illustrates the diverse routes for transporting and distributing hydrogen across extensive distances. The supply chain route encompasses seven key phases: hydrogen production, conditioning, loading, transportation, unloading, re-conditioning, and final distribution [2]. The transportation of liquid hydrogen (LH₂) via road trailers or ships provides a range of options in the realm of hydrogen transport. For shorter distances, utilizing trucks for compressed gaseous hydrogen (CGH₂) proves to be notably cost-effective. Various research studies have identified LH₂ trucks and CGH₂ pipelines as the most economical choices for transporting hydrogen over land for extended distances. Additionally, these studies confirmed that shipping LH₂ stands out as the most cost-effective method for transporting hydrogen across oceans, with liquid organic hydrogen carriers (LOHC) shipping following closely as the next most economical option [4].

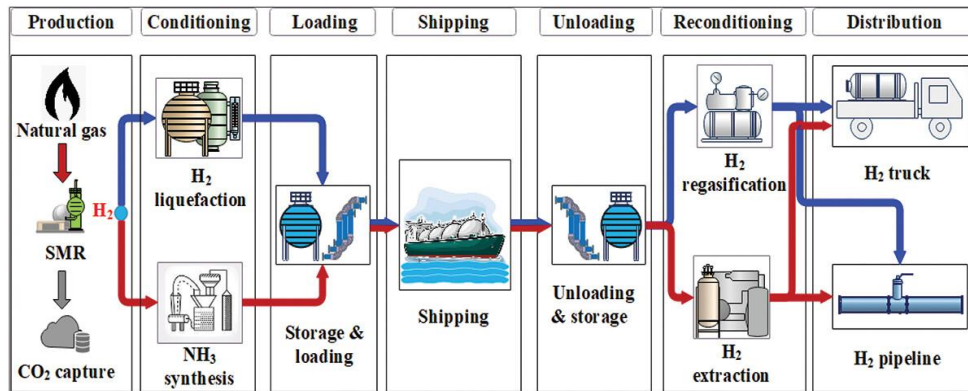


Fig. 1. Flow diagram of LH₂ supply chain [2]

In the LH₂ pathway, hydrogen undergoes a regasification and compression process for its transportation as CGH₂. This can be accomplished through either tube trailers or pipeline systems. Tube trailers are configured to transport hydrogen within the pressure range of 200 to 500 bar, accommodating varying payload capacities ranging from 300 to 1100 kg, contingent upon the specific carrier employed. Tube trailers present a pragmatic solution particularly well-suited for scenarios characterized by modest demand and transportation distances up to 160 km. Alternatively, the utilization of tanker trucks instead of CGH₂ emerges as a viable option offering potential cost advantages attributed to the high density of LH₂. However, a notable technical challenge arises in the form of storage losses associated with LH₂, commonly known as boil-off gas losses (BOG). Conversely, the deployment of pipelines stands out as the most financially feasible solution for extensive H₂ transportation necessitating long distances and catering to substantial demand. While the establishment of pipelines demands considerable capital investment, their operational and maintenance (O&M) costs are notably low, rendering them economically attractive over an extended operational lifespan of around 40 years [2].

Table 1. provides a comparison of various hydrogen transportation methods. Among the various choices for transportation, cryogenic tankers, and pipelines demonstrate the highest efficiency. However, substantial initial investments and transmission costs are required. As depicted in Table 1, the costs associated with transporting and distributing liquid hydrogen (LH₂) are noticeably less than those for compressed gaseous hydrogen (CGH₂). Additionally, Table 1 emphasizes that pipelines can become the most cost-effective solution for conveying CGH₂ when large quantities of H₂ need to be transported over considerable distances.

Table 1. Comparison of different hydrogen transport methods

Parameter	Pipelines	Road			Shipping	References
		CGH ₂ trailer	LH ₂ trailer	Cryogenic Tankers		
Storage Pressure (MPa)	2-3	20-50	0.1-0.4	0.1 to 0.7	0.1 to 0.7	[4]–[6]
Storage Capacity (Maximum)	100 tons /hour	400 kg per trailer	400 kg per trailer	4000 kg per trailer	10,000 tons per ship	[4], [6], [7]
Boil off losses (Maximum)	0.8% per 100 km	6% per 100 km	6% per 100 km	1% per 100 km	0.3% per day	[4], [7]
CAPEX cost (\$)	\$200K-\$1 M per km	\$300K + per truck	\$300K + per truck	\$300K-\$400K per truck	\$465M-\$620M for each barge	[1], [7], [8]
OPEX cost (% of CAPEX) / year	4-4.7%	2%	2%	\$ 16634K + 4%	\$ 10553746 + 4%	[6], [7], [9]
Transportation cost (\$) per kg per 100 km	\$0.10 - \$1.0	\$0.50 - \$2.0	\$0.50 - \$2.0	\$0.30 - \$0.50	\$1.80 - \$2.0	[7], [8]

However, the large-scale transportation of H₂ poses notable challenges in technological and economic dimensions, that must be tackled within current energy infrastructures. Consequently, this research investigates and compares four distinct modes of hydrogen energy carriers: liquid hydrogen (LH₂), ammonia (NH₃), methanol (MeOH), and dimethyl ether (DME). The comparison of techno-economic evaluations of these hydrogen transportation pathways is analytically conducted to advance the cost-effectiveness and expansive development of hydrogen energy carriers.

METHODOLOGY

This section presents the modeling equation to assess the various pathways. Each pathway consists of seven phases from production to distribution. Each stage of the hydrogen supply chain is evaluated based on its specific energy consumption (SEC), the levelized cost of H₂ (LCOH), and CO₂ emission intensity. The modeling of hydrogen transportation and distribution channels is done in this section on techno-economic evaluation (TEE). For the process of hydrogen production, steam methane reforming (SMR) integrated with carbon capture (CC) is assumed in this study. The SEC was determined for the H₂ generation process based on the amount of natural gas utilized to power the operations for producing H₂ and capturing CO₂. Eq. (1) to Eq. (3) are developed to take into account the impact of CC on capital expenditure (CAPEX) and operational expenditure (OPEX) as well as the CO₂ intensity [2][10][11][12].

$$CAPEX_{H_2,generation} [million \$] = Plant\ capacity [TPD] \times [1.014 + 0.0142 \times CC\%] \quad (1)$$

$$OPEX_{H_2,generation} [million \$ / year] = Plant\ capacity [TPD] \times \{0.0493 + 0.0043 \times CC\% \} \quad (2)$$

$$CO_2\ Intensity_{H_2,generation} \left[\frac{kg_{CO_2}}{kg_{H_2}} \right] = 10.63 - 0.0467 \times CC\% \quad (3)$$

The SEC and CAPEX of the conditioning process are calculated using Eq. (4) and Eq. (5), respectively [10];

$$SEC_{H_2,liquefaction} \left[\frac{kWh}{kg_{H_2}} \right] = 13.92 \times (plant\ capacity [TPD])^{-0.1} \quad (4)$$

$$CAPEX_{H_2,liquefaction} [million \$] = 9.3 \times (plant\ capacity [TPD])^{0.8} \quad (5)$$

The number of tanks needed at the loading process for the storage is calculated using Eq. (6) [10][2];

$$Number\ of\ Storage\ tanks = \frac{Specific\ volume \left[\frac{m^3}{kg} \right] \times plant\ capacity [TPD] \times 10^3 \times storage\ duration [days]}{Single\ tank\ capacity [m^3]} \quad (6)$$

Using Eq. (7), the cost of H₂ shipping is determined as [10][2];

$$Shipping\ cost \left[\frac{\$}{kg_{H_2}} \right] = 0.0000286 \times shipping\ distance [km] + 0.158 \quad (7)$$

Similarly, using Eq. (8), the cost of transportation via pipelines is determined;

$$Pipeline\ cost \left[\frac{\$}{kg_{H_2}} \right] = 0.00022 \times transportation\ distance [km] + 0.00564 \quad (8)$$

Using Eq. (9), the SEC of the overall pathway can be determined [10][2];

$$SEC = \sum_{s=a}^{s=g} \left[\frac{Energy\ input}{Delivered\ H_2} \right]_s \quad (9)$$

where *s* is the rank of the process (*a* for production unit, *b* for conditioning unit, *c* for loading and storage unit, *d* for shipping unit, *e* for unloading and storage unit, *f* for reconditioning unit, and *g* for distribution unit).

Using Eq. (10), the levelized cost of hydrogen (LCOH) can be determined;

$$LCOH = \sum_{s=a}^{s=g} \left[\frac{\sum_{t=1}^n (CAPEX_t + OPEX_t)(1+i)^{-t}}{\sum_{t=1}^n P_{H_2}(1+i)^{-t}} \right]_s \quad (10)$$

where t refers to the year. The first year of operation is taken as 1 and n is the last year depending upon the lifetime. P_{H_2} is the quantity of H_2 delivered annually and i is the discount rate.

Using Eq. (11), the CO_2 intensity of the overall pathway can be determined [2];

$$CO_2 \text{ intensity} = \sum_{s=a}^{s=g} \left[\frac{\sum CO_2 \text{ emissions}}{\text{Delivered } H_2} \right]_s \quad (11)$$

RESULTS AND DISCUSSION

The results of TEE are presented in terms of performance indicators including the SEC, LCOH, and CO_2 intensity of various pathways in this section. The SEC of various pathways is illustrated in Fig. 2. It is estimated using equations defined above and input data from the literature [2][13][14]. The conditioning and shipping phase have the highest SEC compared to all other stages in the LH_2 route shown in the Fig.2. SEC for the shipping and liquefaction are 4.40 kWh/kg- H_2 and 7.34 kWh/kg- H_2 , respectively. The main causes of this are the -253°C temperature at which H_2 turns into a liquid and the significant losses incurred from H_2 boil-off during LH_2 transportation. Similar to this, the SEC of ammonia synthesis in the NH_3 process is 2.86 kWh/kg- H_2 . MeOH and DME have corresponding SEC of 6.30 kWh/kg- H_2 and 6.30 kWh/kg- H_2 for methanol and DME synthesis. The total SEC of the LH_2 approach is greater than the other methods during the whole procedure. NH_3 has a total SEC of 7.67 kWh/kg- H_2 , which is less than that of other modes. As a result, compared to the LH_2 technique, the operational costs of other methods most notably NH_3 are significantly cheaper. This shows that for LH_2 to become competitive with the other routes, improvements in reducing its energy usage are necessary.

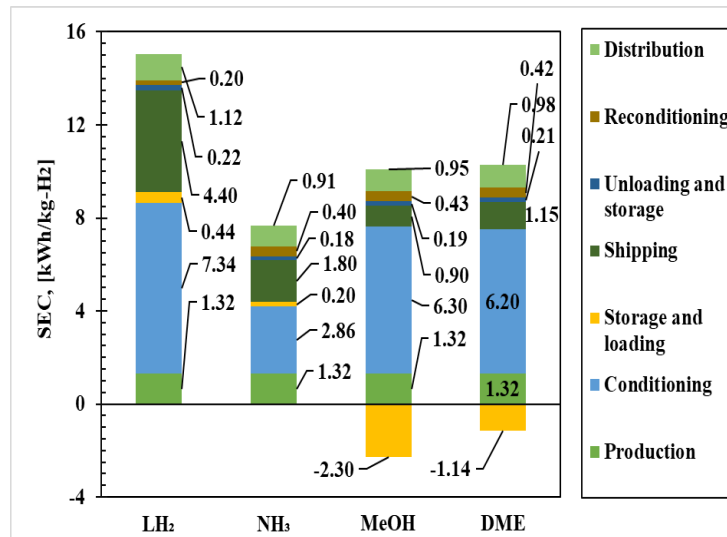


Fig.2. Specific Energy Consumption (SEC) for all seven stages of H_2 pathways for LH_2 , NH_3 , MeOH and DME

The LCOH of various energy carriers is illustrated in Fig.3. It is calculated using Eq. (10) and input data from the literature [2][13][14]. The overall LCOH for LH_2 , DME, and MeOH is 5.17, 7.51, and 6.52 \$/kg- H_2 , respectively which is higher than NH_3 pathway. The least cost of LCOH is NH_3 pathway which is 4.76 \$/kg- H_2 . It can be noted that the main cost in LCOH for MeOH and DME is conditioning and reconditioning which is higher than all others. It is worth observing that the gap in the LCOH between the LH_2 and NH_3 routes is narrower compared to the gap in the SEC. This is mainly because reconditioning involves regasification, which is less expensive than the NH_3 cracking process needed to remove H_2 . Considering the current state of technology and its future direction, it is currently impractical to use NH_3 directly as fuel in power plants and the transportation sector unless the issues with high NO_x emissions and low combustion efficiency of NH_3 are successfully resolved.

About 52% of the carbon emissions in the SMR process used to produce hydrogen are produced at the reactor unit, and 33% are produced at the reformer step [10]. Consequently, using Eq. (11) to compute the CO_2 intensity of the LH_2 , NH_3 , MeOH, and DME route process for hydrogen transportation and distribution at a CC fraction of 52% is shown in Fig. 4. It can be observed from the figure, the maximum CO_2 intensity is 8.18 kg- CO_2 /kg- H_2 for the production stage, which is greater than other processes since SMR is used for generation of H_2 . Moreover, because the hydrogen liquefaction process requires a significant amount of energy, its CO_2 intensity is 3.99 kilogram- CO_2 per kg of hydrogen (kg- H_2).

However, the CO₂ intensity of the LH₂ route would decrease if the H₂ liquefaction process was fueled by a renewable energy source that produced zero CO₂ emissions. The CO₂ intensity of the DME and MeOH routes is 9.96 kg-CO₂/kg-H₂ and 9.95 kg-CO₂/kg-H₂, respectively, which is lower than the other pathways.

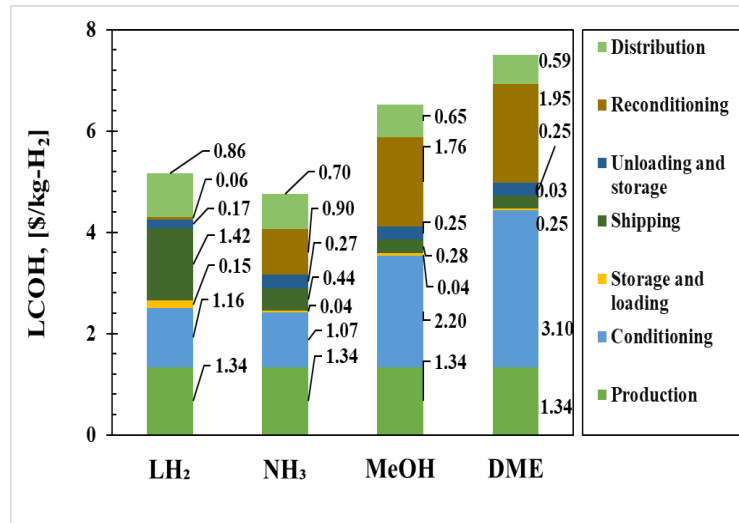


Fig. 3. Levelized cost of Hydrogen for all seven stages of H₂ pathways for LH₂, NH₃, MeOH and DME.

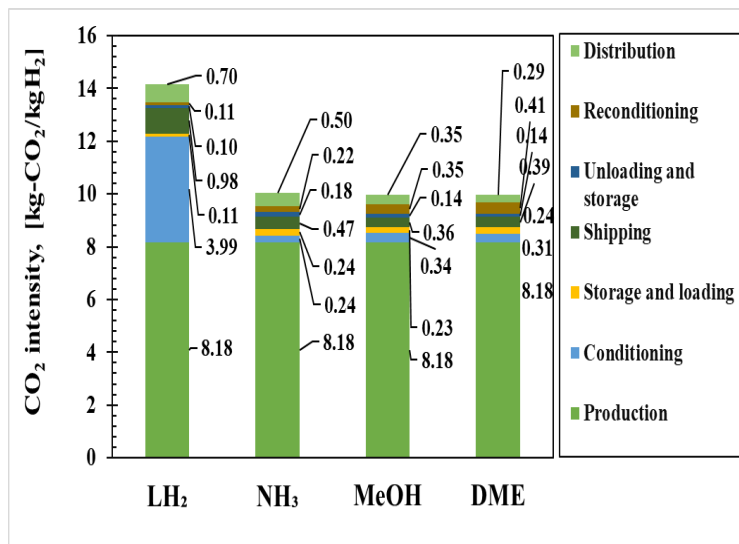


Fig.4. CO₂ intensity for all seven stages of H₂ pathways for LH₂, NH₃, MeOH and DME.

From the above investigation, it becomes evident that the SEC, LCOH, and CO₂ intensity of the NH₃ pathway are all lower in comparison to the other pathways. Further, this LCOH can be reduced more by adopting advancement measures for NH₃ pathway. Some of the measures proposed in the literature to mitigate the LCOH of NH₃ pathway are summarized in Table 2.

Table 2. Improvement measures for the reduction in LCOH for NH₃ pathway

Stage	Measures	Current Cost (\$/kg.H ₂)	Future cost (\$/kg.H ₂)	References
Production	Integrating the SMR, supercritical carbon dioxide (sCO ₂) power cycle and pressure swing adsorption (PSA)	1.34	1.10	[15][16]
Conditioning		1.07	0.71	
Shipping	NH ₃ as a fuel including the boil-off gas (BOG) from NH ₃ storage	0.44	0.31	[17]
Storage and Loading	Invested CAPEX for the LNG terminal can be repurposed for NH ₃	0.04	0.02	[18]
Unloading and Storage		0.27	0.13	
Distribution		0.70	0.35	

After incorporating the improvement measures given in Table 2. to the TEE of the NH₃ pathway as shown in Fig.3, the LCOH will be reduced by 15.3% from 4.76 to 3.52 \$/kg-H₂ as shown in Fig.5.

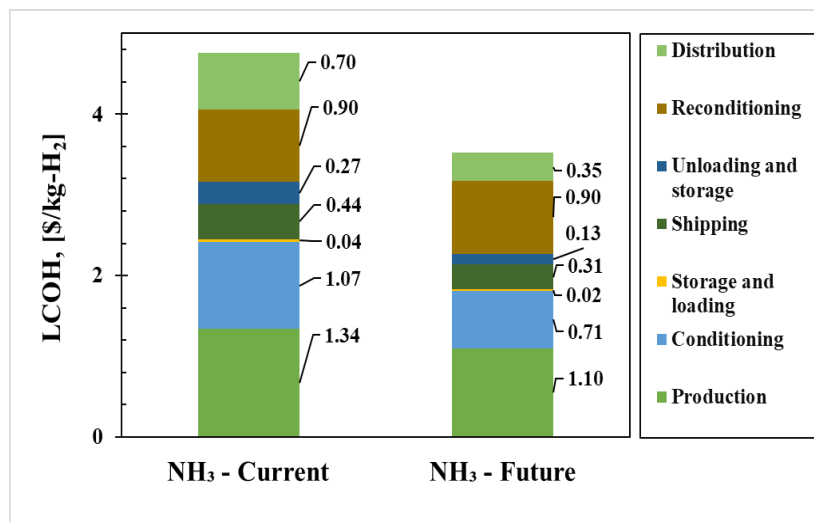


Fig.5. Comparison between current and future reduced LCOH of the NH₃ pathway

CONCLUSION AND FUTURE DIRECTIONS

This paper investigates and compares four different pathways of hydrogen energy carriers namely liquid hydrogen (LH₂), ammonia (NH₃), methanol (MeOH), and dimethyl ether (DME). Each pathway consists of seven phases from production to distribution. The techno economic performance is evaluated in terms of the specific energy consumption (SEC), levelized cost of hydrogen (LCOH), and CO₂ intensity. The main findings of this research are:

- NH₃ followed by LH₂ are the most cost-effective option compared to MeOH and DME energy carrier pathways.
- The total SEC of NH₃ pathway is 7.67 kWh/kg-H₂ which is 51% lower than LH₂ pathway.
- Based on the present status of the NH₃ technologies, the overall LCOH for NH₃ pathway is 4.76 \$/kg-H₂, which can be reduced to 3.52 \$/kg-H₂ (reduced by 26%) by implementing new integrated cycles and repurposing of LNG technologies.
- The main reason for the low LCOH of NH₃ pathway is that for MeOH and DME pathways cost of conditioning and reconditioning stages is much higher.

In the future, it is imperative to conduct further research studies on the commercial feasibility of H₂ transportation for a sustainable hydrogen economy. NH₃ options stand out as promising alternatives for sustainable energy transport for the efficient hydrogen economy. While these options may entail

considerable initial capital investment but as transportation distances increase it may become suitable for long-distance transport needs.

ACKNOWLEDGMENT

The work presented in this publication was made possible by grant QUPD – CENG – 23/24 – 537 from the Qatar University. The findings herein reflect the work, and are solely the responsibility, of the authors.

NOMENCLATURE

BOG	Boil off gas
CC	Carbon capture
CO ₂	Carbon Dioxide
CAPEX	Capital expenditure
CGH ₂	Compressed gaseous hydrogen
DME	Dimethyl ether
LH ₂	Liquid Hydrogen
LOHC	Liquid organic hydrogen carrier
LCOH	Levelized cost of hydrogen
MeOH	Methanol
NH ₃	Ammonia
OPEX	Operating expenditure
O&M	Operational and maintenance
SMR	Steam methane reforming
SEC	Specific energy consumption
TEE	Techno-economic evaluation
TPD	Tons per day

REFERENCES

- [1] H. Nazir *et al.*, "Is the H₂ economy realizable in the foreseeable future? Part II: H₂ storage, transportation, and distribution," *Int. J. Hydrogen Energy*, vol. 45, no. 41, pp. 20693–20708, 2020, doi: <https://doi.org/10.1016/j.ijhydene.2020.05.241>.
- [2] A. K. Sleiti, W. A. Al-Ammari, F. Musharavati, and M. Azizur Rahman, "Techno-economic assessment of low-carbon hydrogen exports from the Middle East to the Asia-Pacific, and Europe," *Energy Sources, Part B Econ. Planning, Policy*, vol. 18, no. 1, p. 2254764, Dec. 2023, doi: [10.1080/15567249.2023.2254764](https://doi.org/10.1080/15567249.2023.2254764).
- [3] A. K. Sleiti, W. A. Al-Ammari, and F. Musharavati, "Theoretical and experimental study on the selection of pure and mixed refrigerants for a power-cooling system driven by ultra-low-grade heat," *Therm. Sci. Eng. Prog.*, vol. 43, p. 101962, 2023, doi: <https://doi.org/10.1016/j.tsep.2023.101962>.
- [4] W. Alsaba, S. A. Al-Sobhi, and M. A. Qyyum, "Recent advancements in the hydrogen value chain: Opportunities, challenges, and the way Forward–Middle East perspectives," *Int. J. Hydrogen Energy*, vol. 48, no. 68, pp. 26408–26435, 2023, doi: <https://doi.org/10.1016/j.ijhydene.2023.05.160>.
- [5] F. Ustolin, J. J. Lamb, O. S. Burheim, and B. G. Pollet, "Chapter | eight - Energy and Safety of Hydrogen Storage," in *Hydrogen and Fuel Cells Primers*, J. J. Lamb and B. G. B. T.-H. Pollet Biomass and Bioenergy, Eds., Academic Press, 2020, pp. 133–153. doi: <https://doi.org/10.1016/B978-0-08-102629-8.00008-6>.
- [6] M. Yang, R. Hunger, S. Berrettoni, B. Sprecher, and B. Wang, "A review of hydrogen storage and transport technologies," *Clean Energy*, vol. 7, no. 1, pp. 190–216, Feb. 2023, doi: [10.1093/ce/zkad021](https://doi.org/10.1093/ce/zkad021).
- [7] B. C. Tashie-Lewis and S. G. Nnabuife, "Hydrogen Production, Distribution, Storage and Power Conversion in a Hydrogen Economy - A Technology Review," *Chem. Eng. J. Adv.*, vol. 8, p. 100172, 2021, doi: <https://doi.org/10.1016/j.cej.2021.100172>.
- [8] T. Galimova, M. Fasihi, D. Bogdanov, and C. Breyer, "Impact of international transportation chains on cost of green e-hydrogen: Global cost of hydrogen and consequences for Germany and Finland," *Appl. Energy*, vol. 347, p. 121369, 2023, doi: <https://doi.org/10.1016/j.apenergy.2023.121369>.
- [9] D. Teichmann, W. Arlt, E. Schlücker, and P. Wasserscheid, "Transport and Storage of Hydrogen via Liquid Organic Hydrogen Carrier (LOHC) Systems," in *Hydrogen Science and Engineering: Materials, Processes, Systems and Technology*, 2016, pp. 811–830. doi: <https://doi.org/10.1002/9783527674268.ch33>.
- [10] A. Okunlola, T. Giwa, G. Di Lullo, M. Davis, E. Gemechu, and A. Kumar, "Techno-economic assessment of low-carbon hydrogen export from Western Canada to Eastern Canada, the USA, the Asia-Pacific, and Europe," *Int. J. Hydrogen Energy*, vol. 47, no. 10, pp. 6453–6477, 2022, doi: <https://doi.org/10.1016/j.ijhydene.2021.12.025>.
- [11] A. O. Oni, K. Anaya, T. Giwa, G. Di Lullo, and A. Kumar, "Comparative assessment of blue hydrogen from steam methane reforming, autothermal reforming, and natural gas decomposition technologies for natural gas-producing regions," *Energy Convers. Manag.*, vol. 254, p. 115245, 2022, doi: <https://doi.org/10.1016/j.enconman.2022.115245>.
- [12] A. K. Sleiti, W. A. Al-Ammari, and S. Ghani, "Novel dual-mixed refrigerant precooling process for high

- capacity hydrogen liquefaction plants with superior performance,” *J. Energy Storage*, vol. 66, p. 107471, 2023, doi: <https://doi.org/10.1016/j.est.2023.107471>.
- [13] P. Schühle *et al.*, “Dimethyl ether/CO₂ – a hitherto underestimated H₂ storage cycle,” *Energy Environ. Sci.*, vol. 16, no. 7, pp. 3002–3013, 2023, doi: 10.1039/D3EE00228D.
- [14] V. L. Meca, R. d’Amore-Domenech, A. Crucelaegui, and T. J. Leo, “Large-Scale Maritime Transport of Hydrogen: Economic Comparison of Liquid Hydrogen and Methanol,” *ACS Sustain. Chem. Eng.*, vol. 10, no. 13, pp. 4300–4311, Apr. 2022, doi: 10.1021/acssuschemeng.2c00694.
- [15] M. Byun *et al.*, “Economically feasible decarbonization of the Haber-Bosch process through supercritical CO₂ Allam cycle integration,” *Appl. Energy*, vol. 307, p. 118183, 2022, doi: <https://doi.org/10.1016/j.apenergy.2021.118183>.
- [16] A. K. Sleiti and W. A. Al-Ammari, “Novel integration between propane pre-cooled mixed refrigerant LNG process and concentrated solar power system based on supercritical CO₂ power cycle,” *Energy Reports*, vol. 9, pp. 4872–4892, 2023, doi: <https://doi.org/10.1016/j.egy.2023.04.012>.
- [17] O. B. Inal, B. Zincir, and C. Deniz, “Investigation on the decarbonization of shipping: An approach to hydrogen and ammonia,” *Int. J. Hydrogen Energy*, vol. 47, no. 45, pp. 19888–19900, 2022, doi: <https://doi.org/10.1016/j.ijhydene.2022.01.189>.
- [18] and J. W. Riemer, Matia, Florian Schreiner, “Conversion of LNG Terminals for Liquid Hydrogen or Ammonia,” 2022. [Online]. Available: <https://doi.org/10.24406/publica-464>.

ICH2P14-OP97

MAXIMIZING POWER GRID RESILIENCE: ROLLING HORIZON CONTROL FOR OUTPUT POWER SMOOTHING IN ISLANDED WIND-SOLAR MICROGRIDS WITH MULTIPLE HYDROGEN STORAGE TANKS

^{1*}Muhammad Bakr Abdelghany, Ahmed Al-Durra

Advanced Power and Energy Center, EECS Department, Khalifa University of Science and Technology, Abu Dhabi, UAE

*Corresponding author e-mail: abdelghany.muhammad@gmail.com

ABSTRACT

This paper introduces a strategic framework based on hierarchical rolling horizon control, also called model predictive control, for efficiently operating a hydrogen-energy storage system (HESS) within a self-contained wind-solar microgrid. The HESS employs an electrolyser to convert renewable-generated electricity into clean hydrogen, subsequently re-electrified using a fuel cell to meet the microgrid's energy demands. A significant innovation lies in incorporating multiple hydrogen storage tanks within the HESS, setting it apart from prior research that typically focused on a single tank. This multi-tank configuration allows for the long-term storage of significant hydrogen volumes, enabling the microgrid to function independently, isolated from the main grid. Optimal device selection at each time-step is crucial to guarantee peak performance. The proposed control strategy considers economic and operational expenses, degradation factors, and physical constraints of the HESS, while concurrently ensuring adherence to reference load demands and the prioritized smoothing of renewable energy fluctuations. Numerical simulations employing actual wind and solar generation profiles demonstrate that the proposed controller adeptly administers the HESS, even when disparities exist between projected and real-time scenarios. This ensures economic efficiency and device cost optimization.

Keywords: Hydrogen-based energy storage systems, energy management, model predictive control.

INTRODUCTION

Renewable energy sources (RESs), specifically wind and solar powers, are increasingly recognized as a viable alternative to fossil fuels [1]. Ongoing research aims to enhance the efficiency and practicality of these technologies for everyday use, addressing inherent challenges [2]. The objective is to seamlessly integrate wind and solar energy into diverse real-world applications, offering a tangible and impactful solutions [3]. Both wind and solar energy face challenges due to their stochastic nature, leading to production-consumption mismatches and cost considerations. The incorporation of technologies such as electrolysers and fuel cells add complexity to plant design, necessitating advanced management strategies. Model predictive control (MPC) strategies for optimal power market management of microgrids coupled with hydrogen-energy storage systems (HESSs) have been proposed in the literature, see, for instances, [4–8]. To the best of the authors' knowledge, the previous studies have not yet investigated the inclusion of multiple hydrogen storage tanks in HESSs, despite the potential advantages. This research aims to address this gap by emphasizing the benefits associated with employing multiple tanks, including enhanced system autonomy, parallel use, scalability, flexibility, and redundancy. Importantly, incorporating multiple tanks allows a microgrid (MG) to operate in islanded mode, i.e., completely independent of the utility grid. This autonomy is particularly crucial for MGs situated in remote areas. With the capacity to store larger quantities of hydrogen, the MG can reliably meet energy demands even during periods of low-RES availability.

MODEL

The operations of the electrolyser and the fuel cell can be depicted using two automata represented in Figure 1. The node set is $\mathcal{S} = \{ON, OFF, STB\}$ and the edge set is $\mathcal{T} = \{(\alpha, \beta) \in \mathcal{S} \times \mathcal{S} | \alpha \neq \beta\}$, where (α, β) denotes the edge from node α to node β . Nodes correspond to device states, and edges represent transitions between them. In the *ON* state, the electrolyser (fuel cell) actively produces (consumes) hydrogen; *OFF* denotes device inactivity; *STB* (standby) indicates a state where the device consumes power despite being inactive. In the following, the electrolyser and the fuel cell are denoted by e and f , respectively, and the generic device is represented by d .

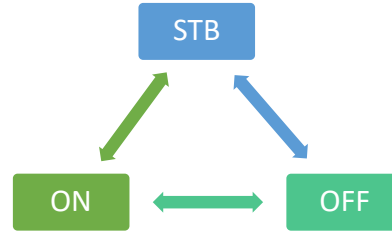


Figure 1: Automaton of the HESS operations.

In line with the mixed logical dynamical (MLD) framework [9], automata modeling incorporates continuous and logical variables. In particular, γ_d^α (for states) is 1 when automaton d is in state α at time-step k , and $\delta_d^{\alpha\beta}$ (for transitions) is 1 when the switch from α to β occurs in automaton d at instant k . Furthermore, it is essential to consider the inclusion of a mutually exclusive condition on state variables, ensuring only one operational state is selected for hydrogen devices at each time-step.

In addition to modeling the operations of the electrolyser and fuel cell, it is important to consider the modeling of hydrogen storage within each tank of the HESS, which is given by

$$H_i(k+1) = H_i(k) + \eta_e \zeta_{e_i}(k)\tau - \frac{\zeta_{f_i}(k)\tau}{\eta_f},$$

where H_i denotes the hydrogen level of tank i , η_e and η_f represent the efficiencies of the electrolyser and the fuel cell, respectively, $\zeta_{e_i} \geq 0$ is the power stored as hydrogen in tank i , $\zeta_{f_i} \geq 0$ is the power extracted from tank i , and τ is the sampling time.

Selecting optimal tanks and power values require the definition of some physical constraints. For instance, each tank must meet specific conditions to ensure hydrogen levels stay within defined thresholds. Moreover, when the electrolyser is active, enforcing constraints guarantees all produced hydrogen is stored. Similar constraints apply to fuel cell power.

CONTROL STRATEGY

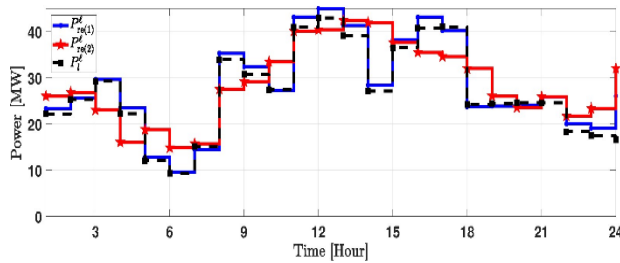
The control strategy employed is a cascade MPC [10] with two layers: the high layer control (HLC) and the low layer control (LLC). The primary goal of the HLC is to plan daily electricity transactions while fulfilling local load demands, maximizing the HESS lifespan, and minimizing operational costs. On the other hand, the LLC receives references from the HLC, adjusting in real-time and focusing on power smoothing.

The global cost function governing the optimization of the HESS management system at both the HLC and the LLC includes three components: HESS cost function, load tracking cost, and tank selection cost function. The degradation aspects, encompassing component depreciation, life cycle reduction, and energy consumption, determine the HESS cost function, which is crucial to minimize due to the high costs associated with the electrolyser and the fuel cell. The load tracking cost minimizes the cumulative square error between available system power and the reference signal, ensuring optimal load fulfillment. The tank selection cost function is included in the global cost function in order to optimize the hydrogen allocations in the tanks. In particular, these cost functions allow to prioritize tanks nearing full capacity for storage and those closest to being empty for extraction. At the LLC, the global cost function also includes an additional term related to power smoothing. This smoothing strategy minimizes variations in the available power in the system in order to enhance stability. In particular, the controller considers a fixed number of consecutive past samples to achieve power smoothing while complying with a given threshold, thus ensuring the system meets stringent power quality standards over hourly intervals.

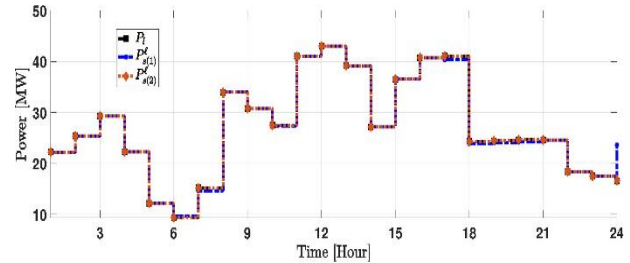
NUMERICAL ANALYSIS

In order to show the effectiveness of the proposed control strategy, a simulation analysis is conducted by considering two RES profiles and a specified electrical load depicted in Figure 2(a). In the

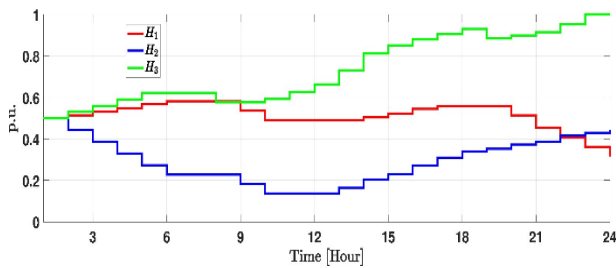
simulations, it is assumed that the HESS includes three hydrogen tanks, and the results are presented in Figure 2(b)–(d). Figure 2(b) illustrates the power scenarios and load reference, by showing the controller's effectiveness in filtering available power to meet the user's requested demand, even in the presence of varying solar and wind profiles. In Figure 2(c) and (d), the hydrogen levels corresponding to the two RES profiles are presented, indicating activated hydrogen production during high RES hours and efficient consumption during periods of low-RES generation.



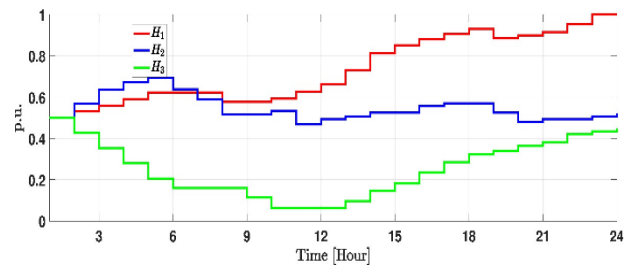
(a) RESs and operator power profiles



(b) Smoothed available power profiles and tracked reference demand



(c) Stored hydrogen in the multiple tanks according to the first RES profile



(d) Stored hydrogen in the multiple tanks according to the second RES profile

Figure 2: Simulation results.

REFERENCES

- [1] Foda, A., Abdelaty, H., Mohamed, M., & El-Saadany, E. (2023). A generic cost-utility-emission optimization for electric bus transit infrastructure planning and charging scheduling. *Energy*, 277, 127592.
- [2] Ge, Y., Hu, H., Chen, J., Wang, K., & He, Z. (2023). Hierarchical Energy Management of Networked Flexible Traction Substations for Efficient RBE and PV Energy Utilization within ERs. *IEEE Transactions on Sustainable Energy*.
- [3] Moustafa, A. M., Abdelghany, M. B., Younis, A. S. A., Moness, M., Al-Durra, A., & Guerrero, J. M. (2023). Software-defined control of an emulated hydrogen energy storage for energy internet ecosystems. *International Journal of Hydrogen Energy*.
- [4] Valverde, L., Rosa, F., Bordons, C., & Guerra, J. (2016). Energy management strategies in hydrogen smart-grids: A laboratory experience. *International Journal of Hydrogen Energy*, 41(31), 13715-13725.
- [5] Abdelghany, M. B., Al-Durra, A., Daming, Z., & Gao, F. (2024). Optimal multi-layer economical schedule for coordinated multiple mode operation of wind-solar microgrids with hybrid energy storage systems. *Journal of Power Sources*, 591, 233844.
- [6] Zou, B., Peng, J., Yin, R., Luo, Z., Song, J., Ma, T., ... & Yang, H. (2023). Energy management of the grid-connected residential photovoltaic-battery system using model predictive control coupled with dynamic programming. *Energy and Buildings*, 279, 112712.
- [7] Abdelghany, M. B., Mariani, V., Liuzza, D., Natale, O. R., & Glielmo, L. (2023). A unified control platform and architecture for the integration of wind-hydrogen systems into the grid. *IEEE Transactions on Automation Science and Engineering*.
- [8] Abdelghany, M. B., & Al-Durra, A. (2023, May). A coordinated model predictive control of grid-connected energy storage systems. In *2023 American Control Conference (ACC)* (pp. 1862-1867).
- [9] Bemporad, A., & Morari, M. (1999). Control of systems integrating logic, dynamics, and constraints. *Automatica*, 35(3), 407-427.
- [10] Garcia, C. E., Prett, D. M., & Morari, M. (1989). Model predictive control: Theory and practice—A survey. *Automatica*, 25(3), 335-348.

ICH2P14-OP098

ELECTRO-BIOMEMBRANE REACTOR FOR CONCURRENT HYDROGEN PRODUCTION AND DESALINATION

¹A. Faruk Kilicaslan, ^{1,2}A. Yagmur Goren, ¹Ibrahim Dincer, ³Ali Khalvati

¹Clean Energy Research Laboratory (CERL), Faculty of Engineering and Applied Science, Ontario Tech. University, 2000 Simcoe Street North, Oshawa, Ontario L1G 0C5, Canada

²Izmir Institute of Technology, Department of Environmental Engineering, Urla, Izmir, 35430, Türkiye

³Viona Consulting Inc., Agro-Environmental Innovation and Technology, Thornhill, Ontario, L3T 0C6, Canada

*Corresponding author e-mail: ahmet.kilicaslan@ontariotechu.net

ABSTRACT

This study has presented a novel reactor for producing both renewable bio-H₂ using poplar leaves and hydrogen from water electrolysis and water desalination simultaneously. The effects of voltage and CO₂ gas on hydrogen production rates were investigated, and the maximum hydrogen production rates were 18.86 mg/min for the dark fermentation chamber and 78.53 mg/min for the electrolysis chamber at an operating voltage of 8V with a total production rate of 97.39 mg/min in the electro-biomembrane reactor. The hydrogen production in the dark fermentation chamber was increased 1.2 times in the presence of CO₂ gas due to its positive effect on the growth of anaerobic microorganisms.

Keywords: Biohydrogen, Biomass, Electrolysis, Dark fermentation, Desalination.

INTRODUCTION

Fossil fuels continue to be a key energy source for countries with industrialized economies due to their low cost, benefits from storage, constancy, and higher energy content. [1]. However, the excessive usage of non-renewable fossil fuels causes significant global energy shortages and loss of biodiversity, which is the most important obstacle to achieving sustainable development of human society. Recently, the investigations on renewable green energy sources that can replace fossil fuels have become a global consensus [2]. Namely, many environmentally friendly and sustainable approaches can be considered to deal with the world energy challenge. Among these renewable energy sources, hydrogen energy stands out with its high energy density and carbon-free characteristics. There are various eco-friendly hydrogen production methods; among these methods, biohydrogen production technologies such as dark and photo fermentation and microbial electrolysis cell processes offer a relatively cost-effective and environmentally sustainable way to produce hydrogen compared to fossil fuel-based hydrogen production methods [3]. Although they have positive effects, low hydrogen production efficiencies reveal that these processes do not perform sufficiently when used alone and need to be developed to be commercialized. Therefore, this study aimed to develop a unique electro-biomembrane system for hydrogen production based on electrochemically driven dark fermentation with a naturally selected mixed culture of electrochemically active anaerobic microorganisms and water electrolysis. Furthermore, the desalination of saline water in the desalination chamber and the energy production with degradation of biomass by microorganisms were considered. In this context, the cylindrical hydrogen generator was designed to facilitate concurrent water and biomass-based hydrogen production, energy generation, and desalination to enhance the overall performance of the system considering sustainability. The capability of the generator to produce hydrogen from acid-treated poplar leaves and directly from water under different potentials and CO₂ concentration was evaluated.

MATERIALS AND METHODS

The electro-biomembrane reactor includes three cells made of plexiglass: dark fermentation, desalination, and electrolysis cells (10 cm × 15 cm × 10 cm each) with an operated volume of 2 L (Fig. 1). To ensure airtightness, cells were clamped together. Anode and desalination cells were separated by an anion exchange membrane (AEM, AMI-7001, Membrane International Inc., USA), and desalination and cathode cells were separated by a cation exchange membrane (CEM, CMI-7000, Membrane International Inc., USA). The anode and cathode electrodes are composed of flexible carbon graphite plates. Conductive copper wires were wound across the electrodes once 2 mm-diameter holes were punched into them. Dark fermentation cell included equal volumes of anaerobic-activated sludge from domestic wastewater treatment facility, and acid-treated poplar leaves hydrolysate as a biomass resource. 1 M potassium hydroxide (KOH) solution was utilized as the electrolyte solution in the electrolysis cell to enhance the desalination and current generation performance of the reactor and the hydrogen production. In the desalination chamber, the specified amount of sodium chloride (NaCl) solution was fed, and the desalination performance of the reactor was measured based on the conductivity of the solution in the

desalination cell. Finally, the produced hydrogen gas from the reactor was analyzed with an H₂ gas sensor. Moreover, a digital multimeter was used to record voltage in the open circuit, which is produced by microorganisms in dark fermentation cell.

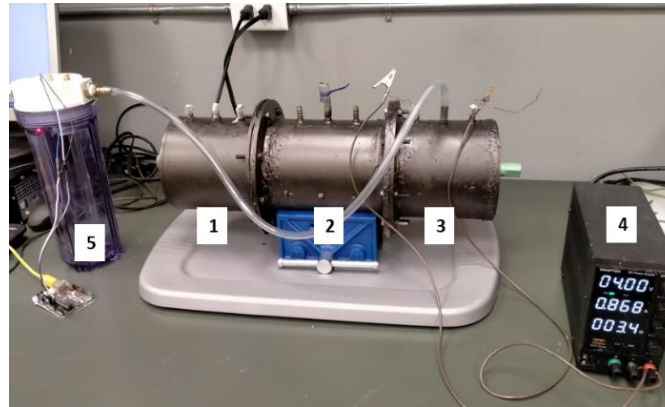


Fig. 1. Actual view of the electro-biomembrane reactor: 1: Anode chamber, 2: Desalination chamber, 3: Cathode chamber, 4: DC power supply, and 5: Hydrogen sensor.

RESULTS AND DISCUSSION

This study evaluated the hydrogen production performances in dark fermentation and electrolysis chambers at different voltage values (Fig. 2). In an electrochemically driven dark fermentation cell, the hydrogen production value is increased from 0.176 to 0.566 g/L with increasing voltage value from 2 to 8 V at operating time of 30 min. Similarly, the hydrogen production increased with the increasing voltage value in the electrolysis cell and provided the highest hydrogen production of 0.785 g/L at an operating voltage of 8 V and operational time of 10 min. Moreover, the hydrogen production rates of the chambers at different voltage values were calculated, and the highest values were 18.86 mg/min for the dark fermentation chamber and 78.53 mg/min for the electrolysis chamber at an operating voltage of 8V. Under the applied voltage of 8 V, the total hydrogen production rate of the electro-biomembrane reactor was 97.39 mg/min. In addition, the effect of CO₂ gas on hydrogen production efficiency in a dark fermentation chamber was investigated under 4 V potential. Our results revealed that the hydrogen production efficiency in the dark fermentation chamber was increased 1.2 times with the addition of CO₂ gas in the chamber since it directly affects microbial growth. Moreover, the desalination efficiency of the reactor was evaluated at 4 V considering its conductivity value, and the initial conductivity of the saline water was decreased from 7706 to 3778 $\mu\text{S}/\text{cm}$. This result proved that the reactor effectively reduced the salinity by approximately 51%. In addition, the initial amount of chemical oxygen demand was recorded as 1452.6 mg/L in the dark fermentation chamber. The final chemical oxygen demand (COD) level decreased to 358.7 mg/L, demonstrating a valuable COD removal efficiency of approximately 75%.

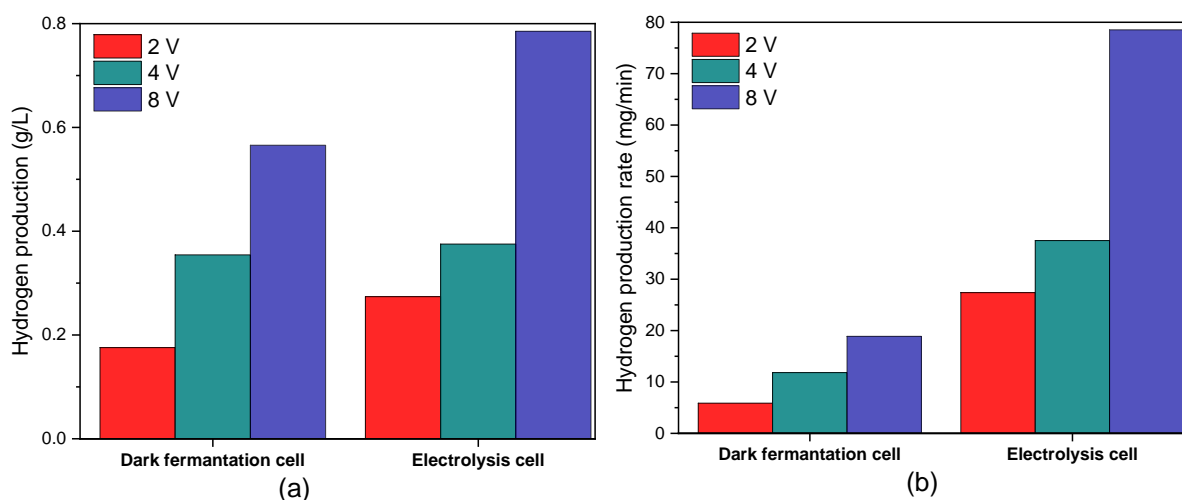


Fig. 2. Hydrogen production amount (a) and hydrogen production rate (b) of the electro-biomembrane reactor at different voltage values.

CONCLUSIONS

This study concerns the development of a novel reactor for producing both renewable bio-H₂ using poplar leaves and hydrogen from water electrolysis and water desalination simultaneously. The overall hydrogen production rate is obtained as 97.39 mg/min in the electro-biomembrane reactor at an operating voltage of 8V. Moreover, the desalination efficiency appears to be 51% at an operational time of 30 min under 4V. The results also prove that the hydrogen production in the dark fermentation chamber was increased in the presence of CO₂ gas. The results further reveal that this electro-biomembrane reactor provides promising benefits based on an environmentally friendly and sustainable point of view with effective hydrogen production and saline water desalination.

REFERENCES

1. Abbasi KR, Shahbaz M, Zhang J, Irfan M, Alvarado R. 2022. Analyze the environmental sustainability factors of China: The role of fossil fuel energy and renewable energy. *Renewable Energy* 187:390–402.
2. Deora PS, Verma Y, Muhal RA, Goswami C, Singh T. 2022. Biofuels: An alternative to conventional fuel and energy source. *Materials Today: Proceedings* 48:1178–84.
3. Goren AY, Dincer I, Khalvati A. 2023. A Comprehensive Review on Environmental and Economic Impacts of Hydrogen Production from Traditional and Cleaner Resources. *Jornal of Environmental Chemical Engineering* 111187.

ICH2P14-OP106

AN INTEGRATED LIFE CYCLE ASSESSMENT AND SUPPLY CHAIN ANALYSIS OF A MULTI-GENERATION SYSTEM FOR RENEWABLE CLEAN POWER AND GREEN HYDROGEN PRODUCTION

**Tahir Abdul Hussain Ratlamwala, Sheikh Muhammad Ali Haider, Khurram Kamal*

National University of Sciences and Technology, H-12, Islamabad, Pakistan

*Corresponding author e-mail: tahir.ratlamwala@pnec.nust.edu.pk

ABSTRACT

Energy crisis across the globe is leading towards an unstable future where the scarcity of energy shall create huge problems at domestic and commercial levels. The need of the hour is to develop and implement sustainable energy production methods which can overcome the crisis. With the depletion of fossil fuels, conventional power production methods are becoming outdated. Environmental crises such as carbon footprints and global warming pose a serious threat to the existence of mankind as well. In this alarming situation, renewable energy sources like biomass, solar, geothermal and wind energy can prove to be sustainable and reliable sources of energy generation with aided advantage of least carbon emissions. This research presents a biomass sourced multigeneration system which produces power and hydrogen as main outputs and cooling, heating, fresh water, and hot water as its by-products. The system consists of a Cogeneration Cycle, a Triple Effect Vapor Absorption Cycle, and a Double Flash Desalination Cycle. The thermal efficiency of the system is 33.36% while the energetic and exergetic efficiencies are 64.82% and 80.99%, respectively. The system produces 33 MW of power, 0.04037 kg of hydrogen per second, 4960 kW of cooling, 37274 kJ/s of space heating, and 34.99 kg/s of freshwater, respectively. Engineering Equation Solver (EES) is used to perform energy and exergy analyses. Multi-objective optimization of the system has also been carried out.

Keywords: Green Hydrogen, Clean Power, Renewable Energy, Multigeneration Systems, Sustainable Energy.

INTRODUCTION

The growing population in the World is causing a massive increase in demands of energy. With current population of 8 billion people, these numbers are expected to rise to 9.7 billion and 10.4 billion in 2050 and in mid-2080, respectively [1]. According to the Intergovernmental Panel on Climate Change (IPCC), the current practices of power generation are leading us towards a disastrous future [2]. With increasing global warming, researchers are focused on inventing new technologies for energy production. Renewable energy generation can prove to be a cutting-edge technology to overcome the increasing energy crisis [3,4]. Enhanced biomass systems, combining solar and biomass sources, demonstrate superior energy and exergy efficiencies compared to single-source systems. A study by Khalid et al found that the hybrid system achieved 66.5% energy efficiency and 39.7% exergy efficiency, surpassing biomass-only (64.5%, 37.6%) and solar-only (27.3%, 44.3%) configurations. Exergy destruction was highest in the combustion chamber (85 MW) [5]. A multigeneration system by Soltani et al, using sawdust as biomass fuel, achieved 60% energy efficiency and 25% exergy efficiency for all outputs, with 3535 kW electricity, 1124 kW heating load, and 29.41 kg/s hot water. Adding more heat recovery units did not affect system efficiency [6].

This study introduces an innovative multigeneration system fuelled by biomass, consisting of three subsystems: (a) Cogeneration Cycle, producing power and hydrogen for domestic, commercial, and fuel cell applications, (b) a triple effect vapor absorption cycle for cooling in hot, humid regions, and (c) a double flash desalination cycle, generating fresh and hot water. The research employs a comprehensive approach, utilizing mathematical modeling, parameter optimization, and exergy analysis for all subsystems. Thermal and exergetic analysis is conducted using the Engineering Equation Solver (EES) software, including an assessment of exergy destruction within the system.

SYSTEM DESCRIPTION

This proposed multigeneration system comprises of integrated power cycle, cooling cycle, desalination cycle and hydrogen production unit. A cogeneration cycle is used as a power cycle, triple effect vapour

absorption cycle as cooling cycle and double flash desalination cycle as freshwater production cycle. The primary products of the proposed system are power and green hydrogen. The by-products include cooling, space heating, freshwater and hot water. The source is rice straw, which is burnt in a biomass combustion chamber to produce high temperature gas which in turn exchanges heat with the cycle fluid of the power cycle. A fraction of the power produced by the cogeneration cycle is utilized to produce hydrogen gas by integrating a PEM electrolyzer with the low low-pressure turbine (LPT). The temperature and pressure at the boiler exit as supposed to be 1500 K and 20 MPa, respectively.

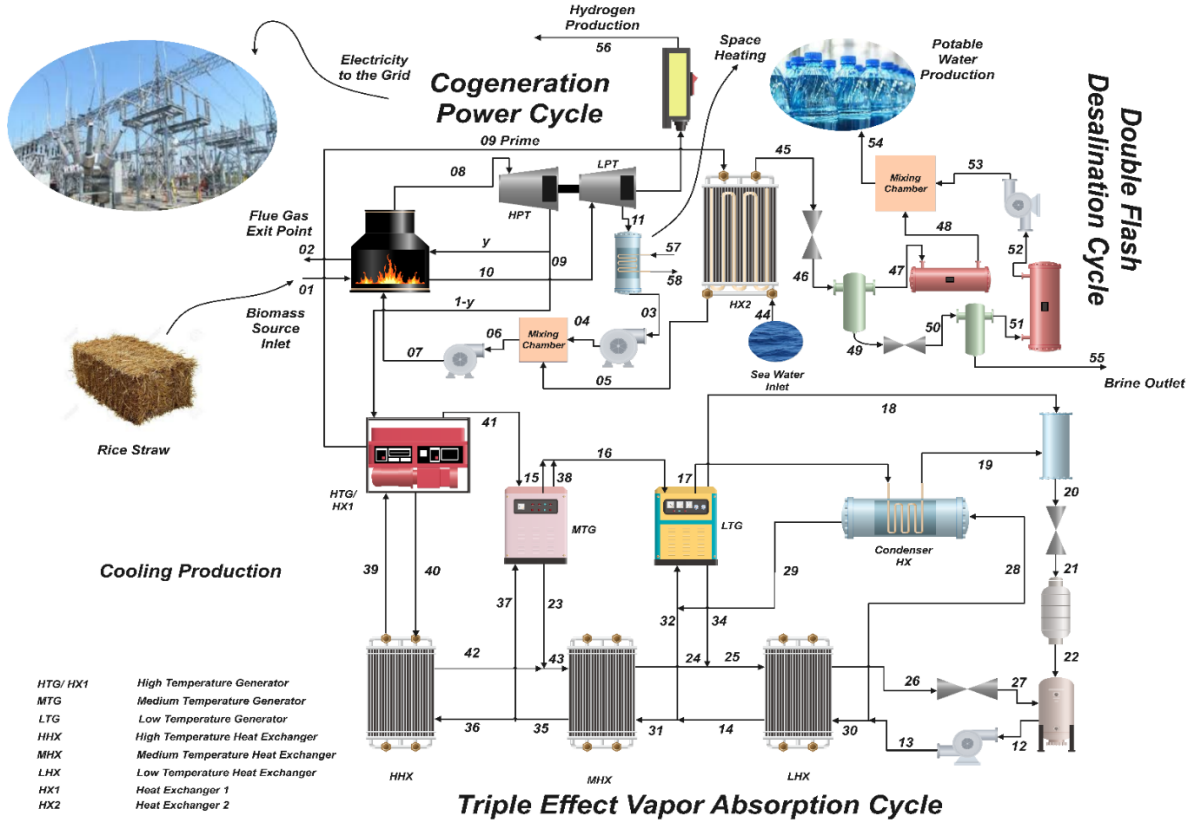


Figure 1: System Drawing of the Proposed Biomass Fed Multigeneration System

ANALYSIS

Equation 1, 2 and 3 are used to calculate energy efficiency, exergy efficiency, and exergy destruction of the system, respectively.

$$\eta_{en,sys} = \frac{\dot{W}_{net} + (\dot{m}_{54} \times h_{54}) + \dot{Q}_{eva} + \dot{m}_{57} \times (h_{58} - h_{57})}{\dot{Q}_{in} + \dot{W}_{pump}} \quad (1)$$

$$\eta_{ex,sys} = \frac{\dot{W}_{net} + \left(1 - \frac{T_0}{T_{11}}\right) \times \dot{Q}_{con} + \left(1 - \frac{T_0}{T_{21}}\right) \times \dot{Q}_{eva} + \dot{m}_{54} \times ex_{54}}{\left(1 - \frac{T_0}{T_1}\right) \times \dot{Q}_{in} + \dot{W}_{pump}} \quad (2)$$

$$\begin{aligned} & \left(1 - \frac{T_0}{T_1}\right) \times \dot{Q}_{in} + \dot{W}_{pump} + \dot{m}_{54} ex_{54} + \left(1 - \frac{T_0}{T_{26}}\right) \dot{Q}_{eva} \\ & = \dot{m}_2 ex_2 + \dot{W}_{turbine} + \dot{m}_{53} ex_{53} + \left(1 - \frac{T_0}{T_{20}}\right) * \dot{Q}_{cond} + \left(1 - \frac{T_0}{T_{11}}\right) * \dot{Q}_{con} \\ & + \dot{E}x_{des.sys} \end{aligned} \quad (3)$$

RESULTS AND DISCUSSION

The relation between biomass mass flow rate and net work output is demonstrated in Figure 2a. When a greater amount of biomass is burnt in the combustion chamber, it increases the energy input to the system

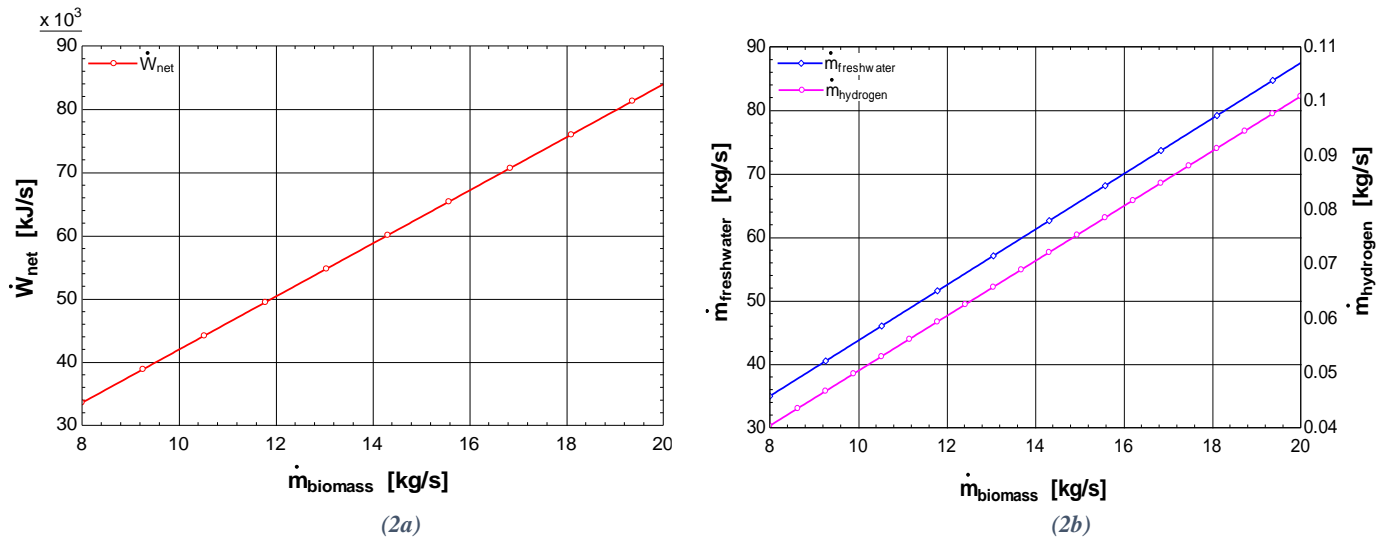


Figure 2: Effect of Biomass Mass Flow Rate (2a) Net Work Output (2b) Hydrogen and Freshwater Production

[7]. This increased biomass flow rate resultantly increases energy efficiency of the system which leads to greater power production in the multigeneration systems [8]. An increase in biomass mass flow rate also enhances exergy efficiency thus increasing useful energy available to do work, which in turn affects power production in a positive manner. PEM electrolyzer being directly attached to the LPT also works more efficiently when power production increases thus increasing the hydrogen production at a significant rate.

CONCLUSIONS

This study proposes a novel multigeneration system sourced by biomass source rice straw which produces power and hydrogen as its main outputs. The by-products of this system include cooling, space heating, freshwater and hot water which are also produced at a significant rate. The energy and exergy (2E) analyses have been carried out. The system produces 33 MW of electric power with producing hydrogen at a rate of 0.04037 kg/s. The cooling produced by the system is 4960 kW and space heating is 37274 kW. The fresh water is produced a rate of 34.99 kg/s at a significant temperature of 313 K, due to which a fraction of it can be used as hot water. The energy efficiency of the system is 64.82% while the exergy efficiency is 80.99%. The exergy destroyed by the system was found to be 8748 kW. Major exergy destruction areas have also been identified. The combustion chamber displayed highest exergy destruction of 21021 kJ/s among all the components indicating a significant amount of entropy generation.

REFERENCES

1. <https://www.un.org/en/global-issues/population>. Accessed on October 18, 2023.
2. <https://unfoundation.org/> Accessed on October 18, 2023.
3. <https://www.ipcc.ch/report/ar5/wg1/> Accessed on October 18, 2023.
4. Cengel, Y.A.; Boles, M.A. Thermodynamics: An Engineering Approach 4th Edition in SI Units; McGraw-Hill: Singapore, 2002.
5. F. Khalid, I. Dincer, and M. A. Rosen, "Energy and exergy analyses of a solar-biomass integrated cycle for multigeneration," Solar Energy, vol. 112, pp. 290–299.
6. R. Soltani, I. Dincer, and M. A. Rosen, "Thermodynamic analysis of a novel multigeneration energy system based on heat recovery from a biomass CHP cycle," Applied Thermal Engineering, vol. 89, pp. 90–100.
7. I. Dincer, C. Zamfirescu, Advanced Power Generation Systems, Elsevier, 2014.
8. T.A.H. Ratlamwala, I. Dincer. Comprehensive Energy Systems, Elsevier, 2018.

ICH2P14-OP110

DEVELOPMENT OF A HYBRID POWERING SYSTEM WITH AMMONIA FUEL CELLS AND INTERNAL COMBUSTION ENGINE FOR SUBMARINES

¹Ibrahim Akgun, ^{1,2}Ibrahim Dincer

¹Mechanical Engineering Department, Yildiz Technical University, Istanbul, 34349, Turkey

²Clean Energy Research Laboratory, Ontario Tech. University, Oshawa, Ontario, L1G 0C5, Canada

*Corresponding author e-mail: iakgun@yildiz.edu.tr

ABSTRACT

To overcome the limitations of current hydrogen storage technologies in submarines, this paper proposes a novel, integrated system that utilizes ammonia as a fuel source. The system combines Direct Ammonia Fuel Cell (DAFC) and Internal Combustion Engine (ICE) technology to generate power, freshwater, and cooling. The system is designed to recover waste heat and utilize it efficiently to produce power, freshwater, and cooling. The study aims to evaluate the performance of the system using thermodynamic energy and exergy analysis tools and conduct a parametric study to investigate the impact of varying system parameters and operating conditions on system efficiency. The proposed integrated system can produce 4,069 kW of net power, provide 5.895 kW of cooling, and generate 1.269 kg/s of freshwater under specified conditions. The energy and exergy efficiencies of the system are 33.96% and 39.39%, respectively.

Keywords: Ammonia, Hydrogen, Submarine, Exergy, Direct Ammonia Fuel Cell.

INTRODUCTION

Submarines play a crucial role in naval warfare. Propulsion and stealth are vital for military success, and conventional submarines rely on internal combustion engines for both. However, engines require air and are vulnerable to detection near the surface. To overcome this limitation, Air Independent Propulsion (AIP) systems were developed, which do not require air. AIP systems suffer from low power outputs, limiting speed and mobility. Increasing AIP power would require reducing conventional diesel power and battery storage. The right balance must be established in the design of submarine power systems [1]. Different nations have AIP submarines in operation, including closed-cycle diesel engines, closed-cycle steam turbines, Stirling cycle engines, fuel cell systems, and nuclear power systems [2]. Academic studies on these systems have been extensively researched in the literature from various perspectives. Nikiforov and Chigarev [3] examined hydrogen storage and generation for FC-based power plants in submarines, concluding that hydrolysis of aluminium in the submarine is a favourable method for hydrogen generation. Han et al. [4] conducted a study on a PEM fuel cell stack for underwater vehicle propulsion. Ammonia has a higher volumetric density and energy density than hydrogen, is cost-effective, and has a strong smell for easy leak detection. Both fuel combustion and fuel cell technologies can generate power using ammonia fuel. Siddiqui and Dincer introduced an innovative combined FC-ICE system driven by ammonia, which recovers waste heat for both energy and cooling purposes. Their system's overall energy efficiency is 59.9%, and its exergy efficiency is 51.9% [5]. The primary goal of this research is to develop a new ammonia-based AIP system that merges DAFC and ICE technology for production of power, freshwater, and cooling. Furthermore, the study aims to evaluate the performance of this system using thermodynamic energy and exergy analysis tools, and to conduct a parametric study to investigate the impact of varying operating conditions on the system efficiency.

ANALYSIS

The proposed system is analysed thermodynamically to identify the mass flow rates, enthalpies, pressures, and temperatures of flows entering and exiting the system. The exergy destruction rate is determined to locate irreversible losses within each component of the system. The modelling is done using the EES software under specific assumptions:

- The reference state at $T_0 = 25\text{ °C}$ and $P_0 = 101\text{ kPa}$.
- Adiabatic operation is assumed for all pumps and turbines, and the isentropic efficiency of the pumps and turbines is taken as 90%, with negligible pressure losses in the heat exchangers.
- The heat losses in the ICE are assumed to be 30% to the cooling system, 30% in the exhaust gases, and 10% in the friction and oil heating, and 30% of the heat produced is converted to work.

The balance equations, particularly those for mass, energy, entropy, and exergy, which are applied to each component of the overall system are presented in Eq. (1), (2), (3) and (4) respectively:

$$\sum \dot{m}_{in} = \sum \dot{m}_{out} \quad (1)$$

$$\dot{m}_{in} h_{in} + \dot{Q}_{in} + \dot{W}_{in} = \dot{m}_{out} h_{out} + \dot{Q}_{out} + \dot{W}_{out} \quad (2)$$

$$\dot{m}_{in} s_{in} + \frac{\dot{Q}_{in}}{T_s} + \dot{S}_{gen} = \dot{m}_{out} s_{out} + \frac{\dot{Q}_{out}}{T_b} \quad (3)$$

$$\dot{m}_{in} ex_{in} + \dot{E}x_{in}^{Q} + \dot{W}_{in} = \dot{m}_{out} ex_{out} + \dot{E}x_{out}^{Q} + \dot{W}_{out} + \dot{E}x_d \quad (4)$$

The parameters employed in the examination of the ammonia-hydrogen fuelled ICE are listed in Table 1. The combustion equations of ammonia and hydrogen in ICE are respectively Eq. (5) and (6):

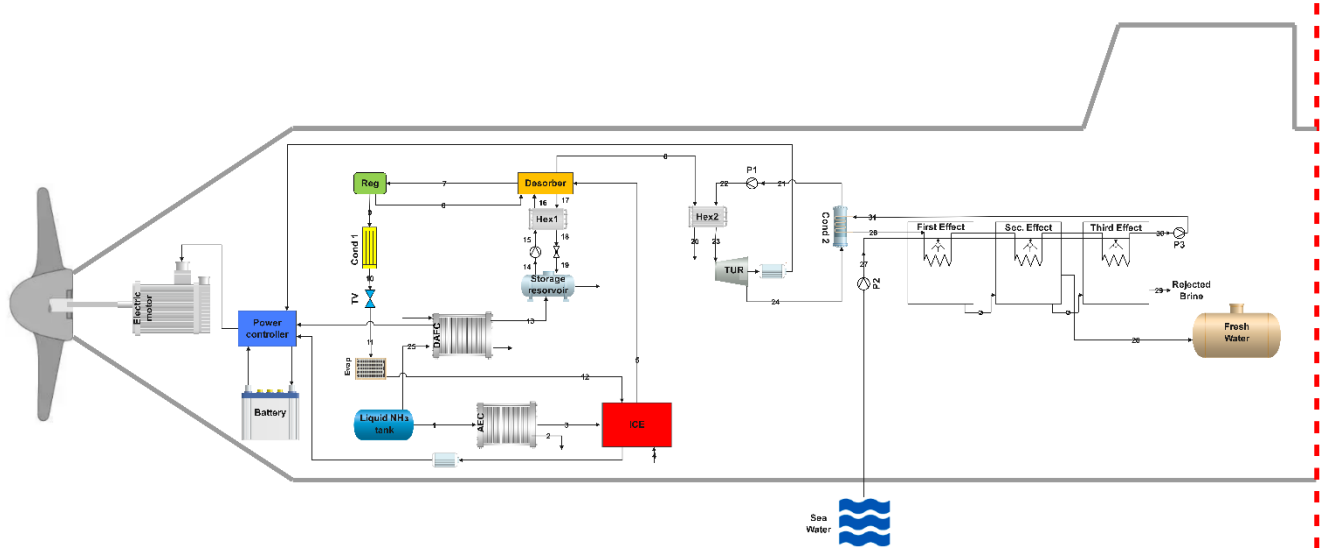


Fig. 1. Schematic view of the integrated system proposed for air independent propulsion system.

Table 1. Design parameters used for ICE [6].

Internal Combustion Engine	
Parameter	Value
ICE Operating pressure	250 kPa
Hydrogen mass fraction	1%
Stoichiometric O ₂ and N ₂ -to-fuel ratio	Ammonia: 6.06 (kg /kg)
	Hydrogen: 34.2 (kg /kg)
Auto ignition temperature	Ammonia: 651 °C
	Hydrogen: 571 °C
Lower heating value	Ammonia: 18.8 MJ/kg
	Hydrogen: 120 MJ/kg

Table 2. Design parameters used for AEC [7].

Ammonia Electrolyte Cell	
Parameter	Value
Ammonia input pressure	870 kPa
Ammonia input temperature	20 °C
Electrolyte thickness	0.0040 cm
Cathode thickness	0.0020 cm
Anode thickness	0.0020 cm
Operating pressure	250 kPa
Operating temperature	25 °C
Cell area	1 m ²
Current density	2,500 A/m ²
Exchange current density	0.37 A/m ²

The overall energetic and exergetic efficiencies of the system are determined by

$$\eta_{en,ovr} = \frac{\dot{W}_{net} + \dot{Q}_{Evap} + \dot{Q}_{PF} + \dot{m}_{fw} \times h_{fw}}{\dot{m}_{NH_3} LHV_{NH_3} + \dot{m}_{sw} \times h_{sw} + \dot{W}_{AEC}} \quad (7)$$

$$\eta_{ex,ovr} = \frac{\dot{W}_{net} + \dot{Q}_{Evap} \left(1 - \frac{T_0}{T_{Evap}}\right) + \dot{m}_{fw} \times ex_{fw}}{\dot{m}_{NH_3} ex_{NH_3} + \dot{m}_{sw} \times ex_{sw} + \dot{W}_{AEC}} \quad (8)$$

where \dot{W}_{net} is net power produced by the proposed system and is calculated as

$$\dot{W}_{net} = \dot{W}_{ICE} + \dot{W}_{DAFC} + \dot{W}_{TUR} - \dot{W}_{Pump1} - \dot{W}_{Pump2} - \dot{W}_{Pump3}$$

RESULTS AND DISCUSSION

A parametric study was conducted to evaluate the performance of the integrated system, taking into account the first and second laws of thermodynamics. The study examined the impact of varying the mass flow rate of ammonia supplied to the internal combustion engine, the steam flow rate of the Rankine cycle, and the effect of changing the ambient temperature on system performance. Fig. 2a and 2b show the effect of temperature on the system's energy and exergy efficiencies and net power output. As the temperature increases from -10 to 50°C, the energy efficiency improves from 32.11 to 35.27%, exergy efficiency increases from 36.44 to 41.56%, and the net power output grows from 3,835 to 4,235 kW.

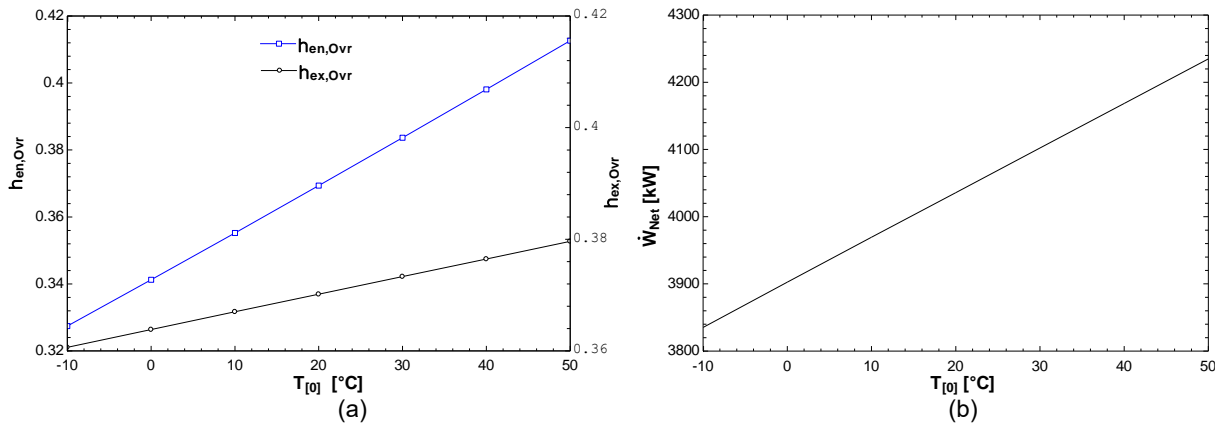


Fig. 2. Variation of the ambient temperature with (a) overall energy and exergy efficiencies, (b) net power generated.

Fig. 3a shows the impact of modifying the ammonia mass flow rate on the overall system energy and exergy efficiency. It indicates that increasing the flow rate from 0.2 kg/s to 2 kg/s results in a significant improvement in both energy and exergy efficiencies. Fig. 3b shows how the power generated by the internal combustion engine varies with the ammonia flow rate. As the flow rate increases from 0.2 kg/s to 2 kg/s, the power output of the engine rises from 3,065 kW to 4,715 kW, and the net power output increases from 3,883 kW to 5,532 kW.

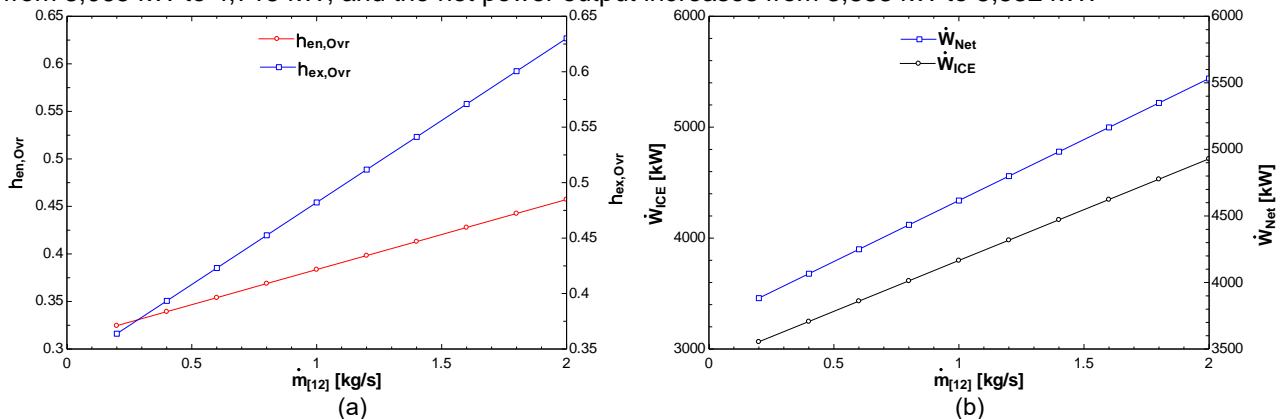


Fig. 3. Variation of the ammonia flow rate with (a) overall energy and exergy efficiencies, (b) ICE and net output power.

CONCLUSIONS

The following are the main conclusions drawn from the proposed integrated system for submarines: (a) The net power produced, cooling provided, and freshwater flow rate produced under specified conditions are 4,069 kW, 5.895 kW, and 1.269 kg/s, respectively. (b) The energy efficiency and exergy efficiency of the system are calculated to be 33.96% and 39.39%, respectively.

REFERENCES

- [1] D. Andrews, *Submarine Design*. John Wiley & Sons, 2017.
- [2] R. R. Menon, R. Vijayakumar, and J. K. Pandey, "Selection of Optimal Air Independent Propulsion System using Forced Decision Matrix," *Def. Sci. J.*, vol. 70, no. 1, pp. 103–109, 2020, doi: <https://doi.org/10.14429/dsj.70.13678>.
- [3] B. V. Nikiforov and A. V. Chigarev, "Problems of designing fuel cell power plants for submarines," *Int. J. Hydrogen Energy*, 2010, doi: 10.1016/j.ijhydene.2010.06.117.
- [4] I. Han, B. Kho, and S. Cho, "Development of a polymer electrolyte membrane fuel cell stack for an underwater vehicle," *J. Power Sources*, vol. 304, pp. 244–254, 2016, doi: 10.1016/j.jpowsour.2015.11.049.
- [5] O. Siddiqui and I. Dincer, "Development and Assessment of a Novel Integrated System Using an Ammonia Internal Combustion Engine and Fuel Cells for Cogeneration Purposes," *Energy Fuels*, vol. 33, no. 3, pp. 2413–2425, 2019, doi: 10.1021/acs.energyfuels.8b04323.
- [6] C. S. Mørch, A. Bjerre, M. P. Gøttrup, S. C. Sorenson, and J. Schramm, "Ammonia / hydrogen mixtures in an SI-engine : Engine performance and analysis of a proposed fuel system," *Fuel*, 2011, doi: 10.1016/j.fuel.2010.09.042.
- [7] F. Mulder, "Electrolytic Cell for the Production of Ammonia," 2014.

ICH2P14-OP111

AN INTEGRATED SOLAR-DRIVEN CHLOR-ALKALI SYSTEM FOR HYDROGEN AND CHLORINE PRODUCTION

^{*2,3}Sümeyya Ayça, ^{1,2}Ibrahim Dincer¹Ontario Tech University, Clean Energy Research Laboratory, Oshawa, Ontario, Canada²Yildiz Technical University, Department of Mechanical Engineering, Istanbul, Turkey³Istanbul Health and Technology University, Faculty of Engineering and Applied Science, Sutluce, Istanbul, Türkiye

*Corresponding author e-mail: smyayca@gmail.com

ABSTRACT

This paper deals with a review of the chlor-alkali process, an industrial application with significant promise for hydrogen production. In this process, the 2.6 MWh of power required for the operation of the system is met by an ingenious approach using a photovoltaic-based energy system. The research includes a comprehensive simulation of a chlor-alkali production system with the operating temperature set to 88°C using the Aspen Plus. The results demonstrate the remarkable potential of this system with a hydrogen production rate of 82.5 kg/h.

Keywords: Hydrogen, hydrogen production, chlor-alkali process, photovoltaic-based energy system.

INTRODUCTION

The chlor-alkali process, primarily responsible for the production of chlorine, sodium hydroxide (commonly referred to as caustic soda), and hydrogen, exemplifies an efficient and environmentally sustainable industrial procedure. This method, which boasts numerous advantages for hydrogen generation, operates as an electrolysis-based process involving anode and cathode reactions, ultimately yielding chlorine (Cl₂), sodium hydroxide (NaOH), and hydrogen gas (H₂). Notably, the generation of hydrogen stands as a valuable byproduct in conjunction with the production of hydrogen, chlorine, and sodium hydroxide. A plethora of environmentally friendly and highly efficient energy systems may be selected as the energy source for such processes. In a study conducted by Wang et al., they fulfilled the energy requirements of the system through a combination of wind, solar, and fuel cell technologies [3]. Pravin et al., also proposed a similar hybrid system in their study. A review of the existing literature reveals that the endeavor to meet the power needs commonly involves the utilization of multiple energy sources [2]. In this study, however, solar energy, a singular source, is employed. The power requirements of the system are satisfied by harnessing solar energy, which stands as a more abundant resource compared to other alternatives. The strategic placement of photovoltaic systems, essential for enhancing sustainability in energy production, is instrumental in achieving significant advantages in terms of energy efficiency. This endeavor commences with the harnessing of solar energy through photovoltaic panels, ensuring the efficient capture of solar radiation. Subsequently, this solar energy undergoes conversion into electrical energy, thereby serving as the primary energy source for chlor-alkali electrolysis. The envisioned end products in this system encompass chlorine gas, sodium hydroxide, and hydrogen gas.

SYSTEM AND ASSESSMENT

The schematic representation of the proposed system is shown in Figure 1. In this system, sodium chloride (NaCl) and hydrochloric acid (HCl) solutions are selected for the product feed. The purified brine is acidified with HCl before entering the electrolysis process. As shown in Figure 1, a photovoltaic system was selected to fulfill the energy requirement of the system. In this solar energy utilisation system supported by solar panels, heat transfer is provided from the segment designated as PV through the S6 line. This method is necessary to provide the power required for the operation of chlor-alkali production plants. The product is then fed into the Stoichiometric reactor, which acts as an anode. In this reactor, chloride ions (Cl⁻) are transformed into chlorine gas (Cl₂) and reactions for the production of water (H₂O) and oxygen (O₂) are defined. Subsequently, Cl₂ output takes place in the Gibbs reactor, the so-called anolyte, where the production of Cl₂ gas takes place. After this process, other products enter the membrane as separators, allowing sodium ions (Na⁺) to pass through the membrane. Na⁺ ions leaving the membrane acting as a separator, where the separation of sodium chloride (NaCl) and Na⁺ ions takes place, enter the Stoichiometric reactor acting as a cathode. Here the H₂O component is separated into hydrogen gas (H₂) and hydroxide ions (OH⁻). Then, OH⁻ ions are separated in the membrane acting as a separator and cyclically return to the system and enter the Stoichiometric reactor acting as an anode. This process step is important for the system. Following the feedback process, the remaining products are separated by Flash, which undergoes a Split process, resulting in the extraction of H₂. Following the extraction of H₂, sodium hydroxide (NaOH) is obtained by a Split procedure. The remaining products are then re-introduced into the system. During the re-feed process, water is introduced into the Mixer and H₂ production is restarted by reintroducing all products into the cathode. In this study establishes an optimal applied current density within the chlor-alkali plant, falling within the defined range of 6x10⁵ to 7x10⁵ A/m². Concurrently, the voltage parameters

are ascertained to be within the range of 2-3 V. A comprehensive review of pertinent literature, encompassing both experimental and numerical inquiries, reveals that the identified current density and voltage values align satisfactorily with the stipulated requirements for the system's power demand.

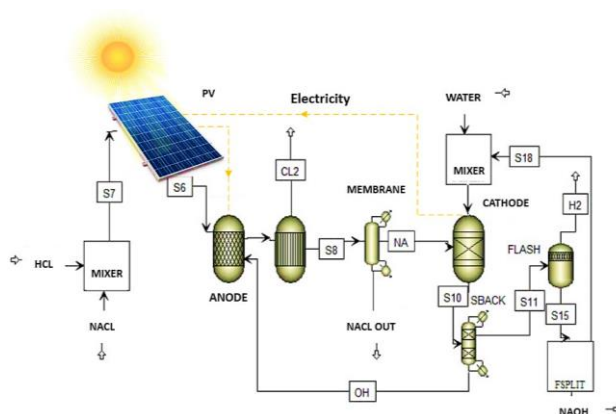


Figure 1. Schematic representation of the system.

RESULTS AND DISCUSSION

This section presents the results obtained in this study. The quantities of HCl and NaCl components introduced into the system were set at 0.0272 kg/h and 111.612 kg/h, respectively, based on the data acquired through the literature review. The operating temperature of 88 °C was determined using the energy supply line from the PV section, which is the system's energy source. This temperature was chosen as it was found to be suitable for the chlor-alkali production industry according to the results of the literature review. As depicted in Figure 2, the Cl₂ gas produced from the Gibbs reactor, functioning as the anolyte, amounted to 64.97 kg/h. Furthermore, the production of Na ions in the membrane section was measured at 43.90 kg/h. When considering the products obtained in this section, a total of 780 kg/h of water and other products were generated. In accordance with the cathode process, hydrogen production is achieved through the introduction of Na into the reactor and the re-entry of all products from the feedback. Figure 2. illustrates the production of 82.5 kg/h of hydrogen. Additionally, another product of the system, the NaOH component, was obtained at a rate of 47.56 kg/h.

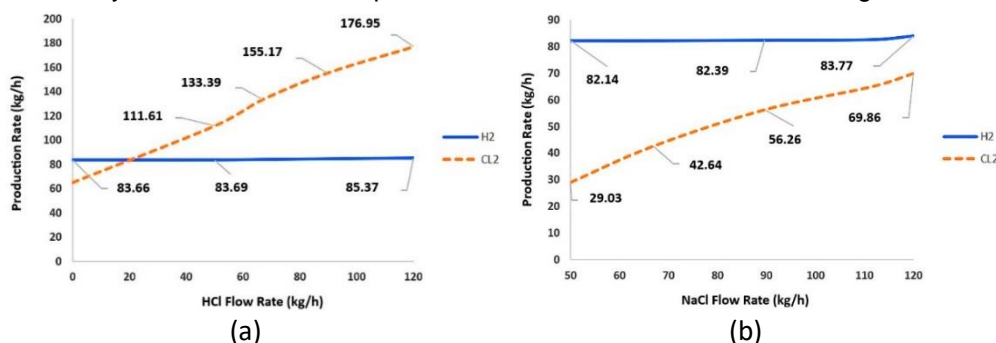


Figure 2. Graphical representation of a) hydrogen b) chloride products produced by NaCl and HCl feeding.

CONCLUSIONS

In this study, hydrogen and chlorine productions through an integrated chlor-alkali system are investigated as a clean and reliable energy production method where the photovoltaic panel systems in an innovative approach for energy production were combined. For the efficient operation of the system, the temperature value was determined as 88°C with the panels integrated into the system. With the feedbacks made, the system has been made to work more efficiently. When we look at the products obtained as a result, the hydrogen yield was recorded as 82.5 kg/h.

REFERENCES

- O'Brien, T. F.; Bommaraju, T. V.; Hine, F. Handbook of Chlor-Alkali Technology; Springer, 2005.
- Erdemir, D., Dinçer, I.; A new solar energy-based system integrated with hydrogen storage and heat recovery for sustainable community. Sustainable Energy Technologies and Assessments. 2022. doi.org/10.1016/j.seta.2022.102355
- Pravin, P.S., Luo, Z., Li, L., Wang, X.,; Learning-based scheduling of industrial hybrid renewable energy systems. Computers & Chemical Engineering. 2022. doi.org/10.1016/j.compchemeng.2022.107665



4. Wang, X., Teichgraeber, H., Palazaoğlu, A., El-Farra, N.; An economic receding horizon optimization approach for energy management in the chlor-alkali process with hybrid renewable energy generation. Journal of Process Control. 2014. doi.org/10.1016/j.jprocont.2014.04.017

ICH2P14-OP112

INFLUENCE OF HYDROGEN UPTAKE ON ADDITIVELY MANUFACTURED AND CONVENTIONAL AUSTENITIC STAINLESS STEELS 316L*¹Qingyang Liu, ¹Sumia Manzoor, ¹Mohammad Tariq, ¹Hanan Farhat, ¹Afroz Barnoush*¹Hamad Bin Khalifa University, Qatar Environment and Energy Research Institute, Corrosion Center, Doha, Qatar

*Corresponding author e-mail: qliu@hbku.edu.qa

ABSTRACT

With increased energy demand in the present-day world, a strong driving force prevails in the transition from existing fossil fuel-based economy to a circular and sustainable renewable energy-based economy. In this context, hydrogen is regarded to play one of the most significant roles in achieving a carbon-neutral society. However, this also poses several major challenges raised by hydrogen-induced metal/alloy degradation during the generation, transportation, and storage of hydrogen.

Additive manufacturing is a promising means of production of austenitic stainless-steel parts for hydrogen service. The hydrogen embrittlement resistance of SS 316L parts by conventionally manufactured and directed energy deposition was examined using tensile testing. For this study, an attempt is made to understand the effect of hydrogen on additively manufactured 316L SS and compare it with conventionally manufactured 316L samples. Therefore, electrochemical hydrogen charging was performed on both AM and CM 316L samples to achieve a comparable hydrogen content in the samples, which were further measured by Thermal Desorption Spectroscopy. A combination of surface characterization techniques; SEM, EDX, XRD, and EBSD are deployed to accurately characterize and gain an improved understanding of the hydrogen embrittlement mechanism in CM and AM stainless steel. The higher presence of hydrogen reduced ductility in the as-built AM sample but did not significantly influence the response in CM materials. Hydrogen-charged samples exhibited a large area of brittle fracture mode, while hydrogen-free samples showed ductile fracture morphology.

Keywords: Additive manufacturing, Hydrogen uptake, Hydrogen embrittlement**Abbreviation:**

AM: Additive manufacturing

SS: stainless steel

SEM: scanning electron microscopy

EBSD: Electron backscatter diffraction

CM: conventionally manufactured

DED: directed energy deposition

XRD: R-ray diffraction

EDX: Energy Dispersive X-ray Spectrometry

INTRODUCTION

In recent years, the hydrogen energy storage has drawn significant attention from government and researchers because hydrogen is one of the most promising green energy sources which has been considered as alternative of hydrocarbon fuels in the potential industrial sectors [1]. There are still some challenges regarding to hydrogen storage, and transportations given that the small size of hydrogen and its interaction with engineering materials [2].

Nowadays, additive manufacturing technology attracted more research interest due to design flexibility and topological optimization of material by tailoring the microstructure to provide the best performance in the hydrogen environments. AM provide great opportunity to meet the best combination of its structure, processing, performance and properties by optimizing the 3D printing parameters [3]. In other word, AM has the potential to accelerate the energy transition by enabling customized and sustainable production of hydrogen-resistant alloys.

However, there is limited understanding of the processing, structure, properties, and performance of AM alloys when interacting with hydrogen. In this paper, we systematically investigate the hydrogen embrittlement of AM and CM stainless steels to better understand the mechanisms of hydrogen interaction with storage materials.

MATERIALS AND METHODS

The materials used in this study were convectional manufacturing (CM) stainless steels 316 and DED additive manufacturing (AM) 316 due to its wide application in industrial area and the composition of SS 316 is provided in Table 3.

Prior of hydrogen charging, the specimens were ground to 1200 grit SiC papers and following with electropolishing with methanolic H₂SO₄ solutions at 25V for 35 seconds to remove the residual stress and contaminations on the surface [4]. Three-electrode configurations were used to perform the ex-situ hydrogen charging in a 2:1 glycerol and phosphoric acid mixture at 75°C under potentiostatic of -2000 mV to preserve a corrosion-free surface for further analysis. In order to study the hydrogen concentration as a function of time, different charging times of 24, 48, 72 and 96 hours were chosen. Tensile test was performed within a miniature module at strain rate of 2×10^{-4} s⁻¹ as shown in Figure 1(a). The Engineering stress and strain could be obtained by tensile test, and the hydrogen embrittlement index can be calculated by the loss of ductility. After the test, TDS (Bruker G4 PHONIX DH) test was performed to determine the global hydrogen content in the sample after hydrogen charging at a heating rate of 80 /min from 25 to 800°C, as shown in Figure 1 (b). X-ray diffraction was used to identify the microstructure phase on the sample before and after hydrogen charging, using monochromatic Co K α radiation ($\lambda = 1.789 \text{ \AA}$). The surface morphology of samples was investigated by SEM integrated with EBSD detectors.

Table 3 Composition of SS 316 (wt.%)

Elements	C	Mn	Si	P	N	Cr	Ni	Mo	Fe
SS 316	0.03	2.00	1.0	0.04	0.1	17.5	12.5	2.3	Bal.

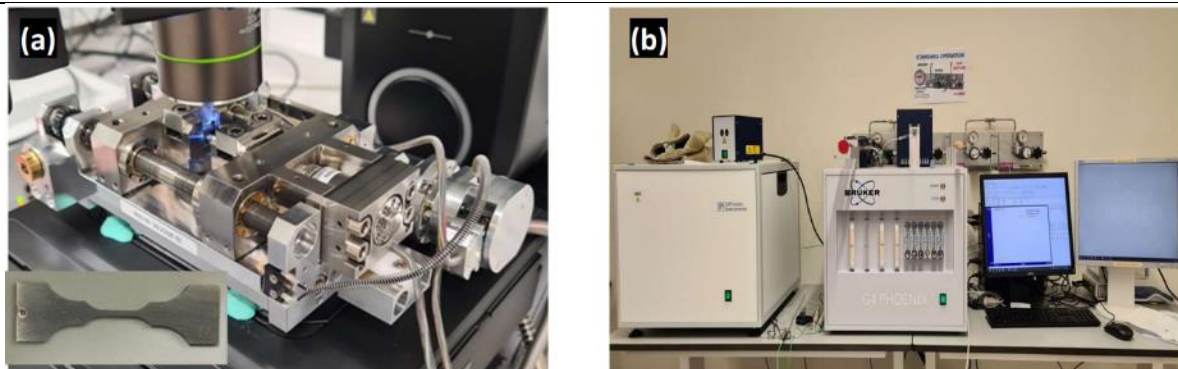


Figure 1 (a) Miniature tensile module under 3D microscopy and (b) thermal desorption spectroscopy.

RESULTS AND DISCUSSION

The surface observation was conducted by SEM and EBSD on both AM and CM samples, the Figure 2 shows the microstructure, inversed polar figure and misorientation angle by SEM and EBSD. As initial microstructure shown in Figure 2, austenite phase was shown on both AM & CM samples and the grain size of AM samples (about 50 μ m) is bigger than that of CM samples (around 10 μ m).

To investigate the potential effects of hydrogen influencing the microstructure or the phase of samples, we performed XRD test on H-free and 24-hour H-charged AM & CM samples, and the results were shown on Figure 3 (a). The XRD patterns of H-charged samples showed the similar peaks with the H-free samples for both AM & CM. The hydrogen concentration of the AM & CM samples after hydrogen charging for different time were plotted on Figure 3 (b). We found that more hydrogen has been absorbed into AM sample with the increase of hydrogen-charging time. For example, the hydrogen content in AM samples reached 250ppm after 96-hour hydrogen charging, while CM sample contained only 25ppm. Despite the larger grain size, the hydrogen solubility in AM 316L is higher than in the CM alloy.

Given the fact that the more hydrogen content in AM than CM samples, the next step is to investigate how the different hydrogen content influences the mechanical properties of alloys. We charged twin dogbone-like samples (shown in Figure 1 (a)) for 24 hours: took one sample into TDS right after hydrogen charging to measure the global hydrogen content and performed slow rate tensile test on another one. Figure 4 (a) showed the engineering stress and strain curve during tensile test until fracture. We found that both samples decreased their strength and ductility after hydrogen charging. AM samples were tested under

as-received condition without any heat treatments and always exhibited a lower ductility and high tensile strength than CM samples.

After the tensile test, we performed SEM to observe and compare the sub-surface of the cracks with and without hydrogen. From Figure 5, we can see some cracks on the H-free sample in Figure 5 (a) (d). And much more cracks were observed on the AM sample (Figure 5 b c) than that on CM sample (Figure 5 e f). From a magnified observation, we can see some isolated cracks on CM sample (Figure 5 f) at the grain boundaries. Compared the Hydrogen free and hydrogen charging sample, it clearly shows that hydrogen reduced the mechanical properties by introducing more cracks. It is important to know hydrogen content in the sample to conclude to what extent hydrogen affecting mechanical properties for both CM and AM samples. As shown in Figure 4 (b), we found 131 ppm hydrogen in AM samples before tensile test, which was almost 10 times higher than that in CM samples. The same trend was also found for the sample after tensile test. The hydrogen embrittlement index (HEI) was introduced to better evaluate the hydrogen embrittlement of samples by calculating the loss of ductility from stress-strain curve in Figure 4 (a). From Equation 1, the HEI is 21.2% and 9.3% for AM and CM samples respectively, which show good agreement with the result from hydrogen concentrations obtained from TDS shown in Figure 4 (b).

Compared with CM samples, more hydrogen was absorbed into AM sample with bigger grain-size and higher amount of misorientation angle in crystal. For AM samples, the higher strength and larger effect of hydrogen on mechanical properties are also surprisingly different than what is expected from the Hall-Petch effect. This anomaly can be related to the high number of small-angle grain boundaries as well as the high dislocation density formed during the additive manufacturing process, as can be seen in the average grain misorientation maps in Figure 2. This misorientation was due to the effect of linear defects (dislocations) within the grains. There are two types of dislocations in the steels: statistically stored dislocations and geometrically necessary dislocations (GNDs). This GNDs affected the hydrogen trapping behavior during hydrogen charging, resulting in hydrogen embrittlement and loss of mechanical properties.

$$HEI = \frac{\epsilon_0 - \epsilon_H}{\epsilon_0} \times 100\%$$

Equation 1

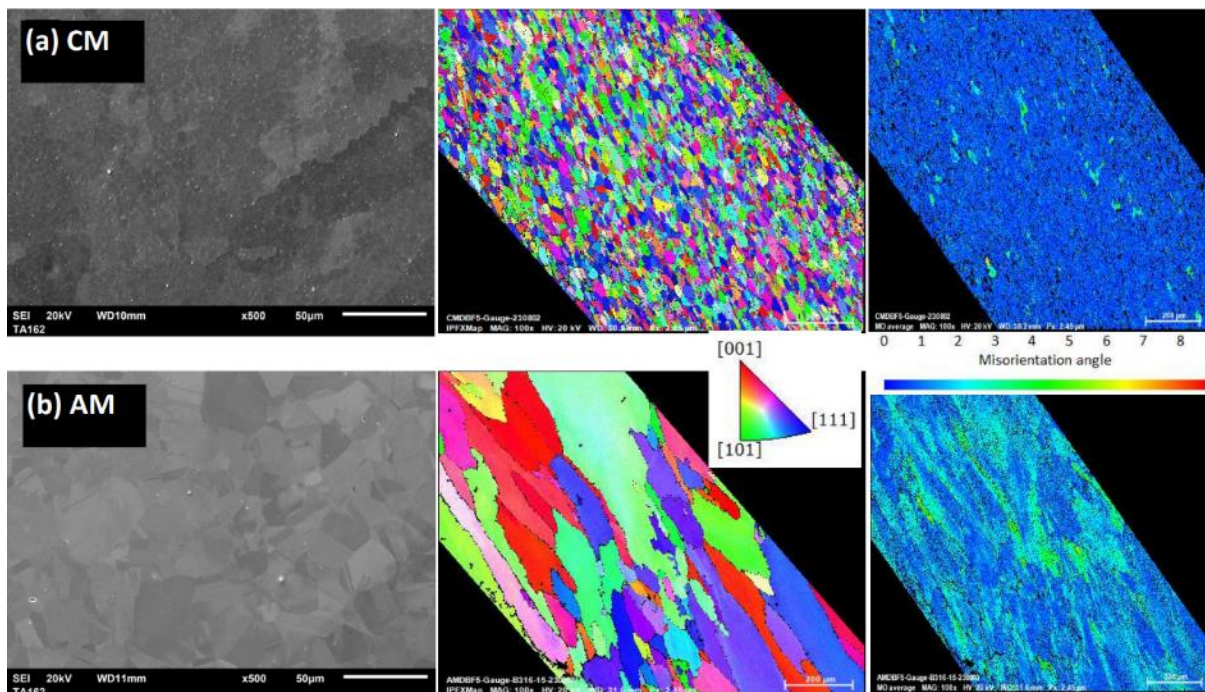


Figure 2 SEM surface observation, EBSD observation on IPF and misorientation angle of AM and CM samples.

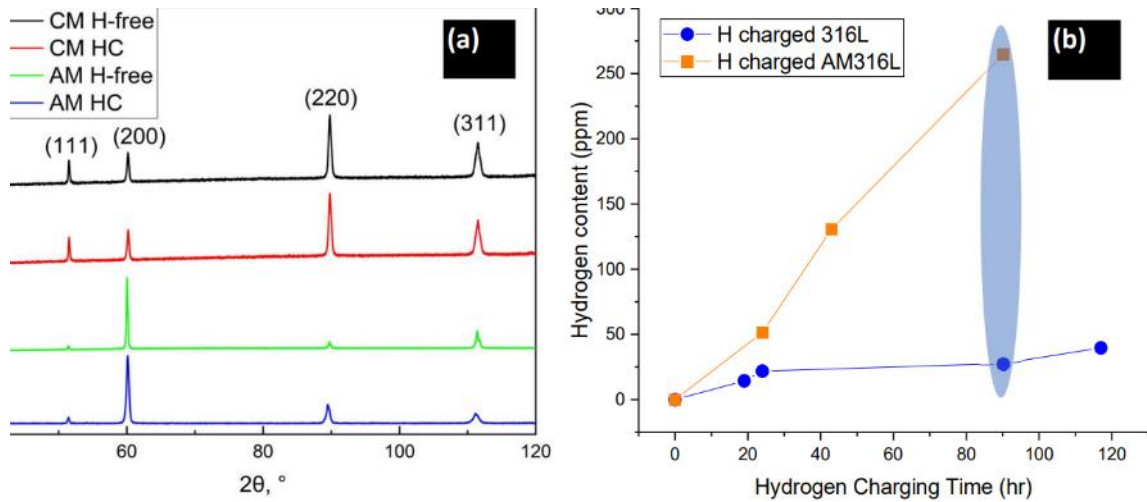


Figure 3 (a): XRD patterns and (b): TDS results after hydrogen charging at different time.

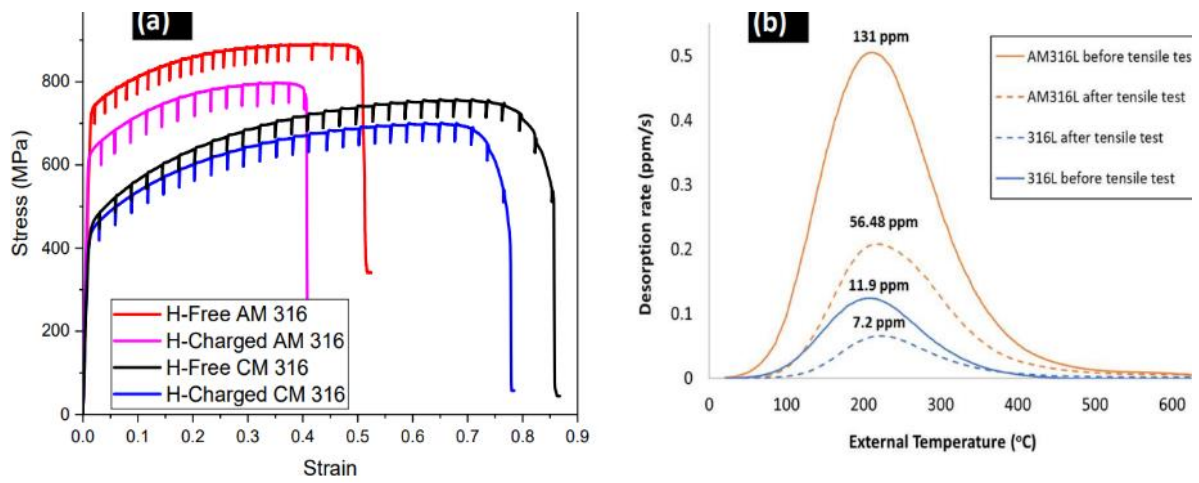


Figure 4: (a) Engineering stress -strain curve for H-free and 24-hour Hydrogen charging AM & CM samples and (b) TDS curves of Hydrogen-charged and hydrogen-free samples.

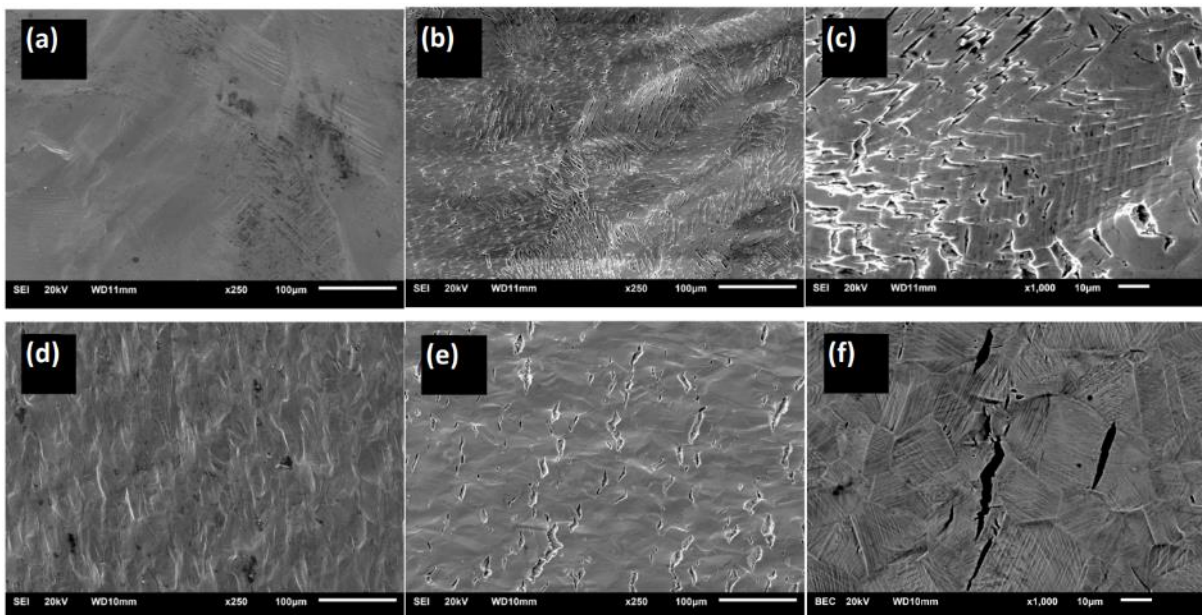


Figure 5: morphology of sub-crack surface of HF and 24-hour HC AM & CM samples, (a): HF AM, (b) HC AM, (c) enlarged HC AM, (d): HF CM, (e) HC CM, (f) enlarged HC CM, respectively.

CONCLUSIONS

We studied and compared the behaviour of DED-AM and conventional manufacturing 316L after electrochemical hydrogen charging. Here are the key conclusions from this study.

1. Increasing demand for hydrogen as an energy vector and the necessity for the safe handling of hydrogen requires the development of novel alloys with superior resistance to HE and AM is a promising manufacturing method to achieve this goal.
2. For the same hydrogen charging duration, the AM alloy absorbs more hydrogen but shows higher strength a comparable reduction in ductility than CM alloy. The higher solubility of AM alloy is related to the higher density of dislocations, as shown by EBSD analysis.
3. Further work is planned to study the hydrogen effect on the am alloys with different build parameters and directions.

REFERENCES

- [1] K.M. Bertsch, A. Nagao, B. Rankouhi, B. Kuehl, D.J. Thoma, Hydrogen embrittlement of additively manufactured austenitic stainless steel 316 L, *Corrosion Science* 192 (2021) 109790.
- [2] M.M. Attallah, R. Jennings, X. Wang, L.N. Carter, Additive manufacturing of Ni-based superalloys: The outstanding issues, *MRS Bulletin* 41(10) (2016) 758-764.
- [3] C. Zhang, F. Chen, Z. Huang, M. Jia, G. Chen, Y. Ye, Y. Lin, W. Liu, B. Chen, Q. Shen, L. Zhang, E.J. Lavernia, Additive manufacturing of functionally graded materials: A review, *Materials Science and Engineering: A* 764 (2019) 138209.
- [4] X. Lu, D. Wang, D. Wan, Z.B. Zhang, N. Kheradmand, A. Barnoush, Effect of electrochemical charging on the hydrogen embrittlement susceptibility of alloy 718, *Acta Materialia* 179 (2019) 36-48.

ICH2P14-OP119

LOW PRICE PHOTO AND THERMAL PRODUCTION OF HYDROGEN FUEL FROM HYDROGEN SULFIDE EXTRACTED FROM PETROLEUM NATURAL GAS

Salah Naman

Dept. of Chemistry, University of Zakho, Kurdistan Region, Iraq
*Corresponding author e-mail: Salah.naman@yahoo.com

ABSTRACT

Photo-Thermal production of hydrogen from hydrogen sulphide from some petroleum natural gas contain 10-13 % H₂S. This gas is very corrosive and poisonous gas to the atmosphere. There were two Claus processes in Iraq to produce 2200 ton/day of pure elemental sulphur and water, the new Claus process can be converted to produce 140 ton/day of hydrogen and elemental sulphur in Iraq by using new catalyst in photo-thermal decomposition of H₂S at low temperature due to fact that energy bonding of the H-S is very low compared with H-O bond in water.

Therefore shortcut production of hydrogen from H₂S is by extraction of this gas from natural petroleum by ethanolamine's solution and direct photolysis of this gas after passing it over trace semiconductors (TiO₂ , ZnO ...etc) at low temperature range (5- 35 °C). H₂S will decomposes to hydrogen and sulphur, therefore three different pilot plants have been built for cheap production of Hydrogen and sulphur in liquid and gas phase at higher temperature.

Keywords: Hydrogen Production; Natural Gas; H₂S; Sensitizer.

INTRODUCTION

Hydrogen sulfide (H₂S) is a smelly, corrosive, highly toxic gas .Beside its other bad habits, it also deactivates industrial catalysts. H₂S is commonly found in natural gas and is also made at refineries, especially if the crude oil contains a lot of sulfur compound (1). Because H₂S is such an obnoxious substance, it is converted to non-toxic and useful elemental sulfur by Claus process at most locations that produce it (2).



In Iraq, a bout 2200 tons a day of sulfur extracted now from H₂S through Claus process .But treating H₂S by Claus process leads to recover only elemental sulfur and hydrogen in H₂S cannot be recovered and is finally wasted in the form of water (3).For that, much attentions began focused on the decomposition of hydrogen sulfide to hydrogen and elemental sulfur, such as thermo chemical, electrolytic and photo chemical process (4).

Because of the low energy of the H-S bond in compared with H-O as shown in figure 1, it is possible that lower cost processes could be devised by making hydrogen from H₂S.

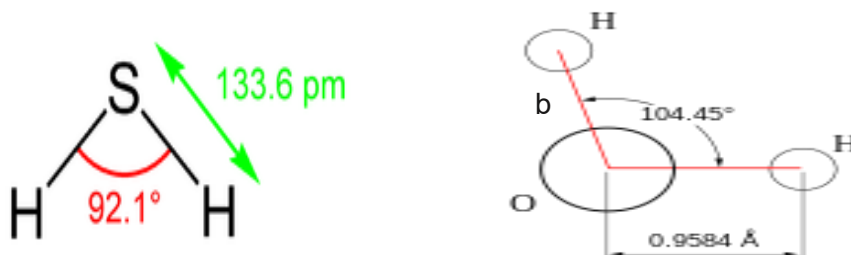
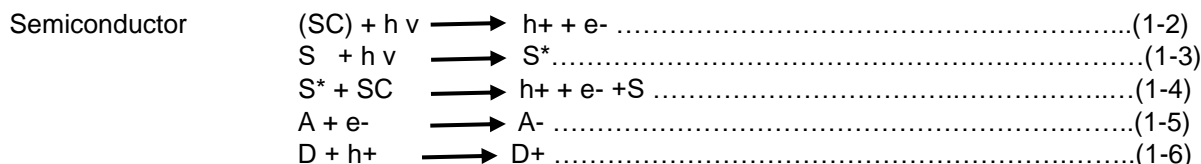


Figure 1: The chemical structure for a: Hydrogen Sulfide, and b: Water

The photo production of hydrogen gas and sulfur deposited in solution may rationalize in terms of the band gap excitation of semiconductor (5). Activation of the semiconductor photo catalysts achieved through the absorption of a photon of ultra- band gap energy, which results in the promotion of an electron e⁻ from the valance band to the conduction band, with the concomitant generation of a positive hole h⁺ in the valance band (6). To increase the percentage decomposition of H₂S, sensitizers have been used with the semiconductor, therefore more light will be absorbed by sensitizers and semiconductor as in the following reactions (7).



In this study, we used titanium dioxide as semiconductor. Anatase is a TiO₂ poly morph which is less stable than rutile, but more efficient than rutile for several applications, including catalysis, photo catalysis, and dye-sensitized, there for riboflavin have been used with TiO₂ .

Ethanol amines are the most frequently used compounds for the removal of H₂S from natural gas, because their reactivity and availability at low cost; alkanol amines have achieved a position of prominence in the gas sweetening industry, e.g. the Claus process in which hydrogen sulfide is converted to sulfur(8). The types of decomposition of H₂S are:

1- Thermochemical production of Sulfur only..

Claus process



2- Photoelectrochemical production of Hydrogen and sulfur.



3- Thermochemical production of hydrogen and sulfur. Different pilot plants.



MATERIALS AND METHODS

H₂S production by kipp's method and cylinder of pure H₂S, TiO₂, ZnO, V₂O₃ have been purchased from Fulge and PDH. Separation of H₂S have been done from natural gas by using ethanol amins at different percentages.

APPARATUS AND PILOT PLANTS

Laboratory experimental have been done using glass apartuse with all options for introducing materials and exposing to radiation and separating the product of the decompositions by physical methods and gas gromotography GLC as in figure 2 for photo radiation decomposition of H₂S and figure 3 for photo and thermal decompositions. And figures 4 and 5 are pilot plants for photo and thermal flow system decomposition of H₂S using GC for analysis of the products.

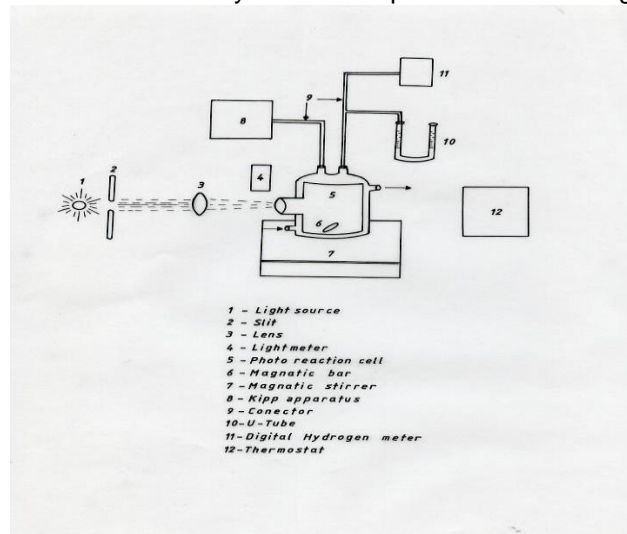


Figure 2: Laboratory glass static photo decomposition.

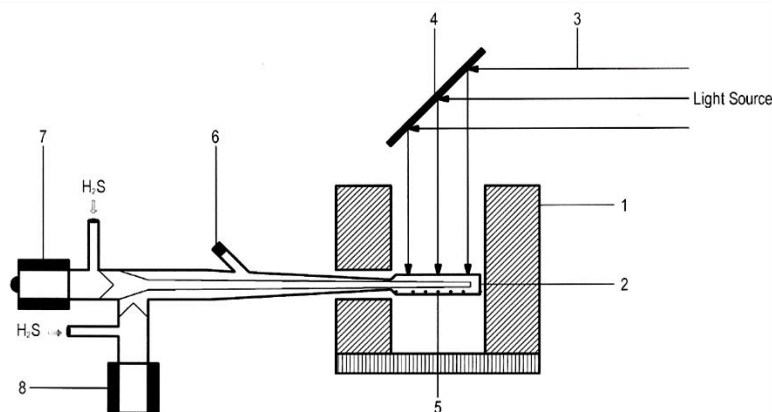


Figure 3: Static Photo thermal Reactor. 1. Furnace, 2. Flat reactor, 3. Light, 4. Mirror, 5. Catalysts on the bottom of reactor, 6. Septum, 7. and 8. Taps for the admission and withdrawal of gas samples.

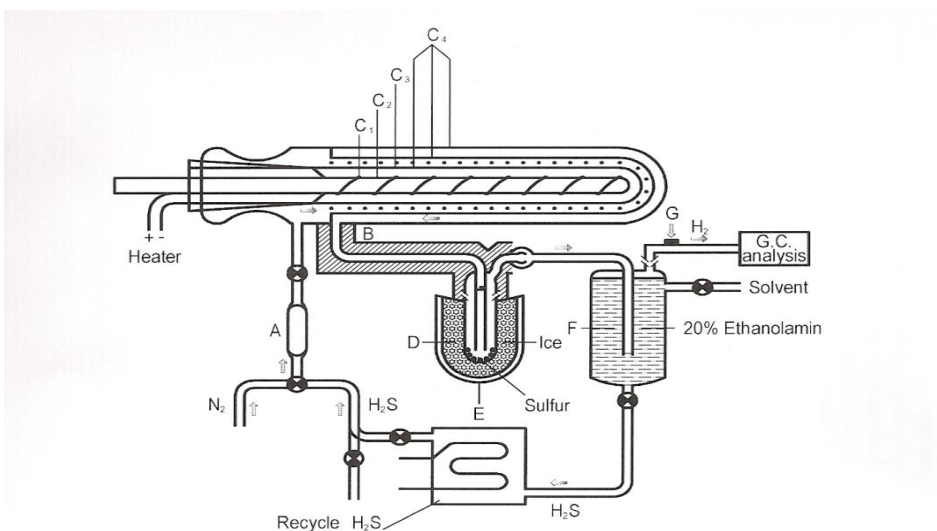


Figure 4: Experimental Apparatus (glass) for flow photothermal pilot plant.

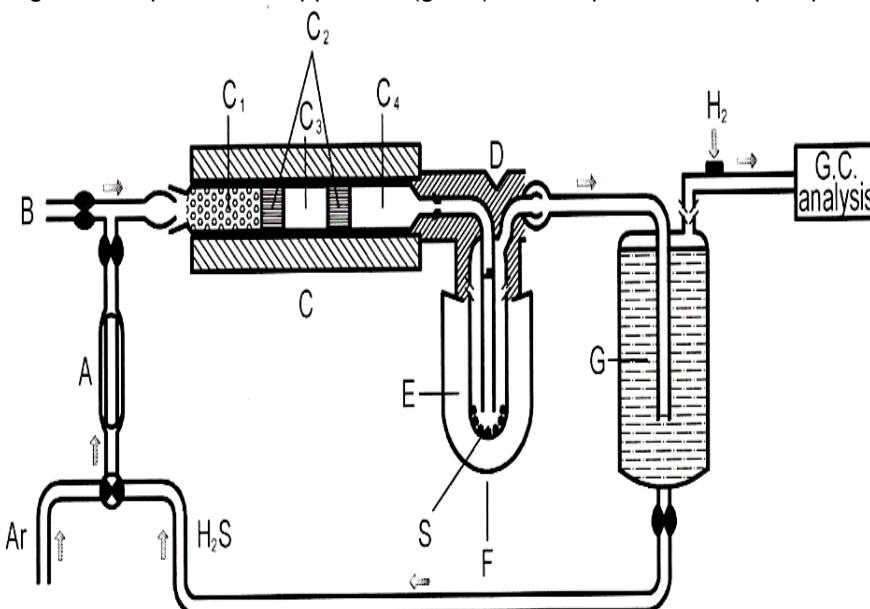


Figure 5: Schematic diagram of experimental apparatus for the decomposition of hydrogen sulfide (furnace)

CONCLUSION

Different methods have been used to convert hydrogen Sulphur to Sulphur and hydrogen using above chemical methods and special pilot for each process. Especially we concentrated on our natural gas as it contains high percentage of H_2S .

REFERENCES

- 1-ATSDR "Toxicological profile for hydrogen sulfide "GA, US Department of Health and Human Services, Agency for Toxic Substances and Disease Registry(1999).
- 2-C.M.Caruna, Chem, Eng.Prog.**92** (1996)63.
- 3-M.J.Atwan, S.T.AL-Ashab, and S.A.Naman, Proc.5th Sci.Conf./SRC-Iraq Baghdad, **3**(1989)187-200.
- 4-S.A.Naman, Int.J.of Hydrogen Energy, **17**(1992)499-504.
- 5-E.Borgarello, K.Kalyanasundaram, M.Gratzel, and E.Pelizzelti, Helv.Chim Acta **65**(1982)243.
- 6-S.A.Naman and M.Gratzel.J.Photochem .Photobiol .A: Chem, (1993).
- 7-A.Mills and S.Hunte.J.Photochem.Photobiol.A: Chem; **1**, (1997)108.
- 8-B.G.Goar and E.Nasato, J. Oil and Gas .**92**(1994)62.

ICH2P14-OP120

A LIFE CYCLE ASSESSMENT OF HYDROGEN PRODUCTION WITH CATALYTS

^{1*}Assem Abdurakhmanova, ^{1,2}Ibrahim Dincer

¹Yildiz Technical University, Clean Energy Technologies Institute, Istanbul, Turkey

²Ontario Tech University, Clean Energy Research Laboratory, Oshawa, Ontario, Canada

*Corresponding author's e-mail: assem.abdurakhman@gmail.com

ABSTRACT

This paper reviews the significant influence of a chemical catalyst in clean hydrogen production on renewable energy technologies. Utilising data from the GREET program, we analyse three pathways: renewable natural gas production from food waste via anaerobic digestion, renewable natural gas for central plant gaseous H₂ production, and renewable natural gas production from fats, oil, and grease via anaerobic digestion. We assess the emissions (CO₂, CH₄, NO_x, PM_{2.5}, SO_x, N₂O) graphically. Our life cycle assessment of the catalyst shows its role in the production of pure hydrogen and highlights its importance for renewable energy. In comparison, conventional hydrogen cyanide production produces CO₂ emissions of 1.96 kg, while the pathways used in cyanide hydrogen production are between 0.19 kg - 0.15 kg.

Keywords: Hydrogen, Life cycle assessment, hydrogen production, Sustainable development.

INTRODUCTION

CO₂ emissions are very significant and have a major impact on the climate, between 2010 and 2020 the use of permanent magnets has resulted in a cumulative increase in global greenhouse gas emissions of 32 billion tonnes of CO₂ equivalent [1]. In this regard, the relationship between clean hydrogen production and renewable energy technologies is a critical element of sustainable energy systems. The chemical catalyst plays a central role in facilitating clean hydrogen production processes, extending its influence beyond chemical reactions into the realm of renewable energy systems. Utilizing data from the Greenhouse gases, Regulated Emissions, and Energy Use in Transportation (GREET) program, this study investigates the complex associations between the chemical catalyst and its impact on various renewable energy pathways. Three specific pathways are considered: the production of renewable natural gas from food waste through anaerobic digestion, the generation of renewable natural gas for hydrogen (H₂) production at a central plant, and the production of renewable natural gas from fats, oils, and grease (FOG) through anaerobic digestion.

METHODOLOGY

This paper employs a methodology that combines a life cycle assessment (LCA) to compare various indicators resulting from the studied processes [2]. The LCA framework allows for a comprehensive evaluation of the environmental impacts associated with clean hydrogen production within the context of selected renewable energy pathways [3]. This assessment encompasses a range of emissions, including carbon dioxide (CO₂), methane (CH₄), nitrogen oxides (NO_x), fine particulate matter (PM_{2.5}), sulfur oxides (SO_x), and nitrous oxide (N₂O). The methodology emphasizes sustainability and the long-term well-being of ecosystems and society. To enhance the accessibility and clarity of data presentation, this paper employs a graphical approach. Graphical representations are used to convey estimates of the environmental impacts associated with CO₂, CH₄, NO_x, PM_{2.5}, SO_x, and N₂O. These graphical tools provide a clear and concise means of presenting the results, with a particular focus on their pertinence to sustainable development. The utilization of graphs facilitates a more intuitive interpretation of the findings, fostering a deeper understanding of the complex interactions between chemical catalysts and their environmental impacts within the broader framework of sustainable development.

RESULTS AND DISCUSSION

This section presents the results obtained in this study. The research will consider the environmental impacts of the three renewable energy pathways analysed: the production of renewable natural gas from food waste through anaerobic digestion, renewable natural gas for hydrogen (H₂) production at a central plant and renewable natural gas from fats, oils and grease (FOG) through anaerobic digestion. The research will also look at CH₄, NO_x, PM_{2.5}, SO_x and N₂O emissions, noting differences between the pathways due to feedstock composition and production processes. The results of these reviews are shown in Figure 1-2. This highlights the complex nature of the effect of chemical catalyst. In figure 1. hydrogen values in cyanide, in figure 2. hydrogen fluoride, both figures show emissions of a few chemical elements, these values were taken per kg.

Further to note that the expected outcome of this study is to elucidate the key role of a chemical catalyst in clean hydrogen production and its broad implications for renewable energy. By combining LCA and analysing the results obtained, this study contributes to the current debate on the integration of clean hydrogen production technologies, providing information for informed decision making. The results of this study should provide a foundation for moving towards a sustainable and durable energy future.

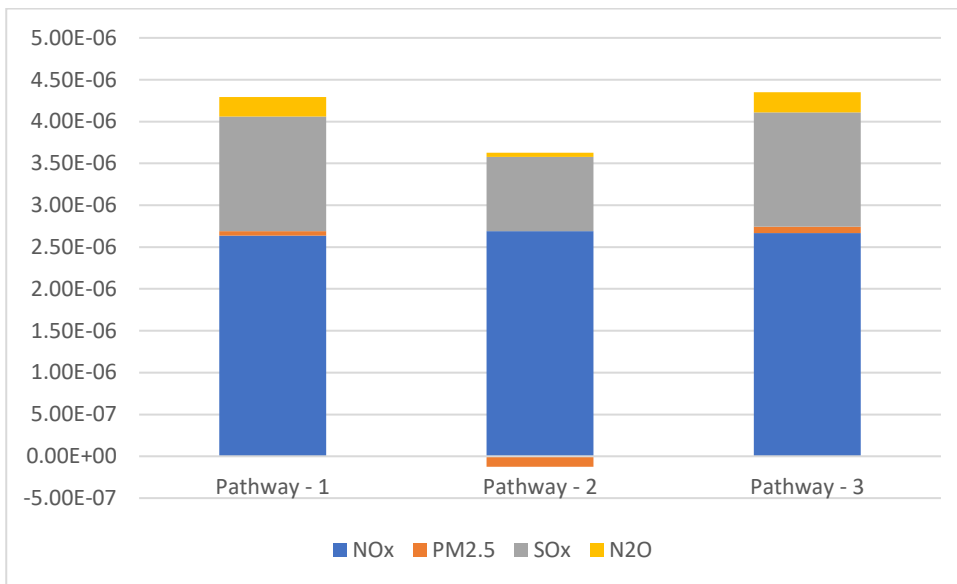


Figure 1. Hydrogen in cyanide

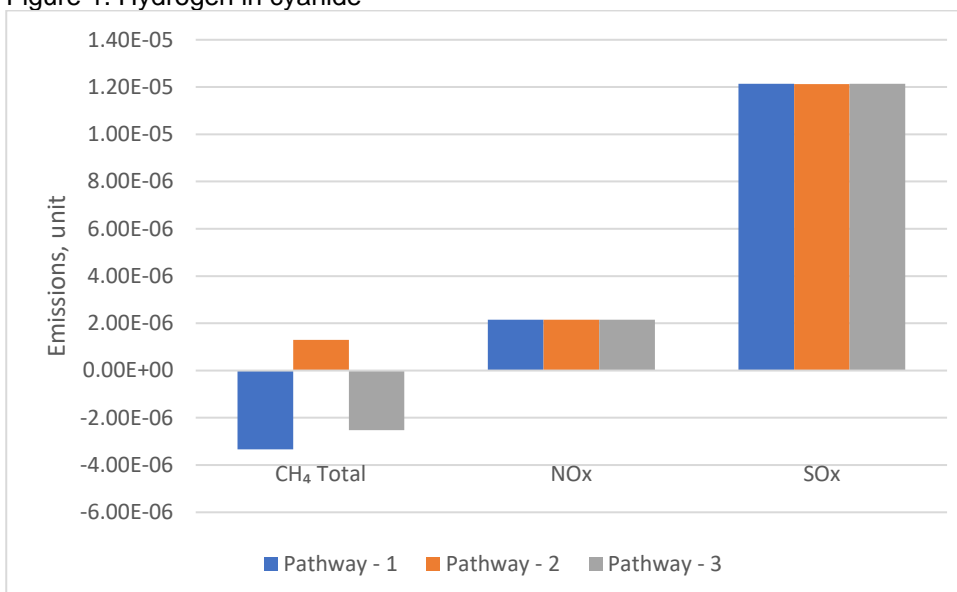


Figure 2. Hydrogen in flouride

CONCLUSIONS

This study aims to conduct a comprehensive analysis of the influence of a chemical catalyst on the production of pure hydrogen, elucidating its impact beyond mere chemical reactions, and extending its ramifications across the broader domain of renewable energy technologies. The evaluation based on data from the GREET programme provides valuable insights into the environmental and economic aspects of this complex relationship. As the subsequent results and discussions will underscore, the multifaceted nature of these conclusions is set to shape the future landscape of renewable energy technologies, providing vital guidance for stakeholders in the field.

REFERENCES

1. Golroudbary, S. R., Makarava, I., Kraslawski, A., & Repo, E. (2022). Global environmental cost of using rare earth elements in green energy technologies. *Science of the Total Environment*, 832. Scopus. <https://doi.org/10.1016/j.scitotenv.2022.155022>.
2. Aydin, M. I., & Dincer, I. (2022). A life cycle impact analysis of various hydrogen production methods for public transportation sector. *International Journal of Hydrogen Energy*, 47(93), 39666–39677. <https://doi.org/10.1016/j.ijhydene.2022.09.125>.
3. Aydin, M. I., & Dincer, I. (2022). An assessment study on various clean hydrogen production methods. *Energy*, 245, 123090. <https://doi.org/10.1016/j.energy.2021.123090>.

ICH2P14-OP122

SYNTHESIS, CHARACTERIZATION, AND APPLICATION OF BIO-TEMPLATED NI-CE/AL₂O₃ CATALYST FOR CLEAN H₂ PRODUCTION IN THE STEAM REFORMING OF METHANE PROCESS

**Mohammad Reza Rahimpour, Maryam Koochi-Saadi*

¹Shiraz University, Department of Chemical Engineering, Shiraz, Iran

*Corresponding author e-mail: Rahimpour23@gmail.com

ABSTRACT

A porous γ -alumina was successfully created using an eco-friendly method, employing Fig leaves as a biotemplate for the first time in this study. Following the confirmation of the porous Al_2O_3 structure using various characterization techniques, it was employed as a support material for Ni-Ce particles to significantly enhance the conversion efficiency of the steam reforming of methane (SRM) process. To achieve this, we fine-tuned the content of Ni, Ce, and the SRM temperature utilizing both bulk and porous Ni-Ce/ Al_2O_3 catalyst structures. The results obtained from field emission scanning electron microscopy (FESEM), temperature-programmed desorption (H_2 -TPD), and N_2 adsorption/desorption indicated the formation of more evenly distributed Ni particles with smaller sizes on the mesoporous alumina (MAI), especially when promoted with CeO_2 . In addition to the effective influence of CeO_2 on Ni particle dispersion, it enhanced the interaction between Ni and Al, thereby increasing the catalysts' activity and reducing coke deposition during the SRM process. Consequently, the 20Ni-3.0Ce/MAI catalyst displayed the highest H_2 yield at 96.02% and CH_4 conversion at 90.20%, with the lowest CO_2 produced to CH_4 consumed ratio of 0.52% at an SRM reaction temperature of 700°C. In contrast, the bulk catalyst with equal Ni and Ce contents exhibited CH_4 conversion, H_2 yield, and CO_2/CH_4 molar ratio of 86.09, 92.30, and 0.56, respectively, at the same temperature. Furthermore, the 20Ni-3.0Ce/MAI catalyst demonstrated the highest stability during a continuous 12-hour SRM reaction at 700°C, with the lowest reductions in CH_4 conversion and H_2 yield, amounting to 3.97% and 5.12%, respectively.

Keywords: Bio-templated Al_2O_3 , Fig leaves template, H_2 production, Steam reforming of methane, Cerium promoter.

1. INTRODUCTION

Steam reforming of methane (SRM) produces hydrogen-rich syngas via an endothermic reaction between methane and water at high pressure and temperature [1, 2]. To downsize SRM for mobile fuel cells [3], a catalyst operating at lower temperatures is needed. Ni-based catalysts are popular due to their activity and cost-efficiency [4]. Understanding the reaction mechanisms is complex, with various proposed models affecting reaction kinetics. Challenges like sintering and coke formation on Ni particles have prompted efforts to improve catalyst efficiency. Strategies involve using high surface area supporting materials like Al_2O_3 and incorporating promoters like CeO_2 to enhance stability and reduce coke deposition [5-7]. Bio-templated materials, particularly from leaves, offer a promising, scalable solution for these catalysts [8, 9]. Research aims to compare bio-templated Ni-based catalysts supported on Fig leaves with conventional ones, assessing their performance in SRM for methanol production and evaluating the impact of a cerium promoter on catalytic activity and coke deposition. Characterization methods are employed to analyze the catalysts and supports before and after the SRM reaction.

2. EXPERIMENTAL SECTION

In the experimental section, various materials including acids, alcohols, and metal compounds were used. Fig leaves served as a bio-template. Catalyst synthesis involved different methods for creating mesoporous and bulk alumina structures and depositing nickel or nickel-cerium particles onto them. Characterization techniques like **XRD**, **EDX**, **FESEM**, **TPR**, and **BET** were used to analyze the synthesized samples. Process activity involved a setup with a fixed-bed reactor for performing catalytic tests in the temperature range of 600–700°C. The reactions and calculations involved methane conversion, hydrogen production yield, and CO_2 to CH_4 consumption ratio.

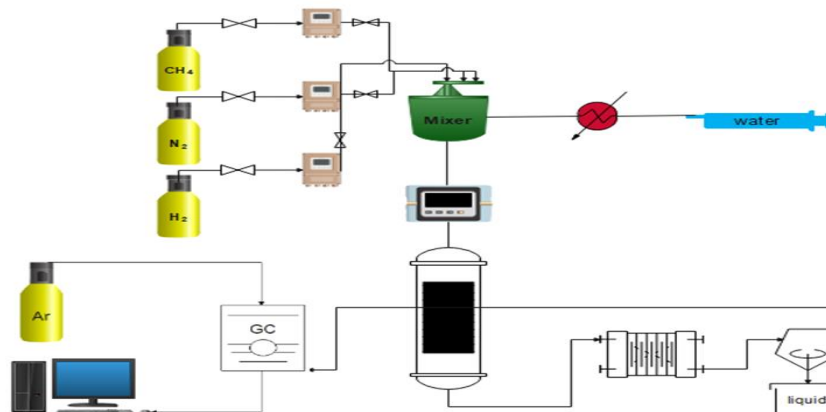
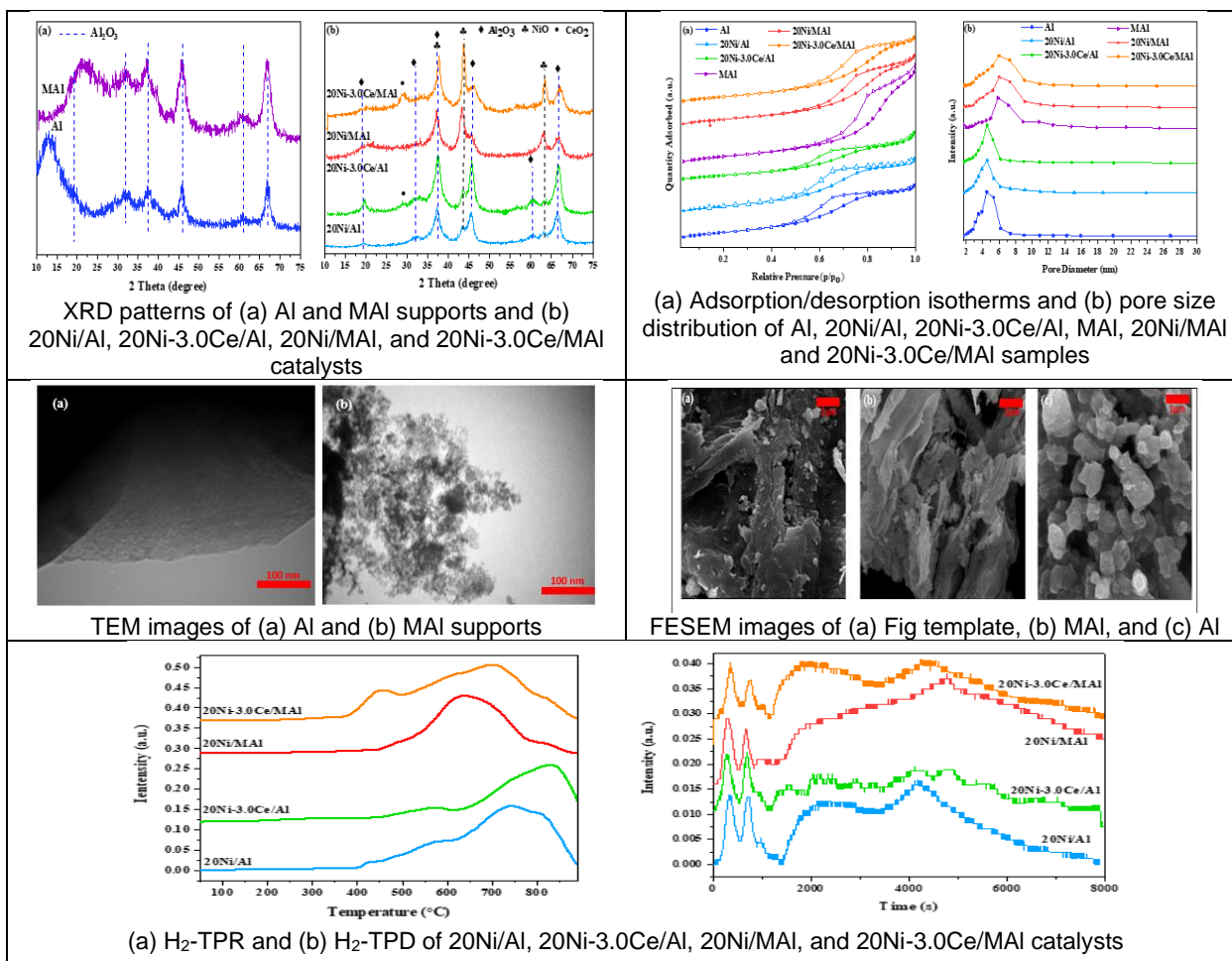


Fig. 1. Schematic of SRM set-up

3. RESULTS & DISCUSSION

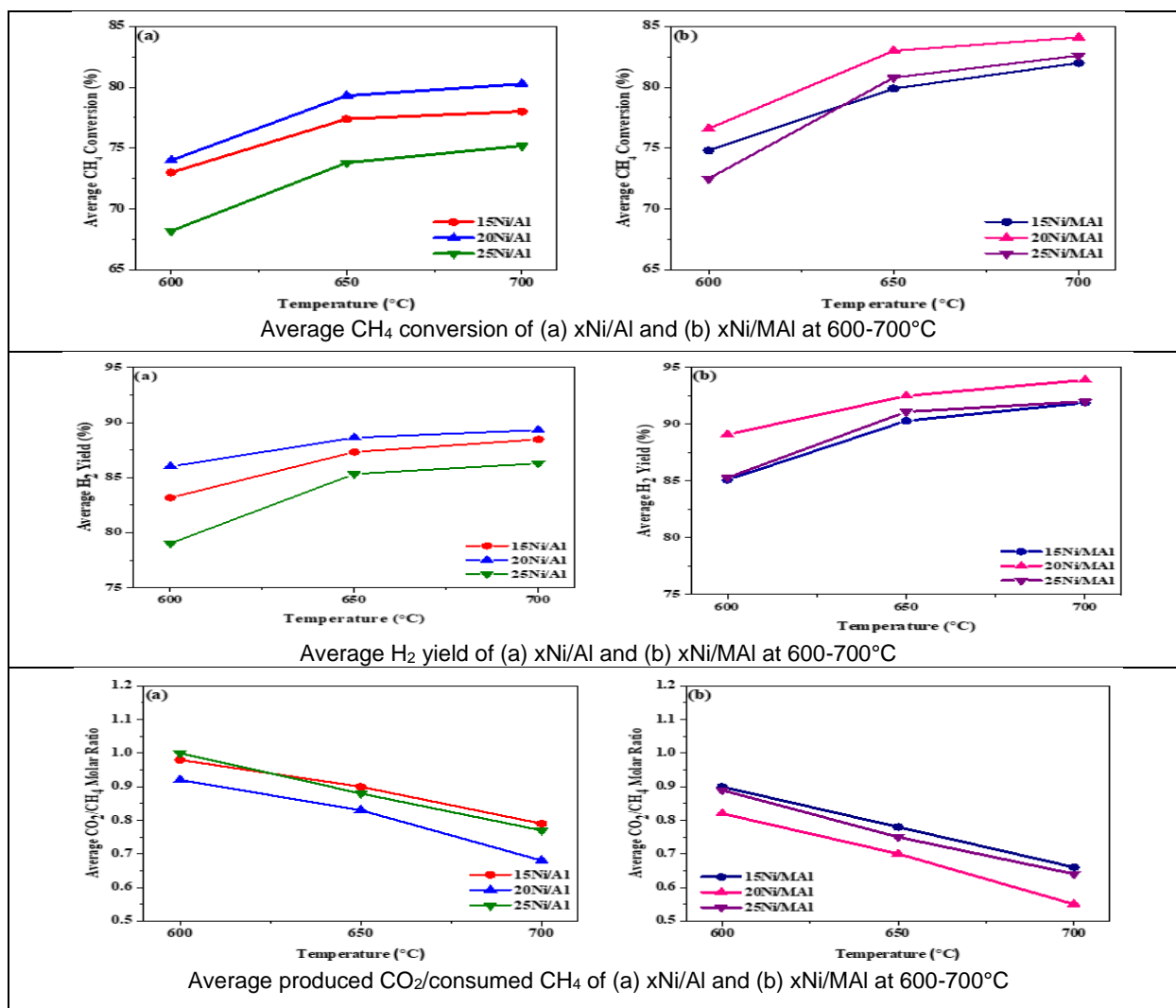
3.1. Fresh synthesized catalysts properties

In assessing fresh synthesized catalysts, XRD analysis revealed γ - Al_2O_3 peaks in support materials and catalysts, along with NiO and CeO_2 phases in the promoted samples. TEM images confirmed the porous structure of the MAI support compared to Al. N_2 adsorption/desorption showed differences in pore sizes and volumes between the supports and catalysts, influenced by impregnation of Ni and Ce. FESEM analysis depicted the morphology and dispersion of NiO particles on the supports, indicating differences between promoted and non-promoted catalysts. H_2 -TPR analysis demonstrated Ni-Al interaction strengths and showed the impact of CeO_2 on enhancing this bond. H_2 -TPD revealed higher Ni dispersion on mesoporous alumina, consistent with BET surface area measurements and FESEM observations.



3.2. Effect of active site loading on the catalyst's activity

The depiction of CH₄ conversion and H₂ yield for Ni-loaded catalysts synthesized at varying temperatures and Ni loadings reveals some interesting patterns. As the temperature increases, CH₄ conversion sees a boost due to the reaction's endothermic nature. The optimal Ni loading at 20wt.% achieves a balance between active sites and particle dispersion, maximizing both H₂ yield and CH₄ conversion. However, higher Ni loading leads to decreased activity owing to particle agglomeration. Notably, at 700°C, the catalyst 20Ni/MAI outperforms others, showcasing higher CH₄ conversion (84.10%) and H₂ yield (93.91%) compared to 20Ni/Al (80.28% CH₄ conversion and 89.31% H₂ yield). These catalysts also exhibit the lowest CO₂/CH₄ ratio, highlighting their environmentally friendly performance. Overall, among the synthesized catalysts, 20Ni/MAI demonstrates the most favorable performance. The trend in CO₂/CH₄ ratio across temperatures for these catalysts is depicted in another illustration.

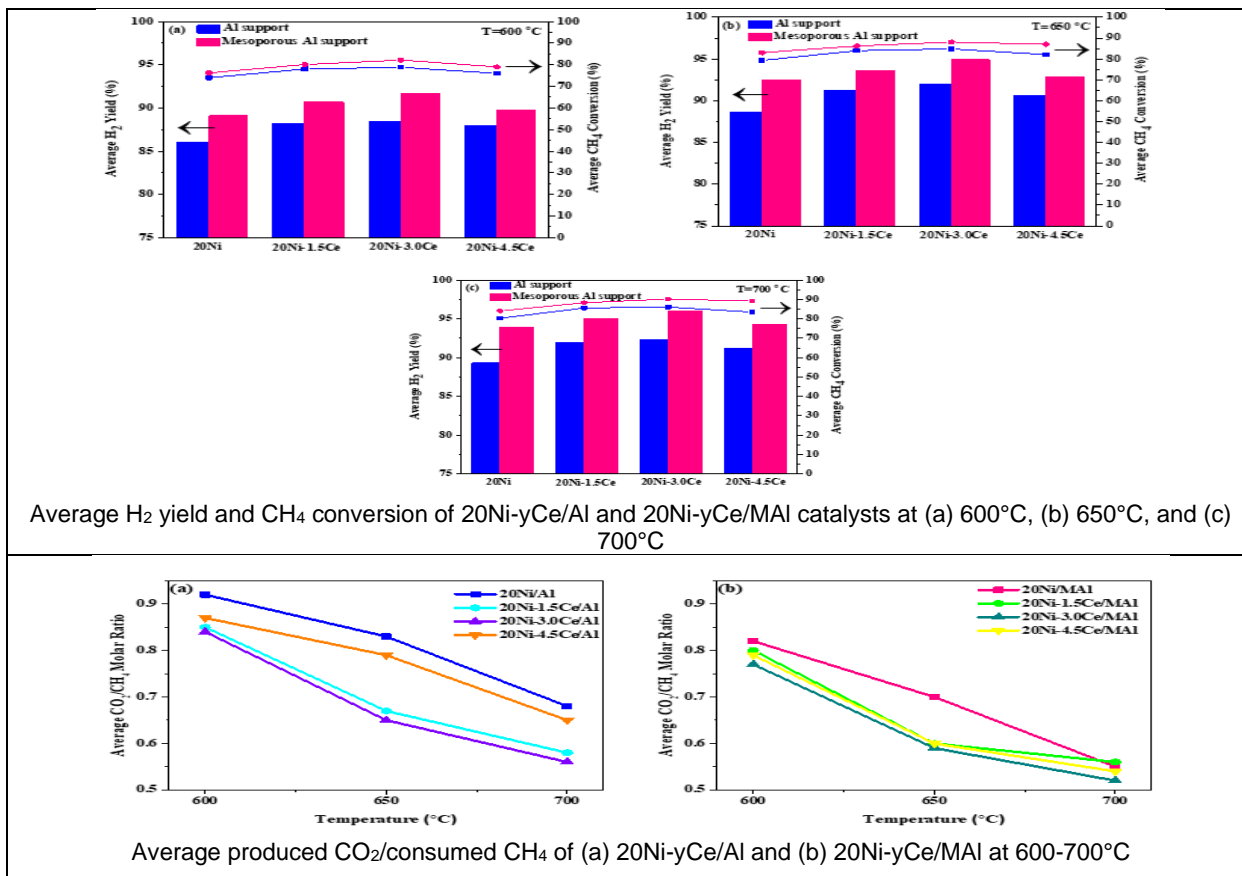


3.3. Effect of Ce loading on the catalytic performance

The examination of promoter loading effects on Ni-weight in alumina-supported catalysts showcases notable differences. When comparing catalysts 20Ni-yCe/Al and 20Ni-yCe/MAI, superior conversions are observed in mesoporous catalysts. The catalyst's optimal performance is achieved with a 3wt.% Ce loading, resulting in enhanced methane conversion and increased hydrogen yield. However, a further increase to 4.5wt.% Ce diminishes the catalytic activity. Particularly noteworthy is the superior performance of the 20Ni-3.0Ce/MAI catalyst across various temperature ranges.

Additionally, the data shows a clear reduction in the CO₂/CH₄ ratio upon the inclusion of Ce in both bulk and mesoporous catalysts. This reduction signifies a shift towards more environmentally favorable behavior, primarily due to enhanced coke oxidation and reverse WGS reactions facilitated by Ce. Notably, the catalysts with 20Ni-

3.0Ce/Al and 20Ni-3.0Ce/MAI compositions exhibit the lowest observed ratios, indicating their heightened efficacy in promoting these desirable reactions.



3.4. Long time-on-stream performance of catalysts

After running the catalyst for 12 hours at 700°C, there was an initial improvement in turning methane into hydrogen, but then it dropped because coke started to form. Some versions of the catalyst, especially the 20Ni-3.0Ce/MAI type, kept performing better. When we looked at the catalysts after using them, X-ray tests showed a carbon coating that affected the CeO₂ peaks. The images from the scanning electron microscope (FESEM) also revealed changes in structure and less buildup of nickel particles on the improved catalysts. Results from the energy-dispersive X-ray spectroscopy (EDX) indicated way less carbon buildup on the better catalysts, especially the 20Ni-3.0Ce/MAI one. Plus, the used catalysts had less surface area because the pores got blocked or they stuck together, but the 20Ni-3.0Ce/MAI type was affected the least. Overall, recent studies in this field have shown that different catalysts can convert methane to hydrogen anywhere between 63% to 100%, depending on the type and how they're used. Adding Ce to the 20Ni/Al and 20Ni/MAI catalysts increased methane conversion by about 7% at 700°C.

CONCLUSION

The article compares mesoporous and bulk Ni-Ce/Al₂O₃ catalysts in the SRM process. Al₂O₃ was synthesized via sol-gel and precipitation, loaded with 15-25wt.% nickel for SRM testing at 600-700°C. Optimal Ni content was determined based on highest CH₄ conversion and H₂ yield. Addition of 1.5-4.5wt.% cerium improved catalyst performance, enhancing active site dispersion and reducing coke deposition. Mesoporous alumina exhibited better catalytic performance due to higher surface area, larger pores, and improved active site dispersion compared to bulk alumina. Addition of 3.0wt.% cerium improved active site dispersion and reduced coke deposition. 20Ni-3.0Ce/MAI showed the best performance with high CH₄ conversion, H₂ yield, and low CO₂ production, making it the most environmentally friendly catalyst for H₂ gas production.

REFERENCES

1. Taji, M., M. Farsi, and P. Keshavarz, *Real time optimization of steam reforming of methane in an industrial hydrogen plant*. International Journal of Hydrogen Energy, 2018. **43**(29): p. 13110-13121.
2. Zangouei, M., A. Zarringhalam Moghaddam, A. Razeghi, and M.R. Omidkhah, *Production of syngas by combination of CO₂ reforming and partial oxidation of CH₄ over Ni/Al₂O₃ catalysts in fixed-bed reactor*. International Journal of Chemical Reactor Engineering, 2010. **8**(1).
3. Di Giuliano, A., et al., *Sorption enhanced steam methane reforming by Ni–CaO materials supported on mayenite*. International Journal of Hydrogen Energy, 2017. **42**(19): p. 13661-13680.
4. Yoo, J., et al., *Hydrogen production by steam reforming of natural gas over butyric acid-assisted nickel/alumina catalyst*. International Journal of Hydrogen Energy, 2017. **42**(47): p. 28377-28385.
5. Meshksar, M., S. Daneshmand-Jahromi, and M. Rahimpour, *Synthesis and characterization of cerium promoted Ni/SBA-16 oxygen carrier in cyclic chemical looping steam methane reforming*. Journal of the Taiwan Institute of Chemical Engineers, 2017. **76**: p. 73-82.
6. San-José-Alonso, D., J. Juan-Juan, M. Illán-Gómez, and M. Román-Martínez, *Ni, Co and bimetallic Ni–Co catalysts for the dry reforming of methane*. Applied Catalysis A: General, 2009. **371**(1-2): p. 54-59.
7. Meshksar, M., M. Farsi, and M.R. Rahimpour, *Effect of Ni active site position and synthesis route on activity, stability, and morphology of Ce promoted Ni/Al₂O₃ catalyst for clean H₂ production*. Journal of Environmental Chemical Engineering, 2022. **10**(5): p. 108471.
8. Hall, S.R., H. Bolger, and S. Mann, *Morphosynthesis of complex inorganic forms using pollen grain templates*. Chemical Communications, 2003(22): p. 2784-2785.
9. Jin, S., et al., *Development of conductive protein-based film reinforced by cellulose nanofibril template-directed hyperbranched copolymer*. Carbohydrate polymers, 2020. **237**: p. 116141.

ICH2P14-OP123

GREEN HYDROGEN BASED AMMONIA PRODUCTION PROCESS: INSIGHT INTO ENERGY AND CO₂ EMISSIONS MINIMIZATION

^{1,2}Swaprabha P. Patel, ^{1*}Ashish M. Gujarathi, ³Piyush Vanzara

¹Petroleum and Chemical Engineering Department, College of Engineering, Sultan Qaboos University, Al Khod, Muscat PC 123, Oman

²Gujarat Technological University, Ahmedabad, India

³Chemical Engineering Department, VVP Engineering College, Rajkot, India

*Corresponding author e-mail: ashishg@squ.edu.om

ABSTRACT

Ammonia is one of the important chemicals, which has a wide range of applications in process industries. The demand for ammonia is expected to increase by 1.5% per year with the increase in demand for global demand for food supply. In this work, the Bare Bones Particle Swarm Optimization (BBPSO) algorithm, which is recognized for solving multimodal and nonlinear optimization problems, is used. BBPSO is an extension of particle swarm optimization, which is considered as one of the successful nature-inspired algorithms. The ammonia production process is modeled using the Promax Software. In this process, hydrogen is produced via the electrolysis of water. This green hydrogen is utilized as a raw material for the production of ammonia. Three single-objective-based objectives, namely minimization of CO₂ emissions (tonnes/year), maximization of profit (million \$/year), and maximization of ammonia flow rate (kg/hr) are individually optimized using BBPSO. Nine decision variables are considered which include five feed temperatures of different streams, two pressures of two different streams, and the flow rate of water and nitrogen. A detailed sensitivity analysis is carried out to determine the dependencies of assigned variables on the targeted objectives. Along with optimum objective values, several other important parameters like energy consumed and the purity of ammonia are also reported. This study not only considers sustainable green production of ammonia but also put light on economics, environmental, and energy-specific criteria for a better tomorrow.

Keywords: Green Hydrogen, Ammonia, BBPSO, CO₂ emissions, Energy.

INTRODUCTION

Owing to a huge 87% share in the fertilizers industry, ammonia is one of the most widely produced inorganic chemicals. Ammonia is a crucial chemical raw material used for modern industrial and agricultural fertilizers and finds applications in almost all sectors of life including refrigeration, air conditioning, acid gas removal capturing agents, raw material for manufacturing papers, plastics, fibers, explosive materials, and acids. Ammonia has a high octane rate, so it can be used as a potential fuel for fuel cells, and internal combustion engines [1,2]. Due to the hazardous effects of fossil fuels, an increase in the concentration of carbon dioxide and methane in the atmosphere, and nitrous oxide adversely affecting climate change global thinking is shifting towards the necessity of carbon-free fuel [3]. To encounter the above challenges along with climate change and greenhouse emissions, alternatives like biomass and renewable electricity are not adequate and thus it needs that we should look for alternatives for carbon-free fuels such as green hydrogen and green ammonia [4,5]. For the de-carbonization of the energy sector, green hydrogen is considered as a capable alternative with an expected forecast of 20 % global energy share by 2050 [5]. As a promising hydrogen derivative, ammonia has attracted the attention of researchers at the current time.

Universally, ammonia is produced by two synthesis processes. The first well-known process is the Haber-Bosch process and the second is the solid state ammonia synthesis process. The current synthesis processes are not environment friendly as they are dependent on the usage of fossil fuels which adds to greenhouse gas emissions in the atmosphere [6]. The Haber-Bosch process is highly energy-demanding and complex in nature. It operates at the higher temperature range of 400-500°C and high pressure of 100-200 atm. In order to control the carbon footprint, ammonia synthesis began to shift towards a greener way by using renewable energy sources like solar and wind [7].

Although the usage of solar and wind energies has their own limitations like reliability, energy storage, sustainability, seasonal fluctuations, and geographical locations it will take time for the complete integration of renewable sources to satisfy the large-scale demand [8]. The ammonia synthesis process was studied from an optimization point of view and various work has been performed in this domain. Recently an optimization study has been carried out for an exothermic reactor of ammonia synthesis by Xie et al. [9] In this study, seven decision variables were selected to minimize the entropy generation rate and to maximize the exothermic rate. The popular NSGA-II algorithm was used and the best optimal reactor conditions are reported by using LINMAP, TOPSIS, and the Shannon entropy method. Another interesting optimization study considers the operational uncertainties caused by wind turbines for the synthesis of the ammonia plant. This study shows the practical problems faced while dealing with renewable energy sources and the need to optimize such processes by using an efficient optimization approach [10]. Biomass is a clean renewable energy source, but its availability is majorly dependent on its geographical location. An optimization study was carried out by Arora et al. [11] considering the location of biomass feedstocks. This study focuses on the environmental and economic aspects of the different feedstock locations in India, Australia, and Brazil for the minimization of manufacturing cost as one of the objectives.

The term Green ammonia suggests that the hydrogen used as a raw material for the manufacturing process for ammonia is synthesized by using a green approach like the electrolysis of water using renewable energy sources which has zero carbon emissions [12]. Recently Campion N. et al. [13] studied the e-ammonia production process in which hydrogen was derived from the electrolysis process. In their study, they primarily focused on modeling, location of production sites for grid electricity, set up of power connections, and estimation of costs for different e-fuels. Olabi AG et al. [14] in detail explain the role of green ammonia in accordance with the sustainable development goals. In their study, recent developments regarding the production process of green ammonia along with its applications are discussed.

With the increasing human population on earth, the food needs are to be fulfilled by expanding agricultural sector products. At the same time, attention should be focused on reducing the carbon burden on the atmosphere with the optimum usage of available resources. So the objectives set for this study are Minimize F1 = minimization of CO₂ emissions (tonnes/year), Maximize F2 = maximization of profit (million \$/year), and Maximize F3 = maximization of ammonia flow rate (kg/hr). All cases were optimized by using an efficient Bare-bones particle swarm optimization (BBPSO) algorithm [15] which is an extension of particle swarm optimization. Particle swarm optimization [16] uses concepts inspired by nature such as fish schooling, and bird flocking. For this optimization study, nine decision variables are considered. The decision variables are the feed temperatures of five different streams, the pressures of two different streams, the flow rate of water, and the flow rate of nitrogen. The manuscript is arranged in the following manner: the next section is on the methodology followed by results and discussions. The output of this study is summarized in the conclusion section and references are cited at the end.

MATERIALS AND METHODS

Fig 1. shows the process flow diagram for the electrolysis and the ammonia synthesis sections of the ammonia production plant. The reacting water (which is recycled back) is cooled to 80°C, and fed to the electrolyzer. In the electrolyzer, the water molecule breaks down into hydrogen and oxygen molecules. In the electrolysis process, electrolyzing 24000 kg/hr of water consumes 1060 kW of energy. The output of the electrolyzer consists of 98.98% water, 0.11 % hydrogen (=27 kg/hr), and 0.91 % oxygen. The process stream is heated to 92°C to facilitate the hydrogen separation process. The membrane separator separates the hydrogen and oxygen with a common carrier of the water molecules. The unreacted water is recycled back to the electrolyzer along with the added makeup water. The 97.5 % of the hydrogen is separated using the flash drum VSSL-101. The exit stream from the flash drum consisting of traces of water is cooled to 30°C and further flashed to achieve a 99.9% of hydrogen-rich stream. The hydrogen is compressed from 31 barg pressure to 131 barg pressure through a series of four compressors and intercooling stages. The high-pressure hydrogen is mixed with a nitrogen stream, which is also compressed and intercooled in four stages to 131 barg pressure. The hydrogen and nitrogen mixture is reacted in a series of three-packed bed reactors. Nitrogen and

hydrogen are reacted over a catalyst bed to produce ammonia. The reaction is modeled using kinetic rate constant information for Langmuir-Hinshelwood type rate expressions. The unconverted reactants are separated in a VSSL-100 separator and ammonia with 99.35 % purity and with a flow rate of 153 kg/hr is produced which results in 1220,000 kg/year of designed production capacity.

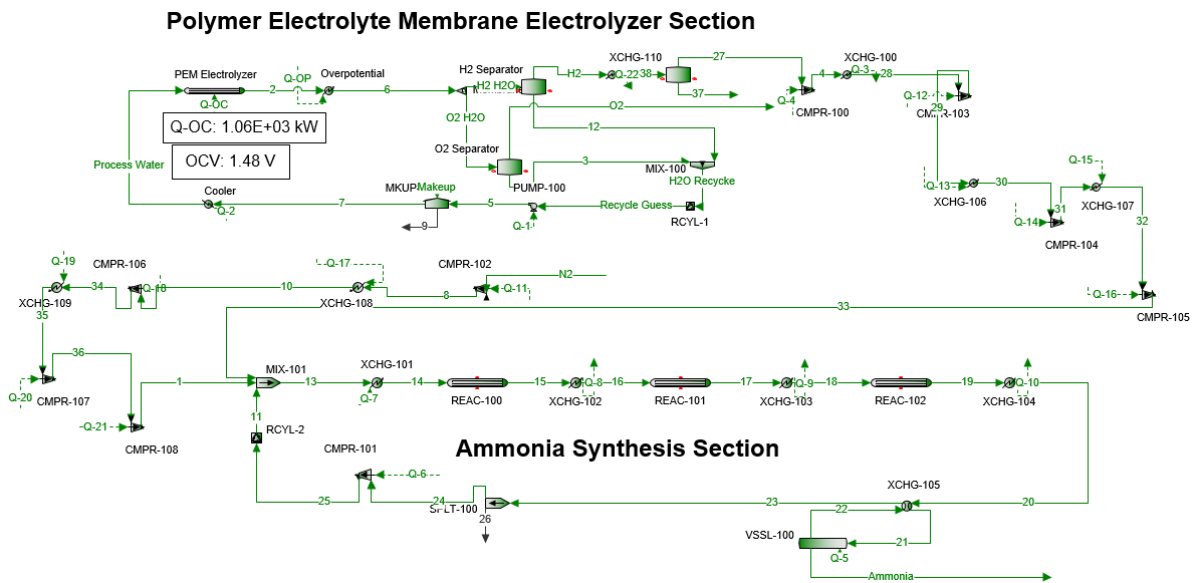


Fig. 1. Process flow diagram of the ammonia synthesis process plant

RESULTS AND DISCUSSION

A detailed sensitivity analysis is carried out to foresee the effect of individual decision variables on the corresponding objectives. Accordingly, five stream temperatures, two stream pressures, and two streams' molar flow rates are considered as decision variables. The upper and lower ranges of decision variables are given in Table 1. For details of stream numbers please refer to Fig. 1 (Process flow sheet). Both water and nitrogen flow rates are considered as important flow rates to achieve the desired objectives.

Table 1. Optimization cases, decision variables, and constraints for the ammonia plant

Objectives	Decision Variables and ranges	Constraints
Case 1: Minimize F1= CO ₂ emissions (tonne/year)	$400 < T_{\text{Stream}_14} \text{ (K)} < 750$	Ammonia Purity > 98%
	$400 < T_{\text{Stream}_16} \text{ (K)} < 750$	
	$400 < T_{\text{Stream}_18} \text{ (K)} < 750$	
Case 2: Maximize F2 = Profit (million \$/year)	$320 < T_{\text{Stream}_20} \text{ (K)} < 620$	
	$150 < T_{\text{Stream}_22} \text{ (K)} < 300$	
Case 3: Maximize F3= Ammonia Flow Rate (kg/hr)	$1950 < P_{\text{Stream}_5} \text{ (kPa)} < 4500$	
	$10200 < P_{\text{Stream}_1} \text{ (kPa)} < 20000$	
	$5000 < F_{\text{Water}} \text{ (kmol/hr)} < 10000$	
	$17 < F_{\text{Nitrogen}} \text{ (kmol/hr)} < 34$	

Three objectives are considered in this study. The first objective is to minimize CO₂ emissions (Minimize F1), the second objective is to maximize profit (Maximize F2), and the third objective is to maximize the flow rate of ammonia (Maximize F3). The amount of CO₂ emitted (tonne /year) is calculated from the electricity consumed in pumps, and compressors and the amount of CO₂ emitted from the heat required

in heaters and coolers by burning natural gas. The detailed profit is calculated by considering the sale value and the cost which consist of costs of equipment, raw materials, utility, construction and equipment costs, royalties, and wages, including depreciation [17]. Ammonia production value is obtained from the exit stream of ammonia with an imposed purity of more than 98% (as a constraint) in this simulation and optimization study.

Table 2: Optimization case results

Objectives and Decision variables		Optimization Cases		
		Case 1: Min CO ₂ Emissions	Case 2: Max Profit	Case 3: Max Ammonia Flow rate
Objectives	CO ₂ emission (tonnes/year)	22322	278637*	27392*
	Profit (million \$/year)	0.02647*	6.39724	0.21121*
	Ammonia Production (kg/hr)	568.03*	352.18*	645.59
	ENG (kW)	11667.73*	1626.21*	14646.59*
	Purity	99.42*	98.19*	99.42*
Decision Variables	T_Stream_14 (K)	680.0766	696.7419	682.5768
	T_Stream_16 (K)	734.0271	400.1884	733.8822
	T_Stream_18 (K)	747.9032	700.4668	739.9084
	T_Stream_20 (K)	543.4261	335.3104	333.6272
	T_Stream_22 (K)	210.8867	254.823	213.7904
	P_Stream_5 (kPa)	2216.78	2195.987	2179.371
	P_Stream_1 (kPa)	13937.24	11982.2	13206.45
	F_Water (kmol/hr)	5031.408	9942.288	5686.492
F_Nitrogen (kmol/hr)	18.4776	30.67103	19.65142	

*= Calculated value, Bold= Optimum value for the given case

Similarly, two additional objectives are also calculated and reported along with the results of F1, F2, and F3 objectives, those objectives are the purity of ammonia and the amount of energy consumed. The energy is calculated using the energy consumed in compressors, pumps, heaters, and coolers. The BBPSO algorithm is used with 100 population points for 100 generations using 9 decision variables and constraints on the purity of ammonia. The optimization runs were executed on the high-speed workstation intel Xeon Processor with 128 GB RAM. Table 2 shows the results of three cases along with other calculated objectives and corresponding decision variables. Case 1 corresponds to the minimization of CO₂ emissions (=22322 tonnes/year), which results in lesser profit with lesser energy consumed. The decision variables trend shows that the water flow rate has approached a lower limit in order to meet the objective of CO₂ emissions minimization.

Case 2 results show that optimum profit also results in the worst value of CO₂ emissions. The higher profit is obtained due to the lesser amount of energy consumed. In case 3, the highest possible ammonia production is obtained (=645 kg/hr). The higher product flow rate also resulted in higher CO₂ emissions and relatively higher energy consumption. Fig. 2 shows the profiles along the length of the reactor for temperature and ammonia production for two different cases. As shown in Fig. 2a. and 2b, the higher production of ammonia demanded a decrease in decision variables values for reactor 2 and 3 temperatures.

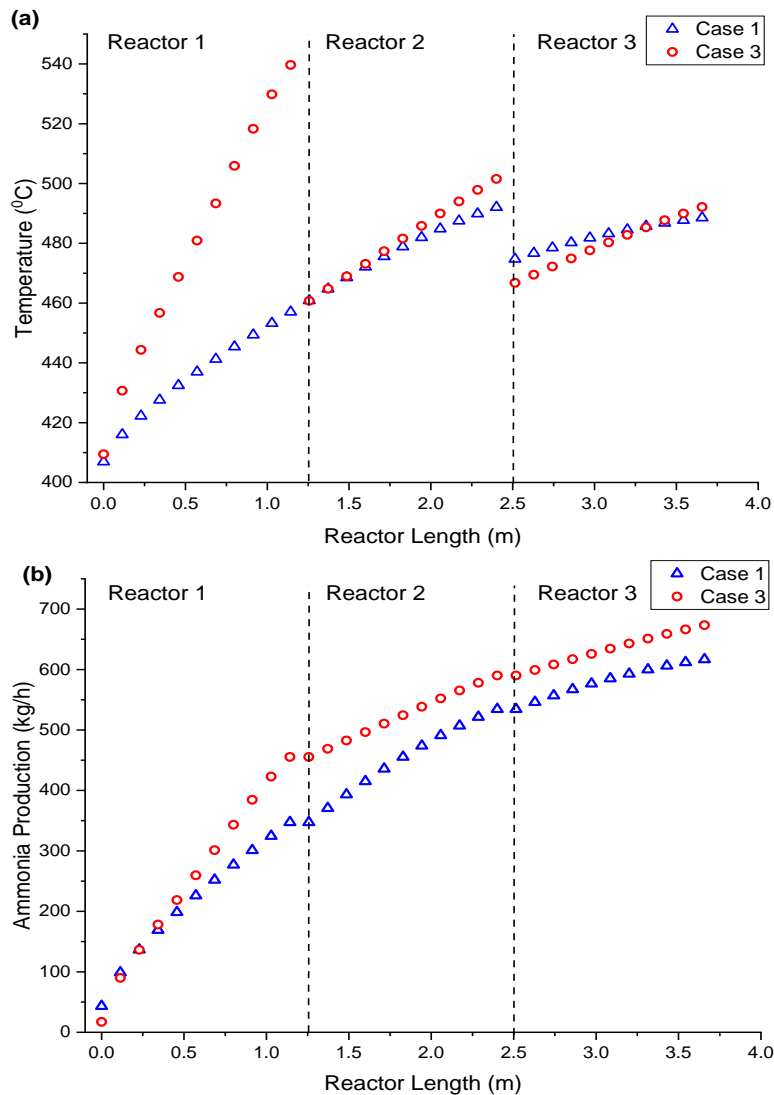


Figure 2: Case 1 and Case 3 results comparison (a) Temperature Vs Reactor length; (b) Ammonia Production Vs Reactor length

CONCLUSIONS

The BBPSO algorithm is used in this study to individually optimized CO₂ emissions, profit, and ammonia production rate. In case 1 minimum value of CO₂ emission is obtained (=22322 tonnes/year) which resulted in profit, ammonia production, and consumed energy values of 264744 (\$/year), 568.03 (kg/hr), and 11667.73 (kW) respectively. For case 2, the objective set was to maximize the profit so the corresponding profit resulted in 63972443 (\$/year) with the highest amount of CO₂ emission (278637 tonnes/year) along with 352.18 (kg/hr) of ammonia production and 1626.21 (kW) energy consumed. Case 3 resulted in the highest amount of ammonia production of 645.59 (kg/hr) with respective 27392 (tonnes/year) CO₂ emission, 211239 (\$/year) of profit, and 14646.59 (kW) of energy utilized. The environmental, economical, and process-related objectives of this study are useful for the ammonia production system for further research-related work. This study is useful to investigate the idea for the production of carbon-free green energy fuels in the coming time for a better tomorrow.

REFERENCES

1. Andersson J, Lundgren J. Techno-economic analysis of ammonia production via integrated biomass gasification. *Appl. Energy*. 2014; 130: 484-490. DOI: 10.1016/j.apenergy.2014.02.029.

2. Zhang H, Wang L, Herle JV, Maréchal F, Desideri U. Techno-economic comparison of green ammonia production processes. *Appl. Energy*. 2020; 259:114135. DOI: [10.1016/j.apenergy.2019.114135](https://doi.org/10.1016/j.apenergy.2019.114135).
3. Chehade G, Dincer I. Progress in green ammonia production as potential carbon-free fuel. *Fuel*. 2021; 299: 120845. DOI:10.1016/j.fuel.2021.120845.
4. Armijo J, Philibert C. Flexible production of green hydrogen and ammonia from variable solar and wind energy: Case study of Chile and Argentina. *Int. J. Hydrog. Energy*. 2020; 45:1541-1558. DOI: 10.1016/j.ijhydene.2019.11.028.
5. Salmon N, Rene B-A. Green ammonia as a spatial energy vector: a review. *Sustain. Energy Fuels*. 2021; 5:2814. DOI: 10.1039/d1se00345c.
6. Bicer Y, Dincer I, Zamfirescu C, Vezina G, Raso F. Comparative life cycle assessment of various ammonia production methods. *J. Clean. Prod.* 2016; 135:1379-1395. DOI:10.1016/j.jclepro.2016.07.023.
7. Wang L, Xia M, Wang H, Huang K, Qian C, Maravelias CT, Ozin GA. Greening Ammonia toward the Solar Ammonia Refinery. *Joule* 2. 2018; 1055–1074. DOI: 10.1016/j.joule.2018.04.017.
8. Demirhan CD, Tso WW, Powell JB, Pistikopoulos EN. Sustainable Ammonia Production Through Process Synthesis and Global Optimization. *AIChE Journal*. 2019; 65, DOI: 10.1002/aic.16498.
9. Xie T, Xia S, Wang C. Multi-Objective Optimization of Braun-Type Exothermic Reactor for Ammonia Synthesis. *Entropy*. 2022; 24, 52. DOI:10.3390/e24010052.
10. Verleysen K, Coppitters D, Parente A, Paepe WD, Contino F. How can power-to-ammonia be robust? Optimization of an ammonia synthesis plant powered by a wind turbine considering operational uncertainties. *Fuel*. 2020;266,117049. DOI:10.1016/j.fuel.2020.117049.
11. Arora P, Hoadley AFA, Mahajani SM, Ganesh A. Multi-objective optimization of biomass based ammonia production- Potential and perspective in different countries. *J. Clean. Prod.* 2017; 148, 363-374. DOI: 10.1016/j.jclepro.2017.01.148.
12. Deng W, Huang C, Li X, Zhang H, Dai Y. Dynamic Simulation Analysis and Optimization of Green Ammonia Production Process under Transition State. *Processes*. 2022; 10, 2143. DOI:10.3390/pr10102143.
13. Champion N, Nami H, Swisher PR, Hendriksen PV, Münster M. Techno-economic assessment of green ammonia production with different wind and solar potentials. *Renew. Sustain. Energy Rev.* 2023; 173, 113057. DOI: 10.1016/j.rser.2022.113057.
14. Olabi AG, Abdelkareem MA, Al-Murisi M, Shehata N, Alami AH, Radwan A, Wilberforce T, Chae KJ, Sayed ET. Recent progress in Green Ammonia: Production, applications, assessment; barriers, and its role in achieving the sustainable development goals. *Energy Convers. Manag.* 2023; 277, 116594. DOI:10.1016/j.enconman.2022.116594.
15. Zhang H, Kennedy DD, Rangaiah GP, Adrián BP. Novel bare-bones particle swarm optimization and its performance for modelling vapor–liquid equilibrium data. *Fluid Ph. Equilibria*. 2011; 301, 33-45. DOI:10.1016/j.fluid.2010.10.025.
16. Kennedy J, Eberhart R. Particle Swarm Optimization. *Proceedings of the Sixth International Symposium Micromachine Human Science, Nagoya, Japan*. 1995; 39–43.
17. Seider WD, Seader JD, Lewin DR. *Product & Process Design Principles: Synthesis, Analysis and Evaluation, (With CD)*. John Wiley & Sons. 2009.

ICH2P14-OP130

EXERGETIC ANALYSIS OF THE PROCESS FOR HYDROGEN RICH SYNGAS PRODUCTION THROUGH BIOMASS GASIFICATION AND ITS ONSITE USE IN HCCI ENGINE FOR LAND TRANSPORTATION

¹Tawfiq Al-Mughanam, ²Abdul Khaliq

¹Department of Mechanical Engineering, College of Engineering, King Faisal University, P.O. Box 380, Al- Ahsa 31982, Saudi Arabia

²Department of Mechanical Engineering, College of Engineering at Yanbu, Taibah University, Yanbu Al-Bahr 41911, Saudi Arabia

*Corresponding author e-mail: talmughanam@kfu.edu.sa

ABSTRACT

This work was aimed to develop and analyze the performance of a system consists of a biomass gasifier producing the syngas rich in hydrogen and its onsite utilization in homogeneous charge compression ignition (HCCI) engine for sustainable transportation. A theoretical formulation for computing the composition of syngas produced after gasification of various biomass materials was developed to predict the percentage of hydrogen appears in the syngas using MATLAB software. The effects of the type of biomass feed and the gasifier operating conditions on exergetic efficiency of the gasifier and on overall performance of the proposed system is examined and a computational method for the investigation based on exergy analysis of the proposed system has also been developed using the EES software. The gasifier operating performance is assessed for the effect of change in equivalence ratio at gasifier (ERG) and steam-to-feed ratio (SFR) and their significant impact is observed on the exergy efficiency of gasifier producing hydrogen. The exergetic efficiency of HCCI engine is also investigated and it is found significantly influenced by the variation of gasifier pressure and type of feed. Among the selected biomass materials, rubber seed derived syngas supplied to HCCI engine resulted in the highest exergy efficiency. The obtained results further show that destruction of fuel exergy is highest in HCCI cylinder 47.73% followed by gasifier 41.72%.

Keywords: Biomass gasification, Hydrogen rich syngas, HCCI engine, Exergy, Sustainable transportation.

INTRODUCTION

The energy used today to satisfy all needs of human is majorly based on combustion of fossil fuels which leads to the generation of pollutant emissions and greenhouse gases. Rapid combustion of fossil fuels to meet the increasing energy demand is resulting into fast depletion of fossil fuel reserves and increased environment degradation. This has drawn increasingly attention for the use of renewable energy source because of the advantages of green environmental protection and inexhaustibility [1]. One of the renewable sources of energy is biomass whose large flexibility as a feedstock is not only recognized to generate heat and power but also to produce hydrogen and biofuel used for transportation. For the conversion of biomass to low-carbon or carbon free fuels, gasification is considered as one of the most attractive technologies as it converts feedstock quite effectively to the transportation fuels such as syngas which is generally a mixture of hydrogen, carbon monoxide, and methane [2]. For small scale applications, biomass gasification using downdraft gasifier is the most effective means of producing syngas and it has gained a new momentum for engine applications. Combustion properties like calorific value, flame speed, and anti-knock behavior of syngas produced in a downdraft gasifier are inferior to conventional hydrocarbon fuels like gasoline and CNG for internal combustion engines [3]. Another concept for biomass gasification is the fluidized bed air-steam gasifier where gasification occurs at higher pressure and temperature in the presence of compressed air and blast steam as a gasifying agent which is expected to produce a syngas having higher hydrogen content which contributes in reducing the pollutant emissions and global warming while maintaining a higher second law efficiency of the engine due to reduced combustion irreversibility [4, 5]. Limited studies are reported regarding the feasibility of using biomass material for producing the hydrogen rich syngas and its utilization in engines for power generation. Most of the syngas fueled engines are downdraft gasifier-based system uses air as a gasifying agent where inner biomass combustion is utilized to supply the required heat of biomass gasification process that leads to the by-products (e.g. SO₂ and NO_x) in the

syngas production, and this restricts the thermal efficiency of biomass used for the production of biofuel [6-8].

To address above stated defects, engine waste heat technology is found as a promising alternative method of utilizing biomass, in which waste heat is used to offer the heat source to generate superheated steam that supplied to biomass gasifier as another gasifying agent along with air which leads to increase the percentage of hydrogen in the syngas produced after gasification [9]. In this regard, this paper aims to propose and investigate a new integrated system consists of air-steam biomass gasification producing the syngas supplied to HCCI engine as this has found as one of the most suitable applications because syngas rich in hydrogen has the characteristics of high flame speed, lower flammability limits, and low auto-ignition temperatures and hence this application results in increasing the utilization efficiency of biomass and in reducing the level of emissions.

SYSTEM DESCRIPTION

Air enters the compressor then part of compressed air goes to gasifier and rest enters the fuel vaporizer after passing through the regenerator. Biomass at ambient conditions fed to the gasifier where it gasifies with superheat steam and compressed air and converts into the hydrogen enriched syngas. The syngas free from tar and char will then enters the fuel-air mixer where it mixes with the compressed and preheated air which enhances the intake temperature and energy content of the charge (fuel-air mixture) which enters the HCCI engine. The charge first compressed then its combustion occurs at constant volume. The combustion products after delivering the power goes to catalytic convertor whose exit at higher temperature enter the gas-turbine which generates power to drive the turbocharger. The turbine exhaust passes through the regenerator where it heats up the compressed air and then routed through the heat recovery steam generator (HRSG) which convert feed water into superheat steam, which is finally delivered to gasifier.

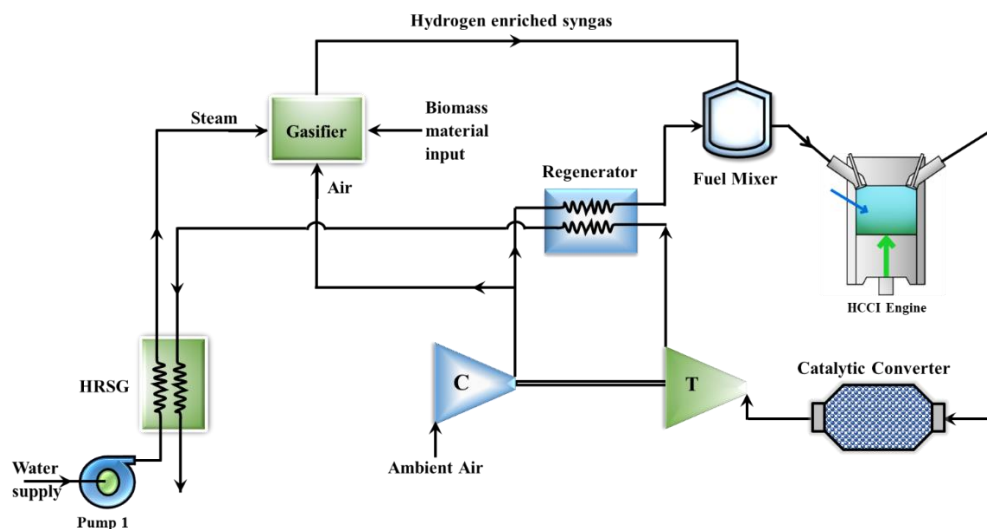
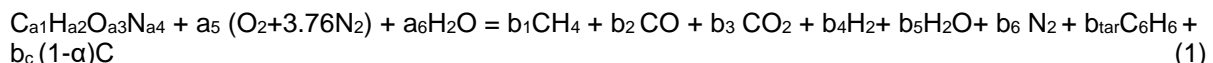


Fig. 1. Schematic diagram of proposed system

MATERIALS AND METHODS

The global chemical reaction inside the fluidized bed gasifier during air-steam gasification process is described as follows



The details of the model developed for the computation of syngas composition and the analysis conducted for the four selected biomass materials gasification can be found in the Ref. [10]. Further, the syngas majorly consists of H₂, CO, and CH₄ is supplied to fuel-air mixer employed before the HCCI engine to prepare the homogeneous mixture of fuel and oxidizer (compressed air). A detailed syngas combustion reaction mechanism used to simulate the HCCI engine is based on the methodology reported in the Ref. [11].

The most common part of exergetic analysis is the physical exergy which deals with the processes having a constant chemical composition during transition from given state to restricted dead state and the physical exergy per unit mass of stream can be expressed as

$$e_{ph} = (h - h_o) - T_o(s - s_o) \quad (2)$$

The change in chemical composition of the working substance is associated with the processes of combustion and gasification, and therefore, the inclusion of chemical exergy has become the integral part of the exergetic evaluation for these two processes.

Chemical exergy of a material stream is computed after employing the expression below

$$\bar{e}_{ch,mix} = \sum y_i \bar{e}_{ch,i} + \bar{R}T_o \sum y_i \ln y_i \quad (3)$$

' y_i ' is the mole fraction of the mixture species and $\bar{e}_{ch,i}$ is the standard chemical exergy of the mixture component per mole, and \bar{R} is the universal gas constant in kJ/kmol-K.

The specific exergy of a flowing stream is the sum of physical and chemical exergy and it is given by

$$e_{total} = e_{ph} + e_{ch} \quad (4)$$

Further detail of exergy formulations developed and utilized to analyze the exergetic performance of a biomass gasifier and the syngas fuelled HCCI engine can be found in the Refs. [10, 12].

RESULTS AND DISCUSSION

A thermodynamic equilibrium model was formulated in this work to simulate the characteristics of a biomass gasifier using the MATLAB Software [10]. Four biomass materials were considered; rubber seed, corn stalk, sawdust, and coconut shell. The impact of steam to feed ratio (SFR) and the equivalence ratio at gasifier (ERG) is investigated on the exergy and exergetic efficiency of gasifier. Furthermore, the impact of change in gasifier pressure is also examined on the exergetic efficiency of HCCI engine coupled with gasifier, and it was evaluated by employing the EES Software [12].

Fig. 2 shows a significant decline in the exergetic efficiency of gasifier with the increase of ERG. This is because increasing the equivalence ratio resulted in the decrease of the concentration of hydrogen in the syngas due to the increased partial combustion when increasing air, i.e., ERG. Since syngas exiting the gasifier carries both physical and chemical exergy, and the chemical exergy of hydrogen is highest among all other constituents of syngas, therefore, a reduction in the contents of hydrogen in the syngas decrease the exergetic output of gasifier and hence its exergetic efficiency reduces at higher ERG. Different types of biomass materials result different composition of syngas with distinct contents of hydrogen when used in the process of gasification. It is observed that promotion of ERG from 0.3 to 0.6 in case of sawdust gasification results in declining the exergy efficiency of gasifier from 51% to 34% and in case of corn stalk it is declined from 45% to 30%.

Fig. 3 shows a decrease in exergy efficiency of gasifier with the promotion of SFR. This is because promotion of SFR results in higher amounts of CH₄. This observation was attributed to the decreased gasification temperature because of increased steam, hindering methane steam reforming and thus increasing the contents of CH₄ in the syngas mixture. It is further argued that higher steam-to-feed ratios decreased the gasification temperature, which subsequently results in a decrease of carbon conversion efficiency. Increasing the concentration of methane compensates the reduction of exergy contents of syngas causes due to the decrease of carbon conversion efficiency but in sum increasing the SFR resulted in the decrease of the exergy accompanied by syngas mixture which is the exergetic output of gasifier. Moreover, the exergy of steam appears in the denominator of expression employed to determine the exergy efficiency of gasifier. Due to these two effects a gradual decline in exergy efficiency of gasifier is observed at the larger increase of SFR. Exergy efficiency of gasifier is influenced by change in type of biomass feed and it is noticed that when biomass feed is changed from sawdust to rubber seed, the exergy efficiency is decreased from 44.8% to 39.5%.

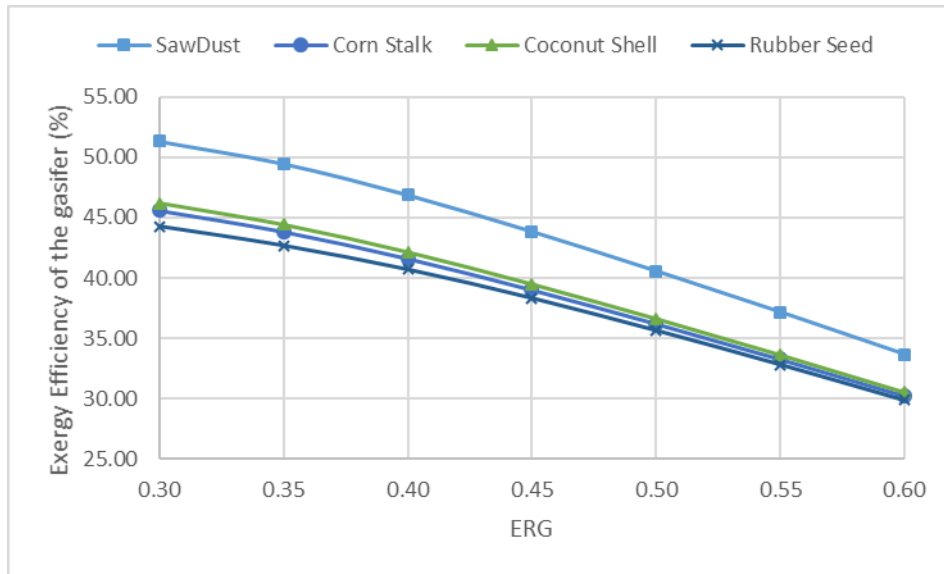


Fig. 2. Effect of gasification equivalence ratio at gasifier (ERG) on exergetic efficiency of gasifier.

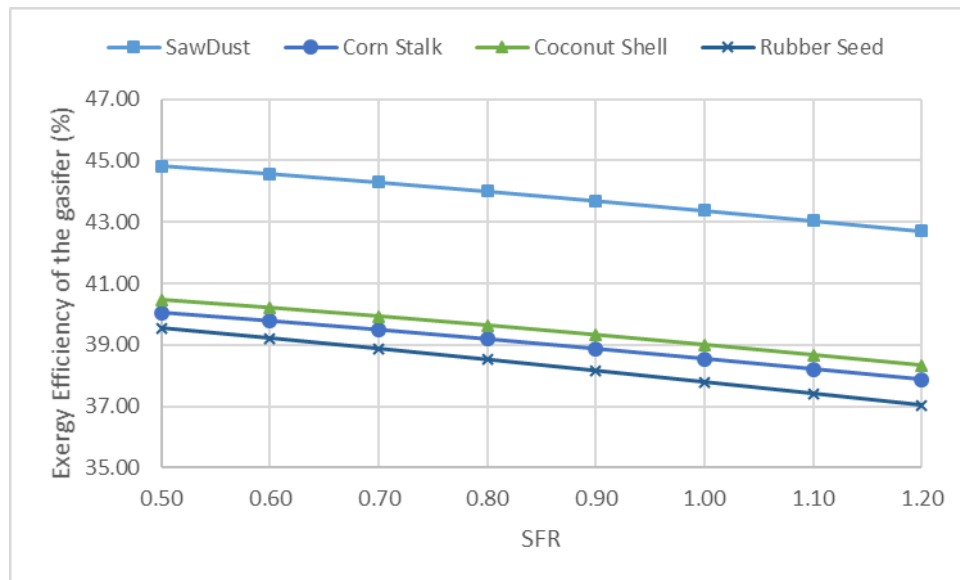


Fig. 3. Effect of steam to feed ratio (SFR) on exergetic efficiency of gasifier.

Fig. 4 illustrates a relationship between the gasifier pressure and the exergy efficiency of HCCI engine which exhibits an upward trend. This occurs because of interplay between charge density and fuel-air mixing which increases if the syngas (fuel supplied to the engine) is produced at elevated pressure. This results in increasing the temperature of mixture inducted into the cylinder that in turn enhances the engine power output which is the exergetic output of the system proposed. In addition, as the gasifier pressure increased, concentration of H₂ and CH₄ in the syngas mixture increased which contributes in increasing the exergy of syngas supplied to HCCI engine and this in turn further increase the engine power output. Input to the system is the chemical exergy of biomass feed which is constant and therefore, due to increase in exergetic output of HCCI engine its exergy efficiency is increasing with the elevation of gasifier pressure.

Fig. 5 shows fuel exergy supplied is destroyed, produced, and loss in the components of the system. Exergy destruction illustrates the internal exergy loss which can be computed in terms of the generation of entropy during the process of gasification and the process of HCCI combustion. Produced exergy is the exergy accompanied by syngas mixture and the HCCI engine output power. Exergy loss is the exergy accompanied by heat transfer to ambient due to difference of temperature between system

boundary and the environment. It is revealed that 41.72% fuel exergy is destroyed in the gasifier which is significantly high because oxidation and reduction reactions occur simultaneously during gasification which increases the entropy of resulting gases and hence the exergy destruction. HCCI engine cylinder attributes highest destruction of exergy of 47.73% and this originate mainly from the irreversible combustion process where entropy is generated via mixing, chemical reaction, and viscous dissipation. As a result, large potential can be achieved to enhance the system exergetic performance by decreasing the gasification and combustion losses.

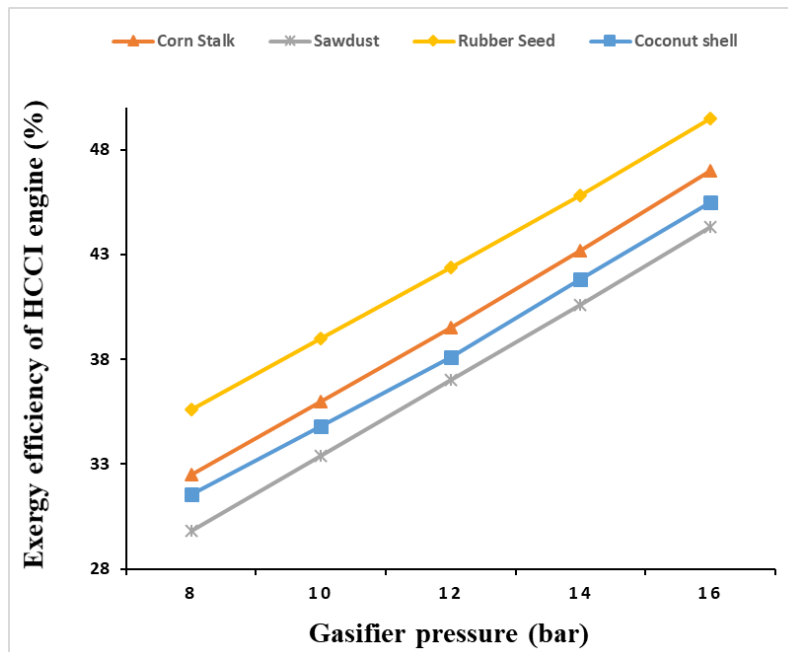


Fig. 4. Effect of gasifier pressure on exergetic efficiency of HCCI engine

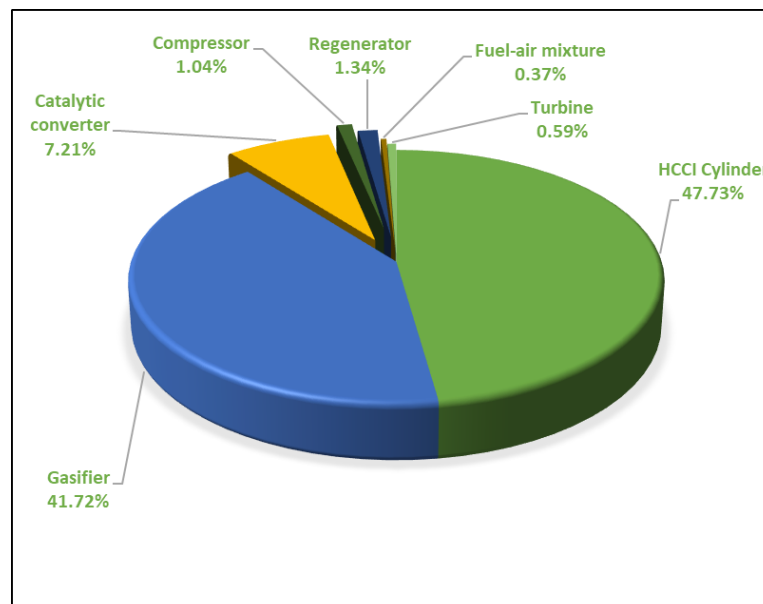


Fig. 5 Percentage of fuel (biomass) exergy distribution in the proposed system

CONCLUSION

Exergetic analysis of the process producing hydrogen rich syngas through air-steam gasification of biomass and its use in HCCI engine for sustainable transportation has been carried out. The system

performance is investigated as a function of equivalence ratio at gasifier, steam-to-feed ratio, and the gasifier pressure. Exergy efficiency of gasifier is found decreasing with increasing of gasification equivalence ratio and steam-to-biomass ratio. The increase of gasifier pressure involves an increase of exergy efficiency of HCCI engine due to enhanced temperature of fuel-air mixture inducted into cylinder as well as due to the increased concentration of hydrogen and methane in syngas mixture. Exergetic analysis identified HCCI engine and gasifier as the largest exergy destructive components 47.73% and 41.72%, respectively, and it is concluded that by reducing losses in these components overall exergetic performance of the proposed system can be improved. Among all the four selected biomass feeds, HCCI engine fuelled by syngas produced through air-steam gasification of rubber seed offers the highest exergy efficiency.

ACKNOWLEDGEMENT

The authors acknowledge the Deanship of Scientific Research, Vice Presidency for Graduate Studies and Scientific Research at King Faisal University, Saudi Arabia, for financial support under the annual funding track [GRANT5138].

REFERENCES

1. Shinnar R and Citro F. 2006. Energy- A road map to U.S. decarbonization. *Science* 313(5791):1243-1244.
2. Guell BM, Sandquist J and Sorum L. 2013. Gasification of biomass to second generation biofuels: A review. *ASME Journal of Energy Resources Technology* 135:014001
3. Mehrpooya M, Khalili M and Sharifzadeh MMM. 2018. Model development and energy and exergy analysis of the biomass gasification process (Based on various biomass sources). *Renewable and Sustainable Energy Reviews* 91:869-887.
4. Samimi F, Marzoughi T and Rahimpour MR. 2020. Energy and exergy analysis and optimization of biomass gasification process for hydrogen production (based on air, steam and air/steam gasifying agents). *International Journal of Hydrogen Energy* 45(58):33185-33197.
5. Olaniyi O, Incer-Valverde J, Tsatsaronis G, Morosuk T. 2023. Exergetic and economic evaluation of natural gas/hydrogen blends for power generation. *Journal of Energy Resources Technology* 145 (6): 062701.
6. Sels BF, Rosen MA, Sharifzadeh A and Shahbeig H. 2022. Exergy sustainability analysis of biomass gasification: a critical review. *Biofuel Research Journal* 33:1592-1607.
7. Viggiano A, Magi V and Fiore M. 2020. Internal combustion engines powered by syngas: A review. *Applied Energy* 276:115415.
8. Sandoval LP and Diaz Gonzalez CA. 2020. Sustainability aspects of biomass gasification systems for small power generation. *Renewable and Sustainable Energy Reviews* 134:110180.
9. Ozveren U and Sezer S. 2021. Investigation of syngas exergy value and hydrogen concentration in syngas from biomass gasification in a bubbling fluidized bed gasifier by using machine learning. *International Journal of Hydrogen Energy* 46(39):20377-20396.
10. Almatrafi E, Khaliq A and Abuhabaya A. 2022. Thermodynamic and exergetic assessment of a biomass derived syngas fueled gas turbine powered trigeneration system. *Case Studies in Thermal Engineering* 35:102099.
11. Saxena M.R, Rajane V and Maurya RK. 2022. Crank angle-based exergy analysis of syngas fuelled homogeneous charge compression ignition engine. *SAE Technical Paper* 2022-01-1037: <https://doi.org/10.4271/2022-01-1037>.
12. Al-Mughanam T and Khaliq A. 2023. Exergy analysis in a HCCI engine powered with hydrogen enriched natural gas. *International Journal of Exergy* 41 (2): 142-166.

ICH2P14-OP133

GRADED GYROID-ENHANCED METAL HYDRIDE CONTAINER FOR EFFICIENT HYDROGEN STORAGE APPLICATION

¹Luthfan Adhy Lesmana, ²Muhammad Aziz

¹Department of Mechanical Engineering, The University of Tokyo, 7-3-1 Hongo, Bunkyo-ku, Tokyo 113-8656, Japan

²Institute of Industrial Science, The University of Tokyo, 4-6-1 Komaba, Meguro-ku, Tokyo 153-8505, Japan

*Corresponding author e-mail: maziz@iis.u-tokyo.ac.jp

ABSTRACT

Hydrogen as an energy storage sector grapples with a pivotal challenge: the imperative to devise efficient hydrogen storage systems. Solid-state compounds such as metal hydrides (MH) emerge as a compelling solution among diverse hydrogen storage technologies, owing to their intrinsic safety attributes and superior hydrogen volumetric density. The limitation of MH lies in its gravimetric density, impeding its applicability in contexts involving mobility.

This study optimizes the designed MH container featuring a gyroid structure and seamlessly integrates the reactor tank into the vehicle's frame and chassis. Subsequently, this design underwent analysis, employing finite element analysis and computational fluid dynamics to evaluate mechanical properties, heat transfer capabilities, and the efficiency of hydrogen charging into the MH within the structure. Through topology optimization of solid isotropic material with the penalization method alongside chamber enlargement through wall offset grading, a 30% augmentation in chamber volume ensued, accompanied by a reduction in the material by nearly 50%. This profound transformation positively impacted the reactor's volumetric and gravimetric density. Despite a measurable reduction in strength, the geometry withstands prescribed mechanical shear loads. The structure also exhibited displacement measuring below 0.2 mm, rendering it suitable for components such as vehicle frames or chassis. Notably, the optimized structure showcased a promising enhancement in the rate of hydrogen charging.

Keywords: Hydrogen Storage, Metal Hydride, Heat Exchanger, Topology Optimisation, Triply Periodic Minimal Surface.

INTRODUCTION

Energy utilities are critical to the shift to sustainable energy sources, assisting with energy security efforts and lowering carbon emissions. Because of its lower greenhouse gas emissions and numerous basic sources, hydrogen appears as a possible alternative energy carrier as countries aim for aggressive CO₂ emission reductions [1]. It offers a compelling alternative for the next generation of automobile and stationary sectors by combustion [2]. However, hydrogen's low volumetric energy density in comparison to other gases creates a storage problem. Metal hydride (MH) technology is considered promising for stationary hydrogen storage, but its low gravimetric hydrogen density causes problems in the mobility industry. MH is produced from a metal complex that is undergoing hydrogen sorption [3]. Just before hydrogen pressure and concentration begin to grow, a solid solution of metal (phase) forms [4]. This reaction can be expressed as Eq(1).



Because of its high hydrogen density per unit volume and safe operating circumstances, MH technology offers potential hydrogen storage possibilities. However, due to its low hydrogen density per unit mass and slow charging and discharging speeds, its use in mobile applications is limited. To address this limitation, one possible solution is to miniaturize and lighten MH reactors and incorporate them into the frame of mobile applications, similar to how lithium batteries are integrated into electric automobiles.

Open-cell porous structures like triply periodic minimal surface (TPMS) structures, on the other hand, have been widely researched for their potential application in the development of bone implants and scaffolds [5]. The TPMS shape is defined by equations that characterize the position of a surface, allowing for the examination of various mathematical functions to improve mechanical qualities while

preserving a high level of porosity. The permeability of TPMS structures promotes bone development and remodeling. TPMS constructions, particularly the gyroid, have been found to have lower levels of stress concentration under compression load when compared to other grid-based lattice [6]

TPMS can be created by arranging mathematically restricted cell shapes asymmetrically in 3D space. These geometries are distinguished by two interlaced networks of spaces with zero-mean curvature. As a result, they have received extensive research for their potential application in heat exchangers, where they have been shown to improve turbulence and heat transfer[7]. TPMS has been cataloged in several forms, including schwartz-p and schoen gyroid, with gyroid have been found effective as metal hydride hydrogen storage containers [8].

METHODS

By optimizing the densities of the elements in a given design domain, the TO method used in this study aims to minimize the volume of the final gyroid structure while meeting stress and displacement constraints. As stated in Eq(2-3), this density optimization serves as a guide for where to reduce volume.

$$\left\{ \begin{array}{l} \text{Find } \rho = (\rho_1 \rho_2 \dots \rho_n)^T \\ \text{Min } V = \sum_{i=1}^n \rho_i v_i \\ \text{S. t. } \left\{ \begin{array}{l} F = Ku \\ u \leq u' \\ \sigma \leq \sigma' \\ 0 \leq \rho_{\min} \leq \rho_i \leq \rho_{\max} \end{array} \right. \end{array} \right. \quad (2)$$

$$E_i = \rho_i^p E^0 \quad (3)$$

Where p is the given design space, V is the gyroid solid volume, F is the given load, K is the global stiffness matrix, u and u' are the global displacement and displacement constraint, σ is the von Mises stress vector, and σ' is the stress constraint. When calculating equilibrium, the optimization objectives use the SIMP method (Wu et al., 2021) to define the density so that it can range from 0 to 1 while maintaining a minimum lower bound of $\min = 0.001$. Furthermore, a penalization power parameter (p) greater than one is introduced; in this study, we use three as the penalization power parameter to increase the resolution of the generated TOed structure. The simple case of a bending problem with a surface load of 5,000N on one face and fixed on the opposite face is used in this study, as shown in Figure 1a. Figure 1a also depicts the 5,030,023 cells used in the TO method. The optimized structure's generated model is used as a scalar function datapoint, and a TPMS gyroid structure thickens the wall based on the density map, as depicted in Figure 1b, with detailed thickness difference observed in Figure 1c. This thickness reduction creates a reactor that has 49% less material than non-TED.

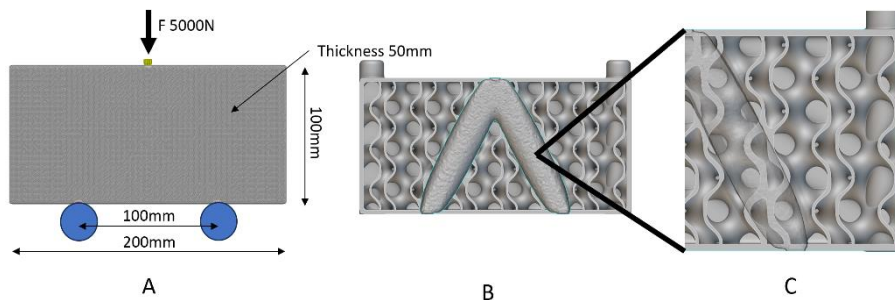


Fig. 1 Visualisation of (A) case studies (B) TO result that overlap with gyroid wall, and (C) zoomed view of differences in wall thickness.

The governing equation is used to simulate the sorption kinetics of hydrogen in the LaNi_5 bed. It includes the volume-averaged energy balance equation, volume-averaged mass balance equation, and reaction kinetics of MH. The energy balance equation is expressed with the following equation.

$$(\rho c_p)_{\text{eff}} \frac{\partial T}{\partial t} = \frac{\partial}{\partial x} \left(k_{\text{eff}} \frac{\partial T}{\partial x} \right) + \frac{\partial}{\partial y} \left(k_{\text{eff}} \frac{\partial T}{\partial y} \right) + \frac{\partial}{\partial z} \left(k_{\text{eff}} \frac{\partial T}{\partial z} \right) - (1 - \varepsilon) \dot{m} \Delta H \quad (4)$$

Where $(\rho c_p)_{\text{eff}}$ is expressed with:

$$(\rho c_p)_{\text{eff}} = \varepsilon(\rho c_p)_{\text{gas}} + (1 - \varepsilon)(\rho c_p)_{\text{mh}} \quad (5)$$

And k_{eff} is defined with:

$$k_{\text{eff}} = \varepsilon k_{\text{gas}} + (1 - \varepsilon) k_{\text{mh}} \quad (6)$$

Mass balance then can be expressed with:

$$(\varepsilon) \frac{\partial \rho}{\partial t} = \dot{m} + (1 - \varepsilon) \frac{\partial}{\partial x} \left(D \frac{\partial \rho}{\partial x} \right) + (1 - \varepsilon) \frac{\partial}{\partial y} \left(D \frac{\partial \rho}{\partial y} \right) + (1 - \varepsilon) \frac{\partial}{\partial z} \left(D \frac{\partial \rho}{\partial z} \right) \quad (7)$$

Where ρ , D , and ε are the density, mass diffusion coefficient, and porosity of MH, respectively, \dot{m} represent hydrogen mass absorbed to MH. Diffusion coefficient D can be expressed as:

$$D = D_o \exp \left(\frac{-H_a}{k_B T} \right) \quad (8)$$

With D_o , k_B , and H_a is the pre-exponential factor, Boltzmann constant, and activation energy respectively and T as temperature. Next, the hydrogen mass rate during absorption per volume can expressed with

$$\dot{m}_a = C_a \exp \left(\frac{-E_a}{RT} \right) \ln \left(\frac{P}{P_{\text{eq}}} \right) (\rho_{\text{sat}} - \rho_{t,a}) \quad (9)$$

ρ_{sat} and $\rho_{t,a}$ is saturated and empty density of MH LaNi_5 . P_{eq} is pressure equilibrium (Vant Hoff equation)

$$\ln(P_{\text{eq}}) = A - \frac{B}{T} \quad (10)$$

A and B denotes Vant Hoff constant. The heat exchanger introduced in the system, coolant at constant flow rate are governed by energy balance equation of

$$(\rho c_p)_f \frac{\partial T_f}{\partial t} + (\rho c_p)_f \vec{u} \text{grad} T_f = \text{div}(k_f \text{grad} T_f) \quad (11)$$

Initially, the MH pressure, density, and temperature are considered to be constant.

$$T = T_o, \quad \rho = \rho_o, \quad P = P_o$$

$$\mathbf{u}_x = \mathbf{u}_y = \mathbf{0}, \quad \mathbf{u}_z = \mathbf{u}_{in}, \quad T = T_{in} \quad (12)$$

RESULTS AND DISCUSSION

3D geometry of the TPMS gyroid MH chamber extracted from the reactor that has been topology optimized is imported as a CAD IGES file into COMSOL Multiphysics. Global parameters and variables' expression of thermophysical for sorption kinetics are set according to Table 1. The study involves three physics component, mass balance, energy balance, and reaction kinetics with time dependent study was selected to investigate the time variation of the reaction. Due to comparison of mesh from normal, to fine to extra fine, fine and extra fine mesh result shows no differences, but the computational time was increased significantly for the extra fine mesh, the fine setting of the mesh is used for this study.

Table 1. LaNi_5 properties

No	Parameters	Value
1.	Density, ρ (kg m^{-3})	8200
2.	Specific heat, c_p ($\text{J kg}^{-1} \text{K}^{-1}$)	419
3.	Thermal conductivity, k ($\text{W m}^{-1} \text{K}^{-1}$)	2.4
4.	Porosity, ε (-)	0.5
5.	Van't Hoff constants used in Eq. (3.8), A (-),	12.99 3704.59
6.	Plateau slope, α (-)	0.038
7.	Hysteresis factor, β (-)	0.137
8.	Initial concentration of MH bed, c_0 (mol m^{-3})	18981.6
9.	Activation energy - Absorption, E_a (J mol^{-1})	21170
10.	Activation energy - Desorption, E_d (J mol^{-1})	16450

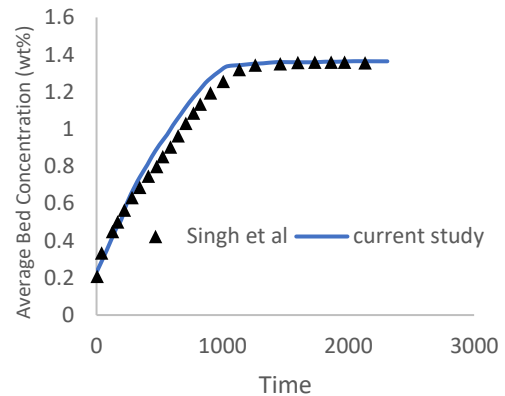


Fig.2 Numerical model and experimental study validation

Numerical simulation study is validated against existing experimental data to validate the model. Singh et.al [9] measured the concentration of MH bed from their model and reacted with hydrogen supply at 15 bar. The comparison in Fig.2 shows that the mathematical model represents the experiment result with the same parameter with the deviation that is assumed caused by the assumption that is being made. The simulation uses a heat transfer coefficient to simulate the cooling condition of $100 \frac{W}{m^2 K}$ to simulate forced convection with water.

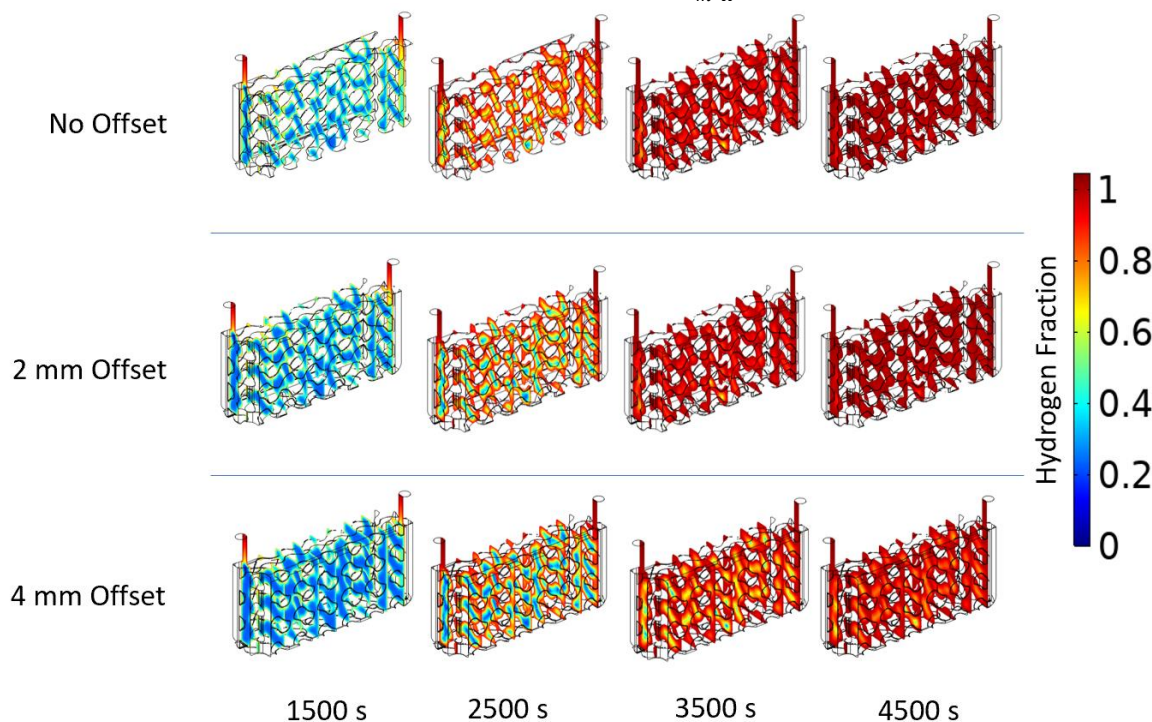


Fig.3 Hydrogen fraction heatmap over time during charging of different values of offset on MH bed chamber

To study the effect of grading the gyroid chamber size, three different chamber size is prepared by increasing the size of the wall offset from the centre. By increasing the wall offset, the MH chamber size is increased, and fluid chamber for cooling and heating the MH is reduced. During charging, it can be seen in Fig. 3 and Fig. 4(left) that the non-offset could reach full hydrogen saturation faster than the 2mm and 4mm offsets. This indicates that the size of the chamber affects the charging time. However, the capacity of hydrogen that can be stored is also considerably better by increasing the offset size of the chamber.

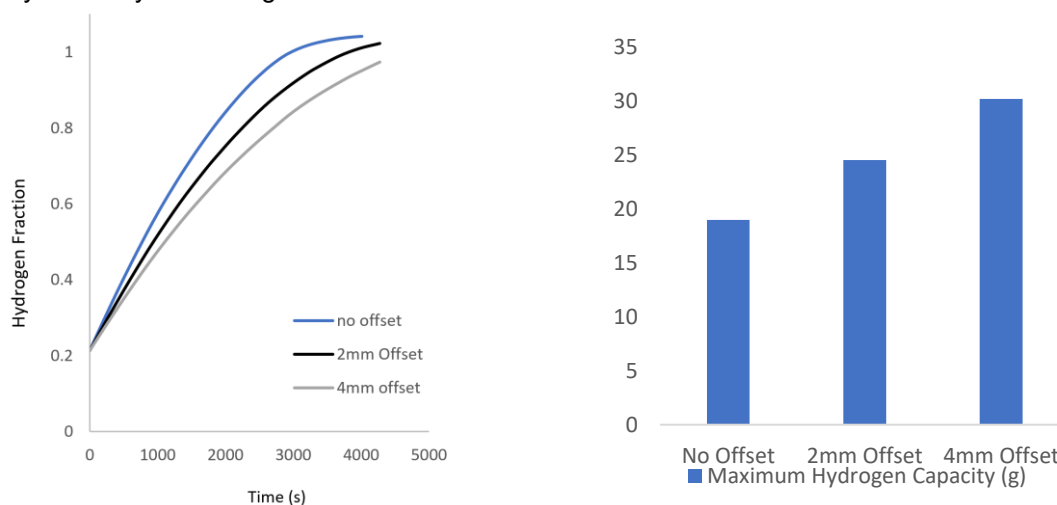


Fig. 4 Hydrogen fraction over time (Left) and maximum hydrogen capacity of each reactor with different chamber offset (Right)



CONCLUSIONS

A reactor containing MH used in hydrogen storage has been generated using the TO method to improve the capacity and reduce the overall reactor volume. The result of the TO generates a structure that can withstand specific loads given during the early stage of design. In this study, the reactor could withstand 5.000 N of bending case while reducing the material by almost 50%. Furthermore, with the use of a mathematical model that has been verified by an existing experiment, the kinetics of hydrogen absorption on the Lani5 MH bed with TPMS gyroid under various graded chamber sizes have been numerically examined. The outcome demonstrates a measurable absorption decrease in charging rate; however, the overall capacity of hydrogen was as good as 30% before becoming unusable due to the missing of another chamber for heat transfer fluid. The current technology availability (additive manufacturing), which is capable of producing a high-strength structure, is good in heat transfer and has multiple chambers, are the major benefits that the TPMS gyroid has. Additionally, given the performance headroom of the present bed reactor, the current analysis might be used to develop a better reactor design for storing hydrogen safely in the mobility sector.

REFERENCES

1. Abe JO, Popoola API, Ajenifuja E, Popoola OM. Hydrogen energy, economy, and storage: Review and recommendation. *Int J Hydrogen Energy* 2019;44:15072–86.
2. Waluyo R, Aziz M. Effects of Chemical Kinetic Mechanism on Pollutant NO Prediction of Turbulent Diffusion Flame Using Large Eddy Simulation 2022;94.
3. Wang H, Prasad AK, Advani SG. Hydrogen storage systems based on hydride materials with enhanced thermal conductivity. *Int J Hydrogen Energy* 2012;37:290–8.
4. Jiao K, Li X, Yin Y, Zhou Y, Yu S, Du Q. Effects of various operating conditions on the hydrogen absorption processes in a metal hydride tank. *Appl Energy* 2012;94:257–69.
5. Dong Z, Zhao X. Application of TPMS structure in bone regeneration. *Engineered Regeneration* 2021;2:154–62. <https://doi.org/10.1016/j.engreg.2021.09.004>.
6. Lu C, Lesmana LA, Chen F, Aziz M. MD-TPMS: Multi-dimensional gradient minimal surface generator [Formula presented]. *Software Impacts* 2023;17:100527. <https://doi.org/10.1016/j.simpa.2023.100527>.
7. Lord EA, Mackay AL, Ranganathan S, Ranganathan S. *New Geometries for New Materials*. Cambridge University Press; 2006.
8. Lesmana LA, Aziz M. Mechanical Behaviour and Fluid Dynamics Analysis of Metal Hydride for Hydrogen Storage Based on Triply Periodic Minimal Surface Structure. *Chem Eng Trans* 2022;94:901–6.
9. Muthukumar P, Singhal A, Bansal GK. Thermal modeling and performance analysis of industrial-scale metal hydride based hydrogen storage container. *Int J Hydrogen Energy* 2012;37:14351–64.



ICH2P14-OP134

THE CORRELATION OF POROUS MATERIAL'S PROPERTIES BETWEEN PARTICLE GEOMETRY FOR HYDROGEN FUEL AND ELECTROLYSIS CELLS

¹Jaeyeon Kim, ¹Luthfan Adhy Lesmana, ²Muhammad Aziz

¹The University of Tokyo, Department of Mechanical Engineering, 7-3-1, Hongo, Bunkyo City, 113-8656 Tokyo, Japan

²The University of Tokyo, Institute of Industrial Science, 4-6-1, Komaba, Meguro City, 153-8505 Tokyo, Japan

*Corresponding author e-mail: maziz@iis.u-tokyo.ac.jp

ABSTRACT

This study focuses on the impact of particle geometry on the properties of porous materials that are crucial to electrochemical devices, such as batteries, electrolysis and fuel cells. There are numerous studies on the properties, but there is little focus on what factor influences these properties and to what extent. Three-dimensional (3D) models with different particle geometry that mimic porous granular with spherical particles and fibrous materials, which are generally utilized for fuel cells, are developed. The particle geometry is as follows: sphere and cylinders with different height-to-diameter ratios of 0.1, 0.5, 1.0, 2.5, 5.0, and 10. Each model exhibits a $43.5 \pm 0.8\%$ porosity, and its particle's volume follows the Gaussian distribution. Through the models, binarized 3D models corresponding to each model have been generated. They consist of 0 or 1 in $400 \times 400 \times 400$ voxels; thus, they are four-dimensional matrixes. Porosity, internal surface area, and tortuosity and chord length of solid and pore phases are figured out and analyzed by utilizing the binarized 3D models and specially written source codes. It is found that specific correlations exhibit Pearson correlation coefficients higher than 0.975 between the particle's sphericity and the internal surface area and chord lengths of solid and pore phases.

Keywords: Porous material, particle sphericity, surface area, chord length, electrochemical devices.

INTRODUCTION

Electrochemical devices including electrolysis and fuel cells play key roles in shifting toward hydrogen society. In these electrochemical devices, porous materials are underlying component to determine behaviors of fluid and resulting electrochemical dynamics. The virtues that they should exhibit are the optimized values for porosity, pore size, high specific surface area, and pore morphology for efficient hydrogen production and utilization.

The porosity is treated as the most basic index; thus, it is a control factor herein. The underlying three indexes (i.e., porosity, specific surface area, and pore size), however, are hard to be measured. For this, several complicated procedures are required, such as gas adsorption method (BET) and mercury intrusion method [1–3].

The pore morphology among the indexes describes pore shape, interconnection, strut, and well and exhibit even more significant impact than pore size [1,4]. Also, this concept can include the morphology of solid phase, and both phases' morphology is closely related. Therefore, we can investigate the effects of the morphology by adjusting particle geometry which organizes entire porous material. In polymer electrolyte membrane fuel cells, powder-based microporous layer and fiber-based gas diffusion backing layer have totally different particle geometry, sphere and cylinder. The morphology is highly likely to affect significantly other indexes or performance of porous material, but other works on particle geometry is almost non-existent in related to fuel cells.

We investigated the correlation between particle geometry and internal surface area, chord length that representative of pore and grain size, and tortuosity under uniform porosity. It is found that there is significant correlation between particle sphericity and porous material properties including internal surface area, chord length of solid and pore phases. The result of the present study can be helpful for understanding and optimizing porous material in electrochemical devices because particle geometry is one of the easiest factors to measure.

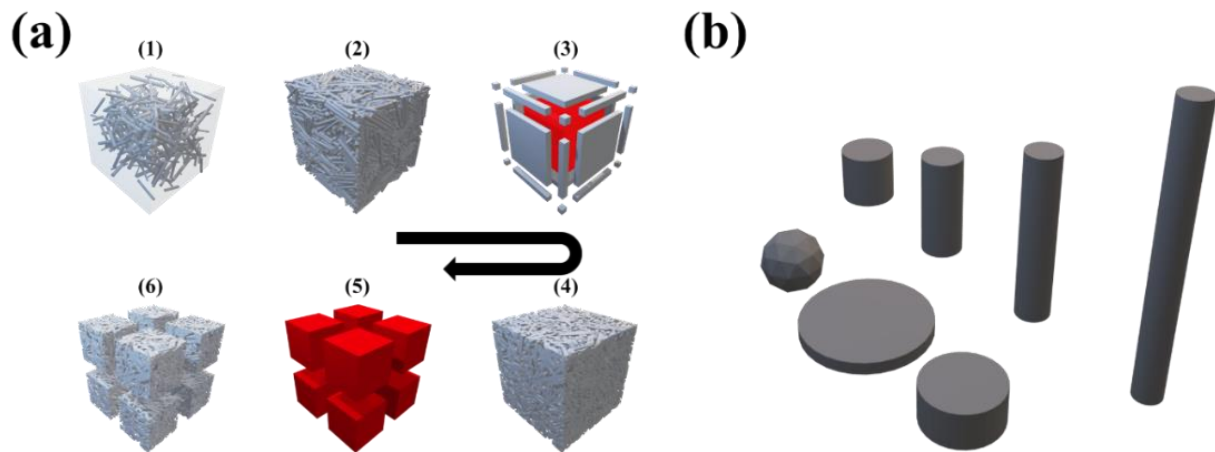


Fig. 1. (a) The process for generating porous materials with different particle geometry, (1) emerging individual rigid particles, (2) forming entire porous material, (3) cutting edges for isotropy, (4) after eliminating the edges, (5) slicing, and (6) the unit sample for analysis and (b) a rendered image of individual particles.

METHODOLOGY

Generation Three-dimensional (3D) Models of Porous Materials

3D models were made by packing spheres and cylinders in a regular hexahedron. The diameter-to-height ratios are differed to 0.1, 0.5, 1.0, 2.5, 5.0, and 10. Each model possesses 3,776 particles with uniform volume distribution of particles. The distribution is according to Gaussian distribution with 5 discrete volumes. Fig. 1 demonstrates the process for generating the 3D models and their particle rendering. Since the particles were generated as rigid body, the overlapping volume between the particles can be negligible.

Generation Binarized Models via the 3D models

The porosity herein is measured by voxel-based method. The 3D models were transformed to 400×400×400 matrixes with each value of 0 (pore) or 1 (solid), it is noted as binarized models. Since the number of coordinates (or voxels) is 6.4e7, the discrimination procedure to distinguish whether each coordinate is in particle or in pore was performed via parallel computing toolbox in MATLAB. The porosity, internal surface area, tortuosity, and chord length for both phases were figured out via the binarized models. The internal surface area and chord length can be delivered by one procedure, since the surface area is directly discovered by the number of chords. In addition, external source codes to discover the distance of two cylinders in 3D space and tortuosity distribution were employed [5,6].

Table 1 Summary of the results and Pearson correlations with sphericity

		Sphere	L/D = 0.1	L/D = 0.5	L/D = 1.0	L/D = 2.5	L/D = 5.0	L/D = 10
Sphericity of Particles		1.0	0.471	0.825	0.874	0.805	0.697	0.579
Porosity (%)		43.02	43.67	43.27	42.95	43.75	44.25	45.49
Specific Internal Surface Area (L²/L³)		27.81	51.95	31.30	30.10	33.39	40.58	44.25
Correlation with Sphericity		$y = 191.96 \cdot \exp(-0.985 \cdot x)$, $R^2 = 0.9776$						
Average Chord Length (L)	Solid	0.140	0.085	0.127	0.134	0.121	0.105	0.095
	Pore	0.106	0.066	0.099	0.099	0.093	0.082	0.079
Correlation with Sphericity		$y = 0.1131 \cdot x + 0.0304$, $R^2 = 0.9732$ (solid phase) $y = 0.0751 \cdot x + 0.0329$, $R^2 = 0.9586$ (pore phase)						
Effective Tortuosity	Solid	1.422	1.287	1.287	1.306	1.332	1.369	1.334
	Pore	1.143	1.327	1.205	1.186	1.168	1.175	1.185

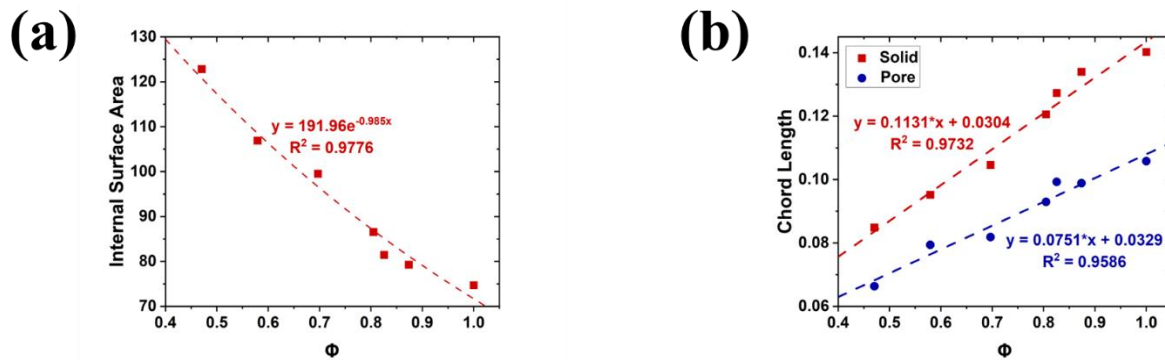


Fig. 2. The correlations between the sphericity and the properties of (a) internal surface area, and (b) average chord lengths of solid and pore phases

RESULTS AND DISCUSSION

The 3D model with spherical particles can mimic granular material based on powder which is prevalent in reality. And the 3D model with cylindrical particle of high height-to-diameter ratio can show behaviors of fibrous materials or provide clues for the generalization by exhibiting intermediate characteristics between that of granular and fibrous materials. All the models have similar porosity and particle volume distribution; thus, we can generalize behaviors of porous materials by solely particle geometry which is an easy-to-know factor.

Table 1 summarizes the properties (i.e., porosity, specific internal surface area, average chord length, and effective tortuosity) of the models. Again, the models herein exhibit negligible overlapping volume between particles, the surface area is directly related to the surface area of individual particles. High surface area leads to high electrochemical active area for hydrogen production and utilization; thus, prediction of surface area is important for manufacturing. The average chord length for solid and pore phases demonstrates the almost same tendency, and they show strong correlation with sphericity. The sphericity, ϕ , is expressed as the following equation (1).

$$\phi = \frac{\pi^{1/3}(6V)^{2/3}}{S} \quad (1)$$

V is particle volume, and S is its surface area. For tortuosity, there is no significant correlation with the sphericity. For solid phase, the model with spheres exhibits the highest tortuosity and it may imply inefficient conduction for heat and electricity. On the other hand, the same model also shows the lowest pore tortuosity, and it means that fluid (e.g., air, vapor, and water) can easy to pass through the model. Fig. 2 demonstrates the relationship between the sphericity and the properties. Based on this, proper prediction can be made for porous material in electrochemical devices

CONCLUSION

It is confirmed that significant correlations certain properties (i.e., specific surface and chord length) between particle's sphericity are exist. By this, precise predictions may be made for more superficial but truly important characteristics such as permeability, diffusivity, and conductivity. They can provide comprehensive understanding and sophisticated application of porous materials.

REFERENCES

1. P.S. Liu and G.F. Chen. 2014. Porous Materials: Processing and Applications. Kidlington. Amsterdam, Elsevier.
2. H. Guo, L. Chen, S.A. Ismail, L. Jiang, S. Guo, J. Gu, X. Zhang, Y. Li, Y. Zhu, Z. Zhang and D. Han. 2022. Gas Diffusion Layer for Proton Exchange Membrane Fuel Cells: A Review, Materials 15:8800.
3. J. Kim, H. Kim, H. Song, D. Kim, G.H. Kim, D. Im, Y. Jeong and T. Park. 2021. Carbon nanotube sheet as a microporous layer for proton exchange membrane fuel cells, Energy 227:120459.
4. Lorna J. Gibson and Micheal F. Ashby. 1997. Cellular solids: Structure and properties, Cambridge, Cambridge University Press.
5. Bruno Luong. 2019. Distance bewteen 2 cylinders in 3D, (<https://www.mathworks.com/matlabcentral/fileexchange/68796-Distance-Bewteen-2-Cylinders-in-3d>), MATLAB Central File Exchange.
6. Ahmet Cecen. 2016. Tortuosity / Connected Path Calculation for 3D Structures, (<https://github.com/Ahmetcecen/Tortuosity-MATLAB>), MATLAB Central File Exchange.



ICH2P14-OP135

PREDICTIVE MODELING OF BIOGAS AND METHANE PRODUCTION FROM COW AND CHICKEN MANURE USING A MODIFIED GOMPERTZ MODEL OPTIMIZED BY PARTICLE SWARM OPTIMIZATION

¹*Nadjiba Sophy*, ²*Nour Elislam Mougari*, ²*Nabil Himrane*, ¹*Luis Le Moyne*

¹Université de Bourgogne, DRIVE, 49 rue Mademoiselle Bourgeois, 58000, Nevers, France

²Laboratory of Energy and Mechanical Engineering, University of M'hamed Bougara, Faculty of technology, cité Frantz. Fanon, 35000, Boumerdes, Algeria

*Corresponding author e-mail: nadjiba.sophy@u-bourgogne.fr

ABSTRACT

In the context of the global energy transition and the imperative of sustainable development, anaerobic digestion of organic waste for biogas recovery presents a compelling alternative. This study aims to develop a robust predictive model for estimating biogas and methane production from organic waste employing advanced optimization techniques. The modified Gompertz model is adopted to characterize the kinetics of biogas production. Parameters optimization of the modified Gompertz model are achieved through the application of the Particle Swarm Optimization algorithm (PSO). To support this research, a comprehensive database sourced from relevant literature is assembled, enabling the creation of predictive models for biogas and methane production. Specifically, this study encompasses the mono-anaerobic digestion of cow and chicken manure, as well as the co-anaerobic digestion of chicken manure blended with sawdust and wheat straw.

Keywords: Biogas, Methane, Anaerobic digestion, Modified Gompertz model, PSO algorithm.

INTRODUCTION

The growth of the world population and economic expansion has led to the issue of waste production, where approximately 1.9 billion tone of solid waste were generated in 2015, with 50% being organic waste [1]. Anaerobic digestion (AD) or methanization is one of the options for the energy valorization principle of organic waste, a well-established and effective biological process that involves the production of biogas as a renewable energy source. However, the production of biogas through such a practice is complex and relies on the interplay of several factors, including changes in operational parameters and monitoring. Understanding the dynamics of these processes is crucial before scaling up AD. Many researchers have focused their attention on and dedicated significant effort to the mathematical modeling of anaerobic digestion. Among the anaerobic digestion models, the Gompertz model has been widely explored in the literature. The kinetic model, and its modified version, have been employed to predict cumulative biogas generation and methane production from various organic waste materials. Matheri et al. [2] applied a modified Gompertz model to establish a relationship concerning biogas generation from pig waste through anaerobic digestion. They demonstrated that the optimal temperature for the digestion process is 37°C. In another research, Deepanraj et al. [3] determined that the Gompertz model outperformed the logistic model in characterizing the kinetic process involved in biogas production from anaerobic digestion of food waste. Zhu, H. et al. [4] utilized the Gompertz model to investigate biogas production resulting from the co-digestion of pig manure and deceased pigs at average temperatures. The obtained results from their model indicated that when the fraction of deceased pigs was under 9%, the anaerobic digestion process was effective, exhibiting a brief lag period and achieving a high rate of raw material utilization. Furthermore, Hansen, B. et al., 2020 [5] explored the integration of machine learning methodologies with the Gompertz model to enhance the accuracy of biogas production prediction, highlighting the potential to improve the precision of models predicting biogas production. The results indicated that the combined model reduced prediction errors by 53% when predicting the methane production one day in advance. Moreover, Lim et al., 2021 [6] demonstrated the suitability of both the modified Gompertz model and logistic-function model in effectively fitting experimental data concerning biogas production from palm oil. Ourradi et al., 2022 [7] demonstrated the accurateness of the Gompertz model in fitting the experimental data for biogas and methane production from date seed showing a correlation coefficient of 0.9331. Ben khedher et al., 2022 [8] employed first order, Gompertz and surface-based models to perform kinetic modeling for the description of anaerobic digestion process of date palm wastes. The results showed that the Gompertz model presented the best fit with the experimental data with a maximum deviation of 6%. Reported literature indicates the effectiveness of employing the Gompertz model for predicting the kinetics of anaerobic digestion processes across diverse waste materials. To the best of our knowledge, there is an absence of reported instances in the literature where the modified Gompertz equation, in conjunction with a particle swarm optimization algorithm, has been utilized to forecast biogas and methane production specifically from the anaerobic digestion of chicken manure with sawdust and wheat straw.

The aim of this work is to develop a hybrid kinetic model based on the modified Gompertz equation to predict cumulative biogas and methane yield. To enhance predictive accuracy, a particle swarm optimization algorithm (PSO) was integrated with the aforementioned model to optimize kinetic parameters. The effectiveness of the proposed model is assessed through statistical performance indicators, specifically the coefficient of determination (R^2) and root mean square error (RMSE), demonstrating the efficacy of the introduced approach.

MODELING AND METHODS

Gompertz modified modeling

There are numerous kinetic models dedicated to AD (Anaerobic Digestion). In general, four types of models can be distinguished. The first-order kinetic model is the simplest and most widely used in anaerobic digestion modeling. It is presented by equation (1) as follows:

$$G(t) = G_0 \times (1 - e^{-Kt}) \quad (1)$$

The Gompertz model, which was originally based on an exponential relationship between a specific growth rate and population density. Gibson et al. [9] modified the Gompertz model to a function that describes cell density during bacterial growth in terms of exponential growth rate and the duration of the lag phase. The function is presented by equation (2) below:

$$G(t) = G_0 \cdot \exp \left\{ -\exp \left[\frac{R_{max} \cdot e}{G_0} (\lambda - t) + 1 \right] \right\} \quad (2)$$

The development of the model for predicting biogas and methane production was carried out in MATLAB. Experimental data on biogas and methane (CH_4) production obtained from the literature [10-14] have been modelled using the modified Gompertz equation identified by equation (2). This equation allows obtaining important digestion parameters (lag phase, specific biogas/methane production, and maximum cumulative biogas/methane production). The equation has been identified as a good empirical model for nonlinear regression and used to simulate the methane accumulation.

To assess the performance and validate the developed model for biogas and methane prediction, the Root Mean Square Error (RMSE) and the coefficient of determination (R^2) have been used, as presented follow:

$$RMSE_{err}^f = \sqrt{\frac{\sum (E_i - P_i)^2}{N \sum E_i^2}} \quad (3)$$

$$R^2 = 1 - \frac{\sum_{i=1}^n (E_i - P_i)^2}{\sum_{i=1}^n (E_i - \bar{P}_i)^2} \quad (4)$$

Optimization of the kinetic parameters of the modified Gompertz equation-PSO

The optimization of the kinetic parameters of the developed model aims to adjust the values of various parameters (G_0 , R_{max} , and λ) to minimize the error and achieve the best possible prediction of experiments while maintaining a correct description of the involved reaction mechanisms.

The objective function to minimize during this operation is the RMSE defined in the equation (4).

In the field of anaerobic digestion, optimizing biogas production from agricultural waste using PSO (Particle Swarm Optimization) has yielded the best results compared to other evolutionary methods. The method remained stable during changes in the number of parameters [15].

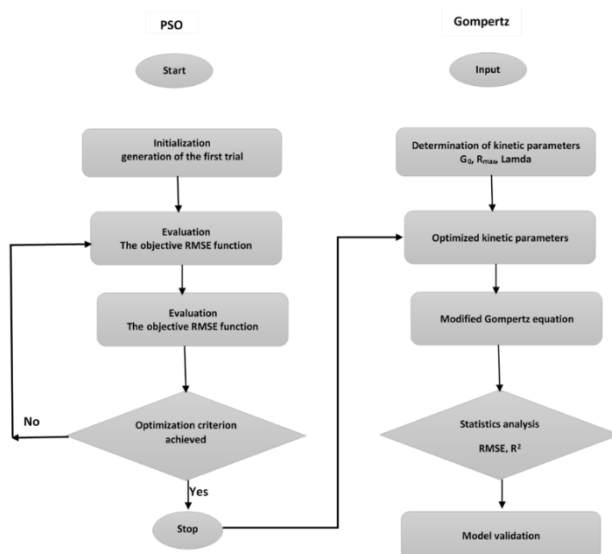


Fig. 1. Optimization algorithm-PSO

Data set

To develop the proposed model for predicting the cumulative production of biogas and methane from the mono-anaerobic digestion of cow and chicken manure, as well as the anaerobic co-digestion of chicken manure with a mixture of wood sawdust and wheat straw, a database of various experiments from previously published works was created.

Experimental data for mono-digestion was obtained from the work of Gopi Krishna Kafle et al., [16]. Five types of manure, including chicken and cow manure, were used to assess the biogas and methane production potential. The experiments have been conducted in a laboratory-scale batch digester at mesophilic temperatures (35-37°C). For experimental data on co-digestion, they were obtained from the work of Darja Pecar et al., [17]. A mixture of chicken manure with wood sawdust and wheat straw at different mass ratios (50:50, 60:40, and 80:20) have been used as substrates for anaerobic digestion. The experiments has been carried out at three temperature levels (35, 40, and 45°C).

RESULTS AND DISCUSSION

Mono-digestion

Using the kinetic parameters optimized by PSO, the fitted curves of biogas and methane production from the mono-anaerobic digestion of cow and chicken manure are presented in figure 2 (a) and (b), and figure 3 (a) and (b), respectively.

The presented results showed a good fit to the experimental data at all phases using the modified Gompertz model optimized by PSO, indicating that the Gompertz equation accurately followed the temporal trend of cumulative biogas and methane production. The RMSE value determined for the cumulative production of biogas and methane from anaerobic digestion of chicken manure is 0.7819 and 0.6021, respectively.

For the cumulative production of biogas and methane from the anaerobic digestion of cow manure, the determined RMSE value is 0.8331 and 0.7253, respectively. It is evident that there is a very small difference between the experimental values and the values predicted by the model, but the RMSE values are close to 0, indicating that the model is well-suited to describe the kinetics of biogas and methane production from anaerobic digestion of poultry and cow manure.

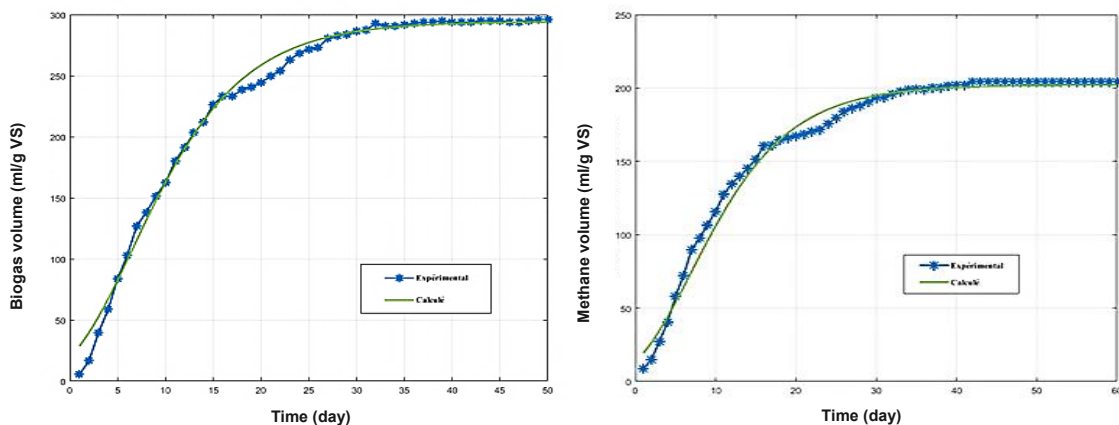


Fig. 2. Cumulative biogas (a) and methane (b) volume from bovine manure

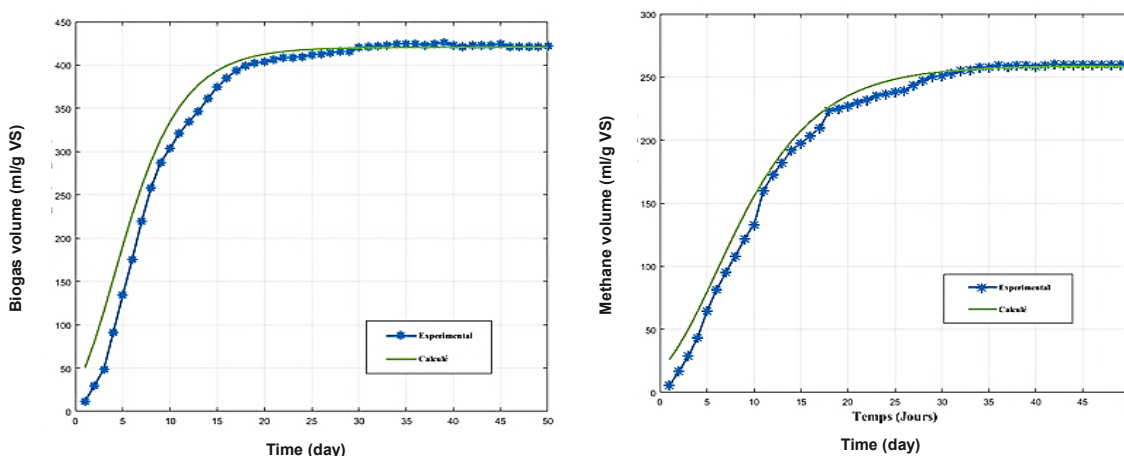


Fig. 3. Cumulative biogas (a) and methane (b) volume from chicken manure.

Co-digestion

The fitted curves of biogas and methane production from the co-digestion of chicken manure and straw for the ratios 80:20, 60:40, and 50:50 are presented in figure 4 (a) and (b), and figure 5 (a) and (b), as well as figure 6 (a) and (b), respectively.

The presented results showed good agreement with the experimental data at all phases using the modified Gompertz model optimized by PSO. The average RMSE values determined for the cumulative production of biogas from the anaerobic co-digestion of chicken manure and straw for the three ratios 80:20, 60:40, and 50:50 are 2.9660, 4.6872, and 2.1887, respectively. The RMSE values for methane are 0.1144, 0.1299, and 0.1026, respectively.

The results indicate that the model is well-suited to describe the kinetics of methane production from the anaerobic co-digestion of chicken manure and straw.

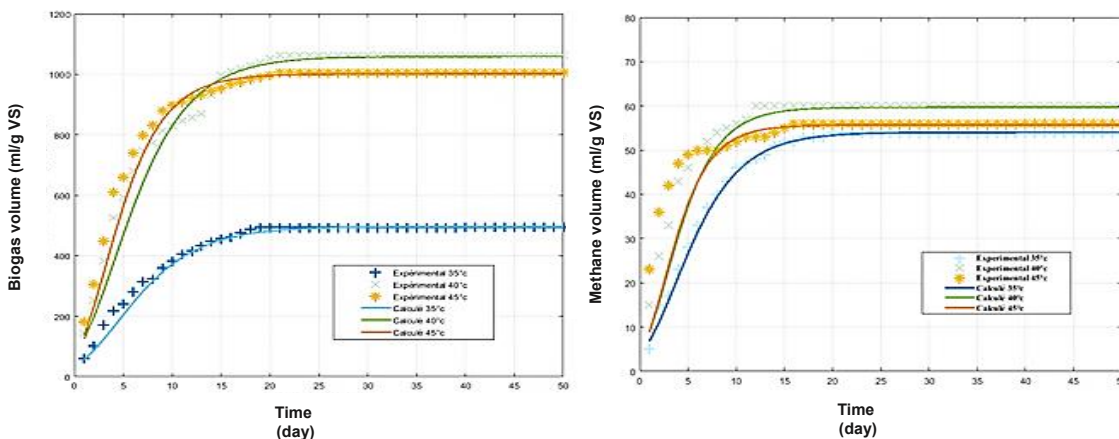


Fig. 4. Cumulative biogas (a) and methane (b) volume of the mixture (80:20)

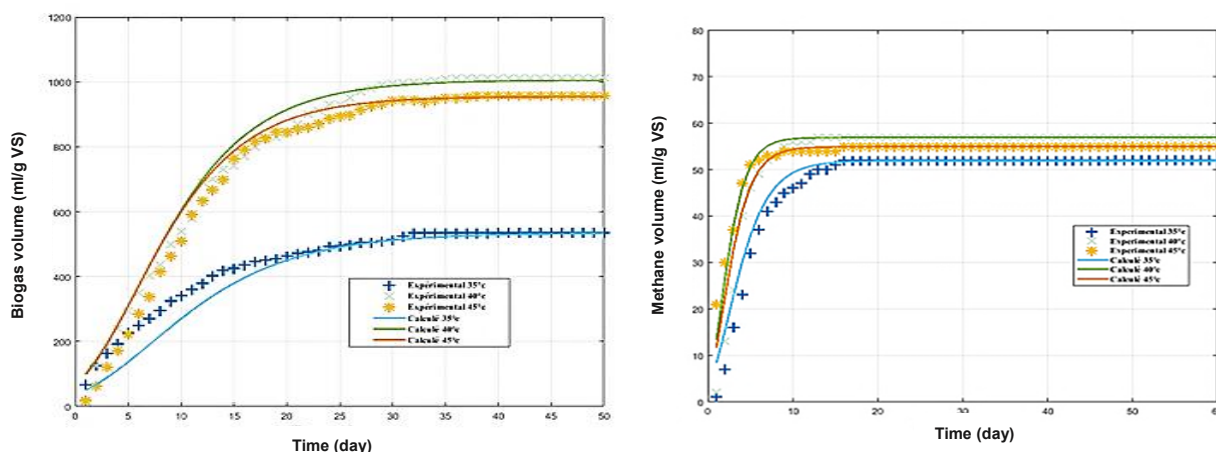


Fig. 5. Cumulative biogas (a) and methane (b) volume of the mixture (60:40)

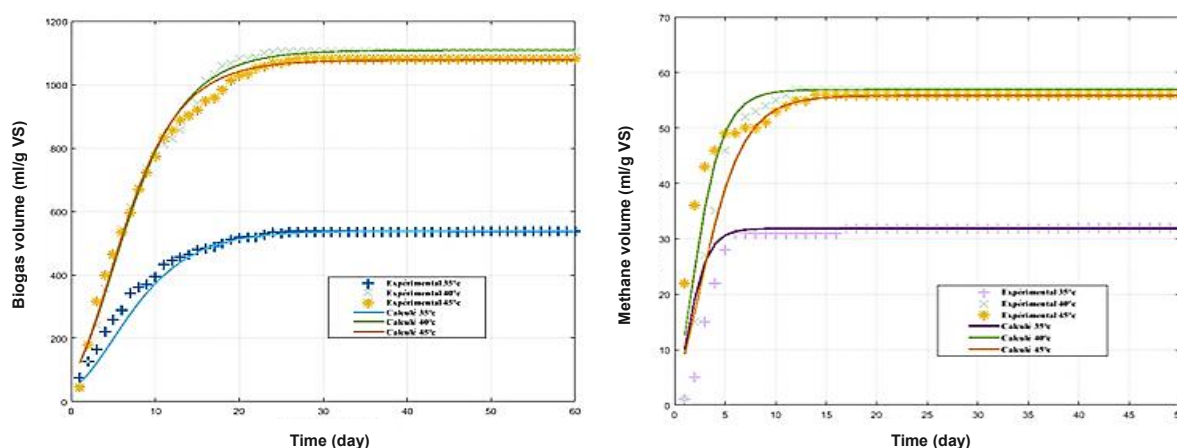


Fig. 6. Cumulative biogas (a) and methane (b) volume of the mixture (50:50)

CONCLUSIONS

In the current context of increasing waste production, the anaerobic digestion and the valorization of the produced biogas, appear as sustainable solutions for waste treatment in the spirit of development. The aim of this work is the prediction of the production of the biogas and the methane in the anaerobic digestion of cow and chicken manure. The biogas production kinetics has been modeled using a modified Gompertz model. This model has been developed based on waste characteristics to facilitate techno-economic studies (maximizing efficiency and economic benefits, stabilizing the AD process, and minimizing costs) or the sizing of a methanization unit at the farm level. A good agreement between this model and experimental data was achieved. Temperature has a proportional influence on methane production kinetics. On the other hand, increasing the biogas volume obtained by adding co-substrates to AD supports the use of co-digestion as a tool for optimizing energy production.

NOMENCLATURE

- G Cumulative yield of biogas/methane at digestion time, ml/g VS
- G_0 Biogas/methane potential of the substrate, ml/g VS
- K Rate constant of biogas/methane production
- t Digestion time, days
- R_{max} Maximal rate of biogas/methane production, ml/g VS

Greek Letters

- λ Lag time, days



REFERENCES

1. Popp, A., 2020. The world's growing municipal solid waste : trends and impacts Recent citations The world ' s growing municipal solid waste : trends and impacts.
2. Matheri, A. N., Belaid, M., Seodigeng, T., & Ngila, C. J. (2016, July). Modelling the kinetic of biogas production from co-digestion of pig waste and grass clippings. In 24th World Congress on Engineering (WCE 2016) London-UK.
3. Deepanraj, B., Sivasubramanian, V., & Jayaraj, S. (2017). Experimental and kinetic study on anaerobic co-digestion of poultry manure and food waste. *Desalination and Water Treatment*, 59, 72-76.
4. Zhao, Y., Sun, F., Yu, J., Cai, Y., Luo, X., Cui, Z., Hu, Y., & Wang, X. (2018). Co-digestion of oat straw and cow manure during anaerobic digestion: Stimulative and inhibitory effects on fermentation. *Bioresource Technology*, 269(July), 143–152.
5. Hansen, B. D., Tamouk, J., Tidmarsh, C. A., Johansen, R., Moeslund, T. B., & Jensen, D. G. (2020). Prediction of the methane production in biogas plants using a combined gompertz and machine learning model. In *Computational Science and Its Applications–ICCSA 2020: 20th International Conference, Cagliari, Italy, July 1–4, 2020, Proceedings, Part I 20* (pp. 734-745). Springer International Publishing.
6. Lim, Y. F., Chan, Y. J., Hue, F. S., Ng, S. C., & Hashma, H. (2021). Anaerobic co-digestion of Palm Oil Mill Effluent (POME) with Decanter cake (DC): Effect of mixing ratio and kinetic study. *Bioresource Technology Reports*, 15, 100736.
7. Ourradi, H., Lahboubi, N., Habchi, S., & Hanine, H. (2022). Methane production from date seed cake (*Phoenix dactylifera* L.) using mesophilic fed-batch anaerobic digestion. *Cleaner Waste Systems*, 2, 100009.
8. Khedher, N. B., Lattieff, F. A., Mahdi, J. M., Ghanim, M. S., Majdi, H. S., Jweeg, M. J., & Baazaoui, N. (2022). Modeling of biogas production and biodegradability of date palm fruit wastes with different moisture contents. *Journal of Cleaner Production*, 375, 134103.
9. Gibson, A. M., Bratchell, N., Roberts, T. A. (1987) The effect of sodium chloride and temperature on the rate and extent of growth of *Clostridium botulinum* type A in pasteurized pork slurry. *Journal of Applied Bacteriology*, 62, 6, 1, 479–490.
10. Nguyen, D. D., Chang, S. W., Jeong, S. Y., Jeung, J., Kim, S., Guo, W., & Ngo, H. H. (2016). Dry thermophilic semi-continuous anaerobic digestion of food waste: Performance evaluation, modified Gompertz model analysis, and energy balance. *Energy Conversion and Management*, 128, 203–210.
11. Hassan, M., Umar, M., Ding, W., Mehryar, E., & Zhao, C. (2017). Methane enhancement through co-digestion of chicken manure and oxidative cleaved wheat straw: Stability performance and kinetic modeling perspectives. *Energy*, 141, 2314–2320.
12. Zhu, H., Yang, J., & Cheng, X. (2019). Application of modified Gompertz model to study on biogas production from middle temperature co-digestion of pig manure and dead pigs. In *E3S Web of Conferences* (Vol. 118). EDP Sciences.
13. Yu, L., Bian, C., Zhu, N., Shen, Y., & Yuan, H. (2019). Enhancement of methane production from anaerobic digestion of waste activated sludge with choline supplement. *Energy*, 173, 1021–1029.
14. Şenol, H., Açikel, Ü., Demir, S., & Oda, V. (2020). Anaerobic digestion of cattle manure, corn silage and sugar beet pulp mixtures after thermal pretreatment and kinetic modeling study. *Fuel*, 263.
15. Gaida, D., Brito, A.L.S., Wolf, C., Baeck, T., Bongards, M., McLoone, S. (2011). Optimal Control of Biogas Plants using Nonlinear Model Predictive Control. In *Proceedings of the ISSC 2011, Dublin, Ireland*, 23–24.
16. Kafle, G. K., & Kim, S. H. (2012). Kinetic Study of the Anaerobic Digestion of Swine Manure at Mesophilic Temperature: A Lab Scale Batch Operation. *Journal of Biosystems Engineering*, 37(4), 233–244.
17. Pečar, D., Pohleven, F., & Goršek, A. (2020). Kinetics of methane production during anaerobic fermentation of chicken manure with sawdust and fungi pre-treated wheat straw. *Waste Management*, 102, 170–178.

ICH2P14-OP137

SODIUM BICARBONATES PRODUCTION THROUGH CARBON MINERALIZATION FOR HYDROGEN STORAGE: A TECHNO-ECONOMIC ASSESSMENT

*Dina Ewis, Zeyad Moustafa Ghazi, Sabla Y. Alnouri, Abdelbaki Benamor, *Muftah H. El-Naas*

Gas Processing Center, College of Engineering, Qatar University, P.O.Box 2713, Doha, Qatar

*Corresponding author e-mail: muftah@qu.edu.qa

ABSTRACT

Hydrogen is a valuable source of energy that can effectively replace fossil fuels. Its combustion mainly yields water, setting it apart from conventional fuels and rendering it a crucial asset for a more sustainable energy future. However, advancements in the utilization of hydrogen fuels remain restricted by the development of efficient storage technologies. In this context, bicarbonates represent a safe and efficient material that can store hydrogen using a catalyst to produce formate, which is well-known for its high storage capacity. Solvay processes produce sodium bicarbonate through the reaction of reject brine and CO₂, providing a pathway for producing an economically attractive product while simultaneously mitigating two major environmental threats. This work reports a systematic techno-economic assessment of the conventional and Ca(OH)₂ modified Solvay processes. The model evaluates the effect of varying the brine salinity, temperature, and pressure on the CO₂ and Sodium ions removal and bicarbonate production. In addition, the process cost associated with each parameter and the effect of carbon tax on the process profitability were analyzed. The results indicate that varying brine characteristics influence sodium removal, CO₂ removal, bicarbonate production, and process profitability. Moreover, the amount of Ca(OH)₂ obtained via the modified Solvay was found to be economically feasible, as it generated a satisfactory annual profit even without the implementation of any carbon tax. However, after the implementation of 40 \$/tonne CO₂ as a carbon tax, the conventional Solvay process was found to break even.

Keywords: Techno-economic, Solvay, modified Solvay, bicarbonates.

INTRODUCTION

The escalating levels of carbon dioxide (CO₂) concentration in the atmosphere as a consequence of fossil fuel combustion for energy production pose a major environmental threat. Besides, the continuous consumption of non-renewable energy sources, considering the current energy demand causes resources' depletion that threatens the life quality of future generations. In this context, the utilization of green energy sources is a critical matter for a more sustainable energy and eco-friendly future. Hydrogen is a valuable energy source that can replace fossil fuels. Unlike fossil fuels, its combustion produces water only. Despite that, its application is limited because of inefficient hydrogen storage technologies. The current storage materials including alanates, ammonia, and amides are limited by the need of complex thermal management during hydrogenation and de-hydrogenation, toxicity, and corrosivity [1].

The Solvay process involves the reaction of reject brin with CO₂ to produce sodium bicarbonate (NaHCO₃) [5]. This process produces economically attractive product that can be used for hydrogen storage while simultaneously mitigating two of the major environmental threats. Bicarbonates represent a safe and efficient material that can store hydrogen in the presence of a catalyst to produce formate. Formate is known for its high storage capacity, good stability, and non-corrosivity [1, 4]. It is worth mentioning that the conventional Solvay process involves the reaction of reject brin with CO₂ in the presence of ammonia (NH₃) producing NaHCO₃. The reaction is followed by NH₃ recovery, which is an energy-intensive process to be introduced back to the reaction. This process was modified by El-Naas [2] in which NH₃ was replaced by Ca(OH)₂ and the recovery unit was eliminated. The reaction of conventional and modified solvay are expressed by Equations (1) and (2), respectively.



This study represents a techno-economic analysis for both the conventional and the Ca(OH)₂ modified Solvay processes. The study is the first to assess the influence of the brine characteristics in terms of temperature, pressure and salinity on the process performance and economic feasibility for NaHCO₃ production. Furthermore, the influence of carbon tax implementation on the economic feasibility of the processes at different salinities was investigated.

METHODS

The conventional and Ca(OH)₂ modified Solvay process were compared by constructing the material and energy balances, assuming a steady state process for each case. The extent of the reaction was calculated according to the Equation (3) below.

$$\varepsilon = \frac{C_{LM} - ((1-FC) * C_{LM})}{v_i} \quad (3)$$

Where C_{LM} is the concentration of the limiting reactant in molar/min, FC is the fractional conversion, and v_i is the limiting reactant stoichiometry.

Table 1 outlines the process parameter used in this study. Besides, the equipment lifetime was assumed to be 20 years. It should be noted that since the process operates at ambient conditions, pumps were the only units that requires energy. However, the energy cost associated with pumps was neglected in this study since it was found to be quite similar for both process. Moreover, for the conventional Solvay case, the ammonia recovery unit is energy intensive, but the cost of ammonia considered in the calculations compensated for the energy requirements. In addition, all gas streams were assumed to be ideal gas with molecular weight corresponds to 29 g/mol. The flow rate of the gas stream was calculated based on 100 gas to liquid ratio. Table 2 shows the cost of chemicals that were utilized. The final profit equation as shown below.

$$\text{Profit} \left(\frac{\$}{\text{yr}} \right) = \text{Revenues} \left(\frac{\$}{\text{yr}} \right) - \text{Cost of equipment} \left(\frac{\$}{\text{yr}} \right) - \text{Cost of chemicals} \left(\frac{\$}{\text{yr}} \right) \quad (4)$$

The profit (\$/yr) was converted to \$/m³ of brine through the equation below.

$$\text{Profit} \left(\frac{\$}{\text{m}^3} \right) = \frac{\text{Profit} \left(\frac{\$}{\text{yr}} \right) \times \frac{1 \text{ yr}}{525600 \text{ min}} \times \dot{m} \left(\frac{\text{kg}}{\text{min}} \right)}{\rho \left(\frac{\text{kg}}{\text{m}^3} \right)} \quad (5)$$

Table 2. List of process parameters.

Process/Parameter	Reagent inlet Ratio	Reagent wt%	Reactor type/ conversion (C)	NH ₃ recovery reactor	
				Fractional conversion	Molar ratio
Conventional	Mass flow ratio 0.03 NH ₃ : NaCl	25%	Bubble reactor, C=0.86	1	Molar ratio of 2 Ca(OH) ₂ : NH ₄ Cl
Ca(OH) ₂ modified Solvay	Molar ratio 0.3 Ca(OH) ₂ : NaCl	2%	Inert-particles spouted bed reactor (IPSBR), C=0.6	-	-

Table 2. Chemicals cost.

Chemical	Cost (\$US/kg)
KOH	0.83
Ca(OH) ₂	0.11
NH ₃	0.45
NaHCO ₃	0.28

The temperature, pressure, and salinity were correlated with the brine density through the model suggested by [3]. The calculations of the brine density in term of temperature, pressure and salinity were carried out via MATLAB [6], whereby the density correlations with respect to temperature, salinity and pressure was taken from [3].

RESULTS AND DISCUSSION

Figure 1 shows the effect of brine temperature, pressure and salinity on conventional Solvay removal capability and the respective economic feasibility. The increase in brine temperature elevates the Inert-particles spouted bed reactor (IPSBR) temperature, thereby, its conversion is reduced considerably. As shown in Figure 1a, as the brine temperature increases from 20 °C to 40 °C, both CO₂, and sodium removal decreases. This reduction is associated with more expenditure due to the reduction in NaHCO₃ production. The removal data are in agreement with the experimental data reported in [5]. On the other hand, the brine pressure does not have an influence on

the process performance due to its negligible effect on the brine density (Figure 1b). Brine salinity has a significant effect on CO₂ and sodium removal. As shown in Figure 1c, the sodium removal reduces as the brine salinity increases, while the CO₂ removal initially increases and then levels out at 80%. The reduction in sodium removal is attributed to the increase in sodium initial concentration while the conversion ratio of the reactor is constant. It is worth noting that the profit per metric tonne of brine rises as the salinity increases from 10 to 30 PSU. The steep increase is attributed to the rise in NaHCO₃ production. The profit remains almost constant afterwards because of the constant production rate of NaHCO₃.

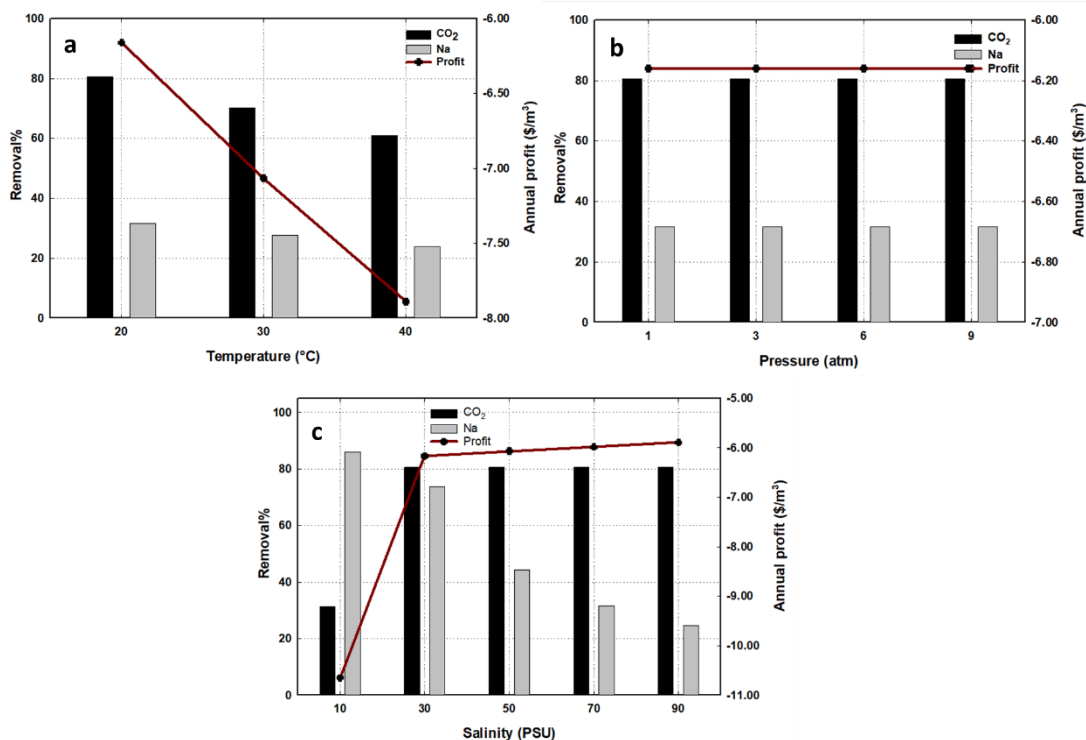


Fig. 1. Effect of reject brine (a) Temperature (b) Pressure (c) Salinity on the conventional Solvay performance and profitability.

The influence of brine temperature, pressure and salinity of Ca(OH)₂ modified Solvay performance and economic feasibility is demonstrated in Figure 2. The increase in brine temperature reduces the reactor conversion, which lead to a reduction in CO₂ and sodium removal (Figure 2A). Thereby, the reduction in the reactor conversion results in less NaHCO₃ production, which causes a drop in annual profit per metric cube of brine. The removal data are in agreement with the experimental data reported in [2]. Figure 2b indicates that pressure does not have an influence on removal percentage of CO₂ and sodium nor the NaHCO₃ production, thereby, the annual profit is not affected. It is worth mentioning that the increasing brine pressure from 1 atm to 9 atm does not influence the brine density significantly. Nevertheless, brine salinity influences the Ca(OH)₂ modified Solvay performance considerably. As the brine salinity increases from 10 PSU to 90 PSU, the CO₂ removal increases from around 12% to almost 100% while the sodium removal remains constant. The removal percentage of sodium is constant as Ca(OH)₂ to NaCl molar ratio shown in table 1 is the optimum ratio that ensure the maximum removal sodium. It is observed that the profit exhibits an upward trend from 1 \$/m³ to an impressive 10\$/m³. This is attributed to the rise in NaHCO₃ production rate from 5.17 kg/min to 46 kg/min with the salinity.

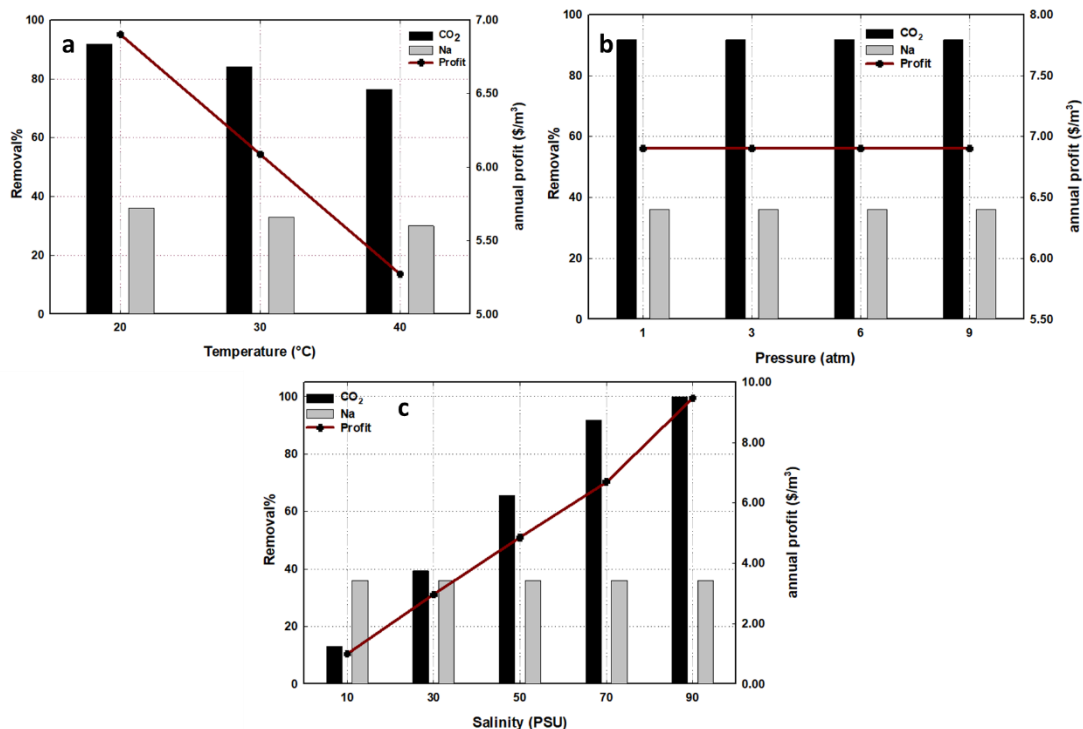


Fig. 2. Effect of reject brine (a) Temperature (b) pressure (c) Salinity on the Ca(OH)₂ modified Solvay performance and profitability.

The effect of implementing carbon tax on conventional and Ca(OH)₂ modified Solvay processes at different brine salinity is shown in Figure 3. The Figure depicts the influence of sea water salinity level as well as reject brine salinity level to assess the processes economic feasibility. As it can be seen, the Ca(OH)₂ modified Solvay process is profitable even without the implementation of carbon tax. In addition, as brine salinity increases, the annual profit increases due to the increase in NaHCO₃ production. For conventional Solvay, the process reaches the break-even point with the implementation of a carbon tax of 40 \$/tonne CO₂. It is worth mentioning that changing the brine salinity does not have a significant influence on the economic status of the conventional Solvay process, which is confirmed by the data obtained from Figure 1c.

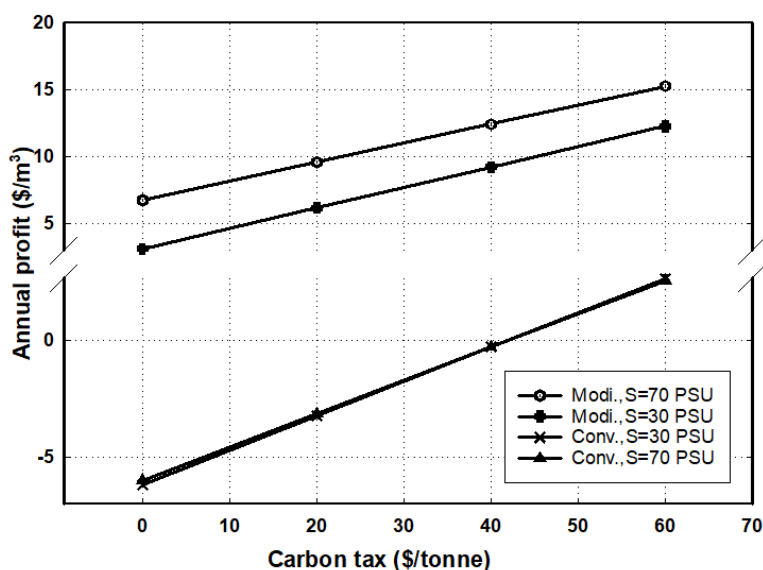


Fig. 3. Effect of Carbon tax implementation on Solvay processes profitability at different reject brine salinity.



CONCLUSIONS

In summary, this study demonstrated a techno-economic assessment on conventional and $\text{Ca}(\text{OH})_2$ modified Solvay process investigating the influence of brine characteristics, including temperature, pressure and salinity on the process. Generally, the results suggested that the conventional Solvay requires a substantial amount of expenditure, while $\text{Ca}(\text{OH})_2$ the modified Solvay generates a moderate profit. In addition, brine temperature reduces the removal capability of the Solvay process due to a reduction in the reactor conversion, thereby, the processes become more non-profitable. Moreover, unlike temperature, the brine pressure does not affect the performance of both Solvay processes. The prominent effect was mainly caused due to brine salinity variations that influenced both processes differently. Lastly, implementing carbon tax causes conventional Solvay to reach a break-even point at 40 \$/tonne CO_2 , while the $\text{Ca}(\text{OH})_2$ modified Solvay becomes more profitable upon carbon tax implementation. Overall, these data suggest the economic feasibility of the $\text{Ca}(\text{OH})_2$ modified Solvay, when compared to the conventional Solvay process.

ACKNOWLEDGEMENT

The authors would like to acknowledge the support of Qatar National Research Fund (a member of Qatar Foundation) through Grant # NPRP 12S-0215-190090. The findings achieved herein are solely the responsibility of the authors.

REFERENCES

- [1] M. Calabrese, D. Russo, A. di Benedetto, R. Marotta, R. Andreozzi, Formate/bicarbonate interconversion for safe hydrogen storage: A review, *Renewable and Sustainable Energy Reviews* 173 (2023) 113102.
- [2] M.H. El-Naas, A.F. Mohammad, M.I. Suleiman, M. Al Musharfy, A.H. Al-Marzouqi, A new process for the capture of CO_2 and reduction of water salinity, *Desalination* 411 (2017) 69-75.
- [3] A.E. Gill, *Atmosphere-ocean dynamics*, Academic press 1982.
- [4] C. Lang, Y. Jia, X. Yao, Recent advances in liquid-phase chemical hydrogen storage, *Energy Storage Materials* 26 (2020) 290-312.
- [5] A.F. Mohammad, M.H. El-Naas, M.I. Suleiman, M.J.I.J.C.E.A. Al Musharfy, Optimization of a solvay-based approach for CO_2 capture, 7(4) (2016) 230.
- [6] G. Ruiz-Martinez, Seawater density from salinity, temperature and pressure, 2023. <https://www.mathworks.com/matlabcentral/fileexchange/85900-seawater-density-from-salinity-temperature-and-pressure>. (Accessed Retrieved November 26, 2023).



ICH2P14-OP138

DESIGN AND PERFORMANCE ANALYSIS OF AMMONIA-BASED POWER GENERATION¹Kazuki Ohira, ¹Rahmat Waluyo, ^{2*}Muhammad Aziz¹Department of Mechanical Engineering, The University of Tokyo, 113-0032, Tokyo, Japan²Institute of Industrial Science, The University of Tokyo, 153-8505, Tokyo, Japan

*Corresponding author e-mail: maziz@iis.u-tokyo.ac.jp

ABSTRACT

In the energy transition from petroleum to carbon-neutral fuel, ammonia appears as a promising energy carrier for power generation using gas turbines, combined cycles, and fuel cells. However, its low reactivity makes ammonia harder to ignite, leading to low combustion efficiency and high NO_x emission when burned in the existing combustion chamber. Mixing ammonia with a more reactive fuel, such as hydrogen from the partial cracking of ammonia, could improve the combustion yield. This paper investigates the performance of ammonia-based combined cycle power generation with an ammonia cracking facility. The proposed system is evaluated by thermodynamic modeling of each component covering heat transfer, pressure change, and ammonia cracking reaction process. The ammonia and hydrogen co-combustion is validated by simulation of laboratory scale pilot combustor. The results obtained show general agreement between the conducted simulation and measurement of the pilot scale combustor, whose results are used to model combustion reaction in the plant scale combustor. In the integrated system, the performance is characterized by the technically feasible turbine inlet temperature, which depends on the operation variables such as equivalence ratio and ammonia cracking ratio.

Keywords: Ammonia combustion, Hydrogen combustion, Ammonia cracking, Combined cycle.

INTRODUCTION

As a non-carbon fuel, hydrogen (H₂) is considered pivotal in realizing a low or zero-carbon society. The utilization of H₂ as a fuel generates no GHGs, as its oxidation produces water. In addition, H₂ can be produced from many available primary energy sources through various conversion technologies, including thermochemical, biological, chemical, and electrical routes [1]. Although H₂ shows a very high gravimetric energy density (lower heating value of 33.3 MJ kg⁻¹), its volumetric energy density is very low (3 Wh L⁻¹) [2]. This observation leads to the challenges of storing and transporting H₂, which is a critical factor for the realization of a successful H₂ economy in the future [3].

There are many media and technology options to store H₂, including compression, liquefaction, metal hydrides [4], liquid organic carriers, ammonia (NH₃), and methanol (CH₃OH). Among proposed alternatives, NH₃ shows advantages in terms of H₂ content (gravimetric and volumetric H₂ contents of 17.8 wt.% and 121 kg-H₂ m⁻³, respectively) [2], high stability during long-term storage [5], possibility for direct use, and established infrastructure and regulation [6]. Wijayanta et al. [7] have performed a techno-economic comparison of high-density H₂ storages, including liquid H₂, methylcyclohexane, and liquid NH₃. They found that liquid NH₃ is the most promising as it exhibits the lowest total cost, the highest total energy efficiency, and the highest volumetric H₂ density.

Although NH₃ is promising as an H₂ carrier, its utilization as a fuel faces several physical and chemical challenges, including high energy demand for both synthesis and decomposition, relatively higher apparent toxicity (about three times of methanol), narrow flammability range (15.15–27.35% at dry air and 15.95–26.55% at 100% relative humidity), and higher risk for NO_x emission [1]. The autoignition temperature of NH₃ is 651 °C, which is higher than H₂ (585 °C) and other conventional hydrocarbon fuels (537 and 232 °C for methane and gasoline, respectively). In addition, the minimum ignition energy for NH₃ is also higher (8.0 mJ) than H₂ (0.011 mJ) and CH₄ (0.28 mJ) [8]. The combustion reaction of NH₃ is slow, as denoted by its laminar burning velocity, which is only 0.07 m s⁻¹ and significantly lower than H₂ (3.51 m s⁻¹) and CH₄ (0.38 m s⁻¹). Due to those characteristics and the possibility of NO_x formation, pure NH₃ combustion does not appear as a viable solution. The co-combustion of NH₃ with other fuels, including H₂ and CH₄, has been actively studied to solve those problems in dedicated NH₃ combustion [9], [10]. In terms of zero-carbon realization, the co-combustion of NH₃ and H₂ is considered promising, as it produces no CO₂ with high combustion performance. In addition, H₂ can be produced from NH₃ decomposition; therefore, a single fuel (NH₃) can be adopted, resulting in better fuel handling, storage, and transportation.

Therefore, this research aims to address the issue of low reactivity of NH₃ by proposing an integrated power generation with NH₃ cracking. The objective of this study is to perform basic combustion simulations of NH₃-H₂

co-combustion on a laboratory scale and to develop a process design that can be applied to actual combustors. The novelty of this study is that it integrates a cracking system in the NH₃-H₂-based power generation system and reflects the basic co-combustion analysis to the integrated system.

METHODS

Model Description

In this work, an NH₃-fired combined cycle with a cracking facility is proposed as a novel power generation system. A portion of NH₃ stream is fed into a cracking reactor, where NH₃ is decomposed into N₂ and H₂. The heat required to sustain the endothermic NH₃ cracking is taken from the combustion products stream through a heat exchanger. Subsequently, both pure and cracked NH₃ are mixed and compressed before being fed into the combustor. After flowing through the NH₃ preheater, the combustion products are expanded in a gas turbine. The outlet of a gas turbine is fed into a heat recovery steam generator (HRSG), which drives the steam Rankine cycle. Fig. 1 illustrates the overall process in the proposed system.

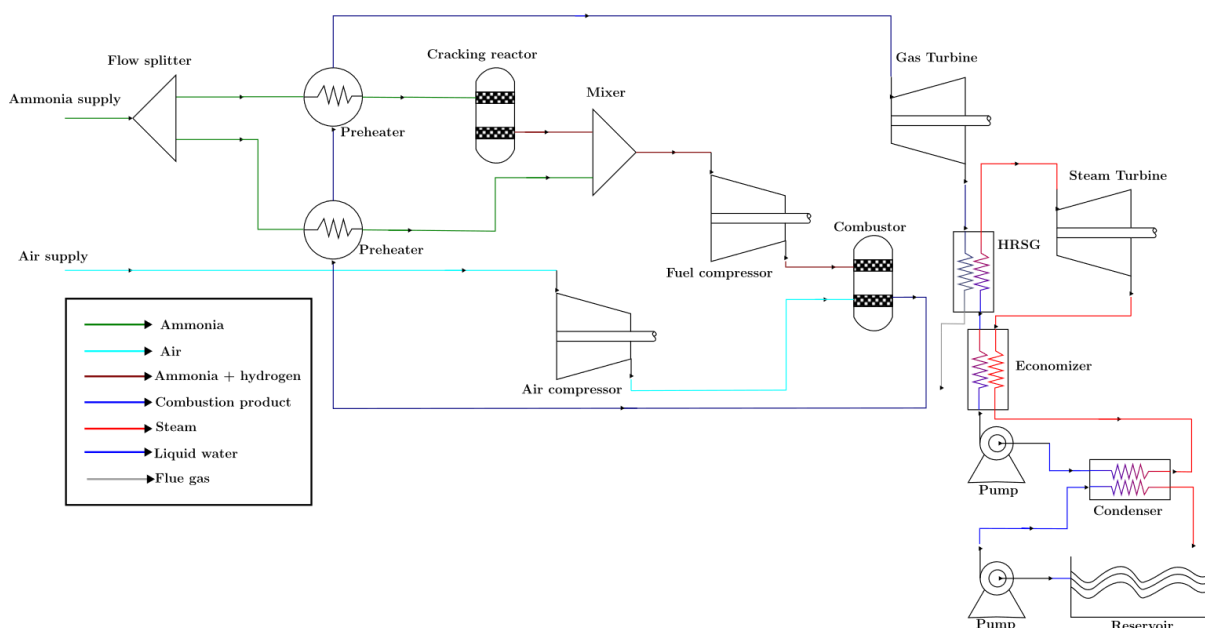


Fig. 1. Schematic of the proposed ammonia-based power generation system

The mass flow of NH₃ in this process simulation is set at 100,000 kg/h with an equivalence ratio ranging from 0.2 to 1.1. The portion of decomposed or NH₃ cracking ratio is also varied from 10 to 40%. The proposed power generation system is modeled by process simulation using Aspen Plus® software. The details of specified parameters for each equipment are summarized in Table 1.

Table 1. Specifications of the equipment adopted during process modeling using Aspen Plus®.

	Adopted module	Specification
Ammonia cracking unit	FSplit+HeatX+RStoic+Mixer	Reactor (RStoic): Cracking temperature: 950°C, Cracking pressure: 1 bar, Split fraction (FSplit): varied from 10 to 40%
Gas cycle	Compr+RStoic	Reactor (RStoic): Inlet temperature: 20°C, Inlet pressure: 20 bar, Compressor (Compr): Discharge pressure: 20 bar, Isentropic efficiency: 0.85, Turbine (Compr): Discharge pressure: 1.5 bar, Isentropic efficiency: 0.9
Steam Rankine cycle	Compr+HeatX+Pump	Coolant Pump (Pump): Discharge pressure 2 bar, Isentropic efficiency: 0.85, Main pump (Pump): Discharge pressure: 200 bar, Isentropic efficiency: 0.85

Combustor Validation

In this study, CFD analysis is performed on a laboratory-scale burner. Experimental results by previous authors [11] are used to validate the accuracy of the analysis results. The analytical condition is the non-premixed combustion of H₂ and ammonia. Reynolds-averaged Navier Stokes (RANS) simulation was conducted using ANSYS Fluent® software.

The mole fraction of fuel composition is NH₃:75.4%, H₂:18.4%, and N₂:6.2%. The velocity of a fuel jet is set to 8.6 m/s, while that of an air jet is 0.24 m/s. The shape of the mesh is shown in Fig. 2. The details of parameters used for simulation are summarized in.

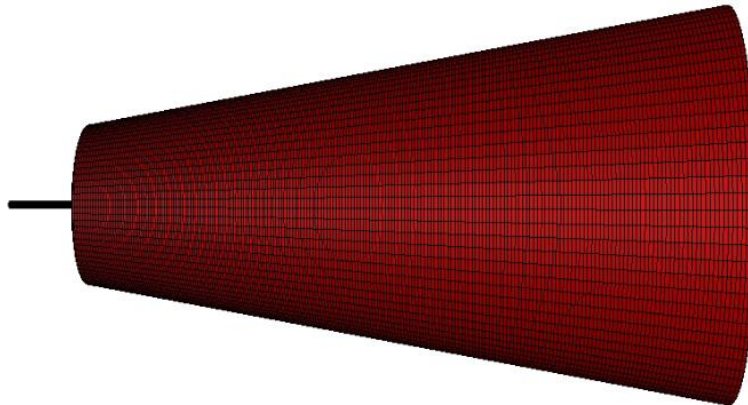


Fig. 2. Hexahedral mesh used for RANS simulation

Table 2. RANS simulation parameters

Simulation	Chemical mechanism	Combustion model	Mesh number	Mesh shape
RANS	Zhang	Flamelet PDF	4.3 million	hexahedral

RESULTS AND DISCUSSION

Performance of Power Generation System

Fig. 3 shows the turbine inlet temperature (TIT) for different ammonia cracking ratios. The maximum operating temperature for state-of-the-art gas turbines is around 1700°C [12]. Therefore, the obtained results show feasible operation conditions at lean combustion mixture.

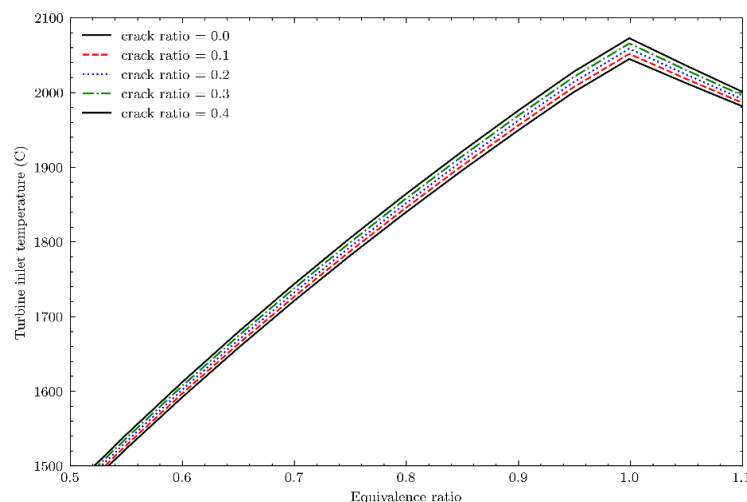


Fig. 3. Turbine inlet temperature (TIT) and overall thermal efficiency (η) as function of equivalence ratio for different ammonia cracking ratio

The introduction of NH₃ cracking leads to slightly lower turbine inlet temperature, which is the direct consequence of heat extraction from combustion products to sustain endothermic ammonia cracking. The maximum temperature is also observed at an equivalence ratio near unity.

Pilot scale combustor simulation

Although the simulation did not converge until 8,000 iterations, several results can be made. The temperature contour diagram is shown in Fig. 4. Maximum temperature is less than 1800 K so there is no need to consider thermal NO.

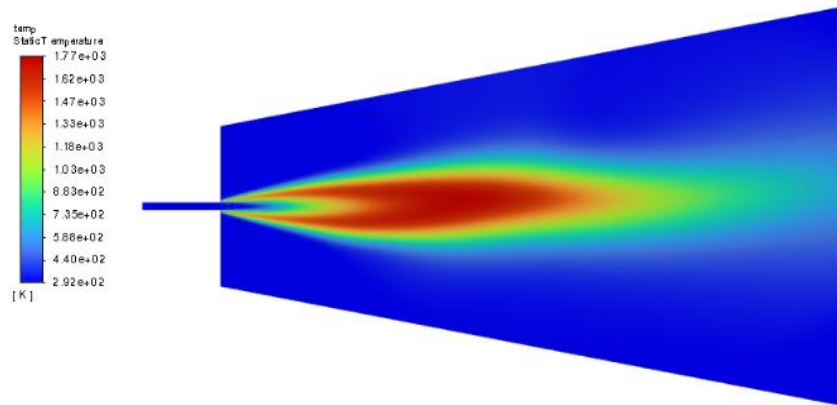


Fig. 4. Temperature contour of pilot combustor

A comparison of simulation and experimental results for temperature, mass fraction of some chemical species, and mixture fraction is shown in Fig. 5. The diameter of the fuel outlet D is 4.58mm. The x-axis of the graph is the radial distance, and it is plotted at the axial distance Z=5D, 20D, 60D. The mole fraction of chemical species and mixture fraction are well simulated at the near area of the inlet. However, temperature is not predicted well.

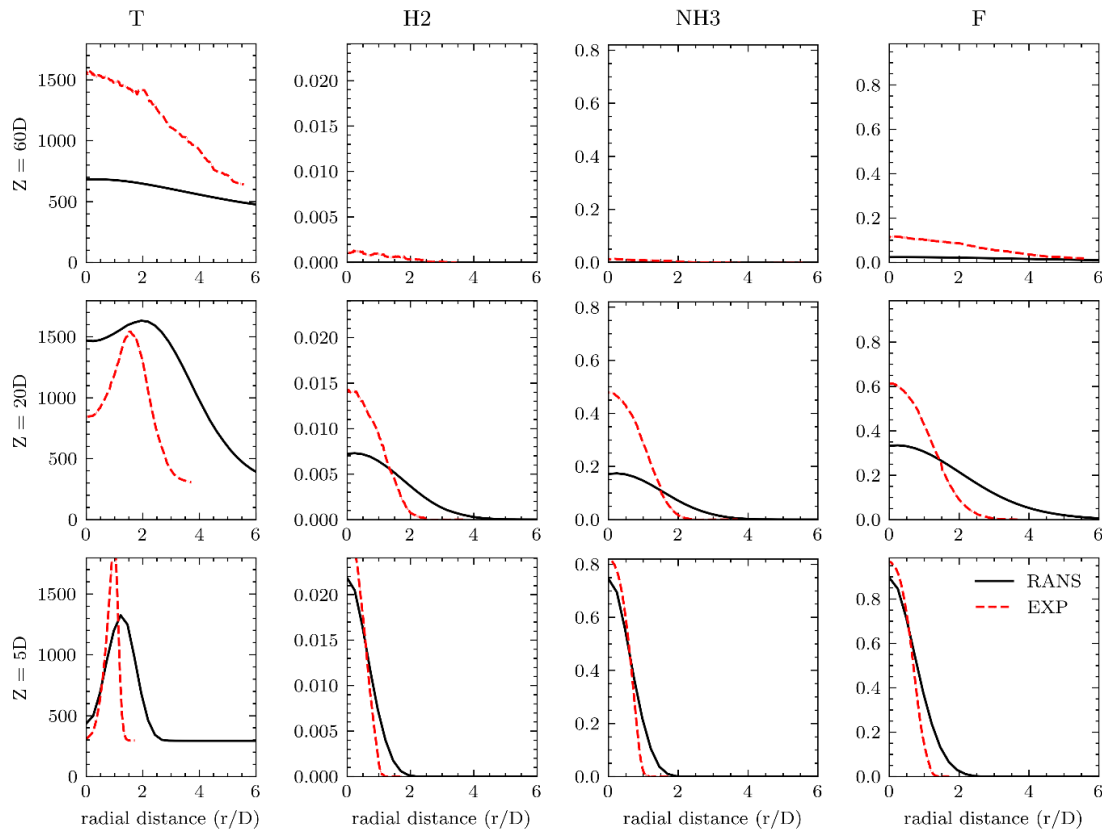


Fig. 5. Radial plot of thermochemical quantities from experimental measurement and numerical simulations

CONCLUSIONS

The design of a plant-scale power generation system using NH₃ with a cracking facility has been proposed. The performance of the system has been evaluated in terms of TIT. Furthermore, a detailed simulation using the CFD method to solve the RANS equation is validated against the experimental measurement of a pilot-scale combustor. The obtained result from this research leads to these points.

- The performance of the proposed system in terms of TIT reduces as part of the heat in the combustion product is used to sustain NH₃ cracking before entering the turbine.
- A model-dependent method such as RANS simulation has not been able to capture the measured thermochemical quantities.

In the future, we would like to use pilot-scale combustor simulation to improve the accuracy of plant-scale process simulation.

ACKNOWLEDGEMENT

This research is supported by the JST/JICA SATREPS program, grant ID JPMJSA2204.

REFERENCES

- [1] M. Aziz, "Liquid hydrogen: A review on liquefaction, storage, transportation, and safety," *Energies*, vol. 14, no. 18. MDPI, Sep. 01, 2021. doi: 10.3390/en14185917.
- [2] M. Aziz, F. B. Juangsa, W. Kurniawan, and B. A. Budiman, "Clean Co-production of H₂ and power from low rank coal," *Energy*, vol. 116, pp. 489–497, Dec. 2016, doi: 10.1016/j.energy.2016.09.135.
- [3] Y. Zhang, Z. Jia, Z. Yuan, T. Yang, Y. Qi, and D. Zhao, "Development and application of hydrogen storage," *International Journal of Iron and Steel Research*, vol. 22, no. 9, pp. 757–770, 2015.
- [4] L. A. Lesmana and M. Aziz, "Structural Topology Optimization of Metal Hydride Gyroid Container for Hydrogen Storage," *Chem Eng Trans*, vol. 103, pp. 469–474, 2023, doi: 10.3303/CET23103079.
- [5] J. Ikäheimo, J. Kiviluoma, R. Weiss, and H. Holttinen, "Power-to-ammonia in future North European 100 % renewable power and heat system," *Int J Hydrogen Energy*, vol. 43, no. 36, pp. 17295–17308, Sep. 2018, doi: 10.1016/j.ijhydene.2018.06.121.
- [6] M. Fecke, S. Garner, and B. Cox, "Review of Global Regulations for Anhydrous Ammonia Production, Use, and Storage," 2016.
- [7] A. T. Wijayanta, T. Oda, C. W. Purnomo, T. Kashiwagi, and M. Aziz, "Liquid hydrogen, methylcyclohexane, and ammonia as potential hydrogen storage: Comparison review," *International Journal of Hydrogen Energy*, vol. 44, no. 29. Elsevier Ltd, pp. 15026–15044, Jun. 07, 2019. doi: 10.1016/j.ijhydene.2019.04.112.
- [8] A. Valera-Medina, H. Xiao, M. Owen-Jones, W. I. F. David, and P. J. Bowen, "Ammonia for power," *Progress in Energy and Combustion Science*, vol. 69. Elsevier Ltd, pp. 63–102, Nov. 01, 2018. doi: 10.1016/j.peccs.2018.07.001.
- [9] C. Brackmann, E. J. K. Nilsson, J. D. Naucclér, M. Aldén, and A. A. Konnov, "Formation of NO and NH in NH₃-doped CH₄ + N₂ + O₂ flame: Experiments and modelling," *Combust Flame*, vol. 194, pp. 278–284, Aug. 2018, doi: 10.1016/j.combustflame.2018.05.008.
- [10] C. S. Mørch, A. Bjerre, M. P. Gøttrup, S. C. Sorenson, and J. Schramm, "Ammonia/hydrogen mixtures in an SI-engine: Engine performance and analysis of a proposed fuel system," *Fuel*, vol. 90, no. 2, pp. 854–864, Feb. 2011, doi: 10.1016/j.fuel.2010.09.042.
- [11] H. Tang *et al.*, "Scalar structure in turbulent non-premixed NH₃/H₂/N₂ jet flames at elevated pressure using Raman spectroscopy," *Combust Flame*, vol. 244, Oct. 2022, doi: 10.1016/j.combustflame.2022.112292.
- [12] A. MAEKAWA, "Evolution and Future Trend of Large Frame Gas Turbine for Power Generation," *Journal of Power and Energy Systems*, vol. 5, no. 2, pp. 161–170, 2011, doi: 10.1299/jpes.5.161.

ICH2P14-OP140

A CRITICAL REVIEW OF HYDROGEN (H₂) FLOW ASSURANCE IN THE PRESENCE OF IMPURITIES

¹Mohammad Azizur Rahman, ²Ibrahim Hassan, ³Rashid Hasan, ⁴Faisal Khan, ³Eduardo Gildin, ⁵Ahmad Sleiti

¹Petroleum Engineering, TAMUQ, Doha, Qatar
²Mechanical Engineering, TAMUQ, Doha, Qatar
³Petroleum Engineering, TAMU, College Station, USA
⁴Chemical Engineering, TAMU, College Station, USA
⁵Mechanical Engineering, QU, Doha, Qatar
*Corresponding author e-mail: marahman@tamu.edu

ABSTRACT

The future of the oil and gas industry relies on the success of the current energy transition initiatives to net-zero carbon production through sustainability and alternative fuel production. In particular, we highlight the circular hydrogen (H₂) economy. To this end, industries need to reduce the carbon footprint and create a sustainable flow assurance of the H₂ value chain from the production to the sequestration site. Hydrogen (H₂) generally flows as a gaseous phase. However, below its critical temperature of -240.17°C and 13 bar pressure, hydrogen can condense into a liquid phase [1]. Below the critical point, the liquid phase of H₂ can coexist with the gas phase. One of the cost-effective transport options for H₂ is to use the existing natural gas pipeline transportation. Due to the environmental and safety constraints, operating condition fluctuations, and thermodynamic phase changes with lengths, transporting H₂ in the existing natural gas pipelines is challenging. During transportation, H₂ poses safety threats due to its low molecular weight, low viscosity, rapid reaction kinetics with the transmission lines, and several flow assurance challenges such as embrittlement, leakage, high diffusivity, high-pressure drop, and cryogenic temperature effect [2-11]. Overcoming the flow assurance challenge involves careful pipeline design. The impact of H₂ transport as multiphase flow is still not well understood. In this study, we provide a literature review on the transport flow behavior of H₂ and its impact on flow assurance challenges.

Keywords: Hydrogen (H₂), Transmission, Multiphase Flow, Phase Envelop, Flow Assurance.

Hydrogen Properties

Depleted oil and gas reservoirs, given their existing infrastructure, present an appealing opportunity for underground hydrogen storage. The primary hurdle in storing hydrogen in these depleted reservoirs lies in ensuring the integrity of wellbores and addressing flow assurance challenges. The depleted oil and gas reservoirs are a potential storage place for H₂ as compared to Salt Cavern and Aquifers. Wellbore integrity is the main challenge for successful hydrogen storage in depleted reservoirs [12]. The excess H₂ after utilization can be stored cost-effectively to subsurface porous media at around 200 bar, 120°C [13]. H₂ is considered the potential "future fuel" as a replacement for traditional fossil fuels due to its superior properties like low mass density, high energy content (142 MJ/kg), and better environmental benefits [14]. Figure 1 presents the comparison of the PVT between CO₂ and H₂.

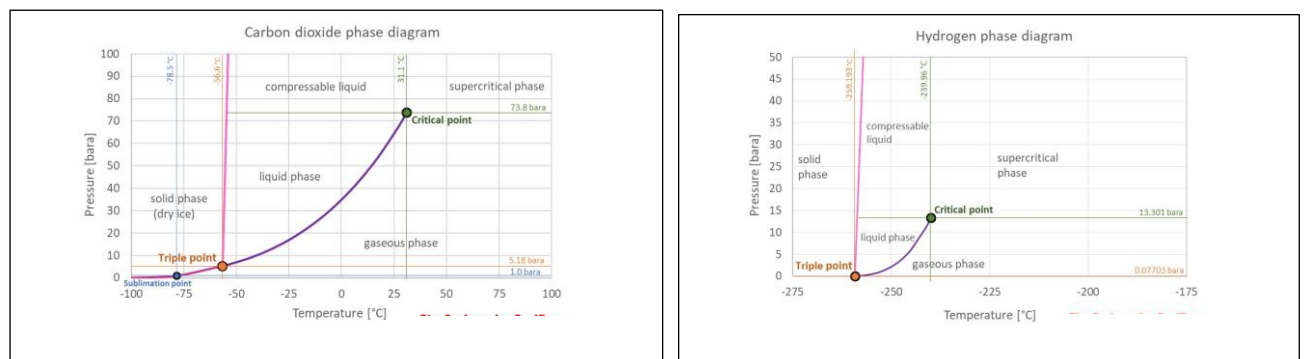


Figure 1: PVT of CO₂ and H₂ [15].

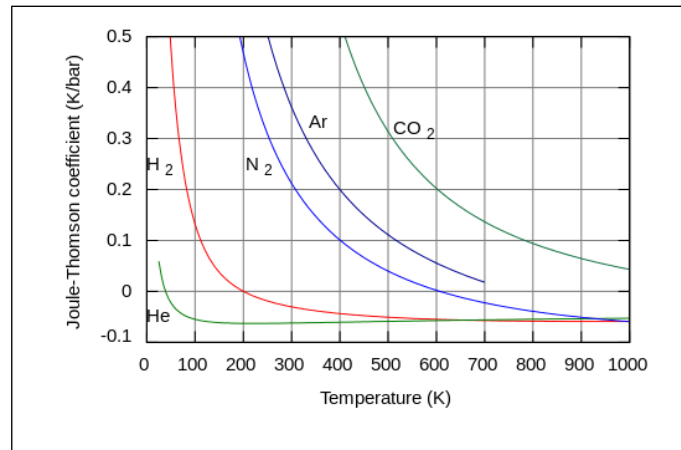


Figure 2: The Joule-Thomson effect for H₂ and CO₂ [16].

Hydrogen has a density of 0.089 kg/m³ at standard temperature (25°C) and pressure (1 bar). At a low temperature (-262 °C), it has a density of 70.6 kg/m³ and acts like a solid. At a temperature of -253 °C it has a density of 70.8 kg/m³ and acts like a liquid. H₂ is about 8 times less dense than CH₄ and 22 times less dense than CO₂ [1]. H₂ lower molecular weight and viscosity impose a threat of leakage from the pipeline and porous media. As presented in Figure 2, the Joule-Thomson (J-T) coefficient for H₂ sometime exhibits negative value as compared to CO₂.

Table 1: Hydrogen, Methane, and Carbon-di-oxide properties [1].

Properties	Hydrogen	Methane	Carbon-di-oxide
Density @25°C and 1 atm, kg/m ³	0.089	0.657	1.98
Viscosity @25°C and 1 atm, Pa.s	0.89×10 ⁻⁵	1.1×10 ⁻⁵	1.49×10 ⁻⁵
Molecular Weight (-)	2.016	16.043	44.09
Boiling Point, °C	-253	-162	-78.44
Critical Temperature, °C	-239.95	-82.3	-31
Critical Pressure, atm	12.8	45.79	72.79
Heating Value, kJ/g	120-142	50-55.5	(-)
Solubility in Pure Water, g/L	16×10 ⁻⁴	22.7×10 ⁻³	1.45×10 ⁻³
Flammability Range, °C	4-75	5-15	(-)

H₂ is stored as a liquid state when the temperature is at -252.8°C at atmospheric pressure. Whereas liquefied natural gas (LNG) is stored at the temperature of -161.5°C at atmospheric pressure. H₂ is also transported at 350-700 bar or 5000-10,000 psi pressure as a gaseous state. The typical H₂ storage in the subsurface is performed at a pressure of 50–100 bar and a temperature of 40–50°C [1]. The critical temperature and pressure of H₂ are -240°C and 13 bar or 188 psi, respectively. The critical temperature and pressure of CH₄ are -82°C and 46 bar or 667 psi, respectively. The critical point of CO₂ is at a temperature of 31°C and a pressure of 74 bar or 1073.28 psi. The CO₂ is transported and injected in critical conditions. Due to the variation of temperature and pressure of the H₂ and CO₂ value chain, both fluids have the possibility to form a two-phase flow.

Hydrogen Transport

During the gray hydrogen production from CH₄, Carbon-di-oxide (CO₂) is produced as a by-product. This CO₂ along with other greenhouse gases can be extracted and injected into the subsurface for permanent storage. The difference between H₂ and CO₂ storage is that H₂ needs to be reused later once it is needed as a potential fuel. The challenge is that after the production of H₂ and the by-product of CO₂, both gases need to be condensed so that a larger volume of gases can be stored in the subsurface cost-effectively. CO₂ is transported and injected into the reservoir under supercritical conditions. At the same time, H₂ is condensed as a very high-pressure gas or liquefied to transport to the desired locations. Keeping H₂ in a liquid phase is difficult during subsurface storage due to the high

temperature in the formation. Therefore, transportation and injection of H₂ into the subsurface are often conducted at very high pressure as a gaseous form. Due to the very low molecular weight and the reaction with the tubing surface of H₂, there is a risk of tubing embrittlement in the transportation line. The existing infrastructure of pipeline or depleted oil and gas wellbore infrastructure can be used when H₂ is mixed with CH₄ in different proportions. Figure 3 represents the pressure and temperature ranges for different H₂ transport mechanisms.

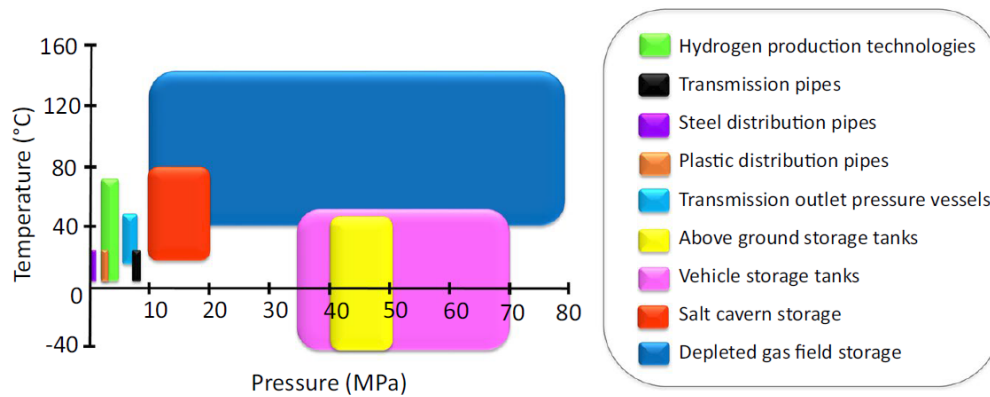


Figure 3: Temperature and pressure ranges of different modes of H₂ transportation and injection. [17]

Machine Learning for H₂ Transport

Developing benign and safer H₂ transport technology will be immensely benefited by reducing the gashouse gas emission, fulfilling the net-zero target. In a recent study, our objective was to determine the most effective machine learning classification algorithms for identifying vertical gas-liquid two-phase flow regimes. To achieve this goal, we conducted a comprehensive review of the literature and gathered data on vertical two-phase flow from more than thirty articles. Additionally, we obtained original flow data from two distinct flow loops, measuring 140 ft. (TAMU) and 18 ft. (TAMUQ) in length, respectively. By combining and refining these datasets through outlier detection and truncation, we produced a final dataset of approximately 2,200 data points, ready for analysis. This dataset comprised fourteen distinct labeled flow regions, serving as the basis for training supervised learning models. We applied various supervised learning models to this dataset, including linear discriminant analysis, quadratic discriminant analysis, K-nearest neighbors (KNN), and multiclass support vector machines (MCSVM). Among these, KNN and MCSVM demonstrated strong performance, with KNN delivering the most favorable outcomes in terms of both classification accuracy and flow map similarity to existing maps, as depicted in Figure 4. The KNN algorithm exhibited a classification accuracy ranging from 92% to 98%, depending on the number of nearest neighbors (K). The class boundaries generated by KNN stabilized after a K value of 35 and showed notable agreement with the flow maps presented by Hasan and Kabir [18]. Due to the experience of different phase envelope during extraction, transportation, utilization, and injection, H₂ also can end up with different multiphase flow regimes. The classification of H₂ multiphase flow regimes can be conducted using the Machine Learning algorithm [19-21].

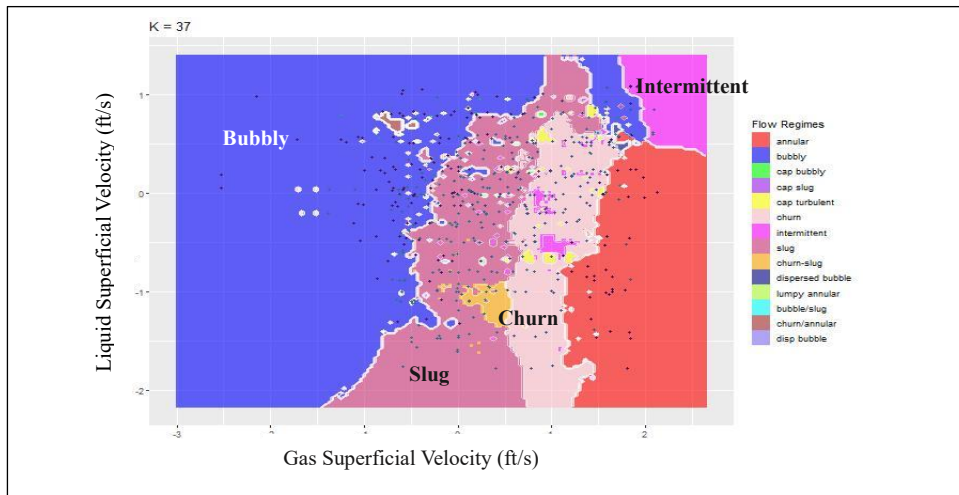


Figure 4. Two - phase flow map generated by the KNN classifier at K = 37[22].

Future Trends

In the future we need to develop a sustainable and innovative H₂ circular economy. Individual study of production, capture, transportation, utilization, and storage is not helpful in developing a meaningful complete technology. A total value chain of H₂ circular economy as presented in Figure 5 is needed. In this context, an innovative interdisciplinary energy research collaboration, including industry participation is essential.

FRAMEWORK:

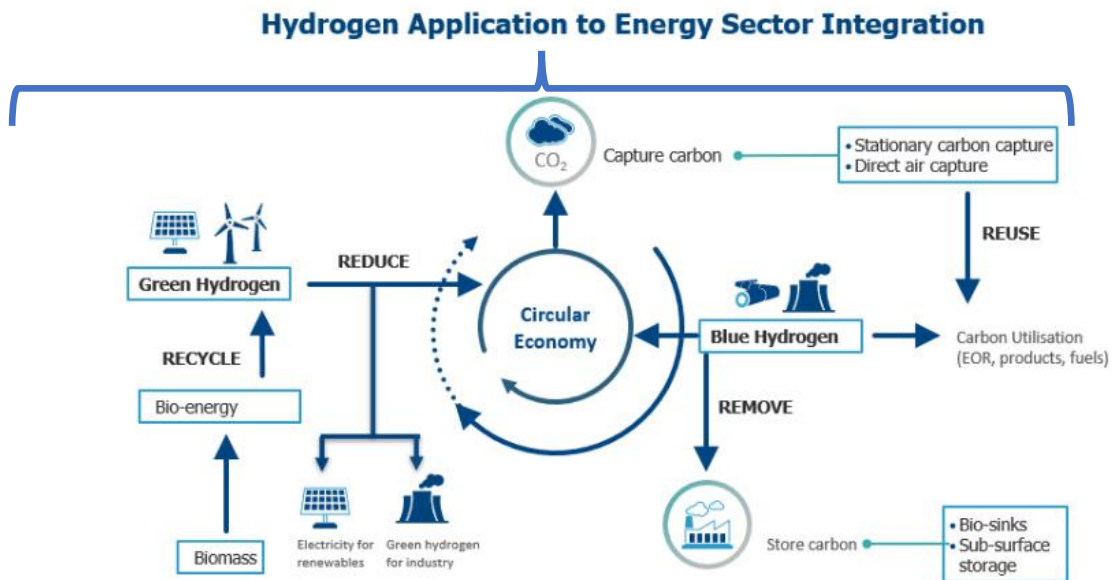


Figure 5: A full H₂ circular economy [23].

Conclusions

From the literature search, it is evident that there are a technology gaps for effective and efficient H₂ transport in industrial scales. To overcome these challenges, we need to better understand the following fundamental concepts:

- 1) To investigate the phase envelope for the H₂ value chain during capture, transport, utilization, and injection.
- 2) To investigate the multiphase flow for the H₂ value chain during capture, transport, utilization, and injection.
- 3) To understand the Joule-Thomson effect during H₂ transportation.
- 4) To develop a safe operating envelope for H₂ value chain from the capture point to the reservoir injection point.

References

1. Muhammed, N.S., et al., *A review on underground hydrogen storage: Insight into geological sites, influencing factors and future outlook*. Energy Reports, 2022. **8**: p. 461-499.
2. Arcangeletti, G., et al. *Advancing Technologies for H₂ and CO₂ Offshore Transportation Enabling the Energy Transition: Design Challenges and Opportunities for Long Distance Pipeline Systems*. in OMC Med Energy Conference and Exhibition. 2021.
3. Arcangeletti, G., et al. *The New Technological Frontiers of CO₂ and Hydrogen Transportation Via Pipelines*. in Abu Dhabi International Petroleum Exhibition & Conference. 2021.
4. Brown, T., et al. *A Study of the Effect on Pipeline Operations of the Addition of Hydrogen to Natural Gas*. in PSIG Annual Meeting. 2022.
5. Davis, B., et al. *Intelligent Hydrogen Gas Monitoring in Natural Gas/Hydrogen Blending*. in Offshore Technology Conference. 2022.
6. Zapukhlyak, V., et al., *Reliability assurance of gas-hydrogen mixture transportation by gas pipeline system*. Procedia Structural Integrity, 2022. **36**: p. 378-385.
7. Galyas, A.B., et al., *Effect of hydrogen blending on the energy capacity of natural gas transmission networks*. International Journal of Hydrogen Energy, 2023. **48**(39): p. 14795-14807.
8. Melaina, M., O. Sozinova, and M. Penev, *Blending Hydrogen into Natural Gas Pipeline Networks: A Review of Key Issues*. 2013.
9. Zhang, H., et al., *Effects of hydrogen blending on hydraulic and thermal characteristics of natural gas pipeline and pipe network*. Oil & Gas Science and Technology - Revue de l'IFP, 2021. **76**: p. 70.
10. Adam, P. *Opportunities and Challenges in Converting Existing Natural Gas Infrastructure for Hydrogen Operation*. in Abu Dhabi International Petroleum Exhibition & Conference. 2021.
11. Zhang, C., et al., *Key Technologies of Pure Hydrogen and Hydrogen-Mixed Natural Gas Pipeline Transportation*. ACS Omega, 2023. **8**(22): p. 19212-19222.
12. Hussain, A., et al. *Experimental Investigation of Wellbore Integrity of Depleted Oil and Gas Reservoirs for Underground Hydrogen Storage*. in Offshore Technology Conference. 2022.
13. Boersheim, E.C., et al. *Experimental Investigation of Integrity Issues of UGS Containing Hydrogen*. in SPE Europec featured at 81st EAGE Conference and Exhibition. 2019.
14. Davoodabadi, A., A. Mahmoudi, and H. Ghasemi, *The potential of hydrogen hydrate as a future hydrogen storage medium*. iScience, 2021. **24**(1): p. 101907.
15. ToolBox, T.E. <https://www.engineeringtoolbox.com/>. 2023.
16. effect, J.T. https://en.wikipedia.org/wiki/Joule%E2%80%93Thomson_effect. 2023.
17. Hassanpouryouzband, A., et al., *Thermodynamic and transport properties of hydrogen containing streams*. Scientific Data, 2020. **7**.
18. Hasan, A.R. and C.S. Kabir, *Fluid Flow and Heat Transfer in Wellbores*. 2nd ed. 2018: Society of Petroleum Engineers.
19. Manikonda, K., et al. *Horizontal Two-Phase Flow Regime Identification with Machine Learning Classification Models*. in International Petroleum Technology Conference. 2022.



20. Obi, C.E., et al. *Flow Pattern, Pressure Gradient Relationship of Gas Kick Under Dynamic Conditions*. in *Offshore Technology Conference*. 2022.
21. Obi, C.E., et al., *A Machine Learning Approach for Gas Kick Identification*. *SPE Drilling & Completion*, 2023: p. 1-19.
22. Manikonda, K., et al., *Application of Machine Learning Classification Algorithms for Two-Phase Gas-Liquid Flow Regime Identification*, in *Abu Dhabi International Petroleum Exhibition & Conference*. 2021. p. D041S121R004.
23. Growth, T.R.o.H.i.S. <https://www.ief.org/news/ief-insight-brief-the-role-of-hydrogen-in-sustainable-growth>. 2020.



ICH2P14-OP141

EXPERIMENTAL AND NUMERICAL ANALYSES OF A CATHODE-SUPPORTED MONOLITHIC SOLID OXIDE ELECTROLYSIS CELL

*¹Hironori Nakajima, ²Yoshihiro Iwanaga, ¹Kohei Ito*¹Kyushu University, Faculty of Engineering, Department of Mechanical Engineering,
744 Motooka, Nishi-ku, Fukuoka 819-0395, Japan²Kyushu University, Graduate School of Engineering, Department of Hydrogen Energy Systems,
744 Motooka, Nishi-ku, Fukuoka 819-0395, Japan

*Corresponding author e-mail: nakajima@mech.kyushu-u.ac.jp

ABSTRACT

In recent years, power-to-gas technology has been in progress. Promising methods include steam electrolysis and co-electrolysis using solid oxide electrolysis cells (SOECs). We have developed a monolithic (honeycomb) electrolytic cell with a larger reactive area for unit volume than the conventional planar and tubular cells. The volumetric density of the fuel production rate can be significantly improved, leading to the development of compact and high performance steam electrolysis systems. This study addresses hydrogen production by steam electrolysis using an SOEC with a porous monolithic cathode support of Ni-YSZ. Current-voltage curves were measured, and we thereby develop and validate a three-dimensional finite element model to clarify the current and temperature distributions that are useful for the optimal design of practical monolithic cells.

Keywords: SOEC, Porous honeycomb support, Volumetric current density, Multiphysics simulation, Current and temperature distributions.

INTRODUCTION

The reduction of CO₂ emissions has been promoted by the introduction of renewable energy. Power- to-Gas (PtG) technology has attracted attention for the use of unstable renewable energy sources by converting excess power into fuel for storage and transport. We focus on the solid oxide electrolytic cell (SOEC), which is the reverse reaction of a solid oxide fuel cell (SOFC), as a promising PtG technology to produce hydrogen and syngas by steam electrolysis and co-electrolysis. Because SOECs operate at high operating temperatures, efficient electrolysis without expensive catalysts and with low overpotential can be achieved [1]. Carbon monoxide and methane productions, in addition to hydrogen production, are also feasible [2]. There have been a number of reports on the development of materials to improve the performance of SOEC, but very few on the development of cell structures. In this study, we thus challenge the development of a monolithic (honeycomb) structure to increase the fuel production rate for a unit cell volume by increasing the reaction area per unit volume. This can lead to the development of compact and high-performance electrolytic systems for practical applications.

Conventionally, planar and tubular SOECs have been developed. The planar type requires improvement in durability against thermal stress and flow channel design, while the tubular type needs further enhancement of volumetric power density. Our previous studies have demonstrated that anode-supported monolithic (honeycomb) SOFCs exhibit promising volumetric power density and enable the design of flow channel arrangements for fuel and air [3][4]. By employing porous electrode support as the cell structure, the electrolyte layer can be thinner, thus reducing internal resistance [5].

In this study, we apply the monolithic structure to test SOECs with a porous cathode support having different hydrogen/air flow channel arrangements. The monolithic structure expands the reaction area for a unit volume compared to the planar cells [6]. With current-voltage characteristics of the test cells, we have constructed and validated three-dimensional (3D) finite element (FE) models to analyze the mass transport in the cells. The numerical model is also beneficial for optimized cell designs.

A 3D FE model (COMSOL Multiphysics) was constructed to reproduce the measured I-V characteristics. Basic equations were the Butler-Volmer equation (electrochemistry), Brinkman equation (viscous flow in the porous media), Navier-Stokes equation (viscous flow in the channels), and Stefan-Maxwell equation (gas diffusion) [6].

EXPERIMENTAL

Fabrication of the Cathode-Supported Monolithic SOEC

The monolithic cathode support consisted of a porous substrate with a porosity of 37%, having 3 x 3 channels (Repton Co. Ltd., Japan). The substrate was made of NiO/YSZ (8 mol% yttria-stabilized zirconia, NiO/YSZ: 65/35 wt%). The substrate was coated with 8YSZ electrolyte slurry using the dip-coating method, followed by co-firing at 1400°C for 2 hours. The monolithic support after the electrolyte sintering is shown in Fig. 1 and allows for various channel arrangements. For the anode, a mixed slurry (10:3 wt%) of $\text{La}_{0.7}\text{Sr}_{0.3}\text{MnO}_3$ and 8YSZ was prepared. The LSM-YSZ composite anode slurry was applied on the electrolyte layer using a brush coating method and fired at 1150°C for 2 hours. Lastly, silver paste was applied onto the anode layer for the current collection, as it becomes porous during the temperature rising process.

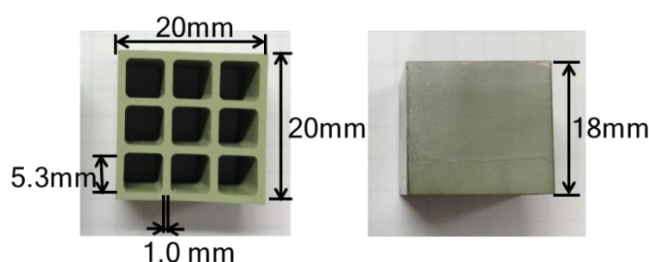


Fig. 1. Electrolyte-coated monolithic porous cathode support of NiO-8YSZ

As illustrated in Fig. 2, the A8C1 cell has one cathode channel and surrounding eight anode channels, while the A4C5 cell has five cathode channels and four anode channels. The entire anode surface was designated as the active reaction area due to the transport of water vapor through the porous cathode support. Thus, those of the A8C1 and A4C5 cells were 17.0 cm² and 8.5 cm², respectively.

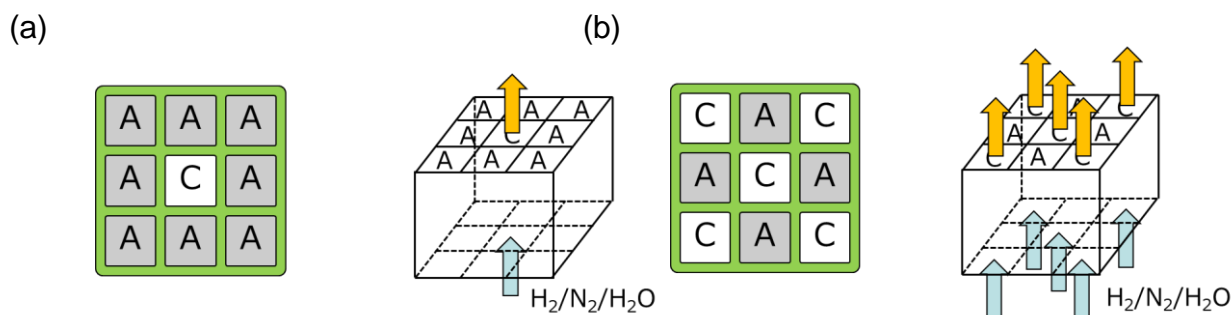


Fig. 2. Flow channel arrangements of the monolithic SOECs. (a) A8C1, (b) A4C5 (A: anode channel, C: cathode channel)

Figure 3 presents a cross-sectional view of the cell, where the flow channels are labeled with the respective letters A and C to represent the anode and cathode flow channels. Platinum (Pt) wires serve as the electrical connection between the anode and cathode. The Pt wires were attached with the silver paste separately to the anode and cathode surfaces at the end of the fuel inlet and outlet.

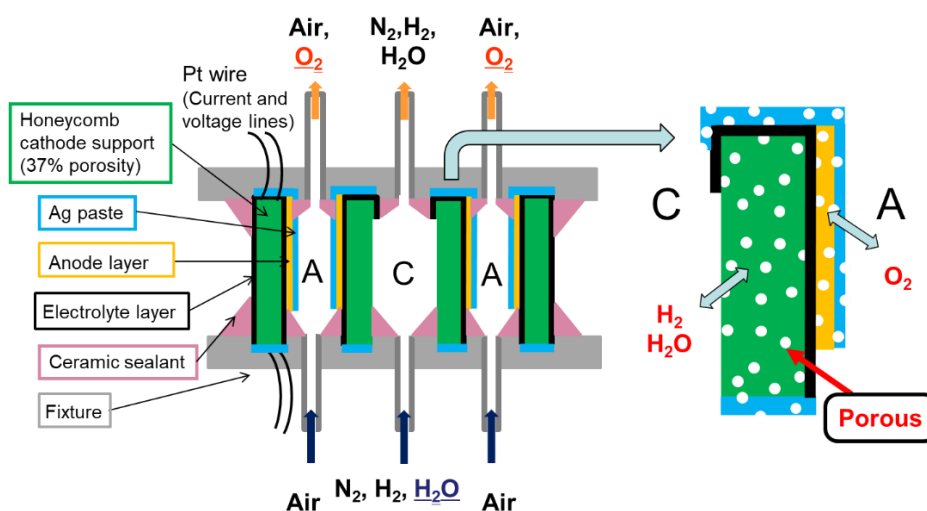


Fig. 3. Cross-sectional drawing of the monolithic cell (A: anode channel, C: cathode channel)

Experimental Conditions

The temperature of the cell was maintained at 800 °C in an electric tube furnace at open circuit voltage (OCV). Mass flow controllers were used to regulate the inlet flow rates of the anode and cathode. Prior to measurements, the NiO cathode was reduced to nickel by feeding a dry H₂/N₂ mixture gas for one hour. During the measurements, the cathode and anode were supplied with H₂/N₂/H₂O mixture and air at constant inlet flow rates, respectively. A humidification bubbler with a controlled temperature of the bubbled gas introduced water vapor into the mixture. The flow conditions of the supplied gas are presented in Table 1.

Table 1 Gas flow rate and bubbler temperature

Inlet flow rate (cm ³ /min at 25 °C, 1atm)			Bubbler temperature (°C)	
Cathode		Anode		
H ₂	H ₂ O	N ₂	Air	42.3
120	20	100	200	

RESULTS AND DISCUSSION

The measured I-V curves are shown in Fig. 4. The main axis of the abscissa shows the current density per unit volume, and the second axis shows the current density per unit area.

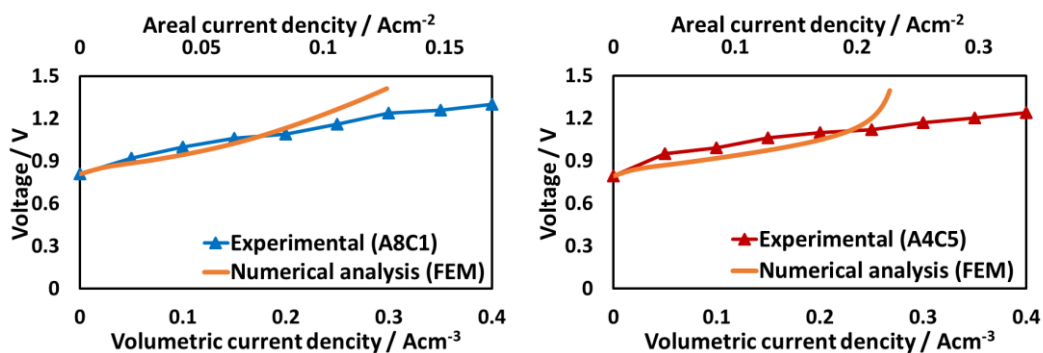


Fig. 4. Predicted and measured I-V curve of the (a) A8C1 (b) A4C5 cells at 800°C. Inlet flow rates (25°C, 1 atm): Cathode: H₂O / N₂ / H₂ = 20 / 100 / 120 cm³/min, Anode: Air = 200 cm³/min

The numerical I-V characteristics are consistent with those of the experiment in the low current density region in Fig. 4. On the other hand, in the high current density region, the numerical model shows an increase in the cell voltage. This is due to increased concentration overpotential with a shortage of water vapor toward the outlets of the flow channels [7]. Rapid increase in the voltage due to the water vapor depletion does not appear in the measurement because the hydrogen generated in the cell possibly produces water vapor with internal short-circuiting through leakage of oxygen [8]. Because the I-V characteristics predicted by the numerical model agree with those measured in the experiments in the low current density region, the model is validated.

3D Distributions in the Cathode-Supported Monolithic SOEC

To consider the optimized design of the monolithic SOEC, 3D distributions in the current density, hydrogen mole fraction, and water vapor mole fraction are predicted by the FE models for the A8C1 and A4C5 cells at 1.7 V when the cathode inlet flow rate was varied from $\text{H}_2\text{O} / \text{N}_2 / \text{H}_2 = 20 / 100 / 120 \text{ cm}^3/\text{min}$ to an increased flow rate at the same partial pressure, $\text{H}_2\text{O} / \text{N}_2 / \text{H}_2 = 60 / 300 / 360 \text{ cm}^3/\text{min}$.

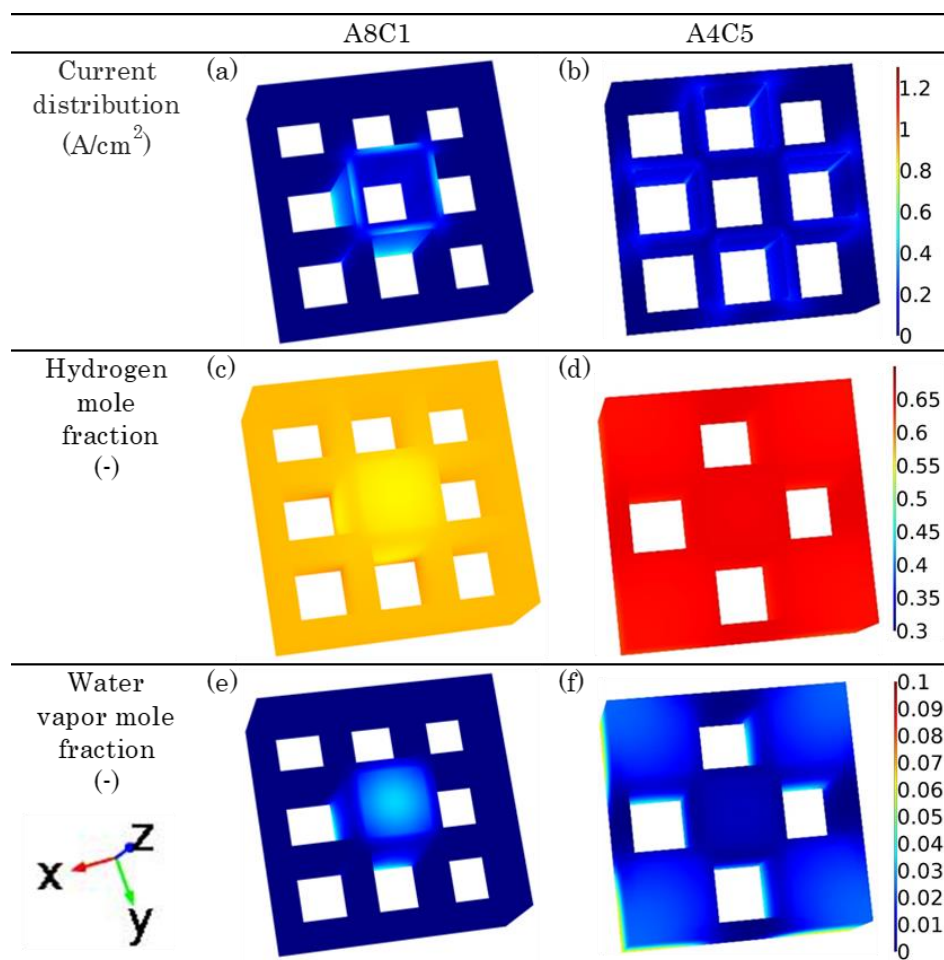


Fig. 5. Comparison of A8C1 and A4C5 cells at 1.7 V and the inlet flow rate of $\text{H}_2\text{O} / \text{N}_2 / \text{H}_2 = 20 / 100 / 120 \text{ cm}^3/\text{min}$, 800°C , (a)(b): current distribution, (c)(d): hydrogen mole fraction, (e)(f): water vapor mole fraction.

Low inlet flow rate

Fig. 5(a) shows that the A8C1 cell has a current distribution around the central channel, while very small current flows around the corner channels. This is because the water vapor from the feed gas does not diffuse much into the porous cathode support. However, the current distribution in the A4C5 cell in Fig. 5(b) differs from that in the A8C1 cell in that a larger current flows around the corner channels than the central channel. The rate of water vapor diffusing in the porous cathode support differs between the corner channels and the central channel. The central channel faces the four anode layers and water vapor can diffuse in all directions, whereas the four corner channels face only two anode layers each, limiting the direction of water vapor diffusion. This leads to reduced current density

due to a decrease in the mole fraction of the reactant water vapor around the central channel as presented in Fig. 5(f). Fig. 5(d) shows that the hydrogen mole fraction in the A4C5 cell is high at the inlet and does not increase much toward the outlet, while the water vapor mole fraction is low from the inlet. In the central channel of the A8C1 cell, the hydrogen mole fraction increases toward the outlet (Fig. 5(c)), but the water vapor mole fraction remained about 0.05 at the outlet (Fig. 5(e)). This is due to the small reaction rate around the central channel because of the difficulty of water vapor diffusion as described above.

High inlet flow rate

In Fig. 6 shows similar distributions at a high inlet flow rate as the low inlet flow rate. Increase in the current density for the A8C1 cell is smaller than that for the A4C5 cell from those at the low inlet flow rate. This result suggests that the A4C5 cell at the low inlet flow rate does not supply enough water vapor to effectively utilize the reaction area, whereas the A8C1 cell at the high flow rate does not enhance the water vapor diffusion toward the corner much as shown in Fig. 6(e).

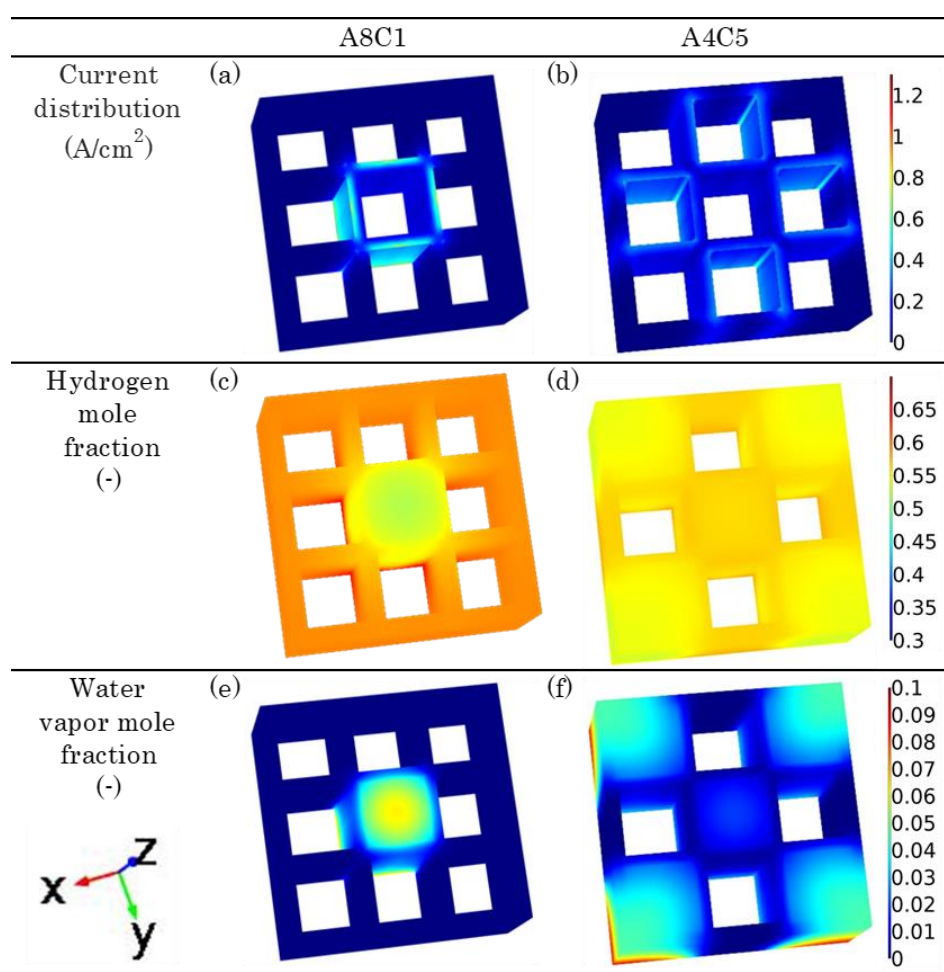


Fig. 6. Comparison of A8C1 and A4C5 cells at 1.7 V and the inlet flow rate of $\text{H}_2\text{O} / \text{N}_2 / \text{H}_2 = 60 / 300 / 360 \text{ cm}^3/\text{min}$, 800°C , (a)(b): current distribution, (c)(d): hydrogen mole fraction, (e)(f): water vapor mole fraction.

Characteristics of the Flow Channel Configuration

A4C5 cell effectively uses the reaction area regardless of the inlet flow rate, whereas the A8C1 cell exhibits insufficient water vapor diffusion. Thus, a structure that can decrease the diffusion distance of water vapor should consist of alternating anode and cathode flow channels, such as the A4C5 cell. In addition, a structure in which the cathode is surrounded by an anode, such as the A8C1 cell, needs more enhancement of the diffusion of water vapor. Increasing the partial pressure of water vapor and smaller flow channels to facilitate vapor diffusion would be



effective. This behavior is coming from the vapor diffusivity, which exhibits different tendency with hydrogen in an anode-supported monolithic (honeycomb) SOFC [4].

CONCLUSIONS

We fabricated cathode-supported monolithic SOECs with different flow channel arrangements, conducted water vapor electrolysis tests, and constructed numerical models to obtain I-V characteristics and design guidelines for the monolithic SOECs. Steam electrolysis was experimentally performed for two flow channel arrangements. Monolithic SOEC model was successfully constructed with FE modeling validated with the measured I-V curves. Analysis using FE models revealed that the diffusion of water vapor in the porous cathode support has a significant effect on the overpotential. Thus, the optimization of the structure and channel arrangement for enhanced water vapor diffusion in the monolithic cathode support will be an important factor in future design guidelines for the cathode-supported monolithic SOECs.

ACKNOWLEDGEMENT

This work is supported by JSPS KAKENHI Grant Number JP21K03916.

REFERENCES

1. A. Brisse, J. Schefold, and M. Zahid, 2008, International Journal of Hydrogen Energy 20: 5375.
2. M. Ni, 2012, Journal of Power Sources 202: 209.
3. S. Kotake, H. Nakajima, and T. Kitahara, 2013. ECS Transactions 57(1): B815.
4. H. Nakajima, S. Murakami, S. Ikeda, and T. Kitahara, 2018. Heat and Mass Transfer 54: 2545.
5. H. Nakajima, T. Kitahara, and T. Konomi, 2010. Journal of Electrochemical Society 157(11): B1686.
6. M. Andersson, H. Nakajima, T. Kitahara, A. Shimizu, T. Koshiyama, H. Paradis, J. Yuan, and B. Sundén, 2014. International Journal of Heat and Mass Transfer 77: 1008.
7. H. Nakajima and T. Kitahara, 2018. Marine Engineering 53: 230–236
8. X. Wang, H. Nakajima, Y. Iwanaga, K. Ito, 2023. Journal of Energy Storage 72:108459



ICH2P14-OP142

OPTIMIZING GREEN HYDROGEN AND POWER GENERATION FROM URBAN SEWAGE SLUDGE IN THE STEEL INDUSTRY: A KERMAN CASE STUDY

**Saeed Edalati, Mohammadreza Khosravirad*

Butia Iranian Steel Company (BISCO), Kerman, Iran

*Corresponding author e-mail: adalati.s@gmail.com

Abstract

In this advanced study focusing on hydrogen production from sewage sludge at a steel industry (HYL III technology), a comprehensive analysis was conducted to determine the most effective technologies. The evaluation centered on green hydrogen production techniques, particularly emphasizing biomass gasification as a promising method considering environmental impacts and resource availability. Key technical results indicated that for simultaneous heat and power production, micro turbines exhibited an output power of 118.209 kW and a maximum annual electricity generation of 1.033 GW. In contrast, Stirling Motors achieved 178.67 kW and 1.55 GW, respectively. For hydrogen and synthesis gas production, the PSA (Pressure Swing Adsorption) technology showed a volumetric flow rate of 393.849 m³/h and a mass flow rate of 480.354 kg/h for hydrogen, indicating high efficiency. The study's economic feasibility analysis revealed the microturbine with PSA unit as the most economically advantageous, primarily due to lower costs in biogas upgrading, coupled with higher profitability in electricity sales. This detailed investigation underscores the potential of utilizing sewage sludge for sustainable hydrogen production, aligning with regional environmental goals and industrial needs.

Keywords: Sewage Sludge management, Anaerobic Digestion technology, Combined Heat and Power (CHP), Sustainable Energy Conversion, Waste-to-Energy Technologies.

1- Introduction

The imperative to confront the challenges posed by climate change is now more critical than ever before. The Inter-governmental Panel on Climate Change (IPCC) has quantified the human contribution to global temperature increase, estimating a rise between 0.8°C and 1.3°C, with a central estimate of 1.07°C[1]. The increasing prevalence of extreme weather events—ranging from heatwaves to tropical cyclones—is increasingly attributed to human influence. This is primarily driven by the high atmospheric concentrations of greenhouse gases like carbon dioxide, methane, nitrous and nitrogen oxides, and other compounds, which significantly contribute to radiative forcing and the resulting global temperature rise. The imperative of rapid decarbonization across all economic sectors to limit the global mean surface temperature increase to 1.5°C by the end of the century is clear[2]. The iron and steel sector, producing 1.86 billion tonnes of crude steel in 2019 alone[3], is a notable contributor to global CO₂ emissions, representing 7% of energy-related global CO₂ emissions[4]. Addressing this industry's emissions is crucial, given the forecasted increase in steel demand. While material efficiency improvements and recycling can help, they are insufficient for meeting the Paris Climate Agreement's emission reduction targets[5]. The sector urgently needs transformative technologies for decarbonization[6] such as Carbon Capture Utilization and Storage (CCUS) and carbon direct avoidance technologies. The industry is exploring novel approaches to mitigate emissions. For instance, ThyssenKrupp's Carbon2chem project[7] and ArcelorMittal's initiative in Belgium[8] aim to utilize off-gases from steel production. Furthermore, the replacement of coke with hydrogen as a reducing agent in a hydrogen direct reduction shaft furnace (H₂-SF) [9] is gaining traction, offering a pathway to emission-free steel production when combined with Electric Arc Furnaces (EAFs) [10]. Additionally, technological advancements are being pursued in electrolysis methods for iron reduction and the use of hydrogen in blast furnaces[11]. However, these technologies are still developing, and their economic feasibility and scalability are under continuous assessment[12–14]. The transition to greener steel production methodologies aligns with global decarbonization goals. This includes the exploration of hydrogen-based steelmaking, as evidenced by the HYBRIT project in Sweden[15] and the HYFOR technology in Austria[16]. These efforts are supported by databases like the Green Steel Tracker, which monitors decarbonization efforts in the steel industry[17]. Therefore, in the broader scope of global decarbonization initiatives, it's noteworthy to mention the substantial efforts of nations such as China and Norway, which are at the forefront of advancing renewable energy and low-carbon technologies[18–21]. It underscores the pivotal role of the steel industry in these initiatives, given its substantial share of global CO₂ emissions and the increasing demand for steel. The paper culminates in a



detailed exploration of the potential for integrating renewable energy into steel production, examining various technology pathways, economic feasibility, and the implications for reducing CO₂ emissions across the globe.

2- Methodology

This research employs a thorough methodological approach, starting with an in-depth analysis of urban sewage sludge, both quantitatively and qualitatively. Understanding the sludge's physical and chemical characteristics is essential for future use. The study then explores how to convert sewage sludge into energy, particularly for the steel industry. It begins with a detailed examination of the sludge, identifying and quantifying its basic components and examining their specific properties and interactions. This dual analysis is crucial for understanding its potential in energy recovery.

The research then examines various strategies for using sewage sludge as an energy source for a steel manufacturing plant, focusing on its electricity or gas requirements. One method involves transforming sewage sludge into natural gas via anaerobic digestion, resulting in biogas with a high natural gas content. This gas can be purified and used either as a primary feedstock for steel production, fulfilling hydrogen needs, or to power a generation unit for the plant's operations. The study conducts a technical-economic evaluation of these methods, including a sensitivity analysis of key factors, to recommend the most effective and economically viable approach for the steel plant.

2-1- Sludge characteristic of this study

In this study, the focus is on analyzing urban sewage sludge from the Kerman wastewater treatment plant, recognizing its critical role in the efficiency of the proposed energy conversion system. Key parameters of the sludge, such as the high solid fraction concentration (98%) and the significant daily volume (182.19 cubic meters), are meticulously determined from preliminary and final analyses[22].

2-2- Thermodynamic simulation of different chains

This section likely delves into the application of thermodynamic simulations to evaluate distinct sequences or processes, which are referred to as 'chains'. These simulations are crucial for understanding how different systems behave under various thermodynamic conditions. The objective is to model and predict the performance, efficiency, and potential outcomes of these chains. This could involve assessing energy transfer, material transformations, or reaction efficiencies. The simulations provide valuable insights, aiding in the optimization and improvement of these processes, and are essential for making informed decisions in system design or modification. The first stage in each of the proposed paths is the anaerobic digestion system for sludge. After biogas production in this system, upgrading process is performed using pressure swing adsorption (PSA). In the next step, various processes for power, heat, and hydrogen production have been investigated based on the available options and the overall objective of the system.

2-2-1-Advanced Modeling of Anaerobic Digestion Systems for Biogas Production: Integrating ADM1 and Fortran in Aspen Plus Simulations

The anaerobic digestion systems simulated in this model are designed based on established models for the anaerobic digestion process, such as the ADM1 model [23,24]. The primary output of this system is biogas produced from the available sludge, which serves as the main feedstock for other processes considered in this study. Therefore, examining the performance of this system and the impact of influencing factors is essential. Given the high performance of thermophilic anaerobic digestion systems compared to other available options, the digester studied in this section is considered to operate under operational conditions at a temperature of 55 degrees Celsius and atmospheric pressure. This temperature selection influences the kinetics of the digestion process and is pivotal in the prediction of biogas composition and yield. Fortran, with its computational efficiency, contributes to the precision of these temperature-dependent calculations, enhancing the reliability of the simulation results.

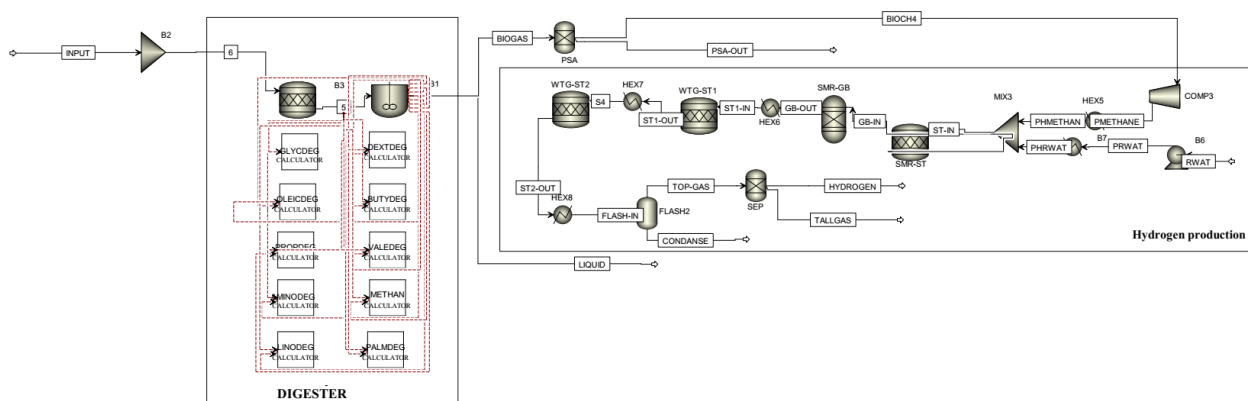


Figure 1 The general layout of a hydrogen production system from sewage sludge utilizing a Pressure Swing Adsorption (PSA)

2-2-2- Technological Analysis and Simulation of CHP Systems for Biogas Energy Recovery

This research section concentrates on the Combined Heat and Power (CHP) system, a vital method for utilizing biogas and biomethane derived from sewage sludge. It focuses on heat and power generation, examining technologies like gas turbines/microturbines and Stirling engines, chosen for their similar modeling approaches and outputs.

The study explores various CHP systems that generate heat and electricity from biogas. The selection of technology depends on system capacity, biogas composition, and heat value. Gas turbines are commonly used in CHP systems, while micro-turbines offer advantages for wastewater treatment plants due to their compact size and quick startup. Stirling engines are suitable for residential areas due to their minimal noise[25–27].

In simulations using Aspen Plus, upgraded biogas is used as fuel in the combustion chamber, with different operational conditions for each system. The output from the combustion chamber is used in micro-turbines and Stirling engines for power and heat generation. The study emphasizes the economic efficiency of micro-turbines for wastewater treatment applications and the suitability of Stirling engines for low-capacity CHP systems.

The research highlights the potential of using biogas from sewage sludge for sustainable heat and electricity generation, contributing to energy efficiency and environmental sustainability. It also considers the importance of gas resources and hydrogen production in steelmaking, especially in colder seasons, with options like hydrogen and methane gas production from anaerobic digestion (Figure 2).

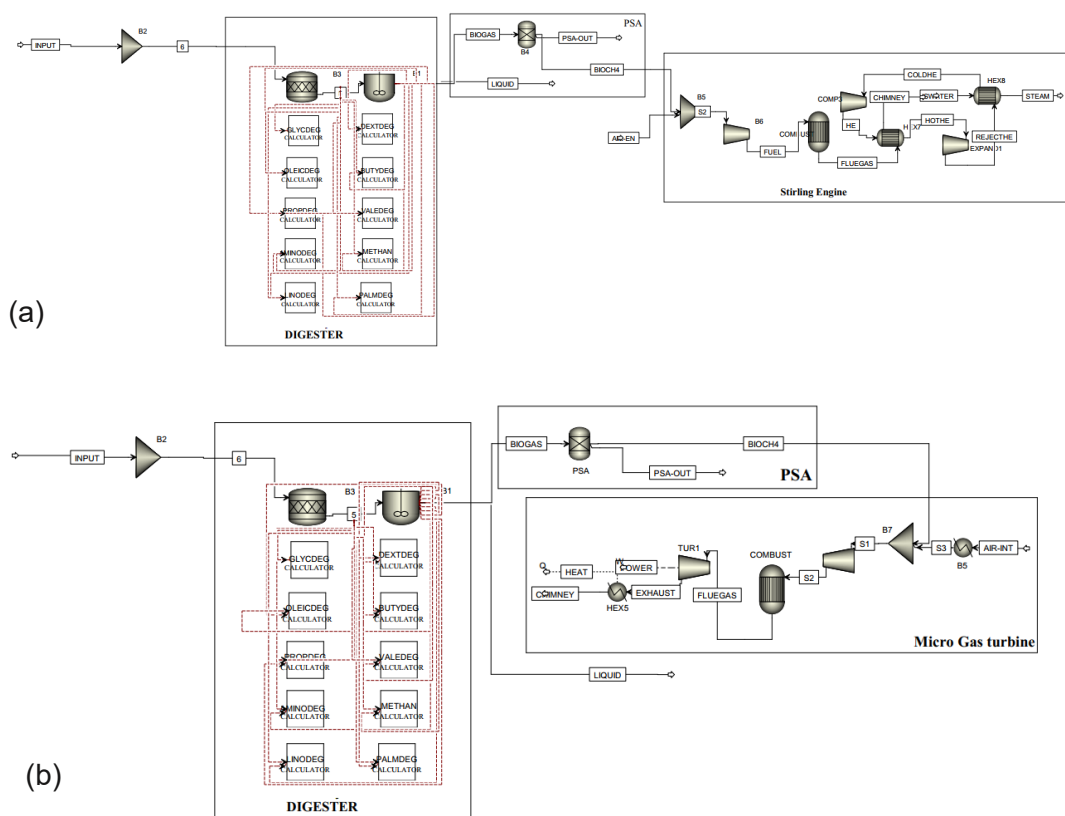


Figure 2 General Overview of the Combined Heat and Power System with Stirling engine with PSA in Aspen Plus Environment(a), General Overview of the Combined Heat and Power System with Gas Turbine/Microturbine with PSA in Aspen Plus Environment(b)

3- Results and discussion

The main objective of this section is to simulate an anaerobic digestion system for the utilization of sewage sludge as an energy source and other valuable products.

3-1- Optimizing Biogas Production: Analyzing the Impact of Sludge Composition and Upgrading Systems on Methane Yield

The results pertaining to biogas production highlight the criticality of implementing an advanced biogas system for enhanced efficiency in subsequent stages. The composition of the input sludge emerges as a crucial factor influencing the output of the anaerobic digestion system. Consequently, this study delves into the methane yield from anaerobic digestion under varying sludge input compositions, identifying it as a principal performance indicator. The study categorizes the input into four primary material groups, scrutinizing the effects of altering the ratios of carbohydrates, proteins, and lipids in the sludge's solid fraction. Figure 3a illustrates the consequences of increasing carbohydrate levels in the sludge input for the anaerobic digestion system. The depicted range reflects a fluctuation from a 10% decrease to a 10% increase in the existing sludge composition, based on the data at hand. Notably, the analysis considers the solid fraction of the sludge in relation to its liquid counterpart. The graph reveals that an upsurge in carbohydrates, leading to a corresponding decrease in proteins and lipids, results in a 5.0% decline in methane generation and a 4.0% increase in carbon dioxide output.

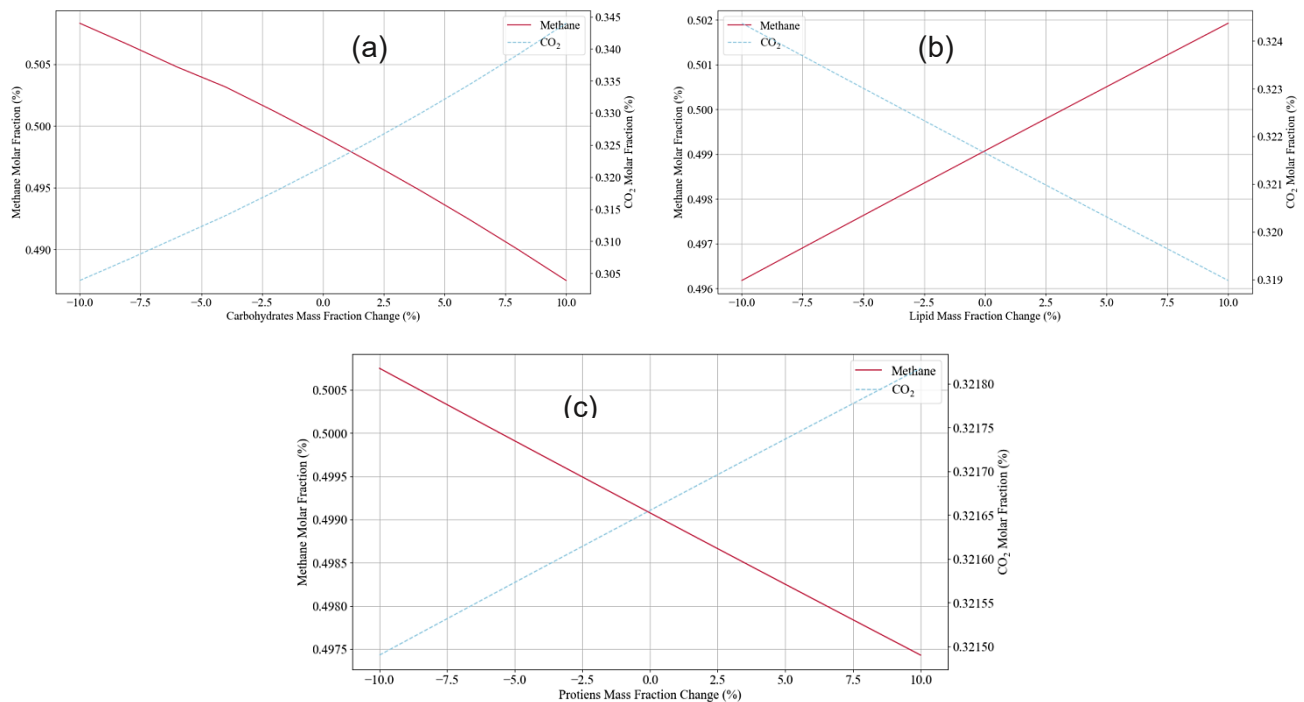


Figure 3 The impact of increasing the share of carbohydrates in the solid fraction of sludge(a), The impact of increasing the proportion of lipids in the solid fraction of sludge(b), The impact of increasing the share of proteins in the solid fraction of sludge(c)

This section delves into the effects of varying the composition of sewage sludge on biogas production, with a focus on methane and carbon dioxide yields. It highlights the influence of changes in the amounts of proteins, lipids, and carbohydrates in the sludge on the efficiency and stability of the biogas production process.

The study reveals that a decrease in the efficiency and stability of amino acid, acidogenic, acetogenic, and methanogenic processes occurs when proteins and lipids are the primary reactants, leading to reduced methane production. In contrast, an increase in the lipid content of the input sludge results in a slight increase in methane production (0.3%) and a decrease in carbon dioxide production (0.5%). This is attributed to the enhanced breakdown of lipids, which boosts acidogenic and acetogenic reactions, crucial in methane production.

Additionally, the intensification of the hydrolysis process, mainly involved in carbohydrate breakdown, leads to an increase in carbon dioxide production, as carbohydrates, especially cellulose, are primary producers of carbon dioxide during hydrolysis.

Furthermore, reducing the protein content in the sludge slightly decreases methane yield (0.25%) and increases carbon dioxide levels. Proteins play a crucial role in generating amino acids during hydrolysis and acidogenic reactions. However, the impact of reducing proteins is somewhat mitigated by the concurrent increase in carbohydrates and lipids, which balances the overall effect on biogas composition.

These findings, illustrated in Figure 3b, and Figure 3c, demonstrate the complex interplay between different components of sewage sludge and their impact on biogas production, particularly in terms of methane and carbon dioxide yields.

3-1-1- Biogas Upgrading System to Biomethane

In this study, a pressure swing adsorption (PSA) system is employed for the upgrading of produced biogas to biomethane. The PSA system, simulated as a separator for the flow streams due to limitations in the Aspen Plus platform for simulating the surface adsorption process, plays a crucial role in the methane extraction process. Table 1 provides a comparison of the input biogas stream and the final gas output stream from the PSA unit.

Table 1 Characteristics of the produced biomethane in the upgrading units

Parameters	Unit	Biomethane (PSA)
Volumetric Flow Rate	Cubic meters per day	2700
Temperature	Celsius degrees	25
Pressure	Bar	2.5
Methane	Mol%	95.6
Carbon Dioxide	Mol%	4.4
Water	Mol%	0
Hydrogen Sulfide	Mol%	0
Ammonia	Mol%	0
Hydrogen	Mol%	0

3-1-2- Steam reforming unit for biomethane upgrading

After upgrading biomethane to bio-methane in the PSA unit, the produced bio-methane enters the steam reforming unit for hydrogen production. The operational conditions of this unit have been detailed in previous sections. Considering the significance of hydrogen as the main output of this unit, a comparison between the hydrogen output stream and the biomethane input is provided in Table 2. It is worth mentioning that, due to the simulation approach for the hydrogen purification unit in the steam reforming biomethane system, the output stream from this system is generally considered to be hydrogen with a purity of 100%.

Table 2 a comparison of the hydrogen flow in different models

Parameter	Unit	Biomethane (PSA)	Hydrogen (PSA)
Volume Flow	m ³ /h	2,700	394
Mass Flow	kg/h	1,524	480
Temperature	Celsius	25	38
Pressure	Bar	1	15.65

The primary external factor affecting the hydrogen production unit through steam methane reforming is the amount of water vapor entering the system. To investigate the impact of this factor on the output of the steam methane reforming system before entering the flash unit, changes in the output model were examined. In the base model, water entering this system is considered to be 40 kilograms per hour. The parameter is studied over the range of 40 to 200 kilograms per hour.

3-2- Combined Heat and Power (CHP) System

One of the primary options for utilizing the produced biogas and subsequently upgraded biomethane is simultaneous production of heat and power. As mentioned at the beginning of this section, the equipment and operational conditions related to biogas production from sewage sludge and its upgrading in this system are entirely similar to the system discussed in the previous section, namely the hydrogen production system. Therefore, this section focuses only on the power and heat production aspect.

Given the results presented above and the studies conducted in previous reports, the use of micro gas turbines as the primary driver for the cogeneration system of heat and power is favored. The reason for this choice is the lower initial and operational costs associated with the micro gas turbine system. Additionally, the operational conditions related to this system are comparatively simpler than other options under consideration.

The study presents detailed results across two tables, Table 3 and Table 4, focusing on various technology outcomes. In the realm of power generation, Stirling engine technology paired with a Pressure Swing Adsorption (PSA) separator emerges as a more apt choice. This preference is based on its effective performance in the given context. Similarly, for hydrogen production, technology integrating a PSA separator is deemed more suitable. A

noteworthy benefit of PSA technology is its lower water consumption, an attribute that significantly enhances its applicability, especially in arid regions. This efficient water usage becomes a vital factor when considering resource allocation and sustainability in such geographical areas.

Table 3 Results of simultaneous heat and power production from sewage sludge

Parameter	Unit	Micro Turbine	Stirling Motor
		(PSA)	(PSA)
Output Power of Turbine	kW	103.34	124.54
Maximum Annual Electricity Production	GW	0.905	0.98
Electrical Efficiency	%	15.208	24.46
Thermal Efficiency	%	17.39	72.29

Table 4 technologies for hydrogen and synthesis gas production

Parameter	Unit	Hydrogen	Synthesis Gas
		(PSA)	(PSA)
Volumetric Flow Rate	m ³ /h	393.849	2523.79
Mass Flow Rate	kg/h	480.354	4605.44
Temperature	°C	38	38
Pressure	bar	15.65	15.65
Hydrogen	mol%	3.4	3.4

3-3- Economic analysis of different chains

This study section focuses on the economic feasibility of various system designs for biogas utilization, using economic indicators to assess their viability. Key factors influencing the economic performance of each system include initial investment and operational costs. The analysis, as shown in Figure 4, reveals that the system combining heat and power production with a Pressure Swing Adsorption (PSA) unit and a microturbine offers the highest net present value. This is due to the lower costs of biogas upgrading, reduced investment for the microturbine, and higher profits from electricity sales. Additionally, the hydrogen production system using a pressure water scrubbing unit is identified as the most economically viable in terms of payback period, owing to its low investment cost and favorable income-to-investment ratio.

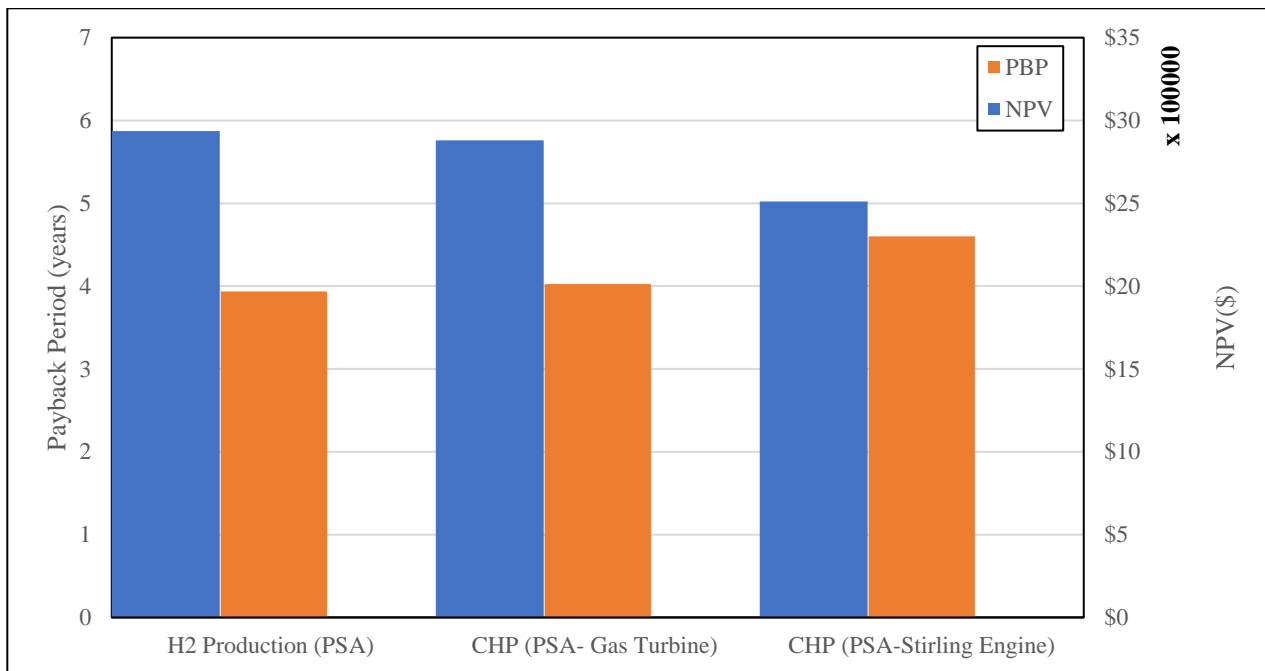


Figure 4 Comparison of different scenarios in terms of economic feasibility

4- Conclusion

This study has significantly advanced the field of sustainable energy production from sewage sludge, focusing on the Iranian Steel Boutia. The evaluation of green hydrogen production techniques identified biomass gasification as a promising method in the context of Kerman. Noteworthy findings include the effectiveness of micro turbines with scrubbing for simultaneous heat and power production, resulting in an output power of 118.209 kW and 1.033 GW in annual electricity generation. Stirling Motors with scrubbing also exhibited superior performance, yielding 178.67 kW and 1.55 GW, respectively.

In terms of hydrogen and synthesis gas production, PSA technology demonstrated high efficiency with a volumetric flow rate of 393.849 m³/h and a mass flow rate of 480.354 kg/h. Economic analysis favored the microturbine with PSA unit as the most economically advantageous choice, driven by lower biogas upgrading costs and higher profitability in electricity sales.

The study underscores the significant potential of sewage sludge for sustainable hydrogen production, aligning with regional environmental goals and industrial requirements. The in-depth exploration of various technologies, along with a focus on technical and economic feasibility, provides valuable insights for the sustainable utilization of waste materials. This research serves as evidence of practical and eco-friendly methods for transforming sewage sludge into valuable energy resources, contributing to both environmental sustainability and regional economic efficiency.

References

- [1] Summary for Policymakers, in: *Clim. Chang. 2021 – Phys. Sci. Basis*, Cambridge University Press, 2023: pp. 3–32. <https://doi.org/10.1017/9781009157896.001>.
- [2] M. Fishedick, J. Marzinkowski, P. Winzer, M. Weigel, Techno-economic evaluation of innovative steel production technologies, *J. Clean. Prod.* 84 (2014) 563–580. <https://doi.org/https://doi.org/10.1016/j.jclepro.2014.05.063>.
- [3] Worldsteel, Major steel-producing countries 2018 and 2019 million. pp. 1–8, 2020 *World Steel in Figures*, Worldsteel Association, (2020).
- [4] IEA, *global energy review 2021*, IEA, Paris., 2021.
- [5] J. Rissman, C. Bataille, E. Masanet, N. Aden, W.R. Morrow, N. Zhou, N. Elliott, R. Dell, N. Heeren, B. Huckestein, J. Cresko, S.A. Miller, J. Roy, P. Fennell, B. Cremmins, T. Koch Blank, D. Hone, E.D.

- Williams, S. de la Rue du Can, B. Sisson, M. Williams, J. Katzenberger, D. Burtraw, G. Sethi, H. Ping, D. Danielson, H. Lu, T. Lorber, J. Dinkel, J. Helseth, Technologies and policies to decarbonize global industry: Review and assessment of mitigation drivers through 2070, *Appl. Energy*. 266 (2020) 114848. <https://doi.org/10.1016/j.apenergy.2020.114848>.
- [6] K. Åhman, M., Olsson, O., Vogl, V., Nyqvist, B., Maltais, A., Nilsson, L.J., Hallding, M. Skånberg, K., Nilsson, Hydrogen steelmaking for a low-carbon economy: A joint LU-SEI working paper for the HYBRIT project., (2018).
- [7] Carbon2chem@CCU as a step toward a circular economy, *Front. Energy Res.* (n.d.). <https://doi.org/10.3389/fenrg>.
- [8] J.-P. Birat, Society, Materials, and the Environment: The Case of Steel, *Metals (Basel)*. 10 (2020) 331. <https://doi.org/10.3390/met10030331>.
- [9] A. Ranzani da Costa, D. Wagner, F. Patisson, Modelling a new, low CO₂ emissions, hydrogen steelmaking process, *J. Clean. Prod.* 46 (2013) 27–35. <https://doi.org/10.1016/j.jclepro.2012.07.045>.
- [10] M. Weigel, M. Fishedick, J. Marzinkowski, P. Winzer, Multicriteria analysis of primary steelmaking technologies, *J. Clean. Prod.* 112 (2016) 1064–1076. <https://doi.org/10.1016/j.jclepro.2015.07.132>.
- [11] J. Suer, M. Traverso, F. Ahrenhold, Carbon footprint of scenarios towards climate-neutral steel according to ISO 14067, *J. Clean. Prod.* 318 (2021) 128588. <https://doi.org/10.1016/j.jclepro.2021.128588>.
- [12] V. Vogl, M. Åhman, L.J. Nilsson, Assessment of hydrogen direct reduction for fossil-free steelmaking, *J. Clean. Prod.* 203 (2018) 736–745. <https://doi.org/10.1016/j.jclepro.2018.08.279>.
- [13] A. Krüger, J. Andersson, S. Grönkvist, A. Cornell, Integration of water electrolysis for fossil-free steel production, *Int. J. Hydrogen Energy*. 45 (2020) 29966–29977. <https://doi.org/10.1016/j.ijhydene.2020.08.116>.
- [14] E. Jacobasch, G. Herz, C. Rix, N. Müller, E. Reichelt, M. Jahn, A. Michaelis, Economic evaluation of low-carbon steelmaking via coupling of electrolysis and direct reduction, *J. Clean. Prod.* 328 (2021) 129502. <https://doi.org/10.1016/j.jclepro.2021.129502>.
- [15] M. Pei, M. Petäjäniemi, A. Regnell, O. Wijk, Toward a fossil free future with hybrit: Development of iron and steelmaking technology in Sweden and Finland, *Metals (Basel)*. 10 (2020) 1–11. <https://doi.org/10.3390/met10070972>.
- [16] Primemetals, Zero-carbon hyfor direct-reduction pilot plant starts operation, (2021).
- [17] G. Vogl, V., Sanchez, F., Gerres, T., Lettow, F., Bhaskar, A., Swalec, C., Mete, J. Åhman, M., Lehne, J., Schenk, S., Witecka, W., Olsson, O., Rootzén, Green steel tracker, (2021).
- [18] IRENA, Geopolitics of the energy transformation: the hydrogen factor., 2022.
- [19] D. Gielen, D. Saygin, E. Taibi, J. Birat, Renewables-based decarbonization and relocation of iron and steel making: A case study, *J. Ind. Ecol.* 24 (2020) 1113–1125. <https://doi.org/10.1111/jiec.12997>.
- [20] H. Trollip, B. McCall, C. Bataille, How green primary iron production in South Africa could help global decarbonization, *Clim. Policy*. 22 (2022) 236–247. <https://doi.org/10.1080/14693062.2021.2024123>.
- [21] A. Moro, L. Lonza, Electricity carbon intensity in European Member States: Impacts on GHG emissions of electric vehicles, *Transp. Res. Part D Transp. Environ.* 64 (2018) 5–14. <https://doi.org/10.1016/j.trd.2017.07.012>.
- [22] Phyllis2 - ECN Phyllis classification, (2023).
- [23] K. Derbal, M. Bencheikh-lehocine, F. Cecchi, A.-H. Meniai, P. Pavan, Application of the IWA ADM1 model to simulate anaerobic co-digestion of organic waste with waste activated sludge in mesophilic condition, *Bioresour. Technol.* 100 (2009) 1539–1543. <https://doi.org/https://doi.org/10.1016/j.biortech.2008.07.064>.
- [24] R.K. Dereli, M.E. Ersahin, H. Ozgun, I. Ozturk, A.F. Aydin, Applicability of Anaerobic Digestion Model No. 1 (ADM1) for a specific industrial wastewater: Opium alkaloid effluents, *Chem. Eng. J.* 165 (2010) 89–94.



<https://doi.org/https://doi.org/10.1016/j.cej.2010.08.069>.

- [25] S. Henry, J. Baltrusaitis, W.L. Luyben, Dynamic simulation and control of a combustion turbine process for biogas derived methane, *Comput. Chem. Eng.* 144 (2021) 107121. <https://doi.org/https://doi.org/10.1016/j.compchemeng.2020.107121>.
- [26] W. Lan, G. Chen, X. Zhu, X. Wang, C. Liu, B. Xu, Biomass gasification-gas turbine combustion for power generation system model based on ASPEN PLUS, *Sci. Total Environ.* 628–629 (2018) 1278–1286. <https://doi.org/https://doi.org/10.1016/j.scitotenv.2018.02.159>.
- [27] P. Brachi, S. Di Fraia, N. Massarotti, L. Vanoli, Combined heat and power production based on sewage sludge gasification: An energy-efficient solution for wastewater treatment plants, *Energy Convers. Manag.* X. 13 (2022) 100171. <https://doi.org/https://doi.org/10.1016/j.ecmx.2021.100171>.



ICH2P14-OP145

HEAT TRANSFER OPTIMIZATION OF A METAL HYDRIDE TANK TARGETED TO IMPROVE HYDROGEN STORAGE PERFORMANCE

¹*Nadhir Lebaal*, ²*Djafar Chabane*, ¹*Alaeddine Zereg*, ¹*Nouredine Fenineche*

¹ICB UMR 6303, CNRS, Université de Bourgogne Franche-Comté, UTBM, 90010, France.

²UTBM, FEMTO-ST Institute, FCLAB, CNRS, Belfort, France.

*Corresponding author e-mail: nadhir.lebaal@utbm.fr

ABSTRACT

In this study, the optimization of heat transfer in a metal hydride hydrogen tank to maximize hydrogen storage was investigated. A finite element model of a quarter tank was developed in COMSOL Multiphysics with parameterized geometry. The main objectives were to maximize stored hydrogen mass and minimize tank filling time while maintaining temperature uniformity within the tank. A design of experiments (DOE) approach was used with the key geometrical parameters. Compared to the base case, the hydride storage mass increased from 26.5 kg to 30.17 kg, and filling time reduced from over 1000 s to 450 s. This demonstrates the potential of optimizing heat transfer to improve metal hydride hydrogen storage performance. The model can be further improved by exploring different cooling designs and materials.

Keywords: Hydrogen storage, Metal hydride hydrogen tank, Kriging optimisation, Heat and mass transfer.

INTRODUCTION

Hydrogen energy, recognized for its clean and efficient nature, has become a cornerstone in the quest for sustainable energy solutions. Central to the utilization of hydrogen as an energy carrier is the effectiveness of its storage, particularly in metal hydride hydrogen tanks. These tanks, while advantageous due to their high-density storage capability and low-pressure operation, are often limited by heat transfer challenges during the hydrogen absorption process.

The quest for efficient hydrogen storage has been a subject of intensive research, with metal hydride hydrogen tanks emerging as a promising solution due to their safety and high energy density [1]. Studies by Tarasov et al. [2] highlight the advantages of metal hydrides for hydrogen storage, emphasizing their low operating pressures and potential for high-density storage. However, these systems are not without their challenges. Eisapour et al. [3] have pointed out the critical issue of heat management during the absorption and desorption processes, which can significantly impact the efficiency and safety of these storage systems.

In addressing these challenges, the role of optimization in enhancing the performance of hydrogen storage systems has been widely recognized. Raju et al. [4] explored various optimization techniques to improve hydrogen storage systems, with a focus on geometrical and operational parameters. Their findings underscore the potential of optimization algorithms to significantly enhance storage efficiency. Furthermore, Lebaal et al. [5] demonstrated the effectiveness of the Design of Experiments (DOE) methodology in systematically exploring and improving system designs, a technique we have adopted in our current study.

The integration of finite element modelling, as utilized in our research, has been previously explored by Suarez et al. [6], who demonstrated its effectiveness in simulating the thermal and physical behaviours of metal hydride tanks. Their work laid the groundwork for detailed analyses of heat transfer and storage dynamics within these systems. The use of COMSOL Multiphysics, in particular, has been noted for its robust capabilities in modelling complex physical phenomena, as evidenced in the work of Chaban et al. [7], they used it to model heat transfer in hydrogen energy storage systems.

Mellouli et al. [8] developed a numerical model for a thermally coupled MH hydrogen storage tank and fuel cell system based on the energy balance between both parts. Simulation results showed a relationship between fuel cell operating temperature and annular metal hydride.

In this study delves into the intricacies of optimizing heat transfer within these tanks, aiming to enhance their hydrogen storage capacity and operational efficiency.

The focus of our research is twofold: firstly, to maximize the mass of hydrogen stored, and secondly, to reduce the time required to fill the tank. Achieving these objectives is crucial for the practical application of metal hydride tanks in various hydrogen-powered systems. To address these challenges, a finite element model of a quarter tank using COMSOL Multiphysics are created, featuring parameterized geometry that allows for extensive analysis under varying conditions.

The innovative approach of this study lies in the application of the Design of Experiments (DOE) method, this methodology enabled us to systematically explore and optimize key geometrical parameters of the tank. The results show a notable increase in hydrogen storage mass, coupled with a substantial reduction in tank filling time. Moreover, this study not only presents an improved tank design but also paves the way for further enhancements.

NUMERICAL MODELING

Geometry and conception

The hydrogen storage tank has a cylindrical geometry with radial symmetry, with an active cooling system using multiple cylindrical tubes (channels) arranged throughout the volume. Due to the presence of two orthogonal symmetry in the overall design, modeling can be simplified by analysing only a quarter of the total system.

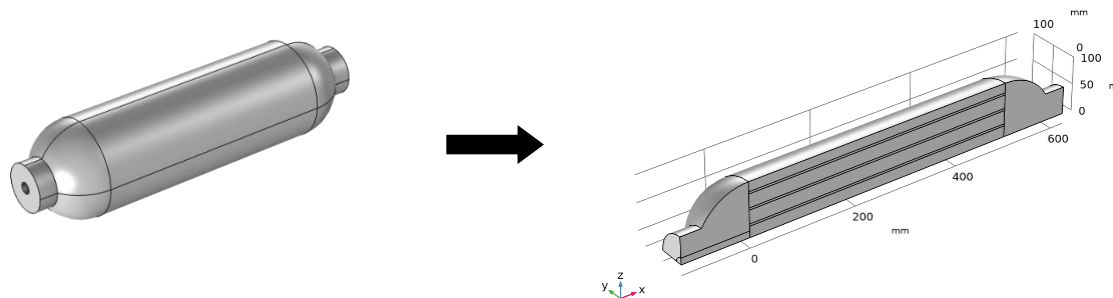


Fig. 1. Tank geometry and symmetry simplification

Table 1 shows the geometric properties of the tank and channels used in the simulation:

Table 1. geometric properties of the tank and channels

Properties	Value
Length of the tank (L_t)	75 [cm]
Diameter of the tank (D_t)	10 [cm]
Thickness of the tank (t_t)	2 [mm]
Water channel length (L_w)	75 [cm]
Water channel diameter (D_w)	5 [cm]
Water channel thickness (t_w)	1 [mm]

Physical properties and boundary conditions

Water domain

The primary purpose of the water is to eliminate the heat produced during the absorption process. The water section comprises a collection of channels equipped with fans, through which the water flows smoothly in a laminar way. These channels and fans come into contact with the hydride material and are constructed from copper.

The mathematical representation of this field includes two equations, reflecting the assumption that the fluid is incompressible. The dynamic equation, which omits the gravitational component, is described as follows:

$$\rho(u_w \cdot \nabla)u_w = \nabla \cdot \{-pI + \mu[\nabla u_w + (\nabla u_w)^T]\} + F \quad (1)$$

This equation is linked with the continuity equation, which is applicable to the steady, laminar flow of an incompressible fluid:

$$\rho \nabla \cdot u_w = 0 \quad (2)$$

u_w is the velocity field, p is the pressure, ρ is the density, μ is the dynamic viscosity and F is the external force applied to the fluid.

Metal hydride domain

The metal hydride domain is the region inside the tank shown in the Figure 1.4, in this domain, the hydrogen reacts with the metal hydride releasing heat during the absorption phase. In the present work, **LaNi5** is considered

a metal hydride. The mass conservation equation for solid metal hydride is shown below:

$$(1 - \epsilon) \cdot \frac{\partial \rho_s}{\partial t} + \nabla \cdot (-\nabla \rho_s) = \dot{m} \quad (3)$$

ρ_s is the metal hydride density.

Energy equation

The heat transfer related to the absorption of hydrogen within the hydride tank is described by the energy equation:

$$(\rho C_p)_{eff} \frac{\partial T}{\partial t} + \rho_{H_2} C_{p_{H_2}} u_{H_2} \nabla T + \nabla \cdot (-\lambda_{eff} \nabla T) = S_m \quad (4)$$

where $(\rho C_p)_{eff}$ is the effective volumetric heat capacity, λ_{eff} is the effective thermal conductivity, $C_{p_{H_2}}$ is the heat capacity of hydrogen in constant pressure and S_m is the heat source term.

The figure 2 shows the boundary conditions for the simulation. Most of the tank volume was filled with metal hydride interspersed with cooling channels (Fig.2a), to absorb heat during hydrogen absorption. To make the calculation time reasonable, the channels, fins, and tank walls were modeled as shell elements (Fig.2b). The table 2 below shows the limit conditions imposed all, while the table 3 shows the physical properties of the materials used in this study.

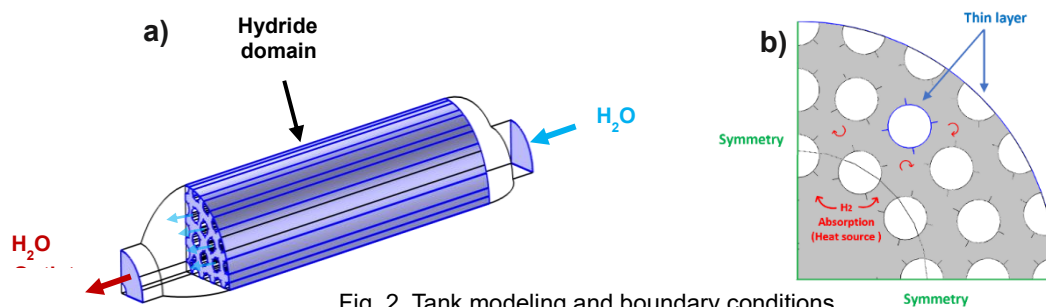


Fig. 2. Tank modeling and boundary conditions

Table 2. Boundary conditions

Domain	Initiale conditions	Boundary conditions
Metal hydride	$\rho_s(t = 0) = \rho_{emp}$ $\frac{\partial \rho_s}{\partial t}(t = 0) = 0$	/
Water	$u_w(t = 0) = 0$ $p(t = 0) = 0$	inlet $u_w = 0.1 [m/s]$ oulet $p = 0$
Tank	$T(t = 0) = T_0$ $p(t = 0) = P_0$	/

Table 3. Model Thermophysical parameters

Water		Metal hydride LiNi5		Copper	
Density (ρ_w)	1000 [kg/m ³]	Density of (ρ_{emp})	8400 [kg/m ³]	Density (ρ_{Cu})	8940 [kg/m ³]
Specific heat capacity (C_{p_w})	4.182 [kJ/kg/K]	Saturation density (ρ_{ss})	8527 [kg/m ³]	Specific heat capacity ($C_{p_{Cu}}$)	0.385 [kJ/kg/K]
Thermal conductivity (λ_w)	0.597 [W/m/K]	Porosity (ϵ)	0.63	Thermal conductivity (λ_{Cu})	400 [W/m/K]

Dynamic viscosity (μ_w)	$10.1 \cdot 10^4$ [Pa.s]	Thermal conductivity (λ_s)	2.4 [W/m/K]
-------------------------------	--------------------------	--------------------------------------	-------------

RESULTS AND DISCUSSION

Initially, a model with channels but no fins was used to determine hydrogen absorption behaviour and saturation time of the hydride. Figure 3 shows hydrogen absorption over time. The results show it takes 1100 seconds to absorb an amount estimated at 1.37% of the total hydride mass.

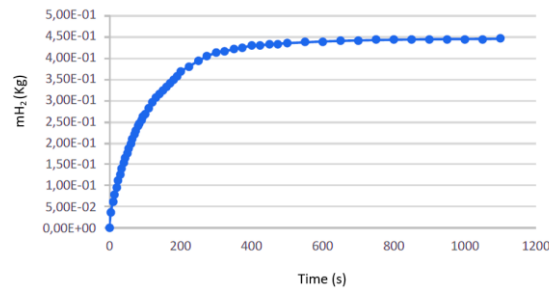


Fig. 3. Evolution of the mass of hydrogen fixed in the tank

To improve the tank's performance, fins were added to the tubes. The model was made parametric through three parameters. This step was important and essential, paving the way for the improvement process.

For that, the following parameters were evaluated (Fig.4):

- "prc": Radius of the tubes in mm.
- "lail": the length of the fins in
- "n": the spacing between the tubes.

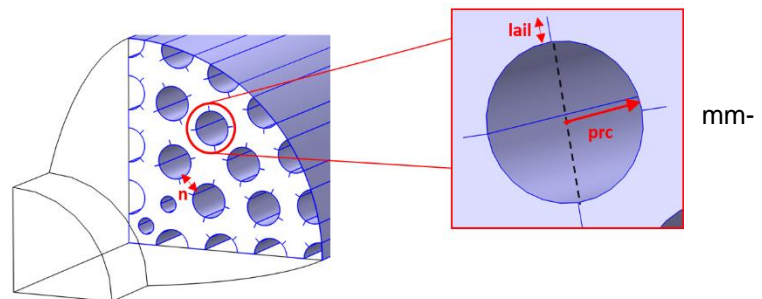


Fig. 4. Different geometrical parameters of channels

As showing in table 4, each parameter is assigned a high and low boundary in order to best study the influence of the parameters and by using a MATLAB code, a design of experiment (DoE) was generated shown below:

Table 4. Low and high boundary values for the parameters

Parametres	Low boundary	High boundary
prc	2	10
lail	2	10
n	2	10

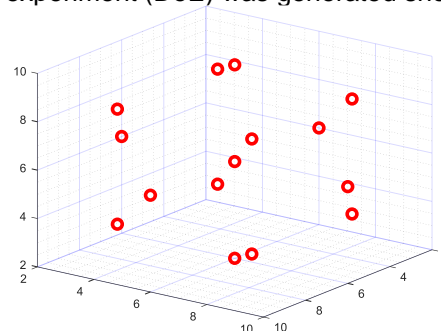


Fig. 5. The Design of experiment obtained.

From this Design, 15 tests (Design points) carried out by varying the parameters within their defined ranges to obtain the deviation, the Hydride mass and the time of charging. The result is showing in the table 5:

Table 5: different design points

Design point	prc	Lail	n	Hydride masse (kg)	Time of charging (s)
1	3,6216	3,6216	3,6216	27,678	375
2	3,6216	3,6216	8,3784	30,014	550
3	3,6216	8,3784	3,6216	30,177	450
4	3,6216	8,3784	8,3784	31,314	850
5	8,3784	3,6216	3,6216	21,558	450
6	8,3784	3,6216	8,3784	25,419	600
7	8,3784	8,3784	3,6216	25,332	550
8	8,3784	8,3784	8,3784	27,215	550
9	2	6	6	31,799	500
10	10	6	6	23,217	500
11	6	2	6	25,072	425
12	6	10	6	28,919	750
13	6	6	2	25,746	450
14	6	6	10	28,897	900
15	6	6	6	27,719	450

The figure 6 presents a comparative result of 15 Design and alongside a base case on their hydride mass and charging time. The aim is to optimize both parameters by maximizing hydride mass (which mean to maximizing the hydrogen absorbed) with minimizing charging time. Design Point 3 stands out as the optimal design, as it exhibits the highest mass at 30,177kg yet a competitive charging time of 450 seconds, achieving the best balance. While some designs like DP2 and DP15 have high mass, their charging times are longer, indicating a trade-off between the two factors. The analysis concludes Design Point 3 is most suitable when mass is prioritized, provided charging time stays reasonable. Interestingly, DP2 also emerges as a viable option with a high mass of 30,014kg and charging time of 450 seconds.

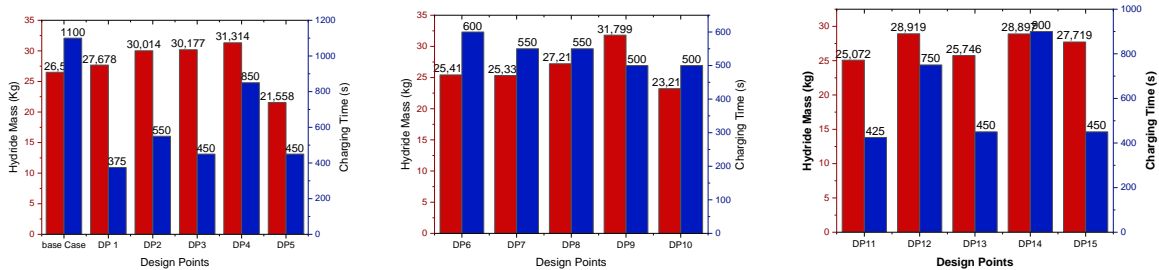


Fig. 6. Hydride mass evolution and charging time for different design points.

CONCLUSIONS

in this study, a demonstration of the potential for optimizing heat transfer design parameters to improve the hydrogen storage performance of a metal hydride tank. A finite element model of the tank was developed using COMSOL Multiphysics in order to investigate the effects of key geometric parameters on stored hydrogen mass and filling time. A Design of Experiments approach was employed to systematically analyse different combinations of parameters. The results showed that optimizing the channels radius, fin length, and channels spacing can significantly increase the amount of hydrogen stored in the tank. The optimal design configuration, as determined from 15 simulations, increased the hydride storage mass by 14% from the base case, reaching a maximum of 30.17 kg. Additionally, the filling time was reduced by over 50% to 450 seconds. This confirmation that heats transfer optimization is a promising approach for enhancing the efficiency and utilization of metal hydride hydrogen tanks. The developed model provides useful insights and can be built upon further to explore additional design configurations and materials. With continued research, it is possible that metal hydrides may meet the stringent requirements for practical onboard and large-scale hydrogen storage applications.

REFERENCES

1.Faye, O., Szpunar, J.A., & Eduok, U. (2022). A critical review on the current technologies for the generation, storage, and transportation of hydrogen. *International Journal of Hydrogen Energy*. 27, 2156-2535.



2. Tarasov, B.P., Fursikov, P.V., Volodin, A.A., Bocharnikov, M.S., Shimkus, Y.Y., Kashin, A.M., Yartys, V.A., Chidziva, S., Pasupathi, S., & Lototsky, M.V. (2020). Metal hydride hydrogen storage and compression systems for energy storage technologies. *International Journal of Hydrogen Energy*.
- Alqahtani, T., Mellouli, S., Bamasag, A., Askri, F., & Phelan, P.E. (2020). Thermal performance analysis of a metal hydride reactor encircled by a phase change material sandwich bed. *International Journal of Hydrogen Energy*, 45, 23076-23092.
3. Eisapour, A., Naghizadeh, A., Eisapour, M., & Talebizadehsardari, P. (2021). Optimal design of a metal hydride hydrogen storage bed using a helical coil heat exchanger along with a central return tube during the absorption process. *International Journal of Hydrogen Energy*.
4. Raju, M.P., & Kumar, S. (2012). Optimization of heat exchanger designs in metal hydride-based hydrogen storage systems. *International Journal of Hydrogen Energy*, 37, 2767-2778.
5. Lebaal N, Settar A, Roth S, Gomes S. Conjugate heat transfer analysis within in lattice-filled heat exchanger for additive manufacturing. *Mech Adv Mater Struct*. 2022;29(10):1361-1369.
6. Suarez, S., Chabane, D., N'Diaye, A., Ait-Amirat, Y., & Djerdir, A. (2021). Dynamic and Static characterization of the absorption process in metal hydride tanks for Mobile Applications. *2021 IEEE Vehicle Power and Propulsion Conference (VPPC)*, 1-
7. Chabane, D., Harel, F., Djerdir, A., Ibrahim, M., Candusso, D., Elkedim, O., & Fenineche, N. (2017). Influence of the key parameters on the dynamic behavior of the hydrogen absorption by LaNi₅. *International Journal of Hydrogen Energy*, 42, 1412-1419.
8. Mellouli, S., Askri, F., Dhaou, H., Jemni, A., & Nasrallah, S.B. (2010). Numerical simulation of heat and mass transfer in metal hydride hydrogen storage tanks for fuel cell vehicles. *International Journal of Hydrogen Energy*, 35, 1693-1705.

ICH2P14-OP149

SUSTAINABLE PROTON-EXCHANGE-MEMBRANE FUEL CELL (PEMFC) SYSTEM EXERGOECONOMIC ANALYSIS

**Rodrigo Raimundo, Carlos Matiolo, Rhayssa Ribas, Lauber Martins, André Mariano, Stephan Och, Vanessa Kava, José Vargas*

Federal University of Paraná, Cel. Francisco H. dos Santos street, 100, Curitiba, Paraná, Brazil

*Corresponding author e-mail: rodrigo.cesar@ufpr.br

ABSTRACT

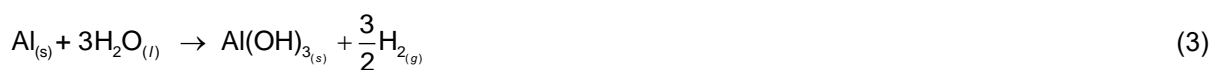
This study presents an exergoeconomic analysis of a sustainable energy generation system comprised of a hydrogen (H₂) generation reactor using recyclable aluminum and water. The system is composed of a batch reactor for greenhouse gas-free hydrogen generation, a gas-liquid separator, a buffer tank, an air booster compressor, a low-pressure filter, a hydrogen storage tank, and a 5 kW proton membrane fuel cell stack. A transient mathematical model for hydrogen generation was conceived based on mass and energy conservation principles, and experimentally validated. Exergetic and exergoeconomic analyses were then conducted to determine the exergetic costs associated with the experimental set up processes, and with the generated H₂ and electricity. The analysis revealed significant commercial and economic potential for the apparatus. Notably, the approach contributes to mitigate adverse environmental effects associated with fossil fuel use, leveraging recycled aluminum – an abundant global waste. In essence, the herein sustainable, on-site production of green hydrogen places the hydrogen generation & fuel cell system technology in the category of a clean energy source. Therefore, the system is expected to be applicable to electric vehicles, electric ships and stationary distributed power generation.

Keywords: Hydrogen Generation, Recycled Aluminum, Sustainable Electrical Generation.

INTRODUCTION

Hydrogen has a high potential as an energy source, being of global interest [1]. The predominant reliance on finite fossil fuel sources in current energy infrastructures has been a primary contributor to the release of greenhouse gases upon combustion [2]. In this context, there exists a critical imperative to actively investigate and develop alternative energy sources, with a distinct preference for those characterized by renewability. Hydrogen emerges prominently in this discourse as a viable and innovative candidate for addressing the challenges associated with traditional energy generation methodologies [3].

Despite being the most abundant element in the universe, hydrogen is not naturally found in its elemental form. Theoretically, the production of hydrogen could be achieved through simple processes such as the breaking of the water molecule (e.g., thermolysis, photolysis, electrolysis). However, establishing an economically viable and competitive methodology presents non-trivial challenges. Presently, 90% of global hydrogen production is derived from methane steam reforming. It is a method not regarded as environmentally optimal for hydrogen synthesis. Consequently, research in the domain of hydrogen synthesis, particularly utilizing recycled aluminum, has garnered attention [4,5]. Water reacts with aluminum according to:



According to Deebika and Saravanakumar (2023) [6], the generation of hydrogen through the reactions of Eqs. (1) – (3) constitutes a method for producing green hydrogen. In this context, green hydrogen synthesis is achieved without greenhouse gases emissions and allowing for the utilization of aluminum scrap. The substantial production of aluminum from bauxite yields approximately 400 billion kilograms

of aluminum scrap annually, available for recycling. Further, the hydrogen obtained through this process attains a high degree of purity, rendering it suitable for diverse applications, such as incorporation into internal combustion engines, gas turbines, or utilization in fuel cells [7].

In recent years, there has been a substantial surge in the adoption of fuel cells. These electrochemical devices exploit redox reactions to convert chemical energy directly into electrical energy, offering a clean and environmentally benign alternative, with advantage of operational viability at moderate temperatures [8]. Within the domain of FCs, the Polymeric Exchange Membrane Fuel (PEMFC) has asserted prominence, demonstrating versatility in applications ranging from portable electronic devices to electric vehicles in transportation and stationary energy systems [9].

This study entails a comprehensive analysis of a newly proposed sustainable H₂ and electricity generation system, encompassing both an energy balance and an exergy analysis, undertaken with the objective of conducting an exergoeconomic assessment. The intricately designed and meticulously constructed system is positioned for prospective integration into the power supply infrastructure of electric vehicles, with the overarching goal of augmenting overall battery autonomy.

MATERIALS AND METHODS

An innovative system composed of a batch reactor for greenhouse gas-free hydrogen generation, a gas-liquid separator, a buffer tank, an air booster compressor, a low-pressure filter, a hydrogen storage tank, and a 5 kW proton membrane fuel cell stack was built in an automotive trailer for high mobility, and it is shown in Figure 1a. The Process Flowchart is depicted in Figure 1b.

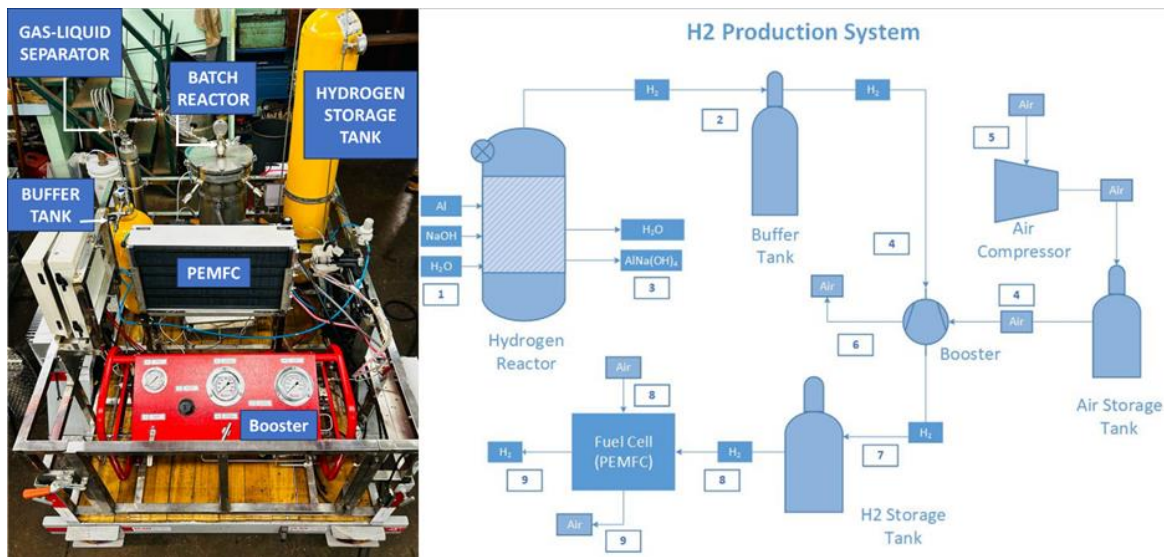


Fig. 1. a) Experimental apparatus (left), b) Process flowchart (right)

A reactor was developed based on the work methodology of Raimundo et al. [3, 4] and the reaction kinetics model was adapted from the work of Noland and Erickson [10] which provides the hydrogen molar rate:

$$r_{H_2} = \frac{P}{RT_R} k_0 S^{b_s} C^{b_c} \exp\left(-\frac{E_a}{RT_R}\right) \quad (4)$$

in which k_0 is the Arrhenius constant, b_c and b_s fitting factors from experimental data, S the Al particles total surface area, C the molality, E_a the reaction activation energy, R the universal gas constant, P the reactor pressure and T_R the reaction temperature.

According to the stoichiometry of the reaction, the reaction rates for the chemical components were reported as following:

$$\frac{r_{Al}}{2} = \frac{r_{H_2O}}{6} = \frac{r_{NaOH}}{2} = \frac{r_{NaAl(OH)_4}}{2} = \frac{r_{H_2}}{3} \quad (5)$$

As a preliminary approximation, the parameters k_0 , b_s , and b_c were initially set to the values of 65,000 J/mol, 24.5 and 0.55, respectively, as reported by Noland and Erickson [10]. Subsequently, an optimization process was undertaken to refine the parameters to better align with the experimental data. The Melder-Mead parameter identification method, implemented in Python, was employed for this purpose. The optimization process aimed at minimizing the squared error between the empirical equation and the experimental data, thereby iteratively adjusting the values of k_0 , b_s , and b_c to enhance the model's accuracy and alignment with the observed outcomes.

Since the system is in batch mode, it was treated as a closed system. Therefore, the energy balance applied to the reactor states that:

$$\frac{dT_R}{dt} = \frac{\dot{Q}_R + \dot{Q}_w + \dot{Q}_{air}}{n_{Al} \bar{c}_{v,Al} + n_{H_2O} \bar{c}_{v,H_2O} + n_{NaOH} \bar{c}_{v,NaOH} + n_{AlNaOH_4} \bar{c}_{v,AlNaOH_4} + n_{H_2} \bar{c}_{v,H_2}} \quad (6)$$

in which n is the number of mols and \bar{c}_v the specific heat at constant volume on a molar basis.

The quantification of heat exchange within the reactor involving water jacket and surrounding air was achieved by utilizing the global heat transfer coefficient (U_i) and the surrounding air or water heat exchange area (A_i), following the fundamental equation $\dot{Q}_R = U_i A_i \Delta T_i$, with $i = \text{air or water}$, so that $\Delta T_i = T_i - T_R$. Cooling water is circulated in closed loop in a control volume inside the water jacket, at a controlled water temperature T_w . The heat released by the reaction was found by utilizing the reaction enthalpy change value (Δh) and the reaction rate (r), as expressed by the equation $\dot{Q}_R = \Delta h r$.

Likewise, an energy balance analysis was conducted for the cooling system, compressor, booster, and battery. However, it is highlighted that in the case of these components, the obtained results were derived under the assumption of system steady state operation.

Subsequently, an exergy balance was meticulously conducted for each individual component within the system framework under consideration. To execute this analysis, the system was analyzed at a specific point, precisely when the system reached steady state in the reactor. Exergy is the actual proportion of energy that can perform mechanical work, as follows:

$$E = (\text{Gibbs free energy}) + (\text{gravitational potential energy}) + (\text{kinetic energy}) \quad (7)$$

Gibbs free energy is the available thermodynamic and chemical energy. Other forms of energy, such as radiation and thermal energy, cannot be completely converted into work and have lower exergy than their energy content [11]. It is emphasized that the chemical exergy values were taken from the work of Bolt et al. [12], ensuring a rigorous and well-founded basis for the system's exergy quantification. Within the exergy accounting, the destroyed exergy (E^d) was subtracted from each component total exergy, computed through $E^d = T_0 S_{gen}$, where S_{gen} represents the entropy generated, and it is multiplied by the ambient (reference) temperature value.

Lastly, endowed with the system's exergy values, exergoeconomic accounting can be systematically carried out for each component k as follows:

$$\sum_e (c_e \dot{E}_e)_k + c_{w,k} \dot{W}_k = c_{q,k} \dot{E}_{q,k} + \sum_i (c_i \dot{E}_i)_k + \dot{Z}_k \quad (8)$$

in which c is the exergetic cost (US\$/kWh), $\dot{Z} = \dot{Z}^{CI} + \dot{Z}^{OM}$ the cost rate encompassing expenses related to equipment (CI), operation and maintenance (OM), i.e., the nonexergetic costs, \dot{W} the power, \dot{E} the exergy rate, subscripts e , and i , the exit and inlet, and q refers to the heat transfer rate. The exergetic cost of each equipment output stream was calculated under the assumption that the purchase cost of each equipment was obtained according to the values of a production line.

The solution to the presented equations was obtained utilizing the Engineering Equation Solver (EES) software. Subsequent sections delineate the results and expound upon the associated discussions.

RESULTS AND DISCUSSION

The integration of the reaction kinetics equation delineated in equation (4) coupled with the ratios in equation (5) resulted in a set of simultaneous differential equations. These equations were systematically solved using the Python programming language. Simultaneously, experimental data was inputted, and an iterative adjustment process was carried out to determine the parameters of equation (4).

Subsequently, Figure 2a illustrates the empirical data concerning hydrogen generation within the reactor, contrasted with the numerical results obtained with equation (4). Moreover, Figures 2b, 2c e 2d illustrate, respectively, the consumption profiles of aluminum, sodium hydroxide, and water, identified as the reactants in accordance with equations (1), (2), and (3).

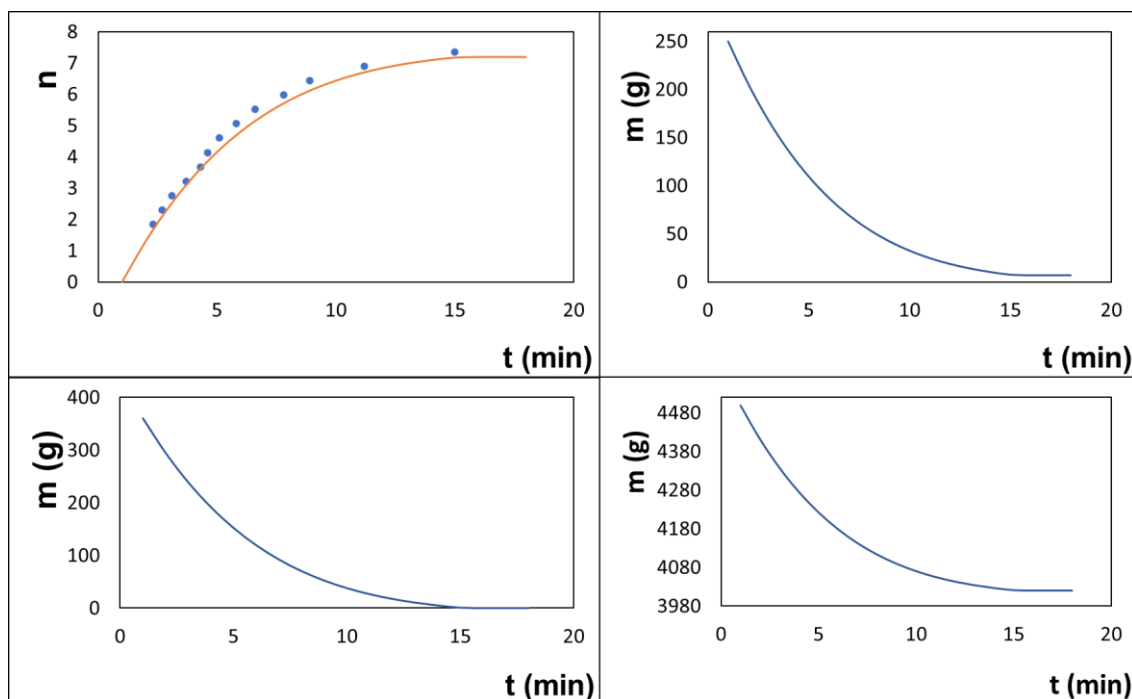


Fig. 2. a) Validation of experimental data with the mathematical model (Top-Left), b) Aluminum (Top-Right), c) Sodium hydroxide (Bottom-Left) and d) water consumption (Bottom-Right)

The results depicted in Figure 2a experimentally validate the developed mathematical model, with good qualitative and quantitative agreement between the computational predictions and empirical observations. By analyzing Figure 2 (a, b, c and d) it is observed that the system attains steady state, within approximately 15 minutes of reaction. This is taken as the operational reference point employed to yield the subsequent results in this work.

Energy balances were executed for all system components, entailing the calculation of heat and work for each equipment when it was relevant. Upon obtaining these results, the exergy accounting, as explained by equation (7) and following text, was conducted. The derivation of the results fundamentally relied on the utilization of internal energy, enthalpy, and entropy values. In this analysis, kinetic and potential energy were neglected, the chemical exergy was considered particularly in the reactor.

Utilizing the heat, energy, work, and exergy values, an exergoeconomic analysis of the project was systematically carried out. Specific exergetic costs assessments were derived for every input and output stream associated with each equipment, and nonexergetic costs as well, according to Figure 1b. Table 1 delineates the resulting exergetic costs of hydrogen at each listed equipment output.

Table 1. Hydrogen exergetic cost at each equipment outlet

Equipment	Price (US\$/kWh)
Reactor	0.04
Buffer Tank	0.05
Booster	0.14
Storage Tank	0.15
PEMFC Stack	0.15

The exergetic cost of hydrogen at the PEMFC stack output amounts to US\$ 0.15 per kWh. By using the data from Table 1, the graph in Figure 3 was plotted, showing the exergetic cost of the hydrogen formed in the reactor (Re), after leaving the buffer tank (Bt), the booster (Bo), the storage tank (ST), and the PEM fuel cell stack (FC). Then, Figure 3 allows for the evaluation of the progression of H₂ costs throughout the process.

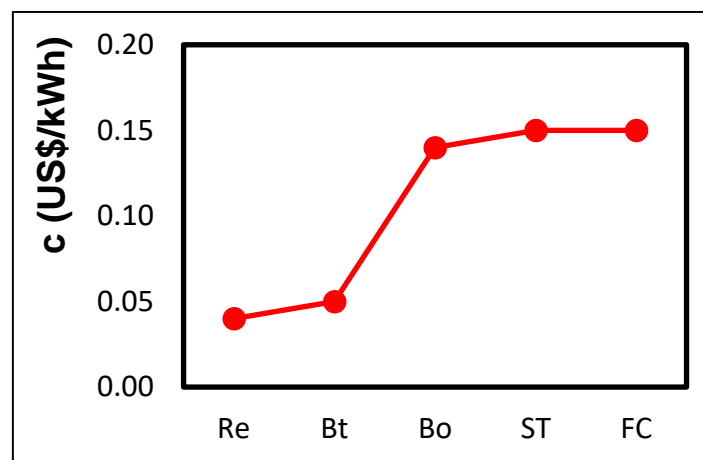


Fig. 3. Hydrogen exergetic cost progression and final electricity exergetic cost.

Through the analysis of Figure 3, it becomes apparent that the hydrogen production from water with the system proposed in Figure 1, employing residual aluminum resulted in an exergetic cost of only US\$ 0.15 per kWh, which is obtained at the storage tank output and equal to the nonconsumed excess H₂ at the PEMFC stack output. The PEMFC generated electricity exergetic cost was calculated as US\$ 0.19 per kWh with equation (8). According to the EnergySave website [13], the price of kWh varies in each region of the United States, e.g., 10.35 ¢/kWh in Idaho and 28.38 ¢/kWh in California. In summary, the average price is 23 ¢/kWh in the United States. This value can be used as a reference for comparison with the value obtained in this work. The graphical representation further reveals that the most pronounced escalation in exergetic cost occurs after the Booster. Referring to data from the Electric Vehicle Database, an electric vehicle (EV) averages an energy consumption of 195 watt-hours per kilometer [14]. Consequently, for an EV to cover 300 km, an energy input of 58.5 kWh would be required, costing around 11.00 dollars based on the hydrogen produced in this project. If it is used a gasoline vehicle as a reference, which needs 30 Liters to cover 300 km, and considering the price of gasoline at 1.99 dollars per Liter, the cost would be 59.70 dollars. It is observed that the value with the herein produced hydrogen is lower than that cost, and also emphasizing that the price of oil has been unstable in recent years.

CONCLUSIONS

The production of hydrogen utilizing residual aluminum with the herein proposed system has shown potential for large-scale application, featuring an economically attractive hydrogen production exergetic cost. Despite the final electricity exergetic cost being smaller than the US average kilowatt-hour price, the system still holds considerable potential for optimization, offering avenues for cost reduction in the overall process. Based on the obtained results, it is reasonable to state that the proposed system yields clean



energy. Notable is the fact that the produced hydrogen exhibits a high level of purity, rendering it directly applicable as an energy source. Furthermore, the system's mobility highlights its adaptability for diverse applications, presenting substantial potential for widespread utilization.

ACKNOWLEDGEMENTS

The authors acknowledge support from the Brazilian National Council of Scientific and Technological Development, CNPq (projects 443823/2018-9, 446787/2020-5, 313646/2020-1, 308460/2020-0, 312516/2019, 408073/2021-7, 300093/2022, 405864/2022-1, and 408080/2022-1), CAPES, Ministry of Education, Brazil (projects 062/14 and CAPES-PRINT-UFPR-88881.311981/2018-01), Araucaria Foundation of Parana, Brazil (project 115/2018, no. 50.579 – PRONEX), Research & Development Foundation, Brazil (project 27192.22 – FUNDEP – ROUTE 2030) and Renault of Brazil.

REFERENCES

- [1] Akdag O. 2023. A compact production plant model for green hydrogen production from medium temperature geothermal resources: A case study of the Van Lake-Zilan location. *International Journal of Hydrogen Energy*. In press. DOI: 10.1016/j.ijhydene.2023.08.037
- [2] Etminanbakhsh M and Allahkaram SR. 2023. Reaction of aluminum particles with superheated steam to generate hydrogen gas as a readily usable clean fuel. *Fuel*. 332:126011.
- [3] Raimundo RC, Vargas JVC, Ordonez JC, Martins LS, Balmant W and Mariano AB. 2022. Optimal sustainable fuel cell stack with cellulosic alkaline membranes. *Fuel Cells*. 22:301-309.
- [4] Raimundo RC, Vargas JVC, Ordonez JC, Balmant W, Polla PTB, Mariano AB and Marino CEB. 2019. A sustainable alkaline membrane fuel cell (SAMFC) stack characterization, model validation and optimal operation. *International Journal of Hydrogen Energy*. 45:5723- 5733.
- [5] Farmani A and Manjili FE. 2023. Modelling and assessment of hydrogen combined cycle power plant using aluminum-water reaction as renewable fuel. *International Journal of Hydrogen Energy*. In press. DOI: 10.1016/j.ijhydene.2023.08.239
- [6] Deebika P and Saravanakumar MP. 2023. Utilization of RO rejects and waste aluminum scraps for hydrogen generation. *International Journal of Hydrogen Energy*. 48: 35516- 35531.
- [7] Urbonavicius M, Varnagiris S, Mezulis A, Lesnicenoks P, Knoks A, Richter C, Milcius D, Meirbekova R, Gunnarsson G and Kleperis J. 2023. Hydrogen from industrial aluminium scraps: Hydrolysis under various conditions, modelling of pH behaviour and analysis of reaction by-product. *International Journal of Hydrogen Energy*. in press. DOI: 10.1016/j.ijhydene.2023.09.065
- [8] Tariq AH, Kazmi SAA, Hassan M, Ali S and Anwar M. 2023. Analysis of fuel cell integration with hybrid microgrid systems for clean energy: A comparative review. *International Journal of Hydrogen Energy*. In press. DOI: 10.1016/j.ijhydene.2023.07.238
- [9] Wu J, Zhang Y, Ruan J, Liang Z and Liu K. 2023. Rule and optimization combined real-time energy management strategy for minimizing cost of fuel cell hybrid electric vehicles. *Energy*. 285:129442
- [10] Noland BMJ and Erickson PA. 2020. Apparent kinetics of hydrogen production with water-slurried aluminum delivery in aqueous sodium hydroxide solutions. *International Journal of Hydrogen Energy*. 45:24285-24299.
- [11] I. Prigogine and D. Kondepudi. 1999. *Thermodynamique*, Éditions Odile Jacob.
- [12] Bolt A, Dincer I, Angelin-Chaab, M. 2020. Energy and exergy analyses of hydrogen production process with aluminum and water chemical reaction. *Energy*. DOI: 10.1016/j.energy.2020.117978
- [13] <https://shorturl.at/dej01>. Accessed on November 25, 2023.
- [14] <https://ev-database.org/cheatsheet/energy-consumption-electric-car>. Accessed on November 23, 2023.

ICH2P14-OP151

REGENERATION ENERGY OPTIMISATION OF POST-COMBUSTION CO₂ CAPTURE (PCC) PROCESS BASED ON AMINE COMPOSITION USING ARTIFICIAL NEURAL NETWORK (ANN)

¹Najamus Sahar Riyaz, ¹Nancy Khalaf AbuZaid, ¹AlAnkaa Al-Harbi, ^{1,2*}Abdelbaki Benamor

¹Gas Processing Center, Qatar University, P.O. Box 2713

²Department of Chemical Engineering, College of Engineering, Qatar University, P.O.Box 2713, Doha, Qatar

*Corresponding author e-mail: benamor.abdelbaki@qu.edu.qa

ABSTRACT

The post-combustion CO₂ capture (PCC) process is largely appraised as being efficient for reducing CO₂ emissions generated from industrial processes. However, one of the most significant drawbacks of the process is its costly nature, attributed to the high energy required for the regeneration of used solvent. Thus, the energy efficiency of this process demands optimization. Such optimization may be achieved among others by Artificial Neural Network (ANN). In this work, we developed an ANN model used to optimize the solvent regeneration energy based on amine solvent composition. The model aims to provide real-time monitoring and optimization for the processes in post-combustion CO₂ capture (PCC) plants considering necessary operational parameters such as flue gas temperature, pressure, as well as amine composition and absorber solvent temperature. The model was developed using available data from literature for different amine compositions and concentrations. Of the total data, 15% was used for testing and 5% for validating with the rest for training. The obtained results showed that the Narrow Neural Network was able to generate energy requirements with a nearly perfect match between experimental and predicted values.

Keywords: CO₂ capture, Artificial Neural Network, Optimization, Solvent, Regeneration Energy.

1. INTRODUCTION

Anthropogenic CO₂ emissions, primarily from burning fossil fuels and industrial processes, have been identified as a significant contributor to global warming and climate change [1]. These emissions have led to intense debates and concerns about the consequences of rising global temperatures [2]. To address this critical issue, it is imperative to explore innovative approaches to carbon capture, such as the post-combustion CO₂ Capture (PCC) process, which holds substantial promise for substantially reducing CO₂ emissions significantly [3].

From the various PCC technologies, some of the most widely used ones are absorption [4], adsorption [5], and membrane separation [6]. Post-combustion CO₂ (PCC) absorption technologies fall into two main categories: chemical absorption and physical absorption. Over many years, chemical absorption has established itself as the most dependable method in the market, recognized for its cost-effectiveness, efficiency, and broad applicability[7]. Typically, a chemical absorption system is built on three primary components: solvent, absorber, and stripper. Flue gases generated from various CO₂ emitters, such as from coal power plants, are in contact with the lean solution in the absorber. Subsequent absorption of the CO₂ on the lean solvent takes place, thereby reducing the concentration of CO₂ in the exhaust gases. From here the CO₂ ridden lean solvent is passed to the stripper which restores the solvent-rich CO₂, and the renewed light solution is returned to the absorber. The compressed CO₂ is returned to the top of the stripper[8]. Many researchers considered that using amines as the reactive chemical solvents for post-combustion CO₂ capture is often seen as the best technology to tackle the elevated levels of CO₂ emissions [9], [10]. Amines are considered as the most mature and advanced option among the different reactive solvents under investigation for post-combustion CO₂ capture (such as hot potassium carbonate, chilled ammonia, and ionic liquid[11]). Amines have different categories encompassing primary, secondary, or tertiary which have different reaction pathways of CO₂ absorption. Typically, monoethanolamine (MEA) (primary amine) is the chemical absorbent most employed in industrial applications[7].

Nevertheless, this process is energy intensive [12], [13], with 3.5–4.5 MJ of heating requirement per kg of captured CO₂ [14], thus research into reducing and optimizing the energy consumption of the amine-based absorption technology is widespread [15]. The energy-intensive nature of PCC necessitates a deeper understanding and optimization, a task where machine learning and artificial intelligence algorithms can play a pivotal role [10]. These sophisticated tools enable a comprehensive analysis of the myriad parameters influencing the process, including temperature, pressure, humidity, and solvent usage. Such tools may be used to generate efficiency models and allow for real-time monitoring of parameters. Artificial Neural Networks (ANN) are becoming increasingly popular for predicting various properties in the CO₂ capture process given that they can process a

variety of parameters which may be formulated rapidly. Therefore, the objective of this study is to develop an Artificial Neural Network (ANN) model for optimizing the solvent regeneration energy in the PCC process and to enhance the energy efficiency of the process through the utilization of an ANN model. This model focuses on real-time monitoring and optimization of PCC plant processes, considering crucial operational parameters such as flue gas temperature, pressure, amine composition, and absorber solvent temperature.

2. DATA COLLECTION & METHODOLOGY

The data used for training the neural network in this study was collected from several studies[16]–[19] focused on optimising the regeneration energy for the post-combustion CO₂ capture process with respect to the amine concentration, in GJ/tonne CO₂. 12 input parameters were used for the model: amine type, amine composition (wt. %), amine flow rate (l/min), lean amine flow rate (L/min), lean loading solvent (mol CO₂/ mol MEA), absorber solvent temperature (°C), flue gas temperature (°C), flue gas flow rate (kg/h), as well as the flue gas compositions with respect to CO₂, SO₂, NO_x, and O₂ (wt. %) in ppm. A 3:1 ratio was maintained between the testing and validation datasets.

Input data were arranged in a matrix and input to MATLAB via the Regression Learner App. A total of 1560 observations were used, of which 15% was used for testing and 5% for validation. A cross-validation approach was used for protection against cross-fitting. The iteration limit was set at 1000, with a ReLu activation for both the narrow and wide neural network.

The analysis followed a comparative approach between the narrow and wide neural networks given that narrow networks are better suited for less complex datasets while wide neural networks are better suited at optimising complex datasets, thus optimisation of both types of neural networks ensure that the developed model may be used for small-scale as well as large-scale plant operations. The networks were first trained using a Levenberg–Marquardt (LM) algorithm and then further optimised using a Bayesian regularisation method thus ensuring the generalisation of the prediction capacity of the model on unseen data. Optimisation using Bayesian regularisation was done using 10 hidden layers with 15% of the data randomly allocated for testing and 5% for validation.

3. RESULTS AND DISCUSSION

Optimisation values from both the Narrow Neural Network (NNN) and Wide Neural Network (WNN) demonstrated an almost perfect response between the predicted values vs actual values for the regeneration energy using the LM algorithm, as depicted in figures 1 and 2.

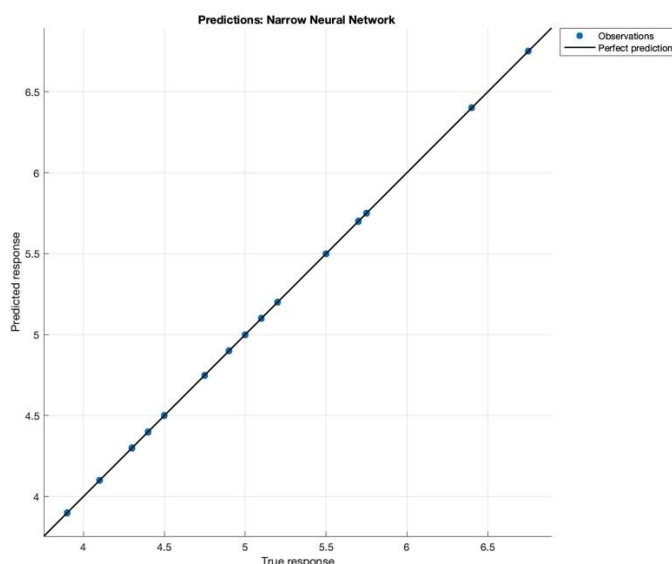


Figure 1 - Predicted response vs. True response of NNN.

NNN demonstrated an almost perfect response between the predicted and actual response. The model displayed high accuracy of validation with an RMSE (Validation) value of 0.0012322 and R-squared (Validation) of 1.

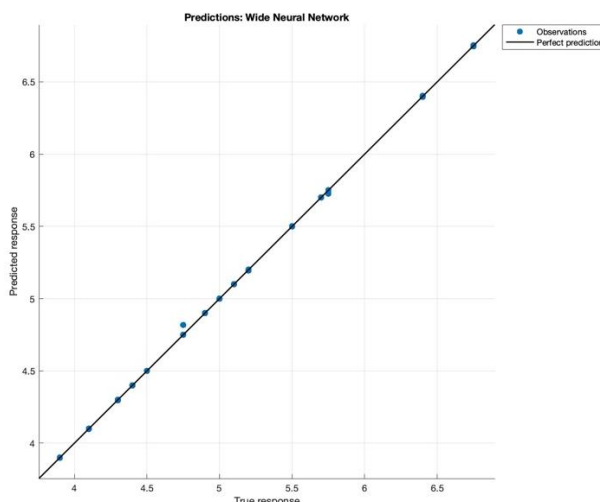


Figure 2 - Predicted response vs Actual response of WNN.

Similarly, WNN displayed high accuracy with the validation values with an RMSE (Validation) value of 0.010574 and R-Squared (Validation) of 1.

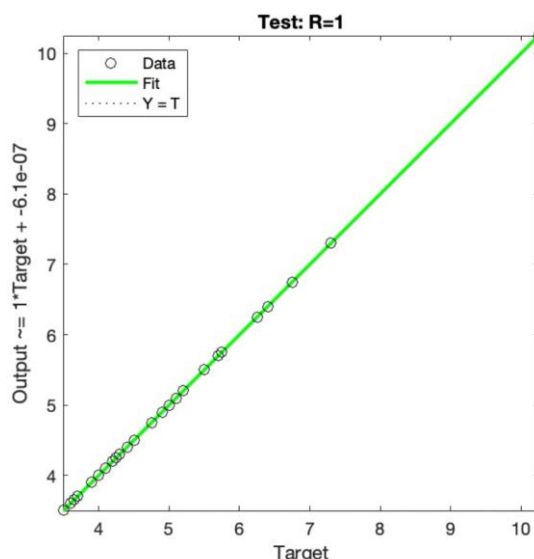


Figure 3 - Testing accuracy via Bayesian Regularisation.

Optimisation results from Bayesian regularisation generated an R-squared testing and validation value of 1 with a testing MSE value of 6.3397 e-13.

Thus, with such high accuracy between the predicted and actual response, such a neural network may be optimised and applicable for predicting, and subsequently optimising values for PCCC regeneration energy. Furthermore, the optimised performance results generated from Bayesian regularisation provide the insight that the model would perform with a high accuracy for unseen data, thereby making it extremely useful for new PCC industrial applications.

4. CONCLUSION

This study presented a neural network optimisation framework for Post-Combustion CO₂ Capture process regeneration energy with respect to amine composition. The optimisation followed a comparative approach between an NNN and WNN. Both models displayed high accuracy between the predicted response vs actual response. With perfect R-Squared validation values of both models, it can be concluded that such a model is applicable for predicting regeneration energy values for both pilot-scale as well as large-scale applications of the PCC capture process. Results from the Bayesian regularisation proved the model's accuracy in predicting responses for unseen data, thereby accounting for the model's generalisation on new applications of the PCC

process. It is thus imperative for the sustainable future of reducing emissions from industrial applications that such models be developed and optimised before the implementation of any CO₂ capture facility so the energy intensity of the process may be optimised.

REFERENCES

- [1] K. O. Yoro and M. O. Daramola, "CO₂ emission sources, greenhouse gases, and the global warming effect," *Advances in Carbon Capture: Methods, Technologies and Applications*, pp. 3–28, Jan. 2020, doi: 10.1016/B978-0-12-819657-1.00001-3.
- [2] O. Khalifa, I. I. I. Alkhatib, D. Bahamon, A. Alhajaj, M. R. M. Abu-Zahra, and L. F. Vega, "Modifying absorption process configurations to improve their performance for Post-Combustion CO₂ capture – What have we learned and what is still Missing?," *Chemical Engineering Journal*, vol. 430, p. 133096, Feb. 2022, doi: 10.1016/J.CEJ.2021.133096.
- [3] O. Otitoju, E. Oko, and M. Wang, "Energy Performance Analysis of Post-combustion Carbon Capture using Piperazine for Large-scale Natural Gas Combined Cycle Power Plants," *SSRN Electronic Journal*, Feb. 2021, doi: 10.2139/SSRN.3814904.
- [4] Ł. Bartela, A. Skorek-Osikowska, and J. Kotowicz, "Economic analysis of a supercritical coal-fired CHP plant integrated with an absorption carbon capture installation," *Energy*, vol. 64, pp. 513–523, Jan. 2014, doi: 10.1016/J.ENERGY.2013.11.048.
- [5] T. E. Akinola, P. L. Bonilla Prado, and M. Wang, "Experimental studies, molecular simulation and process modelling\simulation of adsorption-based post-combustion carbon capture for power plants: A state-of-the-art review," *Appl Energy*, vol. 317, p. 119156, Jul. 2022, doi: 10.1016/J.APENERGY.2022.119156.
- [6] H. Zhang, K. Xue, C. Cheng, D. Gao, and H. Chen, "Study on the performance of CO₂ capture from flue gas with ceramic membrane contactor," *Sep Purif Technol*, vol. 265, p. 118521, Jun. 2021, doi: 10.1016/J.SEPPUR.2021.118521.
- [7] M. Ma *et al.*, "Regulatory mechanism of a novel non-aqueous absorbent for CO₂ capture using 2-amino-2-methyl-1-propanol: Low viscosity and energy efficient," *Journal of CO₂ Utilization*, vol. 67, p. 102277, Jan. 2023, doi: 10.1016/J.JCOU.2022.102277.
- [8] S. D. Peu *et al.*, "A Comprehensive Review on Recent Advancements in Absorption-Based Post Combustion Carbon Capture Technologies to Obtain a Sustainable Energy Sector with Clean Environment," *Sustainability (Switzerland)*, vol. 15, no. 7, Apr. 2023, doi: 10.3390/SU15075827.
- [9] W. Srisang *et al.*, "Evaluation of the heat duty of catalyst-aided amine-based post combustion CO₂ capture," *Chem Eng Sci*, vol. 170, pp. 48–57, Oct. 2017, doi: 10.1016/J.CES.2017.01.049.
- [10] G. T. Rochelle, "Amine Scrubbing for CO₂ Capture," *Science (1979)*, vol. 325, no. 5948, pp. 1652–1654, Sep. 2009, doi: 10.1126/SCIENCE.1176731.
- [11] L. Helei, P. Tantikhajorngosol, C. Chan, and P. Tontiwachwuthikul, "Technology development and applications of artificial intelligence for post-combustion carbon dioxide capture: Critical literature review and perspectives," *International Journal of Greenhouse Gas Control*, vol. 108, p. 103307, Jun. 2021, doi: 10.1016/J.IJGGC.2021.103307.
- [12] S. Vaz, A. P. Rodrigues de Souza, and B. E. Lobo Baeta, "Technologies for carbon dioxide capture: A review applied to energy sectors," *Clean Eng Technol*, vol. 8, p. 100456, Jun. 2022, doi: 10.1016/J.CLET.2022.100456.
- [13] K. Aliyon, F. Rajaei, and J. Ritvanen, "Use of artificial intelligence in reducing energy costs of a post-combustion carbon capture plant," *Energy*, vol. 278, p. 127834, Sep. 2023, doi: 10.1016/J.ENERGY.2023.127834.
- [14] K. Aliyon, A. Hajinezhad, and M. Mehrpooya, "Energy assessment of coal-fired steam power plant, carbon capture, and carbon liquefaction process chain as a whole," *Energy Convers Manag*, vol. 199, p. 111994, Nov. 2019, doi: 10.1016/J.ENCONMAN.2019.111994.



- [15] K. Aliyon, F. Rajaei, and J. Ritvanen, "Use of artificial intelligence in reducing energy costs of a post-combustion carbon capture plant," *Energy*, vol. 278, p. 127834, Sep. 2023, doi: 10.1016/J.ENERGY.2023.127834.
- [16] P. H. M. Feron, A. Cousins, K. Jiang, R. Zhai, and M. Garcia, "An update of the benchmark post-combustion CO₂-capture technology," *Fuel*, vol. 273, p. 117776, Aug. 2020, doi: 10.1016/J.FUEL.2020.117776.
- [17] C. Dinca and A. Badea, "The parameters optimization for a CFBC pilot plant experimental study of post-combustion CO₂ capture by reactive absorption with MEA," *International Journal of Greenhouse Gas Control*, vol. 12, pp. 269–279, Jan. 2013, doi: 10.1016/J.IJGGC.2012.11.006.
- [18] E. Mostafavi, O. Ashrafi, and P. Navarri, "Assessment of process modifications for amine-based post-combustion carbon capture processes," *Clean Eng Technol*, vol. 4, p. 100249, Oct. 2021, doi: 10.1016/J.CLET.2021.100249.
- [19] J. Bravo, D. Drapanauskaite, N. Sarunac, C. Romero, T. Jesikiewicz, and J. Baltrusaitis, "Optimization of energy requirements for CO₂ post-combustion capture process through advanced thermal integration," *Fuel*, vol. 283, p. 118940, Jan. 2021, doi: 10.1016/J.FUEL.2020.118940.

ICH2P14-OP152

DESIGN, DEVELOPMENT AND INVESTIGATION OF SOLAR-INTEGRATED CO-ELECTROLYSIS FOR METHANOL PRODUCTION

¹Muhammad Sajid Khan, ²Muhammad Abid, ³Chen Chen, ²Juliana Hj Zaini, ⁴Tahir Ratlamwala

¹Institute of Innovation Research of Shengzhou, Zhejiang University of Technology, Shengzhou, Zhejiang, 312400 China

²Universiti Brunei Darussalam, Faculty of integrated Technologies, Bandar Seri Begawan, Brunei Darussalam

³College of Mechanical Engineering Zhejiang University of Technology, Hangzhou, Zhejiang, 310032 China

⁴National University of Sciences and technology, Department of Mechanical Engineering, Islamabad, Pakistan

*Corresponding author e-mail: Muhammad.abid@ubd.edu.bn

ABSTRACT

H₂-rich syngas produced from the renewable-driven co-electrolysis of H₂O and CO₂ utilizing solid oxide electrolysis cells (SOEC) have gained huge attraction because of the efficient and high conversion rate. It further delivers opportunities to reduce global warming and CO₂ emissions by storing periodic renewable energies. Solar-integrated co-electrolysis of H₂O and CO₂ via SOEC is considered in the present study to produce H₂-rich syngas, which is used further for methanol synthesis after a series of heat exchangers and compressors. More specifically, parabolic dish solar collectors and photovoltaic modules deliver thermal energy and electricity to the SOEC, respectively. CO₂ from the industry is captured for co-electrolysis and mixed with steam at the inlet of SOEC. The proposed system is developed and modeled in an engineering equation solver, considering mass, energy, and exergy balance equations. The performance of the system is examined by varying certain influential parameters such as direct normal irradiance, heat exchanger effectiveness, current density, cell temperature, and pressure. Solar-to-fuel efficiency and methanol production of the proposed system is 24.27% and 37.85%, respectively. The exergy destruction rate of the system components is investigated to find out the component with maximum irreversibility. In addition, the levelised cost of fuel and payback period of the system is calculated by economic analysis.

Keywords: Solid oxide electrolysis, H₂-rich syngas, Methanol production, Co-electrolysis, Solar dish, Photovoltaic.

INTRODUCTION

Methanol production from renewable energy sources with co-electrolysis in high-temperature electrolyzers promotes a promising way to handle massive electricity storage and carbon capture and utilization issues. Methanol is an important chemical, which is produced globally and can be utilized as a fuel in direct methanol fuel cells and IC (internal combustion) engines [1]. Furthermore, it can be utilized as a raw material for the synthesis of gasoline, Olefins and other chemicals. High-temperature solid-oxide electrolysis is an efficient technology that uses renewable energy and convert CO₂ into syngas with the required H₂ and CO ratio via co-electrolysis of CO₂ and H₂O. SOEC delivers higher electrical efficiency and space of heat integration with the downstream process as compared to low-temperature electrolysis. The previous research work has been proven that the co-electrolysis of H₂O and CO₂ via SOEC produces syngas, convenient for the chemical product synthesis and can be named power-to-chemical process (PtC) [2]. Renewable electricity-based co-electrolysis is crucial to the commercialization of the power-to-methanol (PtM) process as initially, it harvests electricity into syngas via co-electrolysis and then into methanol through syngas methanolization. The integration of exothermic methanol synthesis process with SOEC is important to evaluate the overall process performance specifically, outlet temperature, voltage, current density and operating pressure [3]. In addition, exergo-economic analysis of the proposed system includes economic feasibility, levelised fuel cost, and exergy cost and these have significant influence on the methanol production life cycle assessment and payback period time. To the best knowledge of the authors, the existing literature lack the comprehensively assessment in terms of energetic, thermodynamic and exergo-economic evaluation of renewable methanol production integrated by high temperature SOEC. Therefore, investigation of a renewable-based methanol system with the co-electrolysis of CO₂ and H₂O in a SOEC from the techno and exergo-economical points is addressed in the present study.

SYSTEM DESCRIPTION

Fig. 1 shows the line diagram of the proposed solar-based methanol production unit integrated with co-electrolysis SOEC unit. It includes parabolic dish collectors and PV arrays for thermal energy and DC power supply to the electrolyzer, respectively. In addition, heat exchangers, compressors and methanol production units are the required sub-systems. Solar irradiance provides the required thermal energy to the steam at the inlet of the cathode, while PV modules provide electricity to the electrolyte. On the other side, CO₂ is captured, compressed and mixed with the high-temperature steam just before SOEC inlet. The produced syngas (CO, H₂) is cooled in the heat exchanger and fed to the flash drum, while O₂ flows across the membrane and exits from the anode side. After that, H₂-rich syngas gets compressed in multi-stage compressors and pure methanol is achieved in distillation column. The design input parameters of the proposed system is listed in Table 1.

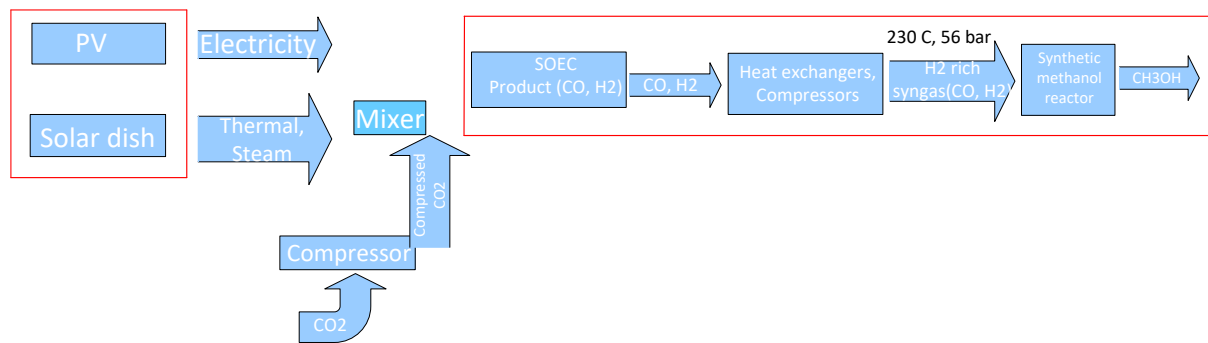


Fig. 1. Solar-integrated co-electrolysis using SOEC for methanol production

METHODOLOGY AND ANALYSIS

This section provides details on the governing equations used for the thermodynamic and exergo-economic analysis of the proposed SOEC-based co-electrolysis for the methanol production system. The system is modelled in the engineering equation solver (EES) considering mass, energy and exergy balance equations [4].

$$\dot{Q} - \dot{W} = \sum(\dot{m} \cdot h)_{in} - \sum(\dot{m} \cdot h)_{out} \quad (1)$$

$$\sum \dot{m}_{in} - \sum \dot{m}_{out} = 0 \quad (2)$$

$$\dot{E}x_{heat} - \dot{W} = \sum(\dot{m} \cdot ex)_{in} - \sum(\dot{m} \cdot ex)_{out} + \dot{E}x_{dest} \quad (3)$$

The energy conversion efficiency of the PV module will be calculated as [5]:

$$\eta_{en} = \frac{P_{max}}{A \times G_b} \quad (4)$$

The collector thermal and exergy efficiencies can be defined by the following equation [6].

$$\eta_{th} = \dot{Q}_u / \dot{Q}_{sun} \quad (5)$$

$$\eta_{ex} = \dot{E}x_u / \dot{E}x_{sun} \quad (6)$$

Solar-to-fuel efficiency can be computed as:

$$\eta_{StF} = \frac{LHV_{Methanol} \times \dot{m}_{Methanol}}{\dot{Q}_{sun}} \quad (7)$$

Table 1. Design parameters of the proposed system

Parameter	Value
SOEC area (m ²)	0.53066
PV array area (m ²)	43.66
Solar dish area (m ²)	6.45
Heat exchanger area (m ²)	0.010621
Solar thermal power (kW)	4.724
Solar PV power (kW)	10.917
SOEC power (kW)	3.909
Solar irradiance (W/m ²)	1000

RESULTS AND DISCUSSION

The current work concentrates on the investigation of solar methanol production integrated with co-electrolysis via SOEC. Major influential operating parameters are DNI, SOEC temperature, pressure, and current density, while solar-to-fuel efficiency, SOEC efficiencies, levelized cost of fuel and cell potential are the desired performance parameters. Fig. 2 shows the variation in the solar-to-fuel efficiency and methanol production against rise in the direct normal irradiance (DNI) value. Both performance parameters increase from 14.17% to 24.27% and 12.83% to 37.85%, respectively with rise in the DNI from 500 to 1000 W/m². It is due to the increase in the useful thermal energy from solar collector at higher DNI. In addition, impact of SOEC operating temperature on the cell potential and SOEC efficiency is plotted in fig. 3. The cell potential is reduced to almost 38.41% due to the decrease in activation and ohmic over-potential is more influential than increase in the concentration over-potential at higher temperatures. This is the main reason that over-potentials are less at higher temperatures. In addition, SOEC efficiency is noticed to be increase in parabolic way (increase from 43.54% to 84.5%) with rise in the SOEC temperature as efficiency is proportional to the current density, which will increase the efficiency.

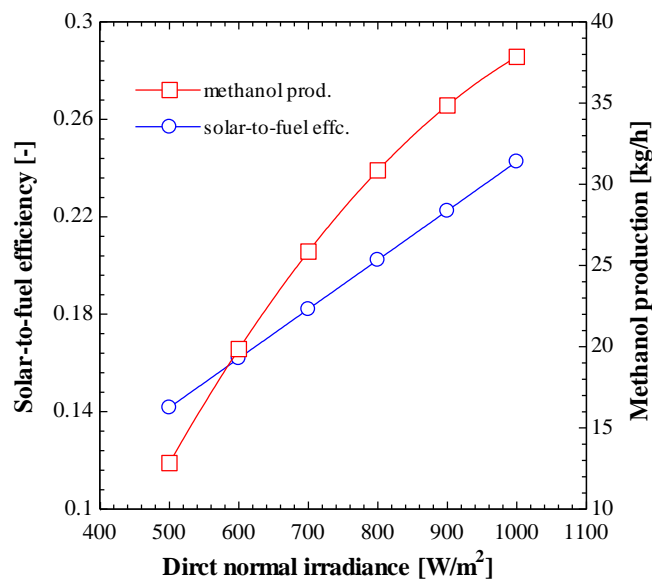


Fig.2. Effect of DNI on solar-to-fuel efficiency and methanol production.

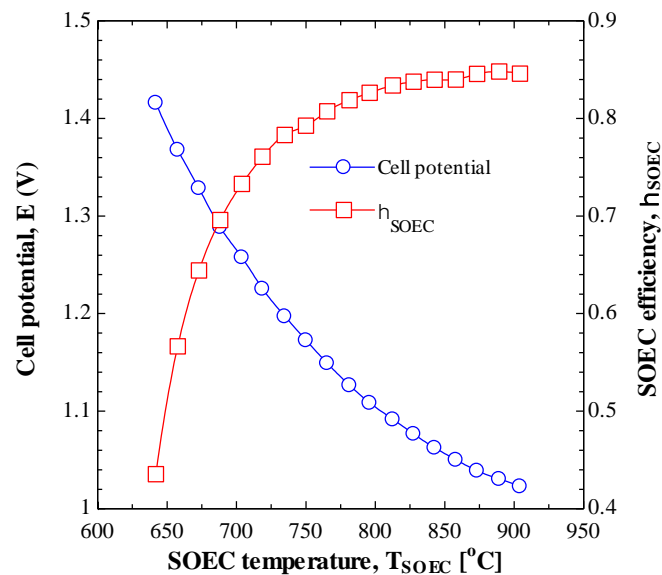


Fig. 3. Impact of electrolyser operating temperature on cell potential and SOEC efficiency.

CONCLUSIONS

The renewable methanol synthesis utilizing co-electrolysis via SOEC technology is an efficient and promising energy storage technology because hydrogen generated from surplus electricity can be used to produce various hydrocarbon fuels after combined with CO₂ captured from different industrial sectors. The present work evaluates a solar-based methanol production using CO₂ and H₂O co-electrolysis via high temperature SOEC. Aim is to investigate the thermodynamic, techno and exergo-economic aspects of the proposed system. Findings of the study can be summarized as:

- Solar-to-fuel efficiency and methanol production of the proposed system is 24.27% and 37.85%, respectively and both performance parameters increase linearly as DNI will enhance.
- The variation in the current density has positive effect on the SOEC efficiencies, solar-to-fuel efficiencies and methanol production rate.
- The cell potential decreases with rise in the SOEC temperature, while SOEC efficiency shows a positive trend against the temperature.

REFERENCES

1. Zhang, H. and Desideri, U., 2020. Techno-economic optimization of power-to-methanol with co-electrolysis of CO₂ and H₂O in solid-oxide electrolyzers. *Energy*, 199, p.117498.
2. Lin, Z., Xia, Q., Ma, K., Khan, M.S., Chen, C. and Liu, Q., 2023. Efficient solar hydrocarbon fuel production by integrating Fischer-Tropsch synthesis with high-temperature solid oxide co-electrolysis and electrolysis. *Energy Conversion and Management*, 294, p.11759.
3. Wei, H., Su, C., Dai, J., Albdeiri, M.S., Alsenani, T.R., Elattar, S., Abed, A.M. and Hua, Y., 2023. Towards a sustainable, and economic production future: Proposing a new process for methanol production based on renewable hydrogen. *Journal of Cleaner Production*, 389, p.135976.
4. Khan, M.S., Abid, M., Bashir, M.A., Amber, K.P., Khanmohammadi, S. and Yan, M., 2021. Thermodynamic and exergoeconomic analysis of a novel solar-assisted multigenerational system utilizing high temperature phase change material and hybrid nanofluid. *Energy Conversion and Management*, 236, p.113948.
5. Amber, K.P., Akram, W., Bashir, M.A., Khan, M.S. and Kousar, A., 2021. Experimental performance analysis of two different passive cooling techniques for solar photovoltaic installations. *Journal of Thermal Analysis and Calorimetry*, 143, pp.2355-2366.
6. Abid, M., Khan, M.S., Ratlamwala, T.A.H., Malik, M.N., Ali, H.M. and Cheok, Q., 2021. Thermodynamic analysis and comparison of different absorption cycles driven by evacuated tube solar collector utilizing hybrid nanofluids. *Energy Conversion and Management*, 246, p.114673.

ICH2P14-OP156
**AN ELECTROLYSER DESIGN FOR MEMBRANELESS ELECTROLYSIS BY
USING 3D PRINTING**

^{1,2*}*Muhammed Iberia Aydin, ^{1,2}Ibrahim Dincer*

¹Yildiz Technical University, Clean Energy Research Institute, Hydrogen Research Center, Esenler, Istanbul, 34220, Türkiye

²Ontario Tech University, Faculty of Engineering and Applied Science, Clean Energy Research Laboratory, Oshawa, Ontario, L1G 0C5, Canada

*Corresponding author e-mail: iberia.aydin@yildiz.edu.tr

ABSTRACT

This study presents a membraneless electrolysis system for hydrogen production. The system leverages fluidic forces to separate gases in electrochemical processes, offering an alternative to membrane separation. Membraneless electrolysis design is more tolerant to impurities in feed water, simplifying the process and reducing costs. The study introduces a unique electrolysis unit, where water is distributed between the anode and cathode through a specially designed layer. This layer, created using 3D printing technology with tough polylactic acid (PLA), ensures continuous flow and increased gas purity by preventing the mixing of oxygen and hydrogen gases. The system's performance, including electrochemical response and gas purity, was tested. Preliminary results show promising efficiency and scalability potential, despite challenges like ohmic losses and less efficient gas separation attributed to membraneless electrolyzers compared to membrane systems. Current density of the system for 15% KOH solution was 100, 188, 318, 470 mA/cm² for 4V, 6V, 8V, and 10V, respectively.

Keywords: Hydrogen production, electrolysis, membraneless, 3D Printing.

INTRODUCTION

The relationship between human development, energy consumption and climate change are the key focus for sustainable development. Human development often means more energy demand. In 2021, a significant 82% of the global electricity demand still be met by using fossil fuels [1]. Although the renewable share is on the rise, it also poses new challenges. Surplus electricity production and counterbalancing the peak-hour demand is a challenge to be addressed for renewable and nuclear energy production methods. Hydrogen is emerging as an energy storage method, especially for storing excess electricity generated from renewable energy sources [2]. Hydrogen with its high energy content is an ideal method for storing energy. Today, 95% of hydrogen production comes from fossil fuels [3]. However, as a result of climate agreements, the research and use of electrolysis technologies using renewable energy as a source has increased. Currently, commercial electrolysis technologies consist of alkaline and proton electrolyte membrane electrolysis methods. Those methods employ physical barriers between the anode and cathode to separate the oxygen and hydrogen evolution inside the cell to prevent mixing these gases. Increased concentration of oxygen in hydrogen feed, or hydrogen in oxygen feed poses risk of explosion under operating conditions. Membrane utilization requires rare earth catalysts like platinum and iridium, which also increases the costs and life cycle footprint of produced hydrogen.

Membraneless electrolyzers take advantage of the fluidic forces to separate gases produced in electrochemical processes instead of solid barriers. Membraneless electrolysis devices are more tolerant to impurities in the feed water that can cause problems in membranes, and the absence of membranes simplifies the process and reduces manufacturing and assembly costs [4]. However, when the membrane electrode assembly is removed from the electrolysis system, the distance that the ions must travel is limited to the distance between the two electrodes. This results in ohmic losses and an increase in the applied voltage. Also, separation of the gases is not efficient as in the membrane systems [5]. In this study, a membrane-less electrolysis system has been designed. In this system, water enters the system through a distributing layer placed between the anode and cathode. The distributor, with its small holes, carries water to the anode and cathode compartments. As the flow is

continuously maintained, it becomes more difficult for oxygen and hydrogen gases to combine, resulting in the increased purity of the gases.

MATERIALS AND METHODS

Designed electrolysis unit was given in Figure 1(a). Stainless steel (316L) electrodes with an active area of 5 cm² were used as both anode and cathode. Flow distributor layer was printed by using an Ultimaker S7 3D printer with tough polylactic acid (PLA). PLA has adequate compressive strength and chemical stability thus it is considered suitable for this study.

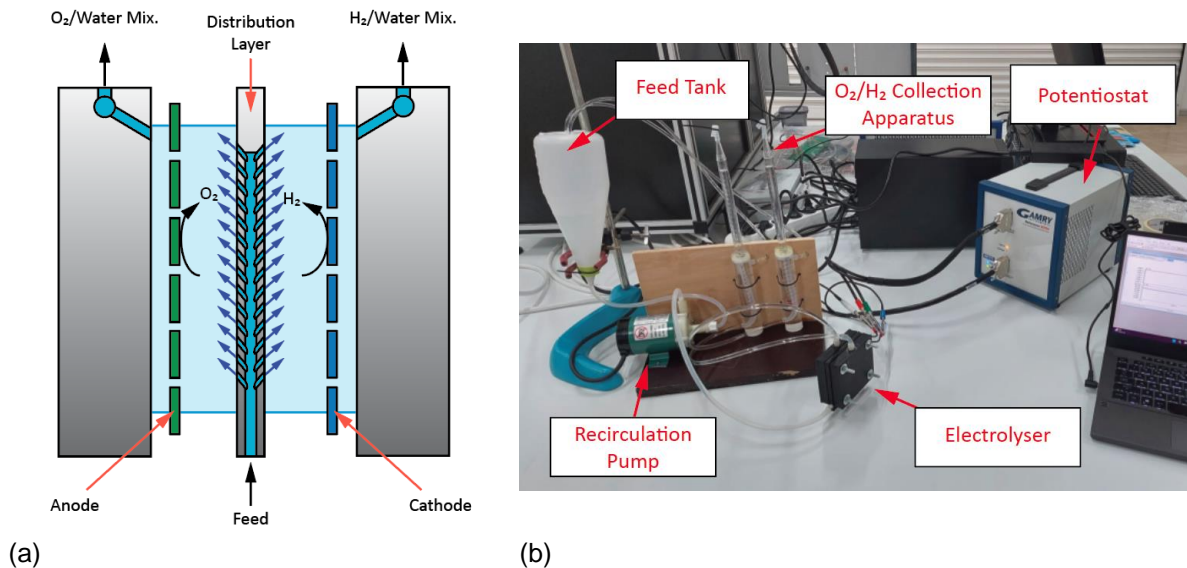


Figure 1. (a) Schematic view of the designed reactor, (b) experimental setup.

Water with varying concentrations of potassium hydroxide (KOH) fed the system through distribution layer and produced gases collected using apparatus given in Figure 1(b). Electrochemical response of the system was observed with a Gamry Reference 3000 potentiostat. Purity of the produced gas was measured with Cubic-Ruiyi Gasboard 3100 gas analyser.

RESULTS AND DISCUSSION

The system responses obtained in the studies with pure water are presented in Figure 2(a). The specific power consumption of the system was obtained as 52 kWh/kg H₂ for 3V. At a KOH concentration of 15%, the current density of the system was 100, 188, 318, 470 mA/cm² for 4V, 6V, 8V, and 10V, respectively.

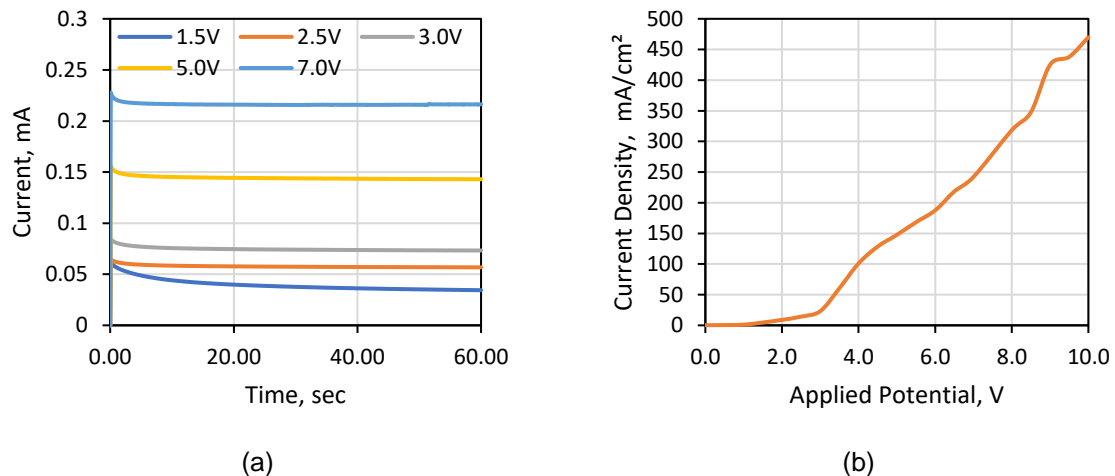


Figure 2. (a) Current response of the electrolyser module with varying voltages (b) current density with varied applied potential



CONCLUSIONS

The study aims to develop a membrane-less electrolysis system for hydrogen production, by using 3D printing technology to design internal parts of the unit. Design of the electrolysis unit utilizes a flow distributor between the anode and cathode that helps effectively separating hydrogen and oxygen gases, thereby enhancing gas purity. The specific power consumption of the system, evaluated under various conditions, indicates its efficiency and potential for scalability. However, challenges such as ohmic losses and less efficient gas separation compared to membrane systems are identified, suggesting areas for future improvement. Overall, this study contributes to the ongoing efforts in sustainable energy production, particularly in the context of hydrogen as a renewable energy storage method, and highlights the importance of innovative approaches.

REFERENCES

- [1] British Petroleum. Statistical Review of World Energy 2022.
- [2] Dincer I, Aydin MI. New paradigms in sustainable energy systems with hydrogen. *Energy Convers Manag* 2023;283:116950. <https://doi.org/https://doi.org/10.1016/j.enconman.2023.116950>.
- [3] Dincer I, Acar C. Review and evaluation of hydrogen production methods for better sustainability. *Int J Hydrogen Energy* 2014;40:11094–111. <https://doi.org/10.1016/j.ijhydene.2014.12.035>.
- [4] Swiegers GF, Hoang AL, Hodges A, Tsekouras G, Lee C-Y, Wagner K, et al. Current status of membraneless water electrolysis cells. *Curr Opin Electrochem* 2022;32:100881. <https://doi.org/https://doi.org/10.1016/j.coelec.2021.100881>.
- [5] Esposito D V. Membraneless Electrolyzers for Low-Cost Hydrogen Production in a Renewable Energy Future. *Joule* 2017;1:651–8. <https://doi.org/https://doi.org/10.1016/j.joule.2017.07.003>.



ICH2P14-OP162

THERMODYNAMIC EVALUATION OF A RENEWABLE ENERGY STORAGE CONCEPT INCORPORATING A SOLID OXIDE ELECTROLYZER AND METAL HYDRIDE COMPRESSOR

*Uday Raj Singh, *Satyasekhar Bhogilla*

Department of Mechanical Engineering, Indian Institute of Technology Jammu, Jammu, 181221, India

*Corresponding author e-mail: satyasekhar6@gmail.com; satya.bhogilla@iitjammu.ac.in

ABSTRACT

Solid oxide electrolysis (SOE) can achieve remarkable efficiency by utilising significant amount of thermal energy. The present study introduces a Metal Hydride (MH) compressor to compress hydrogen generated by SOE. The integrated two-stage MH compressor in this study, effectively elevates H₂ pressure to 350 bar in two steps. The first stage increases the pressure up to 100 bar after which the hydrogen is partially taken for further compression. One half is further compressed to 350 bar whereas the another half can be used for power generation during high electrical energy demand. The compression up to 350 bar is achieved using a heat transfer fluid at approximately 140°C for heating and 20-40°C for cooling. Energy and exergy analysis of the overall system post the integration of the MH compression unit is assessed. The study delves into how critical operating parameters—such as operating temperature, current density, supply pressure, absorption, and heat source temperature—affect the system's energy and exergy efficiency. It was observed that under specific operating conditions, the energy efficiency of SOE alone is approximately 60.57%. This efficiency increases to 66.5% after the system is integrated to the MH compressor.

Keywords: Solid Oxide Electrolyser, Hydrogen storage, Metal Hydride hydrogen Compressor, Energy and Exergy investigation, Thermodynamic assessment.

INTRODUCTION

In light of their environmental drawbacks and significant carbon emissions, fossil fuels remain dominant, providing nearly 80% of global primary energy. Global fossil fuel usage has historically risen with economic growth since the Industrial Revolution. Shifting this pattern will be a pivotal moment in energy history. In the Stated Policies Scenario, fossil fuels will decrease from about 80% to just above 60% of the global energy mix by 2050, leading to a gradual decline in global CO₂ emissions from 37 billion to 32 billion tonnes per year by 2050 [1]. Given the finite nature of these resources, there is a growing imperative to explore alternative energy solutions. Renewable energy sources like solar, wind, and geothermal power offer promising alternatives to finite fossil fuels. However, a significant drawback of these resources is their intermittent nature, leading to the need for effective energy storage solutions to bridge the gap between production and demand. In this context, hydrogen emerges as a compelling alternative to fossil fuels [2–5].

Previous research on hydrogen refuelling stations has predominantly focused on using alkaline electrolyzers for hydrogen production and mechanical compressors to elevate hydrogen pressure. The studies till now have not considered the scope of utilizing thermally driven compressors as an option to store renewable energy. More specifically, the potential of using SOE for hydrogen production and its integration with metal hydrides is rarely explored. Existing literature covers aspects of solar-driven hydrogen generation and high-pressure storage systems. Still, it needs studies on the proposed integrated system, which combines energy production, storage, and compression through thermal compression. Thus, this study evaluates the thermodynamic performance of a high-temperature SOE unit that independently produces hydrogen and oxygen from water and electricity, employing thermodynamics to assess overall system performance. Energy and exergy assessments are of equal significance in high-temperature SOE. A thermodynamic examination of SOE is instrumental in discovering the origins of energy and exergy loss. This, in turn, facilitates the enhancement of SOE plant design to achieve improved efficiency. This paper presents an intricate energy and exergy analysis focused on an integrated hydrogen storage system based on hydrogen production through SOE. It also stores high-pressure storage using a metal hydride-based compressor for refuelling stations. Furthermore, because hydrogen is a key fuel for fuel cells, the system suggests using it in fuel cells to produce electricity and heat.

DESCRIPTION OF THE RENEWABLE ENERGY STORAGE SYSTEM AND SYSTEM MODELLING

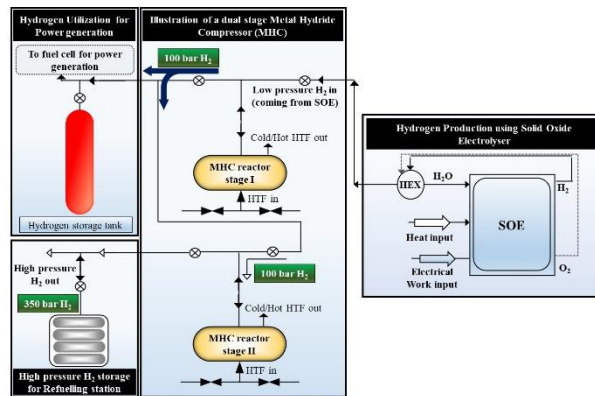


Fig. 1. Schematic representation of the hydrogen storage concept incorporating a SOE and MHC system.

System Energy and Exergy efficiency

The energy and exergy efficiency of the overall system can be evaluated based on some important performance indexes, as discussed below. The energy efficiency can be calculated by considering the heat absorption from the MH compression system during the overall energy release. Moreover, the total thermal requirement is also considered in the efficiency evaluation. The work of compression achieved by utilizing thermal compression is added to the numerator, which improves the system's overall energy efficiency. The overall energy efficiency considering all the factors is given by

$$\eta_{en,sys} = \frac{(LHV \cdot N_{H_2,out}) + W_{comp} + Q_{MH,abs}}{W_{el} + Q_{SOE,heat} + Q_{H_2O,heat} + Q_t} \quad (1)$$

On the other hand, the exergy efficiency of the renewable energy storage system based on SOE can be evaluated using

$$\eta_{ex,sys} = \frac{\dot{E}x_{H_2} \cdot \dot{N}_{H_2,out} + W_{el} + \dot{E}x_{MH,abs}}{\dot{E}x_{W_{el}} + \dot{E}x_{SOE,heat} + \dot{E}x_{H_2O,heat} + \dot{E}x_t} \quad (2)$$

RESULTS AND DISCUSSION

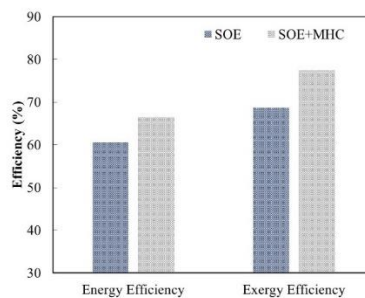


Fig. 2. Energy and exergy efficiencies for electrolyser and overall system (electrolyser+MHC).

Fig. 2 represents the proposed system's theoretical results of energy and exergy investigations. Energy analysis shows that the maximum energy efficiency of the system is calculated to be 60.57%, and it does not account for the amount of work of compression obtained as a result of the thermal compression process. However, with the integration of MH compression, the system's overall energy efficiency experiences a significant improvement, as depicted in Fig. 2. Following the incorporation of MH compression, the energy efficiency increases to 66.50%, marking a remarkable enhancement of approximately 9.8%. This improvement underscores the key role of MH compression in boosting the system's overall energy efficiency. On the other hand, the value of exergy efficiency

is found to be around 68.7%. When the compression effect is added to the exergy efficiency, the value rises by 12.78% to reach 77.47%.

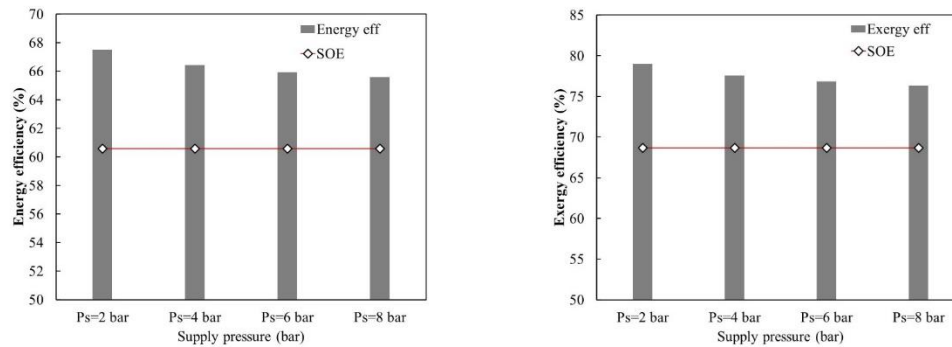


Fig. 3 (a) Energy efficiency for electrolyser and overall system (electrolyser+MHC) at different supply pressures, (b) Exergy efficiency for electrolyser and overall system (electrolyser+MHC) at different supply pressures.

Fig. 3 (a) shows the influence of supply pressure on the system's energy efficiency. The figure represents the comparative analysis of the system with SOE efficiency evaluated to be 60.56% at a current density of 0.5 A/m². The supply pressure does not influence the SOE energy efficiency, as can be seen in Fig. 3 (a). As the supply pressure increases from 2 to 8 bar, the energy efficiency of the overall system is found to reduce from 67.48% to 65.6%. The energy efficiency after considering the absorption heat from the MH compression system results in an 11.43% increment. The change in exergy efficiency with an increase in the supply pressure of the MH compressor from 2 to 8 bar is shown in Fig. 3 (b). It shows that as the supply pressure rises, the exergy efficiency decreases from 78.98% to 76.37%. The overall system's exergy efficiency is improved compared to the exergy efficiency evaluated when the SOE was considered only for hydrogen production. Previously, the SOE efficiency was observed to be 68.69% at a current density of 0.5 A/cm². It is improved by around 15% after incorporating the compression unit with the electrolyser.

CONCLUSIONS

- Influence of key operating parameters, such as temperature, current density, supply pressure, absorption and heat source temperature, on the system's energy and exergy efficiency.
- By employing a combination of V40Ti21.5Cr38.5 and V70Ti7Cr23, it's possible to achieve hydrogen compression, raising the pressure from 2-8 bar to 350 bar, with an absorption temperature of 293-308K and a heat source temperature of 393-408K.
- The energy efficiency of the SOE system was about 60.57%. Integration of MH compression results in a significant increase, raising energy efficiency to 66.5%.
- The SOE system's exergy efficiency was originally measured at 68.69%. When considering compression work and absorption heat from the MH tank, exergy efficiency improves substantially to 77.47%.

REFERENCES

- [1] International Energy Agency. International Energy Agency (IEA) World Energy Outlook 2022. <https://www.iea.org/reports/world-energy-outlook-2022/executive-summary> 2022.
- [2] AlZahrani AA, Dincer I. Thermodynamic and electrochemical analyses of a solid oxide electrolyzer for hydrogen production. *Int J Hydrogen Energy* 2017;42.
- [3] Vinoth Kanna I, Paturu P. A study of hydrogen as an alternative fuel. *International Journal of Ambient Energy* 2020;41.
- [4] Dincer I, Acar C. Review and evaluation of hydrogen production methods for better sustainability. *Int J Hydrogen Energy* 2014;40.
- [5] Singh UR, Bhogilla S, Hauer I. Thermodynamic study of integrated proton exchange membrane fuel cell with vapour adsorption refrigeration system. *Int J Hydrogen Energy* 2023.

ICH2P14-OP163

SEAWATER DESALINATION AND HYDROGEN PRODUCTION USING MONOVALENT SELECTIVE MEMBRANES ASSISTED WITH ION-EXCHANGE RESINS FOR HYDROPONIC SOLUTION PRODUCTION

¹Ragad F. Alshebli, ¹Nadira Salsabila, ^{1,2*}Burak Yuzer, ¹Yusuf Bicer

¹Division of Sustainable Development, College of Science and Engineering, Hamad Bin Khalifa University, Qatar Foundation, Doha, Qatar

²Istanbul University – Cerrahpaşa, Engineering Faculty, Department of Environmental Engineering, Avcilar, Istanbul, Turkiye

*Corresponding author e-mail: byuzer@hbku.edu.qa

ABSTRACT

This study introduces an innovative approach to address the dual challenges of water scarcity and energy demand. The proposed integrated system combines electro dialysis with monovalent selective membranes (ED-MSMs) and ion-exchange resins (IEX-R) to produce hydrogen gas and nutrient-rich solution from seawater simultaneously. ED-MSMs selectively transport monovalent ions over multivalent ions, effectively removing salt and generating a nutrient-rich solution. To enhance the desalination process, IEX-Rs are strategically incorporated to capture magnesium and calcium ions, preventing membrane fouling and electrode scaling. The system demonstrates promise in addressing critical challenges by utilizing abundant seawater as a feedstock for valuable product generation. The generated hydrogen, a clean and renewable energy carrier, can be used for various applications. The results show a net energy consumption of 11.19 kWh/m³ of seawater and a hydrogen production rate of 8.4 mmol/h. This integrated system holds immense potential for sustainable agriculture practices and a resource-efficient future, leveraging the capabilities of ED-MSMs and IEX-Rs.

Keywords: Hydrogen Energy, Ion exchange resins, Membrane fouling, Sustainability.

INTRODUCTION

The dual challenges of water scarcity and energy demand necessitate the development of innovative and sustainable solutions. In this regard, electro dialysis (ED) with monovalent selective membranes (MSMs) and ion-exchange resins (IEX-R) has emerged as a promising technology for simultaneously producing hydrogen gas and nutrient-rich solution for plants while effectively mitigating membrane fouling, and electrode scaling caused by divalent ions. This integrated approach offers a promising strategy to address these critical challenges by utilizing seawater (SW), an abundant and readily available resource, as the feedstock for generating valuable products. A study by Alshebli et al. [1] shows the ability to produce Hydrogen (H₂) gas while desalinating saline water using ED system. Another study was done by Alshebli et al. [2] for Boron (B) and Lithium (Li) recovery from aqueous solutions and hydrogen production using ED assisted with IEX-R.

Electro dialysis (ED) is a mature and efficient desalination technology that utilizes stacked anion-selective and cation-selective semi-permeable membranes. Cation exchange membranes (CEMs) allow cations to pass while blocking anions, while anion exchange membranes (AEMs) allow anions to pass while blocking cations. Under the influence of an electric field, anions and cations migrate toward the anode and cathode, respectively, through the ion-exchange membranes. This process segregates ions from the saline water into the concentrate stream [3]. ED has been employed for various applications, including wastewater treatment in the electroplating industry, desalination of rejected brine, and desalination of water and wastewater [4,5]. According to Al-Amshawee et al. [5], ED desalination capacity worldwide accounts for approximately 4 %.

The ED system's primary advantages include handling high salt concentrations due to its high recovery rate and low propensity for fouling [3,6]. However, as feed stream salinity increases, so does the ED system's energy consumption. Recent research has focused on minimizing ED cell energy consumption. Nam and Choi [7] significantly reduced ED cell operating voltage by employing Bi/BiOCl electrodes. Electrical energy consumption by the ED system has been reported in various studies to range from 4 – 8 kWh/m³ [8–10]. In contrast, Mir and Bicer [11], reported higher electrical energy consumption

values for seawater desalination using the ED process (10 – 25 kW/m³) and brackish water desalination (0.4 – 4 kW/m³). Al-Amshawee et al. [5], reported an energy consumption of 1 – 12 kWh/m³ for the ED process. ED-MSMs are characterized by their ability to selectively transport monovalent ions over multivalent ions, making them ideal for desalination applications. In the context of the integrated system, ED-MSMs are employed to remove salt (NaCl) from SW, effectively producing nutrient-rich solution. To further enhance the desalination process and ensure the production of a nutrient-rich hydroponic solution, IEX-Rs are strategically incorporated into the system. These resins are strategically positioned at the cathode electrode to selectively capture magnesium and calcium ions that may have leaked from the diluate stream to prevent membranes fouling and electrode scaling. The study of Alshebli et al. [2] shows that 95 % and 99.5 % of B and Li removal efficiency, respectively, could be achieved using ED-MSMs system assisted with IEX-R.

Hydrogen gas is produced at the cathode side and captured in a measuring cylinder. The generated hydrogen, a clean and renewable energy carrier, can be utilized for various applications, including power generation, transportation, and industrial processes. Alshebli et al. [1,2] show that 118.8 mg H₂/h·kg Na₂SO₄, and 13.55 mmol/h of H₂ can be produced using ED system in addition to desalination and ion recovery processes. The proposed integrated system holds immense potential in addressing the pressing challenges of water scarcity and energy demand while promoting sustainable agriculture practices. By harnessing the power of ED-MSMs, and IERs, this system paves the way for a more sustainable and resource-efficient future. Alshebli et al. [12] designed and analyzed an integrated system to recover the required nutrients from saline groundwater and produce a nutrient-rich solution with an overall energy and exergy efficiency of 16.1 % and 13.4 %, respectively. The energy consumption consumed by Alshebli et al. [1] is 9.9 kWh/m³ to produce 118.8 mg H₂/h·kg Na₂SO₄ and desalinate Na₂SO₄ solution from an initial conductivity of 21 mS/cm to 1 mS/cm. Furthermore, the energy consumption consumed by Alshebli et al. [2] is 6.1 kWh/m³ to recover 95.1 % and 99.5 % of B and Li from aqueous solution, respectively. By integrating electrodialysis with monovalent selective membranes (ED-MSMs) and ion-exchange resins (IEX-Rs), this study presents a novel approach that simultaneously produces hydrogen gas and nutrient-rich solution from seawater, effectively tackling the dual challenges of water scarcity and energy demand.

MATERIALS AND METHODS

As showing in Figure 1, between the anode and cathode electrodes, there is an arrangement of membranes that selectively allow monovalent ions to pass through. Monovalent ions like sodium (Na⁺), chloride (Cl⁻), and potassium (K⁺) move through these specialized membranes from the input diluate stream to the monovalent concentrate stream. In contrast, divalent ions such as magnesium (Mg²⁺), calcium (Ca²⁺), and sulfate (SO₄²⁻) remain in the diluate stream. Some of Mg²⁺ and Ca²⁺ ions leak through the MSM and move toward the cathode electrode to scale on the electrode and membranes surface which cause membranes fouling. Therefore, IEX-R are strategically positioned at the cathode electrode to selectively capture these leaked ions and prevent membranes fouling and electrode scaling. In addict, to maintain electrical conductivity within the electrodialysis (ED) cell, an electrolyte solution is used. Sodium sulfate (Na₂SO₄) is commonly used as the electrolyte solution, although sodium chloride (NaCl) can be employed in specific applications. It's important to note that when NaCl is used as the electrolyte solution, highly reactive chlorine gas (Cl₂) is generated at the anode, posing a potential risk to the ion-exchange membranes. Ultimately, hydrogen gas (H₂) is produced at the cathode compartment and collected in a graduated cylinder. Different voltages are applied to the system as follow 8, 6, and 4 V, to desalinate 0.25 L of seawater and to study the amount of H₂ produced and the desalinating efficiency. During the experiment the conductivity, pH, resistivity, and TDS are measured. Finally, the nutrients-rich solution is tested and characterized to check the remaining ions concentrations in the produced solution.

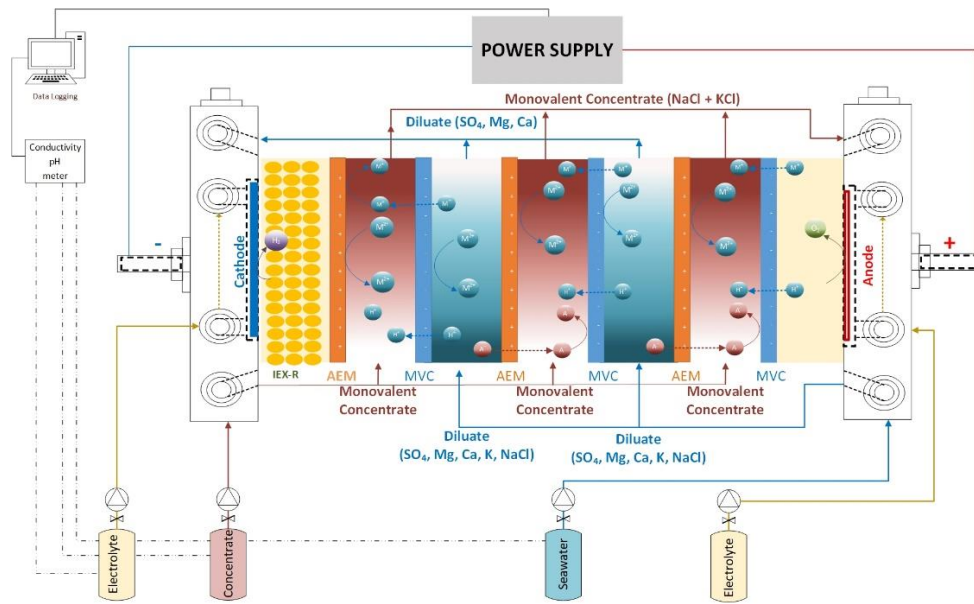
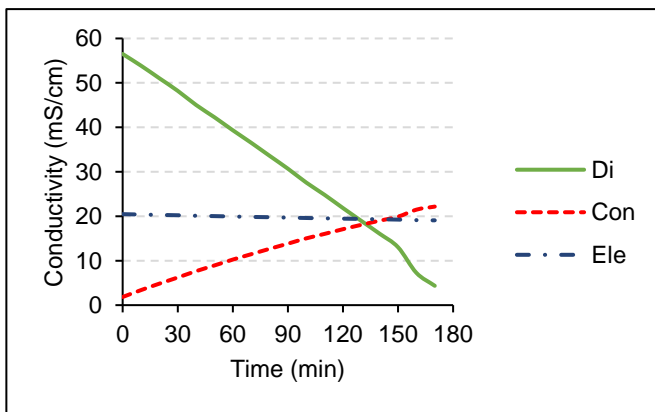


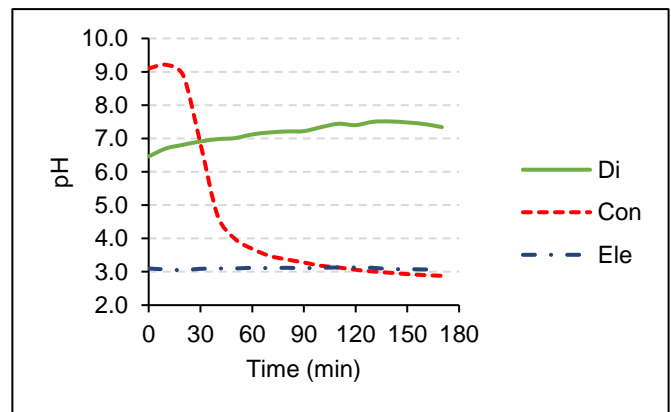
Figure 1 ED-MSM-IEXR System description diagram.

RESULTS AND DISCUSSION

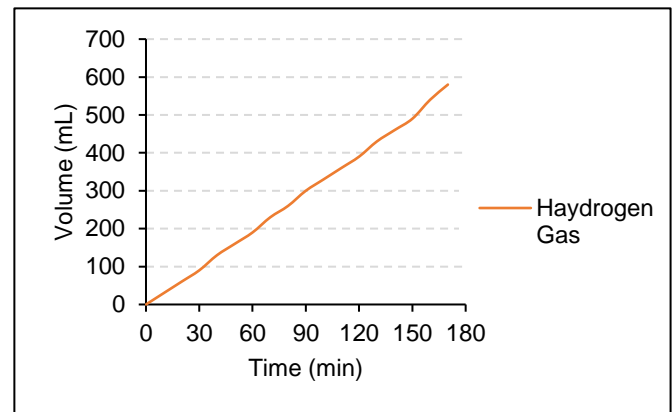
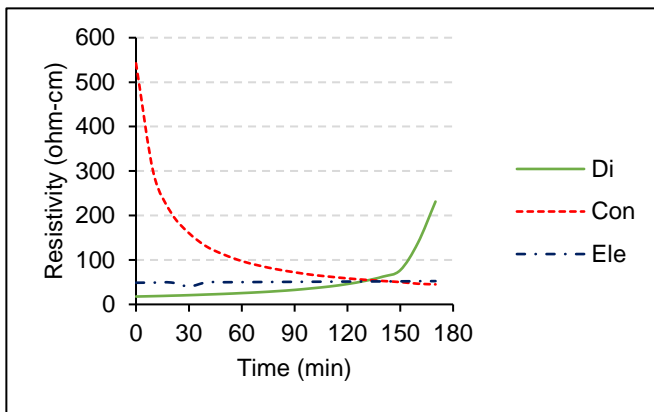
The following figures show the measured results of conductivity (mS/cm), pH, resistivity (ohm-cm), and H₂ volume (mL), during the experiment as shown in Figure 2 a, b, c, and d, respectively. The conductivity of diluate (Di) stream is decreasing during time because the ions are moved and transferred through the membranes toward the concentrate (Con) stream, while the electrolyte conductivity remain constant because of the catholyte, and anolyte streams are mixed in the same containers (see Figure 2 (a)). The pH of the Di stream slightly increases during the experiment while the Con stream pH decreases because of the formation of HCl acid, when the Ele stream pH remain constant even with the formation of OH⁻ and H⁺ ions (see Figure 2 (b)).



(a)



(b)



(c)

(d)

Figure 2 Experimental results (applied voltage = 4 V).

As shown in Figure 2 (c), the relation between the resistivity and conductivity is inversely proportional. Therefore, when the conductivity decreases, the resistivity increases; higher resistivity means it is more resistant to the flow of electric current. In other words, it takes a higher electric field to push the same amount of charge through a material with higher resistivity. This is because the atoms and molecules in the material are more tightly packed together, making it more difficult for electrons to move through them. Figure 2 (d) describes the amount of H₂ produced during the experiment time, the total amount of H₂ gas collected is 580 mL in 180 minutes.

Figure 3 shows the energy consumed during the process with and without the contribution of H₂ energy. For example, the total energy consumed while applying 8 V without H₂ contribution is 42.08 kWh/m³ of seawater, while with the H₂ contribution, the net consumed energy decreases to 34.23 kWh/m³ of seawater. The amount of energy contributed by H₂ energy varied from 6 to 8 kWh/m³ of seawater. In addition, the H₂ production rate are 17.45, 11.60, and 8.43 mmol/h while applying 8, 6, and 4 V, respectively.

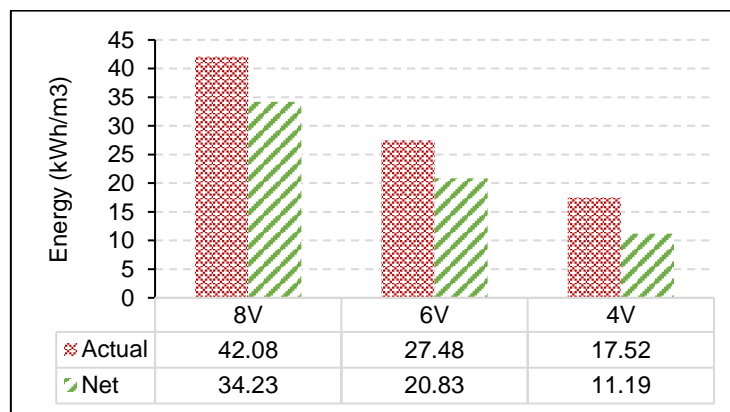


Figure 3 Energy consumption and H₂ contribution.

CONCLUSIONS

This study introduces a new approach to tackle the interconnected problems of water scarcity and energy demand. The proposed integrated system, consisting of ED-MSM and IEX-Rs, provides a dual solution by simultaneously producing hydrogen gas and a nutrient-rich solution from seawater. ED-MSMs selectively transport monovalent ions, effectively desalinating the water and generating a nutrient-rich solution. Moreover, IEX-Rs prevent membrane fouling and electrode scaling by capturing magnesium and calcium ions, improving the overall desalination process.

This innovative system offers promising solutions to critical challenges by utilizing abundant seawater as a valuable resource for product generation. The produced hydrogen, a clean and renewable energy carrier, holds the potential for diverse applications. The study's results, with a net energy

consumption of 11.19 kWh/m³ of seawater and a hydrogen production rate of 8.4 mmol/h, highlight the efficiency of the integrated system. With potential applications in sustainable agriculture and a resource-efficient future, this integrated approach, driven by ED-MSMs and IEX-Rs, represents a significant step toward a more sustainable and resilient global ecosystem.

REFERENCES

- [1] Alshebli RF, Yuzeer B, Bicer Y. Experimental investigation of simultaneous hydrogen production and desalination via electro-dialysis process. *Int J Hydrogen Energy* 2023. <https://doi.org/10.1016/J.IJHYDENE.2022.12.104>.
- [2] Alshebli RF, Salsabila N, Yuzeer B, Bicer Y. Boron and lithium recovery from aqueous solutions by ion-exchange resin stuffed electro-electrodialysis process with hydrogen production. *J Environ Chem Eng* 2023;11:110687. <https://doi.org/10.1016/J.JECE.2023.110687>.
- [3] Mavukkandy MO, Chabib CM, Mustafa I, Al Ghaferi A, AlMarzooqi F. Brine management in desalination industry: From waste to resources generation. *Desalination* 2019;472:114187. <https://doi.org/10.1016/j.desal.2019.114187>.
- [4] Benvenuti T, Siqueira Rodrigues MAA, Bernardes AMM, Zoppas-Ferreira J. Closing the loop in the electroplating industry by electro-dialysis. *J Clean Prod* 2017;155:130–8. <https://doi.org/10.1016/j.jclepro.2016.05.139>.
- [5] Al-Amshawee S, Yunus MYBM, Azoddein AAM, Hassell DG, Dakhil IH, Hasan HA. Electro-dialysis desalination for water and wastewater: A review. *Chem Eng J* 2020;380:122231. <https://doi.org/10.1016/j.cej.2019.122231>.
- [6] Ahmed FE, Khalil A, Hilal N. Emerging desalination technologies: Current status, challenges and future trends. *Desalination* 2021;517:115183. <https://doi.org/10.1016/j.desal.2021.115183>.
- [7] Nam D-H, Choi K-S. Electrochemical Desalination Using Bi/BiOCl Electro-dialysis Cells. *ACS Sustain Chem Eng* 2018;6:15455–62. <https://doi.org/10.1021/acssuschemeng.8b03906>.
- [8] Li Z, Siddiqi A, Anadon LD, Narayanamurti V. Towards sustainability in water-energy nexus: Ocean energy for seawater desalination. *Renew Sustain Energy Rev* 2018;82:3833–47. <https://doi.org/10.1016/j.rser.2017.10.087>.
- [9] Al-Karaghoul A, Renne D, Kazmerski LL. Technical and economic assessment of photovoltaic-driven desalination systems. *Renew Energy* 2010;35:323–8. <https://doi.org/10.1016/j.renene.2009.05.018>.
- [10] Turek M. Cost effective electro-dialytic seawater desalination. *Desalination* 2003;153:371–6. [https://doi.org/10.1016/S0011-9164\(02\)01130-X](https://doi.org/10.1016/S0011-9164(02)01130-X).
- [11] Mir N, Bicer Y. Integration of electro-dialysis with renewable energy sources for sustainable freshwater production: A review. *J Environ Manage* 2021;289:112496. <https://doi.org/10.1016/j.jenvman.2021.112496>.
- [12] Alshebli RF, Bicer Y. Energy and exergy analysis of a renewable energy-driven ion recovery system for hydroponic greenhouses. *Sustain Energy Technol Assessments* 2022;53:102628. <https://doi.org/10.1016/J.SETA.2022.102628>.

ICH2P14-OP165

HYDROGEN GAS AND BIOCHAR PRODUCTION FROM KITCHEN WASTE VIA DARK FERMENTATION

¹*Snigdhendubala Pradhan*, ^{1,2}*Burak Yuzer*, ¹*Yusuf Bicer*, ¹*Gordon Mckay*

¹Division of Sustainable Development, College of Science and Engineering, Hamad Bin Khalifa University, Qatar Foundation, Doha, Qatar

²Department of Environmental Engineering, Engineering Faculty, Istanbul University-Cerrahpasa, Istanbul, Türkiye

*Corresponding author e-mail: spradhan@hbku.edu.qa

ABSTRACT

Food waste including production, supply chain, and consumption, contributes greenhouse gas (GHG) emissions towards global warming. To reduce the risk of global warming, the valorization of food waste for energy production and sustainable agricultural byproducts to reduce fertilizer demand is a major concern worldwide. One of the nutrient recovery techniques involves the dark fermentation method to generate hydrogen (H₂) gas, which serves as a clean energy carrier and could reduce the carbon footprint. Potatoes (*Solanum tuberosum* L.) are the world's fourth most important starchy tuberous vegetable and around 8000 kilotons of potato peel waste are generated yearly with a GHGs emissions of 5 million tonnes of CO₂ equivalent. Another major global economic benefit fruit, watermelon (*Citrullus lanatus*), also generate more than 90% of the rind and is dumped in landfill which constitutes environmental challenges. Therefore, a preliminary study was conducted to produce H₂ gas from potato peels, watermelon rinds, and a mixture of peels and rinds by dark fermentation method by controlling volume and temperature. After the volume analysis of the produced H₂ gas, the leftover residual waste was used to produce biochar. A higher volume of 149 mL of H₂ gas was achieved from potato peels compared to watermelon, while a lower H₂ yield from watermelon rind of 50.6 mL with a biomass pH < 5 was obtained. However, the biochar produced from all types of biomass feedstock was alkaline in nature with a pH of 7.43 to 8.30 by control electrical conductivity (0.358 to 0.418 mS/cm and a zeta (ζ) potential of -18.6 to -35.2 mV. The properties of biochar are found efficient for water, and nutrient retention for agriculture production. The small time span of analysis encourages the scope of food waste for the sustainable production of energy and agriculture production.

Keywords: Hydrogen, Biochar, Dark fermentation, Agriculture, Energy, Environment.

INTRODUCTION

Over the past decade, food waste including production, transportation, consumption, and landfilling released greenhouse gases (GHGs), which is a significant threat to global warming. In order to reduce the risk, the valorization of food waste to clean energy production and agricultural-sustainable byproducts is beneficial worldwide (Foong et al. 2021). According to a survey report by the Food and Agriculture Organization (FAO), approximately 1.3 billion tons per year of food are wasted globally (Seberini 2020). In each year, the largest quantity of food (361 kg per capita is wasted in Australia (Srivastava et al. 2021), while 200 kg per capita of food is wasted in Sweden, 287 kg per capita in the USA, 56 kg per capita in Russia, 44 kg per capita in China and 51 kg per capita wasted in India. However, food waste is a promising biomass to produce energy because of its high content of organics and cellulose. Food waste mainly consists of starch, protein and fat which are good carbon sources for fermentative hydrogen (H₂) gas production (Giroto et al. 2015). Out of all food wastes, a huge quantity of vegetable and fruit wastes especially peels are generated from the kitchen and could be potentially used to produce hydrogen (H₂) gas and biochar (Giroto et al. 2015; Pradhan et al. 2020).

Potatoes (*Solanum tuberosum* L.) are the world's fourth most important starchy tuberous vegetable. According to FAO (Food and Agricultural Organisation of the United Nations), 376 million metric tonnes (mMT) of potatoes were produced worldwide in 2021. It is anticipated that around 8000 kilotons of potato peel waste generated yearly with GHG emissions of 5 million tonnes of carbon dioxide (CO₂) equivalent (Khanal et al. 2023). Watermelon (*Citrullus lanatus*) is one of the major economically beneficial fruits with a global production of 101 million tonnes (mT) in 2020 (Mamiru and Gonfa 2023). Now it has grown to almost 122 countries and many continents.

The watermelon consists of approximately 2% seeds, 30% rind, and flesh. More than 90% of the watermelon rind wastes are dumped as a residue into the environment thereby constituting

environmental challenges (Bellary et al. 2016). Although there are many reports on the potential use of watermelon, but the waste is not used by many industries, household kitchens, and supermarkets. The various social, economic, and environmental concerns associated with the management of food waste especially in terms of GHGs emissions and leachate generation in landfills. Fermentative bacteria hydrolyze and ferment carbohydrates, protein, and lipids to volatile fatty acids to produce H₂ by acetogenic bacteria (Dao et al., 2023). Utilization of watermelon rind is very important for economic value as well as environmental problems as watermelon contains carbohydrates, proteins, fats, minerals, vitamins, etc (Petkowicz et al. 2017).

Dao et al. (2023) conducted a study on H₂ production from peach pulp, examining the influence of hydraulic retention time (HRT) and substrate loading rate (SLR) on the efficiency of H₂ generation. The research revealed that the rate of H₂ formation increased with a reduction in HRT and an elevation in SLR. Notably, a maximum 932 mLH₂/L.d of H₂ formation was achieved with a one-day HRT and a substrate loading rate of 90 g TOC/L.d. In a related study, Cao et al. (2022) utilized potato peel to produce H₂ through the fermentation process employing various pretreated cultures. Their findings indicated a peak hydrogen yield of 71 mL/g of volatile solids (VS) when utilizing aeration-enriched inoculum, coupled with a notable achievement of 29% VS removal with an H₂ yield of 71 mL/g. In another study, a mixture of melon and watermelon substrate was used for H₂ production (Turhal et al., 2019). The study revealed that H₂ gas production exhibited an upward trend with increasing substrate concentration, attributed to a higher initial total sugar content at elevated total solids (TS) concentrations. Specifically, at 37 g TS/L, H₂ gas productivity reached 80.62 mLH₂/L_{reactor}.h with natural microflora. Remarkably, this H₂ significantly rose to 351.12 mLH₂/L_{reactor}.h at the same solid concentration when the fruit mixture was externally inoculated with heat-treated anaerobic sludge.

The literature underscores the significance of several key parameters in H₂ production processes, with HRT, SLR, and the type of inoculum used to be identified as crucial factors influencing H₂ yield. While much of the research has predominantly focused on optimizing H₂ yield, it is essential to note that the environmental impact of the residue generated during the fermentation process deserves attention as well. Efforts in this field should not only prioritize maximizing H₂ yield but also consider the environmental implications of the fermentation by-products. Addressing the residue and its potential environmental impact aligns with broader sustainability goals and ensures a comprehensive understanding of the overall ecological footprint of H₂ production processes.

Furthermore, biochar is a carbonaceous compound available from various biomasses such as wood, sawdust, rice husk, etc. (Abdelaal et al. 2019), and is beneficial for both energy and agriculture practices. Biochar has a high cation exchange capacity (CEC), has a high zeta-potential, large surface area, and steady structure (Pradhan et al. 2020). Biochar application positively affects soil quality, soil water, and nutrient retention and plays a substantial role in enhancing plant growth (Lehmann and Joseph 2009). Biochar prevents nutrient loss by leaching and GHGs emissions (Pradhan et al. 2022). Also, biochar is alkaline in nature and has less electrical conductivity (EC) which is most beneficial to maintain the soil pH and salinity that could be beneficial for seeds germination and plant growth.

However, the H₂ production from starchy food waste such as potato peels and natural sugar fruit waste like watermelon rind and valorize the discarded residue to biochar lack of the study. Also, there is no comparative study reported on the H₂ product quantity of solitary potato peels, watermelon rind, and blended potato peels, watermelon rind. Therefore, this study attempts a preliminary investigation to produce H₂ gas from potato peels, watermelon rind, and a mixture of potato peels and watermelon rind by dark fermentation and the remaining residue to biochar. This study aims to analyze biochar properties that could be beneficial for agriculture practice.

MATERIALS AND METHODS

The solid-state dark fermentation (SSF) process has been employed for the production of H₂ gas using potato peel, watermelon rind, and a combination of both. The primary benefit of these approaches lies in their ability to minimize waste and liquid effluent, thereby posing minimal environmental impact. SSF utilizes uncomplicated natural solids as the medium, offering a low-technology solution with reduced energy requirements and a lower demand for capital investment. A detailed methodology of H₂ gas production from kitchen wastes and recycling of leftover residue to produce biochar is shown in Fig.1.

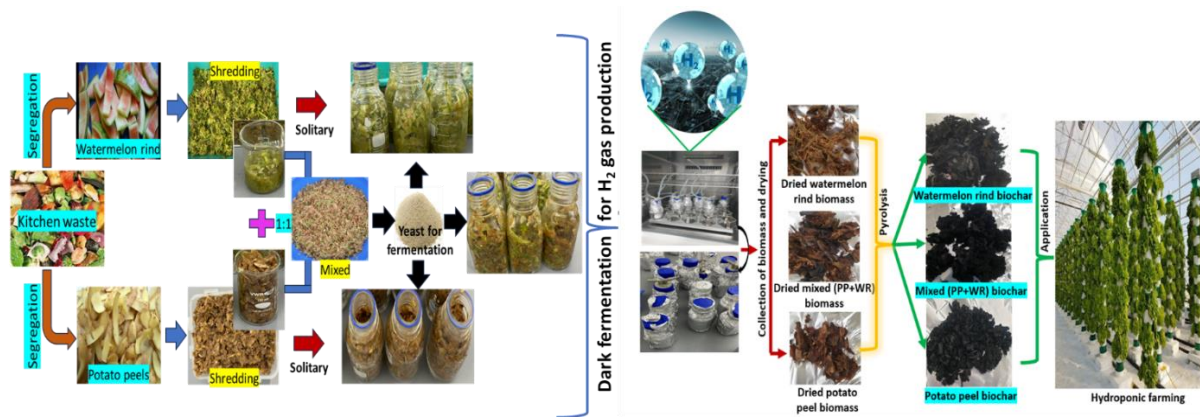


Figure 1 A detailed methodology for H₂ gas and biochar production

Collection of wastes and preparation of feedstock

Potato peels and watermelon rind were collected from the university canteen in Qatar Foundation to produce hydrogen gas by SSF. The peels were chopped into small pieces and prepared solitary and mixed feedstock by 1 to 1 ratio to produce H₂ gas. A list of samples is reported in Table 1.

Table 1 A detailed list of sample notation and sample type

Sample Notation	Sample type
(WR) _B	Watermelon rind blank
(PP) _B	Potato peels blank
(WR+PP) _B	A mixture of watermelon and potato peels blank
(WR) ₁₅	Watermelon rind in addition to 15 mL inoculum solution with a concentration of 500 mg/L
(PP) ₁₅	Potato peels in addition to 15 mL inoculum solution with a concentration of 500 mg/L
(WR+PP) ₁₅	A mixture of watermelon and potato peels in addition to 15 mL inoculum solution with a concentration of 500 mg/L
(WR) ₃₀	Watermelon rind in addition to 30 mL inoculum solution with a concentration of 500 mg/L
(PP) ₃₀	Potato peels in addition to 30 mL inoculum solution with a concentration of 500 mg/L
(WR+PP) ₃₀	A mixture of watermelon and potato peels in addition to 30 mL inoculum solution with a concentration of 500 mg/L

Before proceeding with the H₂ gas and biochar production the initial pH, EC, Total solid (TS), volatile solids (VS), and moisture content (MC) were measured by following different standard procedures (Turhal et al. 2019). Additionally, the pH and EC of the initial biomass of each condition before fermentation was measured.

H₂ gas production

After the preparation of feedstocks, 150 g of each (potato peels, watermelon rind and blended potato peel and watermelon rind) was poured inside the amber bottles (Fig. 1) with triplicates. Anaerobic sludge was employed as an inoculum and subjected to boiling for one hour to eliminate methanogenic bacteria. Then, 1 Liter of treated sludge was mixed with 0.5 g of baker's yeast (*Saccharomyces Cerevisiae*). Subsequently, 15 ml and 30 ml of the prepared inoculum were added to separate sets of triple bottles. No yeast was added to one set to serve as a blank for comparison of the yeast effect. Following inoculation, the samples underwent agitation at 100 rpm within a dark shaker, maintaining a temperature of 35°C for durations of 24, and 48 hours. The amount of H₂ gas produced in the bottle was measured by using a syringe after 24, and 48h. Thereafter, the leftover residue was placed in a Fisher Scientific Isotemp mechanical convection laboratory oven at 105 °C for 24 h for complete drying.

Biochar production

The dried biomass was used to produce biochar at 400 °C by pyrolyzing in the absence of oxygen using a muffle furnace (Lindberg Blue M-3504) at a supply of 0.5L/min N₂ gas (Pradhan et al., 2022). The biomass and biochar were grounded to finer particles to measure the pH, EC, and zeta (ζ) potential by following different standard procedures reported by Pradhan et al. (2022). After the production of biochar at each temperature, the yield was determined using the Eq (1) below:

$$\text{Yield of biochar} = \frac{\text{weight of biochar (g)}}{\text{weight of biomass (g)}} \times 100 \quad (1)$$

The pH, EC, and zeta potential of biomass after fermentation and biochar produced from biomass were determined using an Orion Star A121 pH meter, A329 Thermo Scientific conductivity meter, and Zetasizer Nano-ZS (Malvern) meter respectively. Samples were prepared by mixing media and water at a ratio of 1:10 in a shaker for 1 h at 150 rpm before measuring pH and EC (Dai et al. 2017; Pradhan et al. 2020). To standardize the pH levels, samples with lower pH values were adjusted to 5.5 using a KOH solution.

RESULTS AND DISCUSSION

Characteristics of wastes

The watermelon rind, potato peel, and their combination exhibit approximately 6.8 to 12% TS, 88 to 95% MC and 76 to 88% VS (Fig. 2a). Notably, the VS concentration in potato peels is higher than in watermelon, attributed to the elevated water content in watermelon. The initial pH values of the prepared samples ranged from 4.3 to 5.1, while the EC values were around 2 mS/cm (Fig. 2b).

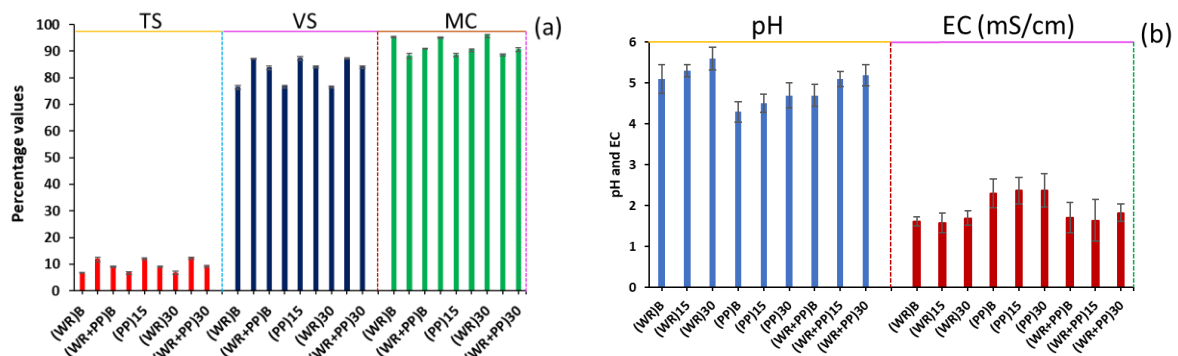


Fig. 2 Characterization of the prepared samples in terms of (a) TS, VS, and MS, (b) pH and EC values.

Quantification of H₂ gas production

Many studies reported the H₂ production rate remains stable beyond the 48-hour mark by the dark fermentation process (Turhal et al., 2019; Dao et al., 2023). Consequently, H₂ production yields were assessed at 24 and 48 hours, and the volumes of generated H₂ gas are illustrated in Figure 3a. Additionally, Figure 3b displays H₂ production rates relative to the amount of VS removal rate. Notably, the introduction of yeast to the inoculum does not confer any advantages to H₂ production. The calculated H₂ production rate stands at approximately 50 mL/g VS removed. It is noteworthy that due to the higher water and sugar content in watermelon, an H₂ production rate exceeding 50.5 mL/g VS removed is achieved. Contrarily, a greater volume of H₂ was obtained with potato peel; however, its production rate was observed to be lower compared to watermelon rind.

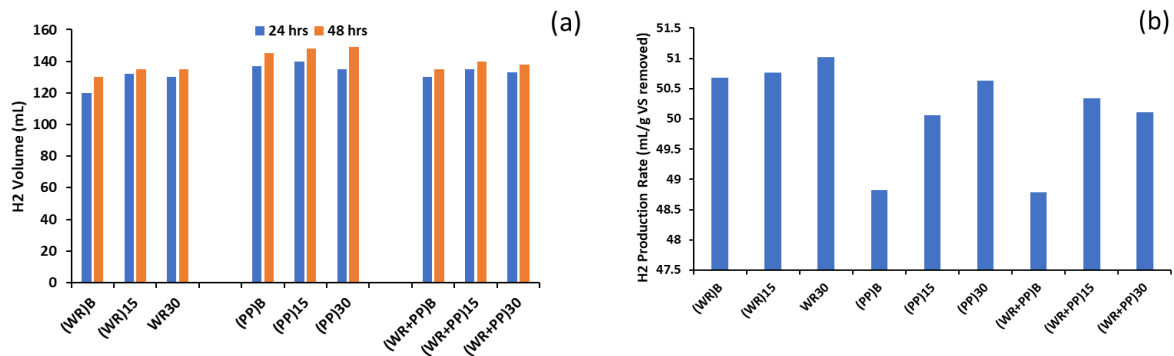


Figure 3 (a) the volume of H₂ gas production and (b) H₂ gas production rate

Yield of Biochar

After H₂ production at two-time intervals (24h and 48h) the leftover residue was used to produce biochar and the yield of biochar was measured. The yield of biochar for different feedstocks is shown in Fig. 4a. The yield of biochar produced from watermelon rind (WR) was found lesser than the potato peel (PP) and mixed (WR+PP) samples. It was observed a slightly reduction in PP biochar yield at 48h in comparison to 24h. However, in the case of watermelon rind and mixed biochar, the yield is almost identical.

pH, EC and zeta-potential

In each type of feedstock biomass, the pH was found <5 after 24h of samples, while a slight reduction in pH was noticed after 48h (Fig. 2b). Compared to WR and WR+PP biomass, the PP showed lower pH values. It demonstrated more acidic compounds formation which reflects the highest volume of H₂ gas production. After biochar production from 24h and 48h feedstocks, the samples are alkaline in nature with pH of more than 7.5 in each feedstock type. Not much significant variation was noticed in the pH of biochar produced at 24h and 48h time span.

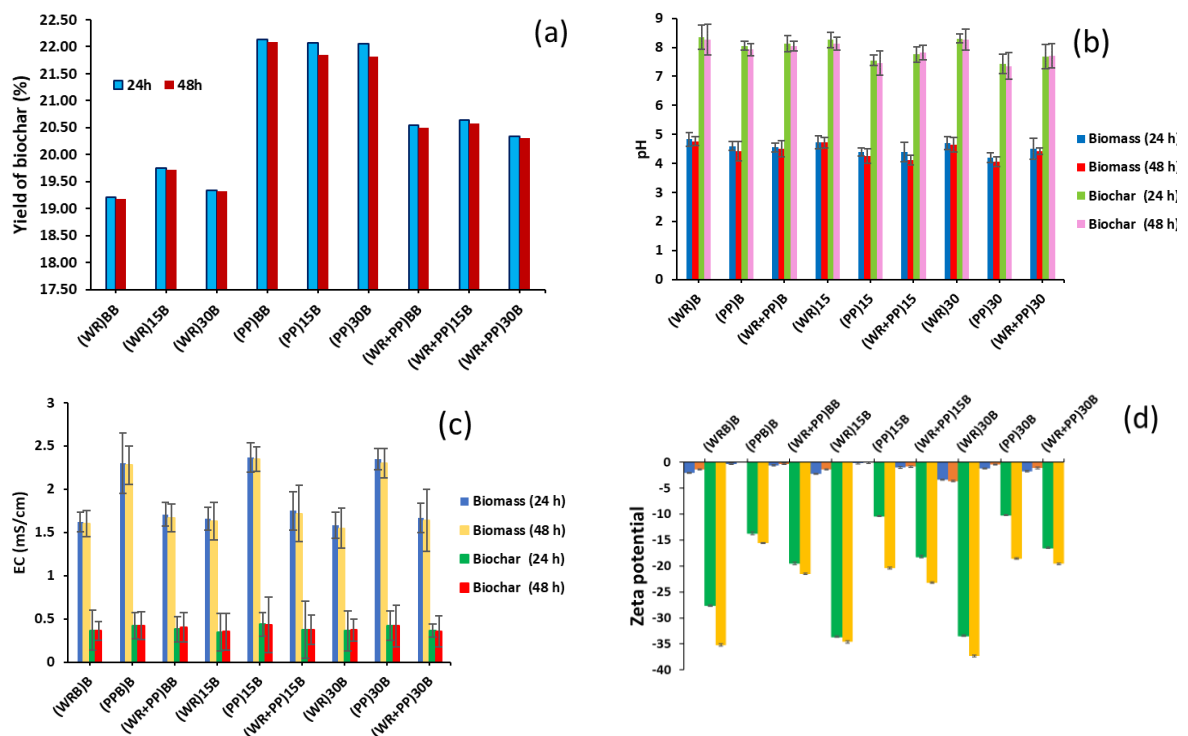


Figure 4 (a)The yield of biochar, (b) pH, (c) conductivity (EC) and (d) ζ-potential of biochar.

It was noticed the application of inoculum solution does not affect the EC of feedstock, therefore in each feedstock type the blank and fermented samples with inoculum solution showed equal EC (Fig. 4c). It

was observed the PP has the highest EC values and all other feedstock biomass has EC more than 1.5 mS/cm. However, a tremendous reduction in EC was noticed in biochar for each feedstock type and was found less than 0.5 mS/cm. A large variation was also noticed for ζ -potential in biochar and biomass (Fig.2d). In each feedstock biomass type the zeta-potential tends to be less *electronegativity strength*, while after biochar production the zeta-potential increased and tends to be more *electronegativity strength* (>-15 mV), which could be beneficial for water and nutrients uptake after amending biochar with soil. Additionally, it will be beneficial for agriculture (especially hydroponic) production with a good yield of crop and plant biomass.

CONCLUSION

This study is a preliminary laboratory-scale investigation on H₂ gas and biochar production from two kitchen wastes which contain a large amount of starch, sugar, and cellulose. A study by Turhal et al. (2019) reported a maximum volume of H₂ gas was produced by dark fermentation. Therefore, by following the research study we produced 150 mL H₂ gas from PP and less in WR. The biochar production from the residue at 400 °C by the pyrolysis process was found to have the most beneficial properties that could be a benefit as a sustainable amendment for soil-based agriculture and hydroponic agriculture. This study emphasizes the future scope to carry the dark fermentation process for the long term to observe the H₂ gas production, the analysis of the concentration of the H₂ gas, and the plant growth after applying biochar.

References

- Abdelaal AH, McKay G, Mackey HR (2019) Food waste from a university campus in the Middle East: Drivers, composition, and resource recovery potential. *Waste Manag* 98:14–20. <https://doi.org/10.1016/j.wasman.2019.08.007>
- Bellary AN, Indiramma AR, Prakash M, Baskaran R, Rastogi NK (2016) Anthocyanin infused watermelon rind and its stability during storage. *Innovative Food Science & Emerging Technologies* 33:554–562. <https://doi.org/10.1016/j.ifset.2015.10.010>
- Cao, J., Xu, C., Zhou, R., Duan, G., Lin, A., Yang, X., You, S., Zhou, Y. and Yang, G. (2022) Potato peel waste for fermentative biohydrogen production using different pretreated culture. *Bioresource Technology*, 362, p.127866.
- Dai Z, Zhang X, Tang C, Muhammad N, Wu J, Brookes PC, Xu J (2017) Potential role of biochars in decreasing soil acidification - A critical review. *Sci Total Environ* 581–582:601–611. <https://doi.org/10.1016/j.scitotenv.2016.12.169>.
- Dao, S., Turanbaev, M., Argun, H. (2023) Dark fermentative hydrogen gas production from waste peach pulp by intermittent feeding: Effects of hydraulic residence time and substrate loading rate. *International Journal of Hydrogen Energy*.
- Fatima A, Basak B, Ganguly A, Chatterjee PK, Dey A (2020) Biohydrogen Production Through Dark Fermentation of Food Wastes by Anaerobic Digester Sludge Mixed Microbial Consortium. In: Kalamdhad AS (ed) *Recent Developments in Waste Management*. Springer, Singapore, pp 57–70
- Foong SY, Chan YH, Cheah WY, Kamaludin NH, Tengku Ibrahim TNB, Sonne C, Peng W, Show P-L, Lam SS (2021) Progress in waste valorization using advanced pyrolysis techniques for hydrogen and gaseous fuel production. *Bioresour Technol* 320:124299. <https://doi.org/10.1016/j.biortech.2020.124299>
- Giroto F, Alibardi L, Cossu R (2015) Food waste generation and industrial uses: a review. *Waste management* 45:32–41
- Khanal S, Karimi K, Majumdar S, Kumar V, Verma R, Bhatia SK, Kuca K, Esteban J, Kumar D (2023) Sustainable utilization and valorization of potato waste: state of the art, challenges, and perspectives. *Biomass Conv Bioref*. <https://doi.org/10.1007/s13399-023-04521-1>
- Lehmann J, Joseph S (eds) (2009) *Biochar for environmental management: science and technology*. Earthscan, London ; Sterling, VA
- Mamiru D, Gonfa G (2023) Extraction and characterization of pectin from watermelon rind using acetic acid. *Heliyon* 9:e13525. <https://doi.org/10.1016/j.heliyon.2023.e13525>
- Petkowicz CLO, Vriesmann LC, Williams PA (2017) Pectins from food waste: Extraction, characterization and properties of watermelon rind pectin. *Food Hydrocolloids* 65:57–67. <https://doi.org/10.1016/j.foodhyd.2016.10.040>



- Pradhan S, Abdelaal AH, Mroue K, Al-Ansari T, Mackey HR, McKay G (2020) Biochar from vegetable wastes: agro-environmental characterization. *Biochar* 2:439–453. <https://doi.org/10.1007/s42773-020-00069-9>
- Pradhan S, Mackey HR, Al-Ansari TA, McKay G (2022) Biochar from food waste: a sustainable amendment to reduce water stress and improve the growth of chickpea plants. *Biomass Conv Bioref* 12:4549–4562. <https://doi.org/10.1007/s13399-022-02575-1>
- Seberini A (2020) Economic, social and environmental world impacts of food waste on society and Zero waste as a global approach to their elimination. *SHS Web Conf* 74:03010. <https://doi.org/10.1051/shsconf/20207403010>
- Srivastava N, Srivastava M, Abd_Allah EF, Singh R, Hashem A, Gupta VK (2021) Biohydrogen production using kitchen waste as the potential substrate: A sustainable approach. *Chemosphere* 271:129537. <https://doi.org/10.1016/j.chemosphere.2021.129537>
- Turhal S, Turanbaev M, Argun H (2019) Hydrogen production from melon and watermelon mixture by dark fermentation. *International Journal of Hydrogen Energy* 44:18811–18817. <https://doi.org/10.1016/j.ijhydene.2018.10.011>

ICH2P14-OP171

Ni-Cu BIMETALLIC CATALYSTS FOR EFFECTIVE SYNGAS PRODUCTION VIA LOW-TEMPERATURE METHANE STEAM REFORMING

¹Martin Khzouz, ²Babak Fakhim, ¹Saleh Babaa, ³Mohammad Ghaleeh, ⁴Farooq Sher, ⁵Evangelos I. Gkanas

¹Department of Systems Engineering, Military Technological College, Al Matar Street, Muscat, 111, Oman

²School of Aerospace, Mechanical and Mechatronic Engineering, The University of Sydney, NSW 2006, Australia

³Department of Engineering, University of Northampton, Northampton NN1 5PH, UK

⁴Department of Engineering, School of Science and Technology, Nottingham Trent University, Nottingham NG11 8NS, UK

⁵Hydrogen for Mobility Lab, Centre for Advanced Low Carbon Propulsion Systems (C-ALPS), UK, Coventry University

*Corresponding author e-mail: marcin.khzouz@gmail.com, marcin.khzouz@mtc.edu.om

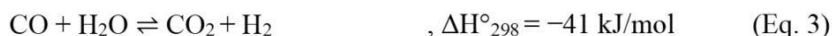
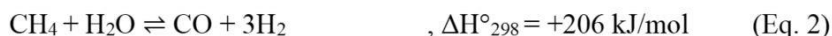
ABSTRACT

In the present work, novel bi-metallic catalysts for syngas production at low temperature steam reforming are developed, characterised and tested. Steam methane reforming by using bi-metallic Ni-Cu catalysts found to balance the product of CO to CO₂ ratios, while affected the water gas shift reaction by increasing the hydrogen selectivity up to 600 °C. The addition of different amounts of Cu (3, 5, 7, 10 wt%) to the Ni catalyst for methane steam reforming showed different reactivity trends. One of the major outcomes of this work is the maximum load capacity of Cu (5wt.%Cu) to maintain the reactivity. For comparison purposes, mono-metallic catalysts of Cu and Ni were developed and tested along with the bi-metallic ones. The activity of the reaction decreased by doping more than 5wt.%Cu which affected the amount of hydrogen produced. This is related to the possible limited number of available sites required for hydrogen adsorption to maintain the reaction of methane steam reforming. Another important outcome of this work is the bi-metallic Ni-Cu catalysts did not decrease the amount of carbon formation.

Keywords: Bimetallic catalysts, steam methane reforming, Heterogeneous catalysts, syngas generation, Bimetallic Ni-Cu/Al₂O₃ catalyst.

INTRODUCTION

Steam-Methane Reforming(SMR) is considered to be the most financially viable technology for syngas production [1]. Methane (CH₄) can be converted to syngas at elevated temperatures, normally above 800 °C [2-4]. However, for the technology of Solid Oxide Fuel Cells (SOFCs), SMR at operating temperatures between 500-700oC is highly desirable, as the generated heat from the SOFCs can be utilised to increase the overall system efficiency [5, 6]. The coupling of Methane steam reformers with SOFCs is already being used via combined heat and power (CHP) systems in residential stationary applications [7]. Residential CHPs use the established methane grid infrastructure, which facilitates the roll out of the Fuel Cell technology [7, 8]. Over 120,000 CHP units have been sold and installed for domestic use in Japan by 2017 [9]. The fuels suitable to operate SOFCs come from a variety and mixture of gases including; H₂, CO and CH₄. The direct use of CH₄, results in the formation of coke at the anode and therefore negatively contributes towards the lifetime of the SOFCs. Therefore, external reforming at comparable temperatures to the operational SOFC temperatures in order to produce syngas has attracted attention for its benefit on SOFCs lifetime with negligible efficiency cost [10, 11]. The overall chemical reaction for methane steam reforming is described in Eq. 1. The reaction from Eq.1 is the result of the combination of the two reactions introduced in Eq. 2 (endothermic SMR) and Eq. 3 (exothermic water gas shift (WGS) reaction).



The aim of the current work is to examine the stability effect when introducing Cu promoters in Ni-based catalysts at low metal loadings (less than 10 wt.%) for methane steam reforming purposes. The work further adds in the understanding of the effect of the Cu addition in terms of mitigation of Ni aggregation and the stability of the catalyst structure. In addition, the reduction of carbon formation during the reaction due to the doping is investigated. For that reason, an experimental approach in the synthesis, characterisation and testing of the Ni-based bimetallic catalysts for methane steam reforming applications is presented. Several loadings of metallic Cu (3, 5, 7, 10 wt%) are introduced and the effects of the methane conversion, water conversion, hydrogen production and carbon production are discussed. The catalysts are characterised after the methane steam reforming reaction by means of XRD, SEM-EDX, TGA and BET analysis. Finally, a carbon formation analysis is introduced, presented and analysed.

MATERIALS AND METHODS

CATALYST PREPARATION

The catalyst was prepared via an impregnation method. The raw materials (Nickel(II) nitrate hexahydrate - $\text{Ni}(\text{NO}_3)_2 \cdot 6\text{H}_2\text{O}$ and Copper(II) nitrate trihydrate - $\text{Cu}(\text{NO}_3)_2 \cdot 3\text{H}_2\text{O}$) were purchased from Alfa Aesar. For the preparation of the mono-metallic catalysts, $\text{Ni}(\text{NO}_3)_2 \cdot 6\text{H}_2\text{O}$ and $\text{Cu}(\text{NO}_3)_2 \cdot 3\text{H}_2\text{O}$ were dissolved in ethanol along with magnetic stirring for 30min. For the case of the bi-metallic catalysts, an additional of 30 min of stirring after the $\text{Ni}(\text{NO}_3)_2 \cdot 6\text{H}_2\text{O}$ was discharged to the $\text{Cu}(\text{NO}_3)_2 \cdot 3\text{H}_2\text{O}$ solution took place. Finally, trilobe Al_2O_3 catalyst carriers (6g) purchased by Johnson Matthey added to the nitrate metal solution and mixed for 120 minutes using ultrasonic mixer at room temperature. Then, the metal supported catalyst left to dry at 100°C for 8 hours. Finally, the catalyst was calcined at 500°C (5°C/min) for 5 hours.

CATALYTIC ACTIVITY MEASUREMENTS

The catalytic reaction took place in the experimental apparatus shown in Fig.1. The prepared catalysts (quantity of 3g) of the prepared catalyst packed in the middle of the reactor furnace (50 mm bed height). The reactor (395 mm length) was made from 316L stainless steel with diameter of 10.9 mm and wall thickness 0.89 mm. Methane (99.99% purity) was supplied to the reactor tube using Brooks mass flowmeter at flow rate of 25 ml/ min. The reaction was carried out between 500-700°C. The steam was injected at a molar ratio of 3:1, generated from water passing through the pipe wrapped with trace heater (OMEGA). A pump (Cole Palmer) controlled the flowrate of water. When the operation stabilised, gas samples were withdrawn for analysis using Refinery Gas Analyser (Agilent 7890A) every 15 minutes for a total duration of four hours. The entire piping system was purged with N_2 before commencing the reaction. Then, hydrogen injected at a flow rate of 10 ml/min for catalyst reduction purposes. As reported previously, the assigned reduction temperature measured by temperature programmed reduction was (650°C for 10% Ni, 250°C for 10% Cu, 350°C for 7% Cu - 3% Ni, 380°C for 5% Cu - 5% Ni, 425°C for 7% Ni - 3% Cu) [12]. The reduction was performed by increasing the temperature to the target value by 5°C/min and maintain the target temperature for 30 minutes. After that, the system was purged again with N_2 .



Fig 1. Experimental apparatus used for catalytic reaction activity test

RESULTS AND DISCUSSIONS

THE EFFECT OF Cu CONTENT ON THE Ni-BASED CATALYTIC REACTIVITY

syngas production were tested at several reaction temperatures. The methane fuel conversion when utilising both the Ni mono-metallic and the Ni-Cu bimetallic catalysts is presented in Fig 2. The bi-metallic catalysts revealed lower conversion at 500-550°C comparing to the Ni mono-metallic catalyst. SMR is an endothermic reaction and thus, it is activated while the temperature is increased. The catalytic reactivity of Ni-based mono-metallic catalysts is enhanced at the temperature range of 500-550°C. The catalytic reactivity at 600°C showed that a small loading with Cu (3%) could lead on a higher conversion rate than the mono-metallic Ni catalyst. The small amount of Cu could enhance the WGS reaction by consuming CO, while extra CO is generated from the steam methane reaction. Increasing the Cu content up to 5% and 7%, resulted in lower methane fuel conversion compared to the mono-metallic Ni catalyst. This behaviour is related to the reduction of the active metal site for the methane steam reforming reaction. The lower methane conversion for 5% Ni - 5% Cu and 3% Ni - 7% Cu catalysts in comparison to the 7% Ni - 3% Cu at 600°C is attributed to the fact that the conversion takes place on the Ni surface and, as seen in Fig. 3, the water consumption was higher for the case of 7% Ni - 3% Cu. For the case of the mono-metallic 10% Cu catalysts, the levels of methane conversion were very low, as presented in Table 1. According to those outcomes, Cu is responsible only for WGS after the SMR takes place. For higher temperatures (650-700°C), it can be observed from Fig. 3 that the water conversion had decreased or remained at similar levels, indicating that the steam is no longer the main contributor for the catalytic methane reaction. This behaviour appears because at elevated operating temperatures, the methane decomposition reaction and the reverse WGS reaction are dominating.

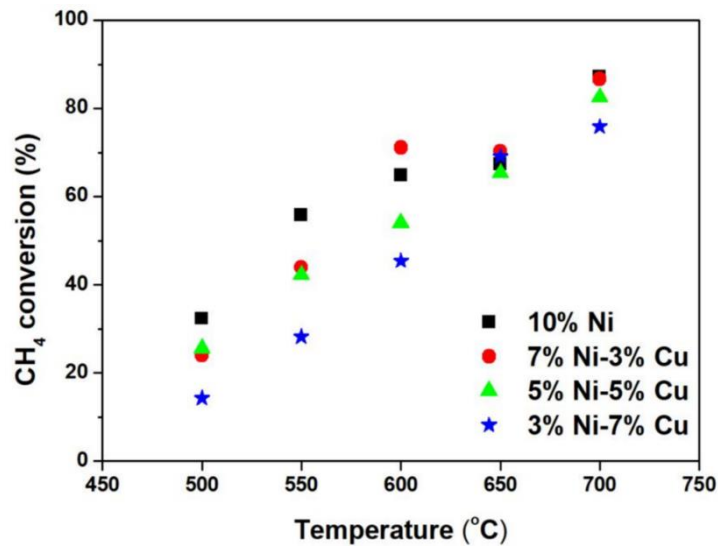


Fig. 2. CH₄ conversion for the mono-metallic and the bi-metallic catalysts at various temperatures between 500-700 °C.

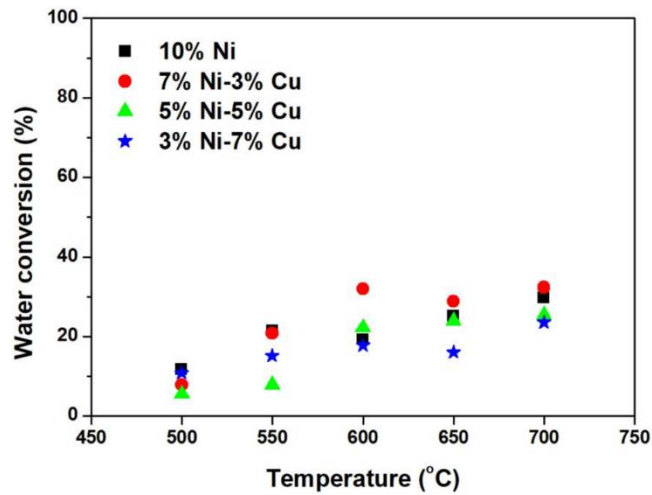


Fig. 3. H₂O conversion for the mono-metallic and the bi-metallic catalysts at various temperatures between 500-700 °C.

Table 1. Activity of catalytic methane reaction for physically mixed monometallic 10% Cu and 10% Ni catalysts

	10%Cu	10%Ni, 10%Cu*	10%Ni, 10%Cu*	10%Ni, 10%Cu*
Temperature (°C)	700	700	600	500
S/C	3	3	3	3
CH ₄ conversion (%)	9.7	87.0	55.8	28.6
Water conversion (%)	0.00	15.1	14.8	10.1
H ₂ yield	0.08	2.19	1.56	0.87
CO ₂ yield	0.01	0.23	0.24	0.17
CO yield	0.00	0.56	0.23	0.04

*Physical mixture of single metal (1.5 g of 10%Cu and 1.5 g of 10%Ni).

HYDROGEN YIELD

The hydrogen yield at the temperature range 500-700°C is presented in Fig 4. As extracted from Fig. 4, a common denominator for all the cases is an increase in the hydrogen yield with the increase of the reaction temperature. At the temperature range of 500-550°C, the mono-metallic Ni catalyst showed the highest hydrogen yield as compared to the performance of the bi-metallic catalysts. The large Ni content enhances the activation of C - H bonds for the SMR. At 600°C and for 7% Ni - 3% Cu, the hydrogen yield was 2.4 mol/mol- CH₄ and achieved the maximum value comparing to the other catalysts. This is mainly related to the WGS reaction. Hydrogen can be produced from both steam methane reforming over Ni and WGS reaction over active Cu. The catalyst becomes less selective to hydrogen at 500-600°C when more than 5 wt.% Cu is added to the catalyst. Thus, the low Ni content could reduce the fuel conversion and therefore the amount of H₂ produced. In addition, it was observed that the bimetallic catalyst has negligible effect on H₂ generated at 650-700°C, as the decomposition reaction is active at higher temperatures.

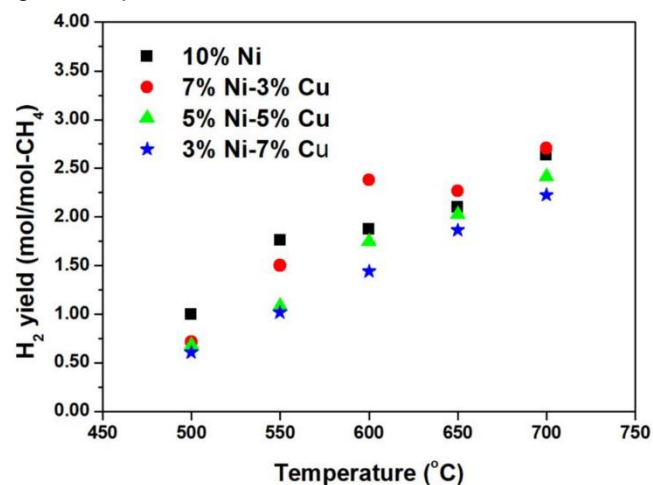


Fig. 4. Hydrogen yield for the mono-metallic and the bi-metallic catalysts at various temperatures between 500-700 °C

CARBON DIOXIDE AND CARBON MONOXIDE YIELDS

The CO₂ yield for the mono-metallic and the bi-metallic catalysts at various temperatures between 500 – 700 °C is presented in Fig. 5. The produced CO₂ is increasing for all the catalysts until 600°C, where the maximum CO₂ yield is achieved. After that point, when the reaction temperature reaches higher values (650-700°C) the CO₂ yield is decreasing. This is related to the nature of WGS reaction, which is less favourable under higher temperatures. The CO yield for the mono-metallic and the bi-metallic catalysts at various temperatures between 500 – 700 °C is presented in Fig. 6. For all the studied catalysts, as the temperature increases, the CO yield also increases. In that case, CO is generated from both the SMR and the reverse WGS reaction. The CO yield at 500 °C is very low for all the catalysts, as under these conditions, the WGS is the favourable reaction. The effect of Cu addition in the bi-metallic catalysts showed that the CO can produced by both the WGS reaction and SMR reaction . For the case of 700°C, the Cu catalytic addition at high temperature encourages strongly the reverse WGS reaction, and as a result, a higher amount of CO is generated from the activated decomposition reaction.

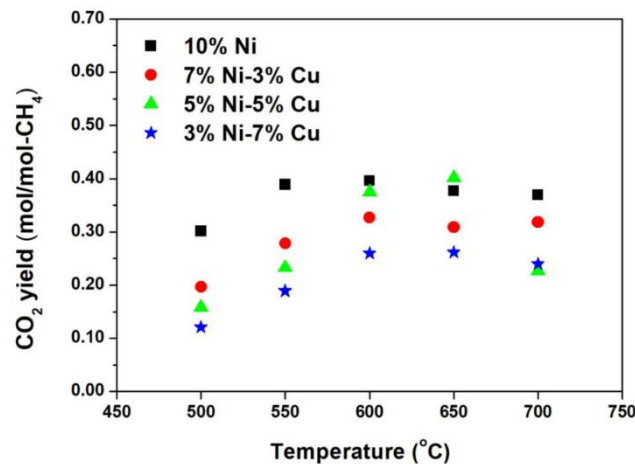


Fig. 5. CO₂ yield for the mono-metallic and the bi-metallic catalysts at various temperatures between 500-700°C

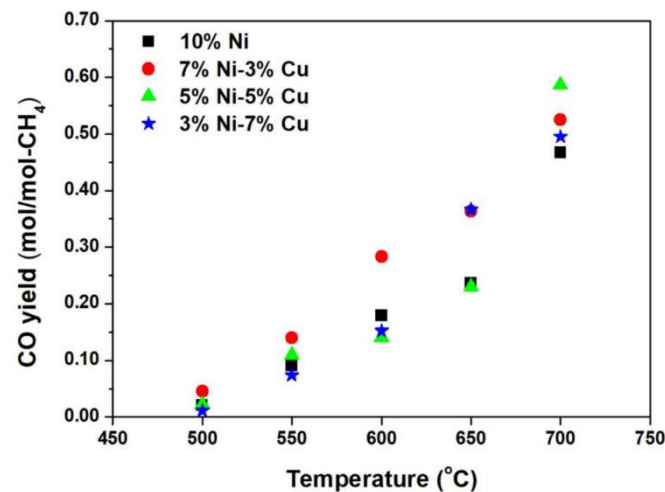


Fig. 6. CO yield for the mono-metallic and the bi-metallic catalysts at various temperatures between 500-700°C

CONCLUSIONS

In this work, various bi-metallic catalysts based on Ni and Cu were developed, characterised and tested under various temperatures in the range of 500-700°C. For comparison purposes, mono-metallic catalysts of Ni and Cu were prepared and tested. All the catalysts were tested regarding their behaviour for methane steam reforming reaction. The loadings considered for the bi-metallic catalysts were 10, 7, 5, and 3%wt. The maximum conversion value (87%) was obtained at the maximum temperature of 700°C for the case of the mono-metallic catalyst (10%Ni). The results showed an increasing amount of CO produced when the reaction temperature was increased due to the reverse WGS and methane decomposition. The bimetallic catalysts improved the catalyst selectivity for WGS reaction at the lower temperatures between 500 – 600 °C. The bi-metallic catalyst with the small amount of Cu (3wt.%) showed good conversion of fuel at 600°C, where the catalyst revealed 71.1% methane conversion and 2.4 mol hydrogen were produced. The prepared bi-metallic catalysts did not find to decrease the carbon formation. The 10%Ni catalyst prepared on this study showed good stability regarding carbon formation compared to the prepared bimetallic Ni-Cu catalysts.

REFERENCES

- Schröders S, Verfondern K, Allelein H-J. Energy economic evaluation of solar and nuclear driven steam methane reforming processes. *Nuclear Engineering and Design*. 2018;329:234-46.
- F. Brown L. A comparative study of fuels for on-board hydrogen production for fuel-cell-powered automobiles. *International Journal of Hydrogen Energy*. 2001;26:381-97.



- Navarro RM, Peña MA, Fierro JLG. Hydrogen production reactions from carbon feedstocks: Fossil fuels and biomass. *Chemical Reviews*. 2007;107:3952-91.
- Steinberg M. Production of hydrogen and methanol from natural gas with reduced CO₂ emission. *International Journal of Hydrogen Energy*. 1998;23:419-25.
- Roh H-S, Jun K-W. Low temperature methane steam reforming for hydrogen production for fuel cells. *Bull Korean Chem Soc*. 2009;30:153.
- Khzouz M, Gkanas E. Experimental and Numerical Study of Low Temperature Methane Steam Reforming for Hydrogen Production. *Catalysts*. 2017;8:5.
- Hou Q, Zhao H, Yang X. Thermodynamic performance study of the integrated MR-SOFC-CCHP system. *Energy*. 2018;150:434-50.
- Irving PM, Pickles JS. Operational requirements for a multi-fuel processor that generates hydrogen from Bio- and petroleum-based fuels for both SOFC and PEM fuel cells. *ECS Transactions*. 2007;5:665-71.
- Ramadhani F, Hussain MA, Mokhlis H, Hajimolana S. Optimization strategies for Solid Oxide Fuel Cell (SOFC) application: A literature survey. *Renewable and Sustainable Energy Reviews*. 2017;76:460-84.
- Zhang X, Chan SH, Li G, Ho HK, Li J, Feng Z. A review of integration strategies for solid oxide fuel cells. *Journal of Power Sources*. 2010;195:685-702.
- Huang Y-L, Hussain AM, Wachsman ED. Nanoscale Cathode Modification for High Performance and Stable Low-Temperature Solid Oxide Fuel Cells (SOFCs). *Nano Energy*.
- Khzouz M, Gkanas EI, Du S, Wood J. Catalytic performance of Ni-Cu/Al₂O₃ for effective syngas production by methanol steam reforming. *Fuel*. 2018;232:672-83.

ICH2P14-OP177

SHADES OF SUSTAINABILITY: AN IN-DEPTH ANALYSIS OF THE DIRECT AND INDIRECT CARBON FOOTPRINT IN BLUE AMMONIA MANUFACTURING

¹Hussein Al-Yafei, ²Ahmed AlNouss, ¹Saleh Aseel

¹Chemical Engineering Department, College of Engineering and Technology, University of Doha for Science and Technology, Doha, Qatar

²College of Science and Engineering, Hamad Bin Khalifa University, Qatar Foundation, Doha, Qatar

*Corresponding author e-mail: hussain.alyafay@udst.edu.qa

ABSTRACT

Integrating sustainability principles into the distribution network process poses a significant challenge for industries aiming to prosper in today's dynamic environment. This challenge is particularly pronounced in the fertilizer industry, given the crucial role of gas as a primary fuel source. Despite extensive research on the environmental implications of such endeavors, there exists a noticeable gap in the literature pertaining to the life cycle assessment (LCA) of Blue Ammonia production and its associated processing units for environmental evaluation. This study addresses this gap by conducting the inaugural LCA of Blue Ammonia production, offering a comprehensive evaluation from the raw material processing stage to the final product. The analysis focuses on direct and indirect greenhouse gas emissions, including carbon dioxide, methane, and nitrous oxides. Notably, our life cycle model incorporates the Aspen HYSYS simulation, which is recognized for its precision in engineering and design contexts. The simulation highlights that a notable 98.9% of GHG emissions in Blue Ammonia stem from carbon dioxide, mainly originating from the Ammonia Converter Unit. The methane and nitrous oxide contribute 0.74% and 0.34%, respectively. More direct GHG emissions were found through the Blue Ammonia process chain than indirect GHG emissions. We propose an integrated framework model based on the insights derived from this study. This model establishes the foundation for a spectrum of sustainability strategies and policy recommendations aligned with broader business sustainability objectives.

Keywords: Life cycle assessment, Blue Ammonia, Carbon footprint, Sustainability, Environmental.

INTRODUCTION

Background

Presently, the production of ammonia on a commercial scale is characterized by high energy consumption and the generation of elevated pollutant levels [1]. The synthesis of ammonia from dinitrogen and dihydrogen is an exothermic process, necessitating low temperatures and high pressures for optimal yield, typically ranging between 400-500°C and 150-300 bar [2]. Nitrogen, sourced from the atmosphere, undergoes separation through cryogenic processes, demanding a substantial amount of energy [3]. Meanwhile, hydrogen is predominantly derived from carbon-based fuel combustion (such as natural gas, coal, and petroleum), resulting in the emission of significant amounts of greenhouse gases [4, 5].

Ammonia holds a crucial role in agriculture as a fertilizer and exhibits potential as an energy carrier, prompting endeavors to develop production methods that are both efficient and environmentally friendly. Furthermore, ammonia is under exploration for long-term energy storage, aiming to facilitate increased integration and utilization of intermittent renewable energy sources like wind and solar power [6]. The versatility of ammonia positions it to play a pivotal role in a future energy landscape characterized by a higher prevalence of renewables. Its ability to balance temporal discrepancies between energy supply and demand in different regions underscores its importance.

Considering the emerging applications of ammonia, there is a potential for a significant increase in global production, potentially reaching orders of magnitude higher than current levels [7]. In the long run, ammonia and other products like biodiesel and hydrogen will inevitably become mainstream alternative fuels for ships [8].

Greenhouse Gas Emissions and Impacts

The production of ammonia constitutes around 2% of global fossil energy consumption, resulting in an annual release of over 420 million tons of CO₂, contributing to approximately 1.2% of the total anthropogenic CO₂ emissions [9, 10]. Addressing the need for decarbonization in the ammonia sector has led to a growing interest in alternative production pathways utilizing renewable resources and industrial by-products.

The entire supply chain of Blue Ammonia relies on distribution networks that connect demand and supply fields. Current efforts by Blue Ammonia manufacturers are directed towards implementing more advanced logistics processes to align with environmentally sustainable practices. The transformation of raw materials through various stages of the Blue Ammonia production chain involves the utilization of a significant amount of fuel, primarily sourced from the feedstock. The combustion of this fuel results in the substantial generation of CO₂, CH₄, and N₂O. As long as Blue Ammonia production persists, the anticipation of greenhouse gas emissions being released into the atmosphere remains a valid concern.

Problem statement, research objective, and research structure

The concept of sustainable development is typically implemented at the policy level, but its extension to the business context is crucial. In response to an increasing demand for sustainably manufactured products driven by environmentally conscious consumers, the fertilizer industrial sector has incorporated sustainability into its growth strategy. The focus is on environmental preservation, particularly in mitigating greenhouse gas emissions, leading to the establishment of a Tank-to-Tank LCA research framework. Among environmental assessment methods, the LCA model stands out as the most comprehensive and illuminating [11].

This research is dedicated to examining and identifying the environmental impact of Blue Ammonia within its value chain. The proposed model, once developed, could serve as the cornerstone for the primary life cycle sustainability assessment for Blue Ammonia businesses.

The structure of this research comprises five sections. Section 1 introduces the background of Blue Ammonia and outlines its environmental impacts. Section 2 offers a comprehensive literature review on both LCA and the Blue Ammonia process chain. Section 3 details the methodology employed in creating the LCA model for Blue Ammonia. Section 4 provides the results and discussions arising from the research outcomes. Finally, Section 5 presents the concluding remarks of the study.

LITERATURE REVIEW

Environmental Life Cycle Assessment

This literature review offers a comprehensive summary of significant studies and insights concerning the environmental LCA of Ammonia production, providing a deeper understanding of sustainability challenges within the industry. The LCA method seeks to evaluate the environmental impact of the product, encompassing aspects such as pollution, resource consumption, and both direct and indirect impacts [11].

The synthesis of ammonia is characterized by high energy intensity, leading to substantial greenhouse gas emissions. A pivotal study by Ghavam, Vahdati [12] underscored the necessity of employing LCA to assess the sustainability of ammonia production. Their research emphasized the critical importance of considering the entire life cycle of ammonia production, spanning from raw material extraction to end-of-life disposal. Furthermore, they explored innovative membrane technologies as potential means to mitigate the environmental footprint associated with ammonia synthesis.

Given the heavy reliance of ammonia production on hydrogen, primarily sourced from carbon-based fuels, the carbon emissions linked to hydrogen production pose a significant environmental concern. Strategies to address these emissions were discussed by Smith, Hill [10], who explored avenues such as carbon capture and utilization (CCU) and renewable hydrogen sources as potential pathways for emission reduction.

In the pursuit of enhancing the sustainability of ammonia production, researchers are investigating waste-based and renewable feedstocks. Ghavam, Taylor [13] introduced a waste-based sustainable ammonia production process that focuses on utilizing waste-derived materials, presenting a promising alternative to reduce greenhouse gas emissions.

Blue Ammonia Process Chain

Figure 1 depicts a flow block diagram illustrating the Blue Ammonia process chain. The units in the diagram are categorized into distinct components, namely the natural gas raw material upstream facility, Stages of Steam Reforming Unit, Auto Thermal Reforming Unit, Water Removal Unit, CO₂ Removal Unit, Ammonia Converter Unit, and the concluding Ammonia Storage Unit. Throughout all these sections, the operation necessitates the use of associated utilities and electrical power [14]. Table 1 summarizes the properties and conditions of the main feedstock, natural gas (NG), and ammonia product {Ullmann, 2011 #517}.

Table 1. Ammonia plant feedstock and product's properties and conditions

NG Feedstock		Ammonia Product	
Flow	1.1 MTPA	Flow	1.2 MTPA
Temperature	30 °C	Temperature	-5 °C
Pressure	2.1 bar	Pressure	5 bar
Components (mol%): Methane (92.00), Ethane (3.00), and N ₂ (5.00)		Components (mol%): Ammonia (100)	

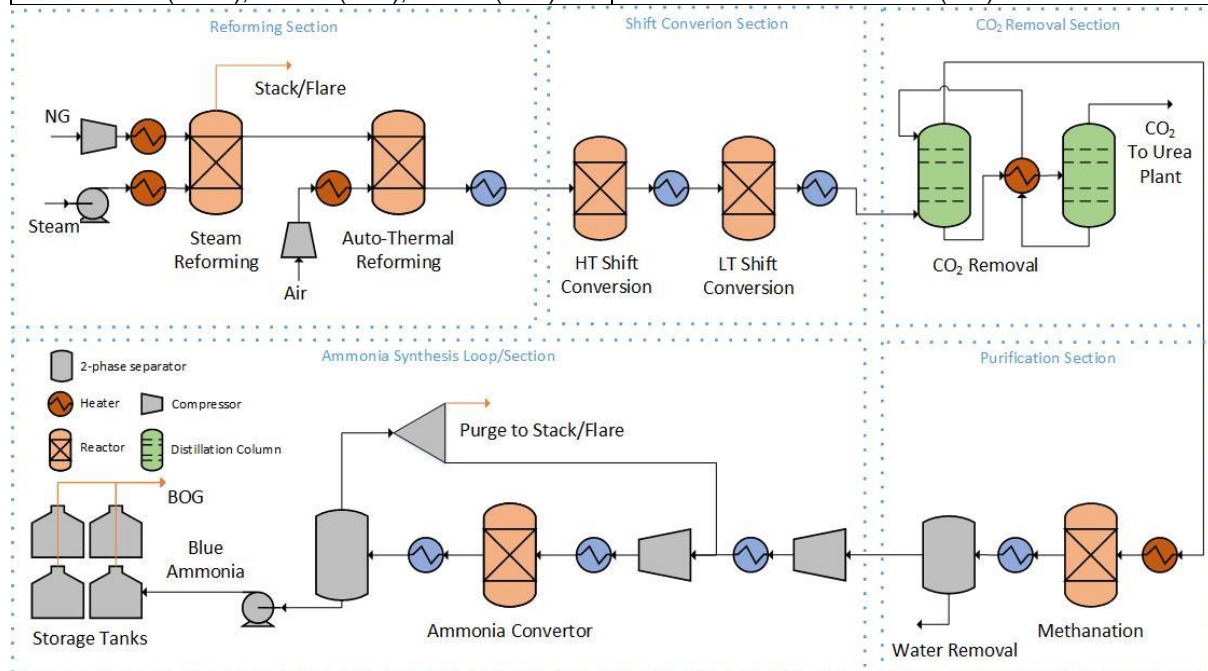


Fig. 1. Block flow diagram of Blue Ammonia Plant

The ammonia process operates at an overall of 19% N₂ conversion and 1/3 N₂ to H₂ ratio, a 7% purging of unreacted recycle N₂ and H₂ stream, and an ammonia separation of 75%. The syngas stream produced from steam and auto-thermal reforming is first directed to a water gas shift reactors to adjust the CO₂ and H₂ content. In addition, air stream is adjusted to ensure the 1:3 desired nitrogen to H₂ ratio. The adjusted syngas passes through a methanol-based acid gas removal unit and a two-phase separator to purify it from CO₂ water. In addition, it undergoes methanation reaction to convert remaining CO into methane and eliminate poisoning the ammonia convertor catalyst. The H₂ and nitrogen presented in the remaining stream enters the ammonia synthesis loop to undergo ammonia production reactions under high temperatures between 480 and 430 °C, and high pressure between 350 and 150 bar. The ammonia product is separated from the loop after refrigeration and is pumped to the urea production loop whilst a

small stream is purged from the unreacted gases before recycling into the reactor inlet. The process takes into account stacks and flares required to burn the discharged gases in addition to boil-off gas collection and recycling system from Ammonia storage tanks which accounts to 0.04% {Belapurkar, #1248} . In addition, the indirect GHG emissions are being considered from the process related electricity only.

Research Gap

After an extensive literature review, it became apparent that numerous studies have delved into the various energy sources employed globally, spanning areas such as transportation and electricity generation. However, a limited number of papers have explored the LCA of Blue Ammonia as a credible, promising, and environmentally friendly energy source when compared to others. Remarkably, no study to date has undertaken a comprehensive LCA, encompassing the entire process from raw material processing to product storage, specifically focusing on direct and indirect carbon footprint aspects.

MATERIALS AND METHODS

Research Flow Chart

Figure 2 illustrates the research methodology employed for the Blue Ammonia LCA. The process begins by defining the primary goal and scope of the research, followed by data collection concerning key indicators. Subsequently, the methodology involves estimating both the direct and indirect carbon footprint arising from the Blue Ammonia manufacturing process.

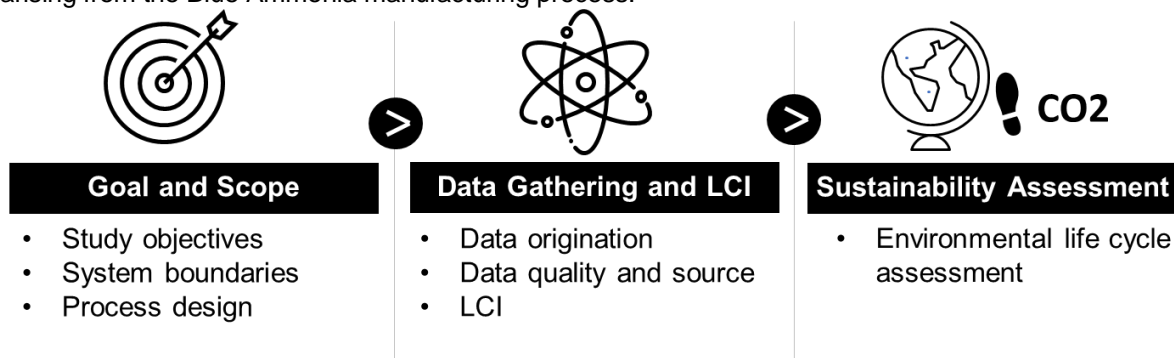


Fig. 2. Research method

LCA Goal and Scope

This study aims to undertake a comprehensive LCA for Blue Ammonia, assessing its performance from the initial feedstock raw materials to the final storage tanks for the Blue Ammonia product. The functional unit chosen for the LCA assessment is one metric ton (MT) of Blue Ammonia produced annually. This approach enables a thorough evaluation of the environmental impact across the entire life cycle of Blue Ammonia production, providing insights into its sustainability performance.

Inventory Analysis

In conducting the assessment, a life cycle inventory (LCI) is compiled for each phase of the Blue Ammonia processing chain, as detailed in Table 1. The case study focuses on Qatar, providing a specific context for the evaluation. To attain this objective, the domain of the Blue Ammonia process chain is considered, with the functional and boundary unit system previously established for estimation purposes. Information and emission data related to the Blue Ammonia process are primarily derived from simulations conducted using the Aspen HYSYS tool.

Table 1. LCI of the study

Impact Area	Impact / Indicator	Conversion Factor	Units
Direct Environmental Global Warming Potential [15]	Carbon Dioxide (CO ₂)	1	Ton CO ₂ to Ton CO ₂ -eq
	Methane (CH ₄)	28	Ton CH ₄ to Ton CO ₂ -eq
	Nitrous Oxides (N ₂ O)	265	Ton N ₂ O to Ton CO ₂ -eq
Indirect Environmental Global Warming Potential [16]	Electricity	0.0005	KWh to Ton CO ₂ -eq

Aspen HYSYS Modelling

This model is a widely used simulation program within the energy industry. The optimization process is the primary purpose of this software; it involves the downstream, upstream, midstream, and utilities processes. The flow process for many industrial operations might include hydrocarbon processes, gas flue enumeration for emission reporting, wastewater treatment, among other operations, process performance troubleshooting and monitoring, and a commonly utilized promising equipment for over 35 years [17].

In this research, the stages starting from the Steam Reforming Unit until the Product Storage Unit, are simulated in the Aspen HYSYS chemical process simulator except for the transportation stage. The Blue Ammonia chain feed conditions and products' specifications are provided by Tjahjono, Stevani [14]. The integrated Blue Ammonia production that has been simulated using the Aspen HYSYS program employed certain assumptions while conducting the steady-state simulation.

RESULTS AND DISCUSSION

Figure 3 provides a detailed breakdown of direct and indirect GHG emissions within the Blue Ammonia process chain. The results are presented as Tons of emissions per Tons of Blue Ammonia product, with the percentage distribution of each emission depicted in Figure 3(a). The simulation reveals that a substantial 98.9% of GHG emissions originate from carbon dioxide, making it the predominant factor. Carbon dioxide results from the combustion of waste gases, routine flaring, Boil off Gas (BOG), and the carbon content present in the feedstock and by-product stream. Notably, the Ammonia Converter Unit emerges as the primary source of carbon dioxide formation. In contrast, methane and nitrous oxide emissions account for 0.74% and 0.34%, respectively. Methane emissions are predominantly associated with the Steam Reforming Unit, while the Ammonia Converter Unit is the primary generator of nitrous oxides in the Blue Ammonia process chain.

In terms of comparing direct and indirect GHG emissions, measured in Tons of CO₂-eq per Tons of Blue Ammonia produced, direct emissions contribute significantly with a 59.8% share, as illustrated in Figure 3(b). This finding underscores the dominance of direct emission sources. The Ammonia Converter Unit is identified as the highest consumer of electricity, whereas the Ammonia Storage Unit has the lowest electricity consumption within the process chain.

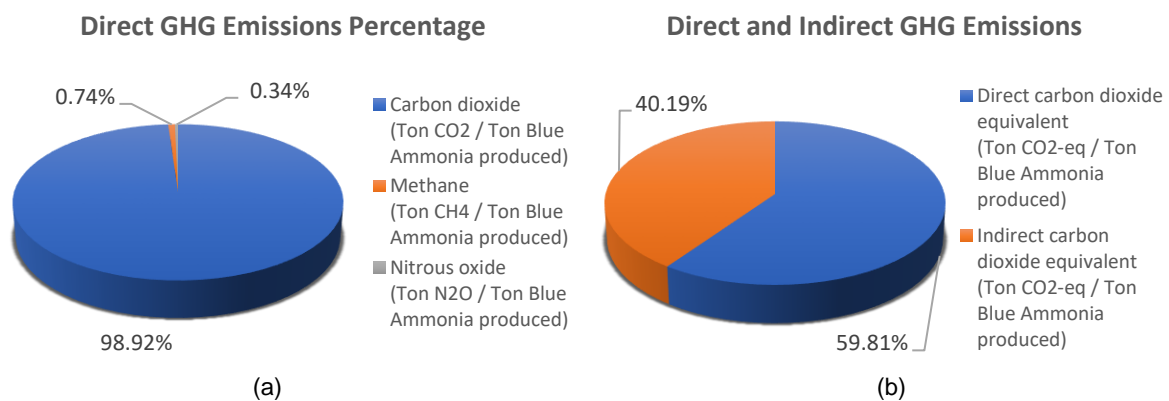


Fig. 3. LCA results of the Blue Ammonia value chain

CONCLUSIONS

Summary of Research and Key Findings

In conclusion, this study delves into the environmental implications of Blue Ammonia production, addressing the critical need for sustainable practices in the ammonia sector. The extensive literature review highlights the scarcity of comprehensive LCA for Blue Ammonia, revealing a research gap that this study aims to fill. The research framework follows a meticulous flowchart to conduct a holistic LCA, considering both direct and indirect carbon footprints. The Aspen HYSYS modeling tool serves as a robust simulation platform for the Blue Ammonia process chain. The detailed breakdown of this research's results reveals that a substantial 98.9% of GHG emissions from Blue Ammonia are carbon dioxide, with the Ammonia Converter Unit as the primary source. Methane and nitrous oxide contribute 0.74% and 0.34%, respectively. Direct and indirect emissions are also assessed. This study underscores the urgent need for sustainable practices in Blue Ammonia production. To bridge the research gap, prioritize policies fostering comprehensive LCAs. To minimize emissions, advocate for sustainable feedstocks, innovative technologies, and renewable energy integration.

Limitations of the Current Research and Recommendations for Future Work

Aspen HYSYS may introduce uncertainty due to equipment design and specification variations, impacting environmental and energy aspects. The tool may not determine maximum equipment capacity or include standby units, which are commonly incorporated in real-world applications. Future research will extend the sustainability assessment of global Blue Ammonia production, encompassing a broader indicator set and addressing import-export dynamics. Additionally, conducting an LCA of the carbon footprint for major Blue Ammonia importers and exporters necessitates thorough carbon footprint accounting, supply chain optimization, and tendering process improvements. The conversion factor for Scope 2 is derived from publicly available information, as acquiring emission factors for the conversion of electricity to CO₂-eq emissions posed difficulties. Implement the carbon capture unit to utilize the CO₂ to form other products such as Methanol or for oil enrichment applications. The application of the Life Cycle Sustainability Assessment (LCSA) to diverse industrial systems can reveal gaps and enhance the methodology, considering inherent uncertainties.

REFERENCES

- [1] Gilbert PR, Thornley P. Energy and carbon balance of ammonia production from biomass gasification. 2010.
- [2] Li K, Chen S, Wang H, Wang F. Plasma-assisted ammonia synthesis over Ni/LaOF: Dual active centers consisting of oxygen vacancies and Ni. *Applied Catalysis A: General*. 2023;650:118983.
- [3] Knapik E, Kosowski P, Stopa J. Cryogenic liquefaction and separation of CO₂ using nitrogen removal unit cold energy. *Chemical Engineering Research and Design*. 2018;131:66-79.
- [4] Timmerberg S, Kaltschmitt M, Finkbeiner M. Hydrogen and hydrogen-derived fuels through methane decomposition of natural gas – GHG emissions and costs. *Energy Conversion and Management*: X. 2020;7:100043.
- [5] Okonkwo E, Al-Breiki M, Bicer Y, Al-Ansari T. Sustainable hydrogen roadmap: A holistic review and decision-making methodology for production, utilisation and exportation using Qatar as a case study. *International Journal of Hydrogen Energy*. 2021;46.
- [6] Liu X, Elgowainy A, Wang M. Life cycle energy use and greenhouse gas emissions of ammonia production from renewable resources and industrial by-products. *Green Chemistry*. 2020;22:5751-61.
- [7] Moghaddam H. Expert Commentary - Potential and Benefits of Blue Ammonia as a Clean Fuel of the Future. Doha, Qatar: Gas Exporting Countries Forum 2021.
- [8] Shi J, Zhu Y, Feng Y, Yang J, Xia C. A Prompt Decarbonization Pathway for Shipping: Green Hydrogen, Ammonia, and Methanol Production and Utilization in Marine Engines. *Atmosphere*. 2023;14:584.
- [9] Giddey S, Badwal SPS, Munnings C, Dolan M. Ammonia as a Renewable Energy Transportation Media. *ACS Sustainable Chemistry & Engineering*. 2017;5:10231-9.
- [10] Smith C, Hill AK, Torrente-Murciano L. Current and future role of Haber–Bosch ammonia in a carbon-free energy landscape. *Energy & Environmental Science*. 2020;13:331-44.



- [11] Al-Yafei H, AlNouss A, Aseel S, Kucukvar M, Onat NC, Al-Ansari T. How Sustainable is Liquefied Natural Gas Supply Chain? An Integrated Life Cycle Sustainability Assessment Model. Energy Conversion and Management: X. 2022;Submitted to
- [12] Ghavam S, Vahdati M, Wilson IAG, Styring P. Sustainable Ammonia Production Processes. Frontiers in Energy Research. 2021;9.
- [13] Ghavam S, Taylor CM, Styring P. The life cycle environmental impacts of a novel sustainable ammonia production process from food waste and brown water. Journal of Cleaner Production. 2021;320:128776.
- [14] Tjahjono M, Stevani I, Siswanto G, Adhitya A, Halim I. Assessing the feasibility of gray, blue, and green ammonia productions in Indonesia: A techno-economic and environmental perspective. International Journal of Renewable Energy Development. 2023;12:1030-40.
- [15] IPCC. Climate Change 2014: Synthesis Report. In: Contribution of Working Groups I and II to the Fifth Assessment Report of the Intergovernmental Panel on Climate Change, R.K. Pachauri and L.A. Meyer (eds.), editor. Geneva, Switzerland 2014. p. 151.
- [16] RenSMART. UK CO₂(eq) emissions due to electricity generation. United Kingdom Wet-Wired.com Ltd.; 2016.
- [17] AspenTechnologyInc. Aspen HYSYS. aspentech.com; 2021.

ICH2P14-OP178

TANK TO TANK LIFE CYCLE ASSESSMENT OF GREENHOUSE GAS EMISSION FROM METHANOL PLANT

¹Hussein Al-Yafei, ^{2*}Ahmed AlNouss, ¹Saleh Aseel, ¹Mohannad AlJarrah, ²Tareq Al-Ansari

¹Chemical Engineering Department, College of Engineering and Technology, University of Doha for Science and Technology, Doha, Qatar

²College of Science and Engineering, Hamad Bin Khalifa University, Qatar Foundation, Doha, Qatar

*Corresponding author e-mail: a.alnouss@hotmail.com

ABSTRACT

Integrating sustainability principles into the distribution network poses a significant challenge for industries aiming to flourish in today's dynamic environment and meet the UN sustainable development goals. This challenge becomes particularly crucial in the additive industry, where natural gas is the primary fuel source. Despite extensive research on the environmental implications of such initiatives, there is a noticeable literature gap concerning the life cycle assessment (LCA) of Methanol production and its associated supply chains regarding environmental evaluation. This research addresses this gap by conducting the first-ever LCA of Methanol production, offering a comprehensive evaluation of its performance from raw material processing to the final product. The LCA includes a particular analysis of both direct and indirect greenhouse gas (GHG) emissions, encompassing carbon dioxide, methane, and nitrous oxides. Significantly, our life cycle model incorporates the reliable Aspen HYSYS simulation, widely recognized for its precision in engineering and design applications. The findings shed light on the primary contributors to carbon dioxide equivalent (CO₂-eq) emissions, known as Scope 1, pinpointing Methanol production, particularly the steam reforming section, as the predominant source with the highest carbon footprint at 81.9% of the overall direct carbon footprint. Moreover, the Methanol Synthesis Loop emerges as the leading contributor to Scope 2 GHG emissions, constituting 52.4% compared to other units in the Methanol production process chain, mainly due to the presence of high energy demand separation columns. Based on the insights garnered from this research, we propose an integrated framework model. This model forms the basis for various sustainability strategies and policy recommendations that align with the broader objectives of business sustainability.

Keywords: Life cycle assessment, Methanol, Greenhouse gas, Sustainability, Environment.

INTRODUCTION

Background

Methanol, also called methyl alcohol, serves as a useful fuel, suitable for internal combustion engines, fuel cells, and stoves. Its high-octane rating makes it a valuable additive or substitute for gasoline, reducing emissions of pollutants. Recent studies explore Methanol's potential in challenging-to-decarbonize sectors like maritime and aviation. The methanol-to-olefins process can also generate light olefins, which are essential for polymer production [1]. Methanol traditionally results from hydrogenating carbon monoxide through a catalytic process with pressurized synthesis gas (syngas). Syngas, generated via steam reforming or partial oxidation, contribute to CO₂ emissions during methanol production, ranging from 0.5 tCO₂ eq. Tri-reforming processes slightly outperform bi-reforming, while renewable energy sources like solar, biomass, hydropower, and wind reduce well-to-wheel GHG emissions by 98% compared to gasoline and diesel. Despite lower environmental impacts in CO₂-based processes, mineral, and water depletion increase [2].

Greenhouse Gas Emissions and Impacts

The production process, reliant on raw materials, involves substantial fuel consumption from feedstock, resulting in noteworthy CO₂, CH₄, and N₂O emissions, posing a persistent concern for greenhouse gas release. Efforts to manage greenhouse gas emissions are pivotal, as evidenced by Kajaste, Hurme [3], and the methanol assessment of methanol production routes using a cradle-to-gate life cycle approach. Findings reveal varying global warming potential (GWP₁₀₀) values, with coal-derived Methanol exhibiting the highest (2.97 kg CO₂eq/kg CH₃OH), contrasting with co-produced Methanol from renewable corn

ethanol displaying negative emissions (0.99 kg CO₂eq/kg CH₃OH). In a study by Khojasteh-Salkuyeh, Ashrafi [4], different methanol production methods, including natural gas reforming and CO₂ utilization, were evaluated. Results emphasize the environmental viability of direct CO₂ hydrogenation only with electricity GHG intensity below 0.17 kg CO₂ equivalent per kWh.

Carbon capture and utilization (CCU) emerged as a strategy for economic and emissions benefits [5]. Utilizing captured CO₂ as a feedstock for Methanol production, especially through thermochemical or electrochemical processes powered by renewable energy, proves environmentally advantageous. Analyzing CO₂-based methanol production in Germany, Kaiser, Siems [6] consider local CO₂ sources, hydrogen import methods, and production impacts. Offshore wind park-derived hydrogen has the least environmental impact, while pipeline import is the most cost-effective method [7]. Methanol's role as a versatile fuel or chemical precursor showcases its potential for sustainable practices in transportation and the chemical industry. This aligns with planetary boundaries, offering significant CO₂ savings and emphasizing Methanol's environmental advantages.

Problem statement, research objective, and research structure

Sustainable development is crucial in meeting the demand for eco-friendly products. The additive industrial sector, responding to environmentally conscious consumers, integrates sustainability into its growth strategy. This research focuses on Methanol's environmental impact, proposing a model for primary life cycle sustainability assessments in Methanol businesses. The five-section structure includes an introduction to Methanol, an LCA literature review, methodology, outcomes, and concluding remarks. The proposed LCA model is deemed a comprehensive environmental assessment method in this context [8]. This research is dedicated to examining and identifying the environmental impact of Methanol within its value chain. The proposed model, once developed, could serve as the cornerstone for the primary life cycle sustainability assessment for Methanol businesses.

The structure of this research comprises five sections. Section 1 introduces the background of Methanol and outlines its environmental impacts. Section 2 offers a comprehensive literature review on both LCA and the Methanol process chain. Section 3 details the methodology employed in creating the LCA model for Methanol. Section 4 provides the results and discussions arising from the research outcomes. Finally, Section 5 presents the concluding remarks of the study.

LITERATURE REVIEW

Environmental Life Cycle Assessment

This literature review offers a comprehensive summary of significant studies and insights concerning the environmental LCA of Methanol production, providing a deeper understanding of sustainability challenges within the industry. The LCA method seeks to evaluate the environmental impact of the product, encompassing aspects such as pollution, resource consumption, and both direct and indirect impacts [8].

Extensive literature, including studies on CCU routes and Green Methanol, delves into economic and environmental aspects. Life cycle assessments (LCAs) reveal trade-offs in environmental indicators, emphasizing the need to broaden the study scope. Analyses of Methanol production highlight trade-offs between carbon footprint, water, and mineral depletion. Overall, CCU routes, especially due to high hydrogen costs and renewable energy demands, are found to be expensive compared to fossil counterparts [9].

Given the heavy reliance of Methanol production on hydrogen, primarily sourced from carbon-based fuels, the carbon emissions linked to hydrogen production pose a significant environmental concern. Smith, Hill [10] discussed strategies to address these emissions and explored avenues such as CCU and renewable hydrogen sources as potential pathways for emission reduction.

Methanol Process Chain and System Boundaries

Figure 1 depicts a flow block diagram illustrating the Methanol process chain. The units in the diagram are categorized into distinct components, namely the natural gas raw material upstream facility, Stages of Steam Reforming Unit, Purification section, which consist of Water Removal Unit and CO₂ Removal Unit, Conditioning Unit, Methanol Converter Unit, and the concluding Methanol Storage Unit. Throughout all these sections, the operation necessitates the use of associated utilities and process-related electrical power [11]. Table 1 summarizes the properties and conditions of the main feedstock, natural gas (NG), and methanol products [12].

Table 1. Methanol plant feedstock and product's properties and conditions

NG Feedstock		Methanol Product	
Flow	1.43 MMTPA	Flow before CO ₂ recovery	1 MMTPA
		Flow after CO ₂ recovery	1.16 MMTPA
Temperature	40 °C	Temperature	60 °C
Pressure	2 bar	Pressure	5 bar
Components (mol%): Methane (93.11), Ethane (1.5), Propane (0.07), n-Butane (0.01), CO ₂ (0.86), and N ₂ (4.45)		Components (mol%): Methanol (99.99) and H ₂ O (0.01)	

Despite increasing demand for Methanol as a transportation fuel in several countries, conventional syngas-based production methods remain dominant [13]. Methanol is typically produced via the traditional route: Carbon Source + Oxygen → Syngas (CO + Hydrogen) → Methanol. Syngas is generated through methods like steam reforming of natural gas [14]. The chemical reactions involved are endothermic, occurring at 5-30 MPa pressure and 300-350°C as can be seen from Eq. (1) through Eq. (3). As far as the fuel type contains more carbon, the emitted CO₂ is going to be higher (e.g., coal is generating more CO₂ than natural gas).

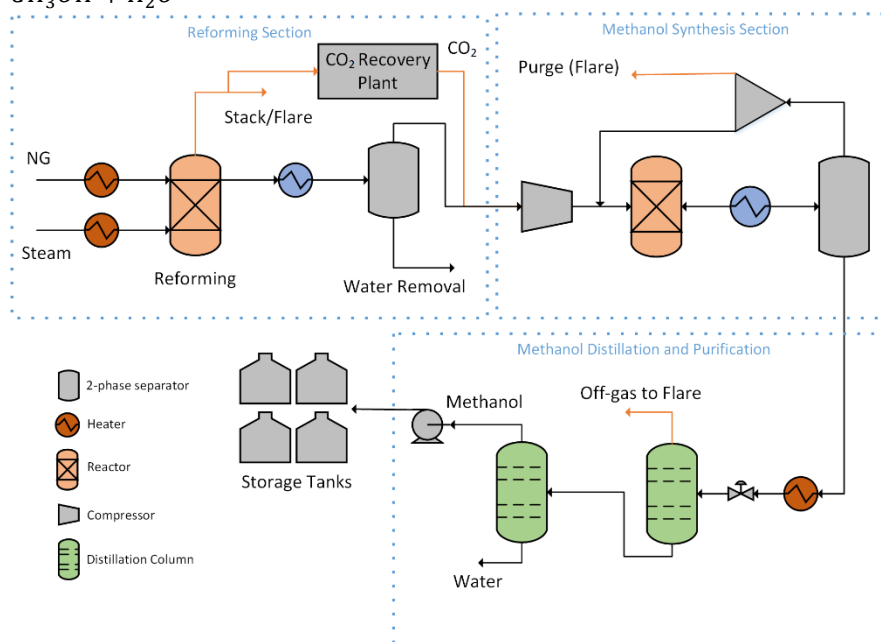


Fig. 1. Block flow diagram of Methanol plant

A steady-state simulation of the Methanol production is conducted under the assumptions of a forward reaction mechanism and a continuous 2% purge from the unreacted recycle gas stream. The syngas produced from NG reforming according to reaction 1 is quenched and purified from water. Before the purified syngas enters the Methanol convertor loop, it is conditioned by a sequence of compressors and coolers. In the Methanol synthesis loop, CO, CO₂, and H₂ are transformed into Methanol and water at high pressures of 100–50 bar following reactions 2 and 3. Once a limited amount has been purged to guarantee process stability, the unreacted components are recycled from a two-phase vessel to the reactor intake. The resultant Methanol is regarded as crude and must go through two columns: one for light ends distillation to eliminate any remaining gases and another for heavy ends distillation to remove water from it. Purified Methanol product is then pumped to storage tanks.

Research Gap

Following an in-depth review of the existing literature, it is marked that numerous studies have investigated global energy sources across transportation and electricity generation. However, there is a scarcity of papers examining the LCA of Methanol as a viable, promising, and eco-friendly energy option compared to alternatives. Notably, no study has conducted a thorough LCA covering the entire process, from raw material processing to product storage, addressing both direct and indirect carbon footprint aspects.

MATERIALS AND METHODS

Research Flow Chart

The research methodology for Methanol LCA is illustrated in Figure 2. It begins by establishing the primary goal and scope, followed by gathering data on key indicators. The subsequent steps involve estimating the direct and indirect carbon footprint associated with the Methanol manufacturing process.

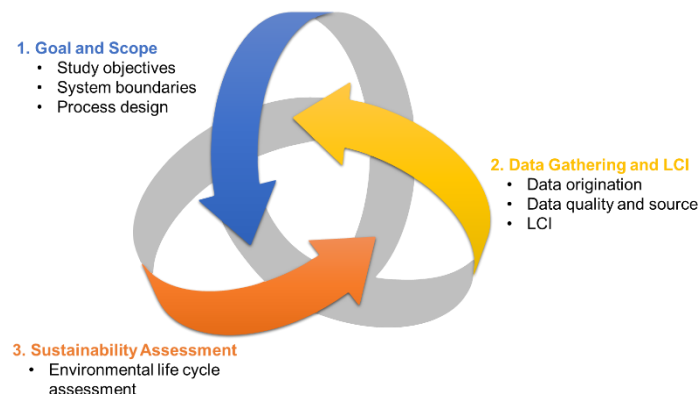


Fig. 2. Research method

LCA Goal and Scope

This study aims to conduct a thorough Tank-to-Tank LCA for the Methanol process, evaluating its performance from raw feedstock to the Methanol product's storage tanks. The selected functional unit is one metric ton (MT) of Methanol produced annually. This approach offers valuable insights into the sustainability performance of Methanol.

Inventory Analysis

A life cycle inventory (LCI) is created in the evaluation, detailed in Table 2. Focused on Qatar, the analysis considers the Methanol process chain domain, aligning with a functional and boundary unit system. The primary source of emissions details is from Aspen HYSYS simulations.

Table 2. LCI of the study

Impact Area	Impact / Indicator	Conversion Factor	Units
Direct Environmental Global Warming Potential [15]	Carbon Dioxide (CO ₂)	1	Ton CO ₂ to Ton CO ₂ -eq
	Methane (CH ₄)	28	Ton CH ₄ to Ton CO ₂ -eq.
	Nitrous Oxides (N ₂ O)	265	Ton N ₂ O to Ton CO ₂ -eq.
Indirect Environmental Global Warming Potential [16]	Electricity	0.0005	KWh to Ton CO ₂ -eq

Aspen HYSYS Modelling

The Aspen HYSYS chemical process simulator, is extensively employed in the energy industry for optimizing processes. With over 35 years of use, it simulates hydrocarbon processes, manages emissions reporting, troubleshoots, and monitors process performance [17]. In our research, we utilized Aspen HYSYS to simulate Methanol production stages, relying on feed conditions and specifications from [12]. The integrated simulation involved steady-state assumptions.

RESULTS AND DISCUSSION

The study was initiated by simulating the Methanol plant to quantify both direct and indirect GHG emissions. Table 3 illustrates the outcomes for direct GHG emissions. Notably, the Steam Reforming Unit exhibits the highest carbon dioxide emission ratio, reaching 76.0 kg per Ton of Methanol produced. Methane emissions peak at Steam Reforming Unit with a factor of 1.55. Nitrous oxide remains minimal across all units in the Methanol process chain. The direct GHG emissions from the Storage and Export Unit are deemed negligible, primarily relying on electricity as a dependable energy source.

Table 3. Direct GHG emission factors from Methanol plant units

Unit	Carbon dioxide (kg CO ₂ / Ton Methanol produced)	Methane (kg CH ₄ / Ton Methanol produced)	Nitrous oxide (kg N ₂ O / Ton Methanol produced)
Steam Reforming Unit	75.998	1.551	0.025
Methanol Synthesis	0.697	-	0.097
Distillation and Purification	0.060	-	0.005
Storage and Export	-	-	-

Figure 3 depicts the indirect carbon dioxide equivalent from the Methanol plant's electricity usage. The findings highlight that the Methanol Synthesis Unit significantly impacts Scope 2 emissions, registering 743.72 Ton of CO₂-eq per Ton of Methanol produced. The Distillation and Purification Unit and the Steam Reforming Unit are the following. The Storage and Export Unit utilizes minimal electricity for its operations to meet operational requirements.

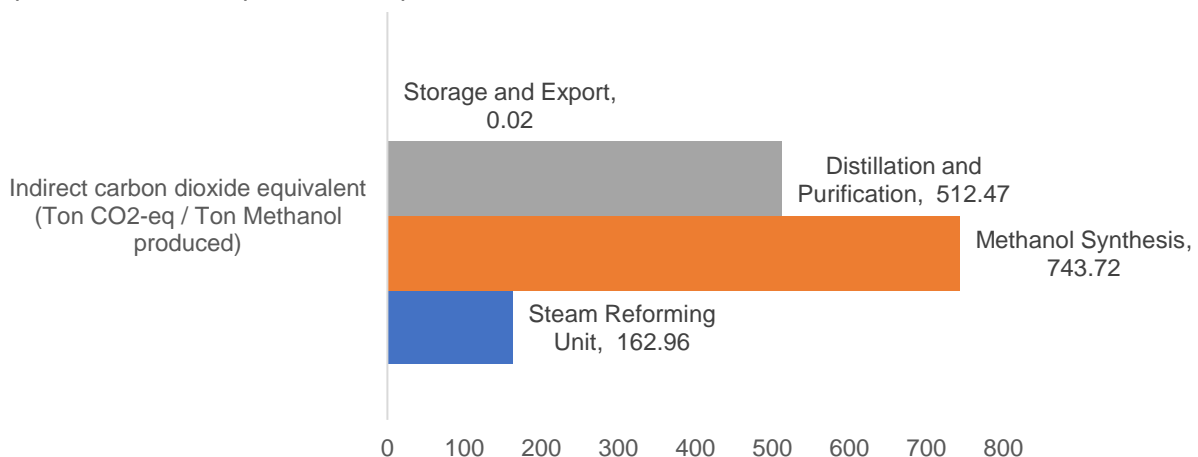


Fig. 3. Indirect carbon dioxide equivalent from the Methanol plant used electricity



CONCLUSIONS

Summary of Research and Key Findings

The study addresses the surging global Methanol demand, presenting a simulated plant producing one million metric tons annually. Using a Tank-to-Tank life cycle model, environmental impacts were assessed with data from Aspen HYSYS. Results categorize CO₂-eq emissions, identifying Methanol production, especially the steam reforming unit and methanol synthesis, as the main Scope 1 and 2 contributors, constituting 81.9% and 52.4%, respectively. Acknowledging Methanol's significance and environmental impact, sustainability measures are proposed. Integrating carbon capture in the Synthesis Loop can cut Scope 1 emissions by 50% while investing in renewable energy and optimizing transportation logistics, promoting a more sustainable methanol supply chain.

Limitations of the Current Research and Recommendations for Future Work

Aspen HYSYS introduces uncertainties in environmental and energy aspects due to variations in equipment design. It may not accurately determine maximum equipment capacity or consider standby units common in real-world applications. Future research on global Methanol production sustainability will consider more comprehensive indicators and address import-export dynamics. A detailed LCA of carbon footprints for major Methanol importers and exporters, accounting for Scope 3 emissions, will require meticulous carbon footprint accounting, supply chain optimization, and improvements in the tendering process. The use of the Life Cycle Sustainability Assessment (LCSA) can reveal gaps and enhance methodology by addressing inherent uncertainties in various industrial systems.

Aspen HYSYS introduces uncertainties in environmental and energy aspects, lacking accuracy in determining maximum equipment capacity and considering standby units common in real-world applications. Studying the import-export dynamics and employing a detailed LCA for the logistics part, accounting for Scope 3 emissions is recommended.

REFERENCES

- [1] Garcia-Garcia G, Fernandez MC, Armstrong K, Woolass S, Styring P. Analytical review of life-cycle environmental impacts of carbon capture and utilization technologies. *ChemSusChem*. 2021;14:995-1015.
- [2] Rumayor M, Dominguez-Ramos A, Irbien A. Innovative alternatives to methanol manufacture: Carbon footprint assessment. *Journal of Cleaner Production*. 2019;225:426-34.
- [3] Kajaste R, Hurme M, Oinas P. Methanol-Managing greenhouse gas emissions in the production chain by optimizing the resource base. *AIMS Energy*. 2018;6:1074-102.
- [4] Khojasteh-Salkuyeh Y, Ashrafi O, Mostafavi E, Navarri P. CO₂ utilization for methanol production; Part I: Process design and life cycle GHG assessment of different pathways. *Journal of CO₂ Utilization*. 2021;50:101608.
- [5] Galán-Martín Á, Tulus V, Díaz I, Pozo C, Pérez-Ramírez J, Guillén-Gosálbez G. Sustainability footprints of a renewable carbon transition for the petrochemical sector within planetary boundaries. *One Earth*. 2021;4:565-83.
- [6] Kaiser S, Siems F, Mostert C, Bringezu S. Environmental and Economic Performance of CO₂-Based Methanol Production Using Long-Distance Transport for H₂ in Combination with CO₂ Point Sources: A Case Study for Germany. *Energies*. 2022;15:2507.
- [7] Iribarren D, Calvo-Serrano R, Martín-Gamboa M, Galán-Martín Á, Guillén-Gosálbez G. Social life cycle assessment of green Methanol and benchmarking against conventional fossil methanol. *Science of The Total Environment*. 2022;824:153840.
- [8] Al-Yafei H, AlNouss A, Aseel S, Kucukvar M, Onat NC, Al-Ansari T. How Sustainable is Liquefied Natural Gas Supply Chain? An Integrated Life Cycle Sustainability Assessment Model. *Energy Conversion and Management: X*. 2022;Submitted to
- [9] Perčić M, Vladimir N, Fan A. Life-cycle cost assessment of alternative marine fuels to reduce the carbon footprint in short-sea shipping: A case study of Croatia. *Applied Energy*. 2020;279:115848.
- [10] Smith C, Hill AK, Torrente-Murciano L. Current and future role of Haber–Bosch ammonia in a carbon-free energy landscape. *Energy & Environmental Science*. 2020;13:331-44.
- [11] Aasberg-Petersen K, Nielsen CS, Dybkjær I, Perregaard J. Large scale methanol production from natural gas. *Haldor Topsoe*. 2008;22.



- [12] Fiedler E, Grossmann G, Kersebohm DB, Weiss G, Witte C. Methanol. Ullmann's Encyclopedia of Industrial Chemistry.
- [13] Chaudhari SM, Meshram RB. A Comparative Life Cycle Assessment (LCA) of Gasoline Blending with Different Oxygenates in India. Nature Environment and Pollution Technology. 2021;20:1947-58.
- [14] Heo JN, Son N, Shin J, Do JY, Kang M. Efficient hydrogen production by low-temperature steam reforming of propane using catalysts with very small amounts of Pt loaded on NiMn₂O₄ particles. International Journal of Hydrogen Energy. 2020;45:20904-21.
- [15] IPCC. Climate Change 2014: Synthesis Report. In: Contribution of Working Groups I and II to the Fifth Assessment Report of the Intergovernmental Panel on Climate Change, R.K. Pachauri and L.A. Meyer (eds.), editor. Geneva, Switzerland 2014. p. 151.
- [16] RenSMART. UK CO₂(eq) emissions due to electricity generation. United Kingdom Wet-Wired.com Ltd.; 2016.
- [17] AspenTechnologyInc. Aspen HYSYS. aspentech.com; 2021.

ICH2P14-OP184

FLEXIBLE NATURAL GAS ALLOCATION TO BLUE-HYDROGEN MONETISED PRODUCTS: AN AGENT-BASED MODELLING APPROACH

¹Noor Yusuf, ²Ahmed AINouss, ¹Tareq Al-Ansari

¹College of Science and Engineering, Hamad Bin Khalifa University, Qatar Foundation, Doha, Qatar

²QatarEnergy LNG, Doha, Qatar

*Corresponding author e-mail: talansari@hbku.edu.qa

ABSTRACT

With the increased demand for cleaner energy resources, natural gas is a bridging fuel for smoothening the transition to renewables. Syngas (hydrogen-rich stream) is a fundamental intermediate for different utilisation routes. The syngas can then be treated for pure hydrogen production or monetised into value-added products. Despite the estimated demand growth in product demand, each utilisation process is subject to exogenous market uncertainties. Hence, accounting for operational flexibility in the early design stages allows the producers to react proactively to market changes. This work evaluates the flexibility of natural gas utilisation to final hydrogen carriers: methanol, MTBE, ammonia, urea and synthetic fuels by investigating plant design configurations and natural gas production allocation to different production routes. Aspen HYSYS is used for process modelling and simulation, followed by identifying each process's costs and operational flexibility. Simulation results and forecasted price and demand data are then used as input into an agent-based model to identify the optimal annual natural gas allocation to different processes subject to environmental and economic objectives. The -results of Qatar's case study revealed the importance of prioritising GTL and the ammonia process to maximise profitability. In comparison, production of the methanol-MTBE route is maximised to reduce the environmental impact.

Keywords: Natural Gas, Grey Hydrogen, Agent-Based Modelling, Hydrogen-Rich Products.

INTRODUCTION

With increased interest in decarbonisation to meet the Paris Agreement climate change goal, investments and deployments in cleaner energy systems have increased rapidly. In the first half of 2023 alone, global investments in renewable energy increased by 22% compared to the previous year's first half. A total global investment value of \$358 billion in renewables was reported, representing an all-time high for the yearly half [1]. Additionally, plans for developing a low-carbon hydrogen economy were accelerated since the Russian-Ukrainian conflict. Earlier this year, a Hydrogen Council/McKinsey Hydrogen Insights report announced the announcement of 680 large-scale hydrogen projects, totalling \$240 billion of investments until 2030 [2]. The reported value represents a 50% increase to the period prior to the Russian-Ukrainian conflict (i.e., late 2021). Yet, more investments in clean hydrogen are needed to achieve the net-zero target by 2050. For countries with rich natural gas reserves and limited renewable capacities, hydrogen production from natural gas represents a valuable investment opportunity. For example, Qatar has a significant potential for producing hydrogen carriers from natural gas, including ammonia, methanol, and synthetic fuels. Moreover, supported by the low natural gas production and processing costs, decarbonisation technologies can be considered for minimising the embodied CO₂ emissions for the production of blue hydrogen-rich products. In practice, dehydrated and treated natural gas is first used to produce a hydrogen-rich intermediate (i.e., syngas) via steam methane reforming (SMR) or autothermal reforming (ATR) technologies. The syngas is then routed to different monetisation technologies, such as separation for pure hydrogen production, and end-use for methanol, ammonia, and synthetic fuels production. Fundamentally, the composition of produced syngas differs based on the final monetisation use. Hence, process parameters of ATR or SMR technologies are maintained based on the final use of syngas. From another perspective, different combinations of technologies in the natural gas to hydrogen carriers are associated with different emissions, capital costs, operating costs, risks, and technical complexities. Yet, with increased demand fluctuations for the products in the final markets, a producer must consider effective strategies to plan and manage the production part of the system in the early design stages of the project. Amongst the several investigated supply management strategies, operational flexibility has been explored as an efficient strategy for strengthening the resilience of supply chains to market uncertainties. Operational flexibility allows for adjusting the capacity of different processes in response to demand and price variations. Which in turn plays a role in enhancing the economic profitability of the business or hedging against risks of oversupply. Although several studies evaluated the operational flexibility of processing systems on a technical level, a gap has been identified in employing the flexibility parameters in a comprehensive strategic study [3,4]. This work investigates the flexibility of natural gas utilisation to final hydrogen

carriers: methanol, MTBE ammonia, urea, and synthetic fuels ,using a simulation agent-based modelling approach. Fundamentally, the data-driven approach relies on forecasted demand and price data, along with process simulation parameters extracted from simulating the processes on the commercial software Aspen HYSYS.

DATA AND METHODOLOGY

The tool used herein to optimise the yearly natural gas allocation to the downstream processes in Qatar is based on an agent-based modelling approach. The framework re-evaluates the optimal allocation strategy in response to demand changes and based on economic and environmental objectives. This section provides an overview of the ABM, the simulation approach, and the main input parameters. Fundamentally, the problem was solved based on economic and environmental objectives, as discussed in the results section.

ABM simulation

An agent is an independent unit with unique characteristics and behaviours. In this work, two major sets of agents were considered to interact for optimal decision-making subject to economic and environmental aspects. The first group is represented by a single agent (i.e., source), which is natural gas. The second group is represented by the processing options (i.e., sinks), which are ammonia, urea, GTL, methanol, and MTBE. The model is run for a planning horizon of 34 years of the primary agent (NG) reacting with the downstream agents (D). Both groups of agents interact in an environment represented by the global economy. Table 1 summarises the characteristics of the agents.

Table 1: Characteristics of agents considered in the model

Agent	Attributes	Behaviours
NG system (NG)	<ul style="list-style-type: none"> - Total NG capacity C (billion cubic meters-BCM). - Yearly NG distribution capacities C_{ng} (BCM) - Yearly NG allocation to Methanol Q_m, GTL Q_n, Ammonia Q_a, MTBE Q_e and Urea Q_u. - Global Warming Potential from generating each product (kg CO₂-eq) 	<ul style="list-style-type: none"> - Allocate NG to methanol (m), GTL (n), Ammonia (a), MTBE (e), Urea (u)
Downstream Industries (Di)	<ul style="list-style-type: none"> - Yearly production capacities Q_{Di} (kg) 	<ul style="list-style-type: none"> - Determine best production sinks.

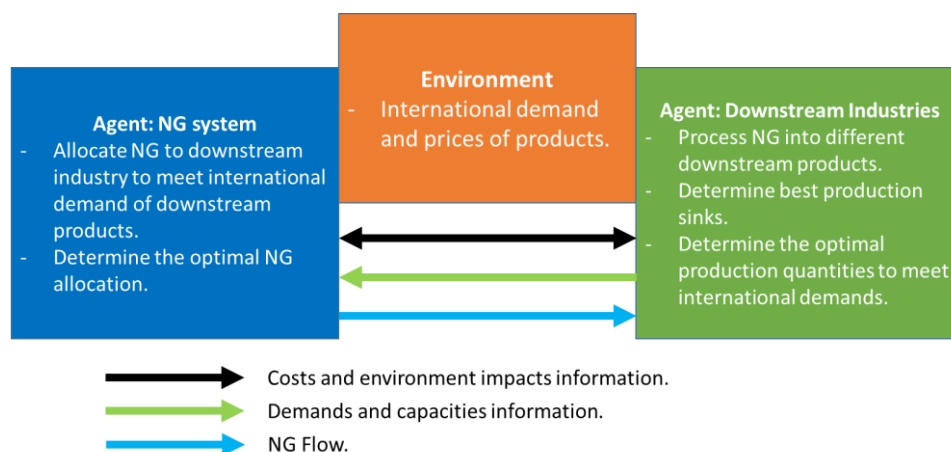


Figure 1: Representation of ABM elements.

Agents

The first group of agent is represented by a single central element, the available natural gas capacity (C_{ng}) to be allocated to different processes at annual basis. To achieve the allocation, NG grid allocates the available natural

gas capacity to 6 sinks: ammonia, urea, methanol, MTBE, and GTL processes to satisfy the allocation of the total NG grid capacity C . A sink is selected with a strategy to optimally allocate NG to downstream processes, including ammonia, urea, methanol, MTBE, and GTL based on forecasted global demand. Each allocation decision is driven by environmental and economic targets and operations limitations of the processes as discussed in the upcoming sections.

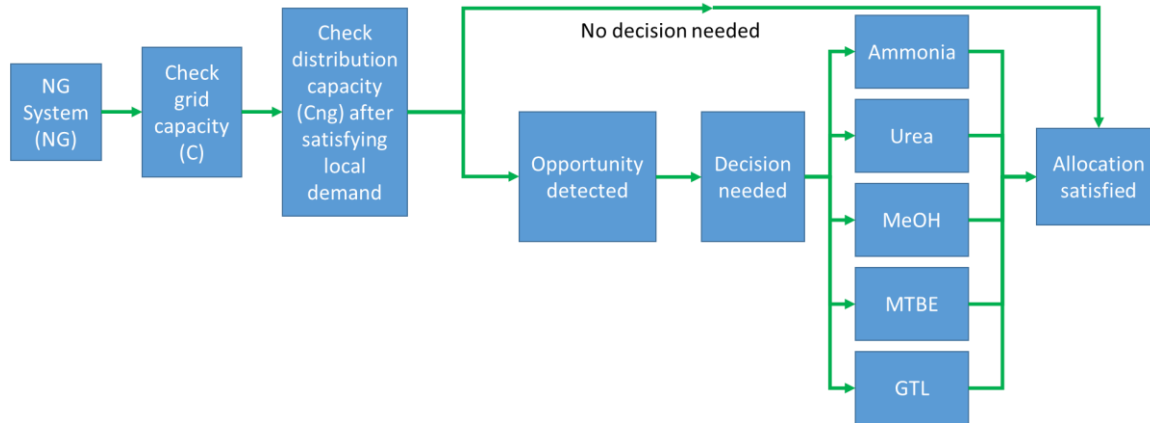


Figure 2: NG system behavior.

The second group of agents is concerned with the downstream processes. In this analysis, five downstream industries are regarded as agents D_i : ammonia, methanol, urea, MTBE, and GTL. The behaviour of D_i is characterised to optimally allocate NG capacity to downstream processes. Fundamentally, the allocated share is determined by factors, including the production capacity of process D_i , and the minimum flexibility production of each industry D_{min} . Figure 3 demonstrate the behavior of the downstream processing system.

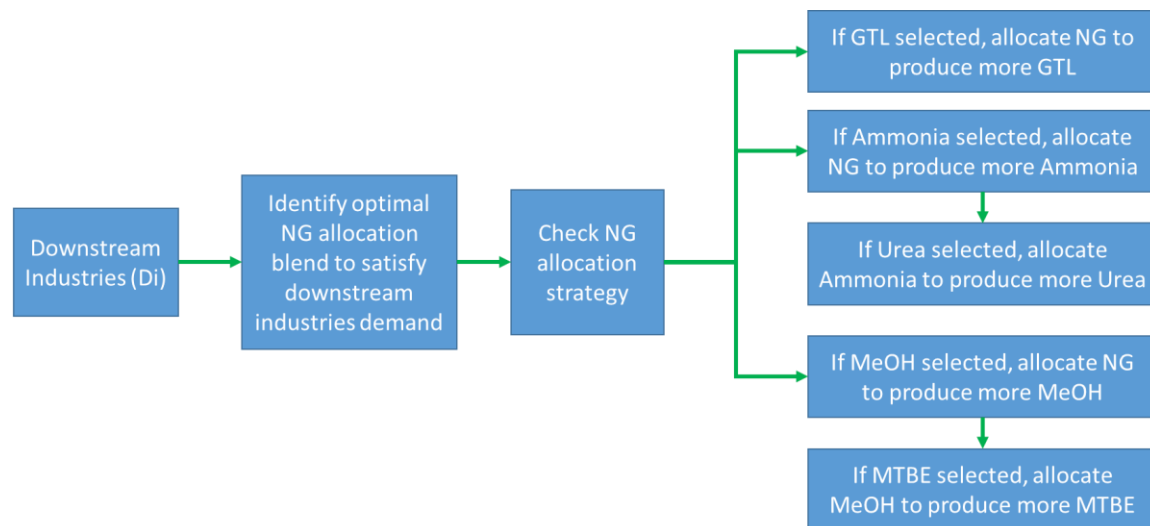


Figure 3: Downstream industries system behavior.

Based on equations (1-4), the economic EC and environmental EI indicators are simulated at each time step n for analysing the performance of NG and D_i . Equations (1-2) are used for the estimating values for the NG strategy, while equations (3-4) are used for the D_i strategy.

$$EC = Q_{i,NG} \times c_{i,NG} \text{ where } i = n (GTL), a (Ammonia), \text{ and } u (Urea), m (methanol), e (MTBE) \quad (1)$$

$$EI = Q_{i,NG} \times e_{i,NG} \text{ where } i = n (GTL), a (Ammonia), \text{ and } u (Urea), m (methanol), e (MTBE) \quad (2)$$

Where $Q_{i,NG}$ is the annual allocation of NG to processes (BCM), and $c_{i,NG}$ is the net cost from the achieved allocation (\$/BCM) computed by HYSYS simulation. While $e_{i,NG}$ is the measure of environmental impact of the processes represented by global warming potential (GWP) and estimated based on HYSYS simulation.

$$EC = Q_{i,D} \times c_{i,D} \quad \text{where } i = n \text{ (GTL)}, a \text{ (Ammonia)}, \text{ and } u \text{ (Urea)}, m \text{ (methanol)}, e \text{ (MTBE)} \quad (3)$$

$$EI = Q_{i,D} \times e_{i,D} \quad \text{where } i = n \text{ (GTL)}, a \text{ (Ammonia)}, \text{ and } u \text{ (Urea)}, m \text{ (methanol)}, e \text{ (MTBE)} \quad (4)$$

Where $Q_{i,D}$ is the annual production of products by the processing units in (MMTPA) and $c_{i,D}$ is the annual profit of products estimated using the economic analyser in Aspen HYSYSin (\$/MT). Meanwhile, $e_{i,D}$ is the GWP for each process estimated using Energy Analyzer in Aspen HYSYS.

Finally, all production processes are subject to a lower operational limit, as illustrated in Table 2.

Table 2: Minimum production flexibilities.

Process	Ammonia	Urea	MeOH	MTBE	GTL
Minimum production flexibility (MMTPA)	3.8	5.6	0.83	0.61	3.75

RESULTS AND DISCUSSION

Economic and environmentally independent scenarios were developed to allocate natural gas optimally to the downstream processes on a yearly basis. While the economic scenario takes into account the cost factor into consideration to decide on the optimal allocation, the environmental scenario solely considers minimising the emissions in the decision-making. Although the allocation strategy differs based on the objective, it was observed that demand and prices had a significant impact on the decision behaviour as illustrated in Figure 4.

Scenario 1: Economic restrictions

To meet the international demand of downstream chemicals, the NG allocation strategy is conducted based on an economic objective. After satisfying the local demand, the majority of the available NG capacity was allocated to GTL in the period between (2000-2014). However, the allocation strategy shifted to preferring ammonia production in the period between (2015-2035) driven by the high anticipated demand for cleaner energy resources. The allocation and associated emissions of the satisfied allocation are demonstrated in Figure 4 & 5.

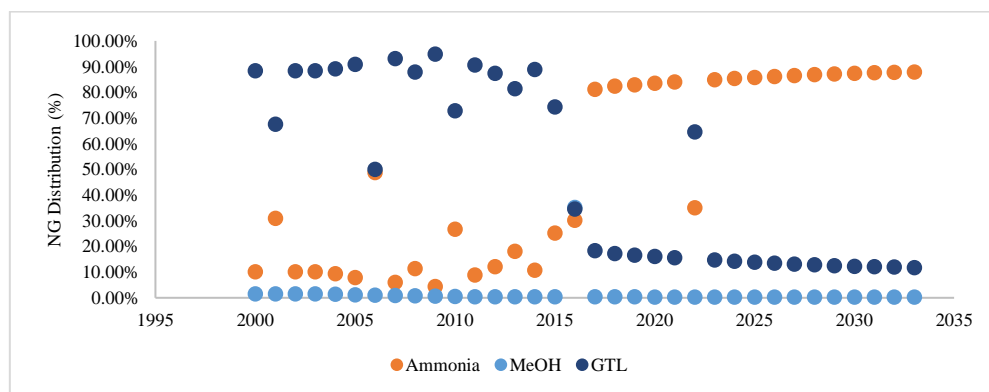


Figure 4. NG allocation mix to downstream industries under scenario 1.

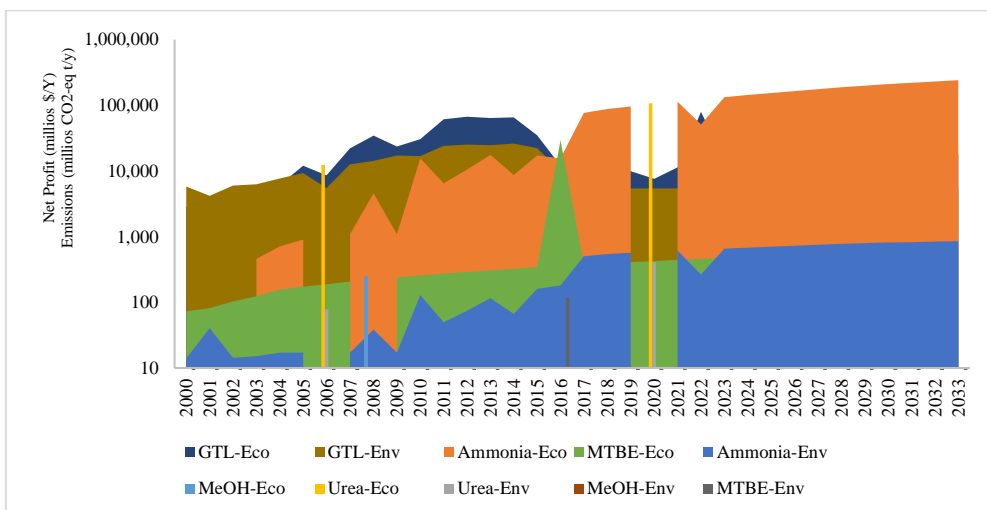


Figure 5. Downstream industries net profit and emissions indicators under scenario 1.

Scenario 2: Environmental restrictions

Subject to environmental conditions, the NG allocation strategy was highly shifted towards methanol production, as demonstrated in Figure 6. Compared to the economic scenario, the NG share allocated to ammonia production was significantly reduced throughout the planning horizon, despite the economic attractiveness of this monetisation route. This decline is driven by the emissions released from the processes, hence the decline in ammonia in turn results in reducing urea production. While the increase in methanol production influences further utilisation of methanol for the production of MTBE as summarised in Figure 7. As illustrated in the figure the overall GWP emissions of each process as per the allocation strategy were reduced compared to the economic scenario.

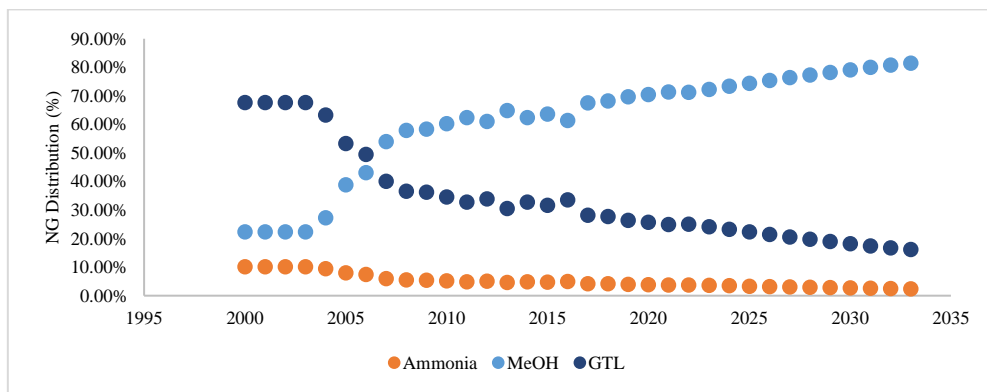


Figure 6. NG allocation mix to downstream industries under scenario 2.

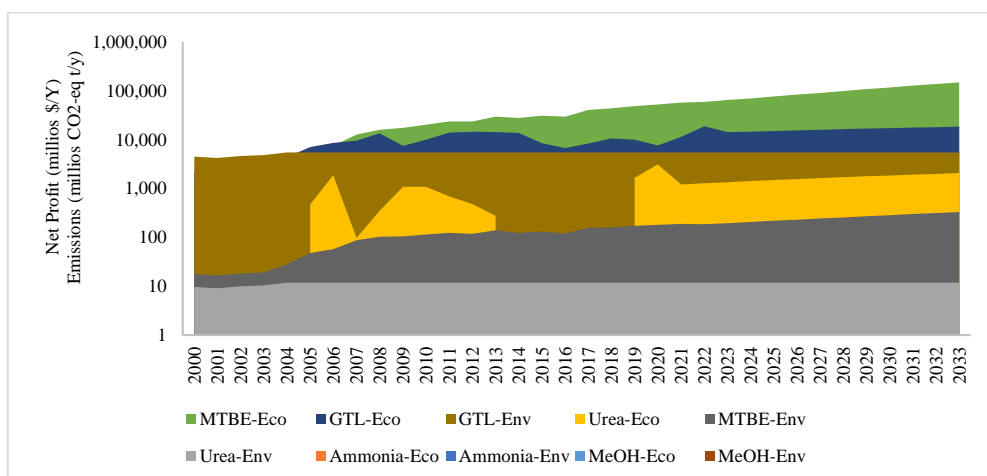


Figure 7. Downstream industries net profit and emissions indicators under scenario 2.



CONCLUSIONS

With the increased shift to cleaner energy resources, hydrogen carriers became crucial for monetising hydrogen for cost-effective transportation to final markets. This work evaluates the optimal annual natural gas allocation to different hydrogen-rich products using forecasted demand and prices, operational flexibility limitations, and HYSYS simulation parameters as main inputs for decision-making. Two independent scenarios were implemented using an agent-based modelling approach to evaluate the optimal allocation strategies. Based on economic considerations, the results revealed a preference to prioritise NG allocation to GTL in the first 14 years of the planning horizon, followed by 16 years of shifting to ammonia due to the increased market demand for ammonia. The increase in ammonia production, in turn, allowed for enhancing the portfolio flexibility by producing urea. On the contrary, the environmental scenario prioritised methanol production due to tackle GWP emissions. This resulted in significantly reducing the NG share allocated to ammonia production. Overall, the allocation strategies based on economic and environmental factors are a trade-off between profitability and emissions. Hence, ABM simulation provides prompt assessments of the influence of different input data and scenarios on the allocation strategy. This in turn supports in decision-making and provides insights on the impact of uncertainties on the operation of existing natural gas production systems.

REFERENCES

- [1] [https://about.bnef.com/blog/renewable-energy-investment-hits-record-breaking-358-billion-in-1h-2023/#:~:text=Renewable Energy Investment Hits Record-Breaking %24358 Billion in 1H 2023,-August 21%2C 2023&text=Global new investment in renewable,for any six](https://about.bnef.com/blog/renewable-energy-investment-hits-record-breaking-358-billion-in-1h-2023/#:~:text=Renewable%20Energy%20Investment%20Hits%20Record-Breaking%20%24358%20Billion%20in%201H%202023,-August%2021%2C2023&text=Global%20new%20investment%20in%20renewable,for%20any%20six). Accessed November 25, 2023
- [2] Hydrogen Council and Mckinsey & Company. Hydrogen Insights 2023. 2023.
- [3] Verleysen K, Parente A, Contino F. How sensitive is a dynamic ammonia synthesis process? Global sensitivity analysis of a dynamic Haber-Bosch process (for flexible seasonal energy storage). Energy 2021;232:121016.
- [4] Di Pretoro A, Montastruc L, Manenti F, Joulia X. Flexibility assessment of a biorefinery distillation train: Optimal design under uncertain conditions. Comput Chem Eng 2020;138:106831.

ICH2P14-OP196

MATHEMATICAL MODELING OF A SUSTAINABLE ENERGY SYSTEM FOR RESTAURANT COMMUNITIES: WASTE-TO-H₂ CONVERSION, CO₂ MITIGATION, CLEAN FUEL PRODUCTION, AND POWER GENERATION

¹Syed Muhammad Aun Rizvi, ¹Khurram Kamal, ¹Tahir Ratlamwala, ²Muhammad Fahad Sheikh

¹National University of Sciences and Technology, Department of Engineering Sciences, Karachi, Pakistan

²College of Science and Engineering, Hamad bin Kahlifa University, Doha, Qatar

Corresponding author e-mail: Ratlamwala.tahir@gmail.com

ABSTRACT

In the world of sustainable energy, our project presents a comprehensive mathematical model for a sustainable energy system within a restaurant community. The restaurant community of 50 restaurants produces waste cooking oil on daily basis that is utilized for biodiesel production, providing power for the community, while the wasted food is processed in an anaerobic biogas digester to produce methane for community's use. Additionally, Glycerol that is produced as a by product in the biodiesel plant is sold to the community. The MFC results in the purification of water and production of little electricity. The community's waste water is also used for hydrogen gas production through electrolysis. The Hydrogen gas produced is reacted with the atmospheric carbon dioxide to produce methanol, which is then used in the production of biodiesel. The mathematical modeling results demonstrate the potential for waste-to-H₂ conversion, CO₂ mitigation from environment, clean fuel production, and green power generation within the restaurant community.

Keywords: sustainable energy, Biodiesel, microbial fuel cell, electrolysis

INTRODUCTION

The increasing amount of waste generated by human activities has become a major environmental concern. Waste-to-energy technologies have emerged as a promising solution to address this issue by converting waste into useful energy. In this project, we aim to develop a sustainable waste-to-energy system that utilizes waste cooking oil from restaurants to produce biodiesel, which can be used to generate power for the restaurant community. The organic waste from the restaurant community will be fed into an anaerobic biogas digester to produce methane, which will be used within the community. Glycerol, a by-product of the biodiesel plant, can be used as a sweetener in the community. The Waste water will be fed into a microbial fuel cell for purification but cannot be reused in the community due to health standards. Some waste water produced is electrolyzed to produce hydrogen, and The hydrogen and CO₂ from the atmosphere will be reacted to produce methanol, which will be used in the production of biodiesel. The project aims to contribute to the development of sustainable waste-to-energy systems that can help reduce the environmental impact of waste while providing a source of renewable energy. The system can be divided into 2 parts one that is directly taking input from the restaurants and other whose input is dependent on other systems. The system taking primary inputs are Biodiesel production plant, Anaerobic Biodigester, MFC and Water electrolyser. The other subsystem include the methanol formation plant.

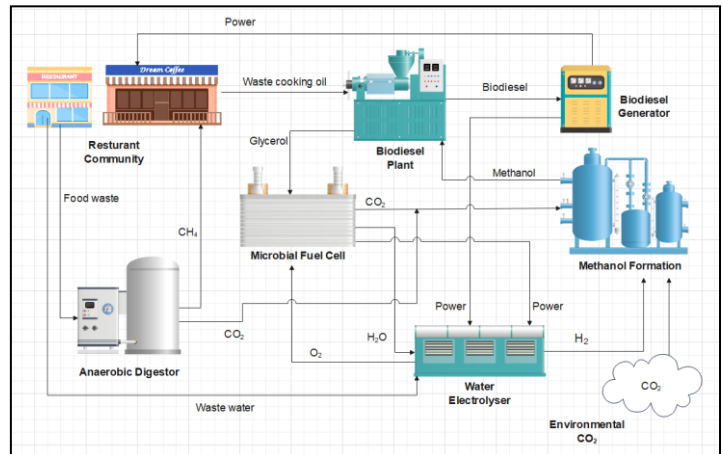


Figure 1: Schematic of the Proposed model

MODELLING

1. Biodiesel Plant

An average restaurant produces 8-10kg of waste cooking oil per day [1]. The Biodiesel Plant was to be fed with 500kg waste cooking produced daily by the community of 50 restaurants. [2] was used to establish the Biodiesel Plant. The molar ratio of methanol to Triglyceride was taken to be 6:1. This means 560 mol of triglyceride was reacted with 3360mol Methanol. So 44kg of methanol will be required daily by the plant. The density of this oil is

0.9192(kg/m³) [3]. The molar mass is 0.872(kg/mol) [4]. The Volume of the reactor is taken 1000L at 60C[differ]. The model is simulated for one day. It must be noted that esterification of the Waste cooking oil is important that reduces the Free Fatty Acids(FFAs) from it to a concentration less than 3%.

The Results showed Biodiesel yield of 435kg using 294.86(g/mol) molar mass of Biodiesel[2] . Glyceride produced as the by-product is 40kg. However the maximum yield was achieved after 2.4 hrs. This means that the daily operating time of the plant will be 2.4 hrs. The methanol utilized per day is 44kg. The glycerol can be used as a sweetener for desserts being sold in the community. A biodiesel generator can produce 1.58kW-h electricity per kg by generator as stated by [5]. This means that the community can use Electricity of 685kWh per day on Biodiesel generators or can produce 17kg of hydrogen from water electrolyses.

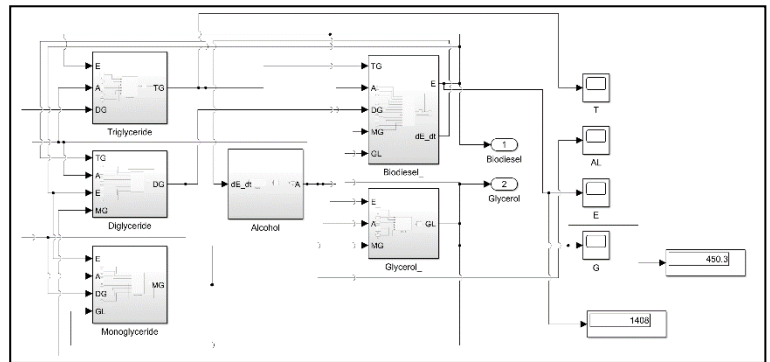


Figure 2: Simulink Model of Biodiesel Plant

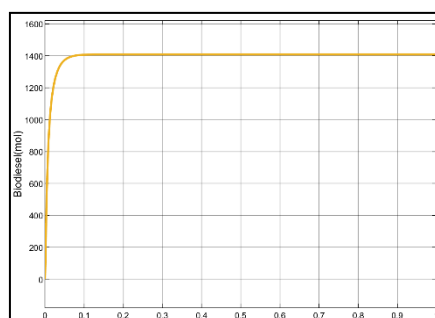


Figure 3 Biodiesel produced per day

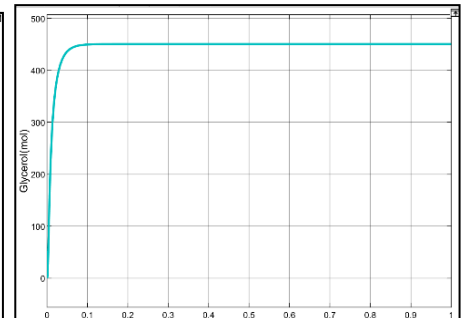


Figure 4: Glycerol produced per day

2. Anaerobic Biogas Digester

According to green restaurant association, [6] a restaurant produce 30kg of waste food daily. This means that our community produces 1500kg of waste food daily that will fed into the Anaerobic Biogas digester daily producing methane gas for restaurant fuel need. Mass balance equations collected by [7] were employed for the simulink model. The simulation was run for a time interval of 30 days and shown methane yield enough for the restaurant demands.

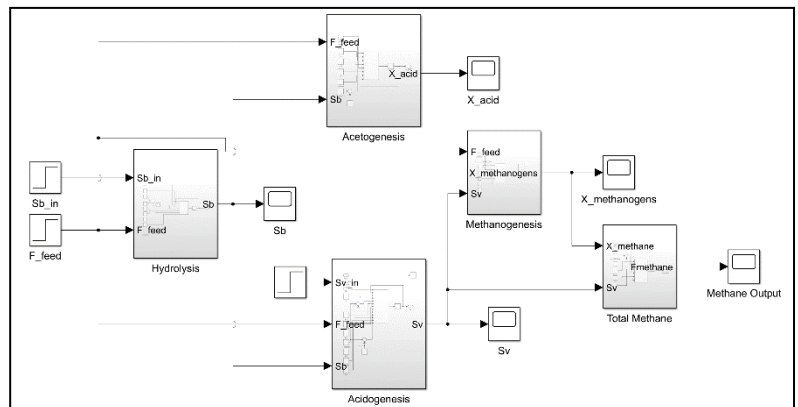


Figure 5: Anaerobic Biogas Digester

3. Microbial Fuel Cell

The microbial fuel cell used is for the water purification purpose. The community produce 25,000L waste water daily. The mathematical model by [pinto] is employed for the Simulink model of the MFC. However the purified water from the MFC will be used in the community due to health standards, but could be transported for washing, irrigation and Industrial purposes. Therefore Its working didn't plays a crucial role in our community.

4. Methanol Production Plant

Methanol formation is done using hydrogenation of carbon dioxide. The model used is taken from [8] that considered 2 reactions. The Simulink model was run for the constants provided in[8]. The aim was to produce minimum 44kg of methanol by the hydrogenation of CO₂ and H₂.

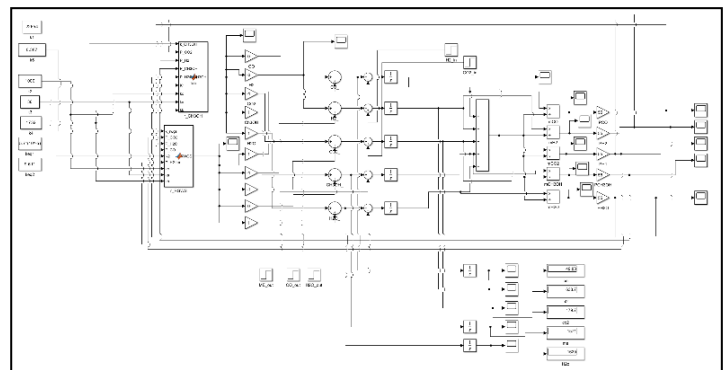


Figure 6: Methanol Plant

The simulation was run iteratively to get the input flow rates of both the reactants. For the H₂ to CO₂ ratio of 3:1 44kg of methanol was produced in 1.5 hours with flow rates of 7.2kg/hr (0.002kg/s) and 52kg/hr (0.014kg/s) for H₂ and CO₂ respectively with



CO₂ conversion efficiency of 90%. Therefore we need hydrogen production of 10.8kg/day for this 1.5 hour running of methanol plant.

5. PEM Water Electrolyser

[9] Reported that 39.4 kW/hr is required per kg production of hydrogen that implies that 425kWh energy is required for the desired amount of H₂ production i.e. 10.8kg/day. Converting 97L of water to hydrogen daily. Priority must be set to use the methane reforming for the methane from the biogas digester or use the power generated from the Biodiesel generator for Electrolysis process for hydrogen production, depending on the prices of methane and Electricity if it is to be bought for the Restaurant.

RESULTS AND DISCUSSION

The model provides a mathematical model to calculate the waste to energy and eventually cost savings. The cost saving depends on the location, availability of the products since the prices hugely depends on the country. In some places Gas is cheap while Electricity is expensive and vice versa. The Community produces 500kg waste cooking oil, 1500kg waste food and 25000L of waste water. The proposed model is capable of predicting conversion of this waste to 435kg of Biodiesel, enough methane for fuelling the community, Purification of the waste water, 10.8kg Hydrogen production, and production of 44kg of Methanol per day. This tells that every waste can be converted into green energy.

CONCLUSIONS

Keeping in point of view the increasing waste production and degradation of fossil fuels, sustainable systems should be focused for increasing the life of planet. Modelled is such a sustainable novel system that could be implemented keeping in view the advantages and limitations of such system. Further work can be done for location specific work for increasing the efficiency and cost effectiveness of the system.

REFERENCES

- [1] "Safeway Used Oil and Grease - Grease Trap Service in Saint Bernard, LA." Accessed: Dec. 05, 2023. [Online]. Available: <https://safewayusedoil.com/>
- [2] B. Y. López Zapata, M. Adam Medina, P. Álvarez Gutiérrez, H. Hernández De León, C. García Beltrán, and R. Meza Gordillo, "Different approaches for the dynamic model for the production of biodiesel," *Chem. Eng. Res. Des.*, vol. 132, pp. 536–550, Apr. 2018, doi: 10.1016/j.cherd.2018.01.048.
- [3] "Energies | Free Full-Text | Density Measurements of Waste Cooking Oil Biodiesel and Diesel Blends Over Extended Pressure and Temperature Ranges." Accessed: Dec. 05, 2023. [Online]. Available: <https://www.mdpi.com/1996-1073/11/5/1212>
- [4] "A Novel qNMR Application for the Quantification of Vegetable Oils Used as Adulterants in Essential Oils - PMC." Accessed: Dec. 05, 2023. [Online]. Available: <https://www.ncbi.nlm.nih.gov/pmc/articles/PMC8470556/>
- [5] T. Suthisripok and P. Semsamran, "The impact of biodiesel B100 on a small agricultural diesel engine," *Tribol. Int.*, vol. 128, pp. 397–409, Dec. 2018, doi: 10.1016/j.triboint.2018.07.042.
- [6] "Green Restaurant Association | Sustainability | Certification." Accessed: Dec. 05, 2023. [Online]. Available: <https://www.dinegreen.com/>
- [7] M. Saeed, S. Fawzy, and M. El-Saadawi, "Modeling and simulation of biogas-fueled power system," *Int. J. Green Energy*, vol. 16, no. 2, pp. 125–151, Jan. 2019, doi: 10.1080/15435075.2018.1549997.
- [8] F. Bezzo and F. Mantoan, "DESIGN AND SIMULATION OF HYDROGENATION PROCESSES FOR CO₂ CONVERSION TO C-1 CHEMICALS".
- [9] K. W. Harrison, R. Remick, and G. D. Martin, "Hydrogen Production: Fundamentals and Case Study Summaries; Preprint".

ICH2P14-OP197

A NET-ZERO EMISSION SYSTEM WITH BIOGAS-FED SOLID OXIDE FUEL CELL FOR HYDROGEN PRODUCTION TO ADVANCE SUSTAINABILITY IN THE TEXTILE INDUSTRY

*Baraka Abbas, Hooreen Ansari, Kabsha Zain, Wasifa Umer, Abeeha Fatima, Khurram Kamal, *Tahir A.H. Ratlamwala*

National University of Sciences & Technology, Karachi, Pakistan

*Corresponding author e-mail: ratlamwala.tahir@gmail.com

ABSTRACT

Increased dependency on non-renewable energy-dependent processes and vast industrialization has led to a drastic increase in the release of greenhouse gases, with very few active efforts to control these emissions. Notably, the textile industry stands as one of Pakistan's largest sectors, generating substantial environmental concerns. In response to these challenges, this study presents an innovative approach by introducing a novel solid oxide fuel cell multigeneration system powered by biomass waste derived from a textile industry and feeding all its energy generation back into that industry, hence achieving net zero emissions. This model aims to reduce waste by limiting greenhouse gas emissions as it uses a renewable energy source as fuel. A biogas purifier is added to the system for eliminating waste by using low-value outputs from the biogas digester. Hydrogen, electricity, and methanol for the textile industry are produced simultaneously by the system, with heat recovery through a simple Rankine cycle for improving efficiency. This multigeneration system has been modelled in MATLAB Simulink to obtain optimized results for the industry. Control systems such as level and feedback controllers have been employed in this model to ensure that best performance is achieved.

Keywords: Hydrogen, Solid Oxide Fuel Cell, Multigeneration, Rankine Cycle, Control Systems.

INTRODUCTION

The ever-increasing demand of textiles has led to a substantial increase in the waste produced by the textile industry. In Pakistan, the textile industry alone is estimated to generate 25 million tons of waste every year, 95% of which can be used as biomass [1]. Currently, the energy supply to operate the textile industry is solely reliant on fossil fuels, and there is a dire need to establish alternative, sustainable energy sources to power the industry. Waste biomass from textile industry, released in large quantities, can be reused to generate electricity and hydrogen.

From the textile industry, the sources of biomass are organic fibres (animal and plant fibres), synthetic fibres, cotton matter (cellulose fibres), synthetic polymers, wool, and sewage sludge [2]. In a study by Muhammad Noman et al [3] on textile waste management in Faisalabad, 850 textile-related industries of the city produced around 80,000 kg/day of solid waste. From this, 87.5% was organic textile waste that can be recycled to generate electricity in a fuel cell. Among the various types of fuel cells, solid oxide fuel cell (SOFC) has been studied for this system. The research by Wanderleiton et al [4] describes solid oxide fuel to have an input temperature be between 600 to 1000°C. The research discusses the two types of fuel injections into a solid oxide fuel cell; direct and indirect injection. In this study, a direct injection is studied, where natural gas can be directly fed into the fuel cell without the need to form a hydrogen-rich mixture. The introduction of PEM water electrolyser into the biogas purification system of the model proposed in this study aims to leverage its capabilities to enhance biogas purification efficiency, support hydrogen production for the methanol plant, and facilitate oxygen supply to the solid oxide fuel cell (SOFC). This integrated approach holds substantial promise in advancing sustainable energy solutions.

The goal is to utilize the waste outputs such that emissions from biomass decomposition are minimized. The two major waste outputs were found out to be carbon dioxide and water, as biogas consists of 50-70% methane and 25-45% carbon dioxide, each of which have been used to generate useful outputs such as hydrogen and methanol within the model. With a Steam Rankine Cycle operating by the exhaust heat of SOFC and powering a Polymer Electrolyte Membrane (PEM) Electrolyser, the model proposed in this system aims to have net-zero emissions by ensuring the release of useful outputs into the textile industry.

SYSTEM DESCRIPTION

Figure 1 on the next page is an overview of the model proposed in this study. Biomass is the input to this system, while hydrogen, methanol, electricity, and heating are the 5 major outputs of this multigeneration model, all of which are utilized in the textile industry. The main components of this system are SOFC stack, Steam Rankine Cycle, PEM electrolyser, and the methanol plant - all of which operate interdependently.

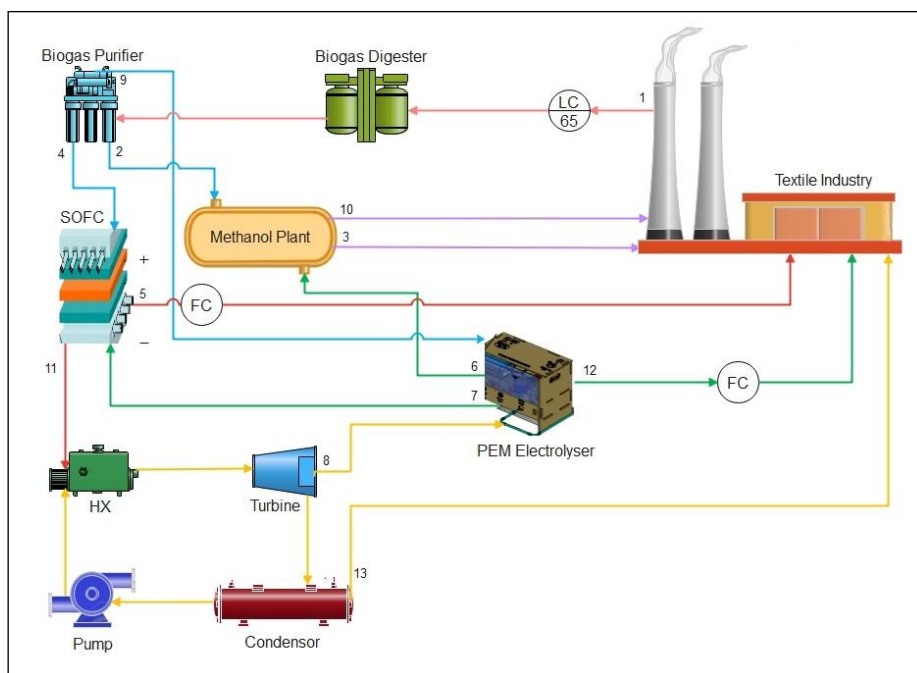


Fig. 1 Overview of the Proposed Model

Biomass from the textile industry at 1 is entering the biogas digester at a rate of 820 kg per day. In the digester tanks, this waste decomposes anaerobically into component-rich biogas and is sent to the biogas purifier where the biogas is purified into its components; namely - natural gas, carbon dioxide, and water. Natural gas at 4 is released at a rate of 0.656 m³ per day, and carbon dioxide at 2 is released at a rate of 328 kg per day. Natural gas from the biogas purifier enters the solid oxide fuel cell, where it powers the cell to produce electricity at 5; this electricity is used in the textile industry to reduce load requirements by powering processes like spinning, printing, weaving & providing lighting. Exhaust energy from the fuel cell at 11, released at a temperature of 600°C [5] is used to power a steam Rankine cycle. In this cycle, a microturbine is used to generate electricity at 8 to power the PEM Electrolyser. Waste heat from the condenser of the cycle at 13 is repurposed to be used in the textile industry for heat setting of fabrics, dye fixation, thermal bonding, and textile printing. Electricity from the turbine at 8 is used to operate the PEM Electrolyser; water released from the biogas purifier at 9 water reacts at the anode of the electrolyser to produce oxygen and hydrogen as outputs. The oxygen released at 7 is used as an input to the SOFC stack while the hydrogen produced by the electrolyser is used in the methanol plant at 6; and in the textile industry at 12, where it is used in polyester production, desizing, hydrogen peroxide production, and pH adjustment. Hydrogen at 6 enters the methanol plant where it is made to react with carbon dioxide at 2, and eventually produce methanol at 3. The methanol produced is used in the textile industry as a base material to make synthetic fibres, and as a solvent in dyeing and printing of textiles. Heat at 10 is also produced as an output from the methanol plant and is utilized within the textile industry for processes mentioned above. Various control systems such as level and feedback controllers have been employed in the system to monitor the inputs and outputs of this model.

ANALYSIS OF HYDROGEN PRODUCTION

The amount of hydrogen produced in this model has been determined by first considering the amount of textile waste available to run the cycle. It has been gathered that 850 textile-related industries from the city of Faisalabad produce 79,4209 kilograms per day of solid waste on average [3]. From this, 87.51% (695,189 kg/day) is organic textile waste. Hence it can be concluded that one textile factory produces approximately 820 kg of biomass per day. This waste will be considered as the input of the proposed system in this paper. Furthermore, C. Sundar Raj et al [6] establishes that 5 kilograms of biomass can generate 0.2 m³ of biogas in 50 days. Using these results, the amount of natural gas produced by 1 kilogram of biomass per day is considered to be 0.008 m³.

Modelling of Methanol Plant

The methanol plant operates with carbon dioxide and hydrogen as its inputs. The amount of carbon dioxide released at 2 has been figured out by assuming that 0.4 kg of carbon dioxide is released when 1 kg of biomass from the textile

industry is burnt [6]. Hence 328 kilograms of carbon dioxide are released when 820 kilograms of biomass decomposes. Molar equation has been used to calculate the moles of carbon dioxide and hydrogen from the relation in equation 1, which are 7454.54 mol and 22363.636 mol respectively. Mass of hydrogen produced per day is thus 44.73 kilograms per day. Hence using equation 1 and the molar equation, the mass of methanol produced is 238.84 kilograms per day.



Modelling of PEM Electrolyser

The amount of hydrogen used in the methanol plant determines how much water is consumed in the Electrolyser to generate the required hydrogen output. This is done using the relation in equation 2, which gives moles of water as 44,727.272, and the corresponding volume of water as 0.805 m³ per day. Required electricity input to the Electrolyser is assumed to be 12.28 kWh [55]. The electrolyser has been modelled on MATLAB Simulink (Figure 2). Temperature setpoint was assumed to be 60°C.

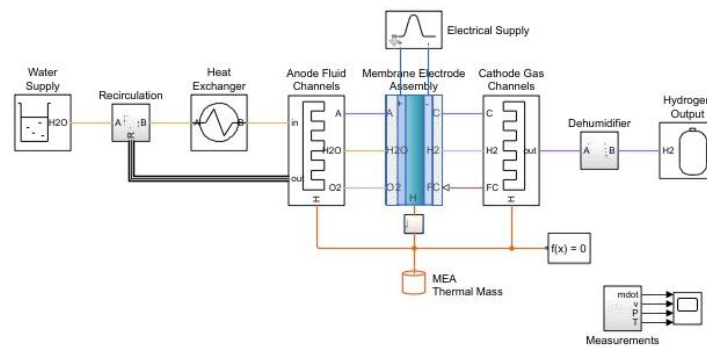
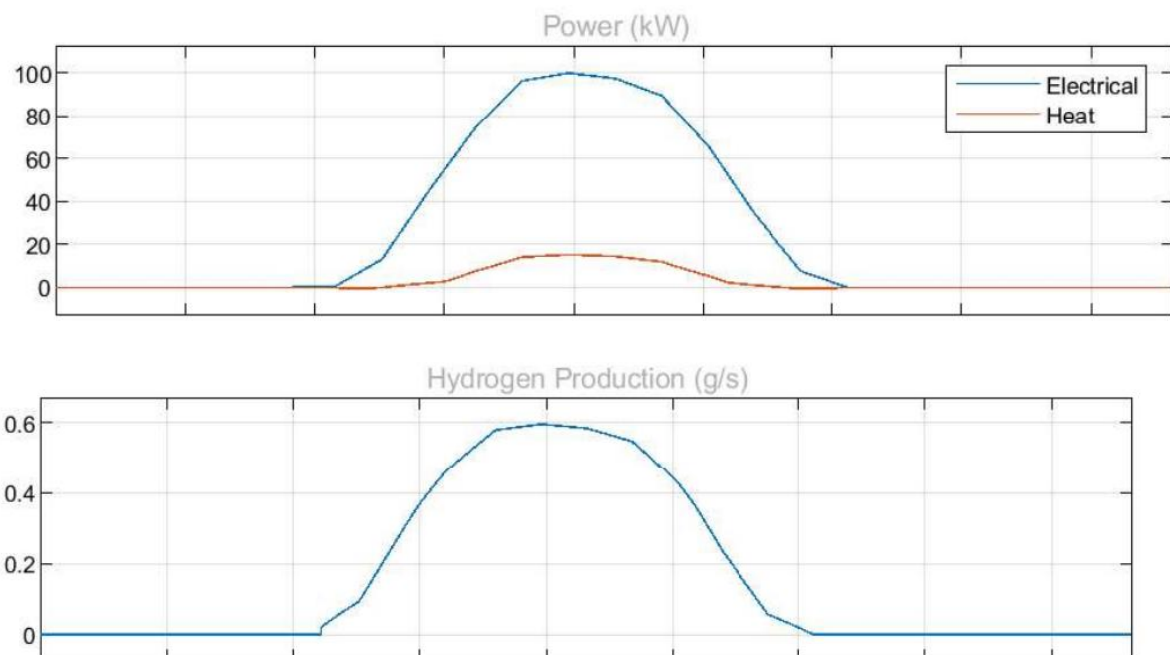


Fig. 3 Simulink Model of PEM Electrolyser

CONCLUSION

It has been concluded by the modelling of PEM Electrolyser that with power varying from 20kW to 100kW (Figure 3), hydrogen production can reach the desired output value of 0.6 g/s i.e. 44.7 kilograms of hydrogen per day for the methanol plant.





REFERENCES

1. INP (2019, April 14). *Fashion industry leading to environmental pollution, says business leader*. Profit <https://rb.gy/6jxehq>
2. Irfan, M., Zhao, Z., Panjwani, M.K., Mangi, F.H., Li, H., Jan, A., Ahmad, M., Rehman, A. (2019). Assessing the energy dynamics of Pakistan: Prospects of biomass energy. *Energy Reports*, 6, 80-93. <https://doi.org/10.1016/j.egy.2019.11.161>
3. Noman, M., Batool, S.A., Chaudhary, M.N., (2013). Economic and employment potential in textile waste management of Faisalabad. *Waste Management & Research: The Journal for a Sustainable Circular Economy*, 31(5), 485-493. <https://doi.org/10.1177/0734242X12474711>
4. Cardoso, W., Felice, R., Baptista, R.C., (2021). Mathematical modeling of a solid oxide fuel cell operating on biogas. *Bulletin of Electrical Engineering and Informatics*, 10(6), 2929-2942. <https://doi.org/10.11591/eei.v10i6.3253>
5. (2020). *Solid Oxide Fuel Cell: Solid oxide fuel cell (SOFC) is interesting device for electricity generation of large scale*. ScienceDirect <https://www.sciencedirect.com/topics/chemistry/solid-oxide-fuel-cell>
6. Raj, S.C., Arul, S., Sendilvelan, S., Saravanan, C.G., (2009). Bio Gas from Textile Cotton Waste - An Alternate Fuel for Diesel Engines. *The Open Waste Management Journal*, 2, 1-5. <http://dx.doi.org/10.2174/1876400200902010001>
7. Fragiaco, P., Genovese, M., (2020). Numerical simulations of the energy performance of a PEM water electrolysis based high-pressure hydrogen refueling station. *International Journal of Hydrogen Energy*, 45(51), 27457-27470. <https://doi.org/10.1016/j.ijhydene.2020.07.007>

14th INTERNATIONAL CONFERENCE ON HYDROGEN PRODUCTION (ICH2P-2023)



December 19 – 21, 2023
Education City, Doha, Qatar

POSTER PRESENTATIONS



ICH2P14-PP008

LONG-TERM ASSESSMENT OF HYDROGEN TECHNOLOGY DEPLOYMENT FOR LARGE SCALE DECARBONISATION OF POWER PRODUCTION

**Kamran Khammadov, Damian Flynn, Eoin Syron*

University College Dublin, College of Engineering and Architecture, School of Chemical and Bioprocess Engineering, Belfield, Dublin, Ireland

*Corresponding author e-mail: kamran.khammadov@ucdconnect.ie

ABSTRACT

At times of low renewable shares in the electrical grid, natural gas is the fuel of choice for power production in many countries. In a bid to further reduce carbon emissions, hydrogen from electrolysis and low-carbon production is an alternative for power production. While low-carbon hydrogen is more competitive in current market conditions, it is essential to take a long-term approach considering the impact of the potential influencing factors and carbon policies. Therefore, this study aims to evaluate the impact of gas prices on the future deployment of hydrogen production technologies to achieve strict emission targets. A cost optimisation model of a power system was developed based on electrical supply-demand balancing and gas balancing. Electricity generation from wind and solar technologies, gas turbines and fuel cells were included in the model. Hydrogen and batteries were the selected energy storage options. The sources of hydrogen were from electrolyzers and the purchase of low-carbon hydrogen. Reducing the gas price from 50 to 35 EUR/MWh, reduced total electrolyser installations from 8 GW to 5.3 GW between 2023 and 2050. However, it did not impact short and mid-terms installations. The levelised electricity cost trends were influenced significantly, while the overall cost reduced by 6%.

Keywords: green hydrogen, electrolyser, decarbonisation, renewable energy, renewable gas.

INTRODUCTION

Transitioning from hydrocarbons to renewable sources for electrical generation is an essential element of global efforts to reduce Greenhouse Gas emissions. Global electricity demand is expected to increase approximately twice of the current level[1] in the upcoming decades and Variable Renewable Energy (VRE) such as wind and solar are the key technologies for decarbonized electricity generation[2]. Existing electrical grids mostly rely on conventional power production plants. Increased VRE shares create challenges for grid operation and energy availability[3]. Renewable energy storage via green hydrogen technologies is technically capable to address the challenges of VRE while achieving decarbonization[4, 5]. On the other hand, green hydrogen technologies are not competitive in the current market conditions. Blue hydrogen from fossil fuel usage with carbon capture and storage technologies (SMR-CCS) provides 2-3 times lower hydrogen costs than from electrolysis[6]. The major cost contributors for hydrogen production via electrolysis are capital cost and electricity price. A study on power-to-gas technology in decentralized energy systems concluded that higher hydrogen demand and VRE availability led to constant H₂ production and a lower levelized cost of H₂ (LCOH) [7]. However, it was still not an economic fuel under current market conditions. Cost optimization of the energy system infrastructures is essential but not sufficient to deploy the systems today. Moreover, an assessment of energy policies to support green hydrogen production using a financial model identified that current policies neither stimulate green hydrogen production nor discourage conventional investments [8]. On the contrary, there are advantages of green hydrogen production compared to conventional technologies. Electrolyser and VRE technology costs are expected to decrease further in the coming years to a lower cost base than over conventional methods[9-11]. Technology advancement in electrolyzers including increasing efficiency is another supporting factor[11]. At the same time, there are ambitious net zero emission goals for the electricity sector, which will drive the demand for the installation of wind, solar and hydrogen technologies [2]. To sum up, there are a number of factors that point toward a commercial future for the green hydrogen technologies, but under what circumstances and conditions is unclear. For example, natural gas price is one of the parameters that has a direct impact on price of hydrogen and electricity generation from fossil fuels. The focus here is to evaluate the potential influence of gas price variations on the long-term technology deployment for hydrogen production via electrolyzers. The study results are expected to add value for investment decisions and policies as part of a decarbonisation pathway.

METHODOLOGY AND MODELING

A mathematical model is representative of an energy system with common features of energy system optimization models in the literature [12]. The model is built for a national coverage in a single node. Overall timeline in the model is between 2023 and 2050 to represent a transition from current system setup to the net-zero emissions in 2050.

Model Components and Balances

The major constraint on the model is the supply-demand balance for the electricity represented as per Eq. (1). Time resolution is combination of hourly (h) balance between power supply and demand and yearly (y) deployment of the various technology options. Renewable and conventional power production technologies such as wind, solar and gas turbine were included in the model together with an option to import electricity within the limits of the interconnectors. Fuel cell deployment was available to utilise hydrogen in power production. Moreover, conventional gas turbines were assumed to burn natural gas with a hydrogen blend up to 5% by volume[13]. Existing gas networks were assumed to handle certain amounts of hydrogen injection without significant changes in operational parameters[14]. Hydrogen (*HSS*) and battery systems (*BESS*) were introduced to take advantages energy storage. However, optimisation of the storage system capacities was not part of the study. Electrolysers were included in the electricity demand side and H₂ production was limited to the total deployed electrolyser size up to a relevant year. Energy loss for H₂ compression (*HSS Comp*) was added to the demand side. The potential power output from VRE sources was assessed based on wind speed and sunlight. Consequently, the supply side in the power balance equation may exceed the demand side, resulting in the dispatch of excess energy or the possibility of electricity export. The model operates on cost optimization without incorporating any revenue streams, therefore electricity exports were excluded from the power balance equation.

$$VRE_{y,h} + GT_{y,h} + FC_{y,h} + BESS_{y,h} + Electricity\ Import \geq User\ Demand_{y,h} + Electrolyser_{y,h} + HSS\ Comp_{y,h} \quad (1)$$

Gas balances were established for natural gas and hydrogen in energy terms. Natural gas used in gas turbines in an hourly timeframe is summed to an annual imported natural gas amount. Two separate sources were available for hydrogen; production via electrolyser deployment (H₂ prod) and imported blue hydrogen (H₂ imp). Hydrogen sent to storage (H₂ to strg) and hydrogen used from the storage (H₂ from strg) are also part of the gas balance. Maximum limit of stored hydrogen in any time was limited to the assigned HSS size per the given year. Hydrogen gas balance is represented in the Eq. (2).

$$H_2\ imp_{y,h} + H_2\ prod_{y,h} + H_2\ from\ strg_{y,h} = H_2\ to\ GT_{y,h} + H_2\ to\ FC_{y,h} + H_2\ to\ strg_{y,h} \quad (2)$$

The model components and interconnection between the gas and electrical balances were described in the Fig. 1. Mathematical models for wind turbines, solar panels, gas turbines, fuel cells, electrolysers and energy storage components are aligned with the common correlations used in the literature[15, 16]. Input data for hourly wind speed, and solar irradiance is based on the data recorded in Ireland in 2022 [17]. Electricity demands were assumed to be according to Ireland current data and electricity outlook [18, 19].

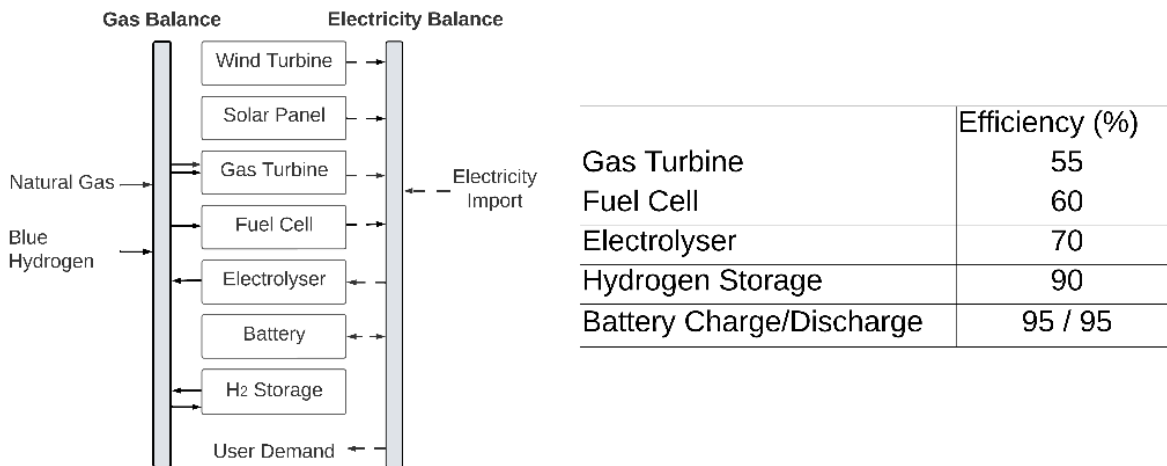


Fig. 1. System Representation and Efficiency parameters

One of the major constraints in the model was yearly carbon emission limit which was based on the Ireland national targets for electricity sector[20]. Emissions factor to burn natural gas was assumed to be 202.9 gCO₂/kWh for gas turbine power production and electricity imports[21]. Moreover, carbon emission penalty was applied with initial value of 47.5 EUR/tCO₂ and increased every year up to 150 EUR/tCO₂ by 2050. Yearly carbon emissions limits and carbon penalties represents ambitious targets for early years as demonstrated in Fig. 2.

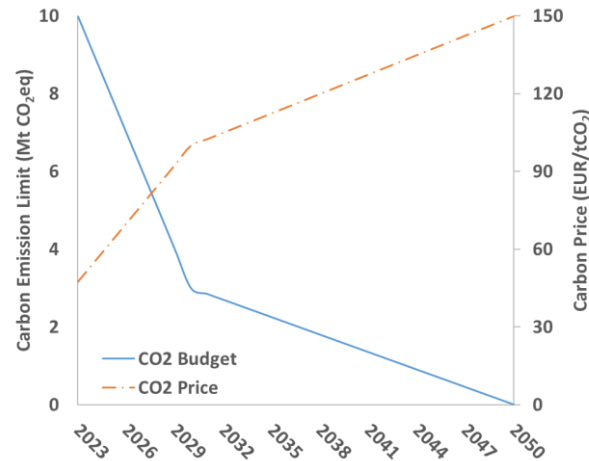


Fig. 2. Projected reduction in carbon emission limit and increase in carbon price to achieve net zero by 2050.

Model Objective

A cost optimisation methodology was used with a single objective function represented in Eq. (3). Net Present Cost (NPC) was calculated including investments, operation and maintenance and replacement costs for technology, carbon emission cost, electricity imports and gas purchases. Remaining lifetime value of the installed technologies at the end of the timeline was subtracted from the overall cost.

$$Net\ Present\ Cost = \sum_{y=2023}^{2050} (Technology\ Cost_y + Fuel\ Cost_y + Carbon\ Cost_y) - Remaining\ Value_{2050} \quad (3)$$

A Mixed Integer Linear Model (MILP) has been developed in a Python Pyomo package[22] utilising a Gurobi solver[23].

Investigated Case Scenarios

The energy system model has been employed to investigate 4 scenarios each with different natural gas price conditions according to European Union gas prices data[24]. A high value of 50 EUR/MWh represents current gas prices while a low value of 35 EUR/MWh was used, based on gas price in prior to extreme price fluctuations. Natural gas price was set to a constant value for each case. The difference in natural gas prices between case 1 (high) and case 4 (low) implies a substantial reduction in price that will enable the examination of potential impacts on results. Purchased hydrogen gas and electricity prices depend on natural gas prices. Table 1 summarizes the complete list of the investigated cases.

Table 1. Summary of the investigated gas price parameter

	Natural Gas Price (EUR/MWh)	SMR-CCS Hydrogen Price (EUR/MWh)	Electricity Import Price (EUR/MWh)
Case 1	50	105 - 102	105
Case 2	45	98 - 95	96
Case 3	40	91 - 88	87
Case 4	35	84 - 80	78

Initial System Conditions

Ireland power production system data has been used as a basis to assign realistic values for user demand, wind installed capacity, interconnector capacity and battery storage systems size [19]. Share of the wind energy at the starting year was 37%. No solar panel capacity was assumed initially. Electricity import was limited to 1000 MW which is equal to 14% of the maximum hourly demand. Interconnector capacity was increased in the subsequent years of the model according to the announced projects[18]. Fossil fuel power production from coal/peat/oil were not part of the model. The system components in the starting year are described in the Table 2. Initial power production CO₂ intensity was 220 gCO₂/kWh.

Table 2. Initial System Summary

Electricity Demand (yearly)	39 TWh
Peak Electricity Demand	6979 MW
Natural Gas Consumption (yearly)	45 TWh
Wind Installed Capacity	5878 MW
BESS Capacity (Size)	2000 MWh (500 MW)

Limitations of the Model

The model has several limitations that must be considered while interpreting the results and conclusions. In this study, fossil fuel used for the blue hydrogen production was not part of the gas balancing and was not considered in emissions. Moreover, power production in the model does not involve the electrical grid operational requirements which are expected to impact any electrical grid modeling. The described energy system refers to Irish grid system but does not represent it.

RESULTS AND DISCUSSION

Impact of the gas prices on the cost optimal decarbonisation pathways for the renewable and hydrogen production technology deployment have been analysed. Results for overall system cost, electrolyzers deployment, hydrogen production and timeline of the optimal electrolyser deployment are discussed in this section. The final system component capacities are summarised in the Table 3 for case 1 and 4. It was observed that low gas prices led to a reduction in the wind and solar technology installation by ~15%.

Table 3. Final System Summary

	Case 1	Case 4
Wind Installed Capacity	21.4 GW	18.2 GW
Solar Installed Capacity	33.2 GW	28.9 GW
Electrolyser Capacity	8 GW	5.3 GW
Fuel Cell Capacity	8.3 GW	8.4 GW
HSS Capacity	2.4 TWh	2.4 TWh
BESS Capacity	20 GWh	20 GWh

Impact on electrolyser deployment and hydrogen production

Results showed that the optimal timeline for the majority of the electrolyser, wind and solar technology installations is between 2030 and 2040 for all investigated case. Main influencing factor was strict carbon restrictions rather than the gas prices. There was demand for hydrogen by 2030, which was met by blue hydrogen purchases. Electrolyser installation became commercially attractive only after the high VRE availability and electrolyser investment cost reduced by 35%. High gas price case led to more electrolyser deployment (~8 GW) than the low gas price (~5.3 GW) case by 2050 as summarised in Fig 3. The difference in the electrolyser capacity installations was only observed after 2040. Lower blue hydrogen prices promoted the hydrogen purchases rather than electrolyser production in the case 4. It has been further discussed together with the hydrogen production trends plotted in the Fig. 4.

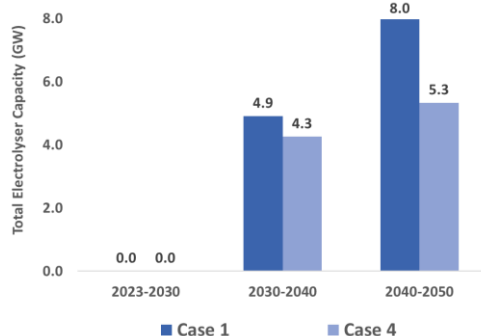


Fig. 3. Total electrolyser capacity installations

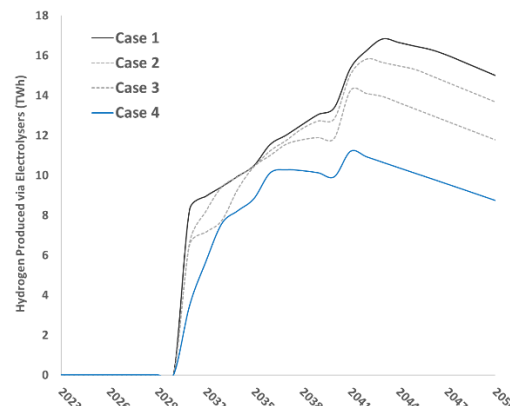


Fig. 4. H2 production trend over the timeline

The overall hydrogen consumption increased by 18% in low gas price case. On the other hand, overall hydrogen production via electrolysis declined by 46%. Lower gas prices led to double the low-carbon hydrogen purchases in comparison to the high gas price case. The results indicated that the gas price change has a significant impact on source of the hydrogen, especially for the last 10 years of the timeline. Moreover, hydrogen production was decreased after 2040 for all the cases. It was observed because of lower electrolyser cost reduction and lack of new VRE capacity additions while electricity demand continues to increase. There was not any significant change in the overall and yearly natural gas consumption between the Case 1 and Case 4 due to being the cheapest fuel option. Although the fuel cell efficiency was slightly higher than gas turbines, additional cost of hydrogen production prevent the significant change in the natural gas consumption.

Impact on system cost

Overall system net present cost includes capital investments for any technology installations, operational and maintenance costs for the installed technology, fuel and electricity purchases and carbon emission costs. It has been observed that there was 6% decrease in overall net present cost between the high and low gas price scenarios while the gas price decreased by 30%. Levelised cost of the electricity (LCOE) has been used to compare the high and low gas price cases in a yearly timeframe and plotted in Fig. 5 for the investigated cases. Obtained results are indicating that the natural gas price has a significant impact on investments in early stages of the energy systems transition period. Electricity demands were increased by 37% until 2030 and by 67% until 2040 where the majority of the technology investments are done in this period. Therefore, high gas prices added significant installation cost into power production in the early timeline to achieve the carbon targets. Lower gas prices resulted in less discrepancy in amount of investments in the near and mid-term. After 2040, there is not extreme differences in LCOE values since the costs are mostly consisted of fuel prices rather than capital investments.

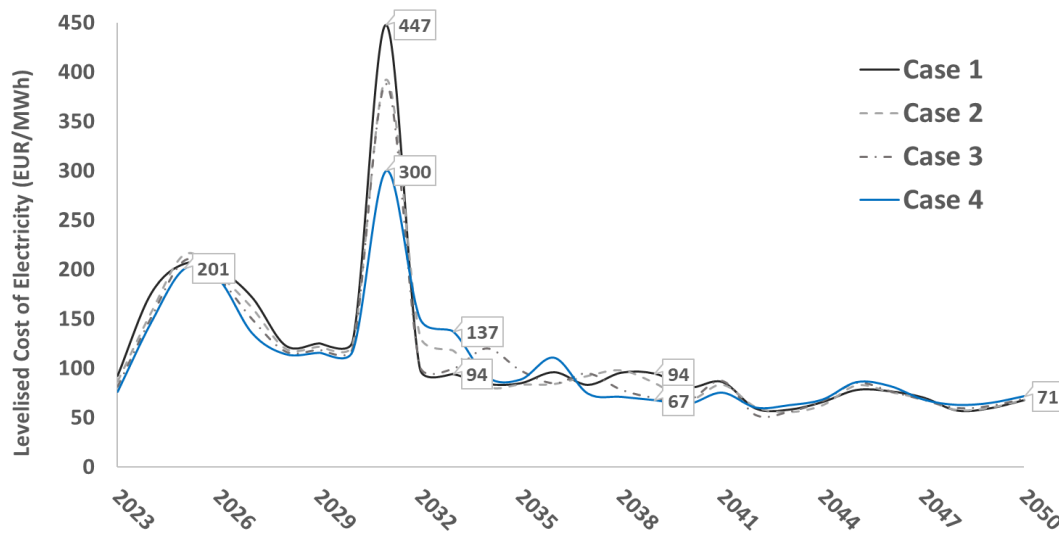


Fig. 5. Levelised Cost of Electricity for Case 1 to Case 4

CONCLUSIONS

Decarbonisation of the power production demands a significant transition in energy systems. Integration of the hydrogen into the energy systems has a potential to support this process. This study aims to investigate a transition timeline and to assess the impact of high and low gas prices on hydrogen production technology integration. The conclusion from the study was that natural gas price did not have significant impact on the electrolyser installation timeline. The main influence on the timeline was from VRE availability which is driven by carbon emissions targets and higher level of cost reduction in electrolysers in the early years. However, low natural gas price has a significant reducing impact on the overall size of the electrolyser installation in the later periods of the energy systems transition. This may suggest that uncertainty in the future gas prices should not impact the investment decisions for electrolysers in mid-term if they are supported by VRE availability. Natural gas price reduction did not impact the overall hydrogen consumption negatively but slowed down hydrogen production by electrolysis. The assumption that blue hydrogen does not lead to carbon emissions disables the impact of carbon restriction on hydrogen purchases. Hydrogen production via electrolyser is also negatively impacted from the lack of new VRE additions in the later term for all gas price cases. The overall cost of the electricity was reduced with lower gas prices which provides advantage in terms of LCOE. Moreover, lower gas prices lead to smoother LCOE fluctuations than higher gas prices. Further analysis of the obtained results might result in deeper findings on potential impact of gas prices.

Given the investigated natural gas prices and discussed results, natural gas price has a significant impact on hydrogen technology deployment in overall the decarbonisation pathway. Potential reduction of the gas prices does not have negative impact on short and mid-term investment decision for hydrogen technology. On the contrary, it may result in more controlled fluctuations for levelised cost of electricity in the early years of the energy transition period.

ACKNOWLEDGEMENT

This work was financially supported by Next Generation Energy Systems (NexSys) research programme funded by Science Foundation Ireland's (SFI) Strategic Partnership Programme.

REFERENCES

1. IEA. 2023. World Energy Outlook 2023. IEA: Paris.
2. IEA. 2021. Net Zero by 2050. Paris.
3. Nordström H, Söder L, Flynn D, Matevosyan J, Kiviluoma J, Holttinen H, et al. 2023. Strategies for Continuous Balancing in Future Power Systems with High Wind and Solar Shares. *Energies* 16(14):5249.
4. Egeland-Eriksen, T., A. Hajizadeh, and S. Sartori. 2021. Hydrogen-based systems for integration of renewable energy in power systems: Achievements and perspectives. *International Journal of Hydrogen Energy* 46(63):31963-31983.
5. Vidas, L. and R. Castro. 2021. Recent Developments on Hydrogen Production Technologies: State-of-the-Art Review with a Focus on Green-Electrolysis. *Applied Sciences* 11(23):11363.
6. IEA. 2023. Global Hydrogen Review 2023. Paris.
7. Jarosch C, Jahnke P, Giehl J, and Himmel J. 2022. Modelling Decentralized Hydrogen Systems: Lessons Learned and Challenges from German Regions. *Energies* 15(4):1322.
8. Joy, O. and J. Al-Zaili. 2021. On effectiveness of current energy policy instruments to make H₂ production projects financially viable for developers: Case of the UK. *International Journal of Hydrogen Energy* 46(65): 32735-32749.
9. National Renewable Energy Laboratory. 2023. 2023 Annual Technology Baseline [Internet] Available from: <https://atb.nrel.gov/>. Accessed on November 25, 2023
10. IEA. 2019. The Future of Hydrogen. Paris.
11. IRENA. 2020. Green Hydrogen Cost Reduction: Scaling up Electrolysers to Meet the 1.5°C Climate Goal. Abu Dhabi.
12. Plazas-Niño, F.A., N.R. Ortiz-Pimiento, and E.G. Montes-Páez. 2022. National energy system optimization modelling for decarbonization pathways analysis: A systematic literature review. *Renewable and Sustainable Energy Reviews* 162:112406.
13. Lorenczik S, Kim S, Wanner B, Bermudez Menendez JM, Remme U, Hasegawa T, et al. 2022. Projected costs of generating electricity-2020 edition. Organisation for Economic Co-Operation and Development.
14. Ekhtiari, A., D. Flynn, and E. Syron. 2022. Green Hydrogen Blends with Natural Gas and Its Impact on the Gas Network. *Hydrogen* 3(4):402-417.
15. Jia K, Liu C, Li S, Jiang D. 2023. Modeling and optimization of a hybrid renewable energy system integrated with gas turbine and energy storage. *Energy Conversion and Management* 279:116763.
16. Zhang Y, Hua QS, Sun L, and Liu Q. 2022. Life Cycle Optimization of Renewable Energy Systems Configuration with Hybrid Battery/Hydrogen Storage: A Comparative Study. *Journal of Energy Storage* 30:101470.
17. MetÉireann. Historical Data. Available from: <https://www.met.ie/climate/available-data/historical-data>. Accessed on October 10, 2023.
18. EirGridGroup. 2022. Ireland Capacity Outlook.
19. EirGridGroup. 2023. System and Renewable Data
20. Government of Ireland. 2022. Climate Action Plan 2023. Department of the Environment, Climate and Communications.
21. SEAI. 2023. SEAI-conversion-and-emission-factors. Sustainable Energy Authority of Ireland.
22. Bynum, M.L.a.H., Gabriel A. and Hart, William E. and Laird, Carl D. and Nicholson, Bethany L. and Sirola, John D. and Watson, Jean-Paul and Woodruff, David L.. 2021. Pyomo--optimization modeling in python. Third ed. Vol. 67. Springer Science & Business Media.
23. Gurobi Optimization LLC. 2023. Gurobi Optimizer Reference Manual.
24. Eurostat, E.C. 2023. Gas prices by type of user. Available from: <http://data.europa.eu/88u/dataset/m836egkc7u1woixzprv7a> Accessed on November 16, 2023.

ICH2P14-PP011
**FIELD INVESTIGATION OF GREEN HYDROGEN PRODUCTION THROUGH THE PEM
ELECTROLYZER IN OUARGLA CITY**

**Ahmed Zouhir Kouache, Ahmed Djafour, Khaled Mohammed Said Benzaoui, Abdelmoumen Gougui*

¹Faculté des Sciences Appliquées, Laboratoire LAGE, Univ Ouargla, Ouargla 30 000, Algeria

*Corresponding author e-mail: kouache.ahmed@univ-ouargla.dz

ABSTRACT

The search for new fuel types to replace fossil fuels has intensified in recent decades within the energy transition context. Moreover, green hydrogen has been classified as one of the most prominent environmental solutions to reduce greenhouse gas emissions due to its many advantages, especially cleanliness and availability, where it is produced cleanly by electrolysis of water using renewable energy sources. Therefore, this paper presents an experimental study of solar hydrogen production by indirect coupling between photovoltaic modules and PEM electrolyzer HG-60 in the Ouargla region, Algeria. In the first part, we present an experimental investigation of the system components' performance under the coupling conditions; however, we found a decrease in the adaptation efficiency between the PV generator and the electrolyzer. Moreover, we present in the second part a coupling via an MPPT controller of the system by developing a program in the MATLAB environment for optimal power transfer to the electrolyzer to determine the system energy potential and the hydrogen volume produced in the actual situation of the system and under the same experimental conditions. The most notable results indicated that the hydrogen production in the experiment phase was 10.88 to 40.5 l/h, resulting in approximately 160,531 liters of hydrogen. However, the MPPT simulation results showed that the production reached 20.28 to 49.72, and the volume of hydrogen was 209 liters during the same experiment periods from 09:47 to 16:30.

Keywords: Hydrogen production, Photovoltaic, PEM electrolyzer, System adaptation, Ouargla region.

INTRODUCTION

Alternative energy sources must be found as quickly as possible, given the depletion of natural resources and the harmful effects of greenhouse gas emissions on the environment resulting from the combustion of fossil fuels. Air pollution is one of the world's major environmental concerns [1]. As a result, exploring new energy sources, techniques for their conversion, and strategies for their use have become key research topics. Renewability and environmental friendliness are essential aspects to consider when considering energy alternatives. In addition to efficient production techniques, efficient storage techniques must also be implemented [2]. Moreover, hydrogen can be an alternative fossil energy source and play an essential role in the energy transition. It can be used as an input for fuel cells to generate electrical energy without greenhouse gas emissions. It can also be utilized in further applications, including mineral processing, petrochemicals, and ammonia [3]. In fact, in nature, this element is found almost systematically with other atoms, such as oxygen in the case of water or carbon in the case of natural gas. Hydrogen has certain physicochemical properties that are useful from a biological point of view. It is a very light gas (density = 0.09 kg/m³, at 0 °C) and has a very high calorific value (33.3 kW/kg, versus about 14 kW/kg for methane; PCI data). It is odorless, colorless, and non-polluting. In the current energy context, hydrogen's physical and environmental properties make it a high-quality energy carrier with electricity [4]. Although hydrogen is the most abundant element in the universe, this component does not occur naturally on Earth. However, it is bound to other atoms similar to (C, O, N), so it has to be created by extracting the H atom from compounds that contain it - mainly water, biological species, and fossil fuels. Hydrogen is the only element that can be produced from the most abundant compound on Earth, water, using various renewable energy sources and different technologies. Recent statistics show that hydrogen production from fossil fuels is the most widespread today, but it cannot be a long-term solution due to the limited lifespan of these fuels. So, it can only constitute a medium-term solution. In addition, this technology generates carbon dioxide. Currently, 48% of the world's hydrogen is produced from natural gas (grey hydrogen), 30% from petroleum, 18% from coal (brown hydrogen), and the remaining 4% comes from the electrolysis of water using renewable energy sources (green hydrogen). As hydrogen technology continues to be researched and developed, it can play an important role in creating a more sustainable and environmentally friendly future. Consequently, the method of hydrogen production is a crucial area of research that should be explored to achieve high hydrogen yields with greater efficiency. Each hydrogen production method has its advantages and drawbacks. Choosing the right procedure depends on energy efficiency, cost, environmental impact, and feedstock availability. Some of these are partial oxidation [5], auto thermal reforming [6], steam methane reforming (SMR) [7], ammonia decomposition [8], biohydrogen, electrolysis [9], biomass gasification [10], photobiological water splitting, plasma

reforming [11], and photoelectrochemical water splitting [12] [13]. Hydrogen can also be stored in three diverse forms, depending on its application, pressure, temperature, and storage volume: (1) compressed in high-pressure gas cylinders [14], (2) stored in liquid form [15], (3) stored in solid form in metallic and non-metallic hydrides [16]. Furthermore, as part of the energy transition project to green hydrogen, in 2020, the Algerian government committed to integrating hydrogen into energy exports by 2030. A roadmap has also been drawn up between Algeria's Sonatrach and Italy's Eni for a joint evaluation of the techno-economic feasibility of a pilot project to generate hydrogen from renewable energies untapped in Algeria, such as solar and wind power [17]. Based on the above, much research has been published about the possibilities of hydrogen production in Algeria. Gougui et al. [18] studied a direct and indirect photovoltaic/water electrolysis system in the Ouargla region. Boudries et al. [19] evaluated the potential for hydrogen energy production using a concentrator photovoltaic (CPV) system for different sites in Algeria. Ghribi et al. [20] studied the technical potential for hydrogen production from a photovoltaic/PEM electrolyzer system. They estimated the amount of hydrogen produced by this system at six different sites in Algeria, using global hourly solar radiation on the horizontal plane and ambient temperature. From the literature in Ouargla, there have been very few field investigations about green hydrogen production. Therefore, the main objective of this article is an experimental study and analysis of the hydrogen production system through the electrolysis of water from a photovoltaic source in the Electrical Engineering Laboratory of the University of Ouargla to know the production capabilities of the system and the potential of the region. For this purpose, some background information and highlights of the importance of the work is provided. Following that, the experimental system description of hydrogen production is presented. Then, the mathematical modeling is offered. After that, the results and discussion are illustrated. Finally, conclusions and future work are provided.

EXPERIMENTAL SYSTEM DESCRIPTION

This experimental part was done in May month. Our installation consists of two photovoltaic modules of polycrystalline types of 220 W mounted in the LAGE laboratory, a PEM electrolyzer (HG-60) of 60 l/h. Moreover, a power management unit includes a DC/DC solar regulator (without MPPT), a DC/AC inverter, two 12 V 55 Ah lead-acid batteries, and a data acquisition unit. The hydrogen delivered during our experiment is collected in special hydrogen tanks. The experimental prototype is presented in Fig.1.



Fig. 1. Hydrogen system components

MATHEMATICAL MODELING

The photovoltaic single diode model equivalent output current is represented in Eq. (1):

$$I = I_{ph} - I_0 \times \left[e^{\left(\frac{V+R_S \times I}{n \times V_T} \right)} - 1 \right] - \left[\frac{V+R_S \times I}{R_p} \right] \quad (1)$$

Where I_{ph} is the photo-current, R_s and R_p represent the series and parallel resistances (Ω), n represents the diode ideality factor, and V_T represents the thermal voltage (V).

The following relations give the adaptation efficiency between the PV generator and the electrolyzer

$$\eta_{adp} = \frac{V \times I}{V_{opt} \times I_{opt}} \quad (2)$$

Where V is the coupling voltage (V), I is the coupling current (A), V_{opt} represents the optimum voltage (V), and I_{opt} represents the optimum current (A).

RESULTS AND DISCUSSION

A set of measurements was taken during May, from 09:47 to 16:30; the results of solar radiation profile, outdoor temperature, and panel temperature are shown in Fig. 2.

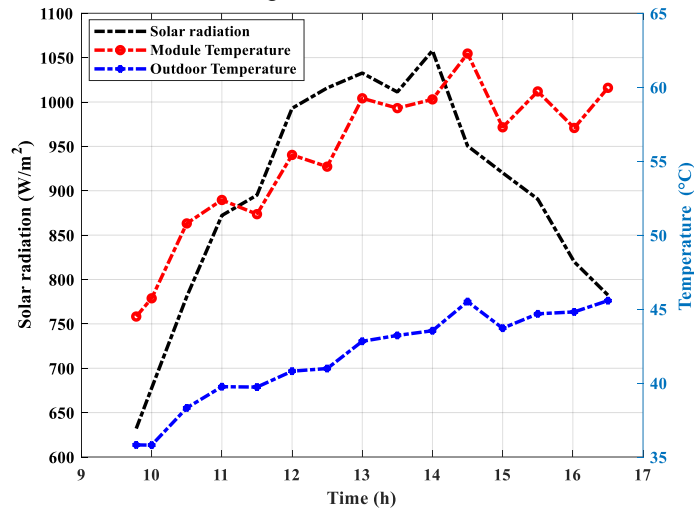


Fig. 2. Solar radiation, outdoor temperature, and panel temperature

After the experimental process and based on the capabilities of the system, we recorded a fluctuation and decrease in the electrical energy produced by the system, which became more apparent in some peak periods due to the lack of a maximum power point tracking system in the experimental prototype, as the maximum energy of the PV generator was not exploited at every moment, and this is confirmed by Fig. 3. Moreover, after the calculation proses, we found that the adaptation efficiency varied from 51.83 to 93.42 % and that confirmed there is a loss of energy. Furthermore, the decrease in the power of the PV generator is due to the decrease in current due to some unintentional partial shading on the PV modules. In addition, the rise in temperature also contributes to a decrease in current values. Therefore, the electricity available to operate the system and electrolyzer to produce hydrogen was less than expected. That also affected the amount of energy stored in the batteries, and it served as a second source in all experiment periods, as shown in Fig. 4 (a).

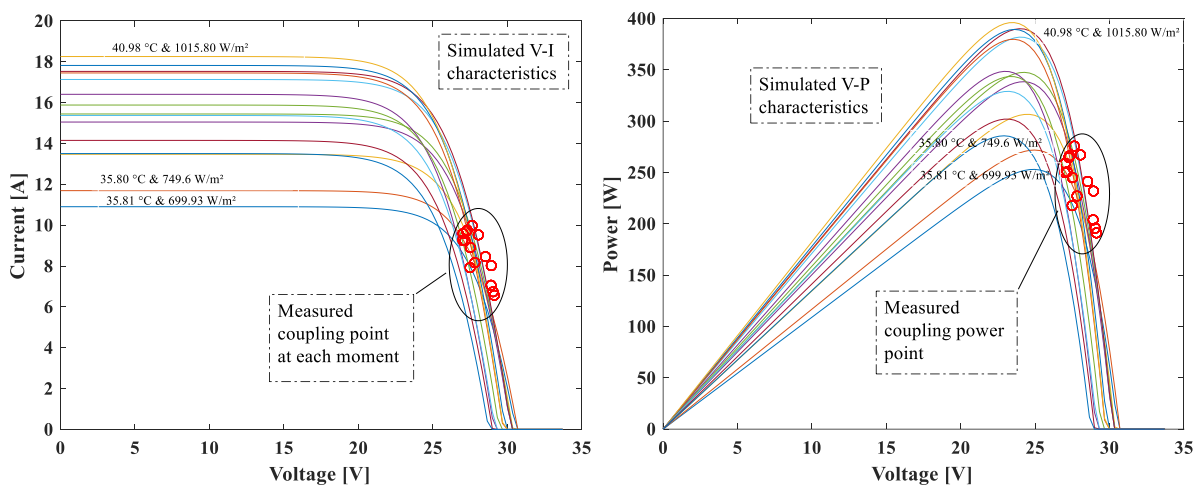


Fig. 3. Simulated V-I and V-P characteristics of the PV generator with the measured coupling point

To address this challenge, a simulation program was developed in the MATLAB environment based on the same experimental conditions but with an MPPT controller to improve energy efficiency and for optimal power transfer to the electrolyzer. The results were presented in Fig. 4(b), and from these results, we recorded a significant improvement in system productivity, contributing to increasing the system's overall efficiency. Moreover, the PV generator production reached 251.7 to 372.5 W watts while not exceeding 275 W in the first stage. In addition, the noticeable improvement in the energy consumed by the electrolyzer leads to increased hydrogen production.

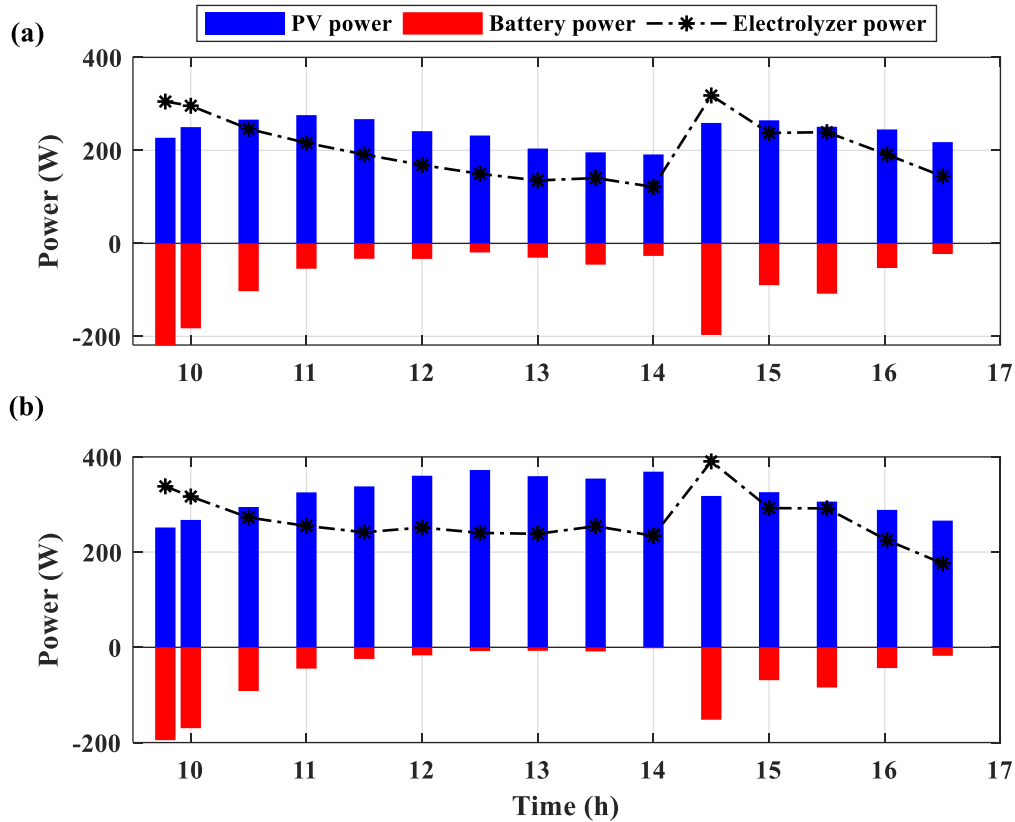


Fig. 4. Power production and consumption, (a) under operating conditions, (b) with MPPT

Fig. 5 shows the hydrogen flow rate for the HG-60 PEM electrolyzer during the experimental periods. The results show that the electrolyzer's output is directly related to the energy supplied because the hydrogen flow is a linear electrical current function within the nominal output limits (60 l/h). Under operating conditions, production was recorded in the range of 10.88 to 40.5 liters per hour. However, with the MPPT controller, the production rate improved from 20.28 to 49.72 l/h. That confirms the direct impact of the absence of the MPPT controller on the electrolyzer production.

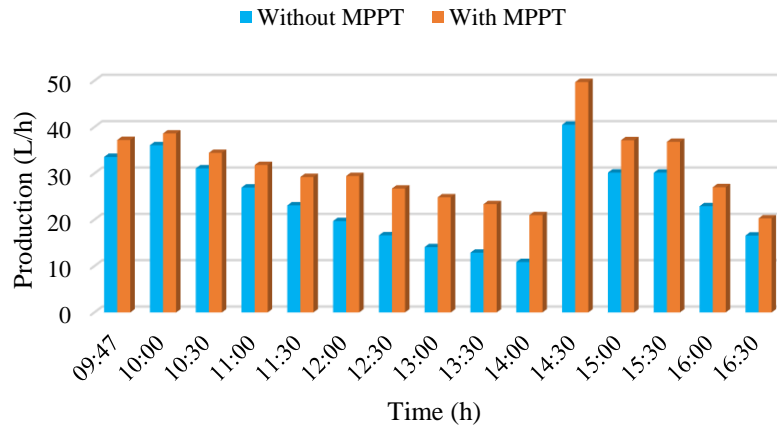


Fig. 5. Hydrogen flow rate

The hydrogen volume refers to the amount of hydrogen produced during the solar water electrolysis process. Furthermore, the trapezes method was used to estimate the volume of hydrogen obtained during the experiment periods from 9:47 a.m. to 4:30 p.m. for the two study cases. The results are shown in Fig.6. Through the results, we found that the volume produced was about 160.5 liters during the experiment periods under operating conditions. In contrast, with the MPPT controller, the produced volume reached 209 liters during the same period.

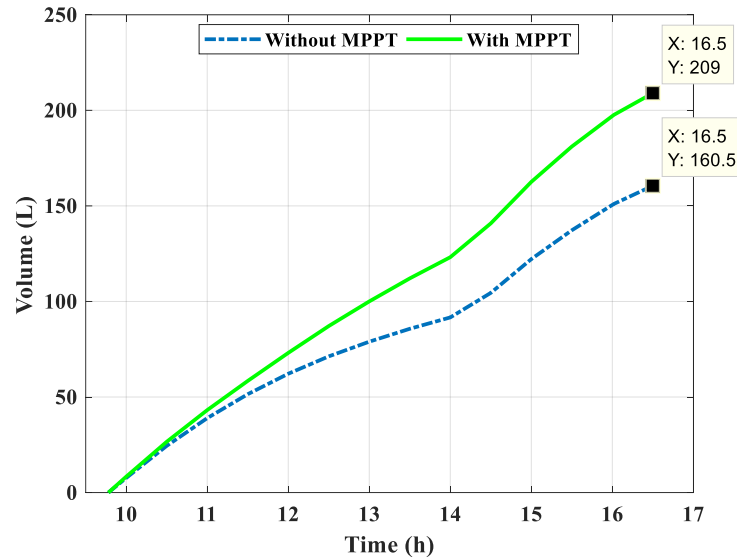


Fig. 6. Hydrogen volume results

In all these results, these variations can be explained by some main factors. An increase in solar radiation increases the total amount of solar energy available to photovoltaic units, thus boosting electricity production. On the other hand, an increase in temperature can hurt PV efficiency. Solar cells work best at low temperatures. A rise in temperature increases the cell's resistance and reduces the available voltage, thus lowering the system's overall efficiency. Moreover, the MPPT technology improves the performance of the PV generator by tracking the maximum power point. Its effect on the performance of solar panels is to increase their efficiency and increase the energy that can be extracted. In addition to some undesirable factors, such as partial shading, these factors primarily affect the electrical current, which is a linear function of the hydrogen flow. Therefore, it affects the solar hydrogen production process.

CONCLUSIONS

In this work, we presented an experimental analysis of a green hydrogen production system in southeastern Algeria using a PEM electrolyzer with a capacity of 60 l/h and a photovoltaic generator with a power of 440 W. Moreover, under normal conditions of the experiment from 09:47 to 16:30, a PV production below 275 W and a hydrogen flow rate of around 40.5 l/h were recorded. Even so, this generated a volume of around 160.5 liters of hydrogen throughout the experiment. Furthermore, to assess the system's true potential, we developed a simulation program in the MATLAB environment under the same experimental conditions and with an MPPT controller. We recorded an improvement in the power transfer to the electrolyzer and, consequently, in the electrolyzer output. The volume of hydrogen reached around 209 liters during the same period of study, which is considered a good value depending on the system available. As a future work, this installation could be developed by adding other elements to the photovoltaic system, such as a fuel cell to make a hybrid system and managing electrical power.

ACKNOWLEDGEMENT

The authors are very grateful to the Laboratory of Electrical Engineering at the University of Ouargla and the general directorate of scientific research, DGRSDT (ALGERIA).

NOMENCLATURE

I	PV output current, A
I_{opt}	PV optimum current, A
I_{ph}	Photo-current, A
I_0	Diode saturation current, A
n	Diode ideality factor
V_{opt}	PV optimum voltage, V
V_T	Thermal voltage, V
R_s, R_p	Series and parallel resistances, Ω

Subscripts

MPPT	Maximum Power Point Tracking
PEM	proton exchange membrane
H ₂	Hydrogen
O ₂	Oxygen
HG-60	Hydrogen Generator 60, sl/h
PV	Photovoltaic

REFERENCES

1. Tleubergenova, A., B.-C. Han, and X.-Z. Meng, *Assessment of biomass-based green hydrogen production potential in Kazakhstan*. International Journal of Hydrogen Energy, 2023.
2. Kumar, D., et al., *Nanocarbon assisted green hydrogen production: Development and recent trends*. International Journal of Hydrogen Energy, 2023.
3. Srettiwat, N., et al., *A techno-economic evaluation of solar-powered green hydrogen production for sustainable energy consumption in Belgium*. International Journal of Hydrogen Energy, 2023.
4. Labbé, J., *L'Hydrogène électrolytique comme moyen de stockage d'électricité pour systèmes photovoltaïques isolés*. 2006, École Nationale Supérieure des Mines de Paris.
5. Buslaev, G., et al., *Hybrid system of hydrogen generation by water electrolysis and methane partial oxidation*. International Journal of Hydrogen Energy, 2023. **48**(63): p. 24166-24179.
6. Gul, H., M.Y. Arshad, and M.W. Tahir, *Production of H₂ via sorption enhanced auto-thermal reforming for small scale Applications- A process modeling and machine learning study*. International Journal of Hydrogen Energy, 2023. **48**(34): p. 12622-12635.
7. Tamilselvan, R. and A.I. Selwynraj, *Model development for biogas generation, purification and hydrogen production via steam methane reforming*. International Journal of Hydrogen Energy, 2023.
8. Su, Z., et al., *Research progress of ruthenium-based catalysts for hydrogen production from ammonia decomposition*. International Journal of Hydrogen Energy, 2023.
9. Hassan, N.S., et al., *Recent review and evaluation of green hydrogen production via water electrolysis for a sustainable and clean energy society*. International Journal of Hydrogen Energy, 2023.
10. Rubinsin, N.J., et al., *An overview of the enhanced biomass gasification for hydrogen production*. International Journal of Hydrogen Energy, 2023.
11. Budhraj, N., A. Pal, and R.S. Mishra, *Plasma reforming for hydrogen production: Pathways, reactors and storage*. International Journal of Hydrogen Energy, 2023. **48**(7): p. 2467-2482.
12. Nabgan, W., et al., *A bibliometric examination and state-of-the-art overview of hydrogen generation from photoelectrochemical water splitting*. International Journal of Hydrogen Energy, 2023.
13. Arsad, S.R., et al., *Patent landscape review of hydrogen production methods: Assessing technological updates and innovations*. International Journal of Hydrogen Energy, 2023.
14. Li, Y., et al., *A comparative analysis of the regulations, codes and standards for on-board high-pressure hydrogen storage cylinders*. International Journal of Hydrogen Energy, 2023.
15. Ahluwalia, R.K., et al., *Liquid hydrogen storage system for heavy duty trucks: Configuration, performance, cost, and safety*. International Journal of Hydrogen Energy, 2023. **48**(35): p. 13308-13323.
16. Boulmrharj, S., et al., *Performance Assessment of a Hybrid System with Hydrogen Storage and Fuel Cell for Cogeneration in Buildings*. 2020. **12**(12): p. 4832.
17. Messaoudi, D., N. Settou, and A. Allouhi, *Geographical, technical, economic, and environmental potential for wind to hydrogen production in Algeria: GIS-based approach*. International Journal of Hydrogen Energy, 2023.
18. Gougui, A., et al., *Field experience study and evaluation for hydrogen production through a photovoltaic system in Ouargla region, Algeria*. International Journal of Hydrogen Energy, 2020. **45**(4): p. 2593-2606.
19. Boudries, R., *Analysis of solar hydrogen production in Algeria: Case of an electrolyzer-concentrating photovoltaic system*. International Journal of Hydrogen Energy, 2013. **38**(26): p. 11507-11518.
20. Ghribi, D., et al., *Study of hydrogen production system by using PV solar energy and PEM electrolyser in Algeria*. International Journal of Hydrogen Energy, 2013. **38**(20): p. 8480-8490.

ICH2P14-PP012

COMPARATIVE STUDY BETWEEN GBO AND BES OPTIMIZATION ALGORITHMS FOR OPTIMAL PEMFC PARAMETERS IDENTIFICATION

**Ahmed Zouhir Kouache, Ahmed Djafour, Khaled Mohammed Said Benzaoui, Mohammed Bilal Danoune*

Faculté des Sciences Appliquées, Laboratoire LAGE, Univ Ouargla, Ouargla 30 000, ALGERIA

*Corresponding author e-mail: kouache.ahmed@univ-ouargla.dz

ABSTRACT

It is known that the functioning of fuel cells necessitates understanding the different phenomena and their properties based on specific mathematical models. So, to deliver a reliable simulation of the properties of a fuel cell system, accurate parameter estimation of the fuel cell model is a crucial step. Due to this reason, a comparative investigation between two robust methods, the Gradient-based Optimizer and the Bald Eagle Search Algorithm, has been presented for the optimum unknown parameters identification of the Proton Exchange Membrane fuel cell (Heliocentris FC-50). The basic concept is to minimize the mean absolute bias error (MABE) between the measured stack voltage and the one predicted by those algorithms. The achievements show that although the algorithms were close, in contrast, the GBO algorithm gives a better superiority than the BES for optimum estimation of the PEMFC model, where the best fitness was recorded with the GBO at 0.036796, compared to 0.036837 with the BES. Also, the GBO has generated the minimum error values in all statistical tests and the lowest deviation with 0.001323 and 0.007040 for the BES algorithm. These results indicate that the GBO method is more stable and robust for PEM fuel cell parameter extraction.

Keywords: PEM fuel Cell, Parameters identification, Gradient-based optimizer, Bald Eagle Search Algorithm, Statistical test.

INTRODUCTION

The growing demand for energy, depletion of fossil resources, and environmental pollution represent a significant challenge to the world's sustainable development. To mitigate these problems, improving energy and developing clean energy technologies is necessary, like fuel cell (FC) systems, which undergo an electrochemical reaction process to generate highly efficient electricity. Fuel cells are clean energy sources because they do not produce harmful pollutants such as CO, CO₂, and SO₂ [1]. Moreover, it is widely applied with numerous advantages such as high efficiency, environmental protection, low pollution, and durability [2]. What is more, there are many different types of fuel cells, and the difference between them according to the type of electrolyte and fuel used, which are Direct methanol fuel cell (DMFC), Alkaline fuel cell (AFC), Molten carbonate fuel cell (MCFC), Proton exchange membrane fuel cell (PEMFC), Phosphoric acid fuel cell (PAFC), Solid oxide fuel cell (SOFC) [3]. In particular, PEMFC technology is essential in creating a safe and efficient energy economy that can contribute to clean energy transition and reduce environmental pollution problems. The PEMFC is a multi-input/output device with a complex structure that requires a continuous hydrogen supply at the anode and oxygen at the cathode under specific temperature and pressure conditions. In addition, a standard PEMFC contains a bipolar plate, a gas diffusion layer, a catalyst layer, and a proton exchange membrane [2]. It has been characterized by fast response and low working temperatures. Further, it has been widely used in many applications, such as electric vehicles [4], microgrid applications [5], domestic applications [6], and micro-combined heat and power applications [7]. It is also used in power systems as distributed generation [8] and in feeding switched reluctance motors [9]. In general, fuel cell operation requires understanding operating dynamics and various phenomena based on distinct mathematical models. Consequently, many mathematical models have been developed to obtain accurate and reliable current and voltage characteristics, but traditional method models need to allow efficient determination of model parameters. Metaheuristic methods, on the other hand, are nature-inspired, population-based search techniques. They have an excellent ability to solve global optimization problems

efficiently. A comprehensive literature review has shown that many meta-methods have been applied in the context of fuel cell modeling. Some of them are: Genetic algorithm [10], Dual objective global optimization [11], Hybrid cuckoo search grey wolf algorithm [12], Fractional order dragonfly algorithm [13], Improved design of crow search optimization algorithm [14], Developed Aquila Optimizer [15], Modified grasshopper algorithm [16], Neural network PSO [17], Levenberg-Marquardt backpropagation algorithm [18], Chaos embedded PSO algorithm [19] and Adaptive Sparrow Search algorithm [20]. Moreover, this short paper compares two identification algorithms: the gradient-based optimizer (GBO) and the Bald Eagle search algorithm. These methods were used to specify PEMFC parameters with the highest possible accuracy. The rest of this paper is organized as follows: Section experimental system description. Moreover, PEMFC mathematical modeling and Fitness functions are introduced in the Section identification strategy. After that, the results and discussion Section. Lastly, conclusions and future work are summarized in Section Conclusion.

EXPERIMENTAL SYSTEM DESCRIPTION

The Heliocentris FC-50 test bench illustrated in Fig. 1 was installed in the LAGE Laboratory at Ouargla University. This platform includes a PEMFC unit of 50W, a cooling fan used as a flow source for oxygen, a Hydrogen tank, a low-pressure regulator valve, an electronic load, a DC/DC converter, and the data acquisition system. The test bench is utilized to characterize, investigate, and validate the different algorithms that ensure optimal operation of the PEMFC-based systems. The field tests were executed at a fixed working temperature and were covered by the automatic cooling fan. In addition, the electrical characteristics of the FC50 fuel cell are drawn by connecting its terminals to a variable electronic load from 0 to 10 amps, then taking the corresponding voltage and current points within the range above, where the measured data can be read directly through the LCD screens or using the data acquisition program provided by the Heliocentris company.

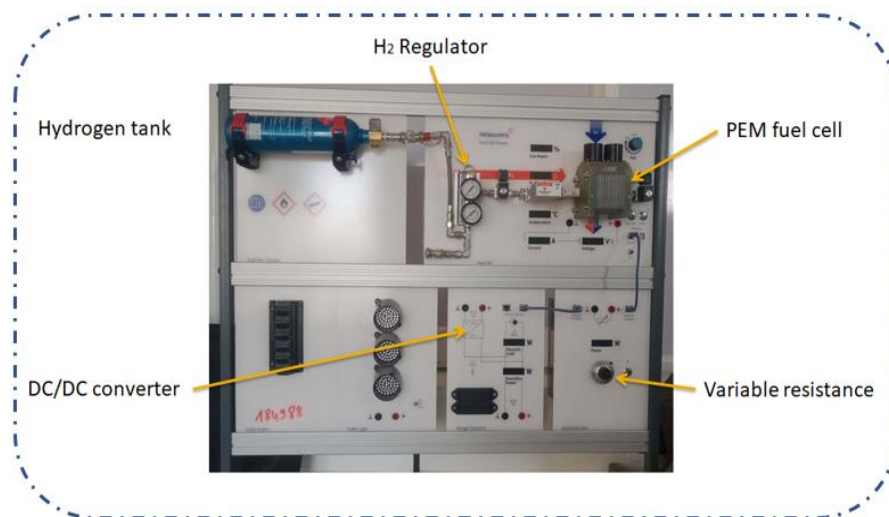


Fig. 1. Heliocentris FC-50 test bench.

In the first step, we review the effect of both temperature and air supply on the electrical characteristics of the fuel cell, where we found that the characteristic of the high-temperature measurement flattened more powerfully, as presented in Fig. 2; it can be noticed that the fuel cell performance was increased with the growing stack temperature. At lower temperatures, the catalytic process was limited. At higher temperatures, the resistance increases, especially from the membranes drying. However, the optimum temperature relies on different factors, e.g., the load current and the airflow. Therefore, the application also affects its optimum temperature. On the other hand, as is displayed in Fig. 3. The performance of the FC with auto fan control continued to rise over the entire measuring range and with values better than the fuel cell with constant fan power (6%).

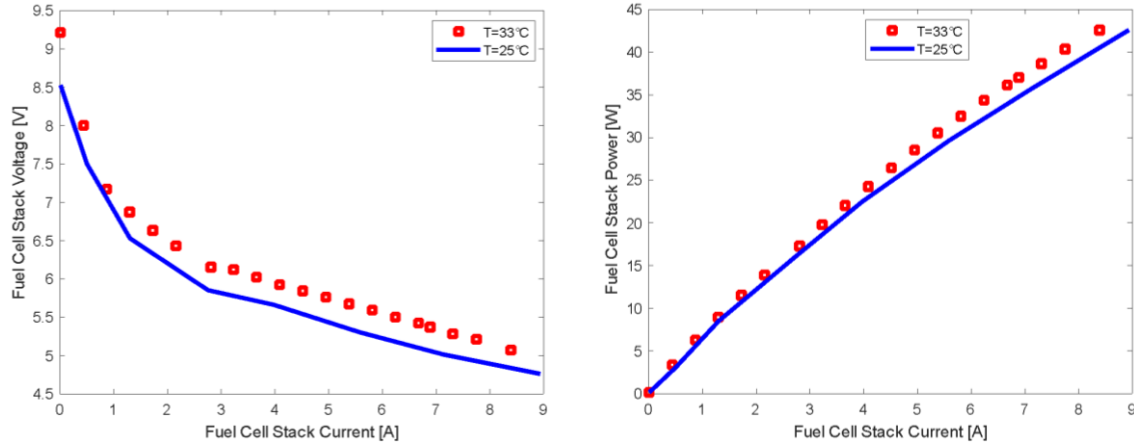


Fig. 2. Impact of temperature on the PEMFC curves.

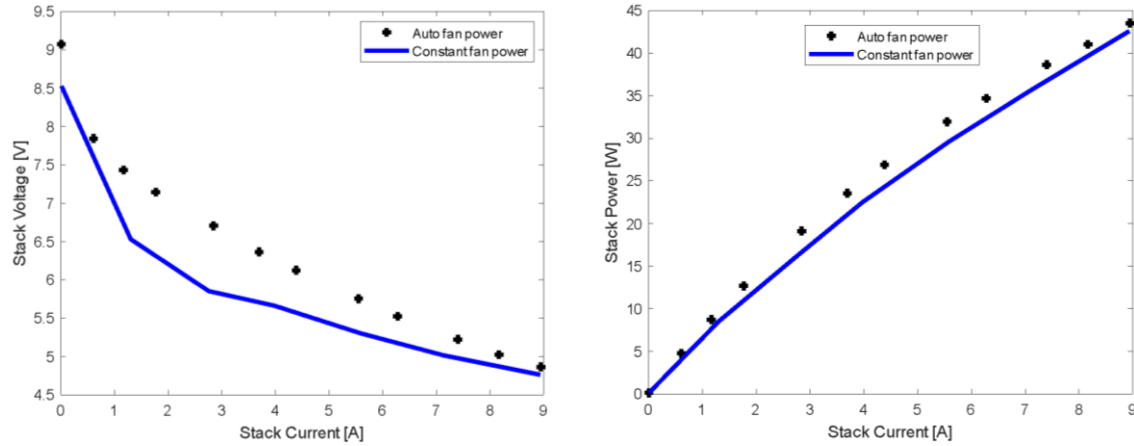


Fig. 3. Impact of air supply on the PEMFC curves.

IDENTIFICATION STRATEGY

PEMFC mathematical modeling

The mathematical model of a proton exchange membrane fuel cell is represented as follows:

$$V_{FC} = n * (E_{nernst} - V_{act} - V_{ohm} - V_{conc}) \quad (1)$$

Where E_{nernst} is the thermodynamic potential, V_{act} is the activation losses, V_{ohm} is the ohmic losses, and V_{conc} is the concentration losses, which can be calculated as follows:

$$E_{nernst} = 1.229 - 0.85 \times 10^{-3}(T - 298.15) + 4.31 \times 10^{-5} \times T \times \ln(P_{H_2}^* \sqrt{P_{O_2}^*}) \quad (2)$$

$$V_{act} = -[\xi_1 + \xi_2 \cdot T + \xi_3 \cdot T \cdot \ln([CO_2^*]) + \xi_4 \cdot T \cdot \ln(I_{FC})] \quad (3)$$

$$V_{ohm} = I_{FC} \cdot (R_m + R_c) \quad (4)$$

$$V_{con} = -\beta \cdot \ln\left(1 - \frac{J}{J_{max}}\right) \quad (5)$$

where T represents the PEMFC temperature (k), $P_{H_2}^*$ and $P_{O_2}^*$ are hydrogen and oxygen pressure values (atm). ξ_1 ; ξ_2 ; ξ_3 ; ξ_4 are semi empirical coefficients; I_{FC} represents the output current; CO_2^* is the oxygen content (mol.cm³), and R_m is the ohmic membrane resistance. J and represents the current density (A/cm²), and β is the electrochemical constant (V).

Fitness function

The mathematical model of PEMFC is defined by eight unknown variables, which are described in Eq 6:

$$X = [\xi_1, \xi_2, \xi_3, \xi_4, \lambda, B, R_c \& J_{max}] \quad (6)$$

These parameters are obtained numerically using the Bald Eagle search optimization algorithm (BES) [21] and the Gradient-based optimizer algorithm (GBO) [22]. A model is accurate if the experimental and estimated

data match each other. Therefore, the mean absolute bias error (MABE) between the measured and predicted points in Eq. (7) is generally viewed as the objective function (OF).

$$OF(V_{exp}, I_{exp}, X) = MABE = \frac{1}{n} \sum_{i=1}^n |V_{exp}(i) - V_{est}(i)| \quad (7)$$

RESULTS AND DISCUSSION

Using the MATLAB environment, the suggested algorithms were used to extract the unknown parameters of the Heliocentris FC-50 stack. Moreover, the program was conducted 30 times during 1000 iterations, and the population number was equal to 50 agents. The optimal parameters results are offered in Table 1. The comparison shows a significant convergence in the values of the optimal parameters recorded. However, the best fitness value was obtained by the GBO algorithm with 0.036796, whereas the BES algorithm achieved a value of 0.036837.

Table 1. - Optimal parameters of PEM FC50 using GBO and BES algorithms

Parameter	Lower bound	Upper bound	GBO	BES	WOA [23]
ξ_1	-1.1997	-0.8532	-1.155790	-1.199328	-1.0837
ξ_2	1e-03	5e-03	0.003656	0.003582	0.0024
ξ_3	3.6e-05	9.8e-05	9.582787e-05	8.239728e-05	5.8816e-5
ξ_4	-26e-05	-9.54e-05	-0.000150	-0.000150	-2.1106e-4
λ	13	23	13.000861	14.933452	16.5558
B	0.0136	0.5	0.499999	0.491618	0.0353
Rc	0.1e-03	0.8e-03	0.000791	0.000799	6.3813e-4
Jmax	0.4	0.5	0.408886	0.402807	0.4996
Best Fitness	-	-	0.036796	0.036837	0.0506

Fig. 4. Shows a comparison between the experimentally measured voltage and power points and those estimated by the GBO and BES algorithms for the FC-50 stack. These results show a good match between the points estimated by these techniques and measured data across the entire operating range. Moreover, this confirms the robustness of the suggested algorithms in extracting the fuel cell's optimal parameters. In addition, with a rapid convergence to the optimal values, as displayed in Figure 5. They have a high potential to explore the search area quickly.

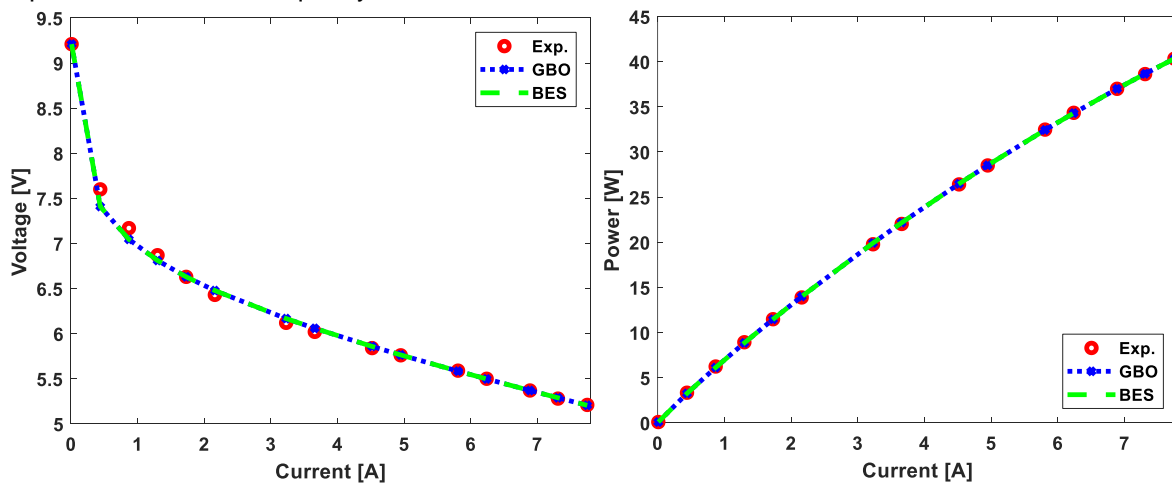


Fig. 4. Output characteristics using the GBO algorithm

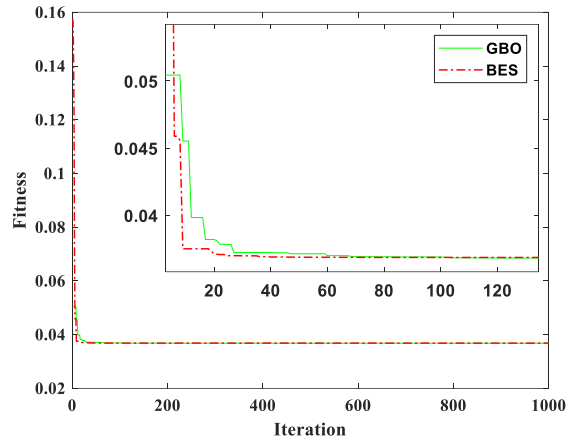


Fig. 5. Convergence speed

Furthermore, the accuracy of the investigated methods was assessed by calculating some benchmarks and statistical indicators. The results are listed in Table 2. The performance was good for all optimizers for the considered PEMFC; However, the GBO results were more suitable than BES. It can be observed that the minimum deviation of 0.001323 was reached by the GBO, followed by the BES with 0.007040. Also, the GBO attained the lowest average MABE value of 0.036980 followed by the BES algorithm with 0.037357. In addition, the results showed that the GBO outperformed the BES, where the value of the determination coefficient was 0.996187, whereas the WOA recorded a value of 0.996182. All that demonstrates the superiority of the GBO in identifying the optimal parameters of the PEM FC50 compared with the BES methods.

Table 2. - Statistical results

Indicator	GBO	BES
Best	0.036796	0.036837
Mean	0.036980	0.037357
Worst	0.050440	0.157631
Std	0.001323	0.007040
Median	0.036798	0.036849
Mode	0.036797	0.036837
Range	0.013643	0.120793
MAPE	0.174109	0.173788
RMSE	0.064200	0.064246
MBE	-0.014727	-0.014710
Rmse	1.017983	1.018701
t-stat	0.881849	0.880105
R ²	0.996187	0.996182
Ranking	1	2

CONCLUSIONS

Hydrogen fuel cells have gotten much attention recently due to their many advantages, high efficiency, and reliability. Therefore, to deliver a reliable simulation of the PEMFC model, accurate parameter estimation is a crucial step. Due to this reason, a comparative analysis of two metaheuristic algorithms, the gradient-based optimizer (GBO) and the bald search eagle algorithm (BES), have been presented for the optimum unknown parameters identification of the PEM fuel cell (FC-50). The primary concept is to lessen the mean absolute

bias error (MABE) between this algorithm's measured and estimated output. The achievements indicate that the GBO algorithms gave a better superiority for optimum PEMFC model estimation, where the best fitness was recorded with 0.036796 and 0.036837 for the BES. Also, the GBO has generated the minimum error values in different statistical tests with the lowest deviation of 0.001323 compared to the BES with 0.007040. These results indicate that the GBO method is more stable and robust for PEMFC parameter extraction. In future work, we aim to use other new optimization algorithms and use them in further fuel cells.

ACKNOWLEDGEMENT

The writers would like to acknowledge and thank the LAGE Laboratory Ouargla Univ and DGRST Algeria for their daily efforts and for financing this project.

NOMENCLATURE

FC	Fuel cell
MABE	Mean absolute bias error
MAPE	Mean absolute percentage error
MBE	Mean bias error
PEMFC	Proton exchange membrane fuel cell
RMSE	Root mean square error
rRmse	Relative Root Mean Squared Error
Std	Standard deviation
t-stat	t-statistic

Symbols

Enernst	Nernst voltage, V
Vact	Activation polarization, V
Vcon	Concentration polarization, V
$V_{est}(i)$	Experimental voltages, V
$V_{exp}(i)$	Estimated voltages, V
Vohm	Resistance polarization, V
R^2	Determination coefficients

REFERENCES

1. Shahril, A.A.D., et al., A review on mode conversion: Dynamic response of unitised regenerative proton exchange membrane fuel cell. *International Journal of Hydrogen Energy*, 2023.
2. Chen, J., H. He, and H. Yue, A review of plateau environmental adaptation for proton exchange membrane fuel cells. *International Journal of Hydrogen Energy*, 2023.
3. Ayar, M. and T.H. Karakoc, Decision mechanism between fuel cell types: A case study for small aircraft. *International Journal of Hydrogen Energy*, 2023. **48**(60): p. 23156-23167.
4. Kannan, R. and V. Sundharajan, A novel MPPT controller based PEMFC system for electric vehicle applications with interleaved SEPIC converter. *International Journal of Hydrogen Energy*, 2023. **48**(38): p. 14391-14405.
5. Samal, K.B., S. Pati, and R. Sharma, A review of FCs integration with microgrid and their control strategies. *International Journal of Hydrogen Energy*, 2023.
6. Bizon, N., et al., Optimization of the proton exchange membrane fuel cell hybrid power system for residential buildings. *Energy Conversion and Management*, 2018. **163**: p. 22-37.
7. Budak, Y. and Y. Devrim, Investigation of micro-combined heat and power application of PEM fuel cell systems. *Energy Conversion and Management*, 2018. **160**: p. 486-494.
8. Sun, L., et al., Efficiency analysis and control of a grid-connected PEM fuel cell in distributed generation. *Energy Conversion and Management*, 2019. **195**: p. 587-596.
9. El-Hay, E.A., M.A. El-Hameed, and A.A. El-Fergany, Improved performance of PEM fuel cells stack feeding switched reluctance motor using multi-objective dragonfly optimizer. *Neural Computing and Applications*, 2019. **31**(11): p. 6909-6924.
10. Yuan, H.-B., et al., Optimized rule-based energy management for a polymer electrolyte membrane fuel cell/battery hybrid power system using a genetic algorithm. *Int. J. Hydrog. Energy*, 2022. **47**(12): p. 7932-7948.
11. Li, Y., et al., A dual objective global optimization algorithm based on adaptive weighted hybrid surrogate model for the hydrogen fuel utilization in hydrogen fuel cell vehicle. *Int. J. Hydrog. Energy*, 2022.
12. Bai, Q. and H. Li, The application of hybrid cuckoo search-grey wolf optimization algorithm in optimal parameters identification of solid oxide fuel cell. *Int. J. Hydrog. Energy*, 2022. **47**(9): p. 6200-6216.



13. Guo, H., et al., Parameter extraction of the SOFC mathematical model based on fractional order version of dragonfly algorithm. *Int. J. Hydrog. Energy*, 2022. **47**(57): p. 24059-24068.
14. Duan, F., et al., Model parameters identification of the PEMFCs using an improved design of Crow Search Algorithm. *Int. J. Hydrog. Energy*, 2022.
15. Wang, S., et al., An optimal configuration for hybrid SOFC, gas turbine, and Proton Exchange Membrane Electrolyzer using a developed Aquila Optimizer. *Int. J. Hydrog. Energy*, 2022. **47**(14): p. 8943-8955.
16. Wen, P., et al., Optimal and stochastic performance of an energy hub-based microgrid consisting of a solar-powered compressed-air energy storage system and cooling storage system by modified grasshopper optimization algorithm. *Int. J. Hydrog. Energy*, 2022. **47**(27): p. 13351-13370.
17. Nasrabadi, A.M. and M. Moghimi, Energy analysis and optimization of a biosensor-based microfluidic microbial fuel cell using both genetic algorithm and neural network PSO. *Int. J. Hydrog. Energy*, 2022. **47**(7): p. 4854-4867.
18. Yang, B., et al., Parameter identification of proton exchange membrane fuel cell via Levenberg-Marquardt backpropagation algorithm. *Int. J. Hydrog. Energy*, 2021. **46**(44): p. 22998-23012.
19. Özdemir, M.T., Optimal parameter estimation of polymer electrolyte membrane fuel cells model with chaos embedded particle swarm optimization. *Int. J. Hydrog. Energy*, 2021. **46**(30): p. 16465-16480.
20. Zhu, Y. and N. Yousefi, Optimal parameter identification of PEMFC stacks using Adaptive Sparrow Search Algorithm. *Int. J. Hydrog. Energy*, 2021. **46**(14): p. 9541-9552.
21. Alsattar, H.A., A.A. Zaidan, and B.B. Zaidan, Novel meta-heuristic bald eagle search optimisation algorithm. *Artificial Intelligence Review*, 2020. **53**(3): p. 2237-2264.
22. Ahmadianfar, I., O. Bozorg-Haddad, and X. Chu, Gradient-based optimizer: A new metaheuristic optimization algorithm. *Information Sciences*, 2020. **540**: p. 131-159.
23. Danoune, M.B., et al., The Whale Optimization Algorithm for efficient PEM fuel cells modeling. *Int. J. Hydrog. Energy*, 2021. **46**(75): p. 37599-37611.

ICH2P14-PP014

INVESTIGATING THE EFFECT OF USING HYDROGEN AS A FUEL ON PERFORMANCES OF GAS TURBINE OPERATING AT LEAN CONDITION IN SITE OF HASSI R'MEL

¹Fethia Amrouche, ¹Bouziane Mahmah, ²Lidya Boudjema, ²Oum Keltoum Bari

¹Centre de Développement des Énergies Renouvelables, CDER, 16340, Algiers, Algeria

²University of Algiers, Benyoucef Benkhedda, Faculty of Sciences

*Corresponding author e-mail: fethia.amrouche@gmail.com

ABSTRACT

Green hydrogen is emerging today as a necessary energy solution to ensure the sustainability of energy resources and to reduce carbon footprint. Electricity production in Algeria is mainly based on gas turbines, therefore the use of green hydrogen, produced from solar sources, in gas turbine is a way to support an efficient transformation of the Algerian energy supply, which is almost exclusively based on natural gas and oil. The aim of this study is to assess the influence of using hydrogen as fuel on the performance of the TG-M5002C gas turbine operating under the specific climatic conditions of the Saharan region. To achieve this goal, a numerical study using THERMOPTIM software was developed to assess the influence of the monthly ambient temperature variations throughout the year on the performance of both natural gas and hydrogen gas turbines, operating at lean conditions with $\lambda=4.5$, under the climatic conditions of the Hassi R'mel gas site. The results have proven the capability of hydrogen as a fuel to improve thermal efficiency, reduce fuel consumption, and decrease pollutant emissions, regardless of the climatic conditions of operation.

Keywords: Hydrogen fuel, Gas turbine, Excess air ratio, Performances and pollutant emissions.

INTRODUCTION

Energy supply and carbon footprint reduction are the major concerns of the century. Nowadays, green hydrogen emerges as a crucial energy solution to ensure the sustainability of energy resources and to reduce carbon footprint, thereby protecting the environment.

Moreover, in the field of advanced combustion, a growing interest in improving combustion in gas turbine combustion chambers through the use of hydrogen pure or mixed with other fuels has been observed [1-2]. Indeed, it is important to notice that the gas turbine performance is highly dependent on ambient air conditions such as temperature, pressure, humidity, and dust. Its power is directly linked to the air density, which decreases with rising ambient temperature, thereby reducing combustion intensity and directly affecting efficiency. Consequently, this machine loses a significant portion of its power during the hot months of the year. According to Cortès et al [3] and Yap et al [4], a high air temperature at the intake increases compressor work and thus produces less power (a decrease of 25 to 35% in the summer) and consumes more fuel. Many methods are used to improve the performance of gas turbines. Hydrogen can be used as a substitute fuel to enhance combustion quality and, consequently, thermal efficiency and reduce fuel consumption [1, 5]. In addition, hydrogen is carbon-free; therefore, burning it will result in zero carbon emissions. Burning hydrogen with a high excess of air will also help to reduce NO_x emissions. Therefore, using hydrogen as a fuel can be an effective method to compensate for the effects of ambient conditions on the gas turbine's performance and emissions.

Various works have been carried out on the combustion of alternative fuels containing hydrogen in gas turbines. Tuncer (2013) [6] has explored the effect of increasing the concentration of hydrogen in syngas on the performance and emissions of a gas turbine; he concluded that increasing the hydrogen concentration allows lean burn operation which results in reduced NO_x emissions. While Cappelletti et al, (2014), [7] described a new dimensioning, carried out by CFD, of the combustion chamber of the Turbec T100 micro-turbine initially operating on natural gas to allow its operation with 100% hydrogen. However, none of these works did a feasibility study of using hydrogen in an existing gas turbine MS5002C implemented in Southern Algeria. Therefore, the aim of this research is to investigate the influence of ambient temperature variations throughout the months of the year on the performance and NO_x emissions

of hydrogen gas turbines, operating under the climatic conditions of the Hassi R'mel gas site. This was done by taking into consideration an optimum excess air coefficient in order to meet the manufacturer's specified operating conditions of the MS5002C gas turbine. The data collected from the natural gas turbine was used as a reference. Air dilution is a simple method that requires no system modifications and allows for the dilution of the hydrogen flame temperature.

THERMODYNAMIC ANALYSIS OF HYDROGEN GAS TURBINE

Description of the MS5002C turbine

The studied gas turbine is an MS5002C turbine, manufactured by the American company GENERAL ELECTRIC. This two-shaft drive turbine operates on a simple cycle. It is used to drive a centrifugal compressor. The section of a gas turbine for mechanical drive is the part in which fuel and air are used to generate power on the shaft. This type of turbine is widely used in the petroleum industry for, among other things, driving the high-powered compressors used in natural gas compression stations. Figure 1 shows the diagram of a two-shaft gas turbine.

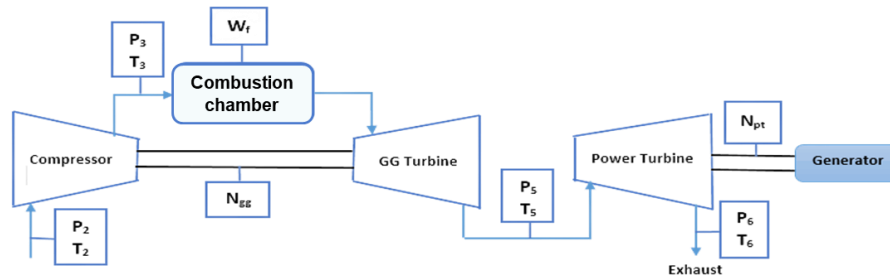


Fig. 1. Diagram of a two-shaft gas turbine

The thermodynamic cycle in gas turbines is based on Brayton cycle. In this cycle, the air is compressed, heated at a constant pressure, expanded through a turbine, and then cooled back to the initial state [8]. Therefore, to model the hydrogen gas turbine the following equations are used:

- **Modeling of the Compressor**

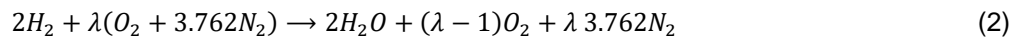
The work required for a unit mass of air is generally expressed by the equation:

$$W_c = \frac{(C_{pa,2} * T_2) - (C_{pa,1} * T_1)}{\eta_m} \quad (1)$$

With: η_m is the mechanical transmission efficiency; C_{pa} is the specific heat of air.

- **Modeling of the combustion chamber**

As combustion is not perfect and unburned components remain in the exhaust gases, therefore, only the flow rate of burned fuel provides energy to the working fluid. This is depicted by the combustion efficiency (η_{cc}). For this work, the used hydrogen is supposed pure and the typical Algerian natural gas is used. The combustion reaction of hydrogen, taken in consideration the excess of air is given by:



Where λ , Is the excess of air ratio,

$$\lambda = \frac{\dot{Q}_{excess\ air}}{\dot{Q}_{Stoichiometric\ air}} = \frac{\dot{Q}_{air}}{(\dot{Q}_c \times \dot{Q}_{Stoichiometric\ air})} \quad (3)$$

\dot{Q}_{air} : Is the mass flow rate of air (kg/h); \dot{Q}_c : is the mass flow rate of the fuel (kg/h)

The adiabatic temperature of the hydrogen flame can be calculated as follows:

$$T_{ad} = \frac{q}{m_r \times C_p} + T_0 \quad (4)$$

With: q is the heat released during combustion; m_r is the mass of the reactants; C_p is the specific heat capacity of the reactants. T_0 is the initial temperature of the reactants.

- **Turbine modeling:** The work of the turbine is defined by the following equation:

$$W_T = h_4 - h_3 \quad (5)$$

- **Specific work:** It is denoted by the contrast between the work generated by the turbine and the work consumed by the compressor. This is represented by the following equation:

$$W_S = W_T - W_C \quad (6)$$

- **Global efficiency:** The thermal efficiency can be defined as the proportion of useful power generated by the gas turbine compared to the heating power generated through the combustion of the fuel used. This relationship is expressed by the following equation:

$$\eta_{glob(TG)} = \frac{W_S}{W_{CC}} \quad (7)$$

Methodology and Calculation

The primary objective of this research is to assess the feasibility of using hydrogen as fuel to power the MS5002C gas turbine. This is done to enhance efficiency while adhering to the operating conditions imposed by the manufacturer. To assess performance metrics and conduct thermodynamic analyses for the integration of hydrogen in the gas turbine, the THERMOPTIM software is employed.

As the first step of this simulation research, the validation of the developed numerical model using manufacturer data is necessary. Then, calculations to investigate the influence of varying ambient temperatures on gas turbine performance and NOx emissions were initiated. The turbine was operated under optimal conditions with an excess air ratio of $\lambda=4.5$ while accounting for the climatic conditions across all twelve months of the year at the Hassi R'mel gas site. The optimal excess of air ratio λ was determined in a previous study based on the manufacturer's specified operating conditions of the MS5002C gas turbine based on combustion and intake temperatures at the specific climate conditions of Hassi R'mel. This was accomplished by using the monthly average temperature data logged over a year. The data collected from the natural gas turbine was used as a reference.

Verification of the model

The model put forward and simulated using Thermoptim Pro software is validated using the data provided by GE, the manufacturer of the TG-M5002C gas turbine. This validation process was carried out under identical operating conditions. Table 1 presents a comparison of the simulation outcomes against the manufacturer's data, facilitating a comprehensive assessment.

Table 1: The Thermoptim simulation outcomes and the manufacturer's data of the TG-M5002C gas turbine.

Parameters	Manufacturer Data [8]	Thermoptim Pro-software
Ambient air temperature	15°C	
Air pressure	1.01325 bar	
Air flow rate	123.61 kg/s	
Isentropic efficiency of the compressor	$\eta_i = 0,87$	
Combustion chamber efficiency	$\eta_{cc} = 0.97$	
Compressor compression ratio	$\pi_c = 8,8$	
Thermal efficiency	28,8 %	28.9%

Developed power	28,377 MW	29.14 MW
-----------------	-----------	----------

According to Table 1, the simulated data have shown very good agreement with those provided by GE manufacturer. Indeed, there is a very small overestimation of the thermal efficiency and developed power, approximately 0.34% and 2.61, respectively. These differences can be attributed to the assumptions made in the theoretical model and simulations, which did not fully account for the real-world complexities of the gas turbine system. Additionally, fluctuations in system behaviour across diverse conditions contribute to this variance. However, for this study, it is evident that there is minimal disparity among the various parameters, underscoring the reliability of the ThermoOptim software and affirming its utility in thermodynamics as well as its use as an industrial tool.

RESULTS AND DISCUSSION

Thermal efficiency

Displayed in Figure 2 below is the cycle efficiency evolution of a pure hydrogen turbine and a natural gas turbine over the twelve months of a year at the Hassi R'mel gas site.

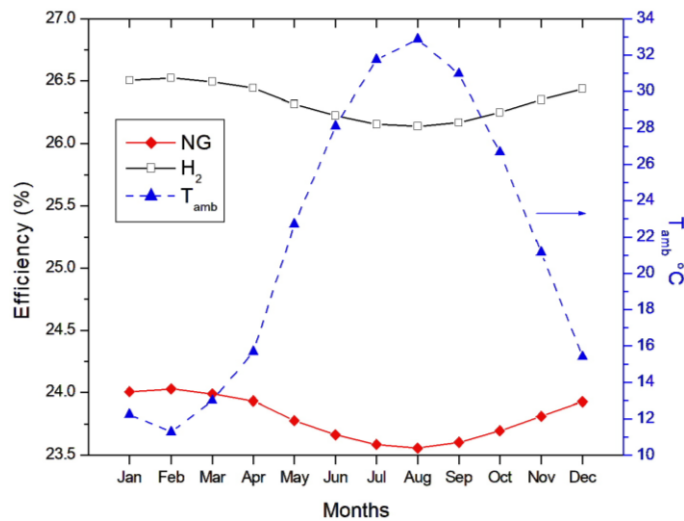
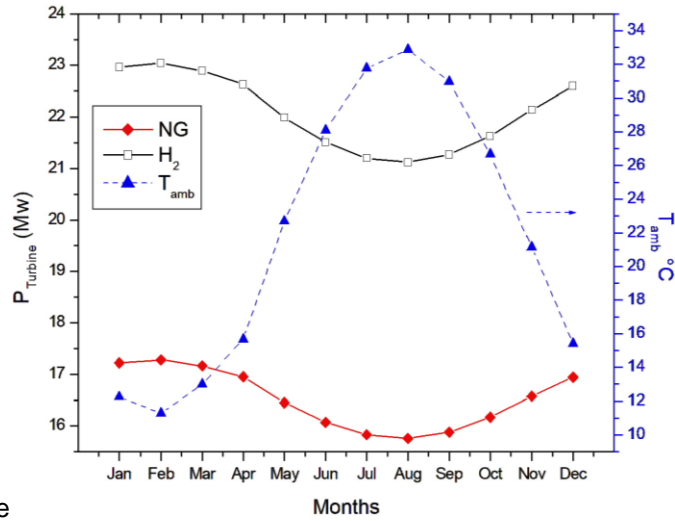


Fig. 2. Variation in thermal efficiency throughout the Twelve Months at Hassi R'mel Gas Site

Figure 2 illustrates a clear pattern. First, it can be observed that the efficiency generated by hydrogen combustion is higher than that produced by natural gas. Indeed, an improvement of about 9.5% was observed for peak efficiency when hydrogen was used instead of natural gas. This is because the use of hydrogen enhances the quality of combustion. Then, for both fuels, as the temperature rises and reaches its peak in August, the efficiency of the system decreases to a minimum. Conversely, efficiency begins to rise during colder months until reaching its maximum in February. A loss in efficiency of about 0.43% was observed when pure hydrogen was used in the fuel mixture between summer and winter, while it is about 1.77% for the natural gas turbine. This means that ambient temperature affected the natural gas turbine more than the pure hydrogen turbine. This can be explained by the fact that the increase in temperature leads to a reduction in the mass of air admitted into the compressor, and consequently, into the combustion chamber. As a result, there is a decrease in efficiency for both modes of operation (pure hydrogen and natural gas). However, because hydrogen improves the combustion quality by enhancing the flammability range, the propagation flame speed, therefore, the efficiency is less affected by air temperature compared to the pure natural gas turbine.

Power output

Figure 3 shows the variation of the turbine power over the twelve months of the year at Hassi R'mel.



gas site
Fig. 3. Variation in power output throughout the Twelve Months at Hassi R'mel Gas Site

According to Figure 3, it can be observed that there is a decrease in the useful energy with the increase in ambient temperature for the two fuels, reaching a minimum value in the middle of August. It is also noteworthy that the energy produced by the combustion of hydrogen is significantly higher than that produced by the combustion of natural gas, exceeding it by 25% in the month of February.

NOx Emissions

Displayed in Figure 4 below is the cycle efficiency evolution of a pure hydrogen turbine and a natural gas turbine over the twelve months of a year at the Hassi R'mel gas site.

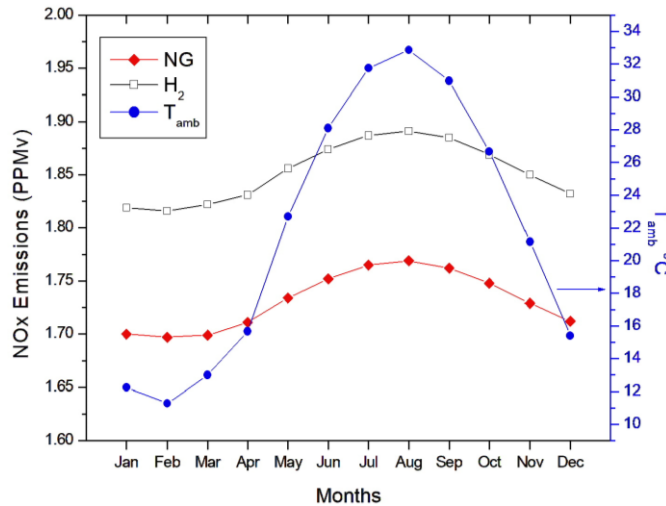


Fig. 4. Variation in NOx Emissions throughout the Twelve Months at Hassi R'mel Gas Site

As can be seen in Figure 4, the maximum NOx emissions generated by hydrogen combustion are approximately 6.45% higher than those produced by natural gas for the month of August. However, these emissions are still acceptable.

These results are predictable due to the higher combustion temperature of hydrogen, which favors the production of thermal NO. Moreover, for both fuels, as the temperature rises and reaches its peak in August, the NO_x emissions exhausted by the turbine increase to their maximum. Conversely, NO_x emissions begin to decrease during colder months until reaching their minimum in February. This is because, first, the temperature is affected by the outdoor temperature, and then, as thermal efficiency decreases, fuel consumption increases.

CONCLUSIONS

The primary objective of this research is to investigate the effect of using hydrogen on the performance and NO_x emissions of the MS5002C gas turbine operating at $\lambda=4.5$ under real-world conditions on the Hassi R'mel gas site. This investigation encompasses the ambient conditions, which have been thoroughly incorporated into the system modelling for comprehensive analysis. This was accomplished by using the monthly average temperature data logged over a year. The data collected from the natural gas turbine was used as a reference. The main findings of this study are as follows:

- The ambient conditions impact the performances of both hydrogen and natural gas turbines.
- An increase in ambient temperature has a negative effect on turbine performance and NO_x emissions.
- The use of hydrogen as fuel effectively improves the thermal efficiency and power output of the M5002C natural gas turbine operating under Saharan climatic conditions.
- The NO_x emissions are higher for the hydrogen turbine compared to those of natural gas. However, the emissions are ultra-low and, therefore, considered negligible for both runs.

This work could demonstrate that the use of hydrogen in the MS5002C gas turbine has effectively improved performance under the selected conditions. However, in order to adhere to the manufacturer's safe operating conditions based on combustion and emission temperatures, a very lean mixture was chosen, which reduces the performance compared to the optimal operating condition for natural gas. Therefore, future research should focus on exploring alternative cooling systems to effectively mitigate this effect and enable the use of a lower excess air ratio to increase power output.

REFERENCES

1. Meziane S, Bentebbiche A. 2019. Numerical study of blended fuel natural gas hydrogen combustion in rich/quench/lean combustor of a micro gas turbine. *Int J Hydrog Energy* 44:15610–21.
2. Yoshimura T, McDonnell V, Samuelsen S. 2005. Evaluation of hydrogen addition to natural gas on the stability and emissions behavior of a model gas turbine combustor. In *Turbo Expo: Power for Land, Sea, and Air* 4725: 573–81.
3. Cortes CR, and Willems DF. 2003. *Gas Turbines Inlet Air Cooling Techniques: An Overview of Current Technologies*. POWER-GEN International.
4. Yap MR and Wang T. 2007. Simulation of producer gas fired power plants with inlet fog cooling and steam injection. *Journal of Engineering for Gas Turbines and Power* 129(3).
5. De Robbio R. 2017. Innovative combustion analysis of a micro-gas turbine burner supplied with hydrogen-natural gas mixtures. *Energy Procedia* 126:858–66.
6. Onur Tuncer, Mendez-Vilas (2013). A premixed combustion of hydrogen and syngas fuels in gas turbine combustors. *J of materials and processes for energy: communicating current research and technological developments, formatex research center, badajoz, spain*, p 946-957.
7. Cappelletti A, Martelli F, Bianchi E, Trifoni E. 2014. Numerical redesign of 100kw MGT combustor for 100% h₂ fueling. *Energy Procedia* 45: 1412 – 1421.
8. GE Energy Oil & Gas, Gas Turbines. Downloaded from www.Manualslib.com manuals search engine. Accessed on September 1, 2023.

ICH2P14-PP015

SORPTION PROPERTIES OF BALL-MILLED POROUS SILICON FOR HYDROGEN STORAGE UP TO 80 BAR

¹Rama Chandra Muduli, ²Paresh Kale

¹Department of Electrical Engineering, NIT Rourkela, 769008, Odisha

²DST-IIT Bombay Energy Storage Platform on Hydrogen, IIT Bombay, 400076, Maharashtra, India

*Corresponding author e-mail: muduliramachandra@gmail.com

ABSTRACT

Solid-state storage is a feasible solution to store hydrogen than commercially available techniques. Porous materials like carbon nanostructures, MOFs, zeolites, and porous polymers possess high surface energy and hydrogen affinity. However, cryogenic temperature operation and low storage at ambient conditions are major demerits for practical storage applications. This study focuses on nanostructuring Si, evaluating its structural characteristics, and investigating its ability to store hydrogen at up to 80 bar. Nanostructuring the hand-grinded porous Si (HGPS) reduces crystallite size, boosts surface energy and enhances thermodynamics. At 80 bar and 120 °C, the ball-milled porous Si (BMPS) exhibits a hydrogen storage capacity of 10.7 wt.%, meeting the hydrogen storage target set by US DOE. Reduced crystallite size, as determined through XRD and Raman spectroscopy, reveals nano-scale pores accessible to hydrogen. This exposure boosts storage capacity, making BMPS an attractive choice for reversible storage applications.

Keywords: Adsorption thermodynamics, Solid-state storage, Isothermic heat, nano-crystallite size, decomposition energy

INTRODUCTION

Hydrogen is often hailed as a promising energy medium with a significant capacity to supplant fossil fuel utilization and aid the transition to net-zero emissions [1]. Hydrogen energy utilization encompasses various stages, including production, storage, and transportation. However, the primary hurdle in hydrogen energy lies in developing effective hydrogen storage methods [2]. Typically, hydrogen can be stored as pressurized gas, cryogenic liquid, and surface bonding [3]. Among the various hydrogen storage systems, solid-state storage systems exhibit significant potential for achieving significant storage capacity in a safe, efficient, compact, and reversible manner [4]. Light metal hydrides demonstrate desirable traits like high storage capacities (above 7 wt.%), recyclability, and reversibility [2,5]. However, the suitability and efficiency of hydrogen storage are hindered by sluggish kinetics, the requirement of elevated temperatures, and higher activation energy for hydrogen uptake and release. Hydrogen storage in several low-temperature hydrides (below 200 °C), like LaNi₅, Ti-Zr alloys, Sb₂Ti, Sn₂Co, and Ti-Fe alloys, is limited to less than 2% by their unit cell volume [6].

Enhancing surface roughness raises surface energy levels, enhancing the capacity for absorbing hydrogen. Typically used large surface area materials adsorb (physisorption) hydrogen on the surface by van der Waals interaction [2,3]. However, the practical application is hindered by the low hydrogen storage capacity under ambient conditions and the need for cryogenic storage temperatures, which are significant constraints [7]. Nanostructured materials significantly impact the thermodynamics and hydrogen adsorption kinetics by increasing the diffusion rate and reducing the diffusion length [8]. Based on prior research, high-energy ball milling is the primary technique for enhancing hydrogen storage by nanostructuring [3,9].

Silicon exhibits a pronounced affinity for hydrogen [4]. However, the low surface area and limited availability of dangling sites in bulk Si restrain its ability to reach the theoretical hydrogen storage capacity (~12.5 wt.%). Nanostructuring Si provides maximum unsaturated dangling sites, enabling higher gravimetric hydrogen storage densities [2,4]. In addition to storage, silicon nanostructures (SiNSs) function as catalysts

to enhance the energy required for formation and decomposition processes [10]. According to Muduli and Kale [4], porous Silicon (PS) is considered the optimal choice for hydrogen storage among different SiNSs. Previous studies on PS for hydrogen storage achieved storage capacities below 2.5 wt.% [11,12]; however, none of the previous works meet the US DOE target of ~5.5 wt.% [13].

The mesoporous sorbents stay below saturation levels when exposed to 20 bar, and their storage capacity continues to increase with charging pressures (exceeding 20 bar) [14]. As the pressure rises, the surface coverage expands, requiring an elevated pressure to completely saturate the surfaces with the target molecule. This study has two main objectives: first, to use ball-milling to transform hand-grounded PS (HGPS) into nanostructured ball-milled PS (BMPS) and study its morphology; and second, to investigate the hydrogen storage capacity of BMPS compared to HGPS at pressures up to 80 bar. The reduction in hydrogen desorption temperature and energy within BMPS is analysed, suggesting its suitability for a wide range of applications in reversible energy storage.

METHODOLOGY AND EXPERIMENTATION

The PS films were synthesized using the electrochemical anodization technique, where boron-doped, single-side polished p-type Si wafers were used as the underlying substrate [4]. The PS films were crushed into powder using mortar and pestle for ten minutes of grinding, called HGPS. HGPS was milled using a high-energy planetary ball mill (Scinomat Solutions India, 2Sx-V04) in an Argon atmosphere for 12 cycles. Each cycle included 45 minutes of milling followed by a 15-minute pause. The sample was mixed with Zirconia milling balls, with diameters of one and two millimeters, at a ratio of 1:40 by weight. The ball-milling jars were set to rotate at 1100 rpm, and the sun speed, where the jars are connected and balanced, was fine-tuned to 220 rpm.

The hydrogen storage properties were analyzed using Sievert's type apparatus using a Pressure Composition Isotherm (PCI) instrument. The measurement process included injecting 99.99% pure hydrogen gas from a reservoir with a predetermined volume into the sample chamber. For both HGPS and BMPS, after performing pre-hydrogenation steps like volume calibration and leak testing, the sample activation procedure involved heat treatment at 300 °C for six hours under vacuum conditions. The previous work by Muduli and Kale [15] discusses the experimental setup of the PCI instrument employed for hydrogen storage. The topology of the material was examined by Field emission scanning electron microscopy (FESEM, make: NOVA NANOSEM 450, FEI). A multifunctional X-ray diffraction system (XRD) measurement was conducted using an Empyrean XRD instrument with a Cu-K α ($\lambda = 1.54 \text{ \AA}$) X-ray source and a step size of 0.02°. The aim was to observe the structural changes and the crystalline/amorphous nature of the sample. The decomposition of hydrogen was analyzed by performing differential scanning calorimetry (DSC, make: NETZSCH-STA409C) at a heating rate of 10 °C/min.

RESULTS AND DISCUSSION

FESEM images display the distinctions in particle dimensions and surface properties that emerge from the techniques of hand-grinding and ball milling (refer to Fig 1). Following manual grinding, particle sizes span from 10 μm to 30 μm (Fig 1 (a)), whereas ball milling leads to a predominant reduction in particle size to the range of 500 nm to 1 μm (Fig 1 (b)). The BMPS particles agglomerate due to the rough surface and elevated surface energy. A rougher surface traps more hydrogen at exposed sites, boosting storage capacity [2].

The PCI measurement characterizes the thermodynamic aspects of hydrogen adsorption and desorption for HGPS (Fig 2 (a)) and BMPS (Fig 2 (b)) across a range of temperatures and pressures, extending up to 80 bar. Due to the non-uniform particle sizes and comparatively larger particle dimensions in HGPS, hydrogen growth within the material occurs irregularly and uncontrolled, reaching a maximum of 0.42 wt.% at 120 °C. As a result of the nanostructuring achieved through ball milling, BMPS enables a maximum

hydrogen storage capacity of approximately 10.7 wt.% at 80 bar and 120 °C. The reduced particle size and exposure of nanopores to the hydrogen facilitates a periodic and smooth uptake behavior.

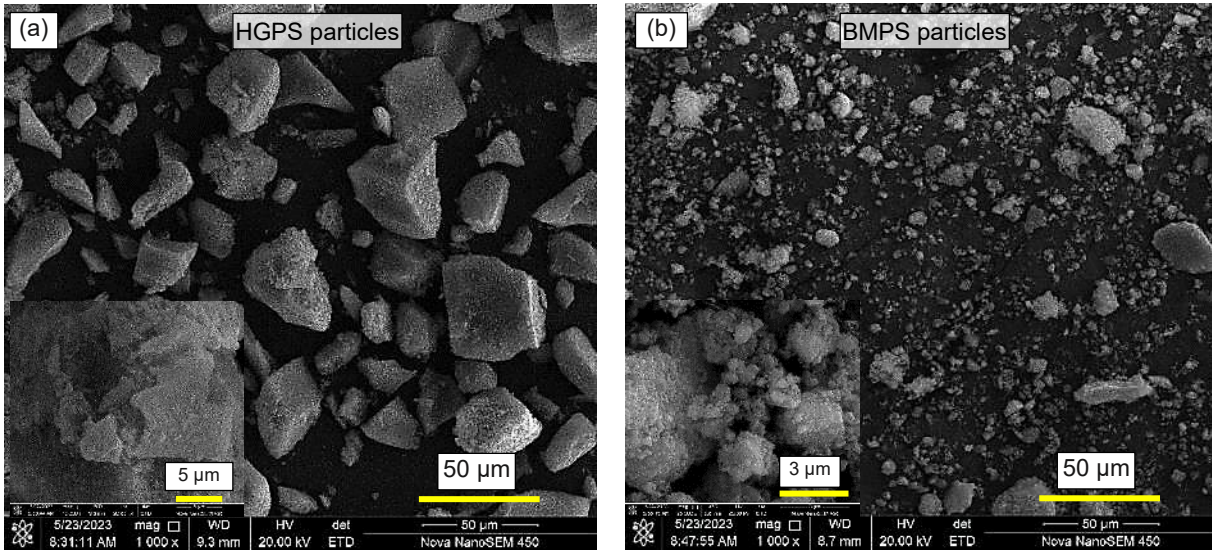


Fig. 1. FESEM images of (a) HGPS particles, (b) BMPS particles

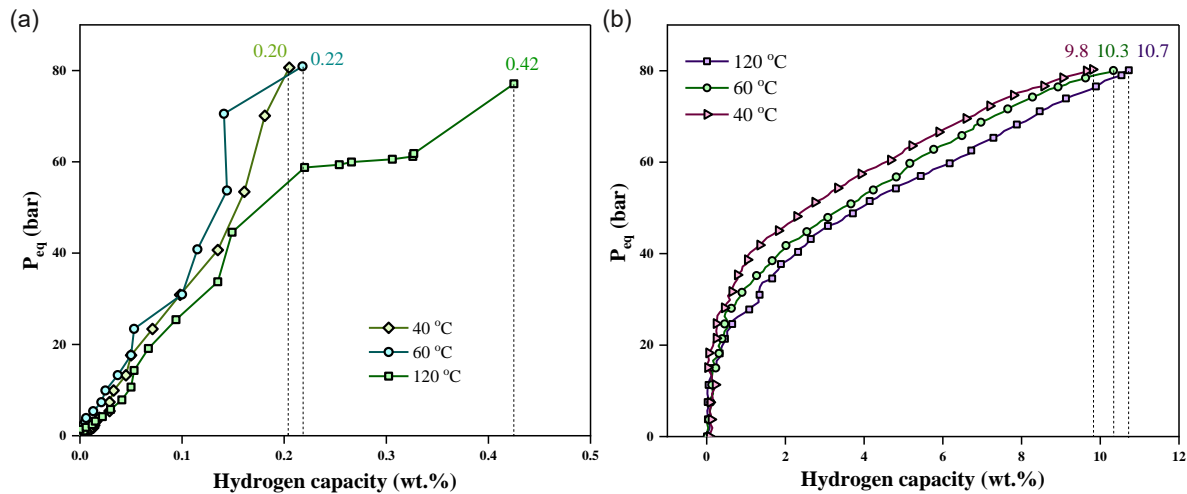


Fig. 2. PCI characterization of (a) HGPS; (b) BMPS at different temperatures and up to 80 bar pressure

Fig. 3 presents a comparative analysis of the crystallite planes and dimensions for HGPS, BMPS, and BMPS subjected to H₂ treatment. Grinding PS led to multiple planes and an augmentation of grain boundary atoms. The broad full width at half maximum (FWHM) in BMPS indicates (refer to Table 1) several changes in its structure, such as elongated grains, altered microstructure, smaller crystallites, and deformation due to ball-milling. The Scherrer equation [16] estimates the nanocrystal size (D_c) by analyzing the broadening of the diffraction line. The average D_c value signifies a 63.2% reduction in crystallite size from 55.1 nm following the ball-milling of HGPS. After undergoing several adsorption and desorption cycles at elevated pressure, the crystallite size of BMPS decreases to 17.7 nm. Crystallinity is quantified by assessing the proportion of the total area beneath crystalline peaks to the total integrated area under the XRD peaks [17].

The thermal decomposition curves provide insights into the stability of the material as the temperature gradually rises from room temperature. Fig. 4 depicts the DSC measurements for HGPS and BMPS conducted in an Argon atmosphere, with the temperature reaching a maximum of 500 °C. The endothermic

peak signifies the complete hydride decomposition, shifting downwards from ~300 °C of HGPS to ~283 °C in BMPS. The lower temperature for hydride decomposition in BMPS reflects the thermodynamic impact of reduced crystallite size. Integrating the endothermic peaks over time determines the enthalpy change (ΔH_d) linked to the decomposition reaction. The ΔH_d value for BMPS drops from 2.30 kJ g⁻¹ in HGPS to 1.56 kJ g⁻¹ following the nanostructuring process through high-energy ball milling.

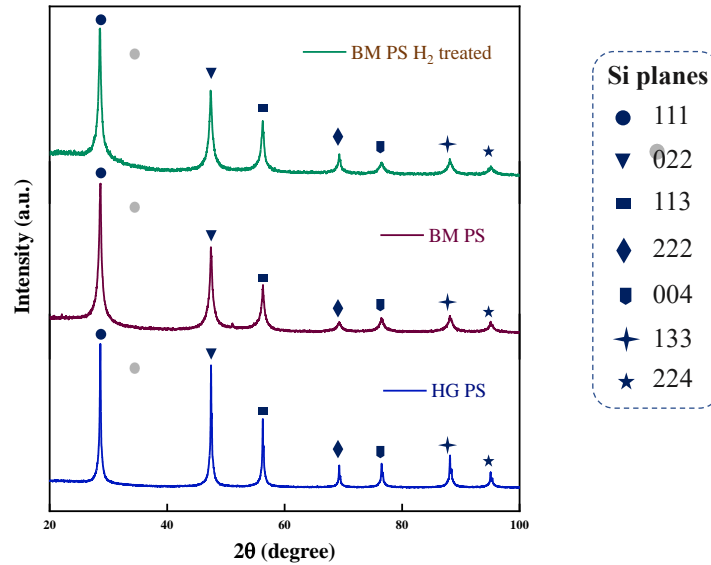


Fig. 3. XRD spectra of HGPS, BMPS, and hydrogen-treated BMPS

Table 1. XRD profile parameters of HGPS, BMPS, and BMPS after H₂-treated

Parameters	HGPS	BMPS	BMPS H ₂ treated
Average D_c considering all planes (nm)	55.11	20.25	17.69
ρ_c (%)	84.46	72.03	71.52
Average FWHM (degree)	0.190	0.574	0.589

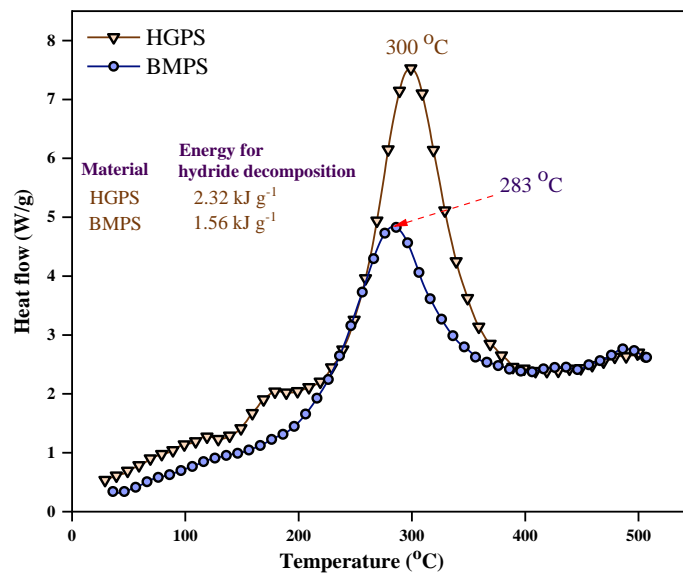


Fig. 4. Thermal decomposition of HGPS and BMPS powders indicating the hydride decomposition endothermic peaks

CONCLUSIONS

The research highlights the structural and functional aspects of BMPS influencing its hydrogen storage properties at high pressures. In BMPS, the smaller crystallite size of ~20 nm maximizes dangling sites, shorter diffusion paths, and increased grain boundary atoms, improving hydrogen adsorption and desorption. At 80 bar pressure and 120 °C temperature, BMPS stores up to 10.7 wt.% of hydrogen, satisfying the US DOE target. The nanocrystalline PS accelerates the rate of hydrogen adsorption and improves the storage capacity by providing multiple activated sites. With increasing pressure, surface and pore volume coverage expands proportionally, requiring higher pressure levels to saturate with the target molecule. The minimal alterations in the BMPS structure following hydrogenation cycles indicate the possibility of enhanced cyclic durability. The hydride decomposition temperature of BMPS drops to ~283 °C, which is lower than the typical temperatures required for commonly used metal and complex hydrides (~400 °C). Therefore, nanostructuring provides feasible conditions to meet the solid-state hydrogen storage objectives and potentially enable applications in reversible storage.

ACKNOWLEDGEMENT

The research is part of a project funded by the DST-IIT Bombay Energy Storage Platform on Hydrogen (DST/TMD/MECSP/2K17/14 (G), 14 February 2019). The authors thank Mr. Dinesh Dashbabu (IIT Tirupati) and Mr. Neeraj Kumar Nishad (NIT Rourkela) for their support in conducting the experiment and technical discussion. The authors thank Dr. Fangqin Guo, Dr. Hiroki Miyaoka, Dr. Ankur Jain, and Zhiwen Chen from Hiroshima University, Japan, for their support in performing PCI isotherms, XPS characterization, and technical discussions.

REFERENCES

- [1] T. Capurso, M. Stefanizzi, M. Torresi, S.M. Camporeale, Perspective of the role of hydrogen in the 21st century energy transition, *Energy Convers. Manag.* 251 (2022) 114898. <https://doi.org/10.1016/j.enconman.2021.114898>.
- [2] R. Chandra Muduli, P. Kale, Silicon nanostructures for solid-state hydrogen storage: A review, *Int. J. Hydrogen Energy.* 48 (2023) 1401–1439. <https://doi.org/10.1016/j.ijhydene.2022.10.055>.
- [3] J.O. Abe, A.P.I. Popoola, E. Ajenifuja, O.M. Popoola, Hydrogen energy, economy and storage: Review and recommendation, *Int. J. Hydrogen Energy.* 44 (2019) 15072–15086. <https://doi.org/10.1016/j.ijhydene.2019.04.068>.
- [4] R. Chandra Muduli, P. Kale, Chemically modified surface of silicon nanostructures to enhance hydrogen uptake capabilities, *Int. J. Hydrogen Energy.* (2022). <https://doi.org/10.1016/j.ijhydene.2022.06.030>.
- [5] A. Jain, H. Miyaoka, T. Ichikawa, Destabilization of lithium hydride by the substitution of group 14 elements: A review, *Int. J. Hydrogen Energy.* 41 (2016) 5969–5978. <https://doi.org/10.1016/j.ijhydene.2016.02.069>.
- [6] P. Prachi R., W. Mahesh M., G. Aneesh C., A Review on Solid State Hydrogen Storage Material, *Adv. Energy Power.* 4 (2016) 11–22. <https://doi.org/10.13189/aep.2016.040202>.
- [7] Z. Chen, K.O. Kirlikovali, K.B. Idrees, M.C. Wasson, O.K. Farha, Porous materials for hydrogen storage, *Chem.* 8 (2022) 693–716. <https://doi.org/10.1016/j.chempr.2022.01.012>.
- [8] M.U. Niemann, S.S. Srinivasan, A.R. Phani, A. Kumar, D.Y. Goswami, E.K. Stefanakos, Nanomaterials for hydrogen storage applications: A review, *J. Nanomater.* 2008 (2008) 1–9. <https://doi.org/10.1155/2008/950967>.
- [9] M.A. Rahmaninasab, S. Raygan, H. Abdizadeh, M. Pourabdoli, S.H. Mirghaderi, Properties of activated MgH₂ + mischmetal nanostructured composite produced by ball-milling, *Mater. Renew. Sustain. Energy.* 7 (2018) 15. <https://doi.org/10.1007/s40243-018-0122-z>.
- [10] A.C. Gangal, P. Kale, R. Edla, J. Manna, P. Sharma, Study of kinetics and thermal decomposition of ammonia borane in presence of silicon nanoparticles, *Int. J. Hydrogen Energy.* 37 (2012) 6741–6748. <https://doi.org/10.1016/j.ijhydene.2012.01.017>.
- [11] S. Merazga, A. Cheriet, K. M'hammedi, A. Mefoued, N. Gabouze, Investigation of porous silicon thin films for electrochemical hydrogen storage, *Int. J. Hydrogen Energy.* 44 (2019) 9994–10002. <https://doi.org/10.1016/j.ijhydene.2019.03.017>.
- [12] P. Kale, A.C. Gangal, R. Edla, P. Sharma, Investigation of hydrogen storage behavior of silicon nanoparticles, *Int. J. Hydrogen Energy.* 37 (2012) 3741–3747. <https://doi.org/10.1016/j.ijhydene.2011.04.054>.
- [13] S.S. Samantaray, V. Sangeetha, S. Abinaya, S. Ramaprabhu, Diatom frustule-graphene based nanomaterial for room temperature hydrogen storage, *Int. J. Hydrogen Energy.* 45 (2020) 764–773. <https://doi.org/10.1016/j.ijhydene.2019.10.155>.
- [14] M. Sevilla, W. Sangchoom, N. Balahmar, A.B. Fuertes, R. Mokaya, Highly porous renewable carbons for



- enhanced storage of energy-related gases (H₂ and CO₂) at high pressures, ACS Sustain. Chem. Eng. 4 (2016) 4710–4716. <https://doi.org/10.1021/acssuschemeng.6b00809>.
- [15] R. Chandra Muduli, P. Kale, Synergetic effect of porous silicon–Nickel composite on its solid-state hydrogen energy storage properties, Int. J. Hydrogen Energy. (2023). <https://doi.org/10.1016/j.ijhydene.2023.05.268>.
- [16] M.K. Sahoo, P. Kale, Role of secondary etching of silicon nanowires towards quantum confinement effect, Superlattices Microstruct. 156 (2021) 106949. <https://doi.org/10.1016/j.spmi.2021.106949>.
- [17] V.K. Hiremath, R.C. Muduli, P. Kale, Investigation of the Stability and Insulating Properties of Mineral Oil-Based Surface Modified Silicon Nanofluid, IEEE Trans. Dielectr. Electr. Insul. (2023) 1–1. <https://doi.org/10.1109/TDEI.2023.3242231>.

ICH2P14-PP016

EVALUATION OF SYNERGISTIC INTEGRATION OF NICKEL, POROUS SILICON, AND THERMALLY REDUCED GRAPHENE OXIDE FOR HYDROGEN STORAGE

^{1,3*}Rama Chandra Muduli, ¹Neeraj Kumar Nishad, ²Dinesh Dashbabu, ^{2,3}E. Anil Kumar, ^{1,3}Paresh Kale

¹Department of Electrical Engineering, National Institute of Technology Rourkela, Odisha, India, 769008

²Department of Mechanical Engineering, Indian Institute of Technology Tirupati, Andhra Pradesh, India, 517619

³DST-IIT Bombay Energy Storage Platform on Hydrogen, IIT Bombay, Maharashtra, India, 400076

*Corresponding author e-mail: muduliramachandra@gmail.com

ABSTRACT

Solid-state hydrogen storage by metal hydrides is a potential way to achieve high storage capacities; yet, high-temperature operations (>400 °C), heat exchange issues, and exothermic formation process are significant drawbacks. Under this perspective, adsorption on porous materials emerges as a viable solution to address these challenges. Carbon nanostructures (such as graphene and graphene oxide (GO) based derivatives) are adequate for hydrogen storage due to their lightweight, low density, and large surface area. However, the poor storage capacity of carbon nanostructures under ambient conditions is the major bottleneck for practical applications. Using a cost-effective transition element like Ni as a catalyst holds significant potential for storing hydrogen in atomic and molecular forms, invoking the spillover mechanism. The porous silicon (PS) stabilizes when decorated on thermally reduced GO (TrGO). PS modifies the surface properties of the graphene sheets and attracts hydrogen toward the surface. The current work evaluates a composition of TrGO, PS, and Ni, synthesized to take advantage of individual properties for hydrogen storage. Field-emission scanning electron microscopy investigates the sheet structure of TrGO and the incorporation of PS and Ni onto its surface. The presence of various phases in the composition is identified using X-ray diffraction. Raman spectroscopy quantifies the degree of disorder in the composition. The pressure-composition isotherms indicate hydrogen storage capacities of 2.43 wt.% for TrGO-PS-Ni composition.

Keywords: Pressure composition isotherm, Isosteric heat energy, Catalytic effect, Thermodynamic stability, adsorption rate

INTRODUCTION

Hydrogen attracts significant research interest due to its potential as a promising energy carrier. It boasts an impressive energy density of 142 MJ kg⁻¹ and serves as a viable and eco-friendly alternative energy source [1]. Solid-state hydrogen storage is preferred over conventional methods due to cost and safety considerations, addressing a major obstacle in advancing hydrogen-based applications [2]. Materials such as metal hydrides and complex metal hydrides offer the potential for hydrogen storage at room temperature and high pressures. Still, their major drawbacks include limited reversibility and slow reaction rates due to strong chemical bonds [3,4]. Porous adsorption materials such as metal-organic frameworks, zeolites, and carbon nanostructures can effectively store hydrogen at extremely low temperatures [5]. However, the common porous materials used for hydrogen storage have limitations under normal conditions, including low storage capacity, cycling issues, and weak binding. Carbon-based nanostructures doped with light heteroatoms and decorated with transition elements are examined to improve storage under ambient conditions [5,6].

The theoretical capacity of hydrogen adsorption as a monolayer on a single side of a graphene sheet is ~3 wt.%. Nevertheless, hydrogen molecules cannot penetrate between the layers of graphite due to their significant thermodynamic stability [7]. Srinivas et al. [8] reported hydrogen adsorption capacities of ~1.2 wt.% and 0.1 wt.% at -196 °C and 25 °C, respectively. Due to the dense layer of oxygen functionalized groups in graphene oxide (GO), the hydrogen storage capacity is poor (i.e., 1.4 wt.% at 50 bar and 25 °C) [9,10]. Thermal reduction of GO (TrGO) efficiently improves the surface area and porous surface, achieving

4.8 wt.% at -196 °C and 90 bar [11]. However, based on recent studies concerning TrGO, it allows poor storage capacities of ~0.35 wt.% (at zero °C) and no storage (at 25 °C) up to 20 bar [5]. Transition materials like Pd decorated activated carbon showed 2.5 wt.% hydrogen uptake at 25 °C and 20 bar [12]. With the addition of Ni and boron to TrGO, the storage capacity is around 0.41 wt.% at 0 °C and 0.16 wt.% at 25 °C [5].

The theoretical hydrogen storage capacity of the Si-decorated graphene layer is ~15 wt.%, surpassing the 6 wt.% target set by the US DOE [13]. Nanostructuring the bulk Si improves the surface energy, enhancing the adsorption capacity [14]. Porous silicon is an optimized Si nanostructure, facilitating significant surface potential for hydrogen storage [1,15]. Honarpazhouh et al. [16] reported the synergistic effect of PS and Pd on GO, resulting in an improved hydrogen storage capacity of 546.1 mAh g⁻¹ (~2.1 wt.%) than individual PS or Pd/PS. The evaluation of hydrogen storage in the Pd-Carbon nanotube/PS/Si structure shows a storage capacity of 537 mAh g⁻¹ (~2.05 wt.%) [17]. The Si and carbon nanotube interface forms shorter C-C bonds, reducing the Si-Si bonds and allowing hydrogen splitting and spillover [18].

Past research on hydrogen storage with carbon nanostructures usually involved cryogenic temperatures, but there is limited information on storage conditions at or above room temperature. Nickel is preferred over palladium and platinum as a cost-effective catalyst for promoting the dissociation of hydrogen adsorption. As per prior findings, in contrast to Pd, Ni retains insignificant hydrogen under ambient temperature and pressure below 100 bar, primarily functioning as a catalyst [5,19]. The study aims to enhance the hydrogen storage capabilities of TrGO by adding PS and Ni decorations.

METHODOLOGY AND EXPERIMENTATION

The graphene oxide was synthesized using the modified Hummers method [20], which entails combining two grams of graphite powder (with particle sizes ranging from 2 to 11 μm, purchased from Sigma Aldrich) with a solution of nitric acid (13.2 ml, 69%) and sulfuric acid (80 ml, 98%) in a 1000 mL volumetric flask. The mixture was continuously stirred for 40 minutes within an ice bath, maintaining a temperature between 10°C and 20°C. Subsequently, 12 grams of potassium permanganate (99% purity) were introduced and stirred for two hours. After removing the ice bath, 100 mL of deionized (DI) water was added to the solution, causing the temperature to rise to 95°C and changing color to brown. Hydrogen peroxide (30% concentration, Merck) was slowly added to the solution to stop oxidation, transforming the color of the solution to greenish-yellow. This mixture was allowed to settle for 16 hours. The remaining graphene oxide (GO) was acquired by washing with hydrochloric acid (36% concentration, Fisher Scientific) and DI water, then exfoliated through 24 hours of sonication. Thermal reduction of the GO was carried out at 180°C for 40 minutes, resulting in the synthesis of TrGO with increased volume and a significant reduction in mass.

PS was synthesized by electrochemical anodization on a silicon wafer, followed by electropolishing to remove the PS film [15,21]. The storage material was crafted by manually grinding together TrGO (237 g), PS (63.2 g), and commercially acquired Ni powder (94.8 g, Thermo Fisher, with particle sizes ranging from 3 μm to 7 μm) in a proportion of 60% TrGO, 16% PS, and 24% Ni. This combination is referred to as the TrGO+Ni+PS composite. During the investigation, structural and elemental analysis was performed using FESEM (FEI Nova Nano SEM 450) equipped with energy-dispersive X-ray Spectroscopy (EDX). A Raman spectroscope (WITec Alpha300) employing a laser power of less than 3 mW, a wavelength of 532 nm, and a diffraction grating setting of 600 grooves/mm was utilized to assess structural and vibrational properties. Hydrogen storage was quantified using a Pressure Composition Isotherm instrument (PCI, by Setaram Instrumentation in France). Applying a pressure of 10 bar at 200°C for six hours triggers the activation of adsorption sites by degassing the material.

RESULTS AND DISCUSSION

The morphology of TrGO, as shown in Fig 1 (a), is characterized by stacked sheets with pores and a crumpled appearance. The surface area of the porous surface improves by partially removing oxygen functional groups (primarily CO and CO₂), introducing defects in the structure. The hand grinding of TrGO, PS, and Ni, as depicted in Fig 1 (b), results in the partial restoration of stacked graphite layers, giving rise to a wavy morphology. The grinding leads to a morphology characterized by loosely stacked and increased crumpling, thereby introducing structural defects. The EDX mapping inset manifests the decoration of both Si and Ni on the TrGO+PS+Ni composite.

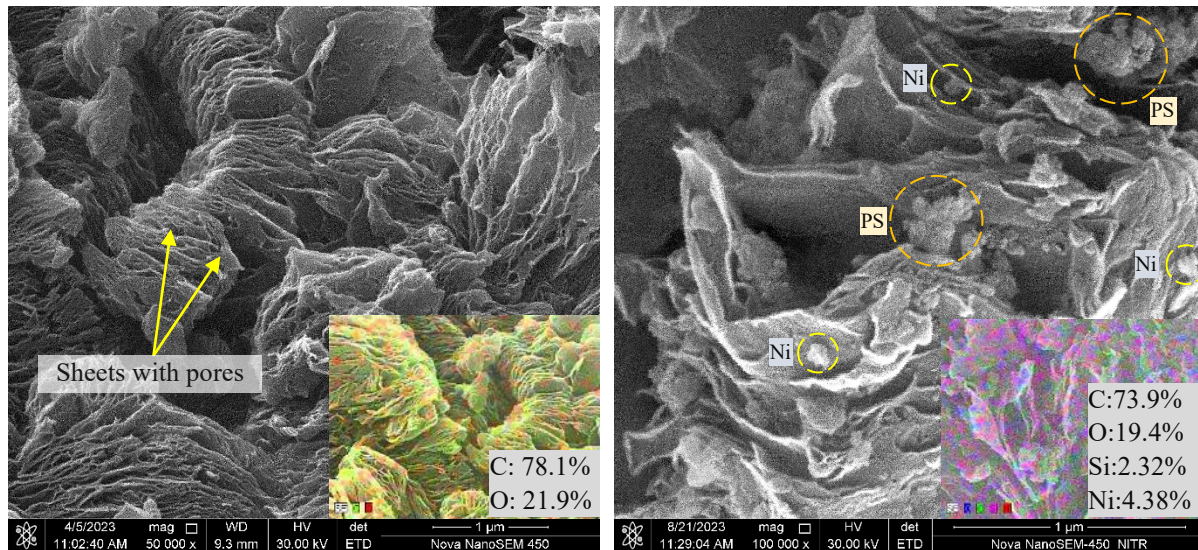


Fig. 1. FESEM images of (a) TrGO with a highly porous surface and EDX mapping inset, (b) TrGO+PS+Ni and its EDX mapping indicating the presence of Si and Ni

Fig. 2 (a) illustrates the PCI evaluation of hydrogen storage capacity within the TrGO+PS+Ni composite, considering different conditions, including pressures up to 50 bar and three different temperatures (40°C, 60°C, and 80°C). The highest storage capacity is observed at 40°C, reaching 2.43 wt% under a pressure of 50 bar. With a consistent charging pressure, the storage capacity diminishes as the temperature increases, suggesting that the bonding stability between carbon and hydrogen weakens as the temperature rises. Since Ni is unable to store hydrogen under standard atmospheric conditions and primarily acts as a catalyst to facilitate hydrogen dissociation [5,19], the storage capacity, excluding the weight of Ni, reaches ~3.1 wt.% at 40°C. The observed capacity is significantly higher than the reported hydrogen storage capacity in the rGO-Ni-B composite (i.e., 0.41 wt.% and 0.16 wt.% at ~ 0 °C and 25 °C at up to 20 bar, respectively) [5].

The gradually sloping plateau indicates the hydride formation involving a combination of physisorption and pore diffusion. The van't Hoff equation [19] provides that the thermodynamic aspects are graphically represented using adsorption temperatures of 40°C, 60°C, and 80°C. The equilibrium pressure (P_{eq}) is characterized by both changes in hydrogenation enthalpy (ΔH) and entropy (ΔS). The slope on the graph indicates a change in enthalpy (ΔH) of ~2.89 kJ mol⁻¹ of H₂, while the intercept represents a change in entropy (ΔS) of ~21.50 J mol⁻¹ of H₂. Lower enthalpy points to physisorption on the surface and suggests a low-temperature necessity for hydride decomposition, signifying low hydride stability [19].

The Raman spectra of carbon composites (refer to Fig. 3) display two noticeable carbon peaks at approximately 1350 cm⁻¹ (D-band) and 1580 cm⁻¹ (G-band) [22]. The G-band is associated with the vibrations of carbon atoms arranged in a hexagonal lattice with sp² hybridization, while the D-band originates from the oscillations of carbon atoms with sp³ hybridization and defects present within the carbon structure. The I_D/I_G intensity ratio (the defect ratio) indicates the level of disorder within the structure, as indicated in Table 1. The introduction of PS and Ni to TrGO leads to an increase in defects, with the ID/IG

ratio rising to 0.98 before PCI and 0.99 after PCI, known as the Tuinstra-Koenig relationship (refer to equation 1 [23]), is employed to calculate the average crystallite size (L_a) in graphene material by utilizing the defect ratio, with λ (532 nm) representing the laser wavelength. Table 1 indicates that the structure with the most defects also have the smallest crystallite size.

$$L_a \text{ (nm)} = (2.4 \times 10^{-10}) \lambda^4 \left(\frac{I_D}{I_G} \right)^{-1} \quad (1)$$

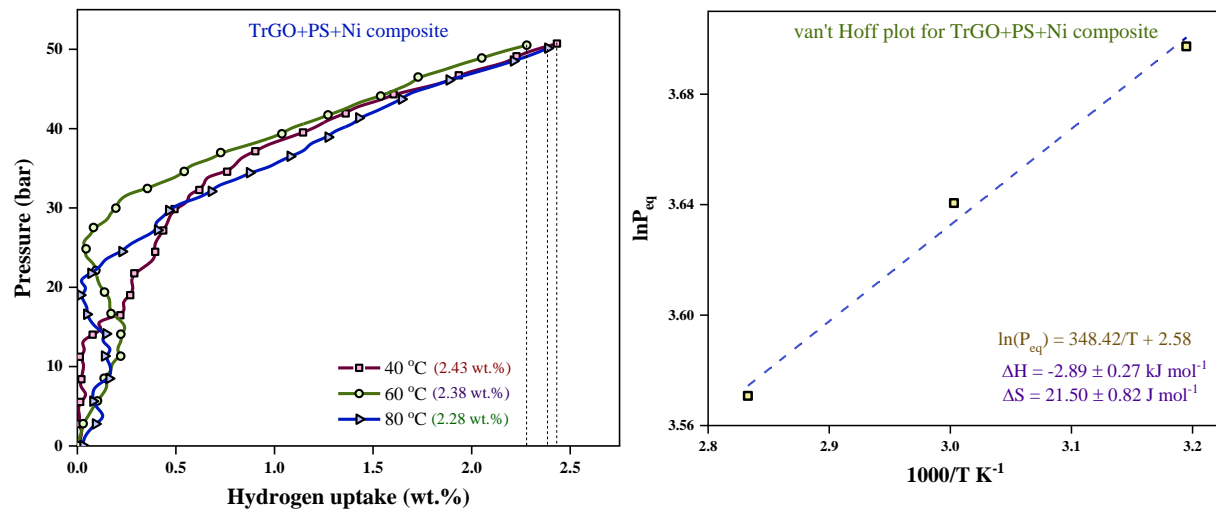


Fig. 2. PCI isotherms of TrGO+PS+Ni composites for hydrogen storage at 50 bar and three different temperatures (40 °C, 60 °C, and 80 °C) and (b) van't Hoff plot for TrGO+PS+Ni composites considering 40 °C, 60 °C, and 80 °C

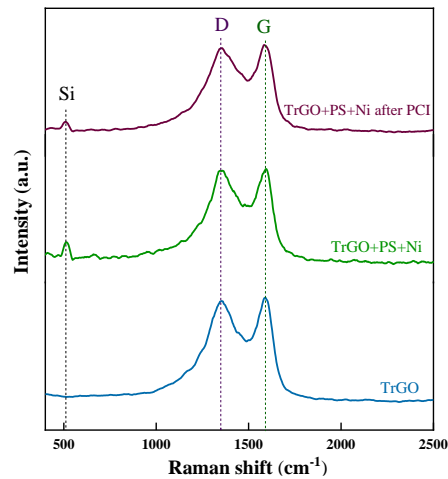


Fig. 3. Raman spectra showing I_D/I_G values of TrGO, TrGO+PS+Ni, and TrGO+PS+Ni composite after PCI characterization

Table 1. The parameters (I_D/I_G and L_a) obtained from Raman spectra

Material	I_D/I_G	L_a (nm)
TrGO	0.93	20.67
TrGO+PS+Ni	0.98	19.61
TrGO+PS+Ni after PCI	0.99	19.42

A transition metal, such as Ni, serves as a solid-state modifier, facilitating the dissociation of hydrogen at charging pressure through the spillover phenomenon. Due to the regular arrangement of carbon atoms by covalent solid bonding and the availability of less active sites for foreign elements [24], individual graphene shows poor hydrogen storage capacity. In contrast, the thermal reduction of GO provides a higher number of active sites for foreign elements. Including foreign elements, such as PS and Ni, enhances storage by serving as stabilizers and catalysts on the surface of TrGO.

CONCLUSIONS

The present study investigates innovative material composition involving functionalized graphene (TrGO) adorned with PS and Ni nanoparticles to enhance solid-state hydrogen storage capabilities. Incorporating PS and Ni into TrGO creates a wavy graphene-layered structure decorated with Si and Ni. The wavy arrangement causes the potential fields of carbon atoms to intersect, thereby increasing the storage capacity. Under the hydrogen charging pressure, molecular hydrogen dissociates on the adorned surface and subsequently permeates into the carbon interlayers. The reduced addition of defects in the TrGO+PS+Ni composite structure after PCI cycles shows its effectiveness in storing hydrogen efficiently for repeated use in cyclic storage applications. The findings indicate that a further improvement in the ratio distribution of PS and Ni with TrGO is essential to boost both the gravimetric storage (hydrogen wt.%) and the rate of hydrogen adsorption in the composite.

ACKNOWLEDGMENT

The research is part of a project funded by the DST-IIT Bombay Energy Storage Platform on Hydrogen (DST/TMD/MECSP/2K17/14 (G), 14-February-2019) and partially funded by the Institution of Engineers (India), 8 Gokhale Road, Kolkata 700020, under the R&D Grant-in-Aid scheme (R.6/2/DR/2022-23/DR2023004, 24-August-2022).

REFERENCES

- [1] R. Chandra Muduli, P. Kale, Silicon nanostructures for solid-state hydrogen storage: A review, *Int. J. Hydrogen Energy*. 48 (2023) 1401–1439. <https://doi.org/10.1016/j.ijhydene.2022.10.055>.
- [2] E. Callini, K.F. Aguey-Zinsou, R. Ahuja, J.R. Ares, S. Bals, N. Biliškov, S. Chakraborty, G. Charalambopoulou, A.L. Chaudhary, F. Cuevas, B. Dam, P. de Jongh, M. Dornheim, Y. Filinchuk, J. Grbović Novaković, M. Hirscher, T.R. Jensen, P.B. Jensen, N. Novaković, Q. Lai, F. Leardini, D.M. Gattia, L. Pasquini, T. Steriotis, S. Turner, T. Vegge, A. Züttel, A. Montone, Nanostructured materials for solid-state hydrogen storage: A review of the achievement of COST Action MP1103, *Int. J. Hydrogen Energy*. 41 (2016) 14404–14428. <https://doi.org/10.1016/j.ijhydene.2016.04.025>.
- [3] M. Hirscher, V.A. Yartys, M. Baricco, J. Bellosta von Colbe, D. Blanchard, R.C. Bowman, D.P. Broom, C.E. Buckley, F. Chang, P. Chen, Y.W. Cho, J.C. Crivello, F. Cuevas, W.I.F. David, P.E. de Jongh, R. V. Denys, M. Dornheim, M. Felderhoff, Y. Filinchuk, G.E. Froudakis, D.M. Grant, E.M.A. Gray, B.C. Hauback, T. He, T.D. Humphries, T.R. Jensen, S. Kim, Y. Kojima, M. Latroche, H.W. Li, M. V. Lototskyy, J.W. Makepeace, K.T. Møller, L. Naheed, P. Ngene, D. Noréus, M.M. Nygård, S. ichi Orimo, M. Paskevicius, L. Pasquini, D.B. Ravnsbæk, M. Veronica Sofianos, T.J. Udovic, T. Vegge, G.S. Walker, C.J. Webb, C. Weidenthaler, C. Zlotea, Materials for hydrogen-based energy storage – past, recent progress and future outlook, *J. Alloys Compd.* 827 (2020) 153548. <https://doi.org/10.1016/j.jallcom.2019.153548>.
- [4] R. Chandra Muduli, Z. Chen, K. Shinzato, F. Guo, T. Ichikawa, A. Jain, H. Miyaoka, P. Kale, Thermodynamic improvement of lithium hydrides for hydrogen absorption and desorption by incorporation of porous silicon, *Int. J. Hydrogen Energy*. (2023). <https://doi.org/10.1016/j.ijhydene.2023.09.015>.
- [5] A. Flamina, R.M. Raghavendra, A. Gupta, A. Subramaniam, Hydrogen storage in Nickel dispersed boron doped reduced graphene oxide, *Appl. Surf. Sci. Adv.* 13 (2023) 100371. <https://doi.org/10.1016/j.apsadv.2023.100371>.
- [6] A. Yadav, M. Faisal, A. Subramaniam, N. Verma, Nickel nanoparticle-doped and steam-modified multiscale structure of carbon micro-nanofibers for hydrogen storage: Effects of metal, surface texture and operating

- [7] conditions, *Int. J. Hydrogen Energy*. 42 (2017) 6104–6117. <https://doi.org/10.1016/j.ijhydene.2016.11.070>.
S. Gadipelli, Z.X. Guo, Graphene-based materials: Synthesis and gas sorption, storage and separation, *Prog. Mater. Sci.* 69 (2015) 1–60. <https://doi.org/10.1016/j.pmatsci.2014.10.004>.
- [8] G. Srinivas, Y. Zhu, R. Piner, N. Skipper, M. Ellerby, R. Ruoff, Synthesis of graphene-like nanosheets and their hydrogen adsorption capacity, *Carbon N. Y.* 48 (2010) 630–635.
<https://doi.org/10.1016/j.carbon.2009.10.003>.
- [9] A. Salehabadi, M.F. Umar, A. Ahmad, M.I. Ahmad, N. Ismail, M. Rafatullah, Carbon-based nanocomposites in solid-state hydrogen storage technology: An overview, *Int. J. Energy Res.* 44 (2020) 11044–11058.
<https://doi.org/10.1002/er.5674>.
- [10] V. Jain, B. Kandasubramanian, Functionalized graphene materials for hydrogen storage, *J. Mater. Sci.* 55 (2020) 1865–1903. <https://doi.org/10.1007/s10853-019-04150-y>.
- [11] B.H. Kim, W.G. Hong, H.Y. Yu, Y.K. Han, S.M. Lee, S.J. Chang, H.R. Moon, Y. Jun, H.J. Kim, Thermally modulated multilayered graphene oxide for hydrogen storage, *Phys. Chem. Chem. Phys.* 14 (2012) 1480–1484. <https://doi.org/10.1039/c2cp23683d>.
- [12] C.I. Contescu, C.M. Brown, Y. Liu, V. V. Bhat, N.C. Gallego, Detection of hydrogen spillover in palladium-modified activated carbon fibers during hydrogen adsorption, *J. Phys. Chem. C.* 113 (2009) 5886–5890.
<https://doi.org/10.1021/jp900121k>.
- [13] M.D. Ganji, S.N. Emami, A. Khosravi, M. Abbasi, Si-decorated graphene: A promising media for molecular hydrogen storage, *Appl. Surf. Sci.* 332 (2015) 105–111. <https://doi.org/10.1016/j.apsusc.2015.01.151>.
- [14] P.G. Kale, P. Sharma, C.S. Solanki, Synthesis and characterization of Si nanoparticles obtained on sonication of porous Silicon multilayer films, *J. Nano Res.* 17 (2012) 13–25.
<https://doi.org/10.4028/www.scientific.net/JNanoR.17.13>.
- [15] R. Chandra Muduli, P. Kale, Chemically modified surface of silicon nanostructures to enhance hydrogen uptake capabilities, *Int. J. Hydrogen Energy*. (2022). <https://doi.org/10.1016/j.ijhydene.2022.06.030>.
- [16] Y. Honarpazhouh, F.R. Astarai, H.R. Naderi, O. Tavakoli, Electrochemical hydrogen storage in Pd-coated porous silicon/graphene oxide, *Int. J. Hydrogen Energy*. 41 (2016) 12175–12182.
<https://doi.org/10.1016/j.ijhydene.2016.05.241>.
- [17] H.G. Shiraz, M.G. Shiraz, Palladium nanoparticle and decorated carbon nanotube for electrochemical hydrogen storage, *Int. J. Hydrogen Energy*. 42 (2017) 11528–11533.
<https://doi.org/10.1016/j.ijhydene.2017.03.129>.
- [18] A.J. Williamson, F.A. Reboledo, G. Galli, Chemisorption on semiconductor nanocomposites: A mechanism for hydrogen storage, *Appl. Phys. Lett.* 85 (2004) 2917–2919. <https://doi.org/10.1063/1.1800274>.
- [19] R. Chandra Muduli, P. Kale, Synergetic effect of porous silicon–Nickel composite on its solid-state hydrogen energy storage properties, *Int. J. Hydrogen Energy*. (2023).
<https://doi.org/10.1016/J.IJHYDENE.2023.05.268>.
- [20] S.P. Muduli, S. Parida, S. Nayak, S.K. Rout, Effect of Graphene Oxide loading on ferroelectric and dielectric properties of hot pressed poly(vinylidene fluoride) matrix composite film, *Polym. Compos.* 41 (2020) 2855–2865. <https://doi.org/10.1002/pc.25581>.
- [21] S. Maurya, S.P. Muduli, S. Nayak, P. Kale, Optimization of Controlling Parameters of Porous Silicon Synthesis Using Taguchi Design of Experiment, *Russ. J. Phys. Chem. A.* 97 (2023) 749–755.
<https://doi.org/10.1134/S0036024423040295>.
- [22] S.K. Jerng, D.S. Yu, J.H. Lee, C. Kim, S. Yoon, S.H. Chun, Graphitic carbon growth on crystalline and amorphous oxide substrates using molecular beam epitaxy, *Nanoscale Res. Lett.* 6 (2011) 1–6.
<https://doi.org/10.1186/1556-276X-6-565>.
- [23] L.G. Cañado, K. Takai, T. Enoki, M. Endo, Y.A. Kim, H. Mizusaki, A. Jorio, L.N. Coelho, R. Magalhães-Paniago, M.A. Pimenta, General equation for the determination of the crystallite size l_a of nanographite by Raman spectroscopy, *Appl. Phys. Lett.* 88 (2006) 163106. <https://doi.org/10.1063/1.2196057>.
- [24] S.K. Tiwari, S. Sahoo, N. Wang, A. Huczko, Graphene research and their outputs: Status and prospect, *J. Sci. Adv. Mater. Devices.* 5 (2020) 10–29. <https://doi.org/10.1016/j.jsamd.2020.01.006>.

ICH2P14-OP041

FAST MODELING METHOD OF GAS DIFFUSION LAYERS OF POLYMER ELECTROLYTE MEMBRANE FUEL CELLS

**Hamid Reza Taheri, Mohsen Shakeri*

¹Babol Noshirvani University of Technology (BNUT), Renewable Energy Research Center, Mechanical Engineering Department, Babol, Iran

*Corresponding author e-mail: H.Taheri@nit.ac.ir

ABSTRACT

Among the most important challenges facing the modelers of diffusion media used in polymer electrolyte membrane fuel cells (PEMFCs), in addition to complexity, we can point out cheapness and fastness of modeling method, closeness to reality and non-simplifying assumptions for microstructures of the composite gas diffusion layer (CGDL). Some previous modeling methods need to graphical interface programs and spend more time and money. Hence, it is very useful to presenting a novel, more efficient and direct method as research application to easily investigating numerically the effective transfer properties such as: effective electrical conductivity/EEC, effective thermal conductivity/ETC and permeability. So, the aims of current article are: (i) to simulating realistically a comprehensive microstructure (GDL, micro porous layer/MPL, PolyTetraFluoroEthylene/PTFE and binder) of a paper CGDL type (SGL 38BC), based on scanning electron microscope (SEM) images' data, in which the essential inputs for geometry generator MATLAB code provided and the reconstructed microstructure in the MATLAB, using the live link technique for subsequent processing is transferred to the COMSOL Multiphysics software, and (ii) to estimating numerically the mentioned effective transfer properties. Thus, a 3D stochastic reconstruction of microstructure of SGL 38BC used to EEC, ETC and permeability estimating in both in-plane (IP) and through-plane (TP) directions. As a validation, the 3D simulation result of the current method is compared with a 3D microstructure reconstructed from the same CGDL, using X-ray micro computed tomography (X-ray μ CT).

Keywords: Micro/Macro Porous Layer, Live Link Modeling Technique, Effective Electrical Conductivity, Effective Thermal Conductivity, Permeability.

INTRODUCTION

The complexity of simulating the porous microstructures of composite gas diffusion layers (CGDLs), is a well-known issue. Some modeling methods need to spend more time and money (e.g., image processing process and the expensive X-ray micro computed tomography / X-ray μ CT) despite less accuracy and more interaction with the user. The studies of Refs. [1-7], simulated the CGDLs' microstructures and have focused on various aspects of CGDLs including improvement of: mechanical properties, thermal-electrical conductivity and mass transfer. Of course, only some of them considered the presence of microporous layer (MPL) and binding agent (polytetrafluoroethylene / PTFE /binder). Although the used methods may lead us to determine characteristic such as: effective electrical/ thermal conductivities (EEC/ETC) and permeability, a more direct and faster method for reconstructing of geometric microstructures is needed to carry out geometric optimization of CGDLs.

METHODS

In order to reconstructing the microstructure of a paper CGDL treated by MPL (SGL 38BC), "first" by using the steps fully explained in Fig. (1), the microstructure of CGDL is reconstructed, "then" each of the mentioned desired properties is calculated.

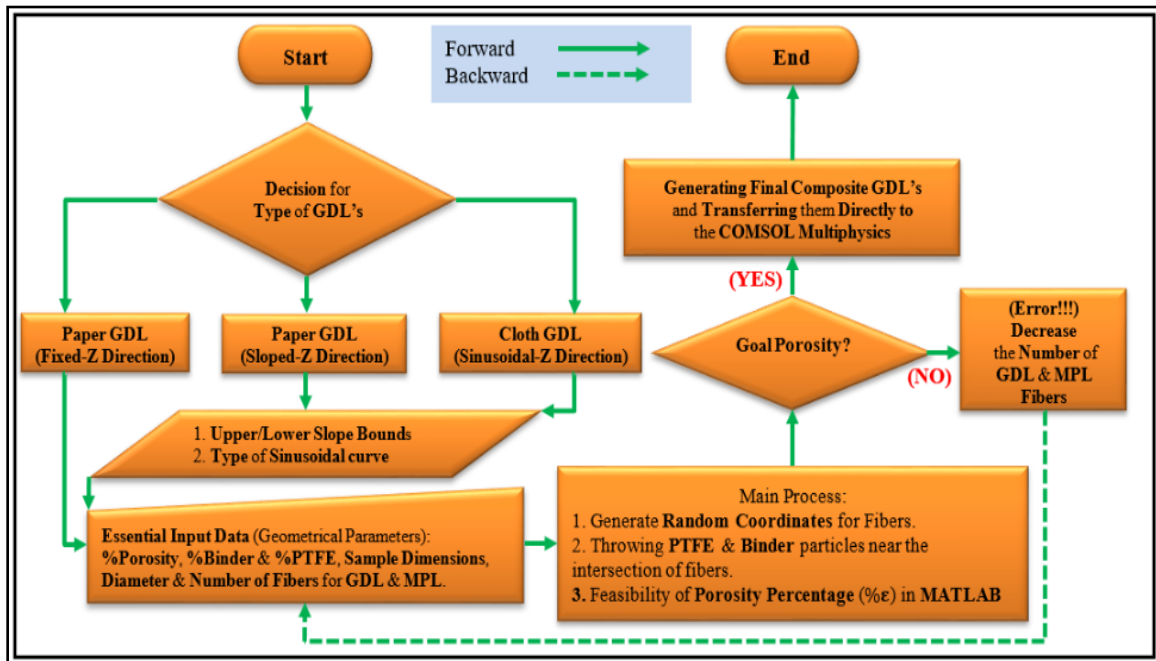


Fig. 1 Flowchart of the summary of the main reconstruction steps of a paper or cloth CGDL.

Numerical Simulation

Using the SEM images of CGDL microstructure, the values of effective geometrical parameters such as: porosity, thicknesses of GDL/MPL layers, diameter and direction of carbon fibers along the all axes are measured and used as inputs to MATLAB geometry generator code. Thus, the microstructure of comprehensive diffusion medium (GDL+MPL) consisting of binding agent will be reconstructed as computational domain (CD) in $600 \times 600 \times 280 \mu\text{m}^3$, as shown in Fig. (2). The probability distribution values of direction of fibers along the X and Y axes were obtained from SEM images and the values of fibers orientation along the Z axis (θ angle), were randomly computed based on $[0 \leq \theta \leq \tan^{-1}(t_{GDL} L_{GDL}^{-1})]$.

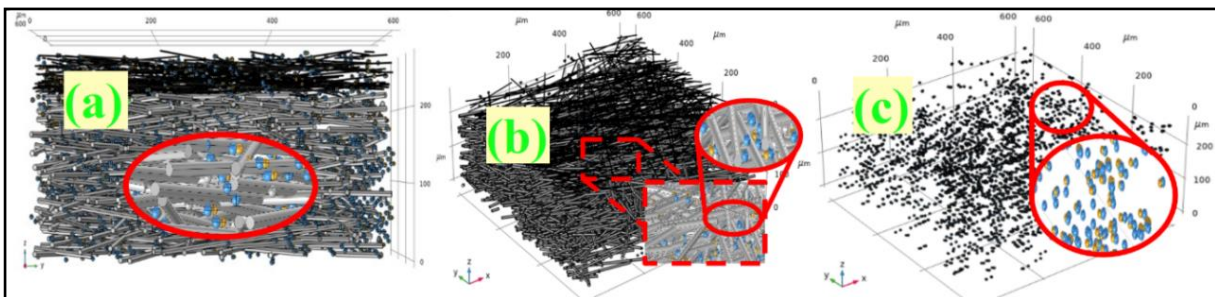


Fig. 2 Schematic of stochastic simulated CD of SGL 38BC. (a) Cross section view, (b) Isometric view and (c) A view of components other than carbon fibers in the reconstructed microstructure, (components include blue spheres for PTFE and yellow ovals for binder).

Solving Procedure: Estimating of the Properties

After ensuring the desired porosity% was gained, by directly linking the MATLAB and the COMSOL multi-physics software, the geometry of the GDL/MPL microstructure along with other components such as PTFE and binder, during reconstruction in the MATLAB and using the live link technique for modeling and subsequent processing, were transferred to the COMSOL. To check the mass transfer property, despite estimating the EEC/ETC, which only need carbon fibers, the space among the fibers is required. Therefore, with the help of the method illustrated in Fig. (3a), the desired CD is obtained. Due to the complexity of the CGDL microstructure, the heuristic method of arbitrarily selecting four unit-cells (UCs) with one-third dimensions at X and Y orient to the main CD as subdomains and averaging over the results was used, as shown in Fig. (3b).

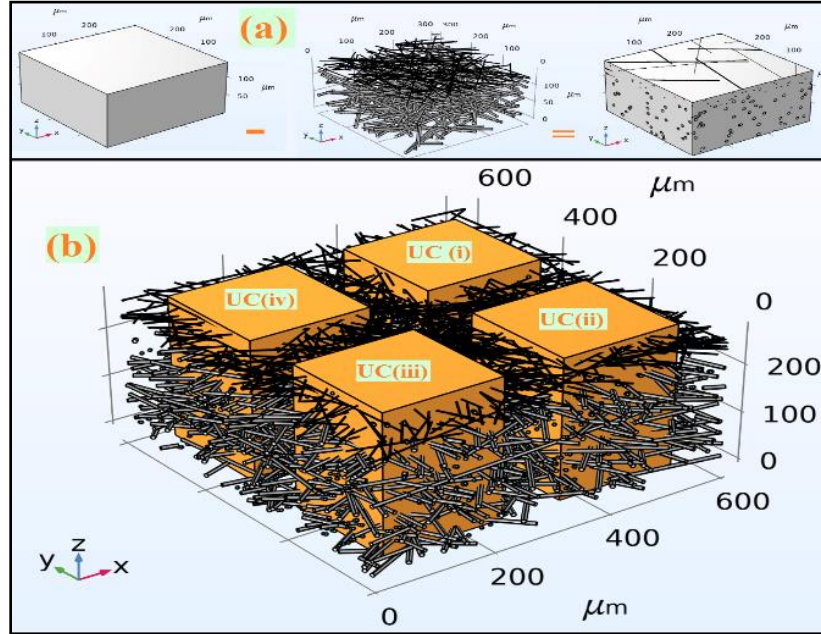


Fig. 3 (a) Production steps of the porous medium in COMSOL software, (produced CGDL with optional dimensions is subtracted from the solid cube with the same dimensions and the porous medium is obtained) and (b) Pickoff UCs from reconstructed CD by orange blocks.

Governing Equations

For calculating the properties of the picked off UCs from the simulated CD, the conservation equations of electron, heat and gas are employed as follows [7]:

$$\nabla \cdot (-\sigma_e \nabla \varphi_e) = 0 \quad (1)$$

$$\nabla \cdot (-\lambda_T \nabla T_T) = 0 \quad (2)$$

$$\nabla \cdot (-D_g \nabla c_g) = 0 \quad (3)$$

RESULTS AND DISCUSSION

Validation of Simulated Microstructure

Using the X-ray μ CT, the simulated CD of SGL 38BC's microstructure validated, as shown in Fig. (4).

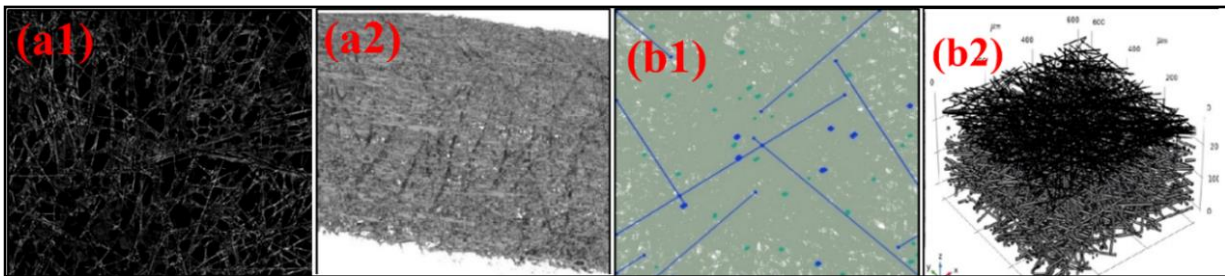


Fig. 4 A visual comparison between 2D/3D images of: (a1), (a2) X-ray μ CT and (b1), (b2) simulated CGDL. (2D images are from the perpendicular sections to the Z direction).

Properties Estimation

By solving the Eqs. (1) to (3) over all of four UCs and averaging on the results, all three effective transport properties of the CD, with the help of Eq. (4), can be calculated [7]. Only TP results of one of the UCs are depicted in Fig. (5).

$$M_{eff} = -\frac{L \cdot J_{ave}}{(B_{in} - B_{out})} \quad (4)$$

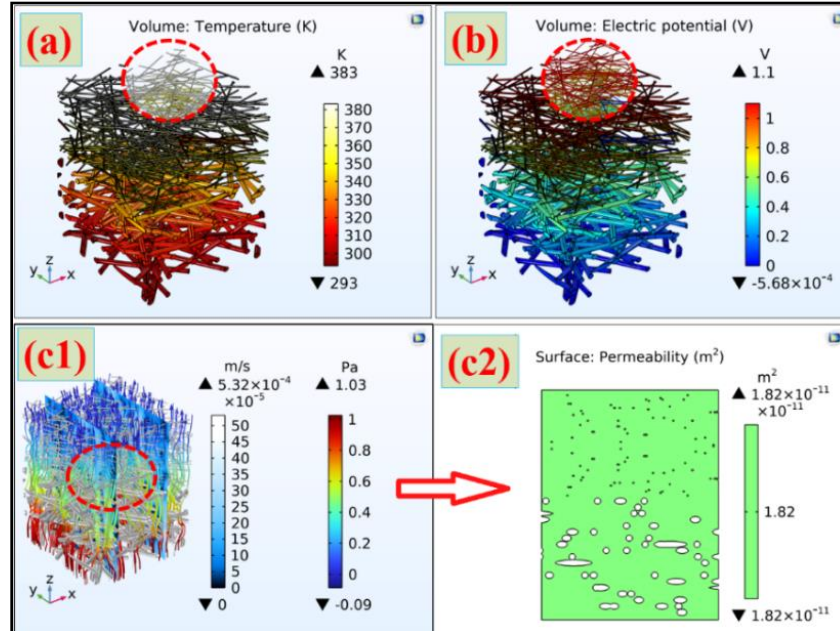


Fig. 5 Schematic of the numerical estimation of properties of reconstructed CD along the thickness /TP direction: (a) ETC, (b) EEC and (c1), (c2) Permeability.

CONCLUSION

Since the current numerical simulation approach, shows low and acceptable difference visually with the obtained results of X-ray μ CT method, and also because of the high power of current method in the quick manipulation of geometric parameters, consequently, to predicting the effective transport properties of the CGDLs more accurately, the current numerical approach is preferred.

REFERENCES

1. Xiao L, Luo M, Zhang H, Zeis R, Sui P-C. 2019. Solid mechanics simulation of reconstructed gas diffusion layers for PEMFCs. *Journal of The Electrochemical Society* 166:F377.
2. Zhang Z, He P, Dai Y-J, Jin P-H, Tao W-Q. 2020. Study of the mechanical behavior of paper-type GDL in PEMFC based on microstructure morphology. *International Journal of Hydrogen Energy* 45:29379-94.
3. Akbar A, Liu J, Chung S-J, Um S. 2021. Statistical characterization of non-linear microscopic mechanical deformation through randomly oriented fibrous porous transport layers for advanced electrochemical energy systems. *Renewable Energy* 178:1106-18.
4. Bahoosh R, Jafari M, Bahrainian SS. 2021. 3-D modeling of proton exchange fuel cell cathode with a novel random generation of gas diffusion porous layer. *Korean Journal of Chemical Engineering* 38:1703-14.
5. Liao J, Yang G, Li S, Shen Q, Jiang Z, Wang H, et al. 2021. Effect of structural parameters on mass transfer characteristics in the gas diffusion layer of proton exchange membrane fuel cells using the lattice Boltzmann method. *Energy & Fuels* 35:2654-64.
6. Zhang H, Zhu L, Harandi HB, Duan K, Zeis R, Sui P-C, et al. 2021. Microstructure reconstruction of the gas diffusion layer and analyses of the anisotropic transport properties. *Energy Conversion and Management* 241:114293.
7. Xiao L, Zhu L, Clökler C, Grünzweig A, Wilhelm F, Scholta J, et al. 2022. Experimental validation of pore-scale models for gas diffusion layers. *Journal of Power Sources* 536:231515.



ICH2P14-PP068

HYDROGEN SULFIDE H₂S – FOR THE SERVICE OF HUMANITY!

**Anatolii Startsev*

Boreskov Institute of Catalysis, Novosibirsk, Russia
*Corresponding author e-mail: anatolii.startsev@gmail.com

ABSTRACT

The main provisions of the recently developed concept of the crucial role of catalysts in the process of low-temperature decomposition of H₂S to produce hydrogen and elemental sulfur are considered. The concept is based on the non-equilibrium thermodynamics of an irreversible process in an open system. Within the framework of this concept, the prospect of using H₂S to solve many scientific and practical problems in the field of chemistry, ecology, energy and economics is analyzed. In particular, one of the most urgent problems is the replacement of the long-outdated technology for the disposal of toxic H₂S by the Claus method with an environmentally safe, highly efficient low-temperature catalytic technology for producing hydrogen from H₂S with an H₂S conversion of up to 100%. This technology will allow obtaining an additional more than 5% hydrogen to existing needs without involving additional H₂S sources in processing. The developed paradigm of catalytic processing of H₂S allows realizing for unexpected chemical reactions that cannot be carried out by traditional methods under normal conditions. First of all, we are talking about the atomic species of hydrogen and sulfur obtained as a result of the H₂S dissociation on the surface of solid catalysts at room temperature. It is shown that atomic hydrogen interacts on the catalyst surface with chemically inert nitrogen and argon molecules to form chemical compounds stable under normal conditions. It is concluded that at present all the prerequisites have been created for initiating full-scale scientific, technological and commercial projects to implement the innovative idea of using the toxic substance H₂S to serve Humanity. Today we have a unique opportunity to use the "gift" of Nature to solve scientific and technological problems that cannot be implemented within the existing paradigm of H₂S processing. A qualitative shift to a new paradigm of the science of catalysis can be achieved if we direct our efforts to create "man-made" irreversible catalytic processes operating under thermodynamically non-equilibrium conditions characteristic of all biological processes.

Keywords: H₂S decomposition, hydrogen production, solid catalysts, non-equilibrium thermodynamics, alternative renewable energy source

INTRODUCTION

Hydrogen sulfide H₂S, the chemical analogue of water H₂O, has been known to mankind since time immemorial "thanks" to its unforgettable disgusting smell. Apparently, the smell is the reason that the chemical properties of this molecule have been studied extremely poorly compared to water, although the chemistry of H₂S was studied already since the 17th century.

At the same time, H₂S is one of the most toxic substances formed as a mandatory and unavoidable by-product in the industry in a total annual amount of tens of millions of tons. The content of H₂S in the bowels and water reservoirs of the Earth is estimated at tens of billions of tons. Unlike water, H₂S is a "useless" substance that has not found practical application in human life. Therefore, it must be removed from wastewater and exhaust gases to the level of sanitary standards.

The processes of H₂S disposal are implemented worldwide by the Claus method (more than 1000 units in the world), developed in the 19th century; as a result, the final products of its disposal are water and solid sulfur. Thus, hydrogen H₂, as a constituent element of H₂S, is irreversibly lost in the form of water H₂O, thereby eliminating the possibility of its use as a pure "green" energy resource. Therefore, the enormous efforts of many generations of researchers have been directed to the decomposition of H₂S in order to obtain the products in demand - hydrogen and sulfur. To achieve this goal, various methods of initiating this reaction have been used; however, none of these technologies has yet reached the level of commercial application [1].

At the same time, already at the end of the 19th century, S.N. Vinogradsky discovered a unique chemical process of chemosynthesis of organic matter from hydrogen sulfide and carbon dioxide, which, unlike photosynthesis known at that time, did not require the energy of sunlight and was carried out under the action of specific microorganisms – bacteria [2]. According to H₂S biochemistry, autotrophic bacteria were the first organisms to produce large amounts of organic matter, and therefore they served as the starting point for the evolution of higher forms of life.

Currently, a wide range of different types of sulfur bacteria with very diverse properties and habitats are known. Colorless sulfur bacteria are found in marine and freshwater sediments, soils and wastewater treatment systems. They grow in an aqueous medium with an acidic or alkaline pH value, at temperatures from +4 to +95 oC, both in aerobic and fully anaerobic conditions.

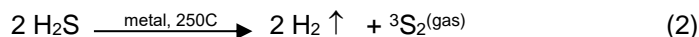
It would seem that this scientific discovery will allow humanity to solve the problem of disposal of toxic H₂S, using it for the synthesis of organic substances by analogy with the process of chemosynthesis, but when studying the mechanism of chemosynthesis, serious problems arose when cultivating sulfur bacteria in the laboratory. It is quite obvious that this process must proceed under the action of biocatalysts - enzymes. However, the complex chemical composition and structure of bacteria did not allow to reveal the nature of the catalytically active centers of the enzyme and, as a consequence, the mechanism of chemosynthesis. Nevertheless, the chemosynthesis process created by Nature gives every reason to assume that there must be catalytic systems capable of efficiently decomposing H₂S into constituent elements under normal conditions, i.e. at room temperature and atmospheric pressure.

CATALYTIC H₂S DECOMPOSITION INTO HYDROGEN AND SULFUR

Really, at the beginning of the 21st century, we discovered that the H₂S decomposition with the production of hydrogen and elemental sulfur takes place on the surface of solid catalysts already at room temperature [3]. As it turned out, there are two types of solid catalysts capable of carrying out the target reaction. On sulfide catalysts, the reaction products are hydrogen and solid sulfur



whereas on metal catalysts, along with hydrogen, diatomic gaseous sulfur is formed in the ground triplet state [4]



In both cases, the H₂S conversion reaches 100% both in the gas-phase mode and when the catalyst is placed in a liquid layer capable of dissolving H₂S and reaction products well. Omitting scientific results and their thermodynamic justification, which are discussed in detail on our website [5] and published in the scientific literature [6], we will highlight here only the nodal points that will help us understand the essence of this scientific problem.

Since both reactions (1) and (2) are carried out at low temperature without the supply of thermal energy from the outside, a reasonable question arises: **where does the energy for these reactions come from?** By special experiments, we proved that the reactions proceed with the same efficiency in the "dark" mode, which excluded the possibility of photo-catalysis.

To solve this very considerable task, we assumed that the energy needed to carry out reactions (1) and (2) is concentrated in the chemical bonds of the H₂S molecule [7]. Indeed, the energy of chemical bonds is an important molecular constant, one of the main characteristics of a molecule that determines the structural features and various properties of chemical compounds. The values of the energies of chemical bonds or, what is the same thing, the energies of dissociation (rupture) of chemical bonds are given in numerous reference tables.

The thermodynamics of H₂S decomposition on sulfide catalysts is considered in detail in [5,6]. The energy profile of the H₂S decomposition reaction on sulfide catalysts at room temperature is as follows (Fig.). The energy reference point is the kinetic energy of H₂S in the gas phase and its potential energy stored in the chemical bonds of the molecule. We see that the first three stages of H₂S decomposition do not require external energy supply and proceed spontaneously with a decrease in the Gibbs free energy. The only

energy-consuming stage is the decomposition of the key surface intermediate, adsorbed disulfane, which occurs through a small energy barrier thanks to the expenditure of free energy accumulated in the previous exothermic stages of H₂S dissociation.

Thus, the catalyst surface acts as a trap and accumulator of the internal (i.e. kinetic and potential) energy of the gas phase molecules, initiating a catalytic process prohibited in the gas phase by "classical" equilibrium thermodynamics. The driving force of this process is the formation of reaction products in the most stable ground electronic state compared to the starting substances (in our case,

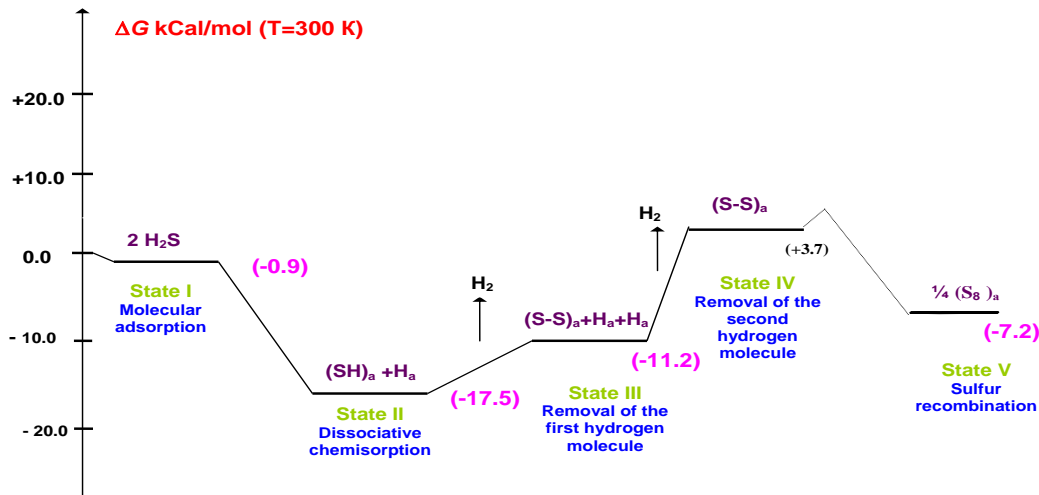
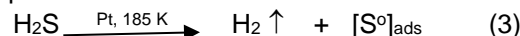


Fig. The energetic profile of H₂S decomposition on sulfide catalysts at room temperature [6,7].

hydrogen and solid sulfur). In general, the catalytic reaction (1) is an exothermic process that occurs **spontaneously** at room temperature.

A remarkable experimental work on the interaction of H₂S with platinum was published in 1986 [8]. It was found that the adsorption of H₂S on the surface of Pt(111) already at 110 K leads to complete dissociation of the molecule with the formation of surface atomic species H_{ads} and S_{ads}. When the sample is heated, molecular hydrogen appears in the gas phase already at a temperature of 185 – 230 K, while sulfur remains on the surface, detected in the form of vibrations of Pt – S bonds.

The chemical state of sulfur is not discussed in this article, so we will try to understand its nature based on the well-known chemical properties of H₂S. The fact is that the appearance of molecular hydrogen in the gas phase can be caused by the decomposition of H₂S to form monatomic sulfur

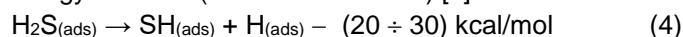


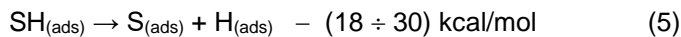
which would lead to the formation of surface platinum sulfide {PtS}, as required by the stoichiometric chemical reaction of platinum **oxidation** with H₂S. However, it is well known that H₂S exhibits only reducing properties, since sulfur is in the lowest oxidation state, therefore, the reaction described above must be **catalytic** with the formation of zero-valence atomic sulfur as a decomposition product of H₂S.

This conclusion is valid for all transition metals.

The energy of H₂S decomposition on metal catalysts is analyzed in detail in [6,7]. Recently, there have been numerous studies of the behaviour of the H₂S molecule on the surface of single crystals, which are based mainly on theoretical calculations by the DFT method. In all cases, it is shown that the interaction of the H₂S molecule with the metal surface begins with a spontaneous exothermic chemisorption process, which proceeds without an activation barrier and, depending on the nature of the metal, varies within – (10 ÷ 21) kcal/mol.

However, the chemisorption of H₂S is accompanied by a further spontaneous process of its dissociation to the surface atomic species of hydrogen and sulfur. Dissociation proceeds through two exothermic stages, each of which has a low energy barrier + (0.2 ÷ 10.0 kcal/mol) [7]:





As a result, potential energy accumulates on the metal surface, which, depending on the nature of the metal, reaches (-70 kcal/mol) or higher. It is important that H_2S dissociation proceeds easily on transition metals and has neither thermodynamic nor kinetic limitations. At the same time, on noble metals, oxides or sulfides, this process may be difficult at any stage. Fundamentally important: *water does not dissociate into atoms on the surface of transition metals* [8].

Thus, the energy "stored" as a result of H_2S dissociation can be spent to carry out the target chemical reaction and desorption of reaction products into the gas phase, which will mean the catalytic nature of the process as a whole. To realize this, it would be necessary to know the desorption energy of the reaction products and the entropy of each of the successive stages for a specific system. Since there are no such calculations in this situation, we will try to substantiate this thesis from the standpoint of thermo-chemistry.

Such an analysis was performed by us for platinum, since, on the one hand, it was on Pt that we discovered the process of low-temperature decomposition of H_2S , and, on the other hand, there is information in the literature about the interaction energy of reaction products (2) with the Pt(111) surface. It turned out [6,7] that the reaction (2) is exothermic $\Delta H = -(20.8 \div 25.8)$ kcal/mol. Moreover, if we take into account that the entropy of reaction (2) increases $\Delta S > 0$ (the number of molecules in the gas phase increases), when the exothermic nature of this reaction $\Delta H < 0$, the change in the Gibbs potential is always negative $\Delta G < 0$, which means the *spontaneous* character of the catalytic process.

In other words, in this case, the First principle of thermodynamics is fully realized – the Law of conservation of energy for open systems: energy does not disappear and does not appear from nothing, i.e., energy conversion from exothermic processes of adsorption and dissociation of the initial H_2S molecules to the chemical transformation into the final products of the reaction – hydrogen and diatomic sulfur, and their desorption into the gas phase. *This process is impossible in the gas phase.*

THE CONCEPT OF THE DECISIVE ROLE OF CATALYSTS IN THE REACTION OF LOW-TEMPERATURE DECOMPOSITION OF HYDROGEN SULFIDE [8]

So, since the processes (1) and (2) are impossible in the gas phase without the participation of solid catalysts, therefore, they cannot be justified by equilibrium thermodynamics. Classical equilibrium thermodynamics considers only isolated systems that exchange neither matter nor energy with the environment. In these systems, chemical processes are carried out by supplying energy from the outside, so the rate and direction of the process depend only on external conditions, and the catalyst does not change the thermodynamics of the process.

At the same time, most of the processes occurring in nature are carried out at ambient temperature and pressure without the supply of thermal energy from the outside. All biological processes are far from equilibrium and are irreversible, therefore, non-equilibrium thermodynamics, or thermodynamics of irreversible processes, was created in the middle of the last century and one of its creators is I.R. Prigozhin [9].

The distinctive features of non-equilibrium thermodynamics are that the systems considered by it are open to flows of matter and energy, and the processes are irreversible and far from equilibrium. The inevitability of the emergence of this science was due to the understanding that the vast majority of processes occurring in Nature and with human participation are irreversible and cannot be described within the existing "classical" equilibrium thermodynamics, which does not take into account the time factor.

Within the framework of non-equilibrium thermodynamics for open systems, we have developed the concept of the decisive role of catalysts in the process of low-temperature H_2S decomposition [7]. Thus, in contrast to the "passive" role of catalysts in equilibrium thermodynamics, a solid catalyst plays a key "active" role in the non-equilibrium irreversible process of low-temperature decomposition of H_2S . In fact, the surface of the solid catalyst captures H_2S molecules from the gas phase, while ensuring their dissociation into atomically adsorbed species of hydrogen and sulfur. Further, these surface atomic species recombine to form reaction products - molecular hydrogen, diatomic gaseous sulfur and solid sulfur. These exothermic processes inevitably caused to an increase in the entropy of the system, which is dissipated into the environment in the

form of bound (waste) energy. It is this circumstance that makes the decomposition of H_2S irreversible. After the bound energy is dissipated, the remaining Gibbs free energy accumulates on the surface of the catalyst and is used to desorb reaction products into the gas phase.

Very important conclusions follow from this concept. First, it was possible to understand the unusual temperature dependence of the reaction under consideration [3,6,7]. Since the key stage of the process is a bimolecular surface reaction between two adsorbed sulfur species, this process is determined by the degree of surface coverage with adsorbed molecules, which, in turn, is a temperature dependent: the lower the temperature, the higher the efficiency of the process.

Second, in an irreversible non-equilibrium process, the efficiency of the catalyst is determined by the number of active centers capable of carrying out the reaction. Therefore, in order to achieve 100% H_2S conversion, it is simply necessary to load the required amount of catalyst.

So, the driving force of the process is the formation of reaction products in the ground electronic state, i.e. having minimal energy - singlet hydrogen, solid sulfur and diatomic gaseous sulfur in the ground triplet state. No less important, a necessary condition of the process is the concentration gradient of the initial substances and reaction products at the inlet and outlet of the reactor. If there is no supply of free energy entering the catalytic cycle, the process stops.

The logical result of our scientific research is a patent [10] describing examples of catalytic systems capable of H_2S decomposing at low temperatures to produce hydrogen and elemental sulfur. This patent contains references to our previous patents on this issue, which indicates a wide variety of catalytic systems that can be used to implement the process in various ways. In addition, the objects of patenting can be both chemical composition and technology of catalyst preparation, as well as the technologies of the process itself. To date, there is no foreign protection of intellectual property rights.

Potential opportunities, challenges and prospects

The main objective of our proposed project is to replace the long-outdated, expensive to operate, metal–and energy-intensive Claus process (more than 1000 units in the world) with an innovative low-temperature technology for processing toxic H_2S to obtain the target product - hydrogen. This will make it possible to obtain at least 5% hydrogen in addition to existing needs without involving new sources of H_2S for processing. The use of this method has no climatic, geographical or other natural restrictions. The technology is applicable anywhere in the world where industrial processing of raw materials with extraction of H_2S takes place.

After the implementation of the proposed project, the main market for sulfur will continue to be its catalytic processing into sulfuric acid. In addition, gaseous sulfur can be used for the synthesis of new chemical compounds of sulfur, analogues of biological objects in medicines, composite materials for various functional purposes, including Li – S batteries, in agriculture, in the rubber industry, for the production of dyes, in industrial and road construction, etc. The market opportunities for the use of gaseous sulfur are far from exhausted due to the lack of scientific research [4].

Along with the commercial attractiveness of the proposed solution for low-temperature decomposition of H_2S , we have discovered the amazing properties of atomic hydrogen formed by H_2S dissociation on the surface of solid catalysts, which has unique properties of interaction with very inert molecules at room temperature and pressure. First of all, this concerns the problem of nitrogen fixation, which leads to the formation of ammonia NH_3 and other nitrogen-containing molecules - N_2H_2 and N_2H_4 .

Another absolutely incredible result is the activation of argon with the formation of hydrogen argonide, H_2Ar , a molecule stable under normal conditions, which can be used for the accumulation, storage and transportation of hydrogen. Moreover, when hydrogen argonide is burned in fuel cells or in the presence of oxygen, water and argon are released, which return to the atmosphere without harm to the environment. There is reason to assume that the chemical analogues of neon and helium (H_2Ne and H_2He) can be obtained in a similar way. Without a doubt, if these compounds really exist under normal conditions, then this scientific discovery will give a huge impetus to the development of noble gas chemistry.

Finally, we have obtained preliminary results on the activation of a carbon dioxide molecule with the formation of carbohydrates - a chemical analogue of chemosynthesis. The urgency of this task is related to solving the problem of global climate warming.



Conclusion

The generally accepted paradigm of H₂S decomposition into constituent elements using external energy sources has not yet allowed to create an acceptable technology for producing hydrogen and sulfur from the point of view of finding the optimal combination of the four 'E' – ecology, economy, efficiency and energy. The proposed paradigm of low-temperature catalytic decomposition of H₂S is, apparently, the very tool for solving the extremely urgent problem of not only the disposal of toxic H₂S with the production of demanded products, but also opens up a wide prospect of using atomic hydrogen and sulfur for the implementation of unexpected chemical reactions and the production of new, previously unknown chemicals. The development potential of the paradigm is limited by the volume of processed H₂S, which, in turn, is limited by the amount of sulfur consumed. The situation may change if new unexpected solutions are found for the use of triplet sulfur as a reagent for the synthesis of new substances and materials in chemistry, industry, mechanical engineering, medicine, pharmacology, etc.

Toxic and "useless" H₂S, which has not found practical application in human life, turned out to be the very substance that underlies the process of chemosynthesis of organic matter from CO₂ created by Nature, which laid the foundation for biological life on Earth. Unlike its chemical counterpart, water, which is the primary basis of the existence of all biological organisms, H₂S is a supplier of hydrogen and energy for the life support processes of these organisms. This extremely important role of H₂S is apparently due to the unique property of this molecule - the standard enthalpy of formation ($\Delta_f H_{298}^\ominus = -4.82$ kcal/mol) is the smallest among all known potential sources of hydrogen, which means minimal energy consumption during the splitting of the molecule. The driving force behind the decomposition of H₂S is the formation of final products in the ground electronic state (i.e. having minimal free energy) – singlet hydrogen, solid sulfur and a diatomic sulfur molecule in the ground triplet state. At the same time, the annual increase in H₂S is hundreds of millions of tons due to the activity of anaerobic sulfate-reducing bacteria, which ensures a continuous cycle of H₂S in Nature.

At the moment, apparently, all the prerequisites have been created for initiating full-scale scientific, technological and commercial projects to implement the innovative idea of using the toxic substance H₂S created by Nature to serve Humanity. Today we have a unique opportunity to use this "gift" of Nature to solve scientific and technological problems that cannot be implemented within the existing paradigm of H₂S processing. For this purpose, we have actually reproduced biological processes carried out in Nature by biocatalysts – enzymes, using heterogeneous catalytic systems. In turn, we have discovered a new phenomenon in heterogeneous catalysis – the use of the internal energy of the chemical bonds of the H₂S molecule to carry out chemical reactions that cannot be carried out in the gas phase in the absence of solid catalysts, which undoubtedly models biological processes.

I would like to emphasize the special role of catalysis for chemistry as a science in general, and for many biological processes occurring under the action of biocatalysts – enzymes. Currently, the role of catalysis in human activity is significantly increasing due to the purposeful search and creation of highly active and selective catalysts capable of effectively solving economic and environmental problems of chemical processes. However, the possibilities of catalysis are far from being exhausted, since NATURE has created unique biocatalysts that, under environmental conditions, are capable of carrying out processes that cannot yet be implemented on an industrial scale. In my opinion, a qualitative shift to a new paradigm of the *science of catalysis* can be achieved if we direct our efforts to create "man-made" irreversible catalytic processes operating in thermodynamically non-equilibrium conditions characteristic of all biological processes.

I really hope that the relevance of the raised scientific problem, as well as the prospect of obtaining new knowledge in previously unknown fields of science will allow us to overcome all obstacles in our very difficult time to solve the problem of sustainable human development.

REFERENCES

1. Hydrogen from Hydrogen Sulphide: Technology Scan and Evaluation Prepared for COSIA by DeLude Consulting Inc. June 8, 2017.
2. Autotrophic Bacteria. (Schlegel HG, Bowien B., Eds.). Sci. Tech Publs., Madison, WI, 1989



3. Startsev AN, Kruglyakova OV, Chesalov YuA, Ruzankin SPh, Kravtsov EA, Larina TV, and Paukshtis EA. 2013. Low Temperature Catalytic Decomposition of Hydrogen Sulfide into Hydrogen and Diatomic Gaseous Sulfur. *Topics in Catalysis.*, 56:969-980.
4. Startsev A. N. 2019. Diatomic sulfur: a mysterious molecule. *Journal of Sulfur Chemistry.* 40:435-450.
5. <http://startsev-an.ru/> , <http://eng.startsev-an.ru/>
6. Startsev AN. 2022. Shift of the H₂S Paradigm. *Journal of Sulfur Chemistry.* 43:671-684.
7. Startsev AN. 2020. The crucial role of catalysts in the reaction of low temperature decomposition of hydrogen sulfide: non-equilibrium thermodynamics of the irreversible process in an open system. *Molec. Catal.* 497:11240.
8. Koestner RJ, Salmeron M, Kollin EB and Gland JL 1986. Adsorption and surface reactions of H₂S on clean and S-covered Pt(111). *Surf. Sci.* 172:668.
9. Prigogine I., 1955. *Introduction to thermodynamics of irreversible processes*, Springfield, Illinois, U.S.A.
10. Startsev AN. Russian Patent No 2,777,440. (11.01.2021).

ICH2P14-PP075

MODELING OF HYDROGEN LIQUIFACTION PROCESS PARAMETERS USING ADVANCED ARTIFICIAL INTELLIGENCE TECHNIQUE

^{1,2}A. Abdallah El Hadj, ¹Ait Yahia, ¹Hamza. K, ²M. Laidi, ²S. Hanini

¹Department of Chemistry, Science Faculty, University of Blida, Road of Somaa, Blida, Algeria

²Laboratoire de biomatériaux et Phénomène de Transport (LBMPT), University of Medea, Medea, Algeria

*Corresponding author e-mail: slamd2005@yahoo.fr

ABSTRACT

The main subject of this work is the application of advanced Artificial intelligence (AI) techniques to predict with accuracy hydrogen liquefaction process parameters. This technique is carried out using a hybrid method based on Neuro fuzzy systems (ANFIS) and particle swarm optimization (PSO). The training and validation strategy has been focused on the use of a validation agreement vector, determined from linear regression analysis of the predicted versus experimental outputs, as an indication of the predictive ability of the ANFIS model. The modelling strategy is performed using the temperature (T), pressure (P), and the mass flowrate (m) as inputs parameters and the stream energy (E) as output parameters.

Statistical analysis of the predictability of the optimized ANFIS model shows excellent agreement with referenced data [1] (coefficient of correlation equal to 0.9988). Also, the comparison between estimated and the referenced values is carried out using average absolute relative deviation objective function (AARD) and shows a high predictive ability of the conceived model with global deviation equal to 1%.

Keywords: Modelling, Hydrogen liquefaction process, ANFIS, PSO, Optimization.

INTRODUCTION

The energy is the driving force of development and the smooth running of the daily life of human beings, without which it will be difficult to imagine the way of living with the various constraints encountered by societies.

The access and availability of energy represents the key to development and progress not only the countries but the entire world. Our suffering is mainly due to the way in which conventional sources and processes of energy production are used and exploited, mainly fossil fuel-based energy sources, despite the high price of the damage caused in particular to the environment.

Here appears the urgent need to search for environmentally friendly energy sources (adopt clean and sustainable processes). The hydrogen is known as one the most important element that can be used in process and ensuring the energy security in green manner [1].

Modelling the different production and exploitation technologies that contain hydrogen is important for the process design, development and sizing. The most efficient methods based on artificial intelligence (AI) are Artificial neural networks (ANNs), the adaptive neuro-fuzzy inference system (ANFIS). The use of these techniques offers many advantages: precision, modelling ability of high non linear problems, the possibility of interpolation and extrapolation where several works in many fields have been carried out [2-4].

The main subject of this work is the application of advanced Artificial intelligence (AI) techniques to predict with accuracy hydrogen liquefaction process parameters. This technique is carried out using a hybrid method based on Neuro fuzzy systems (ANFIS) and particle swarm optimization (PSO)

MODELING WITH ANFIS TECHNIQUES

Jang proposed a multilayer adaptive network-based, first-order Takagi-Sugeno fuzzy inference system called ANFIS [5]. ANFIS structure consists of five layers: fuzzy layer, product layer, normalized layer, de-fuzzy layer and total output layer. The application of ANFIS model for the prediction of stream energy is

performed using the Gaussian function for the inputs and linear function for the output as membership functions (MFs) (Table 1).

Table 1. Details of best the user-defined function for ANFIS model

Training Algorithm	Input		Output	
Levenberg-Marquardt Back-propagation	Number of input	Activation function	Number of output	Activation function
	3	Gaussian	1	Linear

The adaptive neuro-fuzzy inference system (ANFIS) proposed by Jang (1993), is a kind of artificial neural network that is based on the Takagi–Sugeno fuzzy inference system. This technique is a self-tuning and adaptive hybrid controller by the neural network learning algorithms are determined the fuzzy parameters, according to the input data, during accurate and fast learning the output be accurately determined [6]

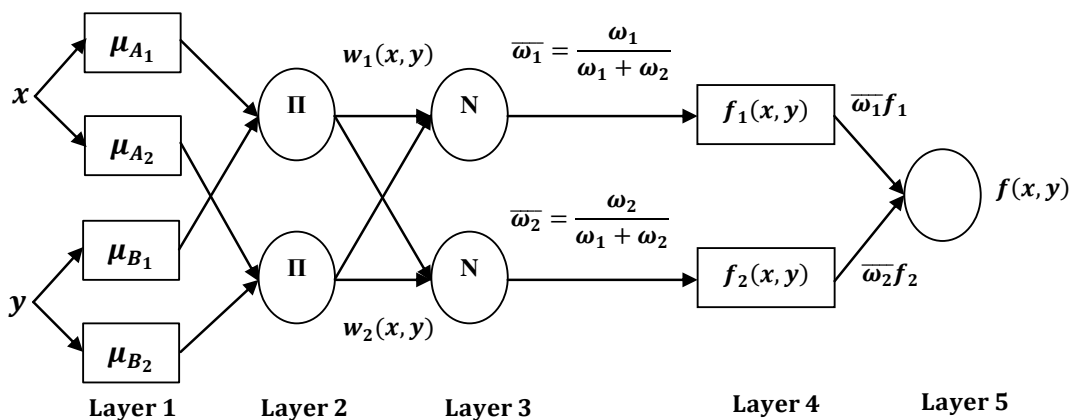


Fig. 1. Architecture of ANFIS model

RESULTS AND DISCUSSION

DATA COLLECTION, PRE-TREATMENT AND ANALYSIS

The experimental data points were collected from literature. Data set was arranged as rectangular matrix (4,1) containing 03 inputs parameters, the temperature (T), pressure (P), and the mass flowrate (m) as inputs parameters and the stream energy (E) as output parameters.

MODEL PERFORMANCE EVALUATION

The performance of the conceived model is evaluated using the following statistical tests [10–15, 42–44]: correlation coefficient (R), a root mean square error for (RMSE) and an average absolute relative deviation of (AARD):

$$R = \frac{\sum_{i=1}^N ((E)_i^{\text{ref}} - \overline{(E)_i^{\text{ref}}}) ((E)_i^{\text{pred}} - \overline{(E)_i^{\text{pred}}})}{\sqrt{\sum_{i=1}^N ((E)_i^{\text{ref}} - \overline{(E)_i^{\text{ref}}})^2 \sum_{i=1}^N ((E)_i^{\text{pred}} - \overline{(E)_i^{\text{pred}}})^2}} \quad (1)$$

$$\text{RMSE} = \sqrt{\frac{1}{N} \sum_{i=1}^N ((E)_i^{\text{ref}} - (E)_i^{\text{pred}})^2} \quad (2)$$

$$\text{AARD} (\%) = \frac{1}{N} \sum_{i=1}^N \frac{|(E)_i^{\text{ref}} - (E)_i^{\text{pred}}|}{(E)_i^{\text{ref}}} \quad (3)$$

Where, i is the number of data points, $(E)_i^{ref}$ is the referenced stream energy and $(E)_i^{pred}$ is the stream energy predicted by the ANFIS model.

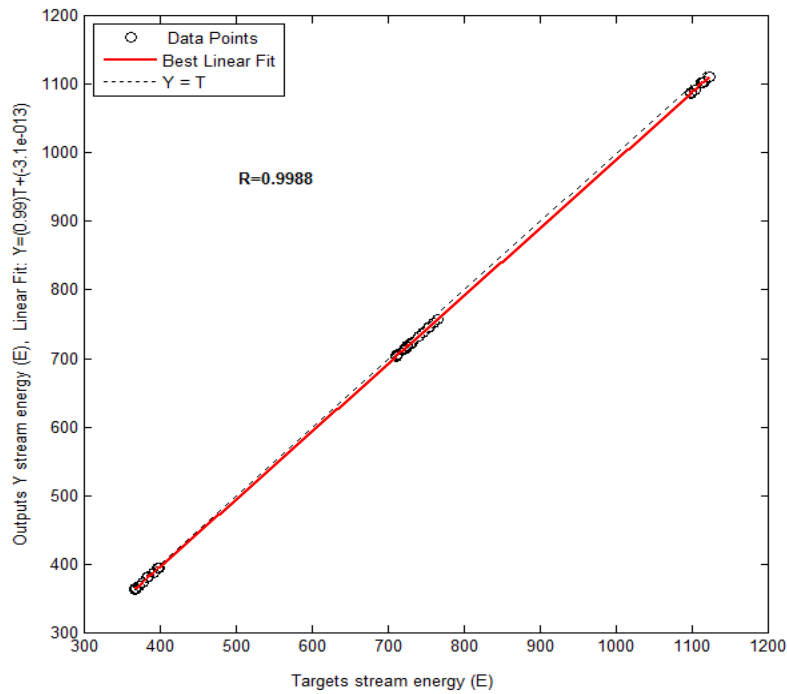


Fig. 2. Global comparison between referenced and estimated output

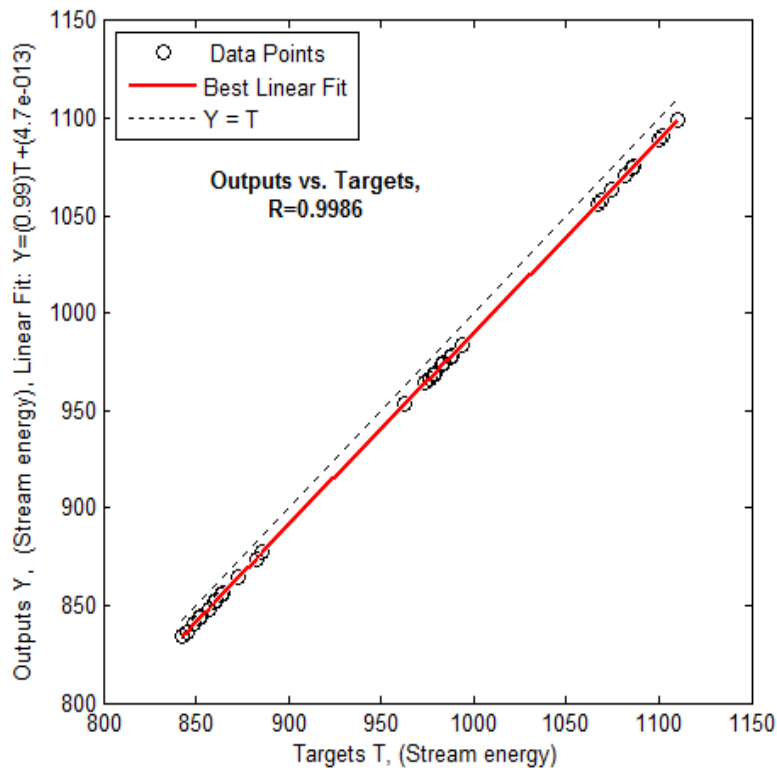


Fig. 3. Regression coefficient obtained between the experimental and estimated output

Figures 2 and 3 give a global comparison in terms of regression coefficient between referenced and the predicted steam energy (E), where the ANFIS model shows excellent agreement with referenced data given coefficient of correlation equal to 0.9988.

CONCLUSIONS

In this work, an advanced artificial intelligence technique to predict with accuracy hydrogen liquefaction process parameters. This technique is carried out using a hybrid method based on Neuro fuzzy systems (ANFIS) and particle swarm optimization (PSO). The ANFIS model is used for modelling the process while the PSO algorithm is used for optimization of model parameters. The modelling strategy is performed using the temperature (T), pressure (P), and the mass flowrate (m) as inputs parameters and the stream energy (E) as output parameters.

The results show that the optimized ANFIS model can predict the stream energy (E) of the hydrogen liquefaction process with high accuracy and the different forms of comparison carried out prove and confirm this .

References:

1. Ansarinassab H, Fatimah M, Khojasteh-Salkuyeh Y. 2023. Conceptual design of two novel hydrogen liquefaction processes using a multistage active magnetic refrigeration system. *Applied thermal eng.* 230: 120771.
2. Abdallah el hadj A Laidi. M, Simoussa. C and Hanini. S. 2017 Novel approach for estimating solubility of solid drugs in supercritical carbon dioxide and critical properties using direct and inverse artificial neural network (ANN). *Neural Comput Appl* 28:87–99.
3. [Mesellem](#) Y, Abdallah el hadj A Laidi. M, Hanini. S and Hentabli. M (2021), "Computational intelligence techniques for modeling of dynamic adsorption of organic pollutants on activated carbon", *Neural Computing and Applications*.
4. Quej VH, Almorox J Arnaldo JA and Saito L 2017. ANFIS, SVM and ANN soft-computing techniques to estimate daily global solar radiation in a warm sub-humid environment. *J Atmos Solar- Terrestrial Phys* 155:62–70
5. Aghav RM, Kumar S and Mukherjee SN. 2011. Artificial neural network modeling in competitive adsorption of phenol and resorcinol from water environment using some carbonaceous adsorbents. *J.Hazard.Mater.*188: 67–77.
6. Jang JR 1993. ANFIS: Adaptive-Network-Based Fuzzy Infer- ence System. 23
7. Aquino G, Zacarias A and Rubio JDJ. 2020. Novel nonlinear Hypothesis for the delta parallel robot modeling. *IEEE Access* 8:46324–46334.
8. Ashfahani A, Pratama M, Lughofer E and Ong YS 2020. DEVDAN: Deep evolving denoising autoencoder. *Neurocomputing* 390:297–314
9. Mukaka MM. 2012. *Statistics Corner : A guide to appropriate use of Correlation coefficient in medical research.* 24:69–71
10. Khair U, Fahmi H, Hakim S Al and Rahim R. 2017 Forecasting Error Calculation with Mean Absolute Deviation and Mean Absolute Percentage Error. *J Phys Conf Ser* 930



ICH2P14-PP117

REDOX REGULATION OF HYDROGEN PRODUCTION IN *ESCHERICHIA COLI* DURING GROWTH ON BYPRODUCTS OF THE WINE INDUSTRY

^{1,2}Lusine Baghdasaryan, ^{1,2}Ofelya Karapetyan, ^{1,2}Karen Trchounian, ³Garabed Antranikian, ^{1,2*}Anna Poladyan

¹Department of Biochemistry, Microbiology and Biotechnology, Faculty of Biology, Yerevan State University, 1 A. Manoogian str., 0025 Yerevan, Armenia

²Scientific-Research Institute of Biology, Yerevan State University, 1 A. Manoogian str., 0025 Yerevan, Armenia

³Hamburg University of Technology, Institute of Technical Biocatalysis, Hamburg, Germany

*Corresponding author e-mail: apoladyan@ysu.am

ABSTRACT

Lignocellulosic wine grape waste (WGW) is considered a suitable medium for *Escherichia coli* growth and H₂ production. The study investigated the growth, H₂ production, and oxidation-reduction potential (ORP) kinetics of the *E. coli* BW25113 wild type when utilizing WGW. Bacteria were cultivated anaerobically on 4 g/L WGW media with dilutions ranging from 0 to 4-fold, pH 7.5. Notably, a 2-fold diluted medium, with pH adjustment using K₂HPO₄, exhibited reduced acidification, prolonged H₂ production, and enhanced biomass formation (OD₆₀₀, 1.5). The addition of the redox reagent DL-dithiothreitol (DTT) was found to positively influence the growth and H₂ production of both the *E. coli* BW25113 wild type and a genetically modified mutant strain. H₂ production started at the 24th h of growth, reaching a maximum yield of 5.10 ± 0.02 mmol/L in the wild type and 5.3 ± 0.02 mmol/L in the mutant strain, persisting until the late stationary growth phase. Intriguingly, the introduction of 3mM DTT induced H₂ production from the early log growth phase, indicating a simultaneous enhancement of H₂ production. These results highlight the potential of medium buffering capacity and ORP as a tool to control the growth and hydrogen production in WGW, highlighting its significance in biotechnological applications.

Keywords: Wine waste pretreatment, bacterial biomass, Hydrogenase enzymes, H₂ production, *Escherichia coli*.

Introduction

Molecular hydrogen (H₂) is considered an environmentally clean, efficient, and renewable source of alternative energy for the future. Obtaining and producing H₂ is of great importance, especially in the field of transport, because only water vapor is released as a result of hydrogen combustion. Considerable research is now being done to obtain bio-H₂ from various industrial wastes as cheap carbon sources. According to scientific and public reports, the total global H₂ demand will reach 614 million t/year by 2050 [1,2]. H₂ can also be easily converted into electricity using fuel cells [3]. It could be a strong contender for a future alternative energy resource [4]. Various biomasses are used for obtaining H₂, the most common are lignocellulosic biomasses, the annual production of which reaches around 200 billion tons [5]. Approximately 80% of the waste is grape skin, 19% grape seeds, and 1% stalks. Grape stems are lignocellulosic and their composition includes mainly lignin (22.9% - 47.3%), cellulose (24.6% - 37.9%), and hemicelluloses (13.9% - 35.3%). Wine waste also contains proteins, oil, and phenolic compounds (11.6 %) [6]. WGW is also used as a fertilizer or animal feed, or simply dumped as natural waste in landfills. Grape phenolic compounds are of great interest as antioxidants, antimicrobials, and enzyme catalysts. It can be effectively used for the extraction of polyphenols, contributing to the development of viticulture eco-economy [7]. H₂ production or oxidation in bacteria is associated with hydrogenase (Hyd) enzymes, which are either cytoplasmic soluble or membrane-bound enzymes. Hyds catalyze the reversible redox reaction of producing H₂ from 2H⁺ + 2e⁻ [8].

Four types of membrane-bound [Ni-Fe] HydS have been identified in *Escherichia coli*, which are synthesized under different physiological conditions [9,10]. As is known, bio-H₂ is produced during dark fermentation, which consists of a series of redox reactions. The decrease in oxidation-reduction potential (ORP) during bacterial growth indicates the enhancement of redox processes, which is probably characteristic of the metabolic processes underlying cell growth and life activity. Facultative anaerobes, in contrast to strict anaerobes, grow in environments with relatively higher ORP values at the expense of the amount of oxygen available. It has been shown that it is possible to affect the metabolic end-product formation by controlling ORP [11]. To establish initial oxidative (~+200 mV) and reductive (~ -250 mV) ORP values, an impermeable oxidizer K₃[Fe(CN)₆] and a membrane-permeating reducer DL-dithiothreitol (DTT) were employed. Ferricyanide provides high positive ORP values in the environment, which strongly suppresses the growth of anaerobic bacteria [12]. Usually, the effect of 1 mM concentration of ferricyanide is observed. Meanwhile, DTT reduces the ORP of the medium, thereby prolonging the lag and log phases of growth. The presence of 3 mM of DTT in the medium lowers its ORP from -60 to -220mV. A relatively high content of DTT in the medium, 10 mM, can have a dangerous effect on bacteria. The work aimed to study the pH and redox regulation of the growth and H₂ production of *E. coli* BW25113 parental strain (PS) and genetically engineered mutant strain (*hyaB hybC hycAfdG ldhA frdC aceE*) (MS) using the WGW hydrolysate. For the first time, the effect of redox reagents on the growth parameters in WGW was observed.

Materials and Methods

Bacterial cultivation conditions

E. coli strains (parental strain (PS)) were provided by Prof. G. Sawers, Institute of Biology/Microbiology, Martin Luther University Halle-Wittenberg, Germany, while the septuple mutant strain (MS) of *E. coli* was provided by Prof. T. Wood, Department of Chemical Engineering, Penn State University, USA. The *E. coli* pre-cultures (inoculate) were grown under fermentative anaerobic conditions in a peptone medium (PM), pH 7.5, 37 °C [9]. Bacterial inoculum (3%) was added to the pre-prepared growth medium and subsequent optical density was measured at 600 nm.

Waste treatment

Pretreatment was carried out by a combination of physical and chemical methods [13]. Solutions containing 4% wine grape waste (pomace) and 0.4% sulfuric acid were autoclaved at 121°C for 20 minutes (Daihan Scientific, South Korea) type autoclave and drained with a thick cotton pad [14]. To remove possible sediments, the solutions were centrifuged for 15 minutes at 7000 rpm in a Thermo Fisher Sorvall LYNX 6000 (Thermo Scientific, Germany) centrifuge. The solutions were then diluted 2 fold and 4 fold. The pH was adjusted with potassium hydro-phosphate (K₂HPO₄) and potassium hydroxide (KOH) until pH 7.5. The pH of the medium was determined with an accuracy of 0.01 units using HJ1131B or Hi2210 pH meters (Hanna Instruments, Portugal) and a counter-selective electrode. To observe the effect of redox reagents, 1 mmol ferricyanide and 3 mmol DTT solutions were added to each medium.

Measurement of bacterial growth

Bacterial growth was determined spectrophotometrically (Spectro UV-VIS Auto, LaboMed, Los Angeles, CA, USA) at a wavelength of 600 nm. The pH of the medium was measured using the pH electrode of an HJ1131B pH-meter (Hanna Instruments, Portugal) and calibrated with 0.1 M NaOH or 0.1 N HCl solutions.

Determination of oxidation-reduction potential (ORP) and H₂

The ORP of the medium was monitored using redox electrodes: Pt-platinum (EPB-1, Measuring Instruments Enterprise, Gomel, Belarus, or PT42BNC, Hanna Instruments, Portugal) and (Ti-Si)-titanium-silicate (EO-02, measuring instruments enterprise, Gomel, Belarus) electrodes [12]. Before measurements, the readings of both electrodes were tested using 0.049 M K₃[Fe(CN)₆] and 0.05 M K₄[Fe(CN)₆]*3H₂O solutions, pH 6.86.

Processing of data and used reagents

Data were obtained from 3 different experiments. Processing of the received data was done using Microsoft Excel 2016. Student's criteria (P) was chosen to indicate the range of error for each experiment. Moreover, the difference was valid when $P < 0.05$.

RESULTS AND DISCUSSION

Cultivation of *E. coli* BW25113 PS and mutant strain in WGW, the effect of redox reagents

As already mentioned, wine production, waste (WGW) is rich in carbohydrates, which makes it a promising and valuable environment for obtaining bio- H_2 through bacterial fermentation. The formation of bacterial biomass and the decline of ORP, followed by acidification of the environment, were observed in WGW. The samples were grown in 0 to 4-fold dilutions of WGW, 7.5 pH. The pH of the media was adjusted with 1 M K_2HPO_4 or KOH solutions. When the pH was adjusted with KOH a pronounced acidification occurred (pH dropped from 7.5 to 4.6) after 24 and 48 h of growth, (Fig. 1).

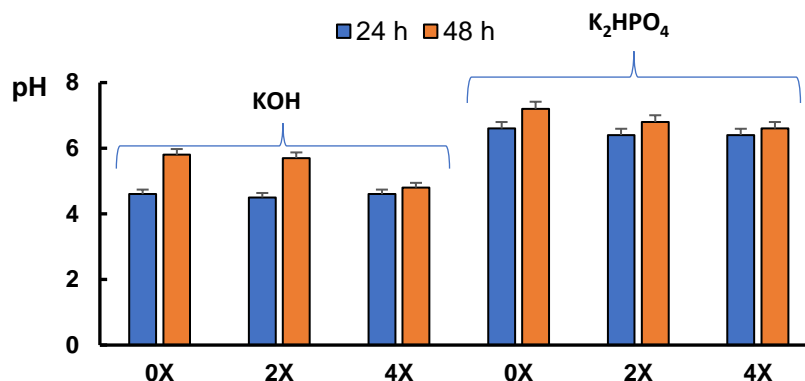


Figure 1. Change in pH during 48 h growth of *E. coli* BW25113 using WGW hydrolysate. The pH of the medium was adjusted by 1 M KOH and K_2HPO_4 . Bacteria were grown anaerobically, pH 7.5, 37 °C.

Whereas in the case of adjustment of pH with K_2HPO_4 , the maximum drop in pH from the initial value was observed after 24 h growth and recorded at 6.6, and after 48 hours, the medium became basic again (Fig. 1). Maximum growth of *E. coli* BW25113 was observed in twice diluted WGW after 48 h growth when the pH of the medium adjusted with K_2HPO_4 . ORP and H_2 production of bacterial cultures were studied with the platinum (Pt) and titanium-silicate (Ti-Si) redox electrodes. During bacterial growth, a decrease from positive values to a negative value of -400 ± 10 mV was observed. After 24 h, both in the control and the 2- and 4-fold diluted WGW samples, the values of ORP were decreased from positive to negative up to -530 mV, which proved the production of hydrogen under WGW fermentation conditions. H_2 production was maintained in all samples even after 48 hours of growth. Hydrogen yield was determined in 2- and 4-fold diluted WGW media when the pH of the media was adjusted with K_2HPO_4 or KOH. H_2 yield was shown to be ~3-fold higher in 2-fold diluted WGW when the pH of the medium was adjusted with K_2HPO_4 , compared to the control. Hydrogen production continued even after 48h in both (control and diluted WGW) media. Meanwhile, hydrogen production was observed only after 24 h in 2- and 4-fold diluted WGW with KOH, and no H_2 production was observed either 24 or 48 h after growth in the control. The results show that the maximum growth and prolonged hydrogen production of *E. coli* BW25113 bacteria in the WGW medium are maintained in the medium with high buffering capacity.

The redox reagents an impermeable oxidizer $K_3[Fe(CN)_6]$ and membrane permeating reducer DL-dithiothreitol were used. The effect of these reagents on the growth parameters and redox kinetics of *E. coli* 25113 bacteria and septuple Mutant strain (MS) was shown. The production of H_2 was stimulated in *E. coli* bacteria in the DTT supplemented samples (Table 1). During *E. coli* PS growth with DTT in WGW, the Pt-Ti electrode reading decreased from the first hour of growth (-470 ± 10 mV) and H_2 production was observed, which continued until the 72nd hour of growth. In the Mutant strain, the ORP value decrease (Pt electrode reading) was also observed from the 3rd h to a value of -430 ± 10 mV (Fig. 2).

Whereas, without DTT, H_2 production was only recorded from the 24th hour of growth. During the 24th hour of growth of PS, under the influence of DTT, the production of hydrogen with a maximum yield of 5.1 mmol/L is observed.

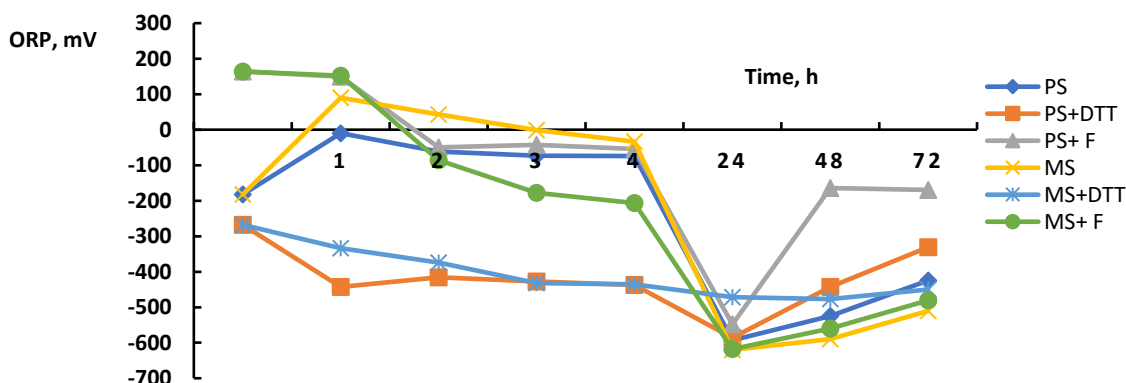


Figure 2. Changes ORP of *E. coli* BW25113 (PS) and mutant strain (MS) in the presence of redox reagents during growth, pH 7.5. Bacteria were grown anaerobically. Bacterial growth in ORP was measured with a platinum electrode (Pt) and expressed in mV (Ag/AgCl (saturated with KCl)). An average of 3 independent experiments are presented. DTT- DL-dithiothreitol, F- ferricyanide.

In the MS, the maximum H_2 yield was recorded at the 24th h of growth in the control and ferricyanide-added samples with values of 5.25 mmol/L and 5.24 mmol/L, respectively. The suppressive effect of ferricyanide on the PS is evident and hydrogen production is observed only at the 24th hour of growth, with a lower yield compared to the other samples (Fig. 2, Table 1). Meanwhile, no special effect due to ferricyanide is observed in the mutant compared to the control. Furthermore, hydrogen production continues until the final stage of growth. In the medium containing DTT ~1.5 times more biomass was formed at 24h and ~2 times at 48 and 72 h compared to the control. In the sample containing ferricyanide, bacterial growth was suppressed ~1.2-fold at 24 hours, ~1.3-fold at 48 hours and at 72 hours it was stimulated ~2 times (Table 1).

Table 1. H_2 yield in *E. coli* PS and mutant strain (MS) during growth in 2x diluted WGW

Medium	1h	2h	24h	48h	72h
PS	-	-	5.10 mmol/L	1.5 mmol/L	-
PS+DTT	1.50 mmol/L	1.40 mmol/L	5.10 mmol/L	1.52 mmol/L	0.80 mmol/L
PS+ F	-	-	1.6 mmol/L	-	-
MS	-	0.80 mmol/L	5.25 mmol/L	3.68 mmol/L	1.50 mmol/L

MS+ DTT	0.75 mmol/L	0.80 mmol/L	5.24 mmol/L	1.36 mmol/L	0.85 mmol/L
MS+ F	-	-	1.40 mmol/L	2.25 mmol/L	1.40 mmol/L

* H₂ yield is presented with an accuracy of ± 0.02 mmol/L

PS- parental strain, MS-mutant strain, DTT- DL-dithiothreitol, F- ferricyanide

It is suggested that ORP can be controlled by supplying oxidants and reductants or mediated by redox stress. As an example, non-penetrating oxidizers by inducing positive ORP values, suppress *Escherichia coli* growth and decrease acidification of the medium. On the other hand, reducing conditions of the environment adjusted with DTT, lead to increased formation of formic acid by *E. coli* [12]. Therefore, culture medium ORP may affect the yields of produced metabolites.

Consequently, ORP could be considered as a tool to monitor growth and changes in the metabolism of aerobically growing bacteria to optimize yields of end metabolites.

CONCLUSION

These results highlight the potential of using lignocellulosic wine grape waste as a medium for H₂ production by *E. coli* and demonstrate the significance of ORP in controlling growth and hydrogen production in this system.

ACKNOWLEDGEMENT

This work was supported by the Foundation of Armenian Science and Technology (FAST) ADVANCE program to LB, AP, KT, and GA and the grant [21AG-1F043] from the State Committee of Science, Ministry of Education, Science, Culture and Sport of Armenia to AP.

REFERENCES

1. Global Hydrogen Review 2022, IEA, Paris <https://www.iea.org/reports/global-hydrogen-review-2022>, License: CC BY 4.0
2. Wang MJ, Wang GZ, Sun ZX, Zhang YK, Xu D. 2019. Review of renewable energy-based hydrogen production processes for sustainable energy innovation. *Global Energy Interconnection* 2:436-443.
3. Zhao J, Patwary AK, Qayyum A, Alharthi M, Bashir F, Mohsin M, Hanif I, Abbas Q. 2022. The determinants of renewable energy sources for the fueling of a green and sustainable economy. *J Energy* 238:0360-5442.
4. Ferrari IV, Pasquini L, Narducci R, Sgreccia E, Di Vona ML, Knauth PA. 2022. Short Overview of Biological Fuel Cells. *Membranes Journal* 12:427.
5. François E, Dumas Ch, Gougeon Régis D et al. 2021. Unexpected high production of biohydrogen from the endogenous fermentation of grape must deposits. *Bioresource Technology* 320, Part A
6. Spinei M, Oroian M. 2021. The Potential of Grape Pomace Varieties as a Dietary Source of Pectic Substances, *References* 217:10, 867.
7. Natolino A. & Da Porto C. 2020. Kinetic models for conventional and ultrasound assistant extraction of polyphenols from defatted fresh and distilled grape marc and its main components skins and seeds. *Chem. Eng. Res. Des.* 156:1–12.
8. Peters JW, Schut GJ, Boyd ES, Mulder DW, Shepard EM, Broderick JB, King PW, Adams MW. 2015. [FeFe]- and [NiFe]-hydrogenase diversity, mechanism, and maturation. *Biochim Biophys Acta (BBA) Mol Cell Res* 1853:1350–69.
9. Trchounian K, Pinske C, Sawers RG, Trchounian A. 2012. Characterization of *Escherichia coli* [NiFe]-hydrogenase distribution during fermentative growth at different pHs. *Cell Biochem Biophys* 62:433–440.



10. Trchounian K, Sawers G, Trchounian A. 2017. Improving biohydrogen productivity by microbial dark- and photo-fermentations: Novel data and future approaches. *Renew Sustain Energy Rev* 80:1201–16.
11. Xue YS, Jian PT, Ning H, Swee KY, Yew WH, Abdullah AIL, Shareena FAIM, Nurul AB, Jamali NS. 2023. Unraveling the effect of redox potential on dark fermentative hydrogen production, *Renewable and Sustainable Energy Reviews* 187113755.
12. Poladyan A, Blbulyan S, Sahakyan M, Lenz O, Trchounian A. 2019, Growth of the facultative chemolithoautotroph *Ralstonia eutropha* on organic waste materials: growth characteristics, redox regulation and hydrogenase activity. *Microb Cell Fact* 18:201.
13. Taylor MJ, Alabdrabalameer HA, Skoulou V. 2019. Choosing Physical, Physicochemical, and Chemical Methods of Pre-Treating Lignocellulosic Wastes to Repurpose into Solid Fuels. *Sustainability* 11:3604.
14. Poladyan A, Trchounian K, Vasilian A, Trchouian A. 2018. Hydrogen production by *Escherichia coli* using brewery waste: Optimal pretreatment of waste and role of different hydrogenases, *Renew Energy* 115:931-936.

ICH2P14-PP118

COMPARATIVE ECONOMIC ANALYSIS OF SMALL MODULAR REACTOR HYDROGEN COGENERATION AND CONVENTIONAL GAS-FIRED PLANT FOR LOAD FOLLOWING: A CASE STUDY

**Derrick Whelan, Lixuan Lu*

Ontario Tech University, Department of Energy and Nuclear Engineering, Faculty of Engineering and Applied Science, 2000 Simcoe St. N, Oshawa, Canada

*Corresponding author email: derrick.whelan@ontariotechu.net

ABSTRACT

Load following by nuclear hydrogen cogeneration is seen as an effective strategy to increase the efficiency and resiliency of future electricity grids, which will contain higher proportions of Variable Renewable Energy Sources (VRES). The Canadian province of Ontario provides an ideal subject for decarbonizing a major industrialized electricity grid using a load following cogeneration strategy. Ontario produces carbon-free baseload power; however, natural gas plants are required to meet peak demand. This paper explores a case study for potentially replacing peak-demand natural gas plants with Small Modular Reactors (SMRs) load following by hydrogen cogeneration. Two peaking plants are compared using Levelized Cost of Electricity (LCOE) to the grid, the First-Of-A-Kind (FOAK) BWRX-300 SMR currently being built with an expected completion date of 2028, and an existing 393 MWe Natural Gas Simple Cycle (NGSC) plant. A subsidized LCOE for a SMR cogenerating hydrogen during “non-peak” grid hours is estimated using the Hydrogen Economic Evaluation Program (HEEP). The results show that a SMR cogeneration strategy produces a lower LCOE than a conventional natural gas plant and can also decrease the SMRs LCOE. Through preliminary economic analysis, research identifying potential SMR applications is expected to help accelerate the deployment of commercially viable, carbon-free small modular nuclear power plants while also facilitating the growth of hydrogen production.

Keywords: Hydrogen production, Small modular reactors, Load following, Cogeneration, HEEP.

INTRODUCTION

Nuclear and hydrogen are recognized as promising carbon-free energy sources. As first-of-a-kind SMR electricity grid additions, Canada’s BWRX-300 builds in Ontario provide the first opportunity for the economic evaluation of SMR assets in the context of a known grid application. Ontario is an ideal example for decarbonizing a large, industrialized electricity grid because it has already significantly lowered carbon emissions, being North America’s first jurisdiction to phase out coal-fired electricity generation. Baseload electricity in Ontario is produced by Canada Deuterium Uranium (CANDU) nuclear reactors and hydroelectric power plants, producing 51% and 25% of the electricity supply, respectively. Furthermore, an increasing proportion of wind and solar-powered Variable Renewable Energy Sources are being added to the grid, providing 9.9% and 2.5%, respectively [1].

The issue of carbon-free load following has recently grown in importance as gas-fired generation increases to address the intermittency of VRES. The increasing proportion of VRES pose a challenge for grids attempting to decrease emissions, as gas-fired plants are often added to provide peak dispatchable electricity during times of lowered VRES output. Attempts to decrease carbon emissions by adding VRES alone have produced unsatisfactory economic outcomes with minimal emissions reductions [2]. Small Modular Reactors are uniquely suited to fill the niche for carbon-free peak power. Providing modularity, lower upfront capital costs, faster construction times, and enhanced operability to enable load following operation with VRES [3].

Load following by nuclear hydrogen cogeneration using SMRs has been looked at extensively due to the simplicity and efficiency of this application. With no need for modifications to the Nuclear Power Plant (NPP), modular units can achieve capacity factors of 95%, providing dispatchable electricity for grid output when needed and switching to hydrogen cogeneration during non-peak hours [4]. This capacity factor is a significant economic benefit, potentially justifying higher upfront capital costs, especially when compared to gas-fired peaking plants, which, on average, operate at a 20% capacity factor [5]. Additionally, depending on the level of carbon tax, nuclear power plants may exhibit better economic performance and lower LCOEs than coal and gas-fired plants [6].

In this study, the LCOE for a conventional Natural Gas Simple Cycle (NGSC) plant is compared with a plant load following by nuclear hydrogen cogeneration to identify the potential for such a system as a peak electricity generator. Hydrogen

cogenerated during off-peak hours provides additional revenue and is incorporated into an adjusted LCOE-SMR-Cogeneration (LCEO-SMR-CG). The analysis uses various hydrogen sales price targets, identified as crucial to successfully implementing hydrogen as a transportation fuel. Carbon tax projections are incorporated into the NGSC-LCOE to compare the long-term economics of the two generation sources within the context of their lifespans. With many SMRs coming to the market, assessing their economic viability and potential applications is imperative to ensure their success, enabling the decarbonization of industry and electricity generation.

METHODS AND ANALYSIS

On/Off Peak Capacity Factors

A 393 MWe NGSC generation plant at the York Energy Centre in Newmarket, Ontario, running under a peaking generation contract, will be compared with a 300 MWe SMR [7]. The Ontario electricity grid follows a time-of-use (TOU) pricing structure, wherein electricity costs to consumers and market clearing prices paid to generators fluctuate based on hourly demand. Peak pricing to consumers is implemented during weekdays, based on a cool season, November to April, with peak hours from 7-11 am and 5-7 pm, and warm season from May to October, with peak hours from 11 am – 5 pm [1]. On-peak and off-peak TOU demand factors, 20% and 80%, respectively, are used to assume yearly capacity factors this analysis. The assumption near the grid's on-peak TOU average is chosen, as it allows for broader assessment of gas-fired peaking plants in general.

LCOE Assumptions and Adjustments

All monetary values from the literature have been inflation-adjusted to 2023 CAD\$. Published LCOE estimates, which account for carbon pricing and radioactive waste management, provide preliminary LCOEs for the two sources. At \$0/tCO₂, the NGSC and SMR-LCOE are 15.7 ¢/kWh and 10 ¢/kWh, respectively [5]. LCOE projections including carbon costs for NGSC generation are estimated using the Government of Canada's benchmark policy, which increases the cost of carbon by \$15/tonne/year until 2030 [8]. The SMR and NGSC plant will be assumed to generate electricity for the grid during on-peak hours. During off-peak hours, the NGSC will be dormant, as is the case for a typical peaking plant, while the SMR will generate hydrogen. A subsidized LCOE for an SMR cogenerating hydrogen (LCOE-SMR-CG) is calculated by discounting the estimated revenue from hydrogen sales from the initial LCOE-SMR, Eq. (1).

$$LCOE\ SMR\ CG = LCOE\ SMR - \frac{Gross\ H_2\ revenue * Wholesale\ Margin * Output * Capacity\ Factor}{BWRX\ 300\ Electricity\ Output * TOU\ Onpeak\ Factor} \quad (1)$$

Hydrogen Production

The IAEA's *Hydrogen Economic Evaluation Program* (HEEP) is used to estimate hydrogen production costs for the BWRX-300. The LCOE-SMR is used as the energy usage cost input for hydrogen plant cogeneration within HEEP, and the NPP cost parameters which have accounted for in the published LCOE-SMR are taken as nil. Tables 1 and 2 provide the assumed HEEP parameters, scaled to match the BWRX-300 from the built-in HEEP case for an Advanced Pressurized Water Reactor using conventional electrolysis (APWR 360 CE04). Hydrogen revenue calculations assume Ontario wholesale fuel margins with carbon taxes credited to the wholesale margin [9], and published 2025 dispensed retail (non-subsidized) hydrogen cost estimates, as seen in Table 3. Dispensed hydrogen sales prices chosen for analysis within the context of this study highlight published price targets that make hydrogen competitive in the North American fuel market [10].

Table 1. Economic Assumptions.

Finance Details	
Discount Rate	5%
Inflation rate	1%
Equity/Debt	70%:30%
Borrowing interest	10%
Tax Rate	10%
Construction Period	5 years
Operating life time/Return Period	60 years

Table 2. Hydrogen Generation Plant HEEP Variables.

Hydrogen Generation Plant Details	
Estimated H ₂ plant capital cost	4.23E+08
H ₂ Generation (kg/yr)	5.10E+07
Electricity required (MWe/unit)	719
Overnight Capital Cost (USD/unit)	4.23E+08
Unit cost of electricity for H ₂ Generation (USD/kWe-h)	0.0729
Other O&M cost (% of capital)	4%
Decommissioning cost (% of capital cost)	10%

Table 3. Target dispensed hydrogen fuel costs excluding subsidies and credits [10].

Cost (\$/kg H ₂)	Dispensed Hydrogen Fuel Cost Target	LCOE-SMR-CG (¢/Kwh)
5.49	Long-term American Department of Energy target	5.1
6.86	Projected target for 2050	12.2
8.23	Fuel-economy-adjusted price parity with gasoline, low end and 2025 midpoint estimate	15.0
11.66	Fuel-economy-adjusted price parity with gasoline, high end	17.8

RESULTS AND DISCUSSION

In comparing the adjusted LCOE for two peak dispatchable electricity generation options, results indicate an SMR load following by hydrogen cogeneration can be economically competitive with a NGSC plant. This finding must be interpreted cautiously, as the LCOE results are jurisdiction dependent, and rely on assumptions regarding plant capacity factor, carbon costs and various other variables such as grid TOU policies. Further analysis of individual plants is needed, since the LCOE will vary significantly based on power plant output, grid demands and initial capital cost requirements. Surprisingly, the LCOE of the NGSC peaking plant is higher than that of the SMR before carbon pricing adjustments are applied. This finding has implications for jurisdictions in need of carbon-free peak electricity generation.

It is apparent from the estimates seen in Figure 1 that the SMR load following strategy lowers the LCOE at various dispensed hydrogen fuel sales targets when compared to the conventional NGSC plant. The LCOE-SMR-CG shows the impact of hydrogen revenue adjustments to the LCOE-SMR. At the estimated upper limit of dispensed hydrogen fuel cost for fuel-economy-adjusted price parity with gasoline, \$11.66/kgH₂, the data show the LCOE-SMR-CG discounted by 4.9 ¢/kWh or 49%. The findings suggest SMR cogenerated hydrogen fuel costs are within a range that makes it potentially competitive in various transportation applications. Furthermore, the SMR load following strategy has the added benefit of decreasing the LCOE to the grid when dispensed hydrogen fuel costs meet a certain threshold, which further work is needed to identify.

The NGSC-LCOE projection to 2030, as seen in Figure 1, shows that the current Canadian carbon pricing policy of \$15/tonne/year can increase peak generation costs by up to 71%. The NGSC-LCOE projection, in conjunction with the apparent economic viability of the load following strategy, implies potential for decarbonizing peak generation grid assets using carbon-free SMRs. This has significant implications for jurisdictions determining the economic feasibility of power generation assets. With 100 of the 190 countries party to the Paris Agreement planning or considering carbon pricing mechanisms in their emissions reduction commitments [11], further investigation is essential to analyse alternative power generation strategies under new carbon cost regimes.

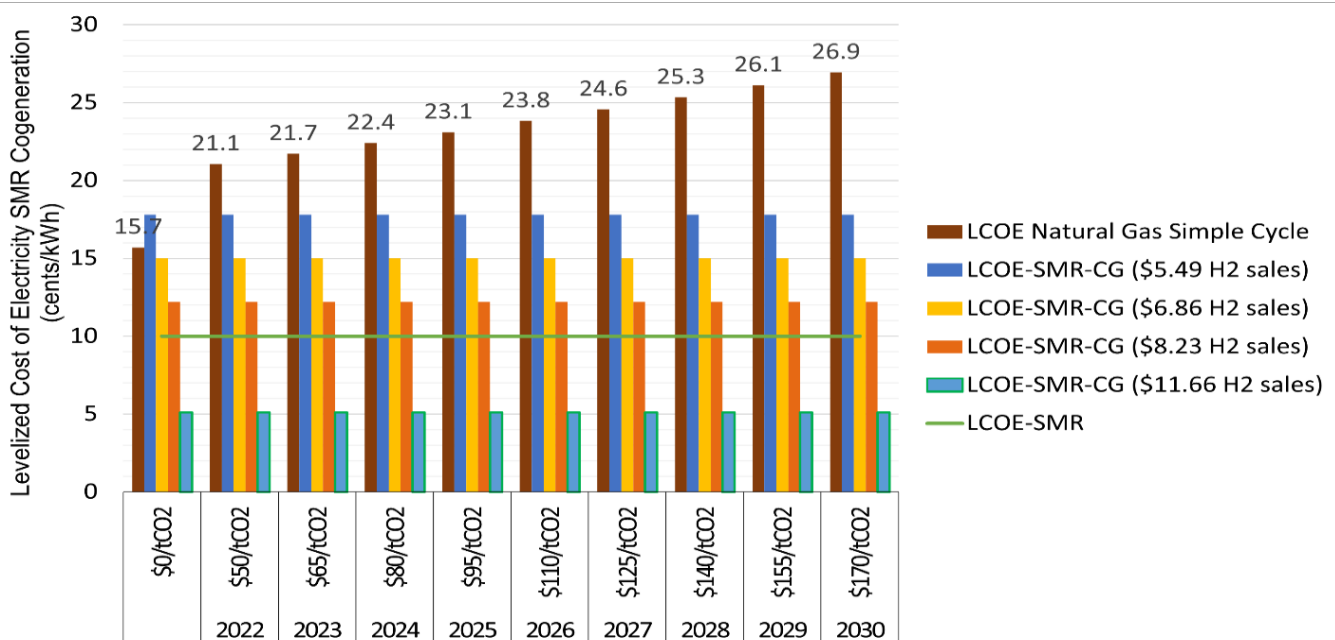


Fig. 1. LCOE adjusted for hydrogen cogeneration revenue and carbon pricing.



CONCLUSIONS

This study compares the LCOE for two peak electricity generation options: a SMR load following by hydrogen cogeneration and a Natural Gas Simple Cycle plant. The electricity grid of Ontario, Canada, provides the context of an industrialised grid, with a high proportion of nuclear and hydroelectric base load power and increasing utilisation of VRES. Various LCOE adjustments and discounts are calculated to determine the effects of carbon pricing, jurisdictional grid policies, and revenue from a load following by nuclear hydrogen fuel cogeneration system. A comparison of the adjusted LCOE estimates for an SMR load following by hydrogen cogeneration and a conventional Natural Gas Simple Cycle peaking plant is made.

The results from the current study are listed as follows:

- As carbon costs increase, an SMR load following by hydrogen cogeneration strategy has a lower adjusted LCOE than an NGSC plant after adjusting for hydrogen revenue. However, further analysis is needed to determine the lowest dispensed hydrogen fuel price that will allow the load following cogeneration system to provide a discount to the initial LCOE input.
- The study has shown preliminary results that a SMR load following strategy has the potential to cogenerate hydrogen fuel for transportation during off-peak hours that is competitive with fuel-economy-adjusted gasoline price parity targets without increasing electricity costs to the grid.
- The lack of a fully built SMRs limits this study, as all capital costs are assumed. There is a need to validate these preliminary findings using known capital costs in new LCOE calculations upon completion of the FOAK BWRX-300.
- SMR modularity and the effectiveness of the load following cogeneration system appear to make SMRs potential candidates for peak dispatchable power generation. Future research should identify nuclear-friendly jurisdictions worldwide in which a load following by nuclear hydrogen cogeneration strategy could be feasible.

ACKNOWLEDGEMENT

We would like to acknowledge the financial support of the Natural Sciences and Engineering Research Council of Canada (NSERC).

REFERENCES

1. <https://www.ontario.ca/files/2023-07/energy-powering-ontarios-growth-report-en-2023-07-07.pdf>. Accessed on October 22, 2023
2. Bahramian P and Jenkins G.P and Milne F. 2021. The displacement impacts of wind power electricity generation: Costly lessons from Ontario. Energy Policy. 10.1016/j.enpol.2021.112211
3. https://aris.iaea.org/Publications/SMR_booklet_2022.pdf. Accessed on September 21, 2023
4. Locatelli G and Fiordaliso A and Boarin S and Ricotti ME. 2017. Cogeneration: An option to facilitate load following in Small Modular Reactors. Progress in Nuclear Energy 10.1016/j.pnucene.2016.12.012.
5. Doluweera G and et. al. 2018. A Comprehensive Guide to Electricity Generation Options in Canada. Canadian Energy Research Institute. ISBN 1-927037-53-9.
6. Locatelli G and Mancini M. 2010. Small-medium sized nuclear coal and gas power plant: A probabilistic analysis of their financial performances and influence of CO2 cost. Energy Policy 10.1016/j.enpol.2010.06.027.
7. <https://www.ieso.ca/en/Power-Data/Supply-Overview/Transmission-Connected-Generation>. Accessed September 1, 2023.
8. Tian X and An C and Chen Z. 2023. The role of clean energy in achieving decarbonization of electricity generation, transportation, and heating sectors by 2050: A meta-analysis review. Renewable and Sustainable Energy Reviews. 10.1016/j.rser.2023.113404.
9. <https://ontario.ca/motor-fuel-prices/>. Accessed September 3, 2023
10. [Roadmap for the Deployment and Buildout of Renewable Hydrogen Production Plants in California | California Energy Commission](#). Accessed September 5, 2023
11. https://unfccc.int/sites/default/files/resource/parisagreement_publication.pdf. Accessed on October 20, 2023.

ICH2P14-PP128

GREEN HYDROGEN PRODUCTION: A COST COMPARISON OF DIFFERENT ELECTROLYSIS TECHNOLOGIES

**Hafiz Muhammad Uzair Ayub, Sabla Y. Alnouri,*

Gas Processing Center, College of Engineering, Qatar University, Doha P.O. Box 2713, Qatar

*Corresponding author e-mail: uzairayub@qu.edu.qa

ABSTRACT

Hydrogen production from conventional fossil fuel-based energy systems often results in CO₂ by-products, and has the potential risk of contributing towards the global greenhouse gas emission (GHG) problem, the primary factor of climate change. Unlike conventional technologies, renewable sources for green hydrogen production are very attractive and environmentally friendly. Green hydrogen is produced through water electrolysis with the integration of renewable electricity generation systems such as wind and solar power. In this study, a cost comparison for green hydrogen production methods has been made by analyzing different types of electrolysis such as alkaline electrolysis (AEL), polymer electrolyte membrane (PEM) electrolysis, and solid oxide electrolysis (SOE). The overall results show that hydrogen production from solar-connected electrolysis technologies is the most cost-efficient when compared to wind solar-connected electrolysis technologies. Moreover, the cost analysis has been categorized into minimum cost and maximum cost cases, using US pricing as a basis for all costing parameters. The hydrogen production cost from AEL is 6.6 \$/kg-H₂ and 10.03 \$/kg-H₂ in both minimum and maximum cost cases respectively which is less than the cost of hydrogen produced from PEM and SOE which in turn ranges from 12.78 \$/kg-H₂ to 20.14\$/kg-H₂ and 8.7\$/kg-H₂ to 12 .26\$/kg-H₂.

Keywords: Green Hydrogen, Hydrogen economy, Electrolysis.

INTRODUCTION

The growing environmental concerns related to climate change as a result of greenhouse gas emissions from conventional energy sources (such as coal and natural gas) has put forth renewable energy sources as one of the potential solutions. In 2020, the International Energy Agency (IEA) reported that 84% of the world's energy demand is supplied using conventional fossil fuel-based energy systems [1]. Therefore, the need to reduce the consumption of fossil fuel-based fuels is necessary to protect the environment. Currently, energy systems that are reliant on renewables like biomass, solar, and wind may possess the capacity to meet global energy needs while simultaneously mitigating the release of greenhouse gas emissions into the environment [2, 3].

Green hydrogen production processes have been reported as very the attractive alternative and sustainable energy option, for the effective transition towards renewable energy systems [4]. Green hydrogen is produced from water splitting powered by renewable electricity generated from wind or solar-based grids [5]. Water covers more than 70% of the earth, and 11.2% of that water consists of hydrogen; thus, water can be considered a very reliable source of hydrogen [6]. Moreover, green hydrogen is considered environmentally friendly due to the zero carbon emissions that result as opposed to the other hydrogen production from the thermochemical conversion of coal and natural gas [7]. Therefore, throughout the past few decades, the evolution towards renewable energy options and viable methods for green hydrogen production has attracted the attention of many researchers and policymakers. As such, the use of green hydrogen energy sources are predicted to have a significant positive long-term impact on the environment as a result of the net-zero carbon emissions from such processes [8].

Electrolysis stands out as being one of the most environmentally efficient processes that can be used for hydrogen production via water splitting, surpassing thermal decomposition of water and thermochemical conversion methods [5]. Electricity is crucial for this process due to the highly endothermic nature of water splitting, demanding substantial energy input to separate it into hydrogen and oxygen. Currently, three

primary electrolysis technologies can be utilized for green hydrogen production: Alkaline Electrolysis (AEL), Proton Exchange Membrane Electrolysis (PEM), and Solid Oxide Electrolysis (SOE) [9].

AEL technology for green hydrogen generation is an established method that has been in constant practice in various hydrogen production plants for more than 100 years [10]. This process is the most cost-effective, extensive, and resilient as compared to the other types of electrolysis. The drawbacks of an AEL process are the hydrogen purity, high amount of electricity requirement for the process operation, lower hydrogen production pressure, and conceded energy efficiency. AEL unit is operated at room temperature to 80 °C and 30 wt% of potassium hydroxide (KOH) basic solution is used as an electrolyte to decompose the water molecule into hydrogen and oxygen [11]. In this technology, the cathode and anode are separated by an ion exchange membrane (IEM); the hydrogen and oxygen gases exit the electrolysis unit and are stored in separate tanks for different processes.

The PEM electrolysis method is an evolved electrolysis technology designed to operate efficiently at appropriate current densities and high input voltages[12]. The purity of the hydrogen produced from PEM is almost 99.995%. In the PEM electrolysis process, the anode and cathode are separated by Nafion-based polymer membranes. This membrane has unique characteristics concerning its conductivity, mechanical firmness, chemical, and thermal stability for the different ranges of process parameters like temperature and pressure. The major disadvantages of the PEM electrolyzer in terms of overall durability are the cost of the electrocatalyst and the PEM conductive membrane [13]. Therefore there is a need to reduce the production cost of the PEM electrolyzer unit for sustainable efficiency and in comparison, the cost of the PEM electrolysis is higher than the cost of the Alkaline electrolysis process.

In the last few years, SOE electrolysis has gained enormous attention due to the deliberation as a most efficient technology regarding the generation of active ions from the provided electrical energy that helps to split the water molecule into the purest hydrogen [14]. On the other hand, this process is operated at very high temperatures of 500 °C to 1000 °C which is the main hurdle in the commercialization of this technology because of the effect on the price of the hydrogen. High operational temperatures improve efficiency over other methods, but material degradation is an important consideration. SOE technology has a faster operational response time than PEM technology because it uses a solid ceramic membrane to separate opposite polar electrodes with high charge transfer rates [15]. Therefore, the main disadvantage of this technology is its energy intensity as compared to the AEL and PEM, which in turn directly affects the cost of green hydrogen production. Fig. 1. shows the difference between AEL, POM and SOE.

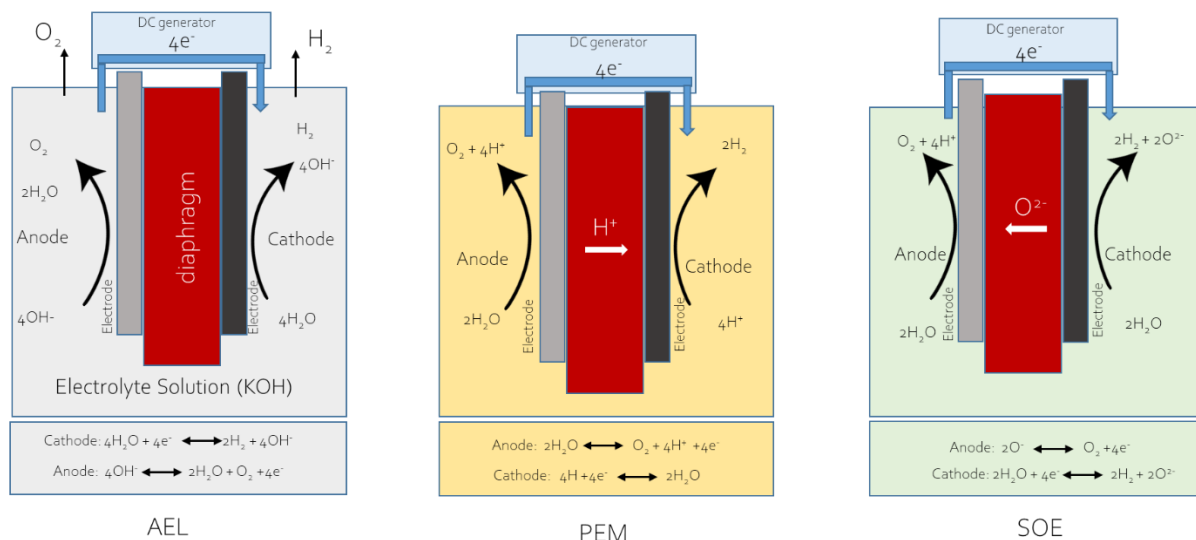


Fig. 1. Illustrative comparison between AEL, PEM and SOE [16].

The cost of producing green hydrogen is directly related to the costs associated with the electricity supplied to the electrolysis units for water splitting [17]. Consequently, the varying costs of electricity from different types of power generation systems, such as wind and solar, also play a significant role. This

study focuses on estimating the cost of green hydrogen production in the United States. The analysis involves determining and comparing the costs of green hydrogen production through AEL, PEM, and SOE electrolysis technologies, utilizing integrated solar and wind electricity generation systems. The comparison is made using both the minimum and maximum cost components and parameters. The findings of this study will serve as a valuable resource for exploring diverse scenarios related to cost components and parameters in the future.

GREEN HYDROGEN COST ESTIMATION

The main objective of this study is to calculate the total green hydrogen production cost from renewable sources such as wind and solar using the three different electrolysis technologies AEL, PEM, and SOE. This hydrogen cost is calculated for the case study of the USA. Figure 2. shows the structure of different routes for green hydrogen production used in this study.

The total cost of per kilogram of hydrogen is calculated as follows:

$$Cost_{H_2,j}^{Total} = Cost_W + Cost_{ES,i} + Cost_{ES,j} \quad (1)$$

Where $Cost_{H_2,j}^{Total}$ is the total hydrogen production cost in \$/kg H₂, $Cost_W$ is the cost of the water required to produce the green hydrogen, $Cost_{E,i}$ is the cost of the electricity from renewable sources such as solar and wind.

$$Cost_W = Cost_{UW} * Water_R \quad (2)$$

Where $Cost_{UW}$ is the unit price of the water and $Water_R$ is the required amount of water for the electrolysis.

$$Cost_{ES,i} = Cost_{UES,i} + Electricity_{R,j} \quad (3)$$

Where $Cost_{UES,i}$ is the unit price of the electricity for the each source and $Electricity_{R,j}$ is the required amount of the electricity needed for the different electrolysis units.

$$Cost_{E,j} = (CAPEX_j + OPEX_j)/t \quad (4)$$

Where $CAPEX_j$ is the total expenditure or the capital cost of the electrolysis units, $OPEX_j$ is the operational expenditures or the operating cost of the electrolysis process and t is the time in hours for a year to produce the hydrogen.

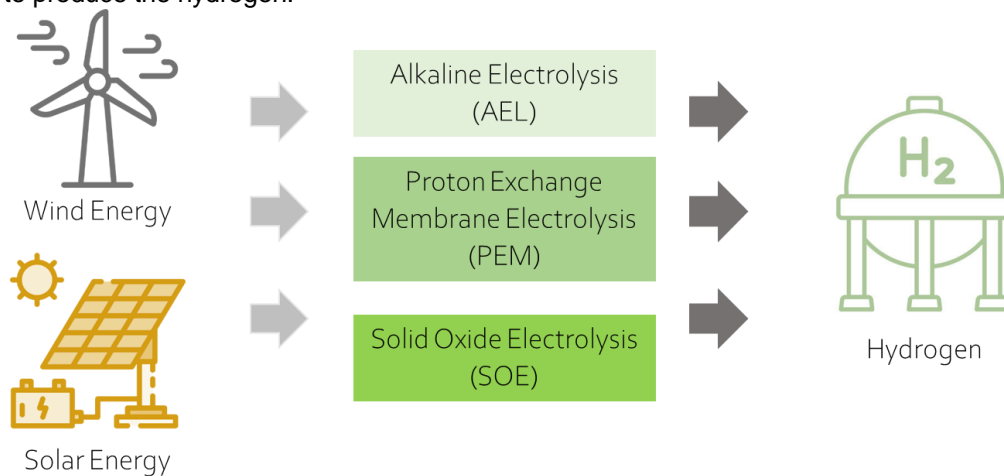


Fig. 2. Green hydrogen production via different electrolysis technologies and different renewable energy routes.

RESULTS AND DISCUSSION

Input parameters and cost components: The input parameters and cost components such as the required electricity, CAPEX, and OPEX to produce the green hydrogen from each type of electrolysis are given in Table 1. The fixed input parameters are provided in Table 2.

Table 1. Input parameters and cost components for US [18].

Minimum Cost Case				
No.	Electrolysis Type	Electricity required (kwh/kg H ₂)	CAPEX (\$/kW)	OPEX (\$/kW)
1	AEL	50	952	28.56
2	PEM	56	1770	53.1
3	SOE	36	1904	57.12
Minimum Cost Case				
1	AEL	65	1142	34.26
2	PEM	72	2208	66.24
3	SOE	45	2311	69.33

Table 2. Fixed input parameters to calculate the hydrogen cost for US [18, 19].

Parameters	Values
Cost of water (\$/m ³)	0.95
water required (kg H ₂ O/kg H ₂)	9.1
Wind Electricity cost (\$/kwh)	0.049
Solar Electricity cost (\$/kwh)	0.02

The hydrogen production from renewable power sources such as wind and solar integrated with the electrolysis units water is considered as the green hydrogen. This green hydrogen is one of the most appealing options for a sustainable environment, but it is also the most expensive when compared to conventional and other thermal-based power generation integrated processes. Table 3 presents the results for two different cases of green hydrogen production (the first case was integrated with wind energy while the second case was integrated with solar energy). For each of those 2 cases, the cost of AEL, PEM, and SOE electrolysis processes were compared using US pricing for electricity and water. Figure 3 shows the hydrogen production cost predicted from the AEL, PEM, and SOE electrolysis processes for the US.

Table 3. Green Hydrogen Production Cost in the US.

Minimum Cost Case				
No.	Electrolysis Type	Electricity Sources	Electricity Cost (\$/kg H ₂)	Hydrogen production cost (\$/kg H ₂)
1	AEL	Wind	8.04	8.05
		Solar	6.59	6.60
2	PEM	Wind	14.39	14.4
		Solar	12.77	12.78
3	SOE	Wind	9.82	9.83
		Solar	8.77	8.78
Maximum Cost Case				
1	AEL	Wind	11.91	11.92
		Solar	10.02	10.03
2	PEM	Wind	22.22	22.22
		Solar	20.13	20.14
3	SOE	Wind	13.47	13.47
		Solar	12.25	12.26

- *Minimum Cost Case:*

The hydrogen production from AEL powered by wind electricity is 8.05 \$/kg H₂ was found to be the most economical option, while the PEM-wind and SOE-wind were reported to be more costly, at 14.4 \$/kg H₂ and 9.83 \$/kg H₂ respectively. Interesting, all integrated solar electrolysis

processes were found to be more cost-effective than the wind-powered electrolysis alternatives. The hydrogen production from AEL powered by solar electricity is 6.6 \$/kg H₂ which is the most economical out of the PEM-solar and SOE-solar (reported to be 12.78 \$/kg H₂ and 8.78 \$/kg H₂ respectively).

- *Maximum Cost Case:*

Hydrogen production through AEL, powered by wind electricity, was found to be the most economical at 11.92 \$/kg H₂ when compared to the costs of PEM-wind (22.22 \$/kg H₂) and the cost of SOE-wind (13.47 \$/kg H₂). On the other hand, the integrated solar electrolysis process was found to be more cost-effective than the wind powered electrolysis process alternatives. AEL, powered by solar electricity, leads with a production cost of 10.03 \$/kg H₂, outperforming PEM-solar (20.14 \$/kg H₂) and SOE-solar (12.26 \$/kg H₂).

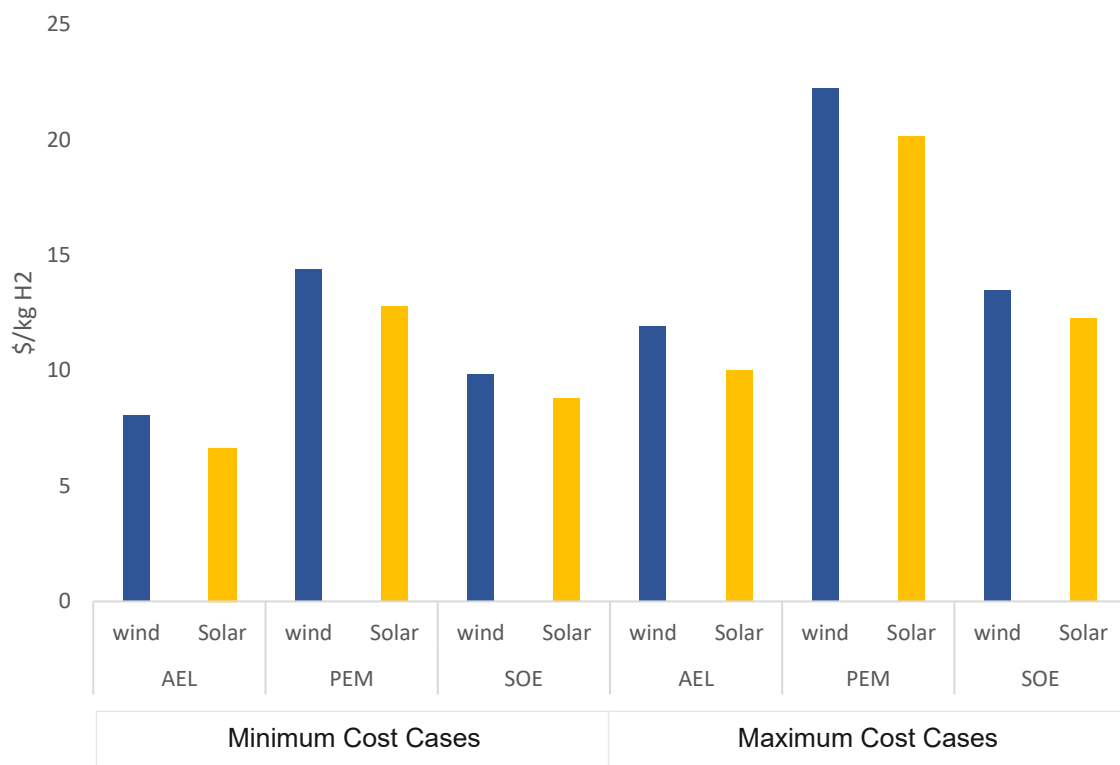


Fig. 3. Total hydrogen production cost (\$/kg H₂).

CONCLUSIONS

Green hydrogen is produced by integrated water electrolysis with renewable energy generation systems such as wind and solar power. This study analyzed different types of electrolysis, such as alkaline electrolysis (AEL), polymer electrolyte membrane (PEM) electrolysis, and solid oxide electrolysis (SOE), to make a cost comparison for green hydrogen production methods. When compared to wind solar-connected electrolysis technologies, the overall results show that hydrogen production from solar-connected electrolysis technologies is the most cost-effective. Furthermore, the cost analysis has been divided into minimum cost and maximum cost cases, with US pricing serving as the foundation for all costing parameters. The cost of producing hydrogen from AEL is 6.6 \$/kg-H₂ in the best case and 10.03 \$/kg-H₂ in the worst case, which is less than the cost of producing hydrogen from PEM and SOE, which ranges from 12.78 \$/kg-H₂ to 20.14\$/kg-H₂ and 8.7\$/kg-H₂ to 12.26\$/kg-H₂, respectively.



REFERENCES

1. Ma, N., et al., *Large scale of green hydrogen storage: Opportunities and challenges*. International Journal of Hydrogen Energy, 2023.
2. Ayub, H.M.U., et al., *Prediction of Process Parameters for the Integrated Biomass Gasification Power Plant Using Artificial Neural Network*. Frontiers in Energy Research, 2022. **10**: p. 894875.
3. Sayed, E.T., et al., *A critical review on environmental impacts of renewable energy systems and mitigation strategies: Wind, hydro, biomass and geothermal*. Science of the total environment, 2021. **766**: p. 144505.
4. Squadrato, G., G. Maggio, and A. Nicita, *The green hydrogen revolution*. Renewable Energy, 2023. **216**: p. 119041.
5. Hassan, Q., et al., *A review of green hydrogen production based on solar energy; techniques and methods*. Energy Harvesting and Systems, 2023(0).
6. Song, H., et al., *Solar-driven hydrogen production: Recent advances, challenges, and future perspectives*. ACS Energy Letters, 2022. **7**(3): p. 1043-1065.
7. Hosseini, S.E. and M.A. Wahid, *Hydrogen production from renewable and sustainable energy resources: Promising green energy carrier for clean development*. Renewable and Sustainable Energy Reviews, 2016. **57**: p. 850-866.
8. van der Spek, M., et al., *Perspective on the hydrogen economy as a pathway to reach net-zero CO₂ emissions in Europe*. Energy & Environmental Science, 2022. **15**(3): p. 1034-1077.
9. Panigrahy, B., K. Narayan, and B.R. Rao, *Green hydrogen production by water electrolysis: A renewable energy perspective*. Materials today: proceedings, 2022. **67**: p. 1310-1314.
10. Bollmann, J., S. Pitchaimuthu, and M.F. Kühnel, *Challenges of Industrial-Scale Testing Infrastructure for Green Hydrogen Technologies*. Energies, 2023. **16**(8): p. 3604.
11. Yue, M., et al., *Hydrogen energy systems: A critical review of technologies, applications, trends and challenges*. Renewable and Sustainable Energy Reviews, 2021. **146**: p. 111180.
12. Demir, M.E. and I. Dincer, *Development of a hybrid solar thermal system with TEG and PEM electrolyzer for hydrogen and power production*. International Journal of Hydrogen Energy, 2017. **42**(51): p. 30044-30056.
13. Zhang, K., et al., *Status and perspectives of key materials for PEM electrolyzer*. Nano Research Energy, 2022. **1**(3): p. e9120032.
14. Biswas, S., et al., *A critical review on cathode materials for steam electrolysis in solid oxide electrolysis*. International Journal of Hydrogen Energy, 2023. **48**(34): p. 12541-12570.
15. Grube, T., et al., *A techno-economic perspective on solar-to-hydrogen concepts through 2025*. Sustainable energy & fuels, 2020. **4**(11): p. 5818-5834.
16. Reduction, G.H.C., *Scaling up electrolyzers to meet the 1.5 C climate goal*. International Renewable Energy Agency, Abu Dhabi, 2020.
17. Ayodele, T. and J. Munda, *Potential and economic viability of green hydrogen production by water electrolysis using wind energy resources in South Africa*. International Journal of Hydrogen Energy, 2019. **44**(33): p. 17669-17687.
18. Katebah, M. and P. Linke, *Analysis of hydrogen production costs in Steam-Methane Reforming considering integration with electrolysis and CO₂ capture*. Cleaner Engineering and Technology, 2022. **10**: p. 100552.
19. Ramadan, M.M., Y. Wang, and P. Tooteja, *Analysis of Hydrogen Production Costs across the United States and over the next 30 years*. arXiv preprint arXiv:2206.10689, 2022.

ICH2P14-PP139

PERFORMANCES OF COMMERCIAL ZEOLITES WITH DIFFERENT ACIDITIES FOR CATALYTIC CO₂ HYDROGENATION TO DIMETHYL ETHER USING COPPER/ZINC/ALUMINA CATALYST

¹Assem. T. Mohamed, ¹Abdul Hakeem Anwer, ¹Dina Ewis, ³Siham Y. Al-Qaradawi, ^{1,2}Mohamed Ali H. Saad, ^{1,2}*Abdelbaki. Benamor

¹Gas Processing Center, College of Engineering, Qatar University, P.O.Box 2713 Doha, Qatar

²Department of Chemical Engineering, College of Engineering, Qatar University, P.O.Box 2713, Doha, Qatar

³Department of Chemistry & Earth Sciences, College of Arts and Sciences, Qatar University, P.P. Box 2713, Doha, Qatar

*Corresponding author e-mail: benamor.abdelbaki@qu.edu.qa

ABSTRACT

In this investigation, we describe the application of three distinct commercially available zeolites—specifically HZSM-5, denoted as Z1, Z2, and Z3 with varying Silica/Alumina ratios, for the direct conversion of carbon dioxide to dimethyl ether (DME) using a Cu/Zn/Alumina (CZA) catalyst. The CZA catalyst, featuring a consistent composition of 60 wt.% Cu, 30 wt.% Zn, and 10 wt.% Alumina, was synthesized utilizing the solution combustion synthesis (SCS) technique. The synthesized catalysts underwent comprehensive characterization through scanning electron microscopy (SEM), transmission electron microscopy (TEM), X-ray diffraction (XRD). Utilizing the prepared catalysts, the CO₂ hydrogenation to dimethyl ether (DME) was conducted through a two-step process in a high-pressure packed bed reactor, employing different pressures (40, 50, and 60 bars), a constant temperature of 250 °C, and a hydrogen to carbon ratio of 3:1. The efficacy of the synthesized catalysts in CO₂ hydrogenation was assessed based on overall CO₂ conversion and product selectivity. The results indicated that CZA/Zeolites exhibited high activity in converting CO₂ to methanol and DME, with CZA/Z3 demonstrating the most noteworthy CO₂ conversion rate at 27.7% and a DME selectivity of 39.5%.

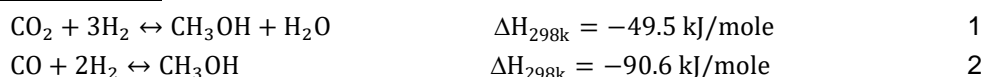
Keywords: CO₂ hydrogenation, Methanol, Dimethyl ether, Catalyst, Zeolites.

1. INTRODUCTION

In response to the escalating global energy demand, the emissions of greenhouse gases (GHG) have been on a consistent rise over the past few decades. Carbon dioxide (CO₂), a prominent GHG, has experienced a substantial increase, reaching concentrations of up to 400 ppm in the atmosphere. Anthropogenic CO₂ emissions are widely acknowledged as a primary contributor to global warming. To address this issue on a global scale, Carbon Capture Utilization and Storage (CCUS) technologies are being explored for CO₂ mitigation [1, 2]. Carbon capture utilization (CCU) aims to convert captured CO₂ into valuable chemicals. Catalytic hydrogenation of CO₂ represents one of the CCU methods, transforming CO₂ into energy products and enabling the substantial recycling of captured carbon dioxide. The conversion of CO₂ into useful products, such as dimethyl ether (DME), hydrocarbons, urea, etc., presents an appealing approach for recycling CO₂ and mitigating its release into the atmosphere.

DME represents a clean fuel distinguished by its hydrogen-rich composition and minimal CO₂ emissions, rendering it highly suitable for clean energy applications. Notably, DME's liquid state at standard ambient temperature facilitates ease of handling. The amalgamation of DME with liquefied petroleum gas (LPG) results in the production of a clean and economically viable fuel applicable to power generation, diesel engines, and fuel cells. The potential advent of DME presents an innovative energy paradigm capable of effectively addressing exhaust gas challenges by markedly reducing both particulate matter and nitrogen oxides (NOX) emissions. DME can be generated through the hydrogenation of CO₂ or CO via two distinct pathways. The initial pathway, structured in two stages, involves the synthesis of methanol in the first stage from CO₂ and H₂, facilitated by a methanol synthesis catalyst as described by Equations 1 and 2. This process necessitates elevated pressure and operates within a specific temperature range of 200-300 °C [3, 4].

Methanol synthesis reactions:



Then, produced methanol is dehydrated to DME on a methanol dehydration catalyst in the second stage according to Equation 3

Methanol dehydration reaction:



In the alternative one-stage route, CO₂ or CO undergoes conversion into dimethyl ether (DME) utilizing a bifunctional catalyst consisting of two components: one for methanol synthesis and another for methanol dehydration. This single-stage process offers enhanced economic viability as the production of DME is not constrained by the thermodynamic limitations of the reactions. Numerous Cu-based catalysts, including CuO-ZnO, CuO-TiO₂-ZrO₂, CuO-ZnO-CrO₃, CuO-ZnO-Al₂O₃, among others, have been evaluated as synthesis catalysts for DME [5] with alumina or HZSM-5 zeolite being the preferred choices for the dehydration component. ZnO is recognized for its role in the CO₂ adsorption step, whereas copper species are acknowledged as the active sites that facilitate the reaction [6, 7]. Consequently, it is crucial to prevent the aggregation of copper sites and maintain the catalyst structure to enhance catalyst activity, elevated dimethyl ether (DME) selectivity, and minimize the formation of undesired by-products. The efficacy of DME production is believed to hinge not only on the metal-oxide phase features of the catalyst, which are responsible for CO₂ activation/hydrogenation, but also on the specific properties of zeolites that influence the activity and stability of hybridized bifunctional catalysts [8]. Through a comprehensive review of existing literature and a comparative assessment of diverse elements and materials, an optimal catalyst combination was identified to achieve elevated CO₂ conversion to DME. The proposed catalyst entails a bimetallic composition of CuZn supported on a high-surface carrier, γ-Al₂O₃. For the methanol dehydration component of the bimetallic synthesis catalyst, HZSM-5 zeolite was selected. This selection was made considering the economic perspective, as Cu and Zn exhibit cost-effectiveness, abundance, and high selectivity toward methanol.

2. MATERIALS AND METHOD

2.1 CATALYST SYNTHESIS

(i) CuZnAl

The catalyst denoted as CZA, consisting of 60 wt% CuO, 30 wt% ZnO, and 10 wt% Al₂O₃, was synthesized using the solution combustion method, as illustrated in Figure 1 and detailed in existing literature. The synthesis process involved dissolving precise weights of (Cu(NO₃)₂·6H₂O, 99.95%), (Zn(NO₃)₂·6H₂O, 99%), Al(NO₃)₃·9H₂O, 99.95%), and glycine (99.5%) in a ratio of 1.3 (Glycine/Nitrates) in 100 ml of deionized water within a 250 ml beaker. Subsequently, the mixture was subjected to heating on a hot plate with stirring until a soft gel formed, leading to a self-ignition reaction. The resulting post-combustion powder underwent calcination at 400°C in air at a rate of 1 degree Celsius per minute for a duration of 2 hours.

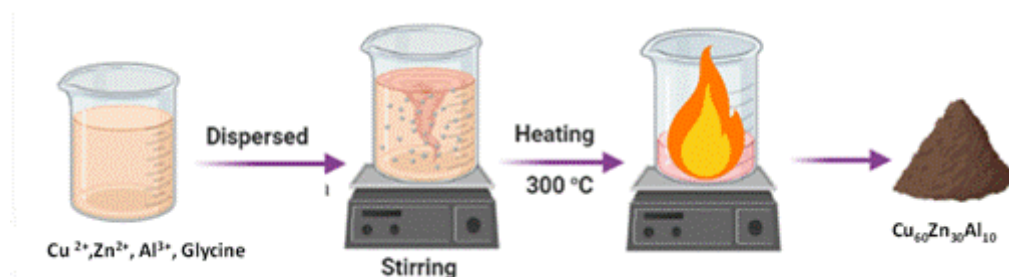


Figure 1. Synthesis procedure of the CZA catalysts.

(ii) Parent Zeolite:

Initially, the precursor ZSM-5 zeolites in NH₄⁺ form were procured from Zeolyst company and designa

ted as follows: (Z1: CBV 2314, Si/Al = 23), (Z2: CBV 3024E, Si/Al = 30), and (Z3: CBV 5524G, Si/Al = 50). To transition them to the acid form (H-ZSM-5), all NH_4^+ forms underwent activation in a muffle furnace at 550 °C, 2dpm, for 2 hours, and were subsequently identified as the parent H-ZSM-5.

(iii) Traditional alkaline treatment (TT)

Based on existing literature, a total of 1.5 grams of the parent HZSM-5 zeolite was introduced into a preheated 80 ml solution containing 0.2 molar sodium hydroxide (NaOH) at a temperature of 65 °C. The mixture was stirred for a 60 minutes. Following this, the zeolite suspension was rapidly cooled by immersion in an ice bath to arrest the desilication process. The resultant suspension underwent multiple washes with deionized water until reaching a neutral pH level (pH 7). The zeolite was subsequently isolated through filtration and then subjected to drying in an oven at 120 °C overnight.

To reactivate the zeolites, a calcination process ensued, subjecting them to a temperature of 550 °C with a heating rate of 2 degrees per minute for 2 h. The resulting zeolite samples were labelled as Z1-TT, Z2-TT, and Z3-TT.

RESULTS AND DISCUSSION

2.2 Catalytic performance

The assessment of CO_2 catalytic hydrogenation performance was conducted in a high-pressure laboratory-scale test unit (PID, Micrometrics) as described in Figure 2. For the experimental trials, 0.5 grams of each zeolite were sealed in the middle of the reactor tube, further 0.5g of CZA, first pelletized and sieved to a size between 100-150 μm , was placed in the upper layer. The catalyst underwent activation by reduction for three hours at 350°C with pure hydrogen. Subsequently, the temperature was lowered to 250°C, and a mixture of hydrogen, carbon dioxide, and nitrogen (in proportions of 67.5%, 22.5%, and 10%) was introduced into the reactor at a flow rate of 30 mL/h, resulting in a Gas Hourly Space Velocity (GHSV) of 3600 h^{-1} .

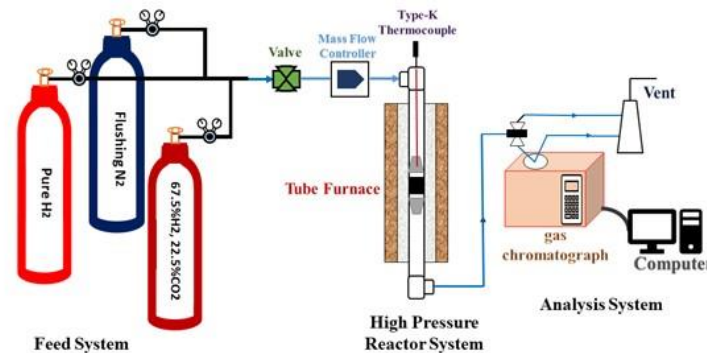


Figure 2. Schematic diagram of the experimental set-up

The conversion of CO_2 through hydrogenation over the prepared catalysts was determined using Equation 6:

$$\text{CO}_2 \text{ conversion (\%)} = \left[\frac{f_{\text{CO}_2(\text{in})} - f_{\text{CO}_2(\text{out})}}{f_{\text{CO}_2(\text{in})}} \right] \times 100 \quad (6)$$

Here, f represents the gas flow rate. The product selectivity, including methanol, CO, and CH_4 , was computed using Equations 7 to 9, respectively:

$$\text{CH}_3\text{OH}_{\text{selectivity}} (\%) = \left[\frac{n_{\text{CH}_3\text{OH}}}{n_{\text{Total product}}} \right] \times 100 \quad (7)$$

$$\text{CO}_{\text{selectivity}} (\%) = \left[\frac{n_{\text{CO}}}{n_{\text{Total product}}} \right] \times 100 \quad (8)$$

$$\text{CH}_4_{\text{selectivity}} (\%) = \left[\frac{n_{\text{CH}_4}}{n_{\text{Total product}}} \right] \times 100 \quad (9)$$

2.3 Result and discussion

2.3.1 Material and characterization

2.4 Physicochemical properties

2.4.1.1 XRD analysis

The X-ray diffraction (XRD) patterns depicting the fresh, reduced, and spent CZA (Copper-Zinc-Aluminum) catalyst are presented in Figure 3. Examination of the XRD data for the fresh catalyst reveals the presence of a CuO phase, as evidenced by diffraction peaks at 2θ angles of 35.2° and 38.5° . Conversely, weak intensity reflections associated with the ZnO phase are observed at 2θ angles of 31.8° and 36.2° [9]. Moreover, faint-intensity Al_2O_3 reflections at 2θ values of 37.6° , 39.5° , 45.8° , and 66.8° [10] become evident in the reduced catalysts. Distinct peaks at 43.4° and 50.3° in the reduced catalyst's XRD pattern are associated with (111) of metallic copper [11].

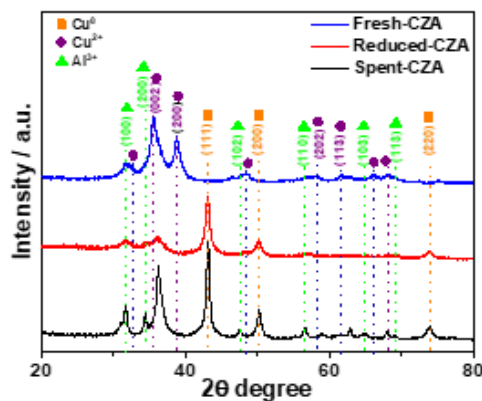


Figure 3. XRD patterns of synthesized catalyst

2.4.1.2 Scanning electron microscope analysis (SEM)

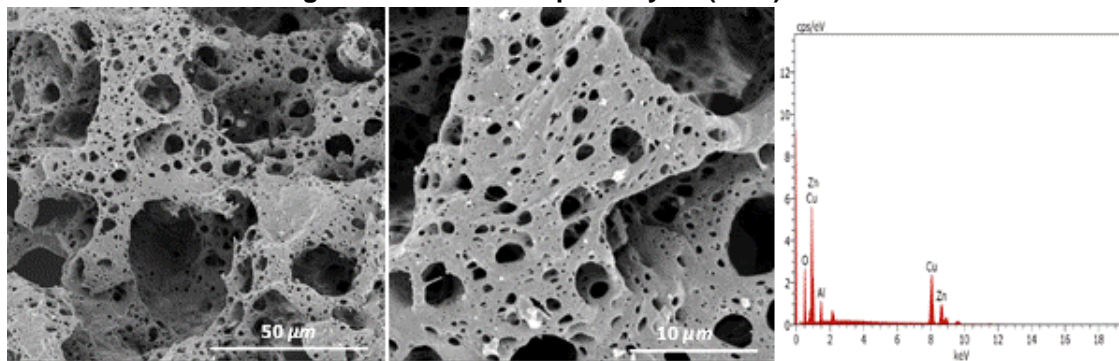


Figure 4. SEM images of synthesized Cu/Zn/Alumina catalyst

The morphology of the CZA catalyst is illustrated in Figure 4, revealing a low-density, spongy-like structure characterized by a notable porous architecture with abundant voids. This structural feature is attributed to the rapid release of gases during the combustion process. Additionally, SEM analysis displayed the morphology of the pristine commercial zeolites and the post-treated zeolite as in (Figure 5).

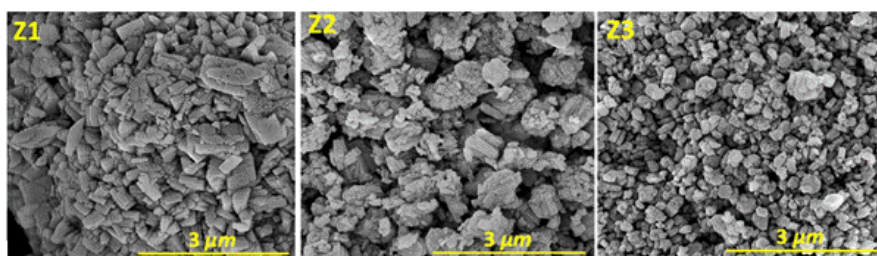


Figure 5. SEM images of zeolites

TEM images in Figure 6 depict the morphology of the three parent zeolites (Z1, Z2, and Z3). All of the samples exhibit a hockey puck-shaped morphology with particle sizes ranging from 300 to 500 nm. Moreover, as illustrated in Figure 7, Z2 and Z3 exhibit a stacked fibrous structure after alkaline treatment, resulting from the removal of Si atoms by NaOH.

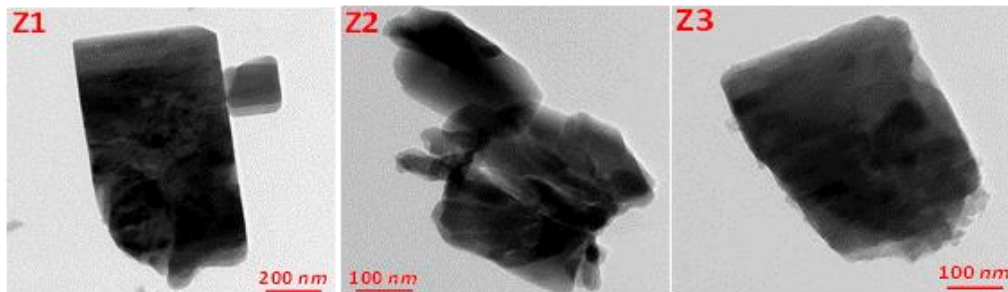


Figure 6. TEM images of zeolite

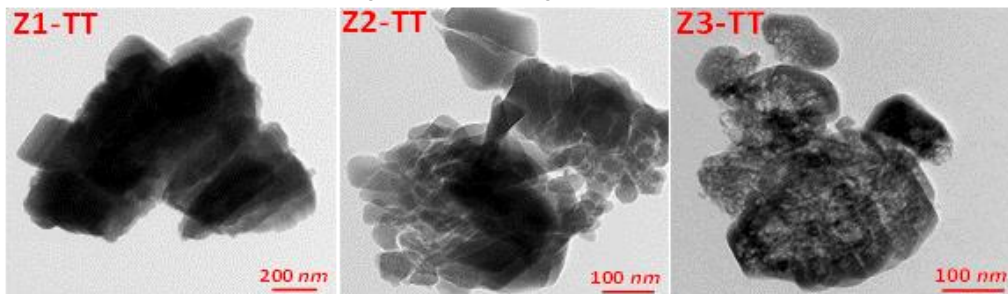


Figure 7. TEM images of treated zeolites

2.4.2 Catalytic performance

Figure 8 illustrates the catalytic performances and product selectivity of the Cu/Zn/Alumina catalyst over alkali-treated commercial zeolites (Z1-TT, Z2-TT, and Z3-TT). In Figure 8a, 8b, and 8c, the selectivity of methanol and DME for the different zeolites were presented. Specifically, in Figure 8a, it was observed that Z1-TT exhibits lower DME selectivity compared to Z2-TT and Z3-TT, with Z3-TT demonstrating the highest selectivity. Notably, Z1-TT experiences a significant decrease in DME selectivity from 34% to 26% as the reaction pressure increases from 40 to 60 bar at a constant temperature of 250°C. This decline was attributed to the lower acidity of Z1-TT. Conversely, methanol selectivity for Z1-TT, Z2-TT and Z3-TT increases from 15.7% to 32%, 17% to 29% and 22.7% to 27.7% respectively. Furthermore, the DME selectivity for Z2-TT and Z3-TT increases from 19.8% to 29.3% and 29.2% to 39.5% this enhancement due to the high acidity of Z3-TT[12].

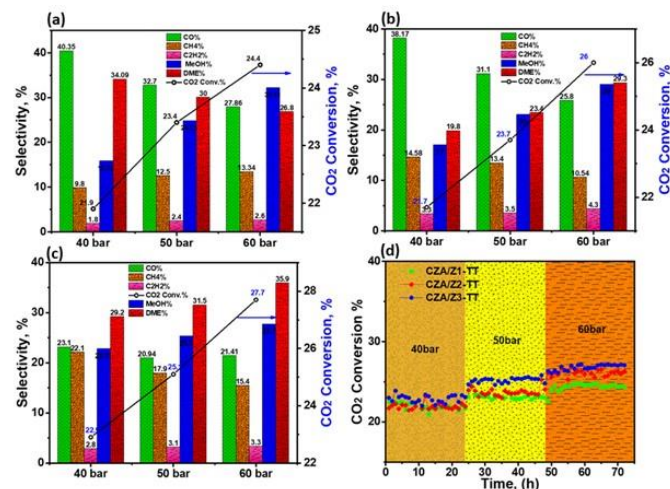


Figure 8. CO₂ conversion and production selectivity for CZA/ treated zeolites.



CONCLUSIONS

The catalytic performance of direct CO₂ conversion to DME was carried out over CZA firstly to get methanol as a product, followed by methanol dehydration over three treated commercial zeolite with different Si/Al ratio. The alkaline treated Z3-TT exhibited the highest induced porosity in terms of material texture, further its showed the best in DME selectivity 39.5%.

ACKNOWLEDGEMENT

This work possible through Qatar University internal grant # IRCC 2023-203. Special thanks go to the CLU staff for their help in providing timely sample analysis.

REFERENCES

- [1] Li Q, Chen Z, Zhang J-T, Liu L-C, Li X, Jia L. Positioning and revision of CCUS technology development in China. *International Journal of Greenhouse Gas Control*. 2016;46:282-93.
- [2] Bachu S. Identification of oil reservoirs suitable for CO₂-EOR and CO₂ storage (CCUS) using reserves databases, with application to Alberta, Canada. *International Journal of Greenhouse Gas Control*. 2016;44:152-65.
- [3] Atsonios K, Panopoulos KD, Kakaras E. Investigation of technical and economic aspects for methanol production through CO₂ hydrogenation. *International Journal of hydrogen energy*. 2016;41:2202-14.
- [4] Kattel S, Ramirez PJ, Chen JG, Rodriguez JA, Liu P. Active sites for CO₂ hydrogenation to methanol on Cu/ZnO catalysts. *Science*. 2017;355:1296-9.
- [5] Wang S, Mao D, Guo X, Wu G, Lu G. Dimethyl ether synthesis via CO₂ hydrogenation over CuO–TiO₂–ZrO₂/HZSM-5 bifunctional catalysts. *Catalysis Communications*. 2009;10:1367-70.
- [6] Sharma P, Sebastian J, Ghosh S, Creaser D, Olsson L. Recent advances in hydrogenation of CO₂ into hydrocarbons via methanol intermediate over heterogeneous catalysts. *Catalysis Science & Technology*. 2021;11:1665-97.
- [7] He Z, Cui M, Qian Q, Zhang J, Liu H, Han B. Synthesis of liquid fuel via direct hydrogenation of CO₂. *Proceedings of the National Academy of Sciences*. 2019;116:12654-9.
- [8] Catizzzone E, Bonura G, Migliori M, Frusteri F, Giordano G. CO₂ recycling to dimethyl ether: State-of-the-art and perspectives. *Molecules*. 2017;23:31.
- [9] Venugopal A, Palgunadi J, Deog JK, Joo O-S, Shin C-H. Dimethyl ether synthesis on the admixed catalysts of Cu-Zn-Al-M (M= Ga, La, Y, Zr) and γ -Al₂O₃: the role of modifier. *Journal of Molecular Catalysis A: Chemical*. 2009;302:20-7.
- [10] Mehmet Tasdemir H, Yagizatlı Y, Yasyerli S, Yasyerli N. The catalytic performance of sol-gel alumina supported Ti-Ce catalysts for H₂S selective oxidation to elemental sulfur. *International Journal of Chemical Reactor Engineering*. 2018;17:20180157.
- [11] Shen W-J, Ichihashi Y, Matsumura Y. A comparative study of palladium and copper catalysts in methanol synthesis. *Catalysis letters*. 2002;79:125-7.
- [12] Rutkowska M, Macina D, Mirocha-Kubień N, Piwowarska Z, Chmielarz L. Hierarchically structured ZSM-5 obtained by desilication as new catalyst for DME synthesis from methanol. *Applied Catalysis B: Environmental*. 2015;174:336-43.

ICH2P14-PP154

FACILITATING PRODUCTION OF ACETATE AND HYDROGEN THROUGH ENHANCED ELECTRON TRANSFER AND SUBSTRATE MASS TRANSFER USING A MULTIFUNCTIONAL PHOTOCATHODE WITH NiO/G-C₃N₄/POLYTHIOPHENE

¹Abdul Hakeem Anwer, ¹Assem Mohamed, ³Nafees Ahmed, ^{1,2*}Abdelbaki Benamor

¹Gas Processing Center, College of Engineering, Qatar University, P.O. Box 2713 Doha, Qatar

²Department of Chemical Engineering, College of Engineering, Qatar University, P.O.Box 2713, Doha, Qatar

³Department of Chemistry, Integral University, Lucknow, 226026, Uttar Pradesh, India

*Corresponding author e-mail: benamor.abdelbaki@qu.edu.qa

ABSTRACT

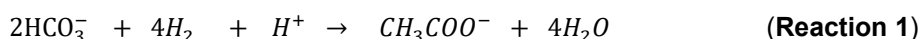
The process of microbial electrosynthesis (MES) represents a promising method for carbon dioxide (CO₂) fixation, wherein biocatalysts derive electrons from electrodes, serving as a driving force for the reduction of CO₂ into more valuable multicarbon products. In this investigation, we designed a novel multifunctional photocatalyst incorporating NiO/g-C₃N₄/Polythiophene, and subsequently established an MES system utilizing a mixed culture as the biocatalyst. Comparative analysis with NiO/g-C₃N₄ revealed that the integration of Polythiophene (PTh) into NiO/g-C₃N₄ not only amplifies the light absorption capacity but also enhances the efficiency of photogenerated electron-hole separation and migration. With an escalating reducing power influence, NiO/g-C₃N₄/PTh manifests the capacity to expedite the electron transport rate to microbes through three distinct pathways: indirect conduits via formate, indirect routes via hydrogen, and direct electron transfer. Moreover, the presence of NiO/g-C₃N₄/PTh proves advantageous in fostering the enrichment of electroautotrophic microorganisms, leading to an augmented abundance of *Acetobacterium* and *Arcobacter*. Additionally, the photocatalyst demonstrates an enhanced CO₂ adsorption capability. Operating at a potential of -0.9 V (versus Ag/AgCl), the MES employing the NiO/g-C₃N₄/PTh photocathode achieves an acetate production rate of 4.12 mM/d, showcasing a remarkable 4.2-fold increase compared to the control. In a controlled environment, the MES system yielded less hydrogen production (0.00905 m³/m³/d) than when utilizing the NiO/g-C₃N₄/PTh combination (0.02105 m³/m³/d). This study presents an innovative approach for semiconductor photocathodes to improve MES performance within mixed cultures.

Keywords: Carbon dioxide sequestration, Bio-photocatalysis, acetate.

1. INTRODUCTION

Fossil fuels, crucial for fulfilling worldwide energy requirements, are gradually diminishing, and their widespread deployment in modern society has substantially augmented the incidence of global warming through the release of carbon dioxide (CO₂) into the atmosphere [1, 2]. In recent times, the decreasing accessibility of fossil fuels has spurred an increasing demand for alternative energy sources. Furthermore, the imperative for reliable alternatives has been intensified by the burgeoning market for portable electronic devices [3]. Addressing these environmental and energy challenges has prompted a heightened awareness and concentration on the investigation of renewable and clean energy sources. Among the auspicious alternatives, bio-photocatalytic CO₂ reduction has surfaced as a feasible and sustainable resolution. This method presents various benefits, encompassing economical, clean energy production, and environmentally favorable attributes. Via the bio-photocatalytic reduction of CO₂, it is possible to convert both carbon dioxide (CO₂) and inorganic carbon (HCO₃⁻) into valuable biofuels, including acetic acid, ethyl alcohol, butyrate, and CH₄, utilizing sustainable radiation. This innovative approach provides a promising pathway for addressing contemporary global environmental and energy challenges, simultaneously presenting a sustainable repository of biofuels with versatile applications. Within the domain of sustainable and advanced methodologies, Microbial Electrosynthesis (MES) has arisen as a propitious and novel technique for transforming inorganic carbon sources, such as bicarbonate (HCO₃⁻) or CO₂, into valuable precursor chemicals. MES systems utilize electro-trophs as biological catalysts, representing a potentially efficient approach for sustainable energy generation and carbon emissions reduction. Electro-trophs are integral to the reduction of CO₂ or bicarbonate (HCO₃⁻) into valuable precursor chemicals within MES systems. These processes entail the employment of electro-trophs as electron acceptors, obtaining electrons either indirectly through the assimilation of soluble electron carriers like H₂ or directly through cathodic electron transfer in MES. Electro-trophs harness electrons in the conversion of CO₂ into reactive acetyl-CoA, a process followed by the oxidation of acetyl-CoA to acetate through ATP phosphorylation utilizing the Wood-Ljungdahl pathway (WLP), elucidated by Ragsdale and Pierce in 2008 [4]. Nonetheless, the interaction between electro-trophs and unmodified electrodes poses a constraint in this procedure, resulting in a reduction in the current density of CO₂ reduction. This limitation stems from the ineffective electron transfer between electro-trophs and unmodified electrodes, constituting a pivotal bottleneck in the overall process. For instance, to enhance the production of chemical compounds like

acetate, it may be advantageous to augment the circuital current or current density of the Microbial Electrosynthesis (MES) cell, leading to a higher abundance of cathodic electrons. An illustration of this concept is evident in the electrochemical reduction of inorganic carbon (IC) to acetate (Reaction 1), a phenomenon demonstrated with varying degrees of success in MES systems employing both monocultures and multispecies inoculations (mixed cultures). MES exhibits potential as a sustainable and pioneering methodology for the generation of valuable chemicals, employing electrotrophs as electron acceptors in the microbial conversion of carbon compound [5, 6]. Usually, cultures are immobilized on various cathodic electrode materials (as delineated in Table S1), including carbon-based metals (Cu, Ni, Au, Fe) and reduced graphene oxides [7]. The fundamental function of these materials is to diminish the resistance to electron transfer between the cathodic electrode and the immobilized electrotrophs. Consequently, there is an elevation in circuital current, facilitating the electrotrophic conversion of inorganic carbon (IC) to acetate, as succinctly outlined in Table S1 [8-10]. An alternative approach to augment the circuital current (current density) essential for the electrotrophic reduction of inorganic carbon (IC) in Microbial Electrosynthesis (MES) biocathodes involves employing photocatalytic semiconductor materials responsive to solar radiation [11-14]. Under favorable conditions, bacteria can obtain supplementary electrons and hydrogen from a stimulated semiconductor, thereby enhancing the electrotrophic process through either indirect means (utilizing H₂ or mediators) or direct reduction of carbon (HCO₃⁻ or CO₂). The integration of artificial and natural platforms offers the potential to create innovative catalytic systems with enhanced functionality compared to the individual catalytic functions in isolation [12]. This methodology utilizes solar radiation to directly activate semiconducting materials, concurrently purging aqueous contaminants from the anodic chambers. Consequently, the approach proves to be an efficient and environmentally sustainable technique for both environmental remediation and renewable energy production. The direct harnessing of solar light as the energy source for stimulating semiconductors, along with the simultaneous removal of aqueous pollutants in the anodic chambers, presents a promising and sustainable strategy with potential applications in mitigating environmental pollution and generating renewable energy [14].



The selection of suitable photocatalytic materials with semiconducting attributes for this application necessitates exemplary biocompatibility with electrotrophs, optimal band gaps, and other favorable characteristics, including low overpotentials, non-toxicity, and long-term stability concerning the electrotrophs. The chosen materials should establish compatibility with the electrotrophs at a biological level and possess advantageous electronic band gaps to facilitate efficient electron transfer processes. Moreover, these materials should demonstrate minimal overpotentials, representing the additional energy requirements for electrochemical reactions to transpire, thereby enhancing the energy efficiency of the system. Factors such as durability over extended durations and non-detrimental effects on electrotrophic microorganisms are also crucial to ensure the sustained efficacy and feasibility of the photocatalytic substances within the system [14, 15].

The groundbreaking study by Liu et al. in 2015 introduced the notion of employing a photoelectrode to assist Microbial Electrosynthesis (MES) in the reduction of carbon dioxide (CO₂) [16]. This inventive method employed a silicon nanowire photocathode and a titanium dioxide (TiO₂) photoanode within a solar-assisted Microbial Electrosynthesis (MES) system. The photoelectrode efficiently captured solar energy and conveyed reducing equivalents to *Sporomusa ovata*, a microorganism recognized for its proficiency in acetate production. Additionally, acetate generated was utilized as a precursor for synthesizing longer carbon chains through recombinant *Escherichia coli* in this strategy [2, 17]. In subsequent investigations, photo-assisted biocathodes, incorporating Z-scheme heterojunctions such as WO₃/MoO₃/g-C₃N₄ [18] and Ag₃PO₄/g-C₃N₄ [19], have been synthesized utilizing *Serratia marcescens* Q1 as the biocatalyst. In this methodology, photo-generated electrons augmented hydrogen production, subsequently facilitating the biocatalyst's carbon dioxide (CO₂) fixation for acetate synthesis. Unlike conventional Microbial Electrosynthesis (MES) systems employing pure bacterial strains as biocatalysts, mixed cultures exhibited heightened acetate production and greater resilience to environmental fluctuations, possibly attributable to synergistic effect [20, 21]. Nevertheless, the comprehension of MES efficiency employing mixed cultures as biocatalysts, in conjunction with photoassisted cathodes, remains limited and necessitates further investigation. Therefore, it is crucial to advance superior and more efficient photocatalysts to optimize CO₂ conversion and enhance yield rates with improved selectivity.

Among numerous photocatalysts, graphitic carbon nitride (g-C₃N₄) stands out as a representative polymer semiconductor extensively employed in the photocatalytic domain due to its notable attributes, including excellent chemical stability, cost-effectiveness, consistent visible light responsiveness, and stable catalytic performance under visible light conditions [22, 23]. Nevertheless, the facile recombination of photogenerated electrons and holes on g-C₃N₄ hampers its overall photocatalytic efficacy. To address this limitation, the coupling of g-C₃N₄ with a narrow-band gap semiconductor represents a viable strategy to enhance the separation of photogenerated electron-hole pairs. Copper oxide, with its narrow band gap and heightened visible light absorption capabilities,

can be integrated with g-C₃N₄ to form heterojunction structures [24]. The combination of metal oxide/g-C₃N₄ exhibits significant potential as a photocatalyst in Microbial Electrosynthesis (MES) by facilitating the separation of photo-induced charge carriers and thereby enhancing photocatalytic efficiency [25].

In this investigation, we propose the utilization of a NiO/g-C₃N₄-modified graphite felt (GF) doped with Polythiophene (PTh) to fabricate a photocathode for chemical (primarily acetate) production from CO₂ in the Microbial Electrosynthesis (MES) system. The incorporation of photocatalysis and electrocatalysis through the NiO/g-C₃N₄/PTh photocathode facilitates the separation of electron-hole pairs, thereby supplying additional reducing power for the conversion of carbon dioxide. Additionally, the photoelectron-generating activity on the NiO/g-C₃N₄/PTh photocathode, capable of modulating the diversity of cathodic microbes, proves advantageous for chemical production. In summary, the incorporation of the NiO/g-C₃N₄/PTh photocathode significantly enhances the performance of MES.

2. MATERIALS AND METHOD

The preparation of NiO/g-C₃N₄/PTh nanocomposites involved the utilization of nickel nanoparticles obtained through a previously reported precipitation method [26]. An electrochemical method was employed for the synthesis of conducting polymer nanocomposites using a potentiostat-galvanostat Autolab system (Autolab 204, Netherland). A standard three-electrode one-compartment cell configuration was adopted for all experiments, with a platinum counter electrode, Ag/AgCl reference electrode, and graphite felt substrates serving as the working electrode. The experiments were conducted at room temperature under an argon atmosphere, and the Ar flow was initiated 15 minutes before each experiment to eliminate dissolved air from the solutions.

The electrochemical polymerization of thiophene and the deposition of PTh/nickel nanocomposites on the graphite electrodes were performed potentiostatically by applying a constant potential of 2.5 V for 120 s. This process took place in an acetonitrile solution (7 ml) containing 1.9 mM thiophene, along with Ni nanoparticles, g-C₃N₄, and tetrabutylammonium tetrafluoroborate (Bu₄NBF₄) as the supporting electrolyte (0.05 g). Following polymerization, the polymer composites coated on the graphite felt substrate underwent rinsing with acetonitrile to eliminate any residue and were subsequently dried in ambient air.

3. Result and Discussion

3.1. Optimizing the Electrode and MES Process Conditions for Acetate Synthesis

3.1.1. MES Operational Parameter Adjustment for Acetate Synthesis

The modified electrode incorporating NiO/g-C₃N₄/PTh demonstrated consistent and reversible photocurrent responses that were 3.19 times greater than those observed with Ni oxide electrodes. This observation implies the existence of varying degrees of electronic interaction between Ni oxide species and g-C₃N₄, particularly when exposed to visible light irradiation. The discernible influence of PTh on enhancing the photocurrent response of the electrode underscores its pivotal role and underscores the potential for synergistic effects within the composite system. In comparison to biotic conditions (Figure 1A), the abiotic controls exhibited significantly higher photocurrents (Figure 1B), indicating a tradeoff between scarification, crucial for photon capture, and the presence of electro-trophs on electrode surfaces for the conversion of inorganic carbon (IC) to acetate. Analogous approaches for methane production involve the use of indium phosphide photocathodes and Methanosarcina barkeri electro-trophs [12].

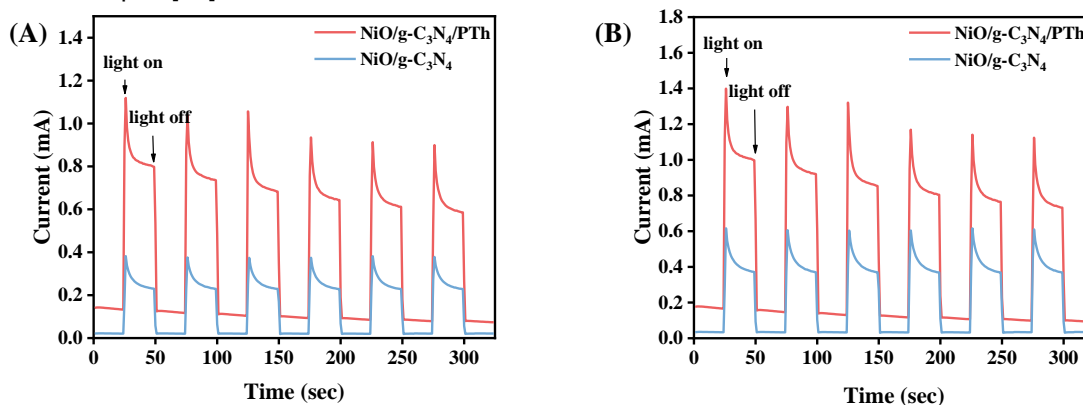


Figure 1. Photocurrent measurements for NiO/g-C₃N₄/PTh graphite felt, NiO/g-C₃N₄ graphite felt setup in 1.0 M Na₂SO₄ solution (A) biotic and (B) abiotic.

The evaluation of NiO/g-C₃N₄/PTh photo-bioelectrochemical systems' performance is fundamentally governed by the intricate balance between light absorption and biocatalysis occurring on the semiconductor-coated electrode surface. Optimal bioelectrocatalytic stability and activity are ensured with a thicker layer of electrotrophs, whereas a thinner layer facilitates superior photon capture and transfer [12]. In subsequent experiments, manipulating the concentration of cultivated mixed microbes within the range of 0.2 to 0.8 of OD₆₀₀ yielded the maximum acetate synthesis (Figure S1A), the highest residual hydrogen (Figure S1B), and the highest photogenerated current (Figure S1C). For the manipulation of the electrode composition and the loading of the composite, the NiO/g-C₃N₄/PTh loadings were incrementally elevated from 0.7 to 1.40 mg/cm², leading to an augmented production of acetate (Figure S3A), accompanied by a concurrent reduction in residual hydrogen levels (Figure S3B). This outcome can be attributed to the enhancement in photo-generated current (Figure S3C). However, an excessive loading of 2.40 mg/cm² resulted in a decline in photo-generated current (Figure S3C), subsequently leading to diminished acetate production and elevated residual hydrogen values (Figure S3A and B).

An optimal ratio of NiO/g-C₃N₄/PTh at 10% (w/w) was attained for the preferred NiO/g-C₃N₄-PTh loading of 1.60 mg/cm², resulting in the highest acetate production (Figure 2A). This configuration corresponded to the lowest residual hydrogen levels (Figure 2B) and the highest photogenerated current density (Figure 2C). Consequently, the heightened cathodic photogenerated holes exerted an additional force, propelling more electrons to the photocathode [27]. In contrast, the supplementary photoinduced current facilitated the reductive generation of hydrogen, thereby amplifying the overall system performance. For this investigation, a NiO/g-C₃N₄/PTh composite loading of 1.60 mg/cm², with a NiO/g-C₃N₄/PTh to PTh ratio of 10% (w/w), was selected for further analyses. These experimental conditions were meticulously chosen to ensure the desired composition and loading of the composite materials, thereby optimizing subsequent analyses.

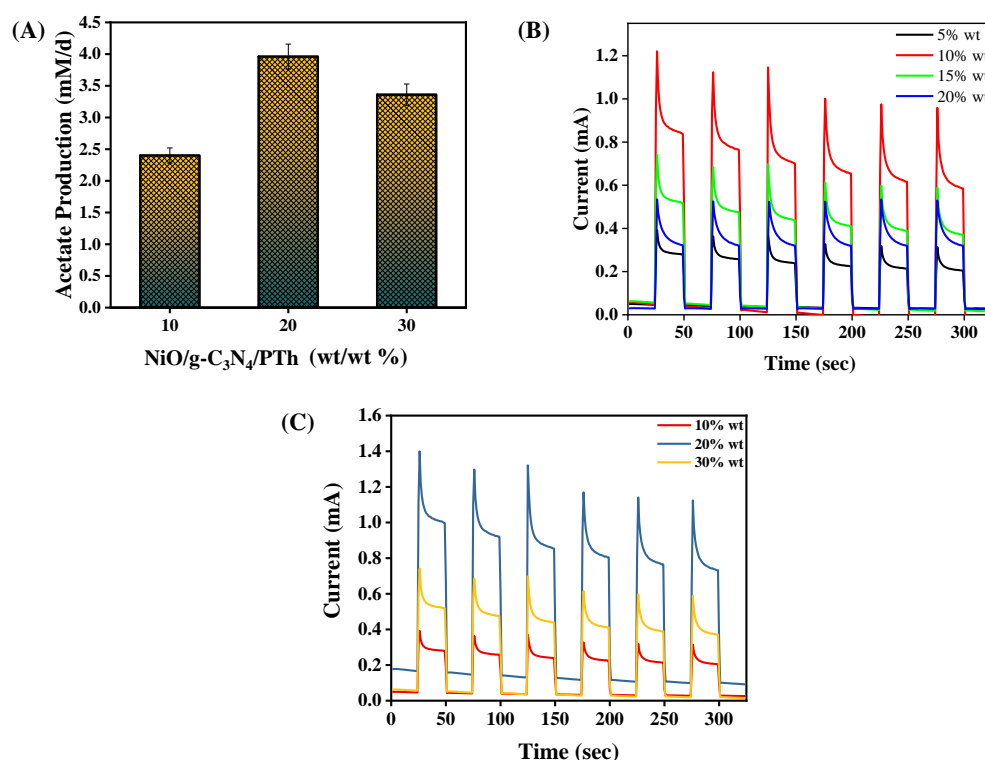


Figure 2 (A) Effect of ratios of NiO/g-C₃N₄/PTh graphite felt on production of Ac (B) Hydrogen of residual (C) photo-response curves.

3.1.2. Long-Term Acetate Formation Kinetics

The Microbial Electrosynthesis (MES) process, extended over 5 days, substantially augmented acetate production to 10.22 ± 0.30 mM, marking a 2.95-fold increase compared to the control using a bare carbon felt electrode as the cathode (Figure 3A). Nevertheless, the rate of acetate synthesis exhibited a gradual decline as the remaining inorganic carbon (IC) in the catholyte was depleted. Furthermore, the acetate production rate of 3.8 mM/d

surpassed that of *Sporomusa ovata* immobilized on surface-modified carbon MES cathodes without light irradiation, achieving a 4.1-fold increase at approximately 2.21 mM/d [8, 9]. Nevertheless, this rate was notably inferior to the reported value of 6.0 mM/d achieved using the same species while incubated in a yeast extracting medium with a continuous CO₂ flow [6]. In line with Reaction 1, the acetate production process in NiO/g-C₃N₄/PTh consumes hydrogen at a heightened rate compared to controls with bare carbon felt cathodes. Consequently, the hydrogen concentration was lower than that in controls with bare carbon felt cathodes, aligning with literature supporting other electrochemical reductions occurring in the absence of light illumination (Figure 3B) [6, 8]. As depicted in Figure 3B, the residual hydrogen exhibited a rapid decline within the initial 1.0 day, aligning with the peak rate of acetate production illustrated in Figure 3A. This suggests that the photocatalytically generated H₂ was effectively utilized through the photoreduction of protons via the heterojunction valence-band electrons. After 5 days of operation, there was a 42 ± 2% current efficiency for acetate production (CE_{acetate}) and a consumption of 95 ± 2% of the supplied HCO₃⁻ (Figure 3C and 3E). These values significantly surpassed the results obtained with controls featuring bare carbon felt cathodes, where the CE_{acetate} was 35 ± 2% and HCO₃⁻ consumption was 85 ± 2%, as depicted in Figure 3D and E. Within a brief operational timeframe, the current efficiency for acetate production (CE_{acetate}) at 0.5 days reached 82 ± 2%, comparable to the performance observed in a hybrid system employing α-NiS photocatalyst and *Methanosarcina barkeri* for methane production with continuous CO₂ supply (74%) [12]. However, the CE_{acetate} declined over time due to an increase in internal resistance, rising from 3.5 Ω (Rs) and 64.17 Ω (Rct) at 0.5 days to 10.4 Ω (Rs) and 54.6 Ω (Rct) at 5 days (Figure 3F). This rise in resistance was attributed to the depletion of the HCO₃⁻ supply after 5 days, aligning with findings in a previously reported hybrid system of *Moorella thermoacetica* and CdS [13]. Nevertheless, a continuous CO₂ sparging approach might provide adequate inorganic carbon (IC) for a high CE_{acetate}, as long as the CO₂ sparging is sustained throughout the entire experiment [6, 8].

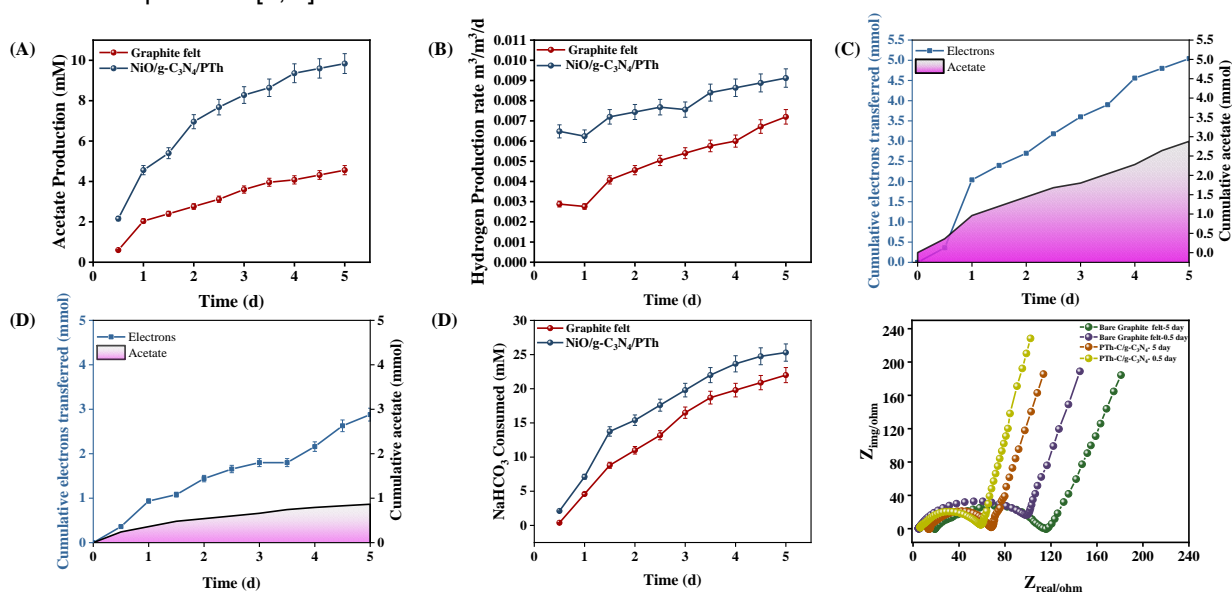


Figure 3. The progress of time (A) acetate synthesis (B) evolution of hydrogen, (C and D) cumulative electrons transferred for PTh/C/g-C₃N₄ and graphite felt respectively (E) IC conversion, (F) Nyquist plots of EIS spectra.

3.1.3. Stability Assessment

Several sequential batch cycles of the MES assembly system were systematically carried out at intervals of 5.0 days, incorporating catholyte refreshment. This rigorous testing regimen was employed to assess the enduring stability of the Ac (acetic acid) production process over an extended timeframe. Throughout 10 operational cycles, each lasting 12 hours over a span of 10 days, the observed Ac production rate ranged from 3.8 to 3.45 mM/d. Notably, this range closely paralleled the residual hydrogen production rate, which fluctuated between 0.0072 and 0.0065 m³/m³/d, as depicted in Figure 9A.

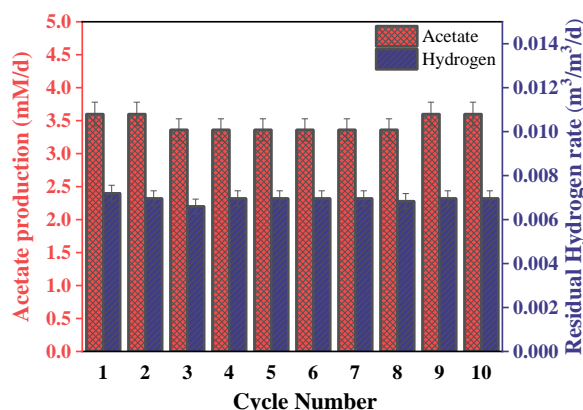


Figure 4. (A) Acetate production and residual hydrogen varies with the number of cycle (each cycle lasts 12 hours).

4. Conclusions

This investigation demonstrates that the NiO/g-C₃N₄/PTh heterojunction-modified cathode profoundly enhances MES performance. Material characterization reveals that the proposed cathode exhibits exceptional visible light absorption and efficient separation of holes and electrons. Photogenerated electrons play a role in promoting biofilm formation and are directly transferred to electroautotrophic microbes, bypassing indirect transfer through hydrogen. Concurrently, photogenerated holes can combine with anodic electrons, providing an additional driving force. Furthermore, the NiO/g-C₃N₄/PTh photocathode enhances biocatalytic activity by increasing the overall amount of biocatalyst and regulating the composition of the cathodic microbial community. The resulting acetate concentration of 5.1 g/L surpasses that of the control group (2 ± 0.1 g/L). Consequently, the NiO/g-C₃N₄/PTh photocathode presents an effective strategy for achieving high acetate accumulation in MES with a mixed culture.

ACKNOWLEDGEMENT

This work possible through Qatar University internal grant # IRCC 2023-203. Special thanks go to the CLU staff for their help in providing timely sample analysis.

REFERENCES

- [1] Peter SC. Reduction of CO₂ to Chemicals and Fuels: A Solution to Global Warming and Energy Crisis. *ACS Energy Letters*. 2018;3:1557-61.
- [2] Shoeb M, Mobin M, Rauf MA, Adnan SM, Ansari MY. Graphene nickelcopper nanocomposite (Gr@NiCu NCs) as a binder free electrode for high energy density supercapacitor and antimicrobial application. *Journal of Materiomics*. 2021;7:815-27.
- [3] Al Shaqsi AZ, Sopian K, Al-Hinai A. Review of energy storage services, applications, limitations, and benefits. *Energy Reports*. 2020;6:288-306.
- [4] Ragsdale SW, Pierce E. Acetogenesis and the Wood–Ljungdahl pathway of CO₂ fixation. *Biochimica et Biophysica Acta (BBA) - Proteins and Proteomics*. 2008;1784:1873-98.
- [5] Rabaey K, Rozendal RA. Microbial electrosynthesis — revisiting the electrical route for microbial production. *Nature Reviews Microbiology*. 2010;8:706-16.
- [6] Blanchet E, Duquenne F, Rafrafi Y, Etcheverry L, Erable B, Bergel A. Importance of the hydrogen route in up-scaling electrosynthesis for microbial CO₂ reduction. *Energy & Environmental Science*. 2015;8:3731-44.
- [7] Anwer AH, Khan N, Khan MD, Shakeel S, Khan MZ. Redox mediators as cathode catalyst to boost the microbial electro-synthesis of biofuel product from carbon dioxide. *Fuel*. 2021;302:121124.
- [8] Zhang T, Nie H, Bain TS, Lu H, Cui M, Snoeyenbos-West OL, et al. Improved cathode materials for microbial electrosynthesis. *Energy & Environmental Science*. 2013;6:217-24.
- [9] Nie H, Zhang T, Cui M, Lu H, Lovley DR, Russell TP. Improved cathode for high efficient microbial-catalyzed reduction in microbial electrosynthesis cells. *Physical Chemistry Chemical Physics*. 2013;15:14290-4.
- [10] Tian S, Wang H, Dong Z, Yang Y, Yuan H, Huang Q, et al. Mo₂C-induced hydrogen production enhances microbial electrosynthesis of acetate from CO₂ reduction. *Biotechnology for Biofuels*. 2019;12:71.



- [11] Anwer AH, Khan MD, Khan N, Nizami AS, Rehan M, Khan MZ. Development of novel MnO₂ coated carbon felt cathode for microbial electroreduction of CO₂ to biofuels. *Journal of Environmental Management*. 2019;249:109376.
- [12] Nichols EM, Gallagher JJ, Liu C, Su Y, Resasco J, Yu Y, et al. Hybrid bioinorganic approach to solar-to-chemical conversion. 2015;112:11461-6.
- [13] Sakimoto KK, Wong AB, Yang P. Self-photosensitization of nonphotosynthetic bacteria for solar-to-chemical production. 2016;351:74-7.
- [14] Fischer F. Photoelectrode, photovoltaic and photosynthetic microbial fuel cells. *Renewable and Sustainable Energy Reviews*. 2018;90:16-27.
- [15] Sasaki K, Sasaki D, Kamiya K, Nakanishi S, Kondo A, Kato S. Electrochemical biotechnologies minimizing the required electrode assemblies. *Current Opinion in Biotechnology*. 2018;50:182-8.
- [16] Liu C, Gallagher JJ, Sakimoto KK, Nichols EM, Chang CJ, Chang MCY, et al. Nanowire–Bacteria Hybrids for Unassisted Solar Carbon Dioxide Fixation to Value-Added Chemicals. *Nano Letters*. 2015;15:3634-9.
- [17] Shoeb M, Mobin M, Adnan SM, Ansari II, Khan MN, Zaidi S, et al. Facile synthesis of a Gr-Ag/PIn nanocomposite as a binder free electrode for high-performance supercapacitor application. *Surfaces and Interfaces*. 2022;28:101650.
- [18] Cai Z, Huang L, Quan X, Zhao Z, Shi Y, Li Puma G. Acetate production from inorganic carbon (HCO₃⁻) in photo-assisted biocathode microbial electrosynthesis systems using WO₃/MoO₃/g-C₃N₄ heterojunctions and *Serratia marcescens* species. *Applied Catalysis B: Environmental*. 2020;267:118611.
- [19] Kong W, Huang L, Quan X, Zhao Z, Li Puma G. Efficient production of acetate from inorganic carbon (HCO₃⁻) in microbial electrosynthesis systems incorporating Ag₃PO₄/g-C₃N₄ anaerobic photo-assisted biocathodes. *Applied Catalysis B: Environmental*. 2021;284:119696.
- [20] Bajracharya S, Srikanth S, Mohanakrishna G, Zacharia R, Strik DP, Pant D. Biotransformation of carbon dioxide in bioelectrochemical systems: State of the art and future prospects. *Journal of Power Sources*. 2017;356:256-73.
- [21] Xiang Y, Liu G, Zhang R, Lu Y, Luo H. High-efficient acetate production from carbon dioxide using a bioanode microbial electrosynthesis system with bipolar membrane. *Bioresource Technology*. 2017;233:227-35.
- [22] Ajiboye TO, Kuvarega AT, Onwudiwe DC. Graphitic carbon nitride-based catalysts and their applications: A review. *Nano-Structures & Nano-Objects*. 2020;24:100577.
- [23] Wang X, Blechert S, Antonietti M. Polymeric Graphitic Carbon Nitride for Heterogeneous Photocatalysis. *ACS Catalysis*. 2012;2:1596-606.
- [24] Mahmood A, Tezcan F, Kardaş G. Photoelectrochemical characteristics of CuO films with different electrodeposition time. *International Journal of Hydrogen Energy*. 2017;42:23268-75.
- [25] Li B, Wang Y, Zeng Y, Wang R. Synthesis of CuO micro-sphere combined with g-C₃N₄ using Cu₂O as precursor for enhanced photocatalytic hydrogen evolution. *Materials Letters*. 2016;178:308-11.
- [26] Pascariu P, Airinei A, Grigoras M, Vacareanu L, Iacomi F. Metal–polymer nanocomposites based on Ni nanoparticles and polythiophene obtained by electrochemical method. *Applied Surface Science*. 2015;352:95-102.
- [27] Hou Y, Gan Y, Yu Z, Chen X, Qian L, Zhang B, et al. Solar promoted azo dye degradation and energy production in the bio-photoelectrochemical system with a g-C₃N₄/BiOBr heterojunction photocathode. *Journal of Power Sources*. 2017;371:26-34.

ICH2P14-PP166

EVALUATION OF HYDROGEN PRODUCTION FROM AMMONIA REFORMING ON Ni/ZnO NANOWIRE CATALYSTS

^{1*}Hiroya Tamai, ^{1,2*}Hironori Nakajima

¹Kyushu University, Graduate School of Engineering, Department of Hydrogen Energy Systems,
744 Motooka, Nishi-ku, Fukuoka 819-0395, Japan

²Kyushu University, Faculty of Engineering, Department of Mechanical Engineering,
744 Motooka, Nishi-ku, Fukuoka 819-0395, Japan

*Corresponding author e-mail: tamai.hiroya.fcsl@gmail.com, nakajima@mech.kyushu-u.ac.jp

ABSTRACT

Ammonia has attracted attention as a hydrogen storage medium for applications such as fuel cells. However, ammonia reforming catalysts suffer from decreased activity due to heating and agglomeration. To suppress agglomeration, we have applied a nanowire structure to improve the durability and efficiency of reforming catalysts. Nickel is supported on two types of ZnO nanowires (rod-like and tree-like) prepared by hydrothermal synthesis. Reforming tests are conducted using these catalysts under different ammonia flow rates to compare the conversions.

Keywords: Ammonia decomposition, Hydrogen storage, Hydrogen carrier, Nanowire, Catalyst.

INTRODUCTION

Ammonia can be easily liquefied by pressurization and cooling. Thus, it has recently attracted attention as a hydrogen storage and transport medium [1]. However, the highly efficient decomposition of ammonia requires high temperatures, and there is concern that conventional particulate catalysts for ammonia reforming (cracking, decomposing) may lose their catalytic activity due to aggregation [2]. In contrast, nanowire (NW) catalysts are expected to suppress the aggregation [3]. Ni/ZnO NW catalysts are prepared by coating Ni on ZnO NWs, and there are two growth modes of ZnO NWs: length growth (LG) and branch growth (BG) [4]. The active surface area of the Ni/ZnO NWs can be increased by introducing the BG mode and highly branching ZnO NWs. In this study, an NW structure is applied to improve the durability and efficiency of the ammonia reforming catalysts and evaluated for hydrogen production for both LG and BG modes.

EXPERIMENTAL

NW Catalysts Preparation [3]

A zinc oxide fine powder (0.05 g)/methanol (10 ml) dispersion was dropped onto a glass plate to fix the zinc oxide particles (particle diameter < 100 nm) as a starting point for nanowire growth. The glass plate was immersed in a zinc nitrate hexahydrate solution (7.437 g/L) and a hexamethylenetetramine solution (3.5 g/L) for hydrothermal synthesis of ZnO nanowires at 90°C. This series of operations was repeated three times to synthesize branched ZnO nanowires. Next, a mixture of nickel nitrate hexahydrate and ethanol was dropped onto the ZnO nanowires, which were then pyrolyzed at 350°C to coat them with a NiO layer on the ZnO nanowires. The concentration of the mixture was 0.3 M. The prepared nanowire catalysts were collected and fixed with quartz wool in a quartz tube (inner diameter of 4 mm) to prepare the catalyst layers (33, 49, 69, 114, and 343 mg).

Ammonia Reforming

Ammonia water (22 mol%) was bubbled with nitrogen gas, and their mixture was fed to the catalyst bed. Flow rates of fed mixture gas of ammonia and nitrogen were controlled with WHSVs of 6000, 18000, 30000, 42000, and 62000 L h⁻¹ kg⁻¹. WHSV is defined by the following equation.

$$WHSV \left[\frac{L}{kg \cdot h} \right] = \frac{\text{Gas flow rate} \left[\frac{L}{h} \right]}{\text{Catalysts mass} [kg]} \quad (1)$$

Reforming temperatures were between 400°C and 700°C, and the catalyst bed was heated using a tubular electric furnace. Exhaust gas from the catalyst bed was collected with a syringe and analyzed by gas chromatography for the composition of the reformed gas. Ammonia conversion in the reforming reaction was determined from the gas composition. The method for determining the ammonia conversion is shown below.

$$\text{Ammonia conversion} [\%] = \frac{\text{moles of ammonia consumed}}{\text{moles of ammonia fed}} \times 100 \quad (2)$$

RESULTS AND DISCUSSION

NW Catalysts Preparation

The fabricated ZnO nanowires are shown in Fig. 1. It can be seen that the nanowires with hexagonal cross sections extend in various directions. Compared to ZnO nanowires in the LG mode (Fig. 1 (b)), the number of nanowires increases with the introduction of the BG mode (Fig. 1 (a)), and the nanowires grow radially. Fig. 2 shows NiO on the fabricated ZnO nanowires, where NiO was deposited to cover the surface of the ZnO nanowires.

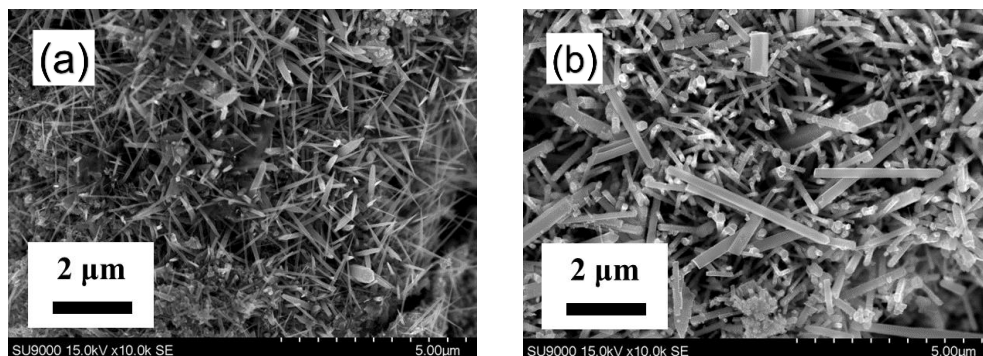


Fig. 1. ZnO NWs of (a) BG mode and (b) LG mode

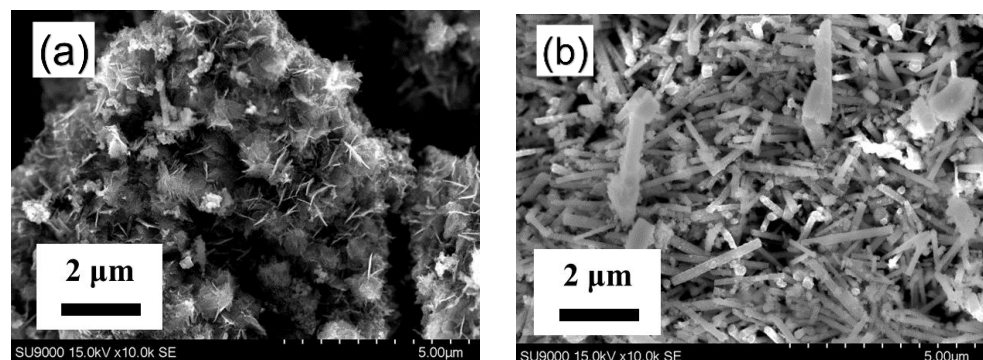


Fig. 2. Ni/ZnO NW catalysts of (a) BG mode and (b) LG mode

Ammonia Reforming

Reforming tests were performed with five catalyst masses packed in the catalyst bed. Hydrogen reduction (99.9% H₂, 1 h) was performed at 500°C prior to the reforming test. Fig. 3 shows the results of the reforming tests. For all WHSVs, it can be seen that the ammonia conversion rate increases with increasing reforming temperature. The WHSV dependence of the ammonia conversion shows that the

conversion reasonably tended to increase with decreasing WHSV; comparing the ammonia conversion rates of the BG and LG modes, the difference is more pronounced at WHSV 6000.

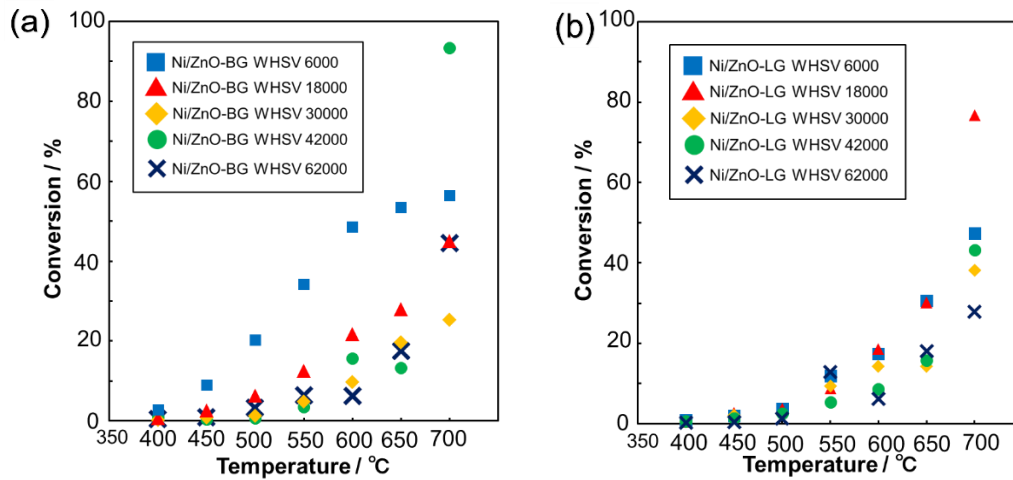


Fig. 3. Ammonia conversion of Ni/ZnO NW catalysts of (a)BG mode and (b) LG mode

The reaction rate constants were estimated from the fundamental equation of the tube reactor to evaluate its catalytic properties [5]. The following equation expresses the basic equation for a tube-type reactor.

$$\tau = \int_{C_{\text{NH}_3,0}}^{C_{\text{NH}_3}} \frac{dC_{\text{NH}_3}}{-r_{\text{NH}_3}} \quad (3)$$

where τ is the residence time of the gas (s), C_{NH_3} is the ammonia concentration (mol m^{-3}), $C_{\text{NH}_3,0}$ is the ammonia concentration at the reactor inlet, and r_{NH_3} is the ammonia decomposition rate (mol s^{-1}). Under isobaric conditions, the volume of gas increases as ammonia decomposition proceeds, so the following equation defines the volume expansion rate, $\varepsilon_{\text{NH}_3}$.

$$\varepsilon_{\text{NH}_3} = \frac{V_{X=1} - V_{X=0}}{V_{X=0}} = \frac{(0.5 + 1.5) - 1}{1} = 1 \quad (4)$$

where X is the ammonia conversion rate (-). The ammonia concentration can be expressed as follows using $\varepsilon_{\text{NH}_3}$ and X .

$$C_{\text{NH}_3} = \frac{(\varepsilon_{\text{NH}_3} - X)}{(\varepsilon_{\text{NH}_3} + X)} C_{0,\text{NH}_3} = \frac{(1-X)}{(1+X)} C_{0,\text{NH}_3} \quad (5)$$

Assuming that the ammonia decomposition reaction is a first-order reaction, the decomposition rate can be expressed by the following equation using the reaction rate constant k .

$$r_{\text{NH}_3} = \frac{-k(1-X)}{(1+X)} C_{0,\text{NH}_3} \quad (6)$$

Substituting equation (6) into equation (3), we obtain the following relationship:

$$k\tau = 2 \ln \frac{1}{1-X} - X \quad (7)$$

Fig. 4(a) and (b) show plots of the relationship in Eq. (7), where the reaction rate constant k is estimated from the slope of the approximate straight line. Fig. 4(c) shows an Arrhenius plot with the natural

logarithm of the obtained rate constant on the vertical axis and the reciprocal of the temperature on the horizontal axis. From the Arrhenius plot, the activation energy and frequency factor for the BG and LG mode nanowire catalysts in this reforming test were estimated to be 81.9 kJ mol⁻¹, 8.96×10⁴ s⁻¹, and 77.8 kJ mol⁻¹, 4.73×10⁴ s⁻¹, respectively. The frequency factor was larger in the BG mode, likely due to the larger catalyst surface area resulting from the tree formation.

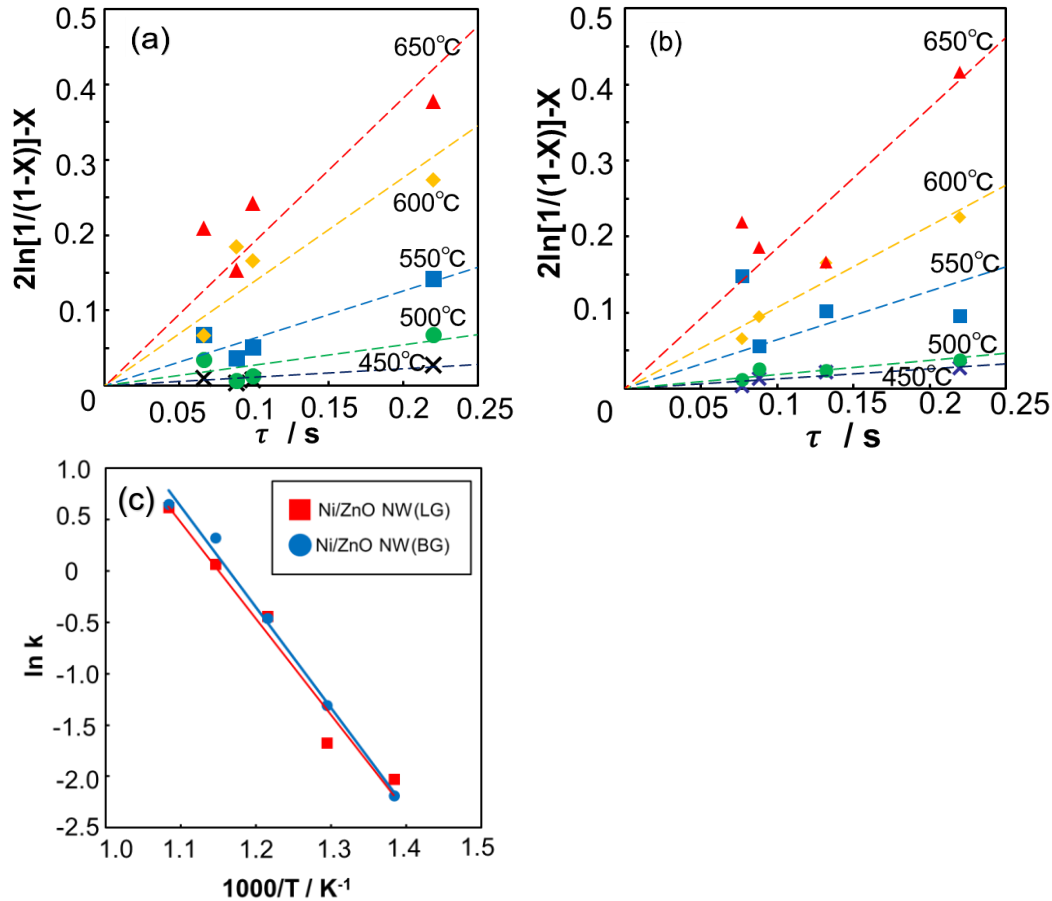


Fig. 4. Plots of $2 \ln[1/(1-XNH_3)] - XNH_3$ against τ for the Ni/ZnO NW of (a) BG mode and (b) LG mode, and (c) Arrhenius plots for the Ni/ZnO NW catalysts (BG and LG) from 723 to 923 K.

Table 1 shows that the obtained activation energy and frequency factor are not significantly different from those of the other reported cases, but the frequency factor is smaller than that of the other reported cases. This may be due to the lack of catalyst surface area; increasing the number of dendritic processes is expected to further expand the catalyst surface area and improve the conversion ratio.

Table 1. Activation energy and frequency factor of each catalyst.

Catalyst	Activation energy (kJ mol ⁻¹)	Frequency factor (s ⁻¹)
Ni/ZnO nanowire (LG)	77.8	4.73×10 ⁴
Ni/ZnO nanowire (BG)	81.9	8.96×10 ⁴
Ni/SiO ₂ [5]	108	4.40×10 ⁷
12%Ni/MRM [6]	72.1	-
Ni/Zr-doped Al ₂ O ₃ [7]	86.44	-



CONCLUSIONS

Ni/ZnO nanowire catalysts for reforming were fabricated, and reforming tests showed that the ammonia conversion tended to increase with decreasing WHSV. The activation energy and frequency factor of Ni/ZnO nanowire catalysts in BG and LG modes were 81.9 kJ mol⁻¹, 8.96×10⁴ s⁻¹, and 77.8 kJ mol⁻¹, 4.73×10⁴ s⁻¹, respectively. The BG mode showed a larger frequency factor, which may be attributed to the increased catalyst surface area due to tree formation. The frequency factor was smaller than that in previous reports, possibly due to the lack of the catalyst surface area. Increasing the number of dendritic processes is expected to further increase the surface area of the catalyst and improve the ammonia conversion.

ACKNOWLEDGEMENT

We would like to thank Professors Kohei Ito and Tatsumi Kitahara of the Department of Mechanical Engineering, Kyushu University, for their invaluable contributions to our discussions.

REFERENCES

1. M. Aziz, A. T. Wijayanta, and A. B. D. Nandiyanto. 2020. Ammonia as Effective Hydrogen Storage: A Review on Production, Storage and Utilization. *Energies* 13:3062-3086.
2. T.V. Choudhary, C. Sivadinarayana and D.W. Goodman. 2001. Catalytic ammonia decomposition: CO_x-free hydrogen production for fuel cell applications. *Catalysis Letters* 72:197-201.
3. H. Nakajima, D. Lee, M. Lee, C. P. Grigoropoulos. 2016. Hydrogen production with CuO/ZnO nanowire catalyst for a nanocatalytic solar thermal steam-methanol reformer. *International Journal of Hydrogen Energy* 41:16927-16931.
4. S.H. Ko, D. Lee, H.W. Kang, K.H. Nam, J.Y. Yeo, S.J. Hong, C.P. Grigoropoulos, and H.J. Sung. 2011. Nanoforest of Hydrothermally Grown Hierarchical ZnO Nanowires for a High Efficiency Dye-Sensitized Solar Cell. *Nano Letters* 11:666-671.
5. R. Atsumi, R. Noda, H. Takagi, L. Vecchione, A. D. Carlo, Z. D. Prete, K. Kuramoto. 2014. Ammonia decomposition activity over Ni/SiO₂ catalysts with different pore diameters. *International Journal of Hydrogen Energy* 39:13954-13961.
6. J.L. Cao, Z.L. Yan, Q.F. Deng, Y. Wang, Z.Y. Yuan, G. Sun, T.K. Jia, X.D. Wang, H. Bala, and Z.Y. Zhang. 2014. Mesoporous modified-red-mud supported Ni catalysts for ammonia decomposition to hydrogen. *International Journal of Hydrogen Energy* 39:5747-5755.
7. S. Henpraserttae, S. Charojrochkul, W. Klysubun, L. Lawtrakul, P. Toochinda. 2018. Reduced Temperature Ammonia Decomposition Using Ni/Zr-Doped Al₂O₃ Catalyst. *Catalysis Letters* 148:1775-1783.

ICH2P14-PP168

CURRENT AND TEMPERATURE DISTRIBUTIONS IN A PLANAR SOLID OXIDE ELECTROLYSIS CELL IN-SITU ASSESSED WITH SEGMENTED ELECTRODES

¹Kentaro Yokoo, ^{1,2*}Hironori Nakajima, ^{1,2}Kohei Ito

¹Department of Hydrogen Energy Systems, Graduate School of Engineering, Kyushu University, 744 Motooka, Nishi-ku, Fukuoka 819-0395, Japan

²Department of Mechanical Engineering, Faculty of Engineering, Kyushu University, 744 Motooka, Nishi-Ku, Fukuoka 819-0395, Japan

*Corresponding author e-mail: yokoo.kentaro.fcs@gmail.com, nakajima@mech.kyushu-u.ac.jp

ABSTRACT

This study investigates current and temperature distributions in solid oxide electrolysis cells (SOECs) for high-temperature steam electrolysis. Segmented anodes enable successful separation of current measurements upstream, midstream, and downstream along the gas flow channels (co-flow) under voltage control. The results are useful to validate three-dimensional finite element models for enhanced SOEC design, improving performance and durability. A cathode-supported planar cell was used for the experiments. The cell consisted of a NiO/YSZ cathode, LSC anode, and YSZ electrolyte. The anode was segmented using silver mesh current collectors and stainless-steel interconnectors. Voltage-controlled current-voltage measurements were performed to simulate a normal cell, while temperature variations with electrolysis voltage were monitored using K-type thermocouples. A low inlet steam flow rate led to a reduced current density downstream owing to the concentration overpotential from the reduced steam concentration with upstream consumption. Temperature changes revealed that heat absorption prevailed at low currents below the thermoneutral voltage, transitioning to heat production at higher currents with more dominant Joule heat from the overpotentials. The segmenting anode allowed successful current separation measurements in different sections, enabling generalized numerical models for improved cell stack performance through operational optimization and interconnector design.

Keywords: SOEC, Hydrogen production, Electrode-segmentation method, Current distribution.

INTRODUCTION

SOEC is an electrochemical device that operates at high temperatures, enabling highly efficient hydrogen production using renewable energy. Because the electrolyte is conductive to oxygen ions, carbon dioxide can be electrolyzed simultaneously with water vapor (co-electrolysis) to produce hydrogen and carbon monoxide synthesis gas. In SOECs, the current and temperature distribution caused by water vapor consumption from the upstream to the downstream of the gas flow channel is problematic, leading to a decrease in efficiency and thermo-mechanical/chemical durability [1][2]. Although many numerical calculations have been reported on the current, temperature, and partial pressure distributions of water vapor in SOECs [3–5], there are few examples of actual measurements [6]. In addition, actual measurements and numerical calculations in co-electrolysis and the direct measurement of the current in each part using the segmented electrode method are scarce [7]. In this study, the oxygen electrode of a steam electrode-supported planar cell was divided along the gas stream in the upstream, midstream, and downstream sections, and direct measurement of the currents at each section was performed.



Fig. 1. Anode of the experimental cell

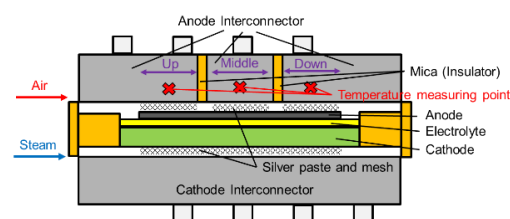


Fig. 2. Cross-sectional drawing of the segmented cathodes and current collectors.

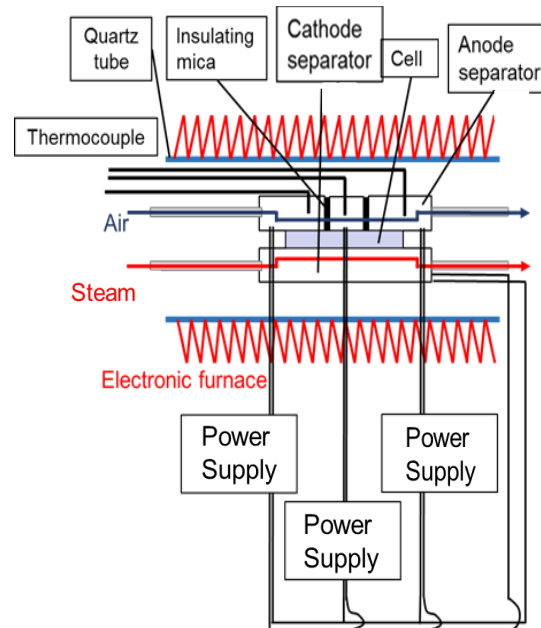


Fig. 3. Experimental set-up

MATERIALS AND EXPERIMENTAL METHODS

Oxygen electrode segmented cell

In this study, experiments were conducted using a planar cell with hydrogen electrode (cathode) support as shown in Figure 1. The hydrogen electrode was NiO/YSZ, oxygen electrode was LSC, electrolyte was YSZ, and intermediate layer was GDC (ASC-400B, Elcogen, Estonia). The hydrogen electrode area was 19.5 (6.5 x 3.0) cm², and the oxygen electrode area was 7.2 (4.8 x 1.5) cm². The oxygen electrode (anode) was divided into three equal areas with segmented silver mesh current collectors fixed with silver paste (Dotite D-500, Fujikura Kasei Co., Ltd.) on the electrode. The interconnector (SUS430) was also divided into three segments on the oxygen electrode side with electrical insulation (mica) between them. In both electrode sides, depth and width of the flow channels were both 1 mm for eight parallel channels along the long side. Because the current and partial pressure distribution of water vapor on the hydrogen electrode is of particular interest in this study, only the oxygen electrode was divided to prevent the influence of the division of the hydrogen electrode on the gas flow in the in-plane direction. Single-electrode segmentation is enough owing to the dominant current flowing in the through-plane (thin) direction.

Electrochemical measurement

A cross-sectional view of the interconnector is shown in Figure 2. A schematic diagram of the experimental setup is shown in Figure 3. Current-voltage (I-V) measurements were performed under voltage control so that the electrodes of each section were under equipotential to reproduce the conditions of a normal single cell, using three power supply units. A four-terminal method with separate current and voltage lines was used for measurements. I-V measurements were taken at each section of the cathode after reduction with H₂O/H₂/N₂ gas mixture (H₂O 240 cm³min⁻¹, H₂ and N₂ 120 cm³min⁻¹ (at 25 °C, 1 atm)). The hydrogen electrode was supplied with H₂O/H₂ gas mixture at inlet flow rates of 40/40, 80/80, and 120/120 cm³min⁻¹ (at 25 °C, 1 atm), while the oxygen electrode was supplied with a constant inlet flow rate of 400 cm³min⁻¹ (at 25 °C, 1 atm) dry air in a co-flow configuration. Experiments were conducted using a tube furnace to maintain the cell temperature at 650 °C at the open-circuit voltage (OCV). Three K-type thermocouples were inserted into the upstream, midstream, and downstream portions of the anode interconnectors, and the temperature in each anode interconnector, 7 mm from the electrode, was measured.

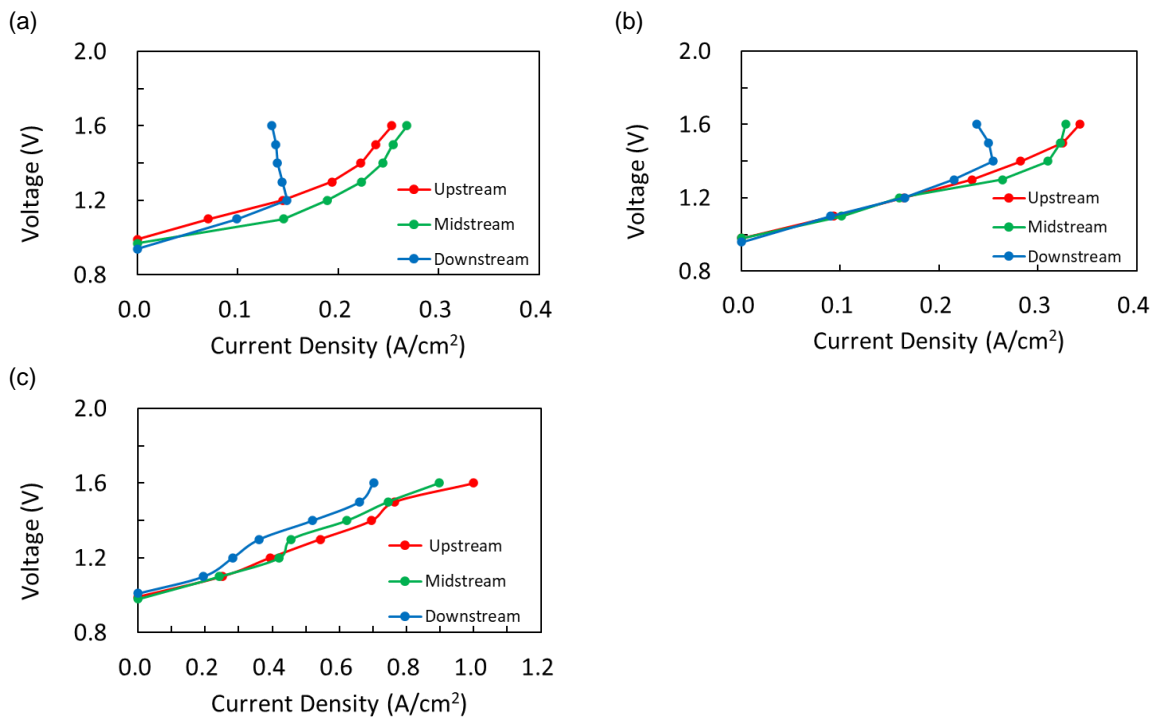


Fig.4 Voltage-controlled I-V characteristics of the cathode-supported SOEC for the up/middle/downstream parts at 650 °C. Inlet flow rates: H₂/H₂O/Air of (a) 40/40/400 (b) 80/80/400 (c) 120/120/400 cm³/min.

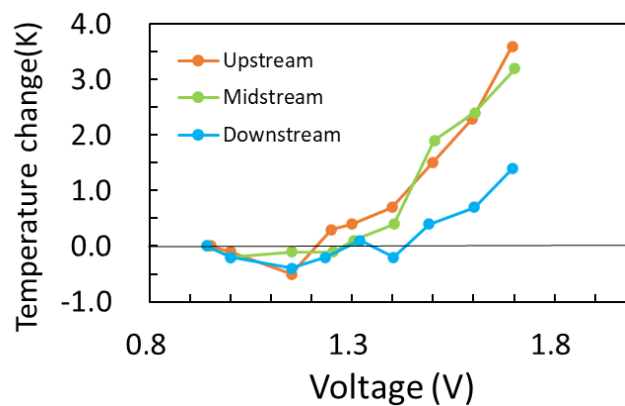


Fig.5 Temperature change from OCV. Inlet flow rates: H₂/H₂O/Air of 40/40/400.

RESULTS AND DISCUSSION

IV characteristics for each flow rate condition are shown in Figure 4. Under high flow rate conditions (b) and (c), the performance was close in the upstream, midstream, and downstream regions, whereas under low flow rate condition (a), the current density decreased in the high voltage region and the decrease was most pronounced in the downstream region. This is possibly due to an increase in the concentration overpotential including the Nernst loss [8], caused by insufficient steam supply to the midstream and downstream segments owing to the reduced inlet flow rate.

Figure 5 shows the temperature change from the open circuit voltage (OCV) versus the electrolysis voltage. The heat balance in the electrolysis consists of the endotherm of the reversible heat $T\Delta S$, the heat production with the total overpotential, including the Ohmic overpotential associated with electron and ion transport, and the reaction overpotentials. Therefore, at low currents, the cell temperature



decreases as the heat absorption rate exceeds the heat production rate, and as the current increases, the heat production rate with the overpotentials increases, resulting in the cell temperature increase.

CONCLUSIONS

To elucidate the current distribution in the gas flow direction in a planar SOEC, a planar cell with three segmented oxygen electrodes was prepared. IV measurements were carried out under voltage control to ensure that the electrodes in each section were equipotential as in a normal cell using three power supply units, and the currents in the upstream, midstream, and downstream sections were successfully measured separately. Numerical modeling based on this measured current distribution can be generalized to optimize the operating conditions and interconnector design guidelines for improving the performance of practical cell stacks.

ACKNOWLEDGEMENT

This work is supported by JSPS KAKENHI Grant Number JP21K03916.

REFERENCES

1. A. Pandiyan, A. Uthayakumar, R. Subrayan, W. Cha, B. Krishna, 2019. *Nanomaterials and Energy* 8(1):2-22
2. A. Nakajo, Z. Wuillemain, J. V. herle, D. Favrat, 2009. *Journal of Power Sources* 193:203-215
3. J. Udagawa, P. Aguiar, N.P. Brandon, 2007. *Journal of Power Sources* 166:127-136
4. D. Gordin, J. Deseure, P. Chabriat, B. Grondin-Perez, A. Brisse, 2013. *Chemical Engineering Research and Design* 91:134-140
5. V. Menon, F. Qingxi, V.M. Janardhanan, O. Deutschmann, 2015. *Journal of Power Sources* 274:768-781
6. T. Mizusawa, T. Araki, M. Mori, 2016. *International Journal of Hydrogen Energy* 41:13888-13900
7. X. Wang, H. Nakajima, Y. Iwanaga, K. Ito, 2023. *Journal of Energy Storage* 72:108459
8. H. Nakajima and T. Kitahara, 2018. *Marine Engineering* 53: 230–236



ICH2P14-PP170

IN-SITU CURRENT DISTRIBUTION MEASUREMENTS OF A PLANAR SOLID OXIDE FUEL CELL FOR A THREE-DIMENSIONAL FINITE ELEMENT MODEL TO TRAIN A MACHINE-LEARNING SURROGATE MODEL

¹Yutaro Ito, ^{1,2}Yingtian Chi, ^{1,3*}Hironori Nakajima

¹Kyushu University, Graduate School of Engineering, Department of Hydrogen Energy Systems,
744 Motoooka, Nishi-ku, Fukuoka 819-0395, Japan

²Tsinghua University, Department of Electrical Engineering, Beijing 100087, China

³Kyushu University, Faculty of Engineering, Department of Mechanical Engineering,
744 Motoooka, Nishi-ku, Fukuoka 819-0395, Japan

*Corresponding author e-mail: nakajima@mech.kyushu-u.ac.jp

ABSTRACT

Solid oxide fuel cells (SOFCs) offer advantages such as high efficiency and fuel flexibility without costly catalysts, owing to their high working temperature. To date, investigating the three-dimensional (3D) distribution of current density, gas concentration, and temperature in cells and stacks has been associated with significant computational expenses. Past efforts involved 3D simulations based on conservation laws to optimize cell and stack designs. In this research, we conduct current distribution measurements on a planar test cell (Ni/8YSZ anode, LSC cathode, and 8YSZ electrolyte) with segmented silver mesh current collectors and stainless-steel interconnectors for upstream, midstream, and downstream parts along the flow channels. They were electrically insulated from one another. Current–voltage characteristics were measured using three electronic loads under voltage control. Thereby, we develop and validate a 3D finite element model. Employing machine learning techniques, we generate a surrogate model from current densities for various cell voltages, inlet gas conditions and cell temperatures as training data predicted by the finite element model. The surrogate model can offer significant computational cost reduction.

Keywords: Solid oxide fuel cell, Multiphysics simulation, Segmented electrodes, Machine learning, Surrogate model.

INTRODUCTION

Solid Oxide Fuel Cells (SOFC) have the advantages of high efficiency, high flexibility in fuel selection, and no need for expensive electrocatalysts. They have advantages such as high efficiency, high fuel flexibility, and no need for expensive electrode catalysts. So far, three-dimensional (3D) simulation analyses using numerical models based on physical laws (conservation laws) have been performed to obtain optimal design guidelines for actual cell stacks. However, such simulations require a large amount of computational time and computer processing power. On the other hand, the construction of a surrogate model by machine learning using conventional simulation data as a teacher is expected to significantly reduce the computational cost of simulation analysis. In this study, a 3D simulation model was constructed using the finite element (FE) method, and the model was verified by actual measurements of the current distribution in a planar test cell with segmented electrodes [1][2]. A surrogate model [3] is generated by machine learning of the current densities for the cell voltages, inlet gas flow rates, and cell temperatures from a finite element model.

EXPERIMENTS AND MODEL BUILDING

SOFC test cell with segmented electrodes

An anode-supported planar cell of NiO/YSZ anode, LSC cathode, and YSZ electrolyte with an intermediate layer of GDC (ASC-400B, Elcogen, Estonia) was used for the measurements. The anode area was 19.5 (6.5 x 3.0) cm², while the cathode area was 7.2 (4.8 x 1.5) cm². A test cell was assembled by dividing the current collector layer (silver mesh) and interconnector (SUS430) for the cathode into three parts in the upstream, midstream, and downstream in the direction of flow channels with electrical insulation between them (mica). In both electrode sides, depth and width of the flow channels were both 1 mm for eight parallel channels along the long side. Cell temperatures were maintained at 600, 650, and 700°C in a tubular electric furnace. Three electronic loads were used to measure the current-voltage (I-V) characteristics at the three segments under

voltage control so that the upstream, midstream, and downstream segments were equipotential to reproduce the operating conditions of actual cells [1][2]. A four-terminal method was used for the measurement, in which the current and voltage lines were separated to exclude voltage drops due to wiring resistance and contact resistance. The center temperatures of the upstream, midstream, and downstream interconnector segments were measured with K-type thermocouples. Inlet hydrogen gas flow rates were 40, 80, and 120 cm³/min (at 25°C, 1atm) and inlet air flow rates were 100, 200, and 400 cm³/min (at 25°C, 1atm) in a co-flow configuration.

Construction and validation of 3D models with finite element method

A 3D FE model was constructed to reproduce the measured I-V characteristics (COMSOL Multiphysics). Basic equations were the Butler-Volmer equation (electrochemistry), Brinkman equation (flow in porous media), Navier-Stokes equation (flow in channel), and Stefan-Maxwell equation (gas diffusion).

Generate surrogate models using machine learning

A surrogate model was generated by machine learning using the output data of current density at various gas supply conditions, cell temperatures, and cell voltages from the constructed three-dimensional finite element model as teacher data. A neural network was used for the machine learning. The surrogate model outputs the current density for the supply gas condition, cell temperature, and cell voltage, and predicts the I-V characteristics. A total of 216 point outputs from the 3D FE model were used as the teacher data. MATLAB was used for machine learning and surrogate model generation.

RESULTS AND DISCUSSION

Current distribution with the segmented electrodes

Fig. 1 shows the I-V characteristics of each part at hydrogen and nitrogen gas flow rates of 120 cm³/min, air flow rates of 400 cm³/min, and 600, 650, and 700°C. As the temperature rises, the current density in each section increases. The current density of each part increases with increasing temperature that promotes ionic conduction and electrode reactions (the overpotentials of each part decrease at the

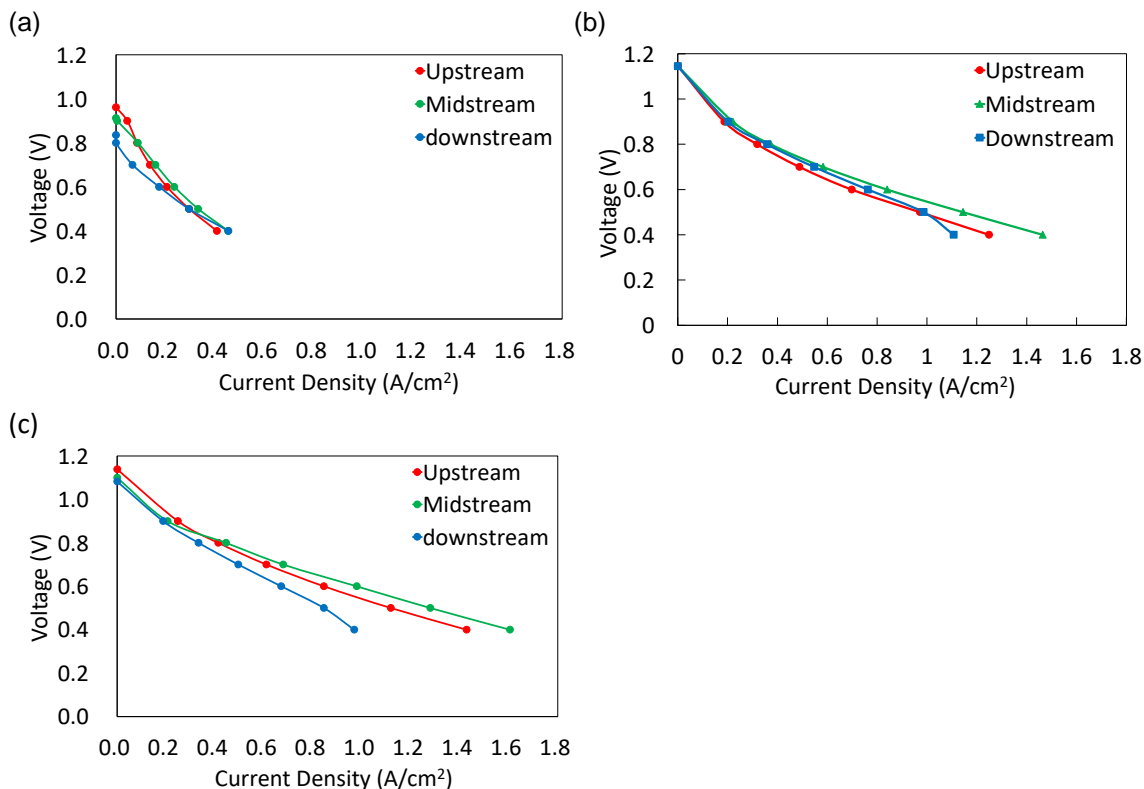


Fig. 1 Voltage-controlled I-V curves for the segments at (a) 600°C, (b) 650°C, and (c) 700°C. Inlet H₂/ N₂/ Air: 120/120/400 cm³/min (25°C, 1 atm).

same current density). It can also be seen that the current distribution is enhanced as the temperature rises, and that the current density downstream relatively does not increase much. The current density increases in the upstream and midstream parts due to the temperature rise, consuming more fuel and supplying insufficient fuel to the downstream part. However, at 600°C, fuel consumption is suppressed in the upstream and midstream parts, feeding sufficient fuel to the downstream part. Similar results were also obtained for other hydrogen gas flow rates and air flow rates. As a result, I-V characteristics were obtained to verify the 3D model. The current density in the midstream tends to be larger than that in the upstream because of the temperature distribution in the tube furnace.

Construction and validation of 3D models by finite element method

A 3D FE model was constructed to reproduce the measured current distributions. The model agrees with the measured I-V curves, and data for machine learning were extracted from the model. Comparisons of the I-V characteristics between the 3D FE model predictions and measurements are presented in Fig. 2.

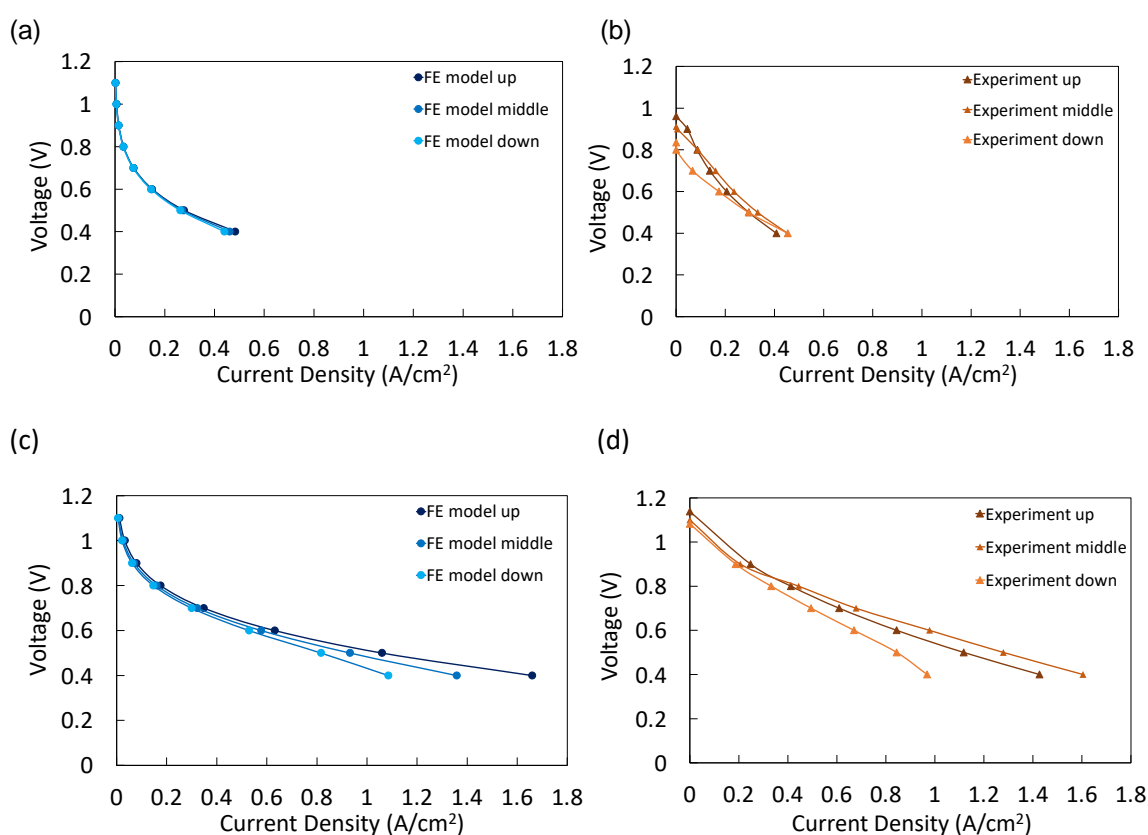


Fig. 2 Predicted (a), (c) and measured (b), (d) I-V curves at 600°C and 700°C, respectively. Inlet H₂/ N₂/ Air: 120/120/400 cm³/min (25°C, 1 atm).

Generate surrogate models using machine learning

From the 3D FE model, multipoint data were exported for the combination of the fed gas flow rates, cell temperatures, cell voltages, and current densities. Surrogate models were generated by machine learning using these data as teacher data. Fig. 3 shows a comparison of the I-V characteristics predicted by the FE and surrogate models under temperature conditions not used for the teacher data.

CONCLUSIONS

The I-V characteristics for various inlet hydrogen and air flow rates, and cell temperatures were measured in the upstream, midstream, and downstream segments along parallel flow channels in a co-flow configuration. As a result, the current density distributions depending on the feed gas flow rate and cell temperature were

obtained. The current density decreases in the downstream segment because of the high consumption of fuel and oxygen in the upstream segment. The current distribution is enhanced at higher temperatures. A 3D FE model was constructed based on the validation with the experimental I-V characteristics. A surrogate model was generated by machine learning using the multipoint data output from the FE model as teacher data. The predicted I-V characteristics from the surrogate model showed.

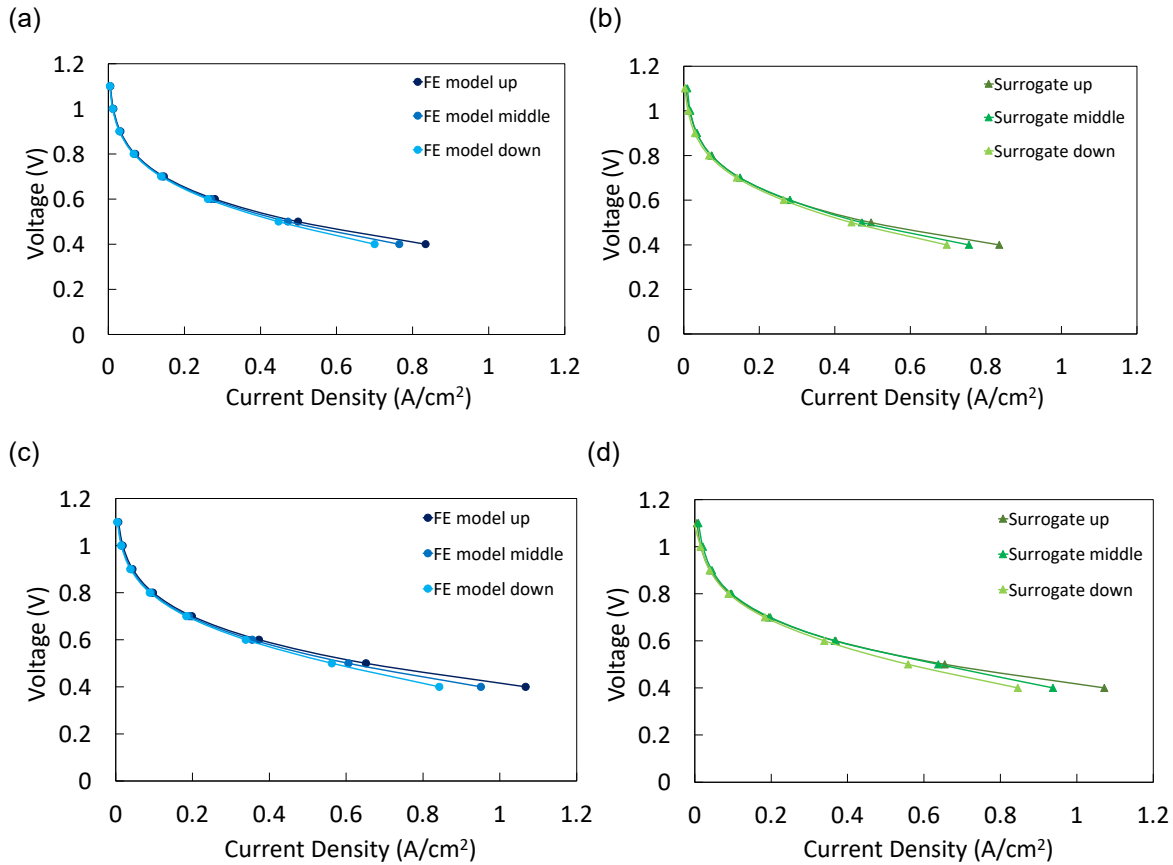


Fig. 3 I-V curves predicted by the FE (a), (c) and surrogate (b), (d) models at 640°C and 660°C, respectively. Inlet H₂/N₂/air: 120/120/400 cm³/min (25°C, 1 atm).

good agreement with the validation data from the FE model, indicating the feasibility of using a surrogate model to reduce computational cost.

ACKNOWLEDGEMENT

We are grateful to Professors Kohei Ito and Tatsumi Kitahara of the Department of Mechanical Engineering, Kyushu University, for their fruitful discussions.

REFERENCES

1. Ö. Aydın, T. Koshiyama, H. Nakajima, and T. Kitahara, *Journal of Power Sources* 279 (2015) 218–223.
2. H. Nakajima, T. Kitahara, and E. Tsuda, *ECS Transactions*, 78 (2017) 2109–2113.
3. Y. Chi, K. Yokoo, H. Nakajima, K. Ito, J. Lin, and Y. Song, *Journal of Power Sources* 562 (2023) 232760.



ICH2P14-PP188

HYDROGEN NAVAL PROPULSION: PROBLEMS AND SOLUTIONS

**Remili Sadia, Mohamed Chaimaa*

University of sciences and technologies, El menouar, Oran, Algeria

*Corresponding author e-mail: remili_sadia@yahoo.fr

ABSTRACT

Main ships emissions in Algeria are nitrogen oxides, sulphur oxides, carbon dioxide, fine particles and polycyclic aromatic hydrocarbons. According to IMO data, ships emissions were estimated around 4.5 million tonnes, which represents an increase of 50% compared to 2012. Algeria has developed a national strategy to combat against climate change aimed at reducing greenhouse gas emissions by 7% by 2030 compared to 2015 levels. The main objective of this work is to highlight the effectiveness of hydrogen propulsion in the field of maritime transport in the fight against air pollution by comparing to other types of propulsion in Algeria.

The hydrogen propulsion system is an effective solution to reduce greenhouse gas ships emissions. It can reduce emissions by 50-100% compared to traditional internal combustion engines. Additionally, hydrogen propulsion system is quiet and requires less maintenance than internal combustion engines, still relatively new and expensive, but it is under development and expected to become more affordable in the future. Many ships using this system are already in service around the world, including ferries and cruise ships. It is a promising solution to reduce greenhouse gas ships emissions and contribute to the fight against climate change. Hydrogen is stored in liquid or gas form on ship board, and when burned in the fuel cell, it produces only water as a by-product.

In longer term, hydrogen, ammonia or methanol could emerge as the future fuels. Carbon neutral, provided they come from clean sources, they still present numerous technical constraints: specific storage conditions (temperatures, adapted tanks and toxicity), larger volume than conventional fuel oil and production costs that are still too restrictive.

The adoption of these new fuels could take ten or even twenty years.

Keywords: Emission, Algeria, Hydrogen propulsion, Reduction, Fuel cell.

1. INTRODUCTION

In the rapidly evolving world of maritime transportation, ship propulsion plays a pivotal role in driving efficiency, sustainability, and safety. As a nation blessed with a rich coastline and a vibrant maritime industry [1], Algeria has embarked on a quest to explore innovative propulsion technologies that not only enhance its shipping capabilities but also align with its commitment to environmental stewardship.

This article delves into the various types of ship propulsion systems and sheds light on the propulsion ships used in Algeria, with a specific focus on hydrogen propulsion.

By understanding the different technologies employed in the maritime sector, we can gain insights into the progress and potential of the Algerian shipping industry. Transition to LNG: In line with global efforts to reduce emissions [2], Algeria's shipping industry has shown a growing interest in LNG propulsion. The National Shipping Company of Algeria (CNAN) has initiated discussions to retrofit some of its vessels with LNG-powered engines, minimizing environmental impact and ensuring compliance with international emission standards.

Green Initiatives: Algeria's commitment to sustainable practices has led to increased investments in research and development of alternative propulsion technologies. Academic institutions, along with public and private entities [3], are exploring collaborations to support green propulsion projects and facilitate knowledge exchange in the field.

Algeria, with its vast hydrogen reserves and commitment to renewable energy, has emerged as a key player in the development of hydrogen propulsion technology. As the demand for cleaner and more efficient transportation grows, Algeria has been exploring the use of hydrogen-powered vehicles and the necessary regulations to promote their adoption. In this article, we will delve into the various aspects of hydrogen propulsion in Algeria and the regulations set forth by the Organization Maritime International (OMI) to ensure safe and environmentally friendly practices, the potential benefits of hydrogen propulsion for the country [3] and the challenges faced in its implementation. Additionally we will examine the specific regulations imposed by OMI to govern the use of hydrogen propulsion on maritime vessels and their importance in ensuring international safety standards

2. MATERIALS AND METHODS

Hydrogen fuel cells offer several advantages over conventional gasoline or diesel engines. FCVs have longer driving ranges and shorter refueling times compared to battery electric vehicles. They also produce no harmful emissions [4], making them a viable option for achieving zero-emission transportation.

However, there are some challenges associated with hydrogen propulsion. Firstly, hydrogen production requires energy-intensive processes and currently relies heavily on fossil fuels. Developing green hydrogen production methods, such as electrolysis powered by renewable energy, is crucial for a sustainable hydrogen economy. Additionally, building a refueling infrastructure for hydrogen is costly and challenging. The limited availability of hydrogen refueling stations can restrict the widespread adoption of FCVs. In this section we discuss different ship propulsion.

2.1. Identification of propulsion types

2.1.1. Traditional Propulsion

Conventionally, ships have relied on diesel engines as the primary source of propulsion. Diesel engines burn fossil fuels, emit greenhouse gases [5] and contribute to marine pollution. However, advancements in engine technology have led to significant improvements in fuel efficiency, reducing the environmental impact.

2.1.2. Liquefied Natural Gas (LNG) Propulsion

LNG-powered ships are gaining popularity due to their lower emissions and reduced operating costs. Natural gas, when burned, produces fewer pollutants and greenhouse gases compared to conventional diesel fuel [6]. LNG-powered engines are gradually being adopted as an alternative propulsion system worldwide.

2.1.3. Electric Propulsion

Electric propulsion systems harness electric motors powered by batteries, fuel cells, or shore-based power. These systems are emission-free during operation and have the potential to revolutionize maritime transport by reducing dependence on fossil fuels [6]. Electric propulsion is being increasingly explored for smaller vessels and futuristic concepts.

2.1.4. Hybrid Propulsion

Combining traditional engines with electric technology, hybrid propulsion systems offer significant fuel savings and emissions reductions. These systems can operate on various power sources, such as diesel generators, batteries, or fuel cells. Hybrid propulsion is emerging as a practical solution for achieving sustainability goals without sacrificing power and efficiency.

2.1.5. Hydrogen propulsion

Hydrogen propulsion is a technology that utilizes hydrogen as a fuel source in various applications, including transportation and energy generation [7]. Its use is gaining attention due to its potential to reduce greenhouse gas emissions and dependence on fossil fuels.

In the context of transportation, hydrogen propulsion typically refers to the use of hydrogen fuel cells to power vehicles. Unlike traditional internal combustion engines that burn fossil fuels [6] fuel cell vehicles (FCVs) convert hydrogen and oxygen into electricity, with water as the only byproduct. This makes them highly efficient and environmentally friendly.

2.2. Analyzing various types of propulsion

Ship propulsion plays a vital role in the maritime industry, determining the efficiency, environmental impact, and overall performance of vessels. In recent years, there has been a growing interest in exploring alternative propulsion technologies that can reduce emissions and improve sustainability. This study aims to provide a comparative analysis of three popular ship propulsion systems: diesel propulsion, electric propulsion, and hydrogen propulsion, based on various factors, including construction and design, efficiency, environmental impact, and operational considerations. By examining the strengths and limitations of each system, we aim to provide insights into the feasibility and suitability of these propulsion technologies in different maritime applications.

2.2.1. Construction and architecture

Diesel Propulsion: Diesel engines are commonly used in ship propulsion systems due to their high power output and efficiency. They require a dedicated engine room for installation [7], which affects the ship's overall design and layout. The engine room needs to be well-ventilated and insulated to minimize noise and vibrations.

Electric Propulsion: Electric propulsion systems use electric motors powered by batteries or generators. They require less space compared to diesel engines, allowing for more flexible ship design and architecture. Electric propulsion systems can be integrated into the ship's structure, resulting in improved space utilization and potentially reducing the overall size of the engine room.

Hydrogen Propulsion: Hydrogen propulsion systems are still in the early stages of development for maritime applications. They require onboard hydrogen storage tanks and fuel cells to convert hydrogen into electricity. The integration of these components into the ship's architecture may require additional space allocation [7], impacting the overall design and construction.

2.2.2. Machine Room Flexibility

Diesel Propulsion: Diesel engines have a well-established infrastructure and are relatively easy to maintain and repair. The machine room layout for diesel propulsion systems is typically fixed, making it less flexible for future upgrades or modifications.

Electric Propulsion: Electric propulsion systems offer greater flexibility in machine room design. The modular nature of electric motors and associated components allows, the length of the response has a limit (we introduced this so that as many people as possible could use the free version of the chat)[6]. To extend this limit and make the responses significantly longer, please consider purchasing the full version of the chat. The lowest cost is only 399USD for one of the most powerful artificial intelligences available today,

Hydrogen Propulsion; essentially, ship propulsion on this basis always entails an electric motor in the drive train. The energy for this drive is generated in fuel cells, for example. Fuel cells are energy converters in which a fuel like hydrogen reacts with an oxidizing agent like oxygen. In the process, water, electrical energy, and heat are generated. In ship drives, the reaction inside the fuel cell is automatic and does not need to be artificially induced, but it is instead catalyzed. All that is needed is a continuous supply of oxygen from the environment and hydrogen [8]. The latter must be stored and carried on the ship in high-pressure or refrigeration tanks. As an alternative to the fuel cell, there are also hydrogen engines. These generate electrical energy in a process that is analogous to that of conventional generators that use fossil fuels. The hydrogen can be used as a gas or bound in a carrier liquid). Table 1 defines the characteristics of each propulsion system.

Table 1. Characteristics of three types of ships propulsion

Characteristics	Hydrogen propulsion	Electric propulsion	Diesel propulsion
Energetic efficiency	High	High	Low
Pollutants emission	Zero	Zero	Important
Cost	High	High	Moderate
Autonomy	Limit	Limit	High
Flexibility	High	High	Low
Construction/Architecture Impact	Important	Important	Low

2.2.3. Size and location of engine room

Diesel Propulsion:

- Size: The size of the engine room compartment for diesel propulsion can vary depending on the size and power requirements of the ship. It typically needs to accommodate the diesel engines, fuel storage tanks, exhaust systems, cooling systems, and other associated equipment [9].
- Location: The engine room compartment is usually located towards the aft (rear) of the ship, below the main deck level. It is positioned to provide easy access for maintenance and to minimize noise and vibration disturbances for passengers or crew.

Electric Propulsion:

- Size: The size of the engine room compartment for electric propulsion is generally smaller compared to diesel propulsion. It mainly houses the electric motors, power converters, batteries or energy storage systems, and control systems.
- Location: The engine room compartment for electric propulsion can be located in various areas of the ship, depending on the design and space availability. It is often situated near the stern or distributed across multiple compartments to optimize weight distribution and reduce cable lengths.

Hydrogen Propulsion;

- Size: The size of the engine room compartment for hydrogen propulsion is typically similar to that of diesel propulsion. It needs to accommodate hydrogen fuel storage tanks, fuel cells or hydrogen combustion engines, cooling systems, and associated equipment.
- Location: The engine room compartment for hydrogen propulsion is generally located towards the aft of similar ship. Figure 1 note the different position of propulsion engine.

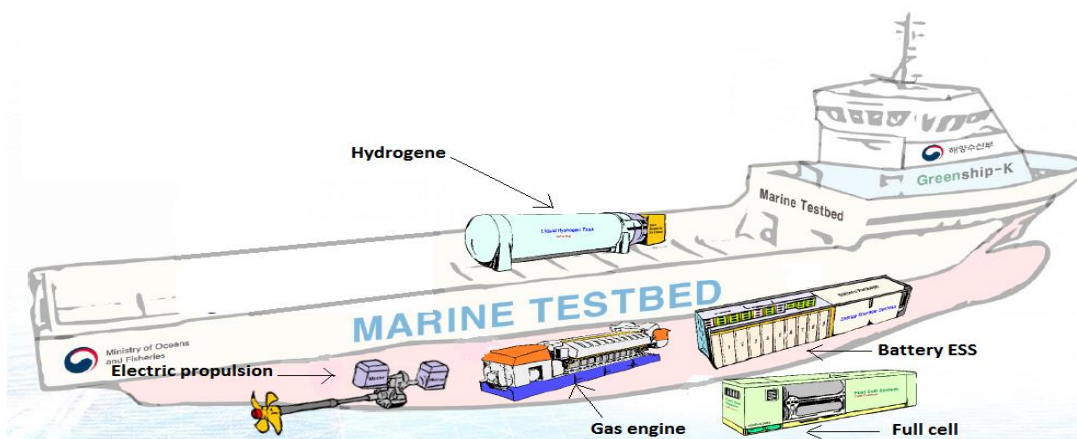


Fig.1. Different positions of propulsion engine.

RESULTS AND DISCUSSION

The maritime sector is responsible for around 2% of global greenhouse gas emissions. To decarbonize the sector, it is necessary to develop cleaner propulsion technologies.

Three emerging naval propulsion technologies (see figure 2) show promise for reducing emissions of greenhouse gases, air pollutants and fine particle matter: diesel propulsion, electric propulsion and hydrogen propulsion. In this section, we will compare propulsion systems to introduce a good solution for gas emission.

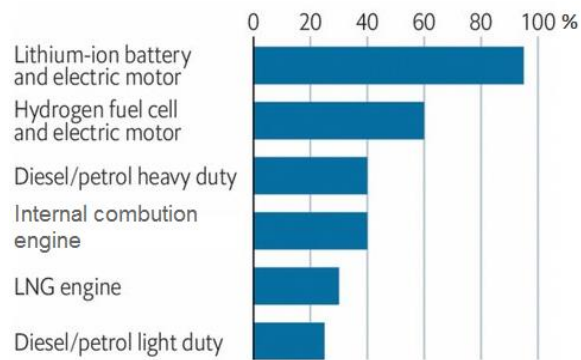


Fig.2. Typical energy efficiency for marine engines

2.3. Diesel propulsion

Diesel engines are known for their high efficiency, resulting in lower fuel consumption and operating costs and can be used for a wide range of ship sizes and types, making them a popular choice in the industry. They are generally reliable and have a long service life, requiring less maintenance and downtime. Diesel engines produce emissions, including greenhouse gases and pollutants, which can have environmental impacts. Significant noise and vibration can be observed in this system, which may require additional insulation and dampening measures. The initial cost of installing a diesel propulsion system can be higher compared to other options, especially for larger ships.

2.4. Electric propulsion

Electric propulsion is a mature technology that is already used on many small and medium-sized vessels. Electric-powered ships do not require significant changes to naval construction and architecture. Electric motors are necessary to propel the ship. Electric motors are generally smaller and lighter than diesel engines, which helps reduce the mass of the vessel. Energy storage system is also necessary. Electric-powered ships typically use batteries to store electrical energy. Electric propulsion systems use electric motors powered by batteries or generators to drive the ship's propellers. In battery-powered electric propulsion, the ship's batteries store electrical energy that is used to power the motors. Electric propulsion offers several advantages, including reduced emissions, improved energy efficiency, and quieter operation. It is commonly used in smaller vessels, such as ferries, yachts, and electric-powered boats. However, the limited energy storage capacity of batteries poses challenges for long-range and large-scale applications.

2.5. Hydrogen propulsion

Hydrogen offers immense potential for ship propulsion in terms of climate footprint, and overall sustainability. And there are many other advantages, such as a high level of safety. The generation, transport, and storage of hydrogen remain a challenge. While these tasks are unproblematic from a technological point of view, the problem is implementing them economically. Solutions to this are well under way and may even reduce costs in the long term.

Hydrogen ship propulsion essentially offers advantages comparable to those for other forms of mobility. The most prominent of these advantages is environmental friendliness. The use of hydrogen engine does not produce any emissions that are damaging to the climate or the environment. Energy only has

to be used for generation and storage. However, this energy can be acquired from green sources. For maritime shipping, wind energy stands out as a particularly obvious choice [10]. Hydrogen propulsion therefore promises climate neutrality for shipping in the long term. We can see in table 3 a comparison between different technical and economical criterion of naval propulsion.

Table 2: Technical and economical criterion of naval engine

Criterion	Hydrogen propulsion	Electric propulsion	Diesel propulsion
Efficiency at loads Max	Relatively Flat	Relatively Flat	Best at > 75%
Response to loads changes	Fuel/reformer dominate	Good	Good
Life	5 year	> 20 year	> 20 year
Noise, Vibration	Low	High	High
Power range	20-2500 kw	5-24MW	> 68 MW
NO _x , CO, HC emission, CO ₂	Very low	Very low	Medium

Another major advantage is the ability to run the system continuously without charging breaks, as would be necessary with purely electric drives. With the ever-improving ability to store cryogenic or highly compressed hydrogen, excellent ranges can be achieved with the ship drive system. Refueling operations are fast and can be easily performed during the loading and unloading of cargo or other berthing activities once an adequate infrastructure is available.

We can find four main types of cells in propulsion system on surface ships, phosphoric acid fuel cell (PAFC), the proton-exchange membrane fuel cell (PEMFC), the molten carbonate fuel cell (MCFC) and solid-oxide ceramic fuel cell (SOFC). The fuels used by these fuel cells are hydrogen, gases with high hydrogen content (see table 3)[11].

Table 3. Types of cells in propulsion system

Fuel cell type	Reactants	Operating temperature (°C)	Efficiency (%)
PEMFC	Air/reformate H ₂	80	39-52
PAFC	Air/reformate H ₂	300	38-42
MCFC	Air/methane	650	40-55
SOFC	Air/methane	900	45-60

Among the currently available fuel cell technologies, MCFC and PEMFC are considered as the most promising options for marine applications as they are available in market size, most of materials used in their manufacturing are available, and the development of their efficiency is high. In addition, SOFC has in theory the highest potential, but is currently not developed far enough.

Ultimately, the choice of propulsion type depends on factors such as environmental concerns, transportation requirements and technological capabilities. Each type of propulsion has its advantages and disadvantages, and the best choice may vary depending on the specific context [12].

3. CONCLUSIONS

The choice of propulsion type for a ship depends on various factors such as the desired speed, fuel efficiency, environmental impact, and initial investment cost. [7] While hydrogen electric ships are currently being tested and developed, they may not be widely adopted in the near future due to challenges in the production and storage of hydrogen.

Therefore, it is recommended to consider a multi-propulsion strategy for future maritime vessels, enabling them to use the most suitable propulsion system based on their operational requirements. The



use of hydrogen propulsion requires in-depth studies on this system on all technical and economic levels. As the maritime sector moves towards a greener future, Algeria is actively seeking propulsion solutions that align with its sustainable development goals. By embracing alternative technology and investing in infrastructure, [4] Algeria aims to bolster its maritime capabilities while minimizing its carbon footprint. The transition to advanced propulsion systems in Algeria not only ensures compliance with international standards but also positions the country as a regional leader in sustainable maritime operations.

However, development in the maritime field in Algeria still remains under examination before moving on to application by analyzing these strong points in relation to electric propulsion.

REFERENCES

1. United Nation. 2022. Review of maritime transport. New York 10017

2. <https://antp.dz>. Accessed on October 18, 2023

3. <https://www.ERENAV.com> . Accessed on September, 2023

4. Angelo O et al. 2023. The future of ship engines: Renewable fuels and enabling technologies for decarbonization. International journal of engine research.

5. Bechlet, M, & Kolbek A. 2017. performance and emissions of a diesel engine fueled with diesel and liquified natural gas (LNG). SAE technical paper 2017-01-0876.

6. Saurabh.S et al. 2016. Study of advancement in marine vessel propulsion system leading to progress of steerable control unit. 1st international conference on automatisisation in industries

7. Onorati A, Payri R, Vaglieco BM, et al. The role of hydrogen for future internal combustion engines. Int J Engine Res 2022; 23(4): 529–540.

8. Hordeski.M.F .2008. Alternative Fuels-The Future of Hydrogen (2nd Ed), Fairmont Press, India (2008), pp. 175-180 ISBN 0-88173-596-5

9. Malmgren E, Brynolf S, Borgh M, Ellis J, Grahn M and Wermuth N. 2020. The HyMethShip concept: An investigation of system design choices and vessel operation characteristics influence on life cycle performance. In: 8th Transport Research Arena, Helsinki, Finland.

10. Baldi S and Brynolf FM. 2019. The cost of innovative and sustainable future ship energy systems. In: Proceedings of the 32nd international conference on efficiency, cost, optimization, simulation and environmental impact of energy systems, Wroc1aw, Poland, pp.23–28.

11. Kumm.W. 1990. Marine and Naval Applications of Fuel Cells for Propulsion: The Process Selection. Journal of Power Sources, 29, pp. 169-179.

12. Yousri. M, Morsi. M and Nader. A. 2011. A comparison between fuel cells and other alternative for marine electric power generation. International journal of naval architecture and ocean engineering.

[cse.hbku.edu.qa](mailto:cse@hbku.edu.qa)

General inquiries:
cse@hbku.edu.qa
inquiry@hbku.edu.qa

P.O. Box: 34110
Doha – Qatar



HBKU



HBKU



Hamad Bin Khalifa University



Hamad Bin Khalifa University



Hamad Bin Khalifa University

Cooperating Institutions



Strategic Partner

Platinum Sponsor



Silver Sponsors





9 786250 082454